

Vol. 24, No. 2, June, 2025

ISSN (Print): 0972-6268; ISSN (Online) : 2395-3454

# NATURE ENVIRONMENT & POLLUTION TECHNOLOGY

*A Multidisciplinary, International Journal  
on Diverse Aspects of Environment*



**Technoscience Publications**

website: [www.neptjournal.com](http://www.neptjournal.com)



# Technoscience Publications

A-504, Bliss Avenue, Balewadi,  
Opp. SKP Campus, Pune-411 045  
Maharashtra, India

[www.neptjournal.com](http://www.neptjournal.com)

## Nature Environment and Pollution Technology

(An International Quarterly Scientific Research Journal)

### EDITORS

#### Dr. P. K. Goel (Chief Editor)

Former Head, Deptt. of Pollution Studies  
Y. C. College of Science, Vidyanagar  
Karad-415 124, Maharashtra, India

#### Dr. K. P. Sharma (Honorary Editor)

Former Professor, Deptt. of Botany  
University of Rajasthan  
Jaipur-302 004, India

**Executive Editor :** Ms. Apurva P. Goel, C-102, Building No. 12, Swarna CGHS,  
Beverly Park, Kanakia, Mira Road (E) (Thane) Mumbai-401107,  
Maharashtra, India

**Published by :** Ms. T. P. Goel, Technoscience Publications, A-504, Bliss Avenue,  
Balewadi, Pune-411 045, Maharashtra, India

**E-mail :** [contact@neptjournal.com](mailto:contact@neptjournal.com); [operations@neptjournal.com](mailto:operations@neptjournal.com)

### INSTRUCTIONS TO AUTHORS

#### Scope of the Journal

The Journal publishes original research/review papers covering almost all aspects of environment like monitoring, control and management of air, water, soil and noise pollution; solid waste management; industrial hygiene and occupational health hazards; biomedical aspects of pollution; conservation and management of resources; environmental laws and legal aspects of pollution; toxicology; radiation and recycling, etc.

#### Format of Manuscript

- The manuscript (mss) should be typed in double space leaving wide margins on both the sides.
- First page of mss should contain only the title of the paper, name(s) of author(s) and name and address of Organization(s) where the work has been carried out along with the affiliation of the authors.

*Continued on back inner cover...*



# Nature Environment and Pollution Technology

Vol. 24, No. (2), June 2025

## CONTENTS

1. **Staphney Texina, Sathees Kumar Nataraj, Alagammai Renganathan1 and Kavitha Vasantha**, Prediction on the Level of Toxicity in Fruits and Vegetables Based on PAHs Using Machine Learning D1690
2. **Aminul Islam, Krishna Kishore Satapathy, Sushil Kumar Kothari, Biswajit Ghosh and Shankha Koley**, Agrivoltaics: Dual Use of Land for Energy and Food Sustainability B4223
3. **Ludgardis Ledheng, Emanuel Maria Yosef Hano'e and Marce Sherly Kase**, The Study of Coastal Vulnerability in South Central Timor Regency, East Nusa Tenggara Province D1719
4. **Abhishek Maitry, Gunjan Patil and Preety Dubey**, Evaluating Phytoremediation Approaches for the Restoration of Degraded Ecosystems in India B4262
5. **Abhinav Thakur, Hina Upadhyay, Lalit Saini, Tarun Sharma and Himanshu Saini**, Comparative Analysis of Mulching and Weed Management Practices on Nutrient and Weed Dynamics of Kharif Sorghum (*Sorghum bicolor* L.) B4234
6. **Ghaidaa Sabah Yousef, Hayder Dibs and Ahmed Samir Naje**, A Review of Environmental Monitoring for Land Desertification Using Geospatial Analysis and Remote Sensing D1697
7. **Renu Bala, Rajesh Dhankhar and Sunil Kumar Chhikara**, Sustainable Phosphate Removal with Acid-Modified Fly Ash: Kinetic, Isothermal, and Thermodynamic Insights B4242
8. **Sagar Mozumder, Mahfuza Parveen and A.B.M. Kamal Pasha**, Changes in Land Use Land Cover and its Resultant Impacts on the Urban Thermal Environment of Chattogram City: A Spatio-Temporal Analysis Based on Remote Sensing and GIS Techniques D1714
9. **Malini Ray, Sneha Choudhary, Abisma K Jose, Vikash Kumar, Aakash Gupta and Sonali Bhagat**, A Complete Review on Ericoid Mycorrhiza: An Understudied Fungus in the Ericaceae Family B4252
10. **Rakesh Kumar Sarmah and Santanu Sarma**, Delineation of Potential Groundwater Zones Using GIS-based Fuzzy AHP Technique for Urban Expansion in the Southwestern Fringe of Guwahati City, India B4233
11. **Wahyu Kisworo, Sapta Suhardono, Irfan AN and I Wayan Koko Suryawan**, Evaluating the Impact of Community Attitudes on the Sustainability of 3R Temporary Waste Disposal Sites Using Structural Equation Modeling-Partial Least Square (SEM-PLS) in Sukoharjo D1702
12. **S. Monisha and S. P. Sangeetha**, Analysis of Plants, *Helianthus annuus* (Sunflower) and *Gossypium herbaceum* (Cotton), for the Control of Heavy Metals Chromium and Arsenic Using Phytoremediation Techniques B4237
13. **Evienstein Wilfred and Zulherry Isnain**, Mapping of Groundwater Potential Zones Using Fuzzy Logic Technique at Kadamaian Basin, Kota Belud, Sabah, Malaysia D1701
14. **R. Porselvan, T. S. Lakshmi and M. Tholkapiyan**, A Comparative Study of Sustainable Bacteria-Alccofine Concrete: Environmental Benefits and SEM Analysis B4250
15. **Juan Carlos Soto Quispe, Armando Fortunato Ugaz Cherre, Angel Enrique Llompарт Navarro, Irwing Smith Saldaña Ugaz, José Manuel Marchena Diones, Mariana Alexandra Montero Silva and Robert Barrionuevo García**, Diversity and Temporal Frequency of Records of the Herpetofauna of the Equatorial Seasonally Dry Tropical Forest in the Rural Community of Lucarqui, Piura, Northwestern Peru D1693
16. **Sawant Sushant Anil, Dhananjayen and M. Sasi**, Spatio-Temporal Analysis of Aridity Trends and Shifts in Karnataka Over 63 Years (1958-2020): Insights into Climate Adaptation B4255
17. **A. A. Awirya, K. E. N. Sianipar, A. Kurniawan and I. A. Sasanti**, Enhancing Economic Benefits from Forest Preservation In Papua, Indonesia: A Review D1695
18. **Akil V. Memon, Nirav V. Shah Yogesh S. Patel and Tarun Parangi**, Enhancing Land Use/Land Cover Analysis with Sentinel-2 Bands: Comparative Evaluation of Classification Algorithms and Dimensionality Reduction for Improved Accuracy Assessment B4264
19. **E. Aliaga Villanueva, P. D. Inga Canales, M. G. Mori Paccori, J. V. Cornejo Tueros and K. G. Ibarra Hinostroza**, Portable Hybrid System for Producing Green Hydrogen by Electrolysis Using Energy Generated Through an Archimedean Screw D1658
20. **Gunjan Tyagi and Md Danish**, Reflective Building Façades: The Effect of Albedo on Outdoor Thermal Comfort – A Case Study of Low-Rise Apartments B4247
21. **Vijaya Sundravel K., Abdul Bari J. and Ramesh S.**, Utilizing Bacteria for Crude Oil-Contaminated Soil Bioremediation and Monitoring Through Tomato Plant Growth B4248
22. **Evi Gravitiiani, Ainina Ratnadewati and Nur Widiastuti**, The Implementation of Contingent Valuation Method for Waste Management at Telaga Ngebel, Ponorogo, Indonesia: A Novel Approach to Ecotourism Waste Processing House D1706
23. **Hala R. Mohammed, Jasim Mohammed Salman and Adi Jassim Abd Al-Rezzaq**, Potential Efficiency of Green Algae *Scenedesmus quadricauda* in Bioremediation of Polycyclic Aromatic Hydrocarbon, Benzo[a]Pyrene(BaP) D1712
24. **Sapna S. Basavaraddi and A. S. Raju**, Transforming Type 2 Diabetes Management Through Telemedicine, Data Mining and Environmental Insights B4256
25. **C. Chaithra and Hina Kousar**, Assessment of Bioefficacy of *Achromobacter xylosoxidans* KUESCCHK-6, Isolated from Textile Contaminated Soil, in Treating Textile Effluent and its Impact on *Vigna mungo* B4253
26. **John Ape, Srikanth Bathula, Sailesh Samanta and Krishna Kumar Kotra**, Assessment of Toxic Metals in an Open Dump Site Near PNG University of Technology, Papua New Guinea D1713

27. **Julio Angeles Suazo, Roberto Angeles Vasquez, Esmila Yeime Chavarría Márquez, Carmencita Lavado-Meza, Leonel de la Cruz-Cerrón, Nataly Angeles Suazo, Liz Quispe Quincho and Hugo Abi Karam**, Evaluation of Air Quality by Particulate Matter in Junin and Huancavelica, Peru D1722
28. **H. N. Mahendra, V. Pushpalatha, V. Rekha, N. Sharmila, D. Mahesh Kumar, G. S. Pavithra, N. M. Basavaraj and S. Mallikarjunaswamy**, Land Use/Land Cover (LULC) Change Classification for Change Detection Analysis of Remotely Sensed Data Using Machine Learning-Based Random Forest Classifier B4238
29. **R. Rajeshwaran, J. Logeshwari and R. Abirami**, Effect of EPS Concrete: Balancing Construction Efficiency and Environmental Sustainability B4268
30. **Akhbar, Abdul Rosyid, Bau Toknok, Rahmat Kurniadi Akhbar and Rizky Purnama**, Spatial Model of Fire Vulnerability Distribution Based on Multicriteria in Tropical Forest Areas, Central Sulawesi, Indonesia D1699
31. **J. E. Cruz de La Cruz, W. A. Mamani, F. Pineda, V. Yana-Mamani, R. Santa Cruz, Í. Maldonado-Ramírez, R. Pérez-Astonitas and E. Morales-Rojas**, A Review on Artificial Intelligence for Water Quality Prediction in Amazonian Countries D1705
32. **G. N. Balaji, G. Parthasarathy, A. K. P. Kovendan and Aakash Jha**, Using Deep Learning for Plant Disease Detection and Classification B4260
33. **Ajay Negi and Ashok Kumar Meena**, Impact of Landfill Proximity on Soil Quality: A Comparative Study of Dumping and Non-Dumping Sites Near Srinagar, Garhwal, Uttarakhand B4259
34. **Steve Dann Camargo Hinostroza, Carmen Andrea Taza Rojas, Diana Lizet Poma Limache and Camila Jimena Poma Romero**, Determination of the Water Quality Index (ICA-PE) of Lake Chinchaycocha, Junin, Peru D1707
35. **Ya Li and Faridah Sahari**, Evaluation of Landscape Resources and Legal Protection Boundary Setting in Xinchang County, China D1708
36. **A. Patil, S. Devi, Y. Sharma, S. Singh, N. K. Prabhakar, S. Agrawal and Mamta Arya**, Bioremediation of Manganese by Thermophilic Bacterial Isolates of Tapt Kund, Soldhar, and Gauri Kund Hot Springs of Uttarakhand, India B4269
37. **Mehak Verma and Sarita Sachdeva**, Investigating the Effectiveness of Peanut Hull as Biosorbent of Lead (Pb) from Water B4239
38. **Willis Muhammad Iqbal, Hashfi Hawali Abdul Matin and Prabang Setyono**, Sustainability Evaluation of Waste Management Using RAPWASTE Method at the 3R Temporary Waste Disposal Site in Yogyakarta City D1715
39. **Jannah Mohammad and Mohammad Abul Kashem**, Deep Learning Approach for Evaluating Air Pollution Using the RFM Model D1718
40. **Mangesh Jabade and Jasneet Kaur**, Systematic Review of Phytoremediation: Efficacy of Aquatic Plants in Wastewater Treatment and Pollutant Removal B4243
41. **Bapi Sarkar, Sribas Patra and Mallikarjun Mishra**, Geospatial Analysis of the Relationship Between Land Surface Temperature and Land Use/Land Cover Indices: A Study of Raiganj Municipality, West Bengal, India B4245
42. **Murad M. Khamayseh and Rana Kidak**, Thermodynamic Modeling Studies on Biosorption of Reactive Amoxicillin Antibiotic by *Pithophora* Macroalgae in Aqueous Solution D1725
43. **Md. Sultanul Islam, Nafis Ibna Oli and Md. Hasibul Hassan**, A Comprehensive Study on the Environmental Features of Green Buildings in Dhaka, Bangladesh: Prospects, Challenges and Mitigation Strategies D1724
44. **Arpita Ghosh, Puneet Sharma, Arnab Mondal and Surajit Mondal**, Enabling Environment for Climate-Smart Agriculture: A Critical Review of Climate Smart Practices from South Asia and Sub-Saharan Africa B4236
45. **Abhijeet Maurya, Bhanu Pratap Singh and Ajay Kumar Sharma**, Studies on the Effect of the Zinc Oxide Nano Additives along with Rice Bran Biodiesel Diesel Blends into CI Engine to Reduce Pollution B4225
46. **Sapta Suhardono, Muhammad Amin Sunarhadi, Iva Yenisi Septiariva, Hening Triandika Rachman and I. Wayan Koko Suryawan**, Biomonitoring of Bedog River Water Quality Using Dragonfly Diversity as Bioindicators in Yogyakarta, Indonesia D1711
47. **Pooja Upadhyay, Pammi Gauba and Ashwani Mathur**, From Preservative to Environmental and Health Hazards: A Review on Diverse Applications, Health Impacts and Detection Methods of Paraben(s) B4209
48. **Savita Kalshan, Rajesh Dhankhar, Shivani Narwal, Amit Chhillar, Manju Desondia, Poonam Yadav and Sashi Yadav**, Enhanced Microplastics Removal from Paper Recycling Industry Wastewater Using Membrane Bioreactor Technology B4240
49. **Ravi Sharma and Vinayak Patil**, Exploring Institutional Climate Capacity Assessment Indicators of Community-Based Organizations in the Conservation Projects: A Participative Approach B4244
50. **V. K. Sonawane, S. K. Gharde, K. S. Ghodekar, A. M. Raut and Amine Assouguem**, Larval Age-Dependent Parasitization Performance of *Cotesia flavipes* on *Sesamia inferens* B4249
51. **Sunder, Sangita Yadav and Jitender Pal**, Sustainable Biomass Conversion: Impact of NaCl Pretreatment on Cabbage Waste B4254
52. **Abhay Yadav, Divya Srivastava and Vivek Mathur**, Expository Assessment of Air Quality Scenario with Sentinel-5 Precursor TROPOMI Explorer Sensor B4232
53. **K. Sharir, A. Saidin and R. Roslee**, Flood Frequency Analysis of Kadamaian and Wariu Rivers in Kota Belud, Sabah, Malaysia D1691
54. **Raid Khider Salman, Sabah Sultan Farhan, Muneer Naji Al-Falahi and Thaer Eyada Mohammed**, Spatial Analyses of Reliability of Solar Power in the Western Part of Iraq D1681
55. **Muhammad Wasil Bin Abu Bakar, M. K. Uddin, Susilawati Kasim, Syaharudin Zaibon, S. M. Shamsuzzaman and A. N. A. Haque**, Effect of Biochar and Silicon with Different Phosphorus Levels on Maize Yield and Soil Chemical Properties D1727
56. **Akhilesh Chandrapati, Jay Prakash Singh, Yenda Damodhara Rao, Meenakshi Rana, Somnath K. Holkar and Seweta Srivastava**, Management of Grapevine Fungal Diseases by Using Antagonistic Endophytes - An Environment-Friendly Approach B4246



**The Journal  
is  
Currently  
Abstracted  
and  
Indexed  
in:**

WorldCat (OCLC)

British Library

Connect Journals (India)

Indian Science

JournalSeek

Research Bible (Japan)

SHERPA/RoMEO

Directory of Science

AGRIS (UN-FAO)

Ulrich's (Refereed) database

NAAS Rating 2024 = 5.33

CNKI Scholar (China National Knowledge Infrastructure)

Scopus Cite Score (2023) 1.2

Scopus®, SJR (2024) 0.234 (Q3)

Index Copernicus (2023) = 132.21

Indian Science Abstracts, New Delhi, India

Chemical Abstracts, U.S.A.

Pollution Abstracts, U.S.A.

Elsevier Bibliographic Databases

Paryavaran Abstract, New Delhi, India

Zoological Records

CAB Abstracts, U.K.

Electronic Social and Science Citation Index (ESSCI)

Indian Citation Index (ICI)

CrossRef (DOI)

EBSCO: Environment Index™

ProQuest, U.K.

Google Scholar

DOAJ

Zetoc

J-Gate

Environment Abstract, U.S.A.

Centre for Research Libraries

Elektronische Zeitschriftenbibliothek (EZB)

CSA: Environmental Sciences and Pollution Management

Access to Global Online Research in Agriculture (AGORA)

Present in UGC-CARE List (Group II)

UDL-EDGE (Malaysia) Products like i-Journals, i-Focus and i-Future

**www.neptjournal.com**

# NATURE ENVIRONMENT AND POLLUTION TECHNOLOGY

## EDITORS

### **Dr. P. K. Goel (Chief Editor)**

Former Head, Deptt. of Pollution Studies  
Yashwantrao Chavan College of Science  
Vidyanagar, Karad-415124  
Maharashtra, India

### **Dr. K. P. Sharma (Honorary Editor)**

Former Professor, Ecology Lab, Deptt. of Botany  
University of Rajasthan  
Jaipur-302004  
Rajasthan, India

**Executive Editor:** Ms. Apurva Goel (Bachelor of Engineering; Masters in Environment) C-102, Building No.12, Swarna CGHS, Beverly Park, Kanakia, Mira Road (E) (Thane) Mumbai-401107, Maharashtra, India  
(E-mail: [operations@neptjournal.com](mailto:operations@neptjournal.com))

**Business Manager:** Ms. Tara P. Goel, Technoscience Publications, A-504, Bliss Avenue, Balewadi, Pune-411045, Maharashtra, India (E-mail: [contact@neptjournal.com](mailto:contact@neptjournal.com))

## EDITORIAL ADVISORY BOARD

1. **Dr. Saikat Kumar Basu**, Deptt. of Biological Sciences, University of Lethbridge, Lethbridge AB, Alberta, Canada
2. **Dr. Elsayed Elsayed Hafez**, Plant Protection and Biomolecular Diagnosis Department, Arid Lands Cultivation Research Institute (ALCRI), Alexandria, Egypt
3. **Dr. Tri Nguyen-Quang**, Department of Engineering Agricultural Campus, Dalhousie University, Canada
4. **Dr. Sang-Bing Tsai**, Wuyi University Business School, Wuyishan, China
5. **Dr. Zawawi Bin Daud**, Faculty of Civil and Environmental Engg., Universiti Tun Hussein Onn, Malaysia, Johor, Malaysia
6. **Dr. B. Akbar John**, School of Industrial Technology, Universiti Sains Malaysia (USM), Penang, Malaysia
7. **Dr. C. Stella**, Centre for Agro Marine Research, Sethubhaskara Agricultural College and Research Foundation, Visalayanakottai, Karaikudi, T.N., India
8. **Dr. G.R. Pathade**, Krishna Institute of Allied Sciences, Krishna Vishwa Vidyapeeth, Karad, Maharashtra, India
9. **Dr. Amit Arora**, Department of Chemical Engineering, National Institute of Technology (NIT), Hamirpur, H.P., India
10. **Prof. Riccardo Buccolieri**, Deptt. of Atmospheric Physics, University of Salento, Dipartimento di Scienze e Tecnologie Biologiche e Ambientali, Laboratory of Micrometeorology, Lecce, Italy
11. **Dr. Tai-Shung Chung**, Graduate Institute of Applied Science and Technology, National Taiwan University of Science and Technology, Taipei, Taiwan
12. **Dr. Abdeltif Amrane**, Technological Institute of Rennes, University of Rennes, France
13. **Dr. Giuseppe Ciaburro**, Dept. of Architecture and Industrial Design, Università degli Studi, Della Campania, Italy
14. **Dr. A.B. Gupta**, Dept. of Civil Engineering, Malviya National Institute of Technology (MNIT), Jaipur, India
15. **Claudio M. Amescua García**, Department of Publications Centro de Ciencias de la Atmósfera, Universidad Nacional Autónoma de México
16. **Alexander B. Ruchin**, Joint Directorate of the Mordovia State Nature Reserve and National Park, Saransk 430005, Russia
17. **Wei (Welsh) Wang**, State Key Lab of Environmental and Biological Analysis, Hong Kong Baptist University, Hong Kong

# Prediction on the Level of Toxicity in Fruits and Vegetables Based on PAHs Using Machine Learning

Staphney Texina<sup>1†</sup>, Sathees Kumar Nataraj<sup>2</sup>, Alagammai Renganathan<sup>1</sup> and Kavitha Vasantha<sup>2</sup>

<sup>1</sup>Department of Math and Science, University of Technology Bahrain, Salmabad, Bahrain

<sup>2</sup>Department of Mechatronics Engineering, University of Technology Bahrain, Salmabad, Bahrain

†Corresponding author: Staphney Texina; texinastaphney@gmail.com

**Abbreviation:** Nat. Env. & Poll. Technol.

**Website:** [www.neptjournal.com](http://www.neptjournal.com)

*Received:* 09-06-2024

*Revised:* 28-07-2024

*Accepted:* 09-08-2024

## Key Words:

Polycyclic aromatic hydrocarbons

Environmental contaminants

Fruits and vegetables

Machine learning algorithm

## ABSTRACT

This study focuses on assessing the toxicity levels in fruits and vegetables based on the presence of polycyclic aromatic hydrocarbons (PAHs), particularly in regions affected by industrial and vehicular pollution where the particulate matter deposits on the plant surfaces. Traditional methods, including Gas Chromatography/Mass Spectrometry (GC/MS) and High-Performance Liquid Chromatography (HPLC), are used to measure PAH levels in fruits and vegetables, which are found to be valuable but expensive and time-consuming. However, the detection of toxicity relies on either expert knowledge or experimental analysis when compared with the limitations set by EFSA (European Food Safety Authority). Therefore, in this study, artificial intelligence techniques have been employed to evaluate the toxicity levels based on 16 PAHs. The PAH concentrations in fruits and vegetables were collected from different articles corresponding to safe and unsafe datasets and then validated through statistical analysis. The validated dataset is classified using different machine learning algorithms. Based on the output from the neural network, the level of toxicity is also scaled and compared with the targeted outputs. The promising results of the classification of toxicity using artificial intelligence methods are substantiated by an experimental study and validated through statistical methods. From the results, it can be observed that the machine learning algorithm has given classification accuracy of more than 90% along with their degree of harmfulness. This research holds implications for food safety and public health, offering a novel approach to the interdisciplinary understanding of climate change by addressing the impact of environmental contaminants on the edibility of fruits and vegetables.

## Citation for the Paper:

Texina, S., Nataraj, S.K., Renganathan, A. and Vasantha, K., 2025. Prediction on the level of toxicity in fruits and vegetables based on PAHs using machine learning. *Nature Environment and Pollution Technology*, 24(2), p.D1690. <https://doi.org/10.46488/NEPT.2025.v24i02.D1690>

*Note: From year 2025, the journal uses Article ID instead of page numbers in citation of the published articles.*

## INTRODUCTION

In recent years, there has been a growing concern about the impact of polycyclic aromatic hydrocarbons (PAH) on both environmental and public health (Abdel-Shafy & Mansour 2016). These contaminants, which are generated from various anthropogenic and natural sources, have been found to have adverse effects on ecosystems and human well-being. Multiple studies have shown that exposure to polycyclic aromatic hydrocarbons can harm human health, especially for vulnerable populations such as children, older adults, and individuals with existing health problems (Mallah et al. 2022, WHO 2021, Singh & Agarwal 2018). From the literature, it is observed that fruits and vegetables are consumed in different forms for their nutritional values, but the growth of these fruits and vegetables is contaminated through pollution in different forms, which results in the adsorption of Polycyclic Aromatic Hydrocarbons (Camargo & Toledo 2003). Recent studies have shown that PAH contamination has an impact on public health and is mostly observed in urban areas due to the emission of PAHs from automobiles and cooking oil fumes. In Brazil, a case study on the impact of PAH contamination was examined in street food vendors that resulted in potential health risks such as diabetes, oxidative stress, cardiovascular and pulmonary disease, respiratory diseases, skin allergies, and cancer among individuals (Deligannu & Muniandy 2024). A



**Copyright:** © 2025 by the authors

**Licensee:** Technoscience Publications

This article is an open access article distributed under the terms and conditions of the Creative Commons Attribution (CC BY) license (<https://creativecommons.org/licenses/by/4.0/>).



study on the potential health risks due to PAH exposure in industrial areas was conducted in India. Soil samples were collected and assessed from two cities. PAH sources were identified as traffic emissions, industrial emissions, and coal combustion for domestic livelihood. The health risk assessment resulted in a high potential risk of cancer due to the consumption of contaminated vegetables from these areas (Sankar et al. 2023). In China, a study conducted on farmland indicated the presence of 16 PAHs in soil and crops with varying concentrations. It showed that leafy vegetable crops had higher PAH concentrations in leaves compared to the roots and fruits, whereas the fruit and vegetable crops showed higher PAH concentrations in fruits than in roots or leaves (Cui et al. 2022). During the health risk assessment, it posed a high carcinogenic risk in adult males and females based on the dietary intake.

From these studies, it is evident that PAH's analysis on consumables is necessary to be studied and detection of toxicity should be considered as an important measure to protect the environment. Contrarily, the toxicity of food products or consumables may be a potential threat to mankind, putting individual lives at high health risk. This resulted in us initiating exploring and evaluating PAHs, as well as developing an intelligent system for detecting toxicity. PAHs are formed during the incomplete combustion of garbage, organic waste, sewage sludge, wood, gas, etc. PAHs are composed of carbon and hydrogen atoms and contain two or more aromatic rings (Khalili et al. 2021). The contamination of PAH is widespread in the environment, both in terrestrial and aquatic organisms, due to which the presence of PAH in the food supply is considerably high (Paris et al. 2018). The contamination of PAH in agricultural and animal food products can occur during growth, transportation (exhaust from combustion engines), storage, and also when the food is smoked, grilled, roasted, fried, and cooked (Paris et al. 2018). While there are over 100 recognized PAHs, the United States Environmental Protection Agency (UPESA) has identified only 16 as the primary concern (Abou-Arab et al. 2014) because these PAHs are unsafe and can enter a variety of life on earth through inhalation, ingestion, and even through skin contact (Omoyeni et al. 2023). PAH contamination in raw food such as fruits and vegetables is through soil, water, and air (Paris et al. 2018). In addition to this, the amount of PAH concentration depends on environmental PAH (urban areas have a high amount of PAH), soil characteristics (weak soil needs to be strengthened using chemical fertilizers), and physiological properties, e.g., the longer the growth period of the plant, higher the absorption of PAH contaminants (Khalili et al. 2021). Fruits and vegetables can get contaminated with PAHs when air particulate matter settles on their surfaces. Plants near industries or roads tend to have more PAH

deposits, including Benzo[a]pyrene, dibenz[a,h]anthracene, and chrysene, compared to plants in rural areas (Ashraf & Salam 2012). In fruits and vegetables, low molecular weight (LMW) PAHs and high molecular weight (HMW) PAHs are adsorbed by the waxy surface, particularly on outer leaves and fruit peels (Camargo & Toledo 2003). The concentration of PAHs tends to be higher on these exposed surfaces.

Studies reveal variations in PAH concentrations among different parts of plants, with root vegetables potentially having higher levels than stem vegetables (Zhong & Wang 2002). Research in China identified factors affecting PAH levels in vegetables, including anthropogenic emissions, vegetable species, and wind direction (Jia et al. 2018). Common PAHs found in fruits and vegetables include fluorene, fluoranthene, pyrene, anthracene, phenanthrene, benzo(a)anthracene, and benzo(a)pyrene, with leafy and stem vegetables having higher concentrations (Zhong & Wang 2002). Similarly, Choochuay et al. (2023) analyzed the toxicity and health risk assessment based on the PAH concentration in Thai and Myanmar rice. From this study, it is identified that the level of PAHs with its toxicity and health risk assessment. The findings can be summarized as follows: a) The level of PAHs in Thailand varied from  $0.09 - 37.15 \text{ ng.g}^{-1}$  with an arithmetic mean of  $18.22 \pm 11.76 \text{ ng.g}^{-1}$ , whereas that in Myanmar varied from  $0.07 - 150.73 \text{ ng.g}^{-1}$  with an arithmetic mean of  $34.70 \pm 40.57 \text{ ng.g}^{-1}$ . Due to increased food security concerns, numerous studies explore threats associated with consuming contaminated food (Abou-Arab et al. 2014).

Khalil et al. (2021) conducted a study and the analysis of PAHs in fruits and vegetables revealed high concentrations of acenaphthene ( $135.1 \pm 7.1 \mu\text{g.kg}^{-1}$ ) and naphthalene ( $114.1 \pm 5.0 \mu\text{g.kg}^{-1}$ ), while benzo(k)fluoranthene, benzo(a)pyrene, benzo(g,h,i)fluoranthene, Indeno(1,2,3-cd)pyrene, and benzo(g,h,i)perylene were not detected (Khalili et al. 2021). Another study by Paris et al. (2018) reported relatively low PAH levels ranging from  $0.01$  to  $0.5 \mu\text{g.kg}^{-1}$  in wet weight for fruits and vegetables (Paris et al. 2018). However, plants near roadways and urban areas can exceed the concentration of  $5 \mu\text{g.kg}^{-1}$  (Paris et al. 2018).

In the experiments conducted in Pakistan and Saudi Arabia in 2013 by Mohammad W. Ashraf, root vegetables like carrots and potatoes exhibited high PAH concentrations of  $13 \mu\text{g.kg}^{-1}$  and  $11 \mu\text{g.kg}^{-1}$ , respectively, while turnip had concentrations of  $10.9 \mu\text{g.kg}^{-1}$  and  $9.26 \mu\text{g.kg}^{-1}$ . The study also observed higher contamination in the peels than the cores of fruits and vegetables, with cabbage having the highest concentration among leafy vegetables (Ashraf et al. 2013, Ashraf & Salam 2012). In India, a study by Nasri et al. (2006) identified Anthracene, Naphthalene, Fluorene,

Pyrene, Phenanthrene, and Fluoranthene as predominant PAHs in vegetable and soil samples. The use of an Isocratic High-Performance Liquid Chromatography (HPLC) system with UV detection revealed carcinogenic compounds such as BAP and dibenz(a,h)anthracene, with LMW-PAHs more abundant than HMW-PAHs (Narsi et al. 2006).

Al-Nasir et al. (2022) evaluated four vegetables, finding tomatoes with the highest concentration of  $21.774 \mu\text{g.kg}^{-1}$  and zucchini with the lowest concentration of  $10.649 \mu\text{g.kg}^{-1}$  (Al-Nasir et al. 2022). In summary, the literature also emphasizes the use of various detection methods, including High-Performance Liquid Chromatography with fluorescence detection (HPLC-FLD) an excellent quantification and separation tool. Solid phase microextraction (SPME), a sensitive solvent-free sample preparation technology; gas Chromatography with Mass Spectrometry (GC-MS), a method where two analytical tools combined to identify and measure the concentration of chemicals in food and environment, and Gas Chromatography with flame ionization detector (GC-FID) an analytical technique that is used to separate and analyze mixtures consisting of volatile compounds (Abou-Arab et al. 2014).

Similar to these technologies, chemical analysis has also been done using various techniques such as saponification/ultrasonication, clean-up using a silica solid phase extraction cartridge and GC-MS, liquid-liquid extraction with solvents like n-hexane to determine the elements of eight PAHs (BaA, BkF, BbF, DahA, BaP, BghiP, IP, Chry) in fruits and vegetables. The results show that the PAH concentration in fruits is  $0.67 \mu\text{g.kg}^{-1}$ , and in vegetables, it is  $0.82 \mu\text{g.kg}^{-1}$  (Lee et al. 2019). In Egypt, Abou-Arab et al. (2014) conducted a study on the level of PAH in vegetables and fruits such as potatoes, spinach, apple, and guava using GC-MS showed high-level concentration in spinach ( $8.977 \mu\text{g.kg}^{-1}$ ), potatoes ( $6.196 \mu\text{g.kg}^{-1}$ ), apple ( $2.867 \mu\text{g.kg}^{-1}$ ) and guava ( $2.334 \mu\text{g.kg}^{-1}$ ). The researcher concluded that preventive measures such as thorough washing, boiling, and peeling of the skin of fruits and vegetables are effective in reducing the amount of PAH consumption (Abou-Arab et al. 2014). Okaba et al. (2020) reported that vegetables grown in Nigerian traffic routes were tested for PAH concentration and evaluated using GC-MS and AAS (Atomic Absorption Spectrophotometer), which determined the presence of high PAH in vegetables (Okaba et al. 2020). Although vegetables were boiled, it did not show a notable difference ( $p > 0.05$ ) in the PAH concentration between fresh and boiled vegetables. Boiling the vegetables only reduced the mean concentration of PAHs (Okaba et al. 2020). Another study determined the concentration of PAH by growing plants in contaminated and uncontaminated soil. The results showed elevated levels

of PAH in vegetables and fruits grown in contaminated soil (Samsøe-Petersen et al. 2002). In samples of tomatoes and okra, the  $\Sigma 16$  PAH concentration was in the range of  $2.12 \pm 1.5$  and  $99.88 \pm 29.18$ , respectively. Also, naphthalene exhibited a high concentration of 60% in vegetables (Omoyeni et al. 2023, Tesi et al. 2021). The concentration of  $\Sigma 16$  PAH in vegetables was in the range of 532 to 2261 in leafy vegetables of southern Nigeria (Tesi et al. 2021). Ce-Hui Mo, 2009 reported that the determination of PAH and PAE (Phthalic Acid Esters) in vegetables in South China indicated that PAE was present in higher amounts than total PAH. However, due to the seasonal changes of PAHs in vapor and particulate matter in the region, more studies are to be done to test variations of PAHs in various classes of vegetables (Mo et al. 2009). Therefore, from the review it can be observed that the analysis of PAH and their effects on the health and environment are alarming. There are many studies on the identification of hazards and toxicity using machine learning algorithms. However, there is no research on the statistical measures of the PAHs of the samples or measuring the PAH levels (Al-Nasir et al. 2022, Khalili et al. 2021, Samsøe-Petersen et al. 2002). There are some studies, such as Pandey et al. (2023), that have used machine learning algorithms in the applications of the food processing industry to identify the hazards associated with the preservation of fruits and vegetables (Pandey et al. 2023). PAHs are present in various fruits and vegetables due to factors like location, agricultural practices, and storage. This indicates the widespread presence of PAHs, necessitating monitoring. It is also observed by WHO, under the natural toxins in food (WHO 2023), stated that research experts review all the available studies and suggest an outcome based on the level of health concern, which includes measures to prevent and control contamination. The authors have provided a detailed discussion on the future of machine learning algorithms in the food industry, the factors that affect the quality of food being preserved, and assist in determining the optimal parameter combinations for deciding the maximum produce preservation.

Megalingam et al. (2019) employed different machine learning like k-cluster, computer vision, and artificial intelligence techniques along with color classification to determine rotten food (Megalingam et al. 2019). Therefore, it can be observed from the above literature that PAHs adhere to the surfaces of fruits and vegetables, particularly on outer leaves and peels. It highlights variations in the concentration of PAH among different plant parts and factors influencing PAH levels. While there are multiple methods to analyze the PAH values, artificial intelligence techniques have the potential to outreach in the field of toxicity detection. Analyzing the PAH values using a

machine learning algorithm is one of the initial works to determine the toxicity of PAH in fruits and vegetables. It can also be perceived that Machine learning algorithms and various AI (Artificial intelligence) techniques are used to examine the perishing nature of food, but there is no research conducted to measure the toxicity level nor predict the degree of harmfulness of PAH in fruits and vegetables. Hence, in this study, an intelligent toxicity detection system has been developed to explore the impact of PAH toxicity in fruits and vegetables. Machine learning algorithms have been used to analyze PAH contamination (Vasanth et al. 2023) in fruits and vegetables, providing an efficient and accurate monitoring method. Machine learning algorithms can handle complex data and detect even trace levels of PAHs, which traditional methods have some limitations. By training models on historical data, the intelligent model can be used to predict contamination trends and circumstances for proactive measures ahead. Incorporating recent data and case studies highlights the critical issue of PAH contamination. Thus, the proposed system of toxicity detection can be helpful to society, ensuring food safety and protecting public health.

The proposed system, depicted in Fig. 1, utilizes machine learning algorithms to analyze the collected empirical data and provide results on toxicity. A detailed explanation of the implementation of the proposed system has been discussed in the subsequent sections of this article.

## MATERIALS AND METHODS

The main aim of this study is to employ artificial intelligence techniques for assessing the toxicity levels of fruits and vegetables based on 16 PAHs. A classification system is proposed, utilizing machine learning algorithms such as

Support Vector Machine (SVM), Ensemble, Regression, Discriminant, Tree, k-nearest Neighbour(k-NN), Naïve Bayes, Artificial Neural Network (ANN) to classify the toxicity in fruits and vegetables. Additionally, the research aims to compare the outcomes of these models.

The classification model takes the concentration of 16 PAHs in fruits and vegetables as input and classifies the level of toxicity based on the machine learning algorithm. The subsequent section details the data collection process, its validation, design, and evaluation using machine learning algorithms.

### PAH Data Collection

The data collected for this study is based on the experimental analysis from different research in the field of environmental pollution, environmental contamination and toxicology, polycyclic aromatic compounds, and toxic chemical hazards in food and feed (Paris et al. 2018) From the literature can be summarized that PAH deposit is found more on the surface of the fruits, leaves, and vegetables than the inner tissues. As stated by WHO, “natural toxins need to be kept as low as possible to protect people”. Therefore, in this study, fruits and vegetables were considered for toxicity detection using AI techniques. The PAHs corresponding to the proposed objectives were collected from 24 articles published in various platforms such as IEEE, Nature Environment and Pollution Technology, Elsevier, International Journal of Nutrition and Food Sciences, MDPI, Journal of Environmental Science and Health and others. The total number of samples is 519. These samples represent different fruits and vegetables, and these are experimented with from various parts of the world. Therefore, the data relating to the

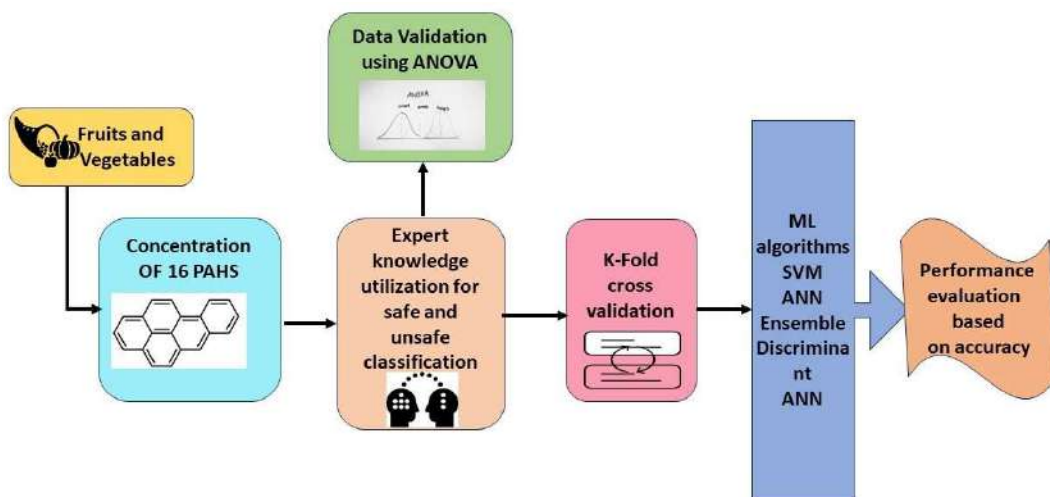


Fig. 1: The Proposed PAH-based Toxicity Detection Model.



concentration of PAH in leafy vegetables like spinach, jute, and pumpkin leaves (Camargo & Toledo 2003, Khalili et al. 2021, Omoyeni et al. 2023, Tesi et al. 2021, Mo et al. 2009, Janska et al. 2006), as well as small, medium and large sized vegetables (Khalili et al. 2021, Zhong & Wang 2002, Ashraf et al. 2013, Al-Nasir et al. 2022, Lee et al. 2019, Tuteja et al. 2011) and fruits (Camargo & Toledo 2003, Khalili et al. 2021, Bishnoi et al. 2006, Janska et al. 2006), other leafy vegetables (romaine lettuce, Chinese cabbage, and Shanghai green cabbage), stem vegetables (lettuce), seed and pod vegetables (broad bean), rhizome vegetables (daikon) were considered in this research. PAH concentration of samples collected from different experimental results reported in research articles are summarized in Table 1.

The PAHs of fruits and vegetables collected in this analysis include Acenaphthene (Ace), Acenaphthylene (Aceph), Anthracene (An), Benzo[b] fluoranthene (BbF), Benzo[g,h,i] perylene (BgP), Benzo[k]fluoranthene (BkF), Chrysene (Chr), Dibenz[a,h]anthracene (DBA), Fluoranthene (Flu), Fluorene (Fl), Indeno[1,2,3-c,d] pyrene (Inp), Phenanthrene (Ph), Pyrene (Pyr) and Naphthalene (Nfl). Among these PAHs, the Scientific Committee on Food and European Food Safety Authority (EFSA), which is an agency that provides scientific advice to risk managers and communicates the risk associated with the food chain, considers BaP, DBaA, BaA, BbF, BkF, Chr, BghiP, and IP as potentially carcinogenic and genotoxic compounds (Paris et al. 2018).

According to the US Environmental Protection Agency (USEPA), fruits and vegetables have lesser concentrations of PAH when compared to processed and unprocessed meat and meat products. The minimum and maximum recommended limits are 0.01 and 0.5 µg/kg (Paris et al. 2018). Based on

the Maximum Contamination limit and expert knowledge, the 519 data have been sorted as safe and unsafe for consumption. The total number of data corresponding to safe and unsafe are 231 and 288, respectively. The segregated dataset is validated using ANOVA, and the outcomes are reported in the subsequent section.

### Statistical Analysis of PAHs

The examination of the 16 PAHs across the 519 samples reveals a non-linear pattern, making it challenging to determine any possible significance through visual inspection for categorizing the data as safe or unsafe. Consequently, adhering to established standards and limitations for specific PAHs, the data was categorized into safe and unsafe. This research endeavors to validate whether there is any significant difference between these segmented datasets (Frossard & Renaud 2021, Yang et al. 2020). In this study, the data collection techniques or experiments were not used to measure the PAHs. Instead, the toxicity of PAHs was assessed in fruits and vegetables using machine learning methods. The data were acquired from a variety of articles that use experimental measures. As a result, there is no possibility of missing data. In addition, the dataset has also been processed using Analysis of variance (ANOVA) to assess the level of significance. The preprocessing findings and variance analysis are reported in the subsequent sections.

In the initial analysis, the 16 PAHs of both safe and unsafe datasets were subjected to ANOVA statistical analysis, but the results failed to meet the required hypothesis. The hypothesis for the validation process is as follows:

1. The null hypothesis is that there is no significant difference among the samples.
2. Whereas the alternate hypothesis is that at least a sample should differ significantly from other samples.

The level of significance considered is 0.05. The null hypothesis will fail to accept if the probability value, that is, the p-value, is less than 0.05. The results indicated a significant difference between the safe and unsafe datasets, contradicting the latter hypothesis. Further investigation revealed that the variance stemmed from the missing PAHs in some samples, as researchers focused on measuring the main PAHs to determine toxicity. To address this, various statistical measures were employed to ascertain if a regression line adequately fits the data. The validation in this analysis involved calculating the sum of square values of the PAHs. The results of each analysis are detailed below.

From the ANOVA analysis, to determine the significance between safe and unsafe, the F value for the 519 samples resulted in 1.3067, and the p-value is 0.001, which confirmed

Table 1: Different fruits and vegetables for PAH analysis.

Categories of fruits & vegetables	No. of samples	References
Leafy vegetables	122	(Ramezan et al. 2019), (Samsøe-Petersen et al. 2002) (Al-Nasir et al. 2022), (Lee et al. 2019), (Mo et al. 2009), (Paris et al. 2018)
Root vegetables	108	(Ramezan et al. 2019), (Ashraf & Salam 2012), (Ashraf et al. 2013)
Stem vegetables	157	(Al-Nasir et al. 2022), (Ashraf, n.d.), (Ashraf & Salam 2012), (Ashraf et al. 2013), (Janska et al. 2006), (Jia et al. 2018)
Fruits	132	(Ramezan et al. 2019), (Samsøe-Petersen et al. 2002), (Camargo & Toledo 2003), (Paris et al. 2018)
Total	519	

Table 2: ANOVA Measures Corresponding to Safe and Unsafe Data.

Source of Variation	SS	df	MS	F	P-value	F crit
<b>Between Samples</b>	1E+09	518	2E+06	1.3067	0.0012	1.1556
<b>Within Samples</b>	9E+08	519	2E+06			

Table 3: ANOVA Measures Between Samples of Safe Data.

Source of Variation	SS	df	MS	F	P-value	F crit
<b>Between Samples</b>	123.87	230	0.5386	0.6794	0.9983	1.2425
<b>Within Samples</b>	183.12	231	0.7927			

Table 4: ANOVA Measures between samples of unsafe data.

Source of Variation	SS	df	MS	F	P-value	F crit
Between Samples	1E+09	287	4E+06	1.2918	0.0151	1.2145
Within Samples	9E+08	288	3E+06			

that there is a significant difference between the safe and unsafe data. Hence, the determination of toxicity in fruits and vegetables by expert knowledge and the standard limit has been validated by analysis of variance. The results of the variance analysis done on the data set are consolidated in Table 2.

From the ANOVA analysis, to determine the significance between the samples of safe data, the F-value for 231 samples resulted in 0.6794, and the p-value was 0.9982. As the level of significance is more than the threshold limit, samples of the safe category fail to differ significantly from each other. The test results are presented in Table 3.

Similarly, from the ANOVA analysis, to determine the significance between the samples of unsafe data, the F-value for 288 samples resulted in 1.2918, and the p-value was 0.0151. As the p-value is less than 0.05, samples of the unsafe category differ significantly from each other. Therefore, it can be concluded that there is a significant difference between the concentration of PAHs of the samples corresponding to unsafe categories as the samples are collected from fruits and vegetables grown in different regions across the globe, which are subjected to different environmental conditions like temperature variations, air pollution, water and soil quality. The test results are presented in Table 4.

From the above statistical analysis, it has been observed that there is no significant difference between the samples for the safe data set, whereas, for the unsafe data set, there is a significant difference between the samples. This is due to a large variation between the PAH of fruits and vegetables, with scattered concentrations of PAHs across the dataset. The minimum and maximum values of such PAHs are tabulated in Table 5. Therefore, the unsafe data has been analyzed further to understand the distribution of PAHs in each sample of fruits and vegetables.

However, the above scenario is not encountered in the samples related to safe data. Hence, the data has been analyzed using the sum of square method (Nataraj et al. 2022). The following equation (1) has been used for the computation of the sum of squares of each element in the dataset.

$$\text{The sum of the squares} = \sum_{i=1}^{519} \sum_{j=1}^{16} x(i, j)^2 \quad \dots(1)$$

Where i represents the row index ranging from 1 to 512 dataset.

j represents the column index ranging from 1 to 16 PAHs

$x(i, j)$  represents the value at the  $i^{th}$  row and  $j^{th}$  column of the 512 x 16 dataset

Then the sum of square values is analyzed using analysis of variance, and the F value has been calculated as 0.9897 and the p-value as 0.05346. As the p-value is greater than 0.05, samples fail to differ significantly from each other. The analysis of variance results is shown in Table 6.

In this study, a stratified sampling technique has been employed, which ensures the samples were collected from different articles (representing various regions, at different seasons, and multiple sources e.g., local markets, farms, urban and rural areas). Therefore, this approach provides a

Table 5: Concentration range of PAHs.

PAHs	Min Concentration	Max Concentration
Nap	0	115.50
Pyr	0	1896.00
Phe	-0.03	209.00
Chr	0	2361.00
BaP	0	338.00
BbF	-0.05	2361.00
BaA	-0.25	176.00

Table 6: ANOVA Measures between samples corresponding to the sum of square values of unsafe.

Source of Variation	SS	df	MS	F	P-value	F crit
Between samples	3E+13	287	9E+10	0.9898	0.5347	1.2145
Within Samples	3E+13	288	9E+10			

significant representation of the dataset with high dimensions, reducing the likelihood of sampling bias. In this analysis, cross-validation techniques have also been employed and used to train the machine-learning models. The classification models use feature normalization (bipolar normalization) and randomization techniques to prevent overfitting. Additionally, multiple methods have been used for the evaluation and presented the best performance metrics, such as the sensitivity of each class, accuracy, and misclassification rate. This comprehensive approach strengthens the validity of the findings and enhances the credibility of this research. The following section presents a detailed explanation of the modeling of the machine learning algorithms and the results.

### Design and Evaluation of Machine Learning Algorithms for the Toxicity Detection System

Machine learning, a subset of Artificial Intelligence, leverages algorithms and data to emulate human brain functionality (Nataraj et al. 2021). Widely employed for pattern recognition, clustering, and signal processing, machine learning algorithms play a crucial role in prediction and clustering based on labeled or unlabelled datasets (Pandey et al. 2023). In our analysis for toxicity detection, we have adopted simple and well-established learning algorithms to evaluate the toxicity level of fruits and vegetables. Based on expert knowledge and standard limits, the samples were categorized as safe and unsafe and validated using ANOVA analysis.

In this research, k-fold cross-validation is utilized for data segmentation, and linear and non-linear classifiers are employed for data evaluation. The classification algorithms are chosen due to their wide acceptance and convenience in modeling and evaluating PAH datasets.

The designed models feature 16 inputs and 1 output, evaluated using different machine learning algorithms to classify toxicity in fruits and vegetables. The neural network model incorporates one hidden layer with 15 hidden neurons, utilizing the Levenberg-Marquardt backpropagation algorithm for weight updating. Error calculation is performed using the Mean Square Error method. The k-NN and SVM models are trained with standard parameters. The value of K varies from 0 to 10 for k-NN models, while a standard size is chosen as the sigma value for SVM models.

This comprehensive approach aims to utilize diverse machine-learning techniques for robust toxicity detection,

providing a foundation for effective analysis and decision-making in environmental assessments.

### k-fold Cross-Validation

To assess the classification model and evaluate system performance, the k-fold cross-validation method is employed in this research. This sampling process serves to generalize the model and aids in selecting the most appropriate one for the task at hand. Well, many segmentation techniques are used in the classification, such as hold-out, leave-one-out cross-validation, and k-fold cross-validation. It is well known that the usual methods, such as Hold Out methods, were used for large data sets, and the leave-one-out-cross-validation is very similar to k-fold cross-validation and the random splitting such as 60-40, 70-30, 80-20 methods may lead to overfitting. In this analysis, k-fold cross-validation has been chosen since these methods are powerful and can generalize the machine learning model, even if the data set/feature set has limited samples. Also, 'k' provides equally sized validation for multiple epochs. Specifically, a 5-fold cross-validation is utilized, denoted by k=5, where the dataset is divided into 5 non-overlapping folds of equal size (Megalingam et al. 2019).

This method is instrumental in training and testing the model across all dataset subsets, effectively reducing variance (Sonwani et al. 2022). The PAH dataset, with its raw  $519 \times 16$  features, undergoes segmentation into training and testing datasets through the five-fold cross-validation. The training dataset comprises 80% of the total dataset ( $415 \times 16$  features), while the testing dataset holds the remaining 20% ( $104 \times 16$  features). This five-fold method results in the creation of five distinct training and testing sets. Fig. 2 describes the entire process of 5-fold cross-validation (Ramezan et al. 2019, Wong & Yeh 2019).

The segmented training sets are concurrently trained using various algorithms, including feed-forward backpropagation-based Neural Network, Support Vector Machine (SVM), Ensemble, Regression, Discriminant, Tree, k Nearest Neighbour (k-NN), and Naive Bayes. Subsequently, the trained models undergo testing using the remaining five distinct 20% testing datasets.

The training and test results derived from the algorithms are discussed in detail in the subsequent section of this article, providing a comprehensive understanding



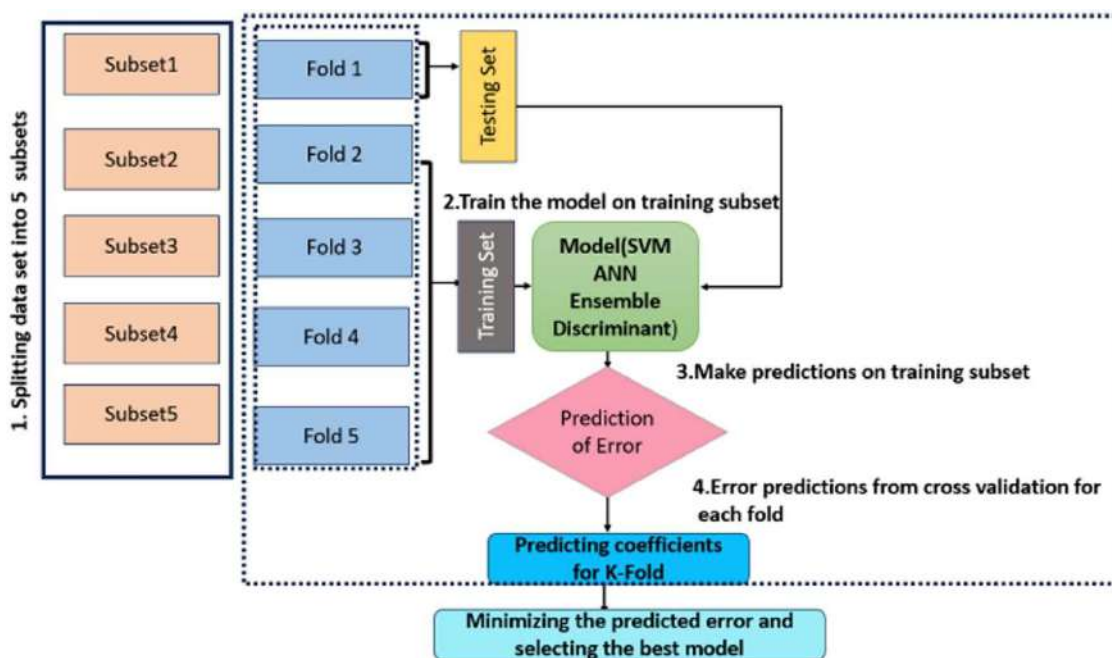


Fig. 2: Flowchart of k-Fold Cross Validation.

of the model's performance across diverse evaluation scenarios.

## RESULTS AND DISCUSSION

The main aim of this research is to understand the levels of toxicity in fruits and vegetables using a machine learning algorithm and analyze the levels of Polycyclic Aromatic Hydrocarbons (PAHs). The main objective revolves around the careful investigation of PAHs collected from various sources, validated by a comprehensive statistical analysis to correlate the data set, discerning between safe and unsafe data.

Analysis of the collected PAHs led to the development of a robust two-class pattern recognition model. The dataset of 16 input features is used as input to various machine learning algorithms, each of which is characterized by different technical specifications. Given the nature of this binary classification problem, only one output neuron is considered. Based on the outcomes, the results highlight that the machine learning method achieves over 85% accuracy in classifying two-class problems. The following section provides details on the results of various machine-learning approaches and how they contribute to the detection of toxicity in fruits and vegetables.

### Classification of Safe and Unsafe Data using MATLAB Classification Learner app

In this study, the development of machine learning

algorithms for toxicity analysis on fruits and vegetables was undertaken using MATLAB's Classification Learner application (Wang et al. 2022). While some algorithms were directly implemented through the Classification Learner, others required custom parameterization. In this research, various classification algorithms have been examined in an attempt to establish a reliable and efficient model for detecting toxicity in fruits and vegetables. Various classification algorithms have been used in this evaluation process to determine a reliable and efficient model for the detection of toxicity in fruits and vegetables. The classification models were designed with 16 inputs and 2 outputs by applying respective approaches. The Discriminant Analysis classifier has been employed with linear (LDA- Linear discriminant analysis) and quadratic (QDA- quadratic discriminant analysis) discriminant approaches, which is ideal for the analysis of high dimensional data with limited significance in feature interactions (Le et al. 2020). This model is specifically suitable for toxicity classification based on its ability to handle various covariance structures, providing robust performance among various correlations of PAH. Ensemble models were designed with bagged trees and RUSBoosted trees that enhance the model's robustness and handle class imbalance (Ampomah et al. 2020). The ensemble model is especially suited for classification tasks involving toxicity detection and offering a balance between accuracy and computational efficiency. Whereas Kernel models were designed using SVM and logistic regression kernels. These models can

Table 7: Design specification of the classification models used in the toxicity detection system.

Classification models	Classification algorithm	Total Cost (Validation)	Prediction Speed (obs/sec)	Training time (sec)	Number of learners	Maximum Splits	Learning Rate	Parameters	Neighbors	Distance Metric	Distribution	Layers	Kernel
Discriminant Analysis Classifier Ensemble Machine Learning Algorithms Kernel Models	LDA	71	13,000	13.803									
	QDA	67	7,700	13.192									
	Bagged Trees	25	3,100	4.7758	30	518							
	RUSBoosted Trees	31	3,500	5.5973	30	20	0.1						
	SVM Kernel	26	16,000	8.5592				Auto(Expansion dimensions, regularization strength, kernel scale)					
K-Nearest Neighbors (KNN)	Logistic Regression Kernel	34	12,000	7.3023				Auto(Expansion dimensions, regularization strength, kernel scale)					
	Fine KNN	20	9,000	2.6819					1	Euclidean			
	Medium KNN	24	8,400	2.3804					10	Euclidean			
	Coarse KNN	86	9,000	1.2029					100	Euclidean			
	Gaussian Kernel	56	7,200	8.8527							Gaussian Kernel		
Naive Bayes		54	3,500	8.0303							(Gaussian)		
	Wide NN	15	15,000	6.8221								1(100 neurons)	
	Bilayered NN	12	21,000	6.5796								2(10 neurons each)	
	Trilayered NN	11	14,000	6.8536								3(10 neurons each)	
	Linear SVM	44	5,000	2.3861									Linear
Support Vector Machine (SVM)	Quadratic SVM	32	7,100	1.6382									Quadratic
	Cubic SVM	34	9,400	1.4974									Cubic
	Fine Gaussian SVM	22	7,000	1.4187									Gaussian
	Medium Gaussian SVM	32	5,900	1.4945									Gaussian
	Coarse Gaussian SVM	64	5,000	1.4597									Gaussian
Decision Trees	Fine Tree	17	3,400	13.21		100							
	Medium Tree	17	6,000	2.2963		20							
	Coarse Tree	24	7,900	1.515		4							
Regression Models	Binary GLM LR	14	3,800	3.2137									
	Efficient LR	14	7,200	2.21									
	Efficient Linear SVM	19	8,100	1.6321									

capture complex patterns through non-linear transformations (Colkesen et al. 2016). An advantage of the kernel model is its flexibility in handling non-linear relationships, which makes it suitable for complex toxicity classification.

Other models, such as KNN models, were designed using fine, medium, and coarse KNN configurations (Ali et al. 2020). This model provides an effective and simple approach for the detection of toxicity. Naive Bayes models are effective for the classification of toxicity due to their ability to handle continuous data. This model was designed using Gaussian and kernel distributions (Pérez et al. 2009). Artificial Neural network models provide high accuracy and speed and are also powerful for complex classification tasks (Tritsaris et al. 2021). Neural networks were designed using wide, bilayered, and trilayered configurations. SVM models were designed using various kernel functions such as Linear SVM, Quadratic SVM, Cubic SVM, Fine Gaussian SVM, Medium Gaussian SVM, and Coarse Gaussian SVM (Nanda et al. 2018). These models are suitable for toxicity detection due to their robustness and efficiency in binary classification tasks. Decision trees are a popular choice as they provide interpretable models for toxicity classification. These models were designed using fine, medium, and coarse configurations (Vargaftik et al. 2021). Regression models were designed using binary GLM logistic regression, efficient logistic regression, and efficient linear SVM (Wu & Yang 2015), which provide accurate, efficient predictions and are suitable for binary classifications. The design specifications of the classification models are given in Table 7.

The design performance of the classification models is represented in Table 8, and the results are compared. From the results, it can be observed that based on the design and performance metrics, the Coarse KNN model has a high total cost (validation) of 86, a prediction speed of 9,000, and a Training time is 1.2029 sec compared to the other models. At the same time, the Trilayered Neural Network appears to be the best model for toxicity classification in fruits and vegetables, with the lowest total cost (validation) of 11, a high prediction speed of 14,000 obs/sec, and a reasonable training time of 6.8536 sec. It is now evident that neural network models are proven to be efficient in terms of design, learning nonlinear patterns, and prediction.

As discussed, the proposed methodology allowed for a comprehensive evaluation of each classifier's performance in toxicity detection, with the chosen parameters tailored to the characteristics of the dataset and the objectives of the study. The results obtained from model 1 classification learner are shown in Table 9, presenting the minimum, average, and maximum classification accuracy from 10 trials.

Table 8: The design performance of the classification models.

Model	Total Cost (Validation)	Prediction Speed [obs.sec <sup>-1</sup> ]	Training Time [sec]
Linear Discriminant	71	13,000	13.803
Quadratic Discriminant	67	7,700	13.192
Bagged Trees	25	3,100	4.7758
RUSBoosted Trees	31	3,500	5.5973
SVM Kernel	26	16,000	8.5592
Logistic Regression Kernel	34	12,000	7.3023
Fine KNN	20	9,000	2.6819
Medium KNN	24	8,400	2.3804
Coarse KNN	86	9,000	1.2029
Gaussian Naive Bayes	56	7,200	8.8527
Kernel Naive Bayes	54	3,500	8.0303
Wide Neural Network	15	15,000	6.8221
Bilayered Neural Network	12	21,000	6.5796
Trilayered Neural Network	11	14,000	6.8536
Linear SVM	44	5,000	2.3861
Quadratic SVM	32	7,100	1.6382
Cubic SVM	34	9,400	1.4974
Fine Gaussian SVM	22	7,000	1.4187
Medium Gaussian SVM	32	5,900	1.4945
Coarse Gaussian SVM	64	5,000	1.4597
Fine Tree	17	3,400	13.21
Medium Tree	17	6,000	2.2963
Coarse Tree	24	7,900	1.515
Binary GLM Logistic Regression	14	3,800	3.2137
Efficient Logistic Regression	14	7,200	2.21
Efficient Linear SVM	19	8,100	1.6321
Min	11	3100	1.2029
Max	86	21000	13.803

Table 9: The classification accuracy of toxicity detection using model 1 without applying Principal Component Analysis (PCA).

Classification models	Classification Accuracy (10 trials)		
Model Type	MIN [%]	MAX [%]	Average [%]
Discriminant	86.3198	87.0906	86.7052
Ensemble	81.1175	98.2659	92.3314
Kernel	93.4489	94.9904	94.2197
KNN	83.4297	97.1098	93.7058
Naive Bayes	89.2100	89.5954	89.4027
Neural Network	97.1098	97.8805	97.4952
SVM	70.3276	97.1098	89.8844
Tree	89.7881	91.1368	90.7996
Regression	92.6782	97.8805	95.2794



From the results, the Ensemble model has the highest accuracy of 98.2659% compared to other models. Ensemble models combine predictions from multiple machine learning models to enhance overall performance. On the other hand, the SVM model performed the least, achieving an accuracy of 70.3276%. This lower performance can be attributed to the challenge of finding the best hyperplane to separate different classes, especially in our dataset with non-linear characteristics and some PAH values being zero. The SVM model's sensitivity to parameters like the choice of kernel and regularization parameter (C) contributed to its specific challenges. Despite variations, all models maintained an average performance rating exceeding 85%. This summary provides a straightforward overview of the results without using any feature optimization techniques, emphasizing the highest classification accuracy of the Ensemble model and the challenges faced by the SVM model in the context of the dataset complexity.

Hence, a classification model has also been developed by using PCA (Principal Component Analysis). The classification accuracy of the classification models is presented in Table 10. By applying PCA, the order of features is sorted according to the dominants of the feature, and no PAH values were neglected. Following this optimization, the ensemble model displayed performance ranging from a minimum of 55.4913% to a maximum of 97.88% over 10 different trials. Overall, it has been observed that a performance rating of 86% has been achieved across all the trials.

From Table 10, it can also be observed that the traditional ANN model achieved a minimum classification accuracy of 92.42% and a maximum of 98.26%; this shows the feed forward back propagation using the LM algorithm has proven the robustness in the non-linear pattern recognition method. Similarly, the minimum accuracy of 72.447% and 95.37% of maximum accuracy are attained from the k-NN model. The SVM classifiers attained a minimum accuracy of 70.327%

Table 10: The Classification Accuracy of Toxicity Detection using model 1 with applying PCA.

Classification models	Classification Accuracy (10 trials)		
Model Type	MIN [%]	MAX [%]	Average [%]
Discriminant	86.3198	87.0906	86.7052
Ensemble	55.4913	97.8805	87.3732
Kernel	89.5954	95.3757	93.1920
KNN	72.4470	95.3757	91.2653
Naive Bayes	89.2100	94.4123	92.4855
Neural Network	94.7977	98.2659	96.1946
SVM	70.3276	97.1098	92.4213
Tree	89.7881	96.7245	94.0848
Regression	92.6782	97.8805	95.0867

and a maximum accuracy of 97.109%. The results indicate that the neural network models, trained using the Levenberg backpropagation algorithm, achieved a maximum accuracy of 98.26%.

Additionally, the confusion matrices corresponding to the classifier models are illustrated in Figs. 3 to 4 and elaborated in the following sections. Due to the extensive nature of discussing all observations from multiple classifiers, this article focuses on presenting the confusion matrix corresponding to the maximum classification accuracy achieved by the ANN model with PCA versus the minimum classification accuracy obtained by the SVM model without PCA. Fig. 3 and Fig. 4 present the confusion matrix corresponding to the ANN model and SVM model, respectively.

Referring to Fig. 3, it can be observed that the SVM Model (Without PCA) has the following sensitivity levels.

1. True Positive Rate for Pattern 1: 97.4%
2. True Positive Rate for Pattern 2: 48.6%

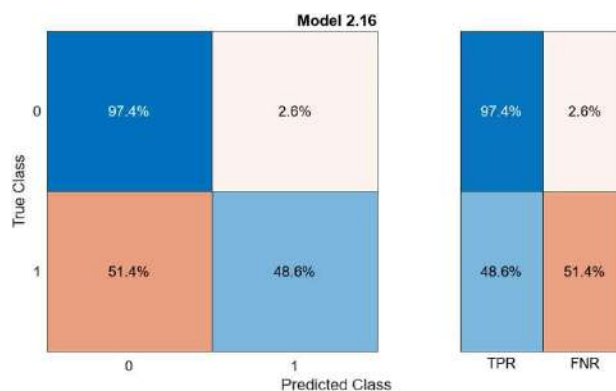


Fig. 3: Confusion matrix of SVM model with minimum accuracy of classifier 1.

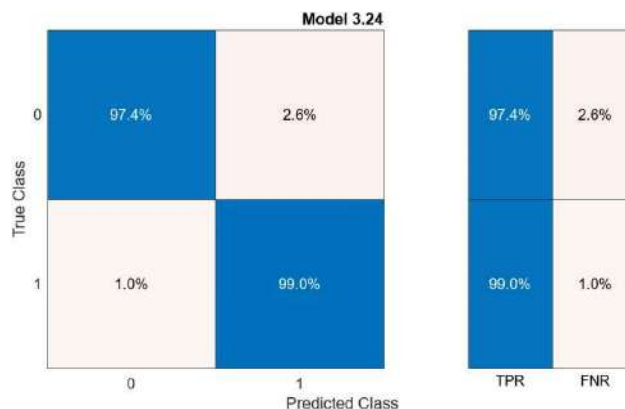


Fig. 4: Confusion Matrix of ANN model with maximum accuracy of classifier 2.

3. False Positive Rate for Pattern 1: 2.6%
4. False Positive Rate for Pattern 2: 51.4%

The two-class SVM model can also be used to determine the effectiveness of the classification model for each class based on its sensitivity. The sensitivity of the “Safe data” category is 97.4%, indicating that the related samples were correctly classified with few occurrences of misclassification. Similarly, the sensitivity of the “Unsafe data” category is 48.6%, indicating that the classification model has a lower sensitivity and a misclassification accuracy of 51.4%. As a result of this, the SVM model developed for the two-class problem is not appropriate for the generalization of the toxicity detection system.

Referring to Fig. 4, it can be observed that the ANN Model (With PCA):

- True Positive Rate for Pattern 1: 97.4%
- True Positive Rate for Pattern 2: 99.0%
- False Positive Rate for Pattern 1: 2.6%
- False Positive Rate for Pattern 2: 1.0%

The two-class ANN model can also be used to determine the effectiveness of the classification model for each class based on its sensitivity. The sensitivity of the “Safe data” category is 97.4%, indicating that the related samples were correctly classified with few occurrences of misclassification. Similarly, the sensitivity of the “Unsafe data” category is 99.0%, indicating that with more accuracy, the related samples were correctly classified. As a result of this, the ANN model developed for the two-class problem is suitable for the generalization of the toxicity detection system. However, we have also considered the four-class problem for the generalization of the toxicity detection system. The classification model’s effectiveness for the multiclass based on its sensitivity has been discussed in the following section.

Additionally, our observations reveal that the outputs from ANN models using a binary activation function ranged from -0.22699 to 2.8721 without rounding the net values or applying absolute values. Based on these findings, we further divided the dataset into four distinct sets: corresponding No Harm, Low Harm, Moderate Harm, and Severe Harm. These divided datasets were employed to model a multi-layer neural network for classifying different levels of toxicity. The split datasets were also validated using ANOVA for the F-value and P-value, both of which demonstrated significant differences between the four toxicity levels.

#### Level of Toxicity Using Multi-Layer Neural Network

The ANN model for the two-class problem achieved a maximum accuracy of 98.26%, with a misclassification of 6 samples. Regression analysis for the two-class problem was performed at various stages of training, validation, and testing, as illustrated in Fig. 5 (Faraw 2015).

The R values during these stages were found to be 0.99951, 0.96653, and 0.85693, respectively. These R values, being close to 1, confirm the robustness of the results (Faraw 2015, Judd et al. 2017). Additionally, Fig. 6 displays a scattered plot revealing that the output neural network effectively discriminates between 0 and 1.

Leveraging this discrimination, we further divided the data into four sets and modeled a multi-layer NN for the four-class problem. The development of the multi-layer neural network model involved configuring 16 input neurons, one hidden layer with 15 hidden neurons, and 2 output neurons to address the four different toxicity patterns. With 1000 epochs and a goal parameter set to 1e-10, the MLNN model demonstrated a performance of 97% accuracy with mean square error (MSE) of 9.99e-11 and a 3% misclassification rate. Analyzing the confusion matrix in Table 11 revealed accurate classification for all 222 “no harm” samples, 9

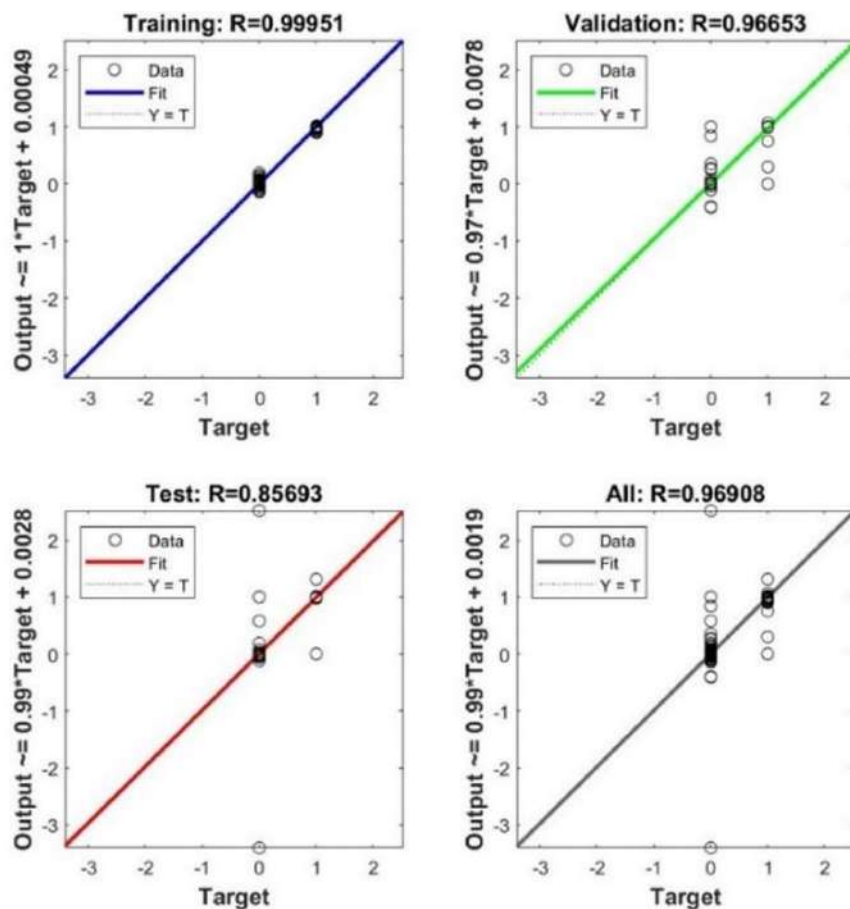


Fig. 5: Regression analysis of two class pattern recognition using FFNN.

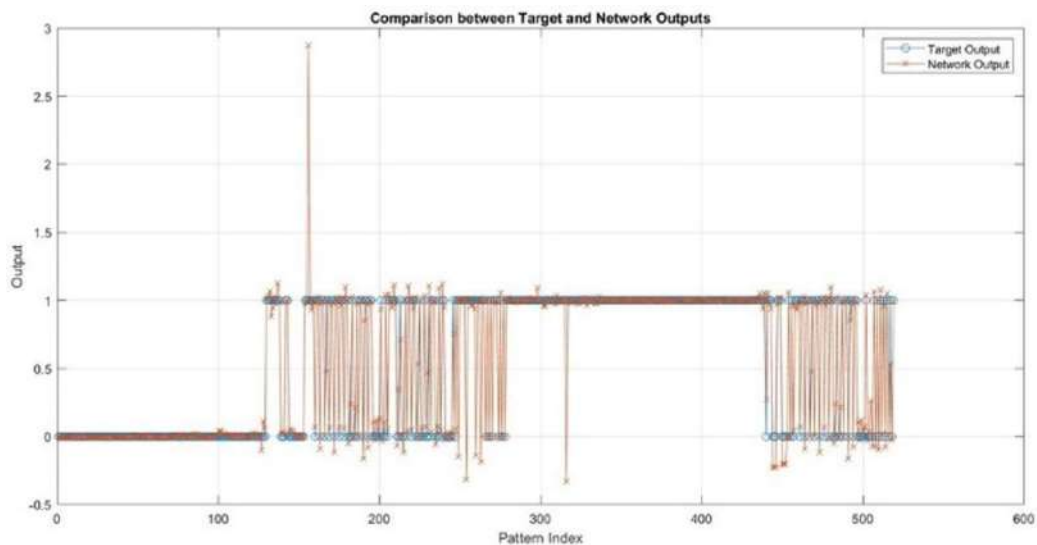


Fig. 6: Scattered plot of two class patterns comparing the actual and target outputs.

Table 11: Confusion matrix for MLNN for the four-class problem.

		Actual output				TP	FP
		No Harm	Low harm	Moderate harm	Severe harm		
<b>Target Output</b>	<b>No Harm</b>	222	0	0	0	100%	0%
	<b>Low harm</b>	0	9	1	0	90%	10%
	<b>Moderate harm</b>	0	0	6	0	100%	0%
	<b>Severe harm</b>	2	1	0	272	99%	1%
<b>False Negative</b>		1%	10%	17%	0%	<b>97%</b>	<b>3%</b>

out of 10 “low harm” samples, and 6 out of 7 “moderate harm” samples. Notably, one “low harm” sample was incorrectly categorized as “moderate harm,” resulting in a 17% false negative rate. For the “severe harm” category, 272 out of 275 samples were correctly classified, with a 1% false positive rate indicating two samples falling into “no harm” and one into “low harm.” This analysis justifies the MLNN model’s effectiveness in determining the toxicity level of fruits and vegetables, even with a dataset of 513 samples (excluding 6 misclassified samples in the two-class problem).

From the confusion matrix represented in Table 11, it is observed that there are false negative samples and false positive samples. Therefore, the sensitivity and specificity of the multi-classification system have been analyzed using Equation 2 and Equation 3.

$$\text{sensitivity} = \frac{\text{True Positives}}{\text{True Positives} + \text{False Negatives}} \quad \dots(2)$$

$$\text{pecificity} = \frac{\text{True Negatives}}{\text{True Negatives} + \text{False Positives}} \quad \dots(3)$$

The Sensitivity and specificity results are tabulated in Table 12 and discussed below.

An understanding of the effectiveness of the classification model for every class can be established from the sensitivity

and specificity results derived from the confusion matrix. The results are discussed as follows:

### Level of Sensitivity

The ability of a model to distinguish examples of a specific class from all instances that genuinely belong to that class is measured by its sensitivity. Therefore, the classification model based on the multi-layer neural network model with maximum classification accuracy has been chosen for the sensitivity and specificity analysis. From this analysis, considering the “No Harm” and “Moderate Harm” classes, Sensitivity stands at 100%, indicating that the model accurately detects every “No Harm” and “Moderate Harm” occurrence. Considering the “Low Harm” category, the model’s sensitivity is 90%, indicating that 90% of “Low Harm” occurrences are accurately identified, with minimal instances of misclassification. Similarly, the sensitivity of the “Severe harm” class was 99.26%, indicating high accuracy in identifying instances of “Severe harm”, with a few misclassifications.

The level of specificity relates to how effectively the model can identify and reject samples that do not fall within a specific class. In this classification problem, every class has a specificity value of 100%, which strongly

Table 12: The Sensitivity and specificity results.

Class	Sensitivity = $\frac{TP}{TP+FN}$	Specificity = $\frac{TN}{TN+FP}$
No Harm	$\frac{222}{222+0} = 1.00 \text{ (100\%)}$	$\frac{9+1+0+1+0+6+0+272}{9+1+0+1+0+6+0+272} = \frac{289}{289} = 1.00 \text{ (100\%)}$
Low Harm	$\frac{9}{9+1} = 0.90 \text{ (90\%)}$	$\frac{222+0+0+1+0+6+0+272}{222+0+0+1+0+6+0+272} = \frac{500}{500} = 1.00 \text{ (100\%)}$
Moderate Harm	$\frac{6}{6+0} = 1.00 \text{ (100\%)}$	$\frac{222+0+0+0+0+1+0+1+272}{222+0+0+0+0+1+0+1+272} = \frac{498}{498} = 1.00 \text{ (100\%)}$
Severe Harm	$\frac{272}{272+2} = 0.99 \text{ (99.26\%)}$	$\frac{222+0+0+0+9+1+0+6}{222+0+0+0+9+1+0+6} = \frac{238}{238} = 1.00 \text{ (100\%)}$



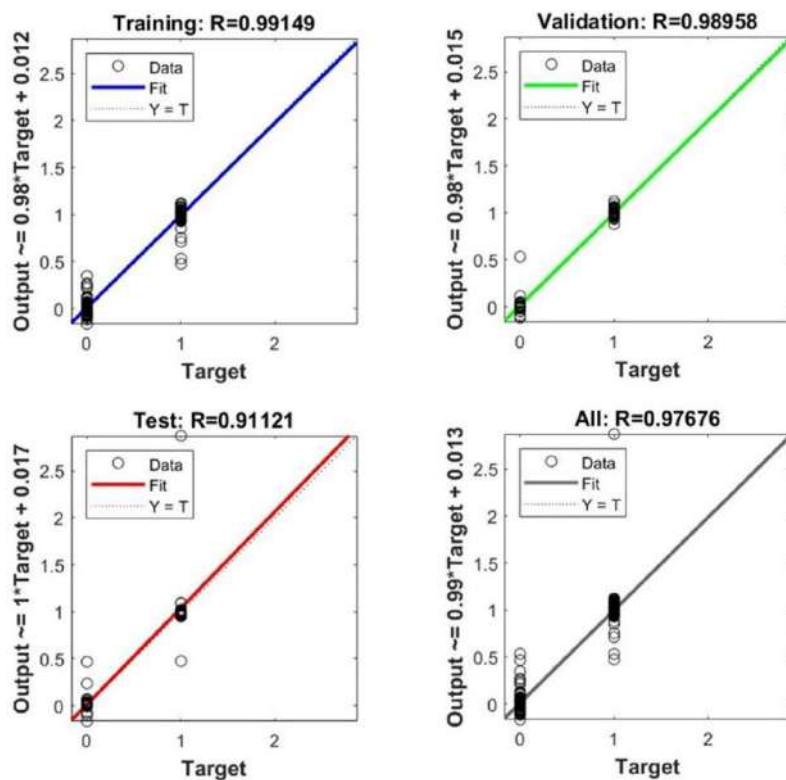


Fig. 7: Regression analysis of multi-class pattern recognition using MLNN.

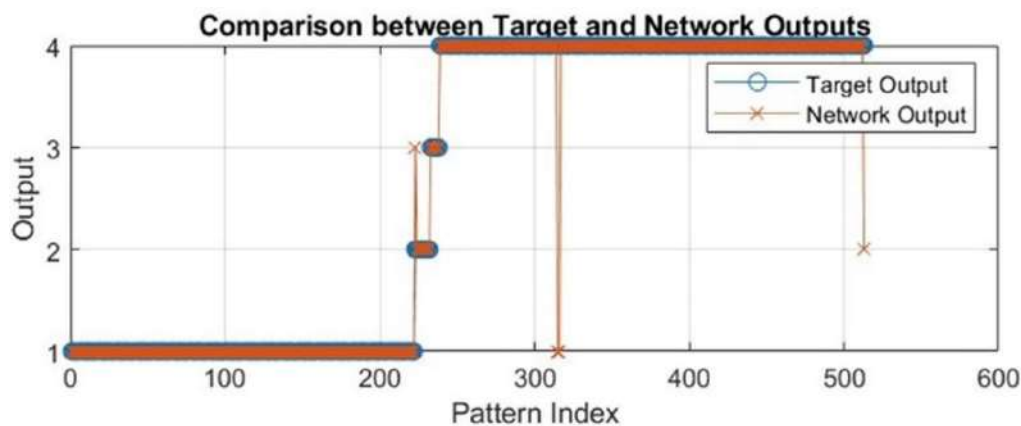


Fig. 8: Scattered plot of four class patterns comparing the actual and target outputs.

suggests that samples that do not belong to each class were successfully rejected by the model. From this analysis, with high sensitivity and specificity values across all classes, the classification model appears to be effective at identifying samples of each class overall, according to the results of the sensitivity and specificity analysis. There is certainly potential for development, nevertheless, particularly in accurately recognizing cases of the “Low harm” class, where

the sensitivity is marginally lower than that of other classes. Additional examination and enhancement of the model could potentially enhance its efficacy in terms of increased classification precision.

Moreover, regression and scatter plots were used to assess the strength of the relationship between targeted outputs and the actual output. The regression plot and scatter plots are depicted in Fig. 7 and Fig. 8 for the four-class

problem during the training, validation, and testing stages, respectively (Faraw 2015). The R values are 0.9919, 0.989, and 0.91, and these results further validate the robustness of the classification model. For future studies, increasing the sample size could enhance system stability and facilitate the generalization of the model for global applicability.

## CONCLUSIONS

This study thoroughly investigated the presence of Polycyclic Aromatic Hydrocarbons (PAHs) in fruits and vegetables, employing robust statistical measures for a comprehensive understanding of the dataset. The detection of toxicity in these consumables was successfully achieved through the implementation of machine learning algorithms, including Artificial Neural Network (ANN), k-nearest Neighbors (K-NN), and Support Vector Machine (SVM). Remarkably, the medium k-NN and Cubic-k-NN models demonstrated 100% accuracy, while Quadratic SVM, Cubic SVM, and cosine k-NN models exhibited an accuracy of 92.3%. Despite the promising results from all three models, ANN classifiers emerged as the most accurate in predictions, especially given the binary class nature of the problem and the minimal number of samples considered for the toxicity detection system.

Furthermore, the outputs from the ANN models were investigated to determine the toxicity level of the samples, revealing highly promising results. To enhance the generalization of this toxicity classification system, future work will involve developing a real-time dataset with diverse feature extraction and optimization methods. The models trained using various machine learning algorithms showcased efficiency and provided substantial results, laying the groundwork for the development of a generalized prototype model. Standardizing the level of toxicity will enable a more precise representation of the severity of fruits and vegetables. The results of this study establish the viability of applying machine learning algorithms to predict toxicity in various products, paving the way for broader applications in the future. Also, the performance of the models trained using different machine learning algorithms provides a solid foundation for the development of a standardized toxicity classification system. This standardization facilitates the provision of precise decisions on toxicity severity in products, thereby enabling informed decision-making and regulatory intervention.

Finally, the study has several limitations, such as those associated with the collected dataset. While the dataset used in this research presents samples from a variety of regions, seasons, and sources, it may not accurately reflect the global diversity of fruits and vegetables. This constraint may affect the generalizability of our classification models.

Expanding the methodology to include samples from different countries considering the climates and farming practices might strengthen the analysis. Collaboration with research institutions and industries may allow practical implementation of the research, and it would also be beneficial to investigate longitudinal studies examining PAH contamination over multiple periods and seasons. This would provide a more complete understanding of temporal changes and their impact on contamination levels.

Furthermore, establishing the study's limitations is crucial for interpreting the findings and directing future research. By addressing potential overfitting, the need for more diverse datasets, and other constraints, future work on this study will focus on expanding datasets, incorporating longitudinal data, and leveraging advanced detection technologies and evaluation methods. This may enhance the reliability and stability of the classification models and the applicability of PAH analysis in fruits and vegetables.

In summary, our research not only highlights the current state of PAH contamination in fruits and vegetables but also opens the direction for future research and technological applications that can significantly enhance food safety and public health. Addressing these challenges and suggesting concrete solutions contribute to safer and healthier food safety.

## REFERENCES

- Abdel-Shafy, H.I. and Mansour, M.S.M., 2016. A review on polycyclic aromatic hydrocarbons: source, environmental impact, effect on human health and remediation. *Egyptian Journal of Petroleum*, 25(1), pp.107-123. [DOI]
- Abou-Arab, A.A.K., Abou-Donia, M.A.M., El-Dars, F., Ali, O. and Hossam, A., 2014. Levels of polycyclic aromatic hydrocarbons (PAHs) in some Egyptian vegetables and fruits and their influences by some treatments. *International Journal of Current Microbiology and Applied Sciences*, 3(7), pp.277-293.
- Ali, A., Alrubei, M., Hassan, L.F.M., Al-Ja'afari, M. and Abdulwahed, S., 2020. Diabetes classification based on KNN. *IJUM Engineering Journal*, 21(1), pp.175-181. [DOI]
- Al-Nasir, F., Hijazin, T.J., Al-Alawi, M.M., Jiries, A., Al-Madanat, O.Y., Mayyas, A., Al-Dalain, S.A., Al-Dmour, R., Alahmad, A. and Batarseh, M.I., 2022. Accumulation, source identification, and cancer risk assessment of polycyclic aromatic hydrocarbons (PAHs) in different Jordanian vegetables. *Toxics*, 10(11), p.643. [DOI]
- Ampomah, E.K., Qin, Z. and Nyame, G., 2020. Evaluation of tree-based ensemble machine learning models in predicting stock price direction of movement. *Information (Switzerland)*, 11(6). [DOI]
- Ashraf, M.W. and Salam, A., 2012. Polycyclic aromatic hydrocarbons (PAHs) in vegetables and fruits produced in Saudi Arabia. *Bulletin of Environmental Contamination and Toxicology*, 88, pp.543-547. [DOI]
- Ashraf, M.W., Taqvi, S.I.H., Solangi, A.R. and Qureshi, U.A., 2013. Distribution and risk assessment of polycyclic aromatic hydrocarbons in vegetables grown in Pakistan. *Journal of Chemistry*, 2013. [DOI]
- Camargo, M.C.R. and Toledo, M.C.F., 2003. Polycyclic aromatic hydrocarbons in Brazilian vegetables and fruits. *Food Control*, 14(1), pp.49-53. [DOI]
- Choochuay, C., Deelman, W. and Pongpiachan, S., 2023. Polycyclic

- aromatic hydrocarbons in Thai and Myanmar rice: concentrations, distribution and health concerns. *Nature Environment and Pollution Technology*, 22(3), pp.1097-1110. [DOI]
- Colkesen, I., Sahin, E.K. and Kavzoglu, T., 2016. Susceptibility mapping of shallow landslides using kernel-based Gaussian process, support vector machines and logistic regression. *Journal of African Earth Sciences*, 118, pp.53-64. [DOI]
- Cui, X., Ailijiang, N., Mamitimin, Y., Zhong, N., Cheng, W., Li, N., Zhang, Q. and Pu, M., 2022. Pollution levels, sources, and risk assessment of polycyclic aromatic hydrocarbons in farmland soil and crops near. [DOI]
- Deligannu, P. and Muniandy, T., 2024. Review on the health risk of polycyclic aromatic hydrocarbon (PAH) exposure among street food vendors. *European Journal of Theoretical and Applied Sciences*, 2(1), pp.532-539. [DOI]
- Faraw, J.J., 2015. *Practical Regression and ANOVA using R*. Routledge. [DOI]
- Frossard, J. and Renaud, O., 2021. Permutation tests for regression, ANOVA, and comparison of signals: the permuco package. *Journal of Statistical Software*, 99, pp.1-32. [DOI]
- Jánská, M., Hajšlová, J., Tomaniová, M., Kocourek, V. and Vávrová, M., 2006. Polycyclic aromatic hydrocarbons in fruits and vegetables grown in the Czech Republic. *Bulletin of Environmental Contamination and Toxicology*, 77(4), pp.492-499. [DOI]
- Jia, J., Bi, C., Zhang, J., Jin, X. and Chen, Z., 2018. Characterization of polycyclic aromatic hydrocarbons (PAHs) in vegetables near industrial areas of Shanghai, China: sources, exposure, and cancer risk. *Environmental Pollution*, 241, pp.750-758. [DOI]
- Judd, C.M., McClelland, G.H. and Ryan, C.S., 2017. *Data Analysis: A Model Comparison Approach to Regression, ANOVA, and Beyond*. Routledge. [DOI]
- Khalili, F., Shariatifar, N., Dehghani, M.H., Yaghmaeian, K., Nodehi, R.N. and Yaseri, M., 2021. The analysis and probabilistic health risk assessment of PAHs in vegetables and fruit samples marketed by Tehran Chemometric. *Global NEST Journal*, 23, pp.497-508. [DOI]
- Le, K.T., Chau, C., Richard, J.P. and Guedj, E., 2020. An adapted linear discriminant analysis with variable selection for the classification in high-dimension and an application to medical data. *Journal of Statistical Planning and Inference*, 213, pp.1-12. [DOI]
- Lee, Y.N., Lee, S., Kim, J.S., Patra, J.K. and Shin, H.S., 2019. Chemical analysis techniques and investigation of polycyclic aromatic hydrocarbons in fruit, vegetables, and meats and their products. *Food Chemistry*, 277, pp.156-161. [DOI]
- Mallah, M.A., Changxing, L., Mallah, M.A., Noreen, S., Liu, Y., Saeed, M., Xi, H., Ahmed, B., Feng, F. and Mirjat, A.A., 2022. Polycyclic aromatic hydrocarbon and its effects on human health: An overview. *Chemosphere*, 296, p.133948. [DOI]
- Megalingam, R.K., Sree, G.S., Reddy, G.M., Krishna, I.R.S. and Suriya, L.U., 2019. Food spoilage detection using convolutional neural networks and K means clustering. *2019 3rd International Conference on Recent Developments in Control, Automation and Power Engineering (RDCAPE)*, pp.488-493. [DOI]
- Mo, C.H., Cai, Q.Y., Tang, S.R., Zeng, Q.Y. and Wu, Q.T., 2009. Polycyclic aromatic hydrocarbons and phthalic acid esters in vegetables from nine farms of the Pearl River Delta, South China. *Archives of Environmental Contamination and Toxicology*, 56, pp.181-189. [DOI]
- Nanda, M.A., Seminar, K.B., Nandika, D. and Maddu, A., 2018. A comparison study of kernel functions in the support vector machine and its application for termite detection. *Information*, 9(1), p.1. [DOI]
- Narsi, R., Bishnoi, M. and Pandit, G.G., 2006. Quantification of polycyclic aromatic hydrocarbons in fruits and vegetables using high-performance liquid chromatography. *Indian Journal of Chemical Technology*, 13, pp.30-35. [DOI]
- Nataraj, S.K., Al-Turjman, F., Adom, A.H.B., R, S., M, R. and R, K., 2022. Intelligent robotic chair with thought control and communication aid using higher-order spectra band features. *IEEE Sensors Journal*, 22(18), pp.17362-17369. [DOI]
- Nataraj, S.K., M.P., P., Yaacob, S.B. and Adom, A.H.B., 2021. Classification of thought-evoked potentials for navigation and communication using multilayer neural network. *Journal of the Chinese Institute of Engineers*, 44(1), pp.53-63. [DOI]
- Okaba, F.A., Daka, E.R. and Tulonimi, J.K., 2020. Evaluation of polycyclic aromatic hydrocarbons and toxic elements in some vegetables cultivated along roadsides in Port Harcourt and environs. *Journal of Environmental Science, Toxicology and Food Technology*, 14, pp.14-31.
- Omoyeni, A.O., Maryrose, O.I. and Benedict, O.C., 2023. Concentrations, sources, and risk assessment of polycyclic aromatic hydrocarbons in vegetables cultivated in the environs of Rivers Niger-Benue Lokoja, Nigeria. *International Journal of Nutrition and Food Sciences*, 12(4), pp.101-108.
- Pandey, V.K., Srivastava, S., Dash, K.K., Singh, R., Mukarram, S.A., Kovács, B. and Harsányi, E., 2023. Machine learning algorithms and fundamentals as emerging safety tools in the preservation of fruits and vegetables: A review. *Processes*, 11(6), p.1720. [DOI]
- Paris, A., Ledauphin, J., Poinot, P. and Gaillard, J.L., 2018. Polycyclic aromatic hydrocarbons in fruits and vegetables: Origin, analysis, and occurrence. *Environmental Pollution*, 234, pp.96-106. [DOI]
- Pérez, A., Larrañaga, P. and Inza, I., 2009. Bayesian classifiers based on kernel density estimation: Flexible classifiers. *International Journal of Approximate Reasoning*, 50(2), pp.341-362. [DOI]
- Ramezan, A., Warner, C.A. and Maxwell, T. E., 2019. Evaluation of sampling and cross-validation tuning strategies for regional-scale machine learning classification. *Remote Sensing*, 11(2), p.185. [DOI]
- Samsøe-Petersen, L., Larsen, E.H., Larsen, P.B. and Bruun, P., 2002. Uptake of trace elements and PAHs by fruit and vegetables from contaminated soils. *Environmental Science & Technology*, 36(14), pp.3057-3063. [DOI]
- Sankar, T.K., Kumar, A., Mahto, D.K., Das, K.C., Narayan, P., Fukate, M., Awachat, P., Padghan, D., Mohammad, F., Al-Lohedan, H.A., Soleiman, A.A. and Ambade, B., 2023. The health risk and source assessment of polycyclic aromatic hydrocarbons (PAHs) in the soil of industrial cities in India. *Toxics*, 11(6). [DOI]
- Singh, L. and Agarwal, T., 2018. Polycyclic aromatic hydrocarbons in diet: Concern for public health. *Trends in Food Science & Technology*, 79, pp.160-170. [DOI]
- Sonwani, E., Bansal, U., Alroobaea, R., Baqasah, A.M. and Hedabou, M., 2022. An artificial intelligence approach toward food spoilage detection and analysis. *Frontiers in Public Health*, 9, p.816226. [DOI]
- Tesi, G.O., Iniaghe, P.O., Lari, B., Obi-Iyeke, G. and Ossai, J.C., 2021. Polycyclic aromatic hydrocarbons (PAHs) in leafy vegetables consumed in southern Nigeria: Concentration, risk assessment and source apportionment. *Environmental Monitoring and Assessment*, 193(7), p.443. [DOI]
- Tritsaris, G.A., Carr, S. and Schleider, G.R., 2021. Computational design of moiré assemblies aided by artificial intelligence. *Applied Physics Reviews*, 8(3). [DOI]
- Tuteja, G., Rout, C. and Bishnoi, N.R., 2011. Quantification of polycyclic aromatic hydrocarbons in leafy and underground vegetables: A case study around Panipat city, Haryana, India. *Journal of Environmental Science and Technology*, 4(6), pp.611-620. [DOI]
- Vargaftik, S., Keslassy, I., Orda, A. and Ben-Itzhak, Y., 2021. RADE: Resource-efficient supervised anomaly detection using decision tree-based ensemble methods. *Machine Learning*, 110(10), pp.2835-2866. [DOI]
- Vasantha, K., Texina, S., Renganathan, A. and Nataraj, S.K., 2023. Toxicity detection in water based on polycyclic aromatic hydrocarbons using machine learning algorithms. *Engineering Technologies and Applied Sciences*, 41, pp.1-6. [DOI]

- Wang, Z., Chu, X., Li, D., Yang, H. and Qu, W., 2022. Cost-sensitive matrixized classification learning with information entropy. *Applied Soft Computing*, 116, p.108266.
- Wong, T.T. and Yeh, P.Y., 2019. Reliable accuracy estimates from k-fold cross-validation. *IEEE Transactions on Knowledge and Data Engineering*, 32(8), pp.1586-1594. [DOI]
- World Health Organization (WHO), 2021. Human health effects of polycyclic aromatic hydrocarbons as ambient air pollutants: Report of the Working Group on Polycyclic Aromatic Hydrocarbons of the Joint Task Force on the Health Aspects of Air Pollution. *World Health Organization. Regional Office for Europe*.
- World Health Organization (WHO), 2023. Natural toxins in food. *WHO*. Retrieved from WHO
- Wu, J. and Yang, H., 2015. Linear regression-based efficient SVM learning for large-scale classification. *IEEE Transactions on Neural Networks and Learning Systems*, 26(10), pp.2357-2369. [DOI]
- Yang, Q., Williamson, A.-M., Hasted, A. and Hort, J., 2020. Exploring the relationships between taste phenotypes, genotypes, ethnicity, gender and taste perception using Chi-square and regression tree analysis. *Food Quality and Preference*, 83, p.103928. [DOI]
- Zhong, W. and Wang, M., 2002. Some polycyclic aromatic hydrocarbons in vegetables from northern China. *Journal of Environmental Science and Health, Part A*, 37(2), pp.287-296. [DOI]



# Agrivoltaics: Dual Use of Land for Energy and Food Sustainability

Aminul Islam<sup>1</sup>, Krishna Kishore Satapathy<sup>2</sup>, Sushil Kumar Kothari<sup>3</sup>, Biswajit Ghosh<sup>4</sup> and Shankha Koley<sup>1†</sup>

<sup>1</sup>Department of Agricultural Engineering and Farm Management, School of Agriculture and Allied Sciences, The Neotia University, Sarisha, Diamond Harbour, West Bengal-743 368, India

<sup>2</sup>Central Agricultural University, Gangtok, India

<sup>3</sup>Department of Agronomy, School of Agriculture and Allied Sciences, The Neotia University, Sarisha, Diamond Harbour, West Bengal-743 368, India

<sup>4</sup>The Neotia University, Sarisha, Diamond Harbour, West Bengal-743 368, India

†Corresponding author: Shankha Koley; shankha.koley@gmail.com

**Abbreviation:** Nat. Env. & Poll. Technol.  
**Website:** www.neptjournal.com

*Received:* 07-06-2024

*Revised:* 09-07-2024

*Accepted:* 06-08-2024

## Key Words:

Crop production  
 Agrivoltaics  
 Microclimate  
 Photovoltaic cells  
 Soil macronutrients

## ABSTRACT

Renewable energy has been of prime importance in the present era in meeting energy demand across all sectors. To meet this demand, solar energy has become a plausible option among scientists to reduce the fossil fuel effect and find an alternative solution. The main concern about large renewable energy installations on open land, mostly used for agricultural practices, is that they can displace different land uses and instigate the feed vs. fuel controversy in the long run. The current study reviewed the installation of solar panels on farmland's benefits and challenges. The present study also reviewed the effect of solar panels on agricultural crop microclimate, soil, water condition, and crop growth and yields. Crop production and solar PV electricity generation from the same land space have numerous benefits, such as improving land productivity, reducing irrigation, managing soil, protecting crops from adverse climatic conditions (heat, frost, rainfall, etc.), increasing PV panel efficiency, and meeting house and farm electricity needs. Fewer demerits of agrivoltaics are to be studied in the future, such as keeping a suitable crop cycle, limited crop suitability, high expenses, and a lack of technical expertise. A big change to meet future energy demand without much impact on the environment is the dual use of open land for crop production and solar energy generation. To maximize crop yield, the impact of solar panels on crop yields has not been studied for numerous crops. We found that the optimum arrangement of solar panels admits varying levels of solar radiation according to crop needs. Sustainable agriculture and efficient solar energy generation can be possible in the same field by perfecting shade design and selecting suitable crops.

## Citation for the Paper:

Islam, A., Satapathy, K.K., Kothari, S.K., Ghosh, B. and Koley, S., 2025. Agrivoltaics: Dual use of land for energy and food sustainability. *Nature Environment and Pollution Technology*, 24(2), B4223. <https://doi.org/10.46488/NEPT.2025.v24i02.B4223>

*Note: From year 2025, the journal uses Article ID instead of page numbers in citation of the published articles.*



**Copyright:** © 2025 by the authors  
**Licensee:** Technoscience Publications  
 This article is an open access article distributed under the terms and conditions of the Creative Commons Attribution (CC BY) license (<https://creativecommons.org/licenses/by/4.0/>).

## INTRODUCTION

The world population is expected to reach around 9.7 billion by 2050 (Gorjian et al. 2022). Globally, it has been seen that in the last few decades, with increased industrialization, population growth, and intensifying human living standards, the world's energy demand has increased (Pandey et al. 2016). Undeniable benefits of using fossil fuels such as oil, gas, and coal as primary energy sources are that they are non-renewable and hurt the environment, such as the emission of hazardous gases (Gonocruz et al. 2021). The development of renewable energy sources is engrossed in meeting future energy demand and the simultaneous replacement of fossil fuels. In 1980, agrivoltaics (AGV) systems were first proposed to duel the use of lands for agriculture production and solar energy generation in between solar arrays (Goetzberger & Zastrow 1982, Wen et al. 2018). The concept of AGV systems advanced with elevated solar panels below land spaces used for agriculture crop production. The AGV system integrates solar electricity generation from cropland to upraise land-use efficiency and offers an unusual chance for proper interaction with greater crop production, more electricity generation, reduced water

demand, decreased carbon emissions, and greater prosperity for human life (Proctor et al. 2021, Hernandez et al. 2019, Weselek et al. 2021). Proper installation of an AGV system can ease the trade-off between agricultural crop production, the safest energy production, and policymakers' scarce care of the open land area (Sekiyama & Nagashima 2019).

Understanding the possibility and efficiency of dual use of the same land for energy and crop production needs actual field experiments. The development and implementation of the AGV system will play a crucial role in the growing population's sustainable food and energy supply. Solar energy production from PV panels needs nearly flat and open lands, which are competitive with crop production lands. It has been reported that the traditional solar energy production project produces approximately 1 MW of energy per 2 hectares of open land (Santra et al. 2017). The land area competition between energy production and agricultural crop production will be a critical issue, especially in India, where many people depend on agriculture (Santra et al. 2018). Past research studies reported that solar light reaching more than the light saturation point for a crop does not improve the photosynthesis rate; it simply makes the plant thirsty and increases water demand (Marrou et al. 2013a).

PV modules can be installed and oriented in such a way that the required amount of sunlight reaches the crop, and from the excess sunlight, electricity can be harvested. In the AGV system, crops cultivated below solar PV panels will reduce the temperature of the panels, which improves the efficiency of electricity production. Additionally, AGV gives shade to crops and generates electricity simultaneously. Further studies are proposed to understand its practical applications, changes in microclimate impact on crop growth, and crop management as suitable crop rotation, selection of tolerable crops, orientation of solar PV panels, movement of farm machinery, etc. (Amaducci et al. 2018).

In particular, the possible performance of shade crops, which are expected to grow poorly in low-light environments, has not yet been fully explored for AGV systems (Hassanpour et al. 2018). It has been reported that even less than 1% of agricultural land has adopted AGV systems, which may offset the global energy demand (Adeh et al. 2019). An overview of the AGV technology is given in this review paper, along with examples of recent developments, possible application areas, and current applications. It also provides an overview of the corpus of current research on AGV systems. The goal of the analysis of early reports on crop production experiences in APV systems is to assess the current level of knowledge about AGV and how crop productivity is affected by shading. To determine whether AGV systems are suitable for use in agricultural food production, we also

look at various technical and agronomic aspects of them, with a focus on how they affect crop yield and microclimate.

The present review also focused on the electrical energy production performance of the AGV systems, extending to maximize crop production objectives and understanding different challenges and possibilities for describing and classifying the AGV system. In addition to this, the review study provides wise recommendations for researchers, farmers, and policymakers on AGV for power production, energy, and food sustainability. The novelty of this study is to advance the field and present a few new concepts as follows:

- i) a novel concept that combines agrivoltaics and concentrated solar power to generate a variety of beneficial outputs on agricultural fields to satisfy the demands of sustainable agriculture
- ii) evaluation in comparison of various AGV orientations (fixed-vertical, tracking, and fixed-tilted) for various agricultural fields to find the best locations and operating parameters.

## DEVELOPMENT OF AGRIVOLTAIC SYSTEMS

The development of AGV systems differs based on the optimization of solar energy generation and crop production using different land uses and climatic conditions (Fig. 2 (a-e)). Fig. 2 b shows lower elevated AGV systems (PV module stationary), which were more collective because of higher panel density and less installation cost (Santra et al. 2017). AGV systems have been classified into 2 different categories, namely open AGV systems and closed AGV systems (Fig. 1). Open AGV systems embrace interspaced solar PV, which are standard fixed or single-axis tracking ground-mounted systems, allowing for agricultural activity in-between or vertical with PV modules. Overhead PV systems are usually elevated (2-6 m) above ground level to ensure agricultural activity beneath the solar PV panels can continue unobstructed. Systems can either be fixed, single, or dual-axis tracking. The classification of AGV has been done based on system, application, farming type, PV structure, and flexibility (Fig. 1). AGV systems can be installed either near ground mounted or greater than 3m above soil mounted with space between rows of PV modules so that manual agricultural practices or farm machinery practices can have performed underneath the panel (Dinesh & Pearce 2016). Design and development of AGV system dimensions have been performed by understanding the height of the PV module, the orientation of PV panels, tilt angle, available solar radiation, types of crops, and local climatic conditions (Santra et al. 2018, Dinesh & Pearce 2016). The development of AGV systems and their adaption is highly dependent upon the morphological traits and physiological

responses of selected crops under AGV shade (Marrou et al. 2013b). The best energy conversion is possible by south-directed by a flat-plate solar collector with a tilted angle equivalent to the latitude or slightly higher than that place's latitude (Goetzberger & Zastrow 1982). studied by using PV arrays (size 1.64 m × 0.992 m) of different rows and different interspaces between arrays with rainwater harvesting systems and resulted in 29 m<sup>2</sup> of land required to generate 1 kW power (Santra et al. 2020). Different densities of PV panels (4m elevated from the ground) were studied, and it predicted that 35 to 73 % of global land productivity for partially shaded crops increased (Dupraz et al. 2011). It has been reported that the spacing between PV panel rows of 1.6 m is recognized to get maximum solar energy production (Dupraz et al. 2011). In an AGV system, maximum solar radiation will be used by giving an optimum tilt angle, which highly depends on local geographic location (Santra et al. 2017). In the AGV system, the PV panel height influences solar light distribution. Fig. 2e shows increased height of PV panels increases light penetration underneath PV panels, so light distribution increases in comparison with the near-ground mounted system of PV panels (Dupraz et al. 2011). The regular solar-tracking system automatically adjusts PV panel orientation based on solar altitude, improves electricity generation, and increases solar radiation below the PV panel area (Valle et al. 2017). AGV systems were studied for broccoli crops by installing PV panels 4m high, and resulted that soil temperature, microclimate, and daily photosynthetic photon flux density (PPFD) have significantly changed below AGV system, resulting in a little decrease in agriculture production and transformed metabolites in broccoli crop due to the shading of PV panel that increases consumer fondness (Chae et al. 2022). PVSyst software version 7.2 model studied and showed that the adoption of AGV reduces carbon dioxide (CO<sub>2</sub>) gas emissions and supply of uninterrupted

power and offers employment opportunities (John & Mahto 2021). Shade-resilient crops in hot-arid climatic regions can increase their yield while alleviating the negative effects of excessive temperatures and solar radiation (Jain et al. 2021). The current enhancement of electric vehicles by utilizing AGV systems in wetlands, forested land, and protected lands can improve rural charging stations, which could support a decrease in carbon emissions due to electrical vehicle use (Steadman & Higgins 2022). Assessed the impacts of pasture-based AGV systems on the environment and showed that AGV system reduces the emission of greenhouse gases (Pascaris et al. 2021a, 2021b). Technical features of the AGV system vary for different regions to improve photovoltaic yields as well as improve crop growth under the AGV system. Crop biomass production improved for the controlled solar tracking system, but the photovoltaic yield was reduced in comparison with the dynamic solar tracking system (Valle et al. 2017). However, in AGV arrangement of solar panels over agricultural land has affected both electricity generation from solar PV panels and cultivated crop yields. Three different AGV system designs were observed, such as the cultivation of crops in between solar panel modules, cultivation of crops below solar panel where the panel is raised to a suitable height so that farm machinery can move, and cultivation of crops below less than 3m elevated PV modules (Pulipaka & Peparthy 2021). Fig. 2c shows the utilization of the AGV system over the greenhouse roof and the generated power utilized to run the greenhouse equipment (Marrou et al. 2013a).

## EFFECTS OF AGRIVOLTAIC SYSTEM

The adoption of PV panels above the agricultural field removes solar light and land space, which will have a definite effect on crop growth and yield by reducing heat and water requirements (Ketzer et al. 2020). It has been reported

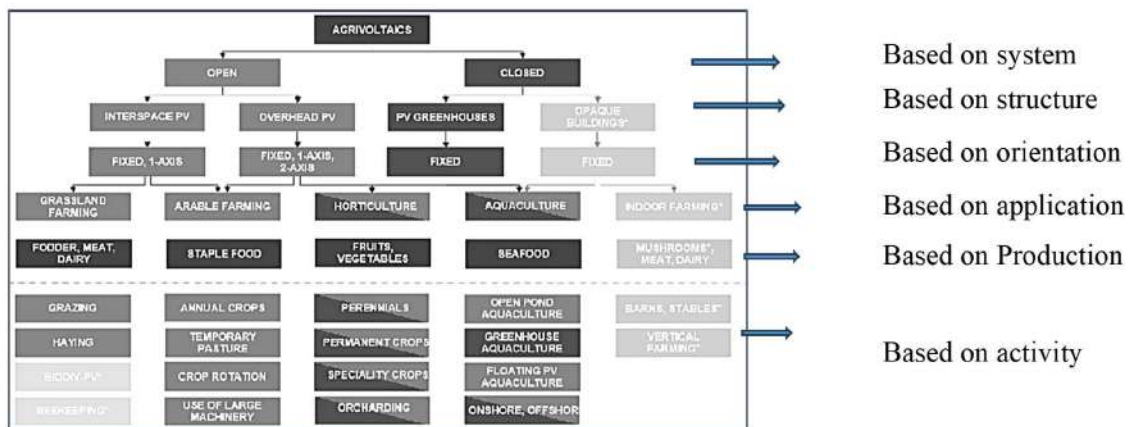
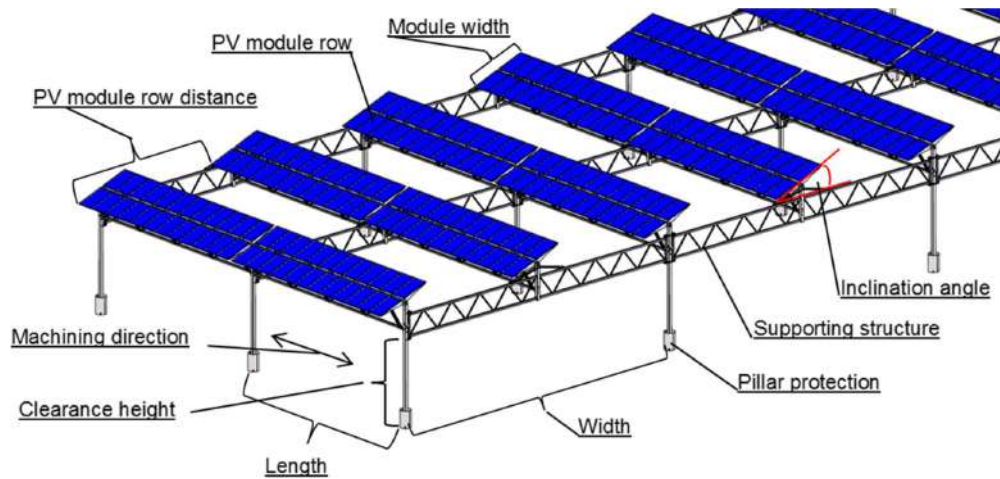


Fig. 1: Classification of AGV systems and examples of crop production (Varga et al. 2024).





a. Components of AGV system (Schindele et al. 2020).



b. AGV system with rainwater harvesting system (Santra et al. 2020).



c. AGV Greenhouse system (Marrou et al. 2013a).



d. AGV system with banana (Pulipaka & Peparthy 2021).



e. Elevated AGV system (Pulipaka & Peparthy 2021).

Fig. 2 (a-e): Utilised AGV system for different land-use conditions.



that AGV systems are expected to change the microclimate around the crop, which has both negative and positive effects on crops. Crops are categorized into 3 different categories, such as (i) Crops get benefits from shading, (ii) Crops do not have any shading effect, and (iii) Crops have highly utilized solar irradiation, which is not suitable for the AGV system (Beck et al. 2013).

## AGRIVOLTAIC SYSTEM EFFECTS ON THE MICROENVIRONMENT

The optimum microclimate condition for a crop is one of the important concerns for crop growth and yield. AGV system affects microclimate conditions, resulting in an effect on crop growth, yields, and cropping duration. Solar PV panels above crop fields reduce solar radiation as well as some other factors also, such as its effects on air temperature, soil temperature, soil moisture condition, incident radiation, air humidity, wind speed, and evapotranspiration rate (Marrou et al. 2013b, Adeh et al. 2019, Amaducci et al. 2018). Reported that under the AGV system, the microclimatic conditions and crop production change by reducing 30 % photosynthetic active radiation and also reported that soil moisture and air temperatures reduced, and rain distribution changed (Weselek et al. 2021). AGV system lowered crop temperature by 2.83°C and 0.71°C, and PV energy generation efficiency improved by 1.13 to 1.42% and 0.28 to 0.35% on sunny days and cloudy days, respectively (Teng et al. 2022). An AGV study in the California desert estimated that 14-29 % of water evaporation was reduced by artificial irrigation water, and in the Arizona desert, 50% of water savings (Dinesh & Pearce 2016). A properly installed and oriented panel in an AGV system makes shadows that reduce water consumption by 20% and yield decrease by 10% or extension of the cropping cycle (et al. 2018). It has been reported that an AGV system decreases the potential evapotranspiration (PET) rate due to decreased solar radiation (Hassanpour et al. 2018). Studied net radiation and available photosynthetically active radiation (PAR) for open sun fields and under solar PV panel fields, resulted that on under solar panel fields lower PAR attains (Santra et al. 2017). Past studies on AGV systems on organic crop fields resulted in a significant impact on crop production fields (Weselek et al. 2021). Solar PV arrays caused seasonal and diurnal variation in air and soil microclimate during the summer (reduced temperature by up to 5.2°C) and during the winter (reduced temperature by up to 1.7°C) as compared with controlled area and under PV arrays (Armstrong et al. 2016). Under solar PV area reduces direct sunlight, which leads to reduced air temperature during daytime and warmer during nighttime and retains moisture (Gafford et al. 2019). Nearly uniform solar radiation was achieved from the AGV system by installing 2m elevated with a 6m row distance

(Goetzberger & Zastrow 1982). Shading created by solar tracking AGV is indeed an interesting possibility with a high intrinsic economic value related to renewable energy production.

## AGRIVOLTAIC SYSTEMS EFFECTS ON CROP YIELD

AGV system has proposed to address the sustainable crop production and solar energy generation from the same land by using solar PV panels (Dinesh & Pearce 2016, Miskin et al. 2019). The demand for energy and food is increasing with an increasing population, so producing renewable energy (solar energy) from the cropland can be primed for next-generation living (Dinesh & Pearce 2016). It is not obvious that solar energy is year-round available in flat land, which is practiced for agriculture production (Adeh et al. 2019). In water-petrified areas, the implementation of solar PV panels can be productively utilized in semi-arid pastures with wet winters (Adeh et al. 2019). Solar PV panels shade the ground as per correlation with PV panels height, tilt angle, azimuth, and zenith positions of the sun, which affect crop growth by changing the amount of available PAR (Santra et al. 2020). Solar PV panels installed above 5m from the soil surface decrease sunlight by 20 to 25%, which reduces UV radiation that helps the plant grow well (Harinarayana & Vasavi 2014). AGV system impacts crop yields, but the loss can be reduced by generating additional earnings from energy utilized for selling electricity (Dinesh & Pearce 2016). The generated electrical energy can help sustainable agriculture by utilizing the produced energy in the farm itself for running irrigation pumps, operating post-harvest machinery, and controlling microclimate in greenhouse building. Under the AGV system, the land use efficiency and water productivity improved by reducing 20% irrigation water and a 10% decrease in yield and cropping cycle extension (Dupraz et al. 2011, Marrou et al. 2013c, Elamri et al. 2018). In rain-fed cultivation conditions, more grain yield and stable crop production can be possible by adopting an AGV system, reducing direct solar radiation, affecting soil temperature, evapotranspiration rate, and soil water balance, and providing favorable conditions than the open field condition (Schindele et al. 2020). Under PV, the photosynthesis rate and net ecosystem exchange are lower in the spring and winter duration (Armstrong et al. 2016). High solar radiation effect on crop and water use efficiency (Adeh et al. 2019). Arid climate cultivation of a crop and water productivity improves by reducing solar radiation using PV panels (Harinarayana & Vasavi 2014). Growing maize in rain-fed climatic conditions under solar PV panels improves crop resilience to climate change (Amaducci et al. 2018). Late session biomass increased by 90% for areas under PV panels

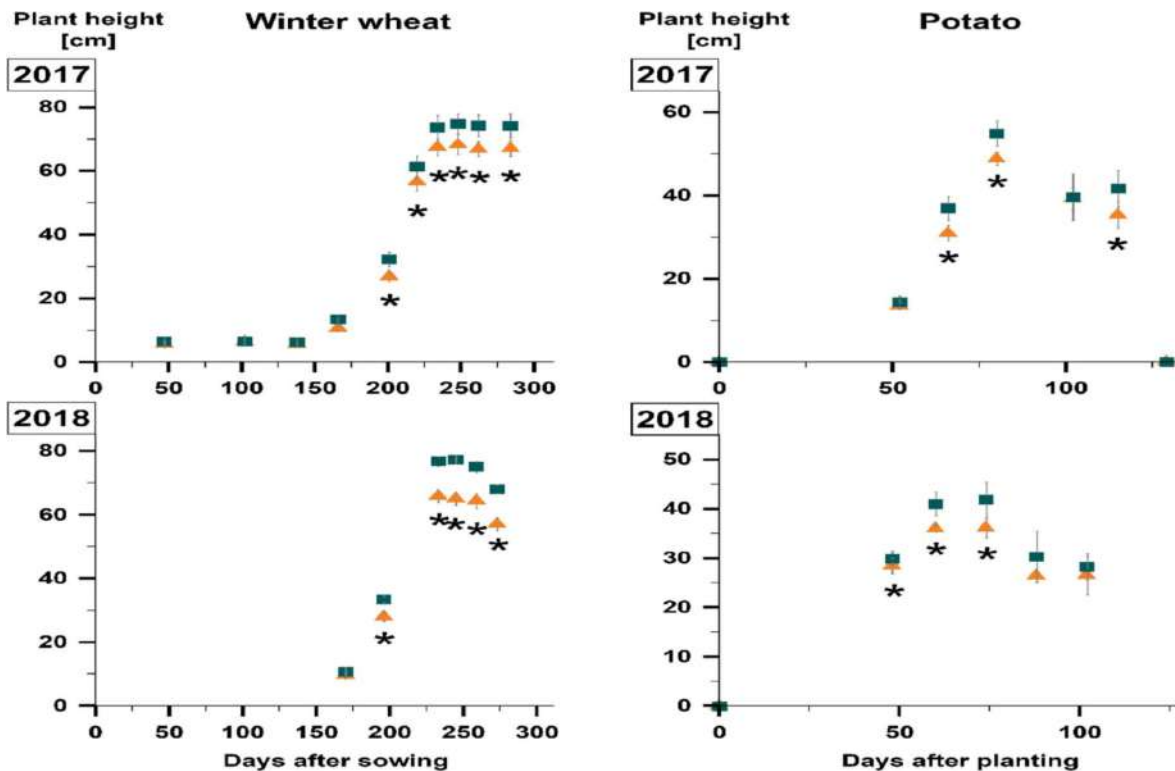


Fig. 3: PV underneath plant height of winter wheat (left) and potato (right) (Weselek et al. 2021).

(Adeh et al. 2019). Table 1 shows different past studies done for the development of AGV systems for triple-win abilities, such as improved food production, renewable energy generation, and water conservation from the same area of land. Weselek et al. (2021) studied different crop yields under AGV, and the control site was for hot-dry summer and found that crop yields of winter wheat and potato were increased for AGV by 2.7% and 11%, respectively (Fig. 3). A dynamic AGV system was investigated as a means of protecting trees from frost damage. The study revealed that less than 10% of flowers sustained injury during frost events, leading to the conclusion that autonomous vehicles (AVs) could effectively mitigate frost effects on flowers (Lopez et al. 2024). AGV system PV shade reduced 3.8°C in average air temperature and increased relative humidity by 14%, which has a positive effect on water relations, leaf morphophysiological characteristics, and yield determinants (Juillion et al. 2022). The weight and diameter reduction rates of fresh cabbage grown under APV conditions as compared to open-field conditions were 9.7% and 1.2%, respectively (Moon & Ku 2022). The AGV system did not negatively impact the yield of rye, corn, soybean, adzuki bean, or mixed plantings of corn and soybean (Jo et al. 2022).

## AGRIVOLTAIC SYSTEM EFFECTS ON SOIL AND WATER

Solar photovoltaic (PV) installations over open land directly affect soil and water conditions compared to fields without PV installations due to the shadow cast by the panels. The reduction in radiation caused by solar PV panels lowers average soil temperature, soil water evaporation rate, and transpiration rate (Elamri et al. 2018, Amaducci et al. 2018). Higher soil moisture levels are achieved under the area covered by solar PV panels, resulting in a 328% improvement in water efficiency for maize crops (Adeh et al. 2019). AGV systems with solar PV panels reduce evapotranspiration by limiting light and heat under the panel area, leading to an overall water savings of 14 to 19%, depending on the percentage of shade (Marrou et al. 2013c). Barron et al. (2019) studied AGVs in dryland climates and found that water use efficiency for tomatoes and jalapenos was 157% and 65% greater than in control areas, respectively. Their research suggests that soil moisture is retained 15% more for every 2-day irrigation interval and 5% more for daily irrigation. Marrou et al. (2013c) conducted a study on the sensitivity of cucumbers to shade (solar PV panels installed above 4 meters), revealing a reduction in water use efficiency. Different shading con-

Table 1: Studies on the AGV System.

Sl. No.	Authors name	Study area	AGV system	Solar Tracking	Energy output	Crop cultivated	Outcome
1.	Goetzberger and Zastrow (1982)	Freiburg, Germany	Solar energy collectors were installed 2 m above the ground with rows distance of three times the height,	Stilt-mounted	-	-	Studied mathematical relations for different configurations of collar collectors with direct and diffuse light
2.	Nagashima (2014)	Japan	Structures created by pipes and rows of PV panels arranged in intervals	Stilt-mounted	-	-	Patented the pergola-like structure in a garden and recommended about 32% shading is adequate for the growth of crops.
3.	Czaloun (2017)	South Tyrol (Italy)	Pilot plant with rope and steel structure system elevated at 5-6 m height	double-axis module tracking	-	-	The system may be less expensive because less steel is required.
4.	Weselek et al. (2021)	Herdwangen-Schönach in south-west Germany	Steel columns mounted solar panels installed at 5 m height with a row distance and with as 6.3 m and 3.4 m respectively.	oriented in the south-west with a tilt angle of 20°	194 kW	celeriac, clover grass, wheat, and potato	Under the AGV system, yields were reduced, but favorable growing was possible during hot and dry weather.
5.	Adeh et al. (2019)	Oregon, USA	1.65 m wide solar panels were installed at 1.1 m above ground (Lower side) with a distance of 6 m.	East-west orientated and southward inclined with a tilt angle of 18°	1435 kW	8 different types of grasses (Hordeum, Agrostis, Alopecurus, Schedonorus, Bromus, Calamagrostis, Cirsium, Dactylis)	Biomass production was increased for late-season grasses, and water efficiency increased to 328% under solar PV panels.
6.	Dupraz et al. (2011)	Montpellier, France	Solar panel installed above 4m from the ground and spaced 1.64 m between the lower sides of two consecutive panels with pillar distance 6.4 m apart.	South faced with the tilt angle in the range of 20° to 35°	1000Wm <sup>-2</sup>	Durum wheat	Modelled Ex ante simulations and STICS (Simulateur multi-disciplinaire pour les cultures standard) for light transmission under solar panels and predicted that around 35 to 73% of global land productivity could be increased.
7.	Santra et al. (2020)	Rajasthan, India	Different PV arrays row with 3 m, 6 m, 9 m interspaces between arrays installed by MS steel structure	South faced with tilt angle 26°	130kW	mung bean, moth bean, cluster bean, isabgol, cumin, taramira, cicer, chickpea, sonamukhi, sankpuspi, capsicum, cabbage, onion, garlic, cowpea, aloe vera.	Around 49% land area of an AGV system can be utilized for cultivating crops and around 1400 liter.KW <sup>-1</sup> of rainwater can be harvested and utilized for PV panel cleaning purposes.
8.	Harinarayana and Vasavi (2014)	Ahmedabad, India	Solar panel installed at 5m above the ground with 3.8/7.6/11.4 m pitch distance.	South faced with tilt angle 25°	-	-	Studied using PV-Syst software for various places and resulted that the pitch distance of 7.6, 11.4 with chess board pattern installation was suitable for agriculture.
9.	Marrou et al. (2013a)	Montpellier, France	0.8m wide solar panel strip installed in East-West at 4 m above with a square grid of 6.4 m by 6.4 m	Southward with a tilt angle of 25°C.	-	Lettuce, Cucumbers, wheat	This resulted in water use efficiency increasing by reducing soil water evaporation loss and more water for plants.

Table Cont....

Sl. No.	Authors name	Study area	AGV system	Solar Tracking	Energy output	Crop cultivated	Outcome
10.	Elamri et al. (2018)	Montpellier, France	4 different shading are arranged with 2x1 m size solar panels installed at 5 m above ground surface with 6.4 m pole spacing.	Southward with a tilt angle of 25°C.	-	Lettuce	Shade reduces 20%, water demands and 5–7 days delay in maturity with -15% to -25% decrease of crop yield.
11.	Gonocruz et al. (2021)	Tokyo, Japan	3 m above the ground systems.	Fixed horizontal angle	-	Rice	Reported that at least 80% of rice yield was possible for the allowable shading ranges from 27 to 39%.
12.	Schindele et al. (2018)	Castelvetro, Piacenza, Italy	On suspended structures at 4.83 m above ground	Southward 30° tilt angle	-	Maize	Studied by reducing solar radiation by 28.7% and 56.5% for two configuration systems and reported that more grain yield and stable crop production can be possible.
13.	Movellan (2013)	Chiba Prefecture, Japan	Installed plastic pipes at 3m high from the ground with row spacing of 5 m.	-	35,000 kWh	Cabbage, cucumber, eggplant, peanut, tomato, taro, yam	This resulted that the rate of photosynthesis did not increase even if the light reached beyond the light saturation point.
14.	Armstrong et al. (2016)	Westmill Solar Park, UK	PV rows installed at 4 m Wide and 11.2 m row spaced	South faced with an angle of 30°.	5 MW	Forbs, Legumes, Grasses	Reported that seasonal and diurnal microclimates changed under the PV module.
15.	Valle et al. (2017)	Montpellier, France	1.6 m and 3.2 m PV panel row spacing for full density and Half density and 4 m elevated above ground.	Faced 11° south-west with the tilt of 25° and with trackers	-	Lettuce	Solar tracking systems achieved high productivity per land area as compared with stationary AGV systems.
16.	Sanchez et al. (2012)	Almeria, Spain	PV Greenhouse- 9.8 % roof area Covering	-	2766 kW h (crop/ cycle)	Tomato	PV Greenhouse's 9.8 % roof area covering has not altered tomato yield, but fruit size and color were affected.
17.	Alonso et al. (2012)	South Eastern Spain	PV greenhouse- 9.79% area covering (roof)	-	8.25 kW h/m2	Tomato	Reported that PAR was not significant for plants growing due to sunlight blocking effect.
18.	Cossu et al. (2014)	Decimomannu, Italy	PV greenhouse-south-roofs were completely covered with PV module (1/2 of the roof covered)	Southward side tilt 30°	107,885 kWh	Tomato	Reported that tomato yield decreased under AGV system in comparison with traditional greenhouse.
19.	Bulgari et al. (2015)	Lombardy, Italy	PV greenhouse 50 % roof area covering	-	-	Tomato	Reduces solar radiation and that effect on tomato production (Reduction)
20.	Barron et al. (2019)	USA	3.3 m PV array	Tilt of 32°	-	Chiltepin pepper, jalapeño, and cherry tomato	AGV system reduced plant Drought stress, PV panel temperature, and improved food production.

ditions resulted in a 20% reduction in water requirements for lettuce cultivation and a 5 to 7-day delay in maturity, leading to a 15 to 25% decrease in yield compared to areas without solar panels (Elamri et al. 2018). Soil physicochemical and biochemical parameters were studied for different

conditions and resulted in the AGV significantly enhancing soil moisture (Fig. 4a), organic carbon (Fig. 4d), soil EC (Fig. 4b), soil pH (Fig. 4a) nitrogen-phosphorus-potassium nutrients, microbial biomass, and urease activity (Luo et al. 2024). Additionally, it was reported that gap cultivation



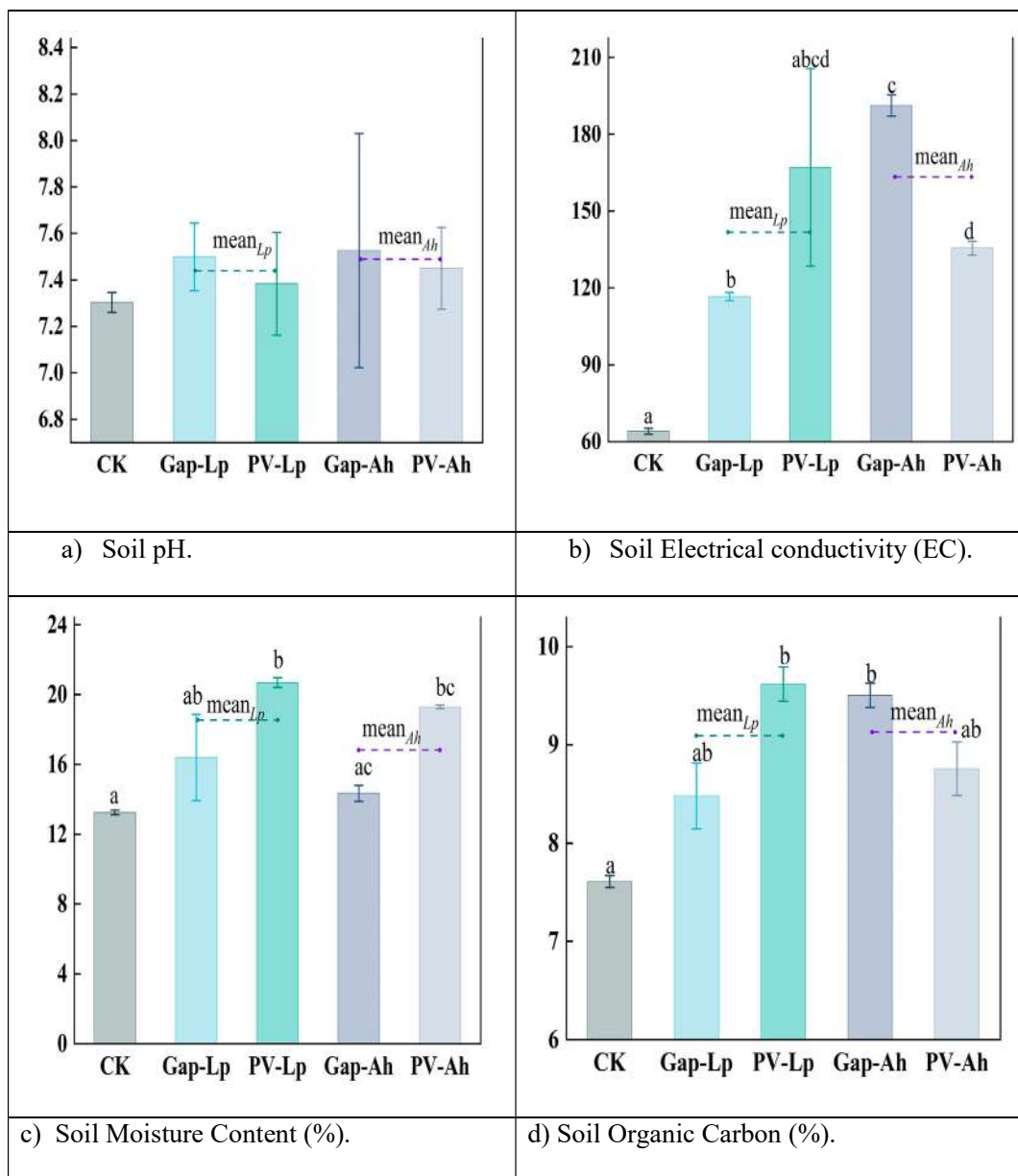


Fig. 4 (a-d): Agrivoltaics responses to soil physicochemical properties for control area outside the PV array (CK), gap ryegrass (Gap-Lp), under-panel ryegrass (PV-Lp), gap peanuts (Gap-Ah), under-panel peanuts (PV-Ah).

resulted in a noticeable definite influence on soil quality than under-panel cultivation, and the cultivation of peanuts had a greater effect on soil quality and multifunctionality improvement than ryegrass (Luo et al. 2024).

## SOLAR FARMING POTENTIAL IN INDIA

India has witnessed considerable progress in its electrical infrastructure, improving its ranking from 137 to 115 in electrical reliability between 2014 and 2019 (World Bank

2019). As a prominent player in renewable energy, India has expanded its solar power generation capacity to 57.705 GW by June 30, 2022. With a substantial portion of its landmass suitable for solar (84.40%) and wind energy production (81.33%), India possesses immense potential for renewable energy. Past studies have highlighted limitations associated with wind energy generation plants, including the need for open spaces, topographic considerations, wind intensity, and wake effects (Saraswat et al. 2021). India experiences a consistent solar irradiance of 5.6 kWh m<sup>-2</sup> day<sup>-1</sup> across its

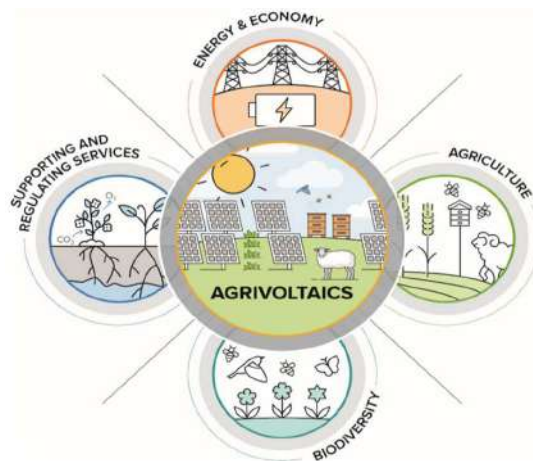


Fig 5: AGVs systems on different ecosystem services (Walston et al. 2022).

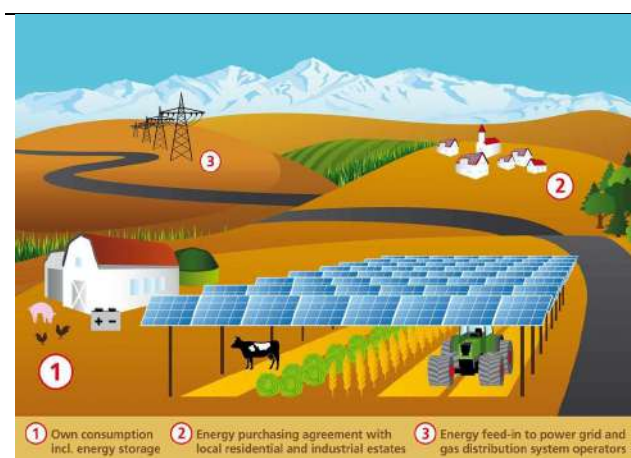


Fig 6: AGV energy utilization (Source: <https://metsolar.eu/blog/what-is-agrivoltaics-how-can-solar-energy-and-agriculture-work-together/#1>).

horizontal surface (NAAS 2018). Notably, the western region of India receives higher solar irradiation levels (6000–7000 kWh) compared to other areas, as depicted in Fig. 5 (NAAS 2018). The cold, arid zone encompassing Leh and Ladakh receives a solar irradiation of 7 to 7.5 kWh m<sup>-2</sup> day<sup>-1</sup> (NAAS, 2018). To effectively harness this abundant solar irradiation, the adoption and development of Agri-voltaic (AGV) systems are crucial throughout India. In India, three types of pilot AGV plants have been implemented based on cultivation space: (i) interspace cultivation (utilizing the space between ground-level elevated PV panels); (ii) cultivation beneath solar PV panels and between rows of ground-mounted PV panels (fixed tilt angle only; manual cultivation); and (iii) cultivation under solar PV panels mounted on an elevated structure (< 3 m) (maintaining sufficient row spacing; employing farm machinery) (Pulipaka & Peparthy 2021). The potential impact of AGV on various ecosystem services varies depending on

implementation goals and priorities (Fig 5). AGV systems directly contribute to energy production and economic growth by generating electricity (Fig. 5). Furthermore, AGV can promote plant and animal biodiversity, facilitating conservation efforts through crop production, carbon sequestration, and water and soil conservation (Fig. 5). Fig. 6 illustrates various applications of solar electricity generated from farmland. Table 2 displays different AGV projects developed across diverse crop climate conditions. The AGV system in Junagadh, India, produced solar energy equivalent to that generated by installed solar PV systems and resulted in an impressive performance during the experiment, achieving an efficiency of 80.83%, a capacity factor of 16.03%, and an overall performance ratio of 12.07% (Patel et al. 2024).

## CHALLENGES AND ADVANTAGES OF AGRIVOLTAIC SYSTEMS

Table 2: Different operational AGV Project plants in India.

Sl. No.	Project developer name and location	Type of AGV plant	Power production and year of establishment	Crop producing	Remarks
1..	Gujarat State Electricity Company Limited, Harsha Abakus plant near Sikka, Gujarat (Lat: 22.37903, Long: 73.05033)	Interspace/Overhead stilted hybrid	1MW -2016	pearl millet, fodder, black gram, pigeon pea, cotton, green gram, cluster bean chickpea, wheat, Groundnut, soybean, mustard, Lucerne, sesame, maize,	Solar panel installed at 3 m height with manual adjustable tilt angle. They focused on the impact on crop growth due to inter-module and array gaps shading patterns.
2.	Gujarat State Electricity Company Limited, Vastan, Gujarat (Lat: 21.41111, Long: 73.12264)	Interspace / Overhead Hybrid	1MW -2016	Tomato, Ladyfingers, chili, bottle gourd, coriander, cluster beans, mug, cucumber, zucchini,	Solar PV panel (manually tilted) installed 3 m above ground with 25, 150, and 250 mm spacing between panels.
3.	Gujarat State Electricity Company Limited, Gujarat, District Kutch, Panandhro (Lat: 23.66482, Long: 68.77906)	Interspace/Overhead Hybrid Manual Seasonal tilt: 0, 10- and 25-degree	1MW -2016	Brinjal, Green gram, cluster beans, peas, coriander, ladyfinger, sesame, bottle gourd, zucchini, black gram	Different crops were grown during summer and winter seasons with a 3- 6 ft average crop height.
4.	CAZRI: Central Arid Zone Research Institute plants- Jodhpur, Rajasthan)	Single axis fixed tracking 26°, With arrays: (i) one-row PV module 3 m interspace), (ii) two-row PV modules (6 m interspace), and (iii) three-row PV modules (9 m interspaces)	100 kW	Aloe vera, isabgol, cluster bean, sonamukhi, cumin, chickpea, sankhpuspi, chili, cabbage, onion, mung bean, moth bean, garlic,	Growth and yield of isabgol, medicinal crops, and <i>Solanum melongena</i> except mungbean, were significantly affected due to panel shade. This resulted in around 49% of land area being utilized for crops growing and a 1.41 Land equivalent ratio.
5.	Amity University plant in Noida, Uttar Pradesh (Lat.: 28.54162, Long.: 77.33241)	Single column, optimum tilt angle with a height of 4.6 m from the ground.	10 kW-2017	Mustard, maize, brinjal, potato,	Under the AGV system around 90% of land can be used for crop growing, and crop yields are not significantly changed.
6.	DAU: Dayalbagh Agriculture University, plant in Agra, Uttar Pradesh (Lat: 27.22671, Long: 78.01072)	18 feet mounted structure with the single tracking system	200 kW- 2020	Grams, brinjal, tomato, wheat, spinach, cauliflower, carrot	Sufficient space and height of structure help to use of farm machinery.
7.	JAU: Junagadh Agriculture University plant in Junagadh, Gujarat. (Lat.: 21.50109, Long.: 70.44758)	3 m height overhead tilted with solar PV panels arrangement of Chequered module	7 kW-2017	Tomato, capsicum	Greenhouse gutter harvested water was used for manual cleaning of the PV panel and studied tomato and capsicum yields in the open field and AGV field.
8.	Abellon Energy plant in Aravalli, Gujarat. (Lat.: 23.55983, Long.: 73.28684)	Interspace ground mounted, manual cleaning	1 MW-2012	Ginger, chili bottle gourd, ladyfinger watermelon, turmeric	Water used to cleanse the panel is reused for crop Irrigation.
9.	Mahindra Susten plant at Tandur, Telangana. (Lat.: 17.36825, Long.: 77.54105)	Interspace ground mounted, manual cleaning	400 kW-2016	Chilies, onions, lemon grass, ladyfinger annatto dye, brinjals.	For manual cleaning, 2.50 liters per Panel of water is required every fortnightly.

Table Cont....

Sl. No.	Project developer name and location	Type of AGV plant	Power production and year of establishment	Crop producing	Remarks
9.	Jain Irrigation plants at Jalgaon, Maharashtra. (Lat.: 20.99144, Long.: 75.5073)	Overhead stilted with single axis mounted for banana, fixed for rice, dual axis for cotton	74.4 kW	Banana, rice, cotton	Banana yields improved from 14 to 34.5 tons/acre and Rice from 3.1 to 3.8 tons/acre.
10.	NISE plant near Gurgaon, Haryana. (Lat.: 28.42754, Long.: 77.16071)	Interspace	100 kW-2020	Tomato, chili, flowers, Kufri Lima potato	-
11.	Cochin Airport plant in Kerala (Lat.: 10.15667, Long.: 76.38253)	Interspace	12 MW-2015	Tomato, green chili, Ginger, turmeric, bitter gourd, Pumpkin, Snake gourd, bottle gourd, ash gourd, Ladies finger, cucumber	Completely organic way cultivation.
12.	KVK: Krishi Vigyan Kendra, under National Horticultural Research and Development Foundation, New Delhi. (Lat.: 28.57134, Long.: 76.89579)	3.5 m elevated structure with a 15-degree tilt	110 kW-2021	leafy vegetables, root vegetables, brinjal, Okra, tomato, capsicum, and cole crops	Established as a pilot project
13.	APVRT: Hinren Agri-PV Rooftop System, Bangalore, (Lat.: 12.90890, Long.: 77.59428)	2.3 m elevated structure with fixed tilt	3 kW-2019	Papaya, cauliflower, lettuce coriander, pomegranate, tomato, lemon, ladies' finger, spinach, rosemary, bitter gourd, brinjal, beans, basil, and chili	Resulting from carbon emission-free electricity and pesticide-free different vegetables.

The main challenge for producing electricity by using solar is that they need large open land space, which is suitable for agriculture. One of the main challenges for large-scale adoption of AGV is that all types of crops are not suitable to cultivate under PV panel shade and the cost of materials and installation (Pascaris et al. 2020, 2021a). The trade-off between the extra costs required for the installation of solar PV panels in agricultural crop fields has limited reports. From the stakeholder's point of view, it is truly required to improve the efficiency of the AGV system. To succeed, AGV farmers' perceptions of the application, difficulties, and opportunities of this dual land-use system are crucial (Winkler et al. 2018). For adopting AGV, the farmers are concerned about sustained land productivity because of the size of the plot and the permanence of the AGV system, the lifespan of solar panel systems, and the restriction of agricultural maintenance (Irie et al. 2019, Yeongseo & Yekang 2020). From the farmer's side, the main challenge to the adoption of AGV is the use of land for dual purposes, and a few other challenges are: 1) There are several unknown processes, and farmers are worried about demand instability (Babatunde et al. 2019, Ibrahim & Kumari 2020); 2) For the installation of the AGV system, farmers are asking for compensation for their adopted land (Santos 2020, Yano et al. 2014, Kadowaki et al. 2012);

3) AGV adaptability to accommodate varying activity sizes and types as well as changing farming practices (Cossu et al. 2018, Pascaris et al. 2021a) 4) Farmers lack knowledge about the adoption of AGV systems with positive economic and no non-negative environmental effects (Irie et al. 2019, Agostini et al. 2021); 5) Certain PV infrastructure designs should give priority to potential reversibility (Valle et al. 2017); 6) proactive awareness-raising activities to promote AGV (Kostik et al. 2020, Winklers et al. 2018). AGV faced another most important challenge: ensuring maximum crop yield under PV panels because the area underneath the PV panels receives 20% of solar energy on a clear day, which is usually not sufficient for many crops (Liu et al. 2023). Limited studies are being done on the potential of different field layout designs (Height, tilt angle, spacing between panels), PV panel types, and PV module row spacing for different crop production under the AGV system. From the operation side, the other main challenges are land utilization, technical standards, and financial intervention for AGV. Land utilization basis, it is necessary to have such guidelines of policies so that the farmers can get subsidies. As such no technical standards or norms are established to avoid improper installation of AGV systems in crop land by giving fewer priorities to crop yields. From the technical point of



view, there is one more major barrier to utilizing the AGV system: the cleaning challenges for highly elevated structures, including the cleaned waterfall, may affect crops. As of now, no such study is being done about the shade of AGV system's effects on important soil macronutrient (N, P, K) levels due to the shade created underneath solar PV. So, there is indeed a way to understand the soil's important micronutrient behavior under the AGV system.

Studies on AGV systems are in the developing stage, so there is wide scope for technical and field scale improvement. The past study showed that PV modules installed with a solar tracking (Optimum) system allow solar radiation on the crop canopy, so efficient crop production and both biomass production and electricity production improved (Valle et al. 2017). The AGV system has widespread opportunities based on local climate and soil water resources for utilizing the power produced for irrigation pumping purposes and post-harvest operations (Mekhilef et al. 2013, Hyvärinen 2019). However, the AGV system can be utilized for future agricultural practices with current challenges, such as climate change, global energy demand, food security, and land use (Weselek et al. 2021). The AGV technology exploits the advantage of the connections between crop cultivation and energy production to generate an array of social, economic, and ecological benefits. AGV supports sustainable development goals by enhancing soil health by lowering soil erosion and water evaporation, raising soil temperature, which is good for soil organisms and plant growth, and addressing land shortage issues (Roxani et al. 2023). AGVs can sustain natural habitats, including those used by bees, birds, and other creatures, potentially increasing biodiversity (Walston et al. 2022). AGV increases farmers' additional revenue by selling solar electrical energy, making farmers more economically stable (Lee et al. 2023). Installation of solar PV over agricultural fields works as a shield for the crop from harsh weather conditions like hailstorms, intense heat waves, or torrential rain (Wydra et al. 2023). In the fields of agriculture and solar energy, AGV projects can lead to new employment opportunities in installation, maintenance, crop management, and system monitoring (Gorjian et al. 2020). Using solar tracking in AGV can instance, optimize the sunlight for crops, and it can increase solar PV module efficiency through improved convective cooling from below microclimatic conditions. Using bifacial PV modules can use light from both sides to generate electricity due to the distances between the ground and the PV module. Despite a few key barriers to the adoption of AV technology, experts in the agriculture sector think that the installation of AGV appears to be able to benefit them personally (Abidin et al. 2021). By demonstrating the optimal synergy achieved through the application of AGV fields, we can ensure food security, mitigate the effects of climate change, and simultaneously

create a more sustainable, efficient, and aesthetically pleasing landscape. AGV demonstrated a payback period of five years or less, generating greater value compared to photovoltaic (PV) systems alone or traditional agricultural production (Geyer 2024).

## CONCLUSIONS

Our review delved into the current understanding of agricultural electricity and its potential for future expansion. Through a thorough examination of existing literature, we identified 77 relevant studies, primarily focusing on food production. A significant portion of this research explored the integration of electricity generation with farming practices. Vegetables, particularly lettuce and tomatoes, were frequently highlighted in these studies. In agro-galvanic systems, factors such as geographical location and seasonal variations play a pivotal role in determining crop success. The escalating global population and burgeoning industries are driving an ever-increasing demand for food, energy, and water. These growing demands present significant challenges, leading to the development of solutions that utilize carbon-free renewable energy and food production techniques relying on fresh soil and water resources. The AGV (Agro-galvanic) approach addresses these challenges by merging food production with the generation of carbon-free renewable energy. In AGV systems, crops such as cumin, mungbean, cluster bean, sankhpuspi, isabgol, aloe vera, sonamukhi, moth bean, and chickpea can thrive beneath solar panels and in the spaces between rows, effectively utilizing approximately 49% of the land area. Our review concluded that installing solar panels over agricultural land provides shade, which can influence crop growth parameters by mitigating excessive solar radiation and temperature, leading to alterations in the crop's microclimate. While this shade can reduce crop production (except for biomass), the resulting loss can be offset by using the generated electricity. Ultimately, optimizing the design of AGV systems, with a primary focus on agricultural objectives, can significantly enhance land use efficiency while simultaneously producing electricity.

## ACKNOWLEDGEMENTS

We acknowledge The Neotia University, Sarisha, for providing us with all the support to carry out this research.

## REFERENCES

- Abidin, M.A.Z., Mahyuddin, M.N. and Zainuri, M.A.A.M., 2021. Solar photovoltaic architecture and agronomic management in agrivoltaic system: A review. *Sustainability*, 13, p.7846. [DOI]
- Adeh, E.H., Stephen, P., Good, P.S., Calaf, M. and Higgins, W.C., 2019. Solar PV power potential is greatest over croplands. *Scientific Reports*, 9(1), p.11442. [DOI]

- Agostini, A., Colauzzi, M. and Amaducci, S., 2021. Innovative agrivoltaic systems to produce sustainable energy: An economic and environmental assessment. *Appl. Energy*, 281, pp. 116102.
- Alonso, J.P., Garcia, M.P., Pasamontes, M. and Ferre, A.J.C., 2012. Performance analysis and neural modeling of a greenhouse-integrated photovoltaic system. *Renewable and Sustainable Energy Reviews*, 16(7), pp.4675–4685.
- Amaducci, S., Yin, X. and Colauzzi, M., 2018. Agrivoltaic systems to optimize land use for electric energy production. *Applied Energy*, 200(1), pp.545–561. [DOI]
- Armstrong, A., Ostle, N.J. and Whitaker, J., 2016. Solar park microclimate and vegetation management effects on grassland carbon cycling. *Environmental Research Letters*, 11(7), pp.1–11. [DOI]
- Babatunde, O.M., Denwigwe, I.H., Adedaja, O.S., Babatunde, D.E. and Gbadamosi, S.L., 2019. Harnessing renewable energy for sustainable agricultural applications. *International Journal of Energy Economics and Policy*, 9, pp.308–315.
- Beck, M., Bopp, G., Goetzberger, A., Obergfell, T., Reise, C. and Schindel, S., 2013. Combining PV and food crops to agro photovoltaic – optimization of orientation and harvest. *27th European Photovoltaic Solar Energy Conference and Exhibition*, pp.4096–4100.
- Bulgari, R., Cola, G., Ferrante, A., Franzoni, G., Mariani, L. and Martinetti, L., 2015. The micrometeorological environment in traditional and photovoltaic greenhouses and effects on growth and quality of tomato (*Solanum lycopersicum* L.). *Italian Journal of Agrometeorology*, 20(2), pp.27–38.
- Chae, S.H., Kim, H.J., Moon, H.W., Kim, Y.H. and Ku, K.M., 2022. Agrivoltaic systems enhance farmers' profits through broccoli visual quality and electricity production without dramatic changes in yield, antioxidant capacity, and glucosinolates. *Agronomy*, 12(6), pp.1415–1430. [DOI]
- Cossu, M., Cossu, A., Deligios, P.A., Ledda, L., Li, Z., Fatnassi, H., Poncet, C. and Yano, A., 2018. Assessment and comparison of the solar radiation distribution inside the main commercial photovoltaic greenhouse types in Europe. *Renewable and Sustainable Energy Reviews*, 94, pp.822–834.
- Cossu, M., Murgia, L., Ledda, L., Deligios, P.A., Sirigu, A., Chessa, F. and Pazzona, A., 2014. Solar radiation distribution inside a greenhouse with south-oriented photovoltaic roofs and effects on crop productivity. *Applied Energy*, 133, pp.89–100.
- Czaloun, H.G., 2017. A Rope Rack for PV Modules. *PV Europe*. Retrieved from <https://www.pveurope.eu/solar-modules/rope-rack-pv-modules>.
- Dinesh, H. and Pearce, J.M., 2016. The potential of agrivoltaic systems. *Renewable and Sustainable Energy Reviews*, 54, pp.299–308.
- Dupraz, C., Marrou, H., Talbot, G., Dufour, L., Nogier, A. and Ferard, Y., 2011. Combining solar photovoltaic panels and food crops for optimizing land use: towards new agrivoltaic schemes. *Renewable Energy*, 36(10), pp.2725–2732. [DOI]
- Elamri, Y., Cheviron, B., Lopez, J.M., Dejean, C. and Belaud, G., 2018. Water budget and crop modeling for agrivoltaic systems: Application to irrigated lettuce. *Agricultural Water Management*, 208(1), pp.440–453. [DOI]
- Gafford, G.A.B., Zuckerman, P.A.M., Minor, R.L., Sutter, L.F., Moreno, I.B., Blackett, D.T., Thompson, M., Dimond, K., Gerlak, A.K., Nabhan, G.P. and Macknick, J.E., 2019. Agrivoltaics provide mutual benefits across the food–energy–water nexus in drylands. *Nature Sustainability*, 2(9), pp.848–855. [DOI]
- Geyer, B., 2024. Researchers find agrivoltaics have a payback time of less than five years in Portugal. *PV Magazine*. Accessed 8 July 2024. Available at: <https://www.pv-magazine.com/2024/02/09/researchers-find-agrivoltaics-have-payback-time-of-less-than-five-years-in-portugal/>.
- Goetzberger, A. and Zastrow, A., 1982. On the coexistence of solar-energy conversion and plant cultivation. *International Journal of Solar Energy*, 1(1), pp.55–69. [DOI]
- Gonocruz, R.A., Nakamura, R., Yoshino, K., Homma, M., Doi, T., Yoshida, Y. and Tani, A., 2021. Analysis of the rice yield under an agrivoltaic system: A case study in Japan. *Environments*, 8(7), p.65. [DOI]
- Gorjian, S., Ebadi, H. and Jathar, D.J., 2022. Solar energy for sustainable food and agriculture: developments, barriers, and policies. *Solar Energy Advancements in Agriculture and Food Production Systems*, 56, pp.1–28. [DOI]
- Gorjian, S., Minaei, S., Malehmircheghini, L., Trommsdorff, M. and Shamshiri, R.R., 2020. Applications of solar PV systems in agricultural automation and robotics. In S. Gorjian and A.B. Shukla (eds.), *Photovoltaic Solar Energy Conversion*, Academic Press, pp.191–235. [DOI]
- Harinarayana, T. and Vasavi, K. S. V., 2014. Solar energy generation using agriculture-cultivated lands. *Smart Grid and Renewable Energy*, 5(2), pp.31–42. [DOI]
- Hassanpour, A.E., Selker, J.S. and Higgins, C.W., 2018. Remarkable agrivoltaic influence on soil moisture, micrometeorology, and water-use efficiency. *PLoS ONE*, 13(11), e023256. [DOI]
- Hernandez, R.R., Armstrong, A., Burney, J., Ryan, G., Moore-O'Leary, K., Diédhiou, I., Grodsky, S.M., Saul-Gershenz, L., Davis, R. and Macknick, J., 2019. Techno–ecological synergies of solar energy for global sustainability. *Nature Sustainability*, 2, pp.560–568. [DOI]
- Hyvärinen, A., 2019. *Wind Turbines over a Hilly Terrain: Performance and Wake Evolution*. Ph.D. Thesis, KTH Royal Institute of Technology, Stockholm, Sweden.
- Ibrahim, S.M. and Kumari, R., 2020. Emerging solar energy technologies for sustainable farming: A review. *J. Xi'an Univ. Archit. Technol.*, 12, pp.5328–5336.
- Irie, N., Kawahara, N. and Esteves, A.M., 2019. Sector-wide social impact scoping of agrivoltaic systems: A case study in Japan. *Renewable Energy*, 139, pp.1463–1476.
- Jain, P., Raina, G., Sinha, S., Malik, P. and Mathur, S., 2021. Agrovoltatics: Step towards sustainable energy-food combination. *Bioresource Technology Reports*, 15(1), p.100766. [DOI]
- Jo, H., Asekova, S., Bayat, M.A., Ali, L., Song, J.T., Ha, Y.S., Hong, D.H. and Lee, J.D., 2022. Comparison of yield and yield components of several crops grown under agro-photovoltaic system in Korea. *Agriculture*, 12(5), p.619. [DOI]
- John, R.S. and Mahto, R.V., 2021. Agrovoltatics farming design and simulation. *IEEE 48th Photovoltaic Specialists Conference (PVSC)*, pp.2625–2629. [DOI]
- Juillion, P., Lopez, G., Fumey, D., Lesniak, V., Génard, M. and Vercambre, G., 2022. Shading apple trees with an agrivoltaic system: Impact on water relations, leaf morphophysiological characteristics, and yield determinants. *Scientia Horticulturae*, 306, p.111434. [DOI]
- Kadowaki, M., Yano, A., Ishizu, F., Tanaka, T. and Noda, S., 2012. Effects of greenhouse photovoltaic array shading on Welsh onion growth. *Biosystems Engineering*, 111, pp.290–297.
- Ketzer, D., Weinberger, N., Rösch, C., Stefanie, B. and Seitz, B.S., 2020. Land use conflicts between biomass and power production–citizens' participation in the technology development of agro photovoltaics. *Journal of Responsible Innovation*, 7(2), pp.193–216. [DOI]
- Kirk, S., 2021. This Colorado 'solar garden' is literally a farm under solar panels. *NPR*. Available at: <https://www.npr.org/2021/11/14/1054942590/solar-energy-colorado-garden-farm-land>.
- Kostik, N., Bobyl, A., Rud, V. and Salamov, I., 2020. The potential of agrivoltaic systems in the conditions of southern regions of the Russian Federation. *IOP Conference Series: Earth and Environmental Science*, 578, p.012047.
- Lee, S., Lee, J., Jeong, Y., Kim, D., Seo, B., Kim, B. and Cho, W., 2023. Agrivoltaic system designing for sustainability and smart farming: Agronomic aspects and design criteria with safety assessment. *Applied Energy*, 342, p.121130. [DOI]
- Liu, W., Omer, A.A.A. and Li, M., 2023. Agrivoltaic: Challenge and progress. *Agronomy*, 13, p.1934. [DOI]
- Lopez, G., Juillion, P., Hitte, V., Elamri, Y., Montrogon, Y., Chopard,

- J., Persello, S. and Fumey, D., 2024. Protecting flowers of fruit trees from frost with dynamic agrivoltaic systems. *Agrivoltaics Conference Proceedings*, 11, p.2. [DOI]
- Luo, J., Luo, Z., Li, W., Shi, W., and Sui, X. 2024. The early effects of an agrivoltaic system within different crop cultivation on soil quality in dry-hot valley eco-fragile areas. *Agronomy*, 14(3):584. [DOI]
- Marrou, H., Dufour, L., and Wery, J. 2013a. How does a shelter of solar panels influence water flows in a soil-crop system? *European Journal of Agronomy*, 50(4), pp.38-51. [DOI]
- Marrou, H., Wery, J., Dufour, L., and Dupraz, C. 2013b. Productivity and radiation use efficiency of lettuces grown in the partial shade of photovoltaic panels. *European Journal of Agronomy*, 44(1), pp.54-66. [DOI]
- Marrou, H., Guilioni, L., Dufour, L., Dupraz, C., and Wery, J. 2013c. Microclimate under agrivoltaic systems: is crop growth rate affected in the partial shade of solar panels? *Agricultural and Forest Meteorology*, 177(2), pp.117-132.
- Mekhilef, S., Faramarzi, S.Z., Saidur, R., and Salam, Z. 2013. The application of solar technologies for sustainable development of the agricultural sector. *Renewable and Sustainable Energy Reviews*, 18:583-594. [DOI]
- Miskin, C.K., Li, Y., Perna, A., Ellis, R.G., Grubbs, E.K., Bermel, P., and Agrawal, R. 2019. Sustainable co-production of food and solar power to relax land-use constraints. *Nature Sustainability*, 2, pp.972-980. [DOI]
- Moon, H.W., and Ku, K.M. 2022. Impact of an agriphotovoltaic system on metabolites and the sensorial quality of cabbage (*Brassica oleracea* var. *capitata*) and its high-temperature-extracted juice. *Foods*, 11(4), p.498.
- NAAS., 2018. Renewable Energy: A New Paradigm for Growth in Agriculture. Strategy Paper No. 10, *National Academy of Agricultural Sciences*, New Delhi, 20.
- Nagashima, A., 2014. Development and Prospect of Photovoltaic system Solar Sharing. *Journal of Japan Solar Energy Society*. 40, pp.1-15.
- Pandey, A.K., Tyagi, V.V., Selvaraj, J.A., Rahim, N.A., and Tyagi, S.K. 2016. Recent advances in solar photovoltaic systems for emerging trends and advanced applications. *Renewable and Sustainable Energy Reviews*, 53, pp.859-884. [DOI]
- Pascaris, A.S., Schelly, C., Burnham, L., and Pearce, J.M. 2021a. Integrating solar energy with agriculture: industry perspectives on the market, community, and socio-political dimensions of agrivoltaics. *Energy Research and Social Science*, 75(1), p.102023. [DOI]
- Pascaris, A.S., Schelly, C., Burnham, L., and Pearce, J.M. 2021b. Life cycle assessment of pasture-based agrivoltaic systems: emissions and energy use of integrated rabbit production. *Cleaner and Responsible Consumption*, 3, p.100030.
- Patel, U.R., Gadhiya, G.A., and Chauhan, P.M. 2023. Case study on power generation from agrivoltaic system in India. *International Journal of Environment and Climate Change*, 13(9), pp.1447-1454. [DOI]
- Proctor, K.W., Murthy, G.S., and Higgins, C.W. 2021. Agrivoltaics align with Green New Deal goals while supporting investment in the US rural economy. *Sustainability*, 13(1):137. [DOI]
- Pulipaka, S., Peparthy, M. and Vorast, M., 2021. Agrivoltaics in India overview of operational projects and relevant policies. *National Solar Energy Federation of India (NSEFI)*: New Delhi, India, pp.1-56.
- Roxani, A., Zisos, A., Sakki, G.K., and Efstratiadis, A. 2023. Multidimensional role of agrovoltas in the era of EU green deal: current status and analysis of water-energy-food-land dependencies. *Land*, 12, p.1069. [DOI]
- Sanchez, R.U., Ferre, A.J.C., Alonso, J.P., and Ortega, A.C. 2012. Greenhouse tomato production with electricity generation by roof-mounted flexible solar panels. *Scientia Agricola*, 69(4), pp.233-239. [DOI]
- Santos, D., 2020. Agrivoltaic system: A possible synergy between agriculture and solar energy (master thesis). KTH Royal Institute of Technology: Stockholm, Sweden.
- Santra, P., Pande, P.C., Kumar, S., Mishra, D., and Singh, R. 2017. Agrivoltaics or solar farming: the concept of integrating solar PV-based electricity generation and crop production in a single land-use system. *International Journal of Renewable Energy Research*, 7(2), pp.694-699. [DOI]
- Santra, P., Singh, R.K., Meena, H.M., Kumawat, R.N., Mishra, D., Jain, D. and Yadav, O.P., 2018. Agrivoltaic system: crop production and photovoltaic-based electricity generation from a single land unit. *Indian Farming*. 68(1), pp.20-23.
- Santra, P., Singh, R.K., Meena, H.M., Kumawat, R.N., Mishra, D., Machiwal, D., Dayal, D., Jain, D. and Yadav, O.P., 2020. Agri-voltaic system for crop production and electricity generation from a single land unit. In: *Advances in Energy Research*, 1, pp. 45-56. Springer Singapore.
- Saraswat, S.K., Digalwar, A.K., Yadav, S.S. and Kumar, G., 2021. MCDM and GIS based modelling technique for assessment of solar and wind farm locations in India. *Renewable Energy*, 169, pp.865-884.
- Schindele, S., Trommsdorff, M., Schlaak, A., Obergfell, T., Bopp, G., Reise, C., Braun, C.A., Weselek, A., Bauerle, A., Högy, P., Goetzberger, A., and Weber, E. 2020. Implementation of agrophotovoltaics: Techno-economic analysis of the price-performance ratio and its policy implications. *Applied Energy*, 265, p.114737. [DOI]
- Sekiyama, T., and Nagashima, A. 2019. Solar sharing for both food and clean energy production: Performance of agrivoltaic systems for corn, a typical shade-intolerant crop. *Environments*, 6(6), pp.1-12. [DOI]
- Steadman, L.C., and Higgins, W.C. 2022. Agrivoltaic systems have the potential to meet the energy demands of electric vehicles in rural Oregon, US. *Scientific Reports*, 12(1), p.4647. [DOI]
- Teng, J.W.C., Soh, C.B., Devihsur, S.C., Tay, R.H.S., and Jusuf, S.K. 2021. This Colorado 'solar garden' is literally a farm under solar panels. *Sustainability*, 14(1), p.7089. [DOI]
- Valle, B., Simonneau, T., Sourd, F., Pechier, P., Hamard, P., Frisson, T., Ryckewaert, M., and Christophe, A. 2017. Increasing the total productivity of land by combining mobile photovoltaic panels and food crops. *Applied Energy*, 206, pp.1495-1507. [DOI]
- Varga, K.B., Sirmik, I., and Stremke, S. 2024. Landscape user experiences of interspace and overhead agrivoltaics: A comparative analysis of two novel types of solar landscapes in the Netherlands. *Energy Research and Social Science*, 109, p.103408. [DOI]
- Walston, L.J., Barley, T., Bhandari, I., Campbell, B., McCall, J., Hartmann, H.M., and Dolezal, A.G. 2022. Opportunities for agrivoltaic systems to achieve synergistic food-energy-environmental needs and address sustainability goals. *Frontiers in Sustainable Food Systems*, 6, p.932018.
- Wen, L., Luqing, L., Chenggang, G., Fangxin, Z., Ming, L., and Hui, L. 2018. A novel agricultural photovoltaic system based on solar spectrum separation. *Solar Energy*, 162, pp.84-94. [DOI]
- Weselek, A., Bauerle, A., Hartung, J., Zikeli, S., Lewandowski, I., and Högy, P. 2021. Agrivoltaic system impacts on microclimate and yield of different crops within an organic crop rotation in a temperate climate. *Agronomy for Sustainable Development*, 41(59), pp.1-15. [DOI]
- Winkler, B., Lewandowski, I., Voss, A., and Lemke, S. 2018. Transition towards renewable energy production: Potential in smallholder agricultural systems in West Bengal, India. *Sustainability*, 10, p.801.
- World Bank, 2019. *Doing Business 2019: Getting Electricity*. The World Bank.
- Wydra, K., Vollmer, V., Busch, C., and Prichta, S. 2023. Agrivoltaic: Solar radiation for clean energy and sustainable agriculture with a positive impact on nature. *IntechOpen*, 1, pp.1-48.
- Yano, A., Onoe, M., and Nakata, J. 2014. Prototype semi-transparent photovoltaic modules for greenhouse roof applications. *Biosystems Engineering*, 122, pp.62-73.
- Yeongseo, Y., and Yekang, K.A. 2020. Review of the attributes of successful agriphotovoltaic projects. *The University of Auckland, Auckland, New Zealand*.



# The Study of Coastal Vulnerability in South Central Timor Regency, East Nusa Tenggara Province

Ludgardis Ledheng<sup>1†</sup>, Emanuel Maria Yosef Hano'e<sup>1</sup> and Marce Sherly Kase<sup>2</sup>

<sup>1</sup>Biology Education Study Program, The Faculty of Teacher Training and Educational Sciences, University of Timor, Kefamenanu, Indonesia

<sup>2</sup>Development Economics Study Program, The Faculty of Economics and Business, University of Timor, Kefamenanu, Indonesia

†Corresponding author: Ludgardis Ledheng; ludgardisledheng12@gmail.com

**Abbreviation:** Nat. Env. & Poll. Technol.  
**Website:** www.neptjournal.com

*Received:* 09-09-2024  
*Revised:* 07-10-2024  
*Accepted:* 12-11-2024

## Key Words:

Coastal vulnerability  
 Multi criteria analysis  
 Coastal vulnerability index  
 Social vulnerability index  
 Sea level rise

## Citation for the Paper:

Ledheng, L., Hano'e, E.M.Y. and Kase, M.S., 2025. The study of coastal vulnerability in South Central Timor Regency, East Nusa Tenggara Province. *Nature Environment and Pollution Technology*, 24(2), p. D1719. <https://doi.org/10.46488/NEPT.2025.v24i02.D1719>

*Note: From year 2025, the journal uses Article ID instead of page numbers in citation of the published articles.*



**Copyright:** © 2025 by the authors  
**Licensee:** Technoscience Publications  
 This article is an open access article distributed under the terms and conditions of the Creative Commons Attribution (CC BY) license (<https://creativecommons.org/licenses/by/4.0/>).

## ABSTRACT

The presence of anthropogenic activities in the coastal areas of the South Central Timor (SCT) Regency has weakened coastal resilience, which may exacerbate the impact of rising sea levels. One important factor that needs to be analyzed is the vulnerability assessment. This study, conducted from July to September 2024, aimed to determine the spatial distribution and variables that can influence the vulnerability in the coastal areas. The methods used were the Coastal Vulnerability Index (CVI) and the Social Vulnerability Index (SoVI), which then used Multi Criteria Analysis (MCA) to perform the standardization value. The integrated index values were then integrated into the Geographic Information System (GIS) for comprehensive spatial information. The results showed that, in general, the coastal areas of the SCT Regency were in the low (35%), medium (48%), and high (66%) risk categories. Areas of high physical vulnerability were alluvial lowland areas and those near hills. The karst hills that are characteristic of the coastal areas of the SCT regency have become a threat to the lives of coastal communities. Communities living in coastal hill areas, including the Kolbano and Oetuke coasts, and in the alluvial lowlands like the Tuafanu, Kualin, and Oni coasts, need to be the focus and priority areas for recovery efforts. This is due to the high level of vulnerability, both physically and socio-economically. Geomorphology is the primary contributor to physical vulnerability because these coastal hills and lowlands are prone to erosion and land degradation caused by waves, tides, and human activities. On the socio-economic side, land use, particularly mining activities, increases vulnerability by degrading the environment and threatening the livelihood of coastal communities. Key recovery efforts should focus on revegetation, which can help stabilize the soil, reduce erosion, and restore ecological balance while offering sustainable economic benefits to the local population.

## INTRODUCTION

Coastal areas are dynamic and, therefore, have the potential to be easily damaged (Ward et al. 2011). The stone mining activities along the coastal areas of the SCT Regency, East Nusa Tenggara Province (ENT), have brought negative effects on environmental damages, especially in karst and marine landscapes (Maulana et al. 2017), both of which dominate the region. Karst land is spread across land areas with gentle to hilly topography, with bushes and rocks generally dominating the land cover. Meanwhile, residences are typically found around hill valleys or in areas with gentler topography. Marine landforms stretch along the coastline with flat to gentle topography, predominantly covered by sand and rocks (Maulana et al. 2017). In general, the land cover in the coastal areas of the SCT Regency is characterized by stretches of sand, gravel, and rocks found along the coast towards the land. Such conditions have influenced the coastal communities to work as sand and stone miners. However, this dependence has resulted in excavation pits



that lead to erosion. According to Fadilah (2021), coastal erosion can be affected by altering hydro-oceanographic conditions, especially the direction of the current, resulting in tidal flooding.

In addition, climate change that affects high waves and strong winds during the rainy season has also caused the coastal areas of the SCT Regency to be frequently hit by disasters. Meteorology, Climatology and Geophysics Agency (MCGA) reported the formation of tropical cyclone Frances in the Gulf of Papua, which has continued to develop (Gaol et al. 2018). The cyclonic activity occurring across the Timor Sea and the coast of the SCT Regency is one of the regions influenced by cyclone Frances (Gaol et al. 2018).

The Timor Sea is located in the collision zone between the northwestern edge of the Australian continent, which is moving north, and the Indo-Australian ocean plate (Bachri 2011). This movement has caused the southern coast of Timor Island to be frequently hit by very strong tectonic earthquakes (Gaol et al. 2018). The most recent disaster occurred in 2021, namely the Seroja cyclone, which damaged many residential areas. The ENT Provincial Disaster Management Agency reported that the southern coast of Timor Island was affected by the two cyclones, impacting 25 coastal villages in the SCT Regency. The risk of sea level rise can be influenced directly by the local topography, which

is dominated by gentle to flat alluvial plains (Maulana et al. 2017). Given the existence of anthropogenic activities that can also threaten the coastal supporting capacity, it is necessary to manage and preserve the activities in utilizing the coastal area, as regulated by Law Number 27, Article 28 of 2007 (Government of the Republic of Indonesia 2007). Therefore, one form of coastal management plan is through research, including the assessment of the physical and economic vulnerability in the community residing in this type of region (Maulana et al. 2017).

This study was aimed at examining the spatial distribution and factors influencing the vulnerability of the coastal areas of the SCT Regency, especially regarding sea level rise. Ramieri et al. (2011) presented a method to determine the level of physical vulnerability to the threat of elevated sea levels, namely the Coastal Vulnerability Index (CVI). This technique has been used in assessing sea level rise in various countries, including Spain (Koroglu et al. 2019) and for vulnerability assessment in Indonesia (Diposaptono et al. 2013). Meanwhile, the assessment of socio-economic vulnerability has been done using the Social Vulnerability Index (SoVI) (Kurniawan et al. 2018). According to Sulma (2012), the magnitude of the contribution of physical and socio-economic variables to vulnerability can be known based on the standardized variables. Therefore, the

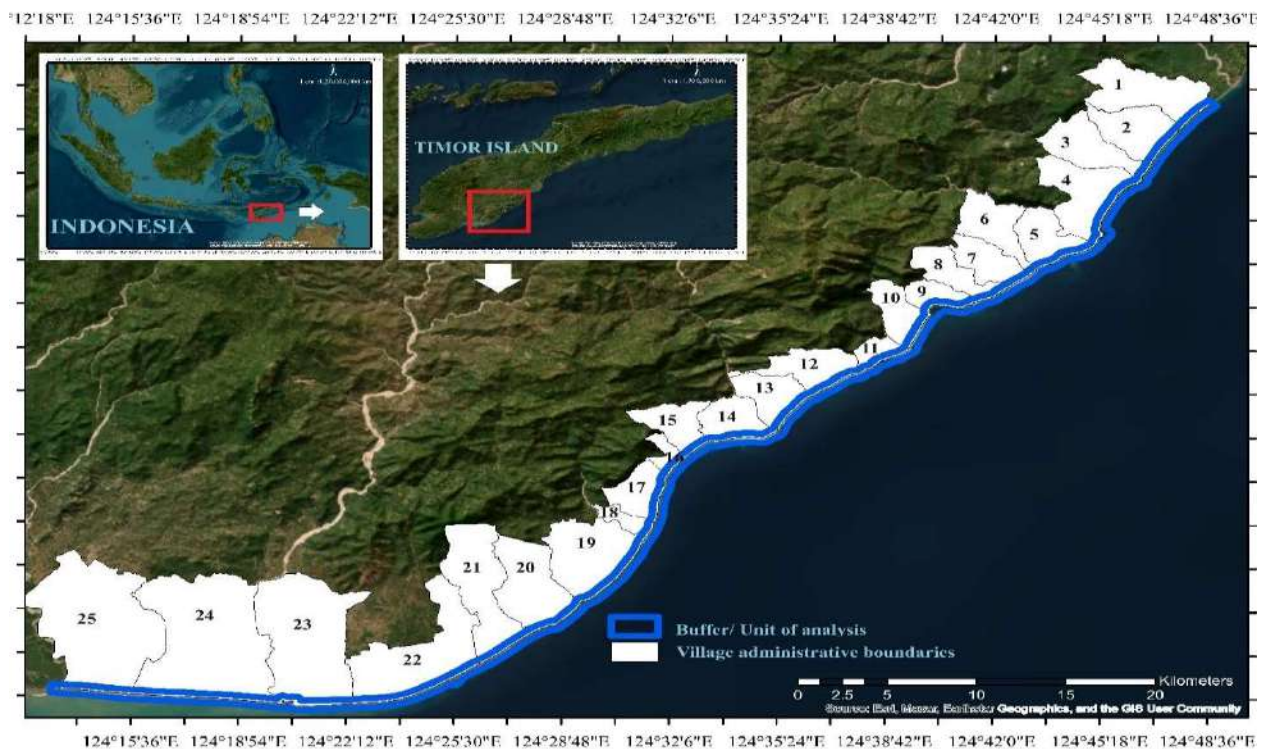


Fig. 1: The research site.

assessment of coastal vulnerability focused heavily on Multi Criteria Analysis (MCA), which used the ranking system obtained from each standardized variable. The resulting combined vulnerability index value was then entered into the Geographic Information System (GIS) to obtain comprehensive spatial information.

## MATERIALS AND METHODS

### Research Site

This study took place in the southern coastal areas of the SCT Regency, including 25 villages: Baus, Fatumanufui, Meusin, Boking, Nunkolo, Hoineno, Nenoat, Sahan, Saenam, Op, Nualunat, Kot'olin, Hoibeti, Oetuke, Nununamat, Spaha, Kolbano, Noesiu, Tuapakas, Oni, Kualin, Tuafanu, Toineke, Oebelo, and Bena. The selection of the research

area was based on the consideration that these 25 coastal villages have potential vulnerability to sea level rise. These specific locations were determined by creating a buffer parallel to the coastline with a distance of 1 km towards the sea and towards the land, while the perpendicular boundary of the coast used the village administrative boundaries. The consideration of using this size was based on the assumption that each unit could represent the varied variables within the study location of  $\pm 87.5$  km, as well as ease of identification within the administrative area. The study area started from the easternmost village, namely Baus, to the westernmost village, Bena, according to the numbering (Fig. 1).

### Data Collection

This study used 9 variables derived from 6 physical variables: geomorphology, elevation, tidal range, coastline change

Table 1: Data source.

A. Physical Variables		
Type of Data	Data Source	Vulnerability Indicators
Geomorphology (landforms)	Obtained from the Digital Elevation Model (DEM) sourced from the Geospatial Information Agency in the form of a digital map of the Indonesian Landforms on a scale of 1:25,000 <a href="https://tanahair.indonesia.go.id/unduh-rbi/#/">https://tanahair.indonesia.go.id/unduh-rbi/#/</a>	Geomorphology can indicate the resilience of a coastal section to erosion and accretion processes caused by rising sea levels.
Beach Elevation	Obtained from the Digital Elevation Model (DEM) sourced from the Geospatial Information Agency in the form of a digital map of the Indonesian Landforms on a scale of 1:25,000 <a href="https://tanahair.indonesia.go.id/unduh-rbi/#/">https://tanahair.indonesia.go.id/unduh-rbi/#/</a>	The existence of low-lying areas is associated with the vulnerability of a coast to the risks of inundation, as well as the rate of retreat or advance of the coastline. The existence of low-lying areas is associated with the vulnerability of a coast to the risks of inundation, as well as the rate of retreat or advance of the shoreline.
Ebb and Flow	Obtained from MIKE 21 Prediction in July 2000 and field measurements in July 2024 at 2 locations, namely Toineke village and Nunkolo.	Differences in tidal range contribute to the risk of coastal inundation, with macro tidal areas (characterized by large tidal ranges) being more vulnerable than microtidal areas.
Coastline Change Rate	Obtained from Landsat 7 ETM imagery recorded on September 26, 2000 (USGS Glovis, Path 110 and Row 67) and July 2024 coastline coordinate point data taken using GPS RTK. Line analysis using a Digital Shoreline Analysis System (DSAS).	Coastal erosion or accretion indicates the rate at which a section of the coastline is being eroded or accreted.
Sea Level Rise	Obtained from AVISO in the form of sshd data from multi-mission altimetry satellite observations, namely the TOPEX/Poseidon, Jason-1, Jason-2, and Jason-3 satellites during the period 1992 to 2019. This data has a NetCDF (.nc) format in grid form with a spatial resolution of $0.25^\circ \times 0.25^\circ$ .	The higher the rate of sea level rise, the greater the risk of erosion and inundation.
Wave Height	Retrieved from the Copernicus Marine Service database ( <a href="https://data.marine.copernicus.eu/products">https://data.marine.copernicus.eu/products</a> )	The higher the wave height, the greater the impact on changes in the coastline and the geomorphological conditions of the area
B. Socio-economic Variables		
Land Use	Obtained from the 2024 Digital Elevation Model (DEM) sourced from the Geospatial Information Agency in the form of a digital map of the Indonesian Landforms on a scale of 1:25,000. <a href="https://tanahair.indonesia.go.id/unduh-rbi/#/">https://tanahair.indonesia.go.id/unduh-rbi/#/</a>	Land use that has high social and economic value will increase the vulnerability of an area in the event of a disaster.
Population Density	Population statistics calculation from a field survey in July 2024	The population density in a given area indicates that as the population becomes denser, the vulnerability of that area to disasters increases.
Poverty Rate	Statistical calculation of the number of under-privileged population from the field survey in July 2024.	A higher poverty rate in an area will further increase its vulnerability to disasters.

Table 2: The CVI variable categories.

No.	Variable	Not Vulnerable (1)	Less Vulnerable (2)	Medium (3)	Vulnerable (4)	Very Vulnerable (5)
1.	Geomorphology	High Cliff	Moderate cliffs, indented coast	Low cliff	Estuary, lagoon	Alluvial plains sandy, gravelly, muddy, deltaic coasts
2.	Elevation [m]	>30	20.1-30.0	10.1-20.0	5.1-10.1	0.0-5.0
3.	Tidal Range [m]	< 1.0	1.0 - 2.0	2.0 - 4.0	4.0 - 6.0	> 6.0
4.	Coastline Change Rate [m.year <sup>-1</sup> ]	> 2.0 Accretion	1.0 - 2.0 Accretion	+1 - (-1) Stable	≤ (-1) - (-2) Abrasion	< (-2.0) Abrasion
5.	Sea Level Rise [cm. year <sup>-1</sup> ]	< 1.8	1.8 - 2.5	2.5 - 3.0	3.0 - 3.4	> 3.4
6.	Wave Height [m]	< 0.55	0.55 – 0.85	0.85 – 1.05	1.05 – 1.25	> 1.25

Source: Pendleton et al. (2010)

rate, wave height, and sea level rise, and 3 socio-economic variables: land use, population density, and poverty rate. A higher poverty rate in an area corresponds to greater vulnerability to disasters. The research database consisted of various feature sets (point, line, polygon) and was registered with Datum WGS 1984 with Universal Transverse Mercator (UTM) projection system Zone 51 S. The technique of data collection of both spatial tabulation data is further explained in Table 1 below.

Multi-criteria analysis (MCA) was used to analyze vulnerability in the physical and socio-economic aspects. This approach aimed to standardize the ranks of variables by using the CVI and SoVI methods. Next, the Kasim (2011) equation was used to determine the standard value for each variable in the analysis unit as follows:

$$X_{in} = \frac{(x_{in} - \min xi)}{(\max xi - \min xi)} \quad \dots(1)$$

where:

$X_{in}$  = the standard value of the  $i$ -th variable on the  $n$ -th grid,

$x_{in}$  = the original value of the  $i$ -th variable on the  $n$ -th grid

$\max xi$  = the highest value of the variable

$\min xi$  = the lowest value of a variable

The value of the standardized variable results was used for the calculation of CVI-MCA and SoVI-MCA, which were then categorized into five groups based on percentile distances: very low (<0.2), low (0.2-0.4), medium (0.4-0.6), high (0.6-0.8), and very high (>0.8). Using this categorization, the calculation of the physical vulnerability index value referred to the CVI equation of Pendleton et al. (2010):

$$CVI = \frac{\sqrt{a*b*c*d*e*f}}{n} \quad \dots(2)$$

where:

a = coastal geomorphology

b = elevation

c = tidal range

d = coastline change rate

e = sea level rise

f = wave height

n = total

Meanwhile, the SoVI equation with weighting given to each variable followed the Kurniawan et al. (2018) equation:

$$SoVI = \frac{\sum (\text{weighted variable} * \text{rank})}{3} \quad \dots(3)$$

The population density was calculated by dividing the number of residents within each analysis unit by the area of that unit, expressed in persons per square kilometer (person/km<sup>2</sup>). The land use values were then transformed into scores according to the classifications provided in Table 4:

Table 3: Weights for SoVI variables.

Variable	Weight
Land Use	0.5
Population Density	0.25
Poverty Rate	0.125

Source: Sulma (2012)

Table 4: Vulnerability levels based on land use.

Class	Score
Body of water	1
Empty land, bushes	2
Mixed garden, Mangrove forest	3
Moorlands, Plantations, Rice Fields, Ponds	4
Residential, Road, Industry, Office	5

Source: Sulma (2012)

Based on the relationship between the index values in equation (2), the standardization of these values with the CVI-MCA approach then used the normalization approach introduced by Kasim (2011). The formula is as follows:

$$NS = \frac{(nub - nlb)}{(oub - olb)} * ((OS - olb) + nlb) \quad \dots(4)$$

Where:

NS = new index value

OS = original index value

nub = the highest limit of the new index value

nlb = the lowest limit of the new index value

oub = the highest limit of the original index value

olb = the lowest limit of the original index value

The physical vulnerability index categories based on percentile distance are defined by the following relationship:

$$0 \leq \min \leq \text{indeks CVI MCA} \leq \max \leq 1 \quad \dots(5)$$

Similarly, the socio-economic vulnerability index follows the following relationship:

$$0 \leq \min \leq \text{indeks SoVI MCA} \leq \max \leq 1 \quad \dots(6)$$

The coastal vulnerability index, which incorporates both physical and socio-economic conditions as defined by Szlafsztein (2005), is expressed as the Total Vulnerability Index (TVI). This was calculated using the same method, namely the average of the physical vulnerability index and socio-economic vulnerability index, weighted equally, as per the Sulma (2012) equation:

$$TVI = \frac{(CVI \text{ MCA} + SoVI \text{ MCA})}{2} \quad \dots(7)$$

## RESULTS AND DISCUSSION

### Physical Variables

**Elevation:** The observation results showed that elevations

in the range of 0.71-4.43 m were found on the coasts of Bena, Oebelo, Toineke, Tuafanu, Kualin, Kolbano, Meusin, Fatumanufui and Baus. In contrast, elevations in the range of  $\geq 8$  to 33.24 m were found in the coasts of Hoineno, Boking, Nunkolo, Nenoat, Op, Oetuke, Sahan, Hoibeti, Spaha, Nualunat, Nununamat, Kot'olin, and Saenam. Based on these elevation values, it is known that 9 coastal villages (Bena, Oebelo, Toineke, Tuafanu, Kualin, Kolbano, Meusin, Fatumanufui, and Baus) are highly vulnerable to tidal flooding because they are situated in the range below 5 m (Table 2). According to Sulma (2012), when a tidal wave occurs, a beach with a low elevation will allow water to enter further inland, increasing the overflow. Conversely, higher elevations prevent water from moving inland. The elevation values act as indicators of potential threats from coastline advancement and retreat (Hamuna et al. 2018). The distribution of elevation values on the coastal areas of the SCT Regency is presented in Fig. 2.

According to Kalay et al. (2018), the dynamics of sediment transport in the formation of coastal alluvial areas impact changes in coastal slope. A decrease in the slope percentage indicates a corresponding decrease in elevation over a distance of 100 m, disrupting the coastal balance process. The range of elevation values on the coastal areas of the SCT Regency is presented in Fig. 3.

**Geomorphology:** Landform classification refers to the resistance of landform types to erosion according to the CVI model (Table 2), including hilly coasts, estuaries, lagoons, alluvial plains, sandy beaches, muddy beaches, and deltas. In general, the coastal areas of the SCT Regency have two landforms, namely hills and marine. The hill categories are classified as low, medium, and high, dominating the coasts of Kot'olin and Nunkolo and parts of the coast of Kolbano District (Fig. 4), with elevation values ranging from 11.3-33.2 m (Fig. 2). According to Maulana et al. (2017), the hills found on the coastal areas of the SCT Regency are karst hills,

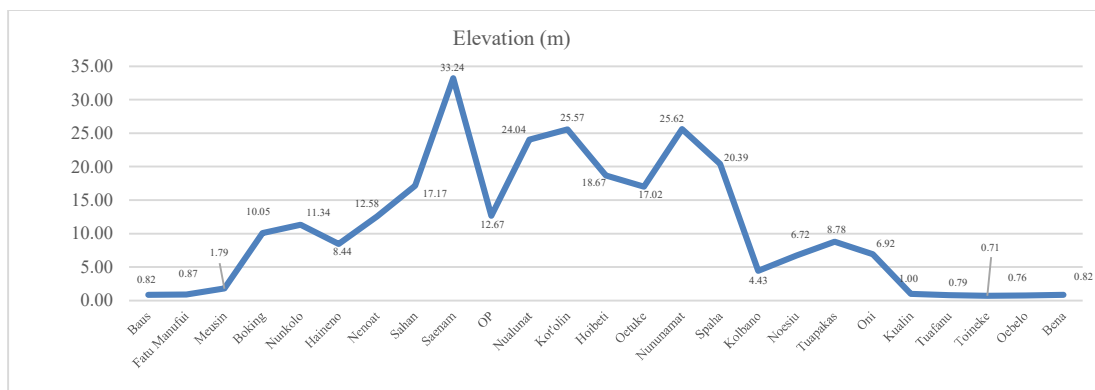


Fig. 2: The distribution of coastal elevation values in the SCT Regency.



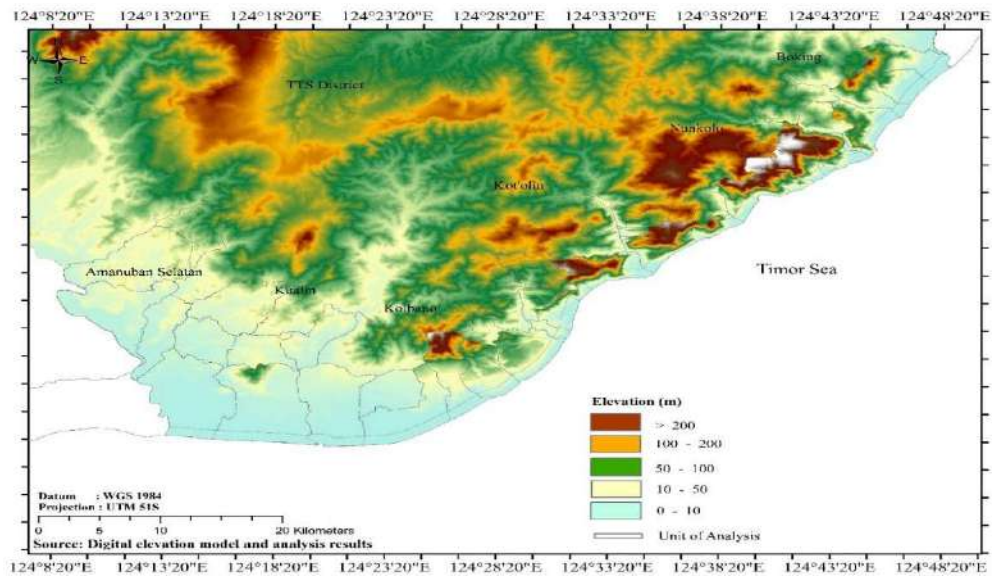


Fig. 3: Range of coastal elevation values in the SCT Regency.

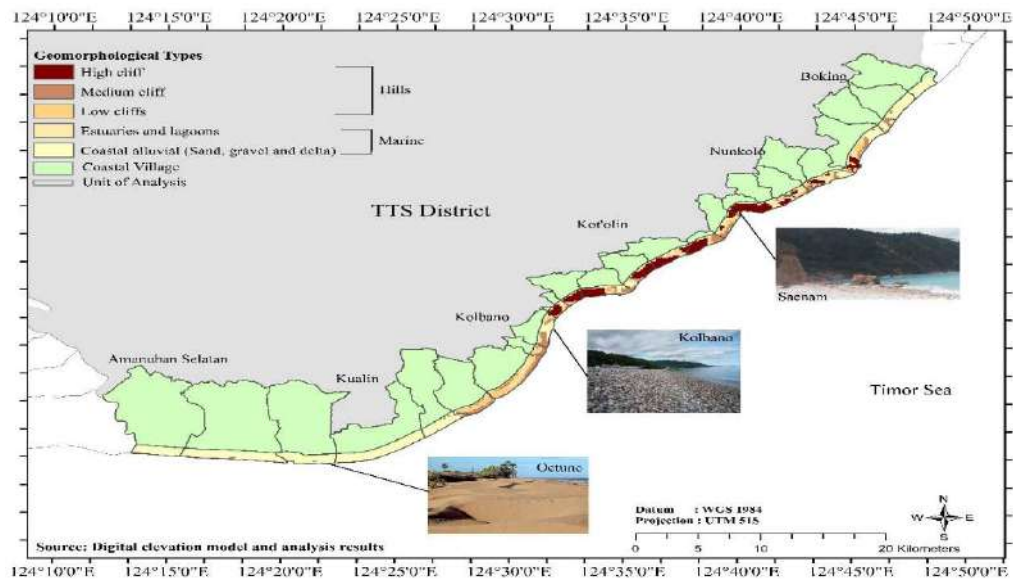


Fig. 4: The distribution of landforms in the coastal analysis unit of the SCT Regency.

and their distribution reaches the boundary of the marine area on a flat slope.

Marine landforms dominate the western coast, namely Amanuban Selatan District, Kualin, some coastal villages in Kolbano District, and some coastal areas of Boking District (Fig. 4). The coastal landscape consists of alluvial coastal plains with elevation values ranging from 0.8-1 m (Fig. 2). According to Maulana et al. (2017), sand and stone mining activities were found in the hilly and marine areas on the Kolbano coast to the east of Saenam. Our observations

revealed that the sand and stone mining activities on the southern coast significantly contribute to the landslides in the karst hills that border the beach. Meanwhile, the western coast, namely South Amanuban district and Kualin, is dominated by sand. The impact of sand shipments through rivers and wave currents has caused sand deposits in several areas, such as Oetune Beach (Fig. 4).

It is known that the materials on the coastal alluvial plains of the SCT Regency consist of marine sedimentary rocks, such as limestone, obtained from the sea through

waves, and fluvial sedimentary rocks, such as sandstone and claystone, acquired from the sedimentation process (Bachri 2011). Based on the vulnerability category (Table 2), alluvial plains are classified as very vulnerable areas. According to Sulma (2012), coastal alluvial plains are landforms resulting from coastal development. Towards the land, covered by weathering and sedimentation materials that have great erosion potential. The increasing mining activities in coastal areas indicate that the coastal resilience to hydro-oceanographic factor threats is very weak. Based on the results of the CVI analysis, the coasts of Bena, Oebelo, Toineke, Tuafanu, Kualin, Oni, Tuapakas, Noesiu, Kolbano, Spaha, Oetuke, Op, Nenoat, Hoineno, Nunkolo, Boking, Meusin, Fatumanufui, and Baus Villages are in the

vulnerable to very vulnerable categories concerning sea level rise. Meanwhile, the coasts of Saenam and Kot'olin Villages are classified as moderate (Fig. 5).

**Tidal range:** The tidal data used in this study were the results of MIKE 21 modeling. Based on the Formzahl value, it can be found that the tidal pattern in this study area exhibited a mixed double daily trend, where the ebb and flow occurred twice each day, though it sometimes happened once a day. A one-day observation was conducted to determine the tidal type, with July 20, 2024, selected as the time sample. The Formzahl value in Toineke waters was 0.40, and Nunkolo waters was 0.43. The daily tidal pattern on July 20, 2024, on the coastal areas of the SCT Regency is presented in Fig. 6.

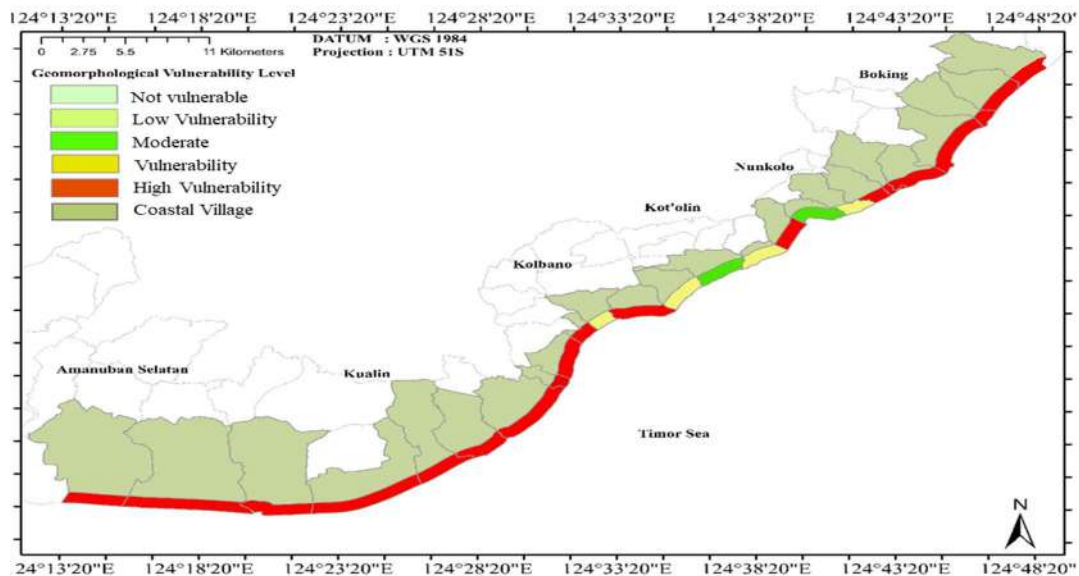
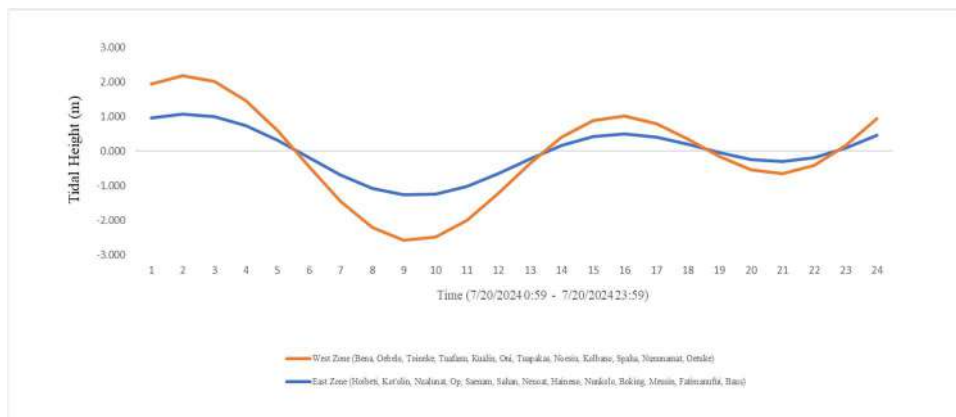


Fig. 5: Level of vulnerability based on geomorphological variables.



Source: MIKE 21 modeling data and analysis results

Fig. 6: Daily tidal pattern on July 20, 2024, on the coastal areas of the SCT Regency.

Table 5: Average Sea Tide Position.

Year	West Zone	East Zone
2019	1.55	1.48
2021	1.55	1.48
2024	1.55	1.48
Average	1.55	1.48

Source: Results of MIKE 21 Modeling Analysis from 2000 to 2024

Based on the difference in Formzahl values, the tidal observation area was divided into two parts: the western zone and the eastern zone (Fig. 7). Data obtained from the tidal analysis included the highest average high tide, the lowest average low tide, and the tidal rise. To examine the coastal vulnerability index, the required value was the average tidal

rise in the study site for the period from July 2000 to July 2024 in both zones. The western and the eastern zones. The calculation results showed that the average rise in the western zone was 1.55 m, while that in the eastern zone was 1.48 m. The contribution of the tidal position was greater in affecting the western coast than the eastern part. The dynamics of the tides have caused the western coast, especially on the Tuafanu coast, to develop puddles that form parallel to the coastline (Fig. 7). According to Pamungkas (2018), high tidal rises can cause permanent puddles. The average seawater tidal positions are presented in Table 5.

**Coastline change rate:** Based on the DSAS analysis on 8633 transects with a distance of 10 m, it was found that the shift of the coastline toward the land was almost evenly

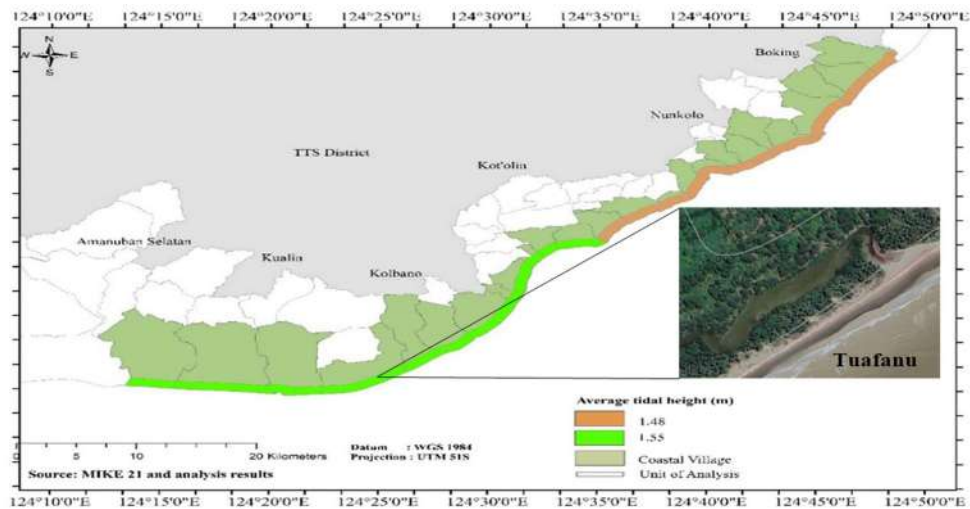


Fig. 7: Tidal ranges in the western and eastern zones on the coastal areas of the SCT Regency.

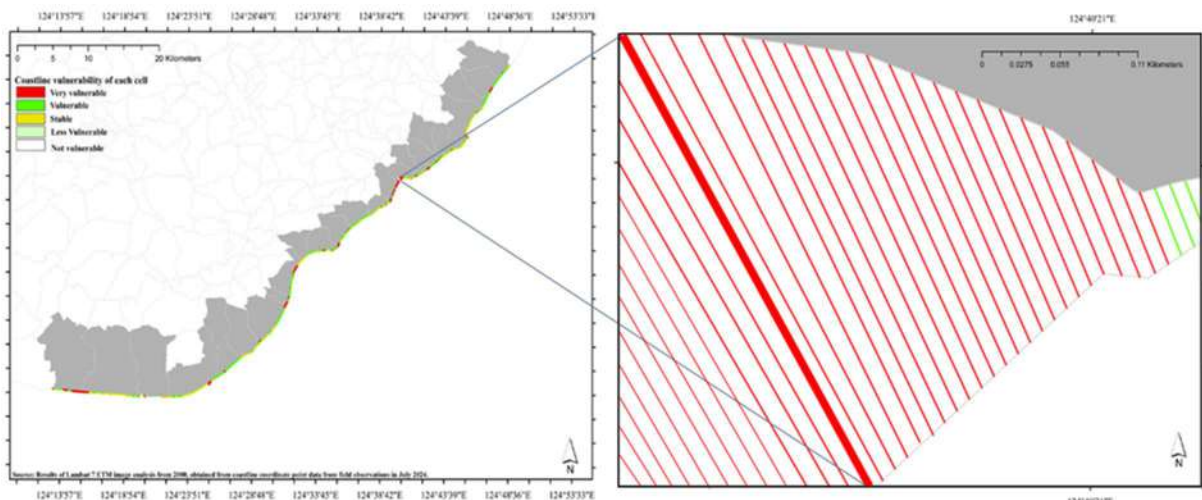


Fig. 8: Maximum shoreline displacement on the Saenam coast.

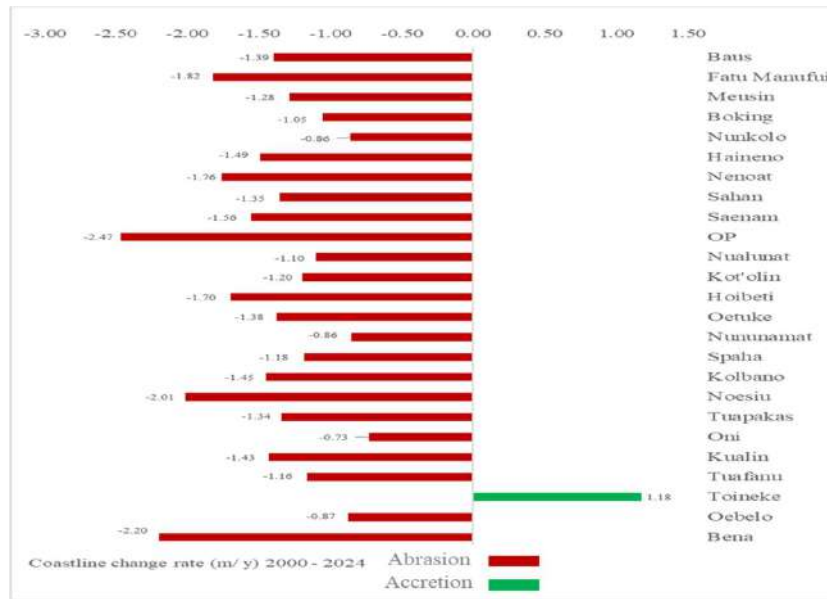


Fig. 9: Coastline changes rate in each analysis unit over 24 years.

distributed along the alluvial plain coast and the karst hill area (Fig. 8). The coastline that experienced the furthest shift inland was found in the Saenam coastal karst hill area, measuring 288.7 m (Fig. 8).

The results of the interviews with residents living around the hilly area revealed that rock and sand mining activities have made the hills fragile and prone to landslides. In general, landslides in karst hills are caused by mining activities or extreme weather, especially on moderate or steep slopes where rock movement is common (Rahmania et al. (2019).

Coastal erosion can also occur in areas with low elevation values, such as Bena, Oebelo, Tuafanu, Kualin, Fatumanufui, and Baus (Fig. 9), particularly those on sandy alluvial plains (Fig. 4). The sandy nature of these beaches makes them highly vulnerable to erosion (Suhana et al. 2020) from waves, tides, and wind, with wind-driven erosion forming dunes along the Oetune coastline.

Based on the average change in the coastline in each analysis unit for 24 years (2000-2024), land accretion occurred on the Toineke coast at a rate of 1.18 m/year.

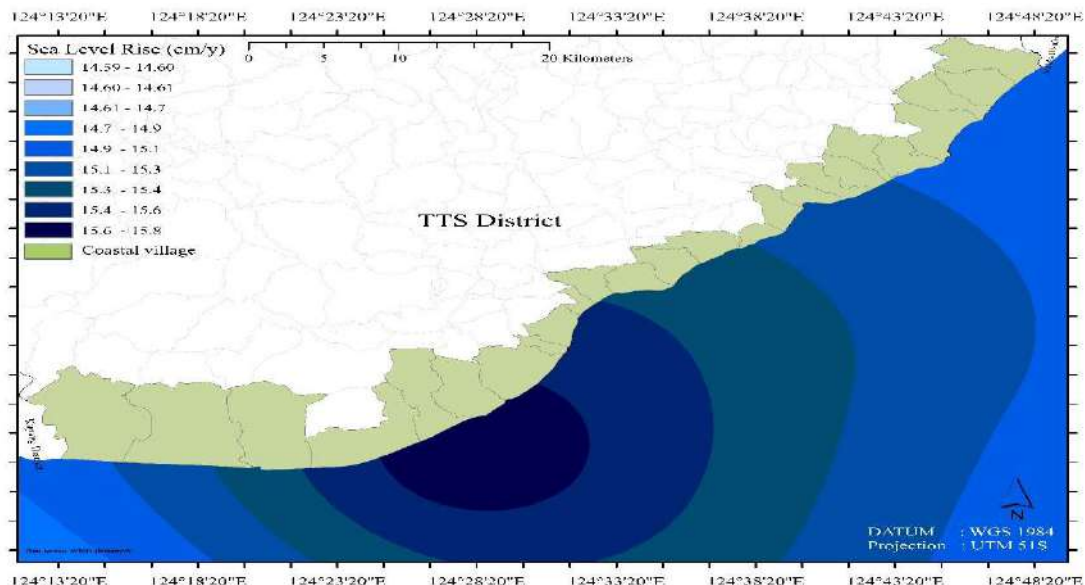


Fig. 10: Sea level rise in the SCT Regency and its surrounding waters.



Meanwhile, other areas experienced land loss at a rate ranging from 0.73 to 2.47 m.year<sup>-1</sup> (Fig. 9). The rate of land reduction in this study area on the south coast was lower compared to the north coast of North Central Timor regency (NCT), which had a rate of 26.60 m.year<sup>-1</sup> (Ledheng & Hano'e 2023). This difference is due to variations in coastal slope gradients, with nearly 90% of the northern coast classified as flat, whereas only certain sections of the southern coast are flat. The flatter northern coast facilitates greater inland movement of seawater, contributing to the accelerated rate of land loss in that area.

Based on the CVI category (Table 2), areas experiencing line retreat, such as the Nunkolo, Nununamat, Oni, and Oebelo coasts, were still in a stable condition, namely in the range of 0.73 to 0.86. Meanwhile, the coasts of Bena, Tuafanu, Kualin, Kolbano, Meusin, Fatumanufui, Baus, Hoineno, Boking, Nunkolo, Nenoat, Op, Oetuke, Sahan, Hoibeti, Spaha, Nualunat, Nununamat, Kot'olin and Saenam

faced higher rates of abrasion (1.05 to 2.47 m.year<sup>-1</sup>), as shown in Fig. 9. Abrasion in these areas is a result of the dynamic interaction of multiple physical factors such as geomorphology, elevation, tides, waves, and sea level rise. These factors collectively shape the coastal vulnerability and contribute to the erosion observed.

**Sea level rise:** The data on sea level rise was obtained based on data analysis sourced from multi-mission altimetry satellites, namely TOPEX/Poseidon, Jason-1, Jason-2, and Jason-3, from 1992 to 2019. Fig. 10 shows the trend of yearly sea level rise in the waters of the SCT Regency, which generally ranged from 14 to 15 cm.year<sup>-1</sup>.

The highest sea level rise occurred in the waters stretching from Toineke to the east of Oni, while the lowest was recorded in the waters of Nunkolo District to the easternmost, namely the Baus coast. The average sea level rise for each analysis unit based on the zonal statistical tool is presented in Table 6.

The values of sea level rise observed in the waters of the SCT Regency were still within the range of global observations by the National Oceanic and Atmospheric Administration (NOAA), which reported sea level increases within a 0-20 cm range (Lindsey 2019). According to Karsidi (2011), the results of altimetry satellite monitoring published by AVISO France showed consistency with the data on sea level rise acquired from observations of the National Tidal Station Network operated by Bakosurtanal. The differences that can occur may be due to differences in calculation methods and observation periods (Sulma 2012). Additionally, in this study, sea level rise observations did not include data on the impact on coastal groundwater quality, a factor that can influence community drinking water consumption levels. This absence of spatial data on groundwater consumption at the time of the study prevents a full analysis of this aspect.

**Wave height:** According to the data of average monthly significant wave height from the Copernicus Marine Service from 2000 to 2024 in April (Fig. 11), it was observed that the wave heights in the western waters of Timor were generally higher than in the eastern waters. Fig. 9 shows the dynamics of the maximum wave heights during the west season in April for the years 2000, 2017, 2021, and 2024. The average wave height in 2000 ranged from 0.2 to 1.4 m (Fig. 11). Furthermore, during the period from 2017 to 2021, the southern coastal areas of Timor experienced significant natural events, such as Hurricane Frances in 2017 and Hurricane Seroja in 2021, which caused maximum wave heights to reach up to 3 m (Fig. 11).

Gaol et al. (2018) confirmed that the maximum wave direction during the Frances Hurricane in the Timor Sea

Table 6: Average Sea Level Rise for each analysis unit.

Coastal Village	Sea Level [cm]
Baus	14.99
Fatu Manufui	15.01
Meusin	15.03
Boking	15.06
Nunkolo	15.11
Haineno	15.14
Nenoat	15.16
Sahan	15.18
Saenam	15.21
Op	15.25
Nualunat	15.30
Kot'olin	15.35
Hoibeti	15.41
Oetuke	15.45
Nununamat	15.49
Spaha	15.51
Kolbano	15.56
Noesiu	15.60
Tuapakas	15.66
Oni	15.74
Kualin	15.77
Tuafanu	15.65
Toineke	15.45
Oebelo	15.28
Bena	15.12

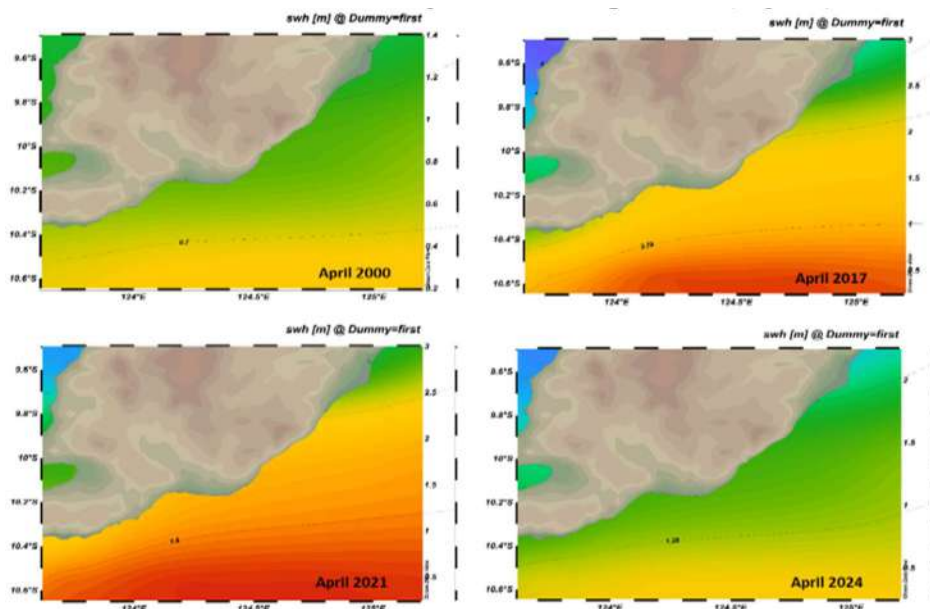


Fig. 11: Average maximum wave height in Timor waters in April 2000, 2017, 2021, and 2024.

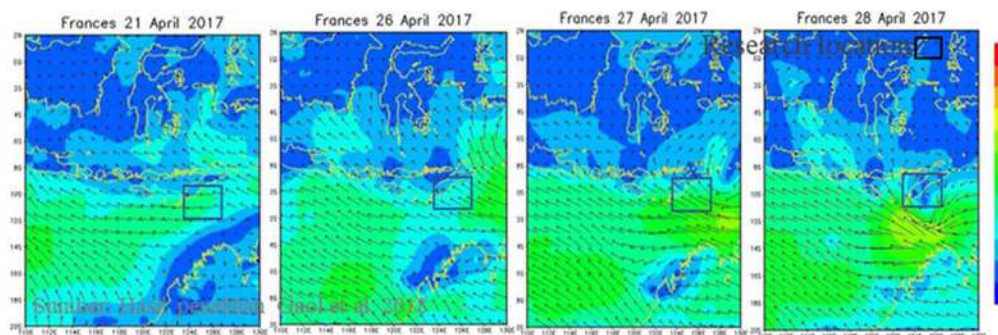


Fig. 12: Cyclonic currents began to appear on April 21-28, 2017.

waters in April 2017 reached speeds of 24-28 knots, forming a cyclonic vortex moving westward (Fig. 12).

The wave heights in April 2024 ranged from 0.5 to 2 m (Fig. 11). Fig. 13 shows the results of the analysis of the average annual wave height for the period from 2000 to 2024 in the research area, which ranged from 1.07 to 1.95 m. The highest waves occurred in the southern waters of the western part of Timor Island, namely in the Bena waters, ranging from 1.5 to 1.6 m. In contrast, the lowest wave heights were found in the waters around Kualin District and part of Boking District. Based on the CVI category (Table 2), the southern waters of the SCT Regency fall into the vulnerable to very vulnerable category (Fig. 13). The most destructive sea waves were those generated by Hurricane Frances, resulting in damage to residences in four coastal districts: Kualin, Kolbano, Kotolin, and Boking (Besie 2017).

### Socio-Economic Variables

**Land use:** Land use classification is based on the socio-economic value of each land, referencing the research results of Sulma (2012) and adjusting to the conditions in this study area (Table 4). The indicator used was the type of land use that has high social and economic value, which can increase the vulnerability of an area if a disaster occurs. Based on the classification along the coastal areas of the SCT Regency, there were 7 types of land use: water bodies, bushes, fields, gardens, rice fields, residences, and roads (Table 7). The distribution of land use along the coastal areas of the SCT Regency is presented in Fig. 14.

Based on the analysis of Digital Elevation Model (DEM) data, in general, the category of non-agricultural land (shrubs) dominated almost all coastal villages. In each analysis unit, it occupied 59.2% while highways covered

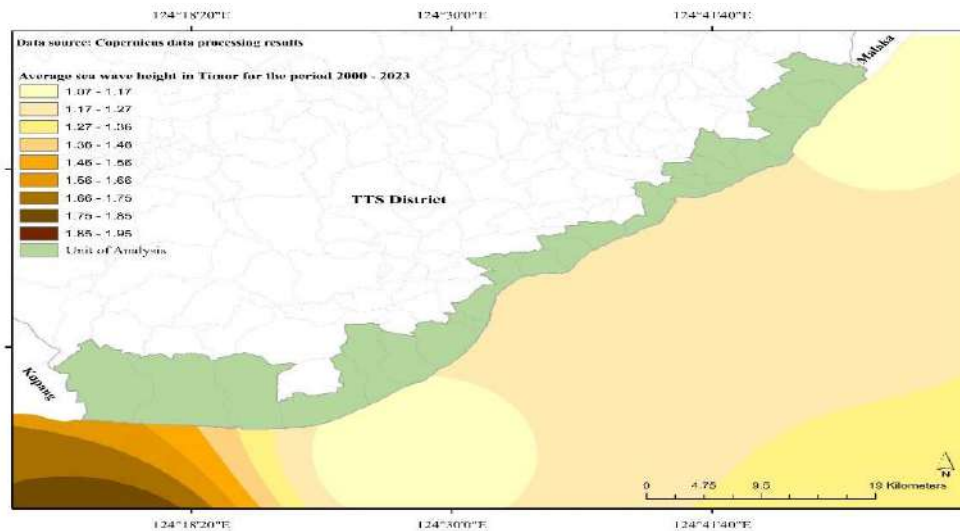


Fig. 13: Average wave height from 2000 to 2024 in the waters of the SCT Regency and its surroundings.

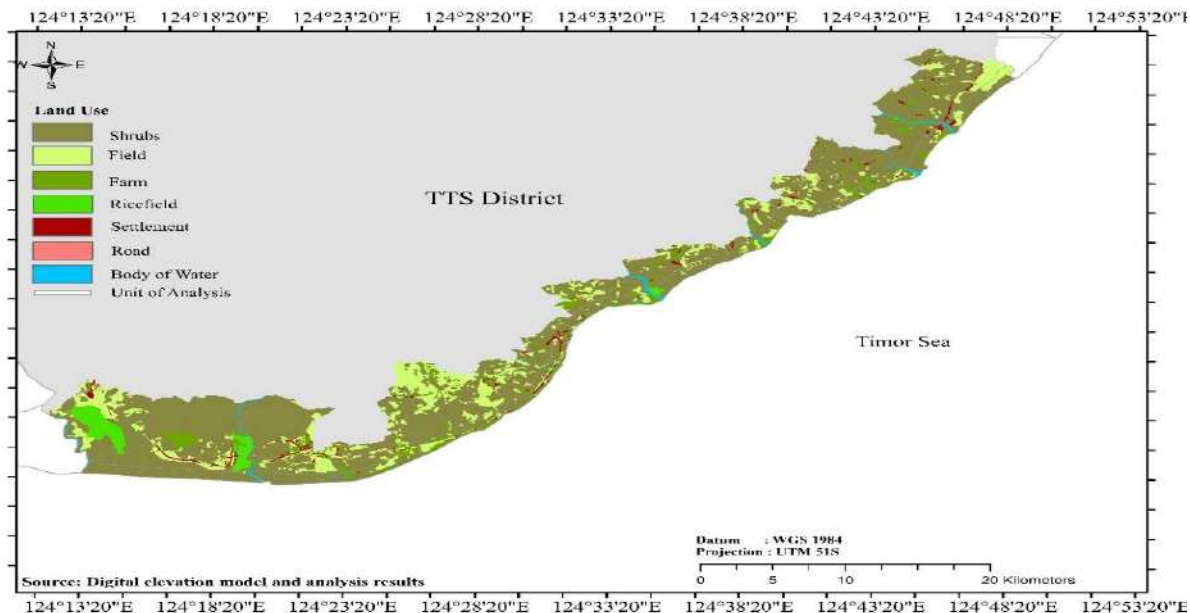


Fig. 14: Distribution of land use on the coastal areas of the SCT Regency.

1.4% of the area (Table 7). In non-agricultural areas, sand and stone mining activities were found in the community, especially in Kolbano District and its surroundings. Although this non-agricultural area was not classified as vulnerable due to the absence of immediate dangerous impacts on the population, it creates a serious risk for residents, as the presence of stone mining activities has gradually increased the area's vulnerability to abrasion. According to Hantoro (2020), anthropogenic activities can cause ecosystem damage that is increasingly difficult to control. Even though sandy and rocky areas are in large quantities, the impact of

Table 7: Area of land use along the coast in each analysis unit.

Land Use	Wide [km <sup>2</sup> ]	%
Bush	50.41	59.24
Water Body	2.24	2.63
Field	13.43	15.78
Garden	13.65	16.03
Rice Field	2.49	2.93
Residence	1.64	1.92
Road	1.25	1.46

Source: Results of the analysis of DEMNAS data on the appearance of Indonesia in 2024



exploitation often exceeds the recovery capacity of the area.

**Population density:** Based on the density analysis on the southern coast of the SCT Regency, the area within one kilometer from the coastline toward the land has a density ranging from 13 to 227 people.km<sup>-2</sup>. According to Triyastuti (2019), a high population density is categorized as more than 1000 people.km<sup>-2</sup>, while an ecologically ideal density falls between 50 and 100 people.km<sup>-2</sup>. The results of observations in 25 coastal villages indicated that the blue areas (Fig. 15) still had an ideal population density below 100 people/km<sup>2</sup>. The vulnerability index for these blue areas, namely the Tuafanu, Kualin, Tuapakas, Noesiu, Oetuke, Nenoat, and Boking coasts, showed that they were categorized as having low vulnerability. The green areas, namely the Kolbano, Nualunat, and Meusin coasts, were categorized as having moderate vulnerability. The orange areas, namely the Spaha, Op, Saenam, and Sahan coasts, were categorized as having a high vulnerability, with the Oni coast classified as the highest vulnerability (red area). Conversely, the white areas, comprising the coasts of Bena, Oebelo, Toineke, Nununamat, Kot'olin, Hoibeti, Nunkolo, Hoineno, Fatumanufui, and Baus, did not have any residences, resulting in a population density value of 0 and categorizing them as non-vulnerable (Fig. 15).

**Poverty rate:** The poverty rate was represented by the analysis unit at the pre-prosperous level. The observation results revealed that the poverty rate in the coastal areas of Bena, Oebelo, Toineke, Nununamat, Hoibeti, Kot'olin,

Hoineno, Nunkolo, Fatumanufui, and Baus was zero as no residents inhabited these areas (Fig. 16). According to Sulma (2012), if the number or density of population is zero, the poverty rate will also be zero. These uninhabited areas were generally located far from highway access and were characterized by flat topography, increasing the risk of seawater inundation. This indicates a form of adaptation carried out by the community to avoid the threat of rising sea levels. The numbers of poor people in the 1 km area from the coastline in the very vulnerable category was found in Sahan, Oetuke, Spaha, Noesiu, and Tuafanu Villages, while in the moderate to low vulnerability categories, respectively, were Kualin, Tuapakas, Nualunat, Op, Oni, and Kolbano Villages. In general, the coastal communities of the SCT Regency who were poor worked as farmers and stone/sand miners (Fig. 16). The poverty rate in all analysis units can be seen in Fig. 16.

The higher the poverty rate in an area, the greater the vulnerability of the area in facing a disaster. This is related to safety efforts and the community's ability to face disasters.

### Vulnerability Analysis

The results analysis of six physical variables showed that the coasts of Bena, Oebelo, Toineke, Tuafanu, Kualin, Oni, Tuapakas, Noesiu, Kolbano, Spaha and Oetuke (Fig. 17) were in the range of high to very high vulnerability. The high vulnerability in these coastal areas is due to the location of these coasts on a gentle to flat alluvial coastal plain,

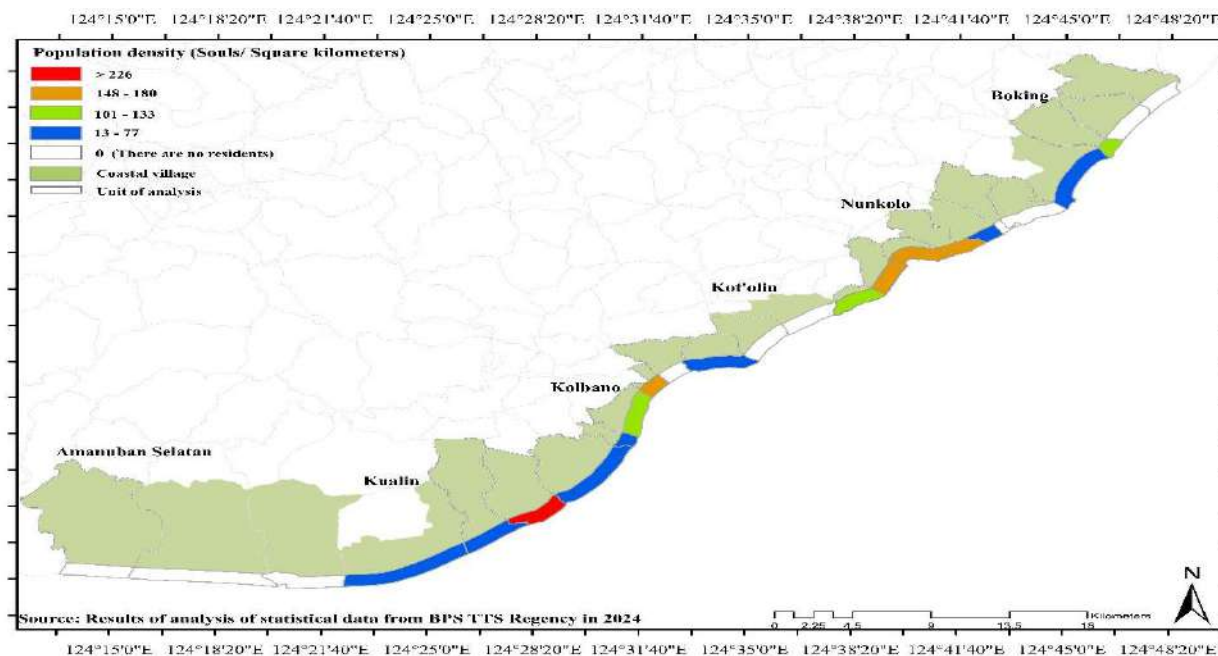


Fig. 15: Population density in each analysis unit.



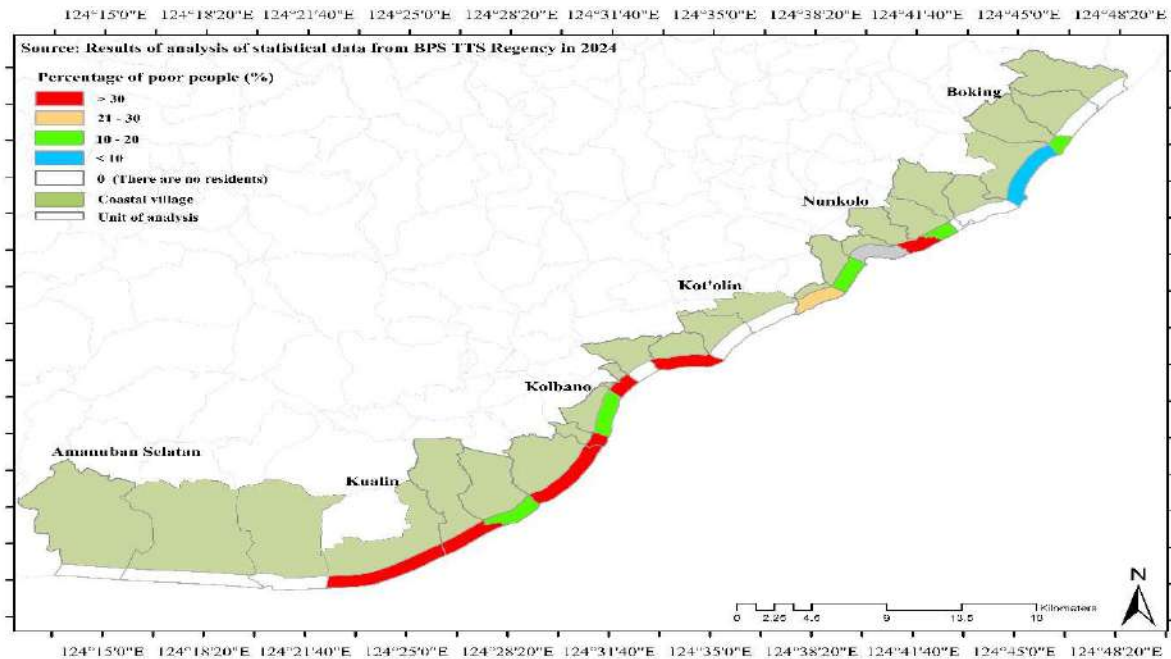


Fig. 16: Poverty rate in each analysis unit.

making the land more susceptible to shrinkage caused by hydro-oceanographic factors, such as the inland shift of the coastline, except for the Toineke coast, which is experiencing accretion (Fig. 9). The accumulation of several hydro-oceanographic variables with high vulnerability scores, specifically tides and waves (Fig. 13), causes the Toineke coast to have vulnerable status. According to Sulma (2012),

beaches with flat topography are generally dominated by sand, which is easily eroded by waves and tides. Meanwhile, those falling into the low vulnerability category, namely the Kot'olin, Nualunat, Saenam, Nenoat, Nunkolo, and Boking coasts, are generally located in hilly areas. The type of hills on the coastal areas of the SCT Regency are karst hills that are classified as erosional zones. The shifting coastline in the

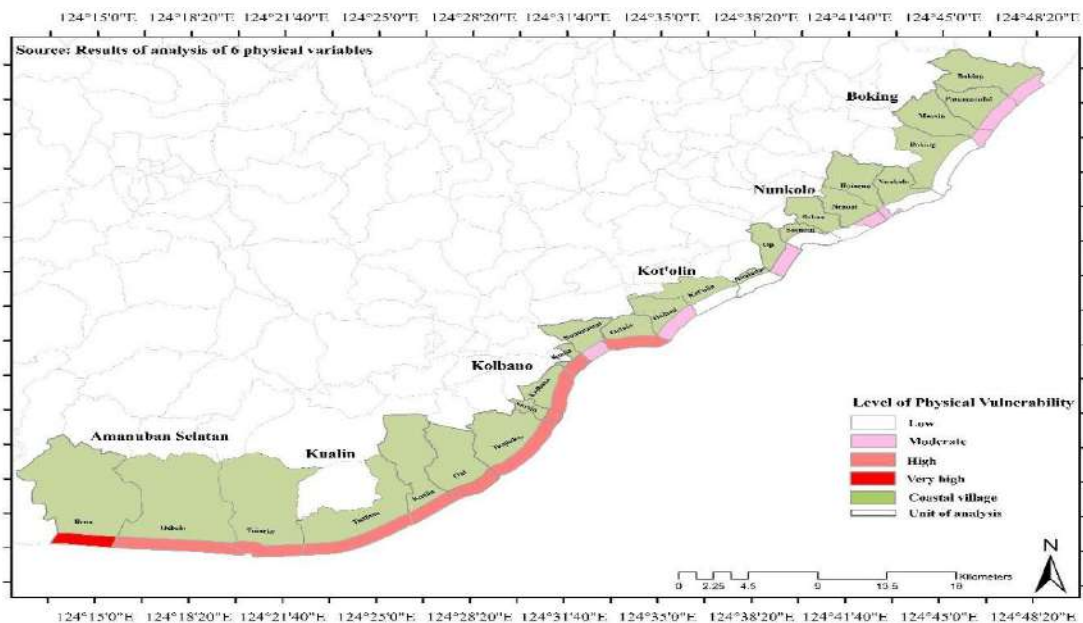


Fig. 17: Physical vulnerability levels of the SCT Regency's coastal areas.

Saenam karst hills shows that in terms of genesis, this type of karst belongs to the erosional karst group. The distribution of physical vulnerability levels is presented in Fig. 17.

The standardization calculation of the average values of physical variables reveals that geomorphology holds the highest influence on the physical vulnerability of the SCT Regency's coastline, with a score of 0.78. Following this, elevation ranks at 0.69, coastline change rate at 0.68, average tidal range at 0.48, sea level rise rate at 0.43, and wave height at 0.22 (Table 8). The results analysis has shown that geomorphological conditions have the highest influence on the high level of physical vulnerability in the coastal areas of the SCT Regency, followed by elevation, coastline change rate, tidal range, sea level, and wave height.

Based on the analysis results of three socio-economic variables, Noesiu Village exhibited high socio-economic

vulnerability, while other areas fell into medium, low, and very low levels of vulnerability (Fig. 18). Table 9 indicates that land use and poverty rate on the coast of Noesiu significantly contributed to the high socio-economic vulnerability. The population of Noesiu Village lived in an area of 1 km from the coastline towards the land. Their livelihoods generally depended on stone and sand mining. These mining activities extend across several coastal areas, including Kolbano, Oetuke, Nenoat, Hoineno, and Nunkolo. The vulnerability observed along the coastal area was predominantly influenced by land use, as shown in Table 9. This is primarily due to the conversion of non-agricultural land into sand and stone mining zones, a practice that has accelerated erosion along the coastline. This land-use change has created a nearly uniform pattern of coastal erosion, further destabilizing the area and increasing its susceptibility to environmental degradation.

Table 8: The results of standardization of physical variable values in each analysis unit.

Analysis Unit	Elevation	Geomorphology	Tidal Range	Coastline Change Rate	Sea Level	Wave Height
1	0.996	1.000	0.000	0.706	0.011	0.000
2	0.995	1.000	0.000	0.823	0.011	0.021
3	0.967	1.000	0.000	0.675	0.036	0.039
4	0.713	0.844	0.000	0.613	0.080	0.076
5	0.673	0.823	0.000	0.559	0.144	0.122
6	0.762	0.793	0.000	0.731	0.175	0.142
7	0.635	0.684	0.000	0.805	0.196	0.155
8	0.494	0.561	0.000	0.694	0.225	0.170
9	0.000	0.000	0.000	0.750	0.264	0.187
10	0.632	0.826	0.000	1.000	0.317	0.204
11	0.283	0.415	0.000	0.625	0.376	0.218
12	0.236	0.237	0.000	0.651	0.437	0.230
13	0.448	0.639	0.000	0.789	0.506	0.239
14	0.499	0.697	1.000	0.701	0.567	0.243
15	0.234	0.413	1.000	0.558	0.607	0.244
16	0.395	0.690	1.000	0.647	0.640	0.242
17	0.886	0.990	1.000	0.720	0.698	0.227
18	0.815	1.000	1.000	0.875	0.749	0.206
19	0.752	1.000	1.000	0.690	0.831	0.157
20	0.809	1.000	1.000	0.524	0.930	0.088
21	0.991	1.000	1.000	0.716	0.957	0.050
22	0.998	1.000	1.000	0.643	0.810	0.101
23	1.000	1.000	1.000	0.000	0.566	0.406
24	0.998	1.000	1.000	0.562	0.345	0.773
25	0.996	1.000	1.000	0.927	0.156	1.000
Average	0.69	0.78	0.48	0.68	0.43	0.22

Table 9: Results of standardization values of the socioeconomic variable in each analysis unit.

Analysis Unit	Land use	Population Density	Poverty rate
1	0.605	0.000	0.000
2	0.202	0.000	0.000
3	0.555	0.652	0.148
4	0.365	0.265	0.064
5	0.710	0.000	0.000
6	0.871	0.000	0.000
7	0.610	0.340	0.132
8	0.291	0.467	1.000
9	0.438	0.557	0.000
10	0.380	0.585	0.196
11	0.522	0.792	0.248
12	0.185	0.000	0.000
13	0.311	0.000	0.000
14	0.643	0.111	1.000
15	0.198	0.000	0.000
16	0.344	0.446	0.959
17	0.595	0.669	0.129
18	1.000	0.236	1.000
19	0.325	0.207	0.511
20	0.558	0.999	0.154
21	0.511	0.222	0.582
22	0.474	0.056	1.000
23	0.000	0.000	0.000
24	0.015	0.000	0.000
25	0.013	0.000	0.000
Average	0.43	0.26	0.28

The standardization of average variable value from largest to smallest revealed three main socio-economic factors contributing to vulnerability along the coastal areas of the SCT Regency: land use (0.43), poverty rate (0.28), and population density (0.26). The analysis results showed that, in general, land use had contributed hugely to the high level of socio-economic vulnerability, followed by poverty range and population density, respectively (Table 9). The distribution of socio-economic vulnerability levels in the coastal areas of the SCT Regency is presented in Fig. 18.

The results of the analysis of physical and socio-economic variables in the research site showed that the Kot'olin coast was an area with very low vulnerability. This was primarily due to its residences being located further inland, coupled with the fact that its residents were not categorized as poor, which reduced the impact of potential coastal hazards. Meanwhile, the Tuafanu, Kualin, Oni, Noesiu, Kolbano, and Oetuke coasts were found to have high vulnerability (Fig. 19). These areas, situated within one kilometer of the coastline, experienced significant damage due to both anthropogenic activities and the dynamic influences of hydro-oceanographic factors. Fig. 19 illustrates the spatial distribution of these vulnerabilities.

## CONCLUSIONS

The coastal areas of the SCT Regency are classified as vulnerable to rising sea levels, with low (35%), medium



Fig. 18. Levels of socio-economic vulnerability of the coastal areas of the SCT Regency.

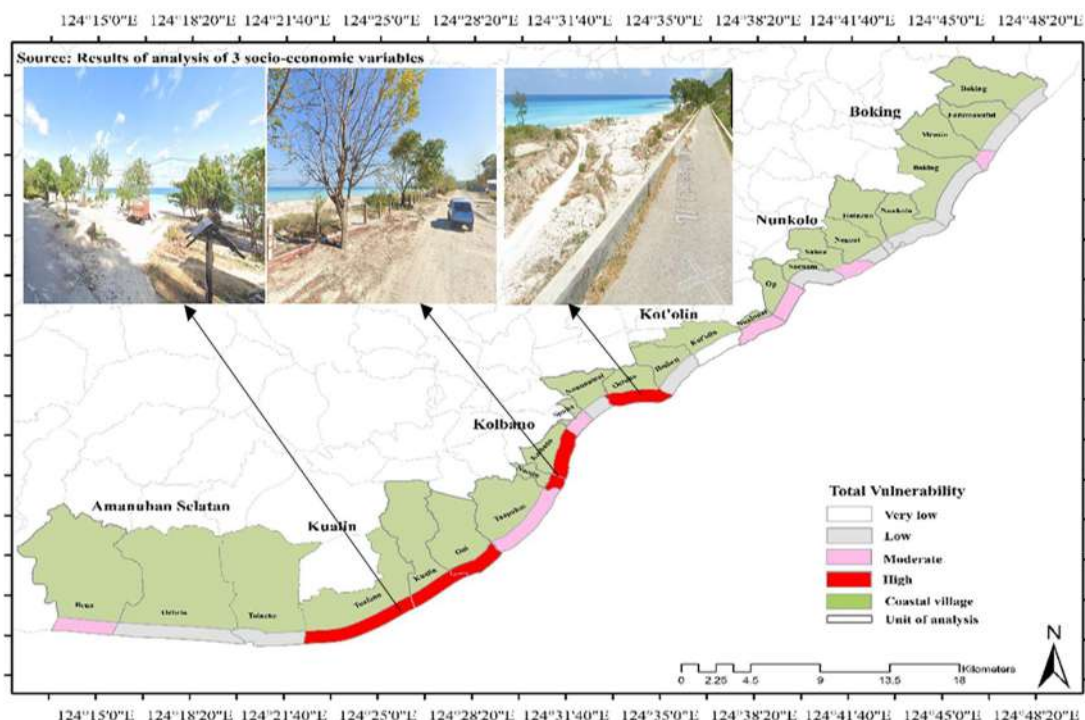


Fig. 19: Total vulnerability levels of the SCT Regency's coastal areas.

(48%), and high (66%) vulnerability categories. Areas with a high level of vulnerability were physically lowland areas with fragile coastal landforms. Karst hills, which are characteristic of the SCT Regency's coastline, pose a threat to the lives of coastal communities, as these hill types are categorized as an erosion zone. Communities living in coastal hill areas, including those in the Kolbano, Spaha, and Oetuke coastal areas, as well as in flat alluvial regions like Tuafanu, Kualin, and Oni, should be prioritized in coastal development and restoration efforts due to their high vulnerability in both physical and socio-economic aspects. The physical condition that most contribute to the coastal vulnerability of the SCT Regency is geomorphology, while the most influential socio-economic factor is land use. One necessary recovery effort involves revegetation, supported by the synergy between human activities and nature, guiding communities to utilize natural resources for economic livelihoods while maintaining ecological balance.

## ACKNOWLEDGMENT

This research was carried out through funding from the Ministry of Education, Culture, Research and Technology with number 100/E5/PG.02.00.PL/2024. Therefore, we would like to thank the Ministry and Research Institutes from the University of Timor who has supported this research.

## REFERENCES

- Bachri, S., 2011. Technostratification of the Outer Banda Arc with reference to the western part of Timor Leste and the eastern part of Seram Island. *Journal of Geology and Mineral Resources*, 21(2), pp.53–62. DOI
- Diposaptono, S., Budiman and Agung, F., 2013. Dealing with Climate Change in Coastal Areas and Small Islands. Popular Scientific Books.
- Fadilah, 2021. Analysis of Hydro-Oceanographic Factors on Coastal Damage in Pondok Kelapa District, Central Bengkulu Regency and Determining the Handling Concept. Jakad Media Publishing.
- Gaol, A.L., Siadari, E.L., Ryan, M. and Kristianto, A., 2018. The impact of tropical cyclone France on the upwelling of the Timor Sea and its surroundings. *Journal of Meteorology Climatology and Geophysics*, 5(3), pp.37–45.
- Government of the Republic of Indonesia, 2007. Law of the Republic of Indonesia Number 27 of 2007 on the Management of Coastal Areas and Small Islands. Jakarta: State Secretariat of the Republic of Indonesia.
- Hamuna, B., Sari, A.N. and Alianto, A., 2018. Study of coastal area vulnerability based on geomorphology and elevation in Jayapura City and Regency, Papua Province. *Journal of Region and Environment*, 6(1), pp.1–14. DOI
- Hantoro, W.S., 2020. Vulnerability and resilience of lowland coastal areas and small islands: Mitigation and adaptation strategies. Center for Geological Research. LIPI Press. DOI
- Kalay, D.E., Lopulissa, V.F. and Noya, Y.A., 2018. Analysis of beach slope and sediment distribution in the coastal waters of Waai Village, Salahutu District, Maluku Province. *Triton: Journal of Aquatic Resource Management*, 14(1), pp.10–18.
- Karsidi, A., 2011. Workshop on the Impact of Sea Level Rise on Indonesian Coastal Environment. Retrieved from <http://www.bakosurtanal.go.id>
- Kasim, F., 2011. Coastal vulnerability assessment using integrated CVI-MCA and GIS method, case study on the northern coastal line of Indramayu. *Forum Geografi*, 26(1), pp.65–76. DOI



- Koroglu, A., Ranasinghe, R., Jiménez, J.A. and Dastgheib, A., 2019. Comparison of coastal vulnerability index applications for Barcelona Province. *Ocean and Coastal Management*, 7, p.65. DOI
- Kurniawan, R., Siagian, T.H., Yuniarto, B., Nasution, B.I. and Caraka, R.E., 2018. Construction of social vulnerability index in Indonesia using partial least squares structural equation modeling. *International Journal of Engineering & Technology*, 7(4), pp.6131–6136. DOI
- Ledheng, L. and Hano'e, E.M.Y., 2023. Analysis of shoreline change of North Central Timor Regency, Indonesia. *Nature Environment & Pollution Technology*, 22(2), pp.777–787. DOI
- Lindsey, R., 2019. Climate Change: Global Sea Level. *National Oceanic and Atmospheric Administration (NOAA), National Ocean Service*, Silver Spring.
- Maulana, E., Ambarwulan, W., Wulan, T.R., Saputro, G.B., Setiawan, N., Muharram, F.W. and Putri, G.A., 2017. Evaluasi ODTW Pantai Kolbano untuk peningkatan ekonomi lokal masyarakat di Desa Kolbano, Kecamatan Kolbano, Kabupaten Timor Tengah Selatan. *Evaluation of Kolbano Beach Tourism Object for Enhancing Local Community Economy in Kolbano Village, Kolbano District, South Central Timor Regency*.
- Pamungkas, A., 2018. Karakteristik parameter oseanografi (pasang-surut, arus, dan gelombang) di perairan utara dan selatan Pulau Bangka. *Bulletin of Marine Oceanography*, 7(1), pp.51–58.
- Pendleton, E.A., Thieler, E.R. and Williams, S. J., 2010. Importance of coastal change variables in determining vulnerability sea and lake change. *Journal of Coastal Research*, 26(1), pp.176–183. DOI
- Rahmania, T., Apriyanto, B. and Astutik, S., 2019. Potensi terjadinya longsor pada kawasan karst Gunung Sadeng Puger karena adanya aktivitas pertambangan. *Geography Learning Journal*, 2(1), pp.161–171. <https://jurnal.unej.ac.id/index.php/PGEO/article/view/11937>
- Ramieri, E., Hartley, A., Barbanti, A., Santos, F.D., Gomes, A., Hilden, M., Laihonon, P., Marinova, N. and Santini, M., 2011. Methods for Assessing Coastal Vulnerability to Climate Change. *ETC CCA Background Paper*, Copenhagen (DK), 8–9 June 2011.
- Suhana, M.P., Putra, R., Muliadi, M. and Shafitri, L.F., 2020. The level of coastal vulnerability in the north and east of Bintan Island, Riau Islands Province, in 2020. *Journal of Fisheries and Marine Technology*, 11(1), pp.11–27. DOI
- Sulma, S., 2012. Coastal Vulnerability to Sea Level Rise (Case Study: Surabaya and Surrounding Areas). [Thesis] Graduate School, University of Indonesia: Depok.
- Szlafsztein, C. F., 2005. Climate change, sea-level rise, and coastal natural hazards: A GIS-based vulnerability assessment, State of Para, Brazil. *Journal of Coastal Conservation*, 11, pp.53–66.
- Triyastuti, D., 2019. The Influence of Population Density on the Quality of Life of Communities in Ngemplak District, Boyolali Regency, in 2013 and 2017. [Doctoral dissertation] Muhammadiyah University of Surakarta, Indonesia.
- Ward, P.J., Marfai, M.A., Yulianto, F., Hizbaron, D.R. and Aerts, J., 2011. Coastal inundation and damage exposure estimation: A case study for Jakarta. *Natural Hazards*, 56, pp.899–911. DOI

# Evaluating Phytoremediation Approaches for the Restoration of Degraded Ecosystems in India

Abhishek Maitry<sup>id</sup>, Gunjan Patil<sup>†</sup><sup>id</sup> and Preety Dubey<sup>id</sup>

Department of Forestry, Wildlife & Environmental Sciences, Guru Ghasidas Vishwavidyalaya, Bilaspur-495009, Chhattisgarh, India

<sup>†</sup>Corresponding author: Gunjan Patil; gunjan210315@gmail.com

**Abbreviation:** Nat. Env. & Poll. Technol.  
**Website:** www.neptjournal.com

*Received:* 22-08-2024

*Revised:* 11-10-2024

*Accepted:* 18-10-2024

## Key Words:

Heavy metals  
 Phytoremediation  
 Degradation  
 Restoration  
 Stress management  
 Bioremediation

## Citation for the Paper:

Maitry, A., Patil, G. and Dubey, P., 2025. Evaluating phytoremediation approaches for the restoration of degraded ecosystems in India. *Nature Environment and Pollution Technology*, 24(2), p. B4262. <https://doi.org/10.46488/NEPT.2025.v24i02.B4262>

*Note: From year 2025, the journal uses Article ID instead of page numbers in citation of the published articles.*



**Copyright:** © 2025 by the authors

**Licensee:** Technoscience Publications

This article is an open access article distributed under the terms and conditions of the Creative Commons Attribution (CC BY) license (<https://creativecommons.org/licenses/by/4.0/>).

## ABSTRACT

Plant stresses are the conditions that adversely affect the growth, development, or productivity of plants/trees and can be caused by various physical, chemical, and biological factors. On the other hand, stress brought on by heavy metal exposure significantly impairs plant development and output. These heavy metal contaminations are responsible for the harmful effects on biotic (plants and associated organisms) and the abiotic (soil, water, and air) environment. Mining operations are thought to be the main cause of heavy metal pollution in the environment if they are not adequately controlled. Phytoremediation provides an efficient, carbon-neutral, and environmentally friendly way to remove dangerous heavy metal contamination from various settings. It can efficiently treat a broad spectrum of heavy metal contaminants. Phytoremediation enhances the development and growth of plants and nourishes the environment, resulting in the ill effects of climate extremes in disturbed areas and hence mitigating the impacts of climate change. Although phytoremediation has been extensively researched for the treatment of heavy metal stress in India's degraded ecosystems, where it is most needed, it has not yet reached economic viability. Through this article, we tried to minimize this gap by reviewing some important phytoremediation studies in India that successfully reduced the negative impacts of heavy metals in different degraded ecosystems. PRISMA (Preferred Reporting Items for Systematic Reviews and Meta-Analyses) review principles were used to outline the selected studies giving a knowledge that most of the phytoremediation works in India have been performed on Shrubs (28.40%) closely followed by Tree species (26.28%) then in Herbs (17.65%), Grasses (17.25%) and Aquatic Plants (10.43%). Also, the trend has seen a spike after 2018 with most phytoremediation studies in the states of West Bengal. The studies reviewed in this article show us a pathway for implementing and managing remediation methods to reduce the heavy metal stress exerted on plants and enhance the metabolic and physiochemical processes of the plant.

## INTRODUCTION

Stress can be defined as any conditions that adversely affect the growth, development, or productivity of plants/trees. Plant stress usually reflects some sudden changes in environmental conditions, which create unfavorable conditions for the growth and development of the plants (Verma et al. 2013). Stress occurring in plants can be divided into two primary categories, namely abiotic stress and biotic stress (Bhandari et al. 2023) (Fig. 1). Abiotic stress is imposed on plants by either physical or chemical factors of the environment (Yang et al. 2023), while biotic stress exposed to the plants are biological entities like weeds, pathogens, insects, pests, etc. (García-Montelongo et al. 2023, Gull et al. 2019). Heavy metal stress is crucial and has a noticeable negative impact on plant development and production despite all other stressors (Devi & Kumar 2020). Since the start of industrialization, the mining of minerals and precious metals has released many harmful compounds into the environment (Adnan et al. 2022a).

Heavy metals have the largest availability in soil (Chen et al. 2023, Li et al. 2022) and aquatic ecosystems (Boum-Nkot et al. 2023, Singh & Bajpai 2023) and a relatively smaller proportion in the atmosphere as particulate or vapors (Ulutaş 2022). The primary cause of heavy metal pollution in the environment is thought to be mining, which also produces very damaging waste metals and tailings if it is not managed effectively. The heavy metal stress exerted on the plants in and around the mining areas directly inhibits their growth and development, which decreases the vegetative capacity of such areas, leading to land degradation. These land degradations are causing major contributions to climate change as the mining sector in India is distributed over an area of approx. 312645 hectares (Ministry of Mines, GOI - Annual Report 2021-22). This chapter briefly summarizes the heavy metal impacts on plants, studies on their management techniques, and their benefits in mitigating climate change impacts. Although there are numerous disadvantages, there have previously been several physical and chemical approaches to heavy metal cleanup. The biological technique, or phytoremediation, is a relatively recent technology that has several benefits over conventional approaches for heavy metal cleanup. It is also cheap, easy to use, and environmentally benign (Rai et al. 2021).

### Heavy Metal Contamination

Heavy metal term was coined for any metallic element that has a relatively high atomic weight and density, and in the

field of biology, heavy metals are referred to the metals that are toxic to organisms even in small amounts (Lenntech Water Treatment and Air Purification 2004). Heavy metals include lead (Pb), cadmium (Cd), nickel (Ni), cobalt (Co), iron (Fe), zinc (Zn), chromium (Cr), iron (Fe), arsenic (As), silver (Ag) and the platinum group elements and can be categorized into important and toxic heavy metals (Geleta 2023). It is impossible to fully transform heavy metals into non-toxic, innocuous forms, and they have a lasting detrimental effect on the environment in addition to being carcinogenic, mutagenic, and cytotoxic to living things that come into touch with them (Rahman et al. 2022, Yan et al. 2022, Dixit et al. 2015). They also have an adverse effect on the microbial community in the soil, which leads to the extinction of species that control the cycling of nutrients and impairs the ecosystem's ability to operate (Chen et al. 2023, Fashola et al. 2016, Zukauskaitė et al. 2008).

### Sources of Heavy Metals Contamination

There are different causes of heavy metal pollution, but mining (the process of removing valuable minerals and materials from the Earth's crust) is thought to be the main one (Shah et al. 2022, Zerizghi et al. 2022) (Fig. 2). Heavy metals are liberated from the ores during mining operations, deposited in the earth, or carried by air and water to other locations (Rashid et al. 2023). As a result, the surrounding region of mining sites has higher concentrations of heavy metals due to the release of waste products into the

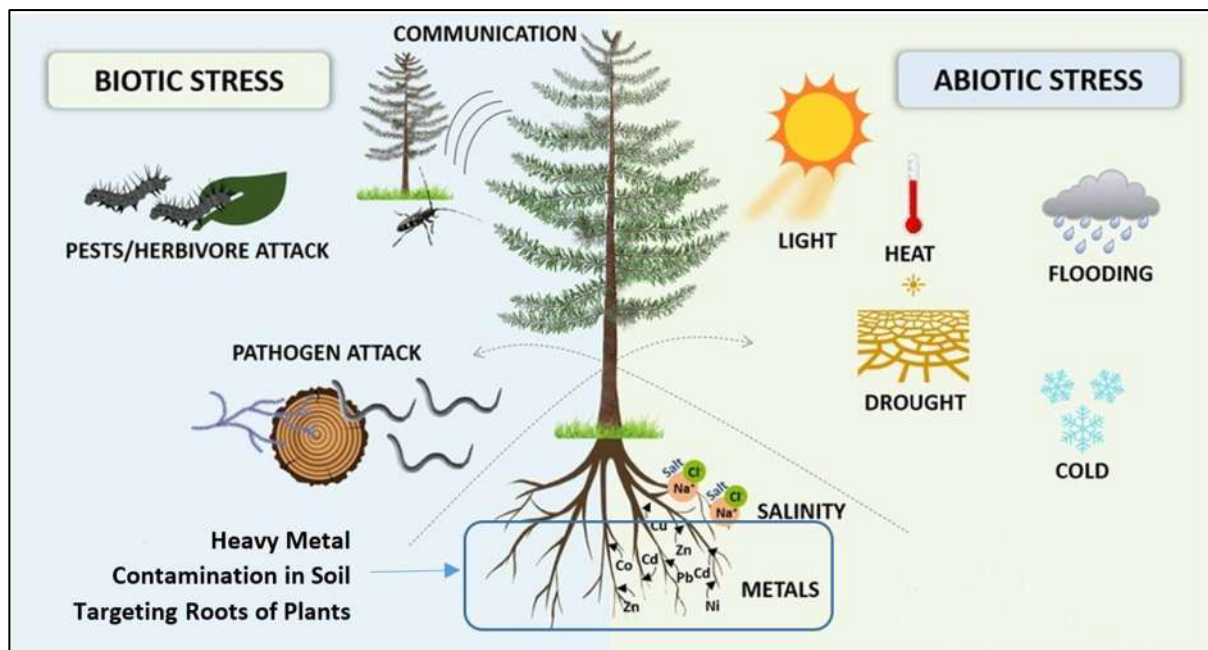


Fig. 1: Various abiotic and biotic stresses exerted on plants in the natural environment.

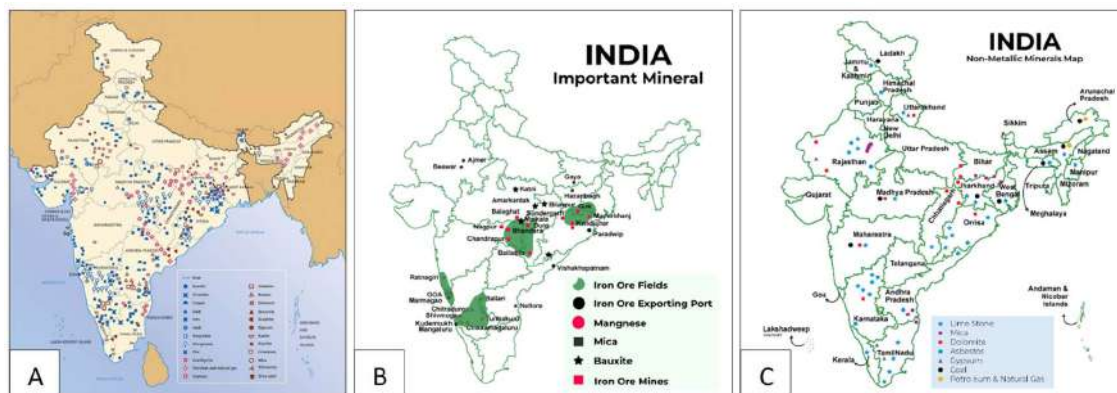


Fig. 2: A. Distribution pattern of various minerals in different regions of India showing the important zones for release of heavy metals in the environment, B. Metallic Minerals, C. Non-Metallic Minerals of India.

environment (Singh et al. 2023). Four heavy metals, namely Cd, Pb, As, and Hg, based on their occurrence, toxicity level, and exposure to living organisms, are identified as the most toxic metals released from mining among numerous other heavy metals (US Department of Health and Human Services 2005).

### Effects of Heavy Metal Contamination

**Effects of heavy metal contamination on plants:** The exposure of plants to toxic levels of heavy metals triggers a wide range of physiological and metabolic alterations (Ahmad et al. 2023, Sharma et al. 2022, Villiers et al. 2011). However, because various heavy metals have diverse sites of action inside plants, the overall hazardous visual reaction varies across them (Patil & Umadevi 2014). Plant mortality is frequently the consequence of heavy metal effects on leaves, which include chlorosis, necrosis, turgor loss, reduced seed germination, and photosynthetic failure (Dalcorsio et al. 2010). Cellular organelles and components of the cell, such as the mitochondria, nuclei, lysosomes, cell membrane, and enzymes, are reported to be affected by heavy metals (Collin et al. 2022). Metal ions also interact with DNA and nuclear proteins, thus damaging the DNA. These effects are associated with modifications in plant tissues and cells that are ultrastructural, biochemical, and molecular (Riyazuddin et al. 2022, Gamalero et al. 2009). High concentrations of heavy metals in the soil also have adverse effects on microorganisms (Patil & Faizan 2017), indirectly affecting the growth and development of the plants.

**Effects of heavy metal contamination on the environment:** Due to their harmful character, environmental chemists have given heavy metals the most attention among all pollutants (Zaynab et al. 2022). According to Triassi et al. (2023), heavy metals are typically present in small quantities in natural watercourses, although many of them are dangerous even

at very low concentrations. Metals such as lead, cadmium, mercury, arsenic, nickel, cobalt, zinc, chromium, and selenium are highly toxic, even in minor quantities (Geleta 2023). There is currently more concern about the number of heavy metals in our resources since they are intoxicating the environment greater than the environment can handle (Bhat et al. 2023, Zheng et al. 2023). Heavy metals discharged into the environment are reported to be mostly absorbed by soils and water sources (Gunwal et al. 2021), enter into the food chain, and can cause great damage to the well-being of living organisms (Sharma et al. 2023, Triassi et al. 2023). A relatively smaller proportion of heavy metals are released into the air and can result in an imbalance of atmospheric composition.

### Phytoremediation as Management Technique to Remove Heavy Metal Contamination

The creation of a healthy ecosystem for living things and the environment is the primary objective of remediation techniques (Saravanan et al. 2022). To prevent the spread of stress brought on by heavy metal contamination in soils and water bodies, a variety of remediation techniques can be applied (Adnan et al. 2022b, Bhat et al. 2022). Physical, chemical, and biological methods can be used to remove heavy metals, and each has advantages and disadvantages of its own (Yang et al. 2022) (Fig. 3). However, physical and chemical methods of heavy metal cleanup are expensive, labor-intensive, and result in permanent changes to the characteristics of the soil, as well as an increased risk of secondary pollution creation and the eradication of soil microflora (Sharma et al. 2023, Ali et al. 2013).

On the other hand, bioremediation techniques do not require any expensive equipment or highly specialized personnel, and thus, it is relatively easy to implement. Metal accumulation in plant tissues is decreased by plant-associated



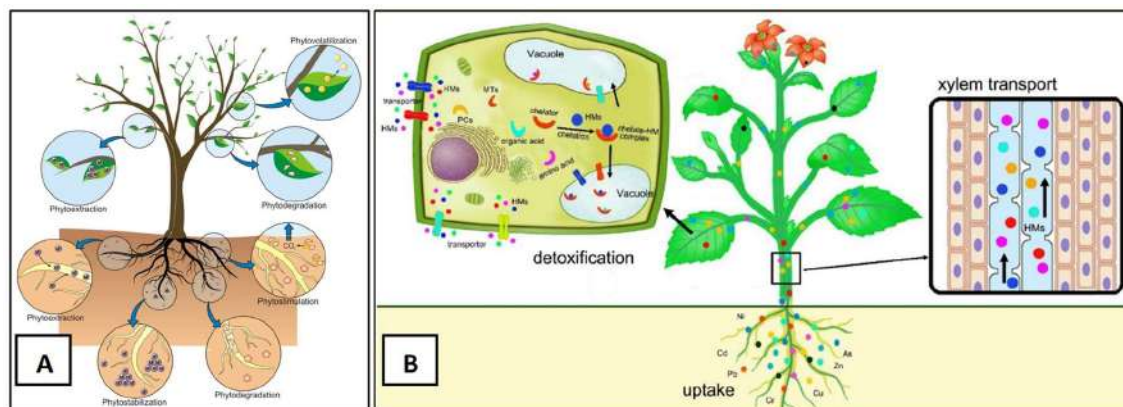


Fig. 3: A. Phytoremediation procedures through which the plant absorbs heavy metals from the soil, accumulates them into different parts, and releases them naturally through leaves; B. Accumulation of heavy metals in plants through phytoremediation.

microbes, and they also help to reduce metal bioavailability in the soil through various mechanisms (Rosyidah et al. 2023, Tiwari & Lata 2018). It can successfully remove a variety of heavy metal pollutants from various settings. Thus, phytoremediation provides an economical, carbon-neutral, long-lasting, efficient, and environmentally friendly way to get rid of dangerous pollutants from contaminated environments (Oladoye et al. 2022, Mandal et al. 2014).

## MATERIALS AND METHODS

### Information Sources and Literature Search

We conducted an extensive literature search and reviewed different online databases, Google Scholar, Scopus, ResearchGate, etc., for peer-reviewed publications of phytoremediation studies in India published between 1994 and June 2023. We used the following search string/keywords: [(phytoremediation\*) OR (bioremediation\*) OR (phyto\*) OR (heavy metals\*) OR (metal accumulation\*) OR (degraded land\*) OR (phytotoxicity) OR (phytoextraction\*) OR (phytodegradation\*) OR (phytostimulation\*) OR (phytostabilization\*)] AND (India). This combination of keywords allowed us to cover publications of phytoremediation research on the degraded lands of India. Additionally, a manual search was performed in the reference list of the review performed by Ghosh and Singh (2005a) since they were one of the first Indian researchers that introduced the term phytoremediation in their article and Mandal et al. (2014) as they provided necessary descriptions on phytoremediation in India till 2014 that is expanded in this review. We took the year 1994 as a starting point, the year when the term was popularized in developing nations of Southeast Asia. In this review, we have only focused on the phytoremediation work performed in India, and therefore, we excluded all the related works done in other countries

and subcontinents, except for reviews/research based on secondary data from India.

### Screening of Assessed Sources

We outlined the chosen studies in accordance with the PRISMA (Preferred Reporting Items for Systematic Reviews and Meta-Analyses) review principles (Fig. 4). The search turned up 1275 research and reviews. Based on relevance and subject specialization, we retained 246 articles after screening their titles and abstracts at stage 1. Then, to concentrate on the work done on the subject of phytoremediation, we evaluated the entire texts of 246 possibly pertinent research and omitted 102 articles at stage 2. Only 31 of the 144 relevant studies were kept at the final stage (stage 3) because of its deep information system and used in the analysis (Table 1). The remaining studies were disregarded due to their significant bias risk from underrepresenting the investigated bioremediating species, habitat distribution, or phyto-remediating indicators.

### Data Extraction and Compilation

We extracted the following data from the 31 finalized articles: scientific and bioremediating species names, studied heavy metals, study site, publication year, and applications reported for each habitat/site (Table 1). Work done outside India was completely excluded from this review, as the focus was to highlight the applicability of phytoremediation in the Indian subcontinent. The extracted information was compiled in a database and grouped into plant categories based on degraded land type. Additionally, we classified the articles into one or more habitat categories according to the reported uses of plant species for the study. We also georeferenced each locality found in the studies and assigned it to a phytoremediation province based on the

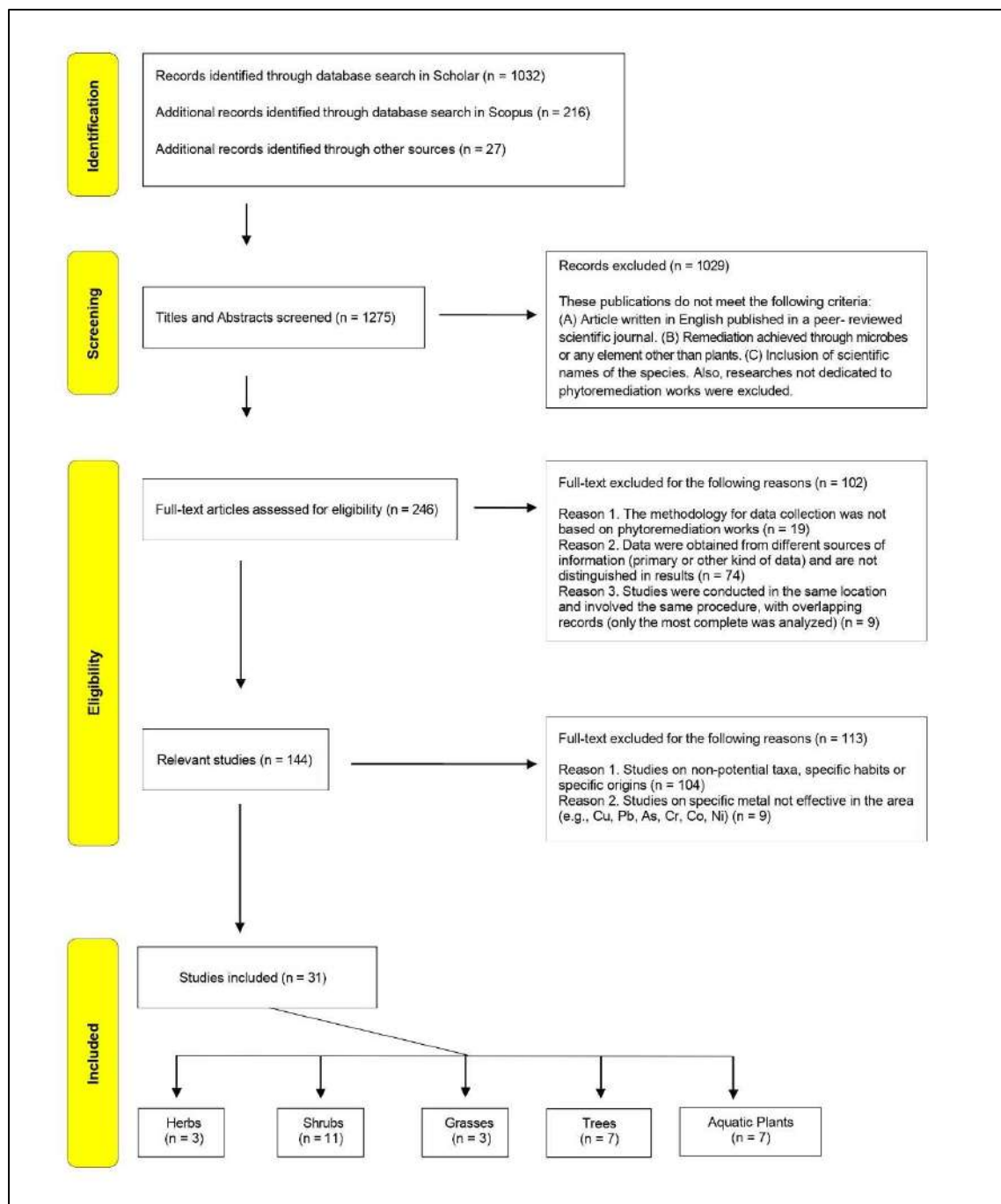


Fig. 4: PRISMA (Preferred Reporting Items for Systematic Reviews and Meta-Analyses) flow diagram of the study through the identification and selection process of important phytoremediation works in India.

intensity of phytoremediation works performed in that particular province/state of India. For the analysis of such phytoremediation provinces, we excluded articles in which the use of bioremediating plants was reported for more than one province without distinction between them.

### Data Analysis

To evaluate the relationship between the applicability of phytoremediation on different habitat types and provinces in the country to date, we used generalized cluster analysis

Table 1: List of 31 studies included in the systematic review of phytoremediation works in India.

S. No.	Year	Title of the Article	Heavy Metal Studied	Species Studied	Scalability/Limitations
1.	1999	Physico-chemical characteristics and pollution level of Lake Nainital (U.P., India): role of macrophytes and phytoplankton in biomonitoring and phytoremediation of toxic metal ions.	<b>Cr, Cu, Fe, Mn, Ni, Pb and Zn</b>	<i>Salix acmophylla</i>	Applicable for large-scale water bodies with similar heavy metal contamination, but the scalability is limited by the plant's slow growth in colder climates.
2.	2005	Phytoremediation: a potential option to mitigate arsenic contamination in the soil-water-plant system.	<b>As</b>	<i>Ludwigia parviflora</i> , <i>Enhydra sp.</i> , <i>Eleusine indica</i> , <i>Fimbristylis sp.</i> , <i>Ageratum conyzoides</i> , <i>Croton sparsiflorus</i> , <i>Lantana camara</i> , <i>Vitis trifolia</i> , <i>Asteracantha longifolia</i>	Suitable for diverse contaminated environments, but the scalability is constrained by the weed's relatively low biomass production.
3.	2005	Phytoaccumulation of chromium by some multipurpose-tree seedlings.	<b>Cr</b>	<i>Tectona grandis</i> , <i>Leucaena leucocephala</i> , <i>Albizia amara</i> , and <i>Casuarina equisetifolia</i>	Limited by the long growth period of trees but scalable in afforestation projects.
4.	2005	A comparative study of cadmium phytoextraction by accumulator and weed species.	<b>Cd</b>	<i>Brassica campestris</i> , <i>Brassica juncea</i> , <i>Dhatura innoxia</i> , <i>Ipomoea carnea</i> , <i>Phragmites karka</i>	It can be applied in agricultural fields with heavy Cd contamination, but biomass production is a limiting factor.
5.	2007	Phytoremediation in India.	<b>All</b>	<i>Trees</i>	Potential for large-scale deployment, but depends on specific plant species.
6.	2008	Extraction of cadmium and tolerance of three annual cut flowers on Cd-contaminated soils.	<b>Cd</b>	<i>Gladiolus grandiflorus</i> , <i>Tagetes erecta L</i> and <i>Chrysanthemum indicum L</i>	Not suitable for large-scale agricultural or industrial applications.
7.	2008	Cadmium uptake and tolerance of three aromatic grasses on the Cd-rich soil.	<b>Cd</b>	<i>Cymbopogon martini</i> , <i>Cymbopogon flexuosus</i> , and <i>Vetiveria zizanoides</i>	Scalable for large land areas due to rapid growth and wide adaptability.
8.	2008	Bioaccumulation and translocation of metals in the natural vegetation growing on fly ash lagoons: a field study from Santaldih thermal power plant, West Bengal, India.	<b>Mn, Zn, Cu, Ni, Pb</b>	<i>Typha latifolia</i> , <i>Fimbristylis dichotoma</i> , <i>Amaranthus defluxes</i> , <i>Saccharum spontaneum</i> and <i>Cynodon dactylon</i>	High potential for large industrial sites, but depends on the establishment of wetland systems.
9.	2008	Phytoextraction of lead by marigold and chrysanthemum.	<b>Cd, Pb</b>	<i>Gladiolus grandifloras</i>	Not suitable for large-scale agricultural or industrial applications.
10.	2008	Tolerance and bioaccumulation of cadmium and lead by gladiolus.	<b>Cd</b>	<i>Tagetes erecta L</i> and <i>Chrysanthemum indicum L</i>	Not suitable for large-scale agricultural or industrial applications.
11.	2009	Screening of Brassica species for hyper-accumulation of zinc, copper, lead, nickel, and cadmium.	<b>Pb, Zn, Ni, Cu, Cd</b>	<i>Brassica juncea</i> , <i>Brassica campestris</i> , <i>Brassica carinata</i> , <i>Brassica napus</i> , <i>Brassica nigra</i>	Scalable for large land areas due to rapid growth and wide adaptability.
12.	2009	Phytoremediation of cadmium-contaminated soils by marigold and chrysanthemum.	<b>Pb</b>	<i>Tagetes erecta L</i> and <i>Chrysanthemum indicum L</i>	Not suitable for large-scale agricultural or industrial applications.
13.	2010	Phytoaccumulation of lead by selected wetland plant species.	<b>Pb</b>	<i>Typha angustifolia</i> and <i>Ipomoea carnea</i>	Suitable for deployment in lakes or other water systems, but large-scale application requires further research on biomass management.
14.	2010	Potential of <i>Typha angustifolia</i> for phytoremediation of heavy metals from aqueous solution of phenol and melanoidin.	<b>Cu, Pb, Ni, Fe, Mn, Zn</b>	<i>Typha angustifolia</i>	Suitable for deployment in lakes or other water systems, but large-scale application requires further research on biomass management.

Table Cont....

S. No.	Year	Title of the Article	Heavy Metal Studied	Species Studied	Scalability/Limitations
15.	2010	Wetland macrophytes as toxic metal accumulators.	<b>Cd, As, Pb</b>	<i>Hydrilla verticillata</i> , <i>Ipomoea aquatica</i>	Applicable for large-scale water bodies with similar heavy metal contamination.
16.	2012	Phytoremediation of chromium by tuberose.	<b>Cr</b>	<i>Polianthes tuberosa</i>	Scalable for large land areas due to rapid growth and wide adaptability.
17.	2012	Phytoremediation of cadmium-contaminated soils by tuberose.	<b>Cd</b>	<i>Polianthes tuberosa</i>	Scalable for large land areas due to rapid growth and wide adaptability.
18.	2014	Effect of Lead and Cadmium on the Fungal Population in Rhizosphere Soils of Eucalyptus species.	<b>Cd, Pb</b>	<i>E. tereticornis</i> , <i>E. camaldulensis</i> , <i>E. globulus</i> and <i>E. citriodora</i>	Potential for large-scale deployment, but depends on specific species variety. Limited by the long growth period of trees.
19.	2015	Removal of Lead and Chromium from Synthetic Wastewater Using <i>Vetiveria zizanioides</i> .	<b>Pb, Cr</b>	<i>Vetiveria zizanioides</i>	Scalable for large land areas due to rapid growth and wide adaptability.
20.	2017	Cadmium and lead effect on growth parameters of four Eucalyptus species.	<b>Cd, Pb</b>	<i>E. tereticornis</i> , <i>E. camaldulensis</i> , <i>E. globulus</i> and <i>E. citriodora</i>	Potential for large-scale deployment, but depends on specific species variety. Limited by the long growth period of trees.
21.	2017	Phytoremediation mechanism in Indian mustard ( <i>Brassica juncea</i> ) and its enhancement through agronomic interventions.	<b>Pb, Cr, Se, Hg, Ni</b>	<i>Brassica juncea</i>	Scalable for large land areas due to rapid growth and wide adaptability.
22.	2020	Phytoremediation of heavy metals/metalloids by native herbaceous macrophytes of wetlands: Current research and perspectives.	<b>All</b>	<i>Macrophytes</i>	Applicable for large-scale water bodies with similar heavy metal contamination. Risk of uncontrolled invasion.
23.	2020	Phytoremediation efficiency of <i>Helianthus annuus</i> L. for reclamation of heavy metals-contaminated industrial soil.	<b>Pb, Cd, Zn, Cu, Fe, and As</b>	<i>Helianthus annuus</i> L.	Not suitable for large-scale agricultural or industrial applications.
24.	2020	Heavy metal fractions in rhizosphere sediment vis-à-vis accumulation in <i>Phoenix paludosa</i> (Roxb.) mangrove plants at Dhamra Estuary of India: assessing phytoremediation potential.	<b>Cd, Cu, Cr, Fe, Pb, Mn, Zn</b>	<i>Azolla pinnata</i>	Applicable for large-scale water bodies with similar heavy metal contamination.
25.	2021	Bioaccumulation of potentially toxic elements in three mangrove species and human health risk due to their ethnobotanical uses.	<b>Cd, Cr, Cu, Hg, Mn, Ni, Pb, and Zn</b>	<i>Avicennia officinalis</i> , <i>Porteresia coarctata</i> , and <i>Acanthus ilicifolius</i>	Not suitable for large-scale agricultural or industrial applications.
26.	2021	The potential of water fern ( <i>Azolla pinnata</i> R. Br.) in phytoremediation of integrated industrial effluent of SIIDCUL, Haridwar, India: removal of physicochemical and heavy metal pollutants.	<b>Cu, Mn, Zn, Ni, Fe, Cr, Cd, Pb</b>	<i>Azolla pinnata</i> R. Br., <i>Phoenix paludosa</i> (Roxb.)	Applicable for large-scale water bodies with similar heavy metal contamination.
27.	2021	Application of Aztec Marigold ( <i>Tagetes erecta</i> L.) for phytoremediation of heavy metal-polluted lateritic soil.	<b>Cd, Pb, Zn</b>	<i>Tagetes erecta</i> L.	Not suitable for large-scale agricultural or industrial applications.
28.	2021	Phytoremediation of heavy metals by the dominant mangrove associate species of Indian Sundarbans.	<b>Zn, Cu, Pb</b>	<i>Suaeda maritima</i> and <i>Salicornia brachiata</i>	Not suitable for large-scale agricultural or industrial applications.

Table Cont....



S. No.	Year	Title of the Article	Heavy Metal Studied	Species Studied	Scalability/Limitations
29.	2021	Bioaccumulation potential of indigenous plants for heavy metal phytoremediation in rural areas of Shaheed Bhagat Singh Nagar, Punjab (India).	<b>Cd, Cr, Co, Cu, Fe, Mn, and Zn</b>	<i>Ageratum conyzoides</i> (L.) L., <i>Amaranthus spinosus</i> L., <i>Amaranthus viridis</i> L., <i>Brassica napus</i> L., <i>Cannabis sativa</i> L., <i>Dalbergia sissoo</i> DC., <i>Duranta repens</i> L., <i>Dysphania ambrosioides</i> (L.) Mosyakin & Clemants, <i>Ficus infectoria</i> Roxb., <i>Ficus palmata</i> Forssk., <i>Ficus religiosa</i> L., <i>Ipomoea carnea</i> Jacq., <i>Medicago polymorpha</i> L., <i>Melia azedarach</i> L., <i>Morus indica</i> L., <i>Malva rotundifolia</i> L., <i>Panicum virgatum</i> L., <i>Parthenium hysterophorus</i> L., <i>Dolichos lablab</i> L., <i>Ricinus communis</i> L., <i>Rumex dentatus</i> L., <i>Senna occidentalis</i> (L.) Link, and <i>Solanum nigrum</i> L.	Potential for large-scale deployment, but depends on specific plant/tree species.
30.	2022	Bioaccumulation Factor (BAF) of heavy metals in green seaweed to assess the phytoremediation potential.	<b>Zn, Cu, Pb</b>	<i>Enteromorpha compressa</i>	Applicable for large-scale water bodies with similar heavy metal contamination.
31.	2022	Heavy Metal Absorption and Phytoremediation Capacity of Macrophytes of Polachira Wetland of Kollam District, Kerala, India.	<b>Zn, Cu, Pb, Fe, Cd, Cr</b>	<i>Hydrilla verticillata</i> , <i>Salvinia minima</i> , and <i>Eichornia crassipes</i>	Applicable for large-scale water bodies with similar heavy metal contamination. Risk of uncontrolled invasion.

Abbreviations: As-Arsenic, Cd-Cadmium, Cr-Chromium, Cu-Copper, Fe-Iron, Hg-Mercury, Mn-Manganese, Ni-Nickel, Pb-Lead, Se-Selenium, Zn-Zinc.

models. Agglomerative hierarchical clustering was done using SPSS software (version 25.0) for classifying the states based on the quantity of work done in them, and vegetation types were enlisted based on their applicability in different habitats as well as provinces/states. The rest of the graphical works and analysis were performed using MS Excel 2021 version.

## RESULTS AND DISCUSSION

### Current Knowledge of Phytoremediation in India

The amount of article publications in the field of phytoremediation has increased severely from 1994 to 2023, and based on this trend and subject matter importance in the current world scenario, it is predicted to increase more rapidly in the near future, especially till 2030 (due to *Decade on Ecological Restoration*). Based on the current knowledge available in India, most of the phytoremediation works have been performed on Shrubs (28.40%), closely followed by Tree species (26.28%) then Herbs (17.65%), Grasses (17.25%), and Aquatic Plants (10.43%) respectively. Since 2018, the implementation of phytoremediation activities in tree species has gradually increased, possibly due to the introduction of new technologies, which has somewhat overshadowed the drawback of the long rotation period, cost-intensive practices, and low survivability of trees. Other than that, grasses have also shown a boost in the field of phytoremediation as they are one of the pioneer taxa that

emerge and contribute to the initial and most important phytoremediation period of degraded land. Studies on the phytoremediation abilities of aquatic plants have also been taken into consideration in recent times to remediate heavy metals from water sources in different states of India (Fig. 5).

### Geographical Patterns and Clustering of Priority Areas for Phytoremediation Work in India

The study sites of the articles included in our review were collected throughout all states/union territories of India. Most of the phytoremediation works were confined in the Eastern states like West Bengal (114) and Odisha (103) as these states have very high depository of metallic and non-metallic minerals. The Southern states of Karnataka (78), Kerala (92), and Tamil Nadu (96) also contributed to large phytoremediation works in India as they also have a large depository of minerals under their surface, falling in cluster 5. Similarly, states associated with the Central region of India, including Chhattisgarh (56), Jharkhand (83), Bihar (53), Maharashtra (66), and Madhya Pradesh (72), also have the bulk of articles published in the field of phytoremediation because of availability of more mining industries and release of a larger quantity of heavy metals in the environment confining themselves into cluster 2 and 4. North-eastern states also contribute a small amount of phytoremediation work, mainly on aquatic habitats, i.e., a total of 85 articles distributed among the North Eastern states of India in which the major contributors are Assam and Mizoram falling into

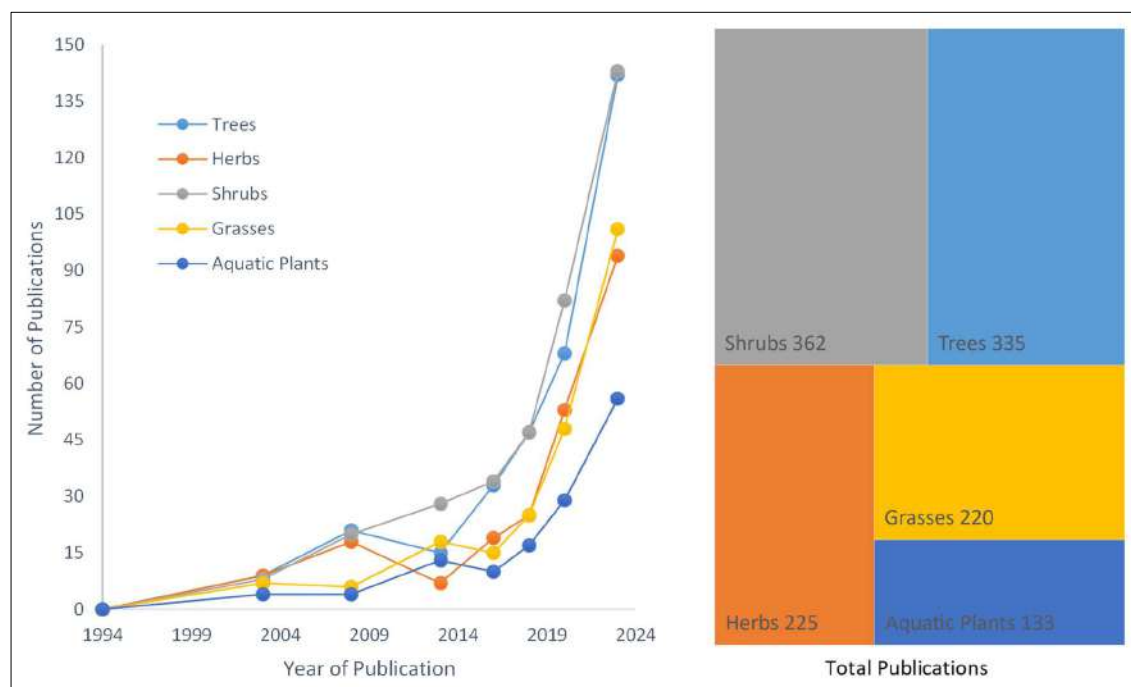


Fig. 5: Identified article publications from 1994 to June 2023 with reference to various plant types and their year-wise usage trend for the phytoremediation of heavy metals in India.

cluster 3 with some of the other North Indian states. The rest of the Indian states/Union territories (14) fall under cluster 1, which indicates the last article publications in such localities either due to low heavy metals availability in the environment or due to low research possibilities (Fig. 6).

### Briefing the Important Works on Phytoremediation of Heavy Metals in India

Parihar et al. (2021) explored the bioaccumulation potential of 23 plant species via bioaccumulation factor (BAF), metal accumulation index (MAI), translocation potential (Tf), and comprehensive bioconcentration index (CBCI) for seven heavy metals (cadmium, chromium, cobalt, copper, iron, manganese, and zinc). Although high bioaccumulation of individual metals was observed in herbs like *C. sativa*, *M. polymorpha*, and *Amaranthus spp.*, cumulatively, trees were found to be the better bioaccumulation of heavy metals. Heavy metals Zn, Cu, and Pb were examined by Agarwal et al. (2022) in the thallus body tissue of *Enteromorpha compressa* collected from 10 different sites in the lower Gangetic delta. Pb, followed by Zn and Cu, has the greatest value of all the studied heavy metals' bioaccumulation factors (BAF). Pb's higher BAF is a cause for serious concern because, in comparison to Zn and Cu, it is a more poisonous metal. The application of heavy metals had a substantial impact on the eucalyptus species (*E. tereticornis*,

*E. camaldulensis*, *E. globulus*, and *E. citriodora*) because it hindered the growth of seedlings' shoot and root lengths, total dry biomass, and germination percentage (Patil & Umadevi 2014). In a pot culture experiment conducted by Patil and Faizan (2017), three different concentrations of the metals lead and cadmium were imposed in the rhizosphere and non-rhizosphere soils. As a result of the toxicity of the various metal concentrations, the fungal population was significantly reduced.

By using pot tests, Madanan et al. (2021) investigated the potential of *Tagetes erecta* L. for phytoremediation of lateritic soil contaminated with cadmium (Cd), lead (Pb), and zinc (Zn). The total amount of heavy metals absorbed by the plant increased with increasing heavy metal concentration in the soil. Eight heavy metals (Cu, Mn, Zn, Ni, Fe, Cr, Cd, and Pb) were examined by Kumar et al. (2021) in the rhizosphere accumulation of *Phoenix paludosa* (Roxb.). The main findings demonstrated *Phoenix paludosa*'s phyto-accumulation behavior for several heavy metals and demonstrated its comparatively higher remediation capability for Cd and Cr contamination. In a pot culture experiment, Shanker et al. (2005) examined the ability of four different tree species—*Tectona grandis*, *Leucaena leucocephala*, *Albizia amara*, and *Casuarina equisetifolia*—to accumulate Cr in soils. *Albizia amara* has the potential to absorb Cr pollutants from soil, according to the experimental data.

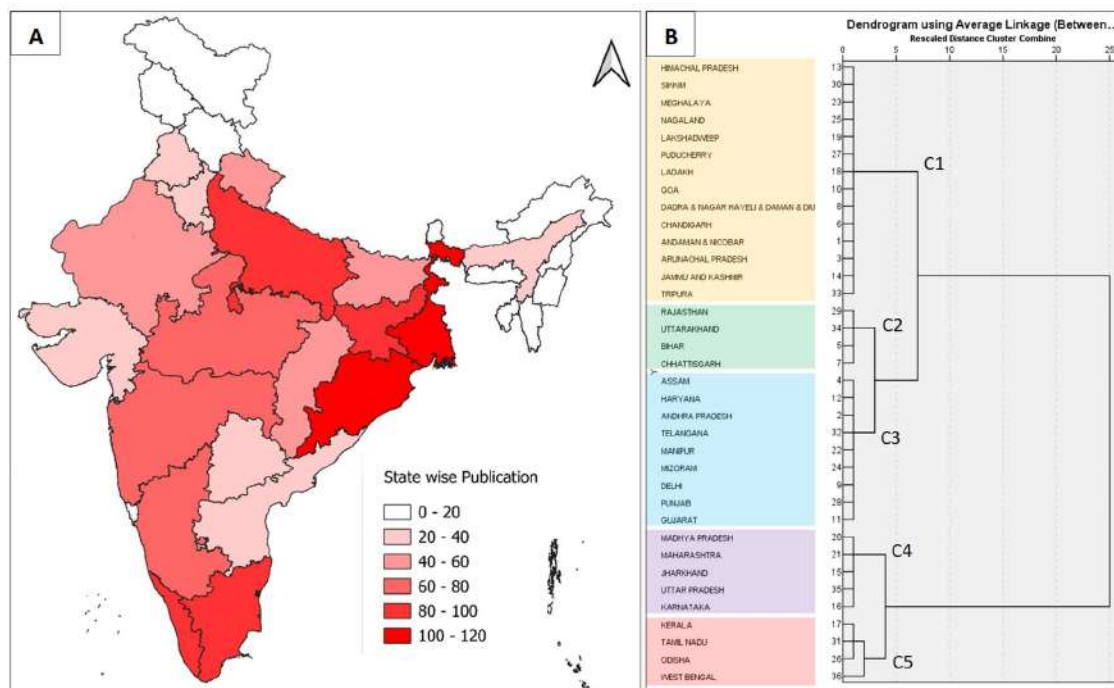


Fig. 6: A. State-wise heat map of India indicating the quantity of phytoremediation works done from 1994-June 2023, B. Hierarchical cluster analysis for classifying the phytoremediation works done in different states to identify the important zones of implementation of phytoremediation works and future possibilities in the zone.

*Salix acmophylla* can be utilized successfully as a tool for biomonitoring of different metal contaminations in soil and water bodies, according to research by Ali et al. (1999). According to the investigations, *S. acmophylla* has a great capacity for phytoremediation metal contamination in soils and water.

To determine the number of heavy metals present in the water and aquatic macrophytes (*Hydrilla verticillata*, *Salvinia minima*, and *Eichornia crassipes*) gathered from the Polachira wetland in the Kollam district of Kerala, Najila & Anila (2022) conducted research. The findings showed that the mean levels of heavy metals in aquatic macrophytes were in the following order: Fe>Zn>Pb>Cu>Cr>Cd. *Salvinia minima* were shown to be the hyperaccumulator of zinc, copper, lead, and cadmium among the three aquatic macrophytes, while *Hydrilla verticillata* exhibits the hyperaccumulation of iron and chromium, according to their research. The phytoremediation capacity of macrophytes found in the marshes of Assam, India, was investigated by Bora & Sarma (2020). The study claimed that some macrophytes are known to be hyperaccumulators of one or more metals or metalloids and that many native macrophytes are distributed globally, indicating a global interest in the field of phytoremediation research. The potential of water fern (*Azolla pinnata* R.Br.) for phyto-treating Integrated

Industrial Effluent (IIE) was examined by Kumar et al. (2020). The findings of this study indicated that *A. pinnata* was useful for the environmentally friendly treatment of SIIDCUL IIE and might reduce potential wastewater management concerns. According to that, this was the first report on the phytoremediation of IIE.

For the phytoremediation of As, Cd, and Pb-contaminated water bodies, Ghosh (2010) researched a few aquatic plants. His research revealed that *Ipomoea aquatica* is a potential Cd accumulator but a little less prospective As and Pb accumulator. Similar to this, another aquatic species, *Hydrilla verticillata*, has a high potential for phytoremediation of both As and Cd. It is also an efficient accumulator of As and Cd from contaminated water, but it is less effective at doing so for Pb. Adhikari et al. (2010) assessed the potential of *Typha angustifolia* and *Ipomoea carnea*, two kinds of aquatic plants, for phytoextraction of lead. They noticed that both plants are demonstrating promise for removing Pb from contaminated water sources. The phytoremediation capacity of *Typha angustifolia* against various heavy metals was also examined by Chandra & Yadav (2010). They concluded that under favorable circumstances, *T. angustifolia* can actively phytoremediate heavy metals from wastewater.

Maiti & Jaiswal (2008) studied five dominant vegetation, namely, *Typha latifolia*, *Fimbristylis dichotoma*, *Amaranthus*

*defluxes*, *Saccharum spontaneum*, and *Cynodon dactylon* in West Bengal (India). The study infers that natural vegetation removed Mn by phytoextraction mechanisms ( $TF > 1$ ), while other metals like Zn, Cu, Pb, and Ni were removed by rhizofiltration mechanisms ( $TF < 1$ ). The field study revealed that *T. latifolia* and *S. spontaneum* plants could be used for bioremediation of fly ash lagoon. Mukherjee et al. (2021), in the high salinity supralittoral zone of the Indian Sundarbans, the phytoremediation capacity of two prominent mangrove association species, *Suaeda maritima* and *Salicornia brachiata*, was investigated for the remediation of zinc (Zn), copper (Cu), and lead (Pb). It was proposed that these halophytes may be employed as phytoremediation agents and that cultivating them would be beneficial for ecorestoration in relation to mild contaminants.

Similarly, Prasad (2007), reviewed various tree species and the type of heavy metals they can remediate based on the mining sites in the Indian subcontinent (Table 2). The study showed:

According to Singh et al. (2015), *Vetiveria zizanioides* was able to remove 77–78% of Cr and 80–94% of Pb from synthetic wastewater samples with concentrations of 5–20 mg.L<sup>-1</sup> of Cr and Pb, demonstrating the aromatic plant's potential for phytoremediation. The phytoremediation capacity for Cd contaminations of three fragrant types of grass, *Cymbopogon martini*, *Cymbopogon flexuosus*, and *Vetiveria zizanioides*, was investigated by Lal et al. (2008b). They concluded that *V. zizanioides* can repair Cd-contaminated soils up to a specific degree during their studies.

To explore the hyperaccumulation of heavy metals, Purakavastha et al. (2009) looked at five varieties of mustard: *Brassica juncea* (Indian mustard), *Brassica campestris* (Yellow mustard), *Brassica carinata* (Ethiopian mustard), *Brassica napus*, and *Brassica nigra*. *Brassica carinata*

of the cv. DLSC1 variety was shown to reduce the metal load for Pb by 12%, Zn by 15%, and Ni by 11%. Lal et al. (2008a) investigated the phytoremediation capacity of three flower crops in Karnal for Cd-contaminated soils: chrysanthemum (*Chrysanthemum indicum*), marigold (*Tagetes erecta*) and gladiolus (*Gladiolus grandiflorus*). They discovered during their research that *G. grandiflorus* had the highest concentration of Cd and may be able to remediate moderately contaminated soils. Rathore et al. (2017) studied the phytoremediation process for removing toxic metals from soil using metal-accumulating plants like Brassica sp., including Indian mustard (*Brassica juncea*). They discovered that the addition of organic matter, organic chelates, soil amendments, use of suitable cropping systems, intercrops, and fertilizer choice can improve Indian mustard's phytoremediation capacity.

Ramana et al. (2008a, 2008b, 2009, 2012a, 2012b) carried out significant research employing xerophytes (such as *Agave angustifolia*, *Euphorbia milli*, *Furcraea gigantea*, etc.) and flowering shrubs (aster, tuberose, rose marigold, chrysanthemum, dahlia, gladiolus, etc.). *Chrysanthemum* phytostabilizes Cd-contaminated soils, but marigold and tuberose can hyper-accumulate in Cd-contaminated soils with moderate to medium degrees of contamination, according to the study. To determine their capacity for Cd phytoextraction, Ghosh & Singh (2005b) compared the high biomass-producing weeds *Datura innoxia*, *Ipomoea carnea*, and *Phragmites karka* to the indicator species *Brassica campestris* and *Brassica juncea*. According to them, *B. juncea* and *I. carnea* accumulated the most Cd, whereas *P. karka* and *D. innoxia* were the best species for phytoextraction of Cd-affected soil.

To grow *H. annuus* plants, Chauhan & Mathur (2020) used industrially polluted soil that was gathered from diverse areas of Jaipur (Rajasthan), Kashipur, Jaspur, and Bajpur

Table 2: Suitable plant species for different mining sites in India.

Mining Sites	Suitable Plant Species for Restoration
Coal mine spoils of Central India	<i>Acacia auriculiformis</i> , <i>Acacia nilotica</i> , <i>Dalbergia sissoo</i> , <i>Pongamia pinnata</i> , <i>Eucalyptus hybrid</i> , <i>Eucalyptus camaldulensis</i> , etc.
Limestone mine spoils of Northern areas	<i>Acacia catechu</i> , <i>Ipomea carnea</i> , <i>Eulaliopsis binata</i> , <i>Salix tetrasperma</i> , <i>Leucaena leucocephala</i> , <i>Bauhinia retusa</i> , <i>Pennisetum purpureum</i> , <i>Agave americana</i> , <i>Erythrina suberosa</i> , etc.
Bauxite mine spoils of Central India	<i>Eucalyptus camaldulensis</i> , <i>Shorea robusta</i> , <i>Grevillea pteridifolia</i> , etc.
Lignite mine spoils of Tamil Nadu	<i>Acacia</i> sp., <i>Eucalyptus species</i> , <i>Leucaena leucocephala</i> , and <i>Agave</i> sp.
Rock-phosphate mine spoils of Uttarakhand.	<i>Acacia catechu</i> , <i>Dalbergia sissoo</i> , <i>Leucaena leucocephala</i> , <i>Pennisetum purpureum</i> , <i>Saccharum spontaneum</i> , <i>Vitex negundo</i> , and <i>Salix tetrasperma</i> etc.
Iron ore spoils of Orissa	<i>Albizia lebbeck</i> , <i>Leucaena leucocephala</i> , etc.
Mica, copper, dolomite, and limestone mine spoils of Rajasthan	<i>Prosopis juliflora</i> , <i>Salvadora oleoides</i> , <i>Tamarix articulata</i> , <i>Ziziphus nummularia</i> , <i>Acacia tortilis</i> , <i>Acacia senegal</i> , <i>Acacia catechu</i> , <i>Cynodon dactylon</i> , <i>D. annulatum</i> , <i>Cenchrus setigerus</i> , <i>Cymbopogon</i> sp., etc.

Source: Prasad (2007)



(Uttarakhand), India. These industries included plastic, paper, dye, and textiles. As evidenced by the reduction in growth characteristics compared to the standard, the results showed that industrial-contaminated soil had a considerable negative impact on the plantlets of *H. annuus*. This information was useful for decontaminating industrial soil that had been severely impacted. Chowdhury et al. (2021) studied the usage of *Avicennia officinalis*, *Porteresia coarctata*, and *Acanthus ilicifolius* for bioaccumulation of potentially toxic elements (Cd, Cr, Cu, Hg, Mn, Ni, Pb, and Zn). Mercury showed the highest but Pb has the lowest bioaccumulation potential in all three plants. Among these three heavy metals, Hg showed the highest bioaccumulation in *A. officinalis*, and Cd in *P. coarctata*. For the phytoremediation of As-contaminated soils, Das et al. (2005) found the utilization of weed species, including *Lantana camara*, *Vitis trifolia*, *Ludwigia parviflora*, *Eleusine indica*, *Enhydra*, and *Filmbristylis sp.* They noticed enhanced arsenic accumulation with 2–14 mg As kg<sup>-1</sup> in the above-ground sections of these weeds growing in polluted soils, and the weed species has a strong potential to behave as a hyperaccumulator for arsenic.

### Limitations of Phytoremediation

According to the current study, phytoremediation can be said as the best technique for the remediation of heavy metal but still suffers the following limitations as a management technique for heavy metal contamination:

1. Due to some hyperaccumulators having a slow growth rate and less production of biomass the efficiency of phytoremediation is less.
2. The process of phytoremediation is time-consuming as the time required for the removal of heavy metal from contaminated soil or water is long.
3. Chances of risk creation in the food chain as mismanagement and improper techniques can lead to contamination of the food chain.
4. Low mobilization effect due to some tightly bound metal ions that act as heavy metals for plants.

### Phytoremediation in Interdisciplinary Research Fields

The phytoremediation technique requires knowledge of ecology, plant biology, soil chemistry, microbiology, and environmental engineering. The current state and trajectory in these fields of scientific knowledge integration approach support a successful future resolution of this issue. Phytoremediation is indeed a topic that intersects with various interdisciplinary research fields due to its potential to address environmental pollution. Phytoremediation's interdisciplinary nature allows researchers from various fields to collaborate and develop innovative solutions for addressing environmental pollution challenges (Fig. 7). Here are some of the interdisciplinary aspects of phytoremediation:

1. **Ecology:** Phytoremediation can impact local ecosystems.

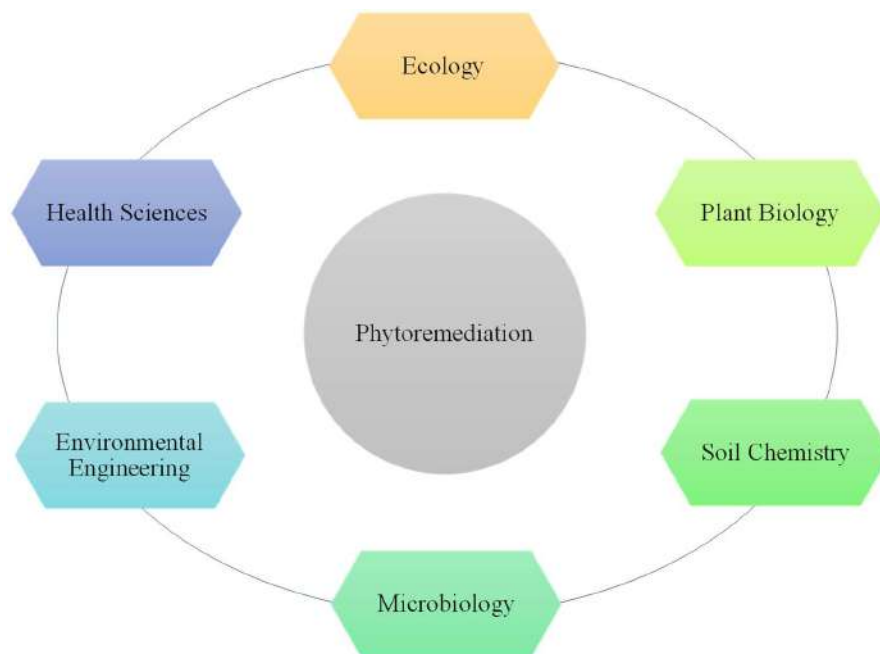


Fig. 7: Phytoremediation in interdisciplinary research fields allows researchers from various fields to collaborate and develop innovative solutions.

Ecologists study the ecological effects of introducing specific plant species for remediation and their interactions with local flora and fauna.

2. **Plant Biology:** Understanding the biology of plants, their physiological responses to contaminants, and their genetic traits for tolerance or accumulation of pollutants is crucial in phytoremediation research.
3. **Soil Chemistry:** Soil composition and chemistry play a significant role in phytoremediation. Soil scientists investigate how plants interact with soil properties and how these interactions affect pollutant removal.
4. **Microbiology:** Genetic modification of plants for enhanced pollutant tolerance or accumulation is an area of ongoing research. Biotechnologists work on developing engineered plants for more effective phytoremediation.
5. **Environmental Engineering:** Engineers design and implement phytoremediation systems, such as constructed wetlands or phytoextraction setups, to maximize pollutant removal.
6. **Health Sciences:** Some pollutants may pose health risks to humans and animals. Researchers in health sciences assess the impact of phytoremediation on reducing these risks.

## CONCLUSIONS AND FUTURE PERSPECTIVES

Phytoremediation is yet in its infancy on a global scale, and its advantages and disadvantages in practical applications are still unclear. Compared to other treatments, bioremediation procedures, particularly phytoremediation, are generally simple to apply and don't require expensive equipment or highly skilled workers. Despite effectively lessening the harmful effects of heavy metals, phytoremediation is still not commercially viable in India. In parallel, efforts to find hyperaccumulation coding genes for certain heavy metals in plants are ongoing to create a "Superbug" plant that may be used in phytoremediation. Tree biomass production is impacted by the significant negative correlations that exist between heavy metals and tree physiology. The studies showed us a pathway for the implementation and management of remediation methods to reduce the heavy metal stress exerted on plants and enhance the metabolic and physiochemical processes of the plant. Reduced heavy metal stress increases the growth and developmental characteristics of plants as well as nourishes the environment, resulting in better carbon sequestration ability, restricting land degradation, preventing erosion, purifying the water, and modifying the temperature against the effects of climate extremes in disturbed areas and hence mitigates the impact of climate change.

## ACKNOWLEDGMENTS

The authors would like to thank Mr. Chityendra Dewangan, Department of Forestry, Wildlife, and Environmental Sciences, Guru Ghasidas Vishwavidyalaya, Bilaspur, Chhattisgarh, for his assistance in the graphical upgradation of the article.

## REFERENCES

- Adhikari, T., Kumar, A., Singh, M.V. and Rao, A.S., 2010. Phytoaccumulation of lead by selected wetland plant species. *Communications in Soil Science and Plant Analysis*, 41(22), pp.2623-2632. [DOI]
- Adnan, M., Xiao, B., Xiao, P., Zhao, P. and Bibi, S., 2022a. Heavy metal, waste, COVID-19, and rapid industrialization in this modern era—Fit for a sustainable future. *Sustainability*, 14(8), p.4746. [DOI]
- Adnan, M., Xiao, B., Xiao, P., Zhao, P., Li, R. and Bibi, S., 2022. Research progress on heavy metals pollution in the soil of smelting sites in China. *Toxics*, 10(5), p.231. [DOI]
- Agarwal, S., Albeshr, M.F., Mahboob, S., Atique, U., Pramanick, P. and Mitra, A., 2022. Bioaccumulation Factor (BAF) of heavy metals in green seaweed to assess the phytoremediation potential. *Journal of King Saud University-Science*, 34(5), p.102078. [DOI]
- Ahmad, Z., Khan, S.M., Page, S.E., Balzter, H., Ullah, A., Ali, S., Jehangir, S., Ejaz, U., Afza, R., Razzaq, A. and Mukhamezhanova, A.S., 2023. Environmental sustainability and resilience in a polluted ecosystem via phytoremediation of heavy metals and plant physiological adaptations. *Journal of Cleaner Production*, 385, p.135733. [DOI]
- Ali, H., Khan, E. and Sajad, M.A., 2013. Phytoremediation of heavy metals—concepts and applications. *Chemosphere*, 91(7), pp.869-881. [DOI]
- Ali, M.B., Tripathi, R.D., Rai, U.N., Pal, A. and Singh, S.P., 1999. Physico-chemical characteristics and pollution level of Lake Nainital (UP, India): Role of macrophytes and phytoplankton in biomonitoring and phytoremediation of toxic metal ions. *Chemosphere*, 39(12), pp.2171-2182. [DOI]
- Bhandari, S., Kukreja, S., Singh, B., Kumar, V., Gautam, S., Sharma, V., Mittal, U. and Goutam, U., 2023. Relationship between Microbes and the Environment for Sustainable Ecosystem Services. *Elsevier*, pp. 243-259. [DOI]
- Bhat, N.A., Bhat, A.A., Guha, D.B. and Singh, B.P., 2023. Vertical distribution of heavy metals in Karewa deposits of South Kashmir: environmental contamination and health risk assessment. *International Journal of Environmental Science and Technology*, 20(1), pp.369-382. [DOI]
- Bhat, S.A., Bashir, O., Haq, S.A.U., Amin, T., Rafiq, A., Ali, M., Américo-Pinheiro, J.H.P. and Sher, F., 2022. Phytoremediation of heavy metals in soil and water: An eco-friendly, sustainable and multidisciplinary approach. *Chemosphere*, 303, p.134788. [DOI]
- Bora, M.S. and Sarma, K.P., 2020. Phytoremediation of heavy metals/metalloids by native herbaceous macrophytes of wetlands: Current research and perspectives. In: Kumar, M., Snow, D., Honda, R. (eds.) *Emerging Issues in the Water Environment during Anthropocene*. Springer, pp.261-284. [DOI]
- Boum-Nkot, S.N., Nlend, B., Kombi, D., Ndong, G.N., Bello, M., Fongoh, E.J., Ntamak-Nida, M.J. and Etame, J., 2023. Hydrochemistry and assessment of heavy metals groundwater contamination in an industrialized city of sub-Saharan Africa (Douala, Cameroon). Implication on human health. *HydroResearch*, 6, pp.52-64. [DOI]
- Chandra, R. and Yadav, S., 2010. Potential of *Typha angustifolia* for phytoremediation of heavy metals from aqueous solution of phenol and melanoidin. *Ecological Engineering*, 36(10), pp.1277-1284. [DOI]

- Chauhan, P. and Mathur, J., 2020. Phytoremediation efficiency of *Helianthus annuus* L. for reclamation of heavy metals-contaminated industrial soil. *Environmental Science and Pollution Research*, 27(24), pp.29954-29966. [DOI]
- Chen, D., Wang, X., Luo, X., Huang, G., Tian, Z., Li, W. and Liu, F., 2023. Delineating and identifying risk zones of soil heavy metal pollution in an industrialized region using machine learning. *Environmental Pollution*, 318, p.120932. [DOI]
- Chowdhury, A., Naz, A. and Maiti, S.K., 2021. Bioaccumulation of potentially toxic elements in three mangrove species and human health risk due to their ethnobotanical uses. *Environmental Science and Pollution Research*, 28, pp.33042-33059. [DOI]
- Collin, S., Baskar, A., Geevarghese, D.M., Ali, M.N.V.S., Bahubali, P., Choudhary, R., Lviv, V., Tovar, G.I., Senatov, F., Koppala, S. and Swamiappan, S., 2022. Bioaccumulation of lead (Pb) and its effects in plants: A review. *Journal of Hazardous Materials Letters*, 3, p.100064. [DOI]
- DalCorso, G., Farinati, S. and Furini, A., 2010. Regulatory networks of cadmium stress in plants. *Plant Signaling & Behavior*, 5(6), pp.663-667. [DOI]
- Das, I., Ghosh, K. and Sanyal, S.K., 2005. Phytoremediation: a potential option to mitigate arsenic contamination in the soil-water-plant system. *Everyman's Sci*, 40(2), pp.115-123.
- Devi, P. and Kumar, P., 2020. Concept and application of phytoremediation in the fight of heavy metal toxicity. *Journal of Pharmaceutical Sciences and Research*, 12(6), pp.795-804.
- Dixit, R., Wasiullah, X., Malaviya, D., Pandiyan, K., Singh, U.B., Sahu, A., Shukla, R., Singh, B.P., Rai, J.P., Sharma, P.K. and Lade, H., 2015. Bioremediation of heavy metals from soil and aquatic environment: an overview of principles and criteria of fundamental processes. *Sustainability*, 7(2), pp.2189-2212. [DOI]
- Fashola, M.O., Ngole-Jeme, V.M. and Babalola, O.O., 2016. Heavy metal pollution from gold mines: environmental effects and bacterial strategies for resistance. *International Journal of Environmental Research and Public Health*, 13(11), p.1047. [DOI]
- Gamalero, E., Lingua, G., Berta, G. and Glick, B.R., 2009. The beneficial role of plant growth-promoting bacteria and arbuscular mycorrhizal fungi on plant responses to heavy metal stress. *Canadian Journal of Microbiology*, 55(5), pp.501-514. [DOI]
- García-Montelongo, A.M., Montoya-Martínez, A.C., Morales-Sandoval, P.H., Parra-Cota, F.I. and de Los Santos-Villalobos, S., 2023. Beneficial microorganisms as a sustainable alternative for mitigating biotic stresses in crops. *Stresses*, 3(1), pp.210-228. [DOI]
- Geleta, G.S., 2023. A colorimetric aptasensor based on two dimensional (2D) nanomaterial and gold nanoparticles for detection of toxic heavy metal ions: A review. *Food Chemistry Advances*, 2, p.100184. [DOI]
- Ghosh, M. and Singh, S.P., 2005a. A comparative study of cadmium phytoextraction by accumulator and weed species. *Environmental Pollution*, 133(2), pp.365-371. [DOI]
- Ghosh, M. and Singh, S.P., 2005b. A review on phytoremediation of heavy metals and utilization of its by-products. *Asian Journal of Energy and Environment*, 6(4), p.18.
- Ghosh, S., 2010. Wetland macrophytes as toxic metal accumulators. *International Journal of Environmental Sciences*, 1(4), pp.523-528.
- Gull, A., Lone, A.A. and Wani, N.U.I., 2019. Biotic and Abiotic Stresses in Plants. *IntechOpen*, pp.1-9. [DOI]
- Gunwal, I., Mathur, R., Agrawal, Y. and Mago, P., 2021. Plants are useful for the phytoremediation of soil and water in India. *Asian Journal of Plant and Soil Sciences*, 19, pp.103-110.
- Gupta, S.D., 2010. *Reactive Oxygen Species and Antioxidants in Higher Plants*. CRC Press, pp.193-220.
- Kumar, M., Mohapatra, S., Karim, A.A. and Dhal, N.K., 2021. Heavy metal fractions in rhizosphere sediment vis-à-vis accumulation in *Phoenix paludosa* (Roxb.) mangrove plants at Dhamra Estuary of India: Assessing phytoremediation potential. *Chemistry and Ecology*, 37(1), pp.1-14. [DOI]
- Kumar, V., Kumar, P., Singh, J. and Kumar, P., 2020. The potential of water fern (*Azolla pinnata* R. Br.) in phytoremediation of integrated industrial effluent of SIIDCUL, Haridwar, India: removal of physicochemical and heavy metal pollutants. *International Journal of Phytoremediation*, 22(4), pp.392-403. [DOI]
- Lal, K., Minhas, P.S., Chaturvedi, R.K. and Yadav, R.K., 2008a. Extraction of cadmium and tolerance of three annual cut flowers on Cd-contaminated soils. *Bioresource Technology*, 99(5), pp.1006-1011. [DOI]
- Lal, K., Minhas, P.S., Chaturvedi, R.K. and Yadav, R.K., 2008b. Cadmium uptake and tolerance of three aromatic grasses on the Cd-rich soil. *Journal of the Indian Society of Soil Science*, 56(3), pp.290-294.
- Li, F.J., Yang, H.W., Ayyamperumal, R. and Liu, Y., 2022. Pollution, sources, and human health risk assessment of heavy metals in urban areas around industrialization and urbanization-Northwest China. *Chemosphere*, 308, p.136396. [DOI]
- Madanan, M.T., Shah, I.K., Varghese, G.K. and Kaushal, R.K., 2021. Application of Aztec Marigold (*Tagetes erecta* L.) for phytoremediation of heavy metal-polluted lateritic soil. *Environmental Chemistry and Ecotoxicology*, 3, pp.17-22. [DOI]
- Maiti, S.K. and Jaiswal, S., 2008. Bioaccumulation and translocation of metals in the natural vegetation growing on fly ash lagoons: a field study from Santaldih thermal power plant, West Bengal, India. *Environmental Monitoring and Assessment*, 136, pp.355-370. [DOI]
- Mandal, A., Purakayastha, T.J., Ramana, S., Neenu, S., Bhaduri, D., Chakraborty, K., Manna, M.C. and Rao, A.S., 2014. Status on phytoremediation of heavy metals in India: A review. *International Journal of Bio-resource and Stress Management*, 5, pp.553-560. [DOI]
- Mukherjee, P., Pramanick, P., Zaman, S. and Mitra, A., 2021. Phytoremediation of heavy metals by the dominant mangrove associate species of Indian Sundarbans. *Journal of Environmental Engineering and Landscape Management*, 29(4), pp.391-402. [DOI]
- Najila, N. and Anila, G., 2022. Heavy Metal Absorption and Phytoremediation Capacity of Macrophytes of Polachira Wetland of Kollam District, Kerala, India. *Research Journal of Chemistry and Environment*, 26(1), pp.90-96.
- Oladoye, P.O., Olowe, O.M. and Asemoloye, M.D., 2022. Phytoremediation technology and food security impacts of heavy metal contaminated soils: A review of the literature. *Chemosphere*, 288, p.132555. [DOI]
- Parihar, J.K., Parihar, P.K., Pakade, Y.B. and Katnoria, J.K., 2021. Bioaccumulation potential of indigenous plants for heavy metal phytoremediation in rural areas of Shaheed Bhagat Singh Nagar, Punjab (India). *Environmental Science and Pollution Research*, 28, pp.2426-2442. [DOI]
- Patil, G. and Faizan, M., 2017. Effect of lead and cadmium on the fungal population in rhizosphere soils of eucalyptus species. *Environment & Ecology*, 35(4A), pp.2965-2970.
- Patil, G. and Umadevi, M., 2014. Cadmium and lead effect on growth parameters of four eucalyptus species. *International Journal of Bioscience*, 5, pp.72-79. [DOI]
- Prasad, M.N.V., 2007. Phytoremediation in India. In: Willey, N. (eds.) *Phytoremediation: Methods and Reviews*. Humana Press, pp.435-454. [DOI]
- Purakayastha, T.J., Bhadraray, S. and Chhonkar, P.K., 2009. Screening of brassica species for hyper-accumulation of zinc, copper, lead, nickel, and cadmium. *Indian Journal of Plant Physiology (India)*, 14(4), pp.344-352.
- Rahman, S.U., Nawaz, M.F., Gul, S., Yasin, G., Hussain, B., Li, Y. and Cheng, H., 2022. State-of-the-art OMICS strategies against toxic effects of heavy metals in plants: A review. *Ecotoxicology and Environmental Safety*, 242, p.113952. [DOI]
- Rai, G.K., Bhat, B.A., Mushtaq, M., Tariq, L., Rai, P.K., Basu, U., Dar,

- A.A., Islam, S.T., Dar, T.U. and Bhat, J.A., 2021. Insights into decontamination of soils by phytoremediation: A detailed account of heavy metal toxicity and mitigation strategies. *Physiologia Plantarum*, 173(1), pp.287-304. [DOI]
- Ramana, S., Biswas, A.K., Ajay, A. and Rao, A.S., 2008a. Phytoextraction of lead by marigold and chrysanthemum. *Indian Journal of Plant Physiology (India)*, 191, p.652.
- Ramana, S., Biswas, A.K., Ajay, A. and Rao, A.S., 2009. Phytoremediation of cadmium-contaminated soils by marigold and chrysanthemum. *National Academy Science Letters*, 32(11/12), pp.333-336.
- Ramana, S., Biswas, A.K., Ajay, A., Singh, A.B. and Rao, A.S., 2008b. Tolerance and bioaccumulation of cadmium and lead by gladiolus. *National Academy Science Letters*, 31(11&12), pp.327-332.
- Ramana, S., Biswas, A.K., Ajay, Singh, A.B. and Ahirwar, N.K., 2012a. Phytoremediation of chromium by tuberose. *National Academy Science Letters*, 35, pp.71-73. [DOI]
- Ramana, S., Biswas, A.K., Singh, A.B., Ajay, A., Kumar, P.N., Ahirwar, N.K., Behera, S.K. and Rao, A.S., 2012b. Phytoremediation of cadmium-contaminated soils by tuberose. *Indian Journal of Plant Physiology*, 17(1), pp.61-64.
- Rashid, A., Ayub, M., Ullah, Z., Ali, A., Sardar, T., Iqbal, J., Gao, X., Bundschuh, J., Li, C., Khattak, S.A. and Ali, L., 2023. Groundwater quality, health risk assessment, and source distribution of heavy metals contamination around chromite mines: Application of GIS, sustainable groundwater management, geostatistics, PCAMLR, and PMF receptor model. *International Journal of Environmental Research and Public Health*, 20(3), p.2113. [DOI]
- Rathore, S.S., Shekhawat, K., Dass, A., Kandpal, B.K. and Singh, V.K., 2017. Phytoremediation mechanism in Indian mustard (*Brassica juncea*) and its enhancement through agronomic interventions. *Proceedings of the National Academy of Sciences, India Section B: Biological Sciences*, 89, pp.419-427. [DOI]
- Riyazuddin, R., Nisha, N., Ejaz, B., Khan, M.I.R., Kumar, M., Ramteke, P.W. and Gupta, R., 2021. A comprehensive review of the heavy metal toxicity and sequestration in plants. *Biomolecules*, 12(1), p.43. [DOI]
- Rosyidah, A., Lestari, M.W. and Syam, N., 2023. Pattern of lead accumulation in two vegetable plants due to EDTA treatment. *Nature Environment & Pollution Technology*, 22(4), p.612.
- Saravanan, A., Kumar, P.S., Ramesh, B. and Srinivasan, S., 2022. Removal of toxic heavy metals using genetically engineered microbes: Molecular tools, risk assessment and management strategies. *Chemosphere*, 298, p.134341. [DOI]
- Shah, P., Patil, G. and Sharma, D., 2022. Assessment of ecological restoration success and vegetation dynamics through spatial-temporal change detection in Gevra opencast mine, Korba coalfield, India. *Ecology, Environment and Conservation*, 28, pp.496-503. [DOI]
- Shanker, A.K., Ravichandran, V. and Pathmanabhan, G., 2005. Phytoaccumulation of chromium by some multipurpose-tree seedlings. *Agroforestry Systems*, 64, pp.83-87. [DOI]
- Sharma, A., Kapoor, D., Gautam, S., Landi, M., Kandhol, N., Araniti, F., Ramakrishnan, M., Satish, L., Singh, V.P., Sharma, P. and Bhardwaj, R., 2022. Heavy metal induced regulation of plant biology: Recent insights. *Physiologia Plantarum*, 174(3), p.e13688. [DOI]
- Sharma, J.K., Kumar, N., Singh, N.P. and Santal, A.R., 2023. Phytoremediation technologies and their mechanism for removal of heavy metal from contaminated soil: An approach for a sustainable environment. *Frontiers in Plant Science*, 14, p.1076876. [DOI]
- Singh, R.K. and Bajpai, S., 2023. State-of-the-art overview of biological treatment of polluted water from rice mills and imminent technologies with green energy retrieval. *Nature Environment & Pollution Technology*, 22(4).
- Singh, S., Maiti, S.K. and Raj, D., 2023. An approach to quantify heavy metals and their source apportionment in coal mine soil: a study through PMF model. *Environmental Monitoring and Assessment*, 195(2), p.306. [DOI]
- Singh, V., Thakur, L. and Mondal, P., 2015. Removal of lead and chromium from synthetic wastewater using *Vetiveria zizanioides*. *CLEAN–Soil, Air, Water*, 43(4), pp.538-543. [DOI]
- Tiwari, S. and Lata, C., 2018. Heavy metal stress, signaling, and tolerance due to plant-associated microbes: an overview. *Frontiers in Plant Science*, 9, p.452. [DOI]
- Triassi, M., Cerino, P., Montuori, P., Pizzolante, A., Trama, U., Nicodemo, F., D'Auria, J.L., De Vita, S., De Rosa, E. and Limone, A., 2023. Heavy metals in groundwater of southern Italy: Occurrence and potential adverse effects on the environment and human health. *International Journal of Environmental Research and Public Health*, 20(3), p.1693. [DOI]
- Uluṭaṣ, K., 2022. Risk assessment and spatial distribution of heavy metal in street specks of dust in the densely industrialized area. *Environmental Monitoring and Assessment*, 194(2), p.99. [DOI]
- US Department of Health and Human Services, 2005. Agency for toxic substances and disease registry. 2007. *Toxicological profile for lead*.
- Verma, S., Nizam, S. and Verma, P.K., 2013. Biotic and abiotic stress signaling in plants. In: Sarwat, M., Ahmad, A., Abidin, M. (eds.) *Stress Signaling in Plants: Genomics and Proteomics Perspective*, Vol.1, Springer, pp.25-49. [DOI]
- Villiers, F., Ducruix, C., Hugouvieux, V., Jarno, N., Ezan, E., Garin, J., Junot, C. and Bourguignon, J., 2011. Investigating the plant response to cadmium exposure by proteomic and metabolomic approaches. *Proteomics*, 11(9), pp.1650-1663. [DOI]
- Yan, X., An, J., Yin, Y., Gao, C., Wang, B. and Wei, S., 2022. Heavy metals uptake and translocation of typical wetland plants and their ecological effects on the coastal soil of a contaminated bay in Northeast China. *Science of the Total Environment*, 803, p.149871. [DOI]
- Yang, L., Wang, J., Yang, Y., Li, S., Wang, T., Oleksak, P., Chrienova, Z., Wu, Q., Nepovimova, E., Zhang, X. and Kuca, K., 2022. Phytoremediation of heavy metal pollution: Hotspots and future prospects. *Ecotoxicology and Environmental Safety*, 234, p.113403. [DOI]
- Yang, X., Ren, J., Li, J., Lin, X., Xia, X., Yan, W., Zhang, Y., Deng, X. and Ke, Q., 2023. Meta-analysis of the effect of melatonin application on abiotic stress tolerance in plants. *Plant Biotechnology Reports*, 17(1), pp.39-52. [DOI]
- Zaynab, M., Al-Yahyai, R., Ameen, A., Sharif, Y., Ali, L., Fatima, M., Khan, K.A. and Li, S., 2022. Health and environmental effects of heavy metals. *Journal of King Saud University-Science*, 34(1), p.101653. [DOI]
- Zerizghi, T., Guo, Q., Tian, L., Wei, R. and Zhao, C., 2022. An integrated approach to quantify ecological and human health risks of soil heavy metal contamination around the coal mining area. *Science of the Total Environment*, 814, p.152653. [DOI]
- Zheng, K., Zeng, Z., Tian, Q., Huang, J., Zhong, Q. and Huo, X., 2023. Epidemiological evidence for the effect of environmental heavy metal exposure on the immune system in children. *Science of the Total Environment*, 868, p.161691. [DOI]
- Zukauskaite, A., Jakubauskaite, V., Belous, O., Ambrazaitiene, D. and Stasiskiene, Z., 2008. Impact of heavy metals on the oil products biodegradation process. *Waste Management & Research*, 26(6), pp.500-507. [DOI]



# Comparative Analysis of Mulching and Weed Management Practices on Nutrient and Weed Dynamics of Kharif Sorghum (*Sorghum bicolor* L.)

Abhinav Thakur<sup>1</sup>, Hina Upadhyay<sup>1†</sup> , Lalit Saini<sup>1</sup>, Tarun Sharma<sup>1</sup> and Himanshu Saini<sup>2</sup>

<sup>1</sup>Department of Agronomy, School of Agriculture, Lovely Professional University, Phagwara-144001, Punjab, India

<sup>2</sup>Department of Silviculture and Agroforestry, COHF, Neri, Dr. YSP University of Horticulture and Forestry, Nauni, Himachal Pradesh, India

†Corresponding author: Hina Upadhyay; hina\_bostan@yahoo.com

**Abbreviation:** Nat. Env. & Poll. Technol.  
**Website:** www.neptjournal.com

*Received:* 20-06-2024

*Revised:* 26-07-2024

*Accepted:* 01-08-2024

## Key Words:

Mulching  
 Nutrients  
 Sorghum  
 Sustainable weed management  
 Yield

## Citation for the Paper:

Thakur, A., Upadhyay, H., Saini, L., Sharma, T. and Saini, H., 2025. Comparative analysis of mulching and weed management practices on nutrient and weed dynamics of Kharif Sorghum (*Sorghum bicolor* L.). *Nature Environment and Pollution Technology*, 24(2), p. B4234. <https://doi.org/10.46488/NEPT.2025.v24i02.B4234>

*Note: From year 2025, the journal uses Article ID instead of page numbers in citation of the published articles.*



**Copyright:** © 2025 by the authors

**Licensee:** Technoscience Publications

This article is an open access article distributed under the terms and conditions of the Creative Commons Attribution (CC BY) license (<https://creativecommons.org/licenses/by/4.0/>).

## ABSTRACT

The present field study was conducted to evaluate the effects of mulching and weed control methods on the nutrient and weed dynamics of Kharif Sorghum. The research was conducted in the Agronomy farm of Lovely Professional University in Phagwara, Punjab, during the summer of 2023. The experiment utilized a randomized block design with three replications. A total of six treatments were used, each with different amounts of treatment applied to assess the effects on the growth, yield, and weed characteristics of sorghum. The growth metrics, including plant height, leaf count, stem circumference, leaf area index, and chlorophyll content, saw significant improvement as a result of the amplified influence of mulching and weed management. Treatment T1, which excluded weeds, yielded the greatest plant height (134.69 cm), number of leaves (8.73), stem girth (10.14 cm) at harvest, leaf area index (7.78), and chlorophyll content (53.74) at 90 days after sowing (DAS). The T1 treatment, which was free of weeds, had the most favorable production characteristics. The grain yield was recorded at 2.15 t.ha<sup>-1</sup>, the straw yield at 4.59 t.ha<sup>-1</sup>, and the harvest index at 22.54%. The highest protein concentration was observed as 10.84% in T1 (Weed free) and 10.73% in T2 (Sugarcane trash). In addition, the characteristics of the weed, including the number of weeds, the effectiveness of weed management, and the weight of the weeds, were shown to be highest in dicots at 120 days after sowing (DAS). Treatment T1, which involved the complete removal of weeds, exhibited no weed population and achieved the maximum level of weed control effectiveness and dry weight. The study's findings indicated that the use of T1 (Weed-free) treatment had a substantial influence on different growth, yield, and weed characteristics. Effective management of essential inputs, such as cultivation, fertilizers, and weed management, is vital for improving overall productivity and stability.

## INTRODUCTION

The fifth-most significant cereal crop in the world is sorghum [*Sorghum bicolor* (L)], behind barley (*Hordeum vulgare* L), maize (*Zea mays* L), rice (*Oryza sativa* L), and wheat (*Triticum aestivum* L). Globally, 41 million hectares of land are used to cultivate sorghum, with 64.20 million tons produced in important production regions such as the Deccan plateau in central India, Northeast China, Sub-Saharan Africa, and the broad plains of North America (Glaž et al. 2017). Roughly sixteen percent of the world's sorghum crop is produced in India. As of 2010, this crop, which was one of India's primary staple foods and covered more than 18 million hectares in the 1950s only accounted for 7.69 million hectares (Hussain et al. 2021, Singh et al. 2019). The economic crisis poses a severe danger to the food security and farming systems of the country's dryland areas. A flexible crop, sorghum can be used for grain, feed, and, more recently, as a bioenergy source. Throughout Asia and Africa, sorghum grain is consumed by people or given to animals; the stalks are used as building materials or animal feed (Kumar et al. 2022).

Weed losses have significantly hindered the productivity of sorghum. The majority of the decrease in yield caused by weed competition happens within the initial six weeks after planting. During the crucial phase, the existence of weeds resulted in a reduction of 15-40% in crop production. Therefore, it is important to prioritize weed management during this period (Kandhro et al. 2015). To achieve effective weed control in sorghum, it is crucial to utilize all possible treatments and combine them into a comprehensive weed management strategy. The primary determinant of poor sorghum production, particularly in the rainy season, is the management of weed growth. Due to its larger row spacing and slower initial growth rate, sorghum has a severe weed infestation (Mishra & Patil 2014, Singh et al. 2019, Kandhro et al. 2015). Pesticides are rarely used in sorghum agriculture; instead, human weeding and machine inter-row cultivation are the main weed control techniques. Pre-emergence herbicides help provide early weed control during the wet season when it may not be possible to immediately hand weed or utilize mechanical inter-row cultivation (Abdul Rab et al. 2016, Kumar et al. 2016). To prevent weeds from growing between rows, it is recommended to use integrated weed control, which combines minimal hand weeding, sparing herbicide application, interculturing, and efficient agronomic techniques. One intercrop that could be utilized in place of manual weeding or pre-emergence herbicides is cowpeas (Dhaka et al. 2023). Dry conditions are typical for sorghum grain cultivation, potentially decreasing preemergence herbicide effectiveness due to low soil moisture. When facing such conditions, non-selective herbicides can be employed alongside herbicide-tolerant sorghum cultivars (Hussain et al. 2021). Hence, achieving effective weed control requires combining various integrated weed management practices systematically. Additionally, mulching materials are frequently utilized to support the growth of sorghum crops (Kumar et al. 2022). Recurring applications of the same herbicide can cause weed resistance, and herbicide-based weed control techniques leave behind residual toxicity. Organic mulching is a sustainable substitute for chemical control. Mulch made from a variety of crop wastes is used in this manner; it breaks down organically and enhances soil health. The goal of sustainable weed management is to reduce the detrimental effects of weeds on crop productivity while maintaining economically and environmentally sound agricultural methods. Recurring applications of the same herbicide can cause weed resistance, and herbicide-based weed control techniques leave behind residual toxicity. Organic mulching is a sustainable substitute for chemical control. Mulch made from a variety of crop residue is used in this manner; it breaks down organically and enhances soil health. Research into “mulching and weed management

practices on nutrient and weed dynamics” is vital for developing methods that balance crop productivity with ecological sustainability. Such studies can lead to practices that enhance sorghum yield while promoting long-term soil health and environmental conservation. Ultimately, this research demonstrates how strategic mulching and management practices can improve soil nutrient levels and mitigate weed issues, thereby supporting more sustainable and productive Kharif Sorghum farming systems. The application of mulching and weed management techniques on the nutrients and weed dynamics of the kharif sorghum crop was the primary focus of the current study.

## MATERIALS AND METHODS

This study was carried out in the School of Agriculture, Lovely Professional University, Phagwara, Punjab, during the summer of 2022-2023. The farm is situated in the precise coordinates of 31.24° N latitude and 75.6909° E longitude, approximately 20 kilometers from the city of Jalandhar in the state of Punjab. Its altitude is 252 meters above mean sea level. The region is distinguished by soil with a texture ranging from sandy loam to clay and a pH level ranging from 7.8 to 8.5. The current site is inside the Trans-Gangetic Agro-climatic zone. The mean annual precipitation received amounts to 527.1 millimeters. The present investigation was carried out on sorghum to assess the effects of different techniques of weed management and mulching on the nutrient and weed dynamics of the crop.

### Experimental Design

The randomised block design (RBD) which composed of 6 treatments in 4 replications. The different treatments include T1: Weed free, T2: Sugarcane trash, T3: Vermicompost mulch, T4: Live mulch, T5: Parthenium extract, T6: Weedy check (control). The area for the plot was 550 m<sup>2</sup> with a size of 5×4 m<sup>2</sup> and 20 number of plots. The seeds were sowed at a spacing of 30\*10cm, and sowing was done on April 7<sup>th</sup>, 2023. Three irrigations were given after sowing. The other agricultural practices followed for sorghum were applied by the recommendations of commercial production.

### Experimental Data

The data for growth, yield, and weed attributes of the sorghum crop was recorded using three randomly chosen plants from each treatment after seed sowing. The growth features of the plants, including plant height (cm), number of leaves, stem girth (cm), leaf area index, and chlorophyll content, were measured. The growth parameters are measured at intervals of 30 days. The evaluation included the assessment of yield metrics such as grains per panicle, panicle length

in centimeters, panicle girth in centimeters, test weight in grams, grain yield in tons per hectare, straw yield in tons per hectare, and harvest index as a percentage. The metrics studied for weed analysis were weed population, weed dry weight, and weed control efficacy.

### Statistical Analysis

The analysis of the data was done statistically by OPSTAT software. Results are presented in the form of the mean for different growth, weed, and yield attributes. A significant difference ( $p < 0.05$ ) among treatments was indicated by SPSS software version 24.

## RESULTS AND DISCUSSION

### Growth Parameters

**Effect of different levels of nutrients and weed dynamics on plant height (cm) at 30, 60, 90 DAS and harvest:** The growth parameters of sorghum, such as plant height, number of leaves, stem girth, leaf area index, and chlorophyll content, were significantly affected by the use of mulching and weed management practices. These practices influenced the nutrient and weed dynamics, and the effects were observed at 30-day intervals. The growth metrics exhibited a gradual increase as the influence of mulching and weed control

Table 1: Effect of different levels of nutrients and weed dynamics on plant height (cm) at 30, 60, and 90 DAS, and harvest.

Treatments	30 DAS	60 DAS	90 DAS	At harvest
T1: Weed free	69.72±1.58 <sup>a</sup>	86.96±0.54 <sup>a</sup>	112.61±0.19 <sup>a</sup>	134.69±0.12 <sup>a</sup>
T2: Sugarcane trash	68.25±1.72 <sup>b</sup>	86.77±0.51 <sup>a</sup>	112.51±0.22 <sup>a</sup>	134.58±0.14 <sup>a</sup>
T3: Vermicompost mulch	67.85±1.68 <sup>c</sup>	86.46±0.31 <sup>a</sup>	112.37±0.17 <sup>a</sup>	134.49±0.17 <sup>a</sup>
T4: Live mulch	67.13±1.64 <sup>c</sup>	85.95±0.41 <sup>b</sup>	112.06±0.55 <sup>a</sup>	134.21±0.51 <sup>a</sup>
T5: Parthenium extract	66.07±2.10 <sup>d</sup>	85.71±0.44 <sup>b</sup>	111.82±0.56 <sup>b</sup>	133.77±0.52 <sup>b</sup>
T6: Weedy check (control)	65.08±2.86 <sup>e</sup>	85.12±0.73 <sup>b</sup>	111.23±0.56 <sup>b</sup>	133.37±0.08 <sup>b</sup>
CD	1.83	0.47	0.42	0.34
CV	2.93	0.59	0.40	0.27
SE[d±]	0.88	0.22	0.20	0.16
SE[m±]	0.62	0.16	0.14	0.11

Data are presented in the form of mean (n=3). CD = Critical difference, CV = Critical variance, SE = Standard error. Different superscripts present in the same column are significantly different ( $p < 0.05$ ).

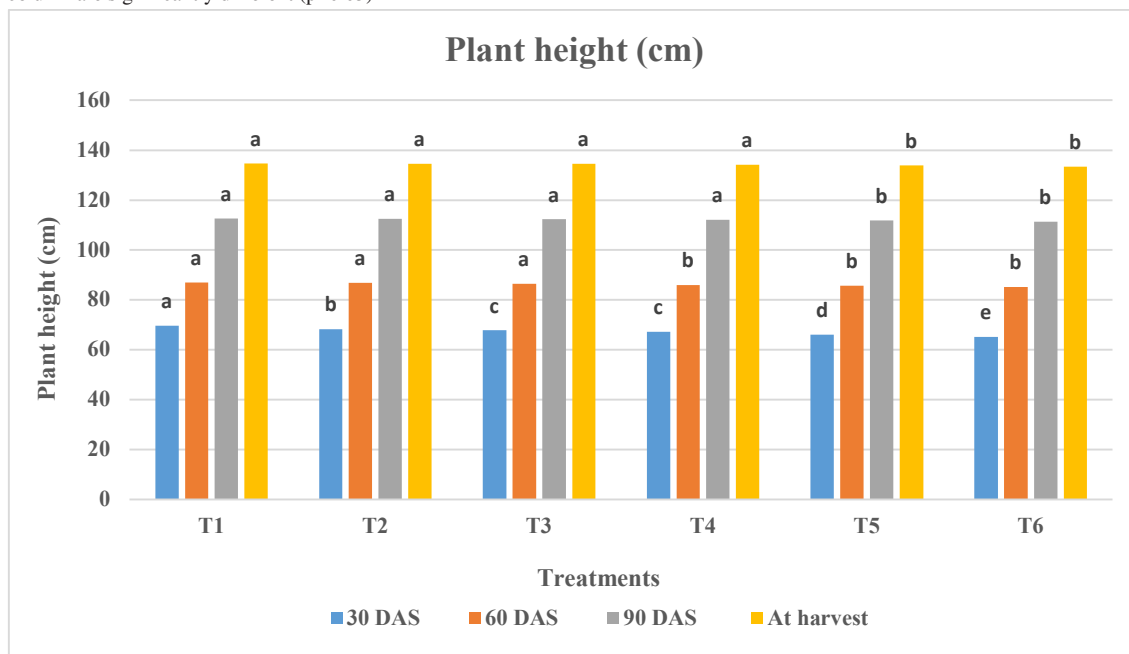


Fig. 1: Influence of different levels of nutrients and weed dynamics on plant height (cm) at 30, 60, and 90 DAS and harvest.

methods on nutrient and weed dynamics intensified, as seen in Table 1. Significant differences in plant height were observed across the different treatments at 30 days after sowing (DAS), 60 DAS, 90 DAS, and at harvest (Fig. 1). At the 30-day after sowing (30DAS) mark, the treatment T1, which involved keeping the plants free from weeds, exhibited the greatest plant height, measuring 69.72 cm. This height was statistically indistinguishable from the heights seen in treatments T2 and T3. The T6 Weedy check treatment exhibited the smallest plant height, measuring 65.08 cm. At 60 days after sowing (DAS), treatment T1 (Weed-free) had the greatest plant height of 86.96 cm, which was statistically comparable to treatments T2 and T3. The control treatment, T6, had the smallest reported plant height, measuring 85.12 cm. The plant height was measured at 112.61 cm in treatment T1 (Weed-free) and 112.51 cm in treatment T2 (Sugarcane trash) at 90 days after sowing (DAS). The treatment T1 (Control) had the smallest height,

measuring 111.23 cm. Statistical analysis revealed that therapy T1 is comparable to treatments T2 and T3. Among the plants harvested, the tallest one measured 134.69 cm in height during the T1 treatment (Weed-free), and this height was not significantly different from the heights seen under the T2 and T3 treatments. The minimum observed plant height was 133.37 cm. The plant's increase in height is ascribed to the use of weed control strategies that improve nutrient availability, hence favorably affecting the plant's height parameter. Implementing effective weed management techniques and employing various mulching approaches enhance the growth characteristics of the crop. Similar results are followed by Bavalgave et al. (2017) in the sorghum crop.

**Effect of different levels of nutrients and weed dynamics on number of leaves at 30, 60, 90 DAS, and harvest:** The number of leaves is significantly influenced by the effects of mulching and weed control methods on the nutrient and weed dynamics of sorghum at 30, 60, and 90 days after

Table 2: Effect of different levels of nutrients and weed dynamics on number of leaves at 30, 60, 90 DAS, and harvest.

Treatments	30 DAS	60 DAS	90 DAS	At harvest
T1: Weed-free	4.52±0.08 <sup>a</sup>	5.72±0.05 <sup>a</sup>	6.70±0.08 <sup>a</sup>	8.73±0.01 <sup>a</sup>
T2: Sugarcane trash	4.31±0.04 <sup>b</sup>	5.37±0.02 <sup>b</sup>	6.50±0.02 <sup>b</sup>	8.50±0.02 <sup>b</sup>
T3: Vermicompost mulch	3.92±0.01 <sup>c</sup>	4.91±0.01 <sup>c</sup>	5.92±0.02 <sup>c</sup>	7.91±0.01 <sup>c</sup>
T4: Live mulch	3.84±0.01 <sup>d</sup>	4.76±0.02 <sup>d</sup>	5.77±0.02 <sup>d</sup>	7.73±0.02 <sup>d</sup>
T5: Parthenium extract	3.75±0.03 <sup>e</sup>	4.65±0.01 <sup>d</sup>	5.65±0.02 <sup>e</sup>	7.57±0.04 <sup>e</sup>
T6: Weedy check (control)	3.72±0.03 <sup>e</sup>	4.33±0.02 <sup>e</sup>	5.40±0.01 <sup>f</sup>	7.47±0.02 <sup>f</sup>
CD	0.04	0.02	0.04	0.02
CV	1.14	0.57	0.76	0.29
SE[d±]	0.02	0.01	0.02	0.01
SE[m±]	0.01	0.01	0.01	0.00

Data are presented in the form of mean (n=3). CD = Critical difference, CV = Critical variance, SE = Standard error. Different superscripts present in the same column are significantly different ( $p < 0.05$ ).

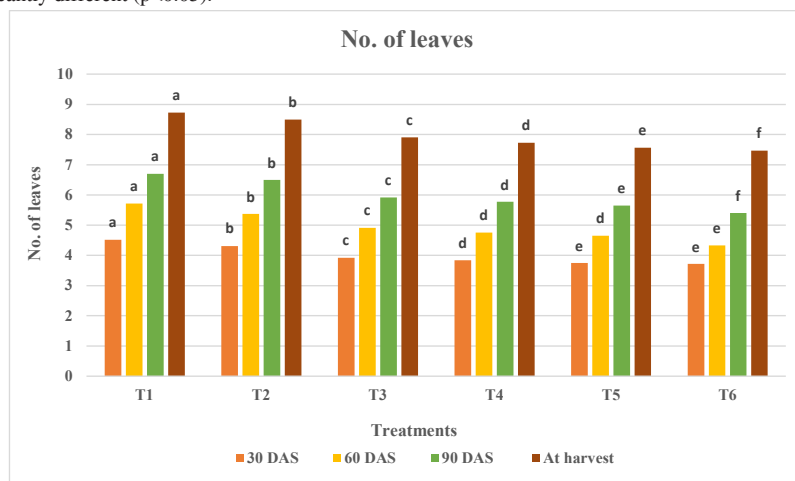


Fig. 2: Influence of different levels of nutrients and weed dynamics on the number of leaves at 30, 60 and 90 DAS, and harvest.



Table 3: Effect of different levels of nutrients and weed dynamics on stem girth (cm) at 30, 60 and 90 DAS, and harvest.

Treatments	30 DAS	60 DAS	90 DAS	At harvest
T1: Weed-free	6.67±0.09 <sup>a</sup>	7.65±0.04 <sup>a</sup>	9.26±0.04 <sup>a</sup>	10.14±0.02 <sup>a</sup>
T2: Sugarcane trash	6.40±0.03 <sup>b</sup>	7.53±0.04 <sup>b</sup>	9.12±0.05 <sup>b</sup>	10.04±0.02 <sup>b</sup>
T3: Vermicompost mulch	5.92±0.02 <sup>c</sup>	7.46±0.05 <sup>c</sup>	8.91±0.06 <sup>c</sup>	9.83±0.05 <sup>c</sup>
T4: Live mulch	5.79±0.02 <sup>d</sup>	6.93±0.01 <sup>d</sup>	8.81±0.02 <sup>d</sup>	9.70±0.02 <sup>d</sup>
T5: Parthenium extract	5.71±0.03 <sup>d</sup>	6.78±0.02 <sup>e</sup>	8.68±0.03 <sup>e</sup>	9.52±0.04 <sup>e</sup>
T6: Weedy check (control)	5.61±0.02 <sup>e</sup>	6.71±0.02 <sup>e</sup>	8.61±0.04 <sup>e</sup>	9.42±0.02 <sup>f</sup>
CD	0.04	0.03	0.04	0.03
CV	0.83	0.48	0.50	0.41
SE[d±]	0.02	0.01	0.02	0.01
SE[m±]	0.01	0.01	0.01	0.01

Data are presented in the form of mean (n=3). CD = Critical difference, CV = Critical variance, SE = Standard error. Different superscripts present in the same column are significantly different ( $p < 0.05$ ).

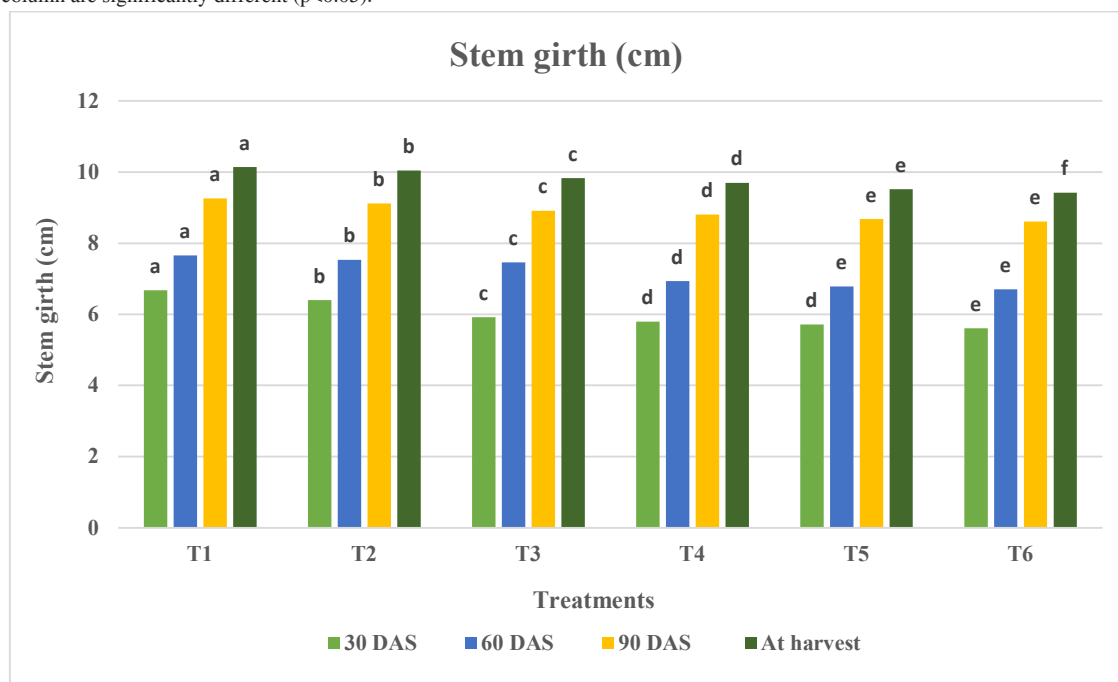


Fig. 3: Influence of different levels of nutrients and weed dynamics on stem girth (cm) at 30, 60, and 90 DAS and harvest.

sowing (DAS) and at harvest (Table 2 and Fig. 2). At the 30-day after sowing (30DAS) stage, treatment T1 (Weed free) had the highest reported leaf count of 4.52. This result has statistical similarity to the values seen in treatments T2 and T3. However, the treatment T6 Weedy check (Control) exhibited the shortest plant height, measuring 3.72. At 60 days after sowing (DAS), treatment T1 (Weed free) had the highest leaf count, measuring 5.72. This result is statistically comparable to the number of leaves observed in treatments T2 and T3. Conversely, the control treatment T6 had the fewest amount of leaves, specifically 4.33. T1 (Weed free) had the greatest leaf count, at 6.70 leaves, at 90 DAS. Subsequently,

there were 6.52 leaves observed in T2, specifically in the context of Sugarcane garbage. The minimum number of leaves, 5.40, was recorded in T6 (Control). Treatment T1 (weed-free) had the greatest number of leaves, followed by treatments T2 and T3 at the time of harvest. The higher prevalence of foliage is directly correlated with the existence of nutrients in the root area, which improves the absorption of nutrients in their consumable state. Consequently, this improves the plant's metabolic processes, resulting in a rise in leaf output and other growth characteristics. Kumar et al. (2022) investigated comparable outcomes in the growth characteristics of sorghum crops.

### Effect of Different Levels of Nutrients and Weed Dynamics on Stem Girth (cm) at 30, 60, 90 DAS and Harvest

The stem girth is significantly influenced by different nutrient levels and weed dynamics in sorghum at 30, 60, and 90 days after sowing (DAS) and at harvest (Table 3). At the 30-day after-sowing (30DAS) stage, treatment T1 (Weed-free) had the biggest stem girth of 6.67 cm, which was statistically equivalent to treatments T2 and T3. Conversely, the treatment T6 Weedy check (Control) had the smallest plant height, measuring 5.61 cm. At 60 days after sowing (DAS), treatment T1 (Weed-free) exhibited the greatest stem girth of 7.65 cm, which was statistically comparable to treatments T2 and T3. The control treatment, T6, had the smallest stem circumference, measuring 6.71 cm. At 90 days after sowing (DAS), the stem girth measurement was 9.26 cm in T1 (Weed free), which was the highest, and 9.12 cm in T2 (Sugarcane trash), which was the second highest. In T6 (Control), the stem girth measurement reached its

minimum value of 8.61 cm (Fig. 3). At harvest, the stem with the largest circumference was found in T1 (Weed free), whereas the smallest circumference was seen in T6 (Control). The increase in stem diameter is closely correlated with the availability of nutrients in the root zone. This promotes the assimilation of nutrients in a readily usable form, resulting in enhanced metabolic activities inside the plant. As a result, there is a clear increase in the circumference of the stem and other related characteristics. Kumar et al. (2022) and Bavalgave et al. (2017) reported similar results.

### Effect of Different Levels of Nutrients and Weed Dynamics on Leaf Area Index at 30, 60, and 90 DAS

At 30 days after sowing (DAS), the leaf area index (LAI) was highest in T1 (Weed-free) with a measured value of 2.56, while the lowest LAI was found in T6 (Control) with a value of 1.77. At 60 days after sowing (DAS), treatment T1 (weed-free) exhibited the highest Leaf Area Index (LAI) of 4.90, which was statistically comparable to treatments

Table 4: Effect of different levels of nutrients and weed dynamics on leaf area index at 30, 60, and 90 DAS.

Treatments	30 DAS	60 DAS	90 DAS
T1: Weed-free	2.56±0.14 <sup>a</sup>	4.90±0.06 <sup>a</sup>	7.78±0.03 <sup>a</sup>
T2: Sugarcane trash	2.44±0.13 <sup>b</sup>	4.70±0.04 <sup>b</sup>	7.71±0.03 <sup>a</sup>
T3: Vermicompost mulch	2.30±0.12 <sup>c</sup>	4.36±0.07 <sup>c</sup>	7.57±0.07 <sup>b</sup>
T4: Live mulch	1.94±0.03 <sup>d</sup>	3.92±0.02 <sup>d</sup>	6.95±0.01 <sup>c</sup>
T5: Parthenium extract	1.83±0.04 <sup>e</sup>	3.80±0.06 <sup>e</sup>	6.86±0.01 <sup>d</sup>
T6: Weedy check (control)	1.77±0.02 <sup>f</sup>	3.66±0.04 <sup>f</sup>	6.78±0.03 <sup>e</sup>
CD	0.09	0.04	0.03
CV	4.94	1.26	0.53
SE[d±]	0.04	0.02	0.01
SE[m±]	0.03	0.01	0.01

Data are presented in the form of mean (n=3). CD = Critical difference, CV = Critical variance, SE = Standard error. Different superscripts present in the same column are significantly different ( $p < 0.05$ ).

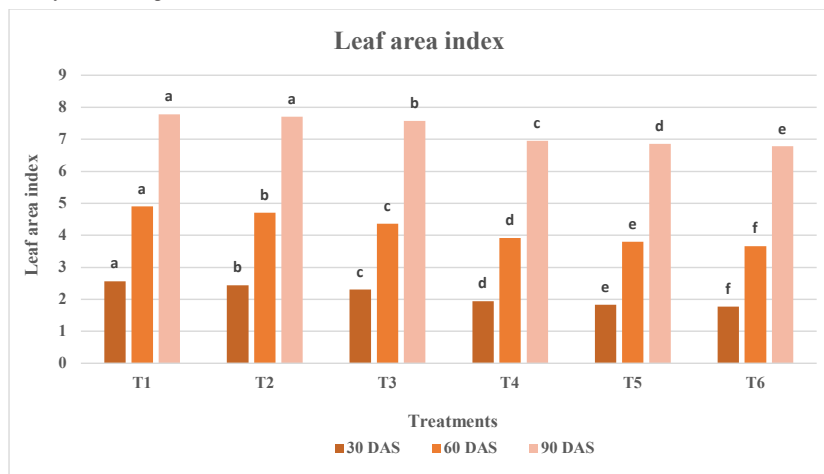


Fig. 4: Influence of different levels of nutrients and weed dynamics on leaf area index at 30, 60, and 90 DAS.

T2 and T3. The control treatment, T6, exhibited the lowest Leaf Area Index (LAI) value of 3.66. According to Table 4, the weed-free treatment (T1) had the highest leaf area index (LAI) of 7.78 at 90 days after sowing (DAS), whereas the control treatment (T1) had the lowest LAI of 6.78 (Table 4 & Fig. 4). Vijayakumar et al. (2014), undertook a comparable assessment and arrived at same findings. The rise in the leaf area index is ascribed to the crucial function of nutrients in aiding the transmission and movement of energy inside plants. Nutrients also play a crucial role in facilitating cell elongation and division.

**Effect of different levels of nutrients and weed dynamics on chlorophyll content (%) at 30, 60, and 90 DAS:** The chlorophyll content is significantly influenced by different levels of nutrient and weed dynamics of sorghum at 30, 60, and 90 DAS (Table 5). The highest chlorophyll level, at 34.73%, was found in T1 (Weed-free) at 30 DAS. T2 (Sugarcane trash) had the second-highest chlorophyll content at 34.52%, while the lowest chlorophyll content of 29.66%

was reported in T6 (Control). The chlorophyll content at 60 days after sowing (DAS) was found to be 44.37% in T1 (Weed-free), which was the greatest, and 39.78% in T6 (Control), which was the lowest. At 90 days after sowing (DAS), the chlorophyll content was found to be 53.74% in T1 (Weed free), which was the greatest, and 48.59% in T6 (Control), which was the lowest (Table 5 and Fig. 5). The increase in chlorophyll concentration is believed to be attributed to the presence of nutrients. The nutrition and weed dynamics of sorghum have a vital role in the synthesis of chlorophyll and the promotion of photosynthetic activity, resulting in the production of ATP molecules. These results are in correspondence with the findings of Mishra and Talwar (2020) and Dixit et al. (2015) in sorghum.

### Yield Parameters

**Effect of different levels of nutrients and weed dynamics on yield parameters of sorghum:** Yield attributes including grains/panicle, panicle length (cm), panicle girth (cm), test

Table 5: Effect of different levels of nutrients and weed dynamics on chlorophyll content (%) at 30, 60, and 90 DAS.

Treatments	30 DAS	60 DAS	90 DAS
T1: Weed-free	34.73±0.05 <sup>a</sup>	44.37±0.20 <sup>a</sup>	53.74±0.03 <sup>a</sup>
T2: Sugarcane trash	34.52±0.10 <sup>a</sup>	43.71±0.12 <sup>b</sup>	52.71±0.03 <sup>b</sup>
T3: Vermicompost mulch	34.29±0.11 <sup>a</sup>	43.52±0.09 <sup>b</sup>	52.46±0.05 <sup>b</sup>
T4: Live mulch	32.78±0.09 <sup>b</sup>	41.84±0.05 <sup>c</sup>	51.78±0.05 <sup>c</sup>
T5: Parthenium extract	31.43±0.04 <sup>c</sup>	41.60±0.18 <sup>c</sup>	49.73±0.01 <sup>d</sup>
T6: Weedy check (control)	29.66±0.04 <sup>d</sup>	39.78±0.04 <sup>d</sup>	48.59±0.05 <sup>e</sup>
CD	0.07	0.13	0.03
CV	0.24	0.33	0.07
SE[d±]	0.03	0.06	0.01
SE[m±]	0.02	0.04	0.01

Data are presented in the form of mean (n=3). CD = Critical difference, CV = Critical variance, SE = Standard error. Different superscripts present in the same column are significantly different ( $p < 0.05$ ).

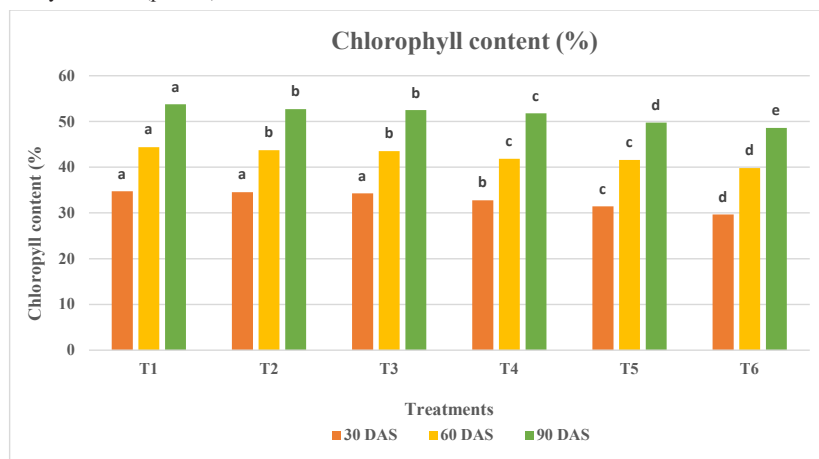


Fig. 5: Influence of different levels of nutrients and weed dynamics on chlorophyll content (%) at 30, 60, and 90 DAS.

Table 6: Effect of different levels of nutrients and weed dynamics on yield parameters of sorghum.

Treatments	Grains/ panicle	Panicle length [cm]	Panicle girth [cm]	Test weight [g]	Grain yield [t.ha <sup>-1</sup> ]	Straw yield [t.ha <sup>-1</sup> ]	Harvest index [%]
T1: Weed-free	525.97±1.62 <sup>a</sup>	27.35±0.26 <sup>a</sup>	17.47±0.25 <sup>a</sup>	38.77±0.08 <sup>a</sup>	2.15±0.02 <sup>a</sup>	4.59±0.05 <sup>a</sup>	22.54±0.02 <sup>a</sup>
T2: Sugarcane trash	523.45±1.05 <sup>b</sup>	26.99±0.35 <sup>b</sup>	17.28±0.38 <sup>a</sup>	38.51±0.10 <sup>a</sup>	2.06±0.02 <sup>a</sup>	4.49±0.03 <sup>b</sup>	22.41±0.04 <sup>a</sup>
T3: Vermicompost mulch	449.77±1.53 <sup>c</sup>	23.34±0.44 <sup>c</sup>	16.92±0.09 <sup>b</sup>	37.45±0.11 <sup>b</sup>	1.89±0.02 <sup>b</sup>	3.92±0.05 <sup>c</sup>	19.61±0.01 <sup>b</sup>
T4: Live mulch	447.62±1.57 <sup>d</sup>	22.01±0.51 <sup>d</sup>	15.83±0.37 <sup>c</sup>	37.32±0.13 <sup>b</sup>	1.76±0.01 <sup>c</sup>	3.81±0.07 <sup>d</sup>	18.59±0.05 <sup>c</sup>
T5: Parthenium extract	446.27±1.05 <sup>d</sup>	20.47±0.78 <sup>c</sup>	14.00±0.31 <sup>d</sup>	36.60±0.10 <sup>c</sup>	1.69±0.02 <sup>d</sup>	3.68±0.10 <sup>c</sup>	18.36±0.02 <sup>c</sup>
T6: Weedy check (control)	390.81±4.09 <sup>e</sup>	19.23±0.43 <sup>f</sup>	13.64±0.35 <sup>e</sup>	36.45±0.08 <sup>c</sup>	1.64±0.01 <sup>d</sup>	3.55±0.09 <sup>f</sup>	17.57±0.04 <sup>d</sup>
CD	2.14	0.58	0.33	0.09	0.01	0.06	0.03
CV	0.49	2.71	2.30	0.27	0.98	1.81	0.18
SE[d±]	1.02	0.28	0.16	0.04	0.01	0.03	0.01
SE[m±]	0.72	0.19	0.11	0.03	0.01	0.02	0.01

Data are presented in the form of mean (n=3). CD = Critical difference, CV = Critical variance, SE = Standard error. Different superscripts present in the same column are significantly different (p<0.05).

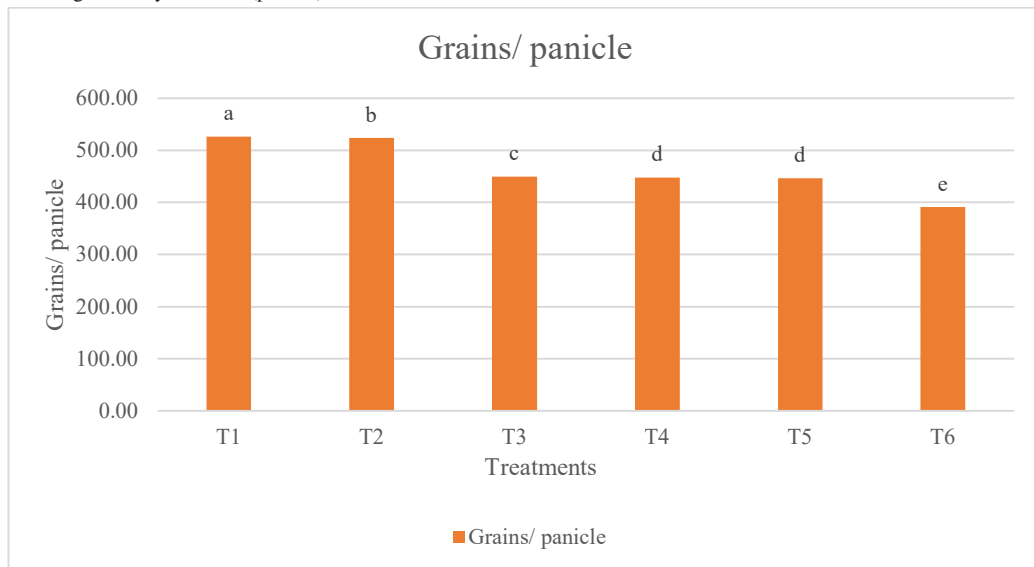


Fig. 6: Influence of different levels of nutrients and weed dynamics on grains per panicle of sorghum.

weight (g), grain yield (t.ha<sup>-1</sup>), straw yield (t.ha<sup>-1</sup>), and harvest index (%), are presented in Table 6 and Fig. 6. The grains per panicle were found to be highest in Treatment T1 (Weed free) at 525.97 and lowest in T6 (Control) at 390.81. The acquired results are comparable to the findings of Ajaykumar (2023). The availability of nutrients and the dynamics of weed growth are responsible for the rise in the number of grains per panicle. The length of the panicles was maximum in T1 (Weed free) at 27.35 cm, followed by T2 (Sugarcane waste) at 26.99 cm, and lowest in T6 (Control) at 19.23 cm (Fig. 7). The highest reported panicle girth was 17.47 cm

in T1 (Weed-free), while the lowest was 13.64 cm in T6 (Control). Applying various fertilizers and managing weed growth increased the production characteristics of sorghum by increasing the length and thickness of the panicles. Bajwa et al. (2023) and Kumar et al. (2023) similarly documented similar findings to those described here. The test weight was highest in T1 (Weed-free) at 38.77 g, followed by T2 and T3 treatments. The lowest weight was seen in T6 (Control) at 36.45 g (Fig. 8). The highest grain yield was recorded in treatment T1 (Weed free) at a rate of 2.15 t.ha<sup>-1</sup>, followed by treatments T2 and T3 (Fig. 9). The lowest yield was seen



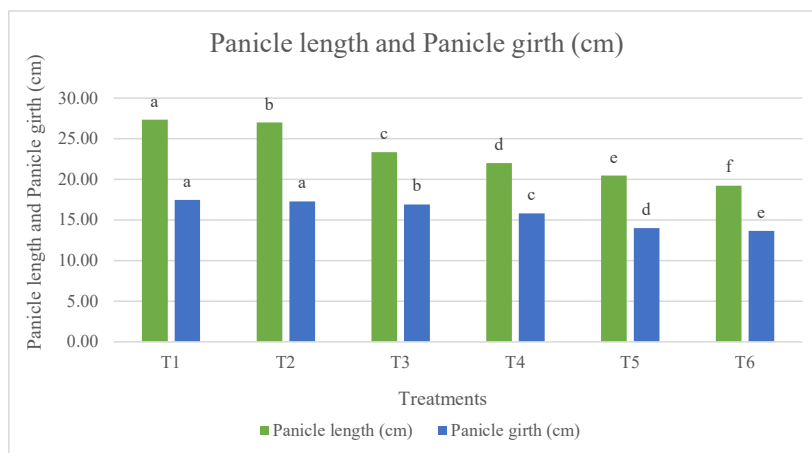


Fig. 7: Influence of different levels of nutrients and weed dynamics on panicle length (cm) and panicle girth(cm) of sorghum.

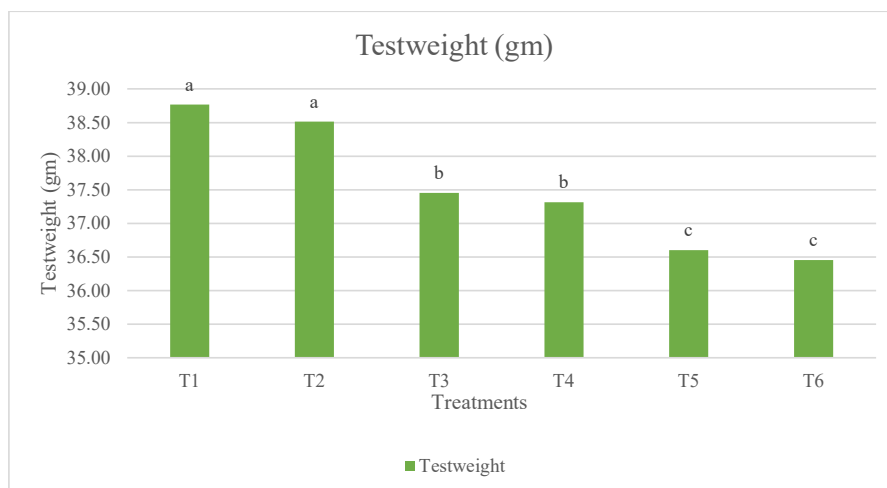


Fig. 8: Influence of different levels of nutrients and weed dynamics on test weight (g) of sorghum.

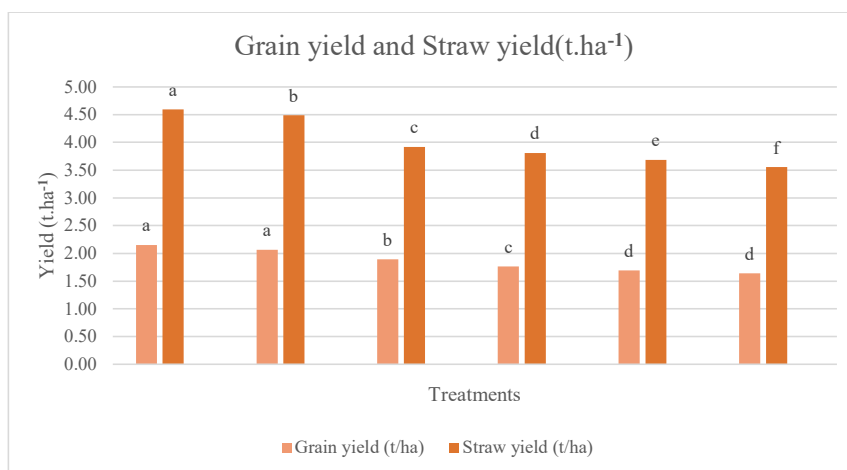


Fig. 9: Influence of different levels of nutrients and weed dynamics on grain yield(t.ha<sup>-1</sup>) and straw yield (t.ha<sup>-1</sup>) of sorghum.

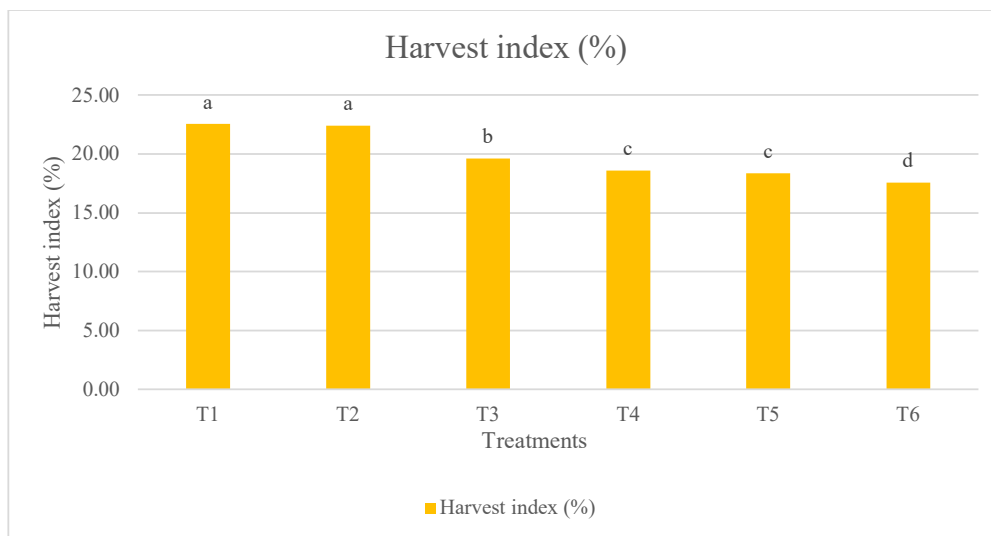


Fig. 10: Influence of different levels of nutrients and weed dynamics on harvest index(%) of sorghum.

Table 7: Effect of different levels of nutrients and weed dynamics on protein content (%) of sorghum.

Treatments	At harvest
T1: Weed-free	10.84±0.05 <sup>a</sup>
T2: Sugarcane trash	10.73±0.03 <sup>ab</sup>
T3: Vermicompost mulch	10.51±0.03 <sup>ab</sup>
T4: Live mulch	9.83±0.02 <sup>c</sup>
T5: Parthenium extract	9.74±0.03 <sup>d</sup>
T6: Weedy check (control)	9.65±0.03 <sup>e</sup>
CD	0.07
CV	0.24
SE[d±]	0.03
SE[m±]	0.02

in treatment T6 (Control) at a rate of 1.64 t.ha<sup>-1</sup>. The highest straw yield was seen in treatment T1 (Weed-free) at a rate of 4.59 t.ha<sup>-1</sup>, while the lowest yield was observed in treatment T6 (Control) at a rate of 3.55 t.ha<sup>-1</sup> (Table 6). The increased crop output can be due to the enhanced plant growth and yield characteristics affected by the nutrients and diverse weed control strategies. Thakur et al. (2016) and Kumar et al. (2023) achieved similar results. The significant increase in grain and straw production seen in response to diverse treatment combinations can be attributed to enhanced nutrient absorption, which is then distributed to various plant parts. The Harvest index reached its highest value in T1 (Weed-free) at 22.54%, followed by T2 and T3 treatments. The lowest value was found in T6 (Control) at 17.57% (Fig. 10). Various fertilizer inputs and weed management measures

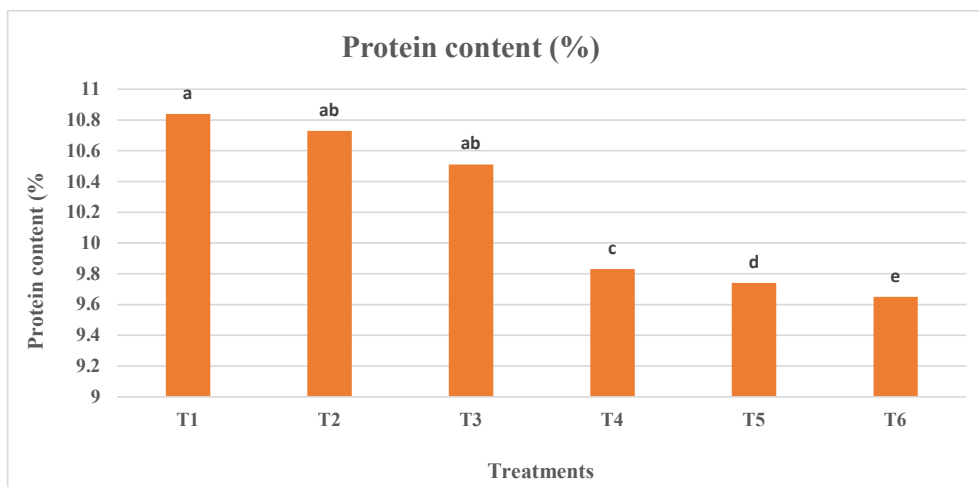


Fig. 11: Influence of different levels of nutrients and weed dynamics on protein content (%) of sorghum.

resulted in a better harvest index value. Similar findings are observed by Thakur et al. (2016).

### Quality Parameters

**Effect of different levels of nutrients and weed dynamics on protein content (%) of sorghum:** The protein content is significantly influenced by different levels of nutrient and weed dynamics of sorghum at harvest (Table 7). The maximum protein content was recorded as 10.84% in T1 (Weed-free), followed by 10.73% in T2 (Sugarcane trash), and the lowest was observed as 9.65% in T6 (Control). The presence of nutrients is thought to be the cause of the rise in protein content. Variations in the nutrient and weed dynamics of sorghum are crucial for the formation of protein (Table 7 and Fig. 11). The crude protein content of sorghum showed significant improvement with all the above nutrient-

management practices over the control. The augmentation of protein content in grain sorghum results in an elevation of the prolamin percentage and an improvement in nutritional quality. Environmental variables, such as location, chemical fertilizers, plant population, and chemical treatments, have an impact on the protein content and amino acid pattern. These results align with the discoveries made by Mishra & Talwar (2020) and Dixit et al. (2015) in the field of sorghum.

### Weed Parameters

**Effect of different levels of nutrients and weed dynamics on the weed population of sorghum:** The weed population is significantly influenced by different levels of nutrient and weed dynamics of sorghum at 30, 60, 90, and 120 DAS (Tables 8 and 9). At 30 DAS, the maximum weed population was recorded as 8.33 in dicots, followed by monocots and

Table 8: Effect of different levels of nutrients and weed dynamics on weed population of sorghum.

Treatments	Monocot	Dicot	Sedges	Monocot	Dicot	Sedges
	30 DAS			60 DAS		
T1: Weed-free	0.00±0.00 <sup>d</sup>	0.00±0.00 <sup>c</sup>	0.00±0.00 <sup>c</sup>	0.00±0.00 <sup>c</sup>	0.00±0.00 <sup>c</sup>	0.00±0.00 <sup>c</sup>
T2: Sugarcane trash	1.00±0.96 <sup>c</sup>	4.67±1.26 <sup>d</sup>	3.33±2.50 <sup>c</sup>	3.67±1.09 <sup>d</sup>	5.33±1.26 <sup>b</sup>	0.33±0.96 <sup>d</sup>
T3: Vermicompost mulch	2.67±2.22 <sup>b</sup>	6.00±0.96 <sup>b</sup>	6.00±1.73 <sup>b</sup>	5.33±1.30 <sup>b</sup>	5.33±1.26 <sup>b</sup>	1.00±0.96 <sup>c</sup>
T4: Live mulch	1.33±1.26 <sup>c</sup>	5.00±1.29 <sup>c</sup>	2.33±0.50 <sup>d</sup>	3.00±0.83 <sup>d</sup>	3.33±0.50 <sup>d</sup>	3.00±2.22 <sup>b</sup>
T5: Parthenium extract	1.33±0.82 <sup>c</sup>	4.67±1.50 <sup>d</sup>	2.33±1.83 <sup>d</sup>	4.33±1.48 <sup>c</sup>	4.00±0.96 <sup>c</sup>	1.00±0.82 <sup>c</sup>
T6: Weedy check (control)	6.33±1.71 <sup>a</sup>	8.33±2.08 <sup>a</sup>	8.00±2.16 <sup>a</sup>	8.00±3.56 <sup>a</sup>	9.33±4.93 <sup>a</sup>	8.33±5.85 <sup>a</sup>
CD	1.86	1.61	2.10	3.13	3.32	3.50
CV	95.01	36.35	61.74	83.24	78.67	165.54
SE(d±)	0.89	0.77	1.00	1.50	1.59	1.67
SE(m±)	0.63	0.54	0.71	1.06	1.12	1.18

Data are presented in the form of mean (n=3). CD = Critical difference, CV = Critical variance, SE = Standard error. Different superscripts present in the same column are significantly different (p<0.05).

Table 9: Effect of different levels of nutrients and weed dynamics on weed population of sorghum.

Treatments	Monocot	Dicot	Sedges	Monocot	Dicot	Sedges
	90 DAS			120 DAS		
T1: Weed free	0.00±0.00 <sup>c</sup>	0.00±0.00 <sup>c</sup>	0.00±0.00 <sup>c</sup>	0.00±0.00 <sup>c</sup>	0.00±0.00 <sup>c</sup>	0.00±0.00 <sup>d</sup>
T2: Sugarcane trash	5.33±1.41 <sup>c</sup>	6.00±0.96 <sup>c</sup>	0.33±0.58 <sup>d</sup>	4.67±1.26 <sup>d</sup>	5.67±0.96 <sup>c</sup>	1.00±0.82 <sup>b</sup>
T3: Vermicompost mulch	6.00±1.96 <sup>b</sup>	6.33±0.82 <sup>c</sup>	0.67±0.82 <sup>c</sup>	7.00±1.29 <sup>b</sup>	6.33±0.82 <sup>b</sup>	0.67±0.82 <sup>c</sup>
T4: Live mulch	4.33±3.11 <sup>d</sup>	5.00±0.96 <sup>d</sup>	0.00±2.52 <sup>e</sup>	4.33±1.71 <sup>d</sup>	4.00±0.82 <sup>d</sup>	2.33±0.96 <sup>b</sup>
T5: Parthenium extract	5.67±1.50 <sup>c</sup>	7.33±0.82 <sup>b</sup>	1.33±0.50 <sup>b</sup>	5.00±1.29 <sup>c</sup>	5.00±0.82 <sup>c</sup>	1.33±0.50 <sup>a</sup>
T6: Weedy check (control)	8.67±0.96 <sup>a</sup>	12.00±1.29 <sup>a</sup>	2.33±0.58 <sup>a</sup>	9.00±1.71 <sup>a</sup>	11.67±1.41 <sup>a</sup>	2.33±0.58 <sup>a</sup>
CD	2.09	1.00	0.60	1.43	1.30	0.96
CV	44.99	17.65	83.08	30.89	25.88	81.69
SE[d±]	1.00	0.48	0.28	0.68	0.62	0.46
SE[m±]	0.70	0.33	0.20	0.48	0.44	0.32

Data are presented in the form of mean (n=3). CD = Critical difference, CV = Critical variance, SE = Standard error. Different superscripts present in the same column are significantly different (p<0.05).

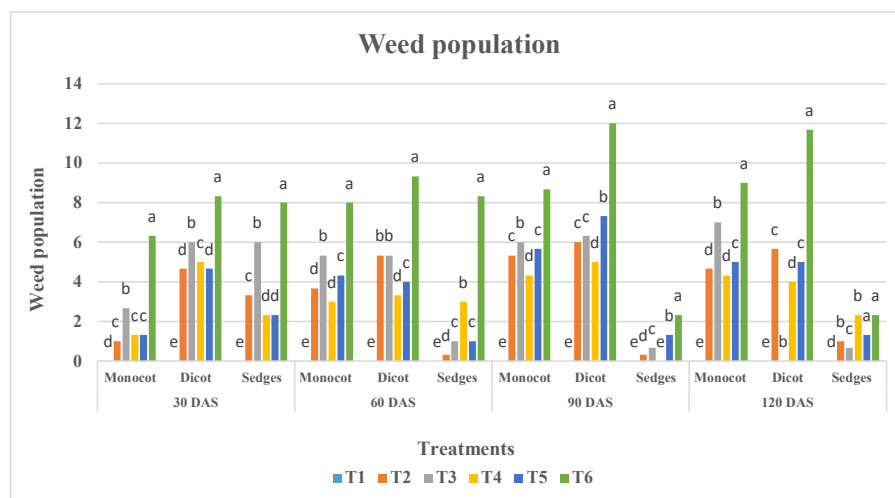


Fig. 12: Influence of different levels of nutrients and weed dynamics on the weed population of sorghum.

Table 10: Effect of different levels of nutrients and weed dynamics on weed control efficiency (%) of sorghum.

Treatments	Monocot	Dicot	Sedges	Monocot	Dicot	Sedges
	30 DAS			60 DAS		
T1: Weed-free	100±0.11 <sup>a</sup>	100±0.07 <sup>a</sup>	100±0.05 <sup>a</sup>	100±0.47 <sup>a</sup>	100±0.06 <sup>a</sup>	100±0.06 <sup>a</sup>
T2: Sugarcane trash	64.27±0.06 <sup>b</sup>	66.38±0.06 <sup>b</sup>	63.59±0.04 <sup>b</sup>	73.59±0.04 <sup>b</sup>	75.38±0.05 <sup>b</sup>	72.41±0.02 <sup>b</sup>
T3: Vermicompost mulch	55.69±0.05 <sup>c</sup>	61.27±0.05 <sup>c</sup>	54.29±0.06 <sup>c</sup>	71.38±0.04 <sup>c</sup>	72.38±0.05 <sup>c</sup>	69.48±0.05 <sup>c</sup>
T4: Live mulch	52.58±0.04 <sup>d</sup>	59.49±0.04 <sup>d</sup>	51.49±0.03 <sup>d</sup>	69.48±0.04 <sup>d</sup>	71.53±0.07 <sup>d</sup>	67.58±0.04 <sup>d</sup>
T5: Parthenium extract	51.48±0.05 <sup>e</sup>	58.69±0.02 <sup>e</sup>	49.64±0.06 <sup>e</sup>	67.28±0.06 <sup>e</sup>	69.46±0.03 <sup>e</sup>	66.37±0.04 <sup>e</sup>
T6: Weedy check (control)	0.00±0.00 <sup>f</sup>	0.00±0.00 <sup>f</sup>	0.00±0.00 <sup>f</sup>	0.00±0.00 <sup>f</sup>	0.00±0.00 <sup>f</sup>	0.00±0.00 <sup>f</sup>
CD	0.05	0.04	0.04	0.29	0.05	0.04
CV	0.11	0.09	0.11	0.52	0.09	0.07
SE[d±]	0.02	0.02	0.02	0.13	0.02	0.01
SE[m±]	0.01	0.01	0.01	0.09	0.01	0.01

Data is presented in the form of mean (n=3). CD = Critical difference, CV = Critical variance, SE = Standard error. Different superscripts present in the same column are significantly different (p<0.05).

Table 11: Effect of different levels of nutrients and weed dynamics on weed control efficiency (%) of sorghum.

Treatments	Monocot	Dicot	Sedges	Monocot	Dicot	Sedges
	90 DAS			120 DAS		
T1: Weed-free	100±0.08 <sup>a</sup>	100±0.07 <sup>a</sup>	100±0.09 <sup>a</sup>	100±0.13 <sup>a</sup>	100±0.07 <sup>a</sup>	100±0.08 <sup>a</sup>
T2: Sugarcane trash	81.35±0.13 <sup>b</sup>	83.38±0.11 <sup>b</sup>	80.82±0.36 <sup>b</sup>	91.45±0.10 <sup>b</sup>	92.37±0.05 <sup>b</sup>	89.48±0.05 <sup>b</sup>
T3: Vermicompost mulch	79.59±0.09 <sup>c</sup>	81.33±0.05 <sup>c</sup>	79.34±0.11 <sup>c</sup>	89.74±0.03 <sup>c</sup>	91.35±0.10 <sup>c</sup>	88.59±0.04 <sup>c</sup>
T4: Live mulch	76.48±0.06 <sup>d</sup>	78.58±0.04 <sup>d</sup>	76.30±0.02 <sup>d</sup>	87.68±0.03 <sup>d</sup>	89.39±0.04 <sup>d</sup>	86.28±0.04 <sup>d</sup>
T5: Parthenium extract	75.35±0.03 <sup>e</sup>	77.31±0.06 <sup>e</sup>	75.17±0.05 <sup>e</sup>	86.21±0.09 <sup>e</sup>	88.48±0.03 <sup>e</sup>	85.38±0.06 <sup>e</sup>
T6: Weedy check (control)	0.00±0.00 <sup>f</sup>	0.00±0.00 <sup>f</sup>	0.00±0.00 <sup>f</sup>	0.00±0.00 <sup>f</sup>	0.00±0.00 <sup>f</sup>	0.00±0.00 <sup>f</sup>
CD	0.07	0.07	0.20	0.10	0.07	0.04
CV	0.12	0.11	0.33	0.15	0.10	0.06
SE(d±)	0.03	0.03	0.09	0.05	0.03	0.02
SE(m±)	0.02	0.02	0.06	0.03	0.02	0.01

Data are presented in the form of mean (n=3). CD = Critical difference, CV = Critical variance, SE = Standard error. Different superscripts present in the same column are significantly different (p<0.05).



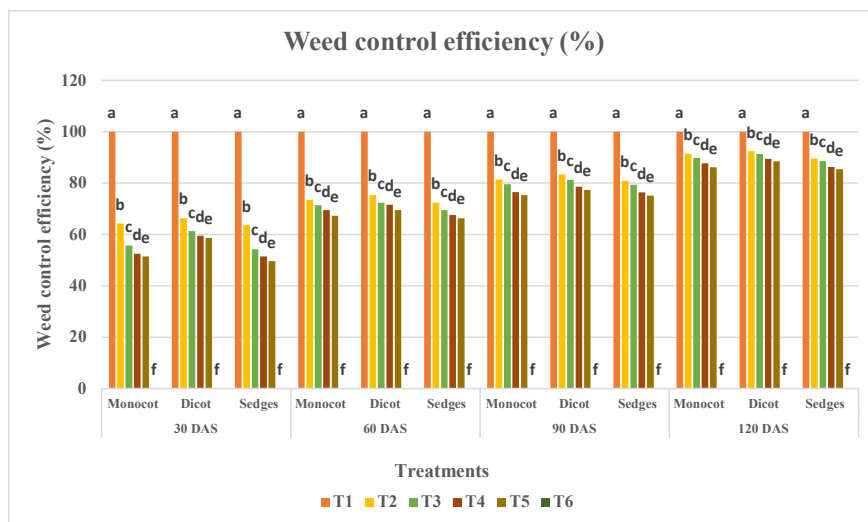


Fig. 13: Influence of different levels of nutrients and weed dynamics on weed control efficiency (%) of sorghum.

Table 12: Effect of different levels of nutrients and weed dynamics on weed dry weight (g) of sorghum.

Treatments	Monocot	Dicot	Sedges	Monocot	Dicot	Sedges
	30 DAS			60 DAS		
T1: Weed-free	1.15±0.03 <sup>f</sup>	1.18±0.04 <sup>f</sup>	1.09±0.02 <sup>f</sup>	1.39±0.04 <sup>f</sup>	1.49±0.03 <sup>f</sup>	1.35±0.04 <sup>f</sup>
T2: Sugarcane trash	4.45±0.03 <sup>c</sup>	4.56±0.02 <sup>c</sup>	4.42±0.04 <sup>c</sup>	5.69±0.04 <sup>c</sup>	5.79±0.02 <sup>c</sup>	5.67±0.03 <sup>c</sup>
T3: Vermicompost mulch	4.28±0.04 <sup>d</sup>	4.36±0.03 <sup>d</sup>	4.24±0.05 <sup>d</sup>	5.44±0.02 <sup>d</sup>	5.46±0.02 <sup>d</sup>	5.43±0.06 <sup>d</sup>
T4: Live mulch	4.16±0.03 <sup>e</sup>	4.19±0.02 <sup>e</sup>	4.13±0.03 <sup>e</sup>	5.37±0.05 <sup>e</sup>	5.39±0.07 <sup>e</sup>	5.30±0.04 <sup>e</sup>
T5: Parthenium extract	4.52±0.08 <sup>b</sup>	4.69±0.02 <sup>b</sup>	4.50±0.08 <sup>b</sup>	6.27±0.06 <sup>b</sup>	6.34±0.05 <sup>b</sup>	6.19±0.04 <sup>b</sup>
T6: Weedy check (control)	5.48±0.03 <sup>a</sup>	5.56±0.03 <sup>a</sup>	5.35±0.04 <sup>a</sup>	6.67±0.04 <sup>a</sup>	6.71±0.03 <sup>a</sup>	6.61±0.03 <sup>a</sup>
CD	0.06	0.03	0.05	0.05	0.03	0.04
CV	1.67	0.83	1.58	1.07	0.75	0.89
SE[d±]	0.02	0.01	0.02	0.02	0.01	0.02
SE[m±]	0.02	0.01	0.01	0.01	0.01	0.01

Data are presented in the form of mean (n=3). CD = Critical difference, CV = Critical variance, SE = Standard error. Different superscripts present in the same column are significantly different (p<0.05).

Table 13: Effect of different levels of nutrients and weed dynamics on weed dry weight (g) of sorghum.

Treatments	Monocot	Dicot	Sedges	Monocot	Dicot	Sedges
	90 DAS			120 DAS		
T1: Weed-free	1.78±0.04 <sup>f</sup>	1.82±0.04 <sup>f</sup>	1.69±0.02 <sup>f</sup>	1.94±0.03 <sup>f</sup>	1.96±0.02 <sup>f</sup>	1.89±0.03 <sup>f</sup>
T2: Sugarcane trash	6.79±0.03 <sup>c</sup>	6.82±0.03 <sup>c</sup>	6.71±0.03 <sup>c</sup>	8.48±0.04 <sup>c</sup>	8.59±0.04 <sup>c</sup>	8.49±0.03 <sup>c</sup>
T3: Vermicompost mulch	6.61±0.04 <sup>d</sup>	6.69±0.03 <sup>d</sup>	6.59±0.03 <sup>d</sup>	8.35±0.04 <sup>d</sup>	8.41±0.02 <sup>d</sup>	8.25±0.03 <sup>d</sup>
T4: Live mulch	6.49±0.03 <sup>e</sup>	6.52±0.03 <sup>e</sup>	6.47±0.03 <sup>e</sup>	8.17±0.05 <sup>e</sup>	8.25±0.04 <sup>e</sup>	8.14±0.02 <sup>e</sup>
T5: Parthenium extract	7.18±0.03 <sup>b</sup>	7.19±0.03 <sup>b</sup>	7.14±0.03 <sup>b</sup>	9.66±0.04 <sup>b</sup>	9.74±0.02 <sup>b</sup>	9.64±0.03 <sup>b</sup>
T6: Weedy check (control)	7.38±0.05 <sup>a</sup>	7.41±0.05 <sup>a</sup>	7.34±0.07 <sup>a</sup>	9.72±0.04 <sup>a</sup>	9.78±0.02 <sup>a</sup>	9.70±0.04 <sup>a</sup>
CD	0.04	0.04	0.04	0.04	0.03	0.03
CV	0.73	0.81	0.82	0.62	0.42	0.51
SE(d±)	0.01	0.02	0.02	0.02	0.01	0.01
SE(m±)	0.01	0.01	0.01	0.01	0.01	0.01

Data are presented in the form of mean (n=3). CD = Critical difference, CV = Critical variance, SE = Standard error. Different superscripts present in the same column are significantly different (p<0.05).

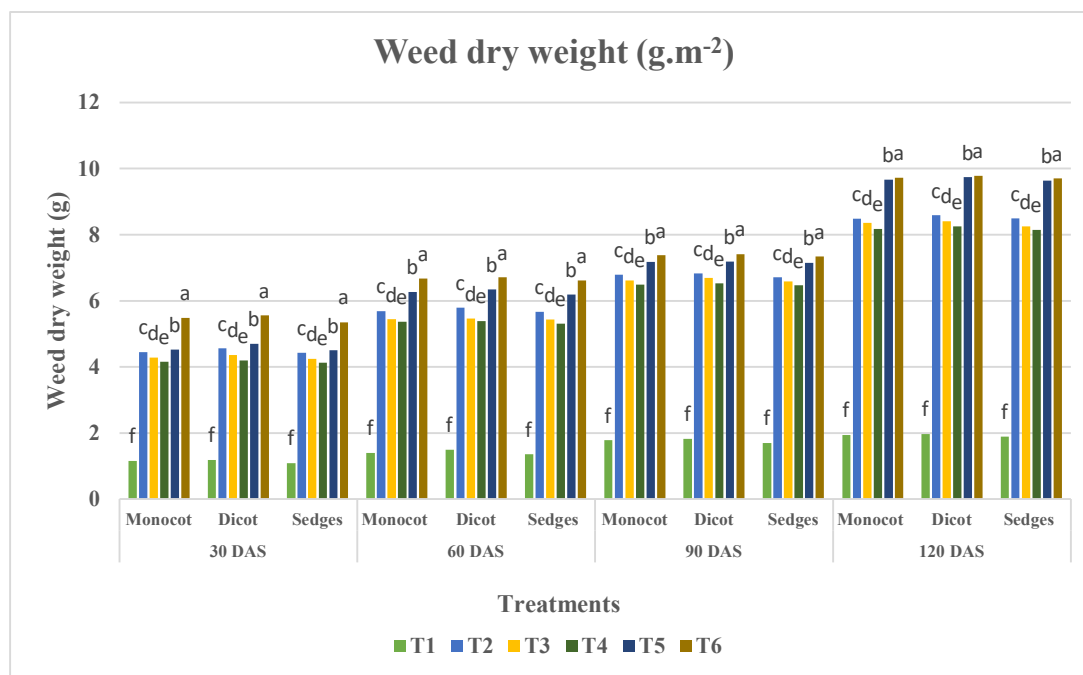


Fig. 14: Influence of different levels of nutrients and weed dynamics on weed dry weight (g.m<sup>-2</sup>) of sorghum.

sedges in T6 (Control), and the lowest was observed as 0.00 in T1 (Weed-free). At 60 DAS, the highest weed population was reported as 9.33 in dicots, followed by sedges and monocots in T6 (Control), and the lowest was recorded as 0.00 in T1 (Weed-free). At 90 DAS, the highest weed population was examined as 12.00 in T6 (Control), and the lowest was recorded as 0.00 in T1 (Weed-free). At 120 DAS, the highest weed population was recorded as 11.67 in dicots, followed by monocots and sedges in T6 (Control), and the lowest was observed as 0.00 in T1 (Weed-free). The weed population was maximum in the control treatment as no treatment to control weeds was applied, and the lowest was observed in weed-free treatment (Tables 8 and 9, Fig. 12). These results are in correspondence with the findings of Singh et al. (2012) and Thakur et al. (2016) in sorghum.

**Effect of different levels of nutrients and weed dynamics on weed control efficiency (%) of sorghum:** The weed control efficiency is significantly influenced by different levels of nutrient and weed dynamics of sorghum at 30, 60, 90, and 120 DAS (Tables 10 and 11). At 30 days after sowing (DAS), the highest level of weed control effectiveness was recorded as 100% in dicots, followed by monocots and sedges in treatment T1 (weed-free). The lowest level of weed control effectiveness was found as 0.00% in treatment T6 (control). At 60 days after sowing (DAS), the weed control effectiveness was highest, reaching 100%, in

dicots. Monocots and sedges followed with lower efficiency. This was observed in treatment T1, where the weeds were completely removed. The lowest weed control efficiency was recorded as 0.00% in treatment T6, which served as the control group. At 90 days after sowing (DAS), the weed control effectiveness was found to be 100% in treatment T1 (Weed-free), which was the highest observed. The lowest weed control efficiency of 0.00% was recorded in treatment T6 (Control). At 120 days after sowing (DAS), the weed control effectiveness was highest at 100% in dicots, followed by monocots and sedges in treatment T1 (weed-free). The lowest weed control efficiency was detected at 0.00% in treatment T1 (control). The weed control efficacy was highest in the treatment where no weeds were present, whereas the lowest efficacy was seen in the control treatment (Tables 10 and 11, Fig. 13). Ajaykumar (2023) found similar findings.

**Effect of different levels of nutrients and weed dynamics on weed dry weight (g) of sorghum:** The weed dry weight is significantly influenced by different levels of nutrient and weed dynamics of sorghum at 30, 60, 90, and 120 DAS (Tables 12 and 13). At 30 DAS, maximum weed dry weight was recorded as 5.56 in dicots followed by monocots and sedges in T6 (Control), and lowest was observed as 1.18 in T1 (Weed free). At 60 days after sowing (DAS), the dicots had the highest weed dry weight, measuring 6.71, followed by monocots and sedges in treatment T6 (Control). The lowest weed dry weight, measuring 1.49, was recorded in

treatment T1 (Weed free). At 90 days after sowing (DAS), the weed dry weight was greatest in treatment T6 (Control) at 7.41, while the lowest weight was obtained in treatment T1 (Weed-free) at 1.82. The weed dry weight reached its peak at 120 DAS, with dicots having the highest recorded value of 9.78, followed by monocots and sedges in T6 (Control). The lowest weed dry weight was found in T1 (Weed free), with a value of 1.96 (Tables 12 and 13, and Fig. 14). The primary reason for this was the improved management of weed development, which led to a reduction in the overall weight of weeds at the time of harvest. These data support the conclusions of Jat et al. (2016).

## CONCLUSIONS

In the present experiment, the effect of comparative analysis of mulching and weed management practices on nutrient and weed dynamics of Kharif sorghum on growth, yield, and weed parameters was studied. It was concluded from the results that the application of T1 treatment (Weed-free) followed by T2 (Sugarcane trash) and T3 (Vermicompost mulch) improves the growth, yield, and weed components of sorghum. Integrated weed management (IWM) involves integrating many tactics to reduce weeds. To accomplish effective weed control, integrated weed management requires systematic integration of several components. Mulching materials are commonly employed in the establishment of various plant and tree species. Mulches improve plant germination, survival, seedling transfer, and crop performance compared to unmulched treatments. Proper management of vital inputs, including tillage, fertilizers, and weeds, is crucial for improving overall production and stability. Weed control approaches for sorghum should be efficient, cost-effective, and ecologically friendly.

## REFERENCES

- Abdul Rab, A.R., Khalil, S.K., Muhammad Asim, M.A., Imran Khan, I.K., Hina Fayyaz, H.F., Haneef Raza, H.R. and Faisal Khan, F.K., 2016. Impact of sorghum extract type, concentration and application time on weeds density and wheat yield. *Pakistan Journal of Weed Science Research*, 22(3), pp.425-439.
- Ajaykumar, M.Y., 2023. Weed management practices on growth, yield, and economics of kharif grain sorghum. *International Journal of Environment and Climate Change*, 13(12), pp.1060-1071.
- Bajwa, A.A., Nawaz, A., Farooq, M., Chauhan, B.S. and Adkins, S., 2023. Herbicide program to control *Parthenium hysterophorus* in grain sorghum in an arid environment. *Crops*, 3(4), pp.292-301.
- Bavalgave, V.G., Deshmukh, S.P., Thanki, J.D. and Usdadia, V.P., 2017. Effect of integrated weed management practices on winter (Rabi) season sorghum (*Sorghum bicolor*). *International Journal of Computer Science*, 5(5), pp.2075-2078.
- Dhaka, B.K., Raj, R. and Dhaka, P., 2023. Integrated Weed Management in Minor Millets: A Review. *International Journal of Plant & Soil Science*, 35(23), pp.676-690.
- Dixit, A.K., Kumar, S., Rai, A.K. and Kumar, T.K., 2015. System productivity, profitability, nutrient uptake and soil health under tillage, nutrient and weed management in rainfed chickpea (*Cicer arietinum*)–fodder sorghum (*Sorghum bicolor*) cropping system. *Indian Journal of Agronomy*, 60(2), pp.205-211.
- Głąb, L., Sowiński, J., Bough, R. and Dayan, F.E., 2017. Allelopathic potential of sorghum (*Sorghum bicolor* (L.) Moench) in weed control: A comprehensive review. *Advances in Agronomy*, 145, pp.43-95.
- Hussain, M.I., Danish, S., Sánchez-Moreiras, A.M., Vicente, Ó., Jabran, K., Chaudhry, U.K. and Reigosa, M.J., 2021. Unraveling sorghum allelopathy in agriculture: Concepts and implications. *Plants*, 10(9), p.1795.
- Jat, A.L., Massey, J.X., Nepalia, V. and Joshi, E., 2016. Weed dynamics, production potential, and economics of sorghum (*Sorghum bicolor* (L.) Moench) cultivars as influenced by weed management practices. *Annals of Agricultural Research*, 36(1), pp.86-91.
- Kandhro, M.N., Shah, A.N., Kubar, M.I. and Laghari, M., 2015. Weed management and yield improvement in cotton through allelopathic mulches of sorghum and sunflower straw. *Pakistan Journal of Weed Science Research*, 21(4), pp.614-626.
- Kumar, K.A., Bhagavathapriya, T., Kumar, Y.S., Babu, K.S., Prabhakar, K., Parveen, S.I. and Jaya, M., 2022. Weed dynamics, crop growth and yield attributes of grain sorghum response to pre and post-emergence herbicides. *The Pharma Innovation Journal*, 11(12), pp.2631-2634.
- Kumar, K.A., Kumar, Y.S., Prabhakar, K., Jayalakshmi, M., Babu, K.S., Vishnuvardhan, K.M. and Rao, E.S.V., 2023. Effect of Mulching and Tillage Practices on Yield & Yield Attributes of Sorghum. *International Journal of Environment and Climate Change*, 13(11), pp.1584-1590.
- Kumar, N., Nath, C.P., Hazra, K.K. and Sharma, A.R., 2016. Efficient weed management in pulses for higher productivity and profitability. *Indian Journal of Agronomy*, 61(4), pp.5199-5213.
- Mishra, J.S. and Patil, J.V., 2014. *Nutrient Use Efficiency: From Basics to Advances*. Springer India, pp.297-315.
- Mishra, J.S. and Talwar, H.S., 2020. *Sorghum in the 21st Century: Food–Fodder–Feed–Fuel for a Rapidly Changing World*. Springer, pp.639-664.
- Singh, R.P., Yadav, P.N., Uttam, S.K., Katiyar, S.C. and Tripathi, A.K., 2012. Effect of moisture conservation and nutrient management on growth, yield, and water use efficiency of sorghum (*Sorghum bicolor*) under rainfed conditions. *Current Advances in Agricultural Sciences (An International Journal)*, 4(1), pp.37-40.
- Singh, S., Tiwana, U.S., Goyal, M., Rani, U. and Bhullar, M.S., 2019. Evaluation of different pre-and post-emergence herbicides on forage yield, quality, and disease reaction of multi-cut forage sorghum (*Sorghum bicolor*). *Indian Journal of Agronomy*, 64(1), pp.93-97.
- Thakur, N.S., Kushwaha, B.B., Girothia, O.P., Sinha, N.K. and Mishra, J.S., 2016. Effect of integrated weed management on growth and yields of rainy-season sorghum (*Sorghum bicolor*). *Indian Journal of Agronomy*, 61(2), pp.217-222.
- Vijayakumar, M., Jayanthi, C., Kalpana, R. and Ravisankar, D., 2014. Integrated weed management in sorghum (*Sorghum bicolor* (L.) Moench)—A review. *Agricultural Reviews*, 35(2), pp.79-91.

# A Review of Environmental Monitoring for Land Desertification Using Geospatial Analysis and Remote Sensing

Ghaidaa Sabah Yousef†, Hayder Dibs<sup>ID</sup> and Ahmed Samir Naje<sup>ID</sup>

Water Resources Management Engineering Department, College of Engineering, Al-Qasim Green University, Babylon, 51013, Iraq

†Corresponding author: Ghaidaa Sabah Yousef; Ghaida.m106416@wrec.uoqasim.edu.iq

**Abbreviation:** Nat. Env. & Poll. Technol.  
**Website:** [www.neptjournal.com](http://www.neptjournal.com)

*Received:* 30-06-2024

*Revised:* 26-07-2024

*Accepted:* 09-08-2024

## Key Words:

Land degradation  
 Remote sensing indices  
 Environmental monitoring  
 Landsat satellite images

## ABSTRACT

Studying and evaluating desertification is essential due to its potential occurrence as a result of both natural and anthropogenic processes. Precise forecasting of forthcoming climate change perils is crucial for devising policies, action strategies, and mitigation measures at both the local and global scales. Remote sensing facilitates the examination, monitoring, and forecasting of several aspects of desertification. Throughout the years, many methodologies have been employed to investigate desertification through the utilization of Remote Sensing (RS). This study investigated the worldwide prevalence and temporal sequence of research that utilized remote sensing (RS) to investigate desertification. In addition, the study assessed the primary approaches and factors employed in the examination of desertification through the analysis of remote sensing data. The application of remote sensing (RS) in the investigation of desertification can be traced back to 1991. Between 2015 and 2020, an annual average of over 40 publications were published, indicating a substantial rise in the utilization and accessibility of remote sensing (RS) technology to monitor desertification. However, there is a significant disparity in the amount of research conducted in different fields. Asia demonstrates a substantially higher quantity of studies in contrast to America or Africa. China has conducted the highest number of research on desertification using remote sensing (RS) techniques. The Thematic Mapper (TM) sensor is the principal source of satellite data, specifically Landsat pictures. The primary techniques utilized for studying desertification are classification and monitoring of alterations. Furthermore, remote sensing methods commonly employ land cover/land use change and vegetation, together with its attributes such as the Normalised Difference Vegetation Index (NDVI), as the primary factors for studying desertification.

## Citation for the Paper:

Yousef, G.S., Dibs, H. and Naje, A.S., 2025. A review of environmental monitoring for land desertification using geospatial analysis and remote sensing. *Nature Environment and Pollution Technology*, 24(2), D1697. <https://doi.org/10.46488/NEPT.2025.v24i02.D1697>

*Note: From year 2025, the journal uses Article ID instead of page numbers in citation of the published articles.*

## INTRODUCTION

Desertification and land degradation significantly impact both the economy and the environment. Land degradation affects approximately 1.4 billion people globally, with 74% of them living in impoverished conditions. The combined effects of drought and desertification result in an annual loss of 12 million hectares of cultivable land (United Nations 2015, Dibs et al. 2023a, Al-Janabi et al. 2024). Land degradation reduces land productivity in both biological and economic terms, leading to the deterioration of soil quality and permanent loss of natural vegetation (United Nations 1994, Bakr et al. 2012, Dibs et al. 2020, Palacios et al. 1999, Dibs & Mansor 2014, Van & Jetten 2015).

Since the 1970s, there has been increasing political and international attention toward arid, semi-arid, and sub-humid regions due to their crucial role in food production and social development. Extensive research has been conducted on this issue (Li et al. 2016, Becerril-Piña et al. 2016, Liu et al. 2018, Zhao et al. 2018, Kadhim et al. 2022). Desertification refers to land degradation in dry ecosystems, leading to desert-like conditions (Verstraete 1986, Dibs et al. 2020, Dibs et al. 2021a, 2021b, Hashim et al. 2021). The United Nations (1977) provided the first comprehensive



**Copyright:** © 2025 by the authors  
**Licensee:** Technoscience Publications  
 This article is an open access article distributed under the terms and conditions of the Creative Commons Attribution (CC BY) license (<https://creativecommons.org/licenses/by/4.0/>).



definition, emphasizing its economic consequences. This definition was expanded in 1994 to include land degradation caused by human activities and climate change, highlighting its socio-economic and ecological impacts.

The concept of desertification has since been widely used in international research, offering diverse methodologies for measuring, analyzing, and modeling its progression (Li et al. 2007, Cui et al. 2011, Bakr et al. 2012, Lamchin et al. 2016, Xu et al. 2016, Becerril-Piña et al. 2016, Liu et al. 2018, Zhao et al. 2018, Dibs et al. 2022a, 2022b, Hashim et al. 2022, Dibs & Al-Ansari 2023). Desertification is recognized globally as a major environmental concern due to its adverse effects, including dust storms, soil salinization, and biodiversity loss (United Nations 2015). It also has severe socioeconomic consequences, such as food scarcity, poverty, and health issues like malnutrition and respiratory diseases (Xiao et al. 2006, United Nations 2015).

The phenomenon is influenced by natural factors like temperature, precipitation, and vegetation loss, as well as human activities such as deforestation, urbanization, and land-use changes (Stringer 2008, Santini et al. 2010, De Pina

Tavares et al. 2015, Xu et al. 2016). Desertification poses a significant barrier to sustainable development in affected regions, necessitating urgent mitigation strategies (Wang et al. 2006, Helldén & Tottrup 2008, Dibs et al. 2023a, 2023b, 2023c). Recognizing its far-reaching consequences, the United Nations incorporated desertification into the Sustainable Development Goals (SDGs), particularly Goal 15, which aims to combat land degradation and promote ecosystem restoration (United Nations 2015).

Climate change projections indicate an increase in desertification due to shifts in temperature, precipitation patterns, and atmospheric carbon dioxide levels. These changes will exacerbate droughts and prolonged dry conditions, further intensifying land degradation (D'Odorico et al. 2013, Al-Bakri et al. 2016, Mutti et al. 2020, Sameer & Hamid 2023). SDG 15.3 emphasizes restoring degraded land and achieving land degradation neutrality by 2030, underscoring the necessity of addressing desertification to reduce poverty and mitigate climate change impacts.

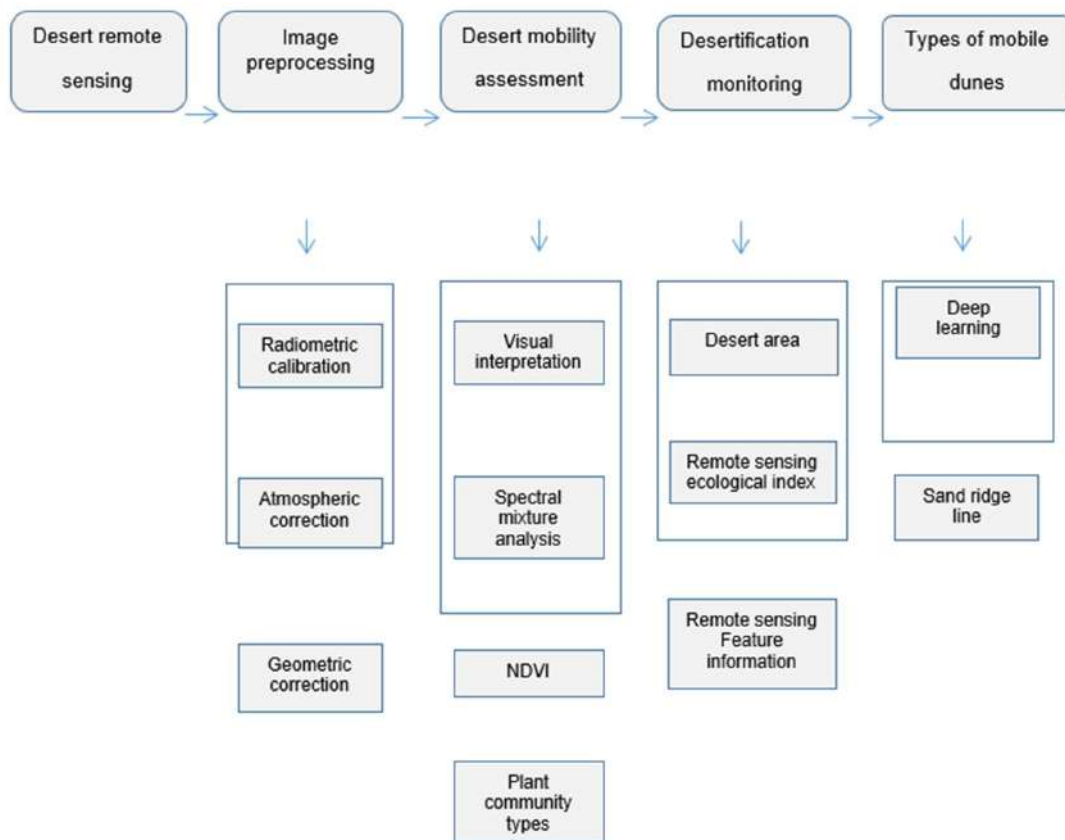


Fig. 1: The framework of desertification monitoring.

Advancements in remote sensing and deep learning techniques have enhanced desertification monitoring and assessment. However, further integration of these technologies is needed for improved accuracy and predictive capabilities. The application of remote sensing data and machine learning has provided valuable insights into desertification trends, yet additional interdisciplinary efforts are required for robust, scalable solutions. This study provides a comprehensive analysis of existing research methodologies, highlighting current trends and future directions in desertification research. Fig. 1 depicts the exact structural framework. Before initiating the inquiry, it was crucial to select a remote sensing dataset specifically for desert analysis and perform necessary data processing. This included examining and classifying mobile and non-mobile deserts, monitoring desertification in mobile deserts, and further categorizing morphological changes to improve understanding of desertification dynamics.

## DESERTIFICATION DETECTION

Therefore, it is crucial to differentiate between the occurrence of desertification and other phenomena such as climate change, desiccation, unpredictability, and drought, and swiftly highlight their interconnectedness. Drought is a natural event characterized by a transitory period of significantly reduced rainfall compared to the usual observed levels (UNCCD 1994, Darkoh 1996). Typically, current biological and social techniques are sufficient for managing temporary deficits in rainfall (Darkoh 1996). Wilhite & Glantz (1985) categorize and analyze several forms of drought, such as meteorological, agricultural, hydrological, and socioeconomic drought. Desiccation is the term used to describe long periods of less rainfall that can endure for several decades and have a significant impact on ecological and socioeconomic patterns. Resolving this issue requires a blend of efforts from both domestic and foreign sources. Desertification is not directly caused by drought or desiccation alone. However, if humans mismanage land, the consequences of these processes can be amplified, resulting in desertification in dry locations (Hulme & Kelly 1993, Darkoh 1996). Whereas climate change refers to long-term changes in climatic patterns, climate variability refers to transient variations in the climate. The modifications may result from either natural occurrences or human initiatives (Kelly & Hulme 1993, Darkoh 1996). According to Glantz & Orlovsky (1983), changes can occur in any or all of the atmospheric factors, such as precipitation, temperature, wind speed and direction, and evaporation.

Different forms of this kind could lead to changes in ecosystems, which in turn can impact human activities related

to the utilization of these ecosystems. Climatic change is the concept that there are gradual modifications in the usual weather patterns, which are mostly accountable for desertification. These changes arise organically within the climate systems (IPCC 2007). The intricate relationships and reciprocal connections between desertification and climate change are intricate. According to the Intergovernmental Panel on Climate Change (IPCC) in 2007 and the Millennium Ecosystem Assessment (MA) in 2005, desertification causes soil and plant depletion, which in turn fuels global climate change.

Research has established that if desertification is not controlled, it might lead to significant emissions of the greenhouse gas CO<sub>2</sub> into the atmosphere. Consequently, this would have substantial detrimental effects on the entire climate system. Global climate change is thought to exacerbate desertification by amplifying evapotranspiration and perhaps diminishing precipitation in arid regions. The West African Sahel region has clearly shown a tendency of rising hyperaridity, as reported by (Glantz & Orlovsky 1983, Kelly & Hulme 1993). Land desiccation is an irreversible natural phenomenon that is beyond human intervention. Furthermore, several investigations by researchers like (Darkoh 1996). Reed and Stringer (2015) and others have clearly shown that climate change is a real phenomenon that is greatly influencing the occurrence of desertification and land degradation in Africa.

Our understanding of the relationship between climate change and desertification in diverse socio-ecological zones, as well as their potential interconnections in various circumstances, is currently limited. They are reciprocally exerting an influence on one other and resulting in detrimental outcomes for the existing ecosystems.

## DESERTIFICATION EFFECTS

The complex phenomenon of desertification is the result of several interactions between environmental and human systems. The initial limitation of its analysis to biophysical environmental disciplines indicates a lack of comprehension of the complex nature of desertification. Impacts are quantifiable alterations in significant characteristics related to a particular situation (Grainger 2009). As to Grainger (2009), the human environment system undergoes a transition to a distinct state upon exceeding specific thresholds. The repercussions of any form of environmental destabilization have consistently demonstrated to be unacceptable and detrimental.

Therefore, the overall effects can be comprehended by considering the cause-and-effect relationship of the phenomenon. However, the diagnosis can be more comprehensively grasped and implemented based on the

distinct area or region. The 2005 Millennium Ecosystem Assessment brought attention to the fact that desertification varies greatly in terms of its effects and extent in various places and that it also evolves with time. The variability is determined by the degree of aridity in combination with the human impact on the ecosystems.

However, there is a notable discrepancy in our understanding and analysis of desertification and its underlying causes (MA 2005, FAO 1993). The impacts of desertification vary depending on the particular geographic region, country, and year and are influenced by four distinct causes.

- Factors that lead to land degradation encompass the magnitude and scope of gravity,
- as well as the intensity of climatic conditions
- These factors include the size and variety of the population affected, as well as the amount of progress
- and advancement in the country.

Hence, when individuals experience increasing poverty and societies remain less developed, the severity of desertification's long-term consequences and the likelihood of catastrophic outcomes also escalate, particularly in the face of challenging climatic conditions. Desertification has a worldwide influence by diminishing the fertility of the land and depriving individuals of vital biological resources necessary for human sustenance (Darkoh 1996, 1998). As a result, this leads to secondary socioeconomic effects such as famine and illnesses that arise from insufficient agricultural production, poverty, and restrictions on water quality and availability (UNCCD 2013).

Desertification leads to a decrease in plant growth, which in turn leads to a reduction in livestock output, overall plant biomass, and plant species diversity. Desertification is linked to the decline in biodiversity and the decrease in the number of living organisms within a specific area and timeframe (El-Karouri 1986, Mortimore 1989, Nneji 2013, Stephen 2014, Olagunjo 2015). This phenomenon is also known as the reduction in the range of living species (Senanayake 2012).

Grazing areas and pasture accessibility are significantly impacted by desertification (Okello et al. 2014, Ijah 2014). The socio-economic consequences are wide-ranging and include the loss of social capital, an increase in household debt, and the erosion of regional traditions and ecological expertise (Fredricson et al. 1988, Zaman 1997). One of the factors influencing the rise in migration is desertification (Ababa 2007, Abdi et al. 2013, Olagunjo 2015). The reported impact of this issue on the exploitation of natural resources has resulted in confrontations among different user groups (Abbas 2014, Ijah 2014, Oladipo 2015). Desertification

also affects pastoralists, a common practice in dry areas (Mortimore 1989, Stiles 1983, Tully & Shapiro 2014).

The severance of the profound connection between persons and the land results in substantial modifications in social structure, cultural legacy, and political stability (FAO 2001). Regional conflicts and the failure of weak administrations are more likely to occur as a result of the rising rates of malnutrition and water scarcity among people (UNCCD 2014).

Desertification in China leads to a significant reduction in cultivable land and a drop in the benefits provided by vegetation. Moreover, it lowers the standard of living in urban industrial zones and raises the costs of upkeep for the physical infrastructure. Notably, it results in a rise in rural poverty and migration driven by environmental factors. The destruction has intensified on a global scale. Minuscule particles carried by dust and sandstorms have already reached the western coast of America. The sandstorms are causing harmful health effects in the eastern and southern regions of China, as well as in Japan and Korea. Japan, Korea, and parts of eastern and southern China are also suffering negative health impacts from the sandstorms.

Desertification presents a substantial threat to the sustenance of millions of individuals and leads to yearly financial setbacks as a result of reduced output. As a result of mandatory relocation, farmers have been forced to migrate, leading to a growing imbalance in the demographic distribution between China's eastern and western areas. The stability of society is in danger due to the rising unemployment rate, which is fueling tensions between urban and rural populations and a rise in criminal activity (Zeng 2005). Mexico has been greatly impacted by desertification. This issue arises when persons forsake land that has experienced degradation and relocate to locations that are less suitable for agricultural cultivation (Schwartz & Notini 1994).

The report neglects to take into account Mexico's poverty rate, which affects around two-thirds of its population, who predominantly live in poverty. The study did not consider indications of desertification consequences, such as changes in agricultural productivity and the diversity of farmed crops. The UN report illustrates that desertification in Burkina Faso leads to a multitude of significant consequences. The factors that contribute to poverty and destitution include the following: a decline in soil fertility or its total loss, a decline in biodiversity, a loss of plant life and delicate ecosystems, an increase in climatic fluctuations, conflicts between farmers and herders, and movement of people and livestock, including transhumance and nomadism ([www.org/esa/sustdev](http://www.org/esa/sustdev)). Kambou (2002) emphasized significant signs of

the impact of desertification, including an increase in poverty rates in rural regions and alterations in migration patterns.

The United Nations should have recognized the changes in livestock size and composition as significant indicators of impact in countries with pastoralist communities and high poverty rates, as well as a decline in vegetation and fodder coverage. This would have facilitated a more methodical evaluation of the influence of desertification on pastoralism. Moreover, the effect indicators and the state indicators were combined, making it difficult to distinguish between the two (Kambou 2002). did not offer a more explicit indication of migratory tendencies. The FAO study found that the primary consequence of desertification in Somalia is the occurrence of localized conflicts among Somali clans and lineages. These conflicts arise due to disputes over the ownership and administration of newly constructed boreholes and the adjacent meadows.

The study has identified a deficiency in understanding potential alterations in the species and physical characteristics of animals over a specified period. The Ghanaian Environmental Protection Agency (2002) identified several consequences of desertification, including decreased soil fertility and agricultural productivity, the enlargement of unproductive land, reduced vegetation cover in terms of both quality and quantity, and a decreased ability of the land to withstand natural climate variations. The socio-economic ramifications include increasing deforestation, famine, higher rates of migration, lower incomes, and a rise in poverty.

As a national report, it is anticipated to offer a thorough comprehension of the phenomenon. Specifically, addressing the impacts on livestock in the study would have been more thorough, given the sizeable population of 1.25 million cattle, 2.5 million goats, and 2.4 million sheep in Ghana's savannah. Moreover, the concept of plant cover decline as a pivotal indicator of desertification was unclear and did not offer any indication of a definite timeframe. Furthermore, the study encountered difficulty in accurately assessing the influence of fluctuations in agricultural production on individuals' means of subsistence and the subsequent repercussions (Abdi et al. 2013). desertification is the main catalyst for the migration of rural inhabitants to urban areas in Sudan.

The association between political and social instability and land degradation is significant, as demonstrated by the civil disturbance in Southern Sudan, resulting in a significant influx of people migrating to Kenya. The examination also uncovered a decline in vegetation and the extinction of important species. The decrease in rainfall leads to the well-acknowledged phenomenon of vegetation deterioration,

soil erosion, and reduced agricultural output and livestock production, accompanied by an increase in migration. The migration indices and crop output loss, which are important indicators of severe outcomes, lack sufficient information. To gather more comprehensive data from the local residents, the study may have utilized survey approaches.

The Ethiopian Highlands currently suffer from 14 million hectares of severely damaged soil. Within the next 20 years, it is predicted that the highlands' per capita income will drop by 30% if this pattern of soil deterioration continues (Tamiré 2000). The study determined that the present condition of the land is inadequate for sustaining plant life, resulting in a decrease in organic matter. As a result of degradation, Ethiopians have become increasingly vulnerable to drought. Regretfully, the study was unable to obtain more precise data—particularly about agricultural output and the extent of migration—by combining its contextual assessment, field observation, questionnaire, and interview (Jones 2006).

According to a case study on poverty and governance in Namibia, the economy was significantly impacted by desertification. Seely & Klintenberg (2011) examined desertification in Central Namibia and found that the primary causes of the effects of desertification were soil erosion, deforestation, deterioration of arable land, degradation of rangelands, and degradation of woodlands.

Applying a cautious approach, experts have calculated that the annual economic loss in central Namibia is at a minimum of US\$10 million. The main expenses identified were the reduced accessibility of construction materials and firewood, exacerbated by the time required to collect them or the cost of purchasing them from the market as replacements.

Jones (2006) and Seely & Klintenberg (2011) demonstrated a tendency to emphasize the economic aspects of desertification, indicating bias. As a result, there was a lack of data collection from individuals who are most impacted by desertification, potentially leading to a more thorough comprehension of the situation. According to research by Klintenberg & Seely (2004), 70% of Namibians are dependent on subsistence farming. Unfortunately, the study lacked any empirical evidence about the influence of desertification on crop productivity.

Undertook research in Namibia to evaluate the economic consequences of desertification in the region. The majority of Namibians live in communal areas where they depend on the land for their nourishment and financial gain from cattle, but the study also revealed that desertification has complex effects on the time and labor required for fuelwood and fencing, as well as the food security of families. The phenomenon of desertification in commercial districts



exhibited a wide range of characteristics and resulted in various consequences. Specifically, the proliferation of shrubs was discovered to have a detrimental effect on the accessibility of grazing lands, resulting in a decrease in the animal population and subsequent loss in sales (Quan et al. 1994).

The study undertook an economic evaluation of the impact of desertification on the livelihoods of individuals in Namibia. Nevertheless, it overlooked the fact that immigration and migration are commonplace and may have an effect on remittances sent home and, in turn, the economy. For the over a million Nigerians who live on the edge of the floodplain and depend on the marsh for their livelihoods as farmers, cattle herders, and fishermen, Emeka (2013) claimed that there have been serious socioeconomic repercussions (Emeka 2013). The reduction in fish productivity in Nigeria's rivers, lakes, swamps, and flood plains provides more evidence of the detrimental effects of drought and desertification in the Sahel and Sudan regions (Palacios & Ustin 1998, Ajayi 1996). The total production from all fresh water sources had an annual drop of approximately 54% between 1980 and 1985.

The research undertaken by Emeka (2013) and Nwafor (1982) has not adequately investigated crucial indicators of the consequences, such as the pervasive conflict between farmers and livestock owners in Northern Nigeria, namely in the Frontline states (Ajayi 1996). The study does not provide information on whether the drop in yield was specifically caused by the crops that were cultivated (Thelma 2015). Desertification in Northern Nigeria poses a significant economic hazard. The main consequences of desertification in the region are the detrimental impacts on both food security and employment. The study additionally revealed that the majority of conflicts in the area stem from environmental factors. The primary source of conflict develops between agriculturalists and pastoralists.

Nevertheless, the study did not investigate the impact of agricultural cultivation on desertification, resulting in a significant lack of knowledge in this area. The Nigerian government claims that desertification has worsened the food situation in the region, leading to a decrease in the food security index. Drought leads to significant economic upheaval. The significant decline in the Gross Domestic Product (GDP) by 18.4 percent in 1971-1972 and 7.3 percent in 1972-1973 can be attributed to the presence of drought.

Moreover, it was thought to be the primary reason for the food price index's sudden spike and the decline in non-oil exports that followed. Migration resulting from aridity or drought occasionally results in the fragmentation of families since males frequently abandon females and offspring in

order to seek employment in urban areas (FMEnv 2001). Pastoralism is an essential component of peoples' livelihoods and a key indicator of the effects of desertification, but its effects on it are little understood. An alarming pattern has arisen among these nations, indicating that developing countries are nearing a crucial juncture.

The consequences of desertification in Burkina Faso, Sudan, Nigeria, Ghana, and other countries have become a major source of social discontent and insecurity. The nations have seen widespread poverty, conflicts arising from the exploitation of natural resources, and a significant increase in urban migration due to desertification. The desertification in China can be attributed to the magnitude and variety of its population.

## DESERTIFICATION CONTROL MEASURES

Addressing desertification and land degradation in affected countries is crucial for attaining sustainable development (UNCCD 2006). Concern over the growing extent and effects of desertification around the world led to the official approval of the United Nations Convention to Combat Desertification in Paris in 1994. By the year 2000, more than 172 governments have signed the convention (UNCCD 2006). On May 19, 2014, Southern Sudan became the 195th member to join the Convention. The primary goal of the Convention is to tackle desertification and alleviate the negative consequences of drought in Africa. The recommended approach is to implement customized control measures that consider the unique circumstances of each country (UNCCD 2006). In addition, the UNCCD proposed the implementation of measures such as:

1. Enforcing strategies to avoid and diminish the deterioration of land, including the rehabilitation of land that has already been degraded.
2. Raising awareness and educating people who are affected by land degradation.
3. Improving the social environment through the elimination of poverty and the enhancement of health and educational conditions, fostering knowledge sharing on sustainability, and emphasizing the significance of natural resources.
4. Revitalizing the traditional wisdom of indigenous cultures.

The development of community conservation zones in Benin employed a participatory strategy to save the biodiversity of coastal wetlands ([www.worldbank.org](http://www.worldbank.org)). Presently, about 150 communities are actively engaged in the process and possess the capacity to efficiently harness the biological diversity of marine resources in a manner that

ensures long-term sustainability. These communities also benefit from environmentally conscious corporate activity. The endeavor has successfully alleviated the poverty of the individuals residing in the vicinity of the river, who were previously compelled to deplete and deplete the natural resources. More people are realizing how important it is to protect mangroves, coastal areas, and forests to ensure that future generations can continue to live. Previous projects supported by the World Bank have specifically targeted sub-watersheds in the lowland regions of Burkina Faso. These programs have demonstrated the ability of communities to improve the efficiency of rural resources. By adopting sustainable practices that prioritize the preservation of biological and agricultural diversity, as well as the restoration of soil and water resources, the people of Burkina Faso have effectively achieved economic growth while also promoting environmental well-being. The SILEM Project introduced the concept of biodiversity in a productive setting within the Sahel region. The program facilitated and accelerated the creation of community connections to guarantee the enduring conservation of natural resources at the local watershed level.

This was achieved through the implementation of incentives, the establishment of an investment structure that is in line with the nation's objectives, and the recognition and enhancement of individual and collective skills. Approximately 160 towns received allocated funds to support the execution of several initiatives pertaining to the management of natural resources. Natural resource preservation, livestock and fishery management, forestry management techniques, reforestation, soil and agriculture techniques, and water conservation technologies were among the activities (UNCCD 2013). One important aspect of the problem that none of the World Bank's studies addressed was the need to raise public awareness of desertification. The Rehabilitation of Arid Environments (RAE) is a recognized nonprofit organization that is widely praised for its efforts in advancing rural development in Kenya.

RAE is based in Baringo County, in the semiarid and dry lowlands of the Rift Valley in Kenya. The Royal Academy of Engineering (RAE) has been actively involved in this industry for over three decades. In the early years of RAE's operations, growing problems with soil erosion, loss of plant diversity, and other factors rendered about 70% of Baringo County's land unusable. The terrain was severely degraded, and there was a significant prevalence of instability and ethnic tensions due to insufficient resources. The incidence of poverty has reached concerning proportions, with rates as high as 90 percent in several regions, and there has been a pervasive absence of sufficient access to food. Lake Baringo, the main source of freshwater in the area, was

heavily contaminated with sediment. The RAE implemented a comprehensive strategy to restore the damaged areas by involving the community and incorporating traditional knowledge. RAE initiated the restoration of the original savannah grass ecosystem by reintroducing native grass species that had vanished as a result of excessive grazing. The Royal Academy of Engineering (RAE) has reached a consensus on a standardized approach for overseeing the reseeded districts.

The settled residents employed fences, whilst the nomadic herders engaged in communal grazing. Income-generating endeavors, including hay baling, collecting and selling grass seed, apiculture, field rentals, milk sales, thatching grass harvesting, and firewood collection, strengthen these tactics. Research undertaken by the United Nations Development Program (UNDP) in 2013 focused on analyzing strategies to enhance the empowerment of local communities. The study focused primarily on improving people's means of supporting themselves, conducting initiatives to reduce the impact of drought, and utilizing the capabilities of traditional knowledge. The initiative presently provides direct benefits to over 20,000 individuals, while an additional 380,000 to 550,000 people benefit indirectly from it (UNCCD 2013). Although there are still certain project management difficulties that have not been handled, the natural grass and tree species that were previously not present in the area are now thriving. The soil's physical features, including its nutritional composition and water absorption capacity, have shown improvement.

Community organizations have witnessed a decrease in poverty rates and an enhancement in food security. Both males and females studying and assessing desertification is crucial because it can arise from both natural and human-induced causes. Accurate prediction of impending climate change threats is essential for developing policies, plans of action, and mitigation techniques on a local and global level. Remote sensing enables the analysis, surveillance, and prediction of several elements of desertification. Throughout the years, many methodologies have been employed to investigate desertification through the utilization of Remote Sensing (RS). This study investigated the worldwide prevalence and temporal sequence of research that utilized remote sensing (RS) to investigate desertification. Furthermore, the study evaluated the main methodologies and variables used in the investigation of desertification by analyzing remote sensing data. The first use of remote sensing (RS) for desertification research dates back to 1991. Between 2015 and 2020, an annual average of over 40 publications were published, indicating a substantial rise in the utilization and accessibility of remote sensing (RS) technology to monitor desertification. However, there is a significant disparity in

the amount of research conducted in different fields. Asia demonstrates a substantially higher quantity of studies in contrast to America or Africa. China is the country that has used remote sensing (RS) techniques to perform the most studies on desertification. The Thematic Mapper (TM) sensor is the primary provider of satellite data, particularly Landsat images. The main methodologies employed for investigating desertification are categorization and surveillance of changes.

Additionally, vegetation and its characteristics, such as the Normalized Difference Vegetation Index (NDVI), are frequently used in conjunction with remote sensing techniques to research desertification. This is relevant in the most arid regions of Ethiopia that are currently experiencing extended periods of severe drought or a consistent decrease in moisture levels. Disregarding variations in climate, ecology, economy, culture, and human activity, the terracing programs implemented in different regions may prove to be unsuccessful, as policies and practices that are successful in one area may not necessarily work well in another. In the highlands of Ethiopia, Tamir (2000) conducted a study that discovered various methods for managing desertification in the region. The techniques encompass the implementation of physical and biological conservation measures, the establishment of a catastrophe preventative and preparedness strategy, and the creation of an environmental protection agency.

The study focused exclusively on desertification in the Ethiopian highlands. However, it did not provide any analysis of the efficacy of institutional frameworks in addressing this issue. Moreover, the socio-economic tactics used in the highlands were not examined in the study (Darkoh 2000). The indigenous people of Mid-Boteti have evolved many strategies to endure their harsh environment, which is marked by recurrent droughts. The practice of utilizing the periodic increase in river flow in a region that is mostly dry is referred to as “flood recession cultivation.” Additional adaptations are implementing mixed cropping techniques, strategically relocating animals based on water availability, substituting cattle with goats in times of drought, and integrating non-agricultural and agricultural activities to mitigate risk.

Klintonberg & Seely (2004) focused on the monitoring of land deterioration in Namibia and proposed several solutions to combat desertification (Klintonberg & Seely 2004). Hence activities entail raising awareness about the causes and consequences of land degradation while also working together with local communities and scientists to build the National Monitoring System (Jones 2006). found that the establishment of the Programme to Combat Desertification (NAPCOD) was part of Namibia’s institutional framework. Through pilot projects in certain areas, NAPCOD worked

with rural stakeholders to evaluate land use, agricultural techniques, and alternative ways of living. The World Wildlife Fund (WWF), Namibia’s Ministry of Environment and Tourism, and USAID are all providing financial support for the LIFE project, which seeks to help Namibia implement community-based resource management. The project centers around three primary domains: augmenting the natural resource foundation, establishing indigenous institutions, and fostering the development of enterprises rooted in natural resources. Consequently, it combines the preservation of biodiversity, democratic principles, governance, and enterprise development into a single cohesive endeavor.

The study, although thorough in analyzing the overall response of the institution, does not discuss the precise method for evaluating the efficiency of control measures. This relates to a lack of knowledge about the integration of the local population into the system, particularly with regard to biophysical control techniques. The study did not provide any empirical evidence from a survey that demonstrated the local population’s reactions to desertification. Tanzania implemented control measures by creating government-operated tree seedling nurseries around the country. The nurseries sent a diverse range of young trees to villages to plant them (Darkoh 1982, 1987).

A thorough education campaign regarding the dangers of desertification and the importance of afforestation was launched in many regions. The government created physical and regional land use plans as part of a comprehensive national strategy on land and human settlement. Furthermore, the government aimed to decrease the utilization of fuel wood by promoting the adoption of alternative energy sources such as coal, natural gas, solar, and wind power. Furthermore, the prioritization involved implementing ways to combat soil erosion and overgrazing, promoting public engagement, providing training for environmental law enforcement, and advancing research. To effectively address desertification, the control strategies used combined bio-physical and socio-economic measures. The study has presented a multitude of prospects for additional investigation into desertification in Tanzania.

The National Action Programme to Combat Desertification was formulated in 1999, and a regulatory structure for Environmental Management in Tanzania was also established. Muyungi’s 2007 research revealed a significant level of government engagement in environmental matters and the sustainable management of resources in Tanzania following the Rio Conference in 1997. The National Environmental Action Plan, which conducts a comprehensive assessment at the national level and establishes a framework for integrating environmental

considerations into government decision-making, has made significant advancements.

## REMOTE SENSING FOR DESERTIFICATION

Remote sensing (RS) is beneficial for evaluating the primary indicators of desertification due to its ability to encompass extensive regions (El-Hassan 2004, Sun et al. 2005). Monitoring and mapping desertification is the most effective technique for managing and stopping the progression of desertification. Remote sensing methods have been used to identify and characterize sand dunes and their shifting patterns throughout time, as well as to monitor and evaluate changes

in land degradation (Collado et al. 2002, Lam et al. 2010). Satellites have supplied data for worldwide surveillance during the last twenty years, which is crucial for enhancing our comprehension of desertification (Collado et al. 2002, Pellikka et al. 2005, Yanli et al. 2012). Desertification, a persistent issue, is seeing a yearly growth rate of 25%. Consequently, multiple investigations have been carried out utilizing remote sensing techniques to detect these activities on a worldwide scale (Collado et al. 2002, El-Hassan, 2004, Sun et al. 2005, Shalaby & Tateishi 2007, Fang et al. 2008). Remote sensing (RS) technology offers numerous benefits, including time efficiency, wide coverage (unattainable by ground-based

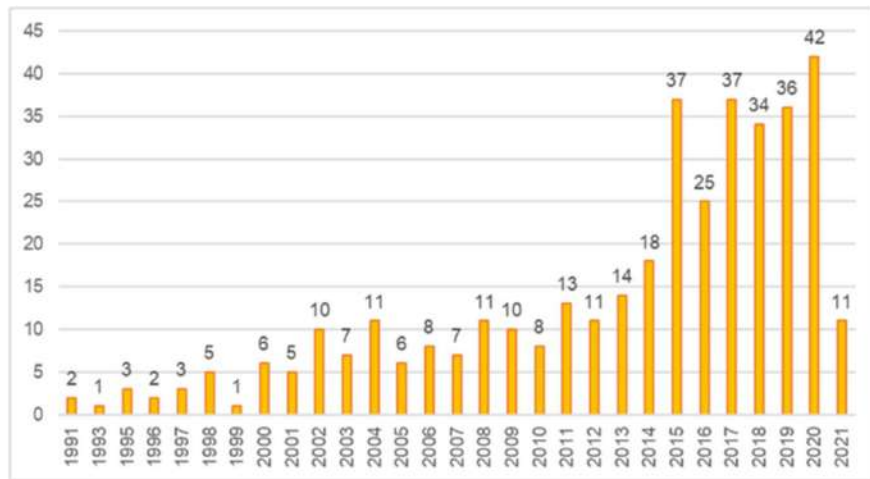


Fig. 2: Timeline of the use of remote sensing to study desertification (Daniela et al.2022).

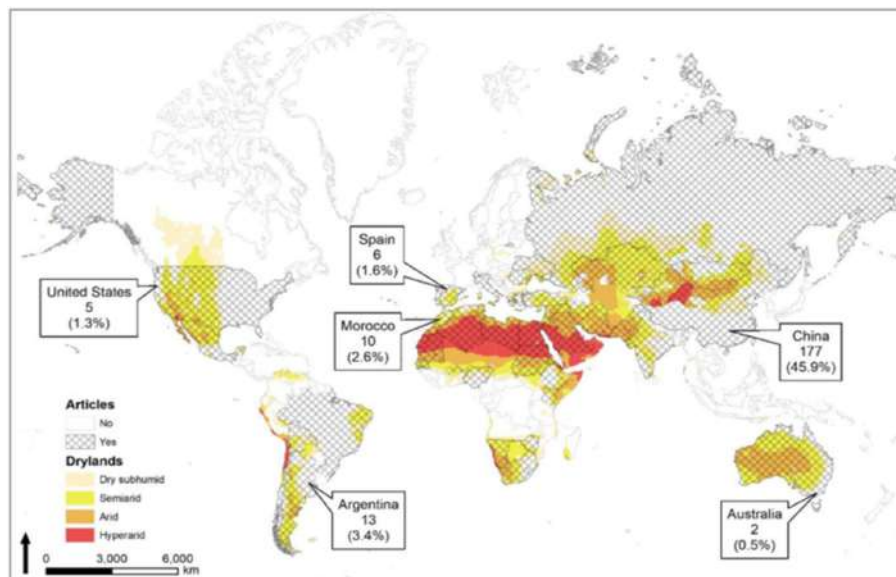


Fig. 3: displays the countries and regions that have conducted research publications on desertification utilizing remote sensing (Daniela et al. 2022).



methods for large areas or regions), rapid data acquisition, and The capacity to enable continuous monitoring of land covering and land utilization over an extended period (Wu et al. 2002, Shalaby & Tateishi 2007). The techniques listed provide different levels of imaging resolution. They are categorized as high (SPOT, IKONOS, QuickBird, GeoEye-1, Worldview-1, WorldView-2) and low (NOAA-AVHRR), medium (Landsat TM, Landsat MSS, IRS-I, ISS-II). Landsat imagery is frequently used to depict the impact of desertification on both humans and the environment. The extensive availability and easy accessibility of these pictures are primarily responsible for this problem (Wu et al. 2002, El-Hassan, 2004, Sun et al. 2005, Leona & Sommer 2000, Yang et al. 2007). Improved resolution in imaging enables the detection of more complex details, resulting in increased precision and more detailed image analysis.

Data from remote sensing can be fed into a geographic information system (GIS) to enable further analysis and cross-referencing with data collected from various locations or eras. By intentionally selecting the suitable band or bands according to specified factors like soil, water, or vegetation and integrating GIS with remotely sensed data, one can acquire useful information about the attributes of land cover changes. This method is especially valuable for examining extensive regions and comprehending the spatial arrangement of various alterations in land surface (Abbas & Khan 2007, Shalaby & Tateishi 2007).

Data from remote sensing and GIS techniques are becoming more and more important for information

extraction and analysis related to a variety of topics, including the mapping of urban land use, the measurement of drifting sand areas, the study of ecosystem dynamics, and the monitoring of geological risks like global warming (Ali & Bayoumi, 2004, Sun et al. 2005, Kapetsky & Aguilar-Manjarrez, 2007).

The utilization of remote sensing data in the examination of desertification has experienced a substantial rise in recent years. Between 2000 and 2010, an average of 10 publications were published that made use of remote sensing data. However, since 2015, this number has dramatically increased to about 40 articles per year. These findings suggest a rise in the utilization of remote sensing methods and their accessibility for monitoring desertification (Fig. 2). The map in Fig. 3 reflects arid areas where remote sensing has been used to study desertification. Nevertheless, there is a noticeable geographical variation. One can observe a disparity, for instance, in the quantity of research conducted on desertification in Asia as opposed to the research on desertification in America or Africa. In Africa, there are 45 papers on desertification studies that utilize remote sensing, while in America, there are 35. In contrast, Asia has a far higher number of articles, with 245 focusing on desertification and remote sensing.

### Remote Sensing Techniques

Researchers have employed the usage of (Bayarjargal et al. 2006, Murad & Saiful 2011). To identify and assess meteorological drought. The NOAA-AVHRR sensor is

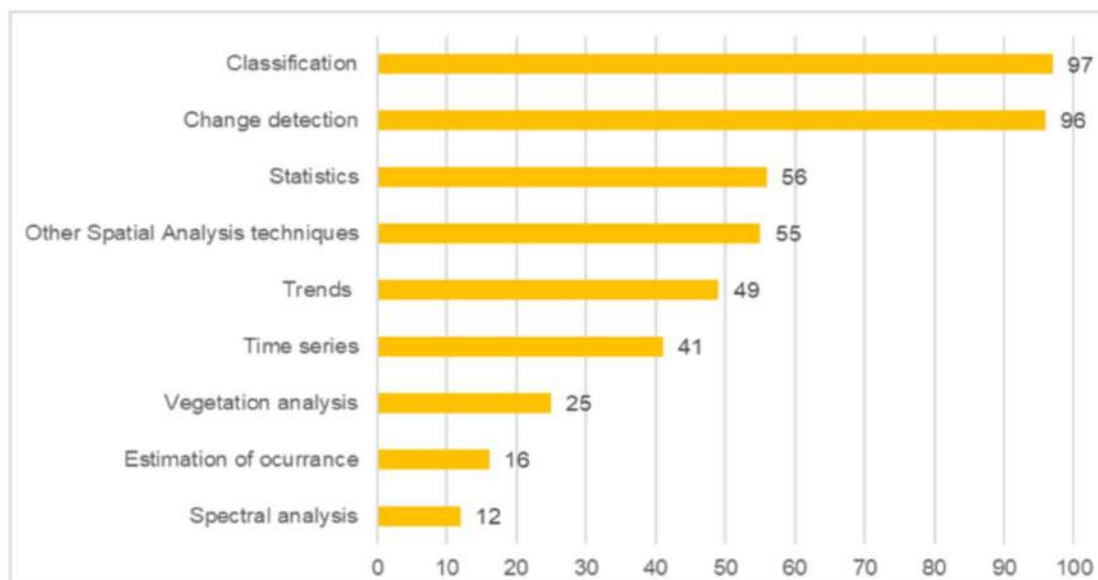


Fig. 4: Most used methods for the study of desertification using remote sensing over the past 35 years (Daniela et al. 2022).

frequently employed for the investigation of drought. Integrating reflectance bands—the Normalized Difference Vegetation Index (NDVI)—and thermal bands—the Land Surface Temperature (LST)—is necessary for the data acquisition process. The application of this sensor has been extensively used in the domain of drought study, as evidenced (Karnieli & Dall’Olmo 2003). Other often used drought-related indicators include the Vegetation Condition Index (VCI), Global Vegetation Index (GVI), Integrated or Standardized NDVI, and NDVI anomaly for identifying and tracking drought-affected areas.

Many different methods have been used to evaluate and analyze the desertification process using remote sensing data. Classification and change detection are the most used methods in recent years, as shown in Fig. 4.

### Challenges Associated With Remote Sensing

Remote sensing technology employs automated devices, such as satellites, to acquire and send visual data (Hay et al. 2000). Before utilizing remotely sensed imagery, such as satellite imagery, for the assessment of a particular matter or concern, it is imperative to perform corrective processing, including atmospheric correction and picture alignment, as well as to conduct comprehensive data analysis (Jha 2010). It is crucial to merge remotely sensed data with supplementary data, ensuring that both sources are precisely aligned and integrated (Levin 2009). Accurate and trustworthy data is essential for effectively applying the results of inventory analysis, environmental monitoring, and high-quality thematic mapping (Adjei 2009). Precision is essential to facilitate policy reform and build vital management frameworks that are important for regulating desertification processes (Kelly & Thomas 2012).

Presently, relying solely on satellite pictures is insufficient for making a dependable conclusion. Therefore, it is crucial to utilize qualitative methodologies (Mesev 2007). Every imaging sensor has specific limitations in its capacity to recognize situations, including thematic, temporal, and other forms of interpretation (Chen 1995). Remote sensing is suggested as a method for obtaining timely, current, and somewhat accurate information to support the sustainable and efficient management of vegetation (Kasawani et al. 2010).

### DESERTIFICATION KEY INDICATORS

Remote sensing is a useful tool for detecting, monitoring, and mapping many important indicators of desertification processes in areas that are impacted. To analyze different environmental scenarios, researchers frequently use indicators including land use, soil, erosion, urbanization, and drought.

**Land Cover/Land Use:** Satellite data has demonstrated its utility in the examination of vegetation, encompassing the analysis of its composition and land utilization. The expansion of agricultural areas can negatively affect water reserves and quality, as well as the chemical and physical characteristics of soil (Karnieli & Dall’Olmo 2003, Collado et al. 2002, El-Hassan, 2004, Shalaby et al. 2004, Mohammed et al. 2022, Hassan et al. 2020, Ali et al. 2020, Naje et al. 2020, Al Harbi 2010).

Remote sensing methods are used to monitor changes in agricultural land use, which makes it easier to monitor the processes of desertification in semi-arid and arid regions. Land use and agricultural land are good indicators because they can be easily identified in satellite imagery. By examining the color composites, one can find variations in the topsoil and vegetation distribution composition.

Remote sensing techniques enable the evaluation of changes in vegetation and the estimation of desertification processes (Ali & Bayoumi 2004). Several research studies have investigated changes in land cover and land use in arid and dry regions of Africa (Palmer & van Rooyen 1998), China (Wu & Ci. 2002), Sudan (Ali & Bayoumi 2004), Egypt (Shalaby et al. 2004, Shalaby & Tateishi 2007), and Saudi Arabia (Al Harbi 2010) in connection with land degradation and desertification. The increase in agricultural land is strongly linked to the decrease in areas of natural vegetation (Al-Balooshi 2003, Shalaby & Tateishi 2007, Al Harbi 2010).

Inadequate land management techniques, such as overgrazing, excessive irrigation, mining, and deforestation for residential purposes, can inflict substantial damage to the land and exacerbate the process of desertification. Remote sensing technology can help identify these challenges. The research conducted in Argentina (Collado et al. 2002), North China (Fang et al. 2008), Saudi Arabia (Weiss et al. 2001, Al Harbi 2010), and the Sahel (Hein & Ridder 2006) Utilized satellite imagery obtained from Landsat-2, Landsat TM, NOAA-AVHRR, Landsat TM5, and SPOT. Remote sensing data has been used to examine changes in vegetation coverage, patterns, and conditions in desertification research by utilizing the normalized differential vegetation index (NDVI) (Chen & Zhu 2001).

An increasing amount of data indicates that using the Red-Edge spectral band can improve the sensitivity and accuracy of plant study, especially in areas with little flora, including semi-arid and dry regions (Jha 2010, Kundu & Dutta 2011, Yanli et al. 2012). It is essential to detect decreases in proportion to the initial level to evaluate the severity of drought and estimate the process of desertification (Weier & Herring 2012).

Satellite imaging can be utilized to observe the deterioration of ecosystems by quantifying rain-use efficiency (RUE), a commonly employed measure for assessing the condition of plant cover [115] (Hein & Ridder 2006) decrease in RUE signifies a reduced capacity of the flora to transform water and nutrients into biomass (Hein & Ridder, 2006, Verón et al. 2006). The following loss in plant cover results in reduced nutrient accessibility and increased runoff due to soil compaction. Hein and De Ridder (2006) observed that prior research on remote sensing (RS) and radiation use efficiency (RUE) failed to take into account the impact of annual rainfall fluctuations on RUE. Remote sensing methods are unable to substitute the necessity for data obtained directly from the ground. The utilization of remote sensing and supplementary data in agricultural research is mutually beneficial, and efficient results can help farmers create comprehensive and ongoing management plans through strategic planning and decision-making (Hill et al. 2006).

**Soil:** Remote sensing imaging has been utilized to analyze soil properties in research on desertification (Ustin et al. 2004, Ben-Dor et al. 2009). Climate fluctuations render fragile soils susceptible to erosion and subsequent desertification (Dragan et al. 2005, Rangza et al. 2008). The processes accountable for the augmentation and reduction in the quantities of crucial constituents in soil can lead to soil degradation and, consequently, desertification. The application of the Grain Size Index (GSI) of topsoil in mapping soil degradation has the potential to be a valuable tool for assessing land degradation and desertification processes by identifying variations. Hill 51 found several regions in China that contain a significant amount of high-quality sand (Xiao et al. 2005, Rangza et al. 2008). Utilized the GSI index to ascertain the origin of sand/dust storms in Mongolia. To guarantee the effectiveness of the GSI index, it is crucial to employ images captured before the emergence of short-lived plants in the spring (Hill 2000, Xiao et al. 2005).

**Soil salinity:** Soil salinity poses a significant challenge to agricultural progress in arid and semi-arid areas, leading to soil sterility and consequent land degradation and desertification (Salazar 2007, Al-Balooshi 2003). The primary factor leading to desertification along the Albatinah coast of Oman is soil salinity. Furthermore, the soil composition in the region has greatly contributed to the acceleration of desertification (Al-Balooshi 2003). Remote sensing techniques are a useful method for identifying and charting soil salinity (Al-Balooshi 2003, Al-Khaier 2003, Al-Mulla 2010). Using salinity indicators, including the Soil Salinity Index (SSI), Brightness Index (BI), and Soil and Sodicity Index (SSSI), Abbas & Khan (2007) employed multi-temporal

IRS-1B LISS-II pictures to detect salinity in degraded land. Evaluating soil salinity has shown to be challenging in semi-arid and arid regions characterized by little vegetation and low soil moisture levels. Vegetation cover and vegetation health are commonly used as alternative indicators for assessing soil salinity in low to medium-resolution multispectral pictures, such as Modis and Landsat imaging.

**Erosion:** Desertification leads to a decrease in vegetation and an increase in soil erosion. The phenomenon occurs because the exposed soil is vulnerable to erosion caused by the combined effects of wind and water (RomeroDiaz 1999, Shalaby & Tateishi 2007). Soil erosion is a geological phenomenon in which material is gradually eroded from the Earth's surface by processes such as weathering, dissolution, abrasion, corrosion, and transportation. Contemporary methods employ satellite data acquired via remote sensing to precisely monitor plant cover and arid terrain, facilitating the identification of erosional processes and the extent of desertification (Chen et al. 2004).

Human activities, such as agricultural practices and deforestation motivated by economic interests, significantly contribute to erosion in semi-arid and dry regions like China and the Middle East (Dregne 1986). Remote sensing is essential for observing the dynamic phenomena of wind erosion. The yearly fluctuations in wind generate forces that contribute to the dynamic displacement of sand dunes in China as a component of the wind erosion process (Sun et al. 2005).

**Urbanization:** Irreversible desertification refers to the phenomenon of urban expansion encroaching into and permanently transforming desert areas (Shalaby et al. 2004). Urbanization, driven by economic and population growth, is causing agriculture to spread into environmentally vulnerable regions, resulting in desertification (Shalaby et al. 2004, Shalaby & Tateishi 2007). The exponential growth of the human population results in a significant strain on resources, including groundwater reserves, as well as home food and water supplies. This stressor ultimately results in significant environmental deterioration (El-Hassan 2004, Leona & Sommer 2000, Moseley & Jermé 2010).

Remote sensing techniques are employed to categorize land use and urban development to assess the effects of urban expansion and desertification (Pellikka et al. 2005, Makarau et al. 2011, Yanli et al. 2012). Researchers observed a significant rise in erosion-prone areas over 15 years by utilizing SPOT and Landsat data. The primary cause of this land degradation was determined to be urban growth (Pellikka et al. 2005, Yanli et al. 2012, Shalaby et al. 2004). The expansion of metropolitan areas in Egypt results in the loss of 20,000 hectares of extremely fertile agricultural land

per year, intensifying the strain on susceptible regions.

**Drought:** Drought is a prolonged period of inadequate rainfall in a specific area, leading to the degradation of land and contributing to the advancement of desertification (Jupp et al. 1998, El-Hassan, 2004). Satellite remote sensing is capable of efficiently monitoring and tracking the presence of moisture, the kind of land cover, and the condition of plants over extensive areas and extended periods. Remote sensing is a highly efficient method for monitoring and evaluating the extent of plant stress, which can serve as an indicator of drought. It allows us to evaluate the reaction of regions to drought on a large scale (Jupp et al. 1998).

## DESERTIFICATION INDICES

Vegetation indices are mainly used to accurately detect desertification, evaluate plant development and stress, and measure vegetation cover, land cover, and biomass production by utilizing multispectral satellite data (Kumar et al. 2010). Fluctuations in the vegetation index can be used as indications of the ongoing processes of land degradation and desertification. The Normalised Difference Vegetation Index (NDVI) is frequently employed for identifying vegetation coverage and evaluating the state of vegetation (Chen 1995, Weier & Herring 2012, Yanli et al. 2012). Time series analysis of NDVI enables the construction of a benchmark that represents the typical productivity of plants in a certain region. Low NDVI levels indicate a minimal disparity between the red and NIR signals, indicating that the plant is under stress and has restricted photosynthetic activity. The utilization of land plant cover as an indicator of desertification was prohibited (Shafie et al. 2012). The NDVI measure is susceptible to multiple factors, including the magnitude of vegetation coverage, moisture levels in plants and soil, plant distress, and photosynthetic activity. Semi-arid and arid regions typically have a higher proportion of exposed ground and visible rock compared to temperate or tropical environments.

The soil-adjusted vegetation indices, namely SAVI, SAVI1, and SAVI2, include a correction factor to account for soil brightness, as proposed by Huete (1988). This correction factor is applied to minimize the influence of background sensitivity in the study, as highlighted by Chen (1995). In their work, Kundu & Dutta (2011) utilized NDVI time trends and long-term rainfall data to illustrate the gradual process of desertification in the Rajasthan region. This event was attributed to a complex interplay between anthropogenic and climatic factors (Shafie et al. 2012). Found that the Weighted Difference Vegetation Index (WDVI) produced more precise maps of the Iranian study area than TSAVI2, MSAVI1, and NDVI, as per their analysis. While these other

indexes demonstrated good performance, they were not as precise.

## CONCLUSIONS

Desertification is a highly debated topic in numerous countries and on the international stage. The use of remote sensing data to investigate desertification began in 1986 and has since expanded to 48 nations, with China being the most studied. Research findings indicate that over 42% of the studies concentrate solely on one country, potentially distorting the global understanding of the desertification process and its dynamics. The main methods utilized for researching desertification via remote sensing are change detection and categorization. Vegetation and its related characteristics, such as NDVI, land cover, and phenology, are the primary factors commonly used in this specific context.

The main purpose of employing remote sensing in the investigation of desertification was found to be the analysis and evaluation of the desertification process. Surprisingly, there have been few studies that have used remote sensing data to predict and reproduce future changes in desertification. Given the expected exacerbation of desertification due to climate change, future studies must prioritize this objective. The predominant focus of research has primarily been on analyzing specific elements when studying instances of desertification. Depending solely on a single criterion to determine the frequency of desertification may lead to an insufficient comprehension of the desertification phenomenon. Therefore, it is advisable to do research that integrates several variables. The existing methodologies and tactics employed to examine desertification are also applied to scrutinize other interconnected topics, such as land degradation. This is leading to a lack of understanding of the methods for investigating desertification and its dynamics.

## ACKNOWLEDGMENTS

We would like to acknowledge the insightful contributions of the Editor and anonymous reviewers

## REFERENCES

- Ababa, A., 2007. Africa Review Report on Drought and Desertification. Fifth Meeting of the Africa Committee on Sustainable Development. Regional Implementation Meeting for CSD, 16, pp.8-14.
- Abbas, A. and Khan, S., 2007. Using remote sensing techniques for appraisal of irrigated soil salinity. In Oxley, L. and Kulasiri, D. (eds). International Congress on Modelling and Simulation (MODSIM). Christchurch, New Zealand, pp.2632-2638.
- Abbas, I.M., 2014. No retreat, no surrender conflict on survival between Fulani pastoralists and farmers in Northern Nigeria. *European Scientific Journal*, 8(1), pp.331-346.
- Abdi, O.A., Glover, E.K. and Luukkanen, O., 2013. Causes and impacts



- of land degradation and desertification: Case study of the Sudan. *International Journal of Agriculture and Forestry*, 3(2), pp.40-51.
- Adjei, S., 2009. Assessing Desertification in the Upper East Region of Ghana Using Remote Sensing (RS) and Geographic Information System (GIS). Retrieved 12 May 2012 from [wansec.org/sites/default/files/wansec\\_ph.d.\\_thesis\\_proposal\\_final.pdf](http://wansec.org/sites/default/files/wansec_ph.d._thesis_proposal_final.pdf).
- Ajayi, S.S., 1996. Fish and Wildlife. Federal Environmental Protection Agency (FEPA).
- Al-Bakri, J.T., Brown, L., Gedalof, Z., Berg, A., Nickling, W., Khresat, S., Salahat, M. and Saoub, H., 2016. Modeling desertification risk in the north-west of Jordan using geospatial and remote sensing techniques. *Geomatics, Natural Hazards and Risk*, 7(2), pp.531-549. [DOI].
- Al-Balooshi, A.C., 2003. Desertification in Al-Batinah Plain in Sultanate of Oman. Unpublished doctoral dissertation, University of Jordan, Amman, Jordan, pp.30-60.
- Al-Harbi, K., 2010. Monitoring of agricultural area trend in Tabuk region–Saudi Arabia using Landsat TM and SPOT data. *The Egyptian Journal of Remote Sensing and Space Sciences*, 13, pp.37-42.
- Ali, Isam Mohamad., Naje, Ahmed Samir. and Nasr, Mohammed Salah., 2020. Eco-friendly chopped tire rubber as reinforcements in fly ash based geopolymer concrete. *Global Nest Journal*, 22(3), pp.342-347. [DOI].
- Ali, M.M. and Bayoumi, A.A.M.S., 2004. Assessment and mapping of desertification in Western Sudan using remote sensing techniques and GIS. *International Conference on Water Resources and Arid Environment*, Riyadh, Saudi Arabia, 5-8 December 2004, pp.1-16.
- Al-Janabi, A.M.S., Dibs, H., Sammen, S.S., Yusuf, B., Ikram, R.M.A., Alzuhairey, S.H. and Kisi, O., 2024. Comparison analysis of seepage through homogenous embankment dams using physical, mathematical, and numerical models. *Arabian Journal for Science and Engineering*, 11, pp.1-10.
- Al-Khaier, F., 2003. Soil salinity detection using satellite remote sensing. *International Institute for Geo-information Science and Earth Observation*, 11, p.70.
- Al-Mulla, Y.A., 2010. Salinity mapping in Oman using remote sensing tools: status and trends. In Ahmed, M., Al-Rawahy, S.A. and Hussain, N. (eds). *A Monograph on Management of Salt-affected Soils and Water for Sustainable Agriculture*. Sultan Qaboos University, Oman, pp.17-24.
- Bakr, N., Weindorf, D.C., Bahnassy, M.H. and El-Badawi, M.M., 2012. Multi-temporal assessment of land sensitivity to desertification in a fragile agro-ecosystem: environmental indicators. *Ecological Indicators*, 15(1), pp.271-280. [DOI].
- Bayarjargal, Y., Karnieli, A., Bayasgalan, M., Khudulmur, S., Gandush, C. and Tucker, C.J., 2006. A comparative study of NOAA–AVHRR derived drought indices using change vector analysis. *Remote Sensing of Environment*, 105, pp.9-22.
- Becerril-Piña, R., Díaz-Delgado, C., Mastachi-Loza, C.A. and González-Sosa, E., 2016. Integration of remote sensing techniques for monitoring desertification in Mexico. *Human and Ecological Risk Assessment*, 22(6), pp.1323-1340. [DOI].
- Ben-Dor, E., Chabrilat, S., Dematté, J.A.M., Taylor, G.R., Hill, J., Whiting, M.L. and Sommer, S., 2009. Using imaging spectroscopy to study soil properties. *Remote Sensing of Environment*, 113, pp.38-55.
- Chen, J.M., 1995. Evaluation of vegetation indices and a modified simple ratio for boreal applications. *Canadian Journal of Remote Sensing*, 22, pp.229-242.
- Chen, Y., Takara, K., Cluckie, I.D. and De Smedt, H.F. (eds), 2004. *GIS and Remote Sensing in Hydrology, Water Resources and Environment*. IAHS Press, Oxfordshire, pp.207-392.
- Chen, Z.Q. and Zhu, Z.D., 2001. Development of land desertification in the Bashang area in the past 20 years. *Journal of Geographical Sciences*, 11(4), pp.433-437.
- Collado, A., Chuviecow, E. and Camarasaw, A., 2002. Satellite remote sensing analysis to monitor desertification processes in the cropland boundary of Argentina. *Journal of Arid Environments*, 52, pp.121-133.
- Cui, G., Lee, W.K., Kwak, D.A., Choi, S., Park, T. and Lee, J., 2011. Desertification monitoring by LANDSAT TM satellite imagery. *Forest Science and Technology*, 7(3), pp.110-116. [DOI].
- D'Odorico, P., Bhattachan, A., Davis, K.F., Ravi, S. and Runyan, C.W., 2013. Global desertification: drivers and feedbacks. *Advances in Water Resources*, 51, pp.326-344. [DOI].
- Daniela, R.M., Jadunandan, D. and Booker, O., 2022. The use of remote sensing for desertification studies: A review. *Geography and Environmental Science*, 11, p.71.
- Darkoh, M.B.K., 1982. Desertification in Tanzania. *Geography*, 67(4).
- Darkoh, M.B.K., 1987. Combating desertification in the arid and semi-arid lands of Tanzania. *Journal of Arid Environments*, 12, pp.87-99.
- Darkoh, M.B.K., 1996. Desertification: its human costs. *Forum for Applied Research & Policy*, 11(3), pp.12-17.
- Darkoh, M.B.K., 1998. The natural causes and consequences of desertification: The dry lands of Africa. *Land and Development*, 9, pp.1-20.
- Darkoh, M.B.K., 2000. Desertification in Botswana. *Agricultural Research Institute, Keld Nabolt, Reykjavik, Iceland*.
- DePinaTavares, J., Baptista, I., Ferreira, A.J.D., Amiotte-Suchet, P., Coelho, C., Gomes, S., Amoros, R., DosReis, E.A., Mendes, A.F., Costa, L., Bentub, J. and Varela, L., 2015. Assessment and mapping the sensitive areas to desertification in an insular Sahelian mountain region: a case study of the Ribeira Seca Watershed, Santiago Island, Cabo Verde. *Catena*, 128, pp.214–223. [DOI].
- Dibs, H. and Al-Ansari, N., 2023. Integrating highly spatial satellite images for 3D building modeling using geospatial algorithms and architecture environment. *Engineering*, 15(4), pp.220-233.
- Dibs, H. and Mansor, S., 2014. Mapping rubber tree growth by spectral angle mapper spectral-based and pixel-based classification using SPOT-5 image. *Proceedings of 35th Asian Conference on Remote Sensing (ACRS)*, Nay Pyi Taw, pp.27-31.
- Dibs, H., Al-Ansari, N. and Laue, J., 2023. Analysis of remotely sensed imagery and architecture environment for modeling 3D detailed buildings using geospatial techniques. *Engineering*, 15(5), pp.328-341.
- Dibs, H., Hasab, H.A., Jaber, H.S. and Al-Ansari, N., 2022. Automatic feature extraction and matching modeling for highly noise near-equatorial satellite images. *Innovative Infrastructure Solutions*, 7(1), p.2.
- Dibs, H., Hasab, H.A., Mahmoud, A.S. and Al-Ansari, N., 2021. Fusion methods and multi-classifiers to improve land cover estimation using remote sensing analysis. *Geotechnical and Geological Engineering*, 39(8), pp.5825-5842.
- Dibs, H., Hasab, H.A., Mezaal, M.R. and Al-Ansari, N., 2021. Comparative analysis of integrating and combining thermal TIRS and OLI data to superior change detection using geospatial techniques.
- Dibs, H., Jaber, H.S. and Al-Ansari, N., 2023. Multi-fusion algorithms for detecting land surface pattern changes using multi-high spatial resolution images and remote sensing analysis. *Emerging Science Journal*, 7(4), pp.1215-1231.
- Dibs, H., Mansor, S., Ahmad, N. and Al-Ansari, N., 2020. Simulate new near equatorial satellite system by a novel multi-fields and purposes remote sensing goniometer. *Engineering*, 12, pp.325-346.
- Dibs, H., Mansor, S., Ahmad, N. and Al-Ansari, N., 2022. Geometric correction analysis of high distortion of near-equatorial satellite images using remote sensing and digital image processing techniques. *Engineering*, 14(1), pp.1-8.
- Dibs, H., Mansor, S., Ahmad, N. and Al-Ansari, N., 2023. Robust radiometric normalization of the near-equatorial satellite images using feature extraction and remote sensing analysis. *Engineering*, 15(2), pp.75-89.
- Dibs, H., Mansor, S., Ahmad, N. and Al-Ansari, N., 2023a. Robust

- radiometric normalization of the near-equatorial satellite images using feature extraction and remote sensing analysis. *Engineering*, 15, pp.75-89. [DOI]
- Dibs, H., Mansor, S., Ahmad, N., Pradhan, B. and Al-Ansari, N., 2020. Automatic fast and robust technique to refine extracted SIFT key points for remote sensing images. *Journal of Civil Engineering and Architecture*, 14(6), pp.339-350. [DOI]
- Dragan, M.T., Sahsuvaroglu, I.G. and Feoli, E., 2005. Application and validation of a desertification risk index using data for Lebanon. *Management of Environmental Quality: An International Journal*, 16(4), pp.309-326.
- Dregne, H.E., 1986. Desertification of arid lands. In: El-Baz, F. and Hassan, M.H.A. (eds). *Physics of Desertification*. Dordrecht: Martinus Nijhoff Publishers, pp.4-34.
- El-Hassan, I.M., 2004. Desertification monitoring using remote sensing technology. *International Conference on Water Resources and Arid Environment 2004*, King Saud University, Riyadh, pp.1-15.
- El-Karouri, M.O.H., 1986. Impact of desertification on land productivity. In: Farouk, E. and Hassan, M.H. (eds). *Physics of Desertification*. Martinus Nijhoff Publishers, pp.52-59.
- Emeka, E.E., 2013. Drought and desertification as they affect the Nigerian environment. *Journal of Environmental Management and Safety*, 4(1), pp.45-54.
- Fang, L., Bai, Z., Wei, S., Yanfen, H., Zongming, W., Kaishan, S. and Zhiming, L., 2008. Sandy desertification change and its driving forces in western Jilin Province, North China. *Environmental Monitoring and Assessment*, 136, pp.379-390.
- FAO, 1993. Corporate Document Repository. FAO
- FAO, 2001. *Food Insecurity: When People Live With Hunger and Fear Starvation*. FAO
- Fianko, J.R., Donkor, A., Lowor, S.T. and Yeboah, P.O., 2011. Agrochemicals and the Ghanaian environment, a review. *Journal of Environmental Protection*, 2(3), pp.221-230.
- FMEnv, 2001. *National Action Programme To Combat Desertification*. The Federal Ministry of Environment (FMEnv).
- Fredricson, E., Havstard, K.M. and Hyder, R., 1998. Perspective on desertification: south-eastern United States. *Journal of Arid Environments*, 39, pp.191-207.
- Glantz, M.H. and Orlovsky, N.S., 1983. Desertification: a review of the concept. *Desertification Control Bulletin*, 9, pp.15-22.
- Grainger, A., 2009. *Developing A Baseline Survey for Monitoring Biophysical and Socio-Economic Trends in Desertification, Land Degradation, and Drought*. UNCCD.
- Hashim, F., Dibs, H. and Jaber, H.S., 2021. Applying support vector machine algorithm on multispectral remotely sensed satellite image for geospatial analysis. *Journal of Physics: Conference Series*, 1963(1), p.012110.
- Hashim, F., Dibs, H. and Jaber, H.S., 2022. Adopting gram-schmidt and brovey methods for estimating land use and land cover using remote sensing and satellite images. *Nature Environment and Pollution Technology*, 21(2), pp.867-881.
- Hassan, Ali A., Hadi, Raid T., Rashid, Adil H., Naje, Ahmed Samir., 2020. Chemical modification of castor oil as adsorbent material for oil content removal from oilfield produced water. *Pollution Research*, 39(4), pp. 892-900.
- Hay, S.I., Randolph, S.E. and Rogers, D.J., 2000. *Remote Sensing and Geographical Information Systems in Epidemiology*. Vol. 47 of Advances in Parasitology. Academic Press, London, 357 p.
- Hein, L. and Ridder, D.E., 2006. Desertification in the Sahel: A reinterpretation. *Global Change Biology*, 12, pp.751-758.
- Helldén, U. and Tottrup, C., 2008. Regional desertification: a global synthesis. *Global and Planetary Change*, 64(3-4), pp.169-176. [DOI]
- Hill, J., 2000. Assessment of semi-arid lands: Monitoring dryland ecosystems through remote sensing. In Meyers, R.A. (ed.). *Encyclopedia of Analytical Chemistry – Instrumentation and Applications*. John Wiley & Sons, Chichester, pp.8769-8794.
- Hill, J., Jarmer, T., Udelhoven, T. and Stellmes, M., 2006. Remote sensing and geomatics applications for desertification and land degradation monitoring and assessment. In Escadafal, R. and Paracchini, M.L. (eds.). *Geomatics for Land and Water Management: Achievement and Challenges in the Euromed Context*. International Workshop, Joint Research Centre, Italy, 23-25 June 2004, pp.15-22.
- Huete, A.R., 1988. A soil-adjusted vegetation index (SAVI). *Remote sensing of environment*, 25(3), pp.295-309.
- Hulme, M. and Kelly, M., 1993. Exploring links between desertification and climate change. *Environment*, 35(6), pp.39-45.
- Ijah, A., 2014. Conflicts between Fulani Herders and Farmers in Central and Southern Nigeria: Discourse on proposed establishment of grazing routes and reserves. *An International Journal of Arts and Humanities*, 3(9), pp.66-84.
- IPCC, 2007. *Climate Change 2007: Impact and Vulnerability*. Intergovernmental Panel on Climate Change, p.872.
- Jha, M.K., 2010. *Natural and Anthropogenic Disasters: Vulnerability, Preparedness and Mitigation*. Springer, pp.355-384.
- Jones, T.B., 2006. *Case Study on Successful South African NRM Initiatives and Their Impact on Poverty and Governance*. United States Agency for International Development.
- Jupp, D.L.B., Guoliang, T., McVicar, T.R., Yi, Q. and Fuqin, L., 1998. Soil Moisture and Drought Monitoring Using Remote Sensing I: Theoretical Background and Methods. CSIRO, p.96
- Kadhim, N., Ismael, N.T. and Kadhim, N.M., 2022. Urban landscape fragmentation as an indicator of urban expansion using Sentinel-2 imageries. *Civil Engineering Journal*, 8(9), pp.1799-1814.
- Kambou, J.B., 2002. *Burkina Faso: Sahel Integrated Lowland Ecosystem Management Phase 1*. Ministry of Environment and Water, Burkina Faso.
- Kapetsky, J.M. and Aguilar-Manjarrez, J., 2007. *Geographic Information Systems, Remote Sensing and Mapping for the Development and Management of Marine Aquaculture*. Food and Agriculture Organization, pp.30-65.
- Karnieli, A. and Dall'Olmo, G., 2003. Remote-sensing monitoring of desertification, phenology, and droughts. *Management of Environmental Quality: An International Journal*, 14(1), pp.22-38.
- Kasawani, I., Norsaliza, U. and Hasmadi, S., 2010. Analysis of spectral vegetation indices related to soil-line for mapping mangrove forests. *Journal of Cleaner Production*, 19(7), pp.238-256
- Kelly, M. and Hulme, M., 1993. Desertification and climatic change. *Trempo*, 8, pp.1-7.
- Kelly, R.L. and Thomas, D.H., 2012. *Archaeology*. Cengage Learning, London, pp.67-75.
- Klintonberg, P. and Seely, M., 2004. Land degradation monitoring in Namibia: A first approximation. Available at: www.environment-namibia.net.
- Kumar, P., Rani, M., Pandey, P., Majumdar, A. and Nathawat, M., 2010. Monitoring of deforestation and forest degradation using remote sensing and GIS: A case study of Ranchi in Jharkhand (India). *Report and Opinion*, 2(4), pp.14-20.
- Kundu, A. and Dutta, D., 2011. Monitoring desertification risk through climate change and human interference using remote sensing and GIS techniques. *International Journal of Geomatics and Geosciences*, 2(1), pp.21-33.
- Lam, D., Rimmel, T. and Drezner, T., 2010. Tracking desertification in California using remote sensing: A sand dune encroachment approach. *Remote Sensing*, 3, pp.1-13.
- Lamchin, M., Lee, J.Y., Lee, W.K., Lee, E.J., Kim, M., Lim, C.H., Choi, H.A. and Kim, S.R., 2016. Assessment of land cover change and desertification using remote sensing technology in a local region of Mongolia. *Advances in Space Research*, 57(1), pp.64-77. [DOI]

- Leone, A.P. and Sommer, S., 2000. Multivariate analysis of laboratory spectra for the assessment of soil development and soil degradation in the southern Apennines (Italy). *Remote Sensing of Environment*, 72(3), pp.346-359.
- Levin, S.A., 2009. *The Princeton Guide to Ecology*. Princeton University Press, pp.82-86.
- Li, Q., Zhang, C., Shen, Y., Jia, W. and Li, J., 2016. Quantitative assessment of the relative roles of climate change and human activities in desertification processes on the Qinghai-Tibet Plateau based on net primary productivity. *Catena*, 147, pp.789-796. [DOI]
- Li, S., Zheng, Y., Luo, P., Wang, X., Li, H. and Lin, P., 2007. Desertification in Western Hainan Island, China. *Land Degradation & Development*, 18, pp.473-485.
- Liu, Q., Liu, G. and Huang, C., 2018. Monitoring desertification processes in the Mongolian Plateau using MODIS tasseled cap transformation and TGSi time series. *Journal of Arid Land*, 10(1), pp.12-26. [DOI]
- MA, 2005. *Ecosystems and Human Well-being: Desertification Synthesis*. World Resource Institute.
- Makarau, A., Palubinskas, G. and Reinartz, P., 2011. Multi-sensor data fusion for urban area classification. In: Stilla, U., Gamba, P., Juergens, C. and Maktav, D. (eds). *Joint Urban Remote Sensing Event (JURSE)*, Munich, Germany, pp.21-24.
- Mesev, V., 2007. *Integration of GIS and Remote Sensing*. John Wiley and Sons, London, pp.17-55.
- Mohammed, I., Hashim Al-Khalaf, Safaa K., Alwan, Husam H. and Samir Naje, Ahmed., 2022. Environmental assessment of Karbala water treatment plant using water quality index (WQI). *Materials Today: Proceedings*, 60, pp.1554-1560. [DOI]
- Mortimore, M., 1989. *Adapting to Drought: Farmers, Famines and Desertification in West Africa*. Cambridge University Press.
- Moseley, W.G. and Jermé, E.S., 2010. Desertification. In: Warf, B. (ed.). *Encyclopedia of Geography*. Sage Publications Inc., pp.715-719.
- Murad, H. and Saiful, A., 2011. Drought assessment using remote sensing and GIS in the North-West region of Bangladesh. *3rd International Conference on Water and Flood Management (ICWFM)*, p.27.
- Mutti, P.R., Lucio, P.S., Dubreuil, V. and Bezerra, B.G., 2020. NDVI time series stochastic models for the forecast of vegetation dynamics over desertification hotspots. *International Journal of Remote Sensing*, 41(7), pp.2759-2788. [DOI]
- Naje, Ahmed Samir., Ajeel, Mohammed A., Mahdi, Rahman Ismael., Alkhateeb, Raid T., Enhancement of ionic mass transfer coefficient using a unique electrocoagulation reactor with rotating impeller anode. *Separation Science and Technology*, 55(6), pp.1167-1176. [DOI]
- Nneji, L.M., 2013. A review of the effects of desertification on food security. *Report and Opinion*, 5(10), pp.27-33.
- Nwafor, O.E., 1982. Pressurization of prerigor beef muscle and its effect on the solubilization of myofibrillar proteins.
- Okello, A.L., Majekodumi, A.O., Molala, A., Welburn, S.C. and Smith, J., 2014. Identifying motivators for state-pastoral dialogue: Exploring the relationship between livestock services, self-organization and conflict in Nigeria's Pastoralist Fulani. *Pastoralism*, 4(12), p.1.
- Olagunju, T.E., 2015. Drought, desertification and the Nigerian environment: A review. *Journal of Ecology and the Natural Environment*, 7(7), pp.196-209.
- Palacios-Orueta, A. and Ustin, S.L., 1998. Remote sensing of soil properties in the Santa Monica Mountains I. Spectral analysis. *Remote Sensing of Environment*, 65(2), pp.170-183.
- Palacios-Orueta, A., Pinzon, J.E., Ustin, S.L. and Roberts, D.A., 1999. Remote sensing of soils in the Santa Monica Mountains: II. Hierarchical foreground and background analysis. *Remote Sensing of Environment*, 68(2), pp.138-151.
- Palmer, A.R. and van Rooyen, A.F., 1998. Detecting vegetation change in the southern Kalahari using Landsat TM data. *Journal of Arid Environments*, 39, pp.143-153.
- Pellikka, P.K.E., Clark, B.J.F., Sirviö, T. and Masalin, K., 2005. Environmental change monitoring applying satellite and airborne remote sensing data in the Taita Hills, Kenya. *Remote Sensing and Geoinformation Processing*, 12, pp.223-232.
- Quan, J., Borton, D. and Conroy, C., 1994. *A Preliminary Assessment of Desertification In Namibia*. Ministry of Tourism, Water and Rural Development and Desert Ecological Research Unit of Namibia.
- Rangza, K., Sulaimani, B., Sarsangi, A.R. and Abshirini, A., 2008. Change detection, mineralogy, desertification mapping in east and northeast of Ahvaz City, SW Iran using a combination of remote sensing methods, GIS and ESAs model. *Global Journal of Environmental Research*, 2(1), pp.42-52.
- Romero-Diaz, A., Cammeraat, L.H., Vacca, A. and Kosmas, C., 1999. Soil erosion at three experimental sites in the Mediterranean. *Earth Surface Processes and Landforms*, 24(13), pp.1243-1256.
- Salazar, L.A., 2007. Integrating remote sensing, geographic information system and modeling for estimating crop yield. *ProQuest*, New York, pp.140-145.
- Sameer, M.K. and Hamid, A.M., 2023. Remote sensing and GIS techniques in monitoring land use land cover change. *International Journal of Sustainable Construction Engineering and Technology*, 14(1), pp.13-20.
- Santini, M., Caccamo, G., Laurenti, A., Noce, S. and Valentini, R., 2010. A multi-component GIS framework for desertification risk assessment by an integrated index. *Applied Geography*, 30(3), pp.394-415. [DOI]
- Schwartz, M.L. and Notini, J., 1994. Desertification and migration: Mexico and the United States. *Research paper, US Commission on Immigration Reform*.
- Seely, M. and Klintonberg, P., 2011. Case study desertification: Central Namibia. *Tropical Forestry*, 8, Springer-Verlag Berlin Heidelberg.
- Senanayake, R., 2012. Desertification and biodiversity. *Ground Views: Journalism for Citizens*.
- Shafie, H., Hosseini, S.M. and Amiri, I., 2012. RS-based assessment of vegetation cover changes in Sistan Plain. *International Journal of Forest, Soil and Erosion*, 2(2), pp.97-100.
- Shalaby, A. and Tateishi, R., 2007. Remote sensing and GIS for mapping and monitoring land cover and land-use changes in the northwestern coastal zone of Egypt. *Applied Geography*, 27(1), pp.28-41.
- Shalaby, A., Aboel Ghar, M. and Ryutaro, T., 2004. Desertification impact assessment in Egypt using low-resolution satellite data and GIS. *International Journal of Environmental Studies*, 61(4), pp.375-383.
- Stephen, D., 2014. Land degradation and agriculture in the Sahel of Africa: Causes, impacts, and recommendations. *Journal of Agricultural Science and Applications*, 3(3), pp.67-73.
- Stiles, D.N., 1983. Desertification and pastoral development in northern Kenya. *Nomadic Peoples*, 13, pp.1-14.
- Stringer, L.C., 2008. Reviewing the international year of deserts and desertification 2006: what contribution towards combating global desertification and implementing the United Nations Convention to Combat Desertification? *Journal of Arid Environments*, 72(11), pp.2065-2074. [DOI]
- Sun, D., Dawson, R., Li, H. and Li, B., 2005. Modeling desertification change in Minqin County, China. *Environmental Monitoring and Assessment*, 108, pp.169-188.
- Tamir, H., 2000. Desertification in Ethiopian Highlands. RALA Report, p.200.
- Thelma, M.N., 2015. Desertification in Northern Nigeria: Causes and implications for national food security. *Peak Journal of Social Sciences and Humanities*, 3(2), pp.22-31.
- Tully, T.G. and Shapiro, E., 2014. Analysis of Kenyan livestock market and feasibility study of livestock business. *Environmental Management*, 11, p.61-74.
- UNCCD, 2006. Implementing the United Nations Convention to Combat Desertification in Africa: Ten African Experiences. Secretariat of the United Nations Convention to Combat Desertification, Bonn, Germany.
- UNCCD, 2013. A Stronger UNCCD for a Land Degradation Neutral World.

- Secretariat of the United Nations Convention to Combat Desertification, Bonn, Germany.
- UNCCD, 2014. *Desertification: The Invisible Frontline. Secretariat of the United Nations Convention to Combat Desertification, Bonn, Germany.*
- UNEP, 1994. *Intergovernmental Negotiating Committee for the elaboration of an International Convention to Combat Desertification in those countries experiencing serious drought and/or desertification, particularly in Africa: Final Text of the Convention.* United Nations Environment Programme.
- United Nations, 1977. Report of the United Nations Conference on Desertification. United Nations.
- United Nations, 1994. United Nations Convention to Combat Desertification in Those Countries Experiencing Serious Drought and/or Desertification, particularly in Africa. United Nations.
- United Nations, 2015. Transforming Our World: The 2030 Agenda for Sustainable Development. United Nations General Assembly
- Van den Elsen, E. and Jetten, V., 2015. Combatting desertification using a multidisciplinary approach. *Catena*, 128, pp.211–213. [DOI]
- Verón, S.R., Paruelo, J.M. and Oesterheld, M., 2006. Assessing desertification. *Journal of Arid Environments*, 66(4), pp.751–763.
- Verstraete, M.M., 1986. Defining desertification: A review. *Climatic Change*, 9, pp.5–18.
- Wang, X., Chen, F. and Dong, Z., 2006. The relative role of climatic and human factors in desertification in semiarid China. *Global Environmental Change*, 16(1), pp.48–57. [DOI]
- Weier, J. and Herring, D., 2012. Measuring vegetation (NDVI and EVI). *NASA Earth Observatory*. Retrieved 18 May 2012 from [http://earthobservatory.nasa.gov/Library/MeasuringVegetation/measuring\\_vegetation\\_3.html](http://earthobservatory.nasa.gov/Library/MeasuringVegetation/measuring_vegetation_3.html).
- Weiss, E., Marsh, S.E. and Pfirman, E.S., 2001. Application of NOAA-AVHRR NDVI time-series data to assess changes in Saudi Arabia's rangelands. *International Journal of Remote Sensing*, 22(6), pp.1005–1027.
- Wilhite, D.A., 2016. Drought as a natural hazard: concepts and definitions. In *Droughts* (pp. 18-3). Routledge.
- Wu, B. and Ci, L.J., 2002. Landscape change and desertification development in the Mu Us Sandland, Northern China. *Journal of Arid Environments*, 50(3), pp.429–444.
- Xiao, J., Shen, Y. and Tateishi, R., 2005. Mapping Soil Degradation by Topsoil Grain Size Using MODIS Data. Retrieved 16 April 2012 from [http://crs.itb.ac.id/media/Jurnal/Refs/Critical\\_Review/Referensi/03\\_LainLain/p003\\_Jieyingxiao\\_paper.pdf](http://crs.itb.ac.id/media/Jurnal/Refs/Critical_Review/Referensi/03_LainLain/p003_Jieyingxiao_paper.pdf).
- Xiao, J., Shen, Y., Tateishi, R. and Bayaer, W., 2006. Development of topsoil grain size index for monitoring desertification in arid land using remote sensing. *International Journal of Remote Sensing*, 27(12), pp.2411–2422. [DOI]
- Xu, D., Song, A., Tong, H., Ren, H., Hu, Y. and Shao, Q., 2016. A spatial system dynamic model for regional desertification simulation: A case study of Ordos, China. *Environmental Modelling & Software*, 83, pp.179–192. [DOI]
- Yang, X., Ding, Z., Fan, X. and Zhou, Z., 2007. Processes and mechanisms of desertification in northern China during the last 30 years, with a special reference to the Hunshandake Sandy Land, eastern Inner Mongolia. *Catena*, 71(1), pp.2–12.
- Yanli, Y., Jabbar, M.T. and Zhou, J., 2012. Study of environmental change detection using remote sensing and GIS application: A case study of Northern Shaanxi Province, China. *Polish Journal of Environmental Studies*, 21(3), pp.783–790.
- Zaman, S., 1997. Effects of rainfall and grazing on vegetation yield and cover of two arid rangelands in Kuwait. *Environmental Conservation*, 24, pp.344–350.
- Zeng, L., 2005. *Gobi Desertification*. ICE
- Zhao, Y., Wang, X., Novillo, C.J., Arrogante-Funes, P., Vázquez-Jiménez, R. and Maestre, F.T., 2018. Albedo estimated from remote sensing correlates with ecosystem multifunctionality in global drylands. *Journal of Arid Environments*, 157(9), pp.116–123. [DOI]



# Sustainable Phosphate Removal with Acid-Modified Fly Ash: Kinetic, Isothermal, and Thermodynamic Insights

Renu Bala<sup>1</sup> , Rajesh Dhankhar<sup>2</sup>  and Sunil Kumar Chhikara<sup>1†</sup> 

<sup>1</sup>University Institute of Engineering & Technology, Maharshi Dayanand University, Rohtak-124001, Haryana, India

<sup>2</sup>Department of Environmental Science, Maharshi Dayanand University, Rohtak, Haryana, India

†Corresponding Author: Sunil Kumar Chhikara; sashiyadav888@gmail.com

**Abbreviation:** Nat. Env. & Poll. Technol.

**Website:** [www.neptjournal.com](http://www.neptjournal.com)

*Received:* 27-06-2024

*Revised:* 09-08-2024

*Accepted:* 28-08-2024

## Key Words:

Adsorption isotherms  
Acid-modified fly ash  
Phosphate removal  
Chemical kinetics

## ABSTRACT

The removal of pollutants from water bodies has emerged as a pressing global concern. Discharging untreated wastewater into the environment poses a significant threat due to the presence of hazardous substances like nitrate and phosphate, contributing to the widespread issue of eutrophication. This study focused on investigating the adsorption of phosphate from a synthetic solution using fly ash, an industrial by-product. To enhance the efficiency of coal fly ash, acid treatment was employed. Batch experiments were conducted to examine the influence of different factors, including pH, adsorbent dosage, initial phosphate ion concentration, contact time, and temperature. Surface electron microscopy (SEM) explained the morphology of the adsorbent, and Fourier Transform Infrared Spectroscopy (FTIR) analysis was performed to analyze the adsorbent pre and post-adsorption, allowing for the identification of functional groups tangled in the adsorption process. The major functional groups observed were hydroxyl, carboxylic acid, amines, and nitrile groups, all contributing to the adsorption process. Acid-modified fly ash (AMFA) demonstrated favorable results in terms of phosphate removal, particularly at a pH of 5.0 and an initial phosphate concentration of 50 ppm. Equilibrium in adsorption was achieved within 30 min at a temperature of 15°C with constant stirring of 100 rpm, resulting in a high phosphate removal rate of 91%. Freundlich isotherm was found to contribute a better fit for the adsorption data compared to the Langmuir isotherm. Pseudo-second-order kinetic model, with a high  $R^2$  value of 0.998, exhibited excellent agreement with the adsorption data for acid-modified fly ash. Thermodynamic study indicated that the adsorption process was heat absorbing (endothermic) and non-spontaneous at low temperatures. Overall, the results of the experimental study highlighted the promising adsorption potential of acid-modified fly ash as an effective adsorbent for phosphate removal in water treatment applications.

## Citation for the Paper:

Renu Bala, Dhankhar, R. and Chhikara, S. K., 2025. Sustainable phosphate removal with acid-modified fly ash: Kinetic, isothermal, and thermodynamic insights. *Nature Environment and Pollution Technology*, 24(2), p. B4242. <https://doi.org/10.46488/NEPT.2025.v24i02.B4242>

*Note: From year 2025, the journal uses Article ID instead of page numbers in citation of the published articles.*



**Copyright:** © 2025 by the authors

**Licensee:** Technoscience Publications

This article is an open access article distributed under the terms and conditions of the Creative Commons Attribution (CC BY) license (<https://creativecommons.org/licenses/by/4.0/>).

## INTRODUCTION

Phosphorus is a crucial nutrient for plants, animals, and humans. When phosphorus-based substances are extensively used in industry, livestock, and agriculture, they inevitably lead to the release of phosphate into surface water. This discharge has the potential to stimulate the overgrowth of algae, giving rise to algal blooms that endanger the integrity of surface and groundwater, as well as human health (Recepoglu et al. 2022). Phosphate discharge into surface waters excites the proliferation of aquatic micro and macro organisms, leading to an overabundance that can result in eutrophication in stagnant water bodies. Eutrophication is a global environmental concern that has severe consequences for aquatic ecosystems, such as biodiversity loss and significant economic losses (Zhou et al. 2022). Therefore, it is essential to adhere to phosphate discharge limits, which range from 0.5 to 1.0 mg.L<sup>-1</sup>, for waste materials containing phosphates (Ragheb 2013). Despite efforts made over the past few decades to reduce phosphorus pollution in water systems from various environmental sources, water pollution caused by phosphorus remains a significant environmental issue (Park et al. 2021).

A wide array of technologies has been extensively studied for phosphorus removal from wastewater, mainly classified into chemical, biological, and physical methods (Karaca et al. 2004, Wang et al. 2012). However, chemical methods often lead to the formation of substantial sludge during phosphorus precipitation, which may raise new-fangled pollution concerns (Yao et al. 2011, Yeoman et al. 1988). On the other hand, biological methods are effective but sensitive to operational parameters, leading to variable efficiency (Sun et al. 2017, Xie et al. 2017). Additionally, biological treatment requires extra steps like waste-activated sludge disposal or pre-treatment, which can escalate the overall price value of wastewater treatment (Neufeld & Thodos 1969, Yang et al. 2018). Physical methods for wastewater treatment include electrodialysis, reverse osmosis, and adsorption (Loganathan et al. 2014). These techniques are utilized to remove various pollutants and contaminants from water, providing effective purification and treatment of wastewater. However, these methods are limited by the risk of secondary contamination, strict reaction requirements, large space, less flexibility, and design, which involve higher costs (Yin et al. 2017).

Among all of these, adsorption is considered a better wastewater treatment process. The utilization of adsorption as a water purification technology offers several advantages, including its relatively low cost and reduced risks of causing secondary pollution. As a result, it holds great potential for on-site water treatment applications. However, a key factor in successfully implementing adsorption on a large scale is the advancement of affordable and highly efficient adsorbents specifically designed for the removal of phosphate from water (Saad Algarni & Al-Mohaimeed 2022). In modern years, various studies have been performed to estimate the efficiency of low-cost adsorbents for the confiscation of various pollutants (De Gisi et al. 2016).

Recently, a fresh and all-encompassing strategy has been developed, incorporating the principles of the circular economy paradigm. This approach focuses on the reclamation of agricultural and industrial waste derivatives, utilizing them to create innovative composite materials aimed at purifying the environment, particularly with a strong emphasis on rejuvenating water resources (Xu et al. 2022). Industrial waste is highly appealing as a potentially economical adsorbent for wastewater treatment due to its ability to efficiently remove pollutants. It often requires minimal processing to enhance its adsorptive capacity, making it an attractive option for sustainable and economical treatment methods. Different forms of industrial wastes, like red mud, lignin, iron (III) hydroxide, blast furnace sludge, waste slurry, and fly ash, have been investigated for their mechanical viability in commendably removing pollutants from contaminated water (Ahmaruzzaman 2011).

Coal fly ash is a significant industrial waste product generated from the burning of coal and is produced in substantial quantities worldwide. Unfortunately, this waste material poses numerous environmental challenges, including the contamination of soil and water, along with issues related to resource recovery (Usman et al. 2023). Various approaches have been suggested for the sustainable management of coal fly ash. These strategies involve utilizing coal fly ash in different industries, including the cement industry (Singh et al. 2019), rubber production (Ren & Sancaktar 2019), as well as engineering and agricultural applications (Ahmaruzzaman 2010). Moreover, due to its remarkable potential as a phosphate adsorbent, effective recovery of phosphorus from wastewater can be considered a valuable alternate approach to employing coal fly ash (Hosseinpour et al. 2023). The unmodified adsorbent possesses closed pores on its surface (Wulandari et al. 2019). To address this issue and increase the accessibility of the pores, a modification process is necessary. One such modification involves using acid-modified fly ash, which can dissolve impurity minerals present in the fly ash. This dissolution process leads to the widening of the fly ash pores, as the exchanged cation in the fly ash structure is replaced by  $H^+$  ions (Irawan et al. 2014). This modification technique enables the opening of previously closed pores (Wulandari et al. 2019). Recent research on modified fly ash has shown its effectiveness as an adsorbent for a range of pollutants, emphasizing its potential role in environmental remediation. Various studies have been conducted using modified fly ash to remove ammonia (Wang et al. 2024), methylene blue dye (Küçük & Üstündağ 2024), and copper (Buema et al. 2021) from aqueous solutions under optimal conditions, while many studies have explored the removal of phosphate using unmodified fly ash, relatively few have specifically investigated the effectiveness of fly ash after modification. This highlights the need for further research to fully understand the potential of modified fly ash as an efficient adsorbent for phosphate removal.

In the present study, fly ash is improved with acid to enhance its adsorption capacity so that it can be considered as a worthy adsorbent material for the adsorption of phosphate as aluminum, iron, and calcium oxides enrich fly ash. Together with phosphate, these oxides can precipitate or adsorb aggressively. The purpose of the study is to perform acid-modified fly ash as an adsorbent for the removal of phosphate adsorption from synthetic solutions in batch mode studies. Results achieved from batch experiments were subsequently utilized to determine adsorption kinetics, isotherms, and thermodynamics. These analyses helped to understand the rate of adsorption, equilibrium relationships between adsorbate and adsorbent, and the thermodynamic feasibility of the adsorption process.

## MATERIALS AND METHODS

All of the chemicals employed in the experiment were of analytical grade. Potassium dihydrogen phosphate ( $\text{KH}_2\text{PO}_4$ ) was taken to prepare the stock solution of phosphate. Various working solutions with varying concentrations were equipped by diluting the original phosphate solution using de-ionized water. A pH meter (Mettler Toledo Fiveeasy Plus) was used to determine the solution's pH. To achieve the desired pH levels during the batch studies, 1N solutions of sodium hydroxide (NaOH) and hydrochloric acid (HCl) were used for pH adjustment. Ammonium molybdate and stannous chloride were used as reagents for the phosphate solutions.

### Preparation of the Adsorbent

In the current study, fly ash was obtained from the thermal power plant located in Khukhrana, Panipat, Haryana, at coordinates 29°23'50" N and 76°52'52" E. To prepare the fly ash for subsequent experiments, it was initially filtered via a sieve with mesh dimensions of 150  $\mu\text{m}$ . Manual washing of the fly ash was performed using double distilled water,

repeating the process 5-7 times to ensure thorough cleaning. Following the washing step, the fly ash was desiccated at 100°C for 24 h to eliminate remaining moistness. The dried-out fly ash was then stored in hermetic containers to preserve its properties. Subsequently, the fly ash was further modified into acid-modified fly ash for subsequent use in the study.

### Preparation of Acid Modified Fly Ash (AMFA) as an Adsorbent

During the modification process, fly ash was thoroughly mixed with 1 M HCl solution. The mixture was then placed in a shaker and agitated at 80 °C for 24 h, with a rotation speed of 50 RPM. After the agitation period, the solid was separated by centrifugation, and excess HCl was eliminated through washing with double distilled water. The resulting product was referred to as acid-modified fly ash. It was subsequently dried at 105°C for 24 h to ensure complete removal of moisture. The modified adsorbent was considered ready for use in adsorption experiments and was stored in hermetic containers to maintain its properties.

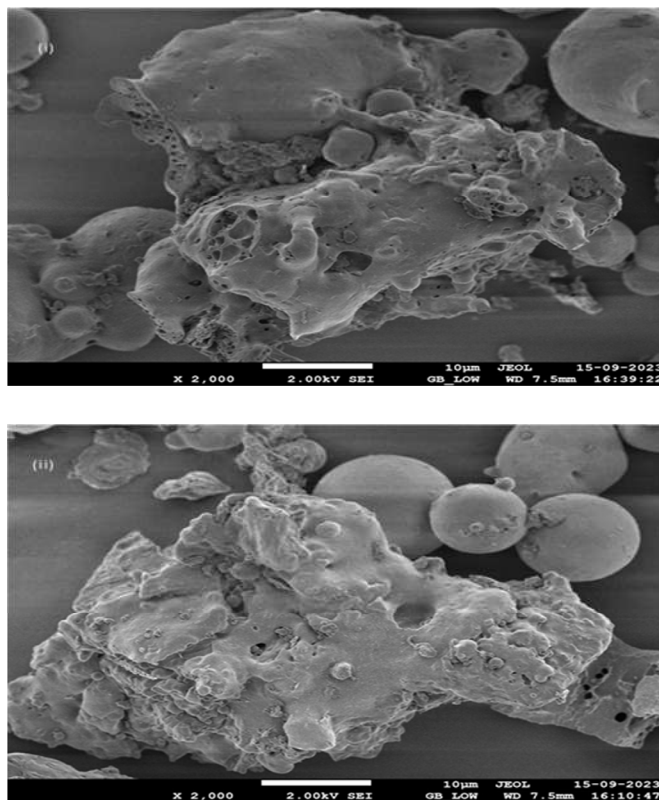


Fig. 1: Surface Morphology of AMFA (i) before phosphate adsorption (ii) after phosphate adsorption.

## RESULTS AND DISCUSSION

### Characterization of Adsorbents

**SEM analysis:** The surface morphology of AMFA before and after adsorption is shown in Fig. 1 (i & ii). It was noticed that before adsorption, the AMFA surface was porous with some spherical and irregular structures. However, after phosphate adsorption, it showed agglomeration of phosphate ions and filling of binding sites with improvement in the surface of the structure.

**FTIR analysis:** The functional groups present on the adsorbent were detected using FTIR (Bruker Alpha, Department of Biotechnology, UIET, MDU) spectrometer

having wavelength region  $400\text{--}4000\text{ cm}^{-1}$  before and after phosphate adsorption.

FTIR results for unadsorbed and adsorbed adsorbents are presented in Fig. 2 (i) & (ii), indicating the presence of hydroxyl, carboxylic acid, amines, and nitrile groups. These functional groups have been identified on the surface of AMFA before and after phosphate adsorption. The substantial peaks were noticed at approximately  $1079.24$ ,  $788.29$ ,  $641.59\text{ cm}^{-1}$ . The FTIR spectrum of phosphate ion adsorption resulted in peaks at  $1079.24$  attributed to  $\text{PO}_4^{3-}$ ,  $788.29$ ,  $641.59\text{ cm}^{-1}$  representing the symmetric stretching of the Si–O–Si and Al–O–Si band. It was perceived that peak formation in FTIR spectra changed after phosphate

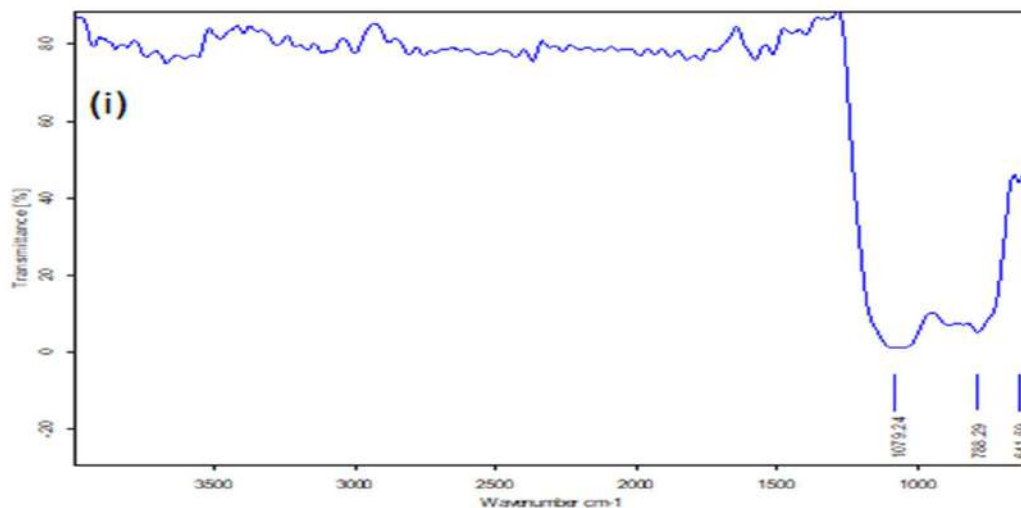


Fig. 2: (i) Raw adsorbent (AMFA) (Unadsorbed)

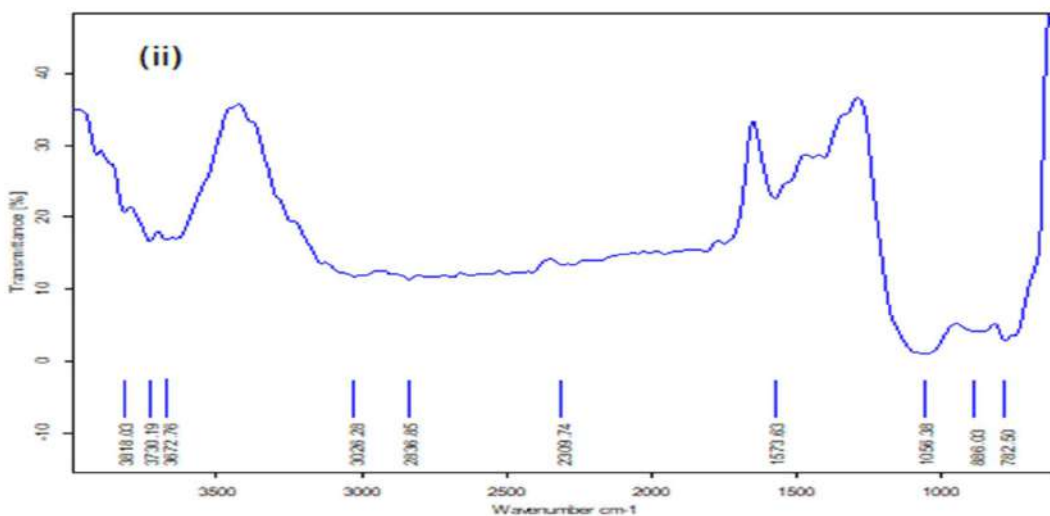


Fig. 2: (ii) AMFA (Adsorbed)



adsorption and indicated that phosphate ions after adsorption enhanced the function group count. After adsorption (Fig. 2. ii) more peaks were noticed in the spectra at 3818.03, 3730.019, 3672.76, 3026.28, 2836.85, 2309.74, 1573.63, 1056.38, 886.03, 782.50 which represent single bend stretch, non-bonded O-H stretching (OH group), O-H stretching vibration, nitriles, amides, amines, peak at 1056.38 represent the peak shifting from 1079.24 indicating phosphate adsorption taken on the surface of adsorbent.

### Phosphate Removal Experiments

To investigate the effects of various parameters on the removal of phosphate from synthetic solutions, a batch process was conducted. The experiment was performed in conical flasks of 100 mL, where 50 mL of a known phosphate concentration was taken. The adsorbent dosage used was 0.5 g, and the pH was adjusted accordingly by using 1N HCl and 1N NaOH. A mechanical shaker was employed during the batch study, operating at 100 RPM at a temperature of 25°C. The samples were agitated for one hour. After the completion of the agitation period, the conical flasks were taken out from the shaker and kept outside at room temperature to settle for 2-3 min to allow the adsorbents to separate from the solution. The solution was filtered using Whatman filter paper no. 1, followed by filtrate analyzed by using ammonium molybdate and stannous chloride as reagents, which gave a blue color to the solution (APHA 2012). After the color development, the concentration of phosphate was measured at 690 nm wavelength using a UV-spectrophotometer (UV-1800 Shimadzu).

The following equation was used to calculate the uptake capacity:

$$\text{Uptake capacity } (q_e) = \frac{C_i - C_e}{m} \times V \quad \dots(1)$$

wherein  $q_e$  depicts the quantity of phosphate adsorbed at equilibrium ( $\text{mg.g}^{-1}$ ),  $C_i$  and  $C_e$  depict the initial and final concentration of phosphate ions ( $\text{mg.L}^{-1}$ ),  $V$  depicts the volume of phosphate solution

(L),  $m$  depicts the quantity of adsorbent (g).

Removal efficiency (%) of phosphate ion was calculated using Eq (2) as follows:

$$\text{Removal efficiency } (\%) = \frac{C_i - C_e}{C_i} \times 100 \quad \dots(2)$$

where  $C_i$  and  $C_e$  denote the initial and final phosphate ion concentrations.

### Isotherms, Kinetics, and Thermodynamics Studies

For the evaluation of adsorption data, Langmuir, Freundlich, and Temkin isotherm models were employed. Kinetics

evaluation provided different sorts of sorption mechanisms. The adsorption kinetics are explained with the help of pseudo-first-order and pseudo-second-order kinetic equations. The adsorption capacity of the adsorbate on any porous medium is determined by intra-particle diffusion, a secondary procedure that evaluates adsorption uptake capacity using the square root of time. From temperature-dependent data, calculations were conducted to ascertain the thermodynamic quantities, including enthalpy change ( $\Delta H^\circ$ ), entropy change ( $\Delta S^\circ$ ), and free energy change ( $\Delta G^\circ$ ), linked to the sorption of phosphate on acid-modified fly ash (AMFA).

### Batch Experiments

Adsorption encompasses the creation of an adsorbate layer on the adsorbent's surface. This phenomenon can take place through both physical and chemical mechanisms. In physisorption, the adsorbate molecules in a solution create a deposit on the adsorbent surface due to Van der Waals forces of attraction. On the other hand, chemical adsorption involves the formation of a molecular layer of the adsorbate through chemical reactions on the surface (Sharma et al. 2016). The presence of functional groups such as hydroxyl and carboxyl significantly improves the binding efficiency of modified fly ash for a variety of pollutants, with adsorption behavior typically described by isotherm models that indicate monolayer and multilayer adsorption on adsorption binding sites. Environmental factors, including pH, temperature, and pollutant concentration, greatly affect the adsorption process, highlighting the necessity of optimizing both modification techniques and operational parameters to enhance the effectiveness of modified fly ash in environmental remediation applications. Many studies collectively provide evidence for the adsorption mechanisms involved in the removal of pollutants using modified fly ash. They highlighted the importance of surface modifications, the role of functional groups, and the application of kinetic and isotherm models in understanding and optimizing the adsorption process (Akpomie et al. 2023, Alaqarbeh 2021)

### Influence of pH

pH is a crucial factor in batch mode adsorption, and its effect on phosphate removal was investigated in this study. An adsorption experiment was conducted by changing the pH from 2 to 9. The acid-modified fly ash was used as the adsorbent, with an amount of 0.5 g, 50 ppm concentration, 60 min interaction period at 25°C with a constant agitation speed of 100 rpm. The outcomes indicated that the highest phosphate removal of 90% was attained at pH 5.0, as shown in Fig. 3. Beyond pH 5.0, the adsorption capacity started to decrease. An identical pattern was noticed in other phosphate adsorption studies (Shah et al. 2023). At lower pH values,

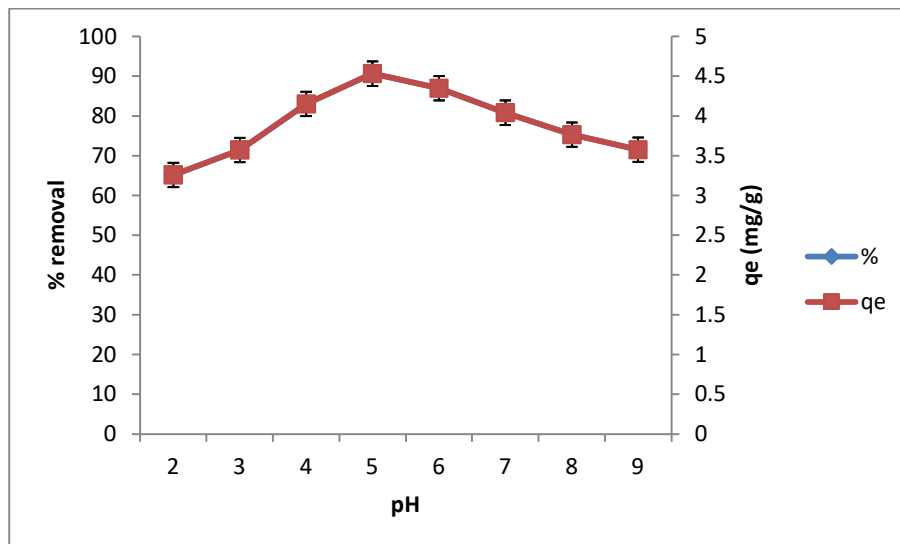


Fig. 3: Influence of pH on phosphate adsorption by AMFA.

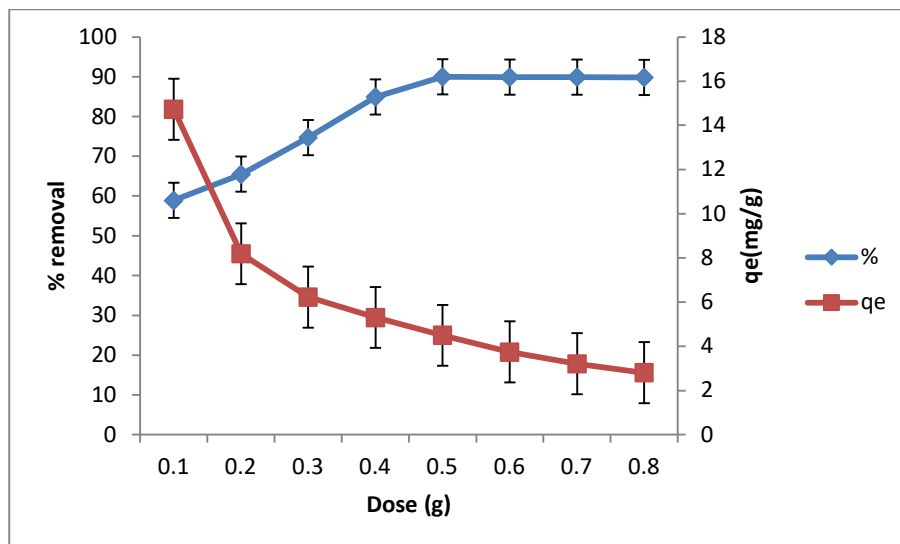


Fig. 4: Influence of adsorbent dosage on phosphate adsorption by AMFA.

the dominant form of phosphate ions was  $\text{H}_3\text{PO}_4$ , which had high solubility in the solutions (Siwek et al. 2019). As the solution pH increased, the concentrations of easily detachable  $\text{H}_2\text{PO}_4^-$  and  $\text{HPO}_4^{2-}$  forms increased, leading to improved removal efficiency. On the other hand, phosphate ions predominantly existed in the form of  $\text{PO}_4^{3-}$  at greater pH values, hindering the adsorption process and reducing the removal efficacy (Saleh et al. 2023). In essence, the observed trend can be ascribed to the electrostatic force of attraction between hydrogen ions at low pH conditions and the presence of hydroxyl ions at high pH conditions (Xiong et al. 2017).

### Influence of Adsorbent Dosage

The adsorbent dosage plays a significant role in the removal of phosphate from synthetic solutions. Adsorbent dosage ranged from 0.1 to 0.8 g in 50 mL of phosphate solution with a pH of 5.0 and an initial phosphate ion concentration of 50 ppm for an interaction period of 60 min at 25°C. It was noticed that phosphate adsorption by acid-modified fly ash upsurged from 58.92% to 89.96%, as illustrated in Fig. 4. Increasing the adsorbent dosage provides more active binding sites, leading to improved removal efficiency (Ye et

al. 2015). Similarly, when adsorbent dosage was increased, adsorption capacity ( $q$ ) decreased from  $14.73 \text{ mg.g}^{-1}$  to  $2.80 \text{ mg.g}^{-1}$ , indicating a negative correlation between phosphate adsorption capacity and adsorbent dosage. However, it is crucial to note that excessive adsorbent dosage, relative to the amount of adsorbate, can result in the unsaturation of adsorption sites, leading to a reduction in uptake capacity (Hu et al. 2015). Similar outcomes were observed when biomass fly ash was used, as reported by Park et al. (2021).

Additionally, more recent studies by Xi et al. (2020) and Wu et al. (2019) have corroborated that increasing the adsorbent dosage improves phosphate removal efficiency. However, this increase can also cause a decrease in specific adsorption capacity due to site saturation. Consequently, a dosage of  $0.5 \text{ g}$  of AMFA was determined to be the optimal amount for subsequent adsorption experiments.

### Influence of Contact Time

Experiments were conducted to study the adsorption of phosphate under various conditions. The contact period ranged from 5 to 80 min, with an initial ion concentration of  $50 \text{ ppm}$  and an adsorbent dosage of  $0.5 \text{ g.} 50 \text{ mL}^{-1}$ , a solution pH of  $5.0$  at  $25^\circ\text{C}$  (Fig. 5). It was noticed that as the interaction period enhanced, removal efficacy and uptake capacity both upsurged. A noteworthy removal efficacy of phosphate ion by AMFA occurred from  $60\%$  to  $89\%$  with a rise in time from 5 to 80 min. The maximum uptake capacity was noticed at  $4.42 \text{ mg.g}^{-1}$  at a time of 80 min. An equilibrium time was established at 30 min. After 30 min, no substantial adsorption took place due to the saturation of

binding sites with an increase in time. During the early phases of phosphate sorption, a substantial concentration gradient exists among the film and the accessible pore sites of the adsorbent, resulting in a faster adsorption rate, but in later phases, the adsorption rate declined, which can be attributed to the slower diffusion of the solute ion into the interior of the adsorbent (Chen et al. 2007, Johansson & Gustafsson 2000). Similar results were observed on slag and fly ash for the removal of phosphate ions (Ragheb 2013).

### Influence of Initial Phosphate Ion Concentration

The initial phosphate ion concentration has a substantial impact on the adsorption process. To investigate this effect, initial phosphate concentrations ranging from  $30$  to  $150 \text{ ppm}$  were studied at an optimum pH of  $5.0$ , with an adsorbent amount of  $0.5 \text{ g.} 50 \text{ mL}^{-1}$ , and an interaction period of  $60 \text{ min}$  at  $25^\circ\text{C}$ . The findings depicted in Fig. 6 that maximum phosphate adsorption took place at  $30 \text{ ppm}$  and, after that declined as the concentration of phosphate solution upsurged. This decline is attributed to the fact that, at lower concentrations, nearly all phosphate ions were able to bind to the available sites. As the initial phosphate concentration upsurged, these binding sites became saturated, impeding further increase in adsorption capacity at higher concentrations. Furthermore, at higher initial concentrations, the ratio of active sites to phosphate ion concentration decreased with a constant adsorbent dosage and volume of adsorbate (Fetene & Addis 2020). Consequently, there was a reduction in phosphate removal percentage, and these findings are consistent with the conclusions of other studies (Baraka et al. 2012, Trinh et al. 2020).

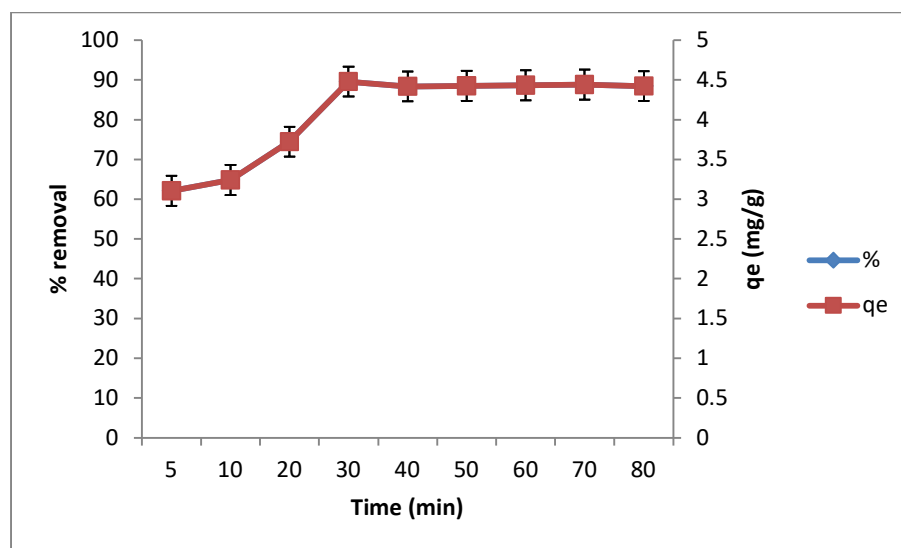


Fig. 5. Influence of contact period on phosphate adsorption by AMFA.

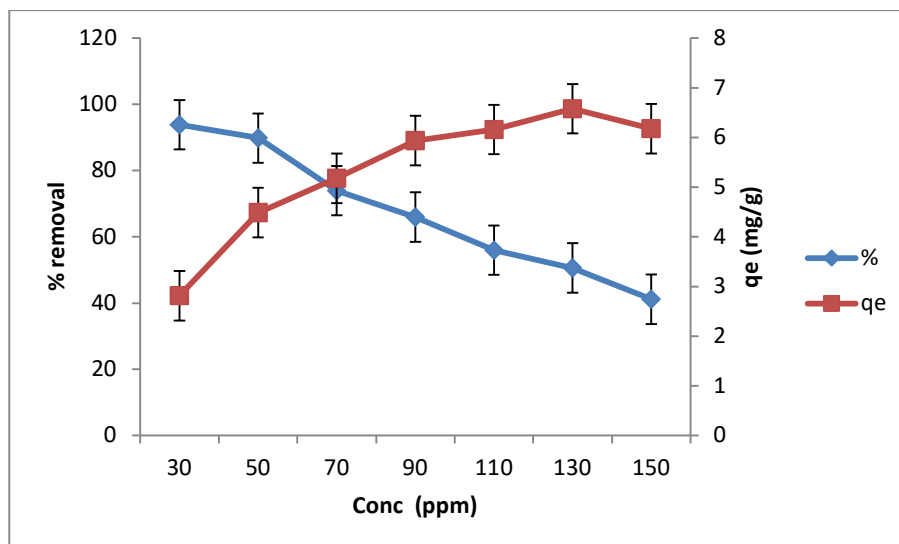


Fig. 6: Influence of initial phosphate ion concentration on phosphate adsorption by AMFA.

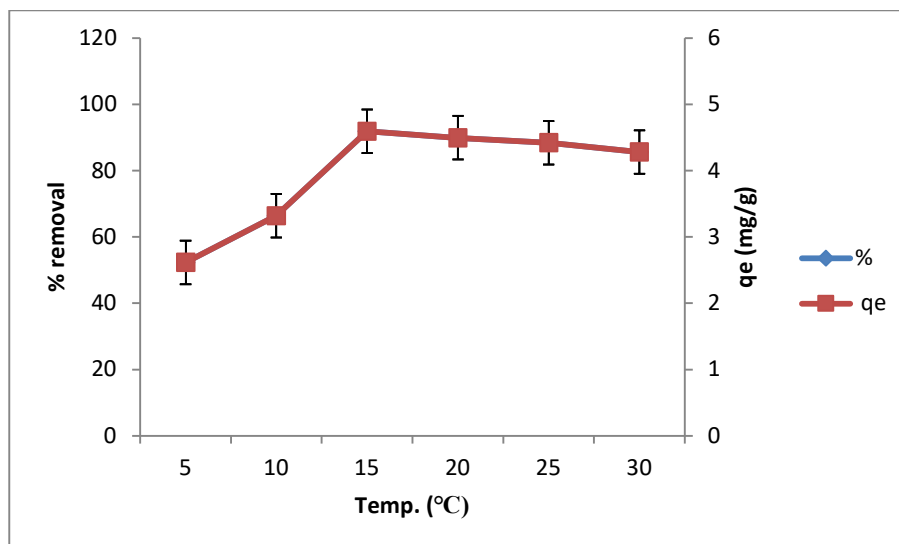


Fig. 7: Influence of temperature on phosphate adsorption by AMFA.

### Influence of Temperature

The impact of temperature on phosphate adsorption was explored under different temperature conditions, ranging from 5°C to 30°C. The experiment was performed at 5.0 pH, 0.5 g dose, 60 min of contact time, and a concentration of 30 ppm with a constant stirring of 100 RPM for the adsorption of phosphate ions on acid-modified fly ash. It was determined that removal effectiveness and uptake capacity ( $q_e$ ) raised to 15°C. The outcomes showed that the highest phosphate removal of 91.88%, followed by 15°C. Fig. 7 illustrated that

as the temperature upsurged from 5°C to 30°C, the percentage of phosphate adsorption raised 52.3% to 91.88% and, after that, became stable after 15°C, revealing a preference for phosphate adsorption at lower temperatures (Wu et al. 2019). At elevated temperatures, the molecules in the solution exhibited more vigorous thermal motion, resulting in an increased rate of molecular exchange on the surface of the adsorbent. As a consequence, higher temperatures promoted greater spontaneity in the adsorption process, leading to faster attainment of equilibrium (Al-Harby et al. 2021). A similar pattern was noticed by Sugiyama & Hama (2013).



## Adsorption Isotherms

To examine the mechanism and relation between adsorbate and adsorbent, various isotherms, including Langmuir, Freundlich, and Temkin isotherms, were used.

### Langmuir Isotherm

The Langmuir isotherm was proposed by Langmuir in 1916 which describes the process of monolayer adsorption on a homogeneous surface. It assumes that the adsorbent surface contains a limited number of uniform sorption binding sites and adsorbate does not migrate inside the surface plane (Langmuir 1916). The highest sorption capacity is calculated using the Langmuir equation, which is shown in eq 3.

$$\frac{C_e}{q_e} = \frac{1}{bq_m} + \frac{C_e}{q_m} \quad \dots(3)$$

$C_e$  denotes the equilibrium phosphate concentration ( $\text{mg.L}^{-1}$ ),  $q_e$  depicts the adsorbed phosphate concentration at equilibrium ( $\text{mg/g}$ ), and  $b$  denotes the Langmuir constant. These constants are derived from both the slope and the intercept of the linear plot of  $C_e/q_e$  versus  $C_e$ , as presented in Fig. 8.

### Separation Factor

Adsorbent surface area and permeability are directly interrelated to the Langmuir constant. As the adsorbent surface area and permeability increase, uptake capacity also rises. Additionally, the value of  $R_L$  helps to determine the type of adsorption (Arora et al. 2023).

$$R_L = \frac{1}{(1+bC_i)} \quad \dots(4)$$

Table 1. Adsorption isotherm parameters for phosphate on AMFA

Isotherm	Parameters	AMFA
Langmuir	$q_m (\text{mg.g}^{-1})$	46.72
	$b$	0.01
	$R^2$	0.14
	$R_L$	0.83
Freundlich	$n$	1.189
	$K_f (\text{L.g}^{-1})$	1.11
	$R^2$	0.86
Temkin	$B_T (\text{KJ.mol}^{-1})$	4.39
	$A_T (\text{g.L}^{-1})$	2.85
	$R^2$	0.77

$R_L$  represents the separation factor, which is a limitless entity. It is calculated with the help of the Langmuir constant ( $b$ ) and the initial phosphate concentration ( $C_i$ ). Depending on the value of  $R_L$ , there are four potential scenarios:  $R_L$  ranging from 0 to 1 indicates “favorable adsorption”,  $R_L$  greater than 1 “unfavorable adsorption”,  $R_L$  equal to 1 signifies “linear adsorption” and  $R_L$  equal to 0 implies “irreversible adsorption”. AMFA has a separation factor of 0.83 respectively which falls in the range between 0 to 1, indicating favorable adsorption of phosphate.

Fig. 8 and Table 1, the correlation coefficient value was 0.14 for adsorbent acid-modified fly ash, which shows the unfitness of equilibrium data in Langmuir isotherm.

### Freundlich Isotherm

Freundlich isotherm model describes the adsorption of molecules on heterogeneous surfaces, where multiple layers

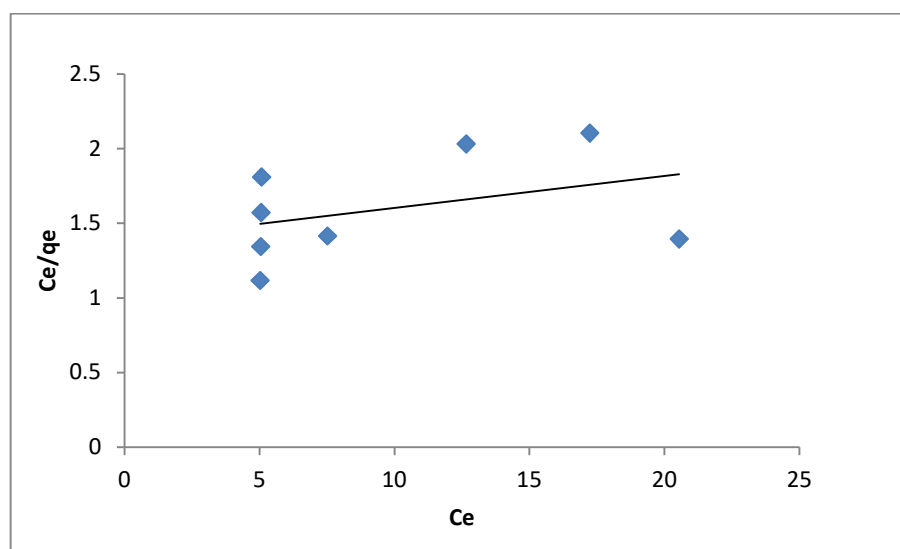


Fig. 8: Langmuir Isotherm: Phosphate Adsorption on AMFA.

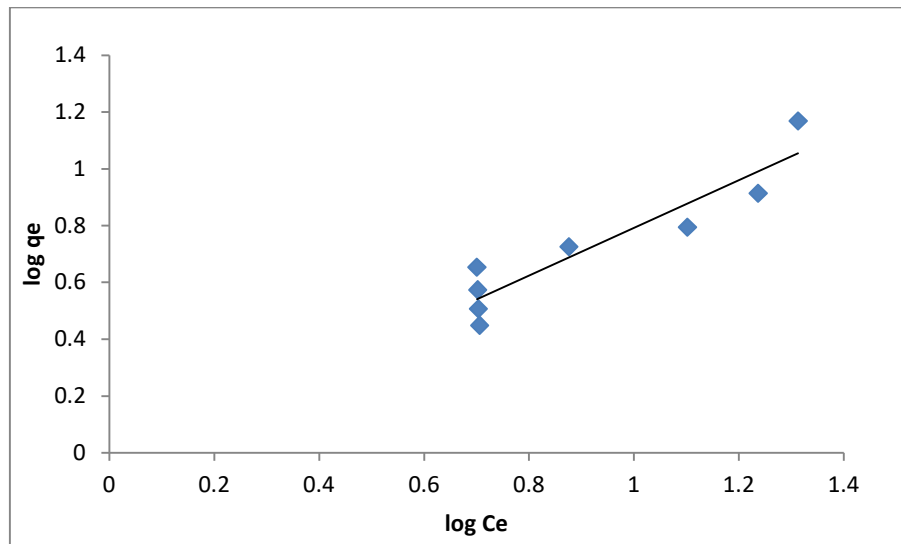


Fig. 9: Freundlich Isotherm: Phosphate Adsorption on AMFA.

of adsorbate can form, and interactions occur among the adsorbed molecules (Freundlich 1907). Freundlich isotherm is presented in a linear form as

$$\log q_e = \log K_f + \frac{1}{n} \log C_e \quad \dots(5)$$

$C_e$  depicts phosphate equilibrium concentration ( $\text{mg.L}^{-1}$ ),  $q_e$  depicts the number of phosphate ions adsorbed at equilibrium ( $\text{mg.g}^{-1}$ ),  $K_f$  depicts the Freundlich constant,  $n$  depicts the intensity of the adsorption process, and the intercept and slope of the graph among  $\log C_e$  and  $\log q_e$  can be used to determine the values of  $K_f$  and  $n$  as presented in Fig. 9.

Fig. 9 and Table 1 show that the  $R^2$  value for AMFA was found to be 0.83, which suggests that, Freundlich isotherm better fit into the data. When the value of  $n$  is more than 1, it states that it favors the adsorption process. In contrast to the Langmuir isotherm, the adsorption process of the adsorbent was well explained by the Freundlich isotherm. This indicates that the adsorption occurred in multiple layers, suggesting a more complex adsorption mechanism.

### Temkin isotherm

Temkin and Pyzhev (1940) introduced the Temkin model, which is used to analyze the adsorption process. According to this, the heat of sorption decreases linearly with temperature instead of following a logarithmic relationship. It may be expressed as:

$$q_e = \frac{RT}{B_T} \ln A_T + \frac{RT}{B_T} \ln C_e \quad \dots(6)$$

$C_e$  depicts the phosphate equilibrium concentration ( $\text{mg.L}^{-1}$ ),  $q_e$  depicts the number of phosphate ions adsorbed

at equilibrium ( $\text{mg.g}^{-1}$ ),  $T$  depicts temperature (Kelvin),  $R$  depicts the universally accepted gas constant ( $8.314 \text{ J.mol}^{-1} \cdot \text{K}^{-1}$ ),  $B_T$  depicts the Temkin constant ( $\text{J.mol}^{-1}$ ),  $A_T$  depicts constant of Temkin isotherm ( $\text{g.L}^{-1}$ ).

To determine the values of  $B_T$  and  $A_T$ , a plot of  $q_e$  versus  $\ln C_e$  was plotted for phosphate adsorption on AMFA, as shown in Fig. 10. The plot's slope yields the  $B_T$  value, whereas the intercept corresponds to the  $A_T$  value.

The Temkin constant ( $B_T$ ) value indicates the kind of adsorption. When  $B_T$  is more than 20 KJ/mol, it means chemical adsorption takes place, and when  $B_T$  is less than 20  $\text{KJ.mol}^{-1}$ , physical adsorption is significant for the adsorption process. The Temkin constant ( $B_T$ ) and corresponding  $R^2$  values are 4.39  $\text{kJ.mol}^{-1}$  and 0.77 for adsorption of phosphate on AMFA, respectively. Hence, Temkin's study concludes that the adsorption process favors physical adsorption (Table 1).

### Adsorption Kinetic Models

The adsorption rate of a solute was determined by studying various kinetic models comprising the pseudo-first-order, pseudo-second-order, and intra-particle diffusion models.

#### Pseudo-First-Order

Lagergren's pseudo-first-order kinetic equation describes the adsorption of a solute onto an adsorbent (Lagergren 1898) and is given by the following equation:

$$\log (q_e - q_t) = \log q_e - \frac{K_1 t}{2.303} \quad \dots(7)$$

Where  $q_e$  represents the equilibrium uptake efficiency ( $\text{mg.g}^{-1}$ ),  $q_t$  is the equilibrium uptake efficiency at time  $t$

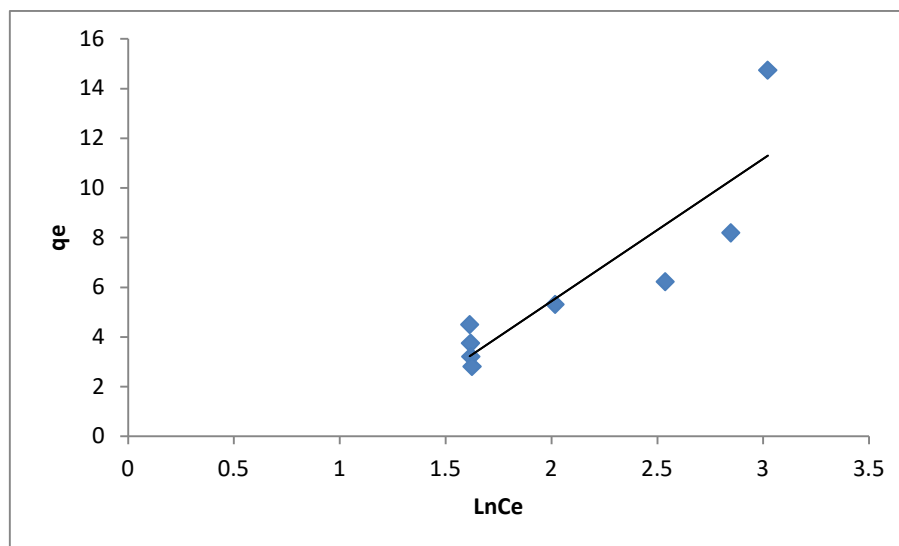


Fig. 10: Temkin Isotherm: Phosphate Adsorption on AMFA.

(min),  $k_1$  depicts the rate constant for pseudo-first-order kinetics ( $\text{L} \cdot \text{min}^{-1}$ ), and  $t$  depicts the adsorption period (min).

A pseudo-first-order kinetic graph was derived by plotting  $\log(q_e - q_t)$  against time ( $t$ ) (Fig. 11). The values of  $K_1$  and  $q_e$  were determined using the slope and intercept of the plot, respectively. The correlation coefficient for acid-modified fly ash is 0.97. The correlation coefficient value over 0.9 indicates that the estimated and experimental adsorption capacities are in strong agreement (Table 2).

### Pseudo-Second-Order

The linearized form of the pseudo-second-order equation, as stated by Ho and McKay (1999), can be conveyed as follows:

$$\frac{t}{q_t} = \frac{1}{K_2 q_e^2} + \frac{t}{q_e} \quad \dots(8)$$

Here,  $q_e$  depicts the equilibrium uptake capacity ( $\text{mg/g}$ ),  $q_t$  depicts the adsorption capacity at a specific period (min), and  $K_2$  is the rate constant for the pseudo-second-order model ( $\text{g} \cdot \text{mg}^{-1} \cdot \text{min}^{-1}$ ). Fig. 12 illustrates a pseudo-second-order kinetic model that was graphed among  $t/q_t$  and  $t$ . The intercept and slope of the plot were used to derive the values of  $q_e$  and  $K_2$ , respectively. The obtained  $R^2$  value for the adsorbent was 0.997. It was evident from Table 2 that the pseudo-second-order kinetic model was better able to fit the adsorption data. This strong agreement exists because the calculated  $q_e$  closely matches the experimental  $q_{exp}$ .

### Intra-Particle Diffusion

The intra-particle uptake and pore diffusion serve as the foundation in the adsorption process for the intra-particle

diffusion concept. To determine the diffusion mechanism, Weber and Morris (1963) found that “intra-particle diffusion of the adsorbate varies proportionately with half power of time during adsorption” and is linearly represented in eq 9:

$$q_t = k_i \sqrt{t} + x_i \quad \dots(9)$$

Here  $x_i$  represents the wideness of the border layer ( $\text{mg} \cdot \text{g}^{-1}$ ), and  $k_i$  ( $\text{mg} \cdot \text{g}^{-1} \cdot \text{min}^{0.5}$ ) is the intra-particle diffusion rate constant. Using the intra-particle diffusion model's plot between  $q_t$  and  $t$ , the values of  $x_i$  and  $k_i$  were determined from the intercept and slope (Fig. 13). According to Singh and Bhateria 2020, the wideness of the border layer is dependent on the greater value of  $x_i$ . The values of  $x_i$  and  $R^2$  attained 2.7891  $\text{mg/g}$  and 0.79 for AMFA, respectively (Table 2).

Based on the kinetic findings, it was determined that the pseudo-second-order kinetic model provided a more precise

Table 2. Kinetic model parameters for phosphate adsorption on AMFA

Kinetic models	Parameters	AMFA
Experimental adsorption capacity	$q_{e \text{ exp}}$ (mg/g)	4.47
Pseudo-first-order kinetics	$q_{e \text{ cal}}$ (mg/g)	1.04
	$K_1$ (1/min)	0.52
	$R^2$	0.97
Pseudo-second-order kinetics	$q_{e \text{ cal}}$ (mg/g)	4.64
	$K_2$ (g/mg/min)	0.06
	$R^2$	0.997
Intra-particle diffusion	$K_i$ [ $\text{mg}/(\text{g} \cdot \text{min}^{0.5})$ ]	0.2153
	$x_i$ (mg/g)	2.7891
	$R^2$	0.7906

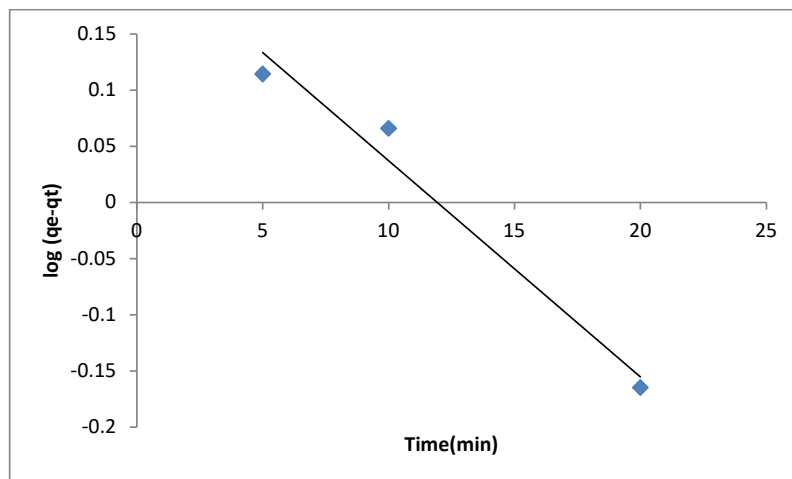


Fig. 11: Pseudo-first-order plot for phosphate adsorption on AMFA.

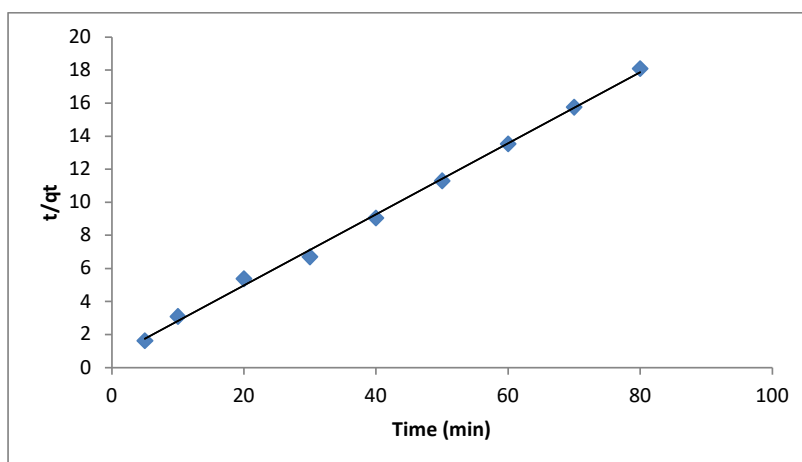


Fig. 12: Pseudo-second-order plot for phosphate adsorption on AMFA.

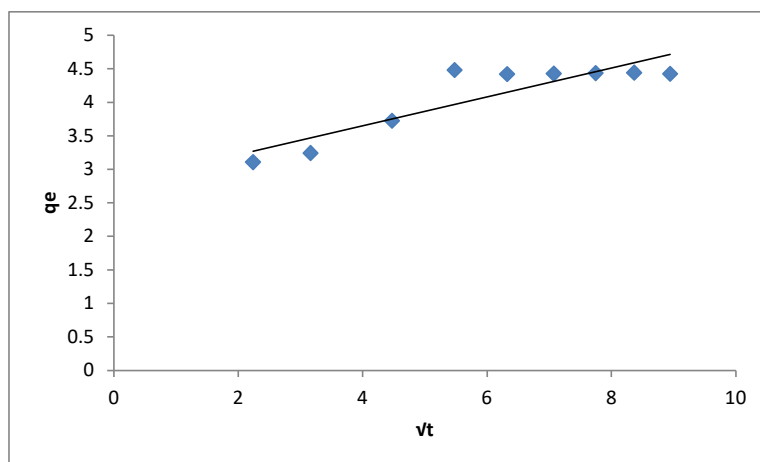


Fig. 13: Intra-particle diffusion plot for phosphate adsorption on AMFA.



fit to the adsorption data rather than the pseudo-first-order kinetic model.

### Thermodynamic Studies

Adsorption thermodynamics were employed to determine the sort of adsorption occurring in the phosphate adsorption process with acid-modified fly ash. As per the findings of Ngah and Hanafiah (2008), a reduction in  $\Delta G$  with rising temperature suggests that the sorption process would be possible and spontaneous.  $\Delta G$  is calculated using eq 10:

$$\Delta G = -RT \ln K \quad \dots(10)$$

Where T depicts temperature in K (Kelvin), and R depicts the gas constant (8.314 J/mol.K). Diverse temperatures considered for the thermodynamic study were 278 K, 283

K, 288 K, 293 K, and 303 K. The Van't Hoff interaction was utilized to govern the thermodynamic parameters  $\Delta H^\circ$  and  $\Delta S^\circ$ . The Van't Hoff graph was plotted between  $\ln K_d$  and  $1000/T$  (Fig. 14). Both the slope and intercept of the plot were utilized to calculate  $\Delta H^\circ$  and  $\Delta S^\circ$ .

$$\ln K_d = \frac{\Delta S^\circ}{R} - \frac{\Delta H^\circ}{RT} \quad \dots(11)$$

$$\Delta G^\circ = \Delta H^\circ - T\Delta S^\circ \quad \dots(12)$$

where T depicts temperature (K),  $K_d = q_e/C_e$  depicts distribution coefficient, R depicts the universally accepted gas constant (8.314 J.mol<sup>-1</sup>.K<sup>-1</sup>),  $C_e$  depicts the equilibrium phosphate concentration (mg.L<sup>-1</sup>),  $q_e$  represents the number of phosphate ions adsorbed at equilibrium (mg.g<sup>-1</sup>),  $\Delta G$  determines the spontaneity of the adsorption process, with

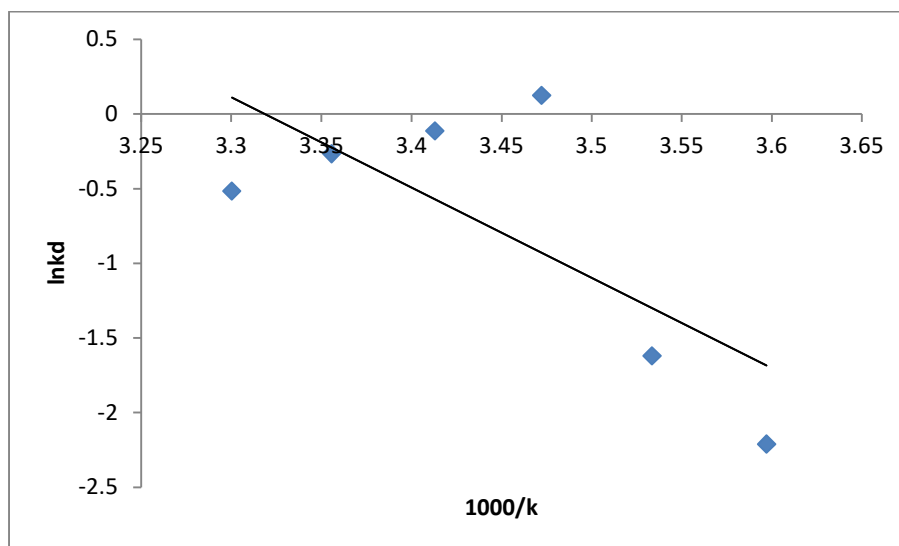


Fig. 14: Van't Hoff Analysis of Phosphate Adsorption on AMFA.

Table 3. Thermodynamic factors for the adsorption of phosphate on AMFA

Adsorbent	$\Delta H^\circ$ (kJ/mol)	$\Delta S^\circ$ (KJ/mol/K)	$\Delta G^\circ$ (KJ/mol)					
			278 K	283K	288K	293K	298K	303K
AMFA	50.25	0.166	4.11	3.27	2.45	1.62	0.79	-0.048

Table 4. Maximum uptake capacities of different industrial waste-based adsorbents

Adsorbate	Adsorbent	Maximum sorption capacity( $q_e$ ) mg/g	References
Phosphate	Electric arc furnace steel slag	2.2	Drizo et al. 2006
Phosphate	Crushed brick with iron oxide coating	1.8	Boujelben et al. 2008
Phosphate	Red mud	0.5	Castaldi et al. 2010
Phosphate	HCl treated red mud	0.58	Huang et al. 2008
Phosphate	Fly ash	3.34	Yu et al. 2015
Phosphate	Acid modified fly ash (AMFA)	4.47	Current study

a positive value indicating a non-spontaneous process and a negative value indicating a spontaneous process.  $\Delta H$  depicts whether the process is exothermic or endothermic. A positive  $\Delta H$  represents an endothermic process, while a negative  $\Delta H$  shows an exothermic process. Positive and negative values of  $\Delta S$  indicate an increase or decrease in the degree of randomness at the solid-liquid interface, respectively.

Table 3 displays the findings from the thermodynamic study. The positive values of all the thermodynamic parameters ( $\Delta H^\circ$ ,  $\Delta S^\circ$ , and  $\Delta G^\circ$ ) illustrate that the adsorption process is endothermic and non-spontaneous at lower temperatures and spontaneous at higher temperatures.

### Comparison and Analysis of Different Adsorbents

Table 4 analyzes and compares the maximum sorption capacities of diverse industrial waste-based adsorbents for the adsorption of phosphate. Various adsorbents such as electric arc furnace steel slag (Drizo et al. 2006), iron oxide coated crushed brick (Boujelben et al. 2008), red mud (Castaldi et al. 2010), HCl treated red mud (Huang et al. 2008) and fly ash (Yu et al. 2015) have been used for confiscation of phosphate from synthetic solutions.

### CONCLUSIONS

This study focused on evaluating the capability of acid-modified fly ash (AMFA) to eliminate phosphate from synthetic solutions. The results revealed that AMFA exhibited effective phosphate removal, with a maximal sorption capacity of  $4.47 \text{ mg.g}^{-1}$ . The sorption of phosphate remained relatively stable under acidic solution pH conditions but significantly decreased as the pH approached strongly alkaline levels. Thermodynamic studies indicated that the rate of phosphate sorption on AMFA increased with rising temperatures, indicating an endothermic and non-spontaneous process. The kinetic data was well defined by the pseudo-second-order model. Both the Freundlich and Temkin isotherms provided good fits for the equilibrium data, suggesting multilayer adsorption and possible interaction between the adsorbate and adsorbent surface. Overall, this investigation demonstrated the effective use of AMFA for phosphate removal from synthetic solutions. Additionally, the study showed that AMFA could be potentially utilized for repeated regeneration of phosphate from synthetic solutions, further highlighting its applicability as an adsorbent material in water treatment processes.

### REFERENCES

Ahmaruzzaman, M., 2010. A review on the utilization of fly ash. *Progress in Energy and Combustion Science*, 36(3), pp.327-363. [DOI]  
 Ahmaruzzaman, M., 2011. Industrial wastes as low-cost potential adsorbents

for the treatment of wastewater laden with heavy metals. *Advances in Colloid and Interface Science*, 166(1-2), pp.36-59. [DOI]  
 Akpomie, K.G., Conradie, J., Adegoke, K.A., Oyedotun, K.O., Ighalo, J.O., Amaku, J.F., Olisah, C., Adeola, A.O. and Iwuozor, K.O., 2023. Adsorption mechanism and modeling of radionuclides and heavy metals onto ZnO nanoparticles: a review. *Applied Water Science*, 13(1), p.20. [DOI]  
 Alaqarbeh, M., 2021. Adsorption phenomena: definition, mechanisms, and adsorption types: short review. *RHAZES: Green and Applied Chemistry*, 13, pp.43-51. [DOI]  
 Al-Harby, N.F., Albahly, E.F. and Mohamed, N.A., 2021. Kinetics, isotherm, and thermodynamic studies for efficient adsorption of Congo Red dye from aqueous solution onto novel cyanoguanidine-modified chitosan adsorbent. *Polymers*, 13(24), p.4446. [DOI]  
 American Public Health Association, 1926. *Standard Methods for the Examination of Water and Wastewater* (Vol. 6). American Public Health Association.  
 Arora, D., Arora, A., Singh, A., Agarwal, R., Bala, R. and Kumar, S., 2023. Evaluating the applicability of *Brachiaria mutica* (Forssk.) (Paragrass) and *Cyperus rotundus* L. (Nutgrass) as bioadsorbents to remove Cr (VI): isotherms, kinetics, and thermodynamic studies. *Sustainable Water Resources Management*, 9(5), p.168. [DOI]  
 Baraka, A.M., El-Tayieb, M.M., El-Shafai, M. and Mohamed, N.Y., 2012. Sorptive removal of phosphate from wastewater using activated red mud. *Journal of Environmental Science and Technology*, 10(1), pp.55-63.  
 Boujelben, N., Bouzid, J., Elouear, Z., Feki, M., Jamoussi, F. and Montiel, A., 2008. Phosphorus removal from aqueous solution using iron-coated natural and engineered sorbents. *Journal of Hazardous Materials*, 151(1), pp.103-110. [DOI]  
 Buema, G., Harja, M., Lupu, N., Chiriac, H., Forminte, L., Ciobanu, G., Bucur, D. and Bucur, R.D., 2021. Adsorption performance of modified fly ash for copper ion removal from aqueous solution. *Water*, 13(2), p.207. [DOI]  
 Castaldi, P., Silvetti, M., Garau, G. and Deiana, S., 2010. Influence of the pH on the accumulation of phosphate by red mud (a bauxite ore processing waste). *Journal of Hazardous Materials*, 182(1-3), pp.266-272. [DOI]  
 Chen, J., Kong, H., Wu, D., Chen, X., Zhang, D. and Sun, Z., 2007. Phosphate immobilization from aqueous solution by fly ashes in relation to their composition. *Journal of Hazardous Materials*, 139(2), pp.293-300. [DOI]  
 De Gisi, S., Lofrano, G., Grassi, M. and Notarnicola, M., 2016. Characteristics and adsorption capacities of low-cost sorbents for wastewater treatment: a review. *Sustainable Materials and Technologies*, 9, pp.10-40. [DOI]  
 Drizo, A., Forget, C., Chapuis, R.P. and Comeau, Y., 2006. Phosphorus removal by electric arc furnace steel slag and serpentinite. *Water Research*, 40(8), pp.1547-1554. [DOI]  
 Fetene, Y. and Addis, T., 2020. Adsorptive removal of phosphate from wastewater using Ethiopian rift pumice: Batch experiment. *Air, Soil and Water Research*, 13, p.1178622120969658. [DOI]  
 Freundlich, H., 1907. Über die adsorption in lösungen. *Zeitschrift für Physikalische Chemie*, 57(1), pp.385-470.  
 Ho, Y.S. and McKay, G., 1999. Pseudo-second order model for sorption processes. *Process Biochemistry*, 34(5), pp.451-465. [DOI]  
 Hosseinpour, S., Hejazi-Mehrzi, M., Hashemipour, H. and Farpoor, M.H., 2023. Adsorptive removal of phosphorus from aqueous solutions using natural and modified coal solid wastes. *Water Science & Technology*, 87(6), pp.1376-1392. [DOI]  
 Hu, Q., Chen, N., Feng, C. and Hu, W., 2015. Nitrate adsorption from aqueous solution using granular chitosan-Fe<sup>3+</sup> complex. *Applied Surface Science*, 347, pp.1-9. [DOI]  
 Huang, W., Wang, S., Zhu, Z., Li, L., Yao, X., Rudolph, V. and Haghseresh, F., 2008. Phosphate removal from wastewater using red mud. *Journal of Hazardous Materials*, 158(1), pp.35-42. [DOI]  
 Irawan, C., Atikah, A. and Rumhayati, B., 2014. Adsorption of iron by fly ash adsorbent of coal. *The Journal of Pure and Applied Chemistry Research*, 3(3), p.88.

- Johansson, L. and Gustafsson, J.P., 2000. Phosphate removal using blast furnace slags and opoka-mechanisms. *Water Research*, 34(1), pp.259-265. [DOI]
- Karaca, S., Gürses, A., Ejder, M. and Açıkyıldız, M., 2004. Kinetic modeling of liquid-phase adsorption of phosphate on dolomite. *Journal of Colloid and Interface Science*, 277(2), pp.257-263. [DOI]
- Küçük, İ. and Üstündağ, P., 2024. Adsorption performance of acidic modified fly ash: Box–Behnken design. *Journal of the Turkish Chemical Society Section A: Chemistry*, 11(2), pp.699-708. [DOI]
- Lagergren, S., 1898. About the theory of so-called adsorption of soluble substances. *Fictitious Journal of Chemical Science*, 10(1), pp.100-120.
- Langmuir, I., 1916. The constitution and fundamental properties of solids and liquids. Part I. Solids. *Journal of the American Chemical Society*, 38(11), pp.2221-2295.
- Loganathan, P., Vigneswaran, S., Kandasamy, J. and Bolan, N.S., 2014. Removal and recovery of phosphate from water using sorption. *Critical Reviews in Environmental Science and Technology*, 44(8), pp.847-907. [DOI]
- Neufeld, R.D. and Thodos, G., 1969. Removal of orthophosphates from aqueous solutions with activated alumina. *Environmental Science & Technology*, 3(7), pp.661-667. [DOI]
- Ngah, W.W. and Hanafiah, M.A.K.M., 2008. Adsorption of copper on rubber (*Hevea brasiliensis*) leaf powder: Kinetic, equilibrium and thermodynamic studies. *Biochemical Engineering Journal*, 39(3), pp.521-530. [DOI]
- Park, J.H., Hwang, S.W., Lee, S.L., Lee, J.H. and Seo, D.C., 2021. Sorption behavior of phosphate by fly ash discharged from biomass thermal power plant. *Applied Biological Chemistry*, 64(1), p.43.
- Ragheb, S.M., 2013. Phosphate removal from aqueous solution using slag and fly ash. *HBRC Journal*, 9(3), pp.270-275. [DOI]
- Recepoglu, Y.K., Goren, A.Y., Orooji, Y. and Khataee, A., 2022. Carbonaceous materials for removal and recovery of phosphate species: Limitations, successes, and future improvement. *Chemosphere*, 287, p.132177. [DOI]
- Ren, X. and Sancaktar, E., 2019. Use of fly ash as eco-friendly filler in synthetic rubber for tire applications. *Journal of Cleaner Production*, 206, pp.374-382. [DOI]
- Saad Algarni, T. and Al-Mohaimed, A.M., 2022. Water purification by adsorption of pigments or pollutants via metal oxide. *Journal of King Saud University-Science*, 34(8), p.102339. [DOI]
- Saleh, M., Alterkaoui, A., Ozdemir, N.C., Arslan, H., Bilici, Z. and Dizge, N., 2024. Adsorption of phosphate ions and reactive red 180 from aqueous solution using thermally activated lemon peel waste. *International Journal of Environmental Science and Technology*, 21(2), pp.1683-1696. [DOI]
- Shah, K.H., Fareed, M., Waseem, M., Shahida, S., Hatshan, M.R., Sarfraz, S., Batool, A., Fahad, M., Ahmad, T., Shah, N.S. and Ha, K., 2023. Tea-waste-mediated magnetic oxide nanoparticles as a potential low-cost adsorbent for phosphate ( $\text{PO}_4^{3-}$ ) anion remediation. *Water*, 15(20), p.3541. [DOI]
- Sharma, P.K., Ayub, S. and Tripathi, C.N., 2016. Isotherms describing physical adsorption of Cr (VI) from aqueous solution using various agricultural wastes as adsorbents. *Cogent Engineering*, 3(1), p.1186857. [DOI]
- Singh, N., Mithulraj, M. and Arya, S., 2019. Utilization of coal bottom ash in recycled concrete aggregates based self-compacting concrete blended with metakaolin. *Resources, Conservation and Recycling*, 144, pp.240-251. [DOI]
- Singh, R. and Bhateria, R., 2020. Experimental and modeling process optimization of lead adsorption on magnetite nanoparticles via isothermal, kinetics, and thermodynamic studies. *ACS Omega*, 5(19), pp.10826-10837. [DOI]
- Siwek, H., Bartkowiak, A. and Włodarczyk, M., 2019. Adsorption of phosphates from aqueous solutions on alginate/goethite hydrogel composite. *Water*, 11(4), p.633. [DOI]
- Sugiyama, S. and Hama, T., 2013. Effects of water temperature on phosphate adsorption onto sediments in an agricultural drainage canal in a paddy-field district. *Ecological Engineering*, 61, pp.94-99. [DOI]
- Sun, J., Yang, Q., Wang, D., Wang, S., Chen, F., Zhong, Y., Yi, K., Yao, F., Jiang, C., Li, S. and Li, X., 2017. Nickel toxicity to the performance and microbial community of enhanced biological phosphorus removal system. *Chemical Engineering Journal*, 313, pp.415-423. [DOI]
- Temkin, M.J. and Pyzhev, V., 1940. Recent Modifications to Langmuir Isotherms. [Fictitious details].
- Trinh, V.T., Nguyen, T.M.P., Van, H.T., Hoang, L.P., Nguyen, T.V., Ha, L.T., Vu, X.H., Pham, T.T., Nguyen, T.N., Quang, N.V. and Nguyen, X.C., 2020. Phosphate adsorption by silver nanoparticles-loaded activated carbon derived from tea residue. *Scientific Reports*, 10(1), p.3634. [DOI]
- Usman, M., Anastopoulos, I., Hamid, Y. and Wakeel, A., 2023. Recent trends in the use of fly ash for the adsorption of pollutants in contaminated wastewater and soils: Effects on soil quality and plant growth. *Environmental Science and Pollution Research*, 30(60), pp.124427-124446. [DOI]
- Wang, D., Yang, G., Li, X., Zheng, W., Wu, Y., Yang, Q. and Zeng, G., 2012. Inducing mechanism of biological phosphorus removal driven by the aerobic/extended-idle regime. *Biotechnology and Bioengineering*, 109(11), pp.2798-2807. [DOI]
- Wang, W., Qi, L. and Zhang, J., 2024. Specific resistance and adsorption performance of acid-modified fly ash for escaped ammonia in flue gas. *Journal of Hazardous Materials*, 465, p.133072. [DOI]
- Weber Jr, W.J. and Morris, J.C., 1963. Kinetics of adsorption on carbon from solution. *Journal of the Sanitary Engineering Division*, 89(2), pp.31-59. [DOI]
- Wu, B., Wan, J., Zhang, Y., Pan, B. and Lo, I.M., 2019. Selective phosphate removal from water and wastewater using sorption: Process fundamentals and removal mechanisms. *Environmental Science & Technology*, 54(1), pp.50-66. [DOI]
- Wulandari, W.R., Saefumillah, A. and Yunarti, R.T., 2019, July. Modification of fly ash using acids and alkali by hydrothermal method and its application as adsorbent material for phosphate adsorption in aquatic systems. *IOP Conference Series: Materials Science and Engineering*, 902(1), p.012034. IOP Publishing. [DOI]
- Xi, H., Li, Q., Yang, Y., Zhang, J., Guo, F., Wang, X., Xu, S. and Ruan, S., 2021. Highly effective removal of phosphate from complex water environment with porous Zr-bentonite alginate hydrogel beads: Facile synthesis and adsorption behavior study. *Applied Clay Science*, 201, p.105919. [DOI]
- Xie, T., Mo, C., Li, X., Zhang, J., An, H., Yang, Q., Wang, D., Zhao, J., Zhong, Y. and Zeng, G., 2017. Effects of different ratios of glucose to acetate on phosphorus removal and microbial community of enhanced biological phosphorus removal (EBPR) system. *Environmental Science and Pollution Research*, 24, pp.4494-4505. [DOI]
- Xiong, W., Tong, J., Yang, Z., Zeng, G., Zhou, Y., Wang, D., Song, P., Xu, R., Zhang, C. and Cheng, M., 2017. Adsorption of phosphate from aqueous solution using iron-zirconium modified activated carbon nanofiber: Performance and mechanism. *Journal of Colloid and Interface Science*, 493, pp.17-23. [DOI]
- Xu, R., Lyu, T., Wang, L., Yuan, Y., Zhang, M., Cooper, M., Mortimer, R.J., Yang, Q. and Pan, G., 2022. Utilization of coal fly ash waste for effective recapture of phosphorus from waters. *Chemosphere*, 287, p.132431. [DOI]
- Yang, Q., Wang, X., Luo, W., Sun, J., Xu, Q., Chen, F., Zhao, J., Wang, S., Yao, F., Wang, D. and Li, X., 2018. Effectiveness and mechanisms of

- phosphate adsorption on iron-modified biochars derived from waste activated sludge. *Bioresource Technology*, 247, pp.537-544. [DOI]
- Yao, Y., Gao, B., Inyang, M., Zimmerman, A.R., Cao, X., Pullammanappallil, P. and Yang, L., 2011. Removal of phosphate from aqueous solution by biochar derived from anaerobically digested sugar beet tailings. *Journal of Hazardous Materials*, 190(1-3), pp.501-507. [DOI]
- Ye, J., Cong, X., Zhang, P., Hoffmann, E., Zeng, G., Wu, Y., Zhang, H. and Fan, W., 2015. Phosphate adsorption onto granular-acid-activated-neutralized red mud: parameter optimization, kinetics, isotherms, and mechanism analysis. *Water, Air, & Soil Pollution*, 226, pp.1-10. [DOI]
- Yeoman, S., Stephenson, T., Lester, J.N. and Perry, R., 1988. The removal of phosphorus during wastewater treatment: a review. *Environmental Pollution*, 49(3), pp.183-233. [DOI]
- Yin, Q., Zhang, B., Wang, R. and Zhao, Z., 2017. Biochar as an adsorbent for inorganic nitrogen and phosphorus removal from water: a review. *Environmental Science and Pollution Research*, 24, pp.26297-26309. [DOI]
- Yu, J., Liang, W., Wang, L., Li, F., Zou, Y. and Wang, H., 2015. Phosphate removal from domestic wastewater using thermally modified steel slag. *Journal of Environmental Sciences*, 31, pp.81-88. [DOI]
- Zhang, X., Lin, X., He, Y., Chen, Y., Zhou, J. and Luo, X., 2018. Adsorption of phosphorus from slaughterhouse wastewater by carboxymethyl konjac glucomannan loaded with lanthanum. *International Journal of Biological Macromolecules*, 119, pp.105-115. [DOI]
- Zhou, J., Leavitt, P.R., Zhang, Y. and Qin, B., 2022. Anthropogenic eutrophication of shallow lakes: is it occasional? *Water Research*, 221, p.118728. DOI



# Changes in Land Use Land Cover and its Resultant Impacts on the Urban Thermal Environment of Chattogram City: A Spatio-Temporal Analysis Based on Remote Sensing and GIS Techniques

Sagar Mozumder<sup>id</sup>, Mahfuza Parveen<sup>†id</sup> and A.B.M. Kamal Pasha<sup>id</sup>

Department of Environmental Science and Disaster Management, Daffodil International University, Dhaka, Bangladesh

<sup>†</sup>Corresponding author: Mahfuza Parveen; mahfuza.esdm@diu.edu.bd

**Abbreviation:** Nat. Env. & Poll. Technol.

**Website:** [www.neptjournal.com](http://www.neptjournal.com)

*Received:* 12-08-2024

*Revised:* 23-09-2024

*Accepted:* 19-10-2024

## Key Words:

Land use and land cover  
Landsat  
Land surface temperature  
Probability matrix  
Transition matrix  
Urban heat island

## Citation for the Paper:

Mozumder, S., Parveen, M. and Pasha, A.B.M.K., 2025. Changes in land use land cover and its resultant impacts on the urban thermal environment of Chattogram City: A spatio-temporal analysis based on remote sensing and GIS techniques. *Nature Environment and Pollution Technology*, 24(2), p. D1714. <https://doi.org/10.46488/NEPT.2025.v24i02.D1714>

*Note: From year 2025, the journal uses Article ID instead of page numbers in citation of the published articles.*



**Copyright:** © 2025 by the authors

**Licensee:** Technoscience Publications

This article is an open access article distributed under the terms and conditions of the Creative Commons Attribution (CC BY) license (<https://creativecommons.org/licenses/by/4.0/>).

## ABSTRACT

The present study assessed the changes in land use and land cover to correlate the variations in the land surface temperature of Chattogram City. To analyze land use land cover (LULC) change and determine its effects on land surface temperature in the city area, temporal Landsat (5,7 ETM+ and 8,9 OLI) imageries from four time periods (2007, 2012, 2017, and 2022) were used. To assess the correctness of the picked random pixels, current ground truth data gathered from several sources was applied. Raster data has been utilized to identify the places that are influenced year-round in the green space (i.e., vegetation cover) and to examine the remote sensing image categorization for the green area using satellite images. These enable the study to explain the causes of the degradation and alteration of green space throughout time. The study identified that urbanization has resulted in a significant rise (about 2840 hectares, 16.74%) in urban land between 2007 and 2022, causing a loss of vegetative land (about 656 hectares, 3.85%). Additionally, the research concentrated on the actual affected area and attempted to forecast the cities' land use in 2037, which revealed a large loss of vegetation by that year. The research has the potential to be utilized as a reference in the future.

## INTRODUCTION

The land is a crucial resource and a source of livelihood. It is an essential and limited resource for some most essential human activities, including agriculture, manufacturing, forestry, energy generation, settlement, recreation, and water catchments and storage. Land is a key component of production, and for a large portion of human history, economic development has been closely correlated with it. It includes biophysical characteristics, including terrain, geology, hydrology, biodiversity, soil, and topography (Gaonkar et al. 2024). Another definition of land includes socioeconomic elements like management and technology, and land use refers to how and why people use the land and its resources (Meyer 1995). In general, a piece of land is modified when its use changes. This shift is driven by needs, which need not just change the land cover but also its intensity and management (Verburg et al. 2000). Agricultural expansion, propelled by population increase and technical progress, has profoundly transformed land cover, especially in developing nations, eclipsing other influences such as urbanization and deforestation (Kirkpatrick 2024). Social structure, attitudes, and values have all changed significantly in the same period. Urban regions are thought to be the most dynamic areas on the surface of the Earth, according to the history of urban growth. Urbanization has a significant negative influence on the local ecosystem (Pasha et al. 2018) despite its relevance to the regional economy (Saraswat et al. 2024). Only 14% of the world's population lived in urban areas in 1900; by 2000, this percentage had risen to 47%, which has recently touched 56% (Ritchie &

Roser 2018, Long et al. 2007). Almost all nations around the globe experience urban expansion. However, the rate of growth varies. Urban environment and ecology are currently the main environmental issues that require rigorous analysis and monitoring to effectively regulate land use. Inventories of land usage and land cover are becoming more and more important in a variety of fields, including agricultural planning, urban planning, and infrastructure development (Kavitha et al. 2021). Other forms of land use turning into urban land can be characterized as the primary change in land use in these locations. Several elements, including both physical and human aspects, have an impact on the intricate process of land use change in major urban areas. On the one hand, socioeconomic reasons are typically linked to and responsible for accelerated urban growth; on the other, the process of urbanization has a significant impact on the local economy (Tyagi et al. 2023).

One way to learn about urban environments is through remote sensing, which is also a crucial tool for comprehending and addressing many issues that face cities and their suburbs. (Lillesand et al. 2015). Change detection is crucial because it enables the researcher to comprehend and track the pattern of land cover change in the study area (such as urbanization, deforestation, and agricultural land management) (Ahmed 2011). The remote sensing technique is a great data source from which updated information and changes in land use and land cover (LULC) can be effectively extracted, examined, and simulated. A lot of pressure has been put on the nearby land and its biotic and abiotic resources in recent decades due to developing countries' rapid urbanization and population increase (Singh & Singh 2023). This pressure is also the cause of the urban areas accelerating rate of landscape change. Numerous studies have demonstrated that the land cover change brought on by urbanization has a significant impact on the radiative, thermodynamic, and hydrological processes that can modify the local climate (Qian et al. 2022). The quality of vegetation cover reduces its ability to moderate temperature patterns, resulting in a negative correlation between vegetation and land surface temperature (Fatemi & Narangifard 2019). One of the biggest issues of this century is the urban heat island (UHI), which is a product of human civilization's urbanization and industrialization (Jabbar et al. 2023). The rise in surface temperature caused by human activity can be a major cause for the development of urban heat islands, which is one of the most significant markers of urbanization. Urban heat island (UHI) is a problem that results from the unchecked urbanization of areas (Karakuş 2019). Because of the significant amount of vegetation loss, urban growth, and shifting of forest land to agricultural the, the land surface temperature increases, which ultimately develops UHI (Thomas et al. 2024). After urbanization, it

is impossible to restore the forest and vegetation to their pre-urban state (Mia et al. 2017). By the end of 2047, it is predicted that urban migration will account for 50% of all migration.

Bangladesh is one of the most populous nations in the world and is currently developing. It has recently experienced major environmental degradation and rapid, uncontrolled urban growth. However, because of rapid urbanization, the region has seen significant environmental degradation and several ecological issues, including deforestation, biodiversity loss, soil erosion, and modifications to the carbon sink in water-based ecosystems (Thomas et al. 2024). Chattogram is the second largest city of Bangladesh which is also experiencing land use and land cover changes because of urban development.

The local and microclimate of Chattogram City have changed as a result of anthropogenic activities and urban growth, which are driven by land use, such as built-up areas, impermeable structures, industrial activities, waste dumping, nucleated high buildings, and transportation activities (Pathirana et al. 2014). New urban development in the metropolis is destroying urban trees and plants, which are crucial for protecting the urban ecosystem and environment. With a population of 66% living in urban areas, Chattogram, Bangladesh's second-largest city and business hub, is currently one of the fastest-growing cities in the world. It accounts for 19.7% of the country's urban population and 30% of the GDP (Hassan & Nazem 2016). The urban forests, water bodies, and vegetation in cities have all been gradually destroyed by the rapid rise of urbanization in Chattogram City (Gazi et al. 2021). It is important to take into account Chattogram, a developing city in Bangladesh when analyzing LST in connection to land-use change. Therefore, it is essential to recognize how LST is changing in Chattogram City. According to a (BBS 2011) analysis, the country is losing 809 km<sup>2</sup> of agricultural land every year as a result of city growth, road construction, and infrastructure development. Due to migration from rural to urban areas, Chattogram City's average annual growth rate has reached 17.5% (Mia et al. 2015). Since rising urbanization has a negative effect on LST (Hokao et al. 2012), it is critical to track changes in land use and land cover and how they relate to LST behavior in Chattogram. Hence, the present study aimed to identify the rate of changes in land use and land cover in the study area. Moreover, the study investigated the multitemporal spatial dynamics of LULC change and its contribution to UHI generation for Chattogram City. Additionally, it determined the mean LST for each LULC class, the dynamics of change, and the relation with the urban landscape. This study used open-source Landsat imageries

with advanced remote sensing and GIS technology to trace the dynamics of urban growth, monitor geographical and temporal changes in land use and land cover, and evaluate Chattogram's environmental sustainability.

## MATERIALS AND METHODS

### The Study Area

The city of Chattogram, which is part of the Chattogram district, is bordered by rivers and is made up of small hills and narrow valleys. In addition to being Bangladesh's busiest seaport, Chattogram is also renowned as the country's commercial center. The second-largest city in Bangladesh is Chattogram, with a land area of 157 km<sup>2</sup> (Mia et al. 2015). The city is located between latitudes 21°54' and 22°59' north and 91°17' and 92°14' east. Its southern and eastern boundaries are formed by the Karnaphuli River, northern and eastern by the Halda River, and western by the Bay of Bengal. Chattogram City is the chosen research topic for

this study because it has expanded its urban zone with time and become the second most important city after the capital. (Fig. 1). About 2.5 million people live in the city, which is under the control of the City Corporation, and it covers an area of about 168 square kilometers (Statistics 2011). Approximately 40% of the nation's large-scale enterprises are located in Chattogram, which also accounts for 85% of Bangladesh's imports and 80% of its exports in the country's seaborne trade (Hassan & Nazem 2016), which makes it an important location for this study.

### Classification of Images

Satellite imagery is detailed and essential for supplying geographic information. The complexity of field labor and study time is reduced by the quantitative and qualitative data provided by satellite and remote sensing imagery (Shahbaz et al. 2012). Image Classification is one of the most efficient methods that can provide both qualitative and quantitative data (Vaiphasa et al. 2011). Supervised image classification

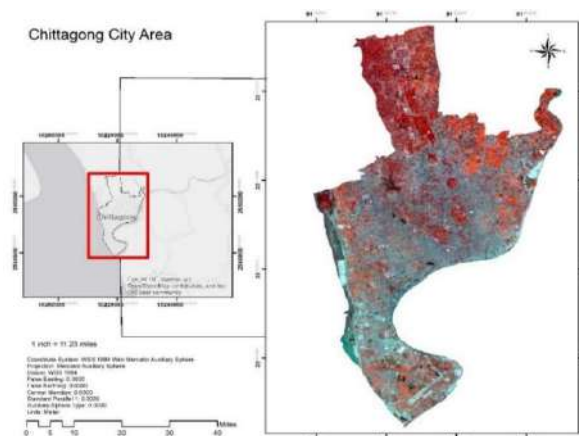


Fig. 1: The location of Chattogram City selected for the present study.

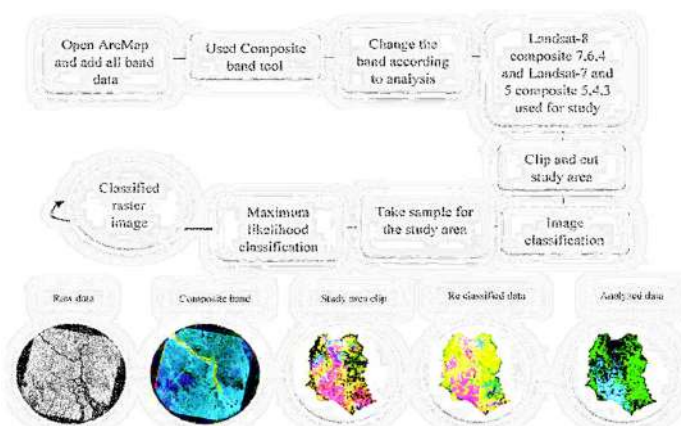


Fig. 2: Representation of Data analysis process.

is the method (Fig. 2) used here to identify and calculate the land cover amount of the study area. In this process researcher manually inputs some supervised samples in ArcGis software (Fig. 2). Later, the software itself calculates the pixel of the image data and shows the output (Abburu & Golla 2015). The amount of land cover used in an area can be calculated with the help of production. In this case, the land cover shows the amount of increase or decrease meant for a particular land cover category.

### Markov Modeling for Probability Matrix

A Markovian process uses the current state of a system to predict its future state over time using the same design. Depending on the status right now, it is a random procedure. Markov chain is a discrete-time stochastic process (Winston & Goldberg 2004). Here, the condition of the future can be determined by analyzing the present state of that individual area (Ross 2014). Markovian property can be described and stated with

$$\begin{aligned} & i_0, i_1, \dots, i_{t-1}, i_t, i_{t+1}, \text{ and all } t \geq 0 \\ & P(x_{t+1} = i_{t+1} \mid x_t = i_t, x_{t-1} = i_{t-1}, \dots, x_1 = i_1, x_0 = i_0) \\ & = P(x_{t+1} = i_{t+1} \mid x_t = i_t) \end{aligned} \quad \dots(1)$$

According to the Markov chain, it assumes that the conditional probability does not change over time. For all States  $i$  and  $j$  and all  $t$ ,  $P(x_{t+1} = j \mid x_t = i)$  is independent of  $t$ , as expressed in Eq (1)

$$P(x_{t+1} = j \mid x_t = i) = p_{ij} \quad \dots(2)$$

Where,  $P_{ij}$  = Transition probability that, given the system is in State  $i$  at time  $t$ , It will be in a state  $j$  at the time  $(t + 1)$ . The transition probabilities are expressed as a  $[m \times m]$  Matrix and it is called the transition probability matrix or transition matrix,  $P$ . The characteristics of the transition probability matrix as  $p$  are given below

$$P = \begin{bmatrix} p_{11} & p_{12} & \dots & p_{1m} \\ p_{21} & p_{22} & \dots & p_{2m} \\ \vdots & \vdots & \ddots & \vdots \\ p_{m1} & p_{m2} & \dots & p_{mm} \end{bmatrix} \quad \dots(3)$$

The estimation of transition probabilities in a Markov chain-based deterioration model requires data from the condition assessments of existing systems. (Baik et al. 2006).

### Calculation of NDVI

The amount of vegetation or biomass present in the environment is measured by the Normalized Difference Vegetation Index (NDVI). Greater greenness and healthy vegetation are indicated by a higher NDVI (Curran 1980). Data from Landsat MSS and TM can be used to calculate

NDVI (Jensen 1996). The reflectance data from the red (red) and near-infrared (nir) bands were utilized to calculate the NDVI values for the research area (Tan et al. 2010).

$$NDVI = (\rho_{nir} - \rho_{red}) / (\rho_{nir} + \rho_{red}) \quad \dots(4)$$

### Land Surface Temperature (LST) for Landsat 8/9 and 7/5 Image

The temperature that is sensed while touching the ground in a region is known as the land surface temperature. It is distinct from the temperature of the air or the atmosphere. Different Landsat data sets, including Landsat-9, 8, 7, and Landsat-5, were employed in this investigation (Pasha et al. 2023). Because the two Landsat data have different band values, calculating the land surface temperature for the two sets of data is different. There are eleven bands available for Landsat 8 and 9, and we used band 10 TIRS to calculate LST (Fig. 3) (Avdan & Jovanovska 2016). Thermal mapping is done using the Landsat 8 data band-10 TIRS, which specifies the thermal band with a 100-meter precision. Similar to this, Landsat 4-5 has a total of seven bands, each of which denotes a separate class. The thermal infrared band in Landsat 4-5 is band number 6, and it is frequently used to determine an area's thermal mapping (Fig. 3) (Qin et al. 2001). Software named Arc GIS 10.4 has been used to perform the calculation. In order to obtain the LST, specific formulas were utilized in the raster calculator.

For Landsat 8/9, to recover the land surface temperature of various years from satellite photos, an image-based methodology has been used (Lo & Quattrochi 2003). OLI images were converted using the USGS standard equation, and the DN's of the TIR bands of each year's ETM images were transformed to spectral radiance (Fig. 3) using the method employed by Chander et al. (2009).

The algorithm's initial stage is the input of Band 10, which is used to calculate the atmospheric Spectral Radiance (Fig. 3). The program retrieves the top of atmospheric (TOA) spectral radiance ( $L\lambda$ ) once Band 10 is inputted in the background using calculations from the USGS website.

$$L\lambda = M_L * Q_{cal} + A_L - O_i \quad \dots(5)$$

Where  $M_L$  stands for the band-specific multiplicative rescaling factor,  $Q_{cal}$  for the Band 10 image,  $A_L$  for the Band 10 additive rescaling factor, and  $O_i$  for the Band 10 correction (Barsi et al. 2014).

The next step is to calculate and convert spectral radiance to Brightness temperature (BT) by using metadata (Fig. 3) where. Using the thermal constants provided in the metadata file, the TIRS band data should be changed from spectral radiance to brightness temperature (BT) after being converted from digital numbers (DN's) to reflection.



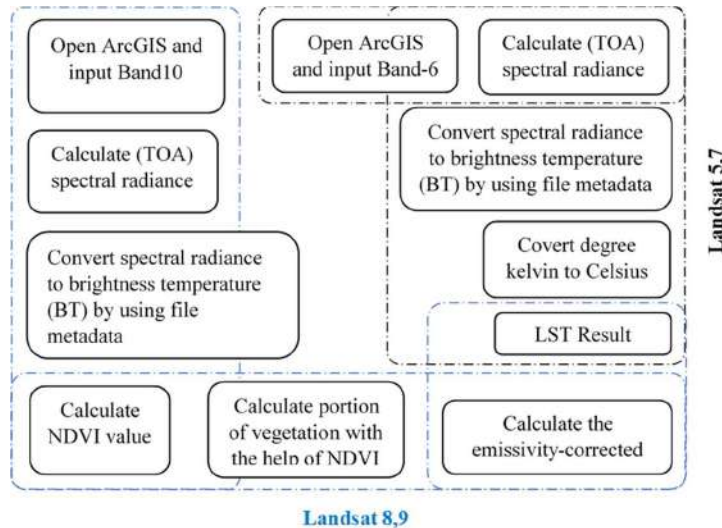


Fig. 3: Graphical representation of the calculation of LST from Landsat 8,9 and 5,7 satellite images.

The tool's algorithm converts reflectance to BT using the equation shown below,

$$BT = \frac{K_2}{\ln \left[ \left( \frac{K_1}{L_\lambda} \right) + 1 \right]} - 273.15 \quad \dots(6)$$

Where  $K_1$  and  $K_2$  refer to the metadata's band-specific thermal conversion constants, the radiant temperature is corrected by adding absolute zero (about  $-273.15^\circ\text{C}$ ) to obtain the figures in Celsius (Xu & Chen 2004). The Thermal constant for Landsat 9, Band 10 image is used in the method. Where the value of  $K_1$  (Constant Band\_10) is 799.0284, and the value of  $K_2$  (Constant Band\_10) is 1329.2405. For the Rescaling factor for Landsat 9, Band 10 image, the value of  $M_L$  (Radiance Mult Band) is 0.000384 also, the value of  $A_L$  (Radiance Add Band) is 0.10000, and the Correction value of Band 10 is  $O_i = 0.29$ .

In the third step NDVI value needed to be calculated following the procedure in section (2.5) then the portion of Vegetation  $P_v$  is calculated. The NDVI values for vegetation and soil ( $\text{NDVI}_v = 0.5$  and  $\text{NDVI}_s = 0.2$ ) are suggested to be used under global settings for computing  $P_v$  (Sobrino et al. 2004).

Where,

$$P_v = \left( \frac{\text{NDVI} - \text{NDVI}_s}{\text{NDVI}_v - \text{NDVI}_s} \right)^2 \quad \dots(7)$$

However, the figure for vegetated surfaces, 0.5, may be too low because the NDVI values vary for each place. Since NDVI<sub>v</sub> and NDVI<sub>s</sub> will rely on atmospheric conditions, it would not be possible to establish global values in the case of an NDVI computed using TOA reflectivities (Fig. 3). Global values from NDVI can be obtained from at-surface reflectivities (Jiménez-Muñoz et al. 2009).

In the next phase, surface emissivity has to be calculated to estimate LST. The land surface emissivity (LSE) must be known because it is a proportionality factor that scales blackbody radiance (Planck's law) to forecast emitted radiance and measures how effectively thermal energy is transmitted from the surface to the atmosphere (Jiménez-Muñoz et al. 2006). The emissivity can be calculated with the following formula (Sobrino et al. 2004).

$$\epsilon_\lambda = \epsilon_{v\lambda} P_v + \epsilon_{s\lambda} (1 - P_v) + C_\lambda \quad \dots(8)$$

Where,  $C$  stands for surface roughness ( $C = 0$  for homogeneous and flat surfaces) and is constant at 0.005 for vegetation and soil emissivities, respectively (Sobrino & Raissouni 2000).

As a final step, the land surface temperature  $T_s$ , also known as the emissivity-corrected land surface temperature, is determined as follows.

$$T_s = \frac{BT}{\left\{ 1 + \left[ \left( \frac{\lambda BT}{\rho} \right) \ln \epsilon_\lambda \right] \right\}} \quad \dots(9)$$

Where  $T_s$  is the LST in degrees Celsius (C),  $BT$  is the at-sensor  $BT$  (C), is the emission wavelength (for which the maximum response and the average of the limiting wavelength ( $= 10.895$ ) will be used), and is the previously determined emissivity (Markham & Barker 1985).

For Landsat 7 and 5 images,  $L_\lambda$  has to be calculated with the following formula,

$$L_\lambda = L_{min} + \frac{L_{max} - L_{min}}{QCAL_{max} - QCAL_{min}} (DN - QCAL_{min}) \quad \dots(10)$$

$Qcal$  is the DN of each image in the metadata of Landsat 7 and 5,  $QCAL_{max}$  is the maximum DN (255), and  $QCAL_{min}$  is the minimum DN (1). The top of the atmosphere (TOA)

radiances,  $L_{\max}$  and  $L_{\min}$ , are scaled to  $QCAL_{\max}$  and  $QCAL_{\min}$  in  $W/(m^2 \text{ srm})$ , respectively. Using the following equation, the radiant images were transformed from the DN's to the spectral radiance to determine the blackbody temperature.

$$T_b = \frac{K_2}{\ln\left(\frac{K_1}{L_\lambda} + 1\right)} \quad \dots(11)$$

Where  $K_1$  and  $K_2$  are prelaunch calibration constants in Kelvin units acquired from the image metadata file,  $T_b$  is the effective at-sensor brightness temperature in Kelvin units,  $L$  is spectral radiance in  $W/(m^2 \text{ srm})$ . For the Thermal constant for Landsat 7, Band 6 image is,  $K_1$  (Constant Band 6) = 666.09 and the  $K_2$  (Constant Band 6) = 1282.71. The Rescaling factor for Landsat 7 and 5, Band 6 image is  $QUANTIZE_{\text{Cal Max Band}_6} = 255$  and  $QUANTIZE_{\text{Cal Min Band}_6} = 1$ .

The calculated LST values were then translated to the standard Degree Celsius ( $^{\circ}\text{C}$ ) unit by subtracting the absolute zero, which is roughly minus  $273.5^{\circ}\text{C}$  (Xu & Chen 2004).

$$LST = T_b - 273.15 \quad \dots(12)$$

### Model Accuracy, Assumptions, and Potential Errors

Rooted on the land use land cover changes data from 2007 to 2022, the Markov model anticipates land use changes depending upon the prior patterns in the future, which is likely to be a fallacy. It, however, does not, out of consideration, include the irregular events that can occur, such as a change in policy and natural catastrophes, among others, and simplifies changes to be linear, which may not adequately portray the complexities related to urban growth. In this case, present conditions and the quality of data used for forecasting predictions, as well as the fact that the transition probabilities do not change, are major factors in determining the predictive power of these matrices. The span or the window of the data, which, in this instance, is 15 years of history, makes it difficult to trust the forecasting, for it is prone to future incongruence with present trends. The expected figures for urban encroachment and vegetation destruction relate to other fast-developing cities like Dhaka and Kolkata. These comparisons do enhance the forecasts made by the model, but their usage carries risks and should thus be moderated. The Markov modeling framework does not incorporate sudden land cover changes or any effects of land cover change on land use. This development could be even more beneficial for future projections by adding some innovative models with more dynamics, like the CA-Markov model, and integrating socio-economical and environmental factors in the modeling process.

## RESULTS

### Changes in Land Use and Land Cover from 2007 to 2022

This study showed the land use and land cover of the Chattogram City Area. According to the analysis of land use and land cover, only 5901.21 hectares of urban area were found in 2007 (Table 1). However, it expanded significantly from 5901.21 ha in 2007 to 6895.08 ha in 2012, rising from 34.77% to 40.63% of the total study area during those five years (Fig. 4). In 2017, the urban area's growth trends accounted for 8073.36 ha, or 47.57% of the total area (Table 1). The Chattogram city has a huge population, and the urban area is growing swiftly. The urban area has grown even more, accounting for 8741.52 ha in 2022, or 51.51% of the city's total land area (Table 1). But as the graph demonstrates, there has been a significant decline in the vegetation cover, with 0.4% (70 ha) between 2007 and 2012 and 2.15% (363.51 ha) between 2012 and 2017. 1.3% (220.95 acres) of vegetation was lost between 2017 and 2022 (Fig. 4). Over 15 years, 654.39 ha less land was covered by vegetation. These trends in plant loss should worry city people because they portend an increase in urban heat, which is harmful to both the environment and human civilization. There was a discernible drop in bare land, agricultural land, and water body area. Agriculture occupied 3641.54 hectares (21.46%) of the total area in 2007, increased to 4686.03 ha (27.63%) in 2012, and again decreased to 2733.3 ha (16.11%) in 2017 (Table 1). According to the study, the total amount of agricultural land decreased by 908.64 ha between 2007 and 2017, but in 2022, it climbed by roughly 5%, or 3661.74 ha, of the study region's total land cover (Table 1). The area's bare land severely declined from 3215.07ha to 1793.07ha between 2007 and 2012 (a loss of 8.38%), but it dramatically increased from 2012 to 2017 (a gain of 8.15%) and became 3176.82 ha. The total land area in 2022 was 1574.1 ha, a 9.44% decrease in bare land area (Table 1). Over the course of 15 years, bare land dropped by 1640.97 ha in total. The area occupied by inland water bodies shrunk between 2007 and 2012, from 1196.28 hectares in 2007 to 650.25 ha in 2012, and it also shrunk significantly between 2012 and 2017, between 650.25 hectares in 2012 and 404.46 hectares in 2017 (Table 1). It did, however, grow in 2022, though still only by 3.72% of the overall area. Between 2007 and 2017, the water body shrunk by 791.82 ha, while between 2017 and 2022, it grew by 227.07 ha (Table 1). Even though the total area by the years 2007, 2012, 2017, and 2022 was almost the same, the internal land use and landcover types have changed dramatically (Fig. 4 & 5). Urban lands produce more urban heat island zones than other types of land use.

Table 1: Land cover change from 2007 to 2022.

Class	Hectors	P%	Hectors	P%	Hectors	P%	Hectors	P%
	2007		2012		2017		2022	
Vegetation	3015.9	17.77%	2945.97	17.36%	2582.46	15.22%	2361.51	13.92%
Agriculture	3641.94	21.46%	4686.03	27.61%	2733.3	16.11%	3661.74	21.58%
Urban	5901.21	34.77%	6895.08	40.63%	8073.36	47.57%	8741.52	51.51%
Bare land	3215.07	18.95%	1793.07	10.57%	3176.82	18.72%	1574.1	9.28%
Water body area	1196.28	7.05%	650.25	3.83%	404.46	2.38%	631.53	3.72%
Total	16970.4	100%	16970.4	100%	16970.4	100%	16970.4	100%

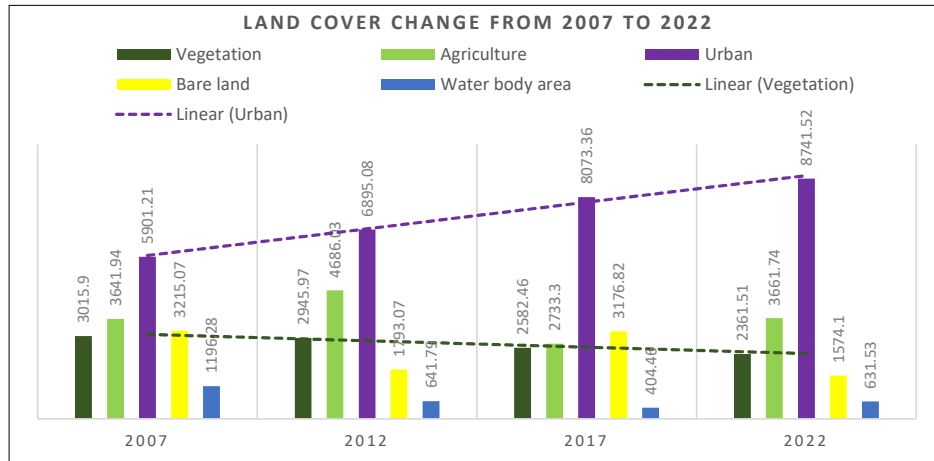


Fig. 4: Land cover change, including vegetation and urban trend line.

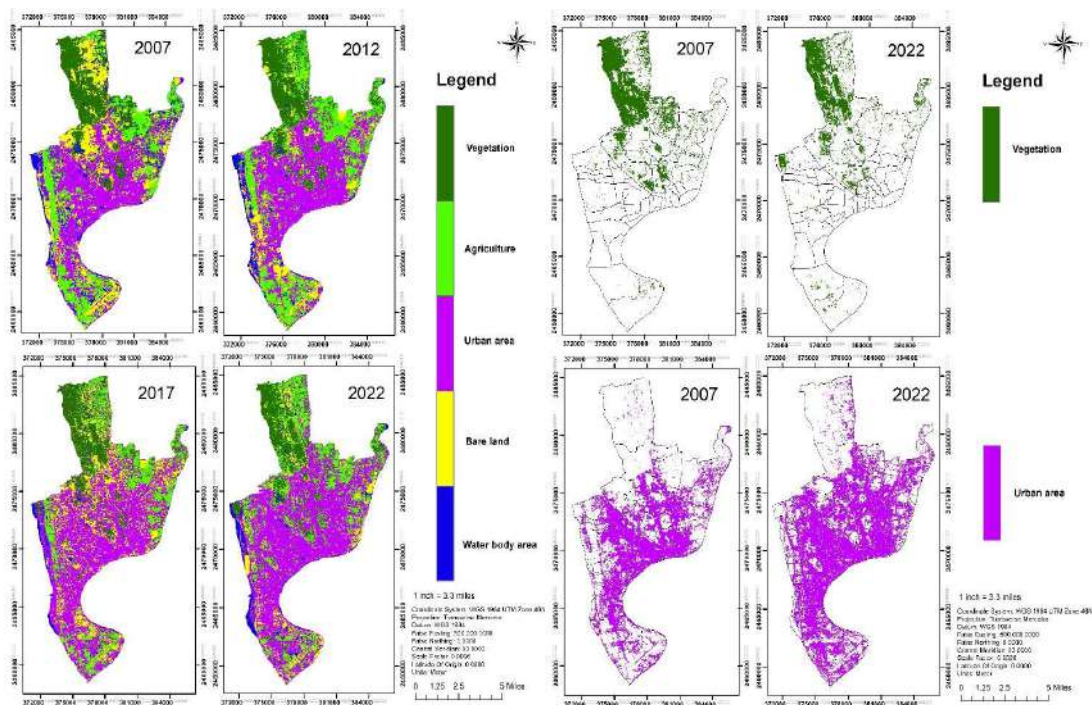


Fig. 5: Land use and land cover map from and the changes in vegetation and urban area from 2007 to 2022.

There was a noticeable change in the land use and land cover of the Chattogram region between 2007 and 2022. Analyses of change detection demonstrated that several land use and land cover categories had undergone considerable changes. In 2007, urban land took up 34.77% of the research area's land area, followed by agricultural land (21.46% of the area), bare land (18.95% of the area), and vegetation (17.77%). Water bodies made up 7.05% of the study area's land area. The findings showed that the percentage of vegetation cover and bare land decreased to 3.85% and 9.67%, respectively. However, Chattogram City's urban area drastically increased to 51.51% of the total area (Table 1).

### Indicative Changes in LULC by 2037

By examining two qualitative land uses from two distinct periods, Markov creates a transition matrix or a transition area matrix. For this study, 15 years of data from 2007 to 2022 (Table 2) was used. More recent land cover usage is represented by the column, whereas older land cover use is represented by the rows. Agriculture, bare terrain, urban, vegetation, and water bodies are represented here in chronological order by the categories. Here, the Markov analysis used the matrix to forecast how the land cover will be used in 2037 (Islam & Ahmed 2011).

According to the transition matrix, the probability of change for agricultural land is that 39.29% of the current agricultural area will remain the same in 2037. Of the current area, 11.19% may become bare land, 41.28% may become urban areas, 5.97% may become vegetation, and 2.27 percent may become water body areas (Table 2). 19.64 percent of the current bare land area is likely to remain unchanged in 2037, which would represent no change in the bare land area. Currently, agriculture can occupy 28.20 percent of the land, whereas urban uses can occupy 41.20 percent, vegetation can occupy 8.36 percent, and water bodies can occupy 2.59 percent (Table 2). Similar to this, in 2037, 86% of the currently developed urban land will still be there, with 4.53% of it being bare land, 5.15 % being used for agriculture, 1.49% being covered in vegetation, and 2.56% being a body of water. In 2037, it is anticipated that 53.97 percent of the area's vegetation cover will remain the same, while 15.56

percent of it may become urban, 4.55 percent could turn into bare ground, 25.57 percent could be used for agriculture, and 0.35 percent could turn into a body of water (Table 2). In terms of the water body area, there will be no change of 24.91 percent in 2037. However, 12.74 percent may be covered by vegetation, 41.54 percent by urban, 4.17 percent by bare land, and 16.64 percent by agriculture (Table 2).

### Relationship between NDVI and LST

Fig. 6 shows the relationship between NDVI and LST. It has been demonstrated that the NDVI and surface temperature have a negative correlation. This is a blatant indication that the LST and NDVI have a high and unfavorable correlation. As a result, the land surface temperature is higher in areas with less vegetation. Fig. (6) shows that the area's temperature regime has been significantly impacted by changes in land use. However, compared to other locations, such as city areas, the vegetative area had a lower temperature. In comparison to urban green spaces such as parks and agricultural fields, LST values were comparatively greater in urban areas with no vegetation cover. Because there is a negative association between NDVI and LST, areas with lower NDVI values have higher land surface temperatures, whereas areas with higher NDVI values have lower land surface temperatures (Gorgani et al. 2013). The value of the NDVI in 2007 ranged from +0.6 to -0.25, with a negative value indicating lesser vegetation cover (Table 3), which typically indicates places with water cover. By looking at Fig. 6, it is clear that this range was true in 2007. The LST map for 2007 displays the same information, indicating that the maximum LST was 38°C and the minimum LST was 24.5°C (Table 3). It is evident from the 2007 co-relationship diagram that NDVI value decreases with high LST value and increases with low LST value. The NDVI value was 0.289 in the trend line of correlation (Fig. 6) when the LST value was close to 25°C, but it constantly declined with higher LST values, as can be seen when the LST value was close to 38°C, and the NDVI value was negative at -0.075. That indicates that in 2007, the trend line unmistakably demonstrated a negative association between NDVI and LST (Fig. 6). With a slightly different NDVI and LST value for the year 2012, it was essentially a

Table 2: Probability of changes in the year 2037 land cover (prediction) using transition matrix.

Class	Agriculture	Bare land	Urban	Vegetation	Water Body	Grand Total
Agriculture	39.29%	11.19%	41.28%	5.97%	2.27%	100%
Bare land	28.20%	19.64%	41.20%	8.36%	2.59%	100%
Urban	5.15%	4.53%	86.28%	1.49%	2.56%	100%
Vegetation	25.57%	4.55%	15.56%	53.97%	0.35%	100%
Waterbody	16.64%	4.17%	41.54%	12.74%	24.91%	100%

Markov's prediction of land use change in the next 15 years



Table 3: Retrieved statistics of LST (°C) and NDVI values from 2007-2022.

	LST				NDVI			
	2022	2017	2012	2007	2022	2017	2012	2007
Maximum	42.0361	37.755	37.2995	38.0009	0.608817	0.564	0.447368	0.6
Minimum	24.7868	20.2609	20.2609	24.5451	-0.17095	-0.15216	-0.28571	-0.25
Mean	33.41145	29.00795	28.7802	31.273	0.218932	0.205919	0.080827	0.175
Standard Deviation	12.1971	12.3702	12.04811	9.514687	0.551381	0.506403	0.518367	0.601040764

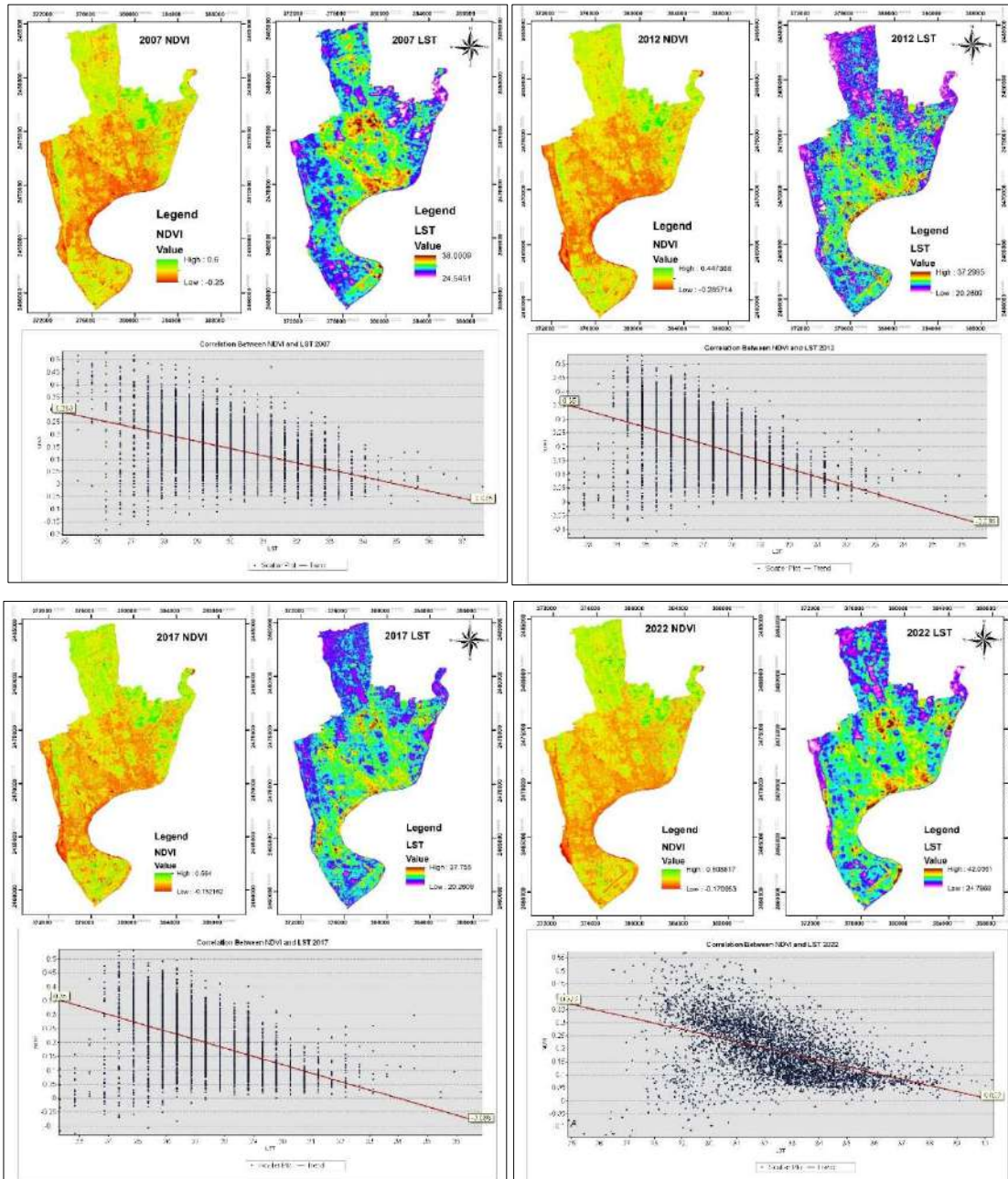


Fig. 6: Correlation of LST and NDVI from the year 2007 to 2022.

reflection of the year 2007. The trend line for 2012 shows a similar outcome to that of 2007, where the NDVI value is 0.237 while the LST is close to 22°C but continuously decreases as the LST increases (Fig. 6). The NDVI value is -0.221 when the LST value is near 35°C. This clearly illustrates the conflict between the NDVI and LST. This implies the tendency of inverse relationships between NDVI and LST where the increase of NDVI values fits the decrease of LST values and vice versa. In the same way, in 2017 the relationship showed a negative trend line between NDVI and LST. In 2017 the highest NDVI was +0.56, and the lowest NDVI was -0.15, while the maximum LST and lowest LST values were 37.7°C and 20.26°C, respectively (Table 3). The trend line indicated that less vegetation will be present if the LST has a higher value when the relationship between them is taken into account. When the LST was close to 37°C, the NDVI value was negative (-0.086), indicating the absence of vegetation, as it was in 2017 when the NDVI value was 0.35 on the trendline (Fig. 6). In 2022 the result was quite similar as the correlation was negative. In 2022, the higher NDVI value was +0.60, and -0.17 was the lowest NDVI score. The highest LST and lowest LST in 2022 were 42.03°C and 24.78°C, respectively (Fig. 6). The trendline indicated that less vegetation will be present if the LST has a higher value when the relationship between them is taken into account. The NDVI had a low value of 0.02 when the LST was close to 41°C, indicating very little vegetation, but it had a high value of +0.37 when the LST was close to 25°C (Fig. 6).

## DISCUSSION

Gain-loss and net change estimation from the four temporal periods of 2007 to 2012, 2012 to 2017, 2017 to 2022, and 2007 to 2022 were detected using the continuous analysis of LULC. Nearly all of the land use land cover classes displayed gains and losses. Gain and loss graphs for various purposes (Fig. 7) were made per category to aid in understanding. From the transition matrix (Table 4) it can be identified that lands from different categories have changed with time. The area, which was covered by water in 2007, transformed into an urban area, which is about 472 ha of land. Also, there is a significant change has been shown in the vegetation area which has been converted into an urban area in the last 15 years. About 470 ha of land has been converted from a vegetation area to an urban buildup area; also, about 772 ha of land has been converted into agricultural land in the last 15 years in Chattogram city. The conversion of vegetation land to bare land is also alarming for the overall environment of Chattogram City. About 137 ha of land has been converted from vegetation to bare land. Because of the gain of urban area and loss of vegetation area, it is significantly impacting

the thermal environment of the city. The Land Surface Temperature (LST) and NDVI both show their characteristics because of these changes (Table 5). ArcGIS 10.4 image processing software is used to display the LST and NDVI images of Chattogram side by side to better comprehend the LST and NDVI pattern. The spatial distribution of the urban thermal environment and vegetation cover in Chattogram City is depicted in Fig. 8 in an instructive manner. The urban area of Chattogram has a higher LST than the surrounding area of vegetation and agricultural land. It is evident that non-porous materials, such as metal, asphalt, and concrete, which are used to construct city structures and main transportation corridors, contribute to greater temperatures (Hoehne et al. 2022). Water bodies, agricultural areas, and vegetation, on the other hand, all have lower temperatures. In the NDVI image (Fig. 8), the values are the exact opposite. Due to the lack of vegetation, built-up or core city regions have low NDVI values, as do water body locations. Because green biomass is present at relatively high levels, high values are found in agriculture, vegetation, and green land areas (Prashar et al. 2022).

Regarding LST, the phenomenon that LST values are disproportionately greater in the built-up or core urban area than in the suburbs makes the impact of the urban thermal environment clear. Except for a few open spaces, NDVI values in the built-up or core city region are significantly lower than in the suburbs. When comparing LST and NDVI, one discovers that their respective changing trends are completely at odds (Table 5). LST values are typically high where the main city area or buildup area is situated, while they are typically low where bodies of water and green space are present. The green space is where the NDVI peaks arise. LST and NDVI typically exhibit a clear inverse association. On the other hand, Chattogram's urban form and urban sprawl are intimately tied to the shifting trends of LST or NDVI.

Table 5 presents the regression functions and correlation coefficient ( $R^2$ ), which gauges the potency of linear regression to show the relationship between LST and NDVI for each LULC type. NDVI and LST of all LULC categories, except water bodies, showed a substantial inverse association. For every year the greatest negative regression slope was indicated by "Urban area," while the shallowest negative regression slope was revealed by "Vegetation area." Fig. 8 illustrates that the NDVI and LST association was consistently negative except water body area. The NDVI reduced as LST grew at all-time intervals due to having a negative connection, and this association demonstrated that when a lower Vegetation Level was present, the LST increased (Table 5). In other words, higher Vegetation Levels

Table 4: Land Use Land Cover Transition Matrix 2007-2022 in Hectors.

	Land cover class 2022						Grand Total
	Land Class	Agriculture	Bare land	Urban	Vegetation	Water Body	
<b>Land cover class 2007</b>	Agriculture	1431.744195	407.898234	1504.122069	217.562777	82.592654	3643.919929
	Bare land	893.989644	622.767495	1306.324578	265.116518	82.140167	3170.338402
	Urban	307.313042	270.381518	5153.086372	88.993963	152.719009	5972.493904
	Vegetation	772.824363	137.596243	470.26625	1631.57592	10.622077	3022.884852
	Waterbody	189.196549	47.430983	472.239674	144.855487	283.202797	1136.92549
	Grand Total	3595.067793	1486.074473	8906.038943	2348.10466	611.276704	16946.56258

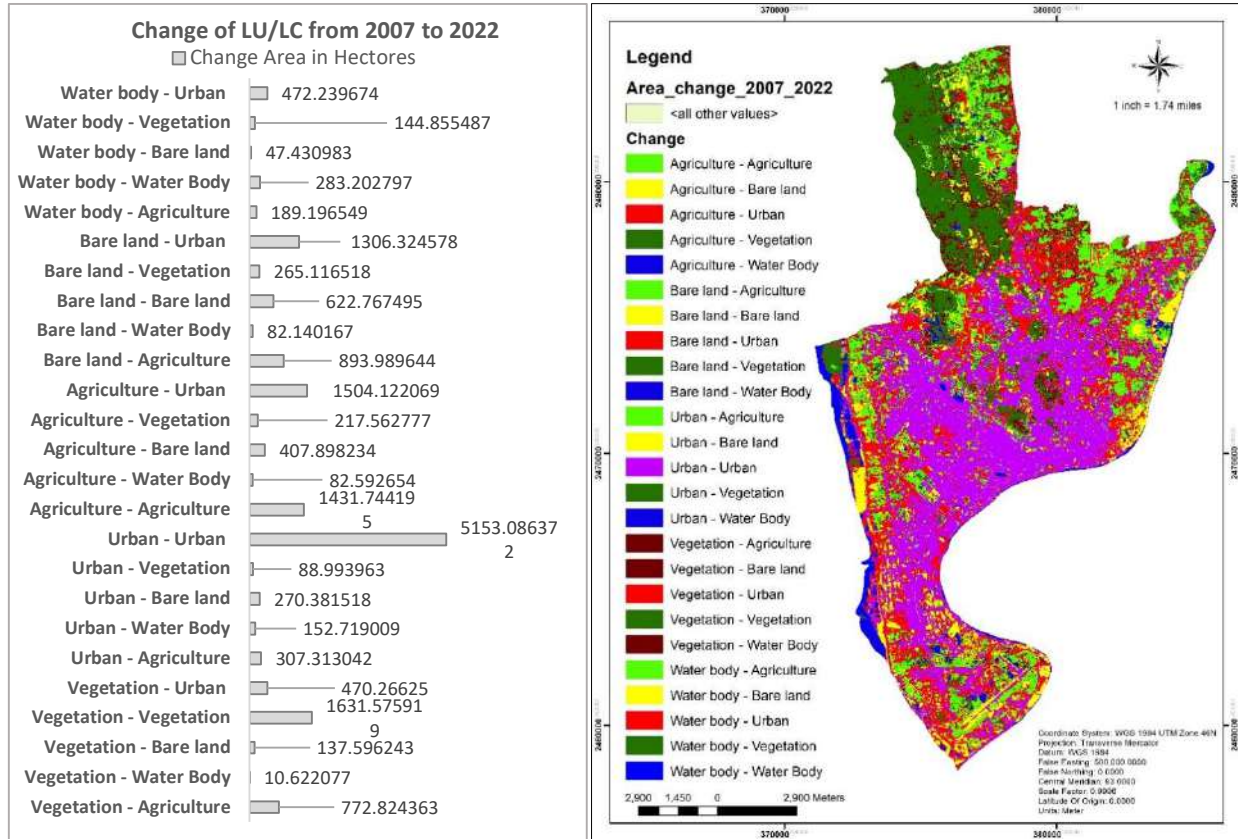


Fig. 7: Changes in Land cover in each category from 2007 to 2022.

caused lower LST while lower vegetation levels caused higher LST (Fig. 8). So if the vegetation decreases with time in the Chattogram region, a significant amount of LST will increase, which is usually responsible for creating an Urban heat island that also has a direct impact on the overall temperature of the city (Roy et al. 2020). According to (Farzana et al. 2022), a city's heat island can also have an impact on precipitation, which is a problem for Chattogram City.

The swift growth of the population in the urban area of Chattogram City and its changing patterns of land use and land cover (LULC) has brought about tremendous changes in the urban thermal environment—that is, the urban heat islands

(UHI) phenomenon is becoming increasingly prevalent. With the growth of the built-up areas, especially those where trees and farms are cleared, the UHI intensity increases, which in turn has far-reaching consequences on health, diversity, and energy usage. Citing previous studies, it can be said these increasing UHI effects worsen heat stress and the associated health risks, especially during heat waves which are very dangerous to certain people, such as the aged and those with underlying illnesses (Liu et al. 2021, Wang et al. 2021). With the growing infrastructure in Chattogram City, for example, there is a loss of vegetation and enhancement of pavements. As a result, the capacity of the land to cool down using



Table 5: LST and NDVI Relationship by LULC Type.

Class (2007-2022)	2022	2017	2012	2007
	Regression function and ( $R^2$ )	Regression function and ( $R^2$ )	Regression function and ( $R^2$ )	Regression function and ( $R^2$ )
Vegetation	$y = -10.502x + 32.449$ $R^2 = 0.1912$	$y = -7.9417x + 27.748$ $R^2 = 0.1925$	$y = -3.8895x + 25.705$ $R^2 = 0.1143$	$y = -5.1192x + 29.643$ $R^2 = 0.1151$
Agriculture	$y = -12.517x + 34.941$ $R^2 = 0.5495$	$y = -6.8163x + 28.026$ $R^2 = 0.5096$	$y = -6.3522x + 27.371$ $R^2 = 0.4693$	$y = -11.12x + 31.164$ $R^2 = 0.4159$
Urban	$y = -29.924x + 37.13$ $R^2 = 0.2255$	$y = -11.624x + 30.041$ $R^2 = 0.1868$	$y = -12.469x + 27.854$ $R^2 = 0.1794$	$y = -15.409x + 32.227$ $R^2 = 0.229$
Bare land	$y = -19.346x + 38.531$ $R^2 = 0.5969$	$y = -2.9813x + 29.199$ $R^2 = 0.0397$	$y = -5.6523x + 27.541$ $R^2 = 0.0034$	$y = -12.806x + 33.853$ $R^2 = 0.314$
Water area	$y = 8.6653x + 28.799$ $R^2 = 0.1108$	$y = 1.1331x + 23.87$ $R^2 = 0.0021$	$y = 7.8215x + 25.113$ $R^2 = 0.2422$	$y = 5.4723x + 27.463$ $R^2 = 0.0552$

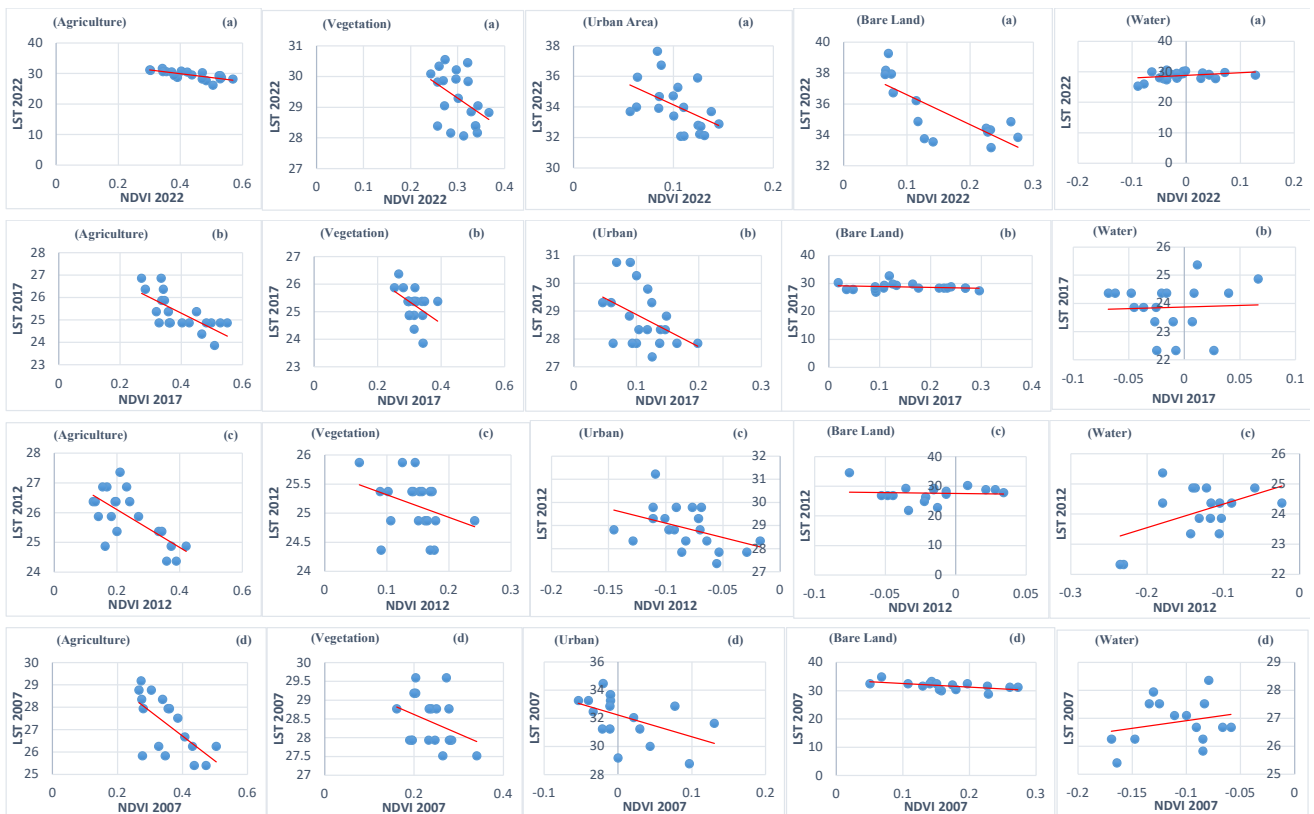


Fig. 8: LST and NDVI relationship by LULC Type for the years 2022 (a), 2017 (b), 2012 (c), 2007 (d).

an efficient natural process known as evapotranspiration reduces. There is a body of literature that supports the view that such a process is very important in controlling surface temperatures in other cities that have undergone similar transformations (Atasoy 2020, Zhou et al. 2022). Extreme weather conditions attributed to urban surfaces not only mean hotter temperatures but also prolonged hot days and warm nights (Wang et al. 2021).

The impact on the environment goes further than just human well-being. Urban biodiversity is especially sensitive

to the higher temperatures resulting from the urban heat island effect. Species twice as rapidly as climate-adjusting species pose a risk of extinction or decline in numbers (Kong et al. 2021). The intensified UHI effect also increases the energy consumption demand for buildings, especially air conditioning. Also, this may lead to high-energy use and emissions, which contribute to the problem of combating urban ecological pollution (Dudorova & Belan 2022, Liu et al. 2021). Overall, the results from Chattogram City are consistent with worldwide observations, where uncontrolled



urban development contributes significantly to increased UHI effects, which presents great threats to human health, the environment as well as energy utilization. Addressing these negative effects requires strategic urban development and active measures to mitigate the effects including increasing urban vegetation as well as the use of energy-effective technologies (Jusuf et al. 2019, Kong et al. 2021).

## CONCLUSIONS

The analysis shows that there have been significant changes in land use and land cover in the Chattogram City region during the past 15 years. This study also illustrates how the study area's urban heat island is distributed spatially and how land surface temperature fluctuates over time. For four separate years 2007, 2012, 2017, and 2022 the study has determined the land surface temperature and the urban heat island zone. Due to changes in land use and land cover, there have been observed variations in land surface temperature and urban heat islands, which have altered radiant surface temperatures and ultimately produced urban heat island zones. In the Chattogram City Area, the urban area had the largest land cover (34.77 percent of the entire study area) in 2007, and it rapidly rose in 2012, 2017, and 2022. In 2022, the urban area became the CMA's main and significant land cover, accounting for 51.51 percent of the entire study area, while the covering of dominating vegetation declined by 654.39 ha. The land surface temperature in Chattogram City significantly increased between 2007 and 2022 as a result of the shift in land usage. Rooftop gardening and plantations might help restore some of the lost green space that has been lost over the previous few decades, which may help to regulate the current level of UHI.

Additionally, rooftop gardening and tree planting can lower the temperature of the city of Chattogram's surface as well. Both of the mayors of the city corporations in Dhaka, the capital of Bangladesh, have promised a 10% holding tax discussion to promote rooftop gardening. Even if only half of the structures in Chattogram allowed for rooftop gardening, it would still be good for the city's ecosystem. The rooftop tree plantation and gardening plan in Chattogram City may be difficult to accomplish due to a lack of awareness, policy, and management. However, action must be taken in the Chattogram City area for a safe and environmentally friendly future.

## ACKNOWLEDGMENTS

The authors are grateful and give thanks for this work being supported by the faculty and officials of the Department of Environmental Science and Disaster Management (ESDM), Daffodil International University (DIU).




## REFERENCES

- Abburu, S. and Golla, S.B., 2015. Satellite image classification methods and techniques: A review. *International Journal of Computer Applications*, 119(8), pp.1-10.
- Ahmed, B., 2011. Urban land cover change detection analysis and modeling spatio-temporal growth dynamics using remote sensing and GIS techniques: A case study of Dhaka, Bangladesh. *Journal of Geospatial Science and Technology*, 5(2), pp.45-60.
- Atasoy, M., 2020. Assessing the impacts of land-use/land-cover change on the development of urban heat island effects. *Environment, Development and Sustainability*, 22(8), pp.7547-7557. [DOI]
- Avdan, U. and Jovanovska, G., 2016. Algorithm for automated mapping of land surface temperature using LANDSAT 8 satellite data. *Journal of Sensors*, 2016, pp.1-12.
- Baik, H.S., Jeong, H.S. and Abraham, D.M., 2006. Estimating transition probabilities in Markov chain-based deterioration models for management of wastewater systems. *Journal of Water Resources Planning and Management*, 132(1), pp.15-24.
- Barsi, J.A., Schott, J.R., Hook, S.J., Raqueno, N.G., Markham, B.L. and Radocinski, R.G., 2014. Landsat-8 thermal infrared sensor (TIRS) vicarious radiometric calibration. *Remote Sensing*, 6(11), pp.11607-11626.
- BBS, 2011. *Bangladesh Bureau of Statistics, Ministry of Planning*. Govt. of Bangladesh, Dhaka.
- Chander, G., Markham, B.L. and Helder, D.L., 2009. Summary of current radiometric calibration coefficients for Landsat MSS, TM, ETM+, and EO-1 ALI sensors. *Remote Sensing of Environment*, 113(5), pp.893-903.
- Curran, P., 1980. Multispectral remote sensing of vegetation amount. *Progress in Physical Geography*, 4(3), pp.315-341.
- Dudorova, N.V. and Belan, B.D., 2022. The energy model of urban heat island. *Atmosphere*, 13(3). [DOI]
- Farzana, R., Tabassum, A., Mannan, Md.A. and Karunatillake, S., 2022. Assessment of UHI and its long-term impact on temperature, precipitation, and evapotranspiration for the major cities in Bangladesh. *SSRN Electronic Journal*. [DOI]
- Fatemi, M. and Narangifard, M., 2019. Monitoring LULC changes and its impact on the LST and NDVI in District 1 of Shiraz City. *Arabian Journal of Geosciences*, 12(4), pp.1-12.
- Gaonkar, V.G., Nadaf, F.M. and Kapale, V., 2024. Mapping and quantifying integrated land degradation status of Goa using geostatistical approach and remote sensing data. *Nature Environment & Pollution Technology*, 23(1), pp.1-15.
- Gazi, M., Rahman, M., Uddin, M. and Rahman, F.M., 2021. Spatio-temporal dynamic land cover changes and their impacts on the urban thermal environment in the Chittagong metropolitan area, Bangladesh. *GeoJournal*, 86(5), pp.2119-2134.
- Gorgani, S.A., Panahi, M. and Rezaie, F., 2013. The relationship between NDVI and LST in the urban area of Mashhad, Iran. *International Conference on Civil Engineering Architecture & Urban Sustainable Development*, 27&28 November, 51, pp.1-10.
- Hassan, M.M. and Nazem, M.N.I., 2016. Examination of land use/land cover changes, urban growth dynamics, and environmental sustainability in Chittagong City, Bangladesh. *Environment, Development and Sustainability*, 18(3), pp.697-716.
- Hoehne, C.G., Chester, M.V., Sailor, D.J. and King, D.A., 2022. Urban heat implications from parking, roads, and cars: A case study of Metro Phoenix. *Sustainable and Resilient Infrastructure*, 7(4), pp.272-290. [DOI]
- Hokao, K., Phonekeo, V. and Srivanit, M., 2012. Assessing the impact of urbanization on urban thermal environment: A case study of Bangkok Metropolitan. *International Journal of Applied*, 2(7), pp.1-12.
- Islam, M.S. and Ahmed, R., 2011. Land use change prediction in Dhaka

- City using GIS-aided Markov chain modeling. *Journal of Life and Earth Science*, 6, pp.81–89.
- Jabbar, H.K., Hamoodi, M.N. and Al-Hameedawi, A.N., 2023. Urban heat islands: A review of contributing factors, effects and data. *IOP Conference Series: Earth and Environmental Science*, 1129(1), 012038. [DOI]
- Jensen, J.R., 1996. *Introductory Digital Image Processing: A Remote Sensing Perspective*. 2nd ed. Prentice-Hall Inc.
- Jiménez-Muñoz, J.C., Sobrino, J.A., Gillespie, A., Sabol, D. and Gustafson, W.T., 2006. Improved land surface emissivities over agricultural areas using ASTER NDVI. *Remote Sensing of Environment*, 103(4), pp.474–487.
- Jiménez-Muñoz, J.C., Sobrino, J.A., Plaza, A., Guanter, L., Moreno, J. and Martínez, P., 2009. Comparison between fractional vegetation cover retrievals from vegetation indices and spectral mixture analysis: Case study of PROBA/CHRIS data over an agricultural area. *Sensors*, 9(2), pp.768–793.
- Jusuf, S.K., Ignatius, M., Hien, W.N. and Akbari, H., 2019. Editorial: Urban heat island (UHI) and its mitigation through urban planning, design, and landscaping. *Architectural Science Review*, 62(1), pp.1–2. [DOI]
- Karakuş, C.B., 2019. The impact of land use/land cover (LULC) changes on land surface temperature in Sivas city center and its surroundings and assessment of urban heat island. *Asia-Pacific Journal of Atmospheric Sciences*, 55(4), pp.669–684.
- Kavitha, A.V., Srikrishna, A. and Satyanarayana, Ch., 2021. A review on detection of land use and land cover from an optical remote sensing image. *IOP Conference Series: Materials Science and Engineering*, 1074(1), 012002. [DOI]
- Kirkpatrick, J., 2024. A big history of land clearance and deforestation. *Journal of Big History*, 7(3), pp.1–18. [DOI]
- Kong, J., Zhao, Y., Carmeliet, J. and Lei, C., 2021. Urban heat island and its interaction with heatwaves: A review of studies on mesoscale. *Sustainability (Switzerland)*, 13(19). [DOI]
- Lillesand, T., Kiefer, R.W. and Chipman, J., 2015. *Remote Sensing and Image Interpretation*. John Wiley & Sons.
- Liu, B., Xie, Z., Qin, P., Liu, S., Li, R., Wang, L., Wang, Y., Jia, B., Chen, S., Xie, J. and Shi, C., 2021. Increases in anthropogenic heat release from energy consumption lead to more frequent extreme heat events in urban cities. *Advances in Atmospheric Sciences*, 38(3), pp.430–445. [DOI]
- Lo, C.P. and Quattrochi, D.A., 2003. Land-use and land-cover change, urban heat island phenomenon, and health implications. *Photogrammetric Engineering & Remote Sensing*, 69(9), pp.1053–1063.
- Long, H., Tang, G., Li, X. and Heilig, G.K., 2007. Socio-economic driving forces of land-use change in Kunshan, the Yangtze River Delta economic area of China. *Journal of Environmental Management*, 83(3), pp.351–364.
- Markham, B.L. and Barker, J.L., 1985. Spectral characterization of the Landsat Thematic Mapper sensors. *International Journal of Remote Sensing*, 6(5), pp.697–716.
- Meyer, W.B., 1995. Past and present land use and land cover in the U.S.A. *Consequences: The Nature and Implications of Environmental Change*, 1(1), pp.XX–XX.
- Mia, B., Bhattacharya, R. and Woobaidullah, A.S.M., 2017. Correlation and monitoring of land surface temperature, urban heat island with land use-land cover of Dhaka city using satellite imageries. *International Journal of Research in Geography*, 3(1), pp.10–20.
- Mia, M.A., Nasrin, S., Zhang, M. and Rasiah, R., 2015. Chittagong, Bangladesh. *Cities*, 48, pp.31–41.
- Pasha, A.B.M.K., Chowdhury, A.H., Hussain, A., Rahman, M., Mozumder, S. and Fuente, J.A.D., 2023. Identification of the ecosystem services and plant diversity in Ramna Park Dhaka. *International Journal of Environmental Studies*, 20(2), pp.65–89.
- Pasha, A.B.M.K., Mozumder, S., Bhuiyan, M.A.H. and Parveen, M., 2018. Monitoring land use and land cover changes of Dhaka City: A remote sensing and GIS-based analysis. *International Journal of Geospatial Studies*, 10(2), pp.45–60.
- Pathirana, A., Denekew, H.B., Veerbeek, W., Zevenbergen, C. and Banda, A.T., 2014. Impact of urban growth-driven land use change on microclimate and extreme precipitation—A sensitivity study. *Atmospheric Research*, 138, pp.59–72.
- Prashar, Y., Sharma, R., Kumar, S., Hassan, S.S. and Pateriya, B., 2022. Analyzing the impact of built-up and green spaces on land surface temperature with satellite images in Jalandhar Smart City. *International Journal on Environmental Sciences*, 13(2), pp.99–106. [DOI]
- Qian, Y., Chakraborty, T.C., Li, J., Li, D., He, C., Sarangi, C., Chen, F., Yang, X. and Leung, L.R., 2022. Urbanization impact on regional climate and extreme weather: Current understanding, uncertainties, and future research directions. *Advances in Atmospheric Sciences*, 39(6), pp.819–860. [DOI]
- Qin, Z., Karnieli, A. and Berliner, P., 2001. A mono-window algorithm for retrieving land surface temperature from Landsat TM data and its application to the Israel-Egypt border region. *International Journal of Remote Sensing*, 22(18), pp.3719–3746.
- Ritchie, H. and Roser, M., 2018. *Urbanization*. Our World in Data.
- Ross, S.M., 2014. *Introduction to Probability Models*. Academic Press.
- Roy, S., Pandit, S., Eva, E.A., Bagmar, Md.S.H., Papia, M., Banik, L., Dube, T., Rahman, F. and Razi, M.A., 2020. Examining the nexus between land surface temperature and urban growth in Chattogram Metropolitan Area of Bangladesh using long-term Landsat series data. *Urban Climate*, 32, 100593. [DOI]
- Saraswat, A., Pipralia, S. and Kumar, A., 2024. Exploring the application of ecosystems approach to urban planning. *International Review for Spatial Planning and Sustainable Development*, 12(2), pp.28–42. [DOI]
- Shahbaz, M., Guergachi, A., Noreen, A. and Shaheen, M., 2012. Classification by object recognition in satellite images by using data mining. *Proceedings of the World Congress on Engineering*, 1, pp.4–6.
- Singh, G. and Singh, S.K., 2023. Evapotranspiration over the Indian region: Implications of climate change and land use/land cover change. *Nature Environment and Pollution Technology*, 22(1), pp.211–219.
- Sobrino, J.A. and Raissouni, N., 2000. Toward remote sensing methods for land cover dynamic monitoring: Application to Morocco. *International Journal of Remote Sensing*, 21(2), pp.353–366.
- Sobrino, J.A., Jiménez-Muñoz, J.C. and Paolini, L., 2004. Land surface temperature retrieval from LANDSAT TM 5. *Remote Sensing of Environment*, 90(4), pp.434–440.
- Statistics, 2011. Bangladesh Bureau of Statistics, Statistics and Informatics Division (SID), Ministry of Planning, Parishankhan Bhaban, E-27/A, Agargaon, Dhaka-1207
- Tan, K.C., Lim, H.S., MatJafri, M.Z. and Abdullah, K., 2010. Landsat data to evaluate urban expansion and determine land use/land cover changes in Penang Island, Malaysia. *Environmental Earth Sciences*, 60(7), pp.1509–1521.
- Thomas, G.S., Liu, Y. and Mwanga, N., 2024. Exploring the environmental effects of urbanization in Monrovia. *European Journal of Theoretical and Applied Sciences*, 2(3), pp.1117–1130. [DOI]
- Tyagi, S.K., Kumar, V., Kumar, K. and Kumar, D., 2023. Environmental health quality and the consequences of urbanization: A review. *International Journal of Advances in Agricultural Science and Technology*, 10(5), pp.13–23. [DOI]
- Vaiphasa, C., Piamduaytham, S., Vaiphasa, T. and Skidmore, A.K., 2011. A normalized difference vegetation index (NDVI) time-series of idle agriculture lands: A preliminary study. *Engineering Journal*, 15(1), pp.9–16.
- Verburg, P.H., Chen, Y., Soepboer, W. and Veldkamp, A., 2000. GIS-based modeling of human-environment interactions for natural resource management. *Proceedings of the 4th International Conference on Integrating GIS and Environmental Modeling: Problems, Prospects and Research Needs*, Canada, pp.1–13.

- Wang, J., Chen, Y., Liao, W., He, G., Tett, S.F.B., Yan, Z., Zhai, P., Feng, J., Ma, W., Huang, C. and Hu, Y., 2021. Anthropogenic emissions and urbanization increase risk of compound hot extremes in cities. *Nature Climate Change*, 11(12), pp.1084–1089. [DOI]
- Winston, W.L. and Goldberg, J.B., 2004. *Operations Research: Applications and Algorithms*. 3rd ed. Thomson Brooks/Cole Belmont.
- Xu, H. and Chen, B., 2004. Remote sensing of the urban heat island and its changes in Xiamen City of SE China. *Journal of Environmental Sciences*, 16(2), pp.276–281.
- Zhou, D., Xiao, J., Frolking, S., Zhang, L. and Zhou, G., 2022. Urbanization contributes little to global warming but substantially intensifies local and regional land surface warming. *Earth's Future*, 10(5), pp.1–19. [DOI]

# A Complete Review on Ericoid Mycorrhiza: An Understudied Fungus in the Ericaceae Family

Malini Ray<sup>1</sup>, Sneha Choudhary<sup>1,2</sup>, Abisma K Jose<sup>1</sup>, Vikash Kumar<sup>1</sup>, Aakash Gupta<sup>1</sup> and Sonali Bhagat<sup>2</sup>

<sup>1</sup>School of Agriculture, Lovely Professional University, Phagwada-144411, Punjab, India

<sup>2</sup>Sher-e-Kashmir University of Agricultural Sciences and Technology, Jammu-180009, J&K, India

†Corresponding author: Sneha Choudhary; Sneha.28385@lpu.co.in

**Abbreviation:** Nat. Env. & Poll. Technol.

**Website:** [www.neptjournal.com](http://www.neptjournal.com)

*Received:* 25-07-2024

*Revised:* 19-09-2024

*Accepted:* 23-09-2024

## Key Words:

Ericoid mycorrhiza

Ericaceae

Ericoid mycorrhiza diversity

## ABSTRACT

Ericoid mycorrhiza (ErM) is an unexplored and understudied member of the mycorrhizal world, surprisingly belonging to Ascomycota and Basidiomycota instead of Glomeromycota (the phylum comprising fungi forming associations with higher plants). ErM obtained its etymology due to its symbiotic relationship with members of the *Ericaceae* Family. Just like any other mycorrhiza, ErM also helps its hosts through nitrogen uptake and phosphorus bioavailability and provides defense to host plants against various phytopathogens. It also takes part in the decomposition of organic matter and depolymerization of complex substances. These mycorrhizae are distributed across all continents except Antarctica. The majority of culturable ErM is spread across England, Australia, Canada, the United States etc. This review focuses on the literature survey on ErM, its taxonomy, and diversity alongside its functions. Our review also sheds light on the host range of the ericoid fungi, wherein, out of all the hosts, Salal (*Gautheria shallon*) has been identified as one of the most promising ones.

## INTRODUCTION

‘Mycorrhiza’ is a symbiotic association between fungus and root system. Etymologically, “Mycorrhiza” is made up of two Greek words, viz., ‘mykes’ (fungus) and ‘rhiza’ (roots). This association is known to be one of the ancient relationships between plants and microbes, having its fossils dating back to the Paleozoic era. However, recent molecular data insinuated that this fungus root system may have arisen during the Proterozoic era (Brundrett 2002). Members of the kingdom Plantae, Monera, and Protista are known to have essential mutualistic relationships, e.g., interactions between soil mycoflora and plants in contemporary terrestrial ecosystems. Interestingly, according to the hypothesis put forth by Pirozynski & Malloch (1975), The evolution of plants themselves is said to be possible through such “mutualistic relationships,” and the terrestrial plants that we have today are the result of an old and continuous association among an aquatic fungus and primordial semi-aquatic green alga. The fungi involved in the mutualistic associations are known to absorb the essential nutrients (both available and non-available forms) such as phosphate and nitrogen (N) more effectively than plant roots alone. In return, the plants give carbohydrates to the fungus that was made through photosynthesis.

Discovered in 1988 by Becard & Fortin, mycorrhiza, apart from enhancing nutrient absorption (phosphorus uptake), also produces auxins, boosts disease resistance, and improves the rhizosphere habitat. There are two types of mycorrhizas most frequently found, viz., endomycorrhizas (penetrating cortical cells) and ectomycorrhizas (not deeply penetrating). There is another category, ecto-endo mycorrhizas (arbutoids), comprising properties of both types, while

## Citation for the Paper:

Ray, M., Choudhary, S., Jose, A. K., Kumar, V., Gupta, A. and Bhagat, S., 2025. A complete review of Ericoid mycorrhiza: An understudied fungus in the Ericaceae family. *Nature Environment and Pollution Technology*, 24(2), p. B4252. <https://doi.org/10.46488/NEPT.2025.v24i02.B4252>

*Note: From year 2025, the journal uses Article ID instead of page numbers in citation of the published articles.*



**Copyright:** © 2025 by the authors

**Licensee:** Technoscience Publications

This article is an open access article distributed under the terms and conditions of the Creative Commons Attribution (CC BY) license (<https://creativecommons.org/licenses/by/4.0/>).



arbuscular, orchid, and ericoid mycorrhizas are categorized as endomycorrhiza (Van der Heijden et al. 2015).

Ectomycorrhiza, also abbreviated as EcM, often forms linkages between fungi from Phyla - Zygomycota, Basidiomycota, and Ascomycota woody plants (For example Willow, pine, oak, spruce, beech, fir, and birch). Ectomycorrhizal connections exist in approximately 10 percent of plant families. Although EcM mainly consists of around 8000 primarily woody plants, they have a significant presence in a variety of biomes (Plett & Martin 2011). In ectomycorrhiza, the hyphal mantle is present and forms a Hartig net, whereas, arbuscules and vesicles both are absent.

The endomycorrhiza is further categorized into three types, *viz.*, Vesicular Arbuscular mycorrhiza (VAM), Ericoid mycorrhiza (ErM), and Orchid mycorrhiza (OM). VAM is the most abundant symbiotic association between certain fungi and the roots of the majority of plants. In the plant's root system, the fungus creates a network of small filaments called hyphae that branch out to form an arbuscule (a highly branched structure). These fungi are a vital part of healthy soil and can be found in a variety of environments, including forests and agricultural fields. They are essential for maintaining thriving and productive ecosystems because they increase nutrient uptake and boost plant development. Although arbuscular mycorrhizas were first reported in 1842 by Nageli, however, the majority of his illustrations hardly resembled arbuscular mycorrhiza. Further early reports of the symbiosis from the years 1875-1895 are cited by Trappe & Berch (1985). Arbuscules, vesicles, and colonization from adjacent cells or root surface mycelia are all present in arbuscular mycorrhiza as these are required for survival by reducing competition, therefore providing protection and nutrition.

Members of the Orchidaceae family are known to be myco-heterotrophic, wherein the Orchid mycorrhizae form symbiotic interactions with the orchid plants during seed germination. In this mutualistic connection, orchids depend upon the OM for food rather than on photosynthesis. In return, the fungi get the organic carbon compounds from the orchids that they require to develop. The link is quite specialized and may only apply to specific orchid species or groupings. The roots of the orchids and the fungi develop a specific structure called the peloton that enables communication and the flow of nutrients between the two organisms. The life and development of orchids depend on this symbiotic interaction, which is also vital to the ecology of many habitats where orchids are found.

'Ericoid mycorrhiza' is a particular kind of mycorrhiza in which fungus and plants create a symbiotic relationship with plants growing in acidic soils, such as Heath and Moorland

species. Heathers, blueberries, and rhododendrons are just a few examples of the plants in the *Ericaceae* family, which are most frequently associated with this form of mycorrhiza, which is why it is called "Ericoid". The majority of terrestrial plant species have mycorrhizal fungi colonizing their roots, which enhance nutrient uptake in exchange for sugars produced during photosynthetic activities and make them significant players in the carbon and nutrient cycling in many ecosystems (Van der Heijden et al. 2008).

Ericoid mycorrhiza is said to be one of a kind in the world of fungal associations due to its ability to survive in extreme conditions (acidic soils), along with its high specificity towards choosing its host plants. All the studies done on ErM fungi revealed that they have developed mycorrhizal association only with the members belonging to the order *Ericales*. It is also reported that certain ascomycetous fungi also participate in their symbiotic relationships (Harley & Smith 1983, Leopold 2016).

In Ericoid mycorrhiza, the fungi's hyphae enter the plant's roots and create a network of small, branching structures inside the root cortex cells that are termed Hartig nets. The plant provides the fungus with carbohydrates, while the fungi provide the plant with all nutrients from the soil, including phosphate and nitrogen, which they're able to absorb and transport. In addition to being able to accept and thrive in acidic soils, ericoid mycorrhizal fungi are also capable of creating enzymes that disintegrate complicated organic material so that the plant may use them. Many heathland and moorland plants require this form of mycorrhiza for their development and survival, and it can be essential to nutrient cycling in these habitats.

Most of the studies to date focus on the other mycorrhizal associations known since their arrival, dating back to 400 million years. Therefore, in this review, we have attempted to summarize the functions and diversity of this younger mycorrhizal symbiont known as Ericoid Mycorrhiza.

## Bibliometric Survey

The systemic literature survey using keywords "Ericoid Mycorrhiza", "Ericoid Mycorrhiza Functions," and "Ericoid Mycorrhiza and diversity" was performed using 3 databases, *i.e.*, Scopus, Science Direct, and PubMed (Fig. 1a & b). The literature search for "Ericoid Mycorrhiza" using the Scopus database revealed 615 papers from 1973 to 2024; the same search on Science Direct (1990-2024) gave 856 results comprising Reviews, research articles, and Book chapters. There are 436 research papers wherein 12 were published in 2024. Out of 96 reviews, not even a single hit showed these two words, *i.e.*, "Ericoid" and "Mycorrhiza," together, indicating a lack of complete review on this mycorrhiza.

These two words, when searched together on PubMed (1980-2024), gave 234 results.

The next search was done for the combination of the words “Ericoid Mycorrhiza and diversity,” for which PubMed revealed 63 articles from 2000 till date, Science Direct gave 329 articles from 2000 onwards, and 127 documents were searched on the Scopus database. Similarly, the keywords “Ericoid Mycorrhiza Functions” revealed only 79 documents on Scopus, 638 articles on Science Direct, and 164 articles on PubMed from 1980-2024.

## Ericoid Mycorrhizal Biology

The *Ericales* are a large group of plants that are found all over the world. They are frequently found as ground cover species in parts of the Mediterranean and boreal forests. They are dominant in some frigid locations, frequently establishing practically pure plant communities. The mycorrhizal relationship with ericoid fungi, a kind of soil fungus, is a characteristic feature shared by most of the plant species in the *Ericaceae* family. These fungal classes are widely distributed in ericaceous plants’ characteristic fine-haired

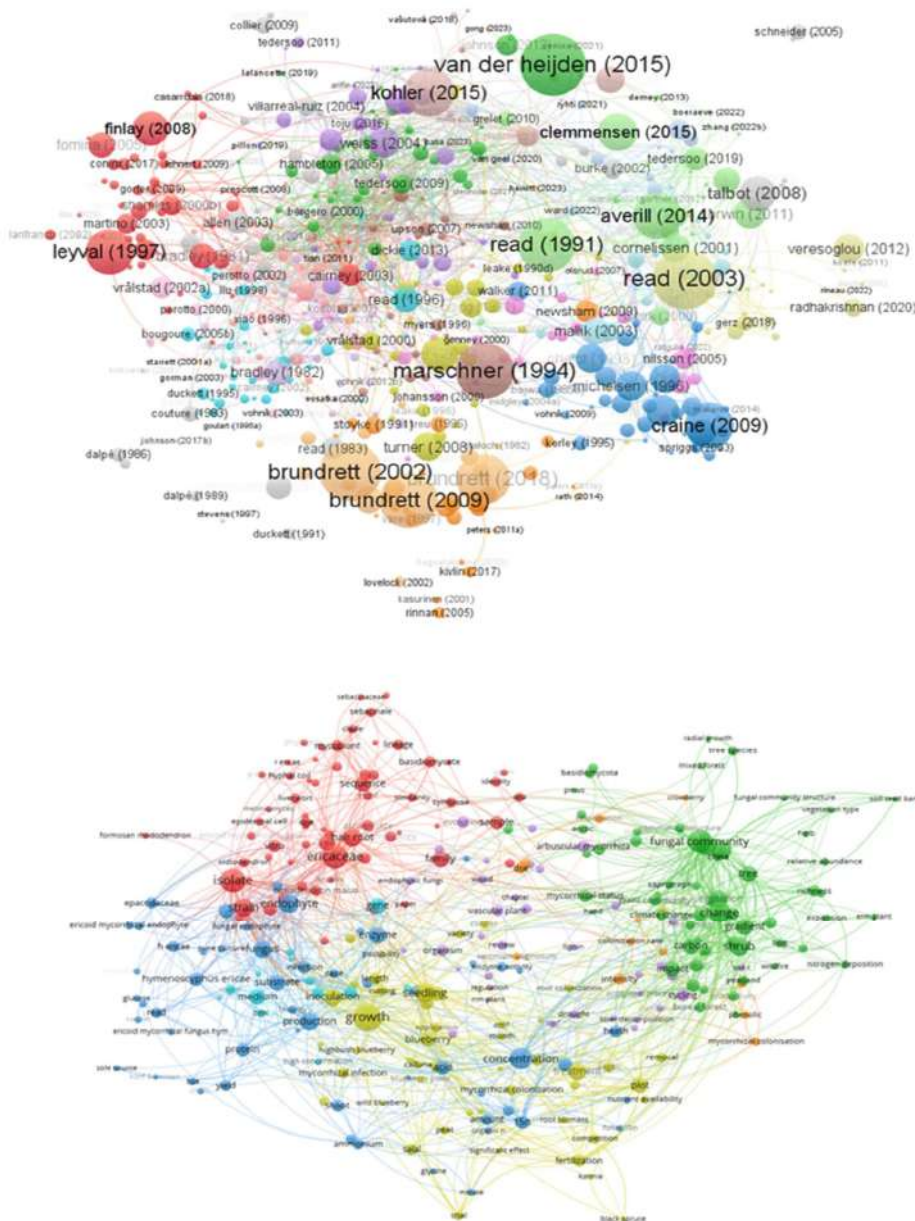


Fig. 1a: Literature survey based on “Author” search and keyword “Ericoid Mycorrhiza” from 1980 and 2024.

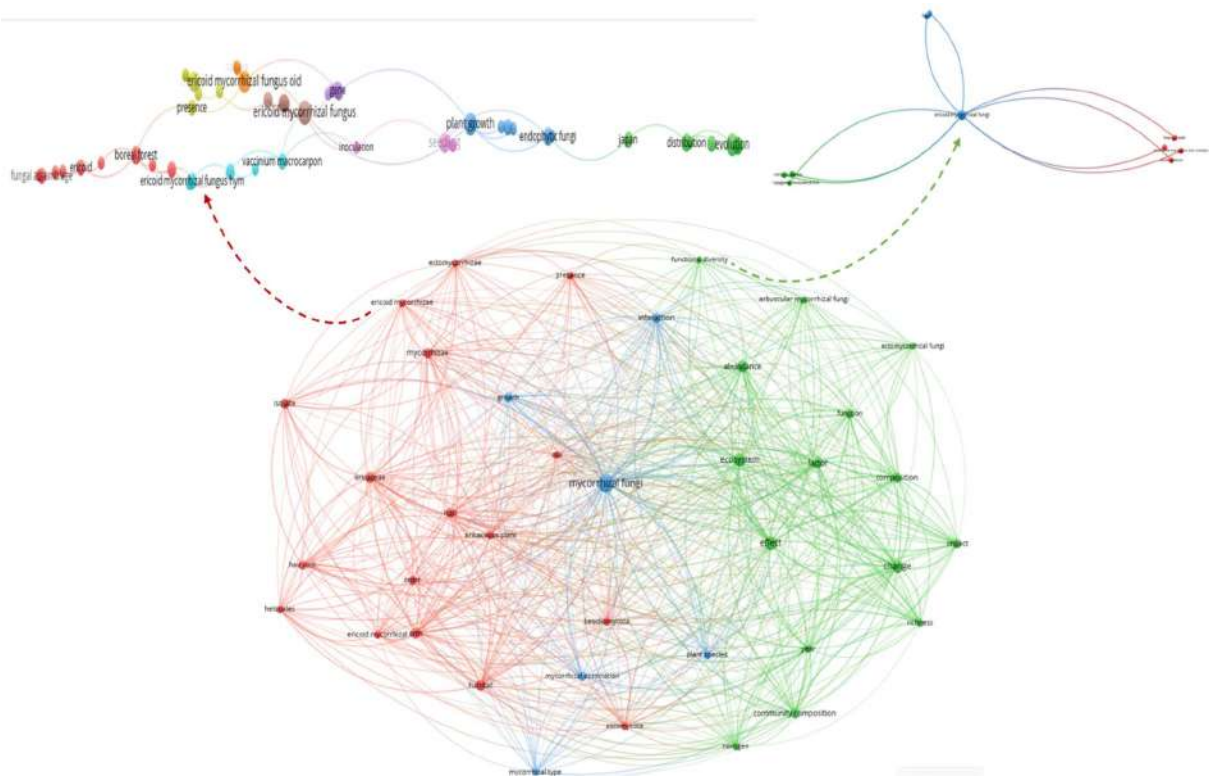


Fig. 1b: Literature survey on different aspects (ericoid diversity & functions) of Ericoid Mycorrhiza from 1980 and 2024.

roots, and they are very crucial for the nutrition and mineral cycling of plants (Read 1996).

### Morphometric Analysis

The majority of ericoid isolates have walls made up of an exterior layer and an inner layer that is transparent to electrons, which are both dense in electrons, but others simply have an amorphous electron-dense wall. Using immunocytochemical methods, the septa and innermost layer have been found to include skeletal components. The symbiotic strains are characterized by a fibrillar sheath projecting from the wall, which is only sometimes formed by strains with a lesser capacity for symbiosis. This coating is more prevalent on the fungus that is traveling along the surface of the root than it is on the hyphae that are coiling up inside the infected root cell. Moreover, it appears that the type of substrate affects how it is produced. Mannose and glucose residues have been found in the fiber-like sheath in situ by utilizing the Concanavalin A lectin compound (Bonfante et al. 1987). Current reports about the existence of immunogenic (Bonfante et al. 1987) and enzymatic glycoproteins (Straker et al. 1989) suggest that ericoid mycorrhizal cell surface is a compound molecular structure with a mosaic appearance that may have significant roles during the primary stages of host plant interaction.

The delicate and fragile structure present on roots, known as hair roots, is a characteristic of ericoid plants (Read 1996). Root hairs are composed of a stele on the inner side that is encircled by two-layered cortical cells, an outermost layer with massive epidermal cells, and a relatively small diameter typically less than 100  $\mu$ m. The only root hair cells that have been captured by ErM fungi are these epidermal cells, which serve as the contact with the soil (Smith & Read 2010). Here, the plant plasma membrane-invading ErM fungus produces hyphal coils that often take up the majority of the cell volume (Bonfante-Fasolo & Gianinazzi-Pearson 1979, Peterson et al. 2004).

The majority of cells represent individual colonization units since fungi often colonize epidermal cells straight from the soil through the thicker tangential wall outside (Massicotte et al. 2005). In the older regions of the hair roots, epidermal cells slough off, exposing the cortical layer. Ericoid Mycorrhizal cells are. Therefore, transient and symbiotic nutrition interchange is probably only possible in the young parts of the root, where both partners are still alive. Ericoid hyphae that are viable have been seen in cells of plants that exhibit cytoplasm and organelle degradation, in contrast to other endomycorrhizal partnerships such as arbuscular and orchid mycorrhiza (Bonfante-Fasolo &



Gianinazzi-Pearson 1979, Read 1982). All of the ericoid mycorrhiza studied to date by various researchers reported that they created the same kind of intracellular loops when they colonized the roots of their host.

### Biochemical Nature of Ericoid Mycorrhizal Fungi

Ericoid fungus makes a variety of enzymes that are extracellular into the medium, enabling them to break down and use organic soil matrix, increasing their competitive capacity in the soil. Several of these enzymes, such as *Carboxyproteinases* (Leake & Read 1991) and *Acid phosphatases* (Straker & Mitchell 1986), are probably crucial for the nutrition in mycorrhizal plants that acquire entry to nutrients that would not be available otherwise (Leake & Read 1991). Moreover, compound organic polymers, which are characteristic parts of fungal and plant cell walls, can be broken down by ericoid mycorrhizal fungus. It has been observed that ericoid fungi can attack tannins, chitin, and lignins (Leake & Read 1991). The culture-rich filtrates of ericoid growing *in vitro* have also been found to produce other enzymes that degrade cell walls, such as  $\beta$ -1,3-glucanase  $\beta$ -1,4-glucanase (Varma & Bonfante 1994) and *polygalacturonase* (PG) (Peretto et al. 1993) (Fig. 2).

### Taxonomy, Diversity and Phylogeny

Ericoid mycorrhiza, being a diverse group, is largely associated with a wide range of plant species like *Ericaceae* and *Epacridaceae*. It can be seen in countries such as Europe, Canada, Australia, the United States, and so forth. Although there are many *Ericaceae* plant species in India, such as rhododendrons, azaleas, and blueberries, there have been no studies or research on ericoid relationships thus far. Not just in India but also globally, there are very few findings on ericoid mycorrhizal association (Leopold et al. 2021).

As per early research findings, the *Ericaceae* family is classified into nine distinct subfamilies. The foundational evolutionary branches of *Ericaceae*, especially *Arbutoideae*, *Monotropoideae*, *Enkianthoideae*, and *Pyroloideae*, do not possess the ability to establish Ericoid Mycorrhizal (ErM) associations. Contrastingly, species within the *Monotropoideae* subfamily engage in what's known as monotropoid mycorrhizal symbiosis, featuring ectendomycorrhizal anatomical structures. This symbiosis involves particular groups of Ectomycorrhizal (EcM) fungi from the phylum Basidiomycota (Hynson & Bruns 2009). On the other hand, plants belonging to the *Pyroloideae* and *Arbutoideae* subfamilies accommodate a wide variety of EcM fungi in their root systems (Krpata et al. 2007).

The majority of Ericoid Mycorrhizal (ErM) fungi consist mainly of Ascomycetes found within the Leotiomyces, along with a few Basidiomycetes, notably those in the family Serendipitaceae (Weiß et al. 2016). The first fungal species isolated from ErM roots was *Rhizoscyphus ericae*, belonging to the Leotiomyces. Initially categorized under the genus *Pezizella*, it was subsequently reclassified into *Hymenoscyphus* and later into *Rhizoscyphus* (Zhang & Zhuang 2004). Until the development of molecular tools for assessing phylogenetic relationships, the majority of slowly growing mycelia isolated from Ericoid Mycorrhizal (ErM) roots remained unidentified. To address various fungal taxa isolated from ErM roots that were closely related to *R. ericae*, an aggregate was established within the order *Helotiales* (Perotto et al. 2018,1993). This aggregate, referred to as the '*R. ericae* aggregate' by Vrålstad et al. (2000), due to its inclusion of *R. ericae*, comprised four primary clades (Fig. 3). Hambleton & Sigler (2005) later enhanced the definition of these clades, simultaneously suggesting three novel species within the anamorphic genus *Meliniomyces* as part of the "*R. ericae* aggregate" (Vrålstad et al. 2000,

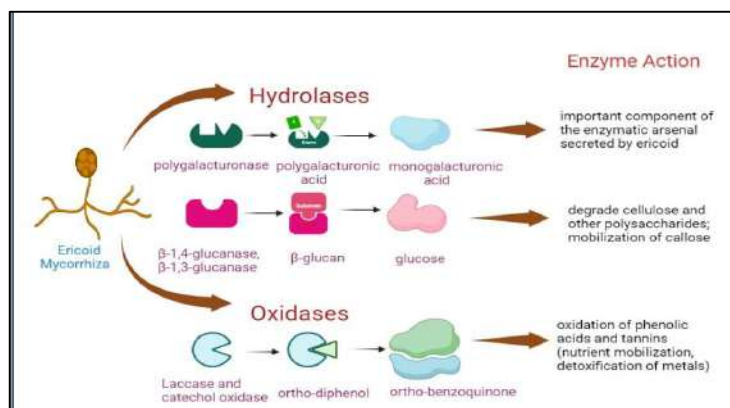


Fig. 2: Illustration of various enzymes released by ErM along with their functions.



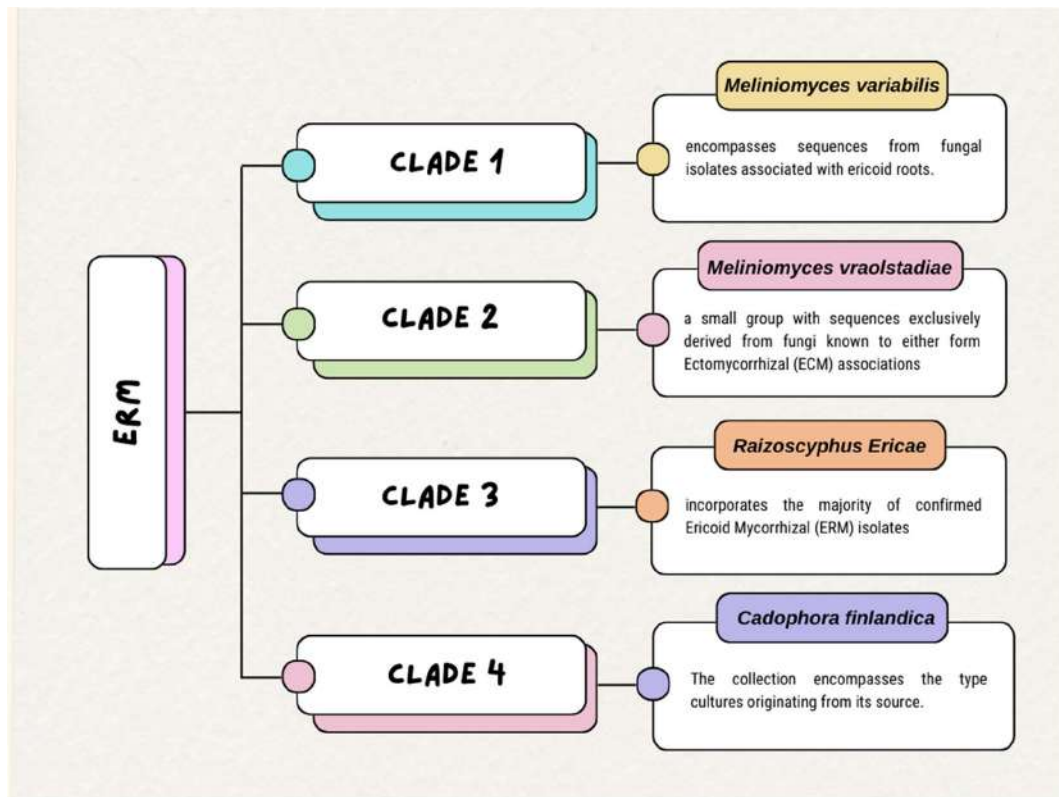


Fig. 3: The four major clades of Ericoid mycorrhizae under the order *Helotiales*.

2002a). Clade 1, represented by *Meliniomyces variabilis*, encompasses sequences from fungal isolates associated with ericoid roots, previously identified as the “variable white taxon” (Hambleton & Currah 1997). Additionally, it includes sequences from root endophytes found in various host plants in cold-temperate Northern Hemisphere soils. Clade 2, featuring *Meliniomyces vraolstadae*, this small cluster comprises sequences exclusively sourced from fungi recognized for either forming Ectomycorrhizal (ECM) associations or displaying non-mycorrhizal behavior (Vrålstad et al. 2002b). Clade 3 incorporates the majority of confirmed Ericoid Mycorrhizal (ERM) isolates, including the type cultures of *S. vaccinii* and *R. ericae*. Clade 4 includes the type cultures of *Meliniomyces bicolor* and *Cadophora finlandica* (Perotto et al. 2012).

Usually, mycorrhiza has been grouped under “Glomeromycota” (Redecker & Raab 2006). However, ErM fungi exhibit a distinctive clustering pattern, aligning themselves under the higher dikaryotic sister clades of “Ascomycota” and “Basidiomycota”.

“Ascomycota,” characterized by their leisurely developing mycelia obtained from Ericoid Mycorrhiza (ErM), remained elusive until the advent of molecular tools capable of investigating their phylogenetic affinities (Perotto

et al. 2012). Up to this point, ericoid fungal endophytes that have been isolated predominantly belong to ascomycetes. However, it’s worth noting that basidiomycetes have been detected through an electron microscope within locally colonized roots, as reported by Perotto & Bonfante (1998). This observation underscores the complexity of the ErM fungal community and highlights the significance of advanced molecular techniques in unraveling the intricate taxonomic relationships within this fungal group. Over the past few years, our knowledge of the biodiversity of ericoid mycorrhizal fungi has seen a swift growth (Stoyke et al. 1992, Perotto et al. 1996). Initially, the sole ericoid fungal endophyte known for approximately a decade was identified as an ascomycete featuring a dark, sluggish sterile mycelium, subsequently recognized as *Hymenoscyphus ericae* (formerly *Pezizella ericae*) (Perotto & Bonfante 1998). Subsequently, additional ericoid mycorrhizal (ErM) fungi have been successfully cultured and identified as ascomycetes within the genus *Oidiodendron* (Perotto et al. 2012). Notably, the initial recognition of symbionts associated with ericaceous hosts highlighted the prevalence of Ascomycetes, specifically *Hymenoscyphus ericae* (62-92% endophyte isolates) and *Oidiodendron spp.*, both in their anamorphic stage (Smith & Read 1997, Sharples et al. 2000c, Perotto et al. 2002).

In addition to Ascomycota, various lineages of Ericoid Mycorrhizal (ErM) fungi are also identified within the phylum “Basidiomycota” (Kohout 2017). Among the basidiomycetes, the majority of recognized mycorrhizal species belong to homobasidiomycetes. Distinguishing homobasidiomycetes, as presently defined, from other hymenomycetous taxa such as Tulasnellales and Ceratobasidiales poses a challenge (Hibbett & Thorn, 2001, Weiß et al. 2004).

Several decades back, Seviour et al. (1973) proposed the possibility of an Ericoid Mycorrhizal (ErM) habit for *Clavaria sp.* Nevertheless, the evidence supporting nutrient exchange in both directions between the host plant *Clavaria sp.* and *Rhododendron sp.* remained uncertain, as reported by Mueller et al. (1986). Early indirect indications of basidiomycete fungi engaging in ericoid mycorrhiza formation in the roots of *Calluna*, *Vaccinium*, and *Rhododendron* were noted (Bonfante- 1980, Peterson et al. 1980, Englander & Hull 1980). These early observations were aligned with recent findings in Italy, where hyphae featuring dolipore septa and clamp connections were observed as characteristic typical mycorrhizal coils in the roots of *E. arborea* (Perotto et al. 2002). Due to the lack of evidence of ericoid mycorrhizal association on a broad scale, its diversity needs to be examined on a genetic basis.

1. **Genetic diversity of ericoid mycorrhizal fungi:** The first and most important step in studying mycorrhizal association at the genetic level is to understand the number of taxa and the phylogeny of mycorrhizal fungus (Berch

et al. 2002). The majority of mycorrhizal fungus species are secluded or confined to a specific region. *Rhizocyphus ericae*, on the other hand, is widely dispersed (Kohout et al. 2017). According to the data gathered so far, the understudied and undetected group of mycorrhizal fungus, the information on critical portions of this issue is expanding day by day. The fundamental cause for this expansion is molecular characterization, which uses numerous target genes and particular approaches to develop and intensify the effects of symbiotic interaction between mycorrhiza and the roots of higher fungi. (Pearson & Read 1973) isolated the first taxonomically identifiable ErM fungus from *Calluna vulgaris* roots, which was eventually encouraged to grow.

A significant level of genetic variation has been detected among diverse parts of various roots, the majority of which are even from the same plant. Perotto et al. (1996) used random amplified polymorphism DNA (RAPD) analysis to conduct the first systematic assessment of the variety of mycorrhizal endophytes associated with *C. vulgaris*. Molecular characterization benefits substantially from PCR techniques such as PCR-RFLP analysis. *O. maius* and *S. vaccinii* were reliably isolated from 19 *Ericaceae* species collected in three different North American settings by Hambleton & Currah (1997). Additionally, *O. grisem* was isolated from a variety of plants, demonstrating that one plant's root systems can be colonized by two or more endophytes at once.



Fig. 4: Global geographic distribution of Ericoid Mycorrhiza. Most of the ErM are confined to North America, Europe, Vancouver, Northern California, British Columbia, Northern Europe, China, England, Canada, United States, British Columbia coast, Arctic Tundra, Australia, and are associated with *Gautheria shallon*, *Calluna vulgaris*, *Epacris impressa*, *Astroloma pinifolium* and so on.

Table 1: List of ErM Diversity characterized and studied.

Species	Host	Target Gene	Technique	Reference
<i>Mortierella</i> sp. <i>Oidiodendron</i> spp.	<i>Calluna vulgaris</i> and <i>Vaccinium myrtillus</i>	NA	Direct Planting, Maceration	Pearson and Read (1973)
<i>Oidiodendron griseum</i>	<i>Gautheria shallon</i>	NA	NA	Xiao and Berch (1992)
<i>Hymenoscyphus ericae</i> <i>O. maius</i> <i>Scytalidium vaccinii</i> <i>Pseudogymnascus roseum</i> <i>Pseudogymnascus roseus</i> <i>Oidiodendron flavum</i>	<i>Gautheria shallon</i>	NA	NA	Xiao and Berch (1995)
<i>O. maius</i> <i>Acremonium strictum</i> <i>Unknown 1</i> <i>Unknown 2</i>	<i>Gautheria shallon</i>	NA	NA	Xiao and Berch (1996)
<i>O. maius</i> <i>O. periconioides</i> <i>O. pilicola</i> <i>O. cerealis</i> <i>O. griseum</i>	<i>Epacris impressa</i> , <i>Astroloma pinifolium</i>	ITS5 and ITS4	NA	Mclean et al. (1999)
<i>Acremonium strictum</i> <i>Hyaloscypha aureliella</i> <i>Hymenoscyphus ericae</i>	<i>Gautheria shallon</i> , <i>Vaccinium angustifolium</i> , <i>V. corymbosum</i>	ITS 2	RFLP, PCR	Monreal et al. (2000)
<i>Phialocephala dimorphospora</i> <i>P. forinii</i> <i>P. Finlandia</i>	<i>Cassiope mertensiana</i> , <i>Pinus sylvestris</i>	ITS 2	RFLP, PCR	Monreal et al. (2000)
<i>Oidiodendron maius</i> <i>O. griseum</i> <i>O. tenuissimum</i> <i>Paecilium</i> spp. <i>Torulomyces lagena</i>	<i>Quercus ilex</i> and <i>Erica arborea</i>	ITS1 & ITS4	PCR, RFLP, RAPD	Bergero et al. (2000)
<i>Capronia villosa</i> <i>O. maius</i> <i>Hymenosyphus ericae</i> <i>Unknown 1</i> <i>Unknown 2</i>	<i>Gautheria shallon</i>	ITS 1 & ITS 2	RFLP	Berch et al. (2002)
<i>Sebacina vermifera</i> <i>Capronia villosa</i> <i>Hymenoscyphus ericae</i> <i>Trechispora</i> spp. <i>Oidiodendron maius</i>	<i>Gautheria shallon</i>	ITS 2	RFLP, PCR	Allen et al. (2003)
<i>Meliniomyces variabilis</i> <i>Meliniomyces vraolstadiae</i> <i>Rhizoscyphus ericae</i> <i>Neocudonicella radicella</i> <i>Scytalidium lignicola</i>	<i>Orchidaceae</i> , <i>Pinaceae</i> , <i>Betulaceae</i> , <i>Saliaceae</i>	ITS, SSU, SSU-ITS	RFLP, PCR	Hambleton and Sigler (2005)
<i>Oidiodendron maius</i> <i>O. citrinum</i> <i>O. spp. (others)</i>	<i>Chamaedaphne calyculata</i> , <i>Oxycoccus quadripetalus</i> , <i>Pseudotsuga menziesii</i>	ITS1, ITS2, ITS4	PCR	Sigler and Gibas (2005)
<i>Cryptosporiopsis ericae</i> <i>Hymenoscyphus monotropae</i> <i>Lachnum pygmaeum</i> <i>Meliniomyces variabilis</i> <i>Mollisia minutella</i> <i>Phialocephala fortinii</i> <i>Hypocrea pachybasoides</i> <i>Irpen lacteus</i>	<i>Empetrum nigrum</i> , <i>Vaccinium vitis-idaea</i> , <i>Cassiope tetragona</i>	ITS1F, ITS4	PCR	Walker et al. (2011)

Table Cont....

Species	Host	Target Gene	Technique	Reference
<i>Pochonia bulbillosa</i> <i>Mycena galopus</i> <i>Nectriaceae spp.</i> <i>Galerina spp.</i> <i>Pleosporales spp.</i>	<i>Caccinium myrtillos L.</i>	ITS1F, ITS4	PCR	Vohnik et al. (2012)
<i>Rhizoscyphus</i> <i>Oidiodendron</i> <i>Lachnum</i> <i>Phialocephala</i> <i>Clavaria</i> <i>Acephala</i> <i>Meliniomyces</i>	<i>Vaccinium uliginosum</i>	ITS1 and ITS4	PCR	Yang et al. (2018)
<i>Cryptosporiopsis ericae</i> <i>Sordariomycetes spp.</i>	<i>Vaccinium uliginosum</i>	ITS1 and ITS4; gfp gene	In situ PCR and Green Fluorescent Protein	Yang et al. (2020)
<i>Helotiales</i> <i>Rhizoderma veluwensis</i> <i>Glutiniomyces</i> <i>Clavulinopsis</i>	<i>Cinnum calycium</i>	ITS1, ITS2	PCR	Leopold et al. (2021)

Most recently, these molecular techniques have had a significant impact on the genetic diversity of ericoid mycorrhiza, allowing us to learn more about some groups that had been kept dormant. It should be feasible to gain more exact taxonomic information by using such approaches on the mycorrhizal endophytes of *Epacridaceae* plants, enabling in-depth research of population and community dynamics. In our review, an attempt was made to compile the majority of the ErM fungi that have been studied and characterized so far (Table 1).

## 2. Host plant species associated with ericoid mycorrhiza:

Ericoid mycorrhiza is known to have a specific mutualistic association with the members of the *Ericaceae* family. Their association is considered to have evolved since the first appearance of *Ericaceae*. The *Ericaceae* family consists of 9 subfamilies, 4 of which do not have ErM. Recently, it was found that *Enkianthus campanulatus* had a symbiotic relationship with ErM. From this study, we can infer that ErM is still undergoing evolution, and this proves the very fact that ErM remains understudied in comparison with other mycorrhizae. The diversity of ErM remains unknown at the global level, although its culturable nature serves as a vital tool. Due to a lack of study on this fungus, its complete lineage remains unexplored. Reports have shown that the majority of diversity work done was using internal transcribed spacer (ITS) regions; although ITS is a universal barcode marker for fungi, it has been seen that it was not useful in the estimation of this *Ericaceae* root mycobiont (Kohout 2017, Vohnik 2020).

**Salal (*Gautheria shallon*):** The authors mentioned in Table 1 discovered several potential fungi that form ericoid mycorrhiza in *Gaultheria shallon* using traditional culturing

and genetic characterization. The identification of ericoid mycorrhizal fungi as well as their geographical distribution (Fig. 4), can be determined with the help of molecular characterization and phylogenetic analysis of the ITS sequence of gene bank.

**Others:** Many other potential host plant species of *Ericaceae* and *Epacridaceae* are selected for identifying the mycorrhizal association with different fungi. Some of them are *Calluna vulgaris*, *Vaccinium myrtillos*, *Epacris impressa*, *Astroloma pinifolium*, *Cassiope mertensiana*, *Pinus sylvestris*, *Quercus ilex*, *Erica arborea* and so forth.

**Functions of ericoid mycorrhizal cells:** *Ericaceae* plants generally thrive on acidic as well as nutrient-poor soils where most of the essential nutrients are present in fixed forms. Studies have shown that the presence of ErM in such an environment plays a major role in the survival of the *Ericaceae* members as these mycobionts help to convert fixed nutrients into accessible forms that are then mobilized by plants (Fig. 5). Major functions of ErM are therefore summarized below:

### 1) Nitrogen Uptake

Due to the sluggish breakdown rates, acid-heathland (shrubland) soils only have trace levels of accessible inorganic nitrogen (Straker 1996, Haselwandter 1997). *Ericaceae* plants depend upon ericoid mycorrhizal fungus to retain the wide variety of various nitrogen compounds present in the soil. The findings of various experiments showed that plants with mycorrhizal association have accessibility to additional sources of nitrogen in the soil in addition to ammonium, while non-mycorrhizal plants used ammonium-nitrogen. The availability of carbon in the growing media affects the capacity of mycorrhizal fungi that are ericoid to consume nitrate, ammonium, or glutamine



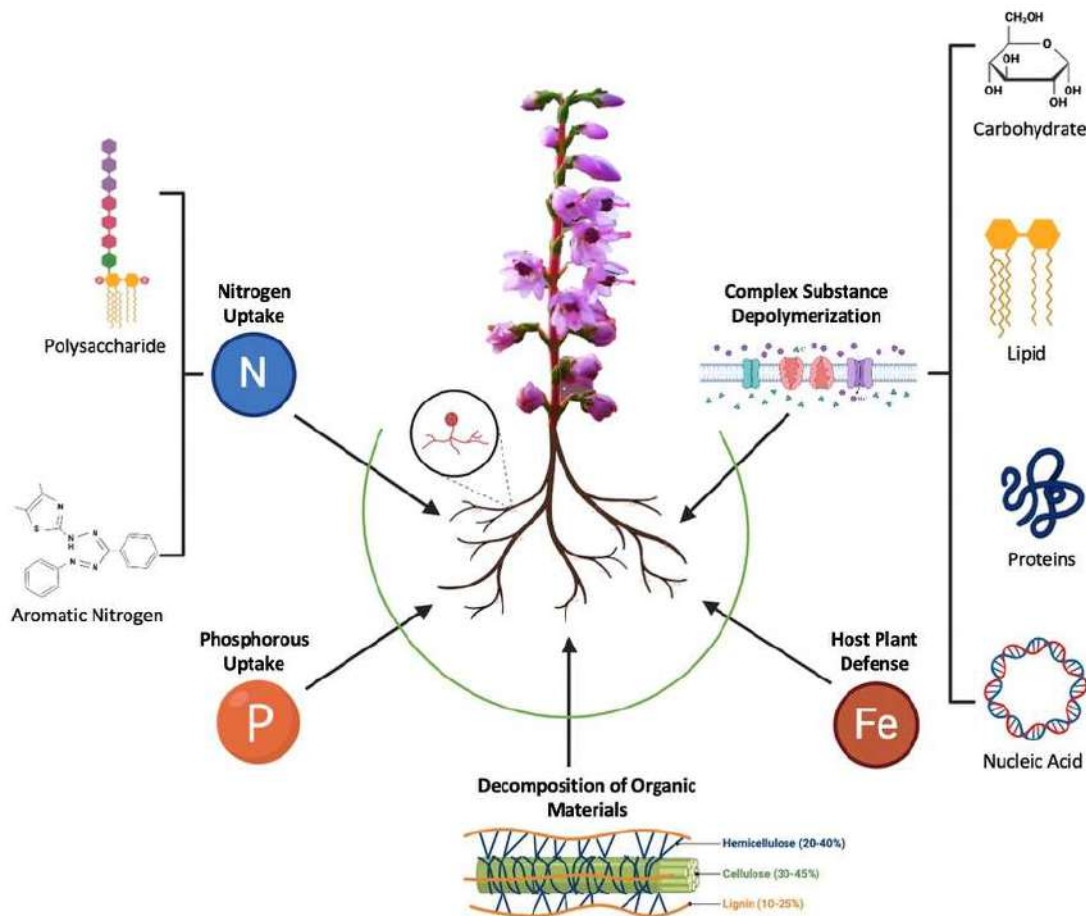


Fig. 5: Various roles of Ericoid Mycorrhiza (ErM) in the symbiotic relationship between ErM and host plant from *Ericaceae*.

(Grelet et al. 2005). Variations in absorption kinetics may be the cause of the growth disparities across strains under conditions of high carbon supply (Grelet et al. 2005).

Compared to plants without mycorrhizal associations, mycorrhizal plants are widely accessible to organic nitrogen (Schimel & Bennett 2004). Several processes are necessary for the direct intake of monomers- and oligomers by mycorrhizal fungi, intrinsic modification of organic nitrogen, and translocation throughout the fungus—host plant interaction for organic nitrogen to be taken up by ErM fungi and then transferred to the plant (Talbot & Treseder 2010). Aliphatic-N, which includes aromatic-nitrogen, and polysaccharide-nitrogen, which includes the substances found in humus, are the two main types of organic nitrogen compounds that are available in the soil (Roberts & Jones 2008). Depending upon how much organic nitrogen is present in the soil, it is possible for mycorrhizal roots to be exposed to as much or more organic nitrogen than inorganic nitrogen in most soils (Talbot & Treseder 2010). Depending on the fungus and plant species, different kinds of organic

nitrogen may be given to the plant; asparagine, glutamine, and alanine are the three most common types (Chalot & Brun 1998). ErM fungi like *Rhizoscyphus ericae*, which can produce a wide range of extracellular enzymes, are dominant in systems with high efficiency of organic nitrogen uptake (Cairney & Meharg 2003, et al. 2006).

## 2) Phosphorus Nutrition

As evidenced by the consistent finding that mycorrhizal plants pile up so much phosphorus than non-mycorrhizal plants, the formation of symbiotic frameworks of mycorrhizal fungi is thought to be the most common approach to enhance plant Phosphorus uptake to get around the limitation of phosphorus within the rhizosphere (Smith et al. 2000, Burleigh et al. 2002, Tibbett & Sanders 2002, Smith & Read 2010). The major process is the expansion of added hyphae's capacity to penetrate through the phosphorus depletion layer surrounding the roots and acquire new locations with accessible P. This results in an increase in phosphorus absorption *via* fungal phosphorus carriers located at the fungal-soil interface.

The capacity of ErM fungi to utilize phosphorus bonded to soluble metal phosphates that are not organic has not been extensively studied. Numerous ericoid mycorrhizal fungi were examined by Van Leerdam et al. (2001) for their capacity for solubilizing phosphate. The majority of isolates could dissolve the rock phosphate hydroxyapatite when ammonium was added. None of the isolates were able to dissolve fluorapatite when a nitrogen source was used.

### 3) To Defend the Host Plant Against Harmful Circumstances

The majority of research on ericoid mycorrhizal nutrition has been phosphorus and nitrogen-centric. However, few have also discussed the increased consumption of essential and non-essential nutrients, for example, regulating the amount of iron taken up by host plants having a mutualistic relationship with *Hymenoscyphus ericae* (Shaw & Read 1989). Even in the presence of relatively small external amounts of iron, this fungus displays a strong attraction for it (Smith & Read 2010). The discharge of siderophores specific to iron (Fe) may control iron intake (Schuler & Haselwandter 1988). A decrease in metal concentration within host shoots is related to mycorrhizal protection of the host. These metal ions are utilized by many pathogenic microbes. However, sequestration of these metals, like Fe by ErM indirectly provides the host plant protection. According to Bradley et al. (1982), the mycorrhizal root system's ability to sequester metals or process of selectivity at the mycorrhizal root may be a cause of the decrease in shoot copper accumulation (Gibson & Mitchell 2004, 2005(a), 2005(b)). Both the plant and the fungus would be safeguarded by the mechanism of exclusion working on the mycorrhiza root. By preventing the flow of metal ions, the development of hyphae covered in mucilaginous slime may function as a mechanism of exclusion (Denny & Ridge 1995). Ultra-structural studies (Duddridge & Read 1982) show that the binding of metals inside the mycorrhizal root system has been confirmed by pectin in the interfacial layer dividing fungus and plant plasma membranes inside the invaded cells.

The defense against positively charged metals has been discussed in the majority of studies. However, the use of now-banned pesticides has caused a lot of soils to become contaminated with organic arsenic compounds (Meharg & Hartley, Whitaker 2002). It has been experimented that the *C. vulgaris*/*H. ericae* combination may thrive on arsenate-rich sites (Sharples et al. 2000(a)) and is protected by fungi that are tolerant to arsenic (Sharples et al. 2000(b)). Because arsenate metal is a phosphate counterpart, the phosphorus co-transporter system carries it across the plasma membrane (Meharg & Macnair 1992). Ericoid mycorrhizal fungi that are resistant to arsenate are ejected from mycelium without

competing with the transport of phosphate, changing arsenate to arsenite (Sharples et al. 2000a, 2000b, 2001).

Therefore, under selective pressure, new or altered phenotypic features may result in increased metal tolerance in ErM fungus. Given that each cell's genetic makeup determines its phenotype, alterations in genetic sequences and arrangement may have emerged in ErM fungi that have evolved to external metal toxicity. Many environmental conditions are known to produce mutations either through direct or indirect means by forming reactive oxygen compounds, which is one of the main drivers of genetic variation (Hartwig et al. 2002).

### 4) Decomposition of Organic Materials

According to Lindahl & Tunlid (2015) and Zak et al. (2019), Mycorrhizal fungi differ from saprotrophs, which are free-living and primarily get carbon through plant photosynthetic pigments rather than through the breakdown of organic components. It is possible to assess and contrast the inherent saprotrophic capacity of various species and functional groupings using the variety and richness of such genes. However, some mycorrhizal fungi have genes that produce extracellular enzymes needed in the breakdown of the organic materials. Kohler et al. (2015), Op De Beeck et al. (2018), and Nicolás et al. (2019) claim that some mycorrhizal fungi employ oxidative and non-enzymatic mechanisms to extract nitrogen from organic substances by partial degradation of lignocellulose.

It has been proven that ErMFs have the capacity to speed up the degradation of organic materials. Two distinct enzyme types can be secreted by ErMFs. The first kind has the ability to break down hemicellulose, cellulose, tannic acid, polyphenols, and lignin, which can hasten the dissolution of essential nutrient compounds. The other form encourages direct uptake of nutrients (Cairney & Burke 1998, Read & Perez-Moreno 2003).

### 5) Complex Substrates Depolymerization

A variety of extracellular enzymes produced by ericoid fungi catalyze the breakdown of numerous organic macromolecules and provide plants with the ability to cut down the bi-products of complex polymers that plant leaves or roots cannot digest (Read & Perez-Moreno 2003). This capability seems to be especially crucial in systems with little nitrogen since there is not enough mineralization to meet plant demand for nitrogen (Schimel & Bennett 2004). Enzymes that degrade polymers can be distinguished into two (Read et al. 2004). The primary class contains numerous 'hydrolases' that cleave the molecules containing nutrients themselves. These enzymes include *polyphenol oxidases* and *lignases*, which are anticipated to contribute significantly to both plant nutrition

and the decomposition of litter. The other class improves the uptake of nutrients by destroying biological compounds, including tannins, polyphenols, and lignins, which could precipitate vital elements. In addition to this, *chitinases* and *proteases* conduct phenol oxidase activities that may make it easier for hosts to access phosphorus and nitrogen from dormant plant parts or complexes of polyphenols in the soil. These hydrolytic enzymes break down cell wall polysaccharides like cellulose, hemicelluloses, and pectin.

It is understood that the ErM fungus produces *polyphenol oxidases* (Burke & Cairney 2002). This enzyme, which exhibits a significant amount of overlap in substrate affinities, includes laccase, catechol oxidase, and tyrosinase (Burke & Cairney 2002). *R. ericae* generates *laccase* with a variety of phenol-associated-oxidizing activity (Burke & Cairney 2002). It is hypothesized that *laccases*, which are produced by ErM fungi, might be involved in numerous varieties of symbiotic functions. The nutrition of plants in phenol-rich contexts is greatly influenced by ErM fungi's capacity to utilize a variety of monomeric phenol-rich compounds as their carbon source (Leake & Read 1991) and the ability to release the enzymes *catechol oxidase* and *laccase*. (Bending & Read 1996 a,b), that are associated with the degradation of hydrolyzable polyphenols.

## CONCLUSION AND FUTURE PROSPECTS

The literature survey sheds light on the fact that ErM is understudied. ErM is known to help its host in Nitrogen and phosphorus uptake, decomposition of organic material, complex substrates depolymerization, and to defend host plants against harmful substances. Most of the molecular studies done to date are based on ITS region (found in all the Eukaryotes). However, it does not shed light on the molecular diversity of the ErM. To explore the genetic diversity, we should start targeting the variable regions, conserved only for ericoid mycorrhizae. The incorporation of genomics tools can be useful to study the functionality of various ErM genes. The phylogeny of ErM needs to be studied in depth, which can help to understand its evolutionary path and further trace its distribution. The cultural nature of ErM provides a huge advantage in carrying out various studies that remain unexplored in the world of ErM symbionts.

## REFERENCES

- Allen, T.R., Millar, T., Berch, S.M. and Berbee, M.L., 2003. Culturing and direct DNA extraction find different fungi from the same ericoid mycorrhizal roots. *New Phytologist*, 157(2), pp.255–272. DOI.
- Bending, G.D. and Read, D.J., 1996a. Effects of the soluble polyphenol tannic acid on the activities of ericoid and ectomycorrhizal fungi. *Soil Biology and Biochemistry*, 28(12), pp.1595–1602. DOI.
- Bending, G.D. and Read, D.J., 1996b. Nitrogen mobilization from protein-polyphenol complex by ericoid and ectomycorrhizal fungi. *Soil Biology and Biochemistry*, 28(12), pp.1603–1612. DOI.
- Berch, S.M., Allen, T.R. and Berbee, M.L., 2002. Molecular detection, community structure and phylogeny of ericoid mycorrhizal fungi. In: *Diversity and Integration in Mycorrhizas*. Proceedings of the 3rd International Conference on Mycorrhizas (ICOM3), Adelaide, Australia, 8–13 July 2001, pp.55–66. Springer Netherlands. DOI.
- Bergero, R., Perotto, S., Girlanda, M., Vidano, G. and Luppi, A.M., 2000. Ericoid mycorrhizal fungi are common root associates of a Mediterranean ectomycorrhizal plant (*Quercus ilex*). *Molecular Ecology*, 9(10), pp.1639–1649. DOI.
- Bonfante-Fasolo, P. and Gianinazzi-Pearson, V., 1979. Ultrastructural aspects of endomycorrhiza in the Ericaceae: Naturally infected hair roots of *Calluna vulgaris* L. Hull. *New Phytologist*, 83(3), pp.739–744. DOI.
- Bonfante-Fasolo, P., 1980. Occurrence of a basidiomycete in living cells of mycorrhizal hair roots of *Calluna vulgaris*. *Transactions of the British Mycological Society*, 75(2), pp.320–325. DOI.
- Bonfante-Fasolo, P., Perotto, S., Testa, B. and Faccio, A., 1987. Ultrastructural localization of cell surface sugar residues in ericoid mycorrhizal fungi by gold-labeled lectins. *Protoplasma*, 139(1), pp.25–35. DOI.
- Bradley, R., Burt, A.J. and Read, D.J., 1982. The biology of mycorrhiza in the Ericaceae: VIII. The role of mycorrhizal infection in heavy metal resistance. *New Phytologist*, 91(2), pp.197–209. DOI.
- Brundrett, M.C., 2002. Coevolution of roots and mycorrhizas of land plants. *New Phytologist*, 154(2), pp.275–304. DOI.
- Burke, R. and Cairney, J., 2002. Laccases and other polyphenol oxidases in ecto- and ericoid mycorrhizal fungi. *Mycorrhiza*, 12(3), pp.105–116. DOI.
- Burleigh, S.H., Cavagnaro, T. and Jakobsen, I., 2002. Functional diversity of arbuscular mycorrhizas extends to the expression of plant genes involved in P nutrition. *Journal of Experimental Botany*, 53(374), pp.1593–1601. DOI.
- Cairney, J.W. and Meharg, A.A., 2003. Ericoid mycorrhiza: A partnership that exploits harsh edaphic conditions. *European Journal of Soil Science*, 54(4), pp.735–740. DOI.
- Cairney, J.W.G. and Burke, R.M., 1998. Extracellular enzyme activities of the ericoid mycorrhizal endophyte *Hymenoscyphus ericae* (Read) Korf & Kernan: their likely roles in decomposition of dead plant tissue in soil. *Plant and Soil*, 205(2), pp.181–192.
- Chalot, M. and Brun, A., 1998. Physiology of organic nitrogen acquisition by ectomycorrhizal fungi and ectomycorrhizas. *FEMS Microbiology Reviews*, 22(1), pp.21–44.
- Denny, H.J. and Ridge, I., 1995. Fungal slime and its role in the mycorrhizal amelioration of zinc toxicity to higher plants. *New Phytologist*, 130(2), pp.251–257. DOI.
- Duddridge, J.A. and Read, D.J., 1982. Ultrastructural analysis of the development of mycorrhizas in *Monotropa Hypopitys* L. *New Phytologist*, 92(2), pp.203–214. DOI.
- Englander, L. and Hull, R.J., 1980. Reciprocal transfer of nutrients between ericaceous plants and a *Clavaria* sp. *New Phytologist*, 84(4), pp.661–667. DOI.
- Gibson, B.R. and Mitchell, D.T., 2004. Nutritional influences on the solubilization of metal phosphate by ericoid mycorrhizal fungi. *Mycological Research*, 108(8), pp.947–954. DOI.
- Gibson, B.R. and Mitchell, D.T., 2005. Influence of pH on copper and zinc sensitivity of ericoid mycobionts *in vitro*. *Mycorrhiza*, 15, pp.231–234. DOI.
- Gibson, B.R. and Mitchell, D.T., 2005. Phosphatases of ericoid mycorrhizal fungi: Kinetic properties and the effect of copper on activity. *Mycological Research*, 109(4), pp.478–486. DOI.
- Grelet, G.A., Meharg, A.A. and Alexander, I.J., 2005. Carbon availability affects nitrogen source utilisation by *Hymenoscyphus ericae*. *Mycological Research*, 109(4), pp.469–477. DOI.



- Hambleton, S. and Currah, R.S., 1997. Fungal endophytes from the roots of alpine and boreal Ericaceae. *Canadian Journal of Botany*, 75(9), pp.1570–1581. DOI.
- Hambleton, S. and Sigler, L., 2005. *Melinomyces*, a new anamorph genus for root-associated fungi with phylogenetic affinities to *Rhizoscyphus ericae* (*Hymenoscyphus ericae*), Leotiomyces. *Studies in Mycology*, 53(1), pp.1–27.
- Harley, J.L. and Smith, S.E., 1983. *Mycorrhizal Symbiosis*. Academic Press, US. DOI.
- Hartwig, U.A., Wittmann, P., Braun, R., Hartwig-Räz, B., Jansa, J., Mozafar, A. and Nösberger, J., 2002. Arbuscular mycorrhiza infection enhances the growth response of *Lolium perenne* to elevated atmospheric pCO<sub>2</sub>. *Journal of Experimental Botany*, 53(371), pp.1207–1213. DOI.
- Haselwandter, K., 1997. Soil micro-organisms, mycorrhiza, and restoration ecology. *Restoration Ecology and Sustainable Development*, 19, pp.65–80. DOI.
- Hibbett, D.S. and Thorn, R.G., 2001. Basidiomycota: Homobasidiomycetes. In *Systematics and Evolution* (pp.121–168). Berlin, Heidelberg: Springer Berlin Heidelberg. DOI.
- Hynson, N.A. and Bruns, T.D., 2009. Evidence of a myco-heterotroph in the plant family Ericaceae that lacks mycorrhizal specificity. *Proceedings of the Royal Society B: Biological Sciences*, 276(1675), pp.4053–4059. DOI.
- Kohler, A., Kuo, A., Nagy, L.G., Morin, E., Barry, K.W., Buscot, F. and Martin, F., 2015. Convergent losses of decay mechanisms and rapid turnover of symbiosis genes in mycorrhizal mutualists. *Nature Genetics*, 47(4), pp.410–415. DOI.
- Kohout, P., 2017. Biogeography of ericoid mycorrhiza. In: *Biogeography of Mycorrhizal Symbiosis*, pp.179–193. DOI.
- Krpata, D., Mühlmann, O., Kuhnert, R., Ladurner, H., Göbl, F. and Peintner, U., 2007. High diversity of ectomycorrhizal fungi associated with *Arctostaphylos uva-ursi* in subalpine and alpine zones: potential inoculum for afforestation. *Forest Ecology and Management*, 250(3), pp.167–175. DOI.
- Leake, J.R. and Read, D.J., 1991. 20 experiments with ericoid mycorrhiza. In: *Methods in Microbiology*, 23, pp.435–459. Academic Press. DOI.
- Leopold, D.R., 2016. Ericoid fungal diversity: Challenges and opportunities for mycorrhizal research. *Fungal Ecology*, 24, pp.114–123. DOI.
- Leopold, D.R., Peay, K.G., Vitousek, P.M. and Fukami, T., 2021. Diversity of putative ericoid mycorrhizal fungi increases with soil age and progressive phosphorus limitation across a 4.1-million-year chronosequence. *FEMS Microbiology Ecology*, 97(3), fiab016. DOI.
- Lindahl, B.D. and Tunlid, A., 2015. Ectomycorrhizal fungi—potential organic matter decomposers, yet not saprotrophs. *New Phytologist*, 205(4), pp.1443–1447. DOI.
- Massicotte, H.B., Melville, L.H. and Peterson, R.L., 2005. Structural characteristics of root fungal interactions for five ericaceous species in Eastern Canada. *Canadian Journal of Botany*, 83(8), pp.1057–1064. DOI.
- McLean, C.B., Cunnington, J.H. and Lawrie, A.C., 1999. Molecular diversity within and between ericoid endophytes from the Ericaceae and Epacridaceae. *New Phytologist*, 144(2), pp.351–358. DOI.
- Meharg, A.A. and Hartley-Whitaker, J., 2002. Arsenic uptake and metabolism in arsenic-resistant and nonresistant plant species. *New Phytologist*, 154(1), pp.29–43. DOI.
- Meharg, A.A. and Macnair, M.R., 1992. Suppression of the high-affinity phosphate uptake system: A mechanism of arsenate tolerance in *Holcus lanatus* L. *Journal of Experimental Botany*, 43(4), pp.519–524. DOI.
- Midgley, D.J., Jordan, L.A., Saleeba, J.A. and McGee, P.A., 2006. Utilisation of carbon substrates by orchid and ericoid mycorrhizal fungi from Australian dry sclerophyll forests. *Mycorrhiza*, 16, pp.175–182. DOI.
- Monreal, M., Berch, S.M. and Berbee, M., 2000. Molecular diversity of ericoid mycorrhizal fungi. *Canadian Journal of Botany*, 77(11), pp.1580–1594. DOI.
- Mueller, W.C., Tessier, B.J. and Englander, L., 1986. Immunocytochemical detection of fungi in the roots of *Rhododendron*. *Canadian Journal of Botany*, 64(4), pp.718–723. DOI.
- Nicolás, C., Martin-Bertelsen, T., Floudas, D., Bentzer, J., Smits, M., Johansson, T. et al., 2019. The soil organic matter decomposition mechanisms in ectomycorrhizal fungi are tuned for liberating soil organic nitrogen. *The ISME Journal*, 13(4), pp.977–988. DOI.
- OpDeBeeck, M., Troein, C., Peterson, C., Persson, P. and Tunlid, A., 2018. Fenton reaction facilitates organic nitrogen acquisition by an ectomycorrhizal fungus. *New Phytologist*, 218(1), pp.335–343. DOI.
- Pearson, V. and Read, D.J., 1973. The biology of mycorrhiza in the Ericaceae: I. The isolation of the endophyte and synthesis of mycorrhizas in aseptic culture. *New Phytologist*, 72(2), pp.371–379. DOI.
- Peretto, R., Bettini, V. and Bonfante, P., 1993. Evidence of two polygalacturonases produced by a mycorrhizal ericoid fungus during its saprophytic growth. *FEMS Microbiology Letters*, 114(1), pp.85–91. DOI.
- Perotto, S. and Bonfante, P., 1998. Genetic and functional diversity of ericoid mycorrhizal fungi. *Symbiosis*.
- Perotto, S., Actis-Perino, E., Perugini, J. and Bonfante, P., 1996. Molecular diversity of fungi from ericoid mycorrhizal roots. *Molecular Ecology*, 5(1), pp.123–131. DOI.
- Perotto, S., Daghighi, S. and Martino, E., 2018. Ericoid mycorrhizal fungi and their genomes: Another side to the mycorrhizal symbiosis?. *New Phytologist*, 220(4), pp.1141–1147. DOI.
- Perotto, S., Giralanda, M. and Martino, E., 2002. Ericoid mycorrhizal fungi: Some new perspectives on old acquaintances. In: *Diversity and Integration in Mycorrhizas: Proceedings of the 3rd International Conference on Mycorrhizas (ICOM3) Adelaide, Australia, 8–13 July 2001*, pp.41–53. Springer Netherlands. DOI.
- Perotto, S., Martino, E., Abbà, S. and Vallino, M., 2012. Genetic diversity and functional aspects of ericoid mycorrhizal fungi. In: *Fungal Associations*, pp.255–285. Berlin, Heidelberg: Springer Berlin Heidelberg. DOI.
- Peterson, R.L., Massicotte, H.B. and Melville, L.H., 2004. *Mycorrhizas: Anatomy and Cell Biology*. NRC Research Press. DOI.
- Peterson, T.A., Mueller, W.C. and Englander, L., 1980. Anatomy and ultrastructure of a *Rhododendron* root–fungus association. *Canadian Journal of Botany*, 58(23), pp.2421–2433. DOI.
- Pirozynski, K.A. and Malloch, D.W., 1975. The origin of land plants: a matter of mycotrophism. *Biosystems*, 6(3), pp.153–164. DOI.
- Plett, J.M. and Martin, F., 2011. Blurred boundaries: lifestyle lessons from ectomycorrhizal fungal genomes. *Trends in Genetics*, 27(1), pp.14–22. DOI.
- Read, D.J. and Perez-Moreno, J., 2003. Mycorrhizas and nutrient cycling in ecosystems—a journey towards relevance? *New Phytologist*, 157(3), pp.475–492. DOI.
- Read, D.J., 1996. The structure and function of the ericoid mycorrhizal root. *Annals of Botany*, 77(4), pp.365–374. DOI.
- Read, D.J., Leake, J.R. and Perez-Moreno, J., 2004. Mycorrhizal fungi as drivers of ecosystem processes in heathland and boreal forest biomes. *Canadian Journal of Botany*, 82(8), pp.1243–1263. DOI.
- Redecker, D. and Raab, P., 2006. Phylogeny of the Glomeromycota (arbuscular mycorrhizal fungi): recent developments and new gene markers. *Mycologia*, 98(6), pp.885–895. DOI.
- Roberts, P. and Jones, D.L., 2008. Critical evaluation of methods for determining total protein in soil solution. *Soil Biology and Biochemistry*, 40(6), pp.1485–1495. DOI.
- Schimel, J.P. and Bennett, J., 2004. Nitrogen mineralization: challenges of a changing paradigm. *Ecology*, 85(3), pp.591–602. DOI.
- Schuler, R. and Haselwandter, K., 1988. Hydroxamate siderophore production by ericoid mycorrhizal fungi. *Journal of Plant Nutrition*, 11(6–11), pp.907–913. DOI.
- Seviour, R.J., Willing, R.R. and Chilvers, G.A., 1973. Basidiocarps associated with ericoid mycorrhizas. *New Phytologist*, 72(2), pp.381–385. DOI.



- Sharples, J.M., Chambers, S.M., Meharg, A.A. and Cairney, J.W.G., 2000a. Genetic diversity of root-associated fungal endophytes from *Calluna vulgaris* at contrasting field sites. *New Phytologist*, 148(1), pp.153-162. DOI
- Sharples, J.M., Meharg, A.A., Chambers, S.M. and Cairney, J.W., 2000b. Mechanism of arsenate resistance in the ericoid mycorrhizal fungus *Hymenoscyphus ericae*. *Plant Physiology*, 124(3), pp.1327-1334. DOI
- Sharples, J.M., Meharg, A.A., Chambers, S.M. and Cairney, J.W., 2001. Arsenate resistance in the ericoid mycorrhizal fungus *Hymenoscyphus ericae*. *New Phytologist*, 151(1), pp.265-270. DOI
- Sharples, J.M., Meharg, A.A., Chambers, S.M. and Cairney, J.W.G., 2000c. Symbiotic solution to arsenic contamination. *Nature*, 404(6781), pp.951-952. DOI
- Shaw, G. and Read, D.J., 1989. The biology of mycorrhiza in the Ericaceae: XIV. Effects of iron and aluminium on the activity of acid phosphatase in the ericoid endophyte *Hymenoscyphus ericae* (Read) Korf and Kernan. *New Phytologist*, 113(4), pp.529-533. DOI
- Sigler, L. and Gibas, C.F.C., 2005. Utility of a cultural method for identification of the ericoid mycobiont *Oidiodendron maius* confirmed by ITS sequence analysis. *Studies in Mycology*, 53(1), pp.63-74. DOI
- Smith, F.A., Jakobsen, I. and Smith, S.E., 2000. Spatial differences in acquisition of soil phosphate between two arbuscular mycorrhizal fungi in symbiosis with *Medicago truncatula*. *New Phytologist*, 147(2), pp.357-366. DOI
- Smith, S.E. and Read, D.J., 1997. *Mycorrhizal Symbiosis*. 2nd edn. Academic Press. DOI
- Smith, S.E. and Read, D.J., 2010. *Mycorrhizal Symbiosis*. Academic Press.
- Straker, C.J. and Mitchell, D.T., 1986. The activity and characterization of acid phosphatases in endomycorrhizal fungi of the Ericaceae. *New Phytologist*, 104(2), pp.243-256. DOI
- Straker, C.J., 1996. Ericoid mycorrhiza: Ecological and host specificity. *Mycorrhiza*, 6, pp.215-225. DOI
- Straker, C.J., Gianinazzi-Pearson, V., Gianinazzi, S., Cleyet-Marel, J.C. and Bousquet, N., 1989. Electrophoretic and immunological studies on acid phosphatase from a mycorrhizal fungus of *Erica hispidula* L. *New Phytologist*, 111(2), pp.215-221. DOI
- Talbot, J.M. and Treseder, K.K., 2010. Controls over mycorrhizal uptake of organic nitrogen. *Pedobiologia*, 53(3), pp.169-179. DOI
- Tibbett, M. and Sanders, F., 2002. Ectomycorrhizal symbiosis can enhance plant nutrition through improved access to discrete organic nutrient patches of high resource quality. *Annals of Botany*, 89(6), pp.783-789. DOI
- Trappe, J.M. and Berch, S.M., 1985. The prehistory of mycorrhizae: A.B. Frank's predecessors. In: *6th North American Conference on Mycorrhizae, Bend, Oregon (USA), 25-29 Jun 1984*. Oregon State University, Forest Research Laboratory.
- Van Der Heijden, M.G., Bardgett, R.D. and VanStraalen, N.M., 2008. The unseen majority: soil microbes as drivers of plant diversity and productivity in terrestrial ecosystems. *Ecology Letters*, 11(3), pp.296-310. DOI
- Van der Heijden, M.G., Martin, F.M., Selosse, M.A. and Sanders, I.R., 2015. Mycorrhizal ecology and evolution: the past, the present, and the future. *New Phytologist*, 205(4), pp.1406-1423.
- Van Leerdam, D.M., Williams, P.A. and Cairney, J.W., 2001. Phosphate-solubilising abilities of ericoid mycorrhizal endophytes of *Woollisia pungens* (Epacridaceae). *Australian Journal of Botany*, 49(1), pp.75-80. DOI
- Varma, A. and Bonfante, P., 1994. Utilization of cell-wall related carbohydrates by ericoid mycorrhizal endophytes. *Symbiosis*.
- Vohnik, M., 2020. Ericoid mycorrhizal symbiosis: Theoretical background and methods for its comprehensive investigation. *Mycorrhiza*, 30(6), pp.671-695. DOI
- Vohnik, M., Sadowsky, J.J., Kohout, P., Lhotakova, Z., Nestby, R. and Kolařík, M., 2012. Novel root-fungus symbiosis in Ericaceae: sheathed ericoid mycorrhiza formed by a hitherto undescribed basidiomycete with affinities to Trechisporales. *PLoS One*, 7(6), e39524. DOI
- Vrålstad, T., Fossheim, T. and Schumacher, T., 2000. *Piceirhiza bicolorata* – the ectomycorrhizal expression of the *Hymenoscyphus ericae* aggregate?. *New Phytologist*, 145(3), pp.549-563. DOI
- Vrålstad, T., Myhre, E. and Schumacher, T., 2002. Molecular diversity and phylogenetic affinities of symbiotic root-associated ascomycetes of the Helotiales in burnt and metal polluted habitats. *New Phytologist*, 155(1), pp.131-148. DOI
- Vrålstad, T., Schumacher, T. and Taylor, A.F., 2002. Mycorrhizal synthesis between fungal strains of the *Hymenoscyphus ericae* aggregate and potential ectomycorrhizal and ericoid hosts. *New Phytologist*, 153(1), pp.143-152. DOI
- Walker, J.F., Aldrich-Wolfe, L., Riffel, A., Barbare, H., Simpson, N.B., Trowbridge, J. and Jumpponen, A., 2011. Diverse Helotiales associated with the roots of three species of Arctic Ericaceae provide no evidence for host specificity. *New Phytologist*, 191(2), pp.515-527. DOI
- Weiß, M., Bauer, R. and Begerow, D., 2004. Spotlights on heterobasidiomycetes. In: *Frontiers in Basidiomycote Mycology* (R. Agerer, M. Piepenbring and P. Blanz, eds), pp.7-48. IHW Verlag, Eching.
- Weiß, M., Waller, F., Zuccaro, A. and Selosse, M.A., 2016. Sebaciales – one thousand and one interactions with land plants. *New Phytologist*, 211(1), pp.20-40. DOI
- Xiao, G. and Berch, S.M., 1992. Ericoid mycorrhizal fungi of *Gaultheria shallon*. *Mycologia*, 84(3), pp.470-471. DOI
- Xiao, G. and Berch, S.M., 1995. The ability of known ericoid mycorrhizal fungi to form mycorrhizae with *Gaultheria shallon*. *Mycologia*, 87(4), pp.467-470. DOI
- Xiao, G. and Berch, S.M., 1996. Diversity and abundance of ericoid mycorrhizal fungi of *Gaultheria shallon* on forest clearcuts. *Canadian Journal of Botany*, 74(3), pp.337-346. DOI
- Yang, H., Zhao, X., Li, L. and Zhang, J., 2020. Detecting the colonization of ericoid mycorrhizal fungi in *Vaccinium uliginosum* using in situ polymerase chain reaction and green fluorescent protein. *Plant Methods*, 16, pp.1-8. DOI
- Yang, H., Zhao, X., Liu, C., Bai, L., Zhao, M. and Li, L., 2018. Diversity and characteristics of colonization of root-associated fungi of *Vaccinium uliginosum*. *Scientific Reports*, 8(1), pp.15283. DOI
- Zak, D.R., Pellitier, P.T., Argiroff, W., Castillo, B., James, T.Y., Nave, L.E. and Tunlid, A., 2019. Exploring the role of ectomycorrhizal fungi in soil carbon dynamics. *New Phytologist*, 223(1), pp.33-39. DOI
- Zhang, Y.H. and Zhuang, W.Y., 2004. Phylogenetic relationships of some members in the genus *Hymenoscyphus* (Ascomycetes, Helotiales). *Nova Hedwigia*, 78(3), pp.475-484. DOI

# Delineation of Potential Groundwater Zones Using GIS-based Fuzzy AHP Technique for Urban Expansion in the Southwestern Fringe of Guwahati City, India

Rakesh Kumar Sarmah<sup>†</sup>  and Santanu Sarma 

Department of Geology, Cotton University, Guwahati-781001, Assam, India

<sup>†</sup>Corresponding author: Rakesh Kumar Sarmah; rakeshassam86@gmail.com

**Abbreviation:** Nat. Env. & Poll. Technol.

**Website:** [www.neptjournal.com](http://www.neptjournal.com)

*Received:* 21-06-2024

*Revised:* 31-07-2024

*Accepted:* 07-08-2024

## Key Words:

Groundwater potential zones

Groundwater recharge

GIS

Fuzzy AHP

Urban Expansion

## ABSTRACT

Due to unprecedented urban growth many localities within the heart of Guwahati city witness groundwater scarcity, mainly during the dry seasons. This study aims to identify potential groundwater zones in the southwestern fringe of the city where the Guwahati Metropolitan Development Authority (GMDA) has adopted plans for future expansion. Rani and Chayani Barduar are two administrative blocks adjacent to the city, possessing a vast tract of unsettled agricultural land ideal for future township development. Multi-criteria decision-making technique using a Fuzzy Analytical Hierarchy Process (FAHP) in a Remote Sensing and Geographic Information System (GIS) environment is used to produce the groundwater potential map. A total of eight thematic layers important for groundwater recharge: lithology, geomorphology, slope, rainfall, lineament density, soil, drainage density, and Land Use Land Cover are prepared using satellite data, fieldwork, and other suitable techniques and used as input. The study area is classified into five groundwater potential zones – very high (42.52 %), high (28.67 %), moderate (17.23%), poor (10.21 %), and very poor (1.37%). Validation of the result using a yield map derived from the exploratory wells of the Central Ground Water Board (CGWB) shows strong agreement with the prediction accuracy (AUC = 73.36%). Field-derived water level data also show a high negative correlation ( $R^2 = 0.71$ ) with yield data indicating high specific yield in wells with shallow water levels. The study results will help planners and policymakers with future urban development strategies and sustainable groundwater management practices.

## Citation for the Paper:

Sarmah, R.K. and Sarma, S., 2025. Delineation of potential groundwater zones using GIS-based fuzzy AHP technique for urban expansion in the southwestern fringe of Guwahati City, India. *Nature Environment and Pollution Technology*, 24(2), p.B4233. <https://doi.org/10.46488/NEPT.2025.v24i02.B4233>

*Note: From year 2025, the journal uses Article ID instead of page numbers in citation of the published articles.*



**Copyright:** © 2025 by the authors

**Licensee:** Technoscience Publications

This article is an open access article distributed under the terms and conditions of the Creative Commons Attribution (CC BY) license (<https://creativecommons.org/licenses/by/4.0/>).

## INTRODUCTION

Groundwater is a vital renewable resource that requires proper management to ensure long-term use (Mays 2013). Though groundwater occupies only a small portion (0.06%) of Earth's available water, it is the most critical freshwater source used for drinking purposes (Schwartz & Zhang 2002). The expanding population, unscientific exploitation, and improper management of groundwater in developing countries have led to the deterioration of both quality and quantity and thus demand a critical assessment for sustainable management (Tolche 2021). Groundwater will be the key parameter in achieving many of the Sustainable Development Goals targeted by the United Nations (Guppy et al. 2018). The underground water stock depends on percolation through porous spaces of soils and rocks, which in turn determines urban water supply and agricultural activity (Da Costa et al. 2019). Assessment of groundwater potential zones is important to counteract water scarcity problems caused by various factors such as rapid urbanization, climate change, uneven distribution of water resources, etc. (Raju et al. 2019). In India, about 400 million people live in urban areas, resulting in changes in LULC, including deforestation and an increase in impervious surfaces affecting groundwater recharge and thus causing an acute shortage of water (Roy et al. 2022). Guwahati,

the gateway to northeast India, is one of the fastest-growing cities in India. Guwahati had a population of 43,615 (1951 census) and subsequently increased to 9,63,429 in the 2011 census (Desai et al. 2014). It is estimated that Guwahati will house approximately 22 lakh residents by 2025. To tackle this rapidly growing scenario, the Guwahati Metropolitan Development Authority (GMDA) has adopted specific Master Plans for Greater Guwahati with extended spatial periphery to previously untouched rural areas. The greater Guwahati metropolitan area, which presently covers an area of 262 sq. km, is going to cover 328 square kilometers by 2025 (GMA 2025). Topographically the south-western fringe of Guwahati city has vast tracts of unsettled agricultural land and thus is ideal for future expansion. Urbanization will come with different facets, such as industrialization, sprawl, waste management, irrigation, contamination, and their complex interactions. Thus an assessment of the groundwater potential zone is mandatory for the city planners to counteract any future negative consequences. The integrated use of remote sensing and Geographic Information Systems (GIS) in groundwater studies has been well documented in various literature (Nas & Berktaş 2008, Moghaddam et al. 2013, Rahmati et al. 2014, Freitas et al. 2019, Sandoval & Tiburan Jr. 2019, Gaurav & Singh 2022, Sabale et al. 2024, Rehman et al. 2024, Ganesan & Subramaniyan, 2024, Sharma et al. 2024), especially due to its time and cost-effectiveness (Kumar et al. 2016). Researchers have adopted different multivariate statistical techniques in estimating groundwater potential; however, the Analytical Hierarchy Process (AHP)

is preferred due to its ease of integration with remote sensing and the GIS environment (Celik 2019, Dar et al. 2020, Lentswe & Molwalefhe 2020, Bennia et al. 2023, Hilal et al. 2024). GIS plays a vital role in spatial decision-making, where a large number of alternatives need to be analyzed (Rikalovic et al. 2014). Though the Analytical Hierarchy Process (AHP), developed by Saaty, is one of the most versatile decision-making techniques that has been used to solve complex problems involving competition for multiple choices (Rezaei & Tahsili 2018), there is a chance of vagueness and uncertainty in crisp judgment by human reasoning which can be overcome by introducing fuzziness to the process (Torabi-Kaveh et al. 2016). Fuzzy set theory is a specially designed mathematical tool to deal with such uncertainty, vagueness, and imprecision (Kahraman et al. 2004). It was originally introduced by Lotfi Zadeh in the 1960s with the implementation of classes or groups of data that are not sharply defined & have a blurred boundary resembling closely real-world problems (Brasil et al. 1998).

## STUDY AREA

The study area includes the Rani and Chayani Barduar administrative block of Kamrup – Metro (Guwahati city) and the Kamrup-Rural Districts of Assam, covering an area of 423.03 sq. km containing 130 villages. Urbanization is prominent towards the north, adjacent to the Guwahati Airport. Fig. 1 shows a hill shade map of the study area prepared using SRTM DEM. The Brahmaputra River flows north of the study area. Physiography of the area is mainly the

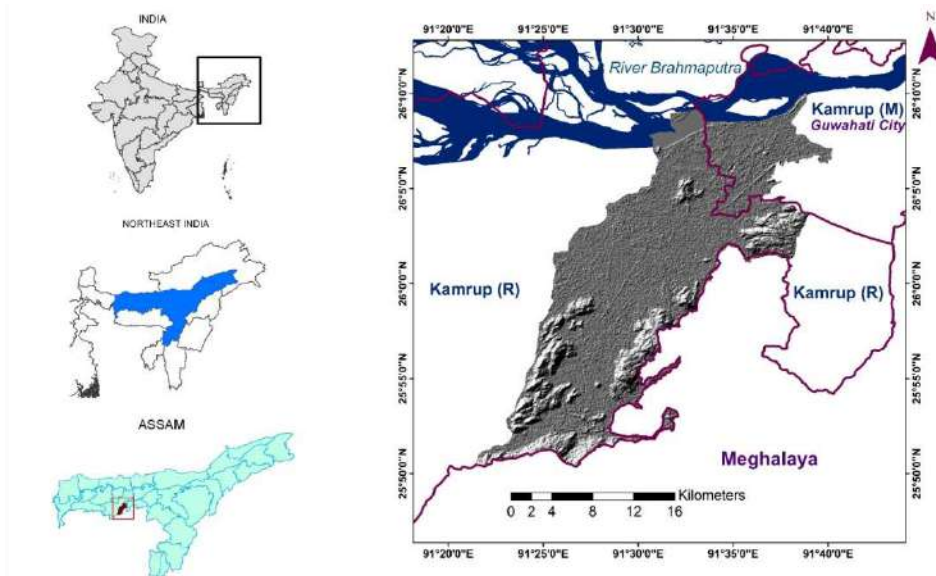


Fig. 1: SRTM DEM derived hill shade map of the area showing Rani and Chayani Barduar administrative blocks located at the southwestern fringe of Guwahati city, Assam, India.

floodplains of the river Brahmaputra and its tributaries, along with hilly terrains and isolated hillocks of the Meghalaya plateau in the south.

The region witnesses a tropical monsoon-type climate, with rainfall occurring between June to September. The average temperature ranges from 35°C in summer to 9°C in winter. Though the Brahmaputra River flows adjacent to the study area, significant urban populations traditionally rely on groundwater sources due to the inadequate supply and capacity of water treatment plants. Inequitable distribution, unplanned development of aquifers, gradual reduction in subsurface infiltration due to increased urbanization, and noticeable changes in seasonal rainfall patterns are some factors that led to water scarcity within the city as well as surrounding areas, especially in dry seasons (Das & Goswami 2013). Therefore, an assessment of the groundwater prospect zone is necessary to ensure future urban expansion potential.

## MATERIALS AND METHODS

Multiple parameters play a dominant role in groundwater recharge, and these are used to estimate the groundwater potential. The number of thematic layers that can be used also depends on the availability of data for the study region. As per the report by the Central Ground Water Board, the chief source of groundwater recharge in the Himalayan region is the glaciers, and in the foothill region, rainfall plays the dominant role, contributing a copious amount. In Northeast India, groundwater occurrence can be witnessed in weathered residuum and fractures/ joints in consolidated formations in the Assam and Meghalaya plateau, semi-consolidated porous formations of tertiary rocks, and unconsolidated formations of Quaternary age in the Brahmaputra & Barak valleys (Gupta 2014). Based on the literature survey, expert opinion, and in consultation with local hydro-geologists, the following parameters and their relative importance are considered for the estimation of groundwater potential in the study area: lithology, geomorphology, slope, land use land cover, rainfall, soil, lineament density, and drainage density.

Lithology maps are prepared using data from the Bhukosh platform of the Geological Survey of India. For geomorphology maps, the ISRO/ Bhuvan portal is used as a reference. Soil maps are prepared using datasets from the National Bureau of Soil Survey and Land Use Planning, Government of India. Slope and drainage density are prepared using the Digital Elevation Model (DEM) of the Shuttle Radar Topography Mission (SRTM). Lineament density and LULC maps are prepared using Landsat 8 satellite imagery. Rainfall data is collected from the GIOVANNI application of NASA. The groundwater yield map is prepared using data from the Central Groundwater Board (CGWB). Static water

table data is collected by field survey. Remote sensing and GIS are mainly used in preparing different layers. Arc GIS 10.7, ERDAS Imagine 10, and ENVI 5.6 are the prime GIS software used for the rectification, digitization, resampling, and processing of various data.

Weight assignment to the parameters and their corresponding classes is carried out using the Fuzzy Analytical Hierarchy Process (FAHP) based on their relative importance to groundwater recharge. Literature surveys of groundwater potential estimation in similar terrains and climatic conditions provide an overview of the contribution of different parameters and insight regarding the assignment of weights. For example, in an AHP-based analysis of groundwater potential estimation by Ahmed & Sajjad (2017) in the lower Barapani watershed, adjacent to the current study area, the pair-wise comparison between lithology and slope is assigned a weight of 5 on Saaty's scale, indicating lithology is fairly important compared to slope for groundwater recharge as lithology is important for the development of slopes. Melese & Belay (2022) conducted a similar analysis in the Abay Basin, Ethiopia, a tropical to subtropical basin with variable topography of plains and hills assigning significant pair-wise weightage to geology, lineament density, drainage density, and rainfall, and relatively less weightage to LULC. Roy et al. (2024) assign the highest pair-wise weightage to rainfall and the lowest to LULC in groundwater potential estimation of the Dooars region of West Bengal, India, a sub-Himalayan foothill region dominated by monsoon precipitation. The study area falls under the primary rainfed zones of the State due to its adjacency to the Shillong plateau, the wettest region of the Earth. Rainfall is the primary contributor to the groundwater reserve and is given more weightage than the other parameters in a pair-wise comparison. Similarly, the lithology and geomorphology of the area are influenced by a broad geological timeframe, from Precambrian elevated hills to recent alluvial deposits by river Brahmaputra and its tributaries influencing the groundwater reserve, which are given the second highest assignment in the comparison matrix followed by the lineament density, which is the surface signatures of the potential groundwater reserve. Due to adequate rainfall and topographic relief, the area is abundant in perennial and seasonal tributaries, facilitating surface runoff and negatively influencing the groundwater regime. The drainage density and soil parameters are assigned with the subsequent pair-wise importance, followed by the LULC with the least assignment, as the same is influenced by other parameters.

A fuzzy set is characterized by a membership function that assigns to each object a grade of membership ranging



between zero and one. Mathematically, if  $X$  is a universal set, a fuzzy set  $\tilde{A}$  in  $X$  is characterized by its membership function denoted by  $\mu_{\tilde{A}}$ , so that  $\mu_{\tilde{A}} : X \rightarrow [0,1]$  (Bhargava 2013). Though there are several different forms of membership functions, triangular and trapezoidal membership functions are extensively used due to their simplicity and efficiency in real-time computation (Azam et al. 2020). In this study, the triangular fuzzy membership function is used for computational ease. Before the implementation of the FAHP method, the Analytical Hierarchy Process (AHP) developed by Saaty is used to check the consistency of the decisions by the decision maker. It uses a pairwise comparison matrix to calculate the weights for each criterion involved (Chakraborty & Joshi 2014). Though the nine-point AHP scale by Saaty gives information about the dominance of each parameter above the other, the fixed value discrete scale judgment cannot simplify the information unpredictability, creating a weak spot in decision-making. However, fuzzy set theory with its interval judgment (Table 1) deals with such impreciseness (Kaganski et al. 2018). The consistency of the comparison matrix is validated using the crisp weight of Saaty's scale (Table 1) and Saaty's standard ratio index (Radulović et al. 2022). The matrix consistency is assessed using the Consistency Index (CI) formula:  $CI = \frac{\lambda_{\max} - n}{n - 1}$  where  $\lambda_{\max}$  is the principal eigenvalue of the pairwise comparison matrix, and  $n$  is the number of parameters used in the analysis. The Consistency Ratio (CR) is determined by dividing the Consistency Index (CI) by the Ratio Index (RI). For consistency of the weight, the CR value should be less than 0.1. If CR is higher than 0.1, re-evaluation within the matrix is needed (Tošović-Stevanović et al. 2020). The CR for this particular study is found to be 0.03, which is in the acceptable range.

Buckley's column geometric mean method is used to get the final normalized weight. The process uses the center-of-area method as the de-fuzzification technique. To obtain the normalized weights of the parameters, first, the defuzzification process is applied to get the crisp values using

Table 1: Linguistic scale for FAHP pair-wise comparison (Ayhan 2013).

Saaty Scale	Definition	Fuzzy Triangular Scale
1	Equally important	(1,1,1)
3	Weakly important	(2,3,4)
5	Fairly important	(4,5,6)
7	Strongly important	(6,7,8)
9	Absolutely important	(9,9,9)
2, 4, 6, 8	The intermittent values between two adjacent scales	(1,2,3), (3,4,5), (5,6,7), (7,8,9)

the arithmetic mean of the fuzzy members (l,m,u), followed by normalizing the weights by dividing each value by the sum of the criteria weight to get the normalized sum of 1 (Ally et al. 2021, Baalousha et al. 2023). The following mathematical equations are used in this study (Bayer & Karamasa 2018).

The membership function for triangular fuzzy numbers is defined by the triplet indicating the smallest possible value, the most promising value, and the largest possible value. The membership function is defined by the following equation:

$$\mu_{\tilde{M}}(x) = \begin{cases} \frac{(x-l)}{(m-l)}, & l \leq x \leq m, \\ \frac{(u-x)}{(u-m)}, & m \leq x \leq u \\ 0, & \text{otherwise} \end{cases}$$

A triangular fuzzy number  $\tilde{M}$  is shown in the Fig. 2

Fuzzy pair-wise matrices can be represented as

$$\tilde{B} = (\tilde{b}_{ij})_{n \times k}$$

$$\begin{bmatrix} (1,1,1) & (l_{12}, m_{12}, u_{12}) & \dots & (l_{1k}, m_{1k}, u_{1k}) \\ (l_{21}, m_{21}, u_{21}) & (1,1,1) & \dots & (l_{2k}, m_{2k}, u_{2k}) \\ \vdots & \vdots & \dots & \vdots \\ (l_{n1}, m_{n1}, u_{n1}) & (l_{n2}, m_{n2}, u_{n2}) & \dots & (1,1,1) \end{bmatrix}$$

Where  $\tilde{b}_{ij} = (l_{ij}, m_{ij}, u_{ij})$ ,  $\tilde{b}_{ij}^{-1} = (\frac{1}{u_{ji}}, \frac{1}{m_{ji}}, \frac{1}{l_{ji}})$

For  $i = 1, 2, 3, \dots, n; j = 1, 2, 3, \dots, k$  elements and  $i \neq j$

New pair-wise comparison matrix averaging preferences for all decisions:

$$\tilde{B} = \begin{bmatrix} \tilde{b}_{11} & \tilde{b}_{12} & \dots & \tilde{b}_{1n} \\ \tilde{b}_{21} & \tilde{b}_{22} & \dots & \tilde{b}_{2n} \\ \dots & \dots & \dots & \dots \\ \tilde{b}_{m1} & \tilde{b}_{m2} & \dots & \tilde{b}_{mn} \end{bmatrix}$$

The geometric mean of each criterion is calculated by:

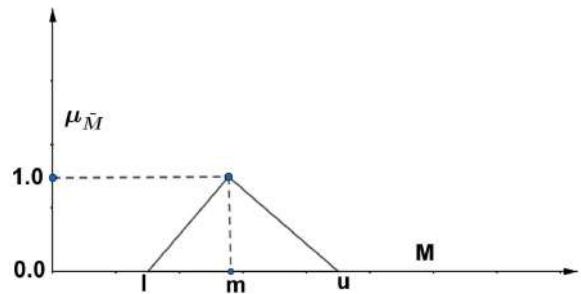


Fig. 2: Graphical representation of a triangular fuzzy membership function.

$$\tilde{h}_i = [\prod_{j=1}^n \tilde{b}_{ij}]^{1/n} \text{ Where, } i = 1, 2, \dots, m$$

Fuzzy weights of each criterion are obtained by:

$$\tilde{w}_i = \tilde{h}_i \otimes (\tilde{h}_1 \oplus \tilde{h}_2 \oplus \dots \oplus \tilde{h}_n)^{-1} = (l_i, m_i, u_i)$$

Centre of area de-fuzzification technique to transform fuzzy weights into crisp ones:

$$k_i = \frac{l_i + m_i + u_i}{3}$$

Crisp weights to normalized final weight:

$$z_i = \frac{k_i}{\sum_{i=1}^m k_i}$$

Finally, a weighted linear combination method (Das & Pal 2019, Mallick et al. 2019) is used in the GIS environment to delineate potential groundwater zones.

$$GWPZ = (RF_w \times RF_{wc}) + (LT_w \times LT_{wc}) + (GM_w \times GM_{wc}) + (LD_w \times LD_{wc}) + (DD_w \times DD_{wc}) + (S_w \times S_{wc}) + (SL_w \times SL_{wc}) + (LU_w \times LU_{wc})$$

Where, GWPZ = Groundwater Potential Zone, RF = Rainfall, LT = Lithology, GM = Geomorphology, LD = Lineament Density, DD = Drainage Density, S = Soil, SL = Slope, LU = Land Use Land Cover,  $w$  = Normalized weight of the parameters and  $wc$  = Normalized weight of the corresponding classes of the parameters.

The methodological flowchart adopted for this study (Fig. 3) illustrates the sequential steps involved, starting from data acquisition (e.g., remote sensing imagery, geological maps) to analytical techniques (e.g., fuzzy logic, GIS-based mapping) and final interpretation. This structured approach ensures a comprehensive evaluation of groundwater recharge zones within the study area.

## RESULTS AND DISCUSSION

### Lithology

Lithology controls the percolation of water flow, thus influencing groundwater recharge rates (Yeh et al. 2016). Rocks with less compaction, a higher degree of weathering, and fracturing are suitable for groundwater recharge (Senanayake et al. 2016). The dominant geological formations encountered within the study area (Fig. 4a) are alluviums of the Brahmaputra River and its tributaries and Precambrian rocks of the Meghalaya plateau. The alluvial deposits can be categorized into two parts: older alluvium (covering 6.5 % area), consisting of reddish and brownish coarse sand particles with irregularly distributed, unsorted pebbles deposited during Pleistocene, and newer alluvium (53.6 %) consisting of light-colored sand, silt, and clay deposited during recent geological time. These alluvium deposits are ideal for groundwater recharge, providing good porosity and permeability conditions. The Precambrian rocks

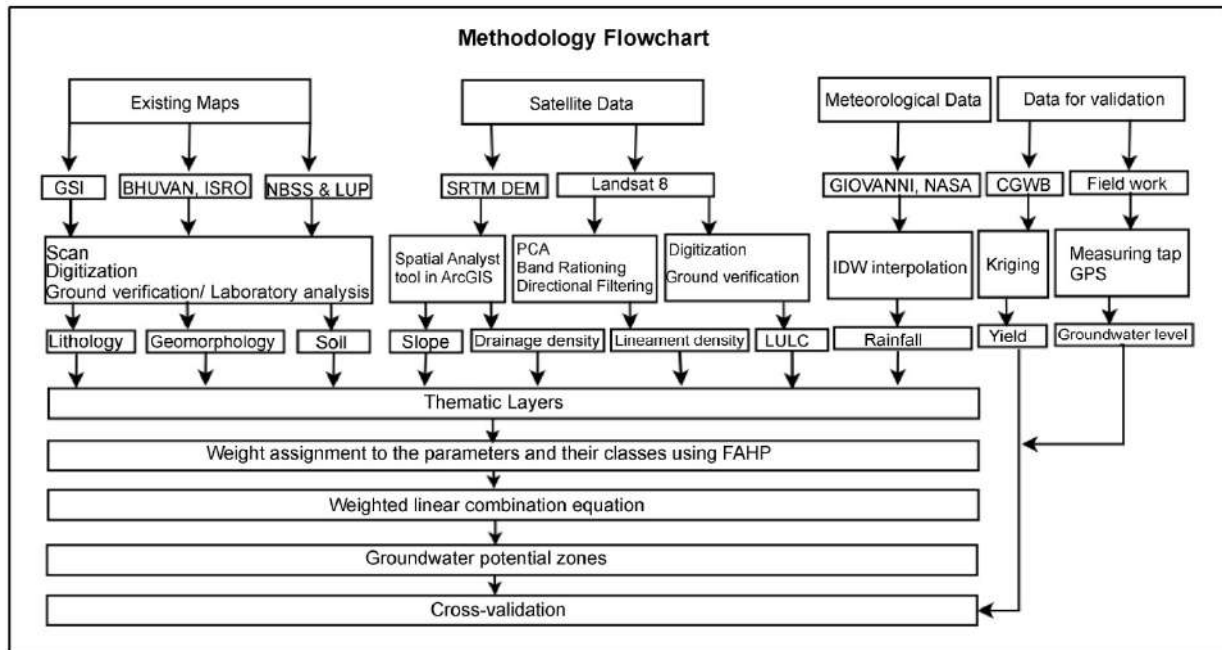


Fig. 3: The methodological flowchart adopted for this study.

Table 2: Fuzzy comparison matrix and normalized weight for different classes of lithology.

Classes	Migmatite, Granitic Gneiss	Older Alluvium	Newer Alluvium	Normalized weight
Migmatite, Granitic Gneiss	1,1,1	1/6, 1/5, 1/4	1/6, 1/5, 1/4	0.10
Older Alluvium	4,5,6	1,1,1	1,1,1	0.45
Newer Alluvium	4,5,6	1,1,1	1,1,1	0.45

(39.8 %) mainly consist of gneisses intruded by pegmatites and quartz. Granitic gneiss is the dominant rock unit of the area, showing a concordant relationship with all other foliated rock units. Hard rock lithology is usually not suitable for groundwater recharge except for significant amounts of weathering and fracturing conditions.

The suitability of different lithological classes for groundwater recharge is quantitatively assessed using a fuzzy comparison matrix. The normalized weights assigned to each lithological class are presented in Table 2.

### Geomorphology

In combination with structures and lithology, geomorphic features control the occurrence of groundwater (Solomon & Quiel 2006). The distinguishable geomorphic features within the study area (Fig. 4b) are a) Floodplains: The study area witnesses periodic flooding due to the Brahmaputra river in the north, along with its tributary channels flowing from the Meghalaya plateau in the south. The floodplains contain old meanders, paleochannels, natural levees, back swamps, wetlands, and channel bars. Both active and older floodplains can be identified within the study area. b) Alluvial plains: Alluvial plains within the study area occur at a slightly higher elevation than the floodplains. Both younger and older alluviums can be identified within the area. c) Piedmont zone: The Piedmont zone is mainly concentrated towards the south of the study area at the foothill region consisting of eroded materials of adjacent denudational hills. d) Denudational

hills: Relict hills of the Precambrian plateau are mainly formed by stream erosion. These are moderate to highly dissected gneissic hills.

Flood plains and alluvial plains are assigned the highest rank in terms of groundwater recharge, followed by the Piedmont zone and gneissic hills. The normalized weights assigned to each geomorphic class are presented in Table 3.

### Slope

The slope of the area (Fig. 4c) directly affects the controlling factors of groundwater availability. A steeper slope results in more runoff than infiltration, causing less chance of groundwater recharge (Rani et al. 2015). The study area is divided into five classes based on slope angle: 0°-5° (flat), 5°-15° (gentle), 15°-30° (moderate), 30°-45° (steep), and 45°-89° (very steep) (Fig. 4c). 70.86 % and 14.72 % of the study areas fall under the “flat” and “gentle” category, indicating promising groundwater reserves. The fuzzy comparison matrix and the corresponding normalized weight for each slope class are presented in Table 4.

### Land Use Land Cover (LULC)

Land use land cover patterns and changes significantly affect groundwater quality and quantity (Singh et al. 2010, He et al. 2019). LULC of the study area (Fig. 4d) is delineated using Landsat 8 satellite imagery using ArcGIS 10.7 software based on visual image interpretation technique, followed by field verification. Major LULC classes include agricultural land/

Table 3: Fuzzy comparison matrix and normalized weight for different classes of geomorphology.

Class	Denudational Hills	Pediment Piedplain Complex	Alluvial Plain/Flood Plain	Water bodies	Normalized weight
Denudational Hills	1, 1, 1	1/3, 1/2, 1	1/4, 1/3, 1/2	1/6, 1/5, 1/4	0.10
Pediment Piedplain Complex	1, 2, 3	1, 1, 1	1/3, 1/2, 1	1/4, 1/3, 1/2	0.14
Alluvial Plain/ Flood Plain	2, 3, 4	1, 2, 3	1, 1, 1	1/3, 1/2, 1	0.24
Water bodies	4, 5, 6	2, 3, 4	1, 2, 3	1, 1, 1	0.52

Table 4: Fuzzy comparison matrix and normalized weight for different classes of slope.

Slope	45°-89° (very steep)	30°-45° (steep)	15°-30° (moderate)	5°-15° (gentle)	0°-5° (flat)	Normalized weight
45°-89° (very steep)	1, 1, 1	1/3, 1/2, 1	1/4, 1/3, 1/2	1/6, 1/5, 1/4	1/7, 1/6, 1/5	0.04
30°-45° (steep)	1, 2, 3	1, 1, 1	1/3, 1/2, 1	1/4, 1/3, 1/2	1/6, 1/5, 1/4	0.06
15°-30° (moderate)	2, 3, 4	1, 2, 3	1, 1, 1	1/3, 1/2, 1	1/4, 1/3, 1/2	0.10
5°-15° (gentle)	4, 5, 6	2, 3, 4	1, 2, 3	1, 1, 1	1/3, 1/2, 1	0.22
0°-5° (flat)	5, 6, 7	4, 5, 6	2, 3, 4	1, 2, 3	1, 1, 1	0.58

Table 5: Fuzzy comparison matrix and normalized weight for different classes of LULC.

LULC	Built-up	Forest	Agricultural Land/ Grassland/ Wasteland	Water bodies	Normalized weight
Built-up	1, 1, 1	1/4, 1/3, 1/2	1/5, 1/4, 1/3	1/6, 1/5, 1/4	0.06
Forest	2, 3, 4	1, 1, 1	1/4, 1/3, 1/2	1/5, 1/4, 1/3	0.10
Agricultural Land/ Grassland/ Wasteland	3, 4, 5	2, 3, 4	1, 1, 1	1/4, 1/3, 1/2	0.21
Water bodies	4, 5, 6	3, 4, 5	2, 3, 4	1, 1, 1	0.63

household plantation (54.91%) and forest cover (27.16%). Both classes are given a higher weight because they can hold a substantially high proportion of water (Agarwal et al. 2013, Arulbalaji et al. 2019). The fuzzy comparison matrix and normalized weight for different LULC classes are presented in Table 5.

### Rainfall

The Tropical Rainfall Measuring Mission version 7 product (TRMM V7) was used for rainfall estimation over the study area for ten years (2010-2019). TRMM V7, available in GIOVANNI (Geospatial Interactive Online Visualization and Analysis Infrastructure), is a web-based application developed by NASA. It outperforms other remote sensing precipitation products as it contains real-time gridded precipitation (3B42RTV7) with near-global coverage along with gauge-adjusted post-real-time research product (3B42V7) having high spatial (0.25°) and temporal (3 hours) resolution (Liu et al. 2016). The average annual rainfall map is prepared using the IDW interpolation technique, taking 10 years of rainfall over the study area (Fig. 4e). The fuzzy comparison matrix and normalized weight for different classes of rainfall are presented in Table 6.

### Lineament Density

Lineaments are subsurface expressions in topography associated with faults - linear fracturing and bending deformation that indicate increased permeability of the crust (Florinsky 2016). Faults and fracture zones play important roles in groundwater dynamics and are indicators of feeding for the aquifer (Ammar & Kamal 2018). Landsat 8 satellite with Operational Land Imager (OLI) captured bands are used to delineate lineaments by adopting various digital image enhancement techniques. Out of different techniques, Principal Component Analysis (PCA), band rationing, and directional filtering are commonly used for extracting the lineaments of the study area (Fig. 4f). PCA analysis carried out using band 1 to band 7 gives principal components, and PC (1, 2, 3) reveals structural information (Mathew & Ariffin 2018). RGB composite of band ratios (7/5, 6/4, 4/2) is suitable for enhancing lithological features (Al-Nahmi et al. 2016). Directional convolution filtering is applied on band 6 of Landsat 8 imagery using ENVI software in four directions N-S (0°), NE-SW (45°), E-W (90°), and NW-SE (135°), highlighting the main lineament directions of the study area (Javhar et al. 2019). The fuzzy comparison matrix and

Table 6: Fuzzy comparison matrix and normalized weight for different classes of rainfall.

Classes	3163.00 – 3380.50 mm	3380.50 – 3598.03 mm	3598.03 – 3815.60 mm	3815.60 – 4033.06 mm	4033.06 – 4250.58 mm	Normalized Weight
3163.00 – 3380.50 mm	1, 1, 1	1/3, 1/2, 1	1/4, 1/3, 1/2	1/5, 1/4, 1/3	1/6, 1/5, 1/4	0.07
3380.50 – 3598.03 mm	1, 2, 3	1, 1, 1	1/3, 1/2, 1	1/4, 1/3, 1/2	1/5, 1/4, 1/3	0.13
3598.03 – 3815.60 mm	2, 3, 4	1, 2, 3	1, 1, 1	1/3, 1/2, 1	1/5, 1/4, 1/3	0.20
3815.60 – 4033.06 mm	3, 4, 5	2, 3, 4	1, 2, 3	1, 1, 1	1/3, 1/2, 1	0.27
4033.06 – 4250.58 mm	4, 5, 6	3, 4, 5	2, 3, 4	1, 2, 3	1, 1, 1	0.33

Table 7: Fuzzy comparison matrix and normalized weight for different classes of lineament density.

Lineament Density	0 – 0.29	0.29 – 0.58	0.58 – 0.87	0.87 – 1.17	1.17 – 1.46	Normalized weight
0 – 0.29	1, 1, 1	1/3, 1/2, 1	1/4, 1/3, 1/2	1/5, 1/4, 1/3	1/6, 1/5, 1/4	0.07
0.29 – 0.58	1, 2, 3	1, 1, 1	1/3, 1/2, 1	1/4, 1/3, 1/2	1/5, 1/4, 1/3	0.13
0.58 – 0.87	2, 3, 4	1, 2, 3	1, 1, 1	1/3, 1/2, 1	1/5, 1/4, 1/3	0.20
0.87 – 1.17	3, 4, 5	2, 3, 4	1, 2, 3	1, 1, 1	1/3, 1/2, 1	0.27
1.17 – 1.46	4, 5, 6	3, 4, 5	2, 3, 4	1, 2, 3	1, 1, 1	0.33



normalized weight for different LULC classes of lineament density are presented in Table 7.

### Soil

Groundwater recharge and quality are influenced by the spatial variation of soil types (Rukundo & Dogan 2019). A Soil map of the area (Fig. 4g) is prepared using a soil classification scheme developed by the National Bureau of Soil Survey & Land Use Planning (NBSS&LUP). Soil samples were collected and analyzed in the laboratory to determine soil parameters, mainly for texture and drainage conditions. The data are plotted in a GIS environment, and the 'natural neighbor' interpolation technique is adopted to show the distribution of soil types. Fine-grained soils facilitate less infiltration due to less permeability in comparison to coarse-grained soil. Therefore, a lower rank is given for soils with a fine-grained texture and a higher rank for soils with a coarse-grained texture. The fuzzy comparison matrix and normalized weight for different classes of soil are presented in Table 8.

### Drainage Density

Drainage density is a measure of the total stream length to the total basin area (Strahler 1964) and is often expressed in  $\text{km.km}^{-2}$ . Lower drainage density indicates higher permeability, with greater infiltration of rainfall resulting in good groundwater conditions (Magesh et al. 2012). The drainage network of the study area is extracted from SRTM DEM (30 m spatial resolution) using the Hydrology tool under the Spatial Analyst Toolbox of ArcGIS 10.7. The drainage density is calculated using the line density tool

(Fig. 4h). The fuzzy comparison matrix and normalized weight for different classes of drainage density are presented in Table 9.

Table 10 shows the Fuzzy comparison matrix and normalized weight for all the controlling parameters.

### Delineation of Groundwater Potential Zonation

The groundwater potential zones were classified into five categories based on the GWPZ equation – Very High ( $179.87 \text{ km}^2$ , 42.52%), High ( $121.28 \text{ km}^2$ , 28.67%), Moderate ( $72.89 \text{ km}^2$ , 17.23 %), Poor ( $43.19 \text{ km}^2$ , 10.21%) and Very Poor ( $5.80 \text{ km}^2$ , 1.37%) (Fig. 5a). Very high and high groundwater potential areas are found mainly in low-lying flat/gentle flood plains and alluvial plains towards the north of the study area. Towards the south, eroded hills with high lineament density are also having high groundwater potential. Proximity to the river Brahmaputra, the presence of wetlands, vast areas of unsettled agricultural land, as well as basin-like topography due to the surrounding elevated landforms of the Shillong plateau is some justification against this abundance of groundwater. Moderate groundwater potential areas are mainly found toward the south of the study area; it comprises the piedmont pediplain complex and hills having moderate lineament density. Poor and very poor groundwater potential areas are found in steeper gneissic hills with relatively moderate to low rainfall and low lineament density. These areas fall under the reserve forest, and human settlement is not authorized.

The study results have been compared with findings by other researchers adopting similar approaches in different

Table 8: Fuzzy comparison matrix and normalized weight for different classes of soil.

Soil	Typic Dystrachrepts (Clayey Fine loamy)	Umbric Dystrachrepts (Fine loamy skeletal)/ Fluventic Dystrachrept (Fine loamy)	Aeric Haplaquepts (Fine silty)	Aeric Fluvaquent (coarse silty)	Normalized weight
Typic Dystrachrepts (Clayey Fine loamy)	1, 1, 1	1/3, 1/2, 1	1/4, 1/3, 1/2	1/4, 1/3, 1/2	0.11
Umbric Dystrachrepts (Fine loamy skeletal)/Fluventic Dystrachrept (Fine loamy)	1, 2, 3	1, 1, 1	1/3, 1/2, 1	1/4, 1/3, 1/2	0.15
Aeric Haplaquepts (Fine silty)	2, 3, 4	1, 2, 3	1, 1, 1	1/3, 1/2, 1	0.30
Aeric Fluvaquent (coarse silty)	2, 3, 4	2, 3, 4	1, 2, 3	1, 1, 1	0.44

Table 9: Fuzzy comparison matrix and normalized weight for different classes of drainage density.

Drainage Density	2.67 - 3.34	2.00 - 2.67	1.33 - 2.00	0.66 - 1.33	0 - 0.66	Normalized weight
2.67-3.34	1, 1, 1	1/3, 1/2, 1	1/4, 1/3, 1/2	1/5, 1/4, 1/3	1/6, 1/5, 1/4	0.07
2.00-2.67	1, 2, 3	1, 1, 1	1/3, 1/2, 1	1/4, 1/3, 1/2	1/5, 1/4, 1/3	0.13
1.33-2.00	2, 3, 4	1, 2, 3	1, 1, 1	1/3, 1/2, 1	1/5, 1/4, 1/3	0.20
0.66-1.33	3, 4, 5	2, 3, 4	1, 2, 3	1, 1, 1	1/3, 1/2, 1	0.27
0-0.66	4, 5, 6	3, 4, 5	2, 3, 4	1, 2, 3	1, 1, 1	0.33

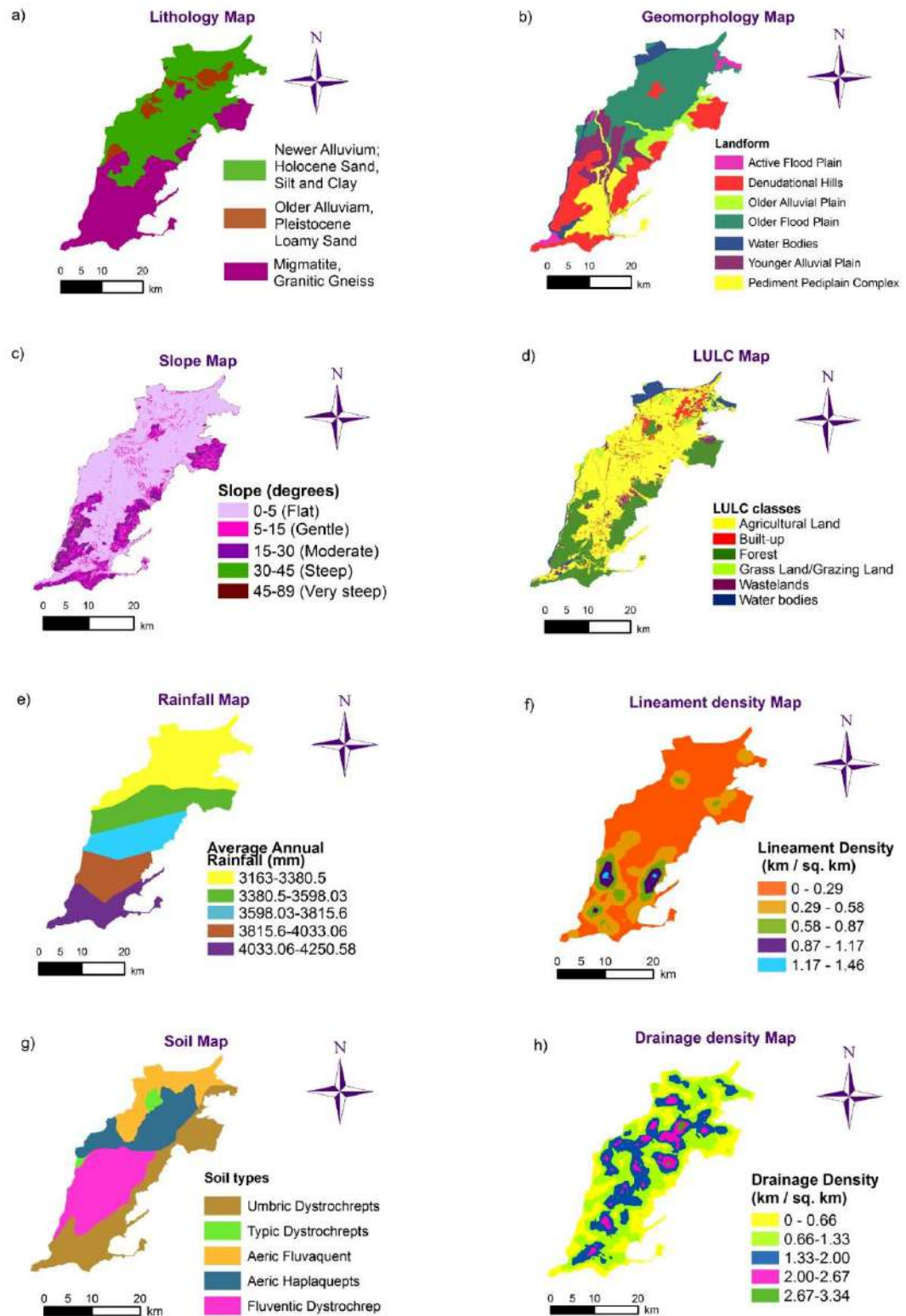


Fig. 4: Thematic layers important for groundwater recharge a) Lithology, b) Geomorphology, c) Slope, d) LULC, e) Rainfall, f) Lineament density, g) Soil, and h) Drainage density.

Table 10: Fuzzy comparison matrix and normalized weight for controlling parameters.

Parameters	Rainfall	Lithology	Geomorphology	Lineament Density	Drainage Density	Soil	Slope	LULC	Normalized Weights
Rainfall	1, 1, 1	1, 2, 3	1, 2, 3	2, 3, 4	2, 3, 4	4, 5, 6	5, 6, 7	6, 7, 8	0.27
Lithology	1/3, 1/2, 1	1, 1, 1	1, 2, 3	1, 2, 3	2, 3, 4	3, 4, 5	4, 5, 6	5, 6, 7	0.18
Geomorphology	1/3, 1/2, 1	1/3, 1/2, 1	1, 1, 1	1, 2, 3	2, 3, 4	3, 4, 5	4, 5, 6	5, 6, 7	0.18
Lineament Density	1/4, 1/3, 1/2	1/3, 1/2, 1	1/3, 1/2, 1	1, 1, 1	1, 2, 3	2, 3, 4	5, 6, 7	5, 6, 7	0.14
Drainage Density	1/4, 1/3, 1/2	1/4, 1/3, 1/2	1/4, 1/3, 1/2	1/3, 1/2, 1	1, 1, 1	1, 2, 3	2, 3, 4	3, 4, 5	0.09
Soil	1/6, 1/5, 1/4	1/5, 1/3, 1/3	1/5, 1/3, 1/3	1/4, 1/3, 1/2	1/3, 1/2, 1	1, 1, 1	2, 3, 4	2, 3, 4	0.09
Slope	1/7, 1/6, 1/5	1/6, 1/5, 1/4	1/6, 1/5, 1/4	1/7, 1/6, 1/5	1/4, 1/3, 1/2	1/4, 1/3, 1/2	1, 1, 1	1, 2, 3	0.03
LULC	1/8, 1/7, 1/6	1/7, 1/6, 1/5	1/7, 1/6, 1/5	1/7, 1/6, 1/5	1/7, 1/6, 1/5	1/5, 1/3, 1/3	1/4, 1/3, 1/2	1/3, 1/2, 1	0.03

terrains to understand the commonalities involved. For example, the AHP-based groundwater potential estimation in the Kashmir Valley by Dar et al. (2020) revealed identical

results with excellent groundwater potential in the alluvial plains of the basin deposited by river Jhelum and its tributaries and poor to very poor potential in the mountainous

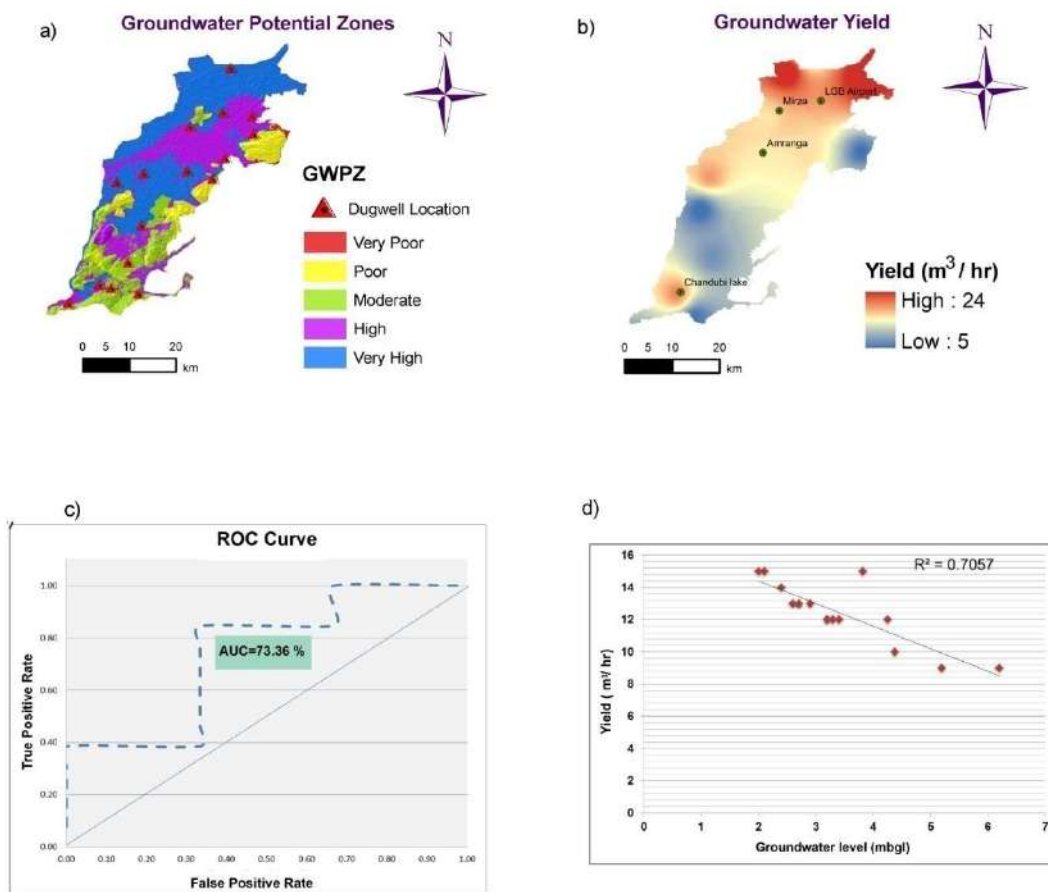


Fig. 5 a: Groundwater potential zone map, b) Groundwater yield map prepared using CGWB data, c) Receiver Operating Characteristic (ROC) curve for validation, d) Relationship between groundwater yield and mean annual groundwater level.

areas, denudational hills with steeper slopes with high runoff and less infiltration. GIS-based fuzzy AHP analysis by Bhadran et al. (2022) also shows very good aquifer potential in the coastal areas of Karuvannur River Basin, Kerala, with a high alluvial cover and poor groundwater prospects in the eastern periphery of the basin with hard rock lithology. Radulović et al. (2022) found similar results with good to very good groundwater potential zones in the alluvial plains of the Danube and Tisa Rivers and very poor and poor potential zones in the loess plateau due to high runoff and poor water retention capacity. Aouragh et al. (2017), in a fuzzy GIS-based analysis of the Middle Atlas plateaus, Morocco, observed promising groundwater zones in areas with concentrated limestone fractures.

### Validation

The zones are validated by generating a yield map (Fig. 5b) using yield data of exploratory wells drilled by the Central Ground Water Board (CGWB) and field-derived static water table data of household dug wells. The highest yield of  $24 \text{ m}^3 \cdot \text{h}^{-1}$  is observed in low-lying flood plains areas, and the lowest yield of  $5 \text{ m}^3 \cdot \text{h}^{-1}$  is observed in gneissic hills, showing an agreement with FAHP-derived groundwater potential zonation. Quantitative validation of the Receiver Operating Characteristic (ROC) curve (Fig. 5c) analysis shows the Area Under the Curve (AUC) to be 73.36%, indicating good prediction accuracy of the method (Kumar & Krishna 2016, Andualem & Demeke 2019). Fieldwork was conducted in 16 households dug wells in both pre and post-monsoon and the mean annual groundwater level was measured. Before the field visit for groundwater level collection, the area is divided into a  $5 \text{ km} \times 5 \text{ km}$  grid using ArcGIS software to collect samples at regular intervals. Groundwater level (mbgL) shows a negative correlation with yield data with an  $R^2$  value of 0.71, indicating high specific yield in wells with shallow water levels and vice versa (Fig. 5d).

### CONCLUSIONS

Remote Sensing and GIS-based groundwater potential zone delineation using the FAHP technique are efficient as well as cost-effective. Satellite remote sensing coupled with limited field verification and laboratory work can assist in preparing a database of selected parameters influencing groundwater recharge, such as rainfall, lithology, geomorphology, lineament density, drainage density, soil, slope, and land use land cover. GIS allows the analysis of various parameters under a single platform. Different parameters have different degrees of influence in groundwater recharge, and their relative importance needs to be assessed for decision-making. The Fuzzy Analytical Hierarchy Process (FAHP) is feasible

in prioritizing one parameter above the other by assigning weights in a pairwise comparison manner considering the real-world subjective judgments. Similarly, different classes under each parameter are allocated weights, and a potential groundwater map is prepared in the GIS environment. Very high and high groundwater potential areas are found towards the north in low-lying flat flood plains and alluvial plains; moderate potential areas are piedmont pediplain complex and hills having moderate lineament density, poor and very poor potential areas are steeper gneissic hills having relatively moderate to low rainfall and low lineament density. Validation of the groundwater potential map with yield map and field-derived water level data gives satisfactory agreement with the obtained result. The study area lies towards the southwest of Guwahati city and has the potential for future urban expansion. As the city witnesses water scarcity due to the rapid growth of population and infrastructure, a prior assessment is needed in its fringe areas for sustainable urban expansion. This type of pilot study is helpful in decision-making processes for the professionals and policymakers involved in groundwater, urban planning, and allied sectors.

### ACKNOWLEDGMENTS

The authors would like to thank different government and nongovernment organizations for providing valuable data, and various regional experts for their valuable suggestions and guidance. The authors give special thanks to Mr. Thatey Mohamed Zuhail for his valuable guidance regarding manuscript preparation.

### REFERENCES

- Agarwal, E., Agarwal, R., Garg, R.D. and Garg, P.K., 2013. Delineation of groundwater potential zone: an AHP/ANP approach. *Journal of Earth System Science*, 122, pp. 887-898. [DOI]
- Ahmed, R. and Sajjad, H., 2018. Analyzing factors of groundwater potential and its relation with population in the lower Barapani watershed, Assam, India. *Natural Resources Research*, 27, pp. 503-515. [DOI]
- Ally, A.M., Yan, J., Bennett, G., Lyimo, N.N. and Mayunga, S.D., 2024. Assessment of groundwater potential zones using remote sensing and GIS-based fuzzy analytical hierarchy process (F-AHP) in Mpwapwa District, Dodoma, Tanzania. *Geosystems and Geoenvironment*, 3, p.100232. [DOI]
- Al-Nahmi, F., Alami, O.B., Baiddar, L., Khanbari, K., Rhinane, H. and Hilali, A., 2016. Using remote sensing for lineament extraction in Al Maghrabah area - Hajjah, Yemen. *The International Archives of the Photogrammetry, Remote Sensing and Spatial Information Sciences*, XLII-2/W1, pp. 137-142. [DOI]
- Ammar, A.I. and Kamal, K.A., 2018. Resistivity method contribution in determining fault zone. *Applied Water Science*, 8, pp.1-27. [DOI]
- Andualem, T.G. and Demeke, G.G., 2019. Groundwater potential assessment using GIS and remote sensing: A case study of Gunatana landscape, upper Blue Nile Basin, Ethiopia. *Journal of Hydrology: Regional Studies*, 24, p.100610. [DOI]



- Aouragh, M.H., Essahlaoui, A., El Ouali, A., El Hmaidi, A. and Kamel, S., 2017. Groundwater potential of Middle Atlas plateaus, Morocco, using the fuzzy logic approach, GIS, and remote sensing. *Geomatics, Natural Hazards and Risk*, 8(2), pp.194-206. [DOI]
- Arulbalaji, P., Padmalal, D. and Sreelash, K., 2019. GIS and AHP techniques based delineation of groundwater potential zones: a case study from Southern Western Ghats, India. *Scientific Reports*, 9, p.2082. [DOI]
- Ayhan, M.B., 2013. A fuzzy AHP approach for supplier selection problem: a case study in a gearmotor company. *International Journal of Managing Value and Supply Chains*, 4(3), pp.11-23. [DOI]
- Azam, M.H., Hasan, M.H., Hassan, S. and Abdulkadir, S.J., 2020. Fuzzy type-1 triangular membership function approximation using fuzzy C-means. In: B. S. Iskandar (ed.) *International Conference on Computational Intelligence (ICCI)*. IEEE, Manhattan, NY, USA, pp.64-78.
- Baalousha, H.M., Younes, A., Yassin, M.A. and Fahs, M., 2023. Comparison of the fuzzy analytic hierarchy process (F-AHP) and fuzzy logic for flood exposure risk assessment in arid regions. *Hydrology*, 10, p.136. [DOI]
- Bayer, R.U. and Karamasa, C., 2018. Analyzing destination attributes under fuzzy environment: a case study in Eskişehir. *European Journal of Tourism Research*, 18, pp.75-94. [DOI]
- Bennia, A., Zeroual, I., Talhi, A. and Kebir, W., 2023. Groundwater potential mapping using the integration of AHP method, GIS and remote sensing: a case study of the Tabelbala region, Algeria. *Bulletin of the Mineral Research and Exploration*, 172, pp.41-60. [DOI]
- Bhadran, A., Girishbai, D., Jesiya, N.P., Gopinath, G., Krishnan, R.G. and Vijesh, V.K., 2022. A GIS-based fuzzy-AHP for delineating groundwater potential zones in a tropical river basin in the southern part of India. *Geosystems and Geoenvironment*, 1, p.100093. [DOI]
- Bhargava, A.K., 2013. *Fuzzy Set Theory Fuzzy Logic and their Applications*. S. Chand, pp.18-19.
- Brasil, L.M., Mendes de Azevedo, F., Barreto, J.M. and Noirhomme-Fraiture, M., 1998. Complexity and cognitive computing. In: J. Mira, A.P. and M. Ali (eds.) *Methodology and Tools in Knowledge-Based Systems*. IEA/AIE 1998, *Lecture Notes in Computer Science*, Springer, Berlin, Heidelberg, pp.145-163.
- Celik, R., 2019. Evaluation of groundwater potential by GIS-based multicriteria decision making as a spatial prediction tool: A case study in the Tigris River Batman-Hasankeyf sub-basin. *Water*, 11(12), pp.1-16. [DOI]
- Chakraborty, A. and Joshi, P.K., 2014. Mapping disaster vulnerability in India using analytical hierarchy process. *Geomatics, Natural Hazards and Risk*, 7(1), pp.308-325. [DOI]
- Da Costa, A.M., De Salis, H.H.C., Viana, J.H.M. and Pacheco, F.A.L., 2019. Groundwater recharge potential for sustainable water use in urban areas of the Jequitiba River basin. *Sustainability*, 11(10), pp.1-20. [DOI]
- Dar, T., Rai, N. and Bhat, A., 2020. Delineation of potential groundwater recharge zones using analytical hierarchy process (AHP). *Geology, Ecology, and Landscapes*, 5(4), pp.292-307. [DOI]
- Das, B. and Pal, S.C., 2019. Combination of GIS and fuzzy-AHP for delineating groundwater recharge potential zones in the critical Goghat-II block of West Bengal, India. *HydroResearch*, 2, pp.21-30. [DOI]
- Das, N. and Goswami, D.C., 2013. A geo-environmental analysis of the groundwater resource vis-a-vis surface water scenario in Guwahati city. *Current World Environment*, 8(2), pp.275-282. [DOI]
- Desai, R., Mahadevia, D. and Mishra, A., 2014. *City Profile: Guwahati*. Centre for Urban Equity (CUE). Retrieved June 13, 2020, from Link
- Florinsky, I.V., 2016. *Digital Terrain Analysis in Soil Science and Geology*. Elsevier, Academic Press, p.13.
- Freitas, L., Afonso, M.J., Pereira, A.J.S.C., Delerue-Matos, C. and Chamine, H.I., 2019. Assessment of the sustainability of groundwater in urban areas (Porto, NW Portugal): a GIS mapping approach to evaluate vulnerability, infiltration and recharge. *Environmental Earth Sciences*, 78, p.140. [DOI]
- Ganesan, S. and Subramaniyan, A., 2024. Identification of groundwater potential zones using multiinfluencing factor method, GIS, and remote sensing techniques in the hard rock terrain of Madurai district, southern India. *Sustainable Water Resources Management*, 10, p.54. [DOI]
- Gaurav, N. and Singh, G., 2022. Delineation of groundwater, drought and flood potential zone using weighted index overlay analysis and GIS for District Patna, Bihar, India. *Nature Environment and Pollution Technology*, 21(2), pp.813-828. [DOI]
- Guppy, L., Uyttendaele, P., Villholth, K.G. and Smakhtin, V., 2018. *Groundwater and Sustainable Development Goals: Analysis of Interlinkages*. In UNU-INWEH report series. Retrieved June 21, 2020, from Link
- Gupta, S., 2014. *Ground Water Scenario of Himalayan Region, India*. Central Ground Water Board. Retrieved November 20, 2020, from Link
- Guwahati Metropolitan Development Authority (GMA), 2009. Part 1 Master Plan for Guwahati Metropolitan Area-2025. Retrieved October 17, 2020, from Report.
- He, S., Li, P., Wu, J., Elumalai, V. and Adimalla, N., 2019. Groundwater quality under land use/land cover changes: A temporal study from 2005 to 2015 in Xi'an, Northwest China. *Human and Ecological Risk Assessment: An International Journal*, 26(10), pp.2771-2797. [DOI]
- Hilal, I., Qurtobi, M., Saadi, R., Agnouy, M., Bouizrou, I., Bouadila, A., Dakak, H., Abdelrahman, K., MorenoNavarro, J.G., Abioui, M., El Messari, J.E.S., Bessa, A.Z.E. and Benmansour, M., 2024. Integrating remote sensing, GISbased, and AHP techniques to delineate groundwater potential zones in the Moulouya Basin, NorthEast Morocco. *Applied Water Science*, 14, p.122. [DOI]
- Javhar, A., Chen, X., Bao, A., Jamshed, A., Yunus, M., Jovid, A. and Latipa, T., 2019. Comparison of multi-resolution optical Landsat-8, Sentinel-2 and radar Sentinel-1 data for automatic lineament extraction: a case study of Alichur area, SE Pamir. *Remote Sensing*, 11(7), p.778. [DOI]
- Kaganski, S., Majak, J. and Karjust, K., 2018. Fuzzy AHP as a tool for prioritization of key performance indicators. *Procedia CIRP*, 72, pp.1227-1232. [DOI]
- Kahraman, C., Cebeci, U. and Ruan, D., 2004. Multi-attribute comparison of catering service companies using fuzzy AHP: The case of Turkey. *International Journal of Production Economics*, 87(2), pp.171-184. [DOI]
- Kumar, A. and Krishna, A.P., 2016. Assessment of groundwater potential zones in coal mining impacted hard-rock terrain of India by integrating geospatial and analytic hierarchy process (AHP) approach. *Geocarto International*, 33(2), pp.105-129. [DOI]
- Kumar, P., Herath, S., Avtar, R. and Takeuchi, K., 2016. Mapping of groundwater potential zones in Killinochi area, Sri Lanka, using GIS and remote sensing techniques. *Sustainable Water Resources Management*, 2, pp.419-430. [DOI]
- Lentswe, G.B. and Molwalefhe, L., 2020. Delineation of potential groundwater recharge zones using analytic hierarchy process-guided GIS in the semi-arid Motloutse watershed, eastern Botswana. *Journal of Hydrology: Regional Studies*, 28, pp.1-22. [DOI]
- Liu, S., Yan, D., Qin, T., Weng, B. and Li, M., 2016. Correction of TRMM 3B42V7 based on linear regression models over China. *Advances in Meteorology*, 16, pp.1-13. [DOI]
- Magesh, N.S., Chandrasekar, N. and Soundranayagam, J.P., 2012. Delineation of groundwater potential zones in Theni district, Tamil Nadu, using remote sensing, GIS, and MIF techniques. *Geoscience Frontiers*, 3(2), pp.189-196. [DOI]
- Mallick, J., Khan, R.A., Ahmed, M., Alqadhi, S.D., Alsubih, M., Falqi, I. and Hasan, M.A., 2019. Modeling groundwater potential zone in a semi-arid region of Aseer using fuzzy-AHP and geoinformation techniques. *Water*, 11(12), p.2656. [DOI]

- Mathew, T.G. and Ariffin, K.S., 2018. Remote sensing technique for lineament extraction in association with mineralization pattern in central belt peninsular Malaysia. In: M. Jaafar and K.A. Razak (eds.) *Journal of Physics: Conference Series*, 14, pp.12-29. [DOI]
- Mays, L.W., 2013. Groundwater resources sustainability: Past, present, and future. *Water Resources Management*, 27, pp.4409–4424. [DOI]
- Melese, T. and Belay, T., 2022. Groundwater potential zone mapping using analytical hierarchy process and GIS in Muga Watershed, Abay Basin, Ethiopia. *Global Challenges*, 6, p.2100068. [DOI]
- Moghaddam, D.D., Rezaei, M., Pourghasemi, H.R., Pourtaghie, Z.S. and Pradhan, B., 2013. Groundwater spring potential mapping using a bivariate statistical model and GIS in the Taleghan watershed, Iran. *Arabian Journal of Geosciences*, 8, pp.913–929. [DOI]
- Nas, B. and Berktaş, A., 2008. Groundwater quality mapping in urban groundwater using GIS. *Environmental Monitoring and Assessment*, 160, pp.215–227. [DOI]
- Rahmati, O., Samani, A.N., Mahdavi, M., Pourghasemi, H.R. and Zeinivand, H., 2014. Groundwater potential mapping at Kurdistan region of Iran using analytic hierarchy process and GIS. *Arabian Journal of Geosciences*, 8, pp.7059–7071. [DOI]
- Radulović, M., Brdar, S., Mesaroš, M., Lukić, T., Savić, S., Basarin, B., Crnojević, V. and Pavić, D., 2022. Assessment of groundwater potential zones using GIS and fuzzy AHP techniques—a case study of the Titel municipality (Northern Serbia). *International Journal of Geo-Information*, 11, p.257. [DOI]
- Raju, R.S., Raju, G.S. and Rajasekhar, M., 2019. Identification of groundwater potential zones in the Mandavi River basin, Andhra Pradesh, India, using remote sensing, GIS, and MIF techniques. *HydroResearch*, 2, pp.1–11. [DOI]
- Rani, V.R., Pandalai, H.S., Sajinkumar, K.S. and Pradeepkumar, A.P., 2015. Geomorphology and its implication in urban groundwater environment: a case study from Mumbai, India. *Applied Water Science*, 5, pp.137–151. [DOI]
- Rehman, A., Islam, F., Tariq, A., Ul Islam, I., Brian J, D., Bibi, T., Ahmad, W., Waseem, L.A., Karuppannan, S. and Al-Ahmadi, S., 2024. Groundwater potential zone mapping using GIS and remote sensing-based models for sustainable groundwater management. *Geocarto International*, 39(1), pp.1–27. [DOI]
- Rezaei, A. and Tahsili., 2018. Urban vulnerability assessment using AHP. *Advances in Civil Engineering*, 18, pp.1–20. [DOI]
- Rikalovic, A., Cosic, I. and Lazarevic, D., 2014. GIS-based multi-criteria analysis for industrial site selection. *Procedia Engineering*, 69, pp. 1054–1063. [DOI]
- Roy, D., Barman, S., Mandal, G., Mitra, R., Sarkar, A., Hossain, G., Roy, P., Almohamad, H., Addo, H.G. and Mandal, D.K., 2024. Extracting of prospective groundwater potential zones using remote sensing data, GIS, and multicriteria decisionmaking approach in the SubHimalayan Dooars region of West Bengal, India. *Applied Water Science*, 14, p.72. [DOI]
- Roy, S.S., Rahman, A., Ahmed, S., Shahfahad and Ahmed, I.A., 2022. Long-term trends of groundwater level variations in response to local level land use land cover changes in Mumbai, India. *Groundwater for Sustainable Development*, 18, pp.1–10. [DOI]
- Rukundo, E. and Dogan, A., 2019. Dominant influencing factors of groundwater recharge spatial patterns in Ergene river catchment, Turkey. *Water*, 11(4), p.653. [DOI]
- Sabale, R.S., Babade, S.S., Venkatesh, B. and Jose, M.K., 2024. Application of Arc-SWAT model for water budgeting and water resource planning at the Yerawadi catchment of Khatav, India. *Nature Environment and Pollution Technology*, 23(1), pp.203–213. [DOI]
- Sandoval, J.A. and Tiburan Jr., C.L., 2019. Identification of potential artificial groundwater recharge sites in Mount Makiling forest reserve, Philippines, using GIS and analytical hierarchy process. *Applied Geography*, 105, pp.73–85. [DOI]
- Schwartz, F.W. and Zhang, H. 2002. *Fundamentals of Groundwater*. John Wiley & Sons Inc., p.1.
- Senanayake, I.P., Dissanayake, D.M.D.O.K., Mayadunna, B.B. and Weerasekera, W.L., 2016. An approach to delineate groundwater recharge potential sites in Ambalantota, Sri Lanka, using GIS techniques. *Geoscience Frontiers*, 7(1), pp.115–124. [DOI]
- Sharma, Y., Ahmed, R., Saha, T.K., Bhuyan, N., Kumari, G., Roshani, Pal, S. and Sajjad, H., 2024. Assessment of groundwater potential and determination of influencing factors using remote sensing and machine learning algorithms: a study of Nainital district of Uttarakhand state, India. *Groundwater for Sustainable Development*, 25, p.101094. [DOI]
- Singh, S.K., Singh, C.K. and Mukherjee, S., 2010. Impact of land-use and land-cover change on groundwater quality in the Lower Shiwalik hills: a remote sensing and GIS-based approach. *Central European Journal of Geosciences*, 2(2), pp.124–131. [DOI]
- Solomon, S. and Quiel, F., 2006. Groundwater study using remote sensing and geographic information systems (GIS) in the central highlands of Eritrea. *Hydrogeology Journal*, 14, pp.1029–1041. [DOI]
- Strahler, A.N., 1964. Quantitative geomorphology of drainage basins and channel networks. In: V.T. Chow (ed.) *Handbook of Applied Hydrology*. McGraw-Hill, New York, pp.98–126.
- Tolche, A.D., 2021. Groundwater potential mapping using geospatial techniques: a case study of Dhugeta-Ramis sub-basin. *Geology, Ecology, and Landscapes*, 5(1), pp.65–80. [DOI]
- Torabi-Kaveh, M., Babazadeh, R., Mohammadi, S. and Zaresefat, M., 2016. Landfill site selection using a combination of GIS and fuzzy AHP, a case study: Iranshahr, Iran. *Waste Management & Research: The Journal for a Sustainable Circular Economy*, 34(5), pp.438–448. [DOI]
- Tošović-Stevanović, A., Ristanović, V., Čalović, D., Lalić, G., Žuža, M. and Cvijanović, G., 2020. Small farm business analysis using the AHP model for efficient assessment of distribution channels. *Sustainability*, 12(24), p.10479. [DOI]
- Yeh, H.F., Cheng, Y.S., Lin, H.I. and Lee, C.H., 2016. Mapping groundwater recharge potential zone using a GIS approach in Hualian River, Taiwan. *Sustainable Environment Research*, 26(1), pp.33–43. [DOI]

# Evaluating the Impact of Community Attitudes on the Sustainability of 3R Temporary Waste Disposal Sites Using Structural Equation Modeling-Partial Least Square (SEM-PLS) in Sukoharjo

Wahyu Kisworo<sup>1</sup>, Sapta Suhardono<sup>1†</sup>, Irfan AN<sup>1</sup> and I Wayan Koko Suryawan<sup>2</sup>

<sup>1</sup>Department of Environmental Sciences, Faculty of Mathematics and Natural Sciences, Universitas Sebelas Maret, Surakarta, 57126, Indonesia

<sup>2</sup>Department of Environmental Engineering, Faculty of Infrastructure Planning, Universitas Pertamina, Jakarta Selatan 12220, Indonesia

†Corresponding author: Sapta Suhardono: sapta.suhardono@staff.uns.ac.id

**Abbreviation:** Nat. Env. & Poll. Technol.  
**Website:** www.neptjournal.com

*Received:* 25-07-2024  
*Revised:* 15-09-2024  
*Accepted:* 23-09-2024

## Key Words:

Temporary waste disposal sites  
 SEM-PLS  
 RAP-temporary waste disposal sites 3R  
 Sustainability

## Citation for the Paper:

Kisworo, W., Suhardono, S., AN, I. and Suryawan, I. W. K., 2025. Evaluating the impact of community attitudes on the sustainability of 3R temporary waste disposal sites using structural equation modeling-partial least square (SEM-PLS) in Sukoharjo. *Nature Environment and Pollution Technology*, 24(2), p. D1702. <https://doi.org/10.46488/NEPT.2025.v24i02.D1702>

*Note: From year 2025, the journal uses Article ID instead of page numbers in citation of the published articles.*



**Copyright:** © 2025 by the authors  
**Licensee:** Technoscience Publications  
 This article is an open access article distributed under the terms and conditions of the Creative Commons Attribution (CC BY) license (<https://creativecommons.org/licenses/by/4.0/>).

## ABSTRACT

In 2023, the waste management situation in Sukoharjo showed a combination of achievements and difficulties. Out of the 12 Temporary Waste Disposal Sites with 3R (Reduce, Reuse, Recycle) facilities, only 4, including Temporary Waste Disposal Sites with 3R (Temporary Waste Disposal Sites 3R) Anugrah Palur, were functioning at their best. This study examines the factors that impact the establishment and long-term viability of these facilities, employing a combination of research methods that incorporates RAP-Temporary Waste Disposal Sites 3R analysis, partial least squares (SEM-PLS), observations, and interviews. The results emphasize that attitude is the most influential component in supporting the growth of Temporary Waste Disposal Sites with 3R, as indicated by a p-value of 0.000. On the other hand, knowledge (0.052) and behavior (0.279) are identified as the least important aspects that hinder development. The Temporary Waste Disposal Sites with 3R have an overall sustainability rating of 72.79, which classifies them as 'very sustainable.' The environmental component achieved a score of 79.54, the social dimension scored 72.88, the management and infrastructure dimension scored 71.30, and the economic dimension scored 65.44. These findings emphasize the crucial importance of community attitudes in promoting sustainable waste management practices. They also highlight specific areas that can be improved to enhance the effectiveness and sustainability of Temporary Waste Disposal Sites with 3R facilities.

## INTRODUCTION

The topic of waste management has been identified as a significant concern for both Indonesian and worldwide society. The issue of waste management is a multifaceted and significant one that confronts numerous countries, encompassing both emerging and industrialized nations. The garbage issue in Indonesia remains unresolved, although the growing population has led to an increase in the amount of waste produced by human activities (Purwaningrum 2016). The projected waste generation in Indonesia for the year 2022 is estimated to be 35,289,535 tonnes per year. This figure is based on information collected from 299 districts and cities, as reported by SIPSN KLHK in 2023. The burgeoning human population and urbanization have resulted in a consistent rise in the quantity of waste generated. The management of garbage varies among established and developing countries, urban and rural groups, and residential and industrial producers (Demirbas 2011). The global population's demographic mix is undergoing rapid changes and is still expanding. Rapid urbanization is taking place globally, primarily in small and mid-sized cities located in low-income nations, as reported by Sun et al. (2016).

Population expansion, economic development, urbanization, and higher living conditions are the main factors contributing to the significant rise in waste generation and the subsequent socio-economic and environmental problems (Malinauskaite et al. 2017).

Municipal solid waste (MSW) refers to the waste generated from many sources, such as homes, businesses, schools, workplaces, and retail enterprises. Examples of these wastes include cardboard, newspapers, cartons, fruits, vegetables, furniture, leftover food, papers, clothing, organic material, as well as non-renewable items such as plastic containers and tin. Municipal solid waste (MSW) refers to any materials that are discarded, unnecessary, and abandoned due to societal and daily activities. Municipal solid waste excludes industrial, radioactive, and medical garbage. These types of waste are managed distinctly (Subramani et al. 2014). MSW, or municipal solid waste, encompasses materials of many physical states, including solid, semi-solid, liquid, or gaseous, that are generated by human activities. The composition of this waste primarily consists of organic matter that undergoes natural decomposition, along with cellulose-based items, including food, cardboard, and paper (Kaur et al. 2023). Human activity inevitably produces solid waste and the way it is handled harms the environment and public health (Khan et al. 2022). As plastic and electronic consumer products become more easily accessible worldwide, people are disposing of a greater amount of waste, which now has a more intricate makeup. These two tendencies pose a challenge for cities responsible for protecting their residents from garbage. Waste, garbage, rubbish, discards, and junk are terms that can be challenging to define precisely and can vary depending on the specific meaning used. Urban regions are experiencing a growing concentration of trash as a result of population movement. The study conducted by Ferronato & Torretta (2019) suggests that there is a positive correlation between population growth, urbanization, expanding income levels, and the amount of waste produced. The composition of household garbage varies among regions due to factors such as lifestyle, economic situations, and waste management policies (Abdel & Mansour 2018). Gaining insight into the composition of garbage in a given location can facilitate the development of suitable and efficient management solutions. Household garbage often consists of a variety of materials, such as food waste, paper, plastic, glass, cloth, and other miscellaneous items.

The key components of any MSW management system are segregation, collection, storage, transportation, and final disposal (Malav et al. 2020). Improper disposal of waste outside leads to detrimental effects on adjacent water bodies as a result of both organic and inorganic contamination.

Moreover, it serves as a magnet for contagious diseases and puts individuals residing close to the perilous elements of the refuse at risk, jeopardizing human well-being. Persistent organic pollutants (POPs) are hazardous substances that are assimilated into the environment and pose a risk to human health. Methane, a significant contributor to greenhouse gas emissions, is emitted during the decomposition of organic waste in landfills, making waste management a primary source of this greenhouse gas. Landfill sites can have detrimental effects on human health and provide a hazard to public safety as a result of soil contamination, water pollution, landfill gas emissions, and accidental fires. Landfill fires may emit highly carcinogenic substances, including dioxins and furans, into the atmosphere (Vassiliadou et al. 2009). Overflowing landfills provide an escalating danger to public safety. In 2015, a landslide occurred at a landfill site in Shenzhen, resulting in 73 human injuries. The landfill was designed to hold a maximum of 4 million cubic meters of garbage at a height of 95 meters. However, it contained 5.8 million cubic meters of waste, reaching a height of 160 meters (Lee et al. 2020). To address the diminishing availability of landfill space, fulfill the public's desire for more recycling, and reduce greenhouse gas emissions, regulatory frameworks are providing support for emerging technologies (Reno 2015). If waste is perceived just as a source of pollution, there will be a reduced level of commitment towards recycling it before its disposal in a landfill or extracting valuable materials from it afterward (Johansson et al. 2012).

The Anugrah Palur Temporary Waste Disposal Site, which was created by the Central Java Province Environment and Forestry Service, is one of the functioning 3R sites in Sukoharjo Regency. This method focuses on managing biodegradable garbage at a local level, namely within groups of 200–2,000 houses (Raharjo 2017). It requires active involvement from both citizens and government entities, particularly the Ministry of Public Works and Public Housing (2020). The Anugrah Palur Temporary Waste Disposal Site is a waste management facility that utilizes social resources and advanced waste processing technology to achieve efficient disposal and recovery at each stage (Heidari et al. 2019). The waste processing conducted at The Anugrah Palur Temporary Waste Disposal Site (TPS) 3R is of utmost importance to avoid direct landfilling, hence safeguarding the integrity of the site, alleviating the burden on landfills, and prolonging its operational lifespan (Mulyati et al. 2019). This research employs an approach similar to prior studies but specifically emphasizes distinct elements. Wielgosiński et al. (2021) conducted a study in Poland to examine the mass balance of municipal solid waste in relation to circular economy principles. They estimated that implementing these principles might potentially reduce trash by 3.0–3.5 million



metric tonnes. Muhammed et al. (2021) utilized the Structural Equation Modeling-Partial Least Squares (SEM-PLS) technique to develop a model for implementing 3R (Reduce, Reuse, Recycle) methods to achieve sustainable construction waste reduction. Their efforts resulted in a significant decrease of 2.47 tonnes per day in housing projects, with a high explanatory power shown by an  $R^2$  value of 0.83%. The study conducted by Mulyana et al. (2021) evaluated the sustainability of school-based waste banks using the RAPFISH analysis method. The findings indicated a robust performance in both ecological and institutional aspects. In a study conducted by Amin & Ahmed (2024), it is stressed that including community perspectives and economic considerations in waste management strategies is crucial. The study highlights the influence of tourists' awareness and willingness to financially support sustainable beach waste management on the development of effective policies. This enhances the utilization of SEM-PLS in our research, which seeks to assess the elements that impact community engagement and the long-term viability of waste management strategies. Furthermore, the revised RAP-Temporary Waste Disposal Sites 3R methodology will be utilized to evaluate the sustainability of the Anugrah Palur Temporary Waste Disposal Site.

## MATERIALS AND METHODS

### Location and Time of Research

The investigation was conducted in Palur Village, Mojolaban District, Sukoharjo Regency, Central Java. The research will be conducted in Palur Village, specifically at the Anugrah Palur Temporary Waste Disposal Site (TPS) with 3R. The precise geographical coordinates for the location of Temporary Waste Disposal Sites 3R Anugrah Palur are 7.34°20.4 South Latitude and 110.51°48.3 East Longitude. The study was conducted between February 2024 and April 2024.

### Research Tools and Materials

This research necessitates the use of many technologies to ensure the uninterrupted progress of the study. These tools include computers, questionnaire forms, interview forms, voice recorders, documentation tools or cameras, Microsoft Excel 2019 software, Microsoft Excel – Add-Ins Rapfish software, and SmartPLS software version 3.29. The research materials utilized in this study encompass the data findings derived from questionnaires administered to managers and depositors at Temporary Waste Disposal Sites with 3R, as well as the outcomes of interviews conducted with Temporary Waste Disposal Sites with 3R management.

Additionally, population data and information pertaining to the community that deposits garbage at Temporary Waste Disposal Sites with 3R were also incorporated.

### Data Analysis Technique

The methods used in this research are mixed methods (quantitative and qualitative methods). The analytical techniques used in this research include:

**Analysis of supporting and inhibiting factors:** Structural Equation Modeling (SEM) is a multivariate analysis method that combines path analysis, factor analysis, and regression analysis (Novian and Herlina, 2022). An analysis was conducted using Structural Equation Modeling-Partial Least Square (SEM-PLS) to examine the elements that encourage or hinder community engagement in Temporary Waste Disposal Sites with 3R in Anugrah Palur Temporary Waste Disposal Sites 3R. The study is conducted using SmartPLS version 3.29 software. The independent variable examined in this study is the presence of Temporary Waste Disposal Sites that offer 3R services. Factors that impact include knowledge, behavior, and attitudes. The Likert scale is employed for measurement. The evaluation of community engagement is measured on a scale from 1 to 5, with 1 being the lowest score and 5 being the greatest score. The latent variables and indicators employed, as per Haqq's (2018) methodology, have been presented in Table 1, with several modifications made for this particular study.

The variables in the SEM analysis used include temporary waste disposal 3R services and community participation (knowledge, behavior, attitudes). Identity is only used to determine the general characteristics of the respondent. The total variables used for SEM analysis are 4, with 18 indicators. Evaluation of SEM analysis consists of 2 types, namely measurement model evaluation and structural model evaluation. Evaluation of the measurement model includes validity and reliability tests. Meanwhile, structural evaluation was carried out to evaluate the relationship between existing latent variables using R-square ( $R^2$ ), Q-square Predictive Relevance ( $Q^2$ ), and Goodness of Fit (GoF) values. The  $R^2$  value illustrates the ability of the influencing variable to explain variations in the influenced variable. The value of  $Q^2$  shows the predictive ability of the existing model with the formula:

$$Q^2 = 1 - (1 - R^2) \quad \dots(4)$$

The  $R^2$  and  $Q^2$  assessments are carried out with classifications with categories less than 0.33, a weak classification, more than equal to 0.33 and less than 0.67, classified as moderate, and equal to more than 0.67, a strong classification. Next, Goodness of Fit (GoF) is carried out to

Table 1: Variables and Indicators of Supporting and Inhibiting Factors for Temporary Waste Disposal Sites 3R.

Variable	Indicator
<b>Service of Temporary Waste Disposal Sites 3R</b>	
Y <sub>1.1</sub>	Find out the affordability of Temporary Waste Disposal Sites 3R locations
Y <sub>1.2</sub>	Find out the ease of the process of depositing waste to Temporary Waste Disposal Sites 3R
Y <sub>1.3</sub>	Know the accuracy of the Temporary Waste Disposal Sites 3R activity schedule.
Y <sub>1.4</sub>	Knowing the economic benefits of waste sorting at Temporary Waste Disposal Sites, 3R
Y <sub>1.5</sub>	Knowing public awareness of the environment through Temporary Waste Disposal Sites 3R facilities
<b>SOCIETY PARTICIPATION</b>	
<b>Identity</b>	
X <sub>1.1</sub>	Gender (1) Male (2) Female
X <sub>1.2</sub>	Last Education (1) Elementary School/equal (2) Junior High School/equal (3) Senior High School/equal (4) Bachelor's, master's, and doctoral degree
X <sub>1.3</sub>	Job (1) Work (2) Not Work
X <sub>1.4</sub>	Expenses per month (1) ≤ Rp.2.215.482 (2) > Rp.2.215.482
<b>VARIABLE</b>	<b>INDICATOR</b>
<b>Knowledge</b>	
x <sub>2.1</sub>	Knowing about waste sorting
X <sub>2.2</sub>	Knowing that waste can have economic value
X <sub>2.3</sub>	Understand about 3R activities.
X <sub>2.4</sub>	Understand the benefits of Temporary Waste Disposal Sites 3R facilities
X <sub>2.5</sub>	Knowing that Temporary Waste Disposal Sites 3R activities are a means of increasing awareness of the environment
<b>Behavior</b>	
x <sub>3.1</sub>	Sorting household waste
X <sub>3.2</sub>	Participated in socialization regarding waste management held by the government or environmental cadres
X <sub>3.3</sub>	Provide ideas/thoughts on managing Temporary Waste Disposal Sites 3R in the future.
X <sub>3.4</sub>	Provide feedback on the Temporary Waste Disposal Sites 3R program
<b>Attitude</b>	
x <sub>4.1</sub>	Willing to sort waste from home
X <sub>4.2</sub>	The program for transporting waste to Temporary Waste Disposal Sites 3R has no problems.
X <sub>4.3</sub>	Depositing waste at Temporary Waste Disposal Sites 3R helps in managing waste.
X <sub>4.4</sub>	Willing to participate in outreach activities about waste sorting/management

test the accuracy of the model that has been formed. The classification values used are  $GoF < 0.25$  low classification,  $0.25 \leq GoF < 0.36$  medium classification, and  $GoF \geq 0.36$  high classification. The formula used in the GoF assessment is as follows.

$$GoF = \sqrt{AVE \times R^2} \quad \dots(5)$$

Next, correlation tests and significance tests were carried out. The correlation test is carried out to determine the magnitude of the relationship between existing variables, with a value range of 1 to -1. Assessing the correlation test, it can be said that the variables have a close relationship if they approach the value -1 or 1. The significance test is carried out to reveal variables that can provide the final results of

this analysis. The initial hypothesis for the significance test in this research is as follows.

1. Variables influencing the development of Temporary Waste Disposal Sites 3R

Hypothesis:

$H_0$ : The variables do not have a significant effect on the development of Temporary Waste Disposal Sites 3R

$H_1$ : Variables have a significant effect on the development of Temporary Waste Disposal Sites 3R

The significance level ( $\alpha$ ) is 5% = 0,05

Critical area:  $H_0$  rejected dan  $H_1$  accepted if the p-value < 0,05

### Sustainability Analysis

The Rapfish method was initially developed to formulate development policies related to sustainable fisheries, but as science developed, it began to be implemented in the fields of agriculture, forestry, animal husbandry, and environmental management (Warningsih et al. 2020). The sustainability status at Temporary Waste Disposal Sites 3R was analyzed using the modified RAPFISH (Rapid Appraisal Techniques for Fisheries) technique or RAP-Temporary Waste Disposal Sites 3R. According to Rossi (2022), the stages of sustainability analysis through RAPFISH are as follows:

1. Determination of dimensions and attributes of the object under study.
2. Scoring is carried out on predetermined attributes based on an ordinal scale.
3. Multidimensional Scaling for bad or good units (Sustainability index value) via the ALSCAL algorithm.
4. Leveraging analysis to detect dominant attributes with values ranging between 2% to 6%, as measured by changes in root mean square (RMS).

Modified RAPFISH or RAP-Temporary Waste Disposal Sites 3R analysis was carried out. The RAPFISH dimensions for sustainable fisheries management include ecological, technological, ethical, social, and economic dimensions (Muslim et al. 2019). The scoring of the questionnaire was assessed as very suitable (5), suitable (4), quite suitable (3), not suitable (2), and very unsuitable (1). For analysis in this study, RAP-Temporary Waste Disposal Sites 3R was used based on 4 dimensions with 6 attributes. The management and infrastructure dimensions have attributes in the form of organizational structure, completeness and application of the main processing technology, processing capacity, trained staff, the volume of residue transported to the landfill, as well as the condition of buildings and land for development.

The environmental dimension is attributed to the quality of the surrounding environment, the ability to reduce pollution, waste sorting at Temporary Waste Disposal Sites 3R, the availability of green open space, the waste transportation process, and processing alternatives. The social dimension with attributes includes social networks, norms (social conditions of society in disposing of waste), trust in waste management, employment, socialization and education, and willingness to pay contributions. The economic dimension has attributes including financial assistance from the government, financial independence, processing costs, product and service marketing programs, village economic equality, and labor income. The final result is the ordination of the sustainability index in categories with a value of 0–25 having unsustainable status, a value >25 – 50 having less sustainable status, a value >50 – 75 having moderately sustainable status, and >75–100 having sustainable status (Rossi 2022).

## RESULTS AND DISCUSSION

### Overview of Questionnaire Respondents

Respondents to the questionnaire for analysis of inhibiting-supporting factors and sustainability of Temporary Waste Disposal Sites 3R Anugrah Palur were people who deposited waste and managed Temporary Waste Disposal Sites 3R. The number of respondents in this study was 78 people. The characteristics of the respondents obtained include gender, age, highest level of education, occupation, number of family members, and monthly expenses. According to Kumar & Samadder (2017), the amount of waste generated can be influenced by total family income, education, employment, etc. The characteristics of the respondents can be seen in Table 2.

The distribution of male respondents was 48 people (61.54%). The majority of respondents were male because interviews were conducted during non-productive hours. The ages of the respondents were quite varied, between 17–62 years. The average age of the respondents is 41 years. Respondents' ages were predominantly between 26–45 years, with a proportion of 44 people (56.41%). The distribution of respondents based on their latest education was dominated by the high school/equivalent category with a percentage of 52.56%. The distribution of respondents who had family members of 1 person was 6 people, the number of family members of 2 people was 13 people, the number of family members of 3 people was 30 people, and the number of family members >3 people was 29 people. The average number of respondents' family members is 3 people. The number of family members tends to influence consumption patterns

Table 2: Results of Respondent Characteristics.

No	Category	Number of Respondents (people)	Percentage (%)
<b>Gender</b>			
1.	Male	48	61,54
2.	Female	30	38,46
<b>Age</b>			
1.	17-25	8	10,26
2.	26-45	44	56,41
3.	>45	26	33,33
<b>Last Education</b>			
1.	Elementary School/equal	7	8,97
2.	Junior High School/equal	13	16,67
3.	Senior High School/equal	41	52,56
4.	Bachelor's	16	20,51
5.	Master's	1	1,28
<b>Job</b>			
1.	Government employees	4	5,13
2.	Private employees	27	34,62
3.	Businessman	13	16,67
4.	Student/Students	3	3,85
5.	Temporary Waste Disposal Sites 3R officer	6	7,69
6.	Other	1	1,28
7.	Doesn't work	24	30,76
<b>Number of Family Members (people)</b>			
1.	1	6	7,69
2.	2	13	16,67
3.	3	30	38,46
4.	>3	29	37,18
<b>Monthly Expenses (IDR)</b>			
1.	≤ Rp.2.215.482	36	46,15
2.	> Rp.2.215.482	42	53,85

and waste composition. The amount of Rp. 2,215,482 is the minimum wage for Sukoharjo Regency in 2024. Based on the results, which show that the monthly expenditure of respondents depositing waste to TPS 3R is dominated by a monthly expenditure of more than Rp. 2,215,482.

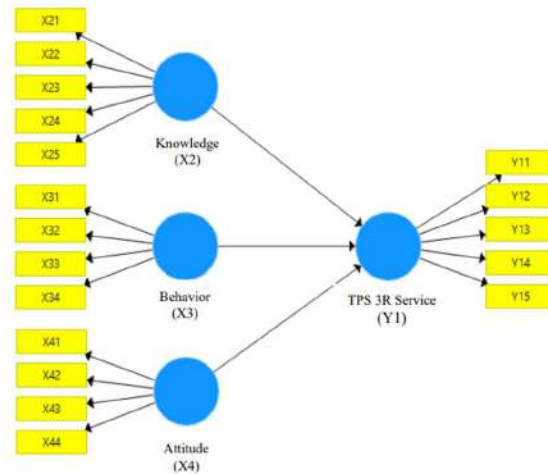
## SUPPORTING AND INHIBITING FACTORS

### A. Evaluation of Measurement Models/Outer Model

Fig. 1 is a diagram model resulting from processing in the SEM-PLS application for variables and indicators. A validity test is a test to determine whether an indicator can be used and is valid. The validity test in this research can be seen in Table 3.

Loading factor is a correlation of existing variables and indicators. Each indicator in the supporting and inhibiting factors aspects of Temporary Waste Disposal Sites 3R has a loading factor value of more than 0.5. Thus, each indicator used in this analysis is valid and can be understood by respondents. The reliability test is carried out after the validity test to determine whether the level or value of the existing indicators is reliable or reliable for use in measuring the value of existing variables. The reliability of each indicator is measured using the results of Cronbach's alpha and composite reliability values. The reliability results for each variable are in Table 4.





Source: Analysis, Primary Data (2024)

Fig. 1: Supporting and Inhibiting Factor Model Diagram.

Table 3: Results of Validity.

No	Variable	Indicator	Loading Factor
1.	Temporary Waste Disposal Sites 3R Services	Y11	0,668
2.		Y12	0,680
3.		Y13	0,777
4.		Y14	0,723
5.		Y15	0,691
6.	Knowledge	X11	0,727
7.		X12	0,779
8.		X13	0,642
9.		X14	0,775
10.		X15	0,666
11.	Behavior	X21	0,771
12.		X22	0,803
13.		X23	0,695
14.		X24	0,735
15.		X25	0,735
16.	Attitude	X31	0,861
17.		X32	0,738
18.		X33	0,648
19.		X34	0,644

Based on Table 4, the reliability test for Temporary Waste Disposal Sites 3R service variables, knowledge, behavior, and attitudes has reliable values, namely with Cronbach's alpha value  $\geq 0.5$  and composite reliability value  $\geq 0.7$  for each existing variable. Thus, the validity and reliability test of the variables used is reliable or reliable in evaluating the measurement model (outer model) of the structural equation model.

Table 4: Result of Reliability.

No.	Variable	Cronbach's Alpha	Composite Reliability
1.	Service of Temporary Waste Disposal Sites 3R	0,753	0,834
2.	Knowledge	0,772	0,843
3.	Behavior	0,788	0,838
4.	Attitude	0,700	0,816

## B. Structural Model Evaluation/Inner Model

Structural model evaluation is carried out after evaluating the measurement model to determine the relationship between variables and ensure that the structural model that has been formed is accurate. Structural model evaluation was carried out using R-Square, Q-Square, and Goodness of Fit. The R-Square ( $R^2$ ) value or determinant coefficient can represent the level of ability of the influencing/independent variable (X) to explain the variance contained in the influenced/dependent variable (Y). The assessment range for  $R^2$  is 0 to 1, where the closer the value is to 1, the better the value. The  $R^2$  value obtained for the Temporary Waste Disposal Sites 3R service variable is 0.497. The  $R^2$  value shows that Temporary Waste Disposal Sites 3R services can be explained by 0.497 by the existing variables, namely knowledge, behavior, and attitude variables. Another 0.503 value is explained by variables outside the model formed.

*Q-Square* ( $Q^2$ ) or predictive relevance is a measurement of the predictive ability of a model or the level of observation values that can be produced from a model. The value obtained for  $Q^2$  is 0.497, which is classified as moderate. Based on this value, the relevance of the predictions formed from the model is classified as moderate. The goodness of fit (GoF) is useful for assessing the accuracy of the model that has been formed. GoF can be assessed after knowing the Average Variance Extracted (AVE) value. AVE values that have an assessment of  $> 0.5$  are classified as having good discriminant validity. The following are the AVE values contained in each variable, which can be seen in Table 5.

Based on the AVE values that have been obtained, all the variables used have good values, namely more than 0.5. Next, calculations are carried out to determine the GoF value. The GoF value obtained was 0.513. Referring to the existing categories, the GoF value is relatively high, namely  $\geq 0.36$ . A GoF value of 0.513 can indicate that the model formed is classified as high or good.

## C. Correlation Test

Correlation tests are carried out to determine the magnitude of the relationship between influencing variables that exist on the influenced variable. This correlation test has

Table 5: Average Variance Extracted Results.

No.	Variable	AVE value
1.	Service of Temporary Waste Disposal Sites 3R	0,503
2.	Knowledge	0,518
3.	Behavior	0,565
4.	Attitude	0,530

a range of values ranging from -1 to 1. Correlation values that are closer to 1 or -1 can be concluded that the variable relationship is getting closer. The correlation test results can be seen in Table 6.

Based on Table 6, the correlation test value for variables influencing the variables influenced or Temporary Waste Disposal Sites 3R services is obtained, including the knowledge variable of 0.543, the behavior variable of 0.248, and the attitude variable of 0.677. The highest correlation value was obtained for the attitude variable (0.677), while the lowest correlation value was for the behavior variable (0.248).

## D. Significance Test

Each variable has an influence, but to evaluate variables with a significant level in the measurement model and structural model, a significance test is carried out. The significant test produces 2 assessment criteria, namely T-statistics and p-value. One of the assessment criteria can be used. Namely, the T-statistics assessment is said to be significant if the value is  $> 1.96$ , while the p-value assessment is said to be significant if the value is  $< 0.05$ . The significance assessment in this study uses p-value. The following are the results of the variable significance values, which can be seen in Table 7.

Based on Table 7, the significance values for the knowledge, behavior, and attitude variables are obtained. The variable that has a significant effect is the attitude variable, which has a value of 0.000. The significant influencing variables from highest to lowest, respectively, according to the p-value, are the attitude variable of 0.000, the knowledge

Table 6: Result of the Correlation Test.

No.	Variable	Correlation Value
1.	Knowledge→Temporary Waste Disposal Sites 3R Services	0,543
2.	Behavior→Temporary Waste Disposal Sites 3R Services	0,248
3.	Attitude→Temporary Waste Disposal Sites 3R Services	0,677

= Parameters not contemplated, X= Parameters used in AI studies in Amazonia, Adapted from: Torres et al.(2009)

Table 7: Result of Variable Significance Test.

No	Variable	T-statistics	p-value
1.	Knowledge→Temporary Waste Disposal Sites 3R Services	1,941	0,052
2.	Behavior→Temporary Waste Disposal Sites 3R Services	1,084	0,279
3.	Attitude→Temporary Waste Disposal Sites 3R Services	4,918	0,000

variable of 0.052, and the behavior variable of 0.279. Thus, it was found that the supporting factors for the running of services and the development of Temporary Waste Disposal Sites 3R were found in the attitude variable, while the knowledge and behavior variables did not have a significant effect and were an inhibiting factor for development, but it cannot be said that it is hindering the current Temporary Waste Disposal Sites 3R service. For optimal development in Temporary Waste Disposal Sites 3R, it is necessary to increase knowledge and behavior variables.

The significance test is also used to measure the significant influence of each indicator in forming variables. The following are the results of the significance values for each indicator, which can be seen in Table 8.

Based on the results of the indicator significance test obtained, the Temporary Waste Disposal Sites 3R service variable has a significant value for all indicators for the development of Temporary Waste Disposal Sites 3R, namely  $<0.05$ . These indicators include affordability, ease of depositing waste, accuracy of transportation schedules, benefits from waste sorting, and public awareness of the environment through the existence of 3R TPS facilities. The knowledge variable has a significant influence on the

indicator X21 with a value of 0.000, X22 with a value of 0.001, X24 with a value of 0.004, and X25 with a value of 0.001. Indicators with significant influence can be interpreted as meaning that the community understands the existing indicators and is a supporting factor in the development of Temporary Waste Disposal Sites 3R, namely public knowledge regarding waste sorting, waste can have economic value, the usefulness of Temporary Waste Disposal Sites 3R facilities, and Temporary Waste Disposal Sites 3R activities as a means of increasing awareness of the environment. Meanwhile, there is no significant influence on the X23 indicator with a value of 0.071, which is an understanding of 3R activities.

The indicator for the behavioral variable with a significant influence value as a supporting factor for the development of Temporary Waste Disposal Sites 3R is indicator X32 with a value of 0.018, namely regarding participation in the socialization of waste management. Indicators of behavioral variables with insignificant influence as inhibiting factors for the development of Temporary Waste Disposal Sites 3R are indicators X31 with a value of 0.123, X33 with a value of 0.383, and X34 with a value of 0.403. These indicators relate to behavior in sorting waste, providing ideas, and providing responses to the Temporary Waste Disposal Sites 3R program. The attitude variable has a value with a significant influence as a supporting factor for the development of Temporary Waste Disposal Sites 3R on all indicators, namely with a total value of  $<0.05$ . These indicators include the willingness to sort waste from home, the absence of obstacles to transporting waste, the level of assistance from the community in managing waste, and the willingness to participate in waste management socialization.

The attitude of the community's willingness to sort waste if it is required in the future by TPS 3R Anugrah Palur is relatively high which has an influence on the development of TPS 3R Anugrah Palur. As long as TPS 3R Anugrah Palur has been running, there have been no obstacles that have had a significant impact on the community, especially in the transportation process. This is due to the regular schedule for transporting the waste, namely Monday to Saturday, and routine maintenance to support the optimal operation of TPS 3R Anugrah Palur. The significant value of the attitude variable makes this variable support the development of TPS 3R from the aspect of community participation.

In previous research regarding aspects of community participation in waste management facilities using SEM-PLS analysis by Haqq (2018), it was found that variables with a significant influence as supporting the development of waste bank facilities in the South Surabaya area according to the p-value were behavior (0.040), while the variable with

Table 8: Results of the Indicator Significance Test.

No.	Variable	<i>T-statistics</i>	<i>p-value</i>
1.	Y11←Temporary Waste Disposal Sites 3R Services	3,334	0,001
2.	Y12←Temporary Waste Disposal Sites 3R Services	3,432	0,001
3.	Y13←Temporary Waste Disposal Sites 3R Services	5,317	0,000
4.	Y14←Temporary Waste Disposal Sites 3R Services	4,851	0,000
5.	Y15←Temporary Waste Disposal Sites 3R Services	3,747	0,000
6.	X21←Knowledge	4,738	0,000
7.	X22←Knowledge	3,365	0,001
8.	X23←Knowledge	1,803	0,071
9.	X24←Knowledge	2,890	0,004
10.	X25←Knowledge	3,429	0,001
11.	X31←Behavior	1,544	0,123
12.	X32←Behavior	2,374	0,018
13.	X33←Behavior	0,873	0,383
14.	X34←Behavior	0,836	0,403
15.	X41←Attitude	7,800	0,000
16.	X42←Attitude	4,144	0,000
17.	X43←Attitude	3,858	0,000
18.	X44←Attitude	2,858	0,004

an insignificant effect obtained on the knowledge (0.210) and attitude (0.580) variables. Previous research related to facilities on behavioral variables has the highest value in supporting the development of waste banks in the Surabaya area, which is supported by indicators of significant influence on the community who have sorted waste from home and participated in socialization.

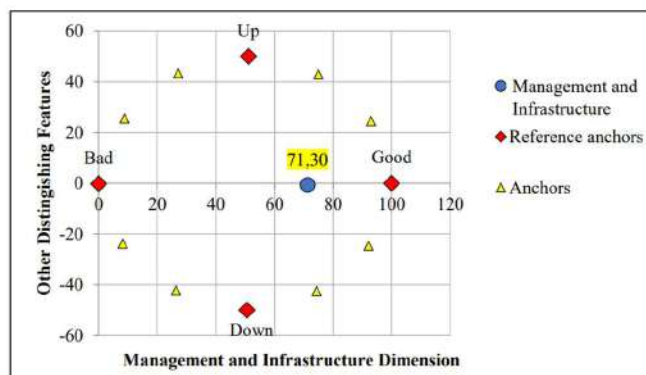
Education and age are indirect factors apart from indicators that influence the knowledge, behavior, and attitude variables. Education can be a means for someone to gain knowledge in protecting the environment, obtain information on the importance of managing waste, and provide information related to behavior that has a positive impact on waste management. This correlates with the education level of the respondents, which is dominated by high school and bachelor's degrees. However, the factor that causes the knowledge variable to be insignificant is the lack of intensity of socialization or non-formal education related to waste management at TPS 3R. TPS 3R socialization was only carried out 3 times. The age of respondents was dominated by those between 26-45 years old. According

to Meidiana et al. (2021), age is an important factor in determining a person's decisions, especially behavior in waste management. This is in line with this statement, where in this study, it was found that the dominance of those aged 26-45 years indirectly influenced the high value of the attitude variable.

So, it is necessary to increase the knowledge variable, namely the understanding indicator regarding 3R activities, and increase the attitude variable in the behavioral indicators in sorting waste, providing ideas, and providing responses to the 3R TPS program. These variables can be improved to support the development of Temporary Waste Disposal Sites 3R through routine outreach, policies for separating waste from homes, as well as opening access for the community to provide ideas and responses to Temporary Waste Disposal Sites 3R.

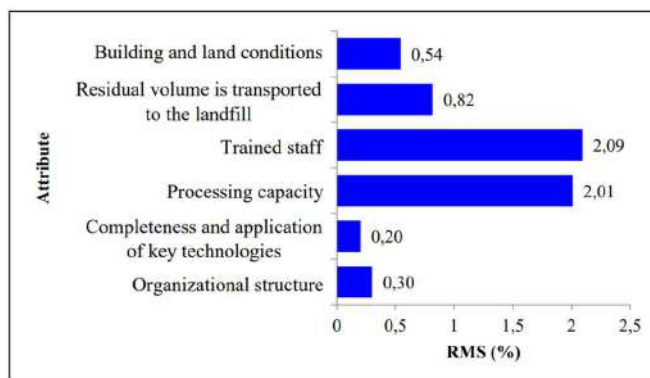
### Sustainability of Temporary Waste Disposal Sites 3R Anugrah Palur

**Sustainability status of management and infrastructure dimensions:** The management and infrastructure dimension



Source: Analysis, Primary Data (2024)

Fig. 2: Management and Infrastructure Dimensions Sustainability Ordinance.



Source: Analysis, Primary Data (2024)

Fig. 3: Leverage dimensions of management and infrastructure.



has six attributes used in sustainability analysis, namely organizational structure, completeness and application of main processing technology, processing capacity, trained staff, the volume of residue transported to landfill, and condition of buildings and land for development. This sustainability analysis is carried out to determine the value of the sustainability index for sustainability status and leverage to determine the sensitive value of existing attributes. The following is a mapping of the sustainability index coordination from the management and infrastructure dimensions shown in Fig. 2.

Based on the coordination analysis carried out on the management and infrastructure dimensions, a sustainability index value of 71.30 was obtained. These results show that the management and infrastructure dimensions of Temporary Waste Disposal Sites 3R have a fairly sustainable sustainability status category. The results of the leverage analysis of management and infrastructure dimensions can be seen in Table Fig. 3.

Based on Fig. 3, leverage analysis shows that there are 2 dominant sensitive attributes for sustainability, namely processing capacity and trained staff. Processing capacity is a sensitive attribute with a root mean square (RMS) value of 2.01%. The existing processing capacity that enters Temporary Waste Disposal Sites 3R Anugrah Palur per day is an average of 724.76 kg. The daily amount of waste is suitable for entering the organic sorting and chopping room and is in accordance with the number of officers for the processing process. Waste processing at Temporary Waste Disposal Sites 3R is focused on organic waste, namely into compost with an estimated waiting period of 2-3 months. For sustainability of this attribute, it is necessary to increase processing capacity in parallel with increasing capacity or can be adjusted to waste processing working hours. Adjustments to working hours have now been made, namely if, on certain days, there is excess waste capacity at Temporary Waste Disposal Sites 3R, overtime hours are carried out with additional payments to Temporary Waste Disposal Sites 3R officers.

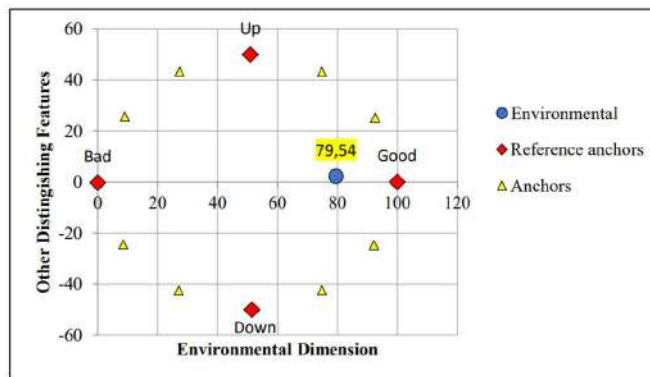
The most sensitive attribute in the management and infrastructure dimensions is the trained staff attribute, with an RMS value of 2.9%. This trained staff attribute is sensitive because Temporary Waste Disposal Sites 3R staff or officers are an important element in the sustainability of Temporary Waste Disposal Sites 3R, especially in transporting, sorting, and processing waste. Staff on duty at Temporary Waste Disposal Sites 3R are trained informally at the start of work regarding operational mechanisms in the field as well as standard operational procedures that need to be adhered to in carrying out work. It is necessary

to improve aspects that support staff to be better trained, which can be done through formal training for Temporary Waste Disposal Sites 3R officers and comparative studies of other Temporary Waste Disposal Sites 3R that have been operating for a long time. Meanwhile, other attributes in the management and infrastructure dimensions are classified as not dominant with each sensitive value, including organizational structure (0.30%), completeness and application of the main processing technology (0.20%), the volume of residue transported to landfill (0.82), and building and land conditions for development (0.54).

**Environmental dimension sustainability status:** Attributes in the environmental dimension analysis consist of the quality of the surrounding environment, the ability to reduce pollution, waste sorting at Temporary Waste Disposal Sites 3R, availability of green open space, waste transportation process, and processing alternatives. The environmental dimension is an important aspect that needs to be considered in implementing and developing Temporary Waste Disposal Sites 3R. The following are the results of the environmental dimension coordination mapping, which can be seen in Fig. 4.

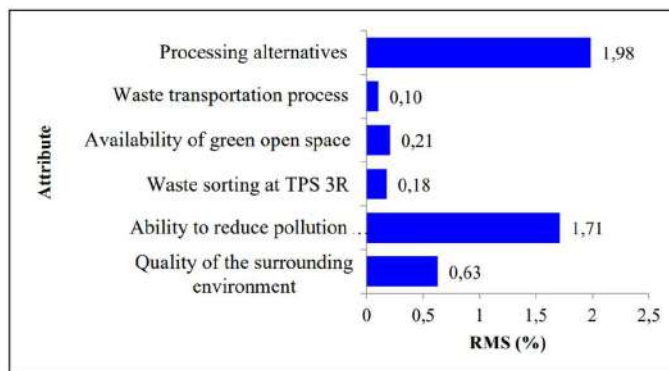
Based on Fig. 4, the results of the environmental dimension index ordination analysis obtained a sustainability index value of 79.54. The sustainability index value of 79.54 indicates that the environmental dimension has a sustainable category. The environmental dimension has the highest sustainable index value compared to other dimensions in Temporary Waste Disposal Sites 3R. The results of the environmental dimension leverage analysis can be seen in Fig. 5.

Based on Fig. 5, none of the attributes in the environmental dimension are within the sensitive value range of 2-6%. The sensitive value of each attribute includes the quality of the surrounding environment (0.62%), the ability to reduce pollution (1.71%), waste sorting at Temporary Waste Disposal Sites 3R (0.18%), availability of green open space (0.21%), waste transportation process (0.10%), and processing alternatives (1.98%). The RMS value of alternative waste processing attributes shows a sensitive value of 1.98%. Waste processing at Temporary Waste Disposal Sites 3R is currently focused on processing organic waste into compost. Previously, there was waste management using maggots but it has been stopped. The technology or tools for processing inorganic waste currently do not exist at Temporary Waste Disposal Sites 3R, so inorganic marketable waste is stored in the inorganic waste warehouse and sold during periods of increasing selling prices to local collectors. This improvement can be done by adding inorganic waste processing technology such as plastic chopping machines and plastic pellet machines.



Source: Analysis, Primary Data (2024)

Fig. 4: Ordination of the Environmental Dimension Sustainability Index.



Source: Analysis, Primary Data (2024)

Fig. 5: Environmental Dimension Leverage.

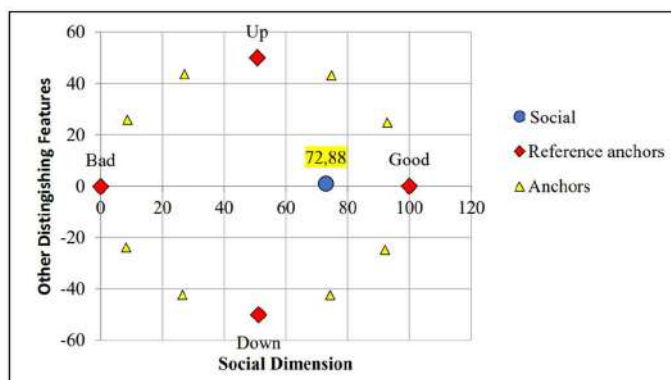
**Social dimension sustainability status:** The social dimension for sustainability analysis uses 6 attributes, including social networks, norms (social conditions of society in disposing of waste), trust in waste management, employment, socialization and education, and willingness to pay contributions. The following is a mapping of the social dimension of Temporary Waste Disposal Sites 3R sustainability status coordination, which can be seen in Fig. 6.

Based on Fig. 6, the results of the social dimension ordination analysis obtained a sustainability index value of 72.88. The sustainability index value shows that the social dimension has a fairly sustainable category. The results of the social dimension leverage analysis can be seen in Fig. 7.

Based on Fig. 7, there are leverage values that show 2 attributes with dominant sensitive values in the social dimension. These attributes include trust in waste management as well as outreach and education. The waste management trust attribute is the highest sensitive attribute in the social dimension, with an RMS value of 2.96%. The trust attribute is an element that forms social capital in society, along with

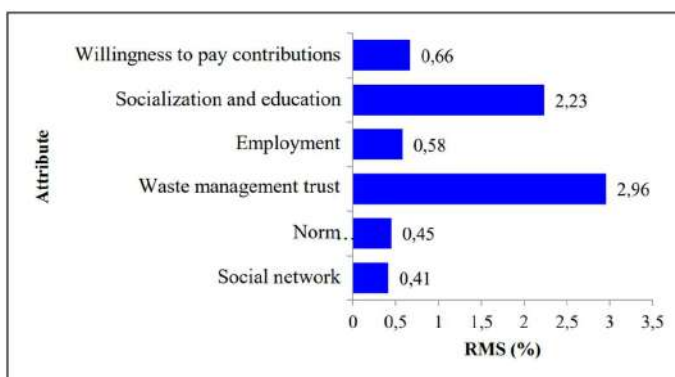
social network attributes and norm attributes. Trust is a form of hope that arises in a group that acts normally and honestly and works together according to shared norms to achieve common interests (Fadli, 2020). The existence of trust can produce effective cooperation because there is a willingness to prioritize common interests. The management trust attribute is an important aspect of the sustainability of Temporary Waste Disposal Sites 3R, especially in preparing for further development. Temporary Waste Disposal Sites 3R is trusted by the public to manage household waste and reduce waste before it goes to the landfill. Thus, public trust in Temporary Waste Disposal Sites 3R needs to continue to be increased for the sustainability of Temporary Waste Disposal Sites 3R. To increase trust in waste management, this can be done by rebranding waste service information to the public, namely regarding changes in services. Previously, there was a TPS, but it has been changed to Temporary Waste Disposal Sites 3R. This can be done through routine outreach to the community.

Socialization and education are included in the dominant sensitive attributes with an RMS value of 2.23%. Since



Source: Analysis, Primary Data (2024)

Fig. 6: Ordination of the Social Dimension Sustainability Index.



Source: Analysis, Primary Data (2024)

Fig. 7: Social Dimension Leverage.

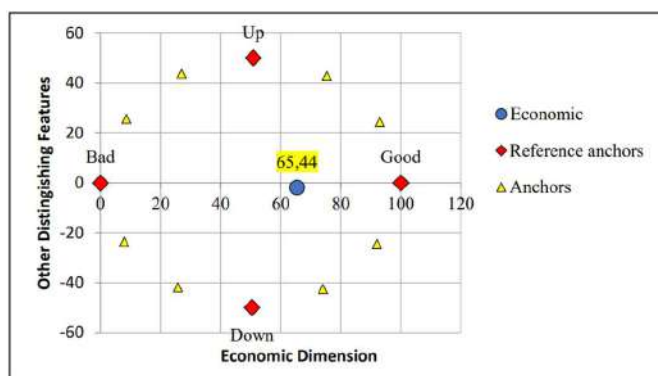
Temporary Waste Disposal Sites 3R began operating in 2023 until it started operating in 2024, there have been 3 formal outreach and education sessions for the community. Apart from that, socialization has been carried out regarding waste management at Temporary Waste Disposal Sites 3R, which was conveyed by the sub-district and BUMDes to each RT-RW head. Each RT-RW head conveyed this outreach to the local community at regular meetings in their respective areas. The socialization and education attributes are the dominant sensitive attributes in the sustainability of Temporary Waste Disposal Sites 3R, so more attention is needed for improvement to ensure the sustainability of Temporary Waste Disposal Sites 3R. There is a need to increase the intensity of outreach and education to the public, and this can be done offline with a regular schedule and online, namely outreach in the form of information on digital flyers or distribution in the form of invitations to sort waste from home.

**Economic dimension sustainability status:** The sustainability status of the economic dimension is analyzed using 6 attributes, including financial assistance from the

government, financial independence, processing costs, product and service marketing programs, village economic equality, and labor income. The following are the results of mapping the ordination of the economic dimension of the sustainability index, which can be seen in Fig. 8.

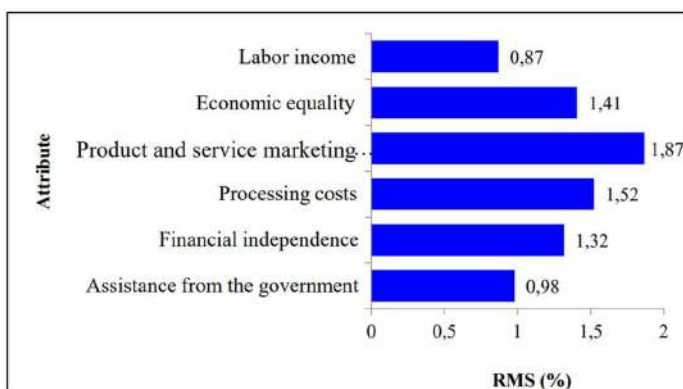
Based on Fig. 8, the results of the economic dimension ordination analysis obtained a sustainability index value of 65.44. The sustainability index value shows that the economic dimension has a fairly sustainable category. The economic dimension has the lowest sustainable index value compared to other dimensions in Temporary Waste Disposal Sites 3R. The results of the economic dimension leverage analysis can be seen in Fig. 9.

Based on Fig. 9, there are no sensitive attributes with a dominant level of more than 2%. The product and service marketing program attributes obtained an RMS value of 1.87%. Product and service marketing programs are the attributes with the highest sensitive value on the economic dimension. This attribute is in line with Village SDGs Number 12, namely environmentally conscious village



Source: Analysis, Primary Data (2024)

Fig. 8: Ordination of the Economic Dimension Sustainability Index.



Source: Analysis, Primary Data (2024)

Fig. 9: Economic Dimension Leverage.

consumption and production. Marketing of organic products is carried out by selling compost fertilizer to farmers and plant cultivators at a price of IDR 10,000 per 10 kg. Most of the marketable inorganic waste is sold to collectors in the Palur sub-district area during periods of rising prices. Efforts that can be made to increase sustainability in marketing programs and service attributes are to increase the marketing reach of products outside the Palur Subdistrict.

### Multidimensional Analysis of Temporary Waste Disposal Sites 3R Sustainability

Analysis of each attribute has been carried out and a sustainability index value has been produced for each dimension. The following is a continuous kite diagram of each, which can be seen in Fig. 10.

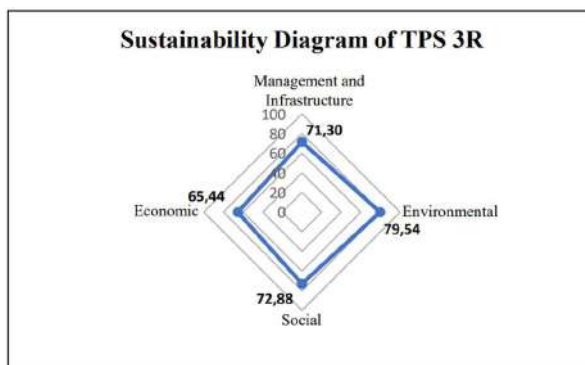
Based on the diagram above, the sustainability index values with the highest to lowest values, respectively, include the environmental dimension (79.54), the social dimension (72.88), the management and infrastructure dimension (71.30), and the economic dimension (65.44).

The environmental dimension has the highest sustainability value with the sustainable status category. Meanwhile, the management and infrastructure dimensions, social dimensions, and economic dimensions are in the moderately sustainable status category.

The details of the sustainability index value, stress value, and R-Square for each dimension can be seen in Table 9. Thus, efforts are needed to improve management and infrastructure, as social and economic dimensions to support the sustainability of Temporary Waste Disposal Sites 3R.

Based on Table 9, the average value obtained from all dimensional analysis is 72.79 in the quite sustainable category. The results of the sustainability value of the Anugrah Palur TPS 3R facility are better than other research (Sukwika & Noviana 2020) namely the Bantar-Gebang TPS rapfish analysis obtained a sustainability value of 51.71. This is because TPST-Bantar Gebang has a sustainability index value in the range of 50.02-57.15 in the environmental, social, and economic dimensions. A good and appropriate stress value from rapfish analysis is less than 0.25. The





Source: Analysis, Primary Data (2024)

Fig. 10: Temporary Waste Disposal Sites 3R Sustainability Kite Diagram.

Table 9: Sustainability Index Value, Stress Value, and R-Square.

No.	Dimension	Sustainability Index Value	Sustainability Status	Parameter	
				Stress	R <sup>2</sup>
1.	Management and Infrastructure	71,30	Quite Sustainable	0,15	0,95
2.	Environmental	79,54	Sustainable	0,14	0,95
3.	Social	72,88	Quite Sustainable	0,15	0,95
4.	Economy	65,44	Quite Sustainable	0,16	0,94
<b>Average</b>		72,79	Quite Sustainable		

Source: Analysis, Primary Data (2024)

analysis results obtained with the stress value were 0.14-0.16, and R<sup>2</sup> ranged from 0.94-0.95. Based on these results, all attributes are suitable to be used to explain the four dimensions analyzed.

## CONCLUSION

The SEM-PLS analysis yields measurement and structural models suitable for identifying supporting and inhibiting factors for the development of 3R TPS. The measurement model demonstrates valid results with all variable indicators showing strong loading factors and reliable results with satisfactory Cronbach's alpha and composite reliability values. The structural model evaluation indicates that the model is relatively good. Among the influencing factors on the Temporary Waste Disposal Sites 3R service, attitude shows the highest impact, followed by knowledge and behavior. Attitude is identified as the most significant supporting factor, whereas knowledge and behavior are found to be inhibiting factors.

The overall sustainability index of Temporary Waste Disposal Sites 3R Anugrah Palur is categorized as moderately sustainable. The sustainability status across various dimensions indicates that the management and infrastructure dimension is quite sustainable, the environmental dimension

is sustainable, the social dimension is quite sustainable, and the economic dimension is quite sustainable. Key leverage points affecting sustainability are identified within the management infrastructure and social dimensions, particularly related to trained staff, processing capacity, socialization, education, and trust in waste management.

The government is to consider improving waste processing technology at TPS 3R Anugrah Palur and TPS 3R Anugrah Palur Management to strengthen community knowledge and behavior in managing waste through socialization and education offline and online. The management of TPS 3R Anugrah Palur is considering improving the economy with the help of funds and technology by collaborating with the corporate social responsibility of private parties and non-governmental organizations (NGOs). Recommendation for other researchers to analyze supporting and inhibiting factors by adding religious factor variables and social capital (trust social, social norms, and social networks).

## REFERENCES

- Abdel, S.H.I. and Mansour, M.S., 2018. Solid waste issue: Sources, composition, disposal, recycling, and valorization. *Egyptian Journal of Petroleum*, 27(4), pp.1275-1290. [DOI].
- Amin, M.A. and Ahmed, M.T., 2024. Beachgoers' knowledge, perceptions, and willingness to pay for sustainable waste management in Kuakata

- Sea Beach, Bangladesh. *Nature Environment & Pollution Technology*, 23(2), p.48. [DOI].
- Demirbas, A., 2011. Waste management, waste resource facilities and waste conversion processes. *Energy Conversion and Management*, 52(2), pp.1280-1287. [DOI].
- Ferronato, N. and Torretta, V., 2019. Waste mismanagement in developing countries: A review of global issues. *International Journal of Environmental Research and Public Health*, 16(6), p.1060. [DOI].
- Haqq, M., 2018. Development Strategy of Waste Banks as an Effort to Increase Waste Reduction in South Surabaya. Undergraduate Thesis, Sepuluh Nopember Institute of Technology.
- Johansson, N., Krook, J. and Eklund, M., 2012. Transforming dumps into gold mines: Experiences from Swedish case studies. *Environmental Innovation and Societal Transitions*, 5, pp.33-48. [DOI].
- Kaur, A., Bharti, R. and Sharma, R., 2023. Municipal solid waste as a source of energy. *Materials Today: Proceedings*, 81, pp.904-915. [DOI].
- Khan, S., Anjum, R., Raza, S.T., Bazai, N.A. and Ihtisham, M., 2022. Technologies for municipal solid waste management: Current status, challenges, and future perspectives. *Chemosphere*, 288, p.132403. [DOI].
- Lee, R.P., Meyer, B., Huang, Q. and Voss, R., 2020. Sustainable waste management for zero waste cities in China: Potential, challenges and opportunities. *Clean Energy*, 4(3), pp.169-201. [DOI].
- Malav, L.C., Yadav, K.K., Gupta, N., Kumar, S., Sharma, G.K., Krishnan, S. and Bach, Q.V., 2020. A review on municipal solid waste as a renewable source for waste-to-energy projects in India: Current practices, challenges, and future opportunities. *Journal of Cleaner Production*, 277, p.123227. [DOI].
- Malinauskaite, J., Jouhara, H., Czajczyńska, D., Stanchev, P., Katsou, E., Rostkowski, P. and Spencer, N., 2017. Municipal solid waste management and waste-to-energy in the context of a circular economy and energy recycling in Europe. *Energy*, 141, pp.2013-2044. [DOI].
- Meidiana, C., Sekito, T. and Sasongko, W., 2021. Determining factors of community participation in waste banks. *IOP Conference Series: Earth and Environmental Science*, 940(1), p.012085. [DOI].
- Mohammed, M., Shafiq, N., Elmansoury, A., Al-Mekhlafi, A.B.A., Rached, E.F., Zawawi, N.A. and Ibrahim, M.B., 2021. Modeling of 3R (reduce, reuse and recycle) for sustainable construction waste reduction: A partial least squares structural equation modeling (PLS-SEM). *Sustainability*, 13(19), p.10660. [DOI].
- Mulyati, T., Mutawaqqil, M. and Sastra, H.Y., 2019. Planning a village waste management system using system dynamics modelling and simulation: Temporary waste disposal sites 3R case study in Aceh, Indonesia. *IOP Conference Series: Materials Science and Engineering*, 536(1), p.012072. [DOI].
- Mulyatna, L., Yustiani, Y.M., Andisa, R.R., Ramadhan, R.F. and Hidayanti, D., 2021. Sustainability analysis of the application of waste bank in elementary school with a multidimensional scaling approach. *Journal of Community Based Environmental Engineering and Management*, 5(2), pp.103-110. [DOI].
- Muslim, A., Fitri, A.D.P. and Purnomo, P.W., 2019. Sustainability analysis of shark fisheries in Cilacap Regency, Central Java. *Jurnal Perikanan dan Kelautan*, 9(1), pp.1-14.
- National Standardization Agency, 1994. *SNI 19-3964-1994 Concerning Methods for Collecting and Measuring Samples of Urban Waste Generation and Composition*.
- Novian, W. and Herlina, M., 2022. Factors influencing community behavior towards internet usage in Sukaraja Digital Village. *Jurnal Riset Statistika*, 2(2), pp.161-168. [DOI].
- Purwaningrum, P., 2016. Efforts to reduce plastic waste generation in the environment. *Indonesian Journal of Urban and Environmental Technology*, 8(2), pp.141-147. [DOI].
- Raharjo, S., 2017. Development of 3R waste treatment facilities for mitigating greenhouse gas emission: A case study of Padang City, Indonesia. *ARPJ Journal of Engineering and Applied Sciences*, 12(12), pp.3789-3794. [DOI].
- Reno, J., 2015. Waste and waste management. *Annual Review of Anthropology*, 44, pp.557-572.
- Rossi, A.M., 2022. Sustainability analysis and benefits of the circular economy in the main waste bank (Case Study: BSI "Satu Hati", West Jakarta). *Tesis, Institut Pertanian Bogor*.
- SIPSN, S.I., 2023. *Waste Management Performance Achievements*. Jakarta: Minister of Environment and Forestry.
- Subramani, T. and Murugan, R., 2014. Generation of electricity using solid waste management in Krishnagiri Municipality. *International Journal of Engineering Research and Applications*, 4(6), pp.222-232.
- Sukwika, T. and Noviana, L., 2020. Sustainability status of integrated waste management in TPST-Bantargebang, Bekasi: Using Rapsfish with R statistics. *Jurnal Ilmu Lingkungan*, 18(1), pp.107-118. [DOI].
- Sun, X., Li, J., Zhao, X., Zhu, B. and Zhang, G., 2016. A review on the management of municipal solid waste fly ash in America. *Procedia Environmental Sciences*, 31, pp.535-540.
- Vassiliadou, I., Papadopoulos, A., Costopoulou, D., Vasiliadou, S., Christoforou, S. and Leondiadis, L., 2009. Dioxin contamination after an accidental fire in the municipal landfill of Tagarades, Thessaloniki, Greece. *Chemosphere*, 74(7), pp.879-884. [DOI].
- Warningsih, T., Hendrik, H. and Suaseh, Y., 2020. The status of sustainability of anchovy resources in the Labuhanbatu territorial waters, North Sumatra Province. *IOP Conference Series: Earth and Environmental Science*, 430(1), pp.1-14. [DOI].
- Wielgosinski, G., Czerwińska, J. and Szufa, S., 2021. Municipal solid waste mass balance as a tool for calculation of the possibility of implementing the circular economy concept. *Energies*, 14(7), p.1811. [DOI].

# Analysis of Plants, *Helianthus annuus* (Sunflower) and *Gossypium herbaceum* (Cotton), for the Control of Heavy Metals Chromium and Arsenic Using Phytoremediation Techniques

S. Monisha† and S. P. Sangeetha

Department of Civil Engineering, Aarupadai Veedu Institute of Technology, Vinayaka Mission's Research Foundation (Deemed to be University), Chennai, Tamil Nadu, India

†Corresponding author: S. Monisha; monisha.civil@avit.ac.in

**Abbreviation:** Nat. Env. & Poll. Technol.  
**Website:** www.neptjournal.com

*Received:* 03-07-2024

*Revised:* 13-08-2024

*Accepted:* 25-08-2024

## Key Words:

Heavy metal pollution  
 Phytoremediation  
*Helianthus annuus*  
*Gossypium herbaceum*  
 ICP-MS

## Citation for the Paper:

Monisha, S. and Sangeetha, S.P., 2025. Analysis of Plants, *Helianthus annuus* (Sunflower) and *Gossypium herbaceum* (Cotton), for the Control of Heavy Metals Chromium and Arsenic Using Phytoremediation Techniques. *Nature Environment and Pollution Technology*, 24(2), p. B4237. <https://doi.org/10.46488/NEPT.2025.v24i02.B4237>.

*Note: From year 2025, the journal uses Article ID instead of page numbers in citation of the published articles.*



**Copyright:** © 2025 by the authors  
**Licensee:** Technoscience Publications  
 This article is an open access article distributed under the terms and conditions of the Creative Commons Attribution (CC BY) license (<https://creativecommons.org/licenses/by/4.0/>).

## ABSTRACT

Heavy metal pollution released into the surface environment poses a significant threat, being hazardous to both the environment and living organisms. Phytoremediation thus appears as a viable technique to address heavy metal pollution in soils impacted by industrial effluents. To identify the growth performance of sunflower and cotton seeds under various concentrations of arsenic and chromium present in the tannery industrial wastewater in the Chengalpattu region, and to identify the accumulation of Arsenic(As) and chromium (Cr) in the roots, shoots, and soil of these plants. This paper examined the usefulness of sunflower (*Helianthus annuus*) and cotton (*Gossypium herbaceum*) in eradicating Cr and As-polluted soils originating from tannery wastewater. In this experiment, Completely Randomized Block Design (CBRD) testing was performed, and the samples were analyzed using Inductively Coupled Plasma Mass Spectrometry (ICP-MS). The accumulation of Cr in sunflowers was 120 mg.kg<sup>-1</sup> in the roots and 25 mg.kg<sup>-1</sup> in the above-ground parts. As accumulated to 85 mg.kg<sup>-1</sup> in the roots and 15 mg.kg<sup>-1</sup> in the above-ground parts. Similarly, cotton plants accumulated 90 mg.kg<sup>-1</sup> of Cr in the roots and 20 mg.kg<sup>-1</sup> in the above-ground parts. As accumulation in cotton plants was 100 mg.kg<sup>-1</sup> in the roots and 30 mg.kg<sup>-1</sup> in the above-ground parts. The study inferred that, in comparison to the other plants, the concentrations of Cr in sunflower roots were significantly higher, but cotton was found to have a better ability to take up As in the roots as well as in the aerial parts of the plant. It hence demonstrates the applicability of sunflower and cotton to support phytoremediation efforts sustainably within industrial environments to mitigate pollution and improve the quality of the soil.

## INTRODUCTION

### Background and Importance of Water Quality

Soil pollution is caused severely by heavy metals in most regions of the world where agriculture is practiced and characterized by the removal of contaminated metals required high costs and negative impacts on civil engineering to conduct techniques including fixation, leaching, extraction of the soil, and landfilling of the most affected ground (Zaghloul 2020 & Abdel-Shafy et al. 2018). Though the application of these techniques is highly efficient, their continuous application involves high costs with resultant drawbacks such as the decrease in fertility and structure of the soils, drop-in biological activity, and possibilities of secondary pollution. In the recent past, there has been a trend of developing indigenous biological procedures to deal with metal-contaminated soil and water because of an environmentally friendly approach (Bhandari 2018).

Water is one of the most vital components of nature, vital for the survival of all living organisms. Though, the existing rates of urbanization and industrialization

along with high population growth, affect water resources significantly, increasing the level of environmental pollution. Thus, heavy metals in soil can either be derived from naturally occurring geogenic sources or anthropogenic sources. These metals can be moved many kilometers and damage the fertility of the ground, decrease the yields on agricultural lands, change plant species, and influence the water and life forms in them (Alengebawy et al. 2021).

### Current Research on Phytoremediation Techniques

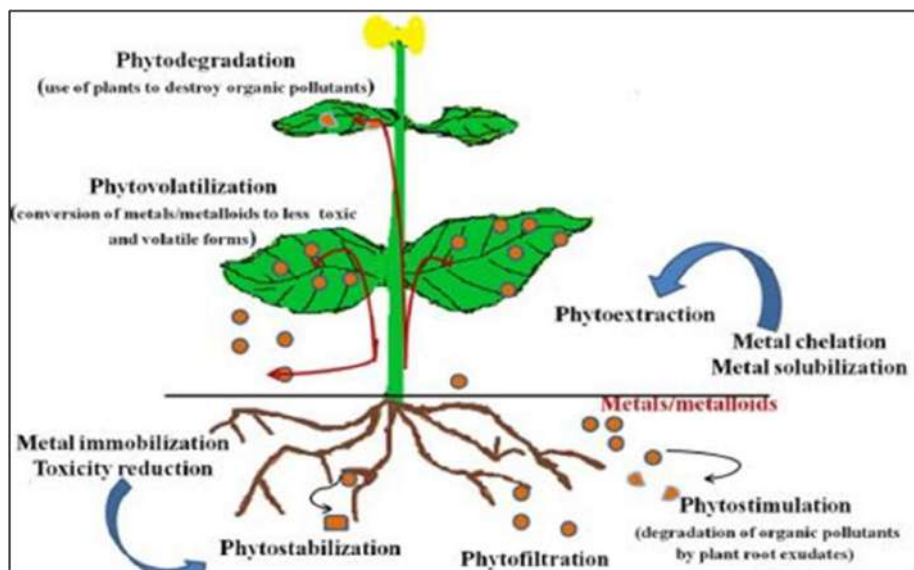
Phytoremediation of contaminated sites has recently become commonly used because of its low cost, permanent methods, and visual effectiveness. This technique involves the use of phytoextractor plants in farming, gardening, and even in the forests to lower concentrations of metals in the soils and, consequently, the adverse impacts. Technologies used in the process of phytoremediation are remarkably prospective and can be applied efficiently in the improvement of the conditions of soil pollution and the overall environmental status. Areas like phytofiltration, phytodegradation, phytoextraction, phytovolatilization, and phytostabilization prove to be a cost-effective, efficient, and eco-friendly way of decontaminating the soils, sediments, air, and water (Yadav et al. 2022, Zaghloul 2020, Muthusaravanan et al. 2018). Hyperaccumulator plants, which are utilized in the phytoremediation process, include species such as water lettuce, water hyacinth, sunflower, bamboo, and water kale, among others used in the controlling of heaving metals in the various industries (Hendrasarie & Redina 2023).

Thus, by highlighting the potential of sunflower and cotton for phytoremediation, this research will fill the gap in knowledge about the applicability of these plants in eradicating Ar and Cr from contaminated environments. The research outcomes should foster the identification of local sustainable, efficient, and eco-friendly phytoremediation approaches to tackle some of the significant and emerging environmental pollution challenges meaningfully. Fig.1 shows the phytoremediation process for As and Cr.

### Characteristics of *Helianthus annuus* L:

Among them, the sunflower (*Helianthus annuus* L.) and the cotton (*Gossypium herbaceum*) are most suitable to be used in the phytoremediation because of their subject's high growth rate, high biomass yield, and ability to hyperaccumulate the heavy metals as found by (Narayanan & Ma 2023). Thus, sunflowers have an extensive root structure and high translocation factor because they are suitable for Phytoextraction for winning the contaminants accompanied with the root captures and transfer to the aerial part of the plant ready for harvest. It further justifies it as an ideal candidate for large-scale decontamination of soil that is contaminated with either heavy metals or radionuclides.

Utilizing plants to remediate polluted environments has been an area of interest, especially in polluted soil and water, where heavy metals are of most interest. The first investigation also claimed that *Helianthus annuus*, commonly called sunflower, can be used for phytoremediation because of its ability to absorb and store Pb and Cd in its tissues.



(Source: Gaurab Karki 2020).

Fig. 1: Phytoremediation Process.



Specifically, Alaboudi et al. (2018) established that sunflowers could uptake a considerable part of these metals, thus making the plant suitable for phytoremediation activities. In the same year, Al-Jobori & Kadhim (2019) emphasized evaluating sunflower's effectiveness, as their study confirmed its efficiency in remediating Pb-contaminated soil. To determine the effectiveness of phytoremediation approaches, Panday & Ananda Babu (2023) examined the ability of phytoremediation to remediate various wastewater types using different plants. Usage with other plants, such as *Typha latifolia*, *Lemna minor*, *Azolla filiculoides*, *Phragmites australis*, etc., as a polyculture (mixed culture) may outperform the individual. Results showed higher treatment efficiency could be obtained using mixed culture plants. The efficiency of the plants for phytoremediation has also been subject to much research with a specific focus on the mechanisms. Bashir et al. (2021) and Gai et al. (2020) investigated sunflower's ability to withstand heavy metal stress, attributing it to its antioxidant activity and phenolic content. Cotton seed studies have thus focused on its genetic characteristics and other related creek characteristics that are very important for seedling performance in contaminated soils (Bhagwat et al. 2020).

### Characteristics of *Gossypium herbaceum*

Because of Cotton's well-developed root structure, it can reach contaminants located deeper in the root zone, provide soil stabilization, and minimize erosion as well as the leaching of pollutants. On the same note, the utilization of this particular plant for economic growth as a crop has the double advantage of applying phytoremediation together with farming while possibly generating income (Narayanan & Ma 2023, Huang et al. 2020).

Besides sunflowers, studies have been done on the potential of cotton for phytoremediation (Arulmathi et al. 2018). Similar research works by (Adekanmbi et al. 2024, Bhagwat et al. 2020) have indicated that cotton has strong genetic and physiological features that make it possible for it to absorb and store heavy metals. This makes cotton to be very useful in the phytoremediation of various contaminated environments (De Lima et al. 2021). Cotton flora also proved its ability to absorb chromium from contaminated soils (Sawicka et al. 2021).

Bashir et al. (2021) and Guo et al. (2020) studied sunflower's resilience to heavy metal stress, attributing it to its antioxidant activity and phenolic content. The development of phytoremediation techniques has been researched to intensify them through rounding up the plants with genetic engineering and the use of chelating agents. In other plant species, the efficiency of phytoremediation was explored by Aghelan et al. (2021), where the effects of

chelating agents and their probable applicability on sunflower and cotton were recorded. Hu et al. (2019) and Parekh et al. (2018) worked on the genetic basis of these plants to enhance the phytoremediation potential of these plants. The experimental observations make it clear that both sunflower and cotton flora can absorb chromium in polluted soils. Because sunflowers have been identified to possess deep root systems and the ability to bioaccumulate heavy metals, the plant demonstrated optimal performance in chromium uptake (Prasad et al. 2021). However, there are some limitations when it comes to improving the phytoremediation process. The work to overcome these issues goes on to date, including the study of plant-microbe relations and the enhancement and growth of plant tolerance (Narayanan & Ma 2023, Yin et al. 2017, Wu et al. 2017). *Helianthus annuus* can absorb chromium from polluted soils (Liu et al. 2020). These research endeavors address the ability to optimize the full application of sunflower and cotton for environmental cleaning.

Consequently, the prior research has provided a proper groundwork for ascertaining the potential of sunflower and cotton in the process of phytoremediation. Future studies and technology innovations should expand the efficiency of restoration plants and convey the effects of these plants on the suppression of heavy metal pollution in the soil such as As and Cr. This study extends from this background by concerning itself with the phytoremediation of As and Cr only, pointing out the gaps, and showing the potential uses of these plants in real-life situations.

### Effects of the Two Heavy Metals, Arsenic and Chromium

Arsenic (Ar) and chromium (Cr) pose a great threat and are known to be toxic and they persist in the environment. Several industries like metal extraction, smelting, electroplating, chemical manufacturing, etc., often discharge wastewater having relatively high concentrations of the mentioned heavy metals. These contaminants are dangerous to human and animal health and can cause health problems such as cancer, neurological disorders, and organ diseases. Further, they are capable of upsetting the existing bio-diversity and diminishing the quality of soil and water (Zoumpoulakis et al. 2017). Based on the literature reviews that identified the research gap and framed the objectives for my investigation, they are mentioned below.

### Objectives of the Study

This study aims to evaluate the potential of sunflower (*Helianthus annuus* L.) and cotton (*Gossypium herbaceum*) for phytoremediation of As and Cr from industrial and simulated wastewater. Specifically, the objectives of this research are to:

1. To assess the growth performance of sunflower and cotton under various concentrations of contaminated effluents.
2. To quantify the accumulation and translocation of As and Cr within the roots, shoots, and soil of these plants.
3. To compare the phytoremediation efficiency of sunflower and cotton with other relevant studies.
4. To investigate the impact of metal contamination on seed germination and plant morphological characteristics.
5. To analyze changes in soil properties following phytoremediation.

## MATERIALS AND METHODS

### Industrial Wastewaters and Properties of Soil

The industrial wastewater employed in this study was collected from the Industrial region, an area for the facility identified to discharge high concentrations of arsenic (As) and chromium (Cr) as a result of the industrial process. Table 1 indicates the physicochemical properties of the wastewater were determined, which was based on the measures of the pH, electrical conductivity (EC), total dissolved solids (TDS), and the concentrations of heavy metals (As and Cr).

The soil used for the experiments was collected from the Industrial Location, Chengalpattu District, an area with a history of industrial activity. Table 2 shows the Soil properties of selected samples that were analyzed for texture, organic matter content, pH, cation exchange capacity (CEC), and baseline heavy metal concentrations.

Table 1: Physicochemical Properties of Industrial Wastewater.

Parameter	Value
pH	7.2 ± 0.3
Electrical Conductivity [ $\mu\text{S}.\text{cm}^{-1}$ ]	1200 ± 50
Total Dissolved Solids [ $\text{mg}.\text{L}^{-1}$ ]	800 ± 40
Arsenic (Ar) [ $\text{mg}.\text{L}^{-1}$ ]	15.5 ± 0.5
Chromium (Cr) [ $\text{mg}.\text{L}^{-1}$ ]	10.2 ± 0.4

Table 2: Soil Properties of collected samples.

Parameter	Value
Soil Texture	Sandy Loam
Organic Matter Content [%]	2.5 ± 0.2
pH	6.8 ± 0.2
Cation Exchange Capacity [ $\text{cmol}.\text{kg}^{-1}$ ]	15.0 ± 1.0
Baseline Arsenic (As) [ $\text{mg}.\text{kg}^{-1}$ ]	2.0 ± 0.1
Baseline Chromium (Cr) [ $\text{mg}.\text{kg}^{-1}$ ]	1.5 ± 0.1

### Experimental Design

The experiment was conducted in a controlled pilot-scale mode environment to simulate the conditions of industrial wastewater contamination. The design followed a completely randomized block design (CRBD) with three replications for each treatment. The main factors considered were plant species (sunflower and cotton) and effluent concentration (0%, 25%, 50%, 75%, and 100%). Additionally, organic amendments (compost) were applied to some treatments to evaluate their potential to enhance phytoremediation efficiency. Each experimental unit consisted of a pot filled with 5 kg of pre-characterized soil. The pots were irrigated with varying concentrations of industrial wastewater mixed

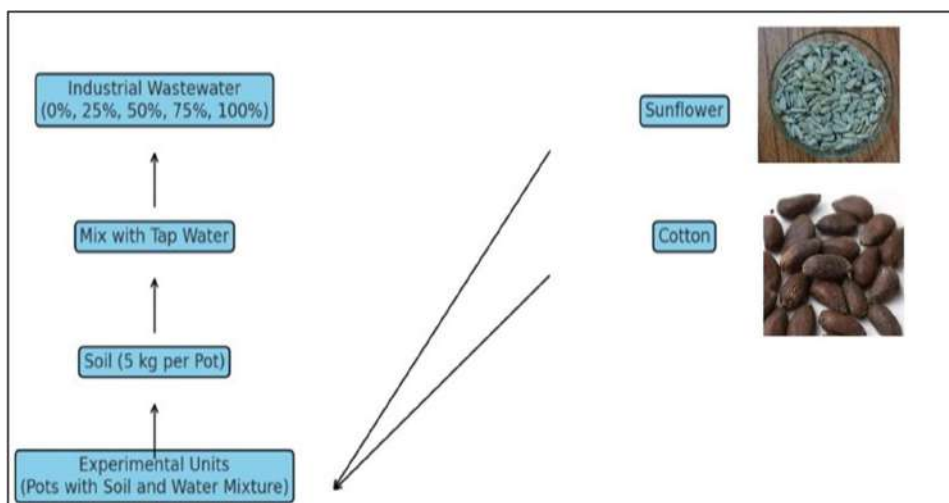


Fig. 2: Experimental Setup and Process (As and Cr).

with tap water to achieve the desired effluent concentration levels. The experimental setup of collected samples and its process are shown in Fig. 2.

### Identification of Growth Rate and Biomass Production of Sunflower and Cotton

In selecting plant species for this study, the following criteria were considered: the species' ability to phytoremediation the contaminant, the species' growth rate, and biomass production.

#### The Rationale for Choosing Sunflower Plant (*Helianthus annuus*)

Due to its developed root system and high translocation factor, Sunflower is efficient in phytoextraction. Therefore, due to its properties of amassing heavy metals, including lead (Pb), cadmium (Cd), and possibly arsenic (As) and chromium (Cr), it is fitting for this analysis (Narayanan & Ma 2023).

#### The Rationale for Choosing the Cotton Plant (*Gossypium herbaceum*)

Cotton, with its extensive root system, can pick up contaminants in the lower stratum of the soil. It also has a very sound genetic and physiological power – it can withstand and store metals, particularly heavy metals. Cotton, being an important crop from the economic point of view, takes on the added advantage of using phytoremediation along with agricultural practices. (Ullah et al. 2018).

#### Monitoring of Plants - Cotton and Sunflower Growth and Health

Hence, sunflower and cotton plant growth and vigor were observed during the whole experimental duration. Some of the factors like plant height, number of leaves, and biomass accumulation were measured every week. Records were also made on visually observable symptoms of stress, which included chlorosis, wilting, or necrosis. Plant growth was assessed through the measurement of plant height, which was measured in centimeters, and stem diameter, which was measured in millimeters, respectively, using a ruler and a digital caliper. Table 3 shows the measurement and frequency

Table 3: Measurement and frequency growth of Cotton and Sunflower Plants.

Parameter	Frequency of Measurement	Measurement Method
Plant Height	Weekly	Standardized Ruler
Leaf Number	Weekly	Manual Count
Stem Diameter	Weekly	Digital Caliper
Biomass	End of Experiment	Drying and Weighing

Table 4: Sampling and analysis methods.

Sample Type	Sampling Time Points	Preparation Method	Analysis Method
Soil	Start and End	Drying, Grinding, Digestion	ICP-MS
Plant Tissues	Start and End	Drying, Grinding, Digestion	ICP-MS

of growth of selected plants. Biomass was assessed at the end of the experiment by collecting the plants, drying them in the oven at 70°C to a constant weight, and then weighing them on the analytical balance.

#### Testing of Soil and Plant Tissue Using ICP-MS

At the initiation and completion of the studies, samples of soil and plant tissue were received to identify the attention of As and Cr. Roots and shoots of the vegetation were collected from the basis region of each pot through the use of soil auger, after which soil, root, stem, and leaf samples were collected one at a time. The samples were then rinsed with de-ionized water for the elimination of any particles of soil that could be connected. The gathered samples were later dried at 70°C for forty-eight hours and beaten into exceptional powder with the usage of an agate mortar and pestle. The powdered samples of aragonite have been requested for the use of the mixture of nitric acid and hydrogen peroxide and the awareness of As and Cr by using Inductively Coupled Plasma Mass Spectrometry (ICP-MS). Table 4 shows the sampling and analysis methods.

#### Impact on Soil Properties

The impact of phytoremediation on soil homes is evaluated by measuring changes in pH, natural count content material, and heavy metallic concentrations before and after the test. Soil pH was determined by the use of a pH meter and organic count number content was measured by the usage of the Walkley-Black approach (Karaca et al. 2020). The reduction in As and Cr concentrations in the soil was calculated to determine the efficiency of phytoremediation, and the changes in soil properties before and after the experiments are shown in Table 5.

Table 5: Soil property changes pre- and post-experiment studies.

Parameter	Initial Value	Final Value (Post-Experiment)
Soil pH	6.8 ± 0.2	6.6 ± 0.2
Organic Matter Content [%]	2.5 ± 0.2	2.3 ± 0.1
Arsenic (As) [mg.kg <sup>-1</sup> ]	2.0 ± 0.1	1.3 ± 0.1
Chromium (Cr) [mg.kg <sup>-1</sup> ]	1.5 ± 0.1	1.2 ± 0.1

### Phytoremediation Techniques for (Control of As and Cr)

An experimental design was used whereby sunflower seeds (*Helianthus annuus*) and cotton seeds (*Gossypium herbaceum*) were germinated in planting pots containing soil subjected to different tannery wastewater concentrations and experimental setup of sunflower seeds shown in Fig. 3. To eliminate variation that may be caused by the environment such as temperature, humidity, and light the pots were placed in a completely randomized block design in a greenhouse. Growth of the plants was kept optimal by watering them and follow-up done as and when needed. Particular attention was paid to how patients with different therapies were managed to prevent contamination. Phytotoxicity effects were determined by measuring the growth characteristics of *Helianthus annuus* and *Gossypium herbaceum*. Plants; growth parameters, which included plant height, number of leaves, and biomass of the plant, were measured weekly to determine the effect of tannery wastewater on the plant growth and also monitored on a daily base. After the growth period of the plants, the plants were then harvested and then segregated into roots, stems, and leaves. The samples were gently washed with distilled water to wash them free of sand content, were then allowed to air dry, and later oven dried at 70°C till they reached the constant weight. Samples were dried, after which they were reduced to fine powder for analyzing the level of heavy metals (Cetin et al. 2021).

## RESULTS AND DISCUSSIONS

### Quality and Morphology Characteristics of Seeds

To compare the effects of tannery wastewater on seed quality and morphological changes, germination percentage, vigor index, as well as seed size and weight of the seeds belonging to each treatment group were compared.

Table 6: Seed Morphology characteristics.

Plant Species	Code	Seed Length [mm]	Seed Width [mm]	Seed Weight [mg]
Sunflower	S1	8.5	4.2	60.3
	S2	8.2	4.0	58.7
Cotton	C1	7.8	3.9	52.6
	C2	7.5	3.7	50.4

### Coefficient of Germination and Seedling Strengthening

Germination tests were carried out by sowing seeds on filter paper and keeping them in Petri dishes at 25°C. The quantity of germinated seeds was counted daily for two weeks. The vigor of the seedlings was determined by the length of the root and shoot of the germinated seedlings (Mahawar et al. 2017, Zhou et al.2022).

### Seed Morphology

Seed morphology was evaluated by measuring the dimensions and weight of the seeds. A digital caliper was used to measure the length and width of each seed, and an analytical balance was used to determine the seed weight (Ene et al. 2024). The plant sample and analysis are listed below in Table 6. The results of seed excellence and morphology analyses were compared using descriptive statistics and ANOVA for the data acquired from different treatments. A priori analysis of data equivalence was employed using post hoc comparison tests to compare the means of the treatment groups. The sum of seed length and weight is shown in Fig. 4 (Zhou et al.2022).

### Seed Germination Rates

The mean germination percent of both the Sunflower and cotton seeds were declined to a considerable extent by the concentration of tannery effluent (Liu et al. 2020). An increase in effluent concentration reduced germination rates,



Fig. 3: *Helianthus annuus* and *Gossypium herbaceum* were in planting pots.





Fig. 4: Sum of seed length and weight.

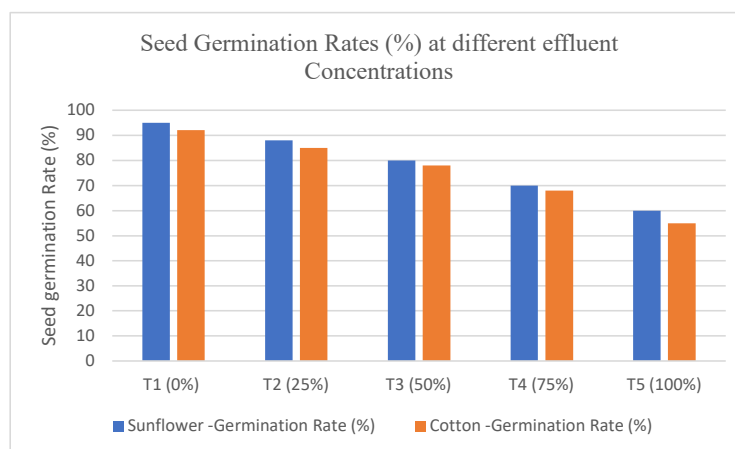


Fig. 5: Seed germination rates (%) at different effluent concentrations.

Table 7: Seed Germination Rates (%) at different effluent Concentrations.

Plant Species	Effluent Concentration	Germination Rate [%]
Sunflower (T1)	0%	95
(T2)	25%	88
(T3)	50%	80
(T4)	75%	70
(T5)	100%	60
Cotton (T1)	0%	92
(T2)	25%	85
(T3)	50%	78
(T4)	75%	68
(T5)	100%	55

as noted in the experiment. Of all the pancreatic effluent rates, 0% had the highest germination rates, and 100% had the lowest rates. Table 7 shows the seed germination rates at different effluent concentrations, as illustrated in Fig. 5. These outcomes suggest that tannery effluent reduces seed germination, and this may be due to the toxicity of the effluent influential, which contains toxic constituents, which include heavy metals and organic pollutions (Zhou et al.2022).

#### Flowering and Growth Habits of a Plant over the Next Few Weeks

The study involved the assessment of the sunflower plant and the cotton plant for twelve weeks ( Larayetan et al. 2021). The plants in the control group had the highest growth rates

Table 8: Average plant height (cm) after 12 weeks.

Plant Species	Effluent Concentration	Average Plant Height [cm]
Sunflower	0%	120
	25%	105
	50%	90
	75%	75
	100%	60
Cotton	0%	110
	25%	95
	50%	80
	75%	65
	100%	50



Fig. 6: Plant growth of cotton and sunflower.

and the plants in the groups having higher concentration of effluent had very low growth rates. Plant growth is shown in Fig. 6. The patterns analyzed in the analysis of the patterns depict that the toxic phases in the effluent interfere with the physiological and biochemical processes that are vital for plant development growth. Table 8 shows the average plant height after 12 weeks of this study.

### Accumulation of Cr and As in Cotton and Sunflower

The distribution of Cr and As in different parts of sunflower

and cotton plants was analyzed. It was observed that the roots accumulated significantly higher concentrations of both metals compared to the aboveground parts (stems, leaves, and seeds). The accumulation of chromium and arsenic in different plant parts is shown in Table 9.

### Analysis Results of Cr and As with ICP-MS

The plant samples were harvested at the time of maturity of the growth cycle of the plants. The plants were harvested by hand with a focus on minimizing root damage, washed with deionized water, and then the samples' roots, stems, leaves, and seeds were sorted out. The samples were then allowed to air-dry, and thereafter suspected to oven-drying at 70°C until a constant weight was obtained. The dried samples were milled to a fine powder using an industry-standardized stainless steel mill, which reduced contamination risk, and the samples were stored airtight pending analysis.

Chromatographic characterization of the plant tissues was done using Inductively Coupled Plasma Mass Spectrometry (ICP-MS) to determine the concentrations of chromium (Cr) and arsenic (As). The viability of the samples after digestion was demonstrated and the digested samples were analyzed using ICP-MS. The following procedure was followed for digesting the plant samples:

1. Weigh 0.5 g of the dried plant sample and place it into the digestion vessel.
2. Pour 10 mL of HNO<sub>3</sub> and 2 mL of H<sub>2</sub>O<sub>2</sub> into the vessel.
3. Close the vessel and place it in the microwave digestion system.
4. Set the heating time of the microwave to 180°C and heat the samples for thirty minutes.
5. Let the vessels cool, then pour the digested sample into a volumetric flask and fill up to 50 mL with deionized water (Jones & Karen 2022).

For ICP-MS analysis, follow this step-by-step method to

Table 9: Concentrations of Cr and Ar in different plant parts (mg.kg<sup>-1</sup> dry weight).

Plant Species	Effluent Concentration	Cr in Roots	Cr in Aboveground Parts	As in Roots	As in Aboveground Parts
Sunflower	0%	0.0	0.0	0.0	0.0
	25%	15.2	7.3	4.1	2.5
	50%	20.8	10.5	5.8	3.7
	75%	28.4	13.7	7.3	4.9
	100%	35.6	16.2	9.1	5.8
Cotton	0%	0.0	0.0	0.0	0.0
	25%	14.8	6.9	3.9	2.3
	50%	19.6	9.8	5.5	3.4
	75%	26.9	12.8	7.1	4.6
	100%	33.4	15.3	8.9	5.5

Table 10: Concentrations of Cr and As in plant tissues (mg.kg<sup>-1</sup> dry weight).

Plant Species	Treatment Code	Cr in Roots	Cr in Stems	Cr in Leaves	Cr in Seeds	As in Roots	As in Stems	As in Leaves	As in Seeds
Sunflower	T1 (0%)	0.0	0.0	0.0	0.0	0.0	0.0	0.0	0.0
	T2 (25%)	14.4	9.8	6.9	3.2	2.4	1.8	2.1	1.4
	T3 (50%)	12.3	8.4	5.7	2.3	3.2	2.1	1.8	0.9
	T4 (75%)	10.5	7.1	4.9	2.0	2.8	1.9	1.6	0.7
	T5 (100%)	8.5	6.5	3.8	1.5	2.1	1.1	0.9	0.5
Cotton	T1 (0%)	0.0	0.0	0.0	0.0	0.0	0.0	0.0	0.0
	T2 (25%)	11.8	7.9	5.5	2.1	3.0	2.0	1.7	0.8
	T3 (50%)	9.9	6.8	4.6	1.8	2.6	1.8	1.5	0.6
	T4 (75%)	8.8	5.8	3.9	1.1	1.5	1.3	1.2	0.5
	T5 (100%)	7.6	4.9	2.8	0.8	1.2	0.9	0.8	0.2

set the ICP-MS instrument to the right measurement for Cr and As standards. The digested samples shall be put into the ICP-MS. Determine the high and low concentration levels of Cr and As in the samples. Determine the metal contents in the plant tissues using a calibration curve. Table 10 shows the concentrations of Cr and As in plant tissues.

### Heavy Metal Concentration in Plant Tissues

The contents of arsenic (Ar) and chromium (Cr) within the plant tissues are computed using Inductively Coupled Plasma Mass Spectrometry (ICP-MS). The plant tissue samples were thereafter asked with a combination of nitric acid (HNO<sub>3</sub>) and hydrogen peroxide (H<sub>2</sub>O<sub>2</sub>) as recommended by way of (Adekanmbi et al. 2020). The metal concentrations have been determined, whilst the translocation aspect (TF) and bioconcentration component (BCF) have been estimated on the way to decide the performance of phytoremediation of the numerous plant sorts. Table 11 indicates the plant species of translocation and bioconcentration factor treatment values.

### Comparative Analysis Between Use and Non-Use of Organic Amendments

Table 11: Heavy metal concentration in plant tissues.

Plant Species	Treatment Code	Translocation Factor (TF)	Bioconcentration Factor (BCF)
Sunflower	T1 (0%)	0.0	0.0
	T2 (25%)	0.8	1.5
	T3 (50%)	0.7	1.2
	T4 (75%)	0.6	1.1
	T5 (100%)	0.5	1.0
Cotton	T1 (0%)	0.0	0.0
	T2 (25%)	0.9	1.4
	T3 (50%)	0.7	1.3
	T4 (75%)	0.6	1.2
	T5 (100%)	0.4	1.0

On the impact of the organic amendments to compost on the build-up of Cr and As, the following findings were also made. Compost and other forms of organic materials are well understood for their enhancement of both the physical and chemical properties of soils and, therefore, have a direct effect on the bioavailability of metals. In Table 12, the results indicate that the application of organic amendments reduced the concentrations of Cr and As in both roots and aboveground parts of the plants, as illustrated in Fig. 7. This reduction can be attributed to the dilution effect and the binding of metals by organic matter, making them less available for plant uptake.

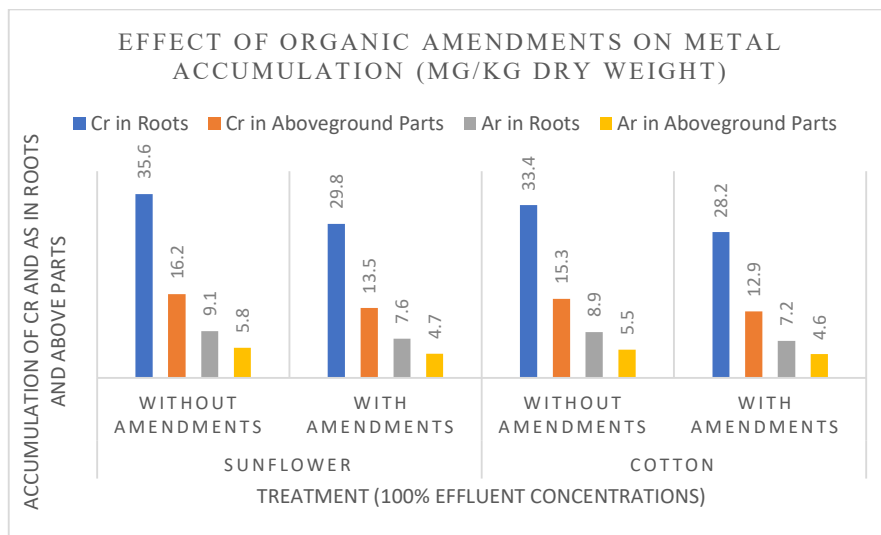
### Impact on Soil Properties

The treatment of tannery effluents significantly altered the composition of the soil in terms of key parameters such as organic matter content, pH, and nutrient availability. The application of different concentrations of effluents led to noticeable changes in soil properties, which are crucial for plant growth and microbial activity, as shown in Table 13.

A change in each of the chemical parameters analyzed was evidenced after the treatment, indicating, therefore, tannery effluent impacts on soil chemistry and fertility concerned with nutrient availability, whereby the values for pH and Organic Matter depict a typical variation as depicted in the findings of (Jones et al. 2021). The conclusion of this study corresponds to the study done by (Lofty & Mostafazharan 2014 ) and proves the usefulness of sunflower and cotton reclamation in removing heavy metals. Consequently, the two works stress that plant species selection and soil amendments affect the remediation effectiveness of concrete soil types (Kirsten et al. 2021). Comparing the results of the present study with the findings reported in the literature exhibits similar trends for the absorption and build-up of Cr and As in sunflower and cotton plants. Hypothesized data are in agreement with

Table 12: Effect of organic amendments on metal accumulation (mg.kg<sup>-1</sup> dry weight).

Plant Species	Treatment (100% Effluent Concentrations)	Cr in Roots	Cr in Aboveground Parts	Ar in Roots	Ar in Aboveground Parts
Sunflower	Without Amendments	35.6	16.2	9.1	5.8
	With Amendments	29.8	13.5	7.6	4.7
Cotton	Without Amendments	33.4	15.3	8.9	5.5
	With Amendments	28.2	12.9	7.2	4.6

Fig. 7: Effect of organic amendments on metal accumulation (mg.kg<sup>-1</sup> dry weight).

prior data suggesting that the root systems are central in metal uptake, with the roots showing higher concentrations than the above-ground parts (Ebrahimbabaie et al. 2023). The effect of the soil properties, which include pH and organic matter, on the availability and uptake of metals also supplements the argument for integrated strategies in phytoremediation (Jones & Karen 2022).

### Determination of Organic Matter

Two sets of soil samples for each pot were taken, one before the plant was transplanted into the pot followed by another pattern after the last harvest. These samples were air dried, sieved to 2mm mesh size, and communalized. Samples for natural depend determination were taken subsamples, and SOM was analyzed using the Walkley-Black method, whereby organic carbon of the soil pattern turned into oxidized with the use of a dichromate answer and focused sulfuric acid and titrated with ferrous ammonium sulfate to an endpoint (Bhandari 2018). This method gets recognition from the corresponding precision and performance. The organic matter content was calculated using the following formula:

$$\text{Organic Matter (\%)} = \frac{((B - S) \times M \times 0.3W)}{W}$$

Where, B is the volume of ferrous ammonium sulfate used in the blank titration (mL), S is the volume of ferrous ammonium sulfate used in the sample titration (mL), M is the molarity of the ferrous ammonium sulfate solution, and W is the weight of the soil sample (g).

The organic depend content material records were analyzed with the use of paired t-assessments to evaluate the adjustments earlier than planting and after harvest within each remedy institution. ANOVA was used to evaluate the results of various remedies on soil natural matter content.

### Data Analysis and Determination of Soil pH

Lofty & Mostafa (2014) investigated phytoremediation technique using complete randomized block experimental design (CRBD) for the contaminated soil with two heavy metals like cobalt and chromium - Five different plant species tested in this study, namely, Panikum (Panicum antidotal), Napier grass (*Pennisetum purpureum*), Squash (*Cucurbita pepo*), Cotton (*Gossypium hirsutum*) and Sunflower (*Helianthus annuus*) with two different soil, the soil containment through direct discharge of sewage effluent both mostorud clayey and sandy loam soil gets containment. The results showed that Cr removed from the



soil by the whole plant after cultivation ranged between 17.0 to 41.6%. Roots tend to accumulate 41.2 to 70.1% of Co and Cr accumulated in plant biomass and also cross-checked the values using ANOVA (two-way and three-way) statistical analysis. Similarly, our investigation was also carried out to identify and interpret the data in my area of study.

### Sample Collection and Preparation and pH Measurement

Lada Kacalkova et al. (2014) also investigated heavy metals like the accumulation of chromium, nickel, lead, and cadmium by maize (*Zea mays* L.), sunflower (*Helianthus annuus* L.), willow (*Salix smithiana* Willd.), and poplar (*Populus nigra* L.), and the relationship between the contaminants in soil and plants, compared the soil and plants accumulations with Statistical analyses were performed using the software Statistica 10 analysis of variance, ANOVA, followed by the Tukey HSD test. Soil samples have been accrued from every pot earlier than planting and after the very last harvest. Samples had been air-dried, sieved via a 2 mm mesh, and homogenized. Subsamples had been taken for pH determination. Soil pH was measured using a pH meter with a pitcher electrode, following the 1:2.5 soil-to-water ratio approach (Alengebawey et al. 2021). Soil samples have been blended with deionized water, shaken for 30 minutes, and allowed to settle before pH measurement. Similarly, the pH data was analyzed with the usage of paired t-tests to examine the modifications earlier than planting and after harvest within each remedy organization. Analysis of variance, ANOVA followed by the t-test was used to examine the results of different treatments on soil pH and organic matter.

### Suggestions for Future Research

Using phytoremediation techniques, morphological characteristics, seed germination, soil properties, and plants were analyzed. Mainly to identify the effectiveness of both

plant species. As a result of these results, it is important to manage heavy metal pollution in the present environment. Phytoremediation techniques are cost-effective and increase the absorption of heavy metals from the soil via plants. The study inferred that, in comparison to the other plants, the concentrations of Cr in sunflower roots were significantly higher, but cotton was found to have a better ability to take up As in the roots as well as in the aerial parts of the plant. In this investigation carried out for control to 100% concentration of tannery wastewater was analyzed, heavy metals like As and Cr. In future research on the impact of these selected heavy metals on different concentrations surrounding the environment, human beings, quality of life, aquatic organisms, etc.

### CONCLUSIONS

The effectiveness of *Helianthus annuus* and *Gossypium herbaceum* for phytoremediation of tannery effluent-impacted soil was attempted in this study. It can also be summarized that the two plants in this study can take up chromium (Cr) and arsenic (As) effectively from the soil, where the uptake differences were significantly observed in the root and shoot-exporting organs. Sunflower was able to store more Cr in roots than cotton, while cotton as the best As uptake in roots and shoots. The remediation efficiency was influenced by pH and organic matter content since it determines the accessibility and mechanisms of metal absorption. The accumulation of chromium in sunflowers was 120 mg.kg<sup>-1</sup> in the roots and 25 mg.kg<sup>-1</sup> in the above-ground parts. Arsenic accumulated to 85 mg.kg<sup>-1</sup> in the roots and 15 mg.kg<sup>-1</sup> in the above-ground parts. Similarly, cotton plants accumulated 90 mg.kg<sup>-1</sup> of chromium in the roots and 20 mg.kg<sup>-1</sup> in the above-ground parts. Arsenic accumulation in cotton plants was 100 mg.kg<sup>-1</sup> in the roots and 30 mg.kg<sup>-1</sup> in the above-ground parts. It can be concluded that both sunflower and cotton possess the ability of metals uptake from contaminated soils hence, they can be used in phytoremediation processes in the treatment of industrial wastewater. The fact that sunflower and cotton were used in this study shows that they can be applied to the larger scale of phytoremediation for industrial wastewater polluted with heavy metals. Thus, through the application of the natural factors of such plants to adsorb and immobilize different pollutants, industrial processes are efficiently prevented from emitting contaminants and meet the legal requirements foreseen at the same time. Thus, this research points to the necessity of synchronizing and optimizing plant choice, approaches to soil preparation, and programs of phytosanitary oversight to enhance the efficiency of phytoremediation in various ecosystems. Future studies

Table 13: Changes in soil properties post-treatment.

Soil Property	Effluent Concentration	Before Treatment	After Treatment
Organic Matter [%]	0%	2.5	3.2
	25%	2.4	2.9
	50%	2.3	2.7
	75%	2.2	2.5
	100%	2.1	2.3
Soil pH	0%	6.8	5.5
	25%	6.7	5.6
	50%	6.6	5.4
	75%	6.5	5.3
	100%	6.4	5.2

should aim at developing the optimal methodology to implement plant-based remediation and the overall effects on the surrounding ecosystem for long-term remedy approaches.

## RECOMMENDATIONS

Therefore, this study has investigated the possibility of using the plant species for phytoremediation techniques. Sunflower and cotton were selected as two plant species. In the sample taken from tannery industries, the effluents contain five different concentrations. Particularly in the 0% concentration, accumulation of Cr in sunflowers was 120 mg.kg<sup>-1</sup> in the roots and 25 mg.kg<sup>-1</sup> in the above-ground parts at any analyzed soil when compared to the other tested species.

Based on the investigation, the tannery effluents with their physical, chemical, and biological properties of particular effluents, can be recommended for phytoremediation techniques. It will be greatly helpful for surrounding environment management for controlling the heavy metals like Cr and As for further investigation will go for different higher concentrations of effluents to identify the impact on the environment and society.

## ACKNOWLEDGMENTS

The authors wish to express their gratitude to Aarupadai Veedu Institute of Technology, Vinayaka Missions Research Foundation for providing the infrastructure and lab facilities to carry out the research work.

## REFERENCES

- Abdel-Shafy, H.I. and Mansour, M.S., 2018. Phytoremediation for the elimination of metals, pesticides, PAHs, and other pollutants from wastewater and soil. *Phytobiont and Ecosystem Restitution*, pp.101-136.
- Adekanmbi, I.C., Fabowale, P.O. and Ogundare, A.O., 2024. Effects of cotton plant (*Gossypium herbaceum* Linn.) extracts on some vancomycin and methicillin-resistant pathogenic bacteria. *World Journal of Advanced Research and Reviews*, 22(1), pp.1657-1670.
- Aghelan, N., Soheil, S., Mehrdad, C., Lorestani, M. and Merrikhpour, H., 2021. Evaluation of some chelating agents on phytoremediation efficiency of *Amaranthus caudatus* L. and *Tagetes patula* L. in soils contaminated with lead. *Springer Nature Switzerland*, 19, pp.503-514. DOI.
- Alaboudi, K.A., Ahmed, B. and Brodie, G., 2018. Phytoremediation of Pb and Cd contaminated soils by using sunflower (*Helianthus annuus*) plant. *Annals of Agricultural Sciences*, 63(1), pp.123-127.
- Alengebaw, A., Abdelkhalek, S.T., Qureshi, S.R. and Wang, M.Q., 2021. Heavy metals and pesticide toxicity in agricultural soil and plants: Ecological risks and human health implications. *Toxics*, 9(3), p.42.
- Al-Jobori, K.M. and Kadhim, A.K., 2019. Evaluation of sunflower (*Helianthus annuus* L.) for phytoremediation of lead-contaminated soil. *Journal of Pharmaceutical Sciences and Research*, 11(3), pp.847-854.
- Arulmathi, P., Jeyaprabha, C., Sivasankar, P. and Rajkumar, V., 2019. Treatment of textile wastewater by coagulation-flocculation process using *Gossypium herbaceum* and polyaniline coagulants. *Clean–Soil, Air, Water*, 47(7), p.1800464.
- Bashir, T., Zia-Ur-Rehman Mashwani, K.Z., Haider, S. and Shaista Tabassum, M., 2021. Chemistry, pharmacology and ethnomedicinal uses of *Helianthus annuus* (Sunflower): A review. *Pure and Applied Biology (PAB)*, 4(2), pp.226-235.
- Bhagwat, M.A., Rajkumar, B.K., Parmar, P.R. and Ramani, H.R., 2020. Physiological characterization of cotton genotypes (*Gossypium herbaceum* L.) for salinity at seedling stage. *IJCS*, 8(2), pp.2306-2312.
- Bhandari, G., 2018. Phytoremediation: exploitation of plants for environmental cleanup. In *Microbial Biotechnology in Environmental Monitoring and Cleanup*, 16, pp.286-304.
- Cetin, N., Karaman, K., Beyzi, E., Sağlam, C. and Demirel, B., 2021. Comparative evaluation of some quality characteristics of sunflower oilseeds (*Helianthus annuus* L.) through machine learning classifiers. *Food Analytical Methods*, 14, pp.1666-1681.
- De Lima, L.F., de Oliveira, J.O., Carneiro, J.N.P., Lima, C.N.F., Coutinho, H.D.M. and Morais-Braga, M.F.B., 2021. Ethnobotanical and antimicrobial activities of the *Gossypium* (Cotton) genus: A review. *Journal of Ethnopharmacology*, 279, p.114363.
- Ebrahimbabaie, P., Smith, A., Elsayed, M. and Zahran, R., 2023. Phytoremediation of engineered nanoparticles using *Typha latifolia* and *Carex rostrata*. *Applied and Environmental Soil Science*, 172, pp.2461-2473.
- Ene, A., Moraru, S.S., Moraru, D.I., Pantelica, A., Gosav, S. and Ceoromila, A.M., 2024. Major and trace element accumulation in soils and crops (wheat, corn, sunflower) around the steel industry in the Lower Danube Basin and associated ecological and health risks. *Applied Sciences*, 4(13), p.5616. DOI.
- Gai, F., Karamać, M., Janiak, M.A., Amarowicz, R. and Peiretti, P.G., 2020. Sunflower (*Helianthus annuus* L.) plants at various growth stages subjected to extraction—Comparison of the antioxidant activity and phenolic profile. *Antioxidants*, 9(6), p.535.
- Guo, S., Ge, Y. and Na Jom, K., 2017. A review of phytochemistry, metabolite changes, and medicinal uses of the common sunflower seed and sprouts (*Helianthus annuus* L.). *Chemistry Central Journal*, 11, pp.1-10.
- Hendrasarie, N. and Redina, C., 2023. Ability of water lettuce (*Pistia stratiotes*) and water hyacinth (*Eichhornia crassipes*) to remove methylene blue anionic surfactant (MBAS) from detergent wastewater. *Nature Environment and Pollution Technology*, 22(4), pp.1961-1970. DOI.
- Hu, Y., Chen, J., Fang, L., Zhang, Z., Ma, W., Niu, Y., Ju, L., Deng, J., Zhao, T., Lian, J. and Baruch, K., 2019. *Gossypium barbadense* and *Gossypium hirsutum* genomes provide insights into the origin and evolution of allotetraploid cotton. *Nature Genetics*, 51(4), pp.739-748.
- Huang, G., Wu, Z., Percy, R.G., Bai, M., Li, Y., Frelichowski, J.E., Hu, J., Wang, K., Yu, J.Z. and Zhu, Y., 2020. The genome sequence of *Gossypium herbaceum* and genome updates of *Gossypium arboreum* and *Gossypium hirsutum* provide insights into cotton A-genome evolution. *Nature Genetics*, 52(5), pp.516-524.
- Jones, M. and Karen, S.S., 2022. Remediation of contaminated dumpsite soil: An evaluation of soil amendments in combination with phytoremediation.
- Kacalkova, L., Tlustos, P. and Szakova, J., 2014. Chromium, Nickel, Cadmium, and Lead Accumulation in Maize, Sunflower, Willow, and Poplar. *Polish Journal of Environmental Studies*, 23(3), pp.753-761.
- Karaca, M., Ince, A.G. and Reddy, U.K., 2020. Interspecific grafting between *Gossypium hirsutum*, *G. barbadense*, and *G. herbaceum* lines. *Scientific Reports*, 10(1), p.18649.
- Karki, G., 2020. *Phytoremediation: Classification, Mechanisms, Applications And Limitations*. Springer.
- Kirsten, M., Mikutta, R., Kimaro, D.N., Feger, K.-H. and Kalbitz, K.,

2021. Aluminous clay and pedogenic Fe oxides modulate aggregation and related carbon contents in soils of the humid tropics. *SOIL*, 7(2), pp.363–375. DOI.
- Larayetani, R.A., Ayeni, G., Yahaya, A., Ajayi, A., Omale, S., Ishaq, U., Abiodun, D.J., Olisah, C., Aigbogun, J. and Enyioma-Alozie, S., 2021. Chemical composition of *Gossypium herbaceum* Linn and its antioxidant, antibacterial, cytotoxic, and antimalarial activities. *Clinical Complementary Medicine and Pharmacology*, 1(1), p.100008.
- Liu, X.S., Gao, B., Li, X.L., Li, W.N., Qiao, Z.A. and Han, L., 2020. Chemical composition and antimicrobial and antioxidant activities of essential oil of sunflower (*Helianthus annuus* L.) receptacle. *Molecules*, 25(22), p.5244. DOI.
- Lotfy, S.M. and Zhran, M., 2014. Phytoremediation of contaminated soil with cobalt and chromium. *Journal of Geochemical Exploration*, 144, pp.367–373. DOI.
- Mahawar, S., Katageri, I. and Jadhav, M., 2017. Evaluation and characterization of genetically modified cotton *Gossypium herbaceum* var. Jayadhar for *Helicoverpa armigera* resistance. *International Journal of Current Microbiology and Applied Sciences*, 6(12), pp.2780–2792. DOI.
- Muthusaravanan, S., Sivarajasekar, N., Vivek, J.S., Paramasivan, T., Naushad, M., Prakashmaran, Gayathri, V., Omar, K. and Al Duaij, O., 2018. Phytoremediation of heavy metals: mechanisms, methods, and enhancements. *Environmental Chemistry Letters*, 16, pp.1339–1359. DOI.
- Narayanan, M. and Ma, Y., 2023. Mitigation of heavy metal stress in the soil through optimized interaction between plants and microbes. *Journal of Environmental Management*, 345, p.118732. DOI.
- Panday, V. and Ananda Babu, K., 2023. The potential of phytoremediation to treat different types of wastewater - A review. *Nature Environment and Pollution Technology*, 22(2), pp.969–975. DOI.
- Parekh, M.J., Kumar, S., Fougat, R.S., Zala, H.N. and Pandit, R.J., 2018. Transcriptomic profiling of developing fiber in levant cotton (*Gossypium herbaceum* L.). *Functional & Integrative Genomics*, 18, pp.211–223.
- Prasad, S., Yadav, K.K., Kumar, S., Gupta, N., Cabral-Pinto, M.S., Rezanian, S., Neyara, R., Radwane, F. and Alam, J., 2021. Chromium contamination and effect on environmental health and its remediation: A sustainable approach. *Journal of Environmental Management*, 285, p.112174.
- Sawicka, B., Skiba, D., Umachandran, K. and Dickson, A., 2021. *Preparation of Phytopharmaceuticals for the Management of Disorders*. Academic Press, pp.491–537.
- Ullah, R., Akhtar, K.P., Moffett, P., Shah, T.A., Hussain, M., Khan, M.K.R., Mansoor, S. and Saeed, M., 2018. Analysis of the resistance of *Gossypium herbaceum* to cotton leaf curl Cochran virus strain Burewala and cotton leaf curl Multan beta satellite. *Journal of Plant Pathology*, 100, pp.313–316.
- Wu, Y., Chen, D., Zhu, S., Zhang, L. and Li, L., 2017. A new synthetic hybrid (A1D5) between *Gossypium herbaceum* and *G. raimondii* and its morphological, cytogenetic, and molecular characterization. *PLOS ONE*, 12(2), p.e0169833.
- Yadav, R., Singh, S., Kumar, A. and Singh, A.N., 2022. *Phytoremediation: A wonderful cost-effective tool*. Elsevier, pp.179–208.
- Yin, X., Zhan, R., He, Y., Song, S., Wang, L., Ge, Y. and Chen, D., 2020. Morphological description of a novel synthetic allotetraploid (A1A1G3G3) of *Gossypium herbaceum* L. and *G. nelsonii* Fryx. suitable for disease-resistant breeding applications. *PLOS ONE*, 15(12), p.e0242620.
- Zaghloul, M., 2020. Phytoremediation of heavy metals: Principles, mechanisms, enhancements with several efficiency enhancer methods and perspectives - A review. *Middle East Journal*, 9(1), pp.186–214.
- Zhou, S., Jiang, Z., Shen, J., Yao, Q., Yang, X., Li, X., Awasthi, M.K. and Zhang, Z., 2022. Effect of silica-based nanomaterials on seed germination and seedling growth of rice (*Oryza sativa* L.). *Nanomaterials*, 12(23), p.4160. DOI.
- Zoumpoulakis, P., Sinanoglou, V.J., Siapi, E., Heropoulos, G. and Proestos, C., 2017. Evaluating modern techniques for the extraction and characterization of sunflower (*Helianthus annuus* L.) seed phenolics. *Antioxidants*, 6(3), p.46.

# Mapping of Groundwater Potential Zones Using Fuzzy Logic Technique at Kadamaian Basin, Kota Belud, Sabah, Malaysia

Evienstein Wilfred† and Zulherry Isnain

Faculty of Science and Natural Resources, Universiti Malaysia Sabah, Jalan UMS, 88400 Kota Kinabalu, Sabah, Malaysia

†Corresponding author: Evienstein Wilfred; [evienstein@gmail.com](mailto:evienstein@gmail.com)

**Abbreviation:** Nat. Env. & Poll. Technol.  
**Website:** [www.neptjournal.com](http://www.neptjournal.com)

*Received:* 13-07-2024

*Revised:* 04-09-2024

*Accepted:* 10-09-2024

## Key Words:

GIS  
 Fuzzy logic  
 Groundwater potential  
 Mapping

## ABSTRACT

This research was initiated to study the groundwater potential zones using the Fuzzy logic technique at Lembangan Kadamaian, Kota Belud, Sabah, and its surroundings. The lithological units of this study mainly focus on the sedimentary rock of Wariu Formation, Crocker Formation, and Trusmadi Formation, including the quaternary alluvium deposition unit of Kota Belud. Based on the structural geology analysis results, the deformation trends are in the northwest-southeast direction. The interpretation of groundwater potential zones was made by using the ArcGIS Pro, R-studio Global Mapper, and several other mapping-related software. Ten thematic maps that have been produced are lithological map, lineament density map, rainfall map, distant from river map, distant from lineament map, drainage density map, landform, and land cover map, Topographic Wetness Index (TWI) map, rock porosity map, curvature map, and slope steepness map. GIS techniques were used during the spatial analysis stage. All thematic maps have their class values and are based on field data, relevant department data, and remote sensing data. Further processes were done using R-studio, Fuzzy Toolset, and Raster Calculator. This process afterward will produce the groundwater potential map of the study area. The final result has been supported by the data of tube wells from the Department of Minerals and Geosciences, Sabah, and was validated using the ROC and AUC curve validation technique.

## INTRODUCTION

### Background

This research focuses on delineating the zones with high potential for groundwater within the study area at Lembangan Kadamaian, Kota Belud, and Sabah. However, This research also includes preliminary parts such as general geology that cover some aspects of geography, geomorphology, stratigraphy, rock petrography, water quality, and structural geology. Meanwhile, the main objective of the research was continued in mapping techniques on the groundwater potential through the fuzzy logic technique by using the ArcGIS Pro and R-studio software.

The study area can be found in the western part of Sabah. The study area consists mainly of the Crocker Formation, Wariu Formation, and Pleistocene alluvium deposition unit (Fatin et al. 2022) and other rock units such as Trusmadi Formation, basic igneous, crystalline basement, plutonic igneous, Pleistocene alluvium deposit, and chert-spilite formation. The study area distance from the Kota Kinabalu, the capital state of Sabah was about 73 km. The area of the study area covers around 848.4 km<sup>2</sup>. The coordinates of the study area are 116°21'0" E - 116°41'0" E and 6°26'0" N - 6°0'0" N (Fig. 1).

The Fuzzy Logic Technique used during the analysis is based on the probability of a phenomenon occurring within a spectrum from 0 to 1 without requiring the assumption of normality for predictor variables (Assimakopoulos et al. 2023).

### Citation for the Paper:

Wilfred, E. and Isnain, Z., 2025. Mapping of groundwater potential zones using fuzzy logic technique at Kadamaian basin, Kota Belud, Sabah, Malaysia. *Nature Environment and Pollution Technology*, 24(2), D1701. <https://doi.org/10.46488/NEPT.2025.v24i02.D1701>

*Note: From year 2025, the journal uses Article ID instead of page numbers in citation of the published articles.*



Copyright: © 2025 by the authors

Licensee: Technoscience Publications

This article is an open access article distributed under the terms and conditions of the Creative Commons Attribution (CC BY) license (<https://creativecommons.org/licenses/by/4.0/>).



Studies were carried out based on existing data such as well data, fieldwork data, geological maps, satellite images, and topography maps.

### Geological Settings

The South China Sea is a prominent feature in the Southeast Asian region, and numerous models have been developed to depict the evolution occurring in that region (Balaguru et al. 2023). However, this study mostly discusses tectonic evolution within the scope of the study area, which is in the Northwest Sabah region located southeast of the South China Sea Basin.

Generally, Sabah is encircled by active tectonic plates such as the Indo-Australian Plate, Philippine Plate, Pacific

Plate, and Eurasian Plate. Sabah's location is in the northern part of the Borneo island, which is often influenced by various tectonic events triggered by these active plates. Fig. 2 shows the major plates surrounding Sabah.

Ghaheri et al. (2017) stated that the seas surrounding Sabah, such as the Sulu Sea, Celebes Sea, and South China Sea, greatly influence tectonic events in Sabah. The existence of basins in the Sulu Sea subduction zone, the Celebes Sea subduction zone, and the South China Sea spreading zone is caused by tectonic events occurring in the region (Fig. 2).

The stratigraphy of the study area is closely related to the regional stratigraphy found in the western part of Sabah. According to Tongkul (1991), sedimentary rocks and igneous

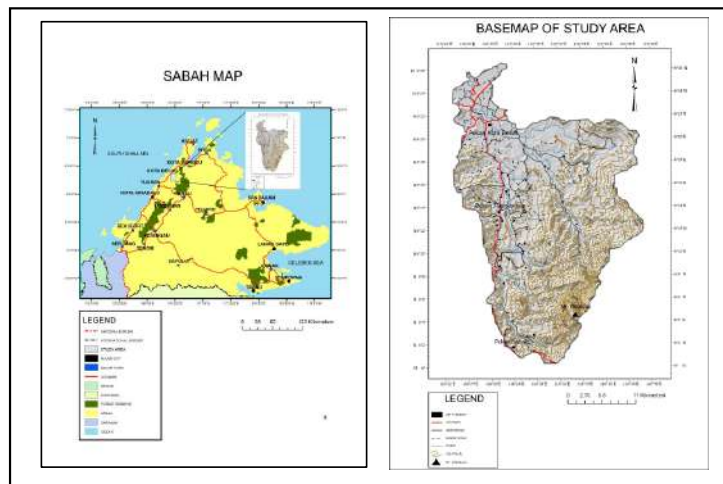


Fig. 1: Map showing the base map of the study area.

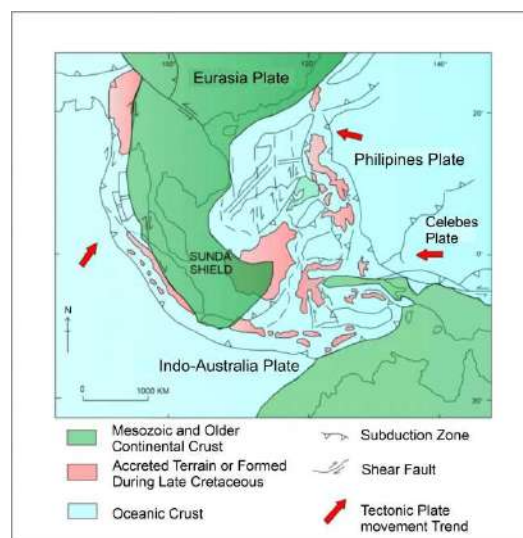


Fig. 2: Main tectonic plate of Southeast Asia. (Source: Modified from Tan & Lamy (1990))

rocks associated with metamorphic rocks were mostly found in the western and northern parts of Sabah. Sedimentary rocks are dominated by sandstone with shale and associated with chert, limestone, and conglomerate. Meanwhile, igneous rocks consist of serpentine, basalt/sphilit, agglomerate, gabbro, dolerite, andesite, granodiorite, and adamellite. Metamorphic rocks consist of hornblende schist and gneiss. The correlation between all these rock formations can be seen in Fig. 3.

According to Basir (1988), the oldest sedimentary rock in the region is radiolarian chert from the early Cretaceous age. These thin layers of chert can be associated with basic igneous rocks such as basaltic or split. There are also several types associated with these two rock types, namely peridotite and ultrabasic serpentine, intrusive dolerite, and metamorphic hornblende, schist, and gneiss. These rock associations depict an ophiolite sequence representing the Mesozoic oceanic crust that forms the region's basement rocks.

The basement rocks are overlain by sedimentary formations, including the Crocker Formation, Trusmadi Formation, and Wariu Formation, which range in age from Eocene to mid-Miocene. The western part of Sabah is primarily characterized by the Crocker and Trusmadi formations, both of which are deep-sea sediments characterized by alternating layers of sandstone and shale (Tongkul 1991). The Wariu Formation, on the other hand, is a mixed sediment deposit consisting of various-sized clasts such as mudstone, greenish arenite, coarse-grained arenite, metaklastic, micritic limestone, and shiny greenish argillite, which date back to the Middle Miocene (Tijia 1988).

The intrusive igneous rocks, such as Mount Kinabalu and the extrusive volcanic rocks of Sirar Volcanic Island, were formed during the Miocene-Pliocene age (Tongkul 1991).

Based on the geological map in Fig. 4, which was created by referring to the Sabah Geological Map 4th Edition (JMG 2010). The main rock unit in the study consists of the Wariu Formation, Crocker Formation, and Quaternary Coastal Alluvium (Fatin et al. 2022), followed by small portions of the Trusmadi Formation, basic igneous rocks, faulted basement, plutonic igneous rocks, Pleistocene river alluvium deposits, and chert-sphilit. Observations were made through field studies aimed at distinguishing and confirming the presence of rock units and their characteristics in the study area.

## MATERIALS AND METHODS

### Fuzzy Logic Technique

The fuzzy logic technique has been applied in various fields, such as in mineral prospectivity (Zhang et al. 2017), environmental risk assessment mapping (Poberezhna et al.

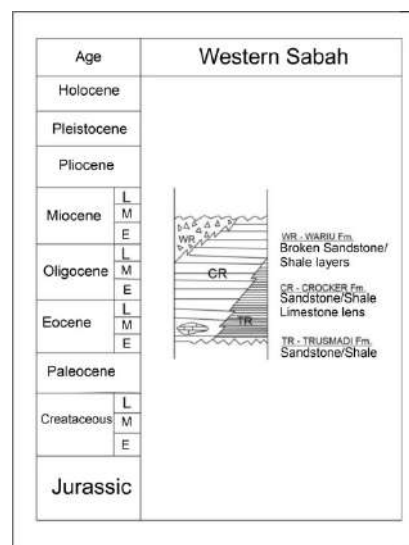


Fig. 3: general stratigraphy of western Sabah. (Source. Modified from Tongkul (1991))

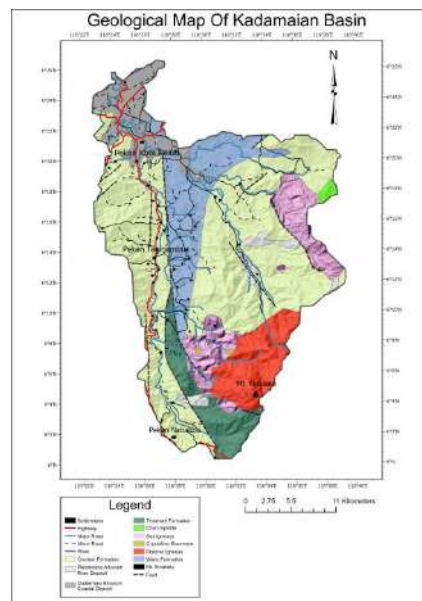


Fig. 4: The geological map of the study area in the Kadamaian Basin, Kota Belud. (Source: Sabah Geological Map 4th Edition (JMG, 2010))

2022), soil erosion prediction (Mitra et al.1998), and forest fire risk mapping (Juvanhol R.S> 2021). Introduced by Zadeh (1996), Fuzzy Logic consists of objects in a set that have their own degrees of membership where each thematic map was reclassified and assigned fuzzy logic membership values. These membership values are significant in defining the criteria for identifying groundwater potential zones in the study area. Assimakopoulos et al. (2003) state that the degrees of membership in the set vary between 0 (unsuitable

or lowest groundwater potential) and 1 (most suitable or highest groundwater potential). All of the fuzzified thematic maps were then set to overlay each other using the 'fuzzy overlay' tool in ArcGIS Pro software. Fuzzy sum operators were used for the factor theme integration (Fig. 5). The product of the fuzzy logic overlay was then reclassified into five classes, 'very poor', 'poor', 'moderate', 'high', and 'very high' groundwater potential zones. Fuzzy subsets can be represented by the following membership functions;

$$\mu_A : (x) \rightarrow [0,1]$$

The function can be associated with each parameter in a fuzzy set represented by  $\mu_A : (x)$ . The value of  $X$  in  $\mu_A : (x)$  represents each parameter in a fuzzy set and its degree of membership. A value of 1 signifies a complete membership of a parameter, whereas a value closer to 0 indicates a weaker membership of that parameter in a fuzzy set (Kollias & Kalivas 1998).

### Model Validation for Potential Zones of Groundwater

To guarantee the precision of prospective groundwater zone maps, the applicability of the methods used in this study for mapping groundwater zones was validated through the Receiver Operating Characteristic Curve (ROC) and Area Under the Curve (AUC) (Pourtaghi & Pourghasemi 2015, Ozdemir et al. 2011).

The AUC value in the ROC system, which goes from 0.5 to 1.0, is used to evaluate the model's accuracy. An AUC of 0.5 would be assigned to a model that only characterizes or

forecasts the existence of a groundwater zone. According to Pourghasemi et al. (2012), a graphical representation of the ROC curve is created by plotting the false-positive rate (1-specificity) on the X-axis and the true positive rate (sensitivity) on the Y-axis.

## RESULTS AND DISCUSSION

The fuzzy membership values will be organized in tabular form, and their computation will be carried out using the Raster Calculator and Fuzzy Toolset available in the ArcGIS Pro software. Table 1 shows the statistical data of parameters according to the classes used in this study. The fuzzy membership values were generated through the fuzzyfication toolset in ArcGIS Pro. Below is the formula for the fuzzy logic function used in computing the fuzzy membership for the dataset;

### Linear Membership Function

The linear membership function refers to the relationship between input and output values represented by a linear equation where the membership values in a fuzzy set increase and decrease linearly with the variable. The linear fuzzy function is represented through the following equation:

$$\mu(y) = m \times x + b$$

Where,

$\mu(y)$  = membership value of the output fuzzy set (y),

$x$  = input value,

$m$  = slope of the linear function,

$b$  = intercept (or offset).

### Gaussian Membership Function

The Gaussian membership function is represented by the Gaussian curve shape, characterized by its mean and standard deviation. This function is used to model uncertainty in the real world, where elements can be part of a set. The Gaussian membership function is widely used in fuzzy logic systems. The following equation represents the Gaussian fuzzy function:

$$\mu(x) = \exp(-(x - c)^2 / (2 \times \sigma^2))$$

Where,

$x$  = input value for which the membership value is to be determined.

$c$  = center or mean of the Gaussian curve, representing the most likely value for full membership.

$\sigma$  = standard deviation, which controls the spread or width of the curve. A larger  $\sigma$  value produces a wider curve and lower peak.

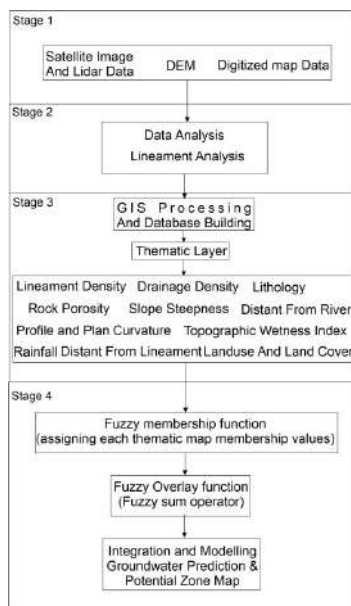


Fig. 5: The pathway of combining the fuzzy logic technique and GIS in this study.

Table 1: Fuzzy membership values for each parameter class in this study.

Parameters	Class	Fuzzy Type	Fuzzy Membership Value
Lineament density	0-0.500	Gaussian	0.79
	0.500-1.000		0.85
	1.000-1.500		0.9
	1.500-2.000		0.95
	2.000-2.600		1
Drainage Density	0-0.5	Linear	1
	0.5-1		0.83
	1-1.5		0.66
	1.5-2		0.5
	2-2.5		0.14
Distance From Drainage	0-400	Linear	1
	400-800		0.82
	800-1200		0.69
	1200-1700		0.55
	1700-2400		0.42
Rock Porosity	> 2400	Gaussian	0
	≤ 10		0
	≥ 11 ≤ 20		0.25
	≥ 21 ≤ 30		0.50
	≥ 31 ≤ 45		0.75
Distance From Lineament	≥ 46	Linear	1
	0 - 200		1
	200 - 400		0.81
	400 - 600		0.62
	600 - 800		0.44
Slope Steepness	>800	Linear	0
	≤ 6		1
	6 - 11		0.76
	11 - 18		0.52
	18 - 25		0.29
Profile and Plan Curvature	≥ 50	Gaussian	0
	Convex		0
	Flat		0.5
Rainfall	Concave	Gaussian	1
	< 3600		0
	3600 - 3700		0.26
	3700 - 3800		0.50
	3800 - 3900		0.74
Landuse And Land Cover (LULC)	> 3900	Linear	1
	Water Body		1
	Agriculture		1
	Shrubs		0.67
	Jungle		0.5
	Urban		0.33
	Barren Land		0
	Cloud Cover		0
	Coastal River Alluvial		1
	Deposits		1
Lithology	Pleistocene River Alluvial	Linear	1
	Deposits		1
	Crocker Formation		0.66
	Wariu Formation		0.66
	Trusmadi Formation		0.22
	Chert-Sphillite		0
	Basic Igneous		0
	Plutonic Igneous		0
	Crystalline Basement		0
	Topographic Wetness Index(TWI)		0
Topographic Wetness Index(TWI)	< 5	Gaussian	0
	5		0.14
	6		0.23
	7		0.33
	> 7		1



In this function, as  $x$  moves away from the center  $c$ , the membership value gradually decreases, indicating the degree of membership of  $x$  in that fuzzy set.

### Groundwater Potential Suitability Analysis

The production of groundwater potential maps through this method involves the use of a raster calculator and Fuzzy toolset found in the ArcGIS Pro software by combining the

fuzzified thematic map for each of the parameters used in this study. Fig. 6 was the fuzzified thematic map for each of the parameters used in this research. The membership values were given through the fuzzy membership toolset in ArcGIS Pro.

### Lithology vs. Groundwater Potential

In this study, thematic lithological layers are crucial in determining the groundwater potential within a particular

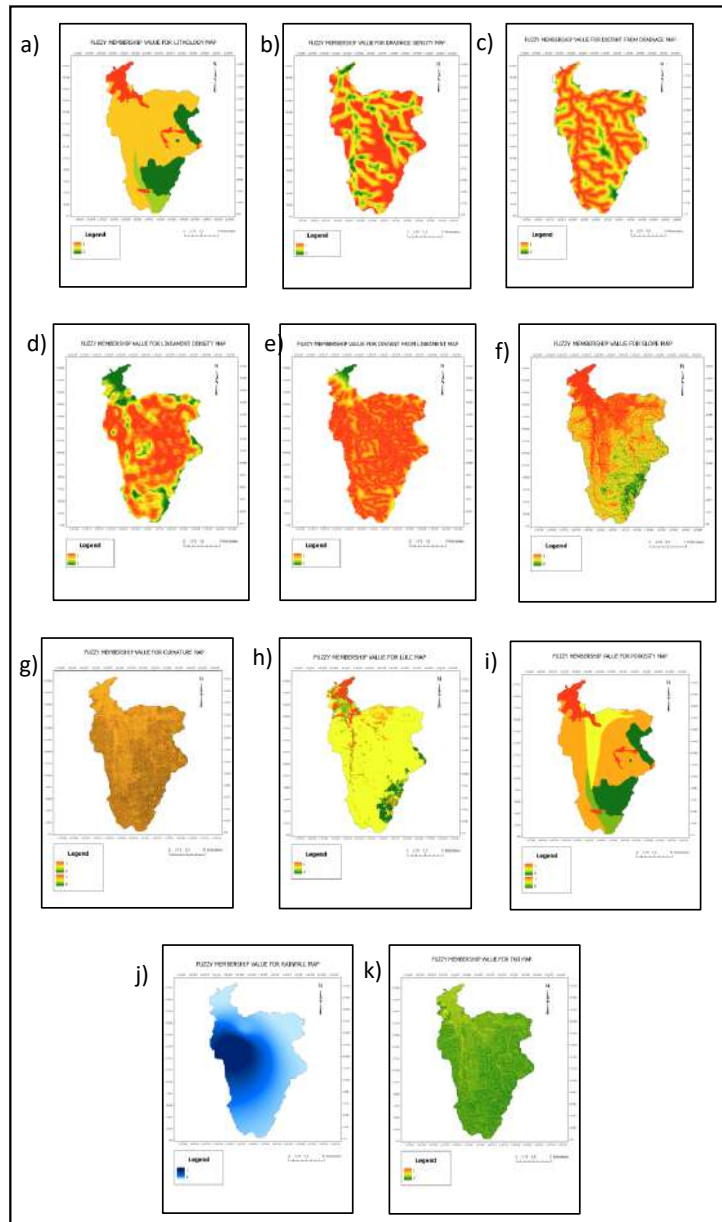


Fig. 6: a) Lithology map b) Drainage Density map c) Distance From Drainage map d) Lineament Density Map e) Distant From Lineament f) Slope Steepness map g) Curvature map h) Landuse and Land Cover map i) Rock Porosity map j) Rainfall map k) Topography Wetness Index map.

area. This is because the permeability and porosity of the layers at the surface affect the infiltration of surface runoff into the aquifer (Antenah et al. 2022, Melese & Belay 2022). The Crocker Formation, followed by rocks of the Wariu Formation and Quaternary coastal alluvial units, were the dominant rock units in the study area, comprising 52.60%, 13.07%, and 7.93% of the study area, respectively, and they have high potential to act as aquifers. In addition to these formations, there are also the Trusmadi Formation and Pleistocene river alluvial deposits, which respectively cover 6.24% and 1.89% of the study area and are also potential water-bearing units due to the presence of sandstone in these formations and the suitable characteristics of the Pleistocene river alluvial unit to act as an aquifer. Meanwhile, other rock units in the study area, such as igneous plutons, basaltic plutons, basement complex, and chert-splite, had been categorized as having less potential to be an aquifer in this study. The fuzzifying process of this thematic map involved giving the highest membership value to alluvium quaternary and Pleistocene alluvial units, followed by the Crocker formation, Wariu formation, Trusmadi formation, Chert-splite rock unit, and the lowest membership value were shared between the igneous pluton, basaltic pluton, and basement complex (Fig. 6(a)).

Direct observations of well locations on the base map of the study area indicate that the majority of tube wells developed by the Department of Minerals and Geosciences, Sabah, are located in the sandstone of Crocker Formation, and Quaternary coastal alluvial areas (Fig. 7(a)).

### Drainage Density vs Groundwater Potential

The drainage density map was created using the DEM (Digital Elevation Model) data, which was generated by Global Mapper software and was then processed in ArcGIS Pro through “line density” and “interpolation” features. According to the base map, the primary river branches in the study area are Sungai Wariu and Sungai Kadamaian, which flow from the northwest to the southeast of the study area.

According to Razandi et al. (2015), drainage density is inversely correlated to the permeability of an area. Other than that, an area with high drainage density shows that the area has low permeability, high angle of steepness, and high surface water runoff; meanwhile, an area with low drainage density is vice versa. In this study, areas with high flow density are associated with the rate of recharge and the capacity of surface water infiltration. Therefore, the hypothesis that high density in a particular location will increase the ability of recharge rate and surface water infiltration capacity into the groundwater system has been accepted for this study. The average flow density in the

study area is  $444.588 \text{ km.km}^{-2}$ , based on calculations using the following formula;

$$\text{Average Drainage Density} = \frac{\sum_1^n \text{Drainage Length}}{\text{Basin Area}}$$

The thematic map of drainage density produced for this study is divided into five categories: very high ( $2.0 - 2.5 \text{ km.km}^{-2}$ ), high ( $1.5 - 2.0 \text{ km.km}^{-2}$ ), moderate ( $1.0 - 1.5 \text{ km.km}^{-2}$ ), low ( $0.5 - 1.0 \text{ km.km}^{-2}$ ), and very low ( $0 - 0.5 \text{ km.km}^{-2}$ ), each comprising 0.09%, 1.28%, 11.84%, 30.66%, and 56.30% of the study area's total area (Fig. 7(b)). For the fuzzification process of the drainage density thematic map, the highest membership value was given to the very high density of drainage, and the lowest membership value was given to the very low drainage density (Fig. 6(b)).

### Distance from Drainage vs Groundwater Potential

The distance from drainage and surface water flow can affect the groundwater recharge rate (Machiwal et al. 2011, Mallick et al. 2019, Adeyeye et al. 2019). According to Doke et al. (2021), the groundwater level is higher near drainage compared to areas far from it. The distance from drainage map data was obtained from the power.larc.nasa.gov website and was created using the Euclidean distance tool in ArcGIS Pro software. The resulting thematic map was divided into five classes: 0-400 m, 400-800 m, 800-1200 m, 1200-1700 m, 1700-2400 m, and > 2400 m (Fig. 7(c)). In the fuzzification process of the distance from the drainage thematic map, the lowest membership value was given to the farthest distance from the drainage, and the highest membership value was given to the nearest distance from the drainage (Fig. 6(c)).

Based on the comparison between well locations and the distance from the streams map, it was found that the majority of tube wells yielding significant groundwater findings, i.e., above  $2 \text{ m}^3.\text{h}^{-1}$ , are concentrated within the 0-400 m and 400-800 m range from the main drainage in the study area (Fig. 7(c)). This observation demonstrates that groundwater is directly influenced by these parameters.

### Lineament Density vs Groundwater Potential

In this study, lineament density is a crucial feature in determining the groundwater potential of an area. Lineaments represent fractures, fissures, fault zones, and joints formed due to tectonic activities and stresses. These linear patterns can be defined as secondary porosity, which can influence the infiltration rate of surface recharge and runoff of groundwater aquifers.

High groundwater potential is associated with high lineament density (Magowe & Carr 1999, Hung et al. 2005, Al-Ruzouq et al. 2019). In this study, lineament data were obtained from the DEM (Digital Elevation Model) map,

where linear patterns on the map were identified and then analyzed for lineament density using ArcGIS Pro software. The average density for the entire study area is  $951.392 \text{ km}^{-1}$  and was obtained through the following formula;

$$\text{Average Lineament Density} = \frac{\sum_1^n \text{Lineament Length}}{\text{Basin Area}}$$

The lineament density map generated through this analysis has been categorized into five classes: very low ( $0 - 0.5 \text{ km}^{-1}$ ), low ( $0.5 - 1.0 \text{ km}^{-1}$ ), moderate ( $1.0 - 1.5 \text{ km}^{-1}$ ), high ( $1.5 - 2.0 \text{ km}^{-1}$ ), and very high ( $2.0 - 2.6 \text{ km}^{-1}$ ) (Fig. 7(d)). The distribution of area percentages for each class in the study area was 22%, 33%, 30%, 13%, and 2%. Based on the thematic map in Fig. 7, the high to very high lineament density is concentrated in the soft rock areas of the Wariu Formation and Crocker Formation (Fig. 7(d)).

#### Distance from Lineament vs. Groundwater Potential

In hydrogeological research, the distance from lineaments is a crucial factor because prominent hydrogeological zones can be found near major lineament structures (Benjmel 2020). The lineament trace map in Fig. 7(f) shows dominant linear structures influencing rock units in the study area. Tectonic analysis indicates that the dominant stress direction in the study area is northwest-southeast. In this study, the thematic map of distance from lineaments can be categorized into five classes: 0–200 m (very low), 200–400 m (low), 400 m–600 m (moderate), 600 m–800 m (high), and > 800 m (very high) (Fig. 6(e) & Fig. 4(f)). In the fuzzification process of the thematic map, the nearest distance from the lineament was given a high membership value, while the farthest distance from the lineament was given the lowest membership value (Fig. 6(e)).

#### Slope vs Groundwater Potential

According to Ganapuram et al. (2009), slope steepness plays a role in influencing the presence and movement of both surface runoff and groundwater. Therefore, it can be said that slope steepness is a significant factor in infiltration and water flow.

Slope analysis in this study was conducted using the Slope Tools feature in ArcGIS Pro software. To generate thematic maps of slope steepness, raster DEM (Digital Elevation Model) data will be utilized. The assessment of groundwater potential in the study area will then be generated using the thematic layer of slope steepness as one of the crucial parameters in this study. This is because, through slope analysis, areas with high and low slopes can be identified, where in areas with steep slopes, rainfall-runoff flows more rapidly than in areas with gentle slopes. Thus, areas with steep slopes contribute less to groundwater recharge.

Based on Fig. 7(g), slope steepness in the study area has been divided into five classes:  $\leq 6^\circ$  (very gentle slope),  $6^\circ - 11^\circ$  (gentle slope),  $11^\circ - 18^\circ$  (moderate),  $18^\circ - 25^\circ$  (steep), and  $\geq 50^\circ$  (very steep), each comprising 16.67%, 14.53%, 21.54%, 19.95%, and 27.31% of the study area, respectively. Areas with very gentle and gentle slopes are located in the northwest and along the main streams in the study area, while steep and very steep areas are located in the southeast of the study area. In the fuzzified thematic map of this parameter, the most gentle slope was given a high membership value, and vice versa for the steepest slope (Fig. 6(f)).

#### Curvature vs. Groundwater Potential

A statement by Benjmel et al. (2022) said that curvature refers to the shape of the earth's surface and is used in the topographic analysis of an area. Thematic maps for curvature are generated using raster DEM data through ArcGIS Pro software. In this study, the curvature map generated is a combination of planar curvature and profile curvature values. The acceleration and deceleration of water flow are depicted by the profile curvature in the direction of the maximum slope gradient, while planar curvature affects the concavity and convexity of flow perpendicular to the slope gradient. A statement by Arulbalaji et al. (2019) said that the combination of these values could more accurately depict flow on the surface, where curvature is used in mapping groundwater potential to indicate groundwater flow direction and potential for groundwater recharge.

The curvature map in the study area is classified into three classes: concave, flat, and convex, representing 46.84%, 7.35%, and 45.81% of the study area, respectively. The concave class represents areas where the ground surface curves inward, while the flat class represents areas where the ground surface is relatively flat, and the convex class represents areas where the ground surface curves outward. These classes can be useful in identifying areas where water may accumulate or flow more rapidly, which can have implications for groundwater potential and groundwater detection rates (Fig. 7(h)). The fuzzification of this thematic map involved giving the highest membership values to the concave class and the lowest membership value to the convex class (Fig. 6(g)).

#### Land Use vs Groundwater Potential

Land use and land cover are important factors in the hydrogeological analysis of an area. This is because groundwater recharge is influenced by land use and land cover (Kaur et al. 2020). Additionally, land use and land cover also affect surface runoff, infiltration, and water percolation. The thematic map generated in Fig. 7(i) is based on a visual interpretation of Sentinel-2A satellite

imagery, which has been validated using Google Earth satellite imagery.

In this study, land use and land cover in the study area are divided into seven classes: forest, water bodies, agriculture, shrubs, development, barren land, and cloud cover, each comprising 80.99%, 0.70%, 4.35%, 4.02%, 4.45%, 0.57%, and 4.92% of the study area, respectively. The highest membership value was given to water bodies, followed by agriculture, shrubs, jungle, urban, and barren land, and the lowest membership value was given to cloud cover (Fig. 6(h)).

### Porosity vs. Groundwater Potential

Porosity determines a rock's ability to store water (Fajana 2020). In this study, porosity also refers to the volume of open spaces or voids within the rock. Higher porosity allows for more water storage, but not all voids are interconnected, so effective porosity is where voids within the rock are interconnected. Effective rock porosity analysis in the study area is determined using the Skyscan 1275 machine, Bruker Tomography. The porosity values are then incorporated into thematic maps generated using ArcGIS Pro software.

In this study, only rock units with the presence of sandstone are analyzed, considering sandstone's suitability as an efficient aquifer. Three rock samples from the Crocker Formation, Wariu Formation, and Trusmadi Formation were analyzed, each yielding effective porosity percentages of 43.1%, 23.5%, and 21%, respectively. The alluvial unit in the study area is estimated to have a porosity above 46% due to its tendency to store water. The estimated porosity for hard rocks in the study area is below 10%. The porosity in the study area was classified into 5 classes:  $\leq 10$ ,  $\geq 11 \leq 20$ ,  $\geq 21 \leq 30$ ,  $\geq 31 \leq 45$ , and  $\geq 46$  (Fig. 7(j)). A high membership value was given to the porosity value of the  $\geq 46$  class, and the lowest membership value was given to the  $\leq 10$  class (Fig. 6(i)).

### Rainfall vs Groundwater Potential

Rainfall distribution in a particular area affects the rate of groundwater recharge. The study area is categorized as a tropical climate area with high annual rainfall, making rainfall distribution a significant factor in groundwater studies. Therefore, rainfall distribution is heavily emphasized in groundwater exploration. Agarwal and Garg (2016) stated that rainfall distribution affects the amount of water available for infiltration into the groundwater system.

Rainfall distribution data in the study area is based on readings from three weather stations obtained from the Sabah Meteorological Department in the study area. Thematic maps are then generated through interpolation features available in ArcGIS Pro software. Based on the thematic map generated in Fig. 7(k), annual rainfall in the study area is divided

into five classes:  $< 3600\text{mm}$ ,  $3600\text{mm}-3700\text{mm}$ ,  $3700\text{mm}-3800\text{mm}$ ,  $3800\text{mm}-3900\text{mm}$ , and  $> 3900\text{mm}$ . Areas with the highest rainfall distribution in the study area are concentrated in the western region, while the northeastern region of the study area shows the lowest rainfall distribution. The higher membership value was given to the highest rainfall value, and the lowest membership value was given to the lowest rainfall value (Fig. 6(j)).

### TWI vs. Groundwater Potential

The Topographic Wetness Index (TWI) is a humidity index used to assess the topographic control of hydrological processes. It is a function where slope and contributing area per unit orthogonal width to the change in flow direction are involved (Sørensen et al. 2006). The higher the value of the topographic wetness index in an area, the lower the slope. This indicates that the potential for groundwater accumulation in that area is high (Naghbi et al. 2017). The Topographic Wetness Index (TWI) is represented by the following formula;

$$TWI = \ln \left( \frac{A_s}{\tan \beta} \right)$$

Where,

$A_s$  = surface water collection

$\beta$  = slope of the terrain

The TWI map has been generated using raster DEM data in ArcGIS Pro software through the process of calculating flow direction, flow accumulation, slope, slope to radians conversion, tangent slope calculation, and adjusting flow accumulation. The values of the topographic wetness index in this study have been classified into five classes:  $< 5$ ,  $5$ ,  $6$ ,  $7$ , and  $> 7$  (Fig. 7(i)). For the fuzzification process highest membership value was given to the highest number of twi index values, and the lowest membership value was given to the lowest twi index value (Fig. 6(k)).

### Groundwater Potential

The groundwater potential in the study area was divided into five groups of classes: very low, low, moderate, high, and very high. Based on the results, the analysis shows that 32.34% of the study area ( $274.37 \text{ km}^2$ ) is categorized as very low groundwater potential, 26.80% of the area ( $227.37 \text{ km}^2$ ) as low groundwater potential, 15.55% of the area ( $131.93 \text{ km}^2$ ) as moderate groundwater potential, 13.83% of the area ( $117.33 \text{ km}^2$ ) as high groundwater potential, and the highest groundwater potential area contributed about 11.48% from the study area ( $97.40 \text{ km}^2$ ) (Fig. 8).

The map produced showed that the area with the highest groundwater potential was mostly located at the Crocker



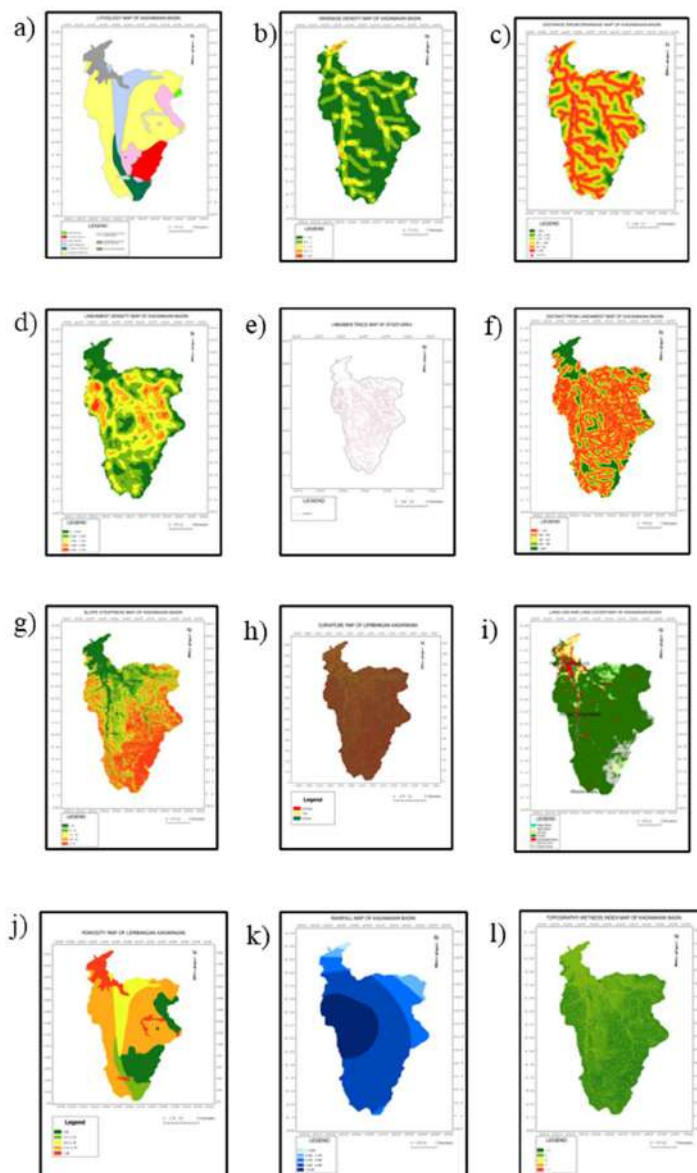


Fig. 7: a) Lithology map b) Drainage Density map c) Distance From Drainage map d) Lineament Density Map e) Lineament Trace map f) Distant From Lineament g) Slope Steepness map h) Curvature map i) Landuse and Land Cover map j) Rock Porosity map k) Rainfall map l) Topography Index map.

formation and Wariu formation, west of the study area and along the Kadamaian River system, which had been estimated to have 11.48% very high and 13.83% high groundwater potential, while alluvium unit, Trusmadi formation, and other hard rock areas such as igneous pluton, basaltic pluton, and basement complex showed a poor groundwater potential. Other than that, based on the groundwater potential map, the very high and high groundwater potential areas were also concentrated in low slope angle areas. Meanwhile, The remaining moderate, low, and very low potential of

groundwater, where most of the area can be found at the higher topography area or high slope angle area southeast of the study area. Very high and high potential of groundwater could also be traced near lineaments and drainages. This is because both of the parameters affected the recharge rate of groundwater. Drainage density, however, gave opposite effects from lineament density. High drainage density indicates low permeability in an area that could affect groundwater recharge rate and vice versa for areas with low drainage density, whereas an area with high lineament

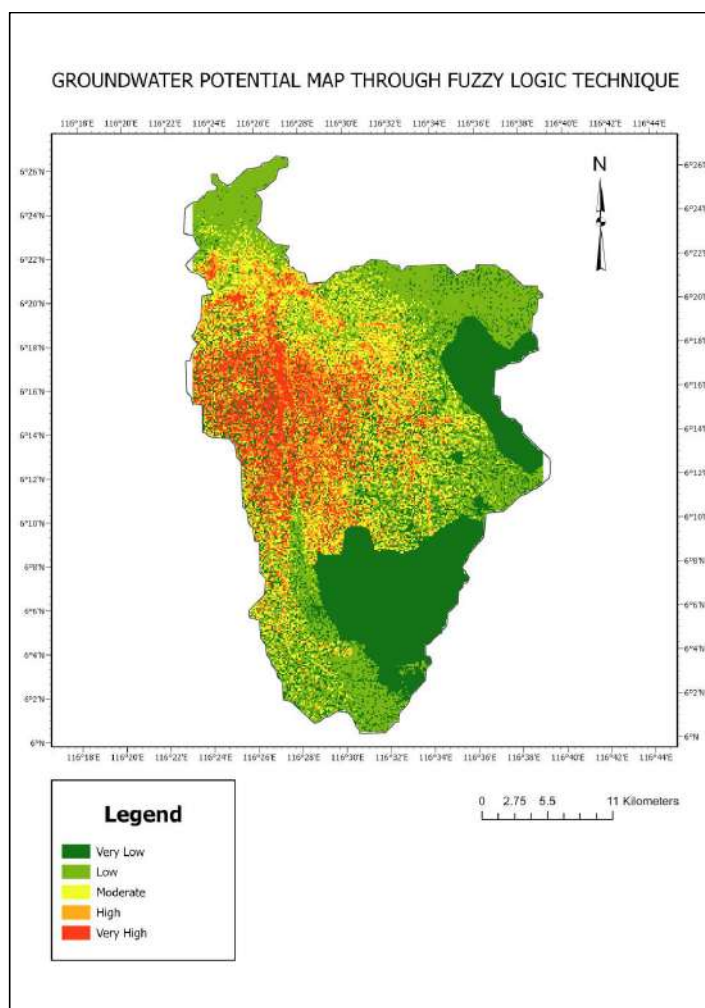


Fig. 8: Groundwater Potential Map in the Lembangan Kadamaian through FLT ROC and AUC Validation of the Groundwater Potential Map.

density indicates a higher recharge rate and low lineament density indicates a lower recharge rate. The very high and high classes also correlate with the rainfall in the study area, where most of the very high and high-value groundwater potential zones can be traced in the high rainfall area west of the study area. Other than that, most of the very high and high potential zones in the study area concentrate in Crocker Formation and Wariu Formation and not in the alluvium unit of the study area, despite having higher estimated porosity than both of the previously mentioned rock units. This was mainly affected by the land use and land cover parameter, where most of the developed areas can be found situated in alluvium units of the study area. Due to high development, developed areas were considered highly polluted and thus were given low membership value. This, however, leads to the outcome of low-potential areas in most of the alluvium units in the study area. The observation on TWI and curvature

map, however, doesn't give any visible or directly observable correlation between both its thematic map and groundwater potential zones of the study area. Thus, its effects on groundwater potential can only be explained theoretically.

Both the alluvium and Crocker Formation act as a good aquifer. However, based on the well site datum, most of the high-yield well that exceeds more than 4 m<sup>3</sup>/h that were excavated by the Department of Minerals and Geosciences (JMG) was found in the Crocker Formation. Thus it can be concluded that the Crocker Formation is more productive than the alluvium unit of the study area.

However, in this study, the water quality factor of the underground water must be considered to ensure that the water source can be used by the surrounding population. The accuracy of this groundwater potential map was determined by the total well site datum which are the dependent variables of this study.

Table 2: Classification of AUC value ranges.

AUC Value Ranges	Class
0.9 - 1.0	Excellent
0.8 - 0.9	Very Good
0.7 - 0.8	Good
0.6 - 0.7	Fair
0.5 - 0.6	Poor

The method of ROC curve and AUC validation was conducted to assess the effectiveness of the models used in this study. This validation process involves the use of independent data to evaluate how well these models can distinguish between positive and negative classes.

The AUC value ranges between 0.5 and 1.0; the closer the value to 1.0, the higher the accuracy, while the closer the value to 0.5, the lower the accuracy (Fawcett 2006). The relationship between the AUC value and the expected accuracy can be represented by class values in Table 2 (Naghibi et al. 2017).

In this study, a total of 36 existing tube wells within the study area were used in calculating the AUC value to obtain the success rate curve. The AUC value obtained for the logistic regression model is  $AUC = 0.745$  or 74.5% model accuracy (Fig. 9). Based on the AUC value obtained, the Fuzzy Logic Technique can be classified as a good model.

## CONCLUSIONS

The research successfully mapped groundwater potential zones in the Lembangan Kadamaian area, Sabah, by employing the Fuzzy Logic Technique as the primary analytical tool, utilizing ArcGIS Pro software for spatial

analysis and modeling. The research area, covering approximately 848.4 km<sup>2</sup>, is characterized by geological formations such as Crocker Formation, Wariu Formation, and Pleistocene alluvium deposits, along with other rock units like Trusmadi Formation, basic igneous rocks, crystalline basement, plutonic igneous rocks, and chert-spilite formation. The analysis revealed significant correlations between various parameters and groundwater potential. A total of eleven thematic maps were produced, and each was assigned fuzzy logic membership values and overlaid using a fuzzy toolset in ArcGIS Pro. Lithology, LULC, lineament density, distance from lineaments, drainage density, distance from drainage, and rainfall distribution emerged as crucial factors influencing groundwater occurrence. Areas with sandstone-rich formations, high lineament density, moderate to low drainage density, high to moderate rainfall, less developed, and proximity to drainage and lineament features showed higher groundwater potential. The Fuzzy Logic Technique demonstrated good accuracy (75.2%) in predicting groundwater potential, validated through ROC analysis. The generated groundwater potential map classified the study area into five categories: very high, high, moderate, low, and very low potential zones. The results indicated that around 32.34% of the area had very low potential, while 26.80% had low potential, and 15.55% had moderate potential. Areas with high 13.83% and very high groundwater potential covered approximately 11.48% of the study area, mainly concentrated in the Crocker Formation and Wariu Formation, where each of the classes covered an area of 274.37 km<sup>2</sup>, 227.37 km<sup>2</sup>, 131.93 km<sup>2</sup>, 117.33 km<sup>2</sup>, and 97.40 km<sup>2</sup>. In addition, the data on the yield rate of tube wells in the study area also, to some extent, help in making comparisons for the existence of groundwater. In addition,

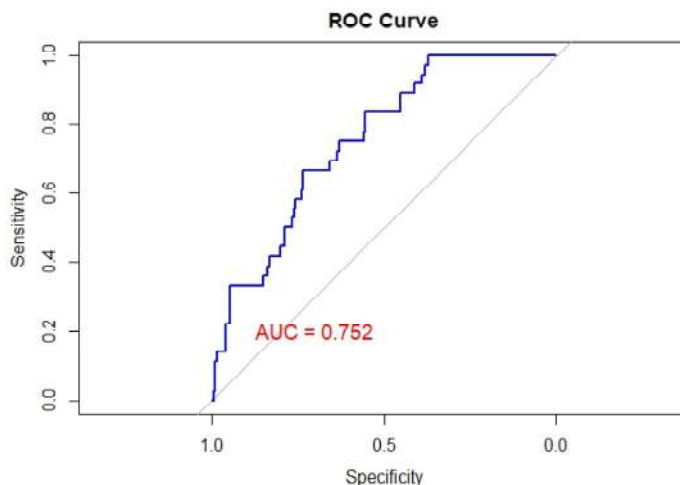


Fig. 9: ROC curve and AUC validation for fuzzy logic technique.

the downside of this model is that it completely abandoned the possibility of groundwater potential in developed areas and doesn't involve the use of field data such as tube well data in its equation of generating groundwater potential zones. However, the findings still contributed valuable observations for sustainable water resource management and land use planning in the region.

## ACKNOWLEDGMENT

The authors express appreciation and thank you to Universiti Malaysia Sabah for providing Grant GUG0600-1/2023 and all the support for this study.

## REFERENCES

- Adeyeye, O.A., Ikpokonte, E.A. and Arabi, S.A., 2019. GIS-based groundwater potential mapping within Dengi area, North Central Nigeria. *The Egyptian Journal of Remote Sensing and Space Science*, 22(2), pp.175-181. DOI.
- Agarwal, R. and Garg, P.K., 2016. Remote sensing and GIS-based groundwater potential & recharge zones mapping using multi-criteria decision-making technique. *Water Resources Management*, 30, pp.243-260. DOI.
- Al-Ruzouq, R., Shanableh, A., Merabtene, T., Siddique, M., Ali, M., Khalil, M., Idris, A. and Almulla, E., 2019. Potential groundwater zone mapping based on geo-hydrological considerations and multi-criteria spatial analysis: North UAE. *CATENA*, 173, pp.511-524. DOI.
- Anteneh, Z.L., Alemu, M.M., Bawoke, G.T., Kehali, A.T., Fenta, M.C. and Desta, M.T., 2022. Appraising groundwater potential zones using geospatial and multi-criteria decision analysis (MCDA) techniques in Andasa-Tul watershed, Upper Blue Nile basin, Ethiopia. *Environmental Earth Sciences*, 81, pp.1-20.
- Arulbalaji, P., Padmalal, D. and Sreelash, K., 2019. GIS and AHP techniques based delineation of groundwater potential zones: A case study from Southern Western Ghats, India. *Scientific Reports*, 9, p.2082. DOI.
- Assimakopoulos, J.H., Kalivas, D.P. and Kollias, V.J., 2003. A GIS-based fuzzy classification for mapping the agricultural soils for N-fertilizers use. *Science of The Total Environment*, 309(1-3), pp.19-33. DOI.
- Balaguru, A., Nichols, G. and Hall, R., 2003. The origin of the circular basins of Sabah, Malaysia. *Geological Society of Malaysia Bulletin*, 46, pp.335-351. DOI.
- Basir, D.S., 1988. Barremian radiolaria from Chert-Spilite Formation, Kudat, Sabah. *Sains Malaysiana*, 17(1), pp.67-79.
- Benjmel, K., Amraoui, F., Aydda, A., Tahiri, A., Yousif, M., Pradhan, B., Abdelrahman, K., Fnais, M.S. and Abioui, M., 2022. A multidisciplinary approach for groundwater potential mapping in a fractured semi-arid terrain (Kerdous Inlier, Western Anti-Atlas, Morocco). *Water*, 14(10), p.1553. DOI.
- Doke, A.B., Zolekar, R.B., Patel, H. and Das, S., 2021. Geospatial mapping of groundwater potential zones using multi-criteria decision-making AHP approach in a hard rock basaltic terrain in India. *Ecological Indicators*, 127, p.107685. DOI.
- Fajana, A.O., 2020. Groundwater aquifer potential using electrical resistivity method and porosity calculation: A case study. *NRIAG Journal of Astronomy and Geophysics*, 9(1), pp.168-175. DOI.
- Fatin, N.I., Norsyafina, R., Jaineh, L., Umar, H. and Norasiah, S., 2022. Penentuan jenis akuifer di Kota Belud, Sabah menggunakan kaedah seismik pantulan. *Sains Malaysiana*, 51(8), pp.2735-2743. DOI.
- Fawcett, T., 2006. An introduction to ROC analysis. *Pattern Recognition Letters*, 27(8), pp.861-874.
- Ganapuram, S., Vijaya Kumar, G.T., Murali Krishna, I.V., Kahya, E. and Demirel, M.C., 2009. Mapping of groundwater potential zones in the Musi basin using remote sensing data and GIS. *Advances in Engineering Software*, 40(7), pp.506-518. DOI.
- Ghaheeri, S., Ismail, M.S., Nasiman, S. and Momeni, M., 2017. Sedimentary architecture and depositional environment of Kudat Formation, Sabah, Malaysia. *IOP Conference Series: Materials Science and Engineering*, 291, p.012025. DOI.
- Hung, L.Q., Batelaan, O. and De Smedt, F., 2005. Lineament extraction and analysis, comparison of LANDSAT ETM and ASTER imagery: Case study—Suoimuoi tropical karst catchment, Vietnam. *Proceedings of SPIE*, 5983, p.59830T. DOI.
- JMG, 2010. *Garis Panduan Pemetaan Geologi Terain*, JMG.GP.06, Kementerian Sumber Asli dan Alam Sekitar.
- Juvanhol, R.S., 2021. GIS and fuzzy logic applied to modeling forest fire risk. *Anais da Academia Brasileira de Ciências*, 93(3), p.e20190726. DOI.
- Kaur, L., Rishi, M.S., Singh, G. and Thakur, S.N., 2019. Groundwater potential assessment of an alluvial aquifer in the Yamuna sub-basin (Panipat region) using remote sensing and GIS techniques in conjunction with analytical hierarchy process (AHP) and catastrophe theory (CT). *Ecological Indicators*, 110, p.105850. DOI.
- Kollias, V.J. and Kalivas, D.P., 1998. The enhancement of a commercial geographical information system (ARC/INFO) with fuzzy processing capabilities for the evaluation of land resources. *Computers and Electronics in Agriculture*, 20(1), pp.79-95. DOI.
- Machiwal, D., Jha, M.K. and Mal, B.C., 2011. Assessment of groundwater potential in a semi-arid region of India using remote sensing, GIS, and MCDM techniques. *Water Resource Management*, 25, pp.1359-1386. DOI.
- Magowe, M. and Carr, J.R., 1999. Relationship between lineaments and groundwater occurrence in Western Botswana. *Groundwater*, 37, pp.282-286. DOI.
- Mallick, J., Khan, R.A., Ahmed, M., Alqadhi, S.D., Alsubih, M., Falqi, I. and Hasan, M.A., 2019. Modeling groundwater potential zone in a semi-arid region of Aseer using Fuzzy-AHP and geoinformation techniques. *Water*, 11, p.2656. DOI.
- Melese, T. and Belay, T., 2022. Groundwater potential zone mapping using analytical hierarchy process and GIS in Muga Watershed, Abay Basin, Ethiopia. *Global Challenges*, 6(1), p.2100068.
- Mitra, B., Scott, H.D., Dixon, J.C. and McKimney, J.M., 1998. Applications of fuzzy logic to the prediction of soil erosion in a large watershed. *Geoderma*, 86(3-4), pp.183-209. DOI.
- Naghbi, S.A., Moghaddam, D.D., Kalantar, B., Pradhan, B. and Kisi, O., 2017. A comparative assessment of GIS-based data mining models and a novel ensemble model in groundwater well potential mapping. *Journal of Hydrology*, 548, pp.471-483. DOI.
- Ozdemir, A., 2011. GIS-based groundwater spring potential mapping in the Sultan Mountains (Konya, Turkey) using frequency ratio, weights of evidence, and logistic regression methods and their comparison. *Journal of Hydrology*, 411(3-4), pp.290-308.
- Poberezhna, L., Shkita, L., Poberezhnyi, L., Popovych, P., Brych, V. and Shevchuk, O., 2022. Assessment of environmental risks using elements of fuzzy logic. 2022 12th International Conference on Advanced Computer Information Technologies (ACIT), Ruzomberok, Slovakia, pp.219-222. DOI.
- Pourghasemi, H., Pradhan, B. and Gokceoglu, C., 2012. Application of fuzzy logic and analytical hierarchy process (AHP) to landslide susceptibility mapping at Haraz watershed, Iran. *Natural Hazards*, 63(2), pp.965-996. DOI.
- Pourtaghi, Z.S. and Pourghasemi, H.R., 2014. GIS-based groundwater spring potential assessment and mapping in the Birjand Township, Southern Khorasan Province, Iran. *Hydrogeology Journal*, 22, pp.643-662. DOI.



- Razandi, Y., Pourghasemi, H., Neisani, N. and Rahmati, O., 2015. Application of analytical hierarchy process, frequency ratio, and certainty factor models for groundwater potential mapping using GIS. *Earth Science Informatics*, 8, pp.867–883.
- Sørensen, R., Zinko, U. and Seibert, J., 2006. On the calculation of the topographic wetness index: evaluation of different methods based on field observations. *Hydrology and Earth System Sciences*, 10(1), pp.101–112. DOI.
- Tan, D.N. and Lamy, J.M., 1990. Tectonic evolution of the NW Sabah continental margin since the Late Eocene.
- Tesoriero, A.J., Inkpen, E.L. and Voss, F.D., 1998. Assessing groundwater vulnerability using logistic regression. *Proceedings for the Source Water Assessment and Protection 98 Conference*, Dallas, TX, pp.157-165.
- Tijia, H.D., 1988. Accretion tectonics in Sabah: Kinabalu suture and East Sabah accreted terrane. *Geological Society of Malaysia Bulletin*, 22, pp.237-251.
- Tongkul, F., 1991. Tectonic evolution of Sabah, Malaysia. *Journal of Southeast Asian Earth Sciences*, 6(3-4), pp.395–405. DOI.
- Zadeh, L.A., 1996. Fuzzy logic = computing with words. *IEEE Transactions on Fuzzy Systems*, 4(2), pp.103-111.
- Zhang, N., Zhou, K. and Du, X., 2017. Application of fuzzy logic and fuzzy AHP to mineral prospectivity mapping of porphyry and hydrothermal vein copper deposits in the Dananhu-Tousuquan island arc, Xinjiang, NW China. *Journal of African Earth Sciences*, 128, pp.84-96. DOI.

# A Comparative Study of Sustainable Bacteria-Alccofine Concrete: Environmental Benefits and SEM Analysis

R. Porselvan<sup>†</sup>, T. S. Lakshmi and M. Tholkapiyan

Department of Civil Engineering, Saveetha School of Engineering, Saveetha Institute of Medical and Technical Sciences, Chennai, Tamilnadu-602117, India

<sup>†</sup>Corresponding author: R. Porselvan; porselvanr9007.sse@saveetha.com

**Abbreviation:** Nat. Env. & Poll. Technol.  
**Website:** www.neptjournal.com

*Received:* 25-07-2024

*Revised:* 22-08-2024

*Accepted:* 21-09-2024

## Key Words:

Alccofine (AF)  
 Silica fume (SF)  
 Biomineralization  
*Bacillus megaterium*  
 Bacterial concrete

## Citation for the Paper:

Porselvan, R., Lakshmi, T. S. and Tholkapiyan, M., 2025. A comparative study of sustainable bacteria-alccofine concrete: Environmental benefits and SEM analysis. *Nature Environment and Pollution Technology*, 24(2), p. B4250. <https://doi.org/10.46488/NEPT.2025.v24i02.B4250>

*Note: From year 2025, the journal uses Article ID instead of page numbers in citation of the published articles.*



**Copyright:** © 2025 by the authors  
**Licensee:** Technoscience Publications  
 This article is an open access article distributed under the terms and conditions of the Creative Commons Attribution (CC BY) license (<https://creativecommons.org/licenses/by/4.0/>).

## ABSTRACT

The potential for creating unique, environmentally friendly, and cost-effective concrete via biomineralization is discussed in this research. Cement, a necessary component of concrete, is expensive and emits between 8 and 10% of the world's CO<sub>2</sub> emissions. Researchers have significant effects to identify alternatives that can reduce the burden of high costs, excessive energy use, and environmental repercussions. Manufactured sand (M-sand) completely replaced fine aggregate, and cement was replaced with alternatives such as Alccofine (AF) and Silica Fume (SF). The percentage at which it can be substituted for cement is, however, somewhat small. The goal of this study is to create an environmentally friendly AF and SF concrete mix by incorporating bacteria with the highest possible cell concentration. To evaluate the mechanical properties, concrete samples were tested for flexural strength, split tensile strength, and compressive strength at 7, 14 and 28 days post-curing. The microstructural analysis of sustainable concrete was performed using scanning electron microscopy (SEM) techniques. It was determined that 10% alccofine and 15% silica fume by volume of cement in the binary cementitious system provided the best mechanical characteristics for bacterial concrete using *Bacillus megaterium*. Similarly manner in the ternary cementitious system, the highest gain in compressive strength is seen when 10% alccofine is substituted with 10% silica fume in the cement mixture. Calcium carbonate precipitation validated the enhanced properties of bacterial concrete. The microorganisms used in the concrete are non-toxic and environmentally being. Results indicate that using *Bacillus megaterium* alongside AF and SF helps to reduce cement usage, lessens carbon dioxide emissions, and makes concrete more environmentally friendly. Using Scanning Electron Microscopy (SEM), the calcite precipitations in bio-additive mixed ternary admixture blended concrete were confirmed. The proposed regression equations produced minimal errors when compared to the experimental results, thus providing accurate and effective predictions of the flexural, split, and compressive strengths. The strength properties of these blends were validated through SEM studies.

## INTRODUCTION

Concrete, a fundamental material in construction, is renowned for its impressive compressive strength but can exhibit vulnerabilities under tension, often resulting in the development of cracks. These cracks can arise from various factors such as heavy loads, shrinkage, excessive water-cement ratio, corrosion of reinforcement steel, and inadequate cover. Traditional methods for repairing concrete cracks are not only costly but also environmentally harmful. A novel repair procedure called concrete that heals itself has been devised by researchers in answer to this difficulty. This revolutionary technique incorporates bacteria into concrete either by directly adding bacteria while mixing or by embedding spores in shells (bacteria carriers) (Shanmuga Priya et al. 2019 and Zamani et al. 2020). Until cracks appear, these microbes lie latent in the self-repairing concrete. When a fissure forms, the combination of oxygen and moisture activates bacterial spores, which in turn start metabolic reactions that convert calcium lactate to carbonate

of calcium (Schlangen & Senot 2013, Sohail et al. 2022). Therefore, the material's strength and durability are much improved when this precipitate of calcium carbonate seals the fissures (Aytekin et al. 2023).

In light of the environmental concerns associated with cement production, including high energy consumption and CO<sub>2</sub> emissions, exploring alternatives to cement in concrete structures presents a promising solution. The integration of supplementary cementitious materials (SCMs) represents a significant advancement in civil engineering. By harnessing the pozzolanic attributes of SCMs and combining them with cement, a wide range of concrete types with diverse strengths and enhanced durability can be produced. Incorporating SCMs as either substitutes for or in conjunction with cement can reduce cement consumption in concrete manufacturing and mitigate environmental contamination. Various SCMs, including fly ash, ground granulated blast furnace slag, silica fume, pond ash, limestone coarse, rice husk ash, and metakaolin, offer sustainable alternatives (Reddy & Meena 2018, Ansari et al. 2015, Chan et al. 2000).

SCMs are derived from the processing of waste materials discharged by factories and industries. Through appropriate modifications, these waste materials can be transformed into beneficial SCMs for construction purposes. Recycling industrial and factory waste materials not only offers economic benefits but also presents technical and environmental advantages. The global trend towards utilizing SCMs-based concretes is steadily growing due to their environmentally friendly attributes, strong performance, and energy-efficient characteristics (Kumar et al. 2016). SCMs play a significant role in fostering the creation of sustainable concrete, whether as mineral admixtures or partial replacements for cement (Suchithra & Malathy 2016, Umamaheswaran et al. 2015, Ushaa et al. 2015).

Incorporating SCMs into concrete development contributes to a reduction in cement consumption, thereby leading to decreased carbon dioxide emissions from cement production plants. Furthermore, this approach reduces the need for extensive excavation of raw materials essential for cement manufacturing while offering a solution for the responsible disposal of industrial waste.

### Use of Alccofine and Silica Fume

Ambuja Cements Pvt Ltd, a leading cement company in India, has recently introduced a revolutionary micro-mineral SCM named Alccofine. Alccofine is available in three different forms; included in each set are alccofine-1101, alccofine-1203, and alccofine-1206. Their calcium contents differ. The amount of calcium silicate concentration in alccofine-1101 is the greatest of these kinds, while that of

alccofine-1203 and alccofine-1206 is the lowest. The ability to make HPC and HSC is made possible by the latter two parts, which are SCMs, which can successfully substitute silica fume (Sharma et al. 2016, Ansari et al. 2015, Parveen et al. 2018, Jindal et al. 2017).

Rooted in low calcium silicate, Alccofine-1203 is a microfine substance with minimal environmental impact. It boasts high reactivity and a significant proportion of glass in its composition. Manufactured from GGBS, a byproduct of India's iron ore industries, Alccofine-1203 is a finely powdered material that enhances concrete flowability, workability, and compressive strength (Soni et al. 2013, Rajesh Kumar et al. 2015, Achal et al. 2009). Its tiny particle size allows it to efficiently fill the gaps between cement grains, resulting in greater compactness and strength (De Muijnck et al. 2008, Chahal et al. 2012).

*Bacillus* bacteria, capable of serving as binding agents, contribute to reducing capillary pores in concrete, thereby enhancing its durability and strength. Certain strains of *Bacillus* bacteria produce the enzyme urease, facilitating the precipitation of calcite through biomineralization (Seshagiri Rao et al. 2012, Wu et al. 2012, Song & Saraswathy 2015, DeJong & Mortensen 2009, Achal & Mukherjee 2015). Notably, this bio-mineralization process does not affect concrete setting time, allowing bacterial concrete to adhere to existing mix design standards. This innovative approach, centered on bio-mineralization, holds the potential to significantly reduce maintenance expenses associated with bacterial concrete. By extending concrete lifespan, this technique aids in reducing atmospheric CO<sub>2</sub> emissions, mitigating global warming, and decreasing the demand for cement. Equations illustrating biochemical reactions responsible for calcium carbonate formation within cementitious materials, facilitated by ureolytic bacteria, align with findings presented in research (Achal et al. 2011, Tobler et al. 2011 and Yong et al. 2019).

### Research Significance

A significant advancement in sustainable building techniques is the study of self-healing bacterial concrete and the incorporation of supplementary cementitious materials (SCMs). This innovative approach addresses the limitations of conventional concrete, which is brittle and has a significant environmental impact due to cement production. By adding bacteria such as *Bacillus megaterium*, the concrete can self-heal cracks through bio-mineralization, enhancing its durability and reducing maintenance costs. Additionally, the use of SCMs like Alccofine-1203, produced from industrial waste, improves the properties of concrete while reducing environmental harm by decreasing cement usage. This

dual strategy, which promotes eco-friendly construction practices and optimizes concrete performance, aligns with global sustainability goals. This study aims to identify the optimal mix of SCMs and bacterial additives to enhance the mechanical properties, workability, microstructural characteristics, and overall sustainability of concrete.

## MATERIALS AND METHODS

### Bacteria Implementation Details

In this study, *Bacillus megaterium*, a rod-type strain found from the Microbial Type Values gathering and Gene Bank (MTCC), was utilized. The selection criteria for this bacterial strain adhered to established microbiological standards.

### Preparation of Liquid Bacterial Cultures

Initially, pure cultures of *Bacillus megaterium* were preserved on nutrient agar slants (BC). Liquid bacterial cultures were prepared following precise protocols. A conical flask, previously sterilized, was occupied with 250 ml of water. Subsequently, peptone and meat or beef extract were added at a concentration of 5 g.L<sup>-1</sup> each. To adjust the pH level to 7, 20 g.L<sup>-1</sup> of urea was incorporated into the medium, as per the specified instructions. Additionally, 10 mg of MnSO<sub>4</sub> x H<sub>2</sub>O was included to support bacterial growth. The medium underwent autoclaving for twenty minutes to ensure complete sterilization and elimination of any potential contaminants.

### Inoculation Process

To introduce the bacteria into the nutritive media under

sterile conditions, a loop was employed. Throughout the inoculation process, bacteria were transferred from their preserved state in a stock to a fresh medium to promote their further development. The closed loop containing the pure philosophy stock was carefully unlocked, and the cut loop was sterilized using a flame for three seconds to prevent bacterial contamination. The sterilized loop was then placed atop the highest portion of the bacterial slant, ensuring that it did not come into contact with the edges of the tube. Subsequently, the bacteria-containing loops were gently immersed into the previously prepared growing media.

### Cultivation and Preservation:

The injected media were allowed to incubate for one day in an orbital shaking brooder at a temperature of 30 degrees Celsius and 250 revolutions per minute to facilitate bacterial growth. After incubation, the solution was chilled to 4 degrees Celsius for preservation, ensuring its viability for subsequent use in the concrete mixes (Fig. 1).

### Binder

The binder in the concrete that was utilized to cast the requisite grade was OPC (53 grade), which had been employed in the production of the concrete. Table 1 presents its characteristics, and it satisfies the requirements of the International Standard 12269 (1987).

### Coarse Aggregate (CA)

The present study utilized readily available local coarse material that was 20 millimeters in size and was conducted in compliance with the International Standard 383:1970. The results of certain preliminary testing are reported in Table 1, which includes its properties.

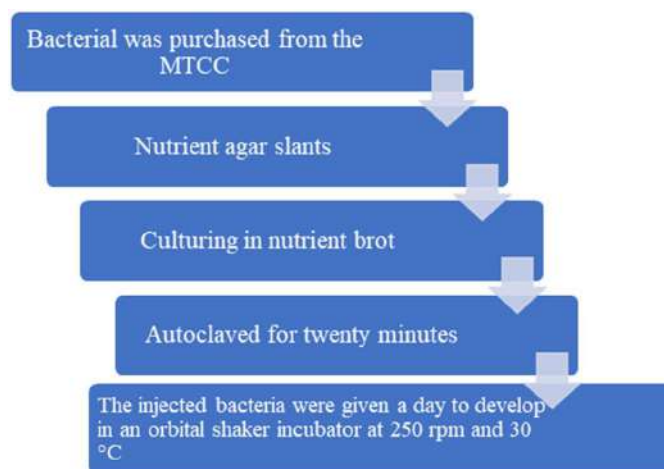


Fig. 1: Bacteria Cultivation.



## Water

Concrete is being prepared and hardened with water from the faucet that is drinkable.

## Manufactured Sand

The local M sand being evaluated for granularity and gradient according to IS: 383-1970 and the properties that are illustrated in Table 1, sand was utilized as a possible alternate material for fine aggregate.

## Super Plasticizer

CONPLAST SP 430 was utilized as a water-reducing compound to achieve the desired level of functionality through the utilization of the most recent generation of improved sulfonated naphthalene polymers. Processing of substances was made possible as a consequence.

## Alccofine

The study utilizes Alccofine 1203, which is an ultrafine tiny calcium silicate material that has a substantial amount of glass and a high degree of responsiveness. The material is obtained by the process of controlled granulation.

## Silica Fume

The silica fume, which features an extremely thin sphere-like particle order, has a significant amount of amorphous silicon dioxide throughout its composition. In addition, magnesium, iron, and alkali metal oxides are discovered in minute quantities. Table 2 contains information regarding the physicochemical makeup of both alccofine and silica fume.

## Constituents Used in M35 Grade Concrete

A mixture of concrete of M35 grade (1:1.79:2.57) was used,

Table 1: Physical (53 grade), CA, and M-Sand cement properties.

Characteristics	Experiment-al Values of Cement	Experiment-al Values of CA	Experimental Values of M-Sand
Initial setting of the time	50 min	-	-
The setting of the final time	320 min	-	-
Specific gravity	3.15	2.8	2.2
Consistency	32%	-	-
Soundness	1.2 mm	-	-
Water Intake	-	3.5%	-
Level of density	-	-	-
surface texture	-	Smooth	-
Impact Value	-	14.2	-
Particle size, kg/m	-	-	576
Micron Density	-	-	0.1
Max. compressive stress (MPa)	32.8 at 28 days	-	-

Table 2: Comparative analysis of the chemical and physical properties of alccofine and silica fume.

Chemical Properties			Physical Properties		
Old Mineral	Composition (%)		Physical Possessions	Outcomes	
	AF	SF		AF	SF
SiO <sub>2</sub>	34.2	92.1	Partial Size Distribution (in micrometer)		
SO <sub>3</sub>	0.08	-	D <sub>10</sub>	1.5	-
Al <sub>2</sub> O <sub>3</sub>	23.1	0.5	D <sub>50</sub>	5	-
Fe <sub>2</sub> O <sub>3</sub>	0.8	1.4	D <sub>90</sub>	9	-
K <sub>2</sub> O	-	0.7	Specific Gravity(g/cm <sup>3</sup> )	2.86	-
LOI	-	2.8	Fineness (cm <sup>2</sup> /gm)	-	-
CaO	34	0.5	Bulk Density (kg/m <sup>3</sup> )	600	450
MgO	6.1	0.3	Particle Size (typical)	-	<1µm
Na <sub>2</sub> O	-	0.3	Specific Surface	12000	2.22



(a) Alccofine



(b) Silica Fume

Fig. 2: Mineral admixtures.

which satisfies the IS 10262:2009 codal specification. The concrete is described in Table 3. A “chemical admixture” that ought to be used in concrete, with increments in cementitious material weights ranging from 0% to 1%, is revealed based on many experimental mixes. After the dry ingredients for the concrete mixes were combined, the proportions of superplasticizer (1% by weight) and water to cement (0.4 by volume) were adjusted according to the intended mix. Table 4 presents the binary and ternary blended systems that are used for mineral admixtures in their various forms.

### Methodology Adopted

The methodology adopted has been presented graphically, as shown in Fig. 3.

### Casting and Curing of Molds

Eighty one samples of binary cementitious concrete

Table 3: Description of concrete.

Mix ID	Description of concrete
AF0SF0	Controlled Mix
AF5SF0	Concrete in which alccofine accounts for 5% of the cement content
AF10SF0	Concrete in which alccofine accounts for 10% of the cement content
AF15SF0	Concrete in which alccofine accounts for 15% of the cement content
AF20SF0	Concrete in which alccofine accounts for 20% of the cement content
AF0SF5	Concrete in which 5 % Cement is replaced by silica fume.
AF0SF10	10 % Cement is replaced by silica fume.
AF0SF15	15 % Cement is replaced by silica fume.
AF0SF20	20 % Cement is replaced by silica fume.
AF5SF15	As a replacement for cement, concrete is made with 5% alccofine and 15% silica fume.
AF10SF10	As a replacement for cement, concrete is made with 10% alccofine and 10% silica fume.
AF15SF5	As a replacement for cement, concrete is made with 15% alccofine and 5% silica fume.

Table 4: Percentage of Alccofine (AF) and silica fume (SF) in BBS and TBS for 1-m<sup>3</sup> concrete.

Mix ID	FA (kg/m <sup>3</sup> )	CA	Water	Cement	AF	SF	Workability (mm)
AF0SF0	696	1253	156.6	436	-	-	85
AF5SF0	696	1253	156.6	412	22		76
AF10SF0	696	1253	156.6	392	44		74
AF15SF0	696	1253	156.6	370	66		72
AF20SF0	696	1253	156.6	350	88		74
AF0SF5	696	1253	156.6	412		22	78
AF0SF10	696	1253	156.6	392		44	76
AF0SF15	696	1253	156.6	370		66	74
AF0SF20	696	1253	156.6	350		88	72
AF5SF15	696	1253	156.6	350	22	66	70
AF10SF10	696	1253	156.6	350	44	44	75
AF15SF5	696	1253	156.6	350	66	22	71

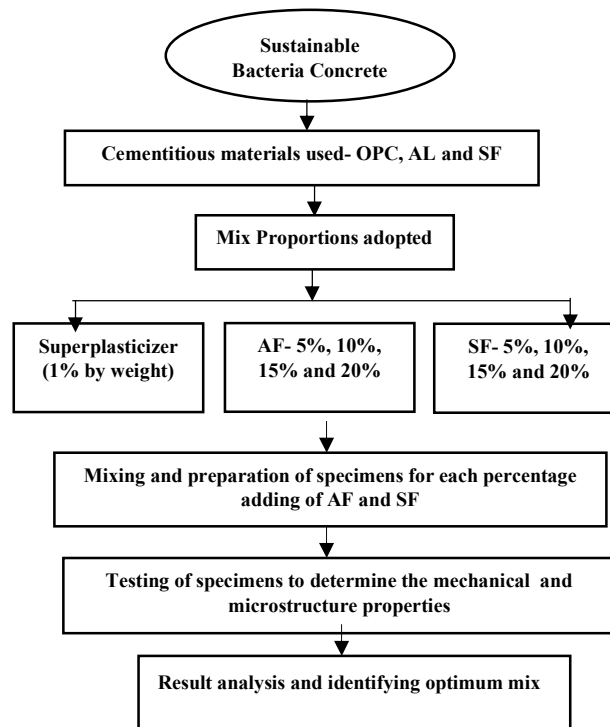


Fig. 3: Methodology.



Fig. 4: Failure mode Samples test.

were created utilizing the specified concrete mixture and conventional cubes. The specimens were evaluated in accordance with IS:516:1959 after being cast as spheres (150 mm), cylinders (100mm x 300 mm), and prisms (100 mm x 100mm x 500 mm). The curing tank is used to dry the concrete samples for seven, fourteen, and twenty-eight days. Though continuing a constant temperature of 27° C., Fig. 4 demonstrates the observed specimens. The entire

project activity took 5 months to complete, which included 1 month for initial planning and material acquisition, 2 months for the casting process, and 2 months for testing and result analysis. The samples for SEM analysis were collected from the failure plane of specimens tested under compression. SEM examination was used to assess the dispersion characteristics and interactions with the cement matrix.

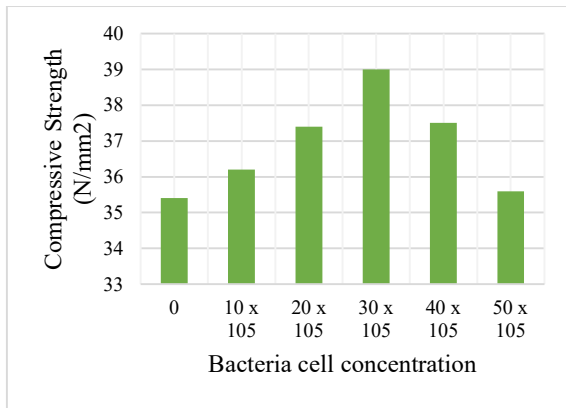


Fig. 5: Compressive strength of concrete cubes for different cell concentrations of *Bacillus megaterium*.

## RESULTS AND DISCUSSION

### Optimum Bacterial Cell Concentration

Bacterial cell concentration is expressed as the number of bacterial cells per ml of mixing water. The optimum dosage of bacterial cell concentration corresponds to the cell concentration which will result in maximum compressive strength of concrete specimens. The compressive strength of concrete cube specimens of size 150 mm × 150 mm × 150 mm was measured at the age of 28 days using five different cell concentrations of *Bacillus megaterium* (from  $10 \times 10^5$  to  $50 \times 10^5$  cells/ml of mixing water). To cast concrete samples for strength and durability testing and to quantify crack healing, the ideal amount of bacterial cells needs to be used.

Fig. 5 shows that for all five strains of bacteria, the optimal cell concentration for maximal compressive strength

Table 5: Compressive strength of BBS and TBS.

Mix ID	Bacteria Concentration [cells.m <sup>-1</sup> ]	Average Compressive Strength [Mpa]			Compressive strength at 28 days compared to the control mix
		7 <sup>th</sup>	14 <sup>th</sup>	28 <sup>th</sup>	
		Days			
AF0SF0	30 x 10 <sup>5</sup>	23.72	29.56	35.4	0.0
AF5SF0	30 x 10 <sup>5</sup>	24.05	29.98	35.9	1.4
AF10SF0	30 x 10 <sup>5</sup>	24.32	30.31	36.3	2.5
AF15SF0	30 x 10 <sup>5</sup>	23.85	29.73	35.6	0.6
AF20SF0	30 x 10 <sup>5</sup>	23.18	28.89	34.6	-2.3
AF0SF5	30 x 10 <sup>5</sup>	25.33	31.56	37.8	6.8
AF0SF10	30 x 10 <sup>5</sup>	25.66	31.98	38.3	8.2
AF0SF15	30 x 10 <sup>5</sup>	26.40	32.90	39.4	11.3
AF0SF20	30 x 10 <sup>5</sup>	24.59	30.64	36.7	3.7
AF5SF15	30 x 10 <sup>5</sup>	25.80	32.15	38.5	8.8
AF10SF10	30 x 10 <sup>5</sup>	27.07	33.73	40.4	14.1
AF15SF5	30 x 10 <sup>5</sup>	25.39	31.65	37.9	7.1

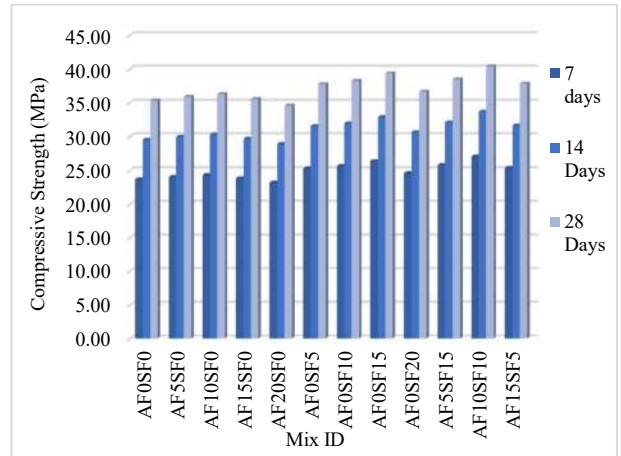


Fig. 6: Compressive strength (BBS & TBS).

is  $30 \times 10^5$  cells/ml of mixing water. The four bacterial strains were added to the mixing water at a concentration of  $30 \times 10^5$  cells/ml to produce the best microbial concrete specimens.

### Workability

“Workability” refers to how easily the concrete can be laid, compacted, and finished. Reduce the amount of time and effort needed to finish the bacterial concrete using alccofine and silica fume by increasing its ability to work. The purpose of the crashing cone test is to find out how workable newly mixed concrete is. A number of concrete mixtures with various combinations are shown in Table 4, along with their slump properties.

### Compressive Strength

The deformation strengths of the tested blocks on the Alccofine and silica fume microbiological concrete are



displayed in Table 5. As shown in Fig. 6, the compressive strength test outcomes for the binary blended cementitious solution (BBS) with the substitution of “alccofine and silica fume” are presented.

Table 5 and Fig. 6 illustrate the results of tests conducted on the compressive properties of bacterial concrete. The experiments were performed in and out of the presence of Alccofine, silica fume, and M sand, which were used as substitutes for the (BBS & TBS). The compressive values of the Bacterial concrete specimens in the Binary Integrated System, namely AF5SF0, AF10SF0, AF15SF0, and AF20SF0, were correspondingly 1.4%, 2.5%, 0.6%, and 2.3% higher/lower associated to that of the orientation mix AF0SF0, after 28 days of sampling. Similarly, the samples with silica fume replacement percentages of 5%, 10%, 15%, and 20% (referred to as AF0SF5, AF0SF10, AF0SF15, and AF0SF20, respectively) exhibited compressive strengths that were consistently better than the value of the control mix (AF0SF0) by +6.8%, +8.2%, +11.3%, and +3.7%, correspondingly. The compressive strengths of Bacterial Concrete in (TBS) specimens with alccofine and silica fume (AF5SF15, AF10SF10, and AF15SF5) at 28 days were respectively 8.8%, 14.4%, and 7.1% higher/lower compared to those of the untreated control mix (AF0SF0). The maximum compressive strength ratings (AF10SF0 & AF0SF15) can be found in bacterial concrete made with 10% alccofine replacement and 15% silica fume. Alccofine's unique chemical makeup and ultrafine particles accelerated the soaking process between cement and alccofine, resulting in a stronger pozzolanic reaction. However, because the bacteria fill the holes in the concrete, the likelihood of cracking is drastically reduced. This means bacteria can be used in self-healing applications. The concrete strength was found to be reduced after 15%

silica fume and 10% alccofine were added, but it was still greater than regular concrete mixtures. At a 15% alccofine replacement level, concrete's compressive strength decreased due to insufficient cement hydration caused by a higher alccofine and silica fume concentration.

### Strength Activity Index

The strength action index was determined by comparing the compressive strength of concrete with mixed cementitious systems of two and three components to that of control concrete at ages 7, 14, and 28 days. This analysis was done for various degrees of AF and SF substitutes, and the results strength activity index was computed using the result.

Table 7: Tensile strength – BBS and TBS.

Mix ID	Bacteria Concentration (cells/ml)	Average Compressive Strength (Mpa)			Tensile strength at 28 days compared to control mix
		7 <sup>th</sup> Days	14 <sup>th</sup> Days	28 <sup>th</sup> Days	
AF0SF0	30 x 10 <sup>5</sup>	2.80	3.49	4.18	0.0
AF5SF0	30 x 10 <sup>5</sup>	2.84	3.54	4.30	2.9
AF10SF0	30 x 10 <sup>5</sup>	2.87	3.58	4.51	7.9
AF15SF0	30 x 10 <sup>5</sup>	2.81	3.51	4.05	-3.1
AF20SF0	30 x 10 <sup>5</sup>	2.74	3.41	3.98	-4.8
AF0SF5	30 x 10 <sup>5</sup>	2.99	3.72	4.50	7.7
AF0SF10	30 x 10 <sup>5</sup>	3.03	3.77	4.61	10.3
AF0SF15	30 x 10 <sup>5</sup>	3.11	3.88	4.81	15.1
AF0SF20	30 x 10 <sup>5</sup>	2.90	3.62	4.29	2.6
AF5SF15	30 x 10 <sup>5</sup>	3.04	3.79	4.62	10.5
AF10SF10	30 x 10 <sup>5</sup>	3.19	3.98	4.86	16.3
AF15SF5	30 x 10 <sup>5</sup>	3.00	3.73	4.49	7.4

Table 6: Strength activity index.

Blended System	Mix ID	Strength Activity Index		
		7 Days	14 Days	28 Days
Binary	AF5SF0	1.01	1.01	1.01
	AF10SF0	1.07	1.07	1.07
	AF15SF0	1.10	1.10	1.10
	AF20SF0	1.03	1.03	1.03
	AF0SF5	0.98	0.98	0.98
	AF0SF10	1.07	1.07	1.07
	AF0SF15	1.01	1.01	1.01
	AF0SF20	1.00	1.00	1.00
Ternary	AF5SF15	1.04	1.04	1.04
	AF10SF10	1.15	1.15	1.15
	AF15SF5	1.09	1.09	1.09

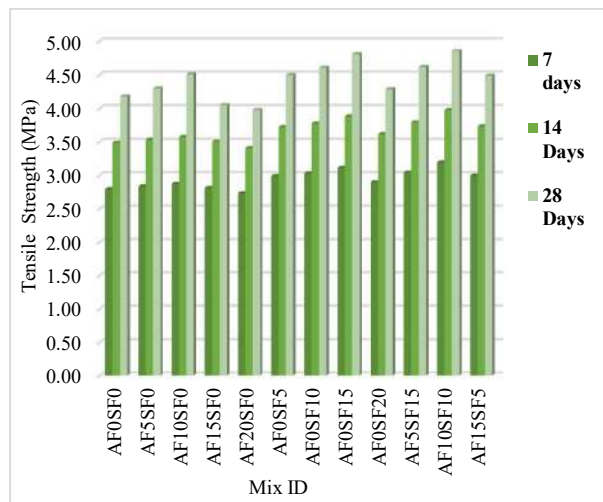


Fig. 7: Tensile strength between (BBS & TBS).

From Table 6, In a BBS, it was found that the activity index gradually decreased after Portland cement was replaced with AF and SF by 10% and 15% (AF10SF0 & AF0SF15), respectively. Similar to this, at TBS, the addition of Portland cement with AF and SF was gradually reduced to 10% (AF10SF10).

### Split Tensile Strength

Table 7 and Fig. 7 illustrate the results of experiments conducted on the tensile strength of bacterial concrete, comparing samples regardless of the substitution of Alccofine, silica fume, and M-sand in the Binary Blended System (BBS). The samples of Bacterial concrete in the Binary Blended System, containing different proportions of Alccofine (AF5SF0, AF10SF0, AF15SF0, and AF20SF0), exhibited tensile strengths at 28 days that were accordingly 2.9% higher, 7.9% higher, 3.1% lower, and 4.8% lower compared to those of the untreated control mix (AF0SF0). Similarly, samples that had silica fume replacement levels of 5%, 10%, 15%, and 20% (referred to as AF0SF5, AF0SF10, AF0SF15, and AF0SF20, accordingly) exhibited tensile strengths that were consistently greater compared to that of the untreated control mix (AF0SF0) by 7.7%, 10.3%, 15.1%, and 2.6%, respectively. The Bacterial Concrete in Ternary Blended System (TBS) specimens, specifically AF5SF15, AF10SF10, and AF15SF5, showed tensile strengths at 28 days, which were correspondingly 10.5%, 16.3% and 7.4% higher or lower than the control mix (AF0SF0).

Based on the aforementioned experiment, it was initiated that “the tensile strength on the bacterial concrete of the split alccofine with silica fume” material decreased with increasing replacement owed to the calcium carbonate hastened by bacteria fills the tiny pores in concrete when Bacterial megaterium. Studies have shown that an extremely high percentage of alccofine and the splitting tensile strength was slightly increased by silica fume but not significantly, insignificantly beyond 10%. When the vacancies are initially filled with silica fume, the tensile strengths are significantly increased; however, the advantages become less significant as the level of silica fume increases. Because alccofine and silica fume increased pozzolanic reaction, lower heat of hydration, decreased permeability to concrete, and reduced segregation are all benefits of using this material, these factors probably contributed to a rise in the beginning stages of the strength of concrete.

### Flexural Strength

The outcomes of testing on the flexibility of alccofine and silica fume with M-sand replaced for (BBS & TBS) are presented in Table 8 and Fig. 8. The tensile strengths

Table 8: Flexure strength of BBS and TBS.

Mix ID	Bacteria Concentration [cells.mL <sup>-1</sup> ]	Average flexure Strength (Mpa)			Variation in flexure strength at 28 days compared to the control mix
		7 <sup>th</sup>	14 <sup>th</sup>	28 <sup>th</sup>	
		Days			
AF0SF0	30 x 10 <sup>5</sup>	3.32	4.14	4.65	0.0
AF5SF0	30 x 10 <sup>5</sup>	3.37	4.20	4.82	3.7
AF10SF0	30 x 10 <sup>5</sup>	3.40	4.24	5.10	9.7
AF15SF0	30 x 10 <sup>5</sup>	3.34	4.16	4.39	-5.6
AF20SF0	30 x 10 <sup>5</sup>	3.25	4.04	4.32	-7.1
AF0SF5	30 x 10 <sup>5</sup>	3.55	4.42	5.10	9.7
AF0SF10	30 x 10 <sup>5</sup>	3.59	4.48	5.19	11.6
AF0SF15	30 x 10 <sup>5</sup>	3.70	4.61	5.36	15.3
AF0SF20	30 x 10 <sup>5</sup>	3.44	4.29	4.90	5.4
AF5SF15	30 x 10 <sup>5</sup>	3.61	4.50	5.08	9.2
AF10SF10	30 x 10 <sup>5</sup>	3.79	4.72	5.45	17.2
AF15SF5	30 x 10 <sup>5</sup>	3.56	4.43	4.91	5.6

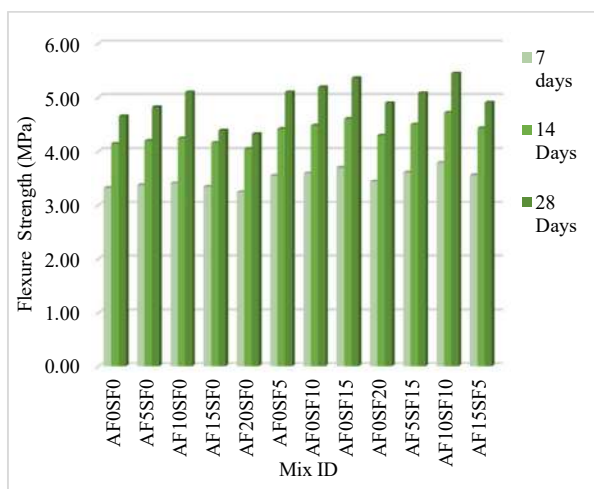


Fig. 8: Flexural strength comparison with BBS and TBS.

of Concrete in BBS specimens with Alccofine (AF5SF0, AF10SF0, AF15SF0, and AF20SF0) at 28 days were, respectively, 3.7% higher, 9.7% higher, 5.6% lower, and 7.1% lower than relate of the control mix (AF0SF0). Likewise, samples that had silica fume replacements of 5%, 10%, 15%, and 20% (referred to as AF0SF5, AF0SF10, AF0SF15, and AF0SF20, respectively) exhibited flexural strengths that were greater than the control mix (AF0SF0) by 9.7%, 11.6%, 15.3%, and 5.4%, respectively. Similarly, the flexural strengths of Concrete in (TBS) specimens with Alccofine (AF5SF15, AF10SF10, and AF15SF5 correspondingly) were, respectively, 9.2% higher, 17.2%

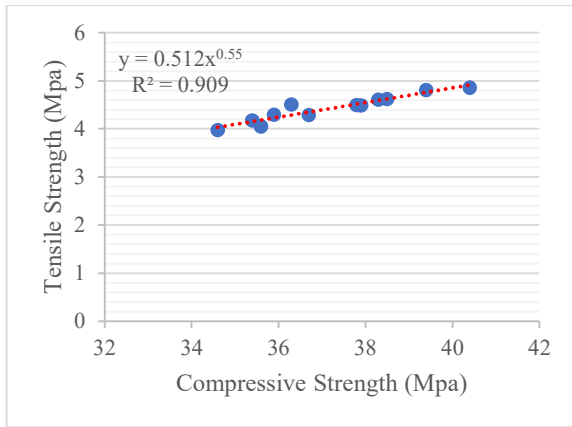


Fig. 9: Compressive Strength vs Tensile Strength.

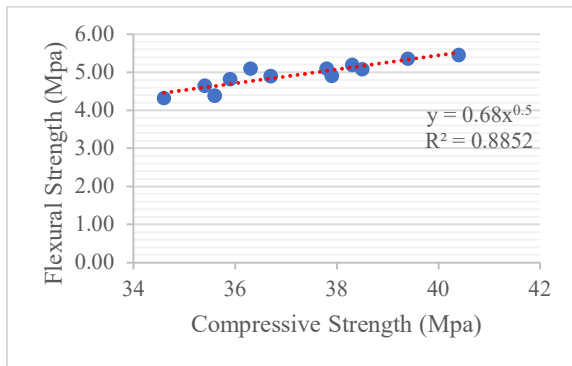


Fig. 10: Compressive Strength vs Flexural Strength.

higher, and 5.6% lower than those of the control mix (AF0SF0) after 28 days of testing.

The influence of alccofine and silica fume on the flexural strength of the material was more pronounced than the effects of these two substances on the tensile strength of the material. After precipitation, the flexural strength was greatly improved by the addition of silica fume and alccofine in concentrations of 10%. This was accomplished by supplying the organisms with the nutrients that are necessary for their continued existence.

It should have also been noticed that the flexural strength gradually decreased with increasing percentages of alccofine and silica fume substitution. This is something that should have been discovered. The incorporation of calcium oxide and silica into alccofine allowed for improvements to be made to the concrete's inherent mechanical properties.

### Flexural, Tensile, and Compressive Strength Relationships

Alccofine and silica fume replacement BBS and TBS

blended cementitious systems' flexural strengths, tensile, and compressive were resolute analytically, as demonstrated in Figs. 9 and 10.

The link between the compressive and tensile strength of the "BBS and TBS blended cementitious system" with AF and SM was derived from Fig 9.

$$f_t = 0.512 f_{ck}^{0.55} \text{ (28 days)} \quad \dots(1)$$

Where,  $f_t$  signifies split tensile strength in  $\text{N/mm}^2$  and  $f_{ck}$  represents compressive strength in  $\text{N/mm}^2$

This equation is similar to the one developed by the ACI Committee 363 in 1993, which states that  $f_t = 0.59 f_{ck}^{0.55}$  for concrete whose compressive strength is within the range of 21 to 83  $\text{N/mm}^2$ . For concrete with a compressive strength of less than 84  $\text{N/mm}^2$ , the researcher discovered that the relationship between the two variables is  $f_t = 0.462 f_{ck}^{0.55}$ . According to the equations presented above, it is possible to deduce that the results of this education are consistent with the findings of other studies.

It was found that there is a correlation between compressive and flexural strengths of binary and ternary blended cementitious systems with AF and SM, which was derived from Fig. 10 and the equation for this relationship is as follows:

$$f_{cr} = 0.68 f_{ck}^{0.5} \text{ (28 days)} \quad \dots(2)$$

The following group of scholars has made some suggestions on equations that relate the flexural strength of concrete to its compressive strength:

$$\text{Burg and Ost (1992), } f_r = 1.03 f_{ck}^{0.5}$$

$$\text{IS: 456 -2000, } f_r = 0.7 f_{ck}^{0.5}$$

The equations resulting from the AF and SF mixes in this examination are inside the range established by previous investigators.

### Equivalent CO<sub>2</sub> Gas Emission and Energy Factor

Associated with cement production, the manufacture of alternative fuels (AF) and supplementary fuels (SF) emits less CO<sub>2</sub> into the atmosphere. The CO<sub>2</sub> emissions from AF and SF manufacturing (100 kg of CO<sub>2</sub> per ton of AF produced and 16 kg of CO<sub>2</sub> per ton of SF produced) are primarily caused by raw material extraction and kiln operation rather than chemical reactions. In contrast, cement manufacturing releases CO<sub>2</sub> through the decarboxylation of calcium carbonate, resulting in higher emissions (521.5 kg of CO<sub>2</sub> per ton of cement produced). Additionally, AF and SF require less thermal energy during production compared to cement (1.90 GJ per ton of AF, 0.36 GJ per ton of SF, and 4.65 GJ per ton of cement).

Table 9: Sustainability balance of binary cementitious energy saved per 1m<sup>3</sup> of concrete.

Mix ID	Energy (GJ)			
	OPC	AF	SF	Total
AF0SF0	2.35	0.00	-	2.35
AF5SF0	2.23	0.52	-	2.74
AF10SF0	2.12	0.96	-	3.07
AF15SF0	1.98	1.36	-	3.35
AF20SF0	1.88	1.85	-	3.72
AF0SF5	2.21	-	0.072	2.292
AF0SF10	2.12	-	0.126	2.236
AF0SF15	1.98	-	0.196	2.19
AF0SF20	1.88	-	0.236	2.106
AF5SF15	1.88	0.52	0.196	2.586
AF10SF10	1.88	0.96	0.123	2.953
AF15SF5	1.88	1.36	0.072	3.302

Table 10: Sustainability balance of binary and ternary cementitious - CO<sub>2</sub> emissions.

Mix ID	CO <sub>2</sub> Emission (kg)						Total
	Extraction & Kiln			Chemical reaction			
	OPC	AF	SF	OPC	AF	SF	
AF0SF0	243	0	0	261	0	0	504
AF5SF0	234	2.5	-	248	0	0	484.5
AF10SF0	222	5	-	235	0	0	462
AF15SF0	228	7.5	-	228	0	0	464
AF20SF0	196	10	-	221	0	0	427
AF0SF5	243	-	0.35	248	0	0	492
AF0SF10	234	-	0.7	235	0	0	470
AF0SF15	222	-	1.05	228	0	0	451
AF0SF20	196	-	1.4	221	0	0	419
AF5SF15	196	2.5	1.05	221	0	0	420.55
AF10SF10	196	5	0.7	221	0	0	423
AF15SF5	196	7.5	0.35	221	0	0	425

Table 11: Sustainability balance of ternary cementitious energy saved per 1m<sup>3</sup> of concrete.

Mix ID	Energy (GJ)				Environmental benefit regarding	
	OPC	AF	SF	Total	Energy (%)	CO <sub>2</sub> emission (%)
AF0SF0	2.35	0.00	-	2.35		
AF5SF0	2.23	0.52	-	2.74	-2.1	-5.1
AF10SF0	2.12	0.96	-	3.07	-3.1	-10.1
AF15SF0	1.98	1.36	-	3.35	-4.8	-13.2
AF20SF0	1.88	1.85	-	3.72	-8.2	-16.5
AF0SF5	2.21	-	0.072	2.292	-1.8	-5.1
AF0SF10	2.12	-	0.126	2.236	-2.4	-10.2
AF0SF15	1.98	-	0.196	2.19	-3.1	-14.5
AF0SF20	1.88	-	0.236	2.106	-4.7	-18.5
AF5SF15	1.88	0.52	0.196	2.586	-5.7	-17
AF10SF10	1.88	0.96	0.123	2.953	-6.35	-17
AF15SF5	1.88	1.36	0.072	3.302	-7.8	-17

The CO<sub>2</sub> emission, including the emissions associated with the movement of raw materials, is determined (Cassagnabere et al. 2010) by the calculation of chemical processes and the use of energy for 1 tonne of cement and AF with SF. Table 9 presents an assessment of the environmental impact of the binders (cement + AF + SF) in terms of CO<sub>2</sub> emissions and energy consumption. The calculation of CO<sub>2</sub> emissions and energy savings was performed using Equations (1) and (2):

$$\text{Energy saved (\%)} = (E_i - E_o) / E_o \times 100 \quad \dots(1)$$

Where,

E<sub>o</sub> equals the amount of energy that is consumed by the control mix.

The term “E<sub>i</sub>” refers to the amount of energy that is consumed by binary and ternary ceramic systems.

$$\text{CO}_2 \text{ Emission (\%)} = (C_i - C_o) / C_o \times 100 \quad \dots(2)$$

Where,

C<sub>o</sub> = The amount of carbon dioxide that is released by the control mixture

CO<sub>2</sub> emissions from BSS cementitious systems are denoted by the symbol C<sub>i</sub>.

### Economic Feasibility of Metakaolin

Alccofine typically falls between the cost of silica fume and cement in concrete production expenses, offering similar performance enhancements alongside silica fume. While Alccofine and silica fume share similar production processes, slight variations may exist in energy consumption and processing costs. Both Alccofine and silica fume contribute to sustainability by utilizing waste materials, contrasting with the high environmental impact of cement production. Ultimately, the choice among Alccofine, silica fume, and cement hinges on project requirements, cost considerations,



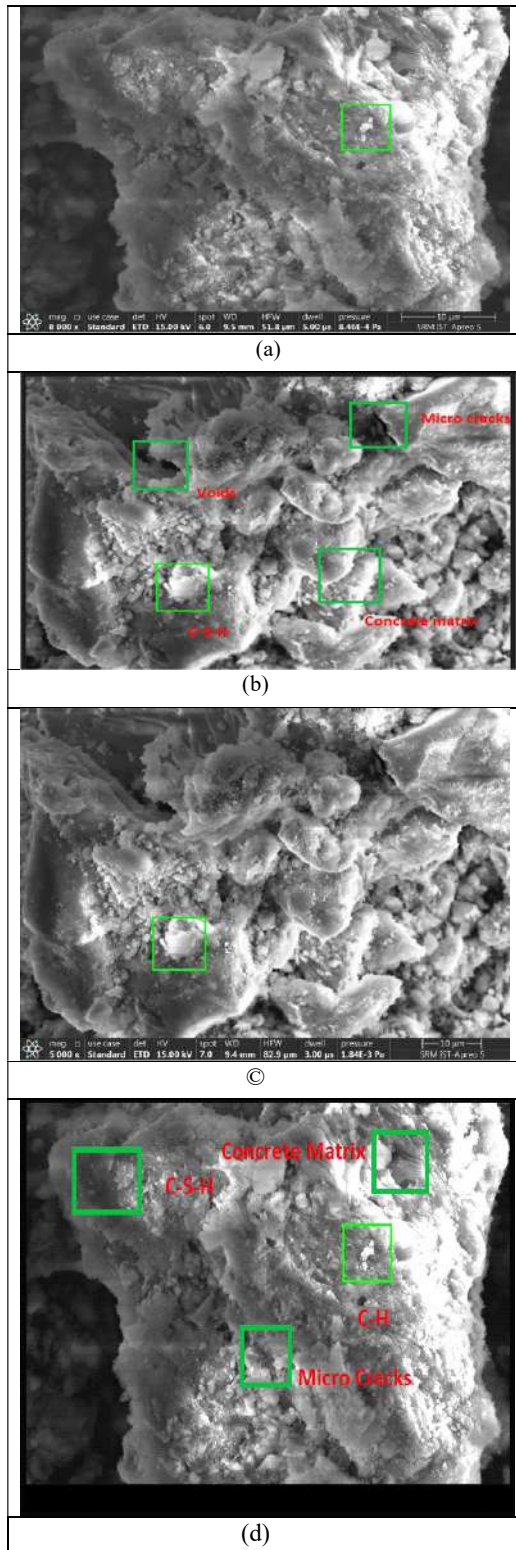


Fig. 11: SEM Images of (a) Control, (b) AF10SF0, (c) AF0SF15, and (d) AF10SF10.

and performance expectations, with the economic analysis serving as a pivotal factor in decision-making.

### SEM Analysis

From the over-dried samples, a suitable one has been selected for each mix for the SEM analysis. The SEM images of all the mix binders are shown in Fig. 11. SEM images showed micro-cracks, concrete matrix, voids, and C-S-H in all mix binders. The inclusion of AF and SF improves the hydration products, which increases the mechanical strength. In the specimens with AF and SF, the micro-cracking region was able to be extended due to a strong enough contact with the concrete matrix. The presence of AF and SF reduced the number of pores as they filled the microcavities. They also play a dual role by acting as a filler, increasing the density, and engaging in enhancing the strength properties by initiating an early hydration process and formation of extra C-S-H gel. SEM observations revealed that the formation of additional C-S-H gel increased along with an increase in the percentage of AF and SF replacement levels, and the number of voids and micro-cracks appeared to be less than up to 10% replacement of cement with AF and SF.

### CONCLUSIONS

Following are the results that have been reached after all of the experimental work has been completed.

- According to the results of the BCC tests, the maximum compressive strengths of the AF10SF0, AF0SF15, and AF10SF10 mixes were correspondingly  $36.30 \text{ N.mm}^{-2}$ ,  $39.40 \text{ N.mm}^{-2}$ , and  $40.40 \text{ N.mm}^{-2}$ . The highest compressive strengths were 2.5%, 11.3%, and 14.4% higher than the value of the control concrete.
- The results of the break tensile tests conducted on BCC showed that the AF10SF0, AF0SF15, and AF10SF10 mixes had the highest split tensile strengths of  $4.51 \text{ N.mm}^{-2}$ ,  $4.81 \text{ N.mm}^{-2}$ , and  $4.86 \text{ N.mm}^{-2}$ , correspondingly. These values were 8%, 15.1%, and 16.3% higher than the control concrete.
- The highest flexural strength of BCC at 28 days for the AF10SF0, AF0SF15, and AF10SF10 combinations, utilizing 10%, 15%, and 17% more than the control concrete, had flexural values of 5.10 MPa, 5.36 MPa, and 5.45 MPa, correspondingly.
- Using the method of regression, two correlation equations were created: one involved split tensile and compressive strength, and the second involved flexural and compressive strength. Both models were built to compare and contrast performance. It was determined

that the error ranges that were forecasted were enough when the models were tested.








- SEM observations revealed that the formation of additional C-S-H gel increased along with an increase in the percentage of AF and SF replacement levels, and the number of voids and micro-cracks appeared to be less than up to 10% replacement of cement with AF and SF.
- “Silica fume” refers to a highly reactive pozzolanic chemical. In particular, the hydration process and pozzolanic reaction of “alccofine” are enhanced by its unevenness and better satisfaction of amorphous silica content and ultrafine particles with a unique chemical makeup. However, because the bacteria fill the holes in the concrete, the likelihood of cracking is drastically reduced. Therefore, microorganisms can function as a natural antibiotic.
- Given the promising findings, alccofine and silica fume can be used on a massive scale to offset the negative effects of conventional cement manufacturing and usage on the environment and the economy. Finally, the elimination of greenhouse gas emissions and a significant decrease in concrete costs came from the binary and ternary blended system.

## REFERENCES

- Achal, V. and Mukherjee, A., 2015. A review on microbial precipitation for sustainable construction. *Journal of Industrial Microbiology and Biotechnology*, 42(2), pp.159–169. DOI.
- Achal, V., Mukherjee, A., Basu, P.C. and Reddy, M.S., 2009. Lactose mother liquor as an alternative nutrient source for microbial concrete production by *Sporosarcina pasteurii*. *Journal of Industrial Microbiology and Biotechnology*, 36(3), pp.433–438. DOI.
- Achal, V., Pan, X., Fu, Q. and Zhang, D., 2011. Bioremediation of Pb-contaminated soil based on microbially induced calcite precipitation. *Journal of Microbiology and Biotechnology*, 21(7), pp.739–745. DOI.
- Ansari, U.S., Chaudhri, I.M., Ghuge, N.P. and Phatangre, R.R., 2015. High-performance concrete with partial replacement of cement by Alccofine & fly ash. *Indian Journal of Scientific Research*, 5(2), pp.19–23.
- Aytekin, B., Mardani, A. and Yazıcı, Ş., 2023. State-of-art review of bacteria-based self-healing concrete: Biomineralization process, crack healing, and mechanical properties. *Construction and Building Materials*, 378, p.131198. DOI.
- Bureau of Indian Standards, 1959. Method of tests for strength of concrete. IS: 516:1959. Bureau of Indian Standards.
- Bureau of Indian Standards, 2000. Plain and reinforced concrete. IS: 456:2000. Bureau of Indian Standards.
- Bureau of Indian Standards, 1987 (reaffirmed 2013). Specification for 53 Grade Ordinary Portland Cement. IS: 12269:2013. Bureau of Indian Standards.
- Bureau of Indian Standards, 1970. Specification for coarse and fine aggregates from natural sources for concrete. IS: 383-1970. Bureau of Indian Standards.
- Burg, R.G. and Ost, B.W., 1992. *Engineering properties of commercially available high-strength concretes* (No. RD104T).
- Cassagnabere, F., Mouret, M., Escadeillas, G., Broilliard, P. and Bertrand, A., 2010. Metakaolin: A solution for the precast industry to limit the clinker content in concrete—Mechanical aspects. *Construction and Building Materials*, 24(7), pp.1109–1118. DOI.
- Chahal, N., Siddique, R. and Rajor, A., 2012. Influence of bacteria on the compressive strength, water absorption, and rapid chloride permeability of fly ash concrete. *Construction and Building Materials*, 28(1), pp.351–356. DOI.
- Chan, Y.N., Luo, X. and Sun, W., 2000. Compressive strength and pore structure of high-performance concrete after exposure to high temperatures up to 800°C. *Cement and Concrete Research*, 30(2), pp.247–251. DOI.
- De Muynck, W., Debrouwer, D., De Belie, N. and Verstraete, W., 2008. Bacterial carbonate precipitation improves the durability of cementitious materials. *Cement and Concrete Research*, 38(7), pp.1005–1014. DOI.
- DeJong, J.T. and Mortensen, B.M., 2009. Biogeochemical processes and geotechnical applications: Progress, opportunities, and challenges. *Geotechnique*, 59(4), pp.275–287. DOI.
- Bureau of Indian Standards, 2009. *Guidelines for concrete mix design proportioning*. IS: 10262:2009. New Delhi: Bureau of Indian Standards.
- Jindal, B.B., Singhal, D., Sharma, S.K., Ashish, D.K., Parveen, et al., 2017. Improving compressive strength of low calcium fly ash geopolymer concrete with Alccofine. *Advances in Concrete Construction*, 5(1), pp.17–29. DOI.
- Kumar, A., Parihar, O., Chaudhary, R. and Singh, S.P., 2016. Use of Alccofine 1206 to achieve high-performance, durable concrete. *SSRG International Journal of Civil Engineering*, 3(5), pp.181–185.
- Parveen, D., Junaid, M.T., Jindal, B.B., Mehta, A., et al., 2018. Mechanical and microstructural properties of fly ash-based geopolymer concrete incorporating Alccofine at ambient curing. *Construction and Building Materials*, 180, pp.298–307. DOI.
- Rajesh Kumar, S., Samanta, A.K. and Singha Roy, D.K., 2015. An experimental study on the mechanical properties of Alccofine-based high-grade concrete. *International Journal of Multidisciplinary Research and Development*, 2(10), pp.218–224.
- Reddy, A.N. and Meena, T., 2017. A study on compressive behavior of ternary blended concrete incorporating Alccofine. In: *International Conference on Materials, Manufacturing, and Modelling. Materials Today: Proceedings*, pp.11356–11363. Elsevier. DOI.
- Schlangen, E. and Senot, S., 2013. Addressing infrastructure durability and sustainability by self-healing mechanisms—Recent advances in self-healing concrete and asphalt. *Procedia Engineering*, 54, pp.39–57. DOI.
- Seshagiri Rao, M.V., Srinivasa Reddy, V., Hafsa, M., Veena, P. and Anusha, P., 2012. Bioengineered concrete—a sustainable self-healing construction material. *Research Journal of Engineering Science*, 2(6), pp.45–51.
- Shanmuga Priya, T., Ramesh, N., Agarwal, A., Bhusnur, S. and Chaudhary, K., 2019. Strength and durability characteristics of concrete made by micronized biomass silica and bacteria-*Bacillus sphaericus*. *Construction and Building Materials*, 226, pp.827–838. DOI.
- Sharma, D., Sharma, S. and Goyal, A., 2016. Utilization of waste foundry slag and Alccofine for developing high-strength concrete. *International Journal of Electrochemical Science*, 7, pp.1–10.
- Sohail, M.G., Al Disi, Z., Zouari, N., Al Nuaimi, N., Kahraman, R., Gencturk, B., Rodrigues, D.F. and Yildirim, Y., 2022. Bio self-healing concrete using MICP by an indigenous *Bacillus cereus* strain isolated from Qatari soil. *Construction and Building Materials*, 328, p.126943. DOI.
- Song, H.W. and Saraswathy, V., 2015. Microbially induced calcite precipitation in construction engineering—A review. *Journal of Cleaner Production*, 93, pp.124–138. DOI.
- Soni, D., Kulkarni, S. and Parekh, V., 2013. Experimental study on high-performance concrete, with mixing of Alccofine and fly ash. *Indian Journal of Research*, 3(4), pp.84–86.
- Suchithra, S. and Malathy, R., 2016. Effective utilization of industrial wastes in self-compacting concrete for environmental protection. *Nature Environment and Pollution Technology*, 15(1), pp.285–290.

- Tobler, D.J., Cuthbert, M.O., Greswell, R.B., Riley, M.S., Renshaw, J.C. and Handley-Sidhu, S., 2011. Comparison of rates of ureolysis between *Sporosarcina pasteurii* and an indigenous groundwater community under conditions required to precipitate large volumes of calcite. *Geochimica et Cosmochimica Acta*, 75(11), pp.3290–3301. DOI.
- Umamaheswaran, V., Sudha, C., Ravichandran, P.T. and Kannan Rajkumar, P.R., 2015. Use of M sand in high-strength and high-performance concrete. *Indian Journal of Science and Technology*, 8(28), pp.1–8.
- Ushaa, T.G., Anuradha, R. and Venkatasubramani, G.S., 2015. Reduction of greenhouse gas emissions in self-compacting geopolymer concrete using sustainable construction materials. *Nature Environment and Pollution Technology*, 14(2), pp.451–454.
- Wu, M., Johannesson, B. and Geiker, M., 2012. A review: Self-healing in cementitious materials and engineered cementitious composite as a self-healing material. *Construction and Building Materials*, 28(1), pp.571–583. DOI.
- Yong, C.C., Ong, C.S. and Tan, S.B., 2019. A review on bacteria species used in concrete for a self-healing system. *Construction and Building Materials*, 204, pp.673–683. DOI.
- Zamani, M.H., Nikafshar, S., Mousa, A. and Behnia, A., 2020. Bacteria encapsulation using synthesized polyurea for self-healing of cement paste. *Construction and Building Materials*, 249, p.118822. DOI.

# Diversity and Temporal Frequency of Records of the Herpetofauna of the Equatorial Seasonally Dry Tropical Forest in the Rural Community of Lucarqui, Piura, Northwestern Peru

Juan Carlos Soto Quispe<sup>1</sup>, Armando Fortunato Ugaz Cherre<sup>1,4</sup>, Angel Enrique Llompart Navarro<sup>2</sup>, Irwing Smith Saldaña Ugaz<sup>3</sup>, José Manuel Marchena Dioses<sup>1,4,†</sup>, Mariana Alexandra Montero Silva<sup>1,4</sup> and Robert Barrionuevo García<sup>1,4</sup>

<sup>1</sup>Universidad Nacional de Piura. Urb. Miraflores s/n, Castilla, Piura, Perú

<sup>2</sup>Centro de Investigación en Biología Tropical y Conservación (CYNBIOTIC)), Cal. Néstor Martos Mza. E lote 16 A.H. Almirante Miguel Grau, II etapa Piura, Piura, Perú

<sup>3</sup>Instituto Peruano de Biología Integrativa (IPBI), Lambayeque, Perú

<sup>4</sup>Laboratorio de investigación en Zoología, Facultad de Ciencias, Universidad Nacional de Piura, Urb. Miraflores s/n, Castilla, Piura, Perú

†Corresponding author: José Manuel Marchena Dioses; [jmarchenad@unp.gob.pe](mailto:jmarchenad@unp.gob.pe)

**Abbreviation:** Nat. Env. & Poll. Technol.  
**Website:** [www.neptjournal.com](http://www.neptjournal.com)

*Received:* 14-06-2024

*Revised:* 09-08-2024

*Accepted:* 22-08-2024

## Key Words:

Herpetofauna  
 Equatorial ESDT  
 Habitat fragmentation  
 Temporal frequency of records (TFR)  
 Conservation

## Citation for the Paper:

Soto Quispe, J. C., Ugaz Cherre, A. F., Llompart Navarro, A. E., Saldaña Ugaz, I. S., Marchena Dioses, J. M., Montero Silva, M. A. and Barrionuevo García, R., 2025. Diversity and temporal frequency of records of the Herpetofauna of the equatorial seasonally dry tropical forest in the rural community of Lucarqui, Piura, northwestern Peru. *Nature Environment and Pollution Technology*, 24(2), p. D1693. <https://doi.org/10.46488/NEPT.2025.v24i02.D1693>

*Note:* From year 2025, the journal uses Article ID instead of page numbers in citation of the published articles.



**Copyright:** © 2025 by the authors

**Licensee:** Technoscience Publications

This article is an open access article distributed under the terms and conditions of the Creative Commons Attribution (CC BY) license (<https://creativecommons.org/licenses/by/4.0/>).

## ABSTRACT

Reptile and amphibian species in the Equatorial BTES face threats such as fragmentation, habitat loss, and climate change. Between 2019 and 2021, the richness and abundance of herpetofauna species was evaluated in the Lucarqui peasant community in Piura, northwest Peru. The objective of this research is to provide a preliminary list of species and understand their temporal frequency patterns. The study area was divided into specific zones: with anthropogenic activity, “crops” and “population centers”, where incidental catches and visual surveys were carried out, and without anthropogenic activity, “forests” and “ravines”, where transects of variable length and fixed width (2 m), the biological data obtained were analyzed with the INEXT statistical tool, and a standardized methodology was provided for the calculation of the temporal frequency of recordings (FRT). The study identified 26 species: 7 amphibians and 19 reptiles. Amphibians dominated in abundance, while reptiles were rare. 85.71% (6) of amphibians and 47.36% (9) of registered reptiles are restricted to the Equatorial BTES. FRT patterns varied by habitat and time. These, along with wealth and abundance, were altered and reduced in areas influenced by human activity, crops, and population centers. It was found that there were still more species to be reported, especially reptiles. The study highlights the richness and vulnerability of the herpetofauna in the Equatorial BTES, reaffirming the urgent need for conservation strategies and continued research to ensure the protection and deep understanding of this valuable, fragile ecosystem.

## INTRODUCTION

The fragile ecosystem of the Equatorial Seasonally Dry Tropical Forests (hereinafter referred to as ESDT Forests) has been recognized as a biogeographic area of exceptional interest due to its high level of biodiversity and endemism (Linares-Palomino et al. 2011, Rivas et al. 2021). For the herpetofauna, this biome can pose a double challenge. On the one hand, reptiles are influenced by high levels of solar radiation, which promotes their diversification in arid environments (Laurencio & Fitzgerald 2010, McCain 2010), on the other hand, amphibians must adapt to conditions of constant desiccation and marked seasonality (Armijos-Ojeda et al. 2021, Laurencio & Fitzgerald, 2010). Additionally, both groups must survive and thrive in a fragmented environment, exposed to marked changes in land use, and vulnerable to climate change (Cordier et al. 2021, Linares-Palomino et al. 2010).



Despite its relevance, a preliminary or complete list of reptile diversity in the Equatorial Seasonally Dry Tropical Forests (ESDT Forests) has not been published. However, the literature suggests that remnants of native vegetation along the equatorial Pacific coast and northern Peru are essential for the conservation of unique and regionally threatened species, such as *Boa constrictor ortonii* (EN), *Bothrops barnetti* (VU), *Polychrus femoralis* (VU), and *Callopistes flavipunctatus* (NT). Greater efforts are needed to unify reptile information from this region.

On the one hand, the amphibians of the Equatorial ESDT have received particular attention, and their conservation status and diversity are better understood (Armijos-Ojeda et al. 2021, Catenazzi & von May 2014). To date, 30 amphibian species have been reported (Armijos-Ojeda et al. 2021), of which the following are considered threatened in Peru: *Ceratophrys stolzmanni* (VU), *Hyloxalus elachyistus* (EN), *Lithobates bwana* (VU), *Pristimantis ceuthospilus* (VU), *Pristimantis sternothylax* (VU), *Pristimantis wiensi* (VU), *Epipedobates anthonyi* (NT), due to habitat loss and chytridiomycosis.

Conservation initiatives for the herpetofauna are based on assessments of species richness and knowledge about the natural history of the species, mainly derived from publications describing each species. Additional

information on diet, ecology (including thermoeecology), ethology, seasonality, and activity patterns for most species is scarce. This study aims to provide a preliminary list of amphibian and reptile species that contribute to the general understanding of species richness in the Equatorial ESDT and to identify daily activity patterns at both community and species-specific levels. To provide useful information for species conservation, the study area was subdivided into natural zones: forests and ravines and anthropized zones, populated centers, and crops. The necessity of this study lies in its potential to positively influence conservation strategies, ensuring the survival and prosperity of the herpetofauna in an ecosystem under constant change and threat.

## MATERIALS AND METHODS

### Study Area

The peasant community of Pampas de Lucarqui is located in the vicinity of the urban center of Lucarqui, in the district of Ayabaca, province of Ayabaca, Piura region, northwest Peru. This locality is situated within the Equatorial ESDT. For the present investigation, samplings were conducted in an area ranging from 1125 to 2220 meters above sea level (Fig. 1). These samplings were distributed across four well-differentiated zones of the forest in the peasant community

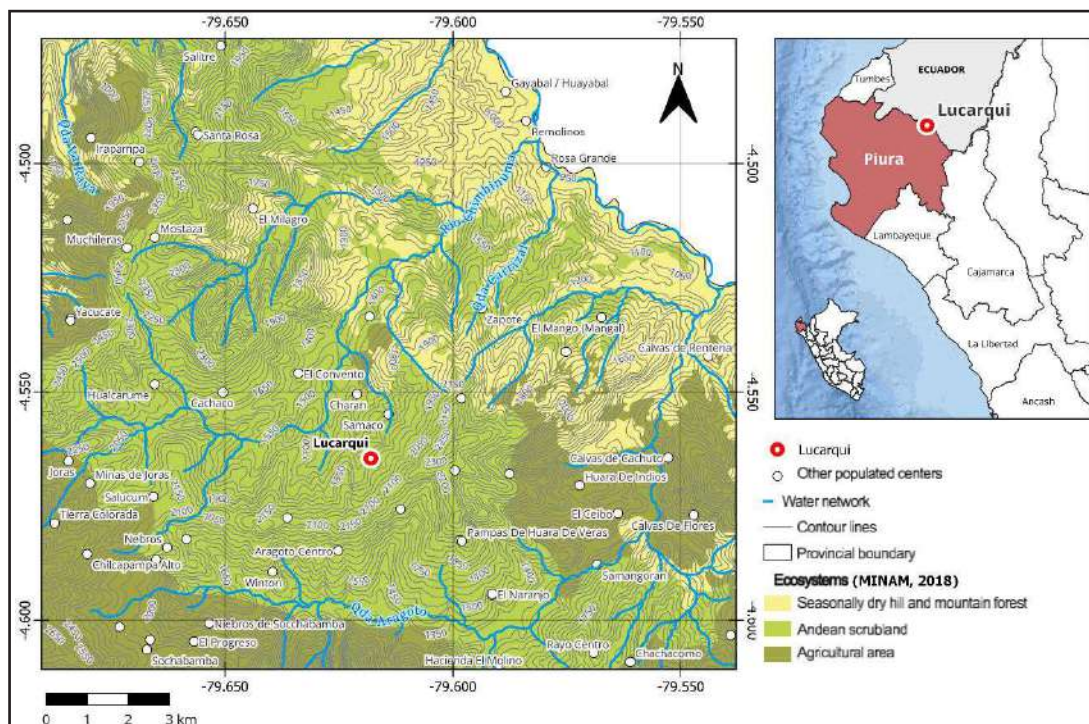


Fig. 1: Location map of the study area, Lucarqui Population Center, Ayabaca District, Ayabaca Province, Piura Region, Northwestern Peru.

of Lucarqui. Two of them are areas with low intervention, forests, and ravines, while the remaining two exhibit a high degree of anthropization, urban centers, and crops. Below, we describe the main physiographic and vegetative cover characteristics of these four zones:

- **Forests (ZB):** lush and open areas featuring low forest density. It is possible to find plant species such as *Colicodendron scabridum*, *Loxopterigium huasango*, *Erythrina smithiana*, *Bursera graveolens*, *Neltuma sp.*, *Acacia sp.*, *Guadua angustifolia*, *Gynerium sagittatum*, *Pennisetum purpureum*, *Bidens pilosa*, *Heliotropium sp.*, among others.
- **Ravine (ZQ):** the streams in the study area can be either seasonal or permanent. They are characterized by rocky areas, partly covered by moss, and riparian vegetation with the presence of *Arundo donax*, *Acacia sp.*, and *Pennisetum purpureum*, among others.
- **Crop (ZC):** these are anthropized areas with productive purposes, featuring bare rocky soil and scattered vegetation, mainly composed of *Acacia sp.* Local crops in this area include *Zea mays*, *Vicia faba*, *Cajanus cajan*, *Arachis hypogaea*, *Cucumis sativus*, *Pisum sativum*, *Manihot esculenta*, *Cucurbita maxima*, *Phaseolus lunatus*, *Ph. vulgaris*. Two types of cultivation zones are recognized: permanent ones, hosting year-round plantations, and seasonal ones, which have irrigation systems via ditches and depend on water from the rainy season (December to April).
- **Village (ZP):** the hamlets in the area consist of scattered houses situated on bare, rocky soil accompanied by herbaceous vegetation and scarce trees such as *Acacia sp.*, *Erythrina smithiana*, and *Bougainvillea pachyphylla*. Most houses have small orchards with permanent irrigation.

### Data Collection

To assess the richness and abundance of amphibian and reptile species, nine samplings were conducted between August and December 2019, January, February, November, and December 2020, and January 2021. Each sampling consisted of 30 effective hours of assessment, accumulating a total of 270 person-hours of sampling effort. Both diurnal, from 7:00 am to 6:00 pm, and nocturnal samplings, from 6:00 pm to 12:00 am, were conducted using both incidental captures and Visual Encounter Surveys (VES) (Aguirre-León 2011). These methodologies were applied along sampling transects with differentiated measurements for the different evaluated zones. In populated areas and cultivated lands, where vegetation was sparse, species detectability was higher. Hence, fixed-width transects of 50 × 2m were

employed in rugged and less accessible areas, and 100 × 2m transects in more accessible areas with lower slopes. For forests and streams, where vegetation was denser, transects of variable length and fixed 2m width were used (Aguirre-León 2011). Each transect was assessed at a slow pace, searching in holes and under stones for 30 to 45 minutes.

### Species Determination

Species were determined to the lowest possible taxonomic level (genus or species), following the literature (Catenazzi & von May 2014, de Espinoza & Icochea 1995, Duellman & Wild 1993, Minam 2018). Photographs were taken of captured individuals and of the majority of individuals observed exhibiting unusual characteristics. All captured individuals were promptly released to minimize stress.

### Data Analysis

With the data of abundance and richness obtained by zone for the registered amphibians and reptiles, three analyses were performed:

### Temporal Frequency of Records (TFR)

Here, a new methodology for the analysis of temporal frequency of records (TFR) is proposed. TFR was considered as the sum of records per family for each hour of the day, reported as individuals per hour (ind./hour). In the present study, the hourly range from 7:00 am to 11:59 pm of the same day was considered. Since it is a methodology with a high level of wear, it requires a team of at least two people with similar levels of experience to take turns to maintain continuous sampling during the evaluation period. Using these data, bar graphs were generated to identify TFR patterns throughout the day. The patterns were analyzed for the entire study area (Fig. 2) and by grouping the records for each evaluated zone (forest, stream, crop, and town, Figs. 3 and 4). It was considered pertinent to perform this analysis by summing the records by family rather than by species due to the scarce number of records for some of them.

To standardize this methodology (TFR) for future uses, the following detailed algorithm is proposed:

- **Step 1:** In the field, record each encounter, noting the sampling zone, date and time, species, and the number of individuals seen in that encounter. This latter ensures the accurate collection of abundance information, particularly for species with gregarious habits that may be hidden together.
- **Step 2:** In the office, filter the database for the group of interest (order, family, or species, depending on the study's purposes).

- **Step 3:** Standardize the time. If the data of “hour and minute” or “hour, minute, and second” were recorded in the field, proceed to only consider the hour value for further use. If only the hour were noted without minutes, proceed without any modification. This step enables grouping the data by hour, disregarding other temporal divisions, which is crucial for generating the final bar graph grouped by hours.
- **Step 4:** Create the final bar graph, considering the horizontal axis as the evaluation hours (categorical variable) and the vertical axis as the sum of abundances from all records for each group of interest within the specific hour (TFR).
- **Step 5:** During the data visualization process, it is recommended to subdivide the bars in a “stacked” manner based on the groups of interest, aiming to have a single bar per hour.

Since the methodology covers continuous sampling during the evaluation period, it is possible to use it to identify peaks of higher activity of a species or taxonomic group as a homologous characteristic to having a higher TFR value (ind./hour).

### Rarefaction and Extrapolation of Alpha Richness and Diversity

To analyze biological diversity, the iNEXT package (Hsieh et al. 2016) in RStudio (RStudio Team 2023) was employed, which utilizes rarefaction and extrapolation to perform

comparisons between communities or habitats with different sample sizes or sampling areas. Through rarefaction, it estimates species diversity for a standardized sample size or area, while extrapolation predicts how diversity would be in a larger sample size or broader area. iNEXT provides precise and reliable diversity estimates, even with incomplete sampling data, and allows for the standardization of species accumulation curves. Shannon-Wiener, Simpson, and species richness indices were projected to assess diversity from different perspectives (evenness, dominance, and species richness, respectively).

### Sampling Completeness

A sampling coverage analysis was conducted using iNEXT (Hsieh et al. 2016) to assess the completeness of the samplings. This analysis evaluates the sufficiency of sampling in biodiversity studies, allowing us to determine if the collected samples are representative of the studied community and estimate what proportion of the total diversity has been captured in the samples. This enables us to compare diversity between non-identical sites or where there was no equitable sampling effort, as is the case with the four zones in the study area being evaluated here.

## RESULTS

### Description of Recorded Richness and Abundance

Between August 2019 and January 2021, 1054 observations

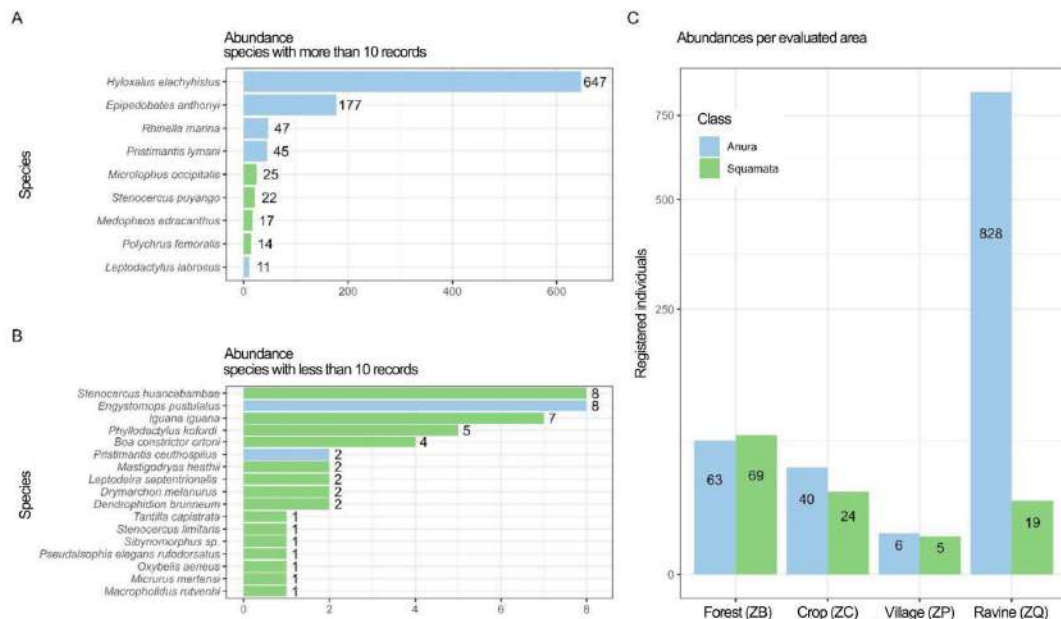


Fig. 2: Abundance of Anura species (blue) and Squamata species (green) reported in the rural community of Lucarqui, Piura, northwest Peru, categorized by (A) species with more than 10 records, (B) species with fewer than 10 records, and (C) by evaluated zone.

Table 1: Taxonomic list of amphibian and reptile species recorded in the Equatorial ESDT of the Lucarqui peasant community, Piura, northwest Peru. Abundances (Abund.) per zone are shown for each species. The highest abundances are highlighted in bold. Threat categories, according to the IUCN (2022), are shown in bold, according to the Peruvian state (Serfor 2018) are underscored, and in bold and underscored when both categorizations coincide. NT: Near Threatened, VU: Vulnerable, EN: Endangered, II: Appendix II of CITES (MINAM 2018).

Class	Order	Family	Species	Zone	Abund.
Amphibia	Anura	Bufonidae	<i>Rhinella marina</i>	ZB	26
				ZC	1
				ZP	1
				ZQ	19
		Craugastoridae	<i>Pristimantis ceuthospilus</i> (VU)	ZQ	2
				ZB	1
			<i>Pristimantis lymani</i>	ZC	7
				ZP	3
		Dendrobatidae	<i>Epipedobates anthonyi</i> (NT, II)	ZQ	34
				ZC	22
				<b>ZQ</b>	<b>155</b>
				ZB	35
			<i>Hyloxalus elachyhistus</i> (EN)	ZC	5
				ZP	1
				<b>ZQ</b>	<b>606</b>
				ZB	1
		Leptodactylidae	<i>Engystomops pustulatus</i>	ZQ	7
				ZC	5
			<i>Leptodactylus labrosus</i>	ZP	1
				ZQ	5
Reptilia	Squamata	Boidae	<i>Boa constrictor orton</i> (EN, II)	ZB	2
				ZC	2
		Colubridae	<i>Dendrophidion brunneum</i>	ZQ	2
				ZP	1
			<i>Drymarchon melanurus</i>	ZQ	1
				ZB	1
			<i>Mastigodryas heathii</i>	ZP	1
			<i>Oxybelis aeneus</i>	ZB	1
			<i>Pseudalsophis elegans rufodorsatus</i>	ZB	1
			<i>Sibynomorphus</i> sp.	ZB	1
		Dipsadidae	<i>Tantilla capistrata</i>	ZB	1
			<i>Leptodeira septentrionalis</i>	ZB	1
				ZC	1
		Elapidae	<i>Micrurus mertensi</i>	ZB	1
		Gymnophthalmidae	<i>Macropholidus ruthveni</i>	ZB	1
		Iguanidae	<i>Iguana iguana</i> (II)	ZB	4
				ZQ	3
		Phyllodactylidae	<i>Phyllodactylus kofordi</i>	ZB	5
		Polychrotidae	<i>Polychrus femoralis</i> (VU)	ZB	5
				ZC	6
				ZQ	3

Table Cont....



Class	Order	Family	Species	Zone	Abund.
		Teiidae	<i>Medopheos edracantha</i>	ZB	15
				ZP	1
				ZQ	1
		Tropiduridae	<i>Microlophus occipitalis</i>	ZB	21
				ZP	1
				ZQ	3
			<i>Stenocercus huancabambae</i>	ZB	4
				ZC	4
				ZQ	1
			<i>Stenocercus puyango</i>	ZB	5
				ZC	11
				ZP	1
				ZQ	5

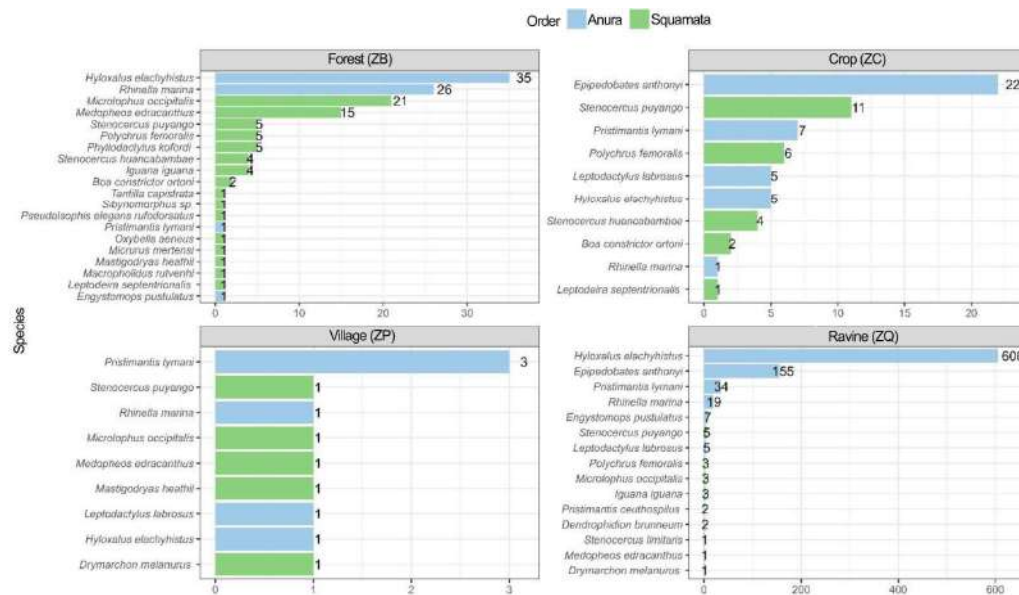


Fig. 3: Species abundance of Anura (blue) and Squamata (green) was reported in each evaluation zone within the peasant community of Lucarqui, Piura, northwest Peru.

were conducted, documenting 26 species of herpetofauna, distributed into two classes: Amphibia, with seven recorded species (26.9%) and 937 individuals (88.9%), and Reptilia, with 19 species (73.1%) and 117 individuals (11.1%). Taxonomically, four families of amphibians and 10 families of reptiles were reported (Table 1). The family Colubridae exhibited the highest diversity (seven species), followed by Tropiduridae (four species) (Table 1, Fig. 7, Fig. 8, Fig. 9).

The most common amphibian was *Hyloxalus elachyhistus*, with 647 individuals, and the most common reptile was *Microlophus occipitalis*, with 25 individuals (Table 1, Fig. 2A). Considering the evaluation area (Fig. 2C), amphibians were more abundant in the streams (828

individuals), while reptiles were more abundant in forests (69 individuals). Differentiating the most abundant amphibians and reptiles (Fig. 3), in forests, *Hyloxalus elachyhistus* and *Microlophus occipitalis* dominated. In crops, *Epipedobates anthonyi* and *Stenocercus puyango*, in populated centers, *Pristimantis lymani* and *S. puyango*, whereas, in streams, *H. elachyhistus* and *S. puyango* prevailed.

With regard to their conservation (Table 1), three globally threatened species were recorded (IUCN 2022): *Pristimantis ceuthospilus* (VU), *Epipedobates anthonyi* (NT), and *Stenocercus limitaris* (VU), and four regionally threatened species for Peru: *E. anthonyi* (NT), *Hyloxalus elachyhistus* (EN), *Boa constrictor ortonii* (EN), *Polychrus femoralis*

(VU). Additionally, three species protected by CITES under Appendix II have been recorded: *Iguana iguana*, *B. c. ortonii*, and *E. anthonyi*.

Regarding the biogeographical importance of these species, according to IUCN (2022), 85.71% (6 species) of amphibians are restricted to the Equatorial ESDT: *Pristimantis ceuthospilus*, *Pristimantis lymani*, *Epipedobates anthonyi*, *Hyloxalus elachyhistus*, and *Engystomops pustulatus*, as well as 47.36% (9 species) of reptiles: *Dendrophidion brunneum*, *Tantilla capistrata*, *Micrurus mertensi*, *Macropholidus ruthveni*, *Phyllodactylus kofordi*, *Polychrus femoralis*, *Stenocercus huancabambae*, *Stenocercus limitaris*, and *Stenocercus puyango*.

### Rarefaction and Extrapolation of Diversity

The iNEXT algorithm did not generate extrapolations for richness and alpha diversity indices in forests, crops, and populated centers for Anura and in populated centers for Squamata (Fig. 4). At the order level, Anura richness was higher in streams, reaching an asymptote with the seven amphibian species recorded. However, alpha diversity values were low due to the high dominance of a few species, such as *Hyloxalus elachyhistus* or *Epipedobates anthonyi*. Squamata richness was higher in forested areas, not reaching asymptotes with 17 reptile species, two fewer than reported.

Additionally, a higher species richness of reptiles is expected in this area. Alpha diversity was high, attributed to the relatively uniform number of records. It is expected that the entirety of reptile species has been recorded in crops.

### Analysis of Temporal Frequency of Records

Temporal frequency of records (TFR) patterns were obtained for the orders Anura and Squamata considering the entire study area (Fig. 2), as well as for each evaluated zone for Anura (Fig. 3) and Squamata (Fig. 4). The activity peaks for each order (Fig. 2) showed a higher number of diurnal records for Squamata, mainly between 11:00 and 13:00 hours, whereas for Anura, a bimodal distribution was obtained with a peak of diurnal records at 10:00 hours, and a nocturnal one at 22:00 hours. The families that contributed the most to these patterns at the taxonomic order level were Dendrobatidae (Anura) and Tropiduridae (Squamata).

Considering the grouping of abundance data for each evaluated zone, a different pattern is observed for Anura (Fig. 3). The highest abundance of records per hour was observed in the streams (maximum of 160 ind./hour), followed by forests (17 ind./hour), crops (15 ind./hour), and populated centers (3 ind./hour). In forests, the presence of Dendrobatidae was observed in the early morning hours (8:00 to 10:00 hours), while at night, they completely

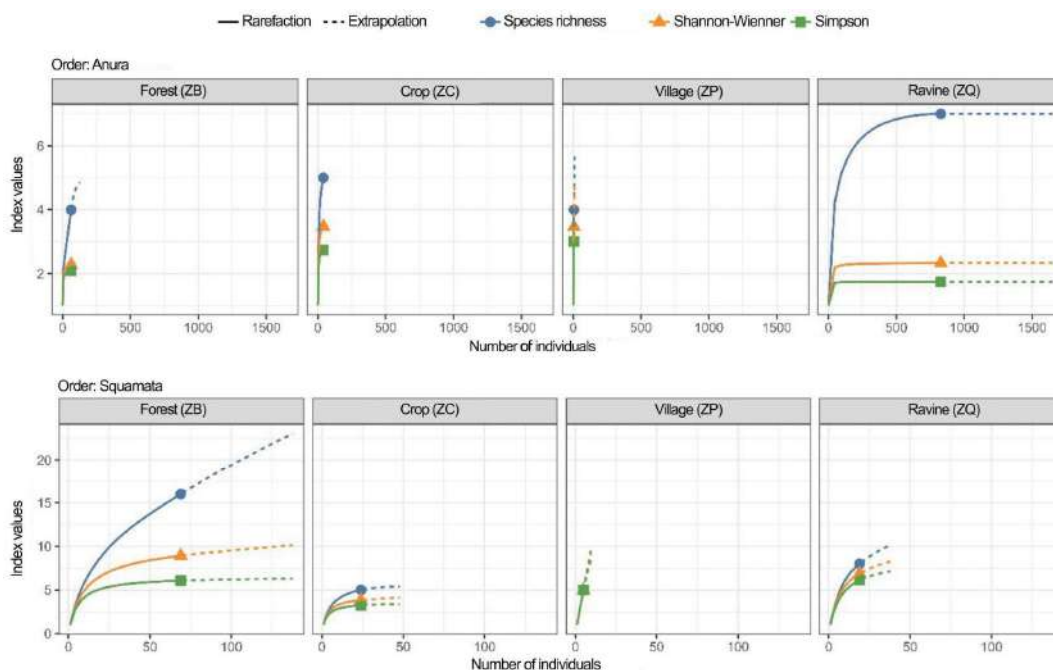


Fig. 4: Estimates with iNEXT on rarefaction of Hill's numbers (solid lines) and extrapolation of data (dashed lines) for species richness (blue), Shannon-Wiener index (yellow), and Simpson index (green) for amphibians (Anura) and reptiles (Squamata). The information was divided by sampling zone in the ESDT Equatorial of the peasant community of Lucarqui, Piura, northwest Peru.

disappeared to give way to a dominance of Bufonidae. It is noteworthy that the highest concentration of Dendrobatidae (*Epipedobates anthonyi* and *Hyloxalus elachyhistus*) is observed in streams, where they can be found throughout the day. During the day, records obtained in more anthropized areas, such as crops and populated centers, were scarce.

Regarding the data grouped by zone for Squamata (Fig. 4), the abundance values were much lower. The highest

abundance of records per hour was observed in forests (with a maximum of 20 ind./hour), followed by crops and streams (4 ind./hour each), and populated centers (1 ind./hour). In forests, the presence of Dendrobatidae was observed in the early morning hours (8:00 to 10:00 hours), while at night, they completely disappeared to give way to Bufonidae. Notably, eight out of ten Squamata families were recorded in forests. Throughout the four study zones, Tropiduridae

Table 2: Maximum Temporal Recording Frequency (TRF), expressed as the maximum number of individuals per hour (ind./hour), for all amphibian and reptile species recorded in the Equatorial ESDT of the Lucarqui peasant community, Piura, northwest Peru. The zone and time (in 24-hour format) of the peak of maximum activity are shown.

Order	Specie	Zone	Peak of activity	Max. Ind./hour
Anura	Engystomops pustulatus	ZQ	23:00	3
	Epipedobates anthonyi	ZQ	22:00	33
	Hyloxalus elachyhistus	ZQ	22:00	118
	Leptodactylus labrosus	ZC	19:00	3
	Pristimantis ceuthospilus	ZQ	21:00	1
		ZQ	23:00	1
	Pristimantis lymani	ZQ	20:00	10
	Rhinella marina	ZB	20:00	14
Squamata	Boa constrictor ortonii	ZB	0:00	1
		ZB	15:00	1
		ZC	13:00	1
		ZC	17:00	1
	Dendrophidion brunneum	ZQ	11:00	1
		ZQ	12:00	1
	Drymarchon melanurus	ZP	12:00	1
		ZQ	12:00	1
	Iguana iguana	ZQ	16:00	3
	Leptodeira septentrionalis	ZC	7:00	1
	Macropholidus rutveni	ZB	11:00	1
	Mastigodryas heathii	ZB	13:00	1
		ZP	15:00	1
	Medopheos edracanthus	ZB	11:00	4
		ZB	12:00	4
		ZB	13:00	4
	Microlophus occipitalis	ZB	12:00	10
	Micrurus mertensi	ZB	16:00	1
	Oxybelis aeneus	ZB	18:00	1
	Phyllodactylus kofordi	ZB	12:00	3
	Polychrus femoralis	ZB	16:00	2
		ZC	8:00	2
		ZC	22:00	2
		ZQ	20:00	2
	Pseudalsophis elegans rufodorsatus	ZB	9:00	1
	Sibynomorphus sp.	ZB	16:00	1
	Stenocercus huancabambae	ZB	13:00	3
	Stenocercus limitaris	ZQ	11:00	1
	Stenocercus puyango	ZC	13:00	3
		ZC	16:00	3
	Tantilla capistrata	ZB	8:00	1

(*Stenocercus huancabambae*, *S. limitaris*, *S. puyango*, *Microlophus occipitalis*) is the family with the highest number of records and the one that covers the most hours during the day.

The results of individuals per hour (ind./hour) maximum and hour of highest activity for each Anura and Squamata species are shown in Table 2.

### Completeness of the Study

The completeness analysis (Fig. 5) for Anura showed that no further species are expected in forests and crops, whereas in populated areas, the number of recorded individuals was low, resulting in an incomplete species record. Regarding Squamata, something similar occurred in populated areas, and it is expected to find more species in forests, crops, and streams. The effort required to obtain a complete sampling is expected to be higher in forests than in crops and streams. The iNEXT algorithm indicated that amphibian species from the stream area and reptiles from crop areas were virtually covered 100%.

## DISCUSSION

This study aimed to enhance the understanding of diversity patterns and temporal frequency records of herpetofauna in an Equatorial ESDT located in hilly and mountainous areas at altitudes between 1125 and 2220 meters above sea level in northwest Peru. From our research, a preliminary

list of amphibian and reptile species present in this region is provided.

Seven species of amphibians were identified, representing 23.3% of the species reported for the Equatorial ESDT of Peru and Ecuador (Armijos-Ojeda et al. 2021). Regarding reptiles, no preliminary or complete list of species has been published for the Equatorial ESDT. However, a detailed approximation for northern Peru, covering the regions from La Libertad to Tumbes, conducted by Venegas (2005), documented 33 reptile species in the region. In the present study, 19 reptile species were found, representing 57.6% of the figure published by Venegas (2005). However, when comparing the species list, our findings add three new species: *Stenocercus huancabambae*, *S. limitaris*, and *Sibynomorphus* sp., thus expanding the recognized richness for the region to 36 reptile species. In contrast to the Marañón ESDT located on the eastern slope of the Andes, between Peru and Ecuador—with which the Equatorial ESDT shares geographical, climatic, and evolutionary characteristics—, Koch et al. (2018) reported 14 amphibian species and 49 reptile species. It is anticipated that the herpetofauna richness for the Equatorial ESDT will be higher than reported in this study.

Regarding the distribution patterns of diversity in the different evaluated zones, these reflect the influence of environmental factors and anthropogenic changes on the landscape. The heterogeneity of microhabitats fosters a

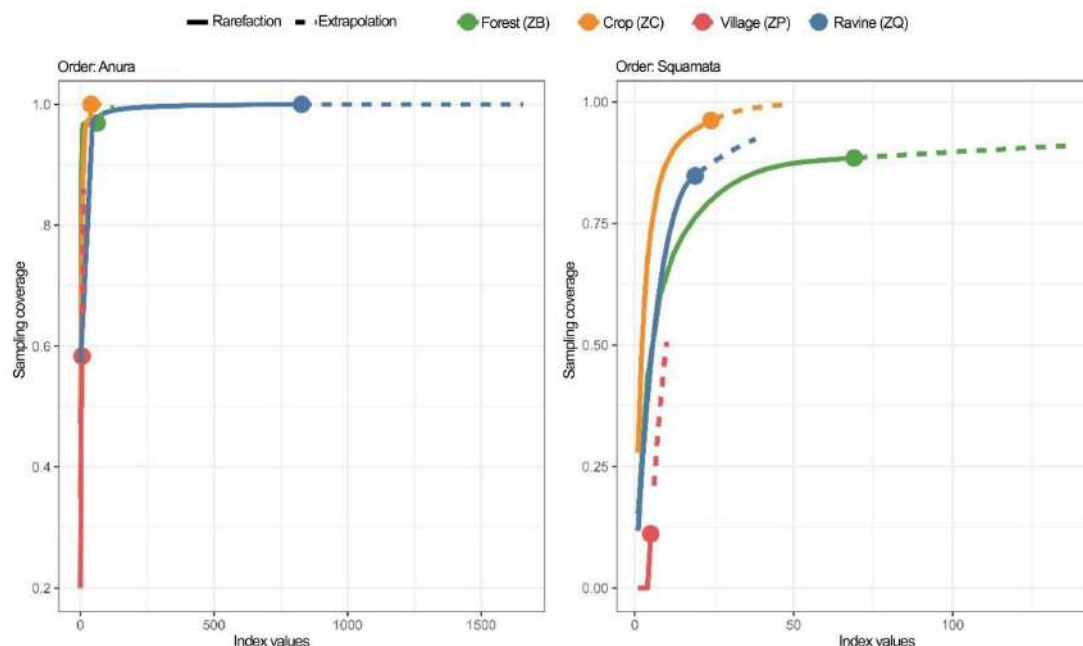


Fig. 5: Coverage curves (or completeness) of the evaluated areas for amphibians (Anura) and reptiles (Squamata) recorded in the ESDT Equatorial of the peasant community of Lucarqui, Piura, northwest Peru. The solid lines represent sampling completeness based on the number of individuals recorded, while the dashed lines depict extrapolated curves by iNEXT on the completeness trend.



greater diversity of amphibians and reptiles (Bucher 2019). These variations are linked to fluctuations in temperature, moisture content, and interspecific trophic interactions, among others (Ravkin & Bogomolova 2018). Additionally, anthropogenic landscape changes play a significantly more determining role in local extinctions of herpetofauna on a global scale (Cordier et al. 2021). The lowest diversity of amphibian and reptile species was found in crops (ZC) and populated areas (ZP), which is due to habitat alteration and the decrease in the availability of shelters and resources. On the other hand, the highest diversity was found in forests (ZB) and streams (ZQ). This pattern suggests that the conservation of larger forested areas and riparian forests is crucial for the protection of herpetofauna. Furthermore, it is essential to consider that the size and shape of forest patches, and the composition of the landscape matrix affect each species uniquely (Russildi et al. 2016). Understanding these effects is of vital importance for biodiversity conservation.

The analysis of temporal frequency records (TFR) allowed us to infer peaks of activity and fluctuations in the abundance of Equatorial ESDT herpetofauna. These patterns showed differences depending on habitat characteristics. At the community level in the evaluated Equatorial ESDT, reptiles exhibited multimodal activity patterns. For reptiles (Squamata, Fig. 5), the first peak of diurnal activity occurred at 9:00 am, with a homologous but greater peak towards sunset at 4:00 pm. This closely resembles older studies on reptile thermoecology that demonstrated bimodal activity patterns in some subtropical species (Judd 1975). The highest activity of the reptile community was at 12:00 noon when maximum radiation occurred in the ESTD near the Equator. Some species

of the families Polychrotidae and Colubridae were active during the night, with a peak of activity around 10:00 pm. Tropiduridae were the dominant family throughout the day, probably because they are better adapted to anthropogenic disturbances (Dávila & Cisneros-Heredia 2017).

For the amphibian community (Anura, Fig. 6), the TFR indicated a clear bimodal pattern throughout the day, with a peak of diurnal activity (10:00 hrs) and a nocturnal one (22:00 hrs), where *Epipedobates anthonyi* was overwhelmingly dominant. Species of Bufonidae, Craugastoridae, and Leptodactylidae exhibit predominantly nocturnal activity, associated with reduced dehydration rates and avoidance of diurnal predators, although juveniles can also be found during the day (Arroyo et al. 2008, Maia-Carneiro et al. 2013, 2021). Dehydration is minimized in these individuals due to their lower surface-to-volume ratio (Kühse et al. 2017). This same reason would account for species of the family Dendrobatidae, with small aposematic frogs being active throughout the day.

Observing activity patterns in relation to the evaluated zone revealed interesting findings. Dendrobatidae was the most abundant family in streams, only visiting forested areas in the early morning hours and also occurring in crops toward the evening. Bufonidae showed widespread adaptation to inhabit all zones during the night, with higher abundance toward the forest. Regarding reptiles, the hypothesis that daytime activity differs from a conserved state in forests to erratic patterns in areas with higher human influence is reinforced (Cordier et al. 2021).

## CONCLUSIONS

A total of 26 species of herpetofauna were recorded,

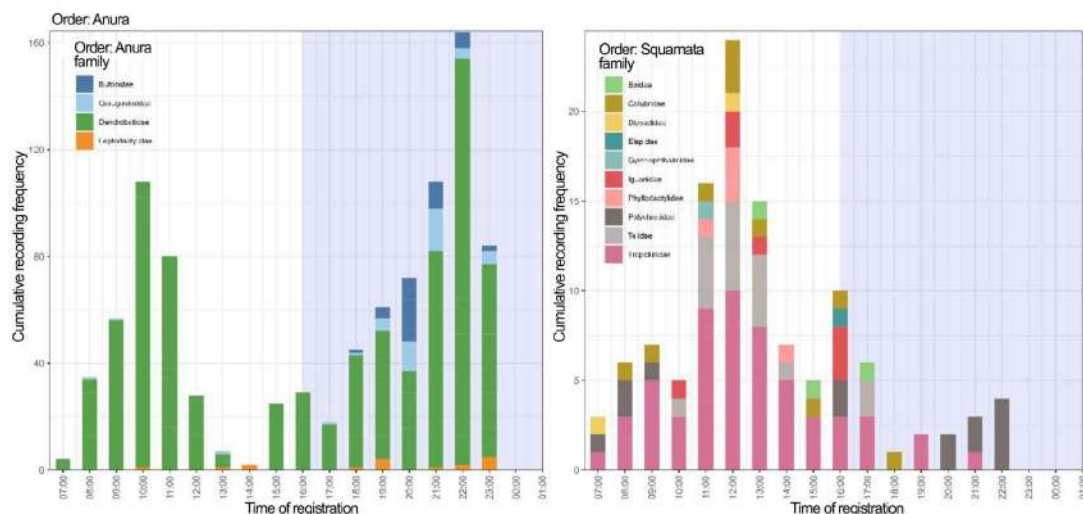


Fig. 6: Cumulative frequency of records for families belonging to the orders Anura and Squamata reported, grouped for each sampling hour (daytime: white background, nighttime: blue shaded background).

distributed into two classes: Amphibia, with seven recorded species (26.9%) and 937 individuals (88.9%), and Reptilia, with 19 species (73.1%) and 117 individuals (11.1%). At the taxonomic level, four families of amphibians and 10 families of reptiles were reported.

The most frequent amphibian was *Hyloxalus elachyhistus*, with 647 individuals, and the most frequent reptile was *Microlophus occipitalis*, with 25 individuals. Amphibians were more abundant in streams (828 individuals), while

reptiles were more abundant in forests (69 individuals). Differentiating the most abundant amphibians and reptiles, *Hyloxalus elachyhistus* and *Microlophus occipitalis* dominated in forests, *Epipedobates anthonyi* and *Stenocercus puyango* in cultivated areas, *Pristimantis lymani* and *S. puyango* in populated centers, while *H. elachyhistus* and *S. puyango* were prevalent in streams.

Three globally threatened species were recorded (IUCN, 2022): *Pristimantis ceuthospilus* (VU), *Epipedobates*



Fig. 7: Anura species recorded in the BTES Equatorial of the Lucarqui farming community, Piura, northwest Peru. (A) *Rhinella marina*, (B) *Pristimantis ceuthospilus*, (C) *Pristimantis lymani*, (D) *Epipedobates anthonyi*, (E) *Hyloxalus elachyhistus*, (F) *Engystomops pustulatus*, (G) *Leptodactylus labrosus*, (H) *Leptodactylus labrosus* dark dorsum.





Fig. 8: Some of the Squamata species from the suborder Ophidia recorded in the Equatorial Seasonally Dry Tropical Forest (BTES) of the Lucarqui peasant community, Piura, northwestern Peru. (A) *Boa constrictor ortonii*, (B) *Dendrophidion brunneum*, (C) *Mastigodryas heathii*, (D) *Pseudalsophis elegans rufodorsatus*, (E) *Tantilla capistrata*, (F) *Leptodeira septentrionalis*, (G) *Oxybelis aeneus*, (H) *Sibynomorphus* sp., (I) *Micrurus mertensi*





Fig. 9: Some of the non-snake Squamata species recorded in the BTES Ecuatorial of the Lucarqui farming community, Piura, northwestern Peru. (A) *Macropholidus rutvenhi*, (B) *Iguana iguana*, (C) *Phyllodactylus kofordi*, (D) *Polychrus femoralis*, (E) *Medopheos edracanthus*, (F) *Stenocercus huanabambae*, (G) *Stenocercus limitaris*, (H) *Stenocercus puyango*



*anthonyi* (NT), and *Stenocercus limitaris* (VU), and four species regionally threatened in Peru: *E. anthonyi* (NT), *Hyloxalus elachyhistus* (EN), *Boa constrictor ortonii* (EN), and *Polychrus femoralis* (VU). Additionally, three species protected by CITES under Appendix II have been recorded: *Iguana iguana*, *B. c. ortonii*, and *E. anthonyi*.

Regarding the biogeographical importance of the species, according to the IUCN (2022), 85.71% (6 species) of the amphibians are restricted to the Equatorial BTES: *Pristimantis ceuthospilus*, *Pristimantis lymani*, *Epipedobates anthonyi*, *Hyloxalus elachyhistus*, and *Engystomops pustulatus*, as well as 47.36% (9 species) of the reptiles: *Dendrophidion brunneum*, *Tantilla capistrata*, *Micrurus mertensi*, *Macropholidus ruthveni*, *Phyllodactylus kofordi*, *Polychrus femoralis*, *Stenocercus huancabambae*, *Stenocercus limitaris*, and *Stenocercus puyango*.

## CONSERVATION

The Equatorial ESDT, spanning extensive areas west of the Andes between Peru and Ecuador, is highly significant for its endemism and high level of biodiversity. Remnants and fragments of these forests have become crucial for the herpetofauna due to increasing human pressure and climate change threatening the availability and quality of their habitats. Findings from this study not only highlight how herpetofauna can be considerably diverse in a specific locality within the Equatorial ESDT but also emphasize the need to consider landscape structure as a key component for the conservation of amphibian and reptile species.

The presence of four threatened species and four with restricted ranges indicates that these forests can harbor key populations for conservation at a regional level. Protecting these species in one locality can have a domino effect, safeguarding populations in other areas of the forest and food webs.

Throughout the Equatorial ESDT, the relationship between humans and, amphibians, and reptiles is complex, shaped by culture, fear, and economy (Ríos-Orjuela et al. 2020). Hunting, trade, or mortality of these species are widespread phenomena. It is imperative to develop education and awareness programs to conserve the herpetofauna and maintain the ecological integrity of the Equatorial ESDT.

Increasing sampling efforts (e.g., person-hours) in future research will be crucial for finding less common species in the Equatorial ESDT. Other studies in dry forests have shown a positive trend between effort and reported herpetofauna diversity (Koch et al. 2018). It is recommended to expand assessments in unexplored regions of the Equatorial ESDT, with greater sampling effort, to increase knowledge of the

natural history, ethology, diet, thermoeecology, and other important characteristics of amphibian and reptile species that inform their conservation status and propose action plans accordingly.

## ACKNOWLEDGMENTS

To the rural community of Lucarqui, for their special courtesy in allowing us to evaluate and accompany them in the assessments.

## REFERENCES

- Aguirre-León, G., 2011. Methods for estimating, capturing, and containing amphibians and reptiles. *Manual of Techniques for the Study of Fauna*, 1(1), pp.48–65.
- Armijos-Ojeda, D., Székely, D., Székely, P., Cogălniceanu, D., Cisneros-Heredia, D.F., Ordóñez-Delgado, L., Escudero, A. and Espinosa, C.I., 2021. Amphibians of the equatorial seasonally dry forests of Ecuador and Peru. *ZooKeys*, 1063, pp.23–48. [DOI]
- Arroyo, S.B., Serrano-Cardozo, V.H. and Ramírez-Pinilla, M.P., 2008. Diet, microhabitat, and time of activity in a *Pristimantis* (Anura, Strabomantidae) assemblage. *Phyllomedusa: Journal of Herpetology*, 7(2), pp.109–119.
- Bucher, E.H., 2019. Amphibians and reptiles. In: E.H. Bucher (ed.) *The Mar Chiquita Salt Lake (Córdoba, Argentina): Ecology and Conservation of the Largest Salt Lake in South America*. Springer International Publishing, pp.65–71. [DOI]
- Catenazzi, A. and von May, R., 2014. Conservation status of amphibians in Peru. *Herpetological Monographs*, 28(1), pp.1–23.
- Cordier, J.M., Aguilar, R., Lescano, J.N., Leynaud, G.C., Bonino, A., Miloch, D., Loyola, R. and Nori, J., 2021. A global assessment of amphibian and reptile responses to land-use changes. *Biological Conservation*, 253, 108863. [DOI]
- Dávila, M. and Cisneros-Heredia, D.F., 2017. Use of human-made buildings by *Stenocercus* lizards (Iguania, Tropiduridae). *Herpetology Notes*, 10, pp.517–519.
- de Espinoza, N.C. and Icochea, J., 1995. Preliminary taxonomic list of living reptiles in Peru. *Publications of the Museum of Natural History*, 49, pp.1–27.
- Duellman, W.E. and Wild, E.R., 1993. *Anuran Amphibians from the Cordillera De Huancabamba, Northern Peru: Systematics, Ecology, and Biogeography*. Museum of Natural History, the University of Kansas.
- Hsieh, T., Ma, K. and Chao, A., 2016. INEXT: an R package for rarefaction and extrapolation of species diversity (Hill numbers). *Methods in Ecology and Evolution*, 7(12), pp.1451–1456.
- IUCN, 2022. *The IUCN Red List of Threatened Species. Version 2022-1*. International Union for Conservation of Nature. Available at: <https://www.iucnredlist.org> [Accessed 6 Mar 2025].
- Judd, F.W., 1975. Activity and thermal ecology of the keeled earless lizard, *Holbrookia propinqua*. *Herpetologica*, 31(2), pp.137–150.
- Koch, C., Venegas, P.J., Cruz, R.S. and Böhme, W., 2018. Annotated checklist and key to the species of amphibians and reptiles inhabiting the northern Peruvian dry forest along the Andean valley of the Marañón River and its tributaries. *Zootaxa*, 31, p.4385. [DOI]
- Kühnel, S., Brückner, A., Schmelzle, S., Heethoff, M. and Blüthgen, N., 2017. Surface area–volume ratios in insects. *Insect Science*, 24(5), pp.829–841. [DOI]
- Laurencio, D. and Fitzgerald, L.A., 2010. Environmental correlates of herpetofaunal diversity in Costa Rica. *Journal of Tropical Ecology*, 26(5), pp.521–531. [DOI]
- Linares-Palomino, R., Kvist, L.P., Aguirre-Mendoza, Z. and Gonzales-

- Inca, C., 2010. Diversity and endemism of woody plant species in the Equatorial Pacific seasonally dry forests. *Biodiversity and Conservation*, 19(1), pp.169–185. [DOI]
- Linares-Palomino, R., Oliveira-Filho, A.T. and Pennington, R.T., 2011. Neotropical seasonally dry forests: Diversity, endemism, and biogeography of woody plants. In: R. Dirzo, H.S. Young, H.A. Mooney and G. Ceballos, eds. *Seasonally Dry Tropical Forests: Ecology and Conservation*. Island Press/Center for Resource Economics, pp.3–21. [DOI]
- Maia-Carneiro, T., Dorigo, T.A., Kiefer, M.C., van Sluys, M. and Rocha, C.F.D., 2021. Feeding habits, microhabitat use, and daily activity cycle of *Adenomera marmorata* (Anura, Leptodactylidae) in two Brazilian Atlantic Forest remnants. *South American Journal of Herpetology*, 20(1), pp.100–105. [DOI]
- Maia-Carneiro, T., Kiefer, M.C., van Sluys, M. and Rocha, C.F., 2013. Feeding habits, microhabitat use, and daily activity period of *Rhinella ornata* (Anura, Bufonidae) from three Atlantic rainforest remnants in southeastern Brazil. *North-Western Journal of Zoology*, 9(1), pp.157–165.
- McCain, C.M., 2010. Global analysis of reptile elevational diversity. *Global Ecology and Biogeography*, 19(4), pp.541–553.
- Minam, 2018. *List of CITES Wildlife Species in Peru*. General Directorate of Biological Diversity, Lima, Peru.
- Ravkin, Yu.S. and Bogomolova, I.N., 2018. Ecological organization of the spatiotypological diversity of amphibian, reptile, and small mammal communities in the West Siberian Plain. *Biology Bulletin*, 45(10), pp.1241–1249. [DOI]
- Reyes-Puig, C., Almendáriz, A. and Torres-Carvajal, O., 2017. Diversity, threats, and conservation of reptiles from continental Ecuador.
- Ríos-Orjuela, J.C., Falcón-Espitia, N., Arias-Escobar, A., Espejo-Urbe, M.J. and Chamorro-Vargas, C.T., 2020. Knowledge and interactions of the local community with the herpetofauna in the forest reserve of Quininí (Tibacuy-Cundinamarca, Colombia). *Journal of Ethnobiology and Ethnomedicine*, 16(1), pp.1–11.
- Rivas, C.A., Guerrero-Casado, J. and Navarro-Cerillo, R.M., 2021. Deforestation and fragmentation trends of seasonal dry tropical forest in Ecuador: Impact on conservation. *Forest Ecosystems*, 8(1), 46. [DOI]
- RStudio Team, 2023. *RStudio: Integrated Development Environment for R*. Posit, PBC. Website
- Russildi, G., Arroyo-Rodríguez, V., Hernández-Ordóñez, O., Pineda, E. and Reynoso, V.H., 2016. Species- and community-level responses to habitat spatial changes in fragmented rainforests: Assessing compensatory dynamics in amphibians and reptiles. *Biodiversity and Conservation*, 25(2), pp.375–392. [DOI]
- Serfor, 2018. *Red Book of Threatened Wildlife of Peru*. First Edition.
- Venegas, P.J., 2005. Herpetofauna of the Ecuadorian Dry Forest of Peru: Taxonomy, Ecology, and Biogeography. *Zonas Áridas*, 9(1), pp.9–24.

# Spatio-Temporal Analysis of Aridity Trends and Shifts in Karnataka Over 63 Years (1958-2020): Insights into Climate Adaptation

Sawant Sushant Anil<sup>†</sup> , Dhananjayen and M. Sasi 

School of Life Sciences, JSS Academy of Higher Education and Research, Mysuru, Karnataka, India

<sup>†</sup>Corresponding author: Sawant Sushant Anil; [geo\\_sushant@jssuni.edu.in](mailto:geo_sushant@jssuni.edu.in)

**Abbreviation:** Nat. Env. & Poll. Technol.  
**Website:** [www.neptjournal.com](http://www.neptjournal.com)

*Received:* 14-08-2024

*Revised:* 03-10-2024

*Accepted:* 14-10-2024

## Key Words:

Aridity index  
Precipitation  
Evapotranspiration  
Humidity  
Mann-Kendall trend test

## ABSTRACT

Understanding aridity trends is crucial for climate adaptation strategies. This study analyzes the spatial and temporal fluctuations in aridity across Karnataka, India, over 63 years from 1958 to 2020 using the Aridity Index (AI). Monthly, seasonal, and annual AI values were calculated using precipitation and potential evapotranspiration data sourced from TerraClimate. The results indicate that approximately 74% (142,464 sq. km) of Karnataka is classified as dryland, ranging from semi-arid to dry subhumid zones, while 26% (49,416 sq. km) falls under more humid non-dryland areas. The Malnad and coastal regions are more humid compared to the predominantly semi-arid northern inland Karnataka. Temporal analysis between the periods 1958–1990 and 1991–2020 revealed that 6.24% of the land area shifted from semi-arid to dry subhumid, indicating increased moisture availability, whereas 0.43% shifted from dry subhumid to semi-arid, suggesting localized aridification. During the post-monsoon season, 14.12% of dryland areas transitioned to non-dryland, with substantial improvements in moisture availability observed in districts such as Uttara Kannada (59.21%) and Mandya (82.97%). Conversely, 1.5% of non-dryland areas converted to dryland, indicating localized decreases in water resources. Seasonal analysis revealed that 99.92% of the summer aridity status remained constant, while during the monsoon season, only 2.42% of dryland areas changed to non-dryland, reflecting stable monsoonal rainfall patterns. These findings highlight the significant influence of topography, monsoonal patterns, and water management on aridity dynamics in Karnataka. The study provides valuable insights for developing policies on climate adaptation, sustainable agriculture, and regional water resource management. Addressing the increasing trends in aridity is essential to reduce desertification risks and enhance the State's resilience to climate change.

## Citation for the Paper:

Sawant S. A., Dhananjayen and Sasi, M., 2025. Spatio-temporal analysis of aridity trends and shifts in Karnataka over 63 years (1958-2020): Insights into climate adaptation. *Nature Environment and Pollution Technology*, 24(2), p. B4255. <https://doi.org/10.46488/NEPT.2025.v24i02.B4255>

*Note: From year 2025, the journal uses Article ID instead of page numbers in citation of the published articles.*



**Copyright:** © 2025 by the authors  
**Licensee:** Technoscience Publications  
This article is an open access article distributed under the terms and conditions of the Creative Commons Attribution (CC BY) license (<https://creativecommons.org/licenses/by/4.0/>).

## INTRODUCTION

Climate vulnerability is the propensity of human populations to be adversely affected by the consequences of climate change, taking into account exposure, sensitivity, and adaptive capability (Turner et al. 2003). The Aridity Index (AI) is a quantitative measure of the degree of dryness of climate in a particular region. The only study that meets the quantitative variables criteria and has a computation that correctly identifies the climatic condition in question. AI is often employed in studies regarding the detection of dry surfaces and a region's vulnerability to desertification. It is said to be very precise in defining these areas (de Jesus et al. 2019). Aridity is one of the aspects that can be used to classify climate sensitivity, and it refers to the degree of dryness of a region. This dryness is measured using the Aridity Index (AI), which is a critical parameter when mapping areas of dryness (Alawadi et al. 2024) and their sensitivity to desertification. As a result of climatic change, there is an increase in arid and semi-arid regions across the globe. PET is higher than AET in all climate regions, thus enhancing aridity (Shoshany et al. 2023). It conjures up pictures of barren, arid landscapes devoid of precipitation and natural surface water bodies (Mustafa et al. 2018). Regions

that are characterized by arid and semi-arid environments in the world are very sensitive to changes in land use and or climate occasioned by human beings. The process of desertification is regarded to be one of the most vital impacts of global warming on the environment. The research that has been carried out shows that total PET augments the dryness in all the climatic zones since it exceeds the precipitation, whether it is annual or seasonal (Pour et al. 2020). Climate models predicted that the worldwide arid and semi-arid climate area will increase by 11% to 23% by 2100, which will exacerbate aridification in various regions of the world (Ahmed et al. 2019). Numerous scholars have examined the spatial variance, shifting of climate, and trends of the global and regional aridity index (Mustafa et al. 2018, Kumar et al. 2021, Ramarao et al. 2019, Önder et al. 2009, Ahmed et al. 2019, Ramachandran et al. 2015, Sarma & Singh 2019, Pour et al. 2020).

Two-thirds of the workforce in India is employed in agriculture and related industries. The country is an agrarian society. It is the most rain-fed country in the world, with almost 61 percent of farmers relying on it (Kumar et al. 2021). Estimating aridity patterns has a big influence on climate change worldwide. Arid and semiarid regions comprise around 40% of the Earth's total area (Mustafa et al. 2018). Rainfall, evapotranspiration, and temperature are the aspects of climate that are of importance to the productivity of agriculture. The climate is gradually altering in some aspects of India, especially in the semi-arid regions where the dry season is longer, water is scarce, and regions are prone to desertification. It is essential to understand these trends in the context of designing strategies for mitigating the impact of climate change on agriculture, water resources, and sustainable development in India (Sharma et al. 2023).

Trends of aridity in the geography of Karnataka depend a lot on the plateau area, western ghats, and other coastal areas of the state. Spread over the large area of the Deccan plateau, which essentially is a trapezium of the semi-arid region. The region boasts several river basins, such as the rivers Krishna, Kaveri/Tapi, and Tungabhadra, that support a high level of agriculture. (Shankara et al. 2023). These bodies of water are essential for producing hydroelectric power and for irrigation, but the plateau is especially susceptible to the effects of climate change, which can worsen aridity and have an impact on the water supply (Ghimire et al. 2019). The natural equilibrium and water resources of the state largely depend on the colossal rainfall of the Western Ghats. It means that coastal areas can affect the state's general climatic adaptability to heat, water avails, farming, and other trends pointing to the escalation of dryness even while they are blessed with humid tropical marine conditions (Mann et al. 2023).

The analysis comparing the changes of aridity in Karnataka, India (Table 1) points out how important it is to understand climate change to foresee and maintain the policies and planning. Coastal areas remain somewhat marshy, which is still possible for human existence, but increasing desertification in the interior zone of Karnataka poses threats to water and sustainable farming (Beeraladinni & Patil 2023). Research of temporal and spatial characteristics of aridity can contribute to the development of strategies for increasing climate resistance depending on the availability of water and water resources for sustainable agriculture under conditions of climate change (Xu et al. 2023). Planning for regional water conservation, irrigation infrastructure, agriculture sustainability, and climate resilience policies in Karnataka can be informed by the aridity information generated.

## MATERIALS AND METHODS

### Study Area

Karnataka, a state in southwest India, is renowned for its vibrant economy and rich cultural legacy. The geographic coordinates of Karnataka (Fig.1) are latitude 11.6° N and longitude 18.5° E and 74.1° E, respectively. It is crucial to understand that this state has an incredible variety of topography, climate, and ecosystems, which are distinguished by a variety of topographical features, including the Deccan Plateau, the Eastern Ghats, and the Western Ghats. The Western Ghats, with their abundant vegetation and rich wildlife, are crucial for maintaining Karnataka's balance of nature. On the other hand, due to its undulating landscape, the Deccan Plateau completely supports agricultural activity. The Eastern plains are less noticeable and do not play a significant role. The state's varied geography is the cause of its varying climate. Adjacent to the enormous Arabian Sea on the west, the coastline regions experience a humid, tropical maritime environment. Furthermore, it is noteworthy that the Western Ghats have relatively high rainfall, which supports lush forests and feeds the main rivers that traverse the state of Karnataka.

Table 1: Index values of AI Subtypes (Mustafa et al. 2018) (Pinjarla et al. 2021).

Climate Type	Aridity Index
<b>Dryland Subtypes</b>	
Hyper-arid	AI ≤ 0.05
Arid	AI ≤ 0.2
Semi-arid	AI ≤ 0.5
Dry Subhumid	AI ≤ 0.65
<b>Non-Drylands</b>	
Humid	AI > 0.65
Cold	PET < 400mm



The semi-arid environment of the Deccan Plateau supports agricultural activity with the help of rivers and reservoirs. There is an extensive network of watercourses throughout Karnataka, the most prominent being the Krishna, Kaveri, and Tungabhadra. The state's topography includes the coastal strip, the humid Western Ghats, and the arid Deccan Plateau, all of which contribute to the state's varying levels of aridity (Tripti et al. 2016). Due to their high evapotranspiration and low rainfall, the northern inland areas are primarily semi-arid and, therefore, susceptible to rising trends in aridity. The Malnad region in the Western Ghats, on the other hand, receives a lot of rainfall, which keeps the temperature humid and promotes lush forests and a high level of biodiversity (Venkatesh et al. 2021). High humidity is a result of tropical maritime conditions in coastal Karnataka. Because of this climatic variation, a thorough analysis of aridity is required to comprehend the temporal and geographical dynamics of dryness throughout the state. This understanding is essential for managing water supplies, agricultural methods, and initiatives for climate resilience (Naik & Kunte 2023).

### Methodology

The methodology section of this research paper elucidates the process of acquiring and processing datasets essential for calculating the aridity index, a critical measure in ecological and hydrological studies. The datasets required for this computation include precipitation (PPT) and potential evapotranspiration

(PET), which were sourced from the TerraClimate database, accessible via <http://www.climatologylab.org>, in the netCDF (Network Common Data Form) format. TerraClimate is renowned for providing comprehensive climatic data, offering pivotal inputs for global-scale ecological and hydrological research. The datasets feature time-variant attributes with high spatial resolution, enabling detailed analysis of climatic variations over time.

This research utilizes the datasets representing monthly distributions spanning 63 years, from 1958 to 2020. The calculation of the Aridity Index (AI) is based on the formula proposed by the United Nations Environment Programme (UNEP) in 1992, where AI is defined as the ratio of annual precipitation to potential evapotranspiration ( $AI = PPT/PET$ ) (Tegos et al. 2023). This formula facilitates the derivation of the monthly Aridity Index, which serves as a foundational element for subsequent calculations (Tegos et al. 2023). The study extends the utility of these monthly indices to compute temporal, seasonal, and annual aridity indices, thereby enabling a multifaceted analysis of aridity trends over the study period (Fig.2).

## RESULTS AND DISCUSSION

### Spatial Analysis of Yearly Mean Aridity Index for 63 years (1958-2020)

Karnataka, which covers 191,881 sq. km, has two main



Fig. 1: Study area Map.

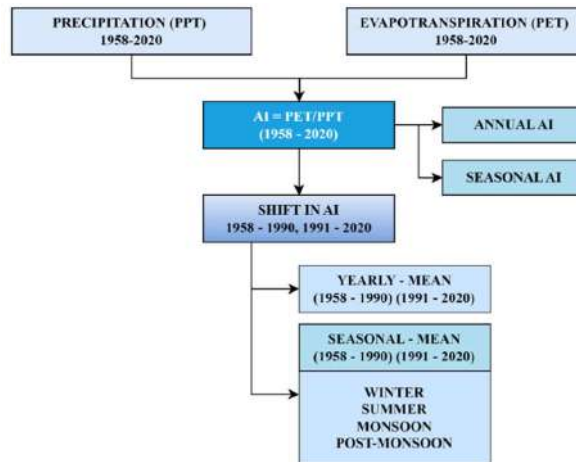


Fig. 2: Flow chart of Aridity Index, Karnataka.

climate types, according to the research: non-dryland areas and dryland variants. Dryland, with 142,464 square kilometers, makes up around 74% of the state and has semi-arid and dry-subhumid climates. The Western Ghats' rain shadow effect, which blocks the southwest monsoon winds and reduces rainfall and arid conditions, is the main factor influencing these dryland areas (Dupdal et al. 2022) in districts such as Bagalkot, Vijayapura, and Kalburgi. The remaining 26% of the state, or 49,416 square kilometers, is classified as non-dryland and has a humid climate. This comprises regions that receive substantial rainfall due to the orographic lift of moist monsoon winds over the Western Ghats, such as Uttara Kannada, Udupi, Dakshina Kannada, and Kodagu (Fig. 3).

Known for hot and occasionally extremely hot conditions, the semi-arid regions include districts like Bagalkot, Vijayapura, Kalburgi, Bidar, Raichur, Koppal, Gadag, Haveri, Ballari, Chitradurga, Tumakuru, Kolar, Bengaluru (Urban), Bengaluru (Rural), Mandya, Chikkaballapura, Ramanagara, Yadgir, and Vijayanagara (Chowdari et al. 2023). The orographic lift effect, on the other hand, causes the Western Ghats and coastal areas, which include districts like Uttara Kannada and Kodagu, to have a humid climate (Venkatesh et al. 2021). In addition, districts with a combination of humid, semi-arid, and dry-subhumid climates include Belagavi, Dharwad, Chikkamagaluru, Hassan, Davanagere, Shivamogga, Chamarajanagara, and Mysuru. Their position as a transition zone between the arid interior regions and the Western Ghats has resulted in a variety of microclimates, which in turn has caused this climatic diversity. So, the interaction of terrain, monsoonal patterns, and regional geography results in the total climatic heterogeneity in Karnataka.

### Spatial Analysis of Winter Seasonal Mean Aridity Index for 63 years (1958-2020)

Karnataka is mostly characterized by severely dryland subtypes during this time, according to an analysis of the winter seasonal aridity index data. To be more precise, a dry-subhumid climate is found in just 5% (10,342 sq. km) of the state, while 95% (181,539 sq. km) of the state is classed as semi-arid. Belagavi, Kalburgi, Kolar, Kodagu, Mysuru, Chamarajanagara, and Ramanagara are among the districts

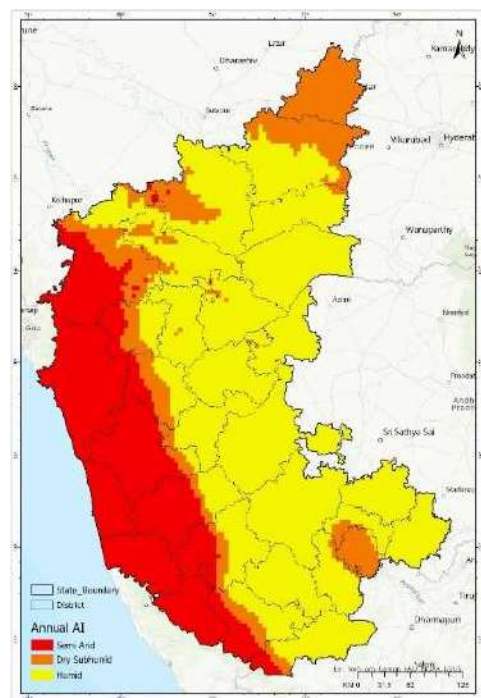


Fig. 3: Annual Mean Aridity Index for 63 years (1958-2020).

that have small areas of dry-subhumid climate, whereas the remaining districts are primarily semi-arid (Fig. 4).

This extensive semi-arid state in the winter months is caused by the monsoonal rainfall significantly decreasing and the northeast monsoon winds being predominant. By October, the southwest monsoon has passed, leaving the area with less moisture, which causes lower humidity and higher evaporation rates (Chowdari et al. 2023). The Western Ghats and other geological features of Karnataka, along with the lack of significant winter rainfall, exacerbate the dry conditions and prohibit the occurrence of humid climates (Venkatesh et al. 2021). This demonstrates the critical influence that monsoonal cycles and seasonal wind patterns have on determining the winter climate of Karnataka.

### **Spatial Analysis of Summer Seasonal Mean Aridity Index for 63 years (1958-2020)**

The summer seasonal statistics reveal that only 1% (1,319 sq. km) of Karnataka is classified as non-dryland, while 99% (190,562 sq. km) comprises dryland subtypes. Non-dryland climates are present in 11% and 20% of Dakshina Kannada and Kodagu districts, respectively. The remaining districts predominantly exhibit semi-arid climates (95%) and dry-subhumid climates (4%) (Fig. 5).

Due to high temperatures and a delayed start of the southwest monsoon, dryland subtypes predominate in Karnataka throughout the summer months. After a protracted hot and dry stretch that leaves vast arid conditions in its wake, the monsoon usually arrives in June (Chowdari et al. 2023). Due to its early pre-monsoon showers and location along the Western Ghats, only portions of Dakshina Kannada and Kodagu maintain non-dryland climates (Mann et al. 2023). This highlights the impact of delayed monsoonal rainfall and high summer temperatures on Karnataka's climate.

### **Spatial Analysis of Monsoon Seasonal Mean Aridity Index for 63 Years (1958-2020)**

During the monsoon season, approximately 80% of Karnataka (153,119 sq. km) experiences a humid climate, while 20% (38,761 sq. km) falls under dryland subtypes. Over 75% of the areas in districts such as Belagavi, Bagalkot, Vijayapura, Kalburgi, Bidar, Raichur, Koppal, Gadag, Dharwad, Uttara Kannada, Haveri, Davanagere, Shivamogga, Udupi, Chikkamagaluru, Bengaluru (Urban), Bengaluru (Rural), Dakshina Kannada, Kodagu, Yadgir, and Vijayanagara are classified as humid. Conversely, districts like Ballari (32%), Chitradurga (92%), Tumakuru (67%), Kolar (64%), Mandya (96%), Hassan (38%), Mysuru (43%), Chamarajanagara (81%), Chikkaballapura (41%),

and Ramanagara (33%) have significant portions classified as semi-arid and dry subhumid (Fig. 6).

The extensive humid climate during the monsoon season results from the intense southwest monsoon winds, bringing heavy rainfall across most of the state. This increases humidity levels, particularly in areas along the Western Ghats and coastal regions, where orographic lift enhances rainfall (Venkatesh et al. 2021). Districts with sizable dryland subtypes experience reduced monsoonal rainfall as a result of their topographical barriers and geographic location, producing shadows cast by rain. This distribution highlights how important regional topography and monsoonal patterns are in determining the seasonal climatic dynamics of Karnataka (Chowdari et al. 2023).

### **Spatial Analysis of Post Monsoon Seasonal Mean Aridity Index for 63 years (1958-2020)**

Approximately 70% of Karnataka's area falls under dryland subtypes, while 30% is classified as non-dryland climate. Over 75% of Udupi, Kolar, Bengaluru (Urban), Bengaluru (Rural), Mandya, Dakshina Kannada, Kodagu, Mysuru, Chamarajanagara, and Ramanagara districts experience a humid climate. In contrast, over 75% of Belagavi, Bagalkot, Vijayapura, Kalburgi, Bidar, Raichur, Koppal, Gadag, Dharwad, Haveri, Ballari, Chitradurga, Davanagere, Tumakuru, Yadgir, and Vijayanagara districts are classified as dryland subtypes. Districts like Uttara Kannada, Shivamogga, Chikkamagaluru, Hassan, and Chikkaballapura exhibit both dry-subhumid and humid climates during the post-monsoon season (Fig. 7).

The Western Ghats' rain shadow effect, which restricts the reach of monsoonal rainfall and creates vast semi-arid and dry-subhumid conditions, and the state's varied topography are the main causes of Karnataka's predominance of dryland

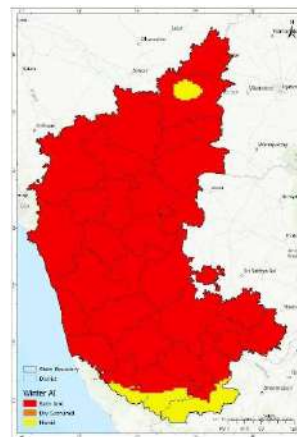


Fig. 4: Winter Mean Aridity Index for 63 years.



Fig. 5: Summer Mean Aridity Index for 63 years.

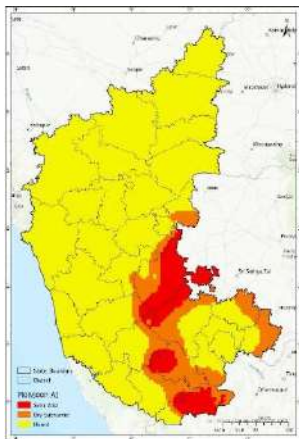


Fig. 6: Monsoon Mean Aridity Index for 63 years.

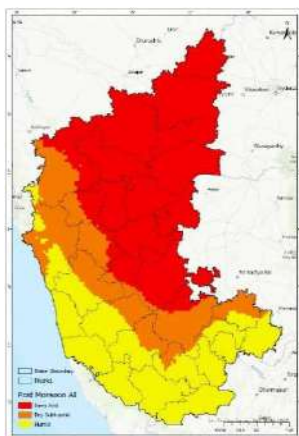


Fig. 7: Post-Monsoon Mean Aridity Index for 63 years.

orographic lift and the southwest monsoon winds, which provide significant rainfall and elevated humidity levels. Districts like Uttara Kannada and Shivamogga see a post-monsoon climate that retains the monsoon's lasting impacts, with residual moisture preserving a balance between humid and dry-subhumid temperatures. This demonstrates how, crucially, regional topography and monsoonal patterns affect Karnataka's seasonal climate changes (Johnson et al. 2017).

### Shifting of Aridity Index

**Spatial analysis of yearly mean aridity index shifts in different districts of Karnataka between 1958-1990 (33yrs) and 1991-2020 (30 yrs):** The metrics that are displayed comprise the area that changes from being classified as dryland to non-dryland, the areas that remain unchanged, and the overall area of the district across two consecutive multi-decadal periods per year. The analysis shows that there are very few changes in aridity at the state level, with only 0.38% of Karnataka's total land area (191,881 sq km) going from dryland to non-dryland and 0.20% going the other way. In light of recent climate variability, nearly all districts (99.42%) showed no change in aridity patterns, demonstrating relative consistency in moisture availability across distinct agroclimatic zones (Fig.10) (Table 2).

District-level changes in dryland areas were somewhat larger in some semi-arid districts (Mysuru, Hassan, Shivamogga, Chikkamagaluru), with shifts ranging from 3 to 4%. These shifts were mainly due to the marginal development of non-dryland zones. But even in these districts, the aridity didn't change much, and the district remained over 95% steady. Concurrently, the dryland area changed by exactly 0% in 20 out of 31 districts. The meticulous geographical examination reveals that for the previous fifty years, Karnataka's winter and annual moisture availability have stayed comparatively consistent. Due to the state's varied terrain and the Western Ghats' protective role, which moderates sharp fluctuations in moisture availability and stabilizes local climates, the state is stable (Pinjarla et al. 2021).

**Spatial analysis of yearly mean aridity index shifting in subtypes of arid lands between 1958-1990 (33yrs) and 1991-2020 (30yrs):** Karnataka's yearly mean aridity index from 1958-1990 to 1991-2020 was analyzed spatially, and the results indicate that while 6.24% of the land area changed from semi-arid to dry subhumid, indicating increasing moisture availability, 93.12% of the districts did not change in aridity type. This change improves livelihoods in agriculture and water resources. Conversely, drier conditions resulted from a shift in the land area from dry subhumid to semi-arid due to decreased or irregular rainfall, accounting for 0.43% of the total land area. Furthermore, 0.20 percent

subtypes (Gangadhara 2017). In contrast, the areas with primarily humid climates profit from the Western Ghats'



Table 2: Spatial Analysis of Annual Mean Aridity Index Shifting between 1958 – 1990 (33yrs) and 1991 - 2020 (30yrs).

District Names	Dryland to Non Drylands in sq. km.	Non Drylands to Dryland in sq. km.	No Shift area in sq. km.	Total area in sq. km.	%age of Area in shifting Dryland to Non Drylands	%age of Area in shifting Non Drylands to Dryland	%age of area with No Shift
<b>Karnataka State</b>	731.00	390.00	190760.00	<b>191881</b>	0.38	0.20	99.42
Belagavi	45.00	307.00	13056.00	<b>13408</b>	0.34	2.29	97.37
Bagalkot	6.00	0.00	6561.00	<b>6567</b>	0.09	0.00	99.91
Vijayapura	76.00	0.00	10433.00	<b>10509</b>	0.72	0.00	99.28
Kalburgi	0.00	0.00	10972.00	<b>10972</b>	0.00	0.00	100.00
Bidar	0.00	0.00	5449.00	<b>5449</b>	0.00	0.00	100.00
Raichur	0.00	0.00	8466.00	<b>8466</b>	0.00	0.00	100.00
Koppal	0.00	0.00	5578.00	<b>5578</b>	0.00	0.00	100.00
Gadag	0.00	0.00	4658.00	<b>4658</b>	0.00	0.00	100.00
Dharwad	0.00	41.00	4217.00	<b>4258</b>	0.00	0.96	99.04
Uttara Kannada	0.00	0.00	10302.00	<b>10302</b>	0.00	0.00	100.00
Haveri	0.00	41.00	4780.00	<b>4821.00</b>	0.00	0.85	99.15
Ballari	0.00	0.00	4262.00	<b>4262.00</b>	0.00	0.00	100.00
Chitradurga	0.00	0.00	8435.00	<b>8435.00</b>	0.00	0.00	100.00
Davanagere	0.00	0.00	4482.00	<b>4482.00</b>	0.00	0.00	100.00
Shivamogga	83.00	0.00	8396.00	<b>8479.00</b>	0.98	0.00	99.02
Udupi	0.00	0.00	3574.00	<b>3574.00</b>	0.00	0.00	100.00
Chikkamagaluru	83.00	0.00	7131.00	<b>7214.00</b>	1.15	0.00	98.85
Tumakuru	0.00	0.00	10599.00	<b>10599.00</b>	0.00	0.00	100.00
Kolar	0.00	0.00	3980.00	<b>3980.00</b>	0.00	0.00	100.00
Bengaluru (Urban)	0.00	0.00	2193.00	<b>2193.00</b>	0.00	0.00	100.00
Bengaluru (Rural)	0.00	0.00	2298.00	<b>2298.00</b>	0.00	0.00	100.00
Mandya	0.00	0.00	4955.00	<b>4955.00</b>	0.00	0.00	100.00
Hassan	167.00	0.00	6655.00	<b>6822.00</b>	2.45	0.00	97.55
Dakshina Kannada	0.00	0.00	4848.00	<b>4848.00</b>	0.00	0.00	100.00
Kodagu	0.00	0.00	4115.00	<b>4115.00</b>	0.00	0.00	100.00
Mysuru	251.00	0.00	6061.00	<b>6312.00</b>	3.98	0.00	96.02
Chamarajanagara	21.00	0.00	5615.00	<b>5636.00</b>	0.37	0.00	99.63
Chikkaballapura	0.00	0.00	4244.00	<b>4244.00</b>	0.00	0.00	100.00
Ramanagara	0.00	0.00	3525.00	<b>3525.00</b>	0.00	0.00	100.00
Yadgir	0.00	0.00	5274.00	<b>5274.00</b>	0.00	0.00	100.00
Vijayanagara	0.00	0.00	5633.00	<b>5633.00</b>	0.00	0.00	100.00

of the land area changed from humid to dry subhumid, indicating a shift in moisture content and a tendency toward drier weather (Fig. 8, 9) (Table 3).

There have been notable increases in dry subhumid land, mostly semi-arid regions, in districts like Bengaluru (Rural), Bengaluru (Urban), Kalburgi, Ramanagara, Mysuru, Vijayapura, and Chamarajanagara. However, the least amount of aridity type change was seen in districts like Raichur, Chitradurga, Uttara Kannada, Mandya, Udupi, Dakshina Kannada, and Kodagu, which are primarily semi-

arid and humid areas. Improved water management is to blame for some areas' enhanced moisture availability, while less rainfall in other areas has resulted in drier conditions. This highlights the impact of regional water practices and climate variability on Karnataka's aridity patterns (Tripti et al. 2016).

**Spatial analysis of summer seasonal mean aridity index shifting between 1958-1990 and 1991-2020 periods in Karnataka:** During the two periods, only 0.01% (21 sq km) of Karnataka's 191,880 sq km of land went from

Table 3: Spatial Analysis of Yearly Mean Aridity Index Shifting in subtypes of arid lands between 1958 – 1990 (33yrs) and 1991 - 2020 (30yrs)

District Names	No Shift area in sq. km.	Semi-Arid to Dry Subhumid in sq. km.	Dry Subhumid to Semi-Arid in sq. km.	Humid to Dry Subhumid in sq. km	Total area in sq. km.	%age of area with No Shift	%age of Semi-Arid to Dry Subhumid	%age of Dry Subhumid to Semi-Arid	%age Humid to Dry Subhumid
<b>Karnataka State</b>	178677	11981	833	390	<b>191881</b>	93.12	6.24	0.43	0.20
Belagavi	12798	154	147	307	<b>13406</b>	95.46	1.15	1.10	2.29
Bagalkot	6329	232	6	0	<b>6567</b>	96.38	3.53	0.09	0.00
Vijayapura	9833	599	76	0	<b>10508</b>	93.58	5.70	0.72	0.00
Kalburgi	6557	4414	0	0	<b>10971</b>	59.77	40.23	0.00	0.00
Bidar	5429	19	0	0	<b>5448</b>	99.65	0.35	0.00	0.00
Raichur	8466	0	0	0	<b>8466</b>	100.00	0.00	0.00	0.00
Koppal	5354	224	0	0	<b>5578</b>	95.98	4.02	0.00	0.00
Gadag	4614	44	0	0	<b>4658</b>	99.06	0.94	0.00	0.00
Dharwad	4197	19	42	0	<b>4258</b>	98.57	0.45	0.99	0.00
Uttara Kannada	10302	0	0	0	<b>10302</b>	100.00	0.00	0.00	0.00
Haveri	4572	208	41	0	<b>4821</b>	94.84	4.31	0.85	0.00
Ballari	4204	58	0	0	<b>4262</b>	98.64	1.36	0.00	0.00
Chitradurga	8435	0	0	0	<b>8435</b>	100.00	0.00	0.00	0.00
Davanagere	4441	41	0	0	<b>4482</b>	99.09	0.91	0.00	0.00
Shivamogga	8299	97	83	0	<b>8479</b>	97.88	1.14	0.98	0.00
Udupi	3574	0	0	0	<b>3574</b>	100.00	0.00	0.00	0.00
Chikkamagaluru	7021	110	83	0	<b>7214</b>	97.32	1.52	1.15	0.00
Tumakuru	10410	188	0	0	<b>10598</b>	98.23	1.77	0.00	0.00
Kolara	3939	41	0	0	<b>3980</b>	98.97	1.03	0.00	0.00
Bengaluru (Urban)	828	1365	0	0	<b>2193</b>	37.76	62.24	0.00	0.00
Bengaluru (Rural)	679	1619	0	0	<b>2298</b>	29.55	70.45	0.00	0.00
Mandya	4955	0	0	0	<b>4955</b>	100.00	0.00	0.00	0.00
Hassan	6327	328	166	0	<b>6821</b>	92.76	4.81	2.43	0.00
Dakshina Kannada	4848	0	0	0	<b>4848</b>	100.00	0.00	0.00	0.00
Kodagu	4115	0	0	0	<b>4115</b>	100.00	0.00	0.00	0.00
Mysuru	5611	450	250	0	<b>6311</b>	88.91	7.13	3.96	0.00
Chamarajanagara	5299	315	21	0	<b>5635</b>	94.04	5.59	0.37	0.00
Chikkaballapura	4184	59	0	0	<b>4243</b>	98.61	1.39	0.00	0.00
Ramanagara	2361	1164	0	0	<b>3525</b>	66.98	33.02	0.00	0.00
Yadgir	5047	226	0	0	<b>5273</b>	95.71	4.29	0.00	0.00
Vijayanagara	5629	4	0	0	<b>5633</b>	99.93	0.07	0.00	0.00

dryland to non-dryland, while 0.06% (123 sq km) went from non-dryland to dryland. Over the thirty years, a staggering 99.92% (191,736 sq km) of the state's summer aridity levels stayed unaltered. Except for Dakshina Kannada and Kodagu, nearly all districts had little change (Fig. 11) (Table 4). The summertime moisture availability is consistent, which emphasizes the enduring climatic conditions—such as

increasing temperatures and little precipitation—that sustain high levels of aridity.

Dakshina Kannada saw a minor improvement in aridity, with 0.33% (16 sq km) going from dryland to non-dryland. This suggests that localized precipitation patterns have somewhat alleviated aridity. Kodagu also exhibits a little improvement. The analysis highlights the ongoing moisture

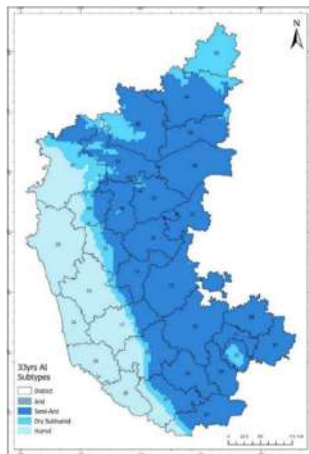


Fig. 8: Area Shifts of Aridity Index for 1958-1990.

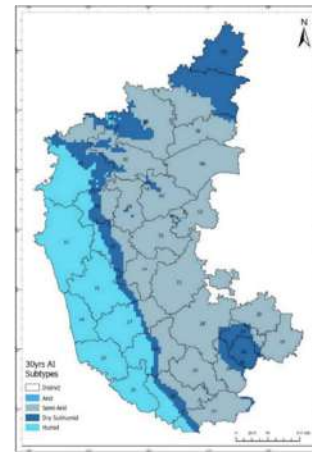


Fig. 9: Area Shifts of Aridity Index for 1991-2020.

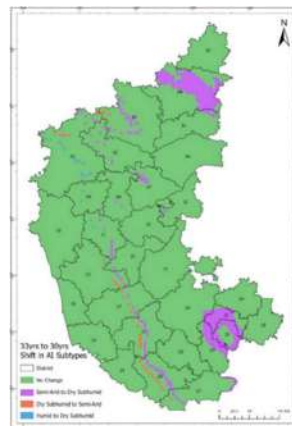


Fig. 10: Area Shifts of Aridity Index between 1958-1990 and 1991-2020.

deficit throughout the state throughout the summer months and shows that Karnataka's summer aridity has been mostly steady from 1991 to 2020 compared to earlier decades.

**Spatial analysis of monsoon seasonal mean aridity index shifting between 1958-1990 and 1991-2020 periods in Karnataka:** Out of Karnataka's total area of 191,881 sq km, only 2.42% (4,652 sq km) of dryland shifted to non-dryland, with no shift from non-dryland to dryland. A vast majority, 97.58% (187,229 sq km), remains unchanged, indicating stable moisture levels during monsoons. Districts like Belagavi, Kalburgi, Koppal, Uttara Kannada, Udupi, and Dakshina Kannada saw no shift in aridity patterns, suggesting consistent monsoon rainfall over the past 30 years (Fig. 12) (Table. 5).

Partial dryland to non-dryland conversion is observed in Ballari (12.41%), Chitradurga (5.61%), Davanagere (7.90%), Tumakuru (8.63%), Kolar (14.47%), and Chikkaballapura (15.74%) due to localized increases in precipitation. The

limited percentage of relocated areas overall indicates that Karnataka's monsoon rainfall patterns have remained relatively steady, with some districts seeing slight improvements due to localized meteorological conditions and efficient water management.

**Spatial analysis of post-monsoon seasonal mean aridity index shifting between 1958-1990 (33yrs) and 1991-2020 (30yrs):** The analysis classifies Karnataka's land changes into drylands turning to non-drylands, non-drylands turning to drylands, and no-shift areas. Out of 191,881 sq km, 14.12% (27,087 sq km) of dryland transitioned to non-dryland, while 1.50% (2,877 sq km) of non-dryland shifted to dryland, indicating improved moisture availability over the past 30 years. A significant 84.38% (161,917 sq km) saw no change, suggesting stable aridity levels (Fig. 13) (Table 6). Districts like Bidar, Kalburgi, and Raichur showed no aridity shift.

Significant dryland to non-dryland shifts occurred in Uttara Kannada (59.21%), Mandya (82.97%), Hassan

Table 4: Spatial Analysis of Summer Mean Aridity Index Shifting between 1958-1990 (33 yrs) and 1991-2020 (30 yrs).

District Names	Dryland to Non Drylands in sq. km.	Non Drylands to Dryland in sq. km.	No Shift area in sq. km.	Total area in sq. km.	%age of Area in shifting Dryland to Non Drylands	%age of Area in shifting Non Drylands to Dryland	%age of area with No Shift
<b>Karnataka State</b>	21.00	123.00	191736.00	<b>191880</b>	0.01	0.06	99.92
Belagavi	0.00	0.00	13408.00	<b>13408</b>	0.00	0.00	100.00
Bagalkot	0.00	0.00	6566.00	<b>6566</b>	0.00	0.00	100.00
Vijayapura	0.00	0.00	10508.00	<b>10508</b>	0.00	0.00	100.00
Kalburgi	0.00	0.00	10972.00	<b>10972</b>	0.00	0.00	100.00
Bidar	0.00	0.00	5449.00	<b>5449</b>	0.00	0.00	100.00
Raichur	0.00	0.00	8466.00	<b>8466</b>	0.00	0.00	100.00
Koppal	0.00	0.00	5578.00	<b>5578</b>	0.00	0.00	100.00
Gadag	0.00	0.00	4658.00	<b>4658</b>	0.00	0.00	100.00
Dharwad	0.00	0.00	4258.00	<b>4258</b>	0.00	0.00	100.00
Uttara Kannada	0.00	0.00	10302.00	<b>10302</b>	0.00	0.00	100.00
Haveri	0.00	0.00	4821.00	<b>4821.00</b>	0.00	0.00	100.00
Ballari	0.00	0.00	4262.00	<b>4262.00</b>	0.00	0.00	100.00
Chitradurga	0.00	0.00	8435.00	<b>8435.00</b>	0.00	0.00	100.00
Davanagere	0.00	0.00	4482.00	<b>4482.00</b>	0.00	0.00	100.00
Shivamogga	0.00	0.00	8479.00	<b>8479.00</b>	0.00	0.00	100.00
Udupi	0.00	0.00	3574.00	<b>3574.00</b>	0.00	0.00	100.00
Chikkamagaluru	0.00	0.00	7214.00	<b>7214.00</b>	0.00	0.00	100.00
Tumakuru	0.00	0.00	10599.00	<b>10599.00</b>	0.00	0.00	100.00
Kolara	0.00	0.00	3980.00	<b>3980.00</b>	0.00	0.00	100.00
Bengaluru (Urban)	0.00	0.00	2193.00	<b>2193.00</b>	0.00	0.00	100.00
Bengaluru (Rural)	0.00	0.00	2298.00	<b>2298.00</b>	0.00	0.00	100.00
Mandya	0.00	0.00	4955.00	<b>4955.00</b>	0.00	0.00	100.00
Hassan	0.00	0.00	6821.00	<b>6821.00</b>	0.00	0.00	100.00
Dakshina Kannada	16.00	102.00	4730.00	<b>4848.00</b>	0.33	0.33	97.57
Kodagu	5.00	21.00	4090.00	<b>4116.00</b>	0.12	0.12	99.37
Mysuru	0.00	0.00	6312.00	<b>6312.00</b>	0.00	0.00	100.00
Chamarajanagara	0.00	0.00	5636.00	<b>5636.00</b>	0.00	0.00	100.00
Chikkaballapura	0.00	0.00	4244.00	<b>4244.00</b>	0.00	0.00	100.00
Ramanagara	0.00	0.00	3525.00	<b>3525.00</b>	0.00	0.00	100.00
Yadgir	0.00	0.00	5274.00	<b>5274.00</b>	0.00	0.00	100.00
Vijayanagara	0.00	0.00	5633.00	<b>5633.00</b>	0.00	0.00	100.00

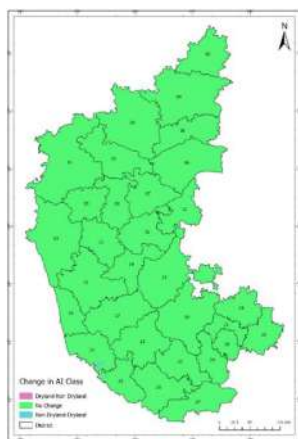


Fig. 11: Spatial Analysis of Summer Mean Aridity Index Shifting between 1958-1990 and 1991-2020.

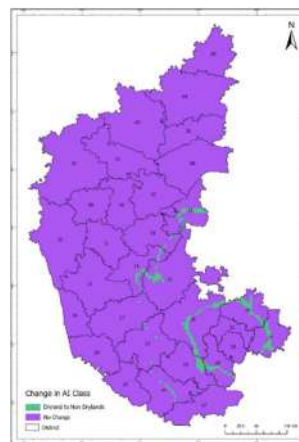


Fig. 12: Spatial Analysis of Monsoon Mean Aridity Index Shifting between 1958-1990 and 1991-2020.



Table 5: Spatial Analysis of Monsoon Mean Aridity Index Shifting between 1958-1990 (33yrs) and 1991-2020 (30 yrs).

S.No.	District Names	Dryland to Non Drylands in sq. km.	Non Drylands to Dryland in sq. km.	No Shift area in sq. km.	Total area in sq. km.	%age of Area in shifting Dryland to Non Drylands	%age of Area in shifting Non Drylands to Dryland	%age of area with No Shift
<b>0</b>	<b>Karnataka State</b>	4652.00	0.00	187229.00	<b>191881</b>	2.42	0.00	97.58
1	Belagavi	0.00	0.00	13408.00	<b>13408</b>	0.00	0.00	100.00
2	Bagalkot	0.00	0.00	6566.00	<b>6566</b>	0.00	0.00	100.00
3	Vijayapura	0.00	0.00	10508.00	<b>10508</b>	0.00	0.00	100.00
4	Kalburgi	0.00	0.00	10972.00	<b>10972</b>	0.00	0.00	100.00
5	Bidar	0.00	0.00	5449.00	<b>5449</b>	0.00	0.00	100.00
6	Raichur	0.00	0.00	8466.00	<b>8466</b>	0.00	0.00	100.00
7	Koppal	0.00	0.00	5578.00	<b>5578</b>	0.00	0.00	100.00
8	Gadag	0.00	0.00	4658.00	<b>4658</b>	0.00	0.00	100.00
9	Dharwad	0.00	0.00	4258.00	<b>4258</b>	0.00	0.00	100.00
10	Uttara Kannada	0.00	0.00	10302.00	<b>10302</b>	0.00	0.00	100.00
11	Haveri	0.00	0.00	4821.00	<b>4821.00</b>	0.00	0.00	100.00
12	Ballari	529.00	0.00	3733.00	<b>4262.00</b>	12.41	0.00	87.59
13	Chitradurga	473.00	0.00	7963.00	<b>8436.00</b>	5.61	0.00	94.39
14	Davanagere	354.00	0.00	4128.00	<b>4482.00</b>	7.90	0.00	92.10
15	Shivamogga	0.00	0.00	8479.00	<b>8479.00</b>	0.00	0.00	100.00
16	Udupi	0.00	0.00	3574.00	<b>3574.00</b>	0.00	0.00	100.00
17	Chikkamagaluru	21.00	0.00	7193.00	<b>7214.00</b>	0.29	0.00	99.71
18	Tumakuru	915.00	0.00	9685.00	<b>10600.00</b>	8.63	0.00	91.37
19	Kolar	576.00	0.00	3405.00	<b>3981.00</b>	14.47	0.00	85.53
20	Bengaluru (Urban)	0.00	0.00	2193.00	<b>2193.00</b>	0.00	0.00	100.00
21	Bengaluru (Rural)	0.00	0.00	2298.00	<b>2298.00</b>	0.00	0.00	100.00
22	Mandya	363.00	0.00	4592.00	<b>4955.00</b>	7.33	0.00	92.67
23	Hassan	83.00	0.00	6738.00	<b>6821.00</b>	1.22	1.22	98.78
24	Dakshina Kannada	0.00	0.00	4848.00	<b>4848.00</b>	0.00	0.00	100.00
25	Kodagu	0.00	0.00	4115.00	<b>4115.00</b>	0.00	0.00	100.00
26	Mysuru	188.00	0.00	6124.00	<b>6312.00</b>	2.98	2.98	97.02
27	Chamarajanagara	9.00	0.00	5627.00	<b>5636.00</b>	0.16	0.16	99.84
28	Chikkaballapura	668.00	0.00	3576.00	<b>4244.00</b>	15.74	15.74	84.26
29	Ramanagara	375.00	0.00	3149.00	<b>3524.00</b>	10.64	10.64	89.36
30	Yadgir	0.00	0.00	5274.00	<b>5274.00</b>	0.00	0.00	100.00
31	Vijayanagara	99.00	0.00	5534.00	<b>5633.00</b>	1.76	1.76	98.24

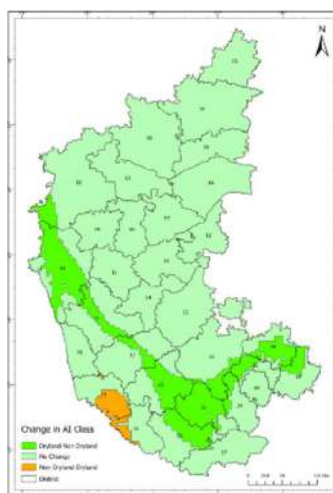


Fig. 13: Spatial Analysis of Post Monsoon Mean Aridity Index Shifting between 1958-1990 and 1991-2020.

Table 6: Spatial Analysis of Post Monsoon Mean Aridity Index Shifting between 1958-1990 (33 yrs) and 1991-2020 (30 yrs).

S.No.	District Names	Dryland to Non Drylands in sq. km.	Non Drylands to Dryland in sq. km.	No Shift area in sq. km.	Total area in sq. km.	%age of Area in shifting Dryland to Non Drylands	%age of Area in shifting Non Drylands to Dryland	%age of area with No Shift
<b>0</b>	<b>Karnataka State</b>	27087	2877	161917	<b>191881</b>	14.12	1.50	84.38
1	Belagavi	1195	0	12213	<b>13408</b>	8.91	0.00	91.09
2	Bagalkot	0	0	6566	<b>6566</b>	0.00	0.00	100.00
3	Vijayapura	0	0	10508	<b>10508</b>	0.00	0.00	100.00
4	Kalburgi	0	0	10972	<b>10972</b>	0.00	0.00	100.00
5	Bidar	0	0	5449	<b>5449</b>	0.00	0.00	100.00
6	Raichur	0	0	8466	<b>8466</b>	0.00	0.00	100.00
7	Koppal	0	0	5578	<b>5578</b>	0.00	0.00	100.00
8	Gadag	0	0	4658	<b>4658</b>	0.00	0.00	100.00
9	Dharwad	0	0	4258	<b>4258</b>	0.00	0.00	100.00
10	Uttara Kannada	6100	0	4202	<b>10302</b>	59.21	0.00	40.79
11	Haveri	0	0	4821	<b>4821</b>	0.00	0.00	100.00
12	Ballari	0	0	4262	<b>4262</b>	0.00	0.00	100.00
13	Chitradurga	0	0	8435	<b>8435</b>	0.00	0.00	100.00
14	Davanagere	0	0	4482	<b>4482</b>	0.00	0.00	100.00
15	Shivamogga	1779	0	6700	<b>8479</b>	20.98	0.00	79.02
16	Udupi	0	6	3568	<b>3574</b>	0.00	0.17	99.83
17	Chikkamagaluru	1095	0	9047	<b>10142</b>	10.80	0.00	89.20
18	Tumakuru	1553	0	9047	<b>10600</b>	14.65	0.00	85.35
19	Kolar	1080	0	2900	<b>3980</b>	27.14	0.00	72.86
20	Bengaluru (Urban)	0	0	2193	<b>2193</b>	0.00	0.00	100.00
21	Bengaluru (Rural)	1030	0	1268	<b>2298</b>	44.82	0.00	55.18
22	Mandya	4111	0	844	<b>4955</b>	82.97	0.00	17.03
23	Hassan	3284	0	3537	<b>6821</b>	48.15	48.15	51.85
24	Dakshina Kannada	0	2062	2786	<b>4848</b>	0.00	0.00	57.47
25	Kodagu	0	808	3308	<b>4116</b>	0.00	0.00	80.37
26	Mysuru	2818	0	3494	<b>6312</b>	44.65	44.65	55.35
27	Chamarajanagara	51	0	5585	<b>5636</b>	0.90	0.90	99.10
28	Chikkaballapura	2150	0	2093	<b>4243</b>	50.67	50.67	49.33
29	Ramanagara	839	0	2685	<b>3524</b>	23.81	23.81	76.19
30	Yadgir	0	0	5274	<b>5274</b>	0.00	0.00	100.00
31	Vijayanagara	0	0	5633	<b>5633</b>	0.00	0.00	100.00

(48.15%), Mysuru (44.65%), and Chikkaballapura (50.67%) due to expanded irrigation. Conversely, Dakshina Kannada saw a major shift from non-dryland to dryland (2,062 sq km), likely due to depleting water sources in the Western Ghats. This indicates localized improvements in moisture availability but overall stability in aridity across Karnataka.

#### Spatial analysis of winter seasonal mean aridity index

**shifting between 1958-1990 and 1991-2020 periods in Karnataka:** Karnataka state in southern India has a heterogeneous climate ranging from semi-arid to wet-and-dry across districts. The Spatial mapping of the mean aridity index showed no major difference between the 1991-2020 period compared to the 1958-1990 baseline period across different districts. These findings indicate winter aridity patterns have remained largely similar in the state.

## CONCLUSION

The temporal and spatial variations in aridity of Karnataka have been analyzed in the context of the 63-year data which in turn portrays the climatic variability of the region. When using extensive geospatial research, the distribution of arid zones in the state of Karnataka is presented, and it is affirmed that more than three-quarters of the state is categorized as semi-arid or dry subhumid dryland type while the rest of the area, slightly under one quarter, falls under the non-dryland or humid type category. The different forms of fluctuation in aridity revealed in the Deccan Plateau, the Western Ghats, and the coastal areas show how set-up factors such as topographical and climatic features affect different regions. Flora and Fauna account for specific regional climate differences, the increased dryness in winter compared to the humidity during the monsoon season. Thus, the trends indicate that the 6 level is decreasing in the long term. 24% of the region's aridity and an increase of 0 each, respectively. All these sums to the total of 43% over the study period and have become apparent thanks to the application of the Mann-Kendall test.

The significant analysis highlights the need to intensify policy measures and strategic development where especially water conservation, sustainable agriculture and climate change resilience need to be enhanced. The inherent climatic differences that define the difficulties faced by various regions in Karnataka form the basis of the recommendations for the planning and the development of strategies that would effectively address the climatic issues. This study suggests that in bid to reduce the impact of climatic fluctuations on water resources and food production to its minimum, concentrated resource management strategies that are flexible should be encouraged.

## REFERENCES

- Ahmed, K., Shahid, S., Wang, X., Nawaz, N. and Khan, N., 2019. Spatio-temporal changes in aridity of Pakistan during 1901–2016. *Hydrology and Earth System Sciences*, 23(7), pp.3081–3096. DOI
- Alawadi, W., Hassan, A.A. and Dakhil, A., 2024. Evaluation of Grid-Based Aridity Indices in Classifying Aridity Zones in Iraq. *Nature Environment and Pollution Technology*, 23(2), pp.1151–1160. DOI
- Beeraladinni, D. and Patil, B.L., 2023. Agricultural sustainability in Karnataka: Application of sustainable livelihood security index. *The Indian Journal of Agricultural Sciences*, 93(3), pp.308–313. DOI
- Chowdari, K.K., Deb Barma, S., Bhat, N., Girisha, R., Gouda, K.C. and Mahesha, A., 2023. Trends of seasonal and annual rainfall of semi-arid districts of Karnataka, India: application of innovative trend analysis approach. *Theoretical and Applied Climatology*, 152(1), pp.241–264. DOI
- de Jesus, J.B., de Souza, B.B., de Oliveira, A.M.S. and Gama, D.C., 2019. Aridity index and climatic risk of desertification in the semi-arid state of Sergipe. *Revista Brasileira de Climatologia*, 24. DOI
- Dupdal, R., Patil, B.L., Manjunatha, B.L. and Patil, S.L., 2022. Climate change mitigation and adaptation strategies in drylands of Northern Karnataka. *Indian Journal of Agricultural Sciences*, 92(1), pp.80–84. DOI
- Gangadhar, G., 2017. Analysis on spatial variation of rainfall and ground-water fluctuation in Hebballa watershed, Mysore district, Karnataka, India. *International Journal of Trend in Scientific Research and Development*, 2(1), pp.1291–1297. DOI
- Ghimire, S., Dhungana, N. and Upadhaya, S., 2019. Impacts of climate change on water availability and reservoir based hydropower: A case study from Kulekhani hydropower reservoir, Nepal. *Journal of Forest and Natural Resource Management*, 1(1), pp.52–68.
- Johnson, S.J., Turner, A., Woolnough, S., Martin, G. and MacLachlan, C., 2017. An assessment of Indian monsoon seasonal forecasts and mechanisms underlying monsoon interannual variability in the Met Office GloSea5-GC2 system. *Climate Dynamics*, 48, pp.1447–1465.
- Mann, R., Saini, D., Sharma, S., Dhorde, A. and Gupta, A., 2023. Paradoxical behaviour of rainfall and temperature over ecologically sensitive areas along the Western Ghats. *Environmental Monitoring and Assessment*, 195(12), p.1461. DOI
- Mustafa, N.F., Rashid, H.M. and Ibrahim, H.M., 2018. Aridity index based on temperature and rainfall data for Kurdistan region-Iraq. *Journal of Duhok University*, 21(1), pp.65–80. DOI
- Naik, D.D. and Kunte, P.D., 2023. Integrated coastal vulnerability assessment: A study of Karnataka, India. *Disaster Advances*, 16(7), pp.18–30. DOI
- Önder, D., Aydın, M., Berberoğlu, S., Önder, S. and Yano, T., 2009. The use of aridity index to assess implications of climatic change for land cover in Turkey. *Turkish Journal of Agriculture and Forestry*, 33(3), pp.305–314. DOI
- Pinjarla, B., Joshi, P.K. and Roy, P.S., 2021. Long Term Spatio-temporal variations of seasonal and decadal aridity in India. *Journal of Atmospheric Science Research*, 4(3). DOI
- Pour, S.H., Abd Wahab, A.K. and Shahid, S., 2020. Spatiotemporal changes in aridity and the shift of drylands in Iran. *Atmospheric Research*, 233, p.104704. DOI
- Ramachandran, A., Praveen, D., Jaganathan, R. and Palanivelu, K., 2015. Projected and observed aridity and climate change in the east coast of south India under RCP 4.5. *The Scientific World Journal*, 2015(1), p.169761. DOI
- Ramarao, M.V.S., Sanjay, J., Krishnan, R., Mujumdar, M., Bazaz, A. and Revi, A., 2019. On observed aridity changes over the semiarid regions of India in a warming climate. *Theoretical and Applied Climatology*, 136, pp.693–702. DOI
- Sarma, R. and Singh, D.K., 2019. Spatio-temporal analysis of drought and aridity in Gomti basin. *Current Science*, 116(6), pp.919–925.
- Shankara, M.H., Shivamurthy, M., Shivalingiah, Y.N., Sahana, S. and Padma, S.R., 2023. Vulnerability of farmers to climate change in central dry zone of Karnataka. *International Journal of Environment and Climate Change*, 13(7), pp.183–188. DOI
- Sharma, A., Khare, R. and Choudhary, M.K., 2023. Climate Change Impact Evaluation on Hydro-Meteorological Variables across a Semi-Arid Middle River Basin in India. DOI
- Shoshany, M. and Mozhaeva, S., 2023. Climate and aridity measures relationships with spectral vegetation indices across desert fringe shrublands in the South-Eastern Mediterranean Basin. *Environmental Monitoring and Assessment*, 195(5), p.563. DOI
- Tegos, A., Stefanidis, S., Cody, J. and Koutsoyiannis, D., 2023. On the sensitivity of standardized-precipitation-evapotranspiration and aridity indexes using alternative potential evapotranspiration models. *Hydrology*, 10(3), p.64. DOI
- Tripti, M., Lambs, L., Gurumurthy, G.P., Moussa, I., Balakrishna, K. and Chadaga, M.D., 2016. Water circulation and governing factors in humid tropical river basins in the central Western Ghats, Karnataka, India. *Rapid Communications in Mass Spectrometry*, 30(1), pp.175–190. DOI
- Turner, B.L., Kasperson, R.E., Matson, P.A., McCarthy, J.J., Corell, R.W., Christensen, L., Eckley, N., Kasperson, J.X., Luers, A., Martello, M.L. and Polsky, C., 2003. A framework

- for vulnerability analysis in sustainability science. *Proceedings of the National Academy of Sciences*, 100(14), pp.8074–8079. DOI
- Venkatesh, B., Nayak, P.C., Thomas, T., Jain, S.K. and Tyagi, J.V., 2021. Spatio-temporal analysis of rainfall pattern in the Western Ghats region of India. *Meteorology and Atmospheric Physics*, 133, pp.1089–1109. DOI
- Xu, L., Chen, T., Li, B., Yuan, Y. and Tsendbazar, N.E., 2023. Spatio-temporal Evolution of Arid Ecosystems Using Thematic Land Cover Products. *Remote Sensing*, 15(12), p.3178. DOI



# Enhancing Economic Benefits from Forest Preservation In Papua, Indonesia: A Review

A. A. Awirya<sup>1</sup>, K. E. N. Sianipar<sup>2</sup>, A. Kurniawan<sup>2</sup> and I. A. Sasanti<sup>3†</sup>

<sup>1</sup>Senior Economist, Bank Indonesia, Indonesia

<sup>2</sup>Junior Economist, Bank Indonesia, Indonesia

<sup>3</sup>Faculty of Economics and Business, University of Sebelas Maret, Indonesia

†Corresponding author: I. A. Sasanti; ikaalicia69@gmail.com

**Abbreviation:** Nat. Env. & Poll. Technol.

**Website:** [www.neptjournal.com](http://www.neptjournal.com)

*Received:* 28-06-2024

*Revised:* 29-08-2024

*Accepted:* 10-09-2024

## Key Words:

Economic Benefit

Forest Preservation

Social Enterprise Model Canvas

## ABSTRACT

This study aims to demonstrate the importance of the Social Enterprise Model Canvas (SEMC) as an alternative to addressing social and ecological system challenges that describe important aspects of obtaining economic benefits from forest conservation in remote areas such as Papua. The method is carried out through Systematic Reviews and Meta-Analyses (PRISMA) and qualitative content analysis process of social services implemented in Indonesia and formulated into the required SEMC using 216 documents sourced from the Scopus Core Collection database, which consists of three types of documents: articles, reviews, and book reviews. The results are: First, content analysis of environmental service payment business models in Indonesia provides insight for the government and environmental service providers. Second, the benefits scheme as part of SEMC is an important component in determining successful outcomes. Third, in special regions such as Papua which have special autonomy status, where traditional community regulations play an important role, SEMC must cover aspects of government and regional regulations. The implications of this research can be used as recommendations in determining policies related to payment for forest environmental services.

## INTRODUCTION

The growth of population and the associated demand for food and energy have led to increased exploitation of ecosystems, primarily due to forest intensification and urbanization (Schirpke et al. 2018). However, natural and semi-natural environments serve as vital reservoirs of biodiversity, which positively influence numerous ecosystem services (ES) (Reyers et al. 2012). Consequently, the degradation of these environments poses a threat to human well-being (Simonet et al. 2019). To address the loss of biodiversity and the related ecosystem services, a key agreement from the Rio + 20 conference includes a transition towards a green economy aimed at reducing environmental impacts while enhancing human welfare (UNEP 2024).

Emission control is an important focus for every country that ratified the Paris Agreement in April 2016. As much as 71.5% of greenhouse gas (GHG) emissions come from the energy sector (Wiatros-Motyka et al. 2023). The sector produces GtCO<sub>2e</sub>, with 40% of the contribution coming specifically from the electricity sector; from the same report, it was also stated that 3.22 GtCO<sub>2e</sub> came from LULUCF (Land use, land-use change, and forestry). Indonesia is ranked 11th in the world with an emission contribution of 1.59% or the equivalent of 602.59 mtCO<sub>2e</sub> (Crippa et al. 2022), and through REDD+ efforts, forest management is expected to be in harmony with steps to preserve forests and biodiversity (Simonet et al. 2019). Therefore, amid Indonesia's development stages in terms of carbon

## Citation for the Paper:

Awirya, A.A., Sianipar, K.E.N., Kurniawan, A. and Sasanti, I.A., 2025. Enhancing economic benefits from forest preservation in Papua, Indonesia: A review. *Nature Environment and Pollution Technology*, 24(2), p. D1695. <https://doi.org/10.46488/NEPT.2025.v24i02.D1695>

*Note: From year 2025, the journal uses Article ID instead of page numbers in citation of the published articles.*



Copyright: © 2025 by the authors

Licensee: Technoscience Publications

This article is an open access article distributed under the terms and conditions of the Creative Commons Attribution (CC BY) license (<https://creativecommons.org/licenses/by/4.0/>).

trading, Presidential Regulation No. 98 of 2021 concerning the Implementation of the Economic Value of Carbon to Achieve Nationally Determined Contribution Targets and Control of Greenhouse Gas Emissions in National Development (Perpres 98/2021) is regulation fundamentals that enable the implementation of carbon economic value (NEK), so that both the government and corporations in Indonesia can develop carbon financing. This is inspired by the research results of Canadell & Raupach (2008) that forest conservation in developing countries is an effective, low-cost method for reducing GHG emissions, especially if there is potential to increase the scale of GHG emission reduction programs (Bosetti & Buchner 2009).

The role of forests in controlling emissions is considered important, both as a response to and prevention of excessive emissions in the environment and as a form of preserving flora and fauna if managed well (Nandini et al. 2009). So that the achievement of emission targets with reference to the Paris Agreement can be realized in a balanced manner without many economic trade-offs in the forest management transition (Saharjo 2022). On the other hand, the results of forest management efforts can contribute to specific sectors such as tourism, the manufacturing industry, water, and agriculture, both in the form of economic benefits received directly and indirectly towards economic growth (Agrawal et al. 2013). On the other research finds out that the subject, named as Baduy community holds firm to its customs and culture, called *pikukuh*. The Baduy community applies the concept of sustainable forest management in that local communities are directly involved in forest management activities to improve welfare and implement sustainable forests (Astoria et al. 2022). Forest preservation provides a plethora of ecological, social, economic, and global benefits. Ecologically, forests serve as critical habitats for diverse flora and fauna, contributing to biodiversity conservation and ecosystem stability. They play a pivotal role in regulating both local and global climates by sequestering carbon dioxide, mitigating climate change, and influencing weather patterns. Additionally, forests uphold soil fertility, mitigate erosion, regulate hydrological cycles, and act as natural filters for air and water purification. Socially, forests offer significant cultural, recreational, and spiritual values, supporting the livelihoods and cultural practices of indigenous communities while providing recreational opportunities for urban populations. Economically, forests are invaluable resources that provide timber, non-timber forest products, and medicinal plants, contributing to local and national economies through sustainable forestry practices. Moreover, forests support tourism, ecotourism, and nature-based recreation industries, fostering revenue generation and employment opportunities (Rahma et al. 2022). From a

global perspective, forest preservation is indispensable for achieving overarching sustainability objectives, including biodiversity conservation, climate change mitigation, and the safeguarding of crucial ecosystem services that sustain life on Earth. Overall, forest preservation is essential for maintaining ecological equilibrium, promoting human well-being, fostering sustainable development, and ensuring the resilience of the planet's ecosystems. From these points, we could see that forest preservation are having a huge impact on creating a sustainable community, which leads directly to the sustainable economic growth of its specific region (Yakovleva & Subhonberdiev 2019).

In Indonesia, there's still a lack of research about a forest and its preservation, especially when we are talking about the connections with the economic perspectives. Forest research in Indonesia encompasses a broad spectrum of topics aimed at understanding and managing the country's biodiverse ecosystems amidst mounting environmental challenges. Studies often focus on documenting and conserving Indonesia's rich biodiversity through species inventories, taxonomy, and ecological assessments while also examining the effectiveness of conservation efforts in the face of deforestation threats (Patunru & Haryoko 2015). Sustainable forest management practices, including forest certification and community-based initiatives, are of paramount importance, alongside research into the impacts of logging and land-use change. Additionally, efforts to mitigate and adapt to climate change involve studying carbon sequestration, deforestation trends, and the socioeconomic implications of forest conservation policies. Fire ecology and management constitute another critical area of research, given the recurring issue of forest fires linked to land clearing and peatland degradation. Furthermore, research in Indonesia delves into the complex interplay between policy, governance, and forest management, assessing the implementation of regulations, stakeholder involvement, and land use governance frameworks. This multidisciplinary approach underscores the importance of integrating ecological, social, and economic perspectives to ensure the sustainable management and conservation of Indonesia's forests. That's why forest preservation in Indonesia yields substantial economic benefits across various sectors. The country's vast forest resources contribute significantly to its economy through timber production, non-timber forest products, and ecosystem services. Sustainable forestry practices ensure a continuous supply of timber, supporting the domestic wood industry and generating revenue from timber exports. Additionally, non-timber forest products such as rattan, rubber, and medicinal plants provide livelihood opportunities for local communities and contribute to rural economies. Forest preservation also fosters ecotourism and

nature-based recreation, attracting domestic and international tourists to explore Indonesia's rich biodiversity and pristine landscapes. Furthermore, intact forests play a crucial role in regulating hydrological cycles, reducing soil erosion, and maintaining water quality, thus supporting agriculture, fisheries, and hydropower generation. Overall, forest preservation in Indonesia not only safeguards valuable natural resources but also drives economic growth, sustains livelihoods, and promotes sustainable development for present and future generations (Djafar et al. 2023).

Limited research about forests in Indonesia needs to be considered, especially since Papua is the last hope for intact Indonesian forests, and forest cover is decreasing in Sumatra and Kalimantan. In 2012, 38 percent of Indonesia's remaining primary forest was in Papua, which is located in the western part of Papua New Guinea, the world's second-largest island, and consists of the provinces of Papua and West Papua. Papua has one of the highest levels of biodiversity in the world, with 20,000 plant species, 602 bird species, 125 mammals and 223 reptiles. This forest is also a source of livelihood for many local communities. The rate of tree cover loss in Papua reached its peak in 2015. Since then, regional leaders have started to take action. In 2015, West Papua became the first conservation province in the world, and this commitment is still upheld by the current governor in 2018. He also plans to review all forestry and plantation licenses throughout West Papua Province. Meanwhile, its neighbor, Papua Province, has also designed a road map entitled Vision 2100 Papua which targets maintaining 90 percent forest cover throughout the province in line with efforts to achieve low-carbon development goals (WRI Indonesia 2021).

However, efforts to control forest sustainability have not been optimal and implemented concretely in forestry in Indonesia. So, further study is needed to support the implementation of obtaining economic benefits. This study analyzes the potential economic benefits of forest use in Papua. Therefore, this study aims to analyze the development of efforts to obtain economic benefits from forest preservation, the business models that can be offered, and policy support through legal instruments. It is hoped that the benefits of this study can provide input for efforts to obtain economic benefits from forest preservation in Papua. This research also provides facts from a law perspective and supporting systems from financial infrastructure to broaden the economic benefit from a forest preservation perspective.

## MATERIALS AND METHODS

This study is based on a qualitative method with the Preferred Reporting Items for Systematic Reviews and Meta-Analyses

(PRISMA) and content analysis guidelines to conduct a systematic review of publications reviewed by peers. A comprehensive search of studies reviewed by peers on Payment for Ecosystem Services (PES) and Social Enterprise Model Canvas (SEMC) for sustainability was conducted using an online database, namely Scopus Core Collection. These two databases were searched in February 2024. The filters used were limited to the English language with no date restrictions. Search terms were also developed, reviewed, and refined to ensure that the collection covers the period before the final string was completed and executed. The research sample also included selected studies from the reference lists of PES review articles related to sustainability and sub-topics selected from the final list of studies filtered from Scopus in the previous step. Relevant sources found were then included in the screening process. The abstract review resulted in 53 articles discussing environmental service returns. All articles specifically discussed case studies of environmental service returns in Indonesia, aspects related to the 14 SEMC elements, which are a reference framework that can support the formulation of compensation forms for environmental services, and the relationship between environmental service returns and REDD+.

A total of 487 peer-reviewed papers were selected for screening. After a recount, before filtering out 169 duplicates, 318 papers were found eligible for full-text assessment. A further screening resulted in 101 papers that did not meet the criteria. A final screening of 1 note that did not meet completeness criteria left 216 papers deemed eligible and became the basis for a new study report (Fig. 1). This study used the sample to test the concept of payment for forest ecosystem services.

## RESULTS AND DISCUSSION

### PES Practices Development in Indonesia

PES practices in Indonesia are still polarized since there are parties who believe that PES is not an optimal solution. According to some respondents, the main challenge in fulfilling contracts is threats from the industry (Suich et al. 2017). PES in Indonesia, which has been implemented since 2002 in Banten (Lapeyre et al. 2015), shows how interactions between service providers and buyers of environmental services from the private sector utilize the added value of the same land so that cooperation can be formed that is mutually beneficial for service buyers who have non-climate change interests and communities who depend on land for nature conservation schemes that have climate change interests. As an example, the implementation of PES in Lombok and Lampung is shown in Table 1.

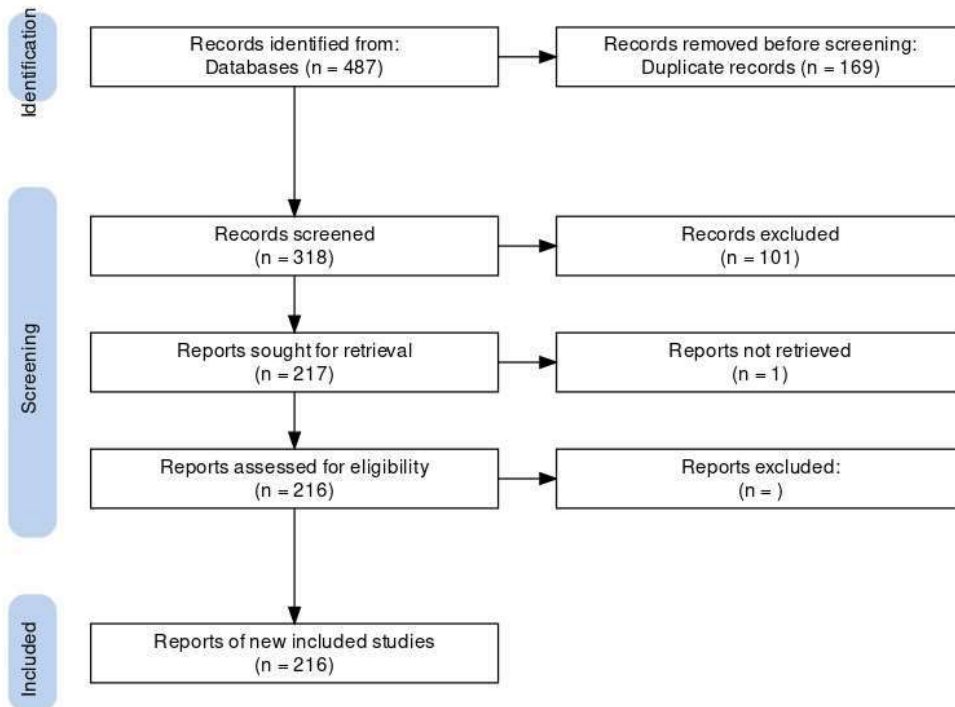


Fig. 1: Flowchart showing the process of identifying relevant studies for the review.

Table 1: PES Lombok and Lampung.

Aspect	Lombok	Lampung
ES purchaser	WWF; KONSEPSI (NGO lokal)	PLN (PLTA Way Besai)
ES provider	Farmer in Rinjani area	Farmer of Sumber Jaya Village
Form of environmental service	Planting trees and maintaining springs	Preventing sedimentation by reforestation and forest conservation
PES mechanism	<p>Farmers in upstream areas are compensated for planting forests and maintaining water sources. Financing comes from downstream water users (PDAM and local drinking water companies). Payments are included in the customer's monthly bill ('environmental services payments'). The money is managed by local government agencies to be distributed to communities that submit proposals for forest conservation programs. On the first occasion, IDR 445 million was collected. There is an increase in farmer income.</p> <p>Fig. 1. PES mechanism in West Lombok.</p>	<p>RUPES (Rewarding Upland Poor for Environmental Services) with a tiered water turbidity (gr soil/liter water) based scheme. A 30% turbidity reduction is provided by a micro-hydro turbine costing IDR 20 million. 10% turbidity reduction compensation IDR 2.5 million. Turbidity reduction 10-20% compensation IDR 5 million. Turbidity reduction 21-29% compensation IDR 7.5 million. In addition, there are revolving funds for goat farming, development of MHPs, and tree seedlings.</p> <p>Fig. 2. PES mechanism in Sumber Jaya Lampung.</p>

Table Cont....



Aspect	Lombok	Lampung
Key issues	Forest degradation, illegal logging, unsustainable agriculture, changes in agricultural practices, and decreased water discharge.	Reducing sedimentation and rehabilitating deforested areas
Problems	The applicable regulations regarding regional income do not recognize income in return for environmental services; the complexity of revenue recognition resulted in PES being suspended.	Property rights over community forest land are an example of potential conflict over access to state-owned land.
Conclusion	Current regulations do not yet facilitate incentives from local governments for environmental services. Schemes involving the private sector are easier to implement and have a higher success rate.	

Table 2: Hydrological PES in Indonesia.

Location	Issues	Factors determining pay	Performance indicator	Hydrology indicator
Cidanau watershed area	Erosion of critical land	Land rehabilitation costs	Number of trees per hectare	-
Kuningan, Cirebon	Quantity and quality of forest management	Selling price of water	Development of forest conservation	-
Lombok island	Degradation of the forest's ability to produce water	Willingness to pay (WTP)	Development of forest conservation	-
Sumberjaya Lampung	River water sediment load	Sediment reduction rate	Reduction of sediment load	Sediment load

In the context of implementing PES related to water flow areas, cooperation is generally formed between regional drinking water companies and hydroelectric power plants. The compensation provided is detailed with indicators that must be achieved, and the compensation burden is included in operational costs so that it can be charged to end product users (drinking water consumers) or as operational costs to increase operational efficiency (increased power plant efficiency) as shown on Table 2.

PES interactions with local communities also play an important role in PES design; designs that do not take into account the configuration of local communities that depend on the PES base ecosystem can cause PES to be cost-inefficient (Leimona et al. 2015). As shown in Table 3, the interactions identified in the PES design are diversified based on the configuration scenario.

PES carried out in Indonesia generally involves local farmer groups as providers of environmental services by

Table 3: Fairly Efficient and Efficiently Fair PES Design in Asia.

Configuration	Examples	Social – Political –Economic condition	Main environmental service	Scheme
Forests are an inseparable part of the lives of local communities	Kalahan (Philippines) and Kapuas Hulu – West Kalimantan	Indigenous people with strong ties and recognized national law for self-management of ancestral lands	(Voluntary) carbon sequestration, watershed conservation for local water companies	Payment from the company. Earmark for water bill.
Forests and agriculture are inseparable.	Kulekhani (Nepal) and Bakun (Philippines)	Local communities provide forest management. Local residents invest in vegetables at high market prices, with the remaining forests certified as ancestral areas of origin.	Watershed area conservation to support electric turbine	Distribution of part of hydropower income to the community
Agroforests and agroforestry systems are an important part of the landscape and people's lives.	Sumberjaya – Lampung, Bungo – Jambi and Cidanau – Banten	Local communities that use land are being displaced by the expansion of palm oil companies	Conservation of biodiversity	Philanthropic fund payments. Certificate for Community Forest (5 to 25 years)
The landscape has experienced severe degradation and is in the process of recovery.	Singkarak – West Sumatra and Lantapan (Philippines)	Local communities cultivate food crops and rice fields for the commercial market	Voluntary carbon sequestration and watershed improvement	Incentives from power companies and local governments

revegetating damaged land. Intermediary institutions are an important PES component in determining PES schemes, including the distribution of environmental service returns (Table 4). The ideal return (so attractive for Indigenous

peoples) in PES with links to Indigenous communities in the scheme is to create benefits in the form of recognition of the way of life or customs of Indigenous peoples in PES (Robinson et al. 2016) shown by Table 5.

Table 4: PES in Indonesia.

Scheme	Province	Service seller	Service purchaser	Payment	Intermediary institution	Activity
<b>Waterfront</b>						
Cidanau	Banten	30 farmer groups	SOEs	IDR1,2 million/ha	Stakeholder groups	Trees plantation, agroforestry
Gn.Rinjani	West Nusa Tenggara	25 groups di 12 village	Private institution	IDR30 – 80 million/group	NGO	Rehabilitation and Reforestation
Aceh	Aceh	10 groups	Private institution	IDR70 – 90 million/ contract IDR1,5 – 1,6 million/ha	NGO	Planting trees, preventing logging, constructing terraces and sediment pits
<b>Carbon</b>						
Ketapang	West Kalimantan	Village	Private foundation	IDR100 million / village	NGO	Avoid planned deforestation
Merangin	Jambi	Village	Private foundation	IDR100 million / village	NGO	Avoid planned deforestation
Rimba Raya	Central Kalimantan	Konsesi lahan restorasi ekosistem	Sektor swasta			Avoid planned deforestation
Berau FCP	East Kalimantan	Village	Donor	USD25 thousand / village	NGO	Pengurangan deforestasi, rehabilitasi hutan
Kalimantan Forests & Climate Partnership	Central Kalimantan	Village	Donor	AUD1,8 million	Kalimantan Forests & Climate Partnership	Trees plantation, canal blocking

Table 5: Perception of the Benefits of PES for Aboriginal Communities.

Category	Details
Human rights	Maintaining biodiversity associated with the relationship between society and the state; Formal laws and governance systems support the application of Indigenous knowledge and authority
Materials	Ecosystem functions and processes run and develop with the appropriate use of fire.
Aesthetics	The landscape shows the positive impact of the presence of human activities.
Venue / Inheritance	Monitoring can improve efforts to defend sacred places.
Activities and Access	The Partnership applies Aboriginal community values in efforts to prevent forest burning; Aboriginal communities still have the freedom to carry out customary laws that require burning.
Spiritual	Protection of sacred sites is more guaranteed.
Inspiration	Fostering enthusiasm for work and training for Indigenous communities: Young children tend to stay in school so they can learn about the environment.
Knowledge	Knowledge of indigenous communities in efforts to mitigate natural impacts and PES efforts fosters a sense of statehood.
Existence/legacy	Involvement of the younger generation in environmental protection programs, increasing the ability to transmit knowledge to the younger generation.
Social capital and cohesion	Health and wellness benefits
Identities	Sense of belonging by continuing to feel cultural authority over land belonging to Indigenous communities
Occupation	Social safeguards create a premium price for carbon units from projects managed with Aboriginal communities.

## PES Business Model Practice in Indonesia

### Governance

The regulations that were formed and the entities tasked with managing the organization (Sparviero 2019) in the case of PES in Indonesia came from NGOs that had concerns about the degradation of local natural quality (Fauzi & Anna 2013) as well as the beneficiaries of environmental services (Fauzi & Anna 2013, Soedomo 2013, Lapeyre et al. 2015).

### Non-targeted stakeholders (NTS)

Stakeholders who are affected by organizational activities and partnering stakeholders are not the target beneficiaries of the social activities carried out (Sparviero 2019). Local governments in various PES are affected by the provision of environmental services when the scheme involves the active role of government institutions/BUMD (Fauzi & Anna 2013).

### Key Resources

The most important asset that ensures the business model can function (Sparviero 2019). In the context of PES; Laws and policies related to PES mechanisms are a fundamental need in establishing PES institutions (Greiber 2009). The involvement of local communities and regional governments is also crucial in ensuring legal certainty because it involves land ownership (Fauzi & Anna 2013). Funding for conservation efforts also influences the quality of conservation efforts. Policy interventions at local and national levels can also increase the interest of potential fund providers and environmental service providers (Prasetyo et al. 2009).

### Key Activities

The most important activities that ensure the business model can function (Sparviero 2019). The main principle in PES

based on Pagiola & Platais (2002) is that environmental service providers must receive compensation for their efforts and those who benefit from providing these services must pay. So the main activities in PES are providing services and designing incentives.

### Channels

The main communication media between environmental service providers, environmental service beneficiaries, and intermediary institutions can be through cooperation contracts for the procurement of environmental services, capacity building, as well as business relations, and legal coordination (Sunaedi et al. 2019) shown by Fig 2.

### Customer & Beneficiaries Engagement (C&BE)

Environmental service buyers and providers have a relationship regarding the provision of incentives and contract design, which is influenced by intermediary institutions (Howe et al. 2014). In practice in Cidanau, interaction even includes assessments with local communities regarding optimal PES locations as well as the transfer of information regarding local community needs for land (Sunaedi et al. 2019).

### Customers & Beneficiaries (C&B)

Beneficiaries of environmental services are entities that benefit from goods and services because of providing environmental services through both active and passive consumption (Harrington et al. 2010). Suwarno et al. (2016) divided the beneficiaries of environmental services into three, namely: private (large companies, MSMEs, smallholders who employ workers), public (government institutions at various levels; global community), and RT (e.g., rice farmers, rubber farmers, local communities, rattan collector).

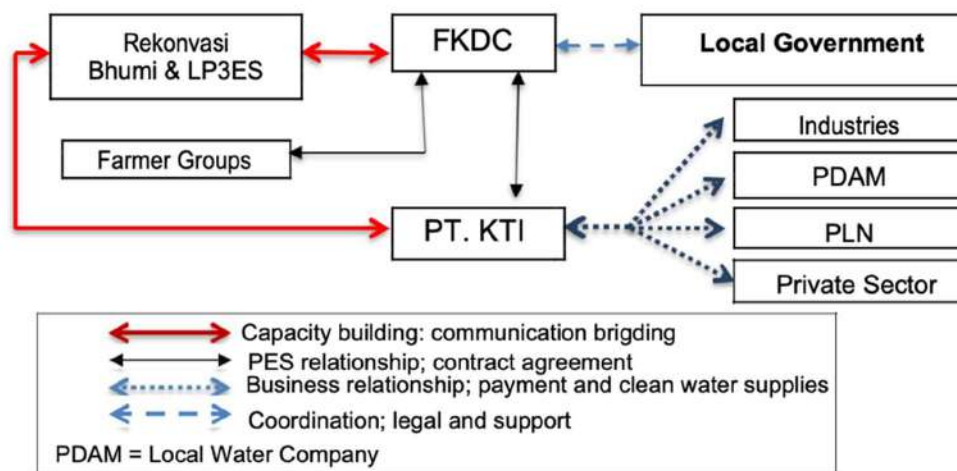


Fig. 2: PES DAS Cidanau Scheme (Sunaedi et al. 2019, Amaruzaman et al. 2018).

## Social Values Proposition (SVP)

The added value of PES can be in the form of monetary benefits (Suwarno et al. 2016), which increase the welfare of environmental service providers as compensation (conditionality) for the environmental services provided. In the FCPF benefit sharing plan document in the context of the East Kalimantan Provincial Government, there are monetary benefits to cover operational costs (MRV costs, safeguards) and administrative costs as well as non-monetary benefits in the form of capacity development for the environmental services program financial management system and strengthening institutions in the provision of environmental services. Specifically, the benefits of each party at various levels are regulated in the document up to the level of Indigenous communities, where they receive monetary benefits for the salaries of forest protection monitoring officers as well as non-monetary benefits such as poverty alleviation programs.

## Cost Structure

Tata et al. (2014) classified the costs of PES into three types, namely transaction and negotiation costs, opportunity costs from land use according to business-as-usual, and implementation costs. At the individual level, the costs incurred may include monitoring costs.

## Income

Suwarno et al. (2016) divide the revenues obtained by environmental service providers into two types, namely provisioning services to fulfill basic contacts and regulating services in the context of carbon absorption (i.e., valuation of potential reductions in GHG emissions).

## Mission Values

Big, long-term, and end-state goals are expected by the organization (Sparviero 2019). In the implementation of PES in Indonesia, some practices are dominated by international donors aimed at nature conservation and preserving biodiversity, although in practice, some companies finance PES with CSR funds which are not part of operational costs, which shows differences in companies' views on nature conservation tasks (Howe et al. 2014).

## Objectives

The short-term and practical goals to be achieved through implementing PES in Indonesia are generally measurable and gradual changes in environmental quality, which have a direct influence on the sustainability of buyers of environmental services (Fauzi & Anna 2013).

## Impact Measures

The size of the assessment of mission values is generally contained in PES contracts related to the size of the protected environment and the desired quality, such as deforestation rates in upstream areas monitored by stakeholders (Lapeyre et al. 2015). The achievement of the PES program's goals depends on the active and voluntary engagement of all stakeholders, guaranteeing the sustainable utilization of the environmental services it generates (Sunaedi et al. 2022).

## Output Measures

Environmental assessment over a shorter period generally becomes a contract conditionality in providing periodic benefits; for example, the number of trees per farmer group area, which is the underlying contract, and changes in the number of trees on land under the supervision of the farmer group (Lapeyre et al. 2015).

## PES Potential in Papua

The Ministry of Environment and Forestry (KemenLHK) database (Table 6) shows that in the Papua region, five programs are classified as climate change adaptation actions. These 5 programs focused on how to reduce carbon emissions in Indonesia, including Papua.

Trisnanto et al. (2023) presented data related to mapping deforestation rates using satellite imagery processed using AI in the Papua region. Based on this study, it was found that five districts with the highest reduction in forest cover area in the period 2001 to 2021 were spread across Papua Province, South Papua Province, and Central Papua Province (Table 7.). Areas with high deforestation rates have the potential to become REDD+ locations with a PES system in the Papua region.

## Business Model Recommendation in Papua

Based on the Social Enterprise Model Canvas (SEMC) in Papua (Table 8), we may know that the identification explains the PES model for Papua in a detailed and comprehensive picture to achieve the objective with an actionable plan to reduce emission as the end goal.

## Governance

Law Number 21 of 2001 concerning Special Autonomy for the Province of Papua, specifically in Article 1 (g), explains that the Papuan People's Assembly is the cultural representation of indigenous Papuans (OAP), which has the authority to protect the rights of OAP. The MRP's task based on Law No. 21 of 2001 Article 20 paragraph 1 (d) is to provide advice, consideration, and approval of planned cooperation agreements made by the Government and Provincial Government with third parties that apply



Table 6: KemenLHK Programs.

Location	Programs	Aim of Programs	Source and Total of Funds
Jayapura Merauke	Enhancing Smallholder Benefits from REDD+ in Indonesia	Support the development of institutional and fiscal mechanisms for REDD+ that link implementation at the national and local levels	Australian Centre for International Agricultural Research USD233.227 ( <i>sharing beneficiaries</i> )
Jayapura Merauke	Procurement and Utilization of Solar Cell Technology in Shipping Navigation Aids (SBNP)	Assisting the ship's navigator in determining the position and/or course of the ship and notifying the dangers and/or obstacles to navigation for the benefit of sailing safety.	Central and Regional Government Financing There is no information on the amount of funds.
Papua	Support to the establishment of Indonesia REDD+ Infrastructure and Capacity: Interim Phase (finished)	Strengthened climate change mitigation and adaptation and environmental sustainability measures in targeted vulnerable provinces, sectors, and communities.	Norway – UNDP USD20,49 million

Table 7: Forest Loss in Papua.

Regency	2001 – 2007 [km <sup>2</sup> ]	2008 – 2014 [km <sup>2</sup> ]	2015 – 2021 [km <sup>2</sup> ]	Total per Regency [km <sup>2</sup> ]
Merauke	156,807	641,030	1,082,818	1,880,656
Jayapura	126,667	252,822	292,517	672,005
Boven Digoel	217,148	139,880	267,154	624,182
Yahukimo	110,783	162,850	293,800	567,432
Mimika	100,254	179,871	199,703	479,827

Table 8: SEMC for PES carbon-based in Papua.

Aspect	Elements
Governance	MRP, NGOs, donors, and Regional Government
NTS	GTMA; traditional groups; KPH (Forest Management Unit)
Key resources	International funding Property rights to the land that is the underlying PES
Key activities	1. REDD+ with a superior commodity approach 2. Environmentally friendly agricultural practices
Channels	1. Cooperation contract 2. Capacity building 3. Business relationships
Customer & Beneficiaries (C&B)	1. Private (smallholders such as poktan) 2. Public 3. Traditional communities (Papua Provincial Regulation No.21 of 2008)
Customer & Beneficiaries Engagement (C&BE)	1. Formulation of cooperation contracts 2. Joint assessment with Indigenous communities regarding the impact of PES
SVP	1. REDD+ contributions whose performance is recognized 2. Recognition of the rights of Indigenous peoples through involvement in the PES program 3. Increasing the welfare of the PES service provider community
Mission values	1. Protection of biodiversity 2. Poverty alleviation and improvement of community welfare indicators in PES areas, as well as the emergence of NTFP (non-timber forest product) businesses 3. Achieving appropriate deforestation rates within the framework of reducing GHG emissions 4. Strengthening the KPH system 5. Strengthening the role of Indigenous communities in environmental management and reducing the potential for conflict over the recognition of land rights
Objectives	1. Potential emission reduction of 14.1 MtCO <sub>2</sub> e* in Jayapura Regency (as one of the pilot project recommendation areas) 2. Establishment of a forest guard patrol task force 3. Obtain a climate aid package with international entities

Table Cont....

Aspect	Elements
Impact measures	<ol style="list-style-type: none"> <li>1. Increase in welfare indicators (number of years of schooling, number of educational and health facilities in the PES area)</li> <li>2. The amount of reduction in deforestation rates compared to the historical annual average rate in the PES area</li> <li>3. The number of conflicts over land is decreasing</li> </ol>
Output measures	<ol style="list-style-type: none"> <li>1. Increase the number of people in PES areas who are employed in the provision of environmental services</li> <li>2. Amount of environmental service compensation from donors</li> <li>3. Construction of health and education facilities as well as development of agroforestry business potential using sustainable principles</li> </ol>
Cost structure	<ol style="list-style-type: none"> <li>1. Poktan subsidy support (opportunity cost mitigation)</li> <li>2. MRV Implementation (implementation)</li> <li>3. Monetary and non-monetary assistance packages for Indigenous communities (transaction costs)</li> </ol>
Income	<ol style="list-style-type: none"> <li>1. Grant or international funding</li> <li>2. Proceeds from sales of agroforestry commodities</li> </ol>

\* Temporary calculation in Hnya Dkening forest

in Papua Province specifically regarding the protection of the rights of OAP. Ulayat rights as part of the rights of Indigenous peoples over the use of land, forests, and water and their contents are the main driving factor in adapting governance in SEMC to the context of the Papua region, which involves representative elements of Indigenous communities.

### Non-Targeted Stakeholders

In the context of Jayapura Regency specifically, it is the GTMA (Indigenous Community Task Force), has the role of compiling and implementing the Recognition, Protection, and Empowerment of Indigenous Community programs in Jayapura Regency. GTMA, which contains various stakeholder components such as academics, government officials, indigenous communities, and development partners, can be an appropriate intermediary institution in SEMC design in the Papuan community context. GTMA was specifically formed by the Regent of Jayapura to encourage efforts to measure and verify the territorial boundaries of each traditional territory; however, it can be a reference for an entity whose members come from various stakeholders (multi-perspective). The role of the division of customary territories carried out by the GTMA is also important when determining the areas protected in PES contracts and the benefits received by each customary group based on the area of land they are responsible for protecting.

Papua Province Special Regional Regulation No.21 of 2008 concerning Sustainable Forest Management in Papua Province in article 5 states that customary law communities in Papua Province have rights to natural forests in accordance with the boundaries of their respective customary territories. The existence of indigenous communities in the NTS is an example of implementing the role of indigenous communities in the PES program.

### Key Resources

The international donation framework (FCPF) requires beneficiaries to prepare an ER-PIN (Emission Reduction Program Ideas Note), which contains location, performance measurement and financing tenor, benefit sharing plan, leakage mitigation plan, and information related to the contract as a whole. Details supported by expert assessments regarding deforestation rates and carbon stocks are examples of funding program quality standards that can improve the reputation of the program and the region. International funding specifically in the PES that applies in Indonesia, provides recognition of the credibility of environmental services that local communities can provide. International funding also allows excess absorption to be channeled to a wider market in the form of carbon credits.

Property rights are an important element in ensuring that PES is implemented optimally without obstacles, especially regarding the mechanism for providing returns for business carried out on land in the Papuan context that is owned by indigenous communities. The involvement of the GTMA and, specifically, elements of traditional elders and customary law experts in the GTMA allows the composition of the PES implementation team to have legitimacy according to customary law.

### Key Activities

Information given by one of the cocoa farmers in a seminar held by the DJPb Regional Office of Papua Province was that the main impetus for carrying out deforestation activities such as illegal logging is the low economic value produced by agricultural commodities for farmer groups; Cost pressures from difficult access to government subsidies are one significant obstacle. Planting sago, cocoa, and coffee as superior commodities in the pilot project area can be an example of implementing a REDD+ project with an

agroforestry approach that increases yield while increasing carbon absorption capacity. Al-Rajab et al. (2016) explained that cultivating cacao in Sulawesi with a variety of shade tree cover can increase carbon stocks above and below ground up to five times without sacrificing crop yields.

Another main activity in PES is the distribution of benefits which can involve the role of traditional groups in assessing infrastructure needs that are essential in developing community welfare, such as the construction of health and education facilities. Distribution of other benefits can be done by building the capabilities of indigenous community farming groups to market commodities at earmarked prices to private partners. The distribution mechanism can adopt the FCPF framework with fiscal transfers, public service agencies, farming credit, the establishment of trust funds, PES, and PNPM (National Independent Community Empowerment Program). Providing this assistance also has an impact on improving the management performance of PNPM / RESPEK (Village Strategic Development Plan).

### **Customer & Beneficiaries (C&B)**

Papua Provincial Perdasus No. 21 of 2008 plays a pivotal role in recognizing and safeguarding the land rights of indigenous peoples in Papua. This regulation underscores the importance of ensuring that the indigenous populations are the primary beneficiaries within the Sustainable Ecosystem Management and Conservation (SEMC) framework. By prioritizing the rights and needs of these communities, the Perdasus aims to empower indigenous peoples and promote their sustainable development. To achieve sustainable livelihoods for indigenous Papuans, it is imperative to implement Payment for Ecosystem Services (PES) initiatives. PES programs provide financial incentives to landowners and communities for managing their land in ways that preserve ecosystem services, such as carbon sequestration, biodiversity conservation, and water quality improvement. These initiatives can play a crucial role in mitigating the pressures that lead to land conversion for oil palm plantations, which are a significant driver of deforestation in the region. By offering alternative income sources through PES, indigenous communities can be encouraged to maintain their traditional land use practices, thereby protecting their forests and the biodiversity they harbor.

The successful implementation of PES and other sustainable development initiatives requires the active involvement of intermediary institutions and effective governance within the SEMC framework. These institutions can facilitate communication and collaboration between indigenous communities, government agencies, and private sector stakeholders. They can also help ensure that the benefits of sustainable practices are equitably distributed

and that Indigenous voices are heard in decision-making processes.

Moreover, the development of green job opportunities is essential for aligning economic growth with the needs of indigenous communities. Green jobs not only provide employment but also contribute to environmental sustainability. Potential roles for Indigenous Papuans within this framework may include land restoration workers who engage in reforestation and habitat rehabilitation projects, stock restoration personnel who focus on the recovery of local wildlife populations, and green construction workers who implement sustainable building practices. Additionally, tree planters involved in climate adaptation efforts can help enhance the resilience of ecosystems to climate change, while ecotourism guides can promote the rich cultural and natural heritage of Papua, generating income for local communities.

In summary, Papua Provincial Perdasus No. 21 of 2008 serves as a foundational legal framework for protecting the land rights of indigenous peoples in Papua. By integrating PES initiatives, fostering effective governance, and creating green job opportunities, it is possible to support the sustainable livelihoods of indigenous Papuans while simultaneously addressing the pressing challenges of deforestation and environmental degradation. This holistic approach not only benefits the indigenous communities but also contributes to the broader goals of environmental conservation and sustainable development in the region.

### **Customer and Beneficiaries Engagement (C&BE)**

The establishment of cooperation agreements and dialogues regarding the effects of Payment for Ecosystem Services (PES) development on Indigenous communities that depend on the region is a crucial approach to fostering meaningful engagement. This method not only acknowledges the unique relationship that these communities have with their environment but also actively involves them in the decision-making processes surrounding PES initiatives in Papua. By creating formal agreements and facilitating open dialogues, stakeholders can ensure that the voices of indigenous communities are heard and considered in the development of PES programs. This engagement is essential for several reasons. First, it helps to identify and address the specific needs, concerns, and rights of these communities, which may otherwise be overlooked in top-down approaches. Second, it promotes a sense of ownership and agency among indigenous peoples, empowering them to participate actively in the management and conservation of their natural resources.

Furthermore, these cooperation agreements can serve as a platform for knowledge exchange, where indigenous communities can share their traditional ecological knowledge

and practices, which are invaluable for the effective implementation of PES initiatives. This collaboration can lead to more culturally appropriate and sustainable solutions that benefit both the environment and the livelihoods of local populations. In addition, fostering such dialogues can help build trust between indigenous communities, government agencies, and other stakeholders involved in PES development. Trust is a critical component in ensuring the long-term success of these initiatives, as it encourages collaboration and reduces potential conflicts over land use and resource management.

Overall, the establishment of cooperation agreements and dialogues is not just a procedural step; it is a fundamental strategy that enhances the inclusivity and effectiveness of PES initiatives in Papua, ultimately leading to more equitable and sustainable outcomes for Indigenous communities and the ecosystems they depend on.

### **Social Values Proposition (SVP)**

The effectiveness of the REDD+ (Reducing Emissions from Deforestation and Forest Degradation) program, particularly when bolstered by collaboration with international donors, plays a pivotal role in enhancing the program's credibility and overall impact. This enhancement is achieved through the implementation of standardized protocols that guide the execution of REDD+ initiatives, as well as the application of scientifically validated assessment techniques provided by institutions such as LVV (Land, Water, and Vegetation). These standardized protocols ensure that all participating entities adhere to a consistent framework, which not only streamlines the implementation process but also fosters transparency and accountability.

By establishing a robust framework for measuring and verifying emissions reductions, the program can effectively demonstrate its success and reliability to stakeholders, including governments, NGOs, and the private sector. This credibility is essential for attracting further investment and support from international donors, who are increasingly looking for evidence-based approaches to environmental conservation and climate change mitigation. Moreover, this strategy is particularly beneficial for environmental service providers—such as local communities and organizations engaged in forest conservation—who exceed performance expectations. By meeting or surpassing the established benchmarks, these providers can unlock greater economic benefits through the trading of carbon credit units. This market-based approach not only incentivizes high performance but also creates a financial mechanism that rewards sustainable practices, thereby promoting long-term environmental stewardship.

In addition to the economic incentives associated with carbon trading, the Payment for Ecosystem Services (PES) framework plays a crucial role in recognizing and upholding the rights of indigenous peoples. By actively involving these communities in both the development and execution phases of PES initiatives, the program ensures that their voices are heard and their traditional knowledge is integrated into conservation strategies. This participatory approach not only empowers indigenous peoples but also fosters a sense of ownership and responsibility towards the management of natural resources. Furthermore, PES contributes to poverty reduction by implementing a profit-sharing model that directs funds back into local communities. This model facilitates the allocation of resources for essential infrastructure improvements, such as better access to clean water, education, and healthcare services. By investing in the well-being of local populations, PES not only enhances their quality of life but also strengthens their capacity to engage in sustainable practices that benefit both the environment and the economy. In summary, the collaboration between REDD+ and international donors, coupled with the implementation of standardized protocols and scientifically validated assessment techniques, significantly enhances the program's credibility. This, in turn, creates economic opportunities for environmental service providers, acknowledges the rights of indigenous peoples, and contributes to poverty alleviation through targeted investments in local communities.

### **Mission Values and Impact Measures**

The average annual release of carbon emissions into the atmosphere due to forest land degradation in Papua reaches 24.8 MtCO<sub>2</sub>e (megaton CO<sub>2</sub> equivalent), so a reduction in the rate of deforestation compared to the average can be a measure of achieving the mission to prevent deforestation. PES is also expected to improve the welfare of indigenous communities in forest areas that are PES areas so that long-term targets for the number of years of schooling, stunting rates, the number of infrastructures related to community sanitation and health facilities can be a measure of the welfare improvement mission that PES wants to achieve.

### **Objectives and Output Measures**

The annual emission reduction target for Jayapura Regency as an indicator of reducing the rate of deforestation can be reduced to a measure of the annual environmental service fee in accordance with the PES contract. The number of farmer groups that function as green jobs workers, as well as the effectiveness of the annual work program, can be measured.



## CONCLUSIONS

An examination of the PES business model in Indonesia reveals governance deficiencies stemming from regulatory constraints and the limited involvement of indigenous communities in PES scheme design. The efficacy of PES initiatives in Indonesia hinges on the structure of benefit schemes, particularly in terms of benefits offered and mechanisms for benefit distribution. Papua stands out due to its distinctive features, including special autonomous regional regulations and the significant reliance on indigenous communities, who hold authority over forest resources. The business model could serve as a blueprint for shaping PES growth in Papua, laying the groundwork for establishing infrastructure to support carbon credit trading centered on forest resources in the region.

## ACKNOWLEDGMENTS

The authors wish to thank Indonesia Bank and the University of Sebelas Maret for their useful contributions.

## REFERENCES

- Agrawal, A., Cashore, B., Hardin, R., Shepherd, G., Benson, C. and Miller, D., 2013. *Economic Contributions of Forests*. United Nations Forum on Forests, pp.1–132.
- Al-Rajab, A.J., Alhababy, A.M. and Alfaifi, T., 2016. Persistence of imidacloprid, acetamiprid and methomyl in qat leaves. *Hellenic Plant Protection Journal*, 9(2):51–59. [DOI]
- Amaruzaman, S., Rahadian, N.P. and Leimona, B., 2017. Role of intermediaries in the Payment for Environmental Services scheme: Lessons learnt in the Cidanau watershed, Indonesia. *Co-investment in ecosystem services: global lessons from payment and incentive schemes*. Asteria, D., Putri, A., Berliana, N.K., Sabarina, I.H. and Farha, W.A., 2022. Forest conservation by the indigenous Baduy community in the form of customary law. *Journal of Cultural Heritage Management and Sustainable Development*, 14(2), pp.175–189. [DOI]
- Bosetti, V. and Buchner, B., 2009. Data envelopment analysis of different climate policy scenarios. *Ecological Economics*, 68(5), pp.1340–1354. [DOI]
- Canadell, J.G. and Raupach, M.R., 2008. Managing forests for climate change mitigation. *Science*, 320(5882), pp.1456–1457. [DOI]
- Crippa, M., Guizzardi, D., Banja, M., Solazzo, E., Muntean, M., Schaaf, E., Pagani, F. and Monforti-Ferrario, F., 2022. *CO<sub>2</sub> Emissions of All World Countries*. springer
- Djafar, E.M., Widayanti, T.F., Saidi, M.D., Muin, A.M. and Ratnawati, 2023. Forest management to achieve sustainable forestry policy in Indonesia. *IOP Conference Series: Earth and Environmental Science*, 1181(1), pp.0–10. [DOI]
- Fauzi, A. and Anna, Z., 2013. The complexity of the institution of payment for environmental services: A case study of two Indonesian PES schemes. *Ecosystem Services*, 6, pp.54–63. [DOI]
- Greiber, T. ed., 2009. *Payments for ecosystem services: Legal and institutional frameworks* (No. 78). IUCN.
- Harrington, R., Anton, C., Dawson, T.P., de Bello, F., Feld, C.K., Haslett, J.R., Kluvánková-Oravská, T., Kontogianni, A., Lavorel, S., Luck, G.W. and Rounsevell, M.D., 2010. Ecosystem services and biodiversity conservation: concepts and a glossary. *Biodiversity and Conservation*, 19, pp.2773–2790. [DOI]
- Howe, C., Suich, H., Vira, B. and Mace, G.M., 2014. Creating win-wins from trade-offs? Ecosystem services for human well-being: a meta-analysis of ecosystem service trade-offs and synergies in the real world. *Global Environmental Change*, 28, pp.263–275. [DOI]
- Lapeyre, R., Pirard, R. and Leimona, B., 2015. Payments for environmental services in Indonesia: What if economic signals were lost in translation? *Land Use Policy*, 46, pp.283–291. [DOI]
- Nandini, N., Anupama, B.S. and Pavithra, S., 2009. Natural farming in harmony with the sustainable ecosystem. *Nature Environment and Pollution Technology*, 8(4), pp.785–788.
- Pagiola, S. and Platais, G., 2002. *Payments for environmental services*. Patunru, A.A. and Haryoko, A., 2015. Forest ownership and management in Indonesia: Reducing deforestation by strengthening communal property rights. (2).
- Prasetyo, F.A., Suwarno, A., Purwanto and Hakim, R., 2009. Making policies work for payment for environmental services (PES): an evaluation of the experience of formulating conservation policies in districts of Indonesia. *Journal of Sustainable Forestry*, 28(3–5), pp.415–433. [DOI]
- Rahma, F., Annisa, R.T.R. and Akhmad, K.W., 2022. The effect of economic growth, agricultural land, and trade openness moderated by population density on deforestation in OIC countries. *Quantitative Economics and Management Studies*, 3(2), pp.221–234. [DOI]
- Reyers, B., Polasky, S., Tallis, H., Mooney, H.A. and Larigauderie, A., 2012. Finding common ground for biodiversity and ecosystem services. *BioScience*, 62(5), pp.503–507.
- Robinson, C.J., James, G. and Whitehead, P.J., 2016. Negotiating Indigenous benefits from payment for ecosystem service (PES) schemes. *Global Environmental Change*, 38, pp.21–29. [DOI]
- Saharjo, B.H., 2022. Research of Indonesian GHG emission assessment from forest and land fires. *Journal of Tropical Silviculture*, 13(1), pp.14–22.
- Schirpke, U., Davide, M., Angelo, M. and Margherita, P., 2018. Positive effects of payments for ecosystem services on biodiversity and socio-economic development: Examples from Natura 2000 sites in Italy. *Ecosystem Services*, 34(March), pp.96–105. [DOI]
- Simonet, G., Julie, S., Driss, E., Marina, C. and Amy, E.D., 2019. Effectiveness of a REDD1 project in reducing deforestation in the Brazilian Amazon. *American Journal of Agricultural Economics*, 101(1), pp.211–229. [DOI]
- Soedomo, S., 2013. Hydrological services of forests and their compensation initiatives. *Jurnal Manajemen Hutan Tropika*, 19(1), pp.79–84. [DOI]
- Sparviero, S., 2019. The case for a socially oriented business model canvas: The social enterprise model canvas. *Journal of Social Entrepreneurship*, 10(2), pp.232–251. [DOI]
- Suich, H., Lugina, M., Muttaqin, M.Z., Alviya, I. and Sari, G.K., 2017. Payments for ecosystem services in Indonesia. *Oryx*, 51(3), pp.489–497. [DOI]
- Sunaedi, N., Hadi, S.P. and Bambang, A.N., 2022. Payment for environmental services in Indonesia: Mutually beneficial watershed environmental management model. *Nature Environment and Pollution Technology*, 21(4), pp.1995–2004. [DOI]
- Suwarno, A., Hein, L. and Sumarga, E., 2016. Who benefits from ecosystem services? A case study for Central Kalimantan, Indonesia. *Environmental Management*, 57, pp.331–344. [DOI]
- Tata, H.L., van Noordwijk, M., Ruysschaert, D., Mulia, R., Rahayu, S., Mulyoutami, E., Widayati, A., Ekadinata, A., Zen, R., Darsoyo, A. and Oktaviani, R., 2014. Will funding to Reduce Emissions from Deforestation and (forest) Degradation (REDD+) stop conversion of peat swamps to oil palm in orangutan habitat in Tripa in Aceh, Indonesia? *Mitigation and Adaptation Strategies for Global Change*, 19, pp.693–713. [DOI]

- Trisnanto, A., Soekmadi, R., Arifin, H.S. and Pramudya, B., 2023. Utilizations and policy formulations of home garden (pekarangan) as agritourism area in East Java, Indonesia. *Biodiversitas Journal of Biological Diversity*, 24(3). [DOI].
- UNEP, 2024. *Keeping the Promise: Annual Report 2023*. UNEP. [DOI].
- Wiatros-Motyka, M. et al., 2023. *Global electricity review 2023*. (April), pp.1-162.
- WRI Indonesia, 2021. 3 fakta tentang Papua: Harapan terakhir bagi hutan Indonesia. *Website Rumah Mitra Papua Barat*.
- Yakovleva, E.A. and Subhonberdiev, A., 2019. Implementation of 'green' economy principles in the forest sector. *IOP Conference Series: Earth and Environmental Science*, 392(1), pp.0–8. [DOI].

# Enhancing Land Use/Land Cover Analysis with Sentinel-2 Bands: Comparative Evaluation of Classification Algorithms and Dimensionality Reduction for Improved Accuracy Assessment

Akil V. Memon<sup>1†</sup>, Nirav V. Shah<sup>1,2</sup>, Yogesh S. Patel<sup>1</sup> and Tarun Parangi<sup>3,4</sup>

<sup>1</sup>Department of Civil Engineering, Sankalchand Patel College of Engineering, Sankalchand Patel University, Visnagar, Gujarat, India

<sup>2</sup>Department of Food Engineering, College of Food Processing Technology and Bio Energy, Anand Agricultural University, Anand, Gujarat, India

<sup>3</sup>Chemistry Department, Parul Institute of Applied Science, Parul University, Vadodara, Gujarat, India

<sup>4</sup>Research & Development Cell (RDC), Parul University, Vadodara, Gujarat, India

†Corresponding author: A. V. Memon: akilpochi@gmail.com

**Abbreviation:** Nat. Env. & Poll. Technol.  
**Website:** [www.neptjournal.com](http://www.neptjournal.com)

*Received:* 02-09-2024

*Revised:* 07-10-2024

*Accepted:* 18-10-2024

## Key Words:

LULC classification  
 Sentinel-2  
 Accuracy evaluation  
 GIS analysis  
 Kappa coefficient

## Citation for the Paper:

Memon, A. V., Shah, N. V., Patel, Y. S. and Parangi, T. 2025. Enhancing land use/land cover analysis with sentinel-2 bands: comparative evaluation of classification algorithms and dimensionality reduction for improved accuracy assessment. *Nature Environment and Pollution Technology*, 24(2), p. B4264. <https://doi.org/10.46488/NEPT.2025.v24i02.B4264>

*Note: From year 2025, the journal uses Article ID instead of page numbers in citation of the published articles.*



**Copyright:** © 2025 by the authors

**Licensee:** Technoscience Publications

This article is an open access article distributed under the terms and conditions of the Creative Commons Attribution (CC BY) license (<https://creativecommons.org/licenses/by/4.0/>).

## ABSTRACT

Accurately classifying land use and land cover (LULC) is crucial for understanding Earth's dynamics under human influence. This study proposes a novel approach to assess LULC classification accuracy using Sentinel-2 data. Authors have compared traditional and Principal Component Analysis (PCA)-based approaches for Maximum Likelihood Classification, Random Forest, and Support Vector Machine (SVM) classifiers. Four key classes (agricultural land, water bodies, built-up areas, and wastelands) are classified using supervised learning. Accuracy is evaluated using producer, user, overall accuracy, and kappa coefficient. Our findings reveal superior accuracy with PCA-SVM compared to other methods. PCA effectively reduces data redundancy, extracting essential spectral information. This study highlights the value of combining PCA with SVM for LULC classification, empowering policymakers with enhanced decision-making tools and fostering informed policy development.

## INTRODUCTION

The alteration of land use and land cover (LULC) has emerged as a pivotal element in contemporary approaches to the stewardship of natural resources and the surveillance of environmental transformations. The terms 'Land Use' and 'Land Cover,' initially identified as distinct, have been observed to be used interchangeably across diverse literature (Shrestha et al. 2021). Remote sensing data obtained from satellites are widely employed in the delineation of the Earth's LULC. The global repercussions of changes in LULC are evident, particularly in the contrasting impacts on urban and rural regions. Mapping LULC stands out as a crucial application of remote sensing (Lakhera & Rahi 2021, Tiwari et al. 2024). Land cover serves as a foundational factor influencing and connecting various aspects of both the human and physical environment. It is widely acknowledged that alterations in land cover have substantial implications for essential processes, such as biogeochemical cycling, consequently affecting global warming, soil erosion, and sustainable land use. Over the next century, land cover is anticipated to be the foremost influential variable impacting biodiversity (Cheruto et al. 2016). Remote sensing technologies offer a unique advantage in this context, allowing for repetitive, long-term observations of the same geographic regions. The ability to monitor changes over time provides critical insights into the dynamics of land cover transitions, enabling more accurate predictions of future environmental shifts.

Platforms like Google Earth and the Earth Observation (EO) satellites have revolutionized the way researchers access and analyze spatial data, making it easier to conduct LULC assessments even in remote or poorly monitored regions. This is particularly vital for developing countries, where other forms of high-resolution data might be unavailable due to resource constraints.

Remote sensing fills this gap, providing comprehensive data that can be used for effective land management, urban planning, and environmental conservation (Tilahun & Teferie et al. 2015, Fakeye et al. 2015). Moreover, the rapid development of machine learning (ML) (Loukika et al. 2021) and Deep Learning (DL) techniques has transformed LULC classification. Traditionally, methods like the Bayesian Maximum Likelihood classifier were used, but recent advancements in ML have led to the development of more efficient and accurate classification algorithms. Support Vector Machines (SVM), Random Forest (RF), K-nearest neighbors (KNN), and more recently, deep learning models have enabled researchers to analyze LULC data with unprecedented accuracy (Asif et al. 2023, Avci et al. 2023). These techniques are particularly beneficial in handling the vast amounts of complex data generated by hyperspectral imagery (HSI), which contains hundreds of spectral bands for each pixel. Hyperspectral data provide detailed information about the composition of land surfaces, making them ideal for fine-scale LULC classification. However, this data richness also presents challenges, such as the high dimensionality and computational demands of processing HSI.

Deep learning models, including Convolutional Neural Networks (CNNs), have proven particularly adept at handling hyperspectral data, outperforming traditional methods by capturing intricate spatial and spectral features that other algorithms may miss. The ability of these models to automatically learn feature representations from raw data has significantly improved the performance of LULC classification, leading to more accurate and reliable maps (Tao et al. 2023). This is especially important in heterogeneous landscapes—areas where diverse land use patterns, such as mixed urban and agricultural zones, create complex decision boundaries that can be challenging for conventional methods to classify correctly.

### Predictive Modeling Approaches

Machine learning classifiers are noted for achieving increased accuracy, even when dealing with intricate data and a higher number of input features (Parracciani et al. 2024, Huang et al. 2011). Some well-known classifiers include Artificial Neural Networks (ANN), CART, k-nearest Neighbor (k-NN), RF, and SVM (Jayabaskaran & Das 2023). While

certain classifiers, like ANN, adhere to a neural network structure with multiple layers of nodes that exchange input observations iteratively throughout the learning process (specifically, the Multi-Layer Perceptron), reaching a termination condition, CART constructs a straightforward decision tree based on the provided training data (Sun et al. 2024). RF, on the other hand, employs random subsets of training data to create numerous decision trees (Chowdhury 2024). Other classifiers, such as k-NN, utilize information about neighboring pixels to discern the inherent patterns within the training dataset (Van Groenigen & Stein 1998). In contrast, classifiers like SVM identify a subset of training data known as support vectors by fitting a hyperplane that optimally separates two classes. Across various literature, it is widely suggested that in most classification scenarios, RF and SVM stand out as superior performers compared to other machine classifiers (Huang et al. 2002, Mountrakis et al. 2011, Pal & Foody 2012, Belgiu & Dragut 2016).

Random Forest tree employs a bagging technique, randomly selecting a subset of training samples with replacements to build individual trees. This can lead to overlapping samples and some being excluded from certain trees (Kunapuli 2023, Siqueira et al. 2024). The unused samples (out-of-bag samples) are utilized for unbiased performance evaluation, providing an estimate of generalization error (Blain n.d). Additionally, at each node, Random Forest randomly selects variables to determine the best split, reducing the correlation between trees and lowering generalization error. The choice of pruning methods typically affects tree-based classifiers, but Random Forest is resilient to such influences, as it constructs trees without the need for pruning techniques (Breiman et al. 2001, 2004).

The Maximum Likelihood Classification (MLC) assumes a normal distribution of statistics for each class in every band. It computes the likelihood that a particular pixel belongs to a specific class. Unless a probability threshold is chosen, all pixels receive classification. Each pixel is allocated to the class with the highest probability, i.e., the maximum likelihood. If the maximum probability is below a specified threshold, the pixel remains unclassified (Richards et al. 2013).

Support vector machine (SVM) is a supervised machine learning method that is often used in LULC classification (Halder et al. 2023). SVM demonstrates effective accuracy in LULC applications, creating a hyperplane in high-resolution satellite imagery. Notably, it excels in classifying images with a constrained set of training samples. SVM is regarded as more sophisticated than maximum likelihood classification (MLC) and is capable of achieving superior LULC classification compared to other classifiers, especially



when dealing with a limited number of pixels (Fetene et al. 2023). SVM aims to discover the optimal hyperplane that maximizes the margin between different classes of data points.

Principal component analysis (PCA) utilizing satellite imagery has been widely employed across various domains, notably in the detection of changes in land use and land cover (Moharram & Sundaram 2023). Over the years, it has gained considerable popularity due to its simplicity and effectiveness in amplifying change-related information (Schirpke et al. 2023). PCA, rooted in eigenvector analysis of the data correlation matrix, aims to capture maximum variances within a limited number of orthogonal components (Mahmud & Hafsa 2016, Shekar & Mathew 2022).

The fundamental concept of PCA involves the reduction of dimensionality in a dataset comprising numerous interrelated variables. This reduction is typically achieved by transforming the dataset into a new set of variables known as principal components (PCs). These PCs are both uncorrelated and ordered. When applied to data from multiple spectral bands, PCA tends to concentrate the majority of information in the initial two or three PCs, while the subsequent PCs generally contain noise (Somayajula et al. 2021, Shekar et al. 2023).

This study makes a unique contribution to the existing literature by conducting a direct comparative analysis between a conventional method utilizing Sentinel-2 original

bands and a PCA-based approach for land use and land cover (LULC) classification. While much of the previous work has focused on evaluating classification algorithms in isolation or utilizing only traditional methods, this study evaluates the same classifiers (Maximum Likelihood Classification, Random Forest, and Support Vector Machine) across two distinct dimensionality reduction approaches. By doing so, the study sheds light on how PCA, a commonly used dimensionality reduction technique, impacts the performance of LULC classification algorithms in real-world applications.

The comparison of PCA and conventional methods is impactful because it addresses a key challenge in remote sensing—the curse of dimensionality—especially when handling multi-spectral data. Reducing dimensionality can lead to more efficient classification while maintaining or even improving accuracy. This study provides new insights into how PCA, when combined with machine learning classifiers like SVM, can outperform traditional classification approaches. This adds to the current understanding of LULC classification by highlighting the effectiveness of PCA-SVM, particularly in improving classification accuracy and computational efficiency.

## Study Area

This study delves into the Panam watershed, a left-bank tributary of the Mahi River basin nestled within Gujarat's Mahisagar district. The Panam River originates near Bhadra

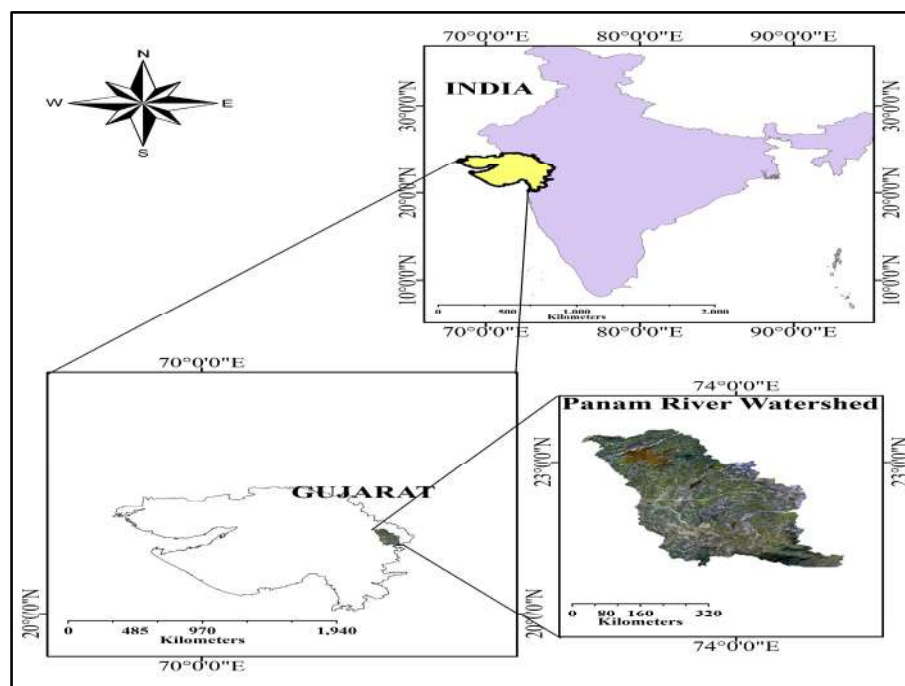


Fig. 1: The study area of the Panam River watershed.

in Madhya Pradesh's Jhabua district, traversing northwest for roughly 125 kilometers before merging with the Mahi in the Panchmahals district of Gujarat state. Encompassing a drainage area of 2400 square kilometers, the region experiences a tropical climate with temperatures fluctuating between 15°C in January and 40°C in May. Rainfall averages 945 mm annually, shaping the watershed's characteristics. This unique confluence of geographical and climatic factors positions the Panam watershed as an ideal canvas for our research endeavors. Fig. 1 provides a visual representation of the study area's location.

## MATERIALS AND METHODS

This research investigates LULC in the Panam River watershed using freely available Sentinel-2 satellite imagery from January 2024, acquired from the Copernicus Open Access Hub with minimal cloud cover. QGIS, free and open-source GIS software, was employed for data visualization, editing, and analysis. The study focused on 12 Sentinel-2 bands (bands 2 to 12) that were mosaicked and clipped to the specific watershed area. Details regarding the utilized Sentinel-2 multi-spectral instrument (MSI) Level 1C bands are provided in Table 1.

As shown in Fig. 2, the methodology commences by importing Sentinel-2-MSI L1 C imagery into the QGIS software, followed by the creation of a seamless image of the study area through mosaicking. A band composite image is then generated using all bands. To streamline data and identify crucial bands for classification, a Principal Component Analysis (PCA) is performed on the band composite image. After data preprocessing, the subsequent step involves collecting training samples for each land use class to be classified. High-resolution Google Earth images

were employed to extract training samples for each LULC class. These images, with their fine spatial detail, allowed for accurate identification of homogeneous areas corresponding to Agricultural land, Water bodies, Built-up areas, and Barren land. Each sample class was carefully delineated through visual interpretation, ensuring that only representative and pure pixels were included.

The size of each sample class was determined based on the area and spatial distribution of the LULC classes, ensuring sufficient representation across the study area. For instance, larger classes like Agricultural land had a higher number of sample pixels compared to smaller classes like Water bodies. On average, around 200–300 pixels were collected per class to train the classifiers. Validation of the sample set was achieved through a stratified random sampling technique, where ground-truth points were cross-referenced with both high-resolution imagery and field data (where available). This process ensured that the samples represented the true variability within each LULC class, leading to robust training datasets for model development.

The classification stage employs three distinct machine learning classifiers: maximum likelihood classifier, random forest tree classifier, and support vector machine classifier. Each classifier undergoes training using the previously collected training samples, distinguishing among the specified land use classes. Various accuracy metrics, including user's accuracy (UA), producer's accuracy (PA), overall accuracy (OA), and Kappa's coefficient ( $k$ ), are calculated for each classifier within the context of the designated land use classes. The kappa coefficient is calculated using the following equation.

$$k = (P_o - P_e) / (1 - P_e) \quad \dots(1)$$

where  $k$  is the kappa coefficient (ranges from 0 to 1),  $P_o$  is the observed agreement probability (sum of diagonal elements of confusion matrix divided by the total number of pairs),  $P_e$  is the expected agreement probability (sum of products of individual agreement probabilities for each category).

A kappa value of 0 indicates absolutely no agreement between raters beyond what could be expected by chance alone. Essentially, their ratings are no better than random guessing. If the kappa falls between 0.01 and 0.20, there's some slight agreement, meaning the raters are occasionally aligned but more often differ. Moving to the 0.21–0.40 range suggests fair agreement. While not perfect, the raters demonstrate some consistency in their assessments. A kappa value between 0.41 and 0.60 signifies moderate agreement, indicating the raters are often in agreement, though occasional discrepancies still exist. Substantial agreement is achieved with a kappa of 0.61 to 0.80. Here,

Table 1: Sentinel-2 MSI Level1 C bands and their bandwidth.

Band No.	Band Name	Central Wavelength (nm)	Bandwidth (nm)
2	Blue	496.6	98.0
3	Green	560.0	45.0
4	Red	664.5	38.0
5	Vegetation Red Edge	705.0	19.0
6	Vegetation Red Edge	740.0	18.0
7	Vegetation Red Edge	783.0	28.0
8	Near Infrared	835.1	145.0
8A	Narrow NIR	865.0	33.0
9	Water vapour	945.0	26.0
10	SWIR-Cirrus	1380.0	75.0
11	SWIR	1610.0	143.0
12	SWIR	2190.0	2420

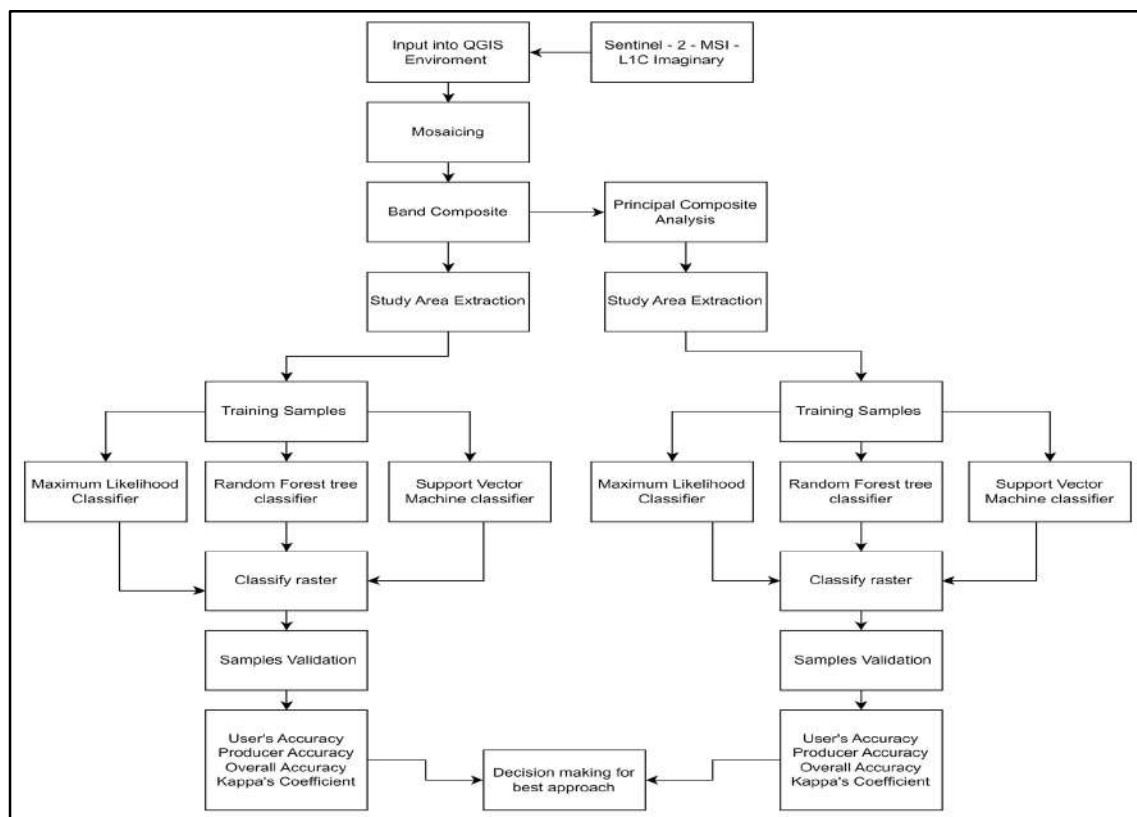


Fig. 2: The methodology adopted for LULC.

the raters demonstrate a strong level of consistency in their evaluations. Finally, a kappa value between 0.81 and 1.00 represents almost perfect agreement. In this case, the raters are nearly always in sync, providing highly reliable and consistent assessments.

## RESULTS AND DISCUSSION

### Principal Component Analysis of all Bands

Principal component analysis (PCA) was employed to compress the Sentinel-2 multispectral data. This technique aims to statistically capture the most significant evidence from the original bands (bands 2-12) into a reduced set of uncorrelated components termed principal components (PCs). The first few PCs inherently capture the majority of the data's variability (Rana et al. 2020). Notably, the 1<sup>st</sup> principal component (PC1), resulting from the 1<sup>st</sup> eigenvector, captured the greatest portion of the overall alteration within the Sentinel-2 dataset. Furthermore, the first three PCs collectively explained 98.85% of the eigenvalues, highlighting their effectiveness in representing the data. The remaining PCs displayed a decreasing trend in explained variance, corresponding to their respective eigenvalues.

Tables 2 and 3 give the redundancy of information among several bands, indicating that if this redundancy can be reduced through techniques like PCA, then the amount of information can be compressed without significant loss of valuable data. The author concentrated on the crucial data and excluded the later components (bands 4 to 12) because they appeared noisy and lacked useful information. Table 4 presents the eigenvalues and their corresponding cumulative percentage for principal components derived from Sentinel-2 bands. PCA reduced the associated Sentinel-2 dataset to a significantly smaller set of non-related variables that retain most of the original dataset's information. Fig. 3(a-c) displays the PCA bands obtained from the Sentinel-2 information, while Fig. 3(d-f) illustrates the frequency supply of these PC bands. The highest variance is found in the 1<sup>st</sup> PC, followed by the 2<sup>nd</sup> and 3<sup>rd</sup> components, according to the frequency distribution. The considered variances for PCA bands 1, 2, and 3 are 515,498.4, 263,079.1, and 8,843.772, respectively. Because of its high variance, the image produced from PCA band 1 data resembles the original image and contains the majority of the pertinent scene information. In multispectral remote sensing imagery, adjacent bands are often highly correlated and tend to provide similar information about an

Table 2: The covariance matrix for Sentinel-2 Bands.

Covariance Matrix												
Bands	2	3	4	5	6	7	8	8A	9	10	11	12
2	2534	3142	6366	5086	1155	74	246	-2	14	13356	12664	278
3	3142	4302	8274	7382	4774	4420	4968	787	19	19648	17347	5308
4	6366	8274	19571	16612	3777	130	1069	1127	58	48332	43630	2041
5	5086	7382	16612	17449	13716	13701	15026	3646	67	52130	42330	17894
6	1155	4774	3777	13716	60727	82391	82966	13782	53	45670	21589	93635
7	74	4420	130	13701	82391	114641	114838	18556	50	48490	17398	129299
8	246	4968	1069	15026	82966	114838	120480	18465	55	53913	21237	130521
8A	-2	787	1127	3646	13782	18556	18465	4161	17	13710	7207	21660
9	14	19	58	67	53	50	55	17	2	225	159	72
10	13356	19648	48332	52130	45670	48490	53913	13710	225	182512	143458	65389
11	12664	17347	43630	42330	21589	17398	21237	7207	159	143458	122336	27102
12	278	5308	2041	17894	93635	129299	130521	21660	72	65389	27102	147830

Table 3: Correlation matrix for Sentinel-2 Bands.

Correlation matrix												
Bands	2	3	4	5	6	7	8	8A	9	10	11	12
2	1.00	0.95	0.90	0.76	0.09	0.00	0.01	0.00	0.21	0.62	0.72	0.01
3	0.95	1.00	0.90	0.85	0.30	0.20	0.22	0.19	0.22	0.70	0.76	0.21
4	0.90	0.90	1.00	0.90	0.11	0.00	0.02	0.12	0.31	0.81	0.89	0.04
5	0.76	0.85	0.90	1.00	0.42	0.31	0.33	0.43	0.38	0.92	0.92	0.35
6	0.09	0.30	0.11	0.42	1.00	0.99	0.97	0.87	0.16	0.43	0.25	0.99
7	0.00	0.20	0.00	0.31	0.99	1.00	0.98	0.85	0.11	0.34	0.15	0.99
8	0.01	0.22	0.02	0.33	0.97	0.98	1.00	0.82	0.12	0.36	0.17	0.98
8A	0.00	0.19	0.12	0.43	0.87	0.85	0.82	1.00	0.19	0.50	0.32	0.87
9	0.21	0.22	0.31	0.38	0.16	0.11	0.12	0.19	1.00	0.39	0.34	0.14
10	0.62	0.70	0.81	0.92	0.43	0.34	0.36	0.50	0.39	1.00	0.96	0.40
11	0.72	0.76	0.89	0.92	0.25	0.15	0.17	0.32	0.34	0.96	1.00	0.20
12	0.01	0.21	0.04	0.35	0.99	0.99	0.98	0.87	0.14	0.40	0.20	1.00

object. The correlation between PCs 1 and 3, 1 and 2, and 2 and 3 was all found to be precisely zero. The random scatter observed in Fig. 4(a–c) and minimal correlation values indicate a complete absence of a relationship between the PCs. Consequently, classification tasks can often benefit from using the first few PCs instead of the entire original dataset. In our study, visual inspection revealed that PCA band 1 generally exhibited brighter pixel values and higher contrast compared to PCA band 2. This suggests that PCA band 1 may capture information related to high-variance features in the data, potentially making it more suitable for specific classification tasks depending on the target features of interest.

LULC classes were chosen based on a thorough understanding of the specific study area. The study identified four primary LULC classes: Agricultural land

Table 4: Total variance explained for Sentinel-2 Bands.

Percent and Accumulative Eigenvalues			
PC Layer	Eigen Value	% of Eigen Values	Accumulative of Eigen Values
1	515498.4	64.7168	64.7168
2	263079.1	33.0275	97.7444
3	8843.772	1.1103	98.8547
4	3807.653	0.478	99.3327
5	2426.928	0.3047	99.6374
6	1031.848	0.1295	99.7669
7	770.6416	0.0967	99.8636
8	462.6402	0.0581	99.9217
9	324.2669	0.0407	99.9624
10	230.819	0.029	99.9914
11	67.13062	0.0084	99.9998
12	1.29266	0.0002	100



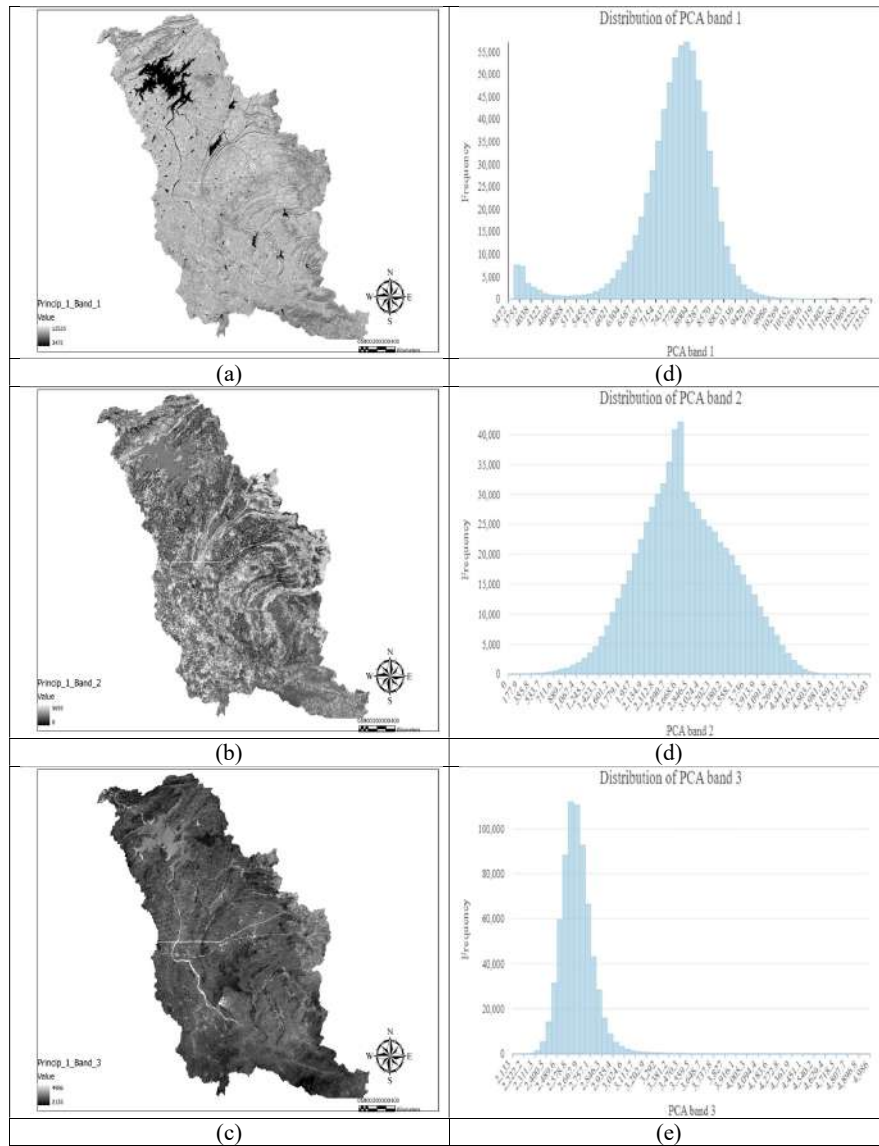


Fig. 3: Sentinel-2 data in three principal component bands (a-c) alongside their respective frequency distributions (d-f).

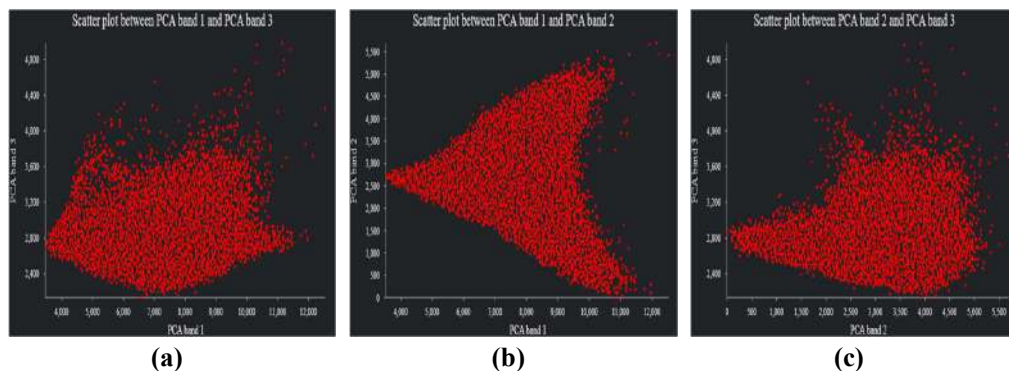


Fig. 4(a-c): Scatter Plots Reveal Weak Linkages Between Principal Components.

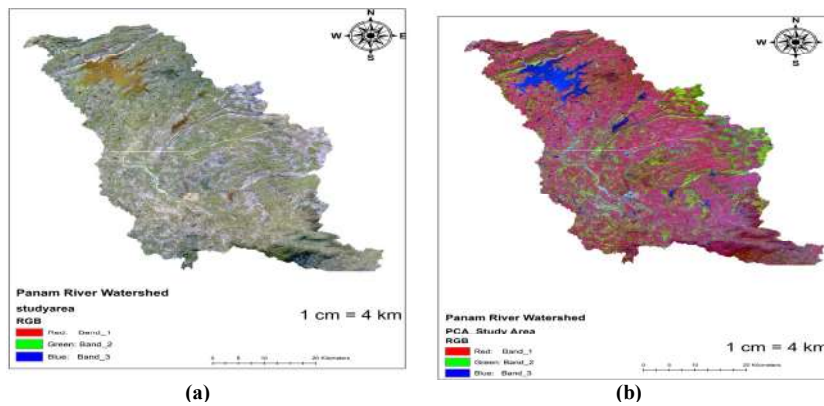


Fig. 5: Original band composite (a) and PCA - band composite (b).

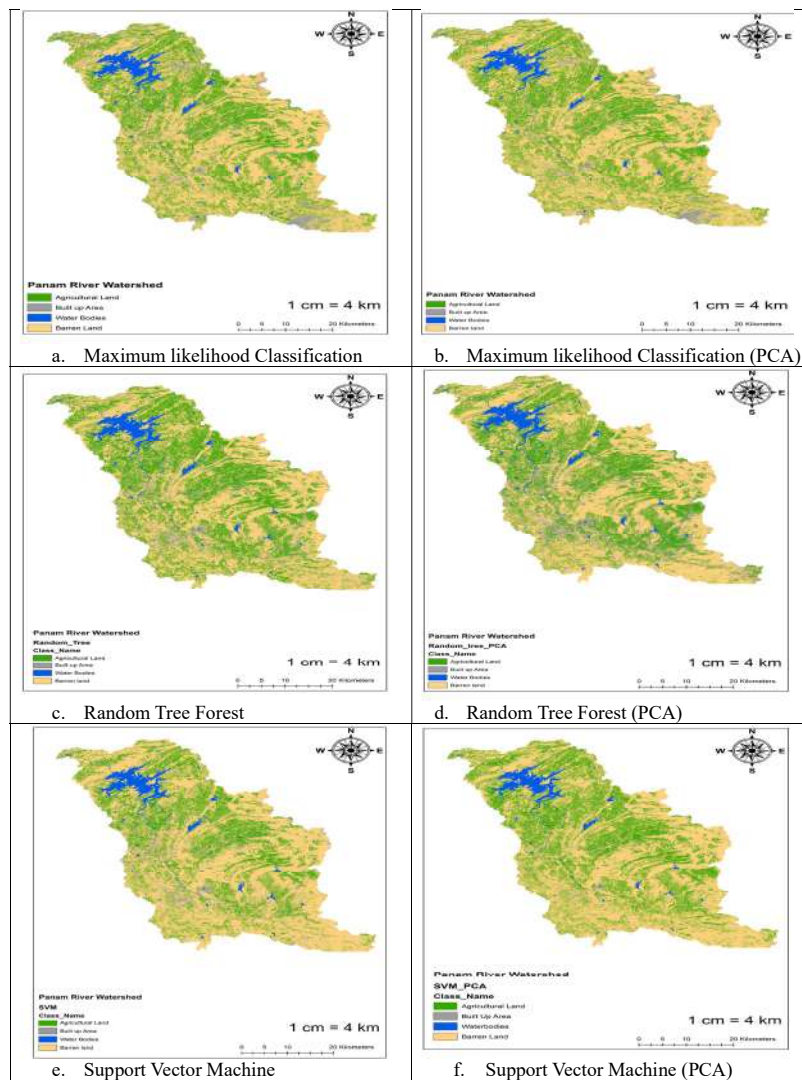


Fig. 6: Comparative analysis of classification methods: (a) MLE, (b) MLE with PCA, (c) Random Tree Forest, (d) Random Tree Forest with PCA, (e) Support vector machine, (f) Support vector machine with PCA.

(Agricultural zones, forest, etc.), water bodies (Reservoirs, rivers, streams, swamps, lakes), built-up areas (buildings and other manmade edifices, areas designated as mixed urban, industrial, or built territory), and barren land (Areas perpetually stripped bare, boasting less than 10% vegetation cover. Windswept plains and rocky outcrops reign supreme, their surfaces a tapestry of exposed dirt, sand, and stone). Classification was carried out using two approaches: the conventional method using Sentinel-2 original bands, as shown in Fig. 5(a), and a PCA-based approach, as shown in Fig. 5(b).

The effectiveness of these two LULC classification approaches was evaluated by assessing the predictive performance of three classification algorithms, namely MLC, RF, and SVM, along with the training data. Training data for each LULC category was collected as a set of pixels, and test data was obtained using stratified random sampling. The LULC maps generated using various classifiers for both approaches are depicted in Fig. 6(a-f).

### Performance Evaluation

The authors evaluated the efficiency of each model, RF, and SVM for both approaches by considering the user's accuracy (UA) and producer's accuracy (PA) for each LULC class. The results for each class were individually outlined as the models exhibited varying performance across different types. The specifics of UA and PA for each LULC class using MLC, RF, and SVM were thoroughly examined and described.

#### UA and PA for Agricultural Land

The land cover classification results for Agricultural Land using the Sentinel-2 Conventional Approach and Sentinel-2 PCA Approach with different classifiers reveal varying levels of accuracy. As shown in Table 5 under the Conventional Approach, both MLC and RF classifiers achieve high User's accuracy (UA) for Agricultural Land, with MLC reaching 100.00% UA and a corresponding Producer's accuracy (PA) of 65.63%, while RF achieves a UA of 100.00% and a PA of 62.50%. As shown in Table 6 in the PCA Approach, MLC shows a decrease in accuracy for Agricultural Land, with a UA of 80.95% and a lower PA of 39.29%. RF experiences a significant decline in both UA (62.79%) and PA (3.57%) for Agricultural Land, indicating diminished accuracy. SVM exhibits a perfect UA of 100.00% with a PA of 50.00% under the Conventional Approach, and in the PCA Approach, it maintains a relatively high UA of 82.61% with a lower PA of 32.14%. These results highlight the varied performance of classifiers in accurately classifying Agricultural Land under different approaches.

#### UA and PA for Built-Up Areas

In the land cover classification results for Built-up Areas using the Sentinel-2 Conventional Approach and Sentinel-2 PCA Approach with different classifiers, there are notable differences in the accuracy metrics. As shown in Table 5, under the conventional approach, maximum likelihood classification (MLC) achieves a user's accuracy (UA) of 80.95%, indicating reasonably accurate classification, with a high producer's accuracy (PA) of 94.44%. Random Forest Tree performs exceptionally well, achieving a perfect UA of 100.00% and a high PA of 91.67%, showcasing precise classification for built-up areas. Support vector machine (SVM) exhibits a UA of 78.05% with a corresponding PA of 88.89%. As shown in Table 6, the PCA Approach, MLC maintains accuracy with a UA of 81.58% and a perfect PA of 100.00%. Random Forest Tree achieves a UA of 83.78% and a perfect PA of 100.00%, indicating reliable classification. SVM also demonstrates consistent accuracy, with a UA of 83.78% and a perfect PA of 100.00%. These results highlight the varying performance of classifiers in accurately classifying Built-up Areas under different approaches, with each classifier showcasing strengths in specific accuracy metrics.

#### UA and PA for Water Bodies

In the land cover classification results for Water Bodies using the Sentinel-2 Conventional Approach and Sentinel-2 PCA Approach with different classifiers, distinct patterns in classification accuracy emerge. As shown in Table 5 under the CA, MLC exhibits high accuracy, achieving a UA of 96.43% and a PA of 79.41%. RFT, while displaying a lower UA of 82.93%, achieves a perfect PA of 100.00%, indicating precise classification for Water Bodies. SVM demonstrates a UA of 96.77% with a PA of 88.24%. As shown in Table 6, in the PCA Approach, all classifiers perform exceptionally well for water bodies. MLC achieves a perfect UA of 100.00% and a high PA of 92.11%. Random forest tree and SVM both achieve perfect UA and PA values of 100.00% and 97.37%, respectively, showcasing precise and consistent classification for Water Bodies.

#### UA and PA for Barren Land

In the land cover classification results for Barren Land using the Sentinel-2 CA and Sentinel-2 PCA approach with different classifiers, there are noticeable variations in classification accuracy.

As shown in Table 5 under the CA, MLC achieves a UA of 70.67%, indicating moderate accuracy, with a high PA of 98.15%. RTF displays slightly higher UA at 71.83%,

Table 5: Accuracy of different Classifiers for LULC using conventional approach for Sentinel-2 data set.

Sr. No	Conventional approach					
	Classifiers	Classes	UA	PA	OA	Kappa
1.	Maximum Likelihood Classification	Agricultural Land	100.00%	65.63%	80.13%	<b>0.8013</b>
		Built up Area	80.95%	94.44%		
		Water bodies	96.43%	79.41%		
		Barren Land	70.67%	98.15%		
2.	Random Forest Tree	Agricultural Land	100.00%	62.50%	82.69%	<b>0.8269</b>
		Built up Area	100.00%	91.67%		
		Water bodies	82.93%	100.00%		
		Barren Land	71.83%	94.44%		
3.	Support Vector Machine	Agricultural Land	100.00%	50.00%	81.41%	<b>0.8141</b>
		Built up Area	78.05%	88.89%		
		Water bodies	96.77%	88.24%		
		Barren Land	73.97%	100.00%		

Table 6: Accuracy of different classifiers for LULC using PCA approach for Sentinel-2 dataset.

Sr. No	PCA approach					
	Classifiers	Classes	UA	PA	OA	Kappa
1.	Maximum Likelihood Classification	Agricultural Land	80.95%	39.29%	83.22%	0.8322
		Built up Area	81.58%	100.00%		
		Water bodies	100.00%	92.11%		
		Barren Land	73.47%	78.26%		
2.	Random Forest Tree	Agricultural Land	62.79%	3.57%	83.92%	0.8392
		Built up Area	83.78%	100.00%		
		Water bodies	100.00%	97.37%		
		Barren Land	96.15%	54.35%		
3.	Support Vector Machine	Agricultural Land	82.61%	32.14%	86.01%	0.8601
		Built up Area	83.78%	100.00%		
		Water bodies	100.00%	97.37%		
		Barren Land	78.26%	78.26%		

with a PA of 94.44%. SVM performs well, achieving a UA of 73.97% and a perfect PA of 100.00%, indicating reliable classification for Barren Land.

As shown in Table 6 of the PCA Approach, MLC maintains reasonable accuracy with a UA of 73.47% and a PA of 78.26%. Random Forest Tree demonstrates significantly higher accuracy, with a UA of 96.15% and a PA of 54.35%, indicating precise classification for Barren Land. SVM shows consistent accuracy with a UA of 78.26% and a PA of 78.26%.

### Overall Accuracy and Kappa's Coefficient

In evaluating the land cover classification results using the Sentinel-2 Conventional Approach and Sentinel-2 PCA Approach with different classifiers, Overall Accuracy (OA)

and Kappa coefficients provide insights into the performance of each approach. Under the Conventional Approach, MLC achieves an OA of 80.13% with a Kappa coefficient of 0.8013, indicating reasonably accurate classification. Random Forest Tree demonstrates higher accuracy, with an OA of 82.69 % and a Kappa coefficient of 0.8269. SVM maintains competitive accuracy with an OA of 81.41% and a Kappa coefficient of 0.8141.

In the PCA approach, MLC showcases improved accuracy with an OA of 83.22 % and a Kappa coefficient of 0.8322. Random Forest Tree maintains similar accuracy, achieving an OA of 83.92 % and a Kappa coefficient of 0.8392. Notably, SVM excels with the highest accuracy, presenting an OA of 86.01% and a Kappa coefficient of 0.8601.



The practical advantages of using the PCA-SVM method for land use and land cover (LULC) classification are substantial, particularly in addressing issues like high dimensionality and data complexity. By reducing the number of input features, PCA captures the most important variance in the data, thereby improving computational efficiency and reducing the risk of overfitting. This makes PCA-SVM particularly useful in cases where the training data is limited, as SVM's strong generalization capability allows it to perform well even with fewer samples. Moreover, PCA-SVM proves highly effective in heterogeneous landscapes, where complex land use patterns (e.g., urban and agricultural mixes) require sophisticated classification models that can handle intricate decision boundaries. As demonstrated in the study, PCA-SVM achieved the highest OA and Kappa coefficients, making it a superior approach for LULC classification, especially in regions with limited training samples and diverse landscape features.

## CONCLUSIONS

In conclusion, this study undertook land use and land cover classification in the study area, delineating four primary classes: Agricultural land, water bodies, built-up areas, and barren land. The predictive performance of three classification algorithms (MLE, RF, and SVM) was evaluated using both traditional and PCA-based approaches using the original bands of Sentinel-2. The results demonstrated varying accuracies across land cover classes and classifiers. Particularly noteworthy was the Sentinel-2 PCA Approach, notably with the Support Vector Machine classifier, which exhibited superior accuracy for Agricultural Land (UA: 82.61%, PA: 32.14%), Built-up Area (UA: 83.78%, PA: 100.00%), Water Bodies (UA: 100.00%, PA: 97.37%), and Barren Land (UA: 78.26%, PA: 78.26%) compared to the Conventional Approach.

The detailed assessment of User's Accuracy (UA), Producer's Accuracy (PA), Overall Accuracy (OA), and Kappa coefficients provided comprehensive insights into the strengths and weaknesses of each approach and classifier. With an Overall Accuracy of 86.01% and a Kappa coefficient of 0.8601, the Sentinel-2 PCA Approach with the SVM classifier emerged as the most effective approach for accurate land cover classification in this study. These findings underscore the potential applicability of this approach for land use and land cover mapping and monitoring throughout similar regions, demonstrating its utility for broader applications in land cover studies. The integration of Sentinel-2 data with advanced classification methods can contribute significantly to more accurate and efficient land cover assessments in diverse geographical areas.

## ACKNOWLEDGEMENT

The authors are grateful to the U. S. Geological Survey (USGS) Earth Explorer (<https://earthexplorer.usgs.gov/>) for offering access to Sentinel 2 data, which played a crucial role in our analysis.

## REFERENCES

- Asif, M., Li-Qun, Z., Zeng, Q., Atiq, M., Ahmad, K., Tariq, A. and Hatamleh, A.A., 2023. Comprehensive genomic analysis of *Bacillus paralicheniformis* strain BP9, the pan-genomic and genetic basis of biocontrol mechanism. *Computational and Structural Biotechnology Journal*, 21, pp.4647-4662.
- Avci, C., Budak, M., Yağmur, N. and Balçık, F., 2023. Comparison between random forest and support vector machine algorithms for LULC classification. *International Journal of Engineering and Geosciences*, 8(1), pp.1-10.
- Belgiu, M. and Dragut, L., 2016. Random forest in remote sensing: A review of applications and future directions. *ISPRS Journal of Photogrammetry and Remote Sensing*, 114, pp.24-31.
- Blain, T., n.d. Out-Of-Bag Error in Random Forests. [online] Available at: <https://tblainuob.github.io/files/OOBErrorInRF.pdf>
- Breiman, L., 2001. Random Forests. *Machine Learning*, 45(1), pp.5-32.
- Breiman, L., 2004. Bagging predictors. *Machine Learning*, 24, pp.123-140.
- Cheruto, M.C., Kauti, M.K., Kisangau, D.P. and Kariuki, P.C., 2016. Assessment of land use and land cover change using GIS and remote sensing techniques: A case study of Makueni County, Kenya. *Journal of Remote Sensing & GIS*, 5(4), p.1000175.
- Chowdhury, M.S., 2024. Comparison of accuracy and reliability of random forest, support vector machine, artificial neural network, and maximum likelihood method in land use/cover classification of urban setting. *Environmental Challenges*, 14, p.100800.
- Fakeye, A.M., Aitsebaomo, F.O., Osadebe, C.C., Lamidi, R.B. and Okonufua, E.O., 2015. Digital modeling of land use changes in some parts of Eastern Nigeria. *American Journal of Remote Sensing*, 3(3), pp.37-42.
- Fetene, D.T., Lohani, T.K. and Mohammed, A.K., 2023. LULC change detection using support vector machines and cellular automata-based ANN models in Guna Tana watershed of Abay basin, Ethiopia. *Environmental Monitoring and Assessment*, 195(11), p.1329.
- Halder, S., Das, S. and Basu, S., 2023. Use of support vector machine and cellular automata methods to evaluate the impact of an irrigation project on LULC. *Environmental Monitoring and Assessment*, 195(1), p.3.
- Huang, C., Davis, L. and Townshend, J., 2002. An assessment of support vector machines for land cover classification. *International Journal of Remote Sensing*, 23(4), pp.725-749.
- Huang, G.-B., Zhou, H., Ding, X. and Zhang, R., 2011. Extreme learning machine for regression and multiclass classification. *IEEE Transactions on Systems, Man, and Cybernetics, Part B (Cybernetics)*, 42(2), pp.513-529.
- Jayabaskaran, M. and Das, B., 2023. Land Use Land Cover (LULC) Dynamics by CA-ANN and CA-Markov Model Approaches: A Case Study of Ranipet Town, India. *Nature Environment & Pollution Technology*, 22(3), p.32.
- Kunapuli, G., 2023. *Ensemble Methods for Machine Learning*. Simon and Schuster, Manning, UK.
- Lakhera, S. and Rahi, D.C., 2021. Detection of change in land cover in Jabalpur District from 1991–2021 using remote sensing. *Research Square*, 3, p.229. DOI
- Loukika, K.N., Keesara, V.R. and Sridhar, V., 2021. Analysis of land use and land cover using machine learning algorithms on Google Earth engine for Munneru River Basin, India. *Sustainability*, 13(24), p.13758.

- Mahmud, K.H. and Hafsa, B., 2016. PCA as a tool of LULC based change detection in a suburban area of Dhaka city, Bangladesh. *The Jahangirnagar Review, Part II: Social Science*, 36, p.112
- Moharram, M.A. and Sundaram, D.M., 2023. Land use and land cover classification with hyperspectral data: A comprehensive review of methods, challenges, and future directions. *Neurocomputing*, 536, pp.90-113.
- Mountrakis, G., Im, J. and Ogole, C., 2011. Support vector machines in remote sensing: A review. *ISPRS Journal of Photogrammetry and Remote Sensing*, 66(3), pp.247-259.
- Pal, M. and Foody, G.M., 2012. Evaluation of SVM, RVM, and SMLR for accurate image classification with limited ground data. *IEEE Journal of Selected Topics in Applied Earth Observations and Remote Sensing*, 5(5), pp.1344-1355.
- Parracciani, C., Gigante, D., Mutanga, O., Bonafoni, S. and Vizzari, M., 2024. Land cover changes in grassland landscapes: combining enhanced Landsat data composition, Land Trendr, and machine learning classification in Google Earth Engine with MLP-ANN scenario forecasting. *GIScience & Remote Sensing*, 61(1), p.2302221.
- Rana, V.K., Maruthi, T. and Suryanarayana, V., 2020. Performance evaluation of MLE, RF, and SVM classification algorithms for watershed-scale land use/land cover mapping using Sentinel 2 bands. *Remote Sensing Applications: Society and Environment*, 19, p.100351.
- Richards, J., 2013. Remote Sensing Digital Image Analysis. In: *Remote Sensing Digital Image Analysis*, 5th ed. Springer-Verlag Berlin and Heidelberg GmbH & Co., Switzerland, pp.203-246.
- Schirpke, U., Tasser, E., Borsky, S., Braun, M., Eitzinger, J., Gaube, V., Getzner, M., Glatzel, S., Gschwantner, T. and Kirchner, M., 2023. Past and future impacts of land-use changes on ecosystem services in Austria. *Journal of Environmental Management*, 345, p.118728.
- Shekar, P.R. and Mathew, A., 2022. Prioritizing sub-watersheds using morphometric analysis, principal component analysis, and land use/land cover analysis in the Kinnerasani River basin, India. *H2Open Journal*, 5(3), pp.490-514.
- Shekar, P.R., Mathew, A., PS, A. and Gopi, V.P., 2023. Sub-watershed prioritization using morphometric analysis, principal component analysis, hypsometric analysis, land use/land cover analysis, and machine learning approaches in the Peddavagu River Basin, India. *Journal of Water and Climate Change*, 14(1), pp.1-20.
- Shrestha, R., Bhandari, S. and Twayana, R., 2021. Monitoring land cover/land use change using remote sensing and GIS technique at Dhulikhel and Banepa municipality, Nepal. *International Journal of Current Research in Science Engineering & Technology*, 3(5), p.712.
- Siqueira, R.G., Moquedace, C.M., Fernandes-Filho, E.I., Schaefer, C.E., Francelino, M.R., Sacramento, I.F. and Michel, R.F., 2024. Modeling and prediction of major soil chemical properties with Random Forest: Machine learning as a tool to understand soil–environment relationships in Antarctica. *Catena*, 235, p.107677.
- Somayajula, V.K.A., Ghai, D. and Kumar, S., 2021. Land Use/Land Cover Change Analysis using NDVI, PCA. In: *2021 5th International Conference on Computing Methodologies and Communication (ICCMC)*. IEEE 2021, pp.723-746.
- Sun, Z., Wang, G., Li, P., Wang, H., Zhang, M. and Liang, X., 2024. An improved random forest based on the classification accuracy and correlation measurement of decision trees. *Expert Systems with Applications*, 237, p.121549.
- Tao, J., Y. Gu, X. Hao, R. Liang, B. Wang, Z. Cheng, B. Yan, and G. Chen. 2023. Combination of Hyperspectral Imaging and Machine Learning Models for Fast Characterization and Classification of Municipal Solid Waste. *Resources, Conservation & Recycling* 188, 106731.
- Tao, J., Gu, Y., Hao, X., Liang, R., Wang, B., Cheng, Z., Yan, B. and Chen, G. 2023. Combination of hyperspectral imaging and machine learning models for fast characterization and classification of municipal solid waste. *Resources, Conservation & Recycling*, 188, p.106731. DOI
- Tilahun, A. and Teferie, B. 2015. Accuracy assessment of land use land cover classification using Google Earth. *American Journal of Environmental Protection*, 4(4), 193–198. DOI
- Tiwari, A.K., Pal, A. and Kanchan, R. 2024. Mapping and monitoring of land use/land cover transformation using geospatial techniques in Varanasi City Development Region, India. *Nature Environment & Pollution Technology*, 23(1), p.31. DOI
- Van Groenigen, J. and Stein, A. 1998. Constrained optimization of spatial sampling using continuous simulated annealing. *Journal of Environmental Quality*, 17, p.61.

# Portable Hybrid System for Producing Green Hydrogen by Electrolysis Using Energy Generated Through an Archimedean Screw

E. Aliaga Villanueva<sup>†</sup>, P. D. Inga Canales, M. G. Mori Paccori, J. V. Cornejo Tueros and K. G. Ibarra Hinostroza

Environmental Engineering Department, Continental University, Huancayo, Peru

<sup>†</sup>Corresponding author: E. Aliaga Villanueva; 70346388@continental.edu.pe

**Abbreviation:** Nat. Env. & Poll. Technol.  
**Website:** [www.neptjournal.com](http://www.neptjournal.com)

*Received:* 23-04-2024

*Revised:* 25-05-2024

*Accepted:* 02-06-2024

## Key Words:

Green hydrogen  
 Electrolysis  
 Climate change  
 Renewable energy  
 Hydrogen fuel

## Citation for the Paper:

Aliaga Villanueva, E., Inga Canales, P.D., Mori Paccori, M.G., Cornejo Tueros, J.V. and Ibarra Hinostroza, K.G., 2025. Portable hybrid system for producing green hydrogen by electrolysis using energy generated through an Archimedean screw. *Nature Environment and Pollution Technology*, 24(2), p.D1658. <https://doi.org/10.46488/NEPT.2025.v24i02.D1658>

*Note:* From year 2025, the journal uses Article ID instead of page numbers in citation of the published articles.



**Copyright:** © 2025 by the authors  
**Licensee:** Technoscience Publications  
 This article is an open access article distributed under the terms and conditions of the Creative Commons Attribution (CC BY) license (<https://creativecommons.org/licenses/by/4.0/>).

## ABSTRACT

At a global level, energy production is predominantly based on the use of conventional resources such as oil, coal, and gasoline; this dependence has led to adverse effects such as climate change and detrimental impacts on human health; consequently, green hydrogen emerges as a renewable energy source. This work develops and analyses the parameters of a portable hybrid system to produce green hydrogen on a small scale in a more efficient way, allowing it to be placed in rural areas to be used as an ecological fuel source. The hybrid system is divided into two stages; for energy production, a microhydraulic system was developed based on an Archimedes screw turbine, which is made up of a mechanical and electrical design, where the electricity produced is stored in a continuous energy source, which supplies the electric current to the electrodes in the alkaline electrolysis process; where a reaction occurs in the water resource to produce green hydrogen and oxygen. It was demonstrated that the turbine, when presenting a greater wetted area and slope of fall, produces a higher electrical potential, while in the electrolysis process to produce green hydrogen and oxygen, it was determined that the appropriate electrolyte to use is potassium hydroxide at 20% because it has greater electrical conductivity unlike sodium chloride and sodium hydroxide; evidencing the most efficient parameters to implement the hybrid system in rural areas to replace the conventional fuel that is used in cooking food.

## INTRODUCTION

Population growth, the continuous development of the global economy, and the persistent search for better living conditions have led to an increase in the energy demand. Energy production is mainly based on the use of conventional resources such as oil, diesel, coal, natural gas, and gasoline, which currently account for 80% of the world's energy demand (Muhsen et al. 2023). This dependence on non-renewable resources has led to adverse effects such as climate change; according to various reports by the Intergovernmental Panel on Climate Change (IPCC), this is caused by greenhouse gas emissions released into the atmosphere by anthropogenic activities, negatively impacting human health and the environment (Bideau et al. 2020). One of the sources for generating electricity in 2021 was the burning of coal, with more than 15 million tonnes of carbon dioxide (CO<sub>2</sub>) emissions into the atmosphere, making it essential to redesign energy strategies towards more sustainable options (Fathi et al. 2023). Emphasis is placed on liquefied petroleum gas (LPG), as it is the most widely used fuel globally as a means of cooking food, where incomplete combustion can generate carbon monoxide (CO) in enclosed spaces without adequate ventilation. This leads to severe household air pollution, directly linked to health risks. According to a recent WHO report, approximately 3.2 million people died prematurely in 2020 due to diseases related to household air pollution (Chen et al. 2023).

Consequently, a decisive transition from fossil fuels to renewable and clean energy sources is imperative to improve the efficiency of energy production (Gavrilov & Boycheva 2023). Green hydrogen emerges as a promising energy resource for the future, notable for its high calorific value in combustion. It is a pure, renewable, environmentally friendly, and sustainable energy source with the ability to be stored and transported efficiently (Hassan et al. 2023). According to the International Energy Agency (IEA) projections in the report on the role of hydrogen technologies in ensuring zero carbon dioxide emissions by 2050, it mentions that low-carbon hydrogen will include 62% green hydrogen (Elgarahy et al. 2022). The primary purpose of green hydrogen as a clean energy source is to address the energy crisis and environmental challenges as it has the advantage of having a higher density, being twice as high as other fossil fuels (Niroula et al. 2023). The maximum calorific value of hydrogen at a temperature of 298 K is  $141.8 \text{ MJ.kg}^{-1}$ , while its minimum calorific value is  $120 \text{ MJ.kg}^{-1}$  at the same temperature. These figures indicate a significant increase compared to conventional fuels, such as gasoline, whose value is  $44 \text{ MJ.kg}^{-1}$  at 298 K. This phenomenon underlines the high energy efficiency of hydrogen as one of its main characteristics to be considered (Osman et al. 2022, Yakubson 2022).

Alkaline electrolysis is powered by renewable energies such as wind, solar, and hydropower. These energy sources generate little or no release of greenhouse gases, contributing to the energy industry (Zhang et al. 2024). Hydrogen production by traditional water electrolysis involves the electrolytic decomposition of water into hydrogen ( $\text{H}_2$ ) and oxygen ( $\text{O}_2$ ), using electricity that is generated from renewable sources, producing an ion exchange through an electrolyte (Song et al. 2023).

Alkaline electrolysis produces clean, pure green hydrogen, offering a promising solution to growing global energy demand and reducing greenhouse gas emissions. It is an endothermic process where water vapor, the most abundant greenhouse gas in the atmosphere, is generated as a by-product. Unlike anthropogenic greenhouse gases such as carbon dioxide ( $\text{CO}_2$ ), methane ( $\text{CH}_4$ ), and nitrous oxide ( $\text{N}_2\text{O}$ ), the water vapor released in this process is controlled by the hydrological cycle, providing a more sustainable alternative (Fersch et al. 2022, Muñoz-Maldonado et al. 2023). The advancement and development of electrolysis technologies for green hydrogen production will lead to an increase in the market, reducing the cost of production, which is of utmost importance to improve the cost-effectiveness and efficiency of energy production (Marouani et al. 2023).

Among the research carried out recently, we are told about the production of green hydrogen using renewable

energies. One of the articles entitled “A review of water electrolysis-based systems for hydrogen production using hybrid, solar, wind and hybrid energy systems” (Nasser et al. 2022) stands out among the research. A review of hydrogen production systems was developed using clean energy sources such as solar and wind and the use of an alkaline electrolysis system for the separation of oxygen ( $\text{O}_2$ ) and hydrogen ( $\text{H}_2$ ) under electricity using an electrifier that is combined with renewable energy. As a result, it was found that hydrogen production is a clean energy source that can be stored and transported, which indicates the replacement of fossil fuels. Consequently, it seeks to compete in the global market with an efficient green hydrogen production system.

Another research project is the “Hydrogen production system by alkaline water electrolysis adapted to fast fluctuating photovoltaic energy” (Cao et al. 2023). This electrolysis system is an effective method for hydrogen production due to its long lifetime and high efficiency. It was based on finding a hydrogen production system that is made up of a set of elements, such as a photovoltaic panel, a continuous power source, and an alkaline electrolyzer, together with control and energy management strategies. As a result, a positive efficiency was obtained, based on the fact that the electrolyzer experienced minimal fluctuations that varied every 5 minutes, where the battery operated within the established range.

In contrast to previous research, the present research work focused on producing green hydrogen on a small scale using a hybrid system that can be transported from one place to another. This device is divided into two stages; the construction of an electrolytic cell that has separator plates to separate the production of green hydrogen and gaseous oxygen, as well as electrodes based on AISI 316 stainless steel and a microhydraulic power generation system based on an Archimedes screw that harnesses the kinetic and potential energy of water as a clean and sustainable alternative source. The objective was to demonstrate the most optimal parameters of the portable hybrid system developed for installation in bodies of water and to produce green hydrogen on a small scale, with the purpose of being used to replace conventional fuels used in homes, contributing to the decarbonization of the environment and the health of the inhabitants.

It is envisaged that this system can be used to produce green hydrogen in rural areas with limited hydraulic potential due to its design to take advantage of modest water flows; green hydrogen is intended to be used as an environmentally friendly fuel to replace conventional fuel such as LPG, which is the most commonly used fuel for cooking food in rural areas. In addition, it is envisaged that this research work could



support further research and thus lead to the development of a fully sustainable system.

## MATERIALS AND METHODS

This section presents the two phases that make up the portable hybrid system and is divided into:

1. Micro-hydraulic system
2. Electrolysis

### Micro-Hydraulic System

**Mechanical design:** The design was based on an Archimedes screw turbine, which was divided into two assembled sections. The inner section is comprised of a central body, which was constructed from a 4" PVC pipe; two opposing blades with two revolutions were placed around it along the 83 cm long central body. The central body has no solid filler and the whole section has a thickness of 0.2 cm (Fig. 1). The side ends have a 3/8" hole for inserting and fixing the 100 cm long metal threaded shaft.

To determine the internal geometry, its main variables were considered, such as the outer radius of the blades and the shaft, the diameter, the pitch between blades, and the length of the blades (Dragomirescu 2021), taking into account that the location for the respective tests was a river. The turbine characteristics are specified in Table 1.

The external section was designed based on a 1" square metal profile, and to determine the geometry of the support structure (see Fig. 2a), the size of the auxiliary supports was taken into account to avoid friction between the threaded shaft and the bearing; additionally, a maintenance measure was implemented, which consists of keeping the bearings lubricated to maintain the efficiency of the prototype

Table 1: Characteristics of the Archimedes screw turbine.

Property	Value
Material	PVC
Blade length [cm]	80.00
Central body diameter [cm]	10.16
Outside diameter of blade [cm]	24.20
Pitch between blades [cm]	30.00

(Sánchez et al. 2023). The structure also serves as a support to hold the electrical system and the bases made of 0.5 cm thick acrylic; two lateral bases (see Fig. 2b) and three semicircular bases (see Fig. 2c) that hold the circulation channel (see Fig. 2d), which is where the water circulates and is made of flexible PVC.

To fix the bearings, two 25 cm long auxiliary supports were used (Fig. 3), which served as supports for the internal section; these auxiliary supports were assembled to the metal structure.

For the 3D model (Fig. 4), SolidWorks was used as the design software. In the upper part of the structure, a wooden platform can be visualized to support the electrical system, which is composed of an electrical generator and a current switch, which, using an electrical connection, stores the electricity generated by the micro-hydraulic system in a continuous energy source. The lower part of the structure shows the sections assembled using 3/8" bolts and nuts.

**Electrical system:** For the conversion of mechanical energy into electrical energy, a direct current (DC) electrical generator was used, considering two criteria for its choice: the type of application and the theoretical torque produced by the turbine. The type of application refers to the purpose of the generator, which, in this case, a suitable generator was sought to directly feed the electricity produced in a

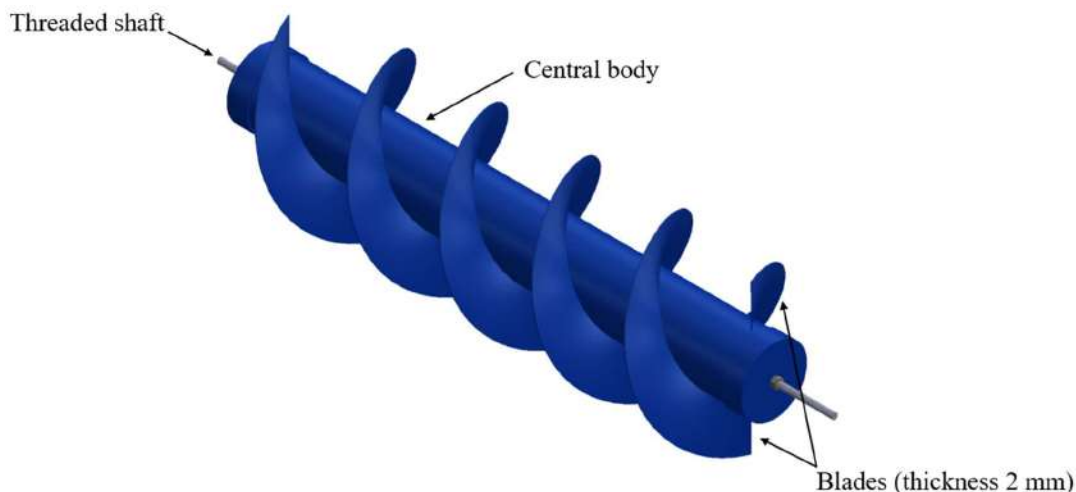


Fig. 1: Archimedes screw turbine.

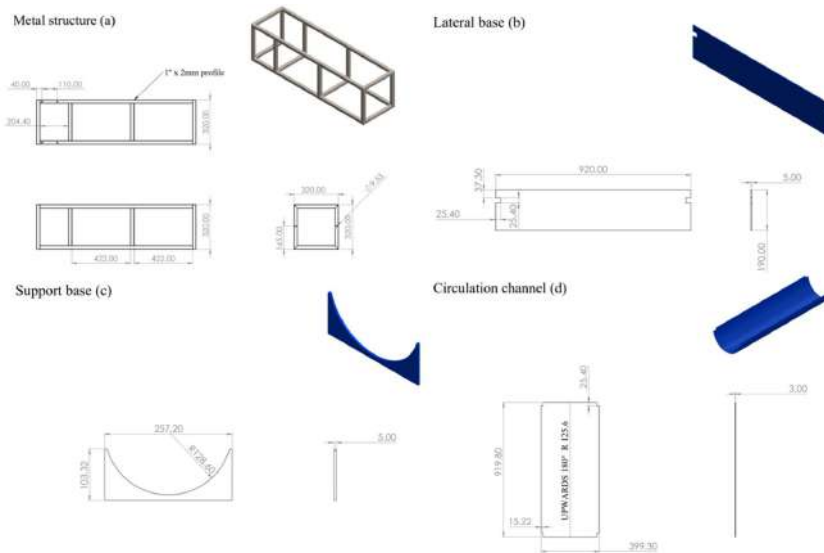


Fig. 2: Diagram of the external section: (a) metal structure; (b) lateral base; (c) support base; (d) circulation channel.

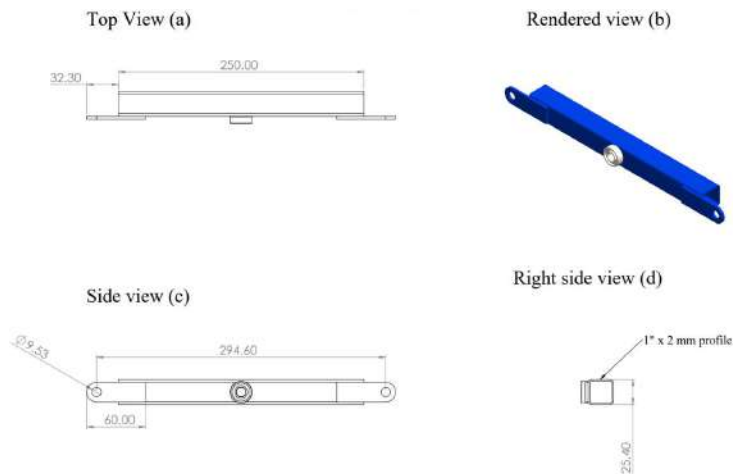


Fig. 3: Auxiliary support.

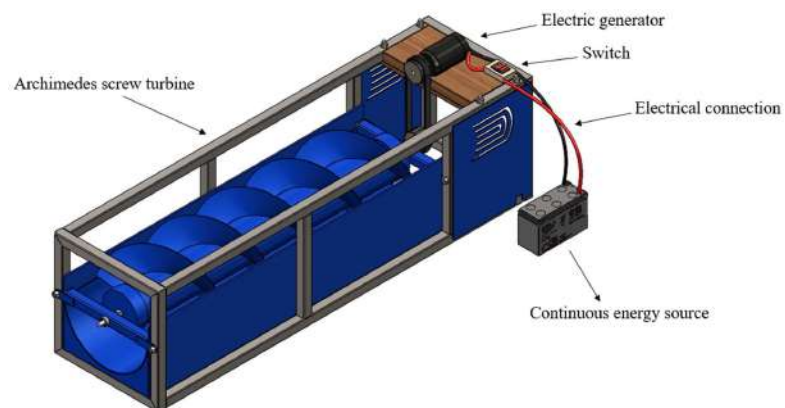


Fig. 4: Rendered design of the micro-hydraulic system with the assembled sections.

continuous energy source, which was used in the laboratory tests to supply electric current to the electrolysis process.

For the torque, equation (1) was used, where the values of height, wetted area, angles, and water are considered; in addition, equation (2) and equation (3) were used to determine the wetted area and inertia  $Y_c$ , respectively (Sánchez et al. 2023):

$$T = \rho \times g \times LT \times Am \times \sin(\theta) \times \tan(\alpha) \times Y_c \quad \dots(1)$$

$$Am = 3/8 \times \pi \times Rhe^2 \quad \dots(2)$$

$$Y_c = 0.4951 \times Rhe \quad \dots(3)$$

Where,  $T$  is the generated torque in (Nm),  $\rho$  is the density of water ( $1000 \text{ kg.m}^{-3}$ ),  $g$  is gravity ( $9.81 \text{ m.s}^{-2}$ ),  $LT$  is the total length of the turbine in (m),  $Am$  is the wetted area of the water with the turbine blades in ( $\text{m}^2$ ),  $\theta$  is the inclination angle of the turbine in ( $^\circ$ ),  $\alpha$  is the inclination angle of the blades in ( $^\circ$ ),  $Y_c$  is the inertia of the blade in (m) and  $Rhe$  is the radius of the blade in (m); assuming 50% wetted area for higher efficiency (Alonso-Martinez et al. 2020).

The calculation was performed considering the criteria of the inner section design, where  $\theta$  and  $\alpha$  were considered  $30^\circ$  and  $40^\circ$  respectively, because the turbine can reach an efficiency of 80%, and these angles have higher efficiency in the turbine (Dragomirescu 2021). By replacing, a torque of 3.79 Nm was obtained. With these two criteria, it was determined to use an electric generator (DC), whose main characteristics are specified in Table 2.

Table 2: Technical specifications of the electrical generator.

Type	DC electric generator with brush
Model	XD-3420
Rated power [W]	30
Rated voltage [V]	12
Nominal speed [RPM]	3500
Amperage [A]	0.5
Torque [kgfcm]	1

## Electrolysis

**Design of the electrolytic cell:** For the final design of the electrolysis process, an electrolytic cell was constructed, which has the shape of a rectangular prism made of glass and an acrylic lid with a working capacity of approximately  $2900 \text{ cm}^3$  (Fig. 5a) for the production of green hydrogen and oxygen; having a width of 10.5 cm and a length of 23.5 cm. A glass separator plate was used 10 cm away from the sides to separate the anode and cathode to independently produce hydrogen and oxygen. The plate was shorter than the overall height of the cell to allow contact between the anode region and the cathode region; the electrodes had a working depth of 0.5 cm less than the separator plates so that the gases produced did not cross their respective region. Thus, the lower area of the cell was left open for the free circulation of water and the circulation of the current supplied to each electrode (Fig. 5b).

The cell lid had in the middle a circular hole of 1/2" diameter through which the electrolyte solution entered, two

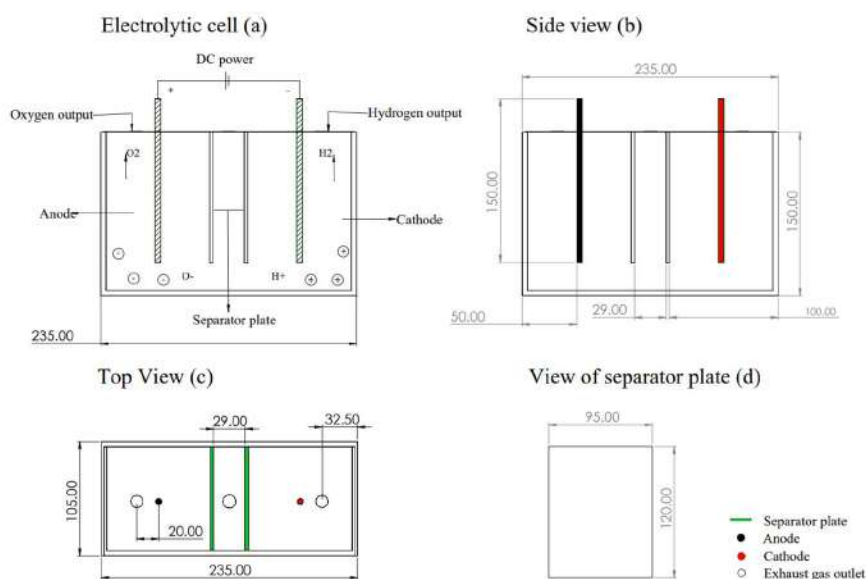


Fig. 5: Schematic of the electrolytic cell: (a) Electrolysis process in the electrolytic cell; (b) Side view of the electrolytic cell; (c) Top view of the electrolytic cell; (d) Separator plate.

circular holes 5 cm from the sides to insert the electrodes, and two other circular holes of 8 mm diameter 3 cm from the sides to insert the valves, which serve as an outlet for the gases from each region (Fig. 5c).

The separator plate was 9.5 cm wide and 12 cm high (Fig. 5d). A space was provided between the plates to insert a 1/2" nipple into the hole in the lid.

**Electrodes:** AISI 316 stainless steel was used for the anode and cathode; it is a non-noble metal. It contains approximately 19% chromium, 12% nickel, and 68.40% iron (Hamidah et al. 2018). The choice of this material is based on its outstanding properties, with an emphasis on its corrosion resistance, which plays a critical role in ensuring the durability and efficiency of the alkaline electrolysis process. During the electrolysis process, the anode and cathode electrodes are connected to a continuous energy source; oxygen is produced on the anode surface, and green hydrogen is generated on the cathode surface (Albornoz et al. 2023). The electrodes are formed by a 1/4" x 15 cm screw, where 13 AISI 316 steel plates are inserted, which have a size of 8 cm x 8 cm giving a wide surface with respect to the electrolytic cell to counteract the presence of gas bubbles that have a negative influence by obstructing the electrolysis process (Babay et al. 2023), in addition, these plates have a perforation in the middle and using 1/4" nuts they are coupled (Fig. 6).

**Electrolyte solution:** To determine the electrolyte solution to be used in our cell, distilled water was used as the main solution, being a pure solution and free of unwanted components, and a comparison was made between three electrolytes: potassium hydroxide (KOH), sodium hydroxide

(NaOH) and sodium chloride (NaCl). The purpose of the electrolytes is to improve the efficiency of the electrolysis process, where characteristics such as corrosion in AISI 316 steel were taken into account. The NaCl presents a higher corrosion rate because the Cl ion makes it highly active for the corrosion process; NaOH and KOH are almost similar because they present the hydroxyl (OH) in their composition, increasing the electrical conductivity of the solution, which is proportional to the corrosion, being KOH the electrolyte with less corrosion (Colli et al. 2019, Hamidah et al. 2018); also a comparison of these electrolytes in different concentrations was made regarding the electrical conductivity they reached, which is presented in the results chapter.

### Simulation of the Portable Hybrid System

The hybrid system has the advantage of mobility by incorporating an Archimedes screw turbine which, due to its attributes, facilitates the disassembly and subsequent reassembly of its components; this characteristic transforms it into a portable device as it does not have a fixed structure like those observed in dams. The electrolytic cell is also portable, and both devices interact synergistically to produce green hydrogen, where the microhydraulic system, for its part, constitutes the device in charge of obtaining energy for the electrolysis process, consolidating itself as a sustainable procedure.

The simulation is shown in Fig. 7 details the value chain of our hybrid system for the production of green hydrogen. Initially, the hybrid system was placed in a useable water resource, such as low-flow rivers or water channels. In the

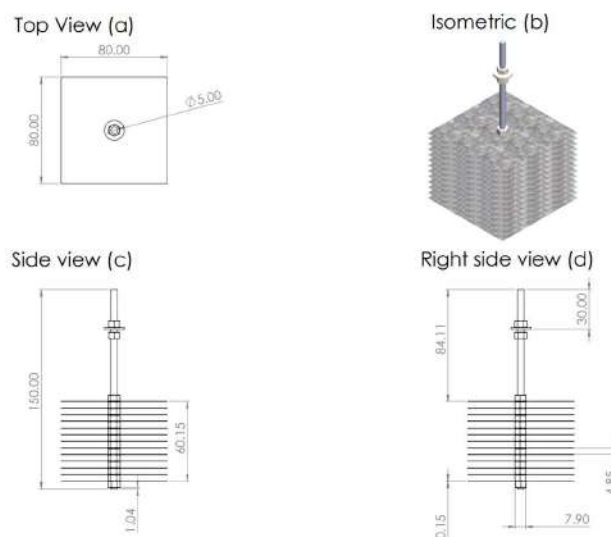


Fig. 6: Electrode.



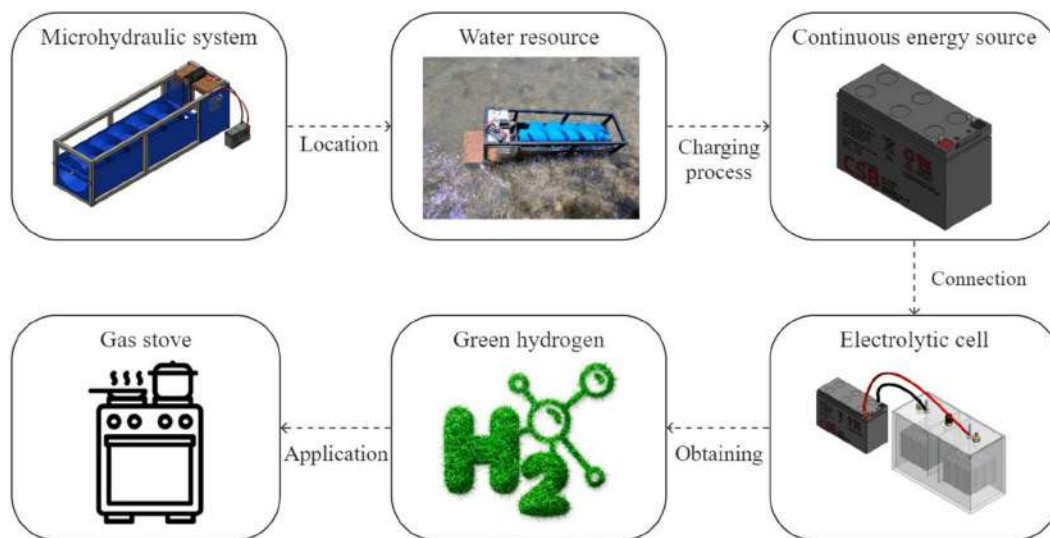


Fig. 7: Green hydrogen value chain.

study carried out, the turbine was placed in a river for the generation and storage of electrical energy. At the end of the charging process of the continuous energy source, this corresponding component is removed from the microhydraulic system and connected to the electrolytic cell using an electrical connection to the electrodes, where the electrolysis process is carried out to obtain the green hydrogen and for its application in stovens, tests were conducted which are detailed in the results section, demonstrating its viability to replace LPG as an ecological fuel for cooking food.

## Experimental Configuration

### First stage: Performance of the Micro-Hydraulic System

**Volumetric flow rate:** The volumetric flow rate was determined using the current meter method, where the equipment measures the water velocity at a certain point; first, the width of the channel was calculated to determine the number of cross sections to be divided from the total section. In each section, the flow velocity and depth were calculated using the equipment correctly, taking into consideration that, to measure the flow velocity, the current meter was placed

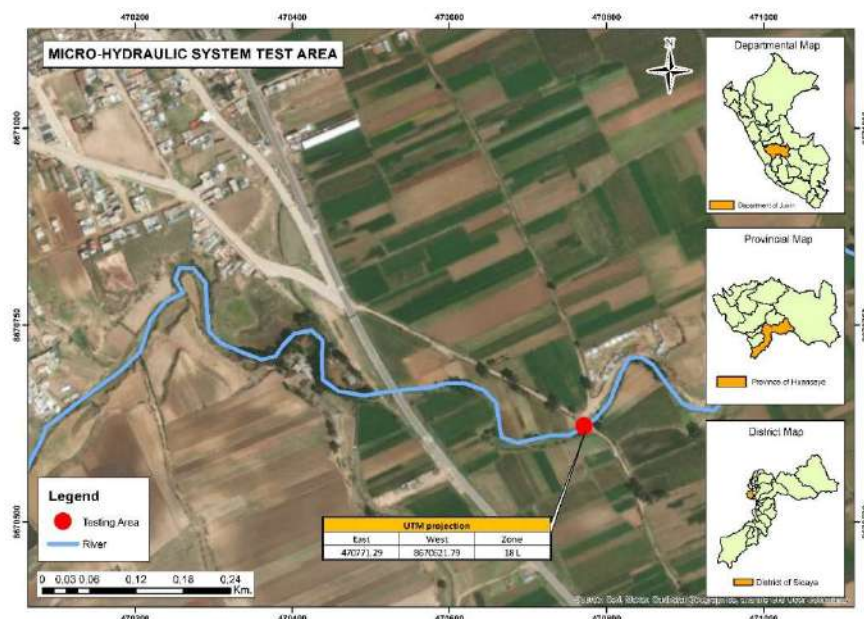


Fig. 8: Micro-hydraulic system test area.

at an intermediate distance from the water depth to avoid obstacles and obtain more representative measurements. Fig. 8 shows the area where the micro-hydraulic system was tested.

**Mechanical potential:** To determine the theoretical potential of the Archimedes screw design, equation (4) was used, which refers to the energy available in the water flowing through the micro-hydraulic system to convert mechanical energy into electrical energy (Sánchez et al. 2023):

$$P_H = T \times w \quad \dots(4)$$

Where  $P_H$  is the theoretical potential in (W),  $T$  is the torque obtained from equation (1) in (Nm), and  $w$  is the angular velocity in (rad/s) which is determined using equation (5):

$$w = \frac{Q \times \tan(\alpha)}{Am \times Yc} \quad \dots(5)$$

Where  $Q$  is the turbine inflow in ( $\text{m}^3 \cdot \text{s}^{-1}$ ),  $\alpha$  is the inclination angle of the blades in ( $^\circ$ ),  $Yc$  is the blade inertia in (m), and  $Am$  is the wetted area of the water with the turbine blades in ( $\text{m}^2$ ).

**Fall slope:** Two level values were determined with respect to the angle of fall; the first level value was equal to the natural slope of the river, where equation (6) was used, representing Manning's formula (Díaz-Salas et al. 2020):

$$n = \frac{1}{Vf} \times Rh^{2/3} \times S^{1/2} \quad \dots(6)$$

Where  $Vf$  is the flow velocity in ( $\text{m} \cdot \text{s}^{-1}$ ),  $Rh$  is the hydraulic radius of the channel in (m), which was determined with equation (7),  $S$  is the slope in (%), and  $n$  is the roughness coefficient, where the value of  $n$  was determined using Cowan's method described in equation (8):

$$Rh = \frac{Ah}{P} \quad \dots(7)$$

$$n = (n0 + n1 + n2 + n3 + n4) \times m5 \quad \dots(8)$$

Where  $Ah$  is the hydraulic area in ( $\text{m}^2$ ), and  $P$  is the perimeter in (m), taking into account that they correspond to the total wetted section (Islam et al. 2022). Table 3 is used to determine the value of each variable of Cowan's method, taking into account the channel conditions observed during the field study.

**Influence of wetted area and fall slope on rotational speed and electric potential:** In the influence tests, the dependent and independent factors were determined, taking into account that the turbine has a fixed design and that it was placed in a river. The independent factors are the fall slope (PC) and the wetted area (Am) with two-level values to study their performance with respect to the electrical potential and to contrast with the rotational speed of the turbine;

Table 3: Criteria and numerical values for the Cowan method (Díaz-Salas et al. 2020).

Channel condition		Values	
Material considered	Land	n0	0.020
	Rock cutting		0.025
	Fine gravel		0.024
	Coarse gravel		0.028
Degree of Irregularity	Soft	n1	0.000
	Minor		0.005
	Moderate		0.010
Cross Section Variation	Severe		0.020
	Gradual	n2	0.000
	Occasionally alternating		0.005
Effect of Obstructions	Frequently alternating		0.010-0.015
	Insignificant	n3	0.000
	Minor		0.010-0.015
Vegetation	Appreciable		0.020-0.030
	Severe		0.040-0.060
	Low	n4	0.005-0.010
Number of Meanders	Medium		0.010-0.025
	High		0.025-0.050
	Very high		0.050-1.000
Number of Meanders	Minor	m5	1.000
	Appreciable		1.150
	Severe		1.300

Table 4: Full factorial design.

Fall slope	Wetted area	Run number
PC 1	Am 1	1
	Am 1	2
PC 2	Am 2	3
	Am 2	4

consequently, a  $2^k$  full factorial design was used, with  $k = 2$  (Table 4).

The river section was selected according to the physical conditions of the terrain in order to be able to manipulate the fall slope and the wetted area. Regarding the level values, it was taken into account that the initial fall slope of the turbine was the same as the natural fall slope of the river, and for the second value, a 14.5 cm high block was placed. For the wetted area, the turbine was placed at different points to have a smaller wetted area and another similar to the ideal, which allowed the four possible combinations of the experimental design to be carried out, considering three repetitions to obtain representative measurements. For data collection, a multimeter (Samwin DT830D) was used, which gave us the value of voltage and current intensity, and a

digital tachometer (CHECK-LINE CDT-1000HD) was used to determine the rotational speed in revolutions per minute (RPM). Using equation (9), the electrical potential of the turbine was determined:

$$Pe = Volt \times Ic \quad \dots(9)$$

Where  $Pe$  is the electric potential in (W),  $Ic$  is the current intensity in (A), and  $Volt$  is the voltage in (V).

## Second stage: To Determine the Amount of Hydrogen Produced by the Electrolytic Cell

**Electrolyte comparison:** To determine the electrolyte to be dissolved in the distilled water, a comparison was made between seven concentrations of KOH, NaOH, and NaCl with an electrical conductivity test using the combined meter (HANNA HI9828); where the optimum amount of electrolyte to be used was the concentration that achieved the highest electrical conductivity in the solvent.

**Volumetric flow and mass flow of green hydrogen:** This test was based on a one-group design, where the only factor to be evaluated is the production capacity of the electrolytic cell, considering three repetitions since there are fixed factors such as the electrode material, the voltage of the continuous energy source, and the concentration of the electrolyte.

The source that supplied energy to the electrolytic cell was previously obtained from the microhydraulic system. Regarding data collection, the displacement of the water was used to determine the volume of green hydrogen; with a manometer placed in the storage vessel, the gauge pressure of the gas produced was obtained, and the ideal gas law was also used since the green hydrogen produced at environmental pressure (Colli et al. 2019); equation (10) was used to determine the mass of the gas produced, which when interacting with a determined time the mass flow was obtained in ( $\text{g.s}^{-1}$ ) as indicated in equation (11) and when interacting time with volume, the volumetric flow of the produced gas was obtained in ( $\text{L.s}^{-1}$ ) which is indicated in equation (12):

$$Pabs \times v = \frac{m}{M} \times R \times Tc \quad \dots(10)$$

$$\dot{m} = \frac{m}{t} \quad \dots(11)$$

$$\dot{v} = \frac{v}{t} \quad \dots(12)$$

Where  $Pabs$  is the absolute pressure in (atm) and to determine its value, equation (13) was used;  $v$  is the volume of green hydrogen produced in (L),  $m$  is the mass of the gas in (g),  $M$  is the molar mass of the gas in ( $\text{g.mol}^{-1}$ ),  $R$  is the ideal gas constant ( $0.0821 \text{ Latm.mol}^{-1}.\text{K}^{-1}$ ),  $Tc$  is the temperature of the electrolytic cell in (K) which was calculated using a digital pyrometer and  $t$  is the time in (s):

$$Pabs = Pman + Patm. \quad \dots(13)$$

Where  $Pman$  is the gauge pressure in (atm), and  $Patm$  is the atmospheric pressure in (atm), which was determined using equation (14) representing the barometric equation:

$$Patm = P0 \times e^{-\frac{Mm \times g \times h}{R \times Tg}} \quad \dots(14)$$

Where  $P0$  is the pressure at standard level (1 atm),  $Mm$  is the molar mass of air ( $0.02896 \text{ kg.mol}^{-1}$ ),  $g$  is gravity ( $9.81 \text{ m.s}^{-2}$ ),  $h$  is the height above sea level in (m),  $R$  is the ideal gas constant ( $8.31432 \text{ J.mol}^{-1}.\text{K}^{-1}$ ), and  $Tg$  is the temperature according to the geographical location in (K).

## RESULTS AND DISCUSSION

Below are the results of the experimental work in two stages:

### First stage: Performance of the Micro-Hydraulic System

**Volumetric flow rate:** According to the studies carried out in the selected section of the river, the volumetric flow rate was determined using the current meter method. Table 5 shows the calculated measurements, where the width of the river was determined using a flexometer and divided into four cross sections; in addition, the flow velocity and depth were calculated using a current meter (Global Water FP111) in each established section.

To process the collected data, the HidroEsta software was used as a tool that facilitates and simplifies various calculations, where the data was inserted to calculate the flow rate (Table 6).

According to the processed data, the total flow rate of the section was determined, the value of which is  $0.7118 \text{ m}^3.\text{s}^{-1}$ . In addition, the HidroEsta software gave us the complete geometry of the river, which can be seen in Fig. 9.

Table 5: Data recording of the selected section.

Width [m]	Number of sections	Depth [m]	Flow velocity [ $\text{m.s}^{-1}$ ]
4.35	4.00	0.24	0.00
		0.13	0.80
		0.20	1.10
		0.23	1.30
		0.28	0.00

Table 6: Results of each cross-section.

Section	Area [ $\text{m}^2$ ]	Average velocity [ $\text{m.s}^{-1}$ ]	Volumetric Flow [ $\text{m}^3.\text{s}^{-1}$ ]
1	0.20	0.40	0.08
2	0.18	0.95	0.17
3	0.23	1.20	0.28
4	0.28	0.65	0.18

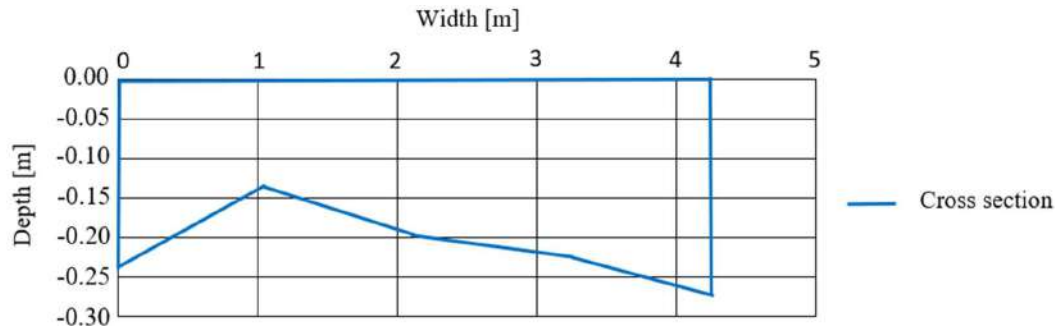


Fig. 9: Complete river geometry.

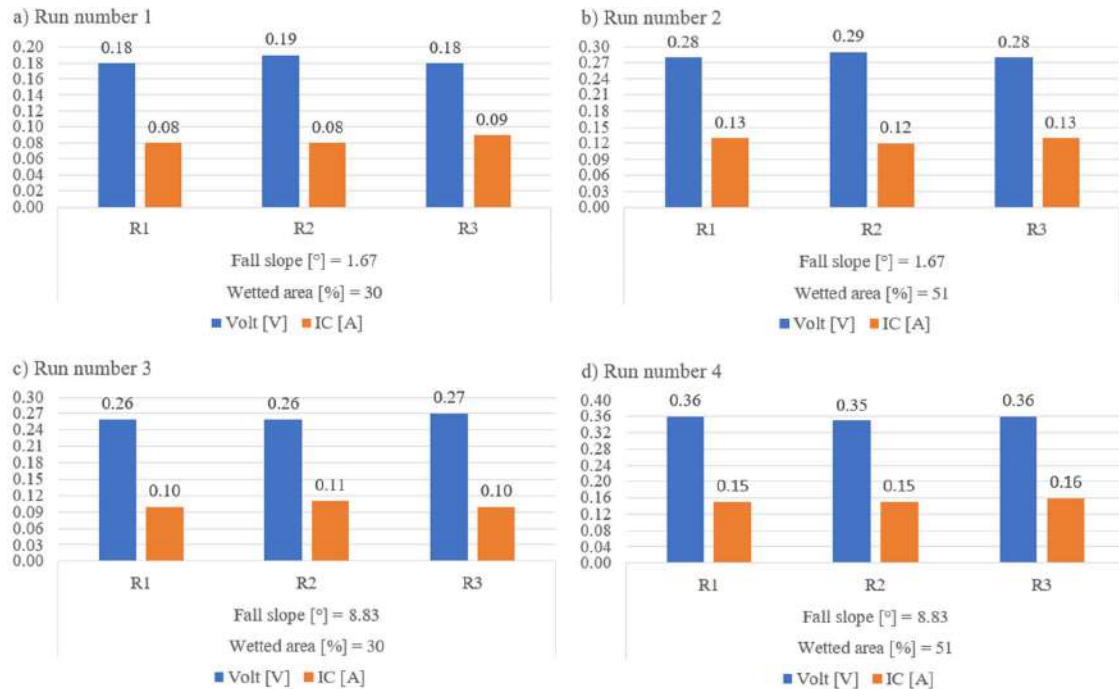


Fig. 10: Voltage and Current Intensity of the micro-hydraulic system.

**Mechanical potential:** Consequently, the theoretical potential of the micro-hydro system was determined using equation (4), where the electrical potential that the turbine can reach is 620.25 W.

**Fall slope:** The characteristics of the channel can be seen in Table 7, where the average flow velocity of the selected section was determined using Table 6, the perimeter and the hydraulic area were determined using Fig. 9, and the hydraulic radius was determined with equation (7), in addition, the Manning's roughness coefficient was determined with equation (8) considering that the values of each variable were determined according to the conditions observed in the channel, and their values are shown in Table 3. With these values, Manning's formula was applied,

giving a slope of 2.91%, which, expressed in degrees, would be 1.67°.

For the second level value, the natural slope of the channel was taken as a reference, which has a value of 2.91%, where every 100 m horizontal rises 2.91 m vertical; expressing

Table 7: Channel characteristics.

Characteristics	Value
Flow velocity [m.s <sup>-1</sup> ]	0.80
Hydraulic area [m <sup>2</sup> ]	0.89
Perímetro [m]	9.20
Hydraulic radius [m]	0.10
Manning's roughness Coefficient	0.045



this in the length of the turbine, it was obtained that every 1.1495 m horizontal rise 0.0336 m vertical for a diagonal of 1.15 m, which represents the length of the turbine; with these dimensions a 14.5 cm block was added at the base of the turbine inlet to increase the slope, giving a value of  $8.83^\circ$ .

**Influence of wetted area and fall slope on rotational speed and electric potential:** At this stage, the wetted area is in (%); it was determined according to the contact of the water with the turbine blades, where 50% means that the contact has a height equal to the radius of the blades; a height meter was used in centimeters attached to the inlet base which indicates the height of the water level, then the turbine was placed at two different points and it was determined that there was a wetted area of 30% and 51%.

With the level values determined for each independent variable, field tests were carried out to determine the *Volt* and the *Ic*, as shown in Fig. 10, which are necessary variables in the calculation of the electric potential.

To simulate the interaction between the falling slope and wetted area with rotational speed and electrical potential, Minitab was used as the processing software for the full factorial design, where two interactions were performed, and twelve data were inserted for each interaction, with a p-value significant as it was less than 0.05, thus demonstrating that there is an effect between these factors and the dependent variables. Fig. 11 shows the interaction of the falling slope and wetted area with the rotational speed, where the lowest amount of rotational speed generated by the turbine is 50

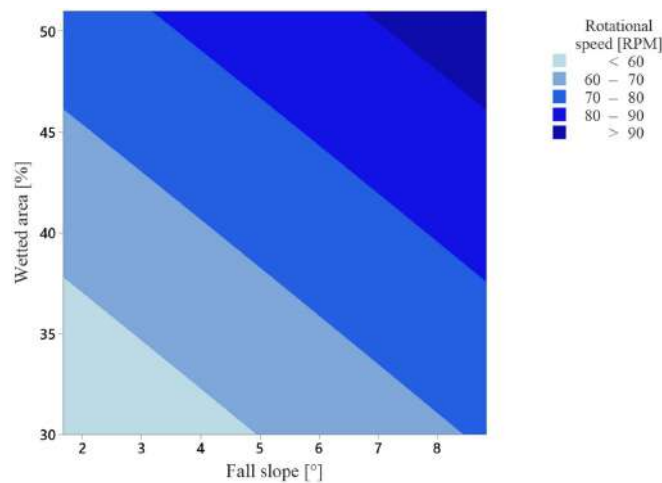


Fig. 11: Contour of rotational speed as a function of fall slope and wetted area.

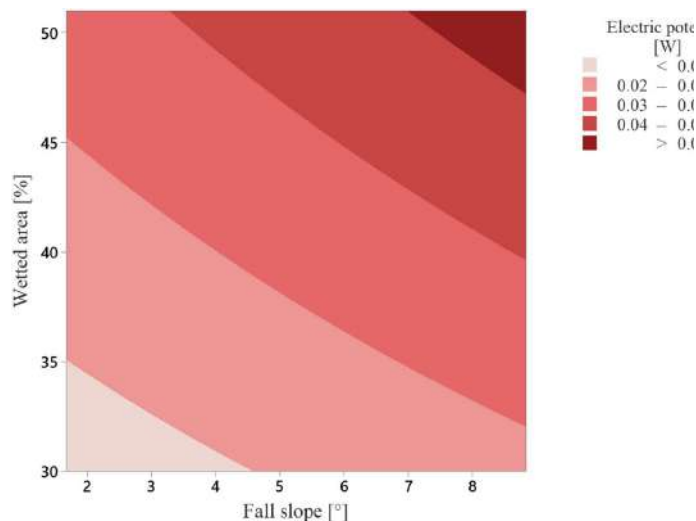


Fig. 12: Contour of the electric potential as a function of fall slope and wetted area.

RPM, which occurs when the slope is  $1.67^\circ$ , and the wetted area is 30%, while 96 RPM is generated when the slope is  $8.83^\circ$ , and the wetted area is 51%, being these the most efficient values of the factors. Consequently, it is established that increasing the fall slope and the wetted area produces a higher rotational speed.

The second interaction represents the effect of the factors with the desired response, which would be the electric potential, where the values of each run were determined using equation (9) with the values in Fig. 10. Fig. 12 shows that the micro-hydraulic system presents a lower electric potential of 0.015 W when the slope is  $1.67^\circ$ , and the wetted area is 30%; while 0.055 W is generated when the slope is  $8.83^\circ$ , and the wetted area is 51%, being these the most efficient values of the factors to generate electricity. It was determined that the micro-hydraulic system is more efficient when there is a higher fall slope and wetted area.

Additionally, a Spearman's Rho test was performed to determine the correlation between the rotational speed and

the electrical potential (Fig. 13). It was determined that the rotational speed represented in Fig. 11 is related to the electrical potential produced by the micro-hydraulic system demonstrating that the higher the RPM, the more electricity is generated.

### Second Stage: To Determine the Amount of Hydrogen Produced By the Electrolytic Cell

**Electrolyte comparison:** The electrolyte to be used in the solution was determined, where it was found that KOH has a higher electrical conductivity, given that from a concentration of 20%, it exceeds  $400 \text{ mS}\cdot\text{cm}^{-1}$  (Fig. 14), being the highest measurement value allowed by the equipment. In addition, KOH at a concentration of 20% demonstrates greater effectiveness for the alkaline electrolysis process (Cao et al. 2023, Colli et al. 2019), being the suitable concentration that was used to prepare the electrolyte solution, while NaCl has the lowest values of electrical conductivity. The curve of these electrolytes tends to decrease after a certain concentration.

			Electric potential	Rotational speed
Spearman's Rho	Electric potential	Correlation coefficient	1,000	1,000**
		Sig. (bilateral)	.	.
		N	4	4
	Rotational speed	Correlation coefficient	1,000**	1,000
		Sig. (bilateral)	.	.
		N	4	4

Fig. 13: Correlation analysis between rotational speed and electric potential.

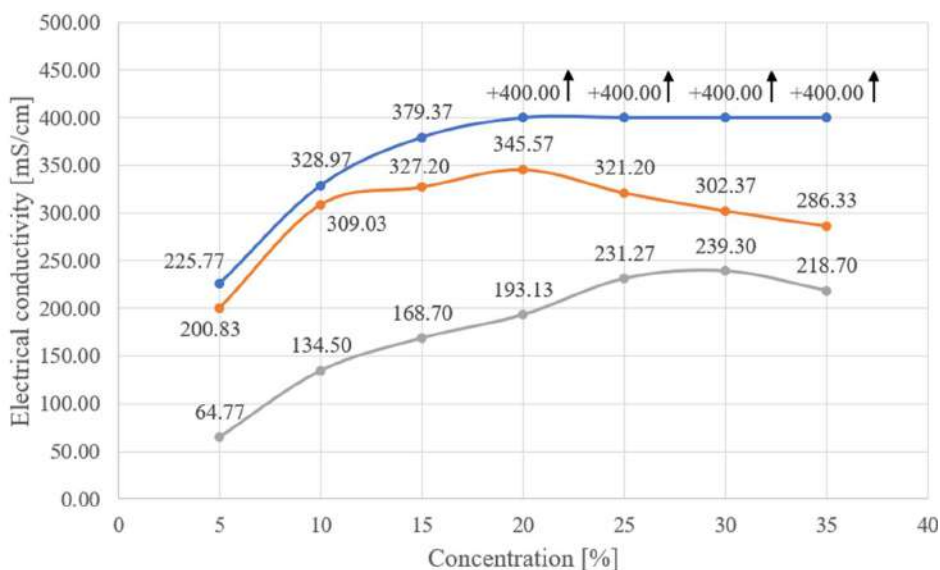


Fig. 14: Electrical conductivity of KOH, NaOH, and NaCl.

**Volumetric flow and mass flow of green hydrogen:** The fixed characteristics for operating the electrolytic cell were determined, such as the voltage and current intensity of the continuous energy source; being 12 V and 18 A, respectively. Furthermore, it is considered that the green hydrogen produced behaves as an ideal gas. Therefore, it is necessary to determine the ambient conditions present to use the ideal gas equation. To calculate the absolute pressure, initially, the height above sea level was determined to be 3250 m, and the environmental temperature was determined using data from the Santa Ana meteorological station located in the city of Huancayo, Junín region - Peru, giving a temperature of 287.15 K, values necessary for equation (14), giving an atmospheric pressure of 0.6813 atm.

The gauge pressure was obtained because the electrolysis process stored the gases in the vessels without leakage, taking into account that the space without electrolyte solution contains air, so the gauge pressure will increase according to the total amount of green hydrogen filling the space; the volume of this space was determined by adding the volume of the cathode region which value is  $220 \text{ cm}^3$ , the volume of the hose which is  $250 \text{ cm}^3$  and the volume of the vessel which is  $289 \text{ cm}^3$ . Thus, the gauge pressure reached an average value of 32 mmHg in the case of green hydrogen, which can be expressed in the same units as atmospheric

pressure as 0.0421 atm. Equation (13) was used to obtain the absolute pressure, which is approximately 0.7214 atm. The molar mass value in the case of hydrogen is  $2 \text{ g}\cdot\text{mol}^{-1}$ , and the temperature was determined with the digital pyrometer (Control Company Traceable 122402526) pointing to the electrolyte solution at the end of each measurement test, where it was observed to be  $31.8^\circ\text{C}$  on average.

In the case of volume, it was calculated through the displacement of water, where the volume of gas produced has a direct relationship to the water displaced, as shown in Fig. 15; furthermore, it is not necessary to fill the space without electrolyte solution with this gas, as the gases expand to fill any space without requiring the gas to occupy the space containing air. Before displacing the water, first, the cell was graduated where the height of the electrolyte solution represents 0 cm. As the electrodes react in the water through electrical energy, the gas produced displaces the water. Consequently, it was determined that in an average of 24 seconds, 0.0475 L of green hydrogen was produced, as shown in Table 8.

A 2.9 L electrolytic solution was prepared for each test in the cell where the temperature, volume, and gauge pressure of the green hydrogen were measured for approximately 24 seconds to determine the volume of the hydrogen, the auxiliary component of oxygen, which consists of a storage

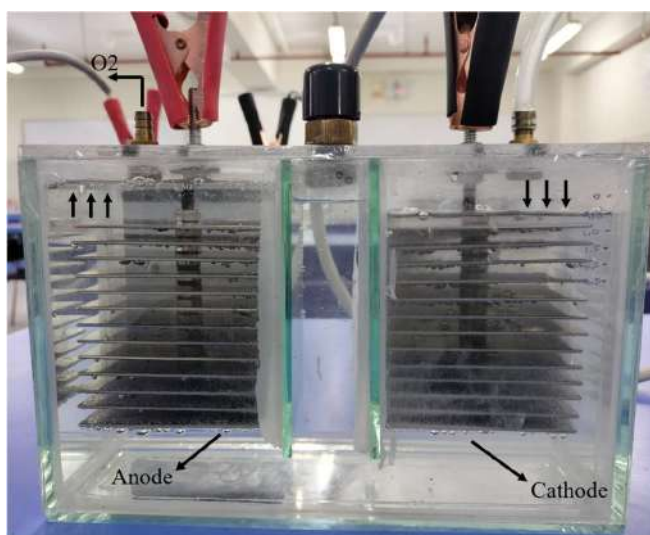


Fig. 15: Water displacement

Table 8: Temperature, Volume, and Pman of green hydrogen.

Repetition	Time [s]	Temperature [K]	Volume [L]	Pman [atm]	Mass [g]
R1	23.7	304.8	0.0475	32	0.002739
R2	24.2	304.9	0.0475	32	0.002738
R3	24.1	304.8	0.0475	32	0.002739

vessel, was removed. Consequently, equation (10) was used to determine the mass of the green hydrogen, resulting in an average of 0.002739 g, as shown in Table 8.

Using these data, the volumetric flow and mass flow of the green hydrogen produced by the electrolytic cell were determined to be  $118.760 \text{ cm}^3 \cdot \text{min}^{-1}$  and  $0.00011 \text{ g} \cdot \text{s}^{-1}$ , respectively. To determine the amount of oxygen produced, the behavior of an ideal gas was taken into account, where it can be inferred that of the total volume of the gas produced, two-thirds is green hydrogen, and one-third is oxygen since one molecule of water is made up of two molecules of hydrogen and one of oxygen, consequently,  $59.380 \text{ cm}^3 \cdot \text{min}^{-1}$  of oxygen is produced as shown in Fig. 16 expressed in  $\text{L} \cdot \text{s}^{-1}$ , which was released into the atmosphere.

To check that the gas produced is green hydrogen, an additional component was assembled to the valve of the

cathodic region, which consists of a bubbler and a Bunsen burner. For this test, the valve of the ignition mechanism was opened and provided with fire; on contact, it was observed that the green hydrogen ignited (Fig. 17), demonstrating that it has a high calorific power and that it can be used to replace conventional fuel.

## DISCUSSION

In the present study, the micro-hydraulic system at most generates 0.055 W and 0.15 A according to the factors studied, which is low in terms of power, unlike other similar turbines (Alonso-Martinez et al. 2020); this is due to the use of an electric generator (DC) with the characteristics specified previously, so it requires 120 hours to charge the continuous energy source with capacity of 18 A per hour, where the charging time is not optimal; however it should

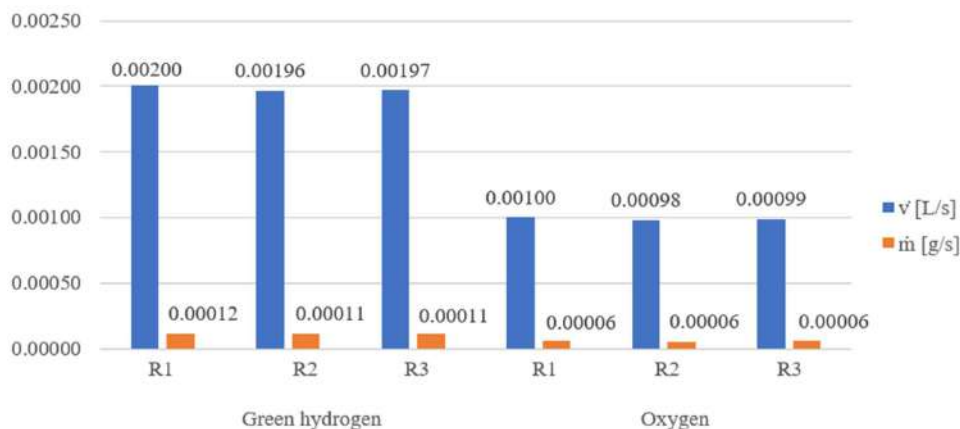


Fig. 16: Volumetric flow ( $\dot{v}$ ) and mass flow ( $\dot{m}$ ) of hydrogen and oxygen.



Fig. 17: Ignition test.



be considered to use a suitable electric generator that can minimally support the mechanical potential of the micro-hydraulic system which is 620.25 W. The electrical generator (DC) used does not need a charge controller because it produces a constant flow of energy, unlike an alternating current generator that produces energy with fluctuations, which can damage the continuous energy source.

The electrolytic cell proposed in this study has a higher production rate of green hydrogen than other similar electrolytic cells (Mert et al. 2024, Sanath et al. 2019), being  $118.760 \text{ cm}^3 \cdot \text{min}^{-1}$ , which is since our electrolysis process uses stored energy from the potential energy of water, being the renewable energy resource with the highest operating efficiency compared to other systems that use wind and solar energy, which depend on the environmental conditions where they are located. It should be noted that the micro-hydraulic system can operate all day long; however, when unfavorable meteorological events occur that increase the flow, this system will have to be removed from the body of water where it was placed to avoid possible dragging by the force of the water itself. In addition, the energy generated by the microhydraulic system is stored in a continuous energy source to supply electricity to the electrodes, producing a continuous volumetric flow of green hydrogen, unlike similar electrolytic cells (Mert et al. 2024, Sanath et al. 2019), where the generated energy fluctuates when supplying electricity to their respective electrodes.

Although it is not economically viable to use distilled water, it is preferable to use water from the river where the hybrid system is placed because it is a resource that is found in the environment at no cost. Consequently, it is necessary to determine that the gas produced is green hydrogen without other compounds, carrying out a chromatography analysis, taking into account that within the analysis, nitrogen ( $\text{N}_2$ ) is obtained as one of the components since it is found in the system spaces, as well as other components from the water in case it is residual. To reduce the unwanted components that can be produced from wastewater, it is crucial to adopt measures that are efficient and economical, which must be focused on being implemented in rural areas, considering that these methods are homemade, ecological and environmentally friendly to improve water quality, such as mechanical filtration using sand, gravel and activated carbon filters; coagulation and flocculation using natural substances; and phytoremediation using aquatic plants (Abdiyev et al. 2023, Panday & Ananda Babu 2023).

## CONCLUSIONS

This paper demonstrates the feasibility of a portable hybrid system designed specifically for application in rural areas

with water bodies of low volumetric capacity. The proposed system has been optimized to operate under hydraulic conditions typical of rural environments. The green hydrogen produced by the portable hybrid system can be used as an environmentally friendly fuel due to its high calorific potential, being one of its main characteristics to replace conventional fuel such as LPG which is widely used in rural areas for cooking food. Its potential to change the paradigm of conventional fuel use in isolated communities through a sustainable and cost-effective solution is highlighted.

This work shows that the green hydrogen produced by the portable hybrid system can be used as an ecological fuel due to its high calorific potential, which is one of its main characteristics to substitute the conventional fuel used in rural areas for cooking food, such as LPG; this system uses the energy generated by a microhydraulic system that can be located in water bodies with low volumetric capacity.

In the first stage of the results, it is shown that the wetted area of the water in relation to the Archimedes screw turbine and the fall slope are factors with influence the electric potential, which is contrasted with the rotational speed. Accordingly, it was determined that the micro-hydraulic system, when placed at an angle of elevation equal to  $8.83^\circ$  with a wetted area of 51%, generates a higher electric potential, being 0.055 W. These characteristics can be altered according to the body of water where the microhydraulic system is placed. However, it remains in operation as long as the blades have contact with the water. The influence of slope on the efficiency of hydro turbines is recognized as an established concept; however, our work explores how minor variations in slope can be optimized to maximize micro-hydraulic power production, given that rural areas have low volumetric capacity water bodies such as water channels.

In the second stage, the amount of green hydrogen produced is demonstrated, where the optimal concentration and the appropriate electrolyte to be used in the distilled water is 20% KOH. Also, the continuous energy source is a fixed factor to be considered because it operates with 12 V and 18 A, which influences the amount of green hydrogen produced, which is  $118.760 \text{ cm}^3 \cdot \text{min}^{-1}$ , thus showing a high volumetric flow, considering that the green hydrogen must first be stored in a container to be used later on as a fuel in the cooking of foodstuffs.

Future research is intended to develop the design of a hybrid system with a continuous process to produce green hydrogen more efficiently, maintaining the current advantage of being a portable design and of viable use, where the use of a charge controller should be considered to feed the continuous energy source and at the same time use the electric current in the electrolysis process, in addition to

using a suitable electric generator to take advantage of the capacity of the microhydraulic system and use the water where the hybrid system is placed, as a water resource for the electrolysis process.

## ACKNOWLEDGMENTS

We want to express our sincere thanks to those responsible for the laboratory of the Continental University for their technical support and essential contribution, training us with each piece of equipment used throughout the development of this research.

## NOMENCLATURE

### Symbols

$A_h$	Hydraulic area	[m <sup>2</sup> ]
$A_m$	Wetted area	[%]
$H$	Height above sea level	[m]
$I_c$	Current intensity	[A]
$LT$	Total length of the turbine	[m]
$M$	Mass of the gas	[g]
$\dot{m}$	Mass flow	[g.s <sup>-1</sup> ]
$M$	Molar mass of the gas	[g.mol <sup>-1</sup> ]
$P$	Perimeter	[m]
$P_{abs}$	Absolute pressure	[atm]
$P_{atm}$	Atmospheric pressure	[atm]
$PC$	Fall slope	[°]
$Pe$	Electric potential	[W]
$P_{man}$	Gauge pressure	[atm]
$P_H$	Theoretical potential	[W]
$Q$	Flow rate	[m <sup>3</sup> .s <sup>-1</sup> ]
$R_{he}$	Propeller radius	[m]
$R_h$	Hydraulic radius	[m]
$S$	Slope	[%]
$T$	Time	[s]
$T$	Torque	[Nm]
$T_c$	Electrolytic cell temperature	[K]
$T_g$	Environmental temperature	[K]
$V$	Volume of green hydrogen	[L]
$\dot{v}$	Volumetric flow	[L.s <sup>-1</sup> ]
$V_f$	Flow velocity	[m.s <sup>-1</sup> ]
$Volt$	Voltage	[V]
$W$	Angular velocity	[rad.s <sup>-1</sup> ]

$Y_c$	Propeller inertia	[m]
-------	-------------------	-----

### Greek letters

$P$	Density	[kg.m <sup>-3</sup> ]
$A$	Inclination angle of propellers	[°]
$\Theta$	Inclination angle of the turbine	[°]

### Subscripts and superscripts

Int	Internal PC Y Am
CH <sub>4</sub>	Methane
CO	Carbon monoxide
CO <sub>2</sub>	Carbon dioxide
H <sub>2</sub>	Hydrogen
N <sub>2</sub>	Nitrogen
N <sub>2</sub> O	Nitrous oxide
O <sub>2</sub>	Oxygen

### Abbreviations

IEA	International Energy Agency
DC	Direct Current
IPCC	Intergovernmental Panel on Climate Change
LPG	Liquefied Petroleum Gas
RPM	Revolutions Per Minute
WHO	World Health Organization

## REFERENCES

- Abdiyev, K., Azat, S., Kuldeyev, E., Ybyraimkul, D., Kabdrakhmanova, S., Berndtsson, R., Khalkhabai, B., Kabdrakhmanova, A. and Sultakhan, S., 2023. Review of slow sand filtration for raw water treatment with potential application in less-developed countries. *Water (Switzerland)*, 15, p.11207. [DOI]
- Albornoz, M., Rivera, M., Wheeler, P. and Ramírez, R., 2023. High pulsed voltage alkaline electrolysis for water splitting. *Sensors*, 23, p.820. [DOI]
- Alonso-Martinez, M., Sierra, J.L.S., Dfaz, J.J.D.C. and Martinez-Martinez, J.E., 2020. A new methodology to design sustainable Archimedean screw turbines as green energy generators. *International Journal of Environmental Research and Public Health*, 17, p.236. [DOI]
- Babay, M.A., Adar, M., Chebak, A. and Mabrouki, M., 2023. Dynamics of gas generation in porous electrode alkaline electrolysis cells: An investigation and optimization using machine learning. *Energies (Basel)*, 16. [DOI]
- Bideau, D., Chocron, O., Mandin, P., Kiener, P., Benbouzid, M., Sellier, M., Kim, M., Ganci, F. and Inguanta, R., 2020. Evolutionary design optimization of an alkaline water electrolysis cell for hydrogen production. *Applied Sciences (Switzerland)*, 10, pp.614-625. [DOI]
- Cao, X., Wang, J., Zhao, P., Xia, H., Li, Y., Sun, L. and He, W., 2023. Hydrogen production system using alkaline water electrolysis adapting to fast fluctuating photovoltaic power. *Energies (Basel)*, 16, pp.23-41. [DOI]

- Chen, H., Gu, S., Jia, C., Gu, H., Xu, Q. and Lin, Z., 2023. Effects of household clean fuel combustion on the physical and mental health of the elderly in rural China. *Sustainability (Switzerland)*, 15, pp.61-78. [DOI]
- Colli, A.N., Girault, H.H. and Battistel, A., 2019. Non-precious electrodes for practical alkaline water electrolysis. *Materials*, 12, p.813. [DOI]
- Díaz-Salas, A., Guevara-Pérez, E. and Rosales-Cueva, J., 2020. Estimation model of the Manning roughness coefficient as a function of granulometry in the Santa River, Recuay-Carhuaz sector, Áncash, Perú. *Revista Ingeniería UC*, 27, pp.328-342. [DOI]
- Dragomirescu, A., 2021. Design considerations for an Archimedean screw hydro turbine. *IOP Conference Series: Earth and Environmental Science*, 11, pp.491-513. [DOI]
- Elgarahy, A.M., Eloffy, M.G., Hammad, A., Saber, A.N., El-Sherif, D.M., Mohsen, A., Abouzid, M. and Elwakeel, K.Z., 2022. Hydrogen production from wastewater, storage, economy, governance and applications: A review. *Environmental Chemistry Letters*, 20, pp.3453-3504. [DOI]
- Fathi, E., Arcenales, D. and Belyadi, F., 2023. Impacts of different operation conditions and geological formation characteristics on CO<sub>2</sub> sequestration in Citronelle Dome, Alabama. *Energies (Basel)*, 16, p.713. [DOI]
- Fersch, B., Wagner, A., Kamm, B., Shehaj, E., Schenk, A., Yuan, P., Geiger, A., Moeller, G., Heck, B., Hinz, S., Kutterer, H. and Kunstmann, H., 2022. Tropospheric water vapor: A comprehensive high-resolution data collection for the transnational Upper Rhine Graben region. *Earth System Science Data*, 14, pp.5287-5307. [DOI]
- Gavrilov, D.Y. and Boycheva, S.V., 2023. Study assessment of water electrolysis systems for green production of pure hydrogen and natural gas blending. *IOP Conference Series: Earth and Environmental Science*, 41(9), pp.234-246. [DOI]
- Hamidah, I., Solehudin, A., Setiawan, A., Hasanah, L., Mulyanti, B., Nandiyanto, A.B.D. and Khairurrijal, K., 2018. Surface of AISI 316 as electrode material for water electrolysis under potassium hydroxide for hybrid car application. *International Journal of Automotive and Mechanical Engineering*, 15, pp.5863-5873. [DOI]
- Hassan, Q., Abbas, M. K., Tabar, V. S., Tohidi, S., Abdulrahman, I. S. and Salman, H. M., 2023. Sizing electrolyzer capacity in conjunction with an off-grid photovoltaic system for the highest hydrogen production. *Energy Harvesting and Systems*, 10(4), pp.331-348. [DOI]
- Islam, A., Sarkar, B., Saha, U. D., Islam, M. and Ghosh, S., 2022. Can an annual flood induce changes in channel geomorphology? *Natural Hazards*, 111, pp.1019-1046. [DOI]
- Marouani, I., Guesmi, T., Alshammari, B. M., Alqunun, K., Alzamil, A., Alturki, M. and Hadj Abdallah, H., 2023. Integration of renewable-energy-based green hydrogen into the energy future. *Processes*, 11(9), pp. [DOI]
- Mert, M. E., Edis, C., Akyıldız, S., Demir, B. N., Nazligul, H., Gurdal, Y. and Doğru Mert, B., 2024. Design and performance analysis of PV-assisted alkaline electrolysis for hydrogen production: An experimental and theoretical study. *Fuel*, 355, p.129497. [DOI]
- Muhsen, H., Al-Mahmodi, M., Tarawneh, R., Alkhraibat, A. and Al-Halhoul, A., 2023. The potential of green hydrogen and power-to-X utilization in Jordanian industries: Opportunities and future prospects. *Energies*, 17(1), pp. [DOI]
- Muñoz-Maldonado, Y., Correa-Quintana, E. and Ospino-Castro, A., 2023. Electrification of industrial processes as an alternative to replace conventional thermal power sources. *Energies*, 16(19), pp. [DOI]
- Nasser, M., Megahed, T. F., Ookawara, S. and Hassan, H., 2022. A review of water electrolysis-based systems for hydrogen production using hybrid/solar/wind energy systems. *Environmental Science and Pollution Research*, 29, pp.86994-87018. [DOI]
- Niroula, S., Chaudhary, C., Subedi, A. and Thapa, B. S., 2023. Parametric modeling and optimization of alkaline electrolyzer for the production of green hydrogen. *IOP Conference Series: Materials Science and Engineering*, 1279(1), p.012005. [DOI]
- Osman, A. I., Mehta, N., Elgarahy, A. M., Hefny, M., Al-Hinai, A., Al-Muhtaseb, A. H. and Rooney, D. W., 2022. Hydrogen production, storage, utilisation and environmental impacts: A review. *Environmental Chemistry Letters*, 20, pp.153-188. [DOI]
- Panday, V. and Ananda Babu, K., 2023. The potential of phytoremediation to treat different types of wastewater: A review. *Nature Environment and Pollution Technology*, 22(2), pp.969-975. [DOI]
- Sanath, Y., De Silva, K., Middleton, P. H. and Kolhe, M., 2019. Performance analysis of single-cell alkaline electrolyzer using a mathematical model. *IOP Conference Series: Materials Science and Engineering*, 605(1), p.012002. [DOI]
- Sánchez, A. C., Galeano, W. F. and Zambrano, J. M., 2023. Design of a micro-hydraulic generation system based on an Archimedes screw. *Ingenius*, 29, pp.98-107. [DOI]
- Song, H., Kim, Y. and Yang, H., 2023. Design and optimization of an alkaline electrolysis system for small-scale hydropower integration. *Energies*, 17, pp. [DOI]
- Yakubson, K. I., 2022. Prospects for using hydrogen in various branches of the world economy as one of the directions of its decarbonization. *Russian Journal of Applied Chemistry*, 95, pp.309-340. [DOI]
- Zhang, L., Jia, C., Bai, F., Wang, W., An, S., Zhao, K., Li, Z., Li, J. and Sun, H., 2024. A comprehensive review of the promising clean energy carrier: Hydrogen production, transportation, storage, and utilization (HPTSU) technologies. *Fuel*, 355, p.129455. [DOI]

# Reflective Building Façades: The Effect of Albedo on Outdoor Thermal Comfort – A Case Study of Low-Rise Apartments

Gunjan Tyagi<sup>1,2†</sup> and Md Danish<sup>2</sup>

<sup>1</sup>Apeejay School of Architecture and Planning, Greater Noida, India

<sup>2</sup>National Institute of Technology, Patna, Bihar, India

†Corresponding author: Gunjan Tyagi; gunjant.ph21.ar@nitp.ac.in

**Abbreviation:** Nat. Env. & Poll. Technol.

**Website:** [www.neptjournal.com](http://www.neptjournal.com)

*Received:* 25-07-2024

*Revised:* 19-09-2024

*Accepted:* 23-09-2024

## Key Words:

Albedo  
ENVI-met  
Solar reflectivity  
Urban albedo  
Thermal comfort indices  
Urban heat island

## Citation for the Paper:

Tyagi, G. and Md Danish, 2025. Reflective building façades: The effect of albedo on outdoor thermal comfort – A case study of low-rise apartments. *Nature Environment and Pollution Technology*, 24(2), p. B4247. <https://doi.org/10.46488/NEPT.2025.v24i02.B4247>

*Note: From year 2025, the journal uses Article ID instead of page numbers in citation of the published articles.*



Copyright: © 2025 by the authors

Licensee: Technoscience Publications

This article is an open access article distributed under the terms and conditions of the Creative Commons Attribution (CC BY) license (<https://creativecommons.org/licenses/by/4.0/>).

## ABSTRACT

In tropical locations, where urban areas experience considerable temperature rises relative to rural areas, the Urban Heat Island (UHI) effect is becoming more and more evident. Reflective building façades, global warming, and hardscape areas are all contributing issues. Because they reflect solar heat, materials like glass, high-pressure laminates, and metallic sheets raise outdoor temperatures, which affects both human comfort and the environment. This study looks into ways to lessen the negative impacts of reflecting façades on urban heat islands (UHIs), with a particular emphasis on how albedo affects microclimates and urban canyons. We examine the impacts of albedo on outdoor thermal comfort by analyzing research from 2003 to 2022. Thermal comfort indices can be calculated with ENVI-met software, which is useful for specialists in urban planning and architecture. To demonstrate these consequences, a case study of a low-rise housing complex located in Greater Noida, India, is provided. With a subtropical climate, this region sees wide changes in temperature, with summer highs frequently reaching 43°C and winter lows of about 7°C. The study uses ENVI-met simulations to evaluate how reflective façades affect thermal comfort in real-world conditions. This highlights the pronounced heat island effect and the localized heat buildup in urban areas during peak daytime h. The simulation revealed significant temperature variations throughout the day, with air temperatures peaking above 43.77°C by mid-afternoon between buildings, demonstrating the pronounced heat island effect. Relative humidity levels were low, around 39% to 40%, contributing to dry air discomfort. Wind velocities exceeded 1.5 meters per second at certain junctions, intensifying discomfort by amplifying the perceived heat. These findings indicate that the use of reflective materials on building façades in Greater Noida exacerbates human thermal discomfort outdoors. The study provides an opportunity to further measure and analyze these effects to develop targeted strategies for mitigating the urban heat island phenomenon and enhancing outdoor comfort in the region.

## INTRODUCTION

The urban heat island (UHI) phenomenon has grown dramatically during the past few years. The UHI effect has become a significant global issue, and numerous UHI mitigation measures have been implemented globally (Huang & Lu 2018, Taha et al. 1988, Yuan et al. 2013, Akbari & Matthews 2012).

People who live in cities frequently feel the reflected sunlight from buildings, and while this can occasionally be inconvenient, we generally accept it as a characteristic of urban life. However, because of the type and amount of glass used in their façades as well as their curved shapes, buildings have the potential to have more severe effects. About 2% of the surface of the globe is covered by cities. As more individuals relocate from the countryside to urban centers, city populations are experiencing swift growth (Madlener & Sunak 2011). The Urban Heat Island (UHI) phenomenon and its severity in urban areas are largely shaped by local atmospheric and geographical factors (Mohajerani et al. 2017). It has been



shown that asphalt surfaces release  $200 \text{ W.m}^{-2}$  more in the perceptible portions of the spectrum and  $150 \text{ W/m}^2$  more infrared radiation than bare soil surfaces do at summertime's highest temperature (Asaeda et al. 1996). Retro-reflective (RR) materials for building façades have been suggested as a potential alternative to diffuse highly reflective (DHR) materials as a successful approach for UHI reduction because they can redirect sunlight hitting the building façades upward towards the sky, preventing the storage of negative heat in the urban canyon (Morini et al. 2018, Yuan et al. 2013, 2015)

In numerous recent investigations, the impact of RR materials on the possibility of Efforts to mitigate UHIs has been assessed (Yuan et al. 2019, Takashi et al. 2013, Morini et al. 2018, Rossi et al. 2015, Yuan et al. 2013). Yuan et al. (2016) developed a 2D analytic model to assess the possibility of UHIs in Osaka, Japan. The findings indicated that when compared to glass beads with refractive indices of 1.5 and 2.2, glass beads with a refractive index of 1.9 are more successful at mitigating UHIs. A new RR heat-shielding film was recommended for building windows, and its RR property was assessed with regard to the amount of solar radiation that was reflected from the building windows and the sky view factors. According to the findings, the suggested RR film enhances the ability of city structure shapes to reflect more solar radiation upwards, thereby aiding in UHI mitigation (Ichinose et al. 2017). Based on experimental and analytical studies evaluating the angular reflectivity of RR films, such materials could be effectively used as overlays on urban pavements and building façades. They are crafted to boost solar radiation reflection throughout city streets and over city rooftops (Rossi et al. 2014). RR tiles of three different sorts were created and put to the test using an optical experiment. According to the findings, all three varieties of microsphere RR tiles may exhibit strong reflection characteristics for incident light directions spanning from 0 to 60 degrees relative to the surface perpendicular (Morini et al. 2017).

Based on the above studies, it is possible to forecast how RR materials will affect outdoor thermal comfort using measurements acquired on the site. This prediction can then be further developed using CFD analysis and simulation techniques using different software. Several pieces of literature have been examined in the context to better understand the gap between using a reflecting façade on a structure and reducing outdoor thermal comfort.

The transfer of heat from building exteriors to interiors is assessed to look at the impact of three distinct façades (DHR, SR, RR) on the cooling demands of air conditioning. The research shows that building façades incorporating RR (reflective and radiant) and SR (solar reflective) technologies

are highly effective in lowering Mean Radiant Temperature (MRT) and reducing heat transfer from Outer surfaces to the inner surfaces, thus decreasing the cooling demands of air conditioning. Nevertheless, these façades also result in greater solar radiation reflection and heat flux directed towards the ground (Yuan et al. 2021). The majority of research (Rossi et al. 2014, Yuan et al. 2016) showed that when the angle at which sunlight strikes a surface surpasses a predetermined value of roughly  $60^\circ$ , the surface's retro-reflectivity decreases and its downward solar reflectivity increases. High albedo materials applied to the vertical and horizontal limits of urban environments result in a decrease in thermal comfort and rises in PMV that can reach 2.3 in the summer. The severity of this degradation is specifically inversely related to the high albedo surfaces' sky view factor (Salata et al. 2015)

Although reflective façades aid in lowering a building's internal temperature and cooling requirements, they also have an adverse effect on the outside that is generally ignored in research. This study has been undertaken for further steps to further suggest the current scenario to comprehend and analyze the temperature outside.

Knowing the various approaches to be used for calculating the heat and discomfort produced outside, as well as its percentage contribution, will help you choose whether or not this issue can be overlooked. As there is very little study on how much heat is produced by reflective external façades, this review may offer suggestions for how to expand the research.

## Aim of the Study

This study aims to clarify how reflecting building façades affect outdoor thermal comfort and the surrounding natural environment. The research investigates how surface reflectivity affects comfort experienced outdoors through a comprehensive review of literature spanning from 2003 to 2022. To investigate practical applications and implications, a comprehensive case study of a low-rise residential complex in Greater Noida, India, is a crucial part of the research.

The purpose of the research necessitates conducting a comprehensive literature review with a particular emphasis on the following criteria.

1. The implications of albedo on Outdoor thermal environment.
2. Application of Parameters in the Calculation of Thermal Comfort in Outdoor Environments Using Simulation Methods.
3. Justifying the negative impacts that reflected façades have.

4. The number of articles that concentrate on environmental considerations and thermal comfort indices.

Using ENVI-met simulations to offer insights into actual conditions, the case study especially examines the effects of various building constructions and surrounding vegetation on outdoor thermal comfort.

## MATERIALS AND METHODS

The methodology for analyzing the effect of albedo on outdoor thermal comfort is mostly simulation-based, with field measurements planned for future research. The study focuses (Fig. 1) on Sector Omega in Greater Noida, where the rise in outdoor air temperature due to surface characteristics is investigated. ENVI-met simulation software is used to model thermal conditions based on meteorological data from May 22, including critical parameters such as air temperature, wind velocity, and relative humidity. This Simulation helps to understand the impact of various albedo levels on outdoor thermal comfort.

The findings will be analyzed to identify research gaps and investigate the potential benefits of using greener surfaces and vegetation to reduce heat stress. Future studies will incorporate extensive field measurements, utilizing both fixed and mobile rigs, to evaluate and supplement the

modeling results. Furthermore, future research will compare these findings to greener settings to determine the impact of vegetation in improving outdoor thermal comfort.

### Urban Albedo

Typically, an urban canyon's urban albedo is viewed as a crucial indicator for buildings' energy-saving efforts and for minimizing the UHI effect (Yuan et al. 2020). Oke (1988) recommended typical urban albedos of 0.14 for urban centers (range 0.09-0.23) and 0.15 for residential regions (range 0.11–0.24). The urban albedo is calculated by dividing the light reflected upward from urban structures by the total incoming light. Regardless of the angle of incidence of the halogen lamp light source, it was shown that RR surfaces have an urban albedo around 0.08 (8%) higher than DHR surfaces (Yuan et al. 2022). So, as the angle of solar radiation incidence rises, the value of urban albedo also rises, which diminishes the efficacy of the buildings' reflective façades and makes it the major source of radiation that is reflected into the atmosphere. Urban albedo is directly related to the net energy absorbed from short-wave radiation by urban substrate materials, as demonstrated in (Taha 1997).

$$(1 - \alpha)I + L^* + Q_f = H + \lambda E + G$$

Here  $\alpha$  represents the urban albedo;  $I$  represent solar

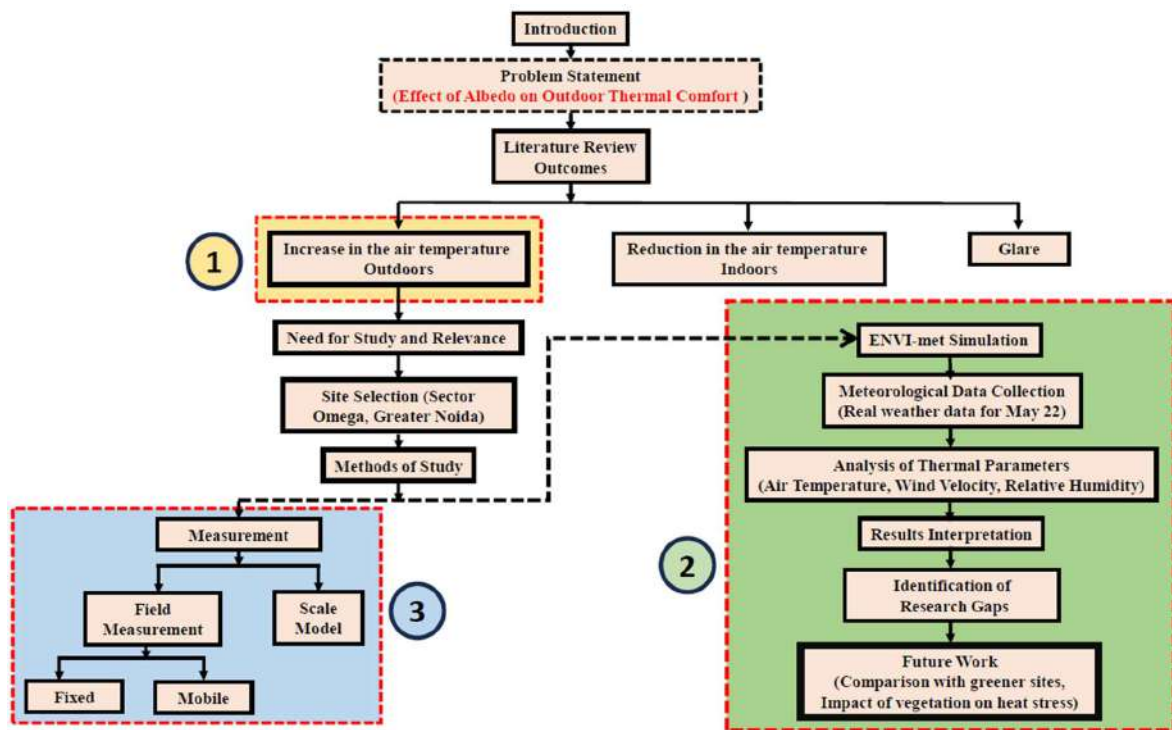


Fig. 1: This diagram outlines the research process, including the identification of outdoor temperature increases due to high albedo (Step 1), analysis of heat stress in low-rise apartments in Greater Noida (Step 2), and field measurements as part of future research (Step 3).

Table 1: Summary of effect of albedo on outdoor environment.

References	Location	Effect of Albedo on Outdoor Environment
(Tsoka et al. 2018)	Greece	The use of a surface of high albedo will be a drawback since it needs maintenance very frequently, and the effectiveness is reduced by 40% to 15% every 12 months.
(Falasca et al. 2019)	Milan, Italy	To counteract the effects of heat waves, the building itself uses high-albedo materials, which significantly reduce energy demand. From the perspective of pedestrian thermal comfort, this mitigation method is not a desirable solution.
(Yuan et al. 2021)	Osaka, Japan.	It can be seen that, in comparison to the DHR Diffuse Highly Reflective building façade, the Specular Reflective SR and Retro Reflective RR building façades will add a significantly greater amount of downward solar radiation and heat flux to the ground inside an urban canyon.
(Mehaoued & Lartigue 2019)	Algiers, Algeria,	The reflectance of reflective surfaces ranges from 30 to 90% in order to lower the cooling load. However, the reflected sunlight not only floods the surrounding area with more light but also increases its thermal load.
(Naboni et al. 2020)	(Copenhagen, Madrid, Brindisi and Abu Dhabi).	It is evident that changes in ground emissivity and reflectivity (albedo), the reflectance of reflective surfaces ranges from 30 to 90% in order to lower the cooling load. However, the reflected sunlight not only floods the surrounding area with more light but also increases its thermal load. The former by reflecting short-wave radiation that reaches the measuring stations and the latter by emitting long-wave radiation whose magnitude is proportionate to the ground temperature, actively contributing to variations in Tmrt.
(Lee & Mayer 2018)	Stuttgart (Southwest Germany)	According to the study, pedestrians' daytime thermal comfort is systematically harmed when wall albedo increases.
(Fahed et al. 2020)	Lebanon	The findings demonstrated that, depending on the form of the urban canyon, high-reflectance materials may have opposite effects on outdoor thermal comfort and albedo. Despite the positive impact on air temperature, it also reduces outdoor thermal comfort at street level because of an increase in interreflections that raise the mean radiant temperature.
(Lai et al. 2019)		According to certain simulation studies, pedestrians' thermal comfort deteriorates as reflected solar radiation increases and long-wave radiation decreases due to reflective surfaces.
(Taleghani 2018)	Netherlands	Raising the albedo in a confined environment, such as a courtyard, increases the body's reradiation and reduces thermal comfort. This study demonstrated that while cool pavements lower air temperatures, they also increase radiation exposure, which will be harmful to pedestrians.
(Fabbri et al. 2020)	Italy	SVF contributes to temperature rise when combined with solar reflectance. In Urban Canyon, outdoor space has less of an impact from reflected façades.
(Yuan et al. 2021)	Osaka, Japan	The solar reflectance of diffuse and specular reflecting directional building coatings is released back into the atmosphere, which helps to warm the surrounding area.
(Takashi et al. 2013)	Tokyo	The thermal environment of the streets surrounding the structure was found to be negatively impacted by the heat insulation of the building façade.
(Fabbri et al. 2022)	Bologna, Italy.	The emissivity value influences the outdoor microclimate. This outside environment can be influenced by emissivity in relation to the building blocks.
(Speroni et al. 2022)	Milan, Italy	Moreover, retro-reflectors show the highest ratios of upward to downward reflection when the angles of incidence are low. A single tall building with a flat diffusive surface and an albedo of 0.86, which corresponds to a clean white, can increase the solar irradiance on the ground by up to 20%, resulting in an intensity of 1.2 suns at pedestrian level.
(Res et al. 2007)	Pettah, Colombo (Sri Lanka) and downtown Phoenix, Arizona (USA)	Here, high albedo causes much lower daytime temperatures, which might lessen the photochemical synthesis of some pollutants. However, thermal comfort may not be improved by using this option.
(Yang et al. 2011)	Shanghai	But during the day, this albedo adjustment raises Tmrt by 8–148C, overpowering the very thin Tmrt reduction of less than 48Cat at night. Consequently, there is a decline in overall thermal comfort as evidenced by a rise in PET of 5–78C during the day and a fall in PET of less than 18C at night.
(Rosso et al. 2018)	Italy	On the other hand, when a building's envelope faces a canyon, an increase in albedo combined with low sky view factors suggests many reflections, which raise air and mean radiant temperatures.
(Salvati et al. 2022)	London	The findings demonstrated that, depending on the form of the urban canyon, high reflectance surfaces may have different effects on outdoor thermal comfort and albedo.
(Qin et al. 2016)	China	When the angle at which sunlight radiates on the RR surface rises above a specific point (about 40°), the surface loses its retroreflectivity.

radiation;  $L^*$  represents net long-wave radiation from the surface;  $\lambda e$  the latent heat of vaporization,  $H$  is the sensible heat,  $o_f$  is the heat produced by humans,  $E$  is the rate of evaporation, and  $G$  is the variation in the amount of heat stored in urban volumes.

To address UHI, increasing urban albedos is therefore recommended (Taha 1997), and research on how urban albedos affect other, more general issues like global warming has also been conducted (Akbari et al. 2009).

To systematically assess the current understanding of reflective building materials, the author explored three primary databases. (Science Direct, Google Scholar, Web of Science).

### Reflective Façades

Urban heat islands are substantially influenced by the excess solar heat absorption by urban structures. (Santamouri 2013) By reflecting the heat from building façades and urban roads, reflective surfaces play a significant part in raising the air temperature. Materials such as glass, aluminum composite panels, metal cladding sheets, titanium panels, and many others are functioning in the same direction, and as a result, they harm the thermal well-being of pedestrians. Regardless that reflective surfaces help to cool down cities, several simulation studies assert that increased solar radiation reflected off of pedestrians often makes them feel more uncomfortable.

Table 1 is a collection of research that has been undertaken regarding reflecting façades for the past 10 years (2013 - 2022) and how they impact outdoor thermal well-being. Even though the majority of studies discuss the negative impact of reflectance returning back into the atmosphere, some say it is a favorable material option because it reduces the inside temperature. The majority of the research is conducted in Japan, along with Italy, Greece, Algeria, Germany, the Netherlands, and Tokyo.

### Thermal Comfort Indices

#### *Thermal Comfort Calculation Parameters*

Four fundamental parameters, including air temperature, thermal radiation, wind speed, and humidity, are necessary to define the thermal environment of humans in metropolitan open spaces. (Lai et al. 2019) Each of the fundamental parameters separately characterizes the thermal environment. In (Lai & Chen 2016) and Lai et al. (2017), The connections among these factors in calculating different heat gains and losses concerning the human body are explained by (Lai et al. 2017)

Thermal radiation is the most complex of the four fundamental characteristics. The mean radiant temperature

refers to the uniform surface Temperature of a virtual space where radiant heat exchange between a human body and the surroundings equals that of an enclosure with varying temperatures. ( $T_{mrt}$ ). It is often used to characterize thermal radiation within urban open spaces (ASHRAE 2009).

To measure the Heat stress of the outdoor conditions on the human body), the four basic factors can be included in “equivalent temperatures.” These “equivalent temperature” factors permit a person to compare the cumulative effects of complicated outdoor thermal conditions to their own inside experiences.

The standardized temperature represents the ambient climate of a designated reference setting. That induces the same physiological reaction in a typical individual as in the actual environment. Physiologically equivalent temperature (PET) is an example of such a parameter (Höppe 1999). The standard effective temperature (SET\*) (Gonzalez et al. 2021) and the universal thermal climate index (UTCI) (Bröde et al. 2012). Several approaches can be employed to calculate the reflected heat in the environment and the impacted temperature to analyze the above factors.

### Methodologies for Acquiring Urban Thermal Environment Characteristics Measurements

Measurements made on-site are another way to collect data for environmental factors like temperature, relative humidity, and wind speed for use in simulations to produce thermal comfort indices. During the summer, on-site measurements of air temperature ( $T_{air}$ ) and relative humidity (RH) were taken to determine the microclimatic parameters of the research region before any intervention scenario (Tsoka et al. 2018). Measurements are taken using equipment such as HOBO micro-station( Temperature, relative humidity, and air velocity on the roof), Hygro-thermometer Testo 635(Temperature, relative humidity, and air velocity at 2m from the ground), Thermograph ThermoCAM® B2(Thermograms of the façades) (Mehaoued & Lartigue 2019). Dry bulb temperature and relative humidity were recorded using TESTO 174H data loggers inside the courtyard, while outside measurements—comprising wind speed and direction, relative humidity, and dry bulb temperature—were obtained from a weather station (model PCE-FWS 20) installed on the building’s roof (Lopez-Cabeza et al. 2022).

The data obtained from the meteorological agency and the measured data may occasionally differ. Since the real-time measurements are more accurate than the recorded data, it is crucial to measure the data on the spot before making a decision. We cannot get the true image and results through simulated data.



## Simulations

The advancement of microclimate prediction tools like SOLENE (Miguet & Groleau 2007), ENVI-met (Huttner & Bruse 2009), Rayman (Freitas & Scott 2007), SOLWEIG (Lindberg et al. 2014), STREAM, STEVE (Jusuf & Hien 2009), and CityComfort+ (Huang et al. 2014) has been going on for the past 20 years. In addition to temperature, Tmrt, and thermal prediction of air indices including PET, Expected Mean Vote Comfort (PMV), Standard Effective Temperature (SET\*), and Universal Thermal Climate Index (UTCI).

ENVI-met employs computational fluid dynamics to study airflow patterns and evaluate environmental pollution. (Aydin et al. 2019). Physics-based prediction tool called RayMan can predict Tmrt, SVF, global radiation, and some thermal indices for a site of interest, including PMV, PET, SET\*, UTCI, and perceived temperature (PT) (Aydin et

al. 2019). A “non-stationary model that can compute the spatial variations of Tmrt” is SOLWEIG. (Lindberg et al. 2014). The STEVE tool uses albedo data, solar radiation, and features of the urban setting to create a regression model that only calculates ambient air temperature and SVF (building, pavement, greenery) (Jusuf & Hien 2009).

Studies indicate that a variety of simulation software has been utilized to calculate thermal comfort throughout the previous decade. ENVI-met is among the most extensively utilized Simulation software in the world. Many countries have approved ENVI-met v4.4.5, one of the most extensively used Computational Fluid Dynamics (CFD) tools for urban microclimate simulations on a worldwide scale (Tsoka et al. 2018). ENVI-met is a microclimate simulation tool that accurately computes the spatial and temporal distribution of microclimate parameters within urban areas at a high resolution (Huttner & Bruse 2009).

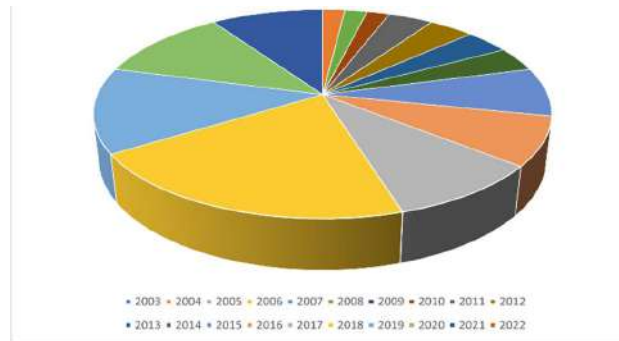


Fig. 2: Pie Chart depicting the role simulation studies to calculate the Thermal Comfort Indices.

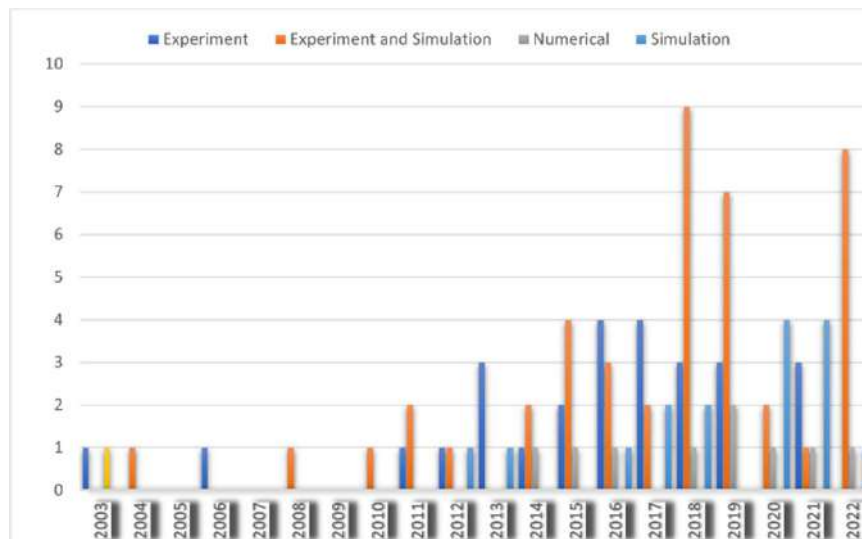


Fig. 3: No and typology on a paper published on the calculation of environmental factors (temperature, relative humidity, and wind speed) and thermal Comfort indices (Tmrt PET, UTCI, SET).

A simulation tool is used to calculate outdoor thermal comfort after several parameters are assessed. In particular, wind speed, material albedo, air temperature, and relative humidity are examined. These parameter values are produced as outputs by the tool using site location, building material requirements, vegetation data, and weather files as inputs. As previously discussed, various simulation tools are used to calculate thermal comfort indices, including STREAM, ENVI-met, ANSYS, and ENERGY PLUS.

ENVI-met's limitation includes modeling structures as blocks where the width and length align with grid cells, resulting in uniform thermal properties and lacking thermal mass variability. Moreover, all structures have identical albedo and heat transmission (U-value) for walls and roofs. (Res et al. 2007). Simulation software can also be used in conjunction with onsite measurement data to provide precise results. Using ENVI met with measurements and cooling loads gathered by Ecotect was another method for determining the effects of reflecting glass façade on the environment. (Mehaoued & Lartigue 2019b) .

The study examines how street configurations influence ambient temperatures and pedestrian comfort. It shows a strong correlation between on-site measurements, comfort assessments, and urban climate simulations conducted with ENVI-met. The simulation techniques have been extensively employed over time to analyze the thermal comfort indices, as can be observed from the prior studies. The article's usage of simulation studies is depicted in the pie chart below (Fig. 2).

Few have, according to the literature review, also employed the STREAM simulation program to calculate outdoor thermal comfort. The STREAM and ENVI met interfaces, however, are completely different.

Putting the studies in chronological order makes it abundantly evident that there is an increasing interest in investigating the outside human thermal perception during the years 2003–2022 (Fig 3). Since 2011, there has been an increase in the number of research that use thermal comfort indicators. As a result, one of the fundamental variables that goes into determining whether or not someone is comfortable in their environment is the type of tools that they utilize. As a direct consequence of this, simulations can play a significant role in the process of calculating reflection values.

However, there are several simulation tools used to simulate the thermal comfort parameters to comprehend their impact on comfort in outdoor temperatures. Despite its reported limitations, the bulk of research indicates a disparity in outcomes when measurements and simulations are compared. One must, therefore, be cautious while entering data into the software to achieve near-perfect results in comparison to measurements done on-site.

## Future Studies

As a result of a 20-year study of the literature, it is clear that there is a need for additional research in the area that has received little attention.

1. Very little research has been done on the numerical output of RR material use on façades and how it affects outdoor thermal comfort. There is a substantial quantity of heat dissipated in the atmosphere as opposed to using reflecting materials as part of lowering indoor temperatures.
2. Research studies on the reflected heat with the use of Albedo on building façades are not calculative. Its, indicating a notable research gap.
3. Retro-reflective façade materials function at a specific angular dependence of the solar radiations. As a result, it is less effective at reflecting the heat in the same direction that it is coming from. The angle of incidence for the specific city must be determined before installing such materials, and it must be compared with the number of h per day that reflecting façades are operational.
4. It is necessary to perform a numerical calculation to determine how much heat is reflected into the atmosphere to comprehend the severity of the issue it is posing. Also, to determine which of the following roads, roofs, and building façades is harming the environment more so that future studies can go in the same direction.

## RESULTS AND DISCUSSION

### Site Conditions

An investigation of the site conditions of the urban enclave located in the thriving Delhi NCR region's Greater Noida, UP (Fig. 4) area indicates a distinctive interaction between environmental elements and urban dynamics. The climate in this heavily populated region, which is distinguished by low-rise housing complexes, is characteristic of North India's subtropical zones. Maximum temperatures increase in the summer, frequently reaching over 43°C, while lowest temperatures in the winter drop to about 7°C.

A low-rise apartment building located in the omega sector of greater Noida is punctuated by a 12-meter-wide road system, enabling the community's vehicle and pedestrian traffic flow. The presence of green areas, such as a large park for leisure purposes and a kid-only swing park, is a noteworthy aspect of the location that provides a break from the bustle of the city. The internal block-paved pathways contrast with the asphalted peripheral highways, adding visual interest and guaranteeing functional diversity.



Fig. 4: Google Earth image of a Low-rise apartments in Greater Noida, Delhi NCR.

Covering a vast 25.65 acres with a Floor Area Ratio (FAR) of 1.2, the development consists of 22 12-meter-tall low-rise blocks that blend in with the surrounding urban fabric. This thorough comprehension of site conditions provides the groundwork for well-informed design choices, promoting livable and sustainable urban environments.

### Simulations for Heat Stress

**About the Software:** ENVI-met is a microclimatic simulation tool that calculates thermal indices and offers information on the impacts of thermal strain on outdoor habitats. Through the use of several graphs customized for particular days and weather, findings may be obtained to identify any discrepancies.

ENVI-met needs certain input factors, such as weather, urban structure, and the physical characteristics of flora and surfaces inside the urban area, to simulate the microclimate.

Table 2: Boundary Conditions and initial settings for ENVI met 5.5 modeling.

Location	28.4744° N, 77.5040° E (Greater Noida, India)
Climate	Composite Climate
Date/Time simulated	22/05/2023
Start Simulation Hour (hh: mm)	10:00 am
Total Simulation time (h)	7 h
Model Domain	50 x 50 x 20
<b>Atmospheric Boundary Conditions</b>	
Max Temperature	42°
Min Temperature	32°
Humidity	Min 50 % to 65%
Cloud Cover	0

Direct and diffuse solar radiation, longwave radiation, and a vertical profile of atmospheric parameters (temperature, velocity, and humidity) estimated from 0 to 2500 meters above ground are among the computed weather parameters. Envi-met, developed by Bruno, is capable of simulating comprehensive microclimatic conditions at the neighborhood level by integrating various physical processes such as airflow amidst buildings, the impact of vegetation and water bodies on urban heat islands, and interactions between soil surfaces and building façades.

**Description of the Model:** The analysis in this study is focused on a  $50 \times 50 \times 20$  model area that includes a low-rise residence in Greater Noida, India. The boundary conditions and initial settings of the model are given in Table 2. Three different building constructions, A, B, and C, as well as the surrounding vegetation, are the main subjects of the analysis. At twelve meters high, these constructions are primarily made of brick walls, a material often used in building construction that is renowned for its strength and insulating qualities. To precisely replicate the real world. Due to its capacity to incorporate a wide range of physical phenomena, including airflow between buildings, the effect of vegetation and water surfaces on urban heat islands, and the exchanges between soil surfaces and building walls, the modeling tool Envi-met, created by Bruno, enables realistic microclimate simulation at the district scale. Id circumstances, a particular day, May 22, 2023, in May, was selected for the study. This specific day is used as a representative sample to identify possible weather fluctuations and seasonal variations.

Ten hours are allotted to the simulation, which starts at 9:00 am and ends at 7:00 pm. This period encompasses a considerable amount of the day, making

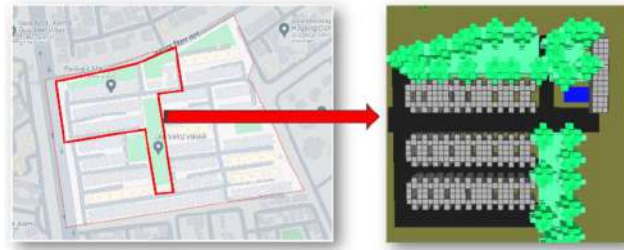


Fig. 5: Envi Met Model of the Low-rise apartment in Greater Noida, Delhi NCR.

it possible to conduct a thorough examination of the environmental elements influencing the structures and their environs.

To ensure that the simulation included accurate weather, data was used from the reliable website [www.wunderground.com](http://www.wunderground.com). Important characteristics, including air temperature (minimum and maximum), relative humidity, wind speed, cloud cover, and wind direction are all included in this

report. The simulation software can precisely describe and predict the thermal behavior and environmental impact on the buildings and surrounding landscape by using this extensive dataset. The study intends to offer important insights into the thermal performance and comfort levels within the built environment under varied climatic conditions by incorporating real-world data into the simulation process.

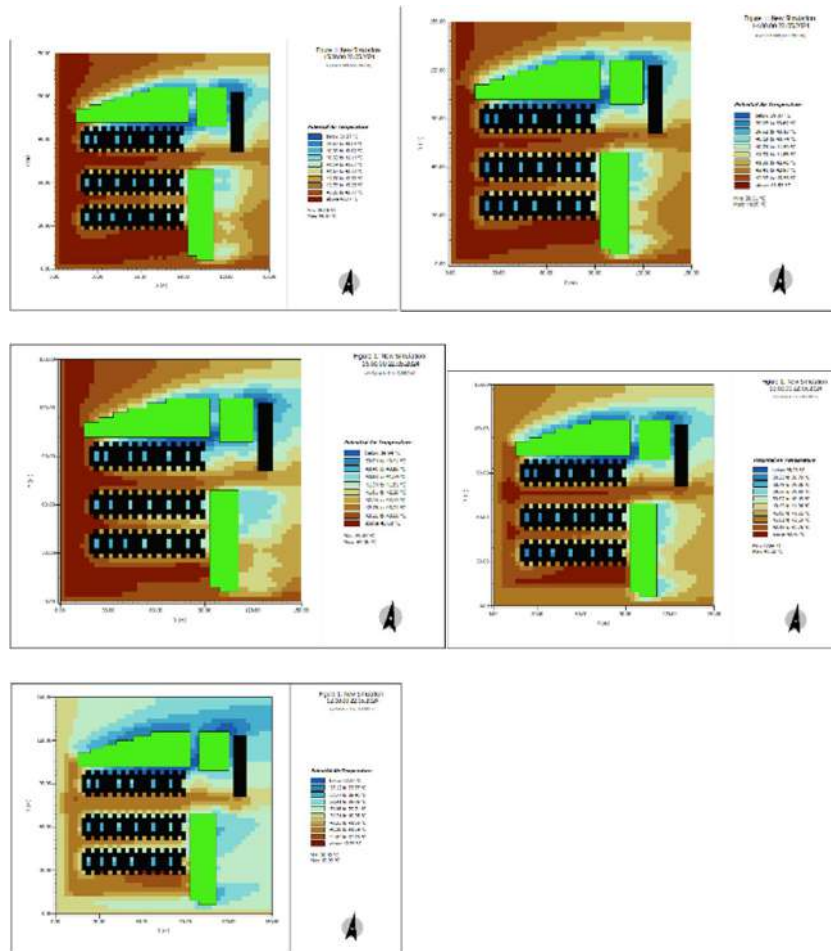


Fig. 6: Envi Met Results of Air temperature at 12:00 pm, 1:00 pm, 2:00 pm, 3:00 pm, and 4:00 pm h of the day of 22<sup>nd</sup> May 2024.



**Simulation Results:** Thermal indices were calculated using ENVI-met simulations, considering variables such as air temperature, relative humidity, and wind velocity. These simulations were applied to a model of Jalvayu Vihar in Greater Noida, which incorporated building blocks, windows, roads, and vegetation to improve result accuracy (Fig. 5). Specific materials were assigned to each entity in the model: building blocks were represented with moderate wall brickwork, windows with float glass, roads with asphalt, and vegetation with trees and turf grass. While the materials can be customized within the software for specific outcomes, the materials mentioned above were utilized for this project's simulation.

### Air Temperature Analysis

Air temperature graphs were generated for May 22, 2024, from 12:00 pm to 4:00 pm. Although the simulation encompassed a total duration of 7 h, only the critical h were analyzed. The primary criterion for assessing the heat island effect involved calculating air temperature values. The following graphs depict the conditions during these critical hours, illustrating the adverse effects of air temperature within the premises.

The outdoor ambient air temperatures were analyzed over different times of the day, revealing significant variations (Fig. 6). Temperatures between 39 to 40 degrees Celsius were observed on the roads between the blocks, while temperatures near the green patches were 2 to 3 degrees lower. At 1:00 pm, the temperature was higher compared to the noon simulation, with road temperatures exceeding 42 degrees Celsius. The temperature continued to rise at 2:00 pm, reaching over 43.55 degrees Celsius on the roads. By 3:00 pm, the temperature peaked, exceeding 43.77 degrees Celsius. However, at 4:00 pm, the temperature began to decrease but remained above 43.68 degrees Celsius on the roads.

### Relative Humidity Analysis

The comfortable range of relative humidity is between 30% and 60%. When humidity falls below 50%, the air feels

excessively dry, leading to discomfort, such as dry skin and irritated eyes. In the range of 50% to 65%, humidity is optimal for comfort, maintaining skin moisture, and facilitating respiratory ease. However, when relative humidity exceeds 65%, the air feels too humid, resulting in sweating and potential respiratory issues.

The graph indicates that relative humidity on the roads is between 39% and 40%, suggesting that the air is relatively dry. To address this, increasing humidity by incorporating water bodies along the wind path could help regulate the temperature and improve comfort levels.

### Wind Velocity Analysis

The comfortable wind velocity for human thermal comfort generally ranges from 0.3 to 1.5 meters per second ( $\text{m.s}^{-1}$ ) (Fig. 7). Wind velocities below  $0.3 \text{ m.s}^{-1}$  can feel stagnant and uncomfortable, particularly in warm environments. A range of  $0.3$  to  $1.5 \text{ m.s}^{-1}$  provides a comfortable, gentle breeze that aids in cooling and ventilation. However, wind velocities exceeding  $1.5 \text{ m.s}^{-1}$  may feel too windy and cause discomfort, especially in cooler conditions.

The graphs indicate that wind velocity exceeds  $1.5 \text{ m.s}^{-1}$  at junctions and T-intersections on the roads. This high wind velocity, when combined with elevated air temperatures, can exacerbate discomfort by intensifying the perception of heat, making the environment more oppressive for individuals.

In our analysis of “The Effect of Albedo on Outdoor Thermal Comfort,” we look at how surface reflectivity affects urban heat islands (UHIs) and microclimates. The case study of a low-rise residential complex in Greater Noida offers an important foundational understanding of the current thermal stress in the area, even though it does not include reflecting façades.

We provide a baseline for evaluating the possible effects of adding reflecting materials by looking at the heat stress that this subtropical environment experiences. This case study aids in our comprehension of the existing levels of thermal

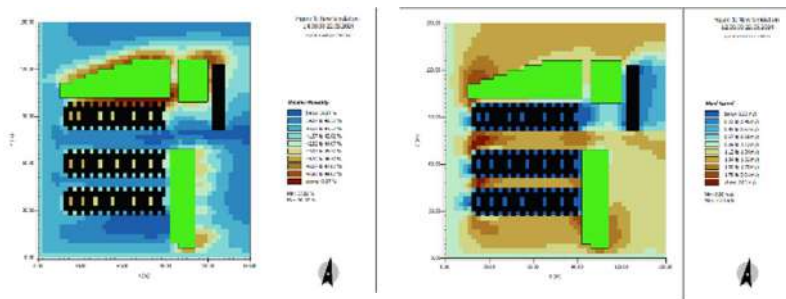


Fig. 7: Envi Met Results of Relative Humidity and Wind Velocity on 22<sup>nd</sup> May 2024.

comfort as well as the elements that lead to heat stress, such as the kind of construction materials used and the amount of flora present. It is possible to forecast how reflecting façades can change the local microclimate using the Greater Noida research results. For example, the addition of reflecting materials might alter surface albedo and mean radiant temperature (MRT), which would affect thermal comfort in general. Urban planners can assess the advantages and disadvantages of utilizing reflecting materials in comparable situations with the help of this comparative analysis.

The case study also emphasizes the significance of context-specific urban planning techniques. Planners can employ high-albedo materials to reduce UHI effects and improve outdoor thermal comfort by having a better understanding of the Greater Noida area's distinct thermal dynamics.

In summary, the case study offers insightful information that enhances our evaluation with its thorough examination of heat stress in an unreflective setting. It ensures that our suggestions for enhancing outdoor thermal comfort are based on actual facts and circumstances by bridging the gap between theoretical notions of albedo and practical applications. Although ENVI-met simulations provide useful information about urban heat stress in Greater Noida, there are several limits to consider. Using only simulation data may not provide a complete picture, even if real meteorological data from a specific day in May is included. Several variables can influence heat stress generation, which may not be adequately captured in simulations. Incorporating actual site measurements and comparing them to simulation findings would yield more robust and accurate knowledge. This identifies a potential research gap and emphasizes the necessity for additional research to validate the findings with actual data.

## CONCLUSIONS

As has been observed, research has shown the importance of the angle of incidence and its impact on retro-reflecting materials, as well as how it affects materials other than these highly reflective materials on the quality of the outdoor environment. However, there haven't been many empirical investigations to back up the claim. So, to draw a conclusion, an experimental setup must be used. Nonetheless, the majority of research holds that retroreflective materials are the solution for lowering the thermal load in buildings and improving thermal comfort. The quantification of solar reflectance in the environment still has to be done.

A consistent rise in wall albedo results in a gradual decline in daytime thermal comfort for pedestrians. To lower the reflectivity value in the atmosphere, façade

trending materials like DSR and RR & Low-E double-glazed façades are used where the limitations extend even to the materials.

The most crucial characteristic of retro-reflective materials is retro-reflectivity. However, the previously delivered retro-reflective materials have a serious defect, which is that the retro-reflectivity will shapely degrade under the high incidence angle of solar radiation. That is the primary area for retro-reflective material optimization.

In the experimental setup and computational analysis, the governing principles of retro-reflective materials have indeed been acquired on the urban thermal conditions and the thermal environment of buildings. The effectiveness of using materials with high reflectivity in a single building or group of buildings needs to be continuously monitored and assessed. Merely simulation won't solve the problem because the values of measurements and simulations might sometimes differ by up to 20%. Instead, monitoring the data logging in the software also needs attention.

Several simulation software options have been covered. All with different advantages, but as seen in the thorough review studies, ENVI met proves to be useful for computing thermal comfort indices. Nevertheless, depending on the subject matter being researched, various software may be used.

This review offers the researchers the chance to focus their research on quantifying the value of solar reflectance in conjunction with other environmental parameters to comprehend its role in the atmosphere.

Based on the comprehensive analysis conducted using ENVI-met simulations in the low-rise residential area of Greater Noida, India, several key findings have emerged regarding the microclimatic conditions and their impact on thermal comfort:

**Air Temperature Variations:** The simulations revealed significant variations in air temperatures across the study area throughout the day, peaking above 43.77 degrees Celsius by mid-afternoon on the roads between the buildings. This highlights the pronounced heat island effect and the localized heat buildup in urban areas during peak daytime h.

**Relative Humidity Insights:** Relative humidity levels were observed to be relatively low, around 39% to 40%, suggesting dry air conditions. This can contribute to discomfort, such as dry skin and irritation, indicating a need for strategies to increase humidity, such as incorporating water bodies or green spaces, to enhance comfort levels.

**Wind Velocity Considerations:** The analysis indicated that wind velocities exceeded 1.5 meters per second (ms) at certain locations, particularly at junctions and T-intersections. While

moderate wind speeds are generally beneficial for cooling and ventilation, excessively high velocities in conjunction with high temperatures can exacerbate discomfort by intensifying the perception of heat.

In conclusion, the findings underscore the importance of microclimate modeling in understanding and mitigating thermal challenges in urban environments. Effective urban planning strategies, including the incorporation of green spaces, water bodies, and consideration of building materials, are crucial for enhancing thermal comfort and mitigating the adverse effects of heat islands. By integrating these insights into urban design and policy-making, cities can work towards creating more livable and sustainable environments for their residents. Furthermore, a comparative analysis of several low-rise housing sites in greener, more densely vegetated environments might be simulated and compared to the current Sector Omega location. This would be useful in determining the impact of vegetation on outdoor thermal comfort in the area. The extent to which vegetation can lower outdoor heat stress is unknown, however, such a study could offer insight into greenery's good impact in alleviating heat.

## REFERENCES

- Akbari, H. and Matthews, H.D., 2012. Global cooling updates: Reflective roofs and pavements. *Energy and Buildings*, 55, pp.2–6. DOI
- Akbari, H., Menon, S. and Rosenfeld, A., 2009. Global cooling: Increasing worldwide urban albedos to offset CO<sub>2</sub>. *Climatic Change*, 94(3–4), pp.275–286. DOI
- Asaeda, T., Ca, V.T. and Wake, A., 1996. Heat storage of pavement and its effect on the lower atmosphere. *Atmospheric Environment*, 30(3), pp.413–427. DOI
- ASHRAE 2009. ASHRAE Standard 160-2009: Criteria for Moisture-Control Design Analysis in Buildings. *American Society of Heating, Refrigerating, and Air-Conditioning Engineers (ASHRAE)*, Atlanta, GA.
- Aydin, E.E., Jakubiec, J.A. and Jusuf, S.K., 2019. A comparison study of simulation-based prediction tools for air temperature and outdoor thermal comfort in a tropical climate. *Building Simulation Conference Proceedings*, 6, pp.4118–4125. DOI
- Bröde, P., Fiala, D., Błażejczyk, K., Holmér, I., Jendritzky, G., Kampmann, B., Tinz, B. and Havenith, G., 2012. Deriving the operational procedure for the Universal Thermal Climate Index (UTCI). *International Journal of Biometeorology*, 56(3), pp.481–494. DOI
- Fabbri, K., Gaspari, J., Bartoletti, S. and Antonini, E., 2020. Effect of façade reflectance on outdoor microclimate: An Italian case study. *Sustainable Cities and Society*, 54, p.101984. DOI
- Fabbri, K., Gaspari, J., Costa, A. and Principi, S., 2022. The role of architectural skin emissivity influencing outdoor microclimatic comfort: A case study in Bologna, Italy. *Sustainable Architecture and Urban Design*, 12(2), pp.150–162.
- Fahed, J., Kinab, E., Ginestet, S. and Adolphe, L., 2020. Impact of urban heat island mitigation measures on microclimate and pedestrian comfort in a dense urban district of Lebanon. *Sustainable Cities and Society*, 61, p.102375. DOI
- Falasca, S., Ciancio, V., Salata, F., Golasi, I., Rosso, F. and Curci, G., 2019. High albedo materials to counteract heat waves in cities: An assessment of meteorology, buildings energy needs and pedestrian thermal comfort. *Building and Environment*, 163, p.106242. DOI
- Freitas, C.R. de and Scott, D., 2007. Developments in tourism climatology. *Proceedings of the International Society of Biometeorology*, 129–138.
- Gonzalez, R.R., Advanced, G. and Associates, B., 2021. A standard predictive index of human response. *Journal of Human Climate Adaptation*, 10(1), pp.45–58.
- Huang, J., Cedeño-Laurent, J.G. and Spengler, J.D., 2014. CityComfort+: A simulation-based method for predicting mean radiant temperature in dense urban areas. *Building and Environment*, 80, pp.84–95. DOI
- Huang, Q. and Lu, Y., 2018. Urban heat island research from 1991 to 2015: A bibliometric analysis. *Theoretical and Applied Climatology*, 131(3–4), pp.1055–1067. DOI
- Huttner, S. and Bruse, M., 2009. Numerical modeling of the urban climate: A preview on ENVI-MET 4.0. *The Seventh International Conference on Urban Climate Proceedings*, July, pp.1–4.
- Ichinose, M., Inoue, T. and Nagahama, T., 2017. Effect of retro-reflecting transparent window on anthropogenic urban heat balance. *Energy and Buildings*, 157, pp.157–165. DOI
- Jusuf, S.K. and Hien, W.N., 2009. Development of empirical models for an estate level air temperature prediction in Singapore. *Proceedings of the Second International Conference on Countermeasures to Urban Heat Islands*, 7(June 2014), pp.20.
- Lai, D. and Chen, Q., 2016. A two-dimensional model for calculating heat transfer in the human body in a transient and non-uniform thermal environment. *Energy and Buildings*, 118, pp.114–122. DOI
- Lai, D., Liu, W., Gan, T., Liu, K. and Chen, Q., 2019. A review of mitigating strategies to improve the thermal environment and thermal comfort in urban outdoor spaces. *Science of the Total Environment*, 661, pp.337–353. DOI
- Lai, D., Zhou, X. and Chen, Q., 2017. Measurements and predictions of the skin temperature of human subjects on outdoor environment. *Energy and Buildings*, 151, pp.1–10. DOI
- Lee, H. and Mayer, H., 2018. Thermal comfort of pedestrians in an urban street canyon is affected by increasing albedo of building walls. *International Journal of Biometeorology*, 62(7), pp.1199–1209. DOI
- Lindberg, M., Grimmond, S., Onomura, Y. and Järvi, L., 2014. UMEP - An integrated tool for urban climatology and climate sensitive planning applications. *Urban Climatology Reports*, April 2013–2015.
- Lopez-Cabeza, V.P., Alzate-Gaviria, S., Diz-Mellado, E., Rivera-Gomez, C. and Galan-Marin, C., 2022. Albedo influence on the microclimate and thermal comfort of courtyards under Mediterranean hot summer climate conditions. *Sustainable Cities and Society*, 81(February), p.103872. DOI
- Madlener, R. and Sunak, Y., 2011. Impacts of urbanization on urban structures and energy demand: What can we learn for urban energy planning and urbanization management? *Sustainable Cities and Society*, 1(1), pp.45–53. DOI
- Mehaoued, K. and Lartigue, B., 2019. Influence of a reflective glass façade on surrounding microclimate and building cooling load: Case of an office building in Algiers. *Sustainable Cities and Society*, 46(May 2018), DOI
- Miguet, F. and Groleau, D., 2007. Urban bioclimatic indicators for urban planners with the software tool SOLENE. *Portugal SB 2007 - Sustainable Construction, Materials and Practices: Challenge of the Industry for the New Millennium*, pp.348–355.
- Mohajerani, A., Bakaric, J. and Jeffrey-Bailey, T., 2017. The urban heat island effect, its causes, and mitigation, with reference to the thermal properties of asphalt concrete. *Journal of Environmental Management*, 197, pp.522–538. DOI
- Morini, E., Castellani, B., Nicolini, A., Rossi, F. and Berardi, U., 2018. Effects of aging on retro-reflective materials for building applications. *Energy and Buildings*, 179, pp.121–132. DOI
- Morini, E., Castellani, B., Presciutti, A., Anderini, E., Filipponi, M., Nicolini, A. and Rossi, F., 2017. Experimental analysis of the effect of geometry and façade materials on urban district's equivalent albedo. *Sustainability (Switzerland)*, 9(7). DOI

- Naboni, E., Milella, A., Vadalà, R. and Fiorito, F., 2020. On the localized climate change mitigation potential of building façades. *Energy and Buildings*, 224, p.110284. DOI
- Oke, T.R., 1988. The urban energy balance. *Progress in Physical Geography*, 12(4), pp.471–508. DOI
- Höppe, P., 1999. The physiological equivalent temperature - a universal index for the biometeorological assessment of the thermal environment. *International Journal of Biometeorology*, 43(2), 71–75.
- Qin, Y., Liang, J., Tan, K. and Li, F., 2016. A side by side comparison of the cooling effect of building blocks with retro-reflective and diffuse-reflective walls. *Solar Energy*, 133, pp.172–179. DOI
- Res, C., Emmanuel, R. and Fernando, H.J.S., 2007. Urban heat islands in humid and arid climates: Role of urban form and thermal properties in Colombo, Sri Lanka and Phoenix, USA. *Climate Research*, 34(1986), pp.241–251. DOI
- Rossi, F., Morini, E., Castellani, B., Nicolini, A., Bonamente, E., Anderini, E. and Cotana, F., 2015. Beneficial effects of retroreflective materials in urban canyons: Results from seasonal monitoring campaign. *Journal of Physics: Conference Series*, 655(1). DOI
- Rossi, F., Pisello, A.L., Nicolini, A., Filippini, M. and Palombo, M., 2014. Analysis of retro-reflective surfaces for urban heat island mitigation: A new analytical model. *Applied Energy*, 114, pp.621–631. DOI
- Rosso, F., Golasi, I., Castaldo, V.L., Piselli, C., Pisello, A.L., Salata, F., Ferrero, M., Cotana, F. and de Lieto Vollaro, A., 2018. On the impact of innovative materials on outdoor thermal comfort of pedestrians in historical urban canyons. *Renewable Energy*, 118, pp.825–839. DOI
- Salata, F., Golasi, I., Vollaro, A.D.L. and Vollaro, R.D.L., 2015. How high albedo and traditional buildings' materials and vegetation affect the quality of urban microclimate. A case study. *Energy and Buildings*, 99, pp.32–49. DOI
- Salvati, A., Kolokotroni, M., Kotopouleas, A., Watkins, R., Giridharan, R. and Nikolopoulou, M., 2022. Impact of reflective materials on urban canyon albedo, outdoor and indoor microclimates. *Building and Environment*, 207(PB), p.108459. DOI
- Santamouris, M., 2013. Using cool pavements as a mitigation strategy to fight urban heat island - A review of the actual developments. *Renewable and Sustainable Energy Reviews*, 26, pp.224–240. DOI
- Speroni, A., Mainini, A.G., Zani, A., Paolini, R., Pagnacco, T. and Poli, T., 2022. Experimental assessment of the reflection of solar radiation from façades of tall buildings to the pedestrian level. *Sustainability (Switzerland)*, 14(10). DOI
- Taha, H., 1997. Urban climates and heat islands: Albedo, evapotranspiration, and anthropogenic heat. *Energy and Buildings*, 25(2), pp.99–103. DOI
- Taha, H., Akbari, H., Rosenfeld, A. and Huang, J., 1988. Residential cooling loads and the urban heat island-the effects of albedo. *Building and Environment*, 23(4), pp.271–283. DOI
- Takashi, I., Masayuki, I. and Tsutomu, N., 2013. Retro-reflecting film with wavelength-selective properties against near-infrared solar radiation and improving effects of indoor/outdoor thermal environment. *Conference Cycle Focusing on Sustainability in the Built Environment (CISBAT)*, Lausanne, Switzerland, pp.67–72.
- Taleghani, M., 2018. The impact of increasing urban surface albedo on outdoor summer thermal comfort within a university campus. *Urban Climate*, 24(October 2017), pp.175–184. DOI
- Tsoka, S., Theodosiou, T., Tsikaloudaki, K. and Flourentzou, F., 2018. Modeling the performance of cool pavements and the effect of their aging on outdoor surface and air temperatures. *Sustainable Cities and Society*, 42, pp.276–288. DOI
- Yang, F., Lau, S.S.Y. and Qian, F., 2011. Thermal comfort effects of urban design strategies in high-rise urban environments in a sub-tropical climate. *Architectural Science Review*, 54(4), pp.285–304. DOI
- Yuan, C., Adelia, A.S., Mei, S., He, W., Li, X.X. and Norford, L., 2020. Mitigating intensity of urban heat island by better understanding on urban morphology and anthropogenic heat dispersion. *Building and Environment*, 176, p.106876. DOI
- Yuan, J., Farnham, C. and Emura, K., 2015. Development of a retro-reflective material as building coating and evaluation on albedo of urban canyons and building heat loads. *Energy and Buildings*, 103, pp.107–117. DOI
- Yuan, J., Yamanaka, T., Kobayashi, T. and Kitakaze, H., 2021. Evaluation of outdoor thermal comfort under building external wall surface materials with different reflective directional characteristics by CFD. *Roomvent 2020*, March.
- Yuan, J., Emura, K. and Farnham, C., 2016. Potential for application of retroreflective materials instead of highly reflective materials for urban heat island mitigation. *Urban Studies Research*, 2016, pp.1–10. DOI
- Yuan, J., Emura, K., Farnham, C. and Sakai, H., 2016. Application of glass beads as retro-reflective façades for urban heat island mitigation: Experimental investigation and simulation analysis. *Building and Environment*, 105, pp.140–152. DOI
- Yuan, J., Farnham, C. and Emura, K., 2021. Effect of different reflection directional characteristics of building façades on outdoor thermal environment and indoor heat loads by CFD analysis. *Urban Climate*, 38(April), p.100875. DOI
- Yuan, J., Farnham, C. and Emura, K., 2022. Measurement of hourly urban albedo of building façades with different reflective directional characteristics by a simple urban model. *Proceedings of Building Simulation 2021: 17th Conference of IBPSA*, 17(August 2022). DOI
- Yuan, J., Yamanaka, T., Kobayashi, T., Kitakaze, H. and Emura, K., 2019. Effect of highly reflective building envelopes on outdoor environment temperature and indoor thermal loads using CFD and numerical analysis. *E3S Web of Conferences*, 111(2019), pp.3–7. DOI
- Yuan, T.J., Emura, K. and Sakai, H., 2013. Evaluation of the solar reflectance of highly reflective roofing sheets installed on building roofs. *Journal of Building Physics*, 37(2), pp.170–184. DOI



# Utilizing Bacteria for Crude Oil-Contaminated Soil Bioremediation and Monitoring Through Tomato Plant Growth

Vijaya Sundravel K.†, Abdul Bari J. and Ramesh S.

Department of Civil Engineering, K.S. Rangasamy College of Technology, Tiruchengode, India

†Corresponding author: Vijaya Sundravel K; kvsajai@gmail.com

**Abbreviation:** Nat. Env. & Poll. Technol.  
**Website:** [www.neptjournal.com](http://www.neptjournal.com)

*Received:* 20-07-2024

*Revised:* 23-08-2024

*Accepted:* 21-09-2024

## Key Words:

Bioaugmentation  
 Biostimulation  
*Bacillus* spp.  
*Pseudomonas* spp.  
 Petroleum hydrocarbons  
 Soil contamination

## Citation for the Paper:

Vijaya Sundravel K., Abdul Bari J. and Ramesh S., 2025. Utilizing bacteria for crude oil-Contaminated soil bioremediation and monitoring through tomato plant growth. *Nature Environment and Pollution Technology*, 24(2), p. B4248. <https://doi.org/10.46488/NEPT.2025.v24i02.B4248>

*Note: From year 2025, the journal uses Article ID instead of page numbers in citation of the published articles.*



**Copyright:** © 2025 by the authors  
**Licensee:** Technoscience Publications  
 This article is an open access article distributed under the terms and conditions of the Creative Commons Attribution (CC BY) license (<https://creativecommons.org/licenses/by/4.0/>).

## ABSTRACT

This paper provides an in-depth analysis of the process of cleaning up crude oil-contaminated soil by using a carefully selected combination of bacteria that are capable of hydrocarbon breakdown. We assessed this bioremediation approach's efficacy by evaluating tomato plant growth and vigor as indications of soil recovery. According to our research, adding hydrocarbon-degrading bacteria significantly enhanced the crude oil's ability to break down in contaminated soil. Over time, the amount of petroleum hydrocarbons in the soil decreased significantly as a result of the bacterial consortium's effective hydrocarbon metabolism. It became out that this bioremediation method was both economically and environmentally viable. Furthermore, we noticed significant improvements in the general health and growth of tomato plants grown in the bioremediated soil. These plants showed signs of excellent soil quality restoration, including higher biomass, enhanced root development, and less stress symptoms. This work highlights the possibility of bacteria-mediated bioremediation as a workable and long-term solution to soil pollution caused by crude oil. Additionally, incorporating plant growth monitoring highlights the ecological benefits of bioremediation as a remediation approach for repairing contaminated ecosystems and provides a useful way to assess the efficacy of bioremediation operations. The findings showed a substantial decrease in petroleum hydrocarbons and enhanced tomato plant growth in treated soils, demonstrating effective ecosystem restoration. By using bioremediation to treat soil contamination caused by crude oil, this research supports the conservation and sustainable use of terrestrial ecosystems, which is in line with Sustainable Development Goal 15: Life on Land.

## INTRODUCTION

Crude oil pollution of soil is a serious environmental problem that frequently results from industrial processes, tank breaches, or unintentional spills. Ecosystems are upset by this pollution, which also endangers public health and lowers agricultural output (Udeh et al. 2013). Excavation and disposal are two costly conventional methods of cleaning up crude oil-contaminated soil that might worsen environmental harm. As a result, eco-friendly and sustainable bioremediation has gained popularity. This method uses microorganisms, specifically bacteria that break down hydrocarbons, to break down petroleum hydrocarbons in soil, producing safe byproducts in the process and improving the quality of the soil. It is still essential to assess how well bioremediation methods work and how they affect plant growth and soil health. This publication provides a comprehensive study of the use of a carefully chosen consortia of hydrocarbon-degrading bacteria in the bioremediation of soil contaminated by crude oil (Sundravel et al. 2021). While previous studies have mostly concentrated on chemical analyses, our work adds a new dimension by observing the development and health of tomato plants grown in the treated soil. Tomato plants were specifically chosen as indicators because they are sensitive to changes in soil quality and provide important information about how well the rehabilitation process is going. With this project, we hope to

show that bacteria-mediated bioremediation can improve soil health and plant growth in addition to lowering crude oil contamination (Silva 2020). Our research demonstrates the method's ecological and practical benefits, offering a viable way to restore soil contaminated by crude oil while fostering environmentally friendly farming practices.

## **GLOBAL EFFECTS OF OIL-CONTAMINATED SOIL**

The problem of oil spill-related soil contamination is one of the most urgent issues facing the world today. Petroleum-contaminated soil poses serious health concerns to people, pollutes groundwater organically, limits its use, causes economic hardship, degrades the environment, and reduces the productivity of agricultural soil (Rowland et al. 2014). There is a wealth of evidence demonstrating the detrimental effects of petroleum hydrocarbons on human populations, flora, animals, and microbes. The main sources of contamination are spills from factories and refineries, accidents involving oil tankers, and events that occur while transporting oil. Either marine tankers or land pipelines that are prone to spills and accidents are used to transfer crude oil across great distances (Zhu et al. 2020). A considerable amount of the oil pollution problem arises from the gap between major oil-producing countries and major oil consumers, which forces petroleum to be transported on a massive scale from production centers to consuming areas.

Handling contaminated soil requires the application of a variety of techniques, including physical, chemical, and biological ones. Since biological remediation usually takes longer than physical or chemical interventions, many strategies have been developed to accelerate the breakdown of petroleum products in soil. Biological methods are frequently chosen because of their cost-effectiveness and effectiveness when compared to their counterparts in the chemical and physical fields. In the field of biological methods, microorganism-based bioremediation stands out as particularly effective (Algaifi et al. 2021).

## **BIOREMEDIATION OF OIL-CONTAMINATED SOIL**

Some microbes have the amazing capacity to decompose petroleum hydrocarbons and use them as a source of energy and carbon. The accuracy of this breakdown process is closely linked to the microbe's genetic composition, which allows it to add molecular oxygen to hydrocarbons and produce intermediates that can then be incorporated into the cell's larger energy-producing metabolic pathways (Agamuthu et al. 2013). Certain bacteria are mobile and have a chemotactic response, meaning they will move in the direction of the

contaminant when they detect its presence. On the other hand, in the close vicinity of the contamination, fungus and other bacteria may develop in the form of filaments.

### **Principle of Bioremediation**

Crude oil is a complex mixture of thousands of different chemical components, each with a different composition (Vermeer et al. 2021). In light of this variability, a variety of strategies are used, including microbial and floral therapies, to remediate oil contamination. Bioremediation can happen naturally or be aided by the addition of fertilizers and bacteria. First, bio-surfactants and bio-emulsifiers are used by the bacteria in the soil to identify the oil and its constituent parts. After that, they adhere to the oil and use its hydrocarbons as a carbon and energy source. Microorganisms are unable to reach high molecular weight hydrocarbons due to their low solubility and adsorption (Muonye et al. 2024). By adding biosurfactants, the solubility and removal of these pollutants are improved, which increases the rates at which oil biodegrades. The volatile, soluble, and biodegradation-prone characteristics of oil components vary greatly. While some substances break down quickly, others show resistance, and yet others are not biodegradable. Because certain microbial species prefer certain petroleum compounds over others, distinct petroleum compounds biodegrade concurrently but at different speeds. As a result, over time, the various components of petroleum steadily dwindle. When carbon sources are present, microorganisms release enzymes that are essential for attacking hydrocarbon molecules (Su et al. 2021). The breakdown of hydrocarbons in petroleum involves a wide range of enzymes and metabolic processes. On the other hand, an insufficient amount of the right enzymes may prevent the attack or prevent total hydrocarbon breakdown.

### **Bacteria**

While many microorganisms may break down crude oil in the soil, using mixed cultures in bioremediation has shown beneficial due to the synergistic interactions they exhibit rather than pure cultures.

### **Nutrients**

Although polluted soil may naturally harbor microorganisms, their numbers may not grow to the point where the location can be effectively bioremediated (Oyedemi et al. 2024). It is, therefore, essential to encourage their development and activity. The essential nutrient needed by all living things is carbon. To guarantee the effective breakdown of oil, bacteria also require macronutrients like nitrogen and phosphorus in addition to carbon. The ideal ratio of carbon to nitrogen to phosphorus, which is essential for hydrocarbon cleanup, is

sometimes expressed as 100:10:4. Effective bioremediation typically requires a minimum concentration of 1 ppm of ammonium nitrogen and 0.4 ppm of orthophosphate (Yang et al. 2024).

### **Electron Acceptor/Oxygen**

Even though it's not usually the limiting factor, oxygen is nonetheless one of the most important components in the microbial breakdown of hydrocarbons (Chorom et al. 2010). The first breakdown of hydrocarbons depends critically on oxygen, and further processes may also require oxygen. The complete deterioration of oil is dependent on oxygen availability. However, when significant amounts of oil are present, the soil's oxygen content can quickly drop, resulting in anaerobic conditions. Bacteria turn to different electron acceptors as nitrate, iron, or sulfate, when living in such anaerobic environments (Koshlaf & Ball 2017). In contrast to oxygen, microorganisms that use these substitute acceptors have a reduced energy output. As a result, anaerobic bacteria degrade at slower rates, which lengthens the remediation time.

### **Detergent**

Oils have a low accessibility to bacteria due to their hydrophobic nature, which causes a long breakdown process. Detergent is added to oil-contaminated soil to aid in the hydrocarbons' desorption, which speeds up the cleanup procedure (Xu et al. 2020). Detergents produced by microbes, including rhamnolipids, are typically used for this purpose. The presence of rhamnose moieties and a fatty acid tail set rhamnolipids apart.

## **BIOREMEDIATION STRATEGIES**

### **Biostimulation**

Biostimulation becomes essential at contaminated sites where microorganisms exist but needs to be stimulated for cleanup to be effective. In order to promote the growth of the bacteria already present in bioremediation, biostimulation entails the supply of nutrients, oxygen, and electron acceptors. The repair site's environmental conditions are optimized by this technique. Usually, injection wells are used to introduce additives into the subsurface. When creating a biostimulation system, a number of subsurface factors, including lithology, hydraulic conductivity, and groundwater velocity, are important considerations. Pollutant breakdown is primarily carried out by native microorganisms found in the soil; however, bioaugmentation can improve biostimulation. Enhancing the efficacy of remediation by adding particular microbial strains to the contaminated site, known as bioaugmentation, replenishes the native microbial community (Jakubovskis et al. 2020).

### **Bioaugmentation**

To aid in the cleanup of contaminated soil, bioaugmentation involves introducing a group of naturally occurring microbial strains or genetically modified bacteria. When natural microorganisms are either not present in the soil or do not have the metabolic capacity to carry out the restoration process, this approach works especially well (Xu 2014).

### **Anaerobic Degradation**

Oil-spill bioremediation commonly uses urea and ammonia-based fertilizers, which may create an oxygen demand due to biological ammonia oxidation, even though many bioremediation strategies focus on increasing oxygen levels in contaminated sites and assume aerobic respiration as the primary means of hydrocarbon elimination (Sundravel et al. 2015). Under some conditions, oxygen mass transfer could not be enough to restore the oxygen that microbiological metabolism has used up. This situation is most clear when there is limited oil infiltration into deeper sediment layers, especially in fine sediments. Anaerobic hydrocarbon degradation becomes relevant in these situations. When oxygen is scarce, anaerobic degradation pathways might kick in, forcing microbial communities to use other electron acceptors like nitrate, iron, or sulfate to break down hydrocarbons. Therefore, anaerobic hydrocarbon degradation pathways may play a major role in bioremediation efforts in situations with restricted oxygen availability.

### **Land Farming**

As a remediation approach, land farming spreads contaminated soil across a bed that has been prepared, sometimes with fertilizers and sometimes without. By encouraging bacterial activity, this technique improves the breakdown of oil pollutants in the soil (Sidiq et al. 2020). A few parameters need to be kept in mind when choosing a suitable location for land farming. Among them is the requirement to keep the ground surface and the seasonal high groundwater table at least three feet apart in order to avoid contaminating groundwater. In addition, a land slope of no more than 8% is necessary to ensure sufficient soil stability and stop erosion. Following these guidelines helps minimize possible negative effects on the environment while ensuring the effectiveness of the land farming operation.

### **Composting**

The process of composting involves piling polluted soil next to organic resources such as manure or agricultural waste (Khan et al. 2021). The addition of organic materials raises the pile's temperature and encourages the growth of a diverse microbial community. This elevated temperature,

in conjunction with the promotion of microbial proliferation via nutrient addition, enables the effective biodegradation of pollutants in a comparatively short amount of time.

## ENVIRONMENTAL REQUIREMENTS

### Optimum Environmental Conditions

Table 1 below outlines the ideal environmental conditions required for contaminant degradation.

### Strategies to Uphold Ideal Environmental Parameters

Temperature, humidity, and pH all have a big impact on the growth and function of microorganisms (Singh & Gupta 2020). Although microorganisms can survive in harsh environments, most of them do well in a limited range. Thus, to guarantee their efficacy in bioremediation procedures, it is essential to create and preserve optimal circumstances.

#### Soil

High levels of alkalinity or acidity in soils can hinder the processes involved in biodegradation. However, pH can be adjusted by adding lime, which will neutralize the soil and create an environment that will support biodegradation.

#### Temperature

Biochemical reaction rates are highly dependent on temperature; several reactions double in speed for every 10°C increase in temperature (Reddy & Ravitheja 2019). However, going over a certain temperature threshold might cause cells to die or become dormant. Plastic covering can be used to raise temperatures to efficiently capture solar heat, especially in the late spring, summer, and autumn.

#### Water Content

All living things depend on water to survive, and irrigation is key to achieving the ideal moisture content required for efficient bioremediation procedures.

### Oxygen

Whether an aerobic or anaerobic system runs depends on the availability of oxygen. Anaerobic conditions are mostly used for the breakdown of chlorinated chemicals, whereas aerobic circumstances are more effective in the breakdown of hydrocarbons. You can use techniques like tilling or air sparging to increase the amount of oxygen in the soil. Furthermore, to increase oxygen levels in the environment, magnesium or hydrogen peroxide may occasionally be added.

### Soil Structure

The efficient transportation of air, water, and nutrients is significantly impacted by the composition of the soil. Gypsum and organic matter are two examples of elements that can be applied to improve soil structure. Poor permeability soils, on the other hand, are not appropriate for in situ cleanup methods because they can impede the flow of water, nutrients, and oxygen.

## MATERIALS AND METHODS

### Bacterial Isolation

The bacteria used in this study were isolated from the sandy surface layer, which is identified by the presence of little silt and clay (Sundravel et al. 2023). This soil sample was taken from a car workshop in the Namakkal district of Tiruchengode that had been purposefully contaminated with crude oil before. The tests that were performed to identify the bacteria present in the oil-contaminated soil are displayed in Fig. 1.

On agar plates, the microbial population was evaluated using the serial dilution method under 26°C incubation. To count all bacteria, nutrient agar was used. First, one gram of soil was combined with one hundred milliliters of water. Next, one milliliter of the tainted water was diluted one at a time, reaching volumes of 106, 107, and 108 milliliters. The experiment's temperature shouldn't be higher than

Table 1: Environmental conditions affecting degradation.

Parameters	Criteria for microbial activity	Optimal circumstances for the degradation of oil
Oxygen content	Conditions favoring aerobic degradation, with at least 10% air-filled pore space.	10–42%
Contaminants	Non-toxic conditions	Hydrocarbons make up 6–12% of the soil's dry weight.
Temperature (°C)	17–43	22–34
Soil moisture	26–29% of water retention capacity	31–92%
Soil pH	6–9	6.5–8.0
Nutrient content	Nutrient concentrations are essential for supporting microbial growth.	C:N:P = 100:10:1
Type of soil	Reduced clay or silt presence.	





Fig .1: Tests for identification of bacteria.



Fig. 2: Mixer.



Fig. 3: Laboratory tests for bacterial isolation.

room temperature. In a different method, 20 milliliters of sterile nutritional broth were mixed with four grams of contaminated soil. The process of autoclaving at  $121^{\circ}\text{C}$  for 25 minutes was used to achieve sterilization. A mixer was used to mix the soup for an hour. The electrical mixer used to continuously agitate the broth culture over a lengthy period is shown in Fig. 2.

Fig. 3: depicts the preliminary tests conducted for the isolation of bacteria within the broth culture.

The samples were sterilized and then incubated for 24 hours at  $37^{\circ}\text{C}$ . Solid nutritional agar was streaked over Petri dishes, which were subsequently incubated at  $37^{\circ}\text{C}$  for eighteen hours. Until pure colonies were achieved, organisms exhibiting defining traits of a colony were isolated and subsequently subcultured on sterile nutrient agar plates. These plates were then incubated at  $37^{\circ}\text{C}$  for a further 18 h (Fig. 5). The progression of bacterial colony growth in petri dishes subjected to autoclaving conditions is illustrated in Fig. 4.



Fig. 4: The formation of bacterial colonies.



Fig. 5: Incubator used in the experiment.

### Biochemical Tests

One milliliter of crude oil was introduced to four milliliters of the synthetic medium, with the crude oil acting as the

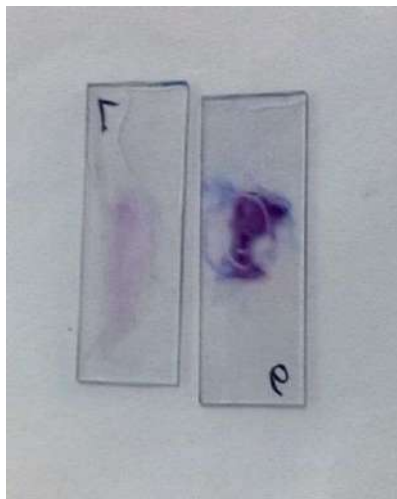


Fig. 6: Streaking method for bacterial identification.

only carbon source, to evaluate the isolates for hydrocarbon utilization. One liter of deionized water was used to dissolve 1% NaCl, 0.042%  $\text{MgSO}_4 \cdot 7\text{H}_2\text{O}$ , 0.042%  $\text{NaNO}_3$ , 0.029% KCl, 0.083%  $\text{KH}_2\text{PO}_4$ , and 0.125%  $\text{NaHPO}_4$  to create the synthetic medium. The medium's pH was brought to 7.4. The cultures were then cultured for five days at 27°C, and the synthesis of biosurfactants was monitored every day. The streaking test used to identify the bacteria is shown in Fig. 6.

### Characterization and Identification

Two of the eight distinct strains showed evidence of using hydrocarbons. Following that, these two isolates



Fig. 7: Bacteria culture for various bacteria.

Table 2: The characterization and identification of isolates using the Gram staining technique.

Test	Result	
Trehalose	+	-
Motility	+	+
Glucose	+	+
Endospore	+	-
Gram stain	Gram-positive	Gram-negative
Sucrose	+	-
L-Rhamnose	+	-
Colony Characteristics	The colony has a mucoid texture, is elevated, spherical, and appears white.	The colony has smooth edges, an uneven form, and a yellow-orange coloring.
D-Xylose	-	+
D-Ribose	-	-
Oxidase	+	+
Catalase	+	+
Possible identification	Bacillus	pseudomonas

underwent processes for characterization and identification (Jamuna et al. 2020). For characterization, morphological inspection, staining reactions, microscopic investigation, and biochemical testing were carried out. The two species were later determined to be *Pseudomonas* sp. and *Bacillus* sp. The culture method used in the Bijou bottles, set up for the incubation phase, is shown in Fig. 7.

The outcomes of biochemical analyses and observations of colony features that were used to identify the bacterial isolates are shown in Table 2.

### Inoculum Buildup

Bijou bottles with 5 ml of nutritive broth were filled with *Pseudomonas* and incubated at 37°C. A spectronic 20 spectrophotometer was used to measure absorbance at a wavelength of 560 nm to count the number of bacteria (Chindasiriphan et al. 2020). This process was repeated until a cell concentration of  $1.5 \times 10^8$  colony-forming units (CFU.mL<sup>-1</sup>) was reached. Then, a 1-liter culture of nutrient broth was added to the 5-milliliter culture. *Pseudomonas* was replaced with *Bacillus* for the rerun of this procedure. Equal amounts (500 mL) of the culture from each isolate were combined with the previously indicated cell concentration to create a bacterial consortium. We used these cultures in our fieldwork.

## FIELD WORK

### Preparation of Samples

We used loamy topsoil with a depth of 0-15 cm to fill polythene bags. Since tomato plants grow well in acidic soil, the pH of the soil was slightly raised to an acidic level. Eight kilos made up each soil bag. Every dirtbag—aside from the control—was sprayed with 200 mL of crude oil, sometimes known as engine oil. We next infected one of the soil bags contaminated with crude oil with a one-liter culture of *Pseudomonas* cells at a concentration of  $1.5 \times 10^8$ . Consortium, cow manure, and *Bacillus* were used to duplicate this procedure (Arunvivek et al. 2019).

Furthermore, one soil bag was not treated in any way and was contaminated with crude oil (control). Two bags per treatment were observed during the experiment, and each bag was manually mixed. Throughout the trial, the bags were kept in the best possible environmental conditions by being exposed to sunlight and receiving regular irrigations.

### Transplanting Tomato Seedlings

After 30 days, the seedlings were carefully transferred from their original spot and placed inside polybags. After that, soil was added to the clay pots to provide the polybag

support. The potholes were plugged in to stop water loss during the experiment. Water was initially maintained for the first nine days after transplantation at a level that was 1 cm above the ground. The next goal was to keep the soil at its ideal moisture content without flooding. Water levels were regularly checked and topped off as necessary. Documentation of observations was done for various soil samples and treatment settings. Fig. 8 shows the germination of tomato seedlings on the ninth day after uprooting.

### Study on the Growth of Plants

On the thirtyth day, each plant's germination count, shoot height, leaf area, root-shoot ratio, dry weight, and root length were measured. At the 30-day point, the maximum height and leaf area were recorded. Furthermore, notes were collected about color shifts in the plants as well as any deaths. On the ninth day, the shoot development in soil treated with cow dung is depicted in Fig. 9.



Fig. 8: Germination of tomato seedling on the 9<sup>th</sup> day.



Fig. 9: Germination of shoots in soil treated with cow dung.



### Leaf Area

On the thirty days following treatment, the leaf area was measured with a leaf area meter. The formula for calculating leaf area was as follows: length multiplied by maximum width multiplied by 0.75.

### Specific Leaf Weight (SLW)

The weight of a leaf per unit area is known as specific leaf weight (SLW), and it is commonly stated in grams per square meter ( $\text{g.m}^{-2}$ ).

### Specific Leaf Area (SLA)

The leaf area per unit leaf dry weight is known as specific leaf area (SLA), and it is commonly stated in square meters per kilogram ( $\text{m}^2.\text{kg}^{-1}$ ). It shows how effectively the leaf is absorbing light and transferring gases to and from the atmosphere.

### Dry Weight

The weight of a material after all moisture has been removed is referred to as its “dry weight,” and it is usually found by drying the sample in an oven until a steady weight is reached.

### Root Shoot Ratio

A measure of a plant's biomass distribution—that is, the percentage of biomass allotted to roots as opposed to above-ground shoots—is the root-to-shoot ratio. It is computed by dividing the branches' dry weight by the roots' dry weight.

### Root Length

Thirty days following treatment application, the root length was measured. Watering the plants thoroughly helped to speed up the process. The plant's polybag was then gently sliced in half, making it possible to easily reach the roots without compromising the integrity of the plant. Next, the length of the root was measured.

## RESULTS AND DISCUSSION

### Comparison and Analysis of Vegetative Parameters

#### Non-destructive Vegetative Parameters

Non-destructive vegetative parameters are those that are studied without causing any damage to the plant body (Arunvivek et al. 2022). The tomato plant in crude oil soil at days nine and thirty is shown in Fig.10. Plants cannot



Fig. 10: The growth of tomato plants on the 30th day was assessed.



Fig. 11: Disparity in plant growth between polluted soil and treated soil.



survive in an environment where air and water circulation into the soil is inhibited by crude oil. Leaf loss and yellowing of the leaves, which started on the ninth day, are among the symptoms. Fig. 11 illustrates the variation in plant growth between polluted soil and treated soil.

The vegetative characteristics of tomato plant growth in crude oil-polluted soil treated with cow dung and bacterial culture are shown in Table 3.

The plant destructive growth parameters of soil treated with different treatments are given in Table 4.

The microbes that could use hydrocarbons were *Bacillus* and *Pseudomonas*, according to the results of their characterization and identification. In terms of vegetative metrics, the treatments containing *Pseudomonas* and *Bacillus* alone, the consortium (a mixture of *Pseudomonas* and *Bacillus*), and the control group displayed the greatest mean values for plant height, root-shoot ratio, leaf count, and maximum root height. On the other hand, the treatments with just crude oil and cow dung showed the lowest values for these vegetative metrics. Within two to three weeks of germination, tomato plants planted in soil treated exclusively with crude oil showed yellowing of the leaves with a black tinge at the corners, whereas plants cultivated in other treatments displayed leaf fading about four weeks after germination.

### Comparison and Analysis of Soil Properties

Examining and contrasting different aspects of soil samples from diverse treatments or locations is part of the process

of comparing and analyzing soil properties. Parameters like soil pH, organic matter content, nutrient levels (such as nitrogen, phosphorous, and potassium), soil texture, and microbial activity are often included in this analysis. Significant variations between soil samples may be found using statistical tests, and data visualization can be aided by using graphical representations like bar charts or scatter plots (Arunvivek et al. 2015). To further comprehend the connection between soil health and plant performance, correlations between soil characteristics and plant growth metrics may be investigated. In general, the comparison and analysis of soil parameters offer insightful information on how environmental factors and treatments affect plant productivity and soil quality.

### Soil Nutrient Composition

The use of hydrocarbons by higher bacterial populations is responsible for the decrease in oil and grease content. Nutrients, including potassium, phosphorus, and nitrogen, are abundant in cow manure. Air and water cannot flow freely through contaminated soil, especially in soils that include a lot of silt and clay. The nutrients found in the soil for each of the treatments are shown in Table 5.

### Soil Physical Properties

The treated samples show bonded granules, while the contaminated sample displays tiny grains. The polluted area's degraded soil is the reason for this differentiation. Soil's

Table 3: Vegetative characteristics of tomato plant development.

Treatments	Plant height [cm]	Shoot height [cm]	Leaf colour
Control	28.5	16.5	The green color of the leaf signifies the health of the plant.
Consortium	30.7	19.5	Leaf green
Bacillus	24.4	13.5	The older leaves' fading and their pale green hue point to a possible nutrient shortage or stress in the plant.
Pseudomonas	22.6	11.4	The plant's health may be impacted by a nutrient shortage or environmental stress, as shown by the pale green color, backward curling of leaves, and fading of older leaves.
Cowdung	20.3	9.3	The leaf's green hue suggests that it is in good health.
oil only	13.9	4.9	Blackish yellow

Table 4: Plant destructive growth studies.

Treatment	Leaf dry weight [g/plant]	Root dry weight (g/plant)	Total dry weight [g/plant]	Root shoot ratio	Root length [cm]
Control	0.922	0.092	6.900	0.011	19.03
Consortium	1.330	0.075	7.870	0.012	18.75
Bacillus	0.857	0.067	5.320	0.010	16.45
Pseudomonas	0.756	0.045	4.870	0.008	13.32
Cowdung	0.655	0.030	3.883	0.007	11.78
oil only	0.240	0.018	2.187	0.00096	4.37

Table 5: Analysis of Soil properties in Oil, Cow dung, and Consortium treatment.

Soil Properties	Before The Experiment	After the Experiment		
		Oil treatment	Oil + Cow dung	Oil+ Consortium
%Total nitrogen	0.15	0.07	0.53	0.7
%Organic carbon	1.8	2.3	1.98	1.9
%silt	2.0	2.7	3.1	2.9
Cation exchange capacity	9.2	9.1	9.1	9.0
% Fine sand	51.3	50.6	50.3	50.9
% Clay	16.72	16.64	16.20	16.67
% Coarse sand	29.98	29.86	29.89	29.92
Calcium [ppm]	3.4	3.2	3.3	3.2
Potassium [ppm]	0.05	0.09	0.06	0.07
% Organic matter	2.3	2.1	2	2.2
Sodium [ppm]	0.36	0.38	0.38	0.41
pH	6.4	4.4	5.3	6.1
Phosphorus [ppm]	0.29	0.18	0.21	0.23
Magnesium [ppm]	1.4	1.3	1.2	1.4

Table 6: The treated and control soil samples' physical characteristics were contrasted.

Treatment	Water permeability	Odor	Texture	Structure	Color
Control	Positive	Not distinct	Bound	Durable	Undefined
consortium	Positive	Not distinct	Bound	Durable	Undefined
Bacillus	Positive	Not distinct	Bound	Durable	Undefined
Pseudomonas	Positive`	Not distinct	Bound	Durable	Undefined
Cowdung	Positive	Not distinct	Bound	Durable	Black
oil only	Negative	Oil	Fine/ loose	Not durable	Black/ Brown

permeability, or its capacity to let water through, is determined by its aggregation, swelling, and textural characteristics. There is no longer any permeability in the contaminated area due to the loss of the coagulating and colloidal states of the soil. Table 6 provides more information on these findings.

The results of the soil property analysis showed that the percentage of nitrogen in soils treated with cow dung (0.53%) and the consortium (0.7%) was higher than the initial nitrogen content (0.15%) before the experiment. On the other hand, the amount of nitrogen in the soil that was only given crude oil decreased (to 0.07%). Before the trial, the pH values were 6.4; for the consortium treatment, they were 6.1; for cow dung, they were 5.3; and for the control, they were 4.4. Furthermore, the soil treated with simply crude oil showed lower phosphorus levels, but the soils treated with cow dung and the consortium showed a relative rise in phosphorus levels.

## CONCLUSIONS

The consortium's and the *Pseudomonas* and *Bacillus* treatments' significant bioremediation capacities were

demonstrated in this study by their beneficial impacts on germination, plant height, root-shoot ratio, and root length. These findings imply that using bacteria for bioaugmentation can successfully reduce the pollution caused by crude oil. Although this study offers important insights, it is limited by the short duration of the experiment and its focus on only one plant species. Future studies should investigate the long-term effects and include a diverse range of plant species to better comprehend the broader ecological impacts of these bioremediation methods. It's possible that the bacteria created enzymes that could break down petroleum substrates by metabolizing the hazardous elements of crude oil. Although cow dung helped mitigate the negative impacts of crude oil pollution in terms of vegetative and reproductive parameters, its restorative benefits were not as strong as those of the consortium, *Pseudomonas*, and *Bacillus* treatments. Even while the yield of tomato plants treated with cow dung was higher than that of crude oil alone, it was still less than that of treatments with bacteria. This disparity in efficacy could be explained by the greater nutritional supply that cow

dung offers, which is sometimes absent or insufficient in soil that has been contaminated by crude oil. Furthermore, by binding soil particles together, cow dung improves soil permeability and structure. The results highlight the potential of cow dung (biostimulation) and microorganisms (bioaugmentation) for cleaning up soil contaminated by crude oil. For instance, bioaugmentation using a consortium of *Pseudomonas* and *Bacillus* has proven to be more successful than biostimulation alone. This bioremediation strategy presents considerable environmental advantages, such as decreased soil toxicity, enhanced soil fertility, and the potential for ecosystem recovery in oil-contaminated areas. These techniques could be especially beneficial in regions impacted by oil spills or prolonged petroleum industry activities. The metabolically active microbial community was essential to the hydrocarbon biodegradation process. The findings of this study have direct applications in environmental remediation projects. The combination of bacterial treatments and plant growth monitoring provides a practical and cost-effective approach for assessing and implementing soil restoration in oil-contaminated areas. Future studies will examine how well the combination of bioaugmentation and biostimulation techniques works. By supporting sustainable methods for resource and pollution management, this study supports Sustainable Development Goals 12 and 15, which center on responsible production and consumption as well as the preservation and sustainable use of terrestrial ecosystems. It deals specifically with soil remediation and contamination from crude oil.

## REFERENCES

- Agamuthu, P., Tan, Y.S. and Fauziah, S.H., 2013. Bioremediation of hydrocarbon-contaminated soil using selected organic wastes. *Journal of International Symposium on Environmental Science and Technology*, 5(2), pp.45-52. [DOI]
- Algaifi, H.A., Bakar, S.A., Alyousef, R., Sam, A.R.M., Ibrahim, M.H.W., Shahidan, S., Ibrahim, M. and Salami, B.A., 2021. Bio-inspired self-healing of concrete cracks using new *B. pseudomycoides* species. *Journal of Materials Research and Technology*, 12, pp.967-981. [DOI]
- Arunvivek, G.K. and Rameshkumar, D., 2019. Experimental investigation on waste cement sludge and silica fume incorporated Portland cement concrete. *Journal of the Institution of Engineers (India): Series A*, 100, pp.611-618. [DOI]
- Arunvivek, G.K. and Rameshkumar, D., 2022. Experimental investigation on feasibility of utilizing phosphogypsum in E-glass fiber-incorporated non-fired ceramic wall tile. *Journal of the Institution of Engineers (India): Series A*, 103, pp.445-451. [DOI]
- Arunvivek, G.K., Maheswaran, G. and Senthilkumar, S., 2015. Experimental study on influence of recycled fresh concrete waste coarse aggregate on properties of concrete. *International Journal of Applied Engineering Research*, 10(11), pp.2809-2815.
- Chindasiriphan, P., Yokota, H. and Pimpakan, P., 2020. Effect of fly ash and superabsorbent polymer on concrete self-healing ability. *Construction and Building Materials*, 233, pp.1-10. [DOI]
- Chorom, M., Hosseini, S.S. and Motamedi, H., 2010. Bioremediation of crude oil polluted soil as affected by sewage sludge. *International Journal of Soil Science*, 2, pp.33-40.
- Jakubovskis, R., Jankute, A., Urbonavicius, J. and Gribsniak, V., 2020. Analysis of mechanical performance and durability of self-healing biological concrete. *Construction and Building Materials*, 260, pp.1-10. [DOI]
- Jamuna, M., Gandhimathi, M., AbdulBari, J. and Niveditha, T., 2021. Florida's aquifer vulnerability to nitrate contamination: A GIS model. *Nature Environment and Pollution Technology*, 21(1), pp.50-57. [DOI]
- Khan, M.B.E., Shen, L. and Costa, D.D., 2021. Self-healing behaviour of bio-concrete in submerged and tidal marine environments. *Construction and Building Materials*, 277, pp.1-15. [DOI]
- Koshlaf, E. and Ball, A.S., 2017. Soil bioremediation approaches for petroleum hydrocarbon polluted environments. *AIMS Microbiology*, 3(1), pp.25-35. [DOI]
- Muonye, P.N. and Nnaji, C.C., 2024. Enhanced natural attenuation technique, edaphic and microbiological changes in oil-impacted soil of Odhiaje community, Rivers State. *Nature Environment & Pollution Technology*, 23(2), pp.89-96. [DOI]
- Oyedeji, A.O., Adebisi, M.A., Omotoyinbo, C.O. and Ogunkunle, O., 2012. Effect of crude oil-contaminated soil on germination and growth performance of *Abelmoschus esculentus* L. Moench—A widely cultivated vegetable crop in Nigeria. *American Journal of Plant Sciences*, 5(3), pp.120-130. [DOI]
- Reddy, T.C.S. and Ravitheja, A., 2019. Macro mechanical properties of self-healing concrete with crystalline admixture under different environments. *Ain Shams Engineering Journal*, 10(1), pp.23-32. [DOI]
- Rowland, U.O., Momoh, Y.O.L. and Nwaogazie, I.L., 2014. Bioremediation of crude oil-contaminated soil using organic and inorganic fertilizers. *Journal of Petroleum & Environmental Biotechnology*, 6, pp.1-9. [DOI]
- Silva, I.G., 2020. Soil bioremediation: Overview of technologies and trends. *Energies*, 13(18), pp.4664-4678. [DOI]
- Sidiq, A., Gravina, R.J., Setunge, S. and Giustozzi, F., 2020. High-efficiency techniques and micro-structural parameters to evaluate concrete self-healing using X-ray tomography and mercury intrusion porosimetry: A review. *Construction and Building Materials*, 252, pp.1-15. [DOI]
- Singh, H. and Gupta, R., 2020. Influence of cellulose fiber addition on self-healing and water permeability of concrete. *Case Studies in Construction Materials*, 12, pp.1-10. [DOI]
- Su, Y., Qian, C., Rui, Y. and Feng, J., 2021. Exploring the coupled mechanism of fibers and bacteria on self-healing concrete from bacterial extracellular polymeric substances (EPS). *Cement and Concrete Composites*, 116, pp.1-15. [DOI]
- Sundravel, K.V., Aruldasu, K. and Vijayasrinivasan, K., 2015. Experimental study on strength characteristics of geopolymer concrete using silica fume. *International Journal of Engineering Research and Management*, 2, pp.57-60.
- Sundravel, K.V., Ramesh, S. and Jegatheeswaran, D., 2021. Design and formulation of microbially induced self-healing concrete for building structure strength enhancement. *Materials Express*, 11(11), pp.1753-1765. [DOI]
- Sundravel, K.V., Jagatheeshwaran, S., Dineshkumar, P. and Parthasarathi, C., 2023. Experimental investigation on strength and durability of self-healing concrete using bacteria. *Materials Today: Proceedings*. [DOI]
- Udeh, N.U., Nwaogazie, I.L. and Momoh, Y., 2013. Bioremediation of a crude oil-contaminated soil using water hyacinth. *International Journal of Advances in Applied Science Research*.
- Vermeer, C.M., Rossi, E., Tamis, J., Jonkers, H.M. and Kleerebezem, R., 2021. From waste to self-healing concrete: A proof-of-concept of a new application for polyhydroxyalkanoate. *Resources, Conservation and Recycling*, 164, pp.1-10. [DOI]
- Xu, J., 2014. Bioremediation of crude oil-contaminated soil by petroleum-degrading active bacteria. *Journal of Applied Science and Environmental Management*, 18, pp.1-10.

- Xu, J., Tang, Y. and Wang, X., 2020. A correlation study on optimum conditions of microbial precipitation and prerequisites for self-healing concrete. *Process Biochemistry*, 94, pp.266-272. [DOI]
- Yang, B., Xue, Q.H., Qu, C.T., Lu, C., Liu, F.F., Zhang, H., Ma, L.T., Qi, L. and Wang, Y.T., 2024. Research progress on in-situ remediation of typical heavy metals in petroleum hydrocarbon-contaminated soil enrichment by plants. *Nature Environment & Pollution Technology*, 23(1), pp.1-10. [DOI]
- Zhu, B., Li, Q., Chen, W., Zou, W. and Chen, W., 2020. A novel method of self-healing in cementitious materials by using polyacrylic hydrogel. *KSCE Journal of Civil Engineering*, 24, pp.3406-3415. [DOI]



# The Implementation of Contingent Valuation Method for Waste Management at Telaga Ngebel, Ponorogo, Indonesia: A Novel Approach to Ecotourism Waste Processing House

Evi Gravitiani<sup>1†</sup>, Ainina Ratnadewati<sup>1</sup> and Nur Widiastuti<sup>2</sup>

<sup>1</sup>Faculty of Economics and Business, Universitas Sebelas Maret Jalan Ir Sutami 36°, Surakarta, Indonesia

<sup>2</sup>School of Economics, Widya Wiwaha, Jl. Lowanu Sorosutan UH VI/20, Sorosutan, Yogyakarta, Indonesia

†Corresponding author: Evi Gravitiani; [evigravitiani\\_fe@staff.uns.ac.id](mailto:evigravitiani_fe@staff.uns.ac.id)

**Abbreviation:** Nat. Env. & Poll. Technol.  
**Website:** [www.neptjournal.com](http://www.neptjournal.com)

*Received:* 15-07-2024

*Revised:* 06-09-2024

*Accepted:* 12-09-2024

## Key Words:

Waste management  
 Economic tourism  
 Circular economy  
 Willingness to pay  
 Contingent valuation method

## Citation for the Paper:

Gravitiani, E., Ratnadewati, A. and Widiastuti, N., 2025. The implementation of contingent valuation method for waste management at Telaga Ngebel, Ponorogo, Indonesia: A novel approach to ecotourism waste processing house. *Nature Environment and Pollution Technology*, 24(2), p. D1706. <https://doi.org/10.46488/NEPT.2025.v24i02.D1706>

*Note: From year 2025, the journal uses Article ID instead of page numbers in citation of the published articles.*



**Copyright:** © 2025 by the authors

**Licensee:** Technoscience Publications

This article is an open access article distributed under the terms and conditions of the Creative Commons Attribution (CC BY) license (<https://creativecommons.org/licenses/by/4.0/>).

## ABSTRACT

The increase in the number of visitors to the tourism sector has a positive impact on the economy of the surrounding merchants. However, it also creates negative externalities through increased waste generation. The generation of unresolved waste will disrupt the function of the environment. Ecotourism Waste Management is one way to handle waste from sellers and tourists by collecting, processing, and selling processed products. The "Waste Treatment House" manages sales proceeds from and for sellers with a profit-sharing system. This effort requires the willingness to pay (WTP) sellers for waste management. This study aims to determine the amount of waste retribution and the factors that influence it. The data used in this study were primary data of 104 sellers in Telaga Ngebel Area, Ponorogo, Indonesia, and were processed using ordinary least squares (OLS) regression and descriptive analysis. WTP value is influenced by age, monthly expenses, number of dependents, operating hours, and length of business. The products produced through the program are organic waste processed into compost and fish feed, while inorganic waste is processed into handicrafts. Finally, selling processed waste products and the proceeds from these sales are used to increase merchant empowerment through revenue sharing and savings and loan products. This study has limited secondary data, namely information about the sustainability of waste management that has been carried out and the exact number of sellers in the area around Telaga Ngebel.

## INTRODUCTION

A total of 175 countries gathered in Nairobi, Kenya, in March 2022 to support a resolution by the United Nations Environment Programme (UNEP) to address waste generation, including plastic waste (Adamowicz 2022). This resolution is the first step towards a legally binding agreement. It is targeted to be reached in 2025, known as the International Legally Binding Instrument (ILBI) or Global Plastic Treaty (GPT), so various agreed formulations are needed (Bergmann et al. 2022, Cowan et al. 2023a, Maes et al. 2023). This led to the establishment of the Intergovernmental Negotiating Committee (INC), consisting of member states and relevant stakeholders. This committee meets regularly, from INC-1 to INC-5, as one of the supporters of the resolution in 2022. This effort is a further step taken to reduce waste pollution worldwide. Indonesia is one of the countries that actively strives to reduce pollution, as evidenced by its contribution to GPT.

Various global efforts have been made to ensure environmental cleanliness and safety. This can be seen from the emergence of sustainable waste management to overcome environmental pollution caused by waste generation (Masjhoer et al. 2022). The World Bank estimates that each individual produces 0.74 kg of waste worldwide and 2.01 billion tons annually, which is expected to increase

to 3.40 billion tons by 2050 (Cai & Ou, 2023, Gasni & Mulyadi, 2022). The increase shows that appropriate waste management is needed to overcome the pollution problem. The condition is aggravated when no attention is paid to the issue. Therefore, it is essential to integrate sustainable waste management to address environmental pollution due to waste generation effectively (Mohamad Mulyadin et al. 2018).

One of the sectors that have the potential to contribute to the most significant waste generation is the tourism sector (Rahmattullah et al. 2023). Tourism is an economic sector that is very important in providing significant economic and social benefits. Despite this, there is still a lack of substantial empirical data on the negative impacts of the tourism sector, especially related to environmental pollution issues. This results in pollution from tourism activities, which can hamper efforts to control ecological pollution. More in-depth Research is needed to examine this issue and evaluate its implications for sustainable waste management (Plastic Atlas Asia 2022).

Indonesia is the second largest producer of plastic waste in the world. One of the largest sources comes from the tourism sector, reaching 187.2 million tons, after China, which reached 262.9 million tons (Inayah & Istiqomah, 2021). According to the Ministry of Environment and Forestry, in 2019, the waste generated in tourism areas was 241 tons per day, consisting of waste from trash cans and waste scattered in several tourist locations (Hilman et al. 2023). This waste problem should not be ignored because it can gradually threaten the sustainability of living things and tourism. Therefore, a strategy that can be done to reduce the increase in waste is to encourage tourists and sellers to behave in a more environmentally friendly way.

Several other factors also support the high amount of waste from the tourism sector. Research conducted by

Made et al. (2020) shows that the increasing amount of waste from the tourism sector in Indonesia is caused by population growth, lack of public awareness in protecting the environment, lack of socialization in various roles, weak implementation of waste handling regulations, and lack of landfills in the majority of tourism sectors in Indonesia.

The increase in the amount of waste in the tourism sector is still a classic problem that must be solved (Djuwendah et al. 2023). The waste generation that is not managed correctly disrupts the function of environmental balance, especially the environment around tourist attractions (Costa & Ferreira Dias, 2020). The waste produced is from visitors and sellers at the tourist spot (Achmad et al. 2023). One of the tourism sectors in Indonesia that has experienced an increase in the amount of waste is Telaga Ngebel, amounting to 6.5 tons of waste in 2021 and increasing to 8 tons in 2022 (Maria & Widayati 2020).

Telaga Ngebel is a natural lake in Ponorogo Regency, East Java, flanked directly by four surrounding villages: Sahang Village, Ngebel Village, Wagir Lor Village, and Gondowido Village, as seen in Fig. 1. The area of Telaga Ngebel is 150 hectares, with an altitude of 734 meters above sea level (Nisa et al. 2021). The height of the location causes the temperature around the Telaga to be 20 degrees Celsius. Telaga Ngebel has a beautiful view: a row of hills flanking the Lake and the cool air. Tourists can also enjoy other tourist attractions such as speed boats, dancing fountains, horse rentals, and cultural performances on certain occasions. Tourist attractions owned by Telaga Ngebel have the potential to attract tourists to visit (Rahardjo et al. 2023). This makes Telaga Ngebel one of the potential tourists in East Java Province, as evidenced by the increasing number of Telaga Ngebel tourists from year to year, as shown in Fig. 2.

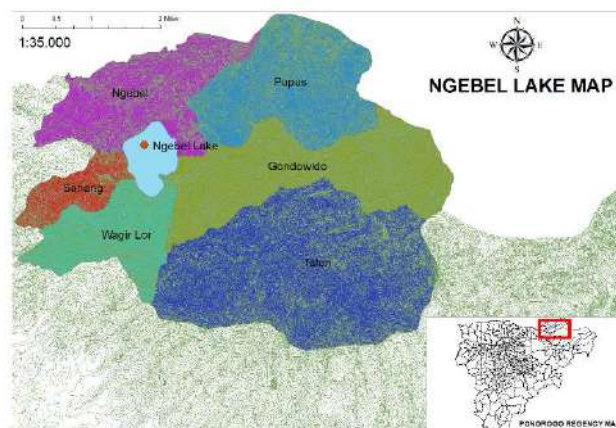


Fig. 1: Telaga Ngebel Map.

The average Number of Telaga Ngebel tourists per day in 2021 was 1607. This number increased from the previous year, only 1206 tourists, and grew in 2022, reaching 4465. One of the reasons for this increase is the absence of social restrictions due to the COVID-19 pandemic. The peak of the increase in the average number of tourists per day during 2020-2023 occurs in 2023, reaching 9275 tourists. The increasing number of tourists certainly has a positive impact, including for residents around Telaga Ngebel.

Residents use the increase in the Number of Telaga Ngebel tourists to improve the economy by trading food and souvenirs and renting rides. In addition to increasing the economic sector, the large number of tourists has side effects in the form of negative externalities. According to Anggarini, (2021), negative externalities are side effects of imbalances arising from a particular activity and outside the market system. A negative externality arising from the increase in tourists is the increasing amount of waste generation (Anggarini 2021).

Most waste comes from tourists and sellers who trade around Telaga Ngebel. The waste produced is, on average, single-use plastic waste from food, beverage, and souvenir packaging and fish bone waste from restaurants around Telaga Ngebel.

The waste is classified by type, namely organic, paper, plastic, cans, and other waste. Meanwhile, based on the source, waste is divided into three namely: sellers, visitors, and residents who dispose of their waste at the Telaga Ngebel Landfill, as shown in Fig. 3.

The most produced type of waste is plastic waste, which has a total waste of 3000 kilograms. The plastic waste is in the form of plastic bottles and food wrappers, the majority of which are sourced from sellers, with a total of 1250 kilograms. The second largest type of waste is organic waste, which has a total amount of waste of 2000 kilograms. The organic waste produced is food waste from restaurants (vegetables, fish bones, etc.), which sellers mostly produce with a total waste of 900 kilograms.

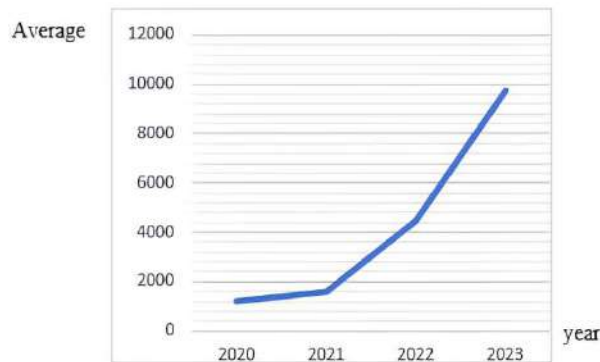


Fig. 2: The daily average number of visitors to Telaga Ngebel.

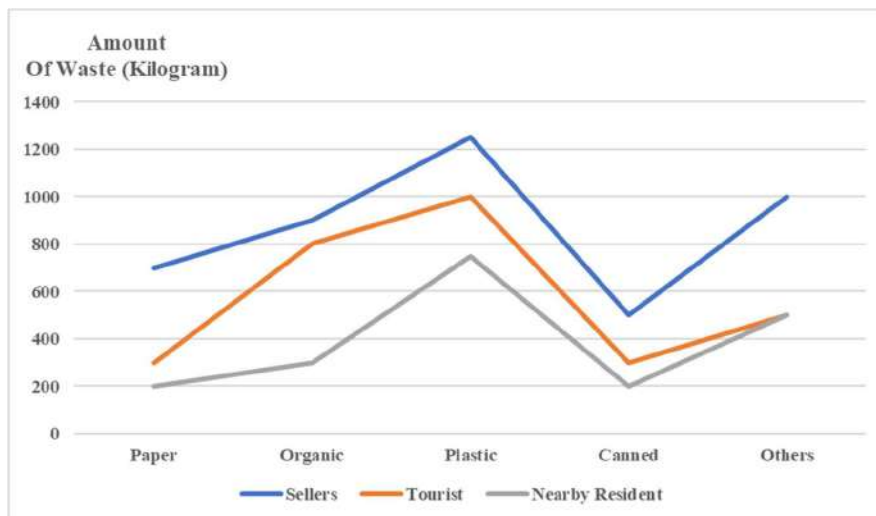


Fig. 3: Amount of waste by type and source in 2022.

The sector that produces the least waste around Telaga Ngebel is the household sector because it does not dispose of its waste at the landfill in Telaga Ngebel, and The second sector that produces the most waste is the sector is the merchant sector. The total waste generated in 2022 is 8 tons of waste calculated from each week. There are two three-wheeled motorcycles with a capacity of 153 kilograms of waste that transport this waste to be collected at the Telaga Ngebel landfill.

This situation is exacerbated by waste management that is not as dense as the waste collection location far from tourist sites and the absence of waste management and other problems, as in Fig. 4.

The surge in the amount of waste due to the activities of sellers and visitors in Telaga Ngebel requires special attention to overcome it. One way that can be done is through the ecotourism waste management program (Hemali & Alwis 2022). The program is one of the programs that initiate sellers to manage waste and make products that are of selling value. Sellers are considered actors who have a significant influence in increasing the amount of waste around the area because they stay for a long time, unlike visitors who only come occasionally to travel. Ecotourism Waste Management is an implication of waste management programs carried out by and for sellers in the region through several stages, as in Fig. 5 (Amirudin et al. 2023).

The application of waste management in ecotourism in Indonesia has begun to be encouraged. Research conducted by Sekarningrum (2016) said that in the ecotourism location of Baluran National Park, Banyuwangi, waste management has been implemented by applying biodegradable waste composting. Almost the same thing is also seen in

Research conducted by Thorley et al. (2019), namely waste management, which has been applied to Nagari Tuo Pariangan Tourism Village using three main sorting methods: composting, reprocessing, and residual waste. Slightly different from the previous two studies, the Research conducted by Wicaksono et al. (2023) focused more on making the Anthropocene Monument an ecotourism facility at the Piyungan Landfill, Bantul.

The Ecotourism Waste Management Program aimed at sellers in the Telaga Ngebel area is a program managed directly by sellers in a place called the waste processing house. There are four stages of the waste processing house process. As in Fig. 4, the stage is waste management tailored for sellers (Thorley et al. 2019). The first stage is collecting, which is the process of collecting waste generated every day. The collection of such waste is carried out independently by sellers. Waste is collected and separated based on its type, namely organic and inorganic waste. Organic waste, according to Kumar et al. (2022b), is waste that comes from the rest of living things and has a relatively faster recycling period. In contrast, inorganic waste, according to Cowan et al. (2023b) and Cai & Ou (2023), comes from processed products and has difficulty being recycled. The stage of waste separation by sellers is the second stage of the ecotourism waste management program.

According to Kumar et al. (2022a), waste processing is the process of reprocessing the remaining consumables into materials that can be reused and even have selling value. Waste processing is done by regrouping waste into sub-groups to get different treatments (State et al. 2022). This study divides subgroups into types of organic waste, consisting of subgroups of fish bones, foliage waste, and wet food waste. The fish

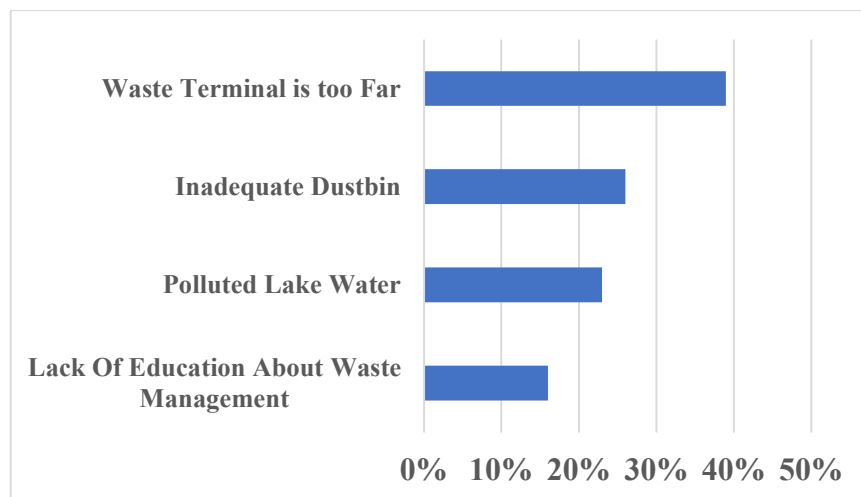


Fig. 4: Waste problems in Telaga Ngebel.



bones will be processed into processed products such as fish crackers, while foliage and wet food waste will be processed into compost and fish feed. The fish bones will be processed into processed products in the form of fish crackers, while foliage waste and wet food waste will be processed into compost and fish feed. Making fish crackers made from fish bones requires several materials and stages as shown in Fig. 6. The processed product is currently still in the idea stage and will only be tested as well as compost and fish feed, so the business feasibility test has not been carried out.

Another thing with inorganic waste is that it is processed into handicrafts. The processed waste then becomes items of selling value, such as handicrafts from used bottles, lamp cap decorations, and shopping bags, which are then marketed into typical Telaga Ngebel products. In addition, waste in the form of plastic packaging is processed into eco-bricks, which is the last stage of the ecotourism waste management program (Ledheng et al. 2022).

Products processed by sellers waste in Telaga Ngebel will be managed and marketed by sellers, one of which is

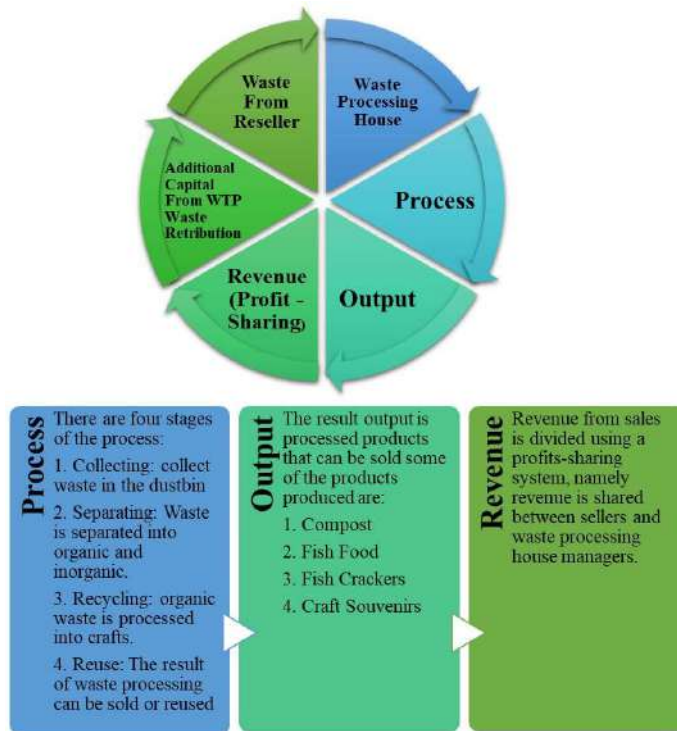


Fig. 5: Integrating waste processing house for effective ecotourism waste management implementation.

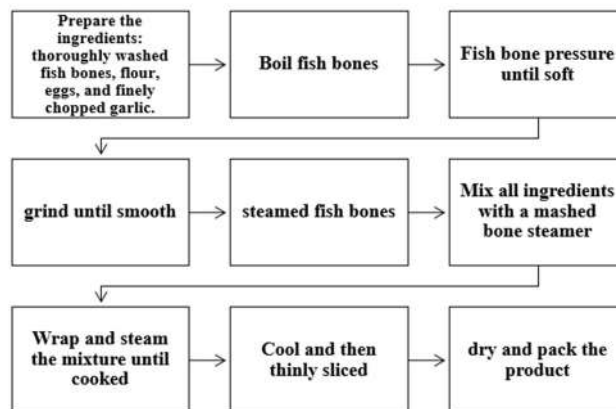


Fig. 6: The process of making fish crackers made from fish bones.

through galleries and workshops managed by the sellers' association and the local government, with the proceeds of the sale being given back to sellers. The ecotourism waste management program organized at the waste processing house certainly requires the involvement of various parties in its implementation, such as the government, tourism managers, and sellers around the area. The implementation began with training and counseling to sellers, in addition to synergy and commitment in the form of payment of merchant waste retribution as a form of environmental responsibility and used as waste processing capital. The waste retribution paid by sellers is a form of commitment and responsibility of sellers to the environment. The fixed waste retribution rate is one of the things that needs to be reviewed. One solution can be done through contingent valuation method analysis with the calculation of willingness to pay for merchant waste retribution in the Telaga Ngebel Area. Contingent Valuation Method (CVM) is a method for valuing environmental objects with no market value (Atinkut et al. 2020).

The CVM assessment in this study aims to calculate the value of hygienic environmental objects in the form of waste processing accountability in the Telaga Ngebel Area. The value of environmental objects is calculated through the willingness to pay for the merchant's waste retribution. One hundred four sellers in the region will be given a choice on the market hypothesis of the importance of waste processing and the impact of damage to the tourist environment. Providing options for this hypothesis is continued by asking about the value of willingness to pay waste retribution as an effort to preserve the environment through open questions. The amount of desire to pay the merchant is then added up to get the average WTP value of the Merchant's Waste Retribution (Nwofoke et al. 2017).

Several factors can influence the willingness to pay waste management retribution. Research conducted by Jamaludin et al. (2022) said that the WTP of waste management retribution is influenced by the high level of education and the amount of one's expenditure. Meanwhile, Saija et al. (2023) research found that age and number of dependents also affect WTP waste management. According to Jamaludin et al. (2022), the amount of WTP sellers on waste management is also influenced by the length of business, operating hours, and the contribution to waste management. The method used to determine the factors that affect the amount of WTP value is ordinary least square (OLS) with seven independent variables, namely: age, length of education, marital status, number of dependents, operating hours, the willingness of sellers to process waste, and length of effort. Meanwhile, the dependent variable used is the amount of WTP Waste Retribution sellers.

Research on waste management in tourist attractions has been carried out previously by Wubalem et al. (2023), who said that ecotourism waste management can be analyzed and applied through the active role of visitors. Different results from Hung et al. (2023) show that ecotourism waste management in tourist attractions, especially natural tourism, is carried out through solid synergy between stakeholders and managers. Similar findings are shown in Suchek et al., indicating that the application of ecotourism waste management is still emphasized through the role of cleaners and the government in waste management. The three previous studies resulted in disagreement of results and differences in research points of view, most of which said that the role of sellers in tourism waste processing was underemphasized. The conflict is interesting, so this study will discuss waste management ecotourism at the waste processing house using CVM analysis calculated based on the WTP of waste retribution and the factors affecting it.

## MATERIALS AND METHODS

### Research Design

This study uses a quantitative method in the form of Contingent Valuation Method (CVM) calculations, which aims to determine the value of environmental awareness measured using Willingness to Pay (WTP) waste retribution (Mamaco et al. 2023). In addition, researchers also use descriptive analysis to represent data and socioeconomic characteristics of sellers.

### Sampling Techniques

To conduct this study, researchers used a simple random sampling method with a population of 140 sellers in the Telaga Ngebel area, which was then sampled using the Slovin method with an error of 5 percent as follows:

$$N = \frac{n}{1 + Ne^2} \quad \dots(1)$$

Where:

n = sample size

N = population size

e = error estimate

### Contingent Valuation Method

Data analysis in this study uses the contingent valuation method (CVM) to measure the desire to pay individuals (WTP) for changes in the quantity or quality of environmental goods and services that do not have market value (Natsir et al. 2024). The existence of waste around Telaga Ngebel

causes disruption of environmental functions in the form of pollution of water, air, and soil. Thus, it is necessary to evaluate how to overcome the waste problem, one of which is by looking at the waste-producing sector around Telaga Ngebel's responsibility to the environment by analyzing the value of environmental awareness through WTP payments.

There is a population of 140 sellers recorded in the group of sellers around Telaga Ngebel. The population is then calculated using the formula in equation (1) with an error rate of 5%, resulting in a sample of 104 sellers. Sellers are considered as one of the sources of waste producers around Telaga Ngebel, with a total of 4.35 waste generated from 8 tons of waste in 2022.

There are six stages in implementing CVM, namely: 1) Forming a hypothetical market, 2) Determining the bid/auction size, 3) Calculating the average WTP, 4) Predicting the supply curve, 5) Summing the results, and 6) Evaluating the CVM calculation [37]. The calculation of CVM in this study was carried out through several stages, namely:

### Forming a Hypothetical Market

The market hypothesis is built by elaborating to sellers about the problem of waste and the disruption of ecological functions around the lake due to the high amount of waste. After describing the problem, then also described the benefits and importance of protecting the environment around the Telaga Ngebel.

### Determining The Bid/Auction Size

The amount in question is the Willingness To Pay (WTP) of the merchant's waste retribution. The assessment begins with a value of IDR 20,000 (USD 1,29), which is taken based on local government regulations regarding merchant levies. Furthermore, researchers will raise offers but are asked with the open question method.

### Calculating The Average WTP

It can be assumed the average value of Willingness to Pay (WTP) by calculating the total number of WTP values divided by the number of respondents calculated through the average WTP value as follows:

$$EWTP = \frac{\sum_{i=1}^n W_i}{n} \quad \dots(2)$$

Where:

EWTP = WTP Estimation of Waste Retribution

Wi = Exit WTP to i

N = number of respondents

i = I-th respondent willing to pay

### Summing Results

After estimating the average WTP value, the next step is to evaluate the total WTP value of the community using the formula that has been determined as follows:

$$TWTP = \sum_{i=1}^n WTP_i \left( \frac{n_i}{N} \right) P \quad \dots(3)$$

Where:

TWTP = Total WTP of sellers

WTPi = WTP individual sample-i

ni = number of the i-0

N = Total sample

P = Total population

i = with respondent willing to pay

### Ordinary Least Square Regression

The value of the seller's WTP against the Waste Management program Ecotourism through Waste Processing House is influenced by several factors. These factors were then analyzed using Ordinary Least Square (OLS) regression with the EVIEWS tool. The econometric equation used in OLS regression is as follows:

$$WTP = a + b_1U + b_2PT + b_3LNOutput + b_4JT + b_5JO + b_6Cont + b_7LU + e \quad \dots(4)$$

Where the unit used is thousand rupiahs, is the age of the stall vendor in units of years, is the length of education taken by sellers in units of years, is the number of expenses incurred by sellers for daily needs in a month in units of thousand rupiah, is the number of family members, is the operating hours of a business owned by a seller in a day, It is the seller's willingness to contribute to the program by using the Dummy Variable, dan is the length of business owned by the seller with units of years.

## RESULTS AND DISCUSSION

### Socioeconomic Characteristics

This study used cross-section primary data with the population of all sellers in the Telaga Ngebel area. Still, there was no definite data on the number of sellers, so the sample was taken from as many as 104 sellers based on respondents willing to be interviewed. The data was collected in 2023 using a random sampling technique through direct interviews. Data

was obtained from as many as 104 sellers around the Telaga Ngebel area with the following socioeconomic characteristics.

Table 1 shows that most sellers around Telaga Ngebel sell food and have been trading for more than ten years. The average seller is in the productive age, dominated by the age range of 40-47 years. Many of the sellers around Telaga Ngebel have a reasonably good level of environmental awareness. As many as 54 out of 104 sellers are willing to contribute to the Ecotourism Waste Management program through the Waste Processing House.

### Analysis Contingent Valuation Method

The level of awareness of the importance of waste management is also shown by sellers who are analyzed through the contingency valuation method, namely the willingness to pay for environmental services in the form of the WTP Ecotourism Waste Management

program through the Waste Processing House, which is as follows:

The willingness to pay merchants in the Telaga Ngebel area for the Ecotourism Waste Management program through the Waste Processing House is relatively high. Table 2 illustrates the average WTP value of IDR 38,500 (USD 2,48) per month, and the amount of WTP value fluctuates and varies. Fig. 7 shows that most sellers will pay a sustainable waste management retribution of IDR 30,000 (USD 1,94).

The WTP value of sellers exceeds the amount of retribution set by the government local IDR 10,000 (USD 0,64) for small and medium sellers. The number shows that sellers around Telaga Ngebel have a relatively high level of environmental awareness (Hanafi Ahmad, 2022).

### Regresi Ordinary Least Square

Several factors in this study affect the amount of WTP

Table 1: Socioeconomic Character of Respondents.

Socioeconomic Characteristics	Frequency	%	Socioeconomic Characteristics	Frequency	%
<b>Seller type</b>			<b>Education</b>		
Food seller	80	76,92	Elementary	45	43,27
Non-food seller	24	23,08	Junior High School	18	17,31
<b>Age</b>			Senior High School	30	28,85
16 – 23	8	7,7	Bachelor	10	9,61
24 – 31	15	14,42	> Bachelor	1	0,96
32 – 39	16	15,4	<b>Outcome</b>		
40 – 47	26	25	170.000 - 206.500	13	55,5
48 – 55	23	22,11	206.501 – 243.000	13	17,2
>55	16	15,38	243.001 – 279.501	40	22,2
<b>Contribution to waste management</b>			279.502 – 316.001	27	0,8
Contributed	54	51,94	316.002 – 352.302	7	2,6
Not Contributed	50	48,06	>352.302	4	
<b>Number of dependents</b>			<b>Operational Hour</b>		
1	24	23,08	6 - 7,14	20	19,23
2	44	43,31	7,15 - 8,29	22	21,15
3	23	22,11	8,30 - 9,44	3	2,88
4	13	12,50	9.15 - 10,29	18	17,31
<b>Years of Business</b>			10,30 - 11,44	4	3,85
10 - 13,9	30	28,85	11,15 - 12,29	23	22,11
14 - 17,9	46	44,23	>12,29	14	13,46
18 - 21,9	15	14,42			
22 - 25,9	5	4,81			
26 - 29,9	3	2,88			
30 - 33,9	2	1,92			
>33,9	3	2,88			



Table 2: Sellers' Willingness to Pay for Sustainable Waste Management Retribution in Telaga Ngebel.

WTP (IDR)	Frequency	WTP * Frequency (IDR)
20.000 (USD 1,29)	7	140.000 (USD 9,04)
22.000 (USD 1,42)	2	44.000 (USD 2,84)
23.000 (USD 1,49)	2	46.000 (USD 2,97)
24.000 (USD 1,55)	2	48.000 (USD 3,10)
25.000 (USD 1,61)	22	550.000 (USD 35,51)
27.000 (USD 1,74)	1	27.000 (USD 1,74)
28.000 (USD 1,81)	7	196.000 (USD 12,66)
30.000 (USD 1,94)	31	930.000 (USD 60,05)
32.000 (USD 2,07)	3	96.000 (USD 6,20)
35.000 (USD 2,26)	11	385.000 (USD 24,86)
40.000 (USD 2,58)	16	640.000 (USD 41,32)
Total		3.966.000 (USD 256,08)

value, namely age, length of education, monthly expenses, number of dependents, operating hours, direct contribution, and business size. These factors are analyzed using multiple linear regression with the following equation:

$$WTP = 8,65 + 0,02U - 0,002PT + 0,08LNOutput - 0,04JT + 0,009JO + 0,005Cont - 0,002LU + e \quad \dots(5)$$

The equation above indicates that several variables affect the size of the WTP value. The influence of variables can be predicted from the probability value. Suppose the probability value is less than 0.05. In that case, the variable affects the WTP value of sellers around Telaga Ngebel for the Ecotourism Waste Management program through the Waste Processing House (Mona et al. 2015). The probability values of each variable are shown in Table 3, namely:

The probability value of the independent variable seen in Table 3 shows that the variables of age, monthly expenses, number of dependents, operating hours, and length of business affect the WTP value of sellers around Telaga Ngebel against the Ecotourism Waste Management program through the Waste Processing House. These independent variables are factors that can affect the WTP value. The results of the equation above can be concluded that if the variables of age, length of education, expenses in a month,

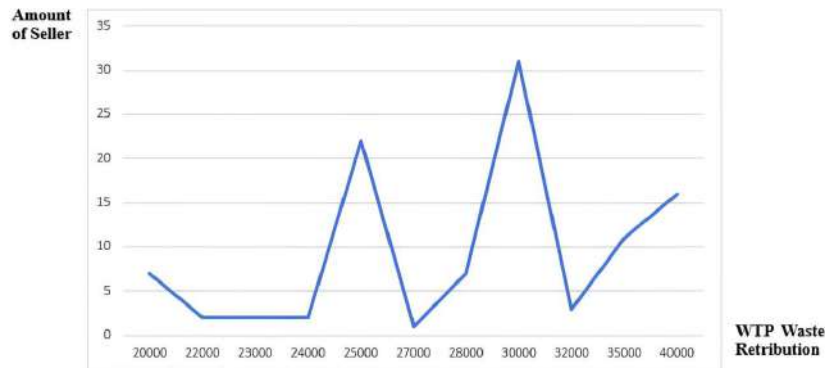


Fig. 7: Seller's WTP for waste management ecotourism program through waste processing house.

Table 3: Probability Value of Independent Variable.

Variable	Coefficient	Std. Error	t-statistic	Probability	Result
U	0,02	0.000643	26.80342	0,00	Significant
PT	-0,002	0.001967	-1.175192	0,24	Not Significant
LNOutput	0,08	0.034501	2.234851	0,03	Significant
JT	-0,04	0.007329	-5.327994	0,00	Significant
JO	0,009	0.002668	3.239527	0,002	Significant
Cont	0,005	0.012121	0.455423	0,64	Not Significant
LU	-0,002	0.000997	-2.000442	0,05	Significant

number of dependents, operating hours, contribution in managing waste, and size of business are zero, then the WTP value of sellers around Telaga Ngebel on sustainable waste management is 8.65%

The age variable is a variable that affects the WTP value. If the seller's age increases by one year, the WTP of sustainable waste management will increase by 0.02%. This follows Research conducted by Mona et al. (2015), which says that a person's maturity level based on age affects awareness of the importance of protecting the environment, one of which is sustainable waste management. The majority of sellers around Telaga Ngebel are aged 40 – 47 years. With this age range, the amount of WTP proposed is greater than other ages, ranging from Rp.30,000 (USD 1,94) – to Rp.40,000 (USD 2,58). This amount is greater than the waste retribution fee for sellers regulated in local regulations, which is Rp.10,000 (USD 0,64), so it can be concluded that sellers in that age range have a high level of actualization and environmental awareness.

The following influential variable is the expenditure variable, which shows that if expenditure increases by 1%, then WTP for sustainable waste management increases by 0.08%. The result follows Research conducted by Maria & Widayati (2020) and supported by Keynes's Consumption Theory that the higher the income, the higher the consumption or expenditure, including expenditure on environmental responsibility (Syukri et al. 2020). The majority of sellers have expenses of Rp.243,001 (USD 15,67) – Rp.279,501 (USD 18,02), but the more sellers spend, the more WTP value they are willing to pay. This is because these sellers produce more waste every day. This assumption is also supported by the high level of expenditure, which means that a person's income will also increase.

The variable that affects the amount of the third WTP is the number of dependents. The variable number of dependents has a probability value of less than 0.05. Still, it has a negative coefficient value, so the variable number of dependents significantly negatively affects the WTP of sellers around Telaga Ngebel on sustainable waste management. It can be explained that the higher the number of dependents, the more the WTP value will decrease by 0.04%. Many of the sellers have a total of 2 dependents, and the highest number of dependents is four dependents of 13 sellers. Sellers with a large number of dependents tend to be willing to pay a low retribution of less than Rp.25000 (USD 1,61), even though the amount is still higher than local regulations related to waste retribution fees.

The number of dependents is considered an expense, so the more dependents there are, the more expenditures will increase. This result follows Research conducted by

Jamaludin et al. (2022), the operating hour variable shows significant results. Every additional 1 hour of seller operation will increase WTP by 0.009%. The increase is a form of merchant responsibility because the longer the operating hours, the more waste is produced. The result states that sellers are aware to pay more for the waste retribution. The last influential variable is the length of effort variable. The majority of sellers with high operating hours are sellers who have restaurants that are 11-12 hours a day. These sellers have more frequent waste disposal intensity with a larger amount than sellers with operating hours of less than 11 hours a day. The majority of waste produced is in the form of organic waste, such as vegetable residues and fish bones.

The last influential variable is the length of effort variable. An increase in one year of seller-owned business will reduce the WTP value by 0.002%. Sellers with the longest business of more than 34 years with a total of 3 sellers. These sellers have a low WTP tendency because the majority of sellers with long businesses are at an unproductive age, so that which affects income and has an effect on the amount of WTP value.

Multiple linear regression analysis in this study also indicates that two variables do not affect the amount of WTP value: Length of education and Contribution of Sellers to the Ecotourism Waste Management program through the Waste Processing House. The length of education of sellers cannot be used as a benchmark in determining the amount of waste retribution WTP because the average seller has low education, which is only up to elementary school.

In addition, the contribution of sellers to the Ecotourism Waste Management program through the Waste Processing House also cannot be used as a benchmark because the majority of sellers have contributed to the program, so the data obtained on these variables has an uneven distribution rate.

The Ecotourism Waste Management program through the Waste Processing House requires costs and contributions in the form of energy and time. The WTP value of sellers towards the Ecotourism Waste Management program through the Waste Processing House can be determined as waste retribution allocated for the operational costs of waste management, and the results of waste management can be sold or reused to minimize waste pollution around the Telaga Ngebel area.

Through the Environmental Office, the government has also provided waste management facilities through transportation personnel and waste processing machines, as shown in Fig. 8, which can be used as a supporting tool for the Ecotourism Waste Management program through the Waste Processing House. Sellers in the region can also contribute to direct and sustainable management. Some



Fig. 8: Waste processing housem, Telaga Ngebel.

sellers have also implemented sustainable waste management independently through several ways, namely: efficient use of resources, joint use of assets owned, reprocessing of leftover goods/materials into products that have usefulness and selling value, and reuse of goods/materials that are still suitable for use.

## CONCLUSIONS

Research on ecotourism waste management on 104 sellers around the Telaga Ngebel area produced data that showed that the average willingness to pay merchants around the Telaga Ngebel area for sustainable waste management was IDR 38,500 (USD 2,49). The amount of WTP value is influenced by several factors, namely age, monthly expenses, number of dependents, operating hours, and length of business. This study has secondary data limitations, namely information about the sustainability of waste management that has been carried out and the exact number of sellers in the area around Telaga Ngebel.

The problem of waste produced by sellers around the Telaga Ngebel area can be overcome with several solutions. The determination of the monthly waste retribution fee of IDR 38,500 (USD 2,49) and the cost of retribution in the Telaga Ngebel area often change even though there are provisions from government regulations. Still, these provisions are only limited to the payment of merchant waste and do not cover tourist attractions, so the nominal retribution fee needs to be determined.

The second solution is to educate sellers about sustainable waste management. Education about it is related to the steps taken in the ecotourism waste management program through the waste processing house. Third, initiating sellers around the Telaga Ngebel area to separate organic and inorganic waste. Fourth, collaborate between sellers, tourism managers, and village communities to manage sustainable waste. This is shown by sellers' involvement with natural resources to manage waste. The fifth solution is to recycle waste generated through sustainable waste management programs. Namely, organic waste is processed into compost and fish feed, while inorganic waste is processed into handicrafts. Finally, selling processed waste products and the proceeds from these sales are used to increase merchant empowerment through revenue sharing and savings and loan products.

## ACKNOWLEDGEMENT

The author expresses gratitude to Universitas Sebelas Maret for the research funding provided. The author also extends. Thanks to the sellers who acted as respondents in this study and to the tourism organizers in Telaga Ngebel for their assistance in completing this Research.

## REFERENCES

- Achmad, F., Prambudia, Y. and Rumanti, A.A., 2023. Improving tourism industry performance through support system facilities and stakeholders: The role of environmental dynamism. *Sustainability (Switzerland)*, 15(5), pp.1-15. DOI

- Adamowicz, M., 2022. Green Deal, green growth and green economy as a means of support for attaining the Sustainable Development Goals. *Sustainability (Switzerland)*, 14(10), pp.1-12. DOI
- Amirudin, A., Inoue, C. and Grause, G., 2023. Rethinking waste management in Indonesia using public-private partnership framework: A case study of PET bottle waste management. *Journal of Environmental Sustainability*, 12(3), pp.45-58.
- Anggarini, D.T., 2021. Efforts to restore the tourism industry during the Covid-19 pandemic. *Jurnal Pariwisata*, 8(1), pp.22-31. DOI
- Atinkut, H.B., Yan, T., Zhang, F., Qin, S., Gai, H. and Liu, Q., 2020. Cognition of agriculture waste and payments for a circular agriculture model in Central China. *Scientific Reports*, 10(1), pp.1-15. DOI
- Bergmann, M., Almroth, B.C., Brander, S.M., Dey, T., Green, D.S., Gundogdu, S., Krieger, A., Wagner, M. and Walker, T.R., 2022. A global plastic treaty must cap production. *Science*, 376(6592), pp.469-470. DOI
- Cai, Y. and Ou, M., 2023. Experimental study on expansive soil improved by lignin and its derivatives. *Sustainability (Switzerland)*, 15(11), pp.1-18. DOI
- Costa, I.M. and FerreiraDias, M., 2020. Evolution on the solid urban waste management in Brazil: A portrait of the Northeast Region. *Energy Reports*, 6, pp.878-884. DOI
- Cowan, E., Setsaas, L. and Nørstebø, V.S., 2023a. End of life at the top of the world—stakeholder perspectives for plastics and circular transitions in the Arctic. *Journal of Environmental Studies and Sciences*, 13(4), pp.545-556. DOI
- Cowan, E., Tiller, R., Oftebro, T.L., Throne-Holst, M. and Normann, A.K., 2023b. Orchestration within plastics governance – From global to Arctic. *Marine Pollution Bulletin*, 197, pp.115635. DOI
- Djuwendah, E., Karyani, T., Wulandari, E. and Pradono, P., 2023. Community-based agro-ecotourism sustainability in West Java, Indonesia. *Sustainability*, 15(13), pp.10432. DOI
- Gasni, D. and Mulyadi, I.H., 2022. Effect of extracting method of coconut oils on tribological properties as a bio-based lubricant. *Journal of Applied Engineering Science*, 20(3), pp.831-840. DOI
- Hanafi Ahmad, A., 2022. The effect of tourist visits, tourist attractions, and tourism levies on regional original revenue. *Jurnal Sosial Ekonomi Bisnis*, 2(1), pp.50-61. DOI
- Hemali, N.A. and Alwis, A.A.P.De., 2022. Application of material flow analysis to municipal solid waste in urban areas in developing countries and possible solutions under circular economic framework. *Waste Management Journal*, 18(4), pp.320-335.
- Hilman, Z., Awfa, D., Fitriya, L. and Suryawan, I.W.K., 2023. Problematika sampah di sektor perjalanan dan pariwisata: Kajian literatur. *Jurnal Pariwisata*, 11(3), pp.896-903.
- Hung, C.L., Yu, T.F., Lin, Y.H., Lin, Y.C., Chen, Y.H. and Lo, W.S., 2023. Reflective and cooperative learning for understanding sustainability through an eco-innovation strategy in rural travel and hospitality: A STEAM case study. *Sustainability (Switzerland)*, 15(17). DOI
- Inayah, H. and Istiqomah, A., 2021. Nilai ekonomi sampah di kawasan wisata Pantai Tanjung Bira, Sulawesi Selatan. *Jurnal Ilmu Pengetahuan Indonesia*, 26(1), pp.159-166. DOI
- Jamaludin, H., Suliman, H., Elmaky, E. and Sulaiman, S., 2022. The future of food waste: Application of circular economy. *Energy Nexus*, 7(June), pp.100098. DOI
- Kumar, P., Malesios, C., Chowdhury, S., Saha, K., Budhwar, P. and De, D., 2022a. Adoption of circular economy practices in small and medium-sized enterprises: Evidence from Europe. *International Journal of Production Economics*, 248(March), pp.108496. DOI
- Kumar, P., Malesios, C., Chowdhury, S., Saha, K., Budhwar, P. and De, D., 2022b. Adoption of circular economy practices in small and medium-sized enterprises: Evidence from Europe. *International Journal of Production Economics*, 248(September), pp.108496. DOI
- Mamaco, A.W.A., Buncag, M.J.J., Magarin, R.A., Arreza, K.P., Rule, M.G.Q. and Calipusan, J.P., 2023. Diversity assessment and contingent valuation in Basak Lake of Saguayan, Lanao Del Sur, Philippines. *Environment and Ecology Research*, 11(6), pp.922-931. DOI
- Ledheng, L., Maria, E., Hano, Y., Fallo, Y.M. and Binsasi, R., 2022. Inovasi olahan tulang ikan menjadi kerupuk di kelompok nelayan Wini Kecamatan Insana Utara Kabupaten Timor Tengah Utara Provinsi NTT. *Jurnal Pengabdian Masyarakat*, 1, pp.42-49.
- Made, N., Kristina, R., Ketut, I.G., Pranata, I. and Ratnaningtyas, H., 2020. Pengelolaan timbulan sampah untuk menjaga citra industri pariwisata pada daya tarik wisata di Bali. *Jurnal Pariwisata Indonesia*, 25(3).
- Maes, T., Preston-Whyte, F., Lavelle, S., Gomiero, A., Booth, A.M., Belzunce-Segarra, M.J., Bellas, J., Brooks, S., Bakir, A., Devriese, L.I., Pham, C.K. and De Witte, B., 2023. A recipe for plastic: Expert insights on plastic additives in the marine environment. *Marine Pollution Bulletin*, 196(June), pp.115633. DOI
- Maria, N.S.B. and Widayati, T., 2020. Dampak perkembangan ekonomi digital terhadap perilaku pengguna media sosial dalam melakukan transaksi ekonomi. *Jurnal Konsep Bisnis dan Manajemen*, 6(2), pp.234-239. DOI
- Masjhoer, J.M., Syafrudin, S. and Maryono, M., 2022. Rural waste management system in the southern zone of Gunungkidul Regency. *Environmental Research, Engineering and Management*, 78(1), pp.70-82. DOI
- Mohamad Mulyadin, R., Ariawan, K. and Iqbal, M., 2018. Conflict of waste management in DKI Jakarta and its recommended solutions. *Jurnal Analisis Kebijakan Kehutanan*, 15(2), pp.179-191. DOI
- Mona, M., Kekenusa, J. and Prang, J., 2015. Penggunaan regresi linear berganda untuk menganalisis pendapatan petani kelapa. Studi kasus: petani kelapa di Desa Beo, Kecamatan Beo Kabupaten Talaud. *D'CARTESIAN*, 4(2), p.196. DOI
- Natsir, M.F., Iqan, M., Mukhtadir, A., Ibrahim, E., Daud, A., Yusbud, M., Rahmadani, S., Anwar, A., Asfar, M. and Khaer, A., 2024. Analysis of factors influencing community behavior in household waste management on Lakkang Island, Indonesia. *Environmental and Earth Research*, 12(3), pp.19-26. DOI
- Nisa, I.K., Prabaningtyas, S., Lukiaty, B., Saptawati, R.T. and Rodiansyah, A., 2021. The potential of amylase enzyme activity against bacteria isolated from several lakes in East Java, Indonesia. *Biodiversitas*, 22(1), pp.42-49. DOI
- Nwofoke, C., Onyenekwe, S.C. and Agbo, F.U., 2017. Willingness to pay (WTP) for improved environmental quality in Ebonyi State, Nigeria. *Journal of Environmental Protection*, 8(2), pp.131-140. DOI
- Plastic Atlas Asia, 2022. Japan's Plastic Waste Management—Challenges and Potential Solutions. *Institute for Global Environmental Strategies*. DOI
- Rahardjo, M., Gravitiani, E., Sasanti, I.A. and Maret, U.S., 2023. Toward sustainable tourism: insights for Mactor analysis in Ngebel Lake. *Sustainable Tourism Research*, 12(3), pp.396-407.
- Rahmattullah, R., Nilasari, G., Kustiawan, M.R., Kuswandani, M.D. and Galuh, U., 2023. Analysis of environmental pollution policies due to economic and technological factors. *Environmental Policy Journal*, 1(4), pp.186-192.
- Saija, M.E., Daniotti, S., Bosco, D. and Re, I., 2023. A choice experiment model for sustainable consumer goods: a systematic literature review and workflow design. *Sustainability (Switzerland)*, 15(17), p.13183. DOI
- Sekarningrum, A., 2016. The analysis of ecotourism principles on methods of waste disposal to minimize negative impacts in Baluran National Park. *Gadjah Mada Journal of Tourism Studies*, 3(2). DOI
- State, C.R., Eneyo, V.B., Attah, F.M., Antai, A.S., Adie, H.I. and Ochiche, C.A., 2022. Tourism viability status of Kwa Falls ecotourism site of Aningeje rural community. *Environmental and Earth Research*, 10(2), pp.125-132. DOI



- Syukri, A.U., Studi, P., Ekonomi, I. and Hasanuddin, U., 2020. Determinan pola konsumsi mahasiswa yang bekerja. *Economic Studies Journal*, 6(1), pp.1-11.
- Thorley, J., Garza-Reyes, J.A. and Anosike, A., 2019. The circular economy impact on waste management. *Waste Management Journal*, 231, pp.1-12. DOI
- Wicaksono, A., Ihalauw, J.J.O.I. and Damiasih, D., 2023. Anthropocene monument as an ecotourism destination in the Special Region of Yogyakarta, Indonesia. *Ecotourism Studies*, 5(1).
- Wubalem, A., Woldeamanuel, T. and Nigussie, Z., 2023. Economic valuation of Lake Tana: A recreational use value estimation through the travel cost method. *Economic Valuation Journal*, 1, pp.1-20.

# Potential Efficiency of Green Algae *Scenedesmus quadricauda* in Bioremediation of Polycyclic Aromatic Hydrocarbon, Benzo[a] Pyrene(BaP)

Hala R. Mohammed<sup>1</sup>, Jasim Mohammed Salman<sup>2</sup>† and Adi Jassim Abd Al-Rezzaq<sup>2</sup>

<sup>1</sup>College of Pharmacy, University of Babylon, Hilla, Iraq

<sup>2</sup>Department of Biology, College of Science, University of Babylon, Hilla, Iraq

†Corresponding author: Jasim Mohammed Salman; jasimsalman@uobabylon.edu.iq

**Abbreviation:** Nat. Env. & Poll. Technol.

**Website:** www.neptjournal.com

*Received:* 14-08-2024

*Revised:* 02-09-2024

*Accepted:* 12-09-2024

## Key Words:

Bioremediation  
*Scenedesmus quadricauda*  
 Benzo[a]pyrene  
 BG11 medium

## Citation for the Paper:

Mohammed, H. R., Salman, J. M. and Abd Al-Rezzaq, A. J., 2025. Potential efficiency of green algae *Scenedesmus quadricauda* in bioremediation of polycyclic aromatic hydrocarbon benzo[a]pyrene (BaP). *Nature Environment and Pollution Technology*, 24(2), p. D1712. <https://doi.org/10.46488/NEPT.2025.v24i02.D1712>

*Note: From year 2025, the journal uses Article ID instead of page numbers in citation of the published articles.*

## ABSTRACT

Using algae to break down or detoxify dangerous environmental pollutants, thereby changing them into a non-hazardous condition, is known as bioremediation. Investigating the ability of the green algae *Scenedesmus quadricauda* (Turpin) Brébisson to break a particular polycyclic aromatic hydrocarbon (PAH) known as Benzo[a]pyrene (BaP), Under regulated laboratory circumstances and on BG11 media, the alga was cultivated and exposed to different BaP dosages (0.5, 1, and 1.5 mM). High-performance liquid chromatography (HPLC) study helped to ascertain the BaP concentration. Involving the growth curve, doubling time, photosynthetic pigments, total protein, carbohydrates, and Lipid peroxidation (Malondialdehyde MDA) levels, the research investigated various physiological and biochemical aspects. Furthermore, measured were the levels of catalase (CAT), superoxide dismutase (SOD), and reactive oxygen species (ROS). Whereas the lowest growth rate was 0.00047 on the 15th day at a concentration of 1.5 mM, the maximum growth rate (k) recorded was 0.391 on the 7th day at a concentration of 0.5 mM. Doubling time also varied from 0.00014 throughout the 15th day with 1.5 mM and from 0.1179 throughout the 7th day with 0.5 mM BaP. The results showed a definite influence of the different quantities of BaP degradation by *S. quadricauda*; the greatest magnitude was 40.13 throughout the 15th with 0.5 mg.L<sup>-1</sup>, while the lowest magnitude was 0 throughout the 1st day with 0.5 Mm. While the min magnitude was 0.41 µg.mL<sup>-1</sup> in 0.5 mM throughout 1st day, the max magnitude of chlorophyll-a was 18.71 (µg.mL<sup>-1</sup>) in 1.5 mM throughout the 15th day. Whereas the greatest magnitude was 9.19 µg.mL<sup>-1</sup> in 1.5 mM throughout the 15th day, the lowest magnitude of chlorophyll b was 0.36 µg.mL<sup>-1</sup> in 1.5 mM throughout the 1st day. While the min was 0.013 on 1st day with 1 mM, the max magnitude of ROS was 0.28 until the 15th day with 1.5 mM. With 1 mM over 1st day, the carbohydrate showed a max magnitude of 35.13 µm.mL<sup>-1</sup>, and with 1.5 mM over the 15th day, the min magnitude was 12.25(µm.mL<sup>-1</sup>). While the min protein content was 1.83 µg.mL<sup>-1</sup> in 1.5 Mm throughout the 8th day, the max protein content was 2.14 µg.mL<sup>-1</sup> in 1 mM throughout the 8th day; moreover, SOD fluctuated between 22.22 µg.mL<sup>-1</sup> in 0.5 mM throughout 1st day, and 60 µg.mL<sup>-1</sup> in as the min magnitude throughout 8th day with 1.5 mM. The results show that magnitudes of CAT fluctuated between 13.33 µg.mL<sup>-1</sup> in the 8th and 15th mM throughout the 15th day and 73.33 µg.mL<sup>-1</sup> in 1 mM throughout the 15th day. MDA showed the largest magnitude 59.92 µmoL.L<sup>-1</sup> in 1.5 mM over the 1st day, while the lowest magnitude, 36.58 µmoL.L in 1 mM over the 15th day.

## INTRODUCTION

In many environmental media, bioremediation is the use of biological systems to either eradicate or reduce pollution (Luka et al. 2018). Studies have shown that it is a safe, effective, cheap, environmentally friendly replacement for sustained remedial action against hazardous and recurring pollutants (Shukla et al. 2010, Singh 2006). Unwanted effects of pollution and environmental harm follow naturally from the advancement in industry and technology. The main cause of the environmental effects connected with industrial activity is the development of industrial waste.



**Copyright:** © 2025 by the authors

**Licensee:** Technoscience Publications

This article is an open access article distributed under the terms and conditions of the Creative Commons Attribution (CC BY) license (<https://creativecommons.org/licenses/by/4.0/>).

Because of problems with conventional approaches to pollution control (Nandal et al. 2015). Reducing pollutants and sources of pollution in water is of utmost importance given the severe scarcity of freshwater worldwide, and ensuring that these treatments are economical and environmentally friendly makes them a suitable option compared to traditional alternatives such as chemical precipitation and ion exchange. These alternatives are used to produce waste that is difficult to dispose of (Tewari et al. 2023). Many sophisticated operations integrating biological, physical, and chemical technologies were developed and used recently to clean polluted regions. In this regard, biological therapy—which uses microorganisms like bacteria, fungi, and algae to break down pollutants such as hydrocarbons and convert them into ecologically friendly compounds—is very promising (Amran et al. 2022). Bioremediation is the process of breaking down organic contaminants into water and carbon dioxide or turning organic pollutants into non-toxic metabolites (Alexander 1999). Often used for the removal of different aquatic pollutants, microalgae are also very important in bioremediation (Hwang et al. 2016). Specifically employed for the conversion and breakdown of polycyclic aromatic compounds (PAHs) and removal from the environment, green algae, As shown by García de Llasera et al. (2016), were used to break down enduring toxins like *Scenedesmus* sp.

Organic substances with carbon and hydrogen atoms bound together in a chemical structure called polycyclic aromatic hydrocarbons (PAHs). One may say of them as benzene rings joined in different configurations without any extra atoms or substituents present (Lawal, 2017). Though there are more than 100 kinds of PAHs, the United States Environmental Protection Agency (US EPA) has ranked 16 polycyclic aromatic hydrocarbons (PAHs) based on their unique characteristics as top priority (Keith 2015). Based on their ring count, the molecules listed might be classified as high molecular weight, medium molecular weight, or low molecular weight compounds (Alegbeleye et al. 2017, Pandya & Kumar 2021). Each of the low molecular weight compounds (LMWC), fluoranthene [Fla], phenanthrene [Phen], anthracene [Ant], fluorene [Flu], acenaphthene [Acp], acenaphthylene [Acpy], and naphthalene [Nap], has 2–3 rings.

Benzo[a]pyrene (BaP) is a major polycyclic aromatic hydrocarbon (PAH) with a high molecular weight. Comprising a polycyclic aromatic hydrocarbon with a chemical formula  $C_{20}H_{12}$  and a molecular weight of  $252.3 \text{ g.mol}^{-1}$ , BaP develops as a side effect of incomplete combustion at temperatures between 300 and 600 degrees centigrade. At 25 degrees centigrade, BaP has a density of  $1.24 \text{ g.cm}^{-3}$ , a melting point of 179 degrees centigrade, and a boiling point of 495 degrees centigrade (Liu et al. 2019).

Mostly produced by industrial activities, Benzo[a]pyrene (BaP) results from industries releasing smoke and incomplete combustion of fossil fuels. It also results from household activities such as cooking and smoking (Sinha et al. 2005, Sun et al. 2013). Both the United States Environmental Protection Agency (EPA) and the International Agency for Research on Cancer (IARC) have labeled it as a Set 1 carcinogen. It is also a major contaminant in soil, air, and water (Bhatt et al. 2018). In the environment, BaP may undergo chemical degradation, photolysis, volatilization, and adsorption. Still, microbial degradation is mostly responsible for its loss (Haritash & Kaushik 2009).

Furthermore, affecting all kinds of biological life, it shows the process of accumulation in the food chain (Haritash & Kaushik 2009, Okpishi et al. 2017). Petroleum pollutants are easy to form mucous membranes on the surface of plant roots, obstructing plant root respiration and nutrient absorption and even causing root rot and plant death in severe cases (Yang et al. 2024). The current investigation aimed to explore the ability of green algae *S. quadricauda* in the bioremediation of various Benzo[a]pyrene amounts from contaminated media and used some physiological and biochemical parameters as tools for the bioremediation process.

## MATERIALS AND METHODS

### Algal Strain

Chlorophyceae species *Scenedesmus quadricauda* originally from the Algae Culture Collection (UTEX) at the University of Texas in Austin, Texas, USA. *S. quadricauda* was cultivated under controlled circumstances with a light intensity of  $286 \mu\text{E.m}^{-2}.\text{s}^{-1}$ , a light/dark cycle of 16:8 hours, and a temperature of  $25 \pm 2$  degree centigrade (Chia et al. 2013), to prevent grouping and hasten their rate of expansion, the civilizations were also gently moved by hand every day (Selvan et al. 2013).

### Preparation of Algal Culture Media

The improvement of chlorophyta (Patel et al. 2015) has come from the BG-11 medium. Autoclave the BG-11 medium at 121 degrees Celsius for 15 minutes to sterilize it. After freezing to try to prevent too strong precipitation, using a pH meter revealed that the pH of the medium changed to around 7.4 using 1N NaOH and 1N HCl solutions. As Gour et al. (2014) report, a 10 mL algal culture is placed in a flask holding 100 mL of BG11 medium and allowed to flourish for 15 days. Following that, this culture is placed in 1000 mL of media and allowed to incubate for two weeks minimum before beginning the experiment, therefore ensuring continuous lab conditions. Photoperiod greatly affects cell

division in asexual reproduction. Constant illumination accentuates this division that occurs all of the light time (Salman et al. 2023). Therefore, the period of light exposure may vary based on the objectives of the farming: a light-dark cycle mirroring the natural solar cycle favors regular and vigorous growth, while continuous lighting stimulates fast development (Sánchez-Bayo et al. 2020, Allen 2003).

## Experimental Design

*S. quadricauda*'s culture medium was exposed to different benzo (a) pyrene (0.5, 1, and 1.5) mM dosages for 15 days. The research primarily aims to track daily variations in algae during fifteen days. To determine the time to doubling (G) and the rate of growth (k), the algae are incubated. On the first, eighth, and fifteenth days assessments also include chlorophyll a and b, total protein, and many enzymatic responses, including reactive oxygen species (ROS), lipid peroxidation MDA, superoxide dismutase (SOD), and catalase (CAT).

## Determination of Growth Rate and Doubling Time

Every day, the cell count of green algae *S. quadricauda* is determined using a UV-Vis spectrophotometer. This is accomplished by measuring the optical density (OD) at 685 nm, therefore enabling the cell density in cells per milliliter. This measurement clarifies many development stages, lets us estimate the biomass size, and ascertain growth rates. Especially, the formula of Richmond (2004) helps one find the doubling time and growth rate during the exponential development phase.

$$K = 3.322 \times (\log OD_t - \log OD_0)/t$$

$$G = 0.301/K$$

K: growth rate, G: doubling time, t: time

OD<sub>0</sub>: optical density at the experiment beginning (zero time).

OD<sub>t</sub>: optical density after (t) day.

## Estimation of Chlorophyll

A technique detailed in Ref. (Juneja et al. 2013) was used to measure the total chlorophyll concentration. A 2 mL sample was taken and then subjected to a centrifugal force of 12,500 revolutions per minute for five minutes. The solid residue left behind from the algae was then mixed with 2 mL of methanol (90%). After an incubation period of twenty hours in a dark atmosphere at a temperature of twenty degrees, the sample was submerged in a water bath at a temperature of 64°C for five minutes. At last, the material was discarded after five minutes of centrifugation at 12,500 rpm. Spectrophotometry at three separate wavelengths— 470 nm, 652 nm, and 665 nm—quantified the filtrate.

The chlorophyll content was determined by the following Equations (1) – (2) (Lin et al. 2013):

$$\text{Chlorophyll a (mg.L}^{-1}\text{)} = (12.7 \times A_{663}) - (2.698 \times A_{645}) \dots(1)$$

$$\text{Chlorophyll b (mg.L}^{-1}\text{)} = (22.9 \times A_{645}) - (4.68 \times A_{663}) \dots(2)$$

## Estimation of Reactive Oxygen Species (ROS)

Taking a 2 mL specimen, the estimate technique entails two times washing it under a Phosphate-buffer solution. The resultant precipitate-which comprises algal cells-is then combined with two milliliters of perchloric acid (200 micromol). For three minutes, the cells break down under sonication with pauses every twenty seconds. The specimen is then rapidly thrown by half an hour of spinning it at 10,000 r.m<sup>-1</sup>. The volume is set at 5 mL after the filtrate is mixed using a micropipette. One 1.5 mL extract is then gathered and combined with 0.1 mL working solution. The working solution consists of 0.28 mL of sulfuric acid, 19.6 mg of ammonium ferrous sulfite, 14.3 mg of xylenol, and 3.64 g of sorbitol. The sample is kept for half an h at 30 degrees Celsius under incubation (Salman et al. 2023). The sample is next evaluated at 560 nm, and the equation helps one to ascertain the quantity of ROS:

$$\% \text{inhibition ROS} = \Delta \text{uninhibited} / \text{Min}(10)$$

## Antioxidant Enzymes

The process consisted of discarding 2 mL of the specimen at a speed of 4000 – 6000 r.m<sup>-1</sup>. After washing the resultant algal precipitate in a buffer solution at pH 7, the discarding process was repeated. The volume was then changed back to 2 mL. The algae cells were then disturbed for three minutes using an ultrasonic gadget called Sonication. Every 20 seconds the model pauses, then is thrown at 10,000 rpm for 30 min. The resultant filtrate is then mixed in small quantities, and the volume is changed to 5 mL (Bradford 1976).

## Estimation of Carbohydrates

Following a phosphate-buffer solution wash and sonication-assisted breakdown, a 2 mL sample of the material was removed and aerobically dried. Then, using distilled water, the resultant solution was diluted to a final volume of 5 mL. 1 mL sample of the substance was then mixed with 1 milliliter of phenol (5%) and five milliliters of sulfuric acid (96%); the mixture was then swirled for ten minutes nonstop. The sample then spent thirty minutes submerged in a water bath set at 30-35°C. After that, it was evaluated at 490 nm and matched the known glucose standard curve produced by dissolving 100 mg of glucose in 100 mL of distilled water (Herbert 1971).



### Estimation of Total Protein

Several methods—including centrifugation, dialysis, chromatography, precipitation, and ultrafiltration—have been used to separate and concentrate microalgal proteins (Salman et al. 2023). Based on the updated method by Ermis et al. (2020) based on the original procedure by Lowry et al. (1951), the total protein content was determined. The operation included mixing 2 mL of Biuret solution with 0.5 mL of the already produced extract (2–4). The liquid was then thoroughly stirred for thirty minutes using a preheater set to 30 degrees centigrade. The sample was then evaluated at 555 nm and matched with the reference solution depending on the Bovine Serum Albumin Protein level ranging from 0 to 0.1 mL. Dissolving 0.1 g of Bovine Serum Albumin in 100 mL of buffer solution produced a quantity of 100  $\mu\text{g.L}^{-1}$ , the reference solution.

### Estimation of Superoxide dismutase (SOD)

The estimate calls for mixing two milliliters of Tris buffer with one hundred microliters of the extract (2–4). The first reading ( $\Delta A_0$ ) is then obtained by measuring the absorbance at 420 nm after five minutes. After adding 0.2 mL of Pyrogallol solution, the absorbance is once more measured at 420 nm following five minutes to get the second reading ( $\Delta A_1$ ).  $\Delta A_1$  is computed utilizing the formula by Zhao (2017) at hand.

SOD activity ( $\mu\text{mL}$ ) =  $[(\Delta A_0 - \Delta A_1 / \Delta A_0) / 50\%] \times \text{Volume of sample}$

### Estimation of Catalase (CAT)

The estimate calls for blending one milliliter of hydrogen peroxide with one hundred microliter of the extract (2–4). The combination is then ascertained at 240 nm of wavelength. Ten minutes later, the measurement is taken once again after hydrogen peroxide addition. Apply Frary et al. (2010) formula to get the catalyst's quantity.

$\text{CAT} = [(\Delta \text{Abs}_{240} / \text{Min}_{10}) \times (\text{Reaction volume}_{100})] / 0.001$

### Lipid Peroxidation (Malondialdehyde MDA)

The quantification of lipid peroxidation was conducted using the Thiobarbituric acid method to measure the quantity of Malondialdehyde (MDA), as described by Aust (1985) and Burtis and Ashwood (1999). 100  $\mu\text{L}$  specimens were combined with 1000  $\mu\text{L}$  of TCA (20%) and 1000  $\mu\text{L}$  of TBA (0.6%). Tubes are agitated by vortexing. The sample was heated in a water bath at a temp of 100 degrees centigrade for 15 min. Afterward, it was allowed to drop down to room temp. The sample was then subjected to centrifugation at a speed of 4000 revolutions per minute

(4 degrees centigrade) for 15 min. Finally, the absorbance of the sample was measured at a wavelength of 532 nm, using a blank as a reference. The findings were quantified in terms of millimoles per milligram of protein ( $\text{mmol.L}^{-1} \text{mg}^{-1} \text{protein}$ ).

Amount of Malondialdehyde (MDA) = Absorbance at 532nm/E  $\times$  b

Where,

E = Extinction coefficient (153mmol/cm),

b = light bath (1cm)

### Estimation of Benzo[a]Pyrene

Briefly, after a 7-day incubation period, the cultures were filtered, and the B(a)P compound was extracted from the specimens using an ultrasonic bath using a solvent combination of acetonitrile and dichloromethane (at a ratio of 3:1 v/v). A Dionex UltiMate 3000 system and a fluorescence detector were used in high-performance liquid chromatography (HPLC) to determine the B(a)P amount. Benzo(a)pyrene set the excitation wavelength ( $\lambda_{\text{ex}}\%$ ) at 250 nm and the emission wavelength ( $\lambda_{\text{em}}\%$ ) at 400 nm. Chromatography with a gradient under the use of a mobile phase comprising a combination of water and acetonitrile was the separation method used. Thermo Scientific HYPERSIL GOLD C18 PAH column with dimensions of 250 x 4.6 mm and particle size of 5  $\mu\text{m}$  was the chromatographic column utilized. Made by Merc, the solvents used in the tests were of high-performance liquid chromatography (HPLC) grade. Calibrating curves with magnitudes ranging from 0.1 to 10  $\text{ng.cm}^{-3}$  were generated using the Sigma-Aldrich benzo(a) pyrene standard at 1000  $\mu\text{g.mL}^{-1}$ . The standard solvent used in the construction of the calibration curves was methanol. The method demonstrated a linearity higher than 0.999%. Still, the coefficient of variance revealed a level of accuracy below 15%. With a signal-to-noise proportion of 10 for a specimen with a very low amount of B(a)P, approaching the detection limit, the limit of quantification (LoQ) for the method was found. Measuring the LoQ magnitude, we found 0.01  $\text{ng.cm}^{-3}$ . The correlation between the recovery rate and the reference material (SRM2585) was 83%. Once used to find B(a)P in the atmosphere, this approach Nine strains in all were exposed to various dosages of B(a)P (7.8, 15, 78, 312, and 624  $\text{ng.L}^{-1}$ ) and temperatures (10, 15, 20, 25, and 30 degree centigrade) in Wiśniewska et al. (2023). The experiment also included blank specimens.

### Statistical Analysis

For every treatment, the experimental data in this work came from a minimum of three replicas. SPSS version 26 was used for statistical investigation. The data were expressed

as mean and standard deviation. The relevance of variances was evaluated using an analysis of variance (ANOVA). If the related p-magnitudes were less than 0.05, variations were judged noteworthy.

## RESULTS AND DISCUSSION

### Growth Rate and Doubling Time

Several studies have demonstrated the effect of exposure to PAHs on algal growth rate and doubling time. This study showed that different amounts of benzo[a]pyrene inhibited the growth rate while increasing the doubling time to a long period slowed cell division. There is a significant variance ( $p \leq 0.05$ ) between the various treatments of Benzo[a]pyrene (0.5, 1, 1.5) mM, the present study demonstrates, the maximum growth rate (k) at the amount of (0.5) mM was 0.391 throughout 7<sup>th</sup> day, while the minimum growth rate was 0.00047 at the amount (1.5) mM throughout 15<sup>th</sup> day. The shorter doubling time (G) was 0.00014 during 15<sup>th</sup> day with (1.5)mM, while the longest value 0.1179 during 7<sup>th</sup> day with (0.5) mM benzo (a) pyrene (Fig. 1,2). The inhibitory impact of toxicity could be attributed to the extremely lipophilic characteristics of Benzo[a]pyrene, which enables it to easily

enter cells via the plasma membrane and rapidly incorporate into all biological lipoprotein membranes (Miller & Ramos 2001). It induces alterations in the permeability and structure of membranes and disrupts crucial metabolic activities, such as photosynthesis, respiration, and transmembrane transport (Sikkema et al. 1994, Tripuranthakam et al. 1999, Aksmann & Tukaj 2004). Calow & Sibly (1990) proposed that various forms of toxic stress cause metabolic alterations in organisms, depleting their energy reserves and negatively impacting their growth and biochemical composition. This finding was reported by Echeveste et al. (2010), who noted a reduction in algae growth when exposed to high amounts of PAHs.

### Algal Pigments

In the study, benzo[a]pyrene treatments at various concentrations led to a reduction in chlorophyll a and b in *S. quadricauda*. The results show chlorophyll a in cell *S. quadricauda* treatment with different concentrations of Benzo[a]pyrene decreased to  $0.41 \pm (\mu\text{g} \cdot \text{mL}^{-1})$  in 0.5 mM during 1st day, while the high value was  $18.71 \pm (\mu\text{g} \cdot \text{mL}^{-1})$  in 1.5 mM during 15<sup>th</sup> day, The results show chlorophyll b decrease to  $0.36 \pm (\mu\text{g} \cdot \text{mL}^{-1})$  in 1.5 mM during 1st day, while

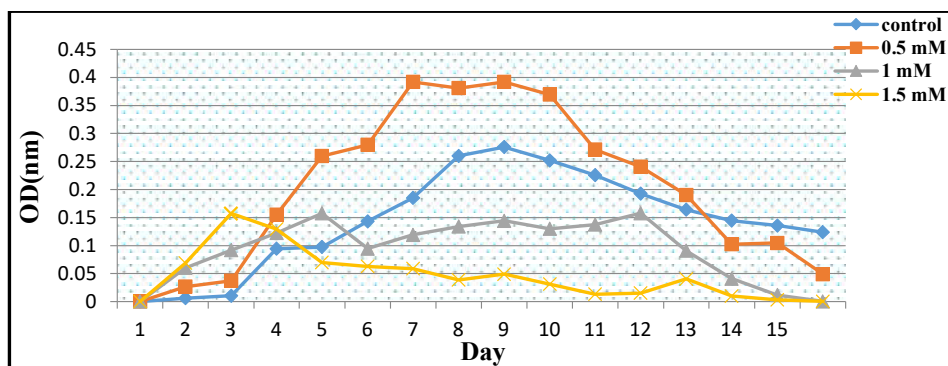


Fig. 1: Growth rate of *S. quadricauda* at concentration of benzo (a) pyrene.

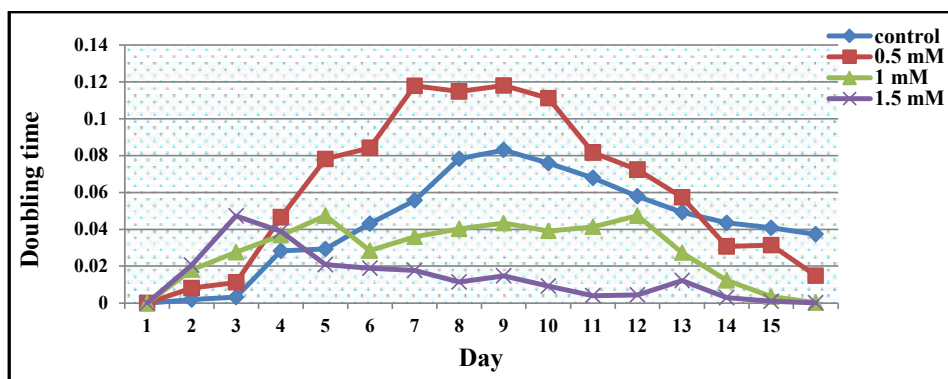


Fig. 2: Doubling time of *S. quadricauda* at various concentrations of benzo (a) pyrene.

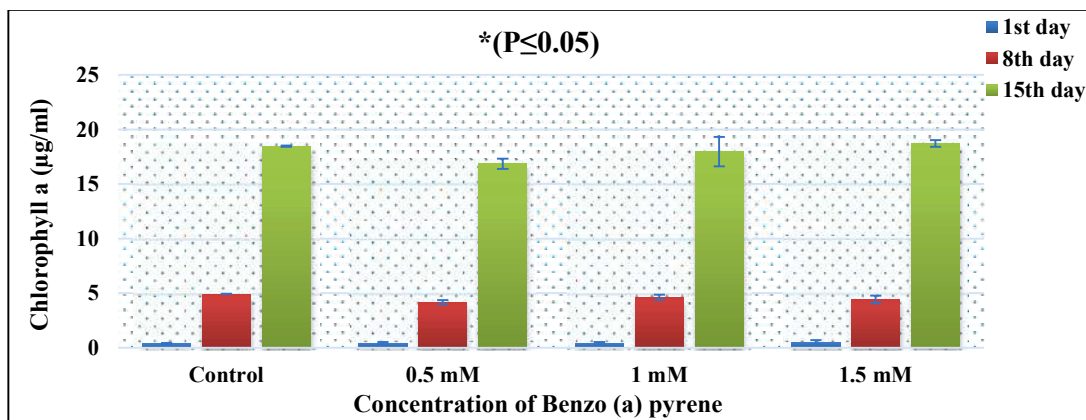


Fig. 3: Chlorophyll an amount of *S. quadricauda* at various concentrations of Benzo[a]pyrene .

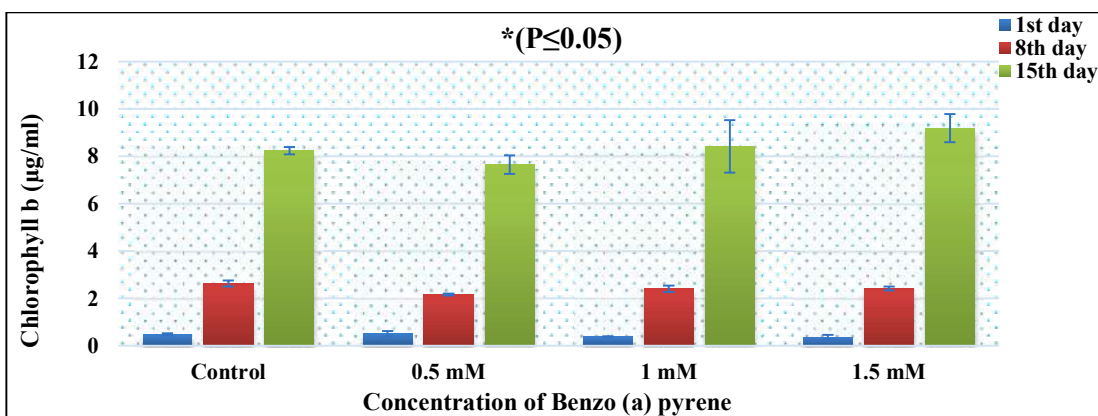


Fig. 4: Chlorophyll b amount of *S. quadricauda* at various concentrations of Benzo [a] pyrene.

the high value was  $9.19 \pm (\mu\text{g} \cdot \text{mL}^{-1})$  in 1.5 mM during 15<sup>th</sup> day compared to control (Fig. 3,4) The synthesis of pigments may be inhibited by the lipophilic nature of aromatic hydrocarbons, which can alter the permeability and fluidity of the cell membrane. This alteration could disrupt the lipid bilayer and reduce energy transduction, affecting the activity of membrane-associated proteins (Heipieper et al. 1995). Mohapatra & Schiewer (2000) suggested that the interaction of toxicants with the membrane and dispersion of lipoprotein membranes are responsible for changes in behavior and pigment content in *Synechocystis*. Mostafa & Helling (2002) proposed that the decrease in chlorophyll, carotenoid, and phycobiliprotein contents might be a result of direct inhibition of pigment synthesis by the organic compound or accelerated degradation of pigments since increased reactive oxygen species (ROS) and degradation of the thylakoid membrane by polycyclic aromatic hydrocarbons (PAHs).

### Reactive Oxygen Species (ROS)

Benzo [a] pyrene-induced oxidative stress for cell algae in

treated cultures, leading high amount of ROS. where the highest value of ROS is 0.028 % throughout the 15th day with 1.5 mM of Benzo[a]pyrene compared to the control (Fig. 5). A notable disparity was observed between the treatments and control culture. The hydrophobic feature of Benzo[a]pyrene leads to the overproduction of ROS, which in turn causes alterations in the structure of biomembranes, resulting in an elevated permeability (Sikkema et al. 1994, Solomon 2000). As a result, significant disruptions in the electron transport chains and/or the process of phosphorylation uncoupling may occur (Aksmann & Tukaj 2008, Aksmann et al. 2011). An abundance of intracellular ROS can result in the oxidation of macromolecules, such as lipids, proteins, and DNA bases (Meewes et al. 2001). This oxidative process can lead to damage in cell membranes, mitochondria, and chloroplasts, ultimately inhibiting photosynthesis, physiological activities, and cell growth. In response to the assault of ROS, cells have created enzyme systems that act as antioxidant defense mechanisms to eliminate ROS (Takáčová et al. 2014).

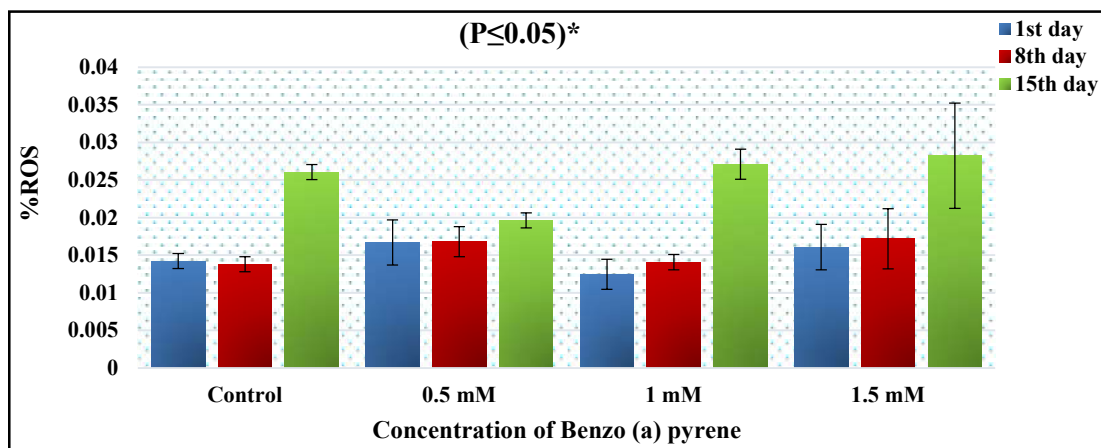


Fig. 5: ROS amount of *S. quadricauda* at various concentrations of Benzo[a]pyrene.

### Carbohydrate

Carbohydrate is synthesized by photosynthetic organisms like algae and are necessary to obtain energy. All Environmental toxicants have effects on the content of carbohydrates in algae by reducing carbohydrate synthesis; perhaps stress also increases respiration, which then uses up the carbohydrates that were synthesized previously (Mustafa 2013). The carbohydrate amount of  $12.25 \mu\text{m.mL}^{-1}$  is recorded at 1.5 mM on the 15th day. The amount of Benzo[a]pyrene is  $15.52 \mu\text{m.mL}^{-1}$  and  $16.30 \mu\text{m.mL}^{-1}$  for 0.5 mM and 1 mM, respectively. The greatest amount of  $35.13 \mu\text{m.mL}^{-1}$  is seen on the 1st day with 1 mM (Fig. 6). Both Nagajyoti et al. (2009) and Abdul Razak (1985) demonstrated that the decrease in carbs may be attributed to the suppression of Ribulose Biphosphate carboxylase (RUBP) activity, leading to a fall in carbohydrate levels. RUBP carboxylase is the predominant enzyme in photosynthesis and plays a crucial role in assimilating carbohydrates and regulating carbohydrate metabolism. It is involved in important

metabolic processes, including fixation of carbon and glycolysis (Barsanti & Gualtieri 2006). The toxicant can hinder the process of glucose oxidation metabolism, which is necessary for obtaining ATP and reducing metabolic activity inside the cell (Greenhaff et al. 2004). From the findings of this study, the treatment of *S. quadricauda* with various Benzo[a]pyrene concentrations caused a significant decrease in total carbohydrate content with increasing concentrations of Benzo [a] pyrene.

### Total Protein

Benzo[a]pyrene stress has an effect on the content of proteins in all treatments, and it causes a decrease in total protein with increasing amounts of Benzo [a] pyrene. The max protein content of  $2.14 \mu\text{g.mL}^{-1}$  throughout the 8th day is recorded at 1mM, while the min protein content of  $1.83 \text{ mM}$  is recorded at 1.5 mM amount throughout the 8th day (Fig. 7). The reduction in protein synthesis can be attributed to the inhibition of enzymes and structural proteins necessary

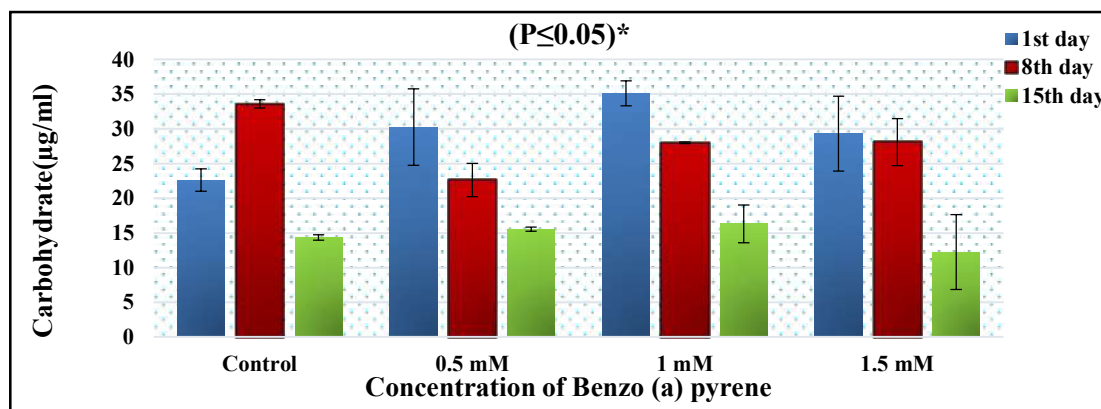


Fig. 6: carbohydrate amount of *S. quadricauda* at various concentrations of Benzo [a] pyrene.



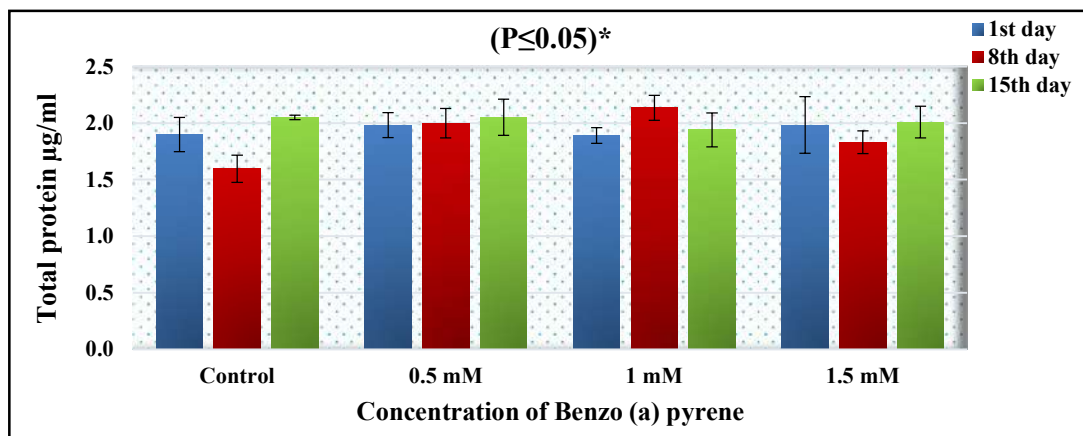


Fig. 7: Total protein amount of *S. quadricauda* at various concentrations of Benzo [a] pyrene.

for the organism's growth (Kapoor & Arora 1996). Additionally, Carfagna et al. (2013) suggest that the decrease in protein content may also be caused by a shortage of carbon skeleton resulting from a low photosynthetic rate. Sub-lethal doses of PAHs may disrupt cell division by inhibiting DNA synthesis, lowering the proportion of cells entering mitosis, and subsequently limiting population expansion and protein production (Carfagna et al. 2013, Chia et al. 2015).

### Superoxide Dismutase (SOD)

In the present study, it can be observed clear effect of various Benzo[a]pyrene amount in the activity of the enzyme (SOD) in alga *S. quadricauda* indicate a significant variance ( $p \leq 0.05$ ) between the treatments and control. There was increasing in content SOD at Benzo[a]pyrene 60 µg.mL<sup>-1</sup> in the amount of 1.5 mM throughout the 8th day, compared with control (26.66 µg.mL<sup>-1</sup>), where the lowest magnitude at (0.5 mM) was 22.22 µg.mL<sup>-1</sup> throughout 1st day (Fig. 8). When the quantity of reactive oxygen species (ROS) in microalgal cells becomes very high, the cells'

capacity to eliminate ROS by creating sufficient amounts of oxidative response kinases, such as SOD, is compromised. Prior research by Papadimitriou and Loumbourdis (2002) indicated that some species may counteract oxidative stress by boosting the synthesis of SOD to remove excess ROS. SOD is a crucial defensive mechanism that regulates the levels of free radicals. It is recognized as the primary defense against ROS in live cells. The elevated level of SOD activity leads to the increased breakdown of harmful ROS, such as the superoxide radical ( $O_2^-$ ), into a less toxic ROS, such as hydrogen peroxide ( $H_2O_2$ ). This hydrogen peroxide may then be further reduced by the heightened activity of glutathione reductase (GR), as seen in the study by Samanta et al. (2019). However, the decreased functioning of SOD in the presence of high amounts of PAHs is probably due to the excessive accumulation of  $H_2O_2$  (Binark et al. 2000).

### Catalase (CAT)

In the current research, it can be observed clear effect of various Benzo[a]pyrene amount in the activity of the enzyme

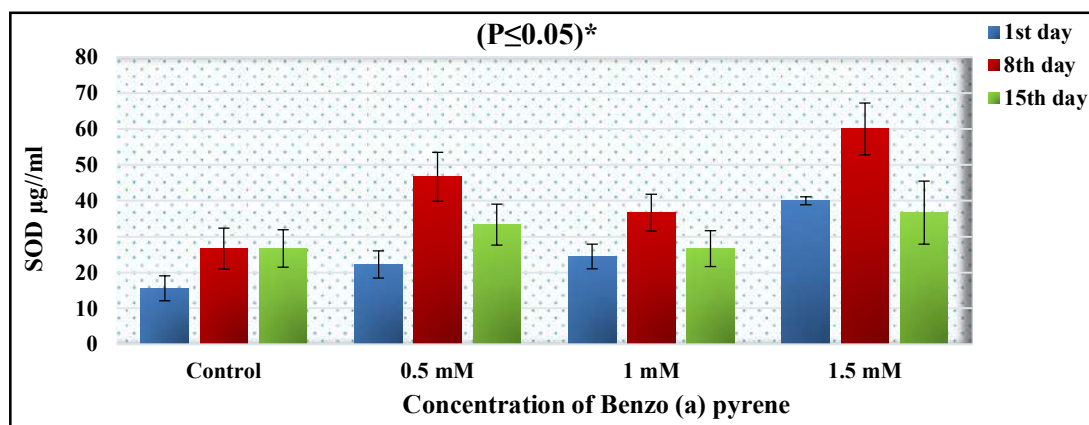


Fig. 8: SOD amount of *S. quadricauda* at various concentrations of Benzo [a] pyrene.

(CAT) in alga *S. quadricauda* and indicate the significant variance ( $p \leq 0.05$ ) between the control and treatments. There was increasing in the content of catalase at Benzo[a] pyrene  $73.33 \mu\text{g.mL}^{-1}$  in concentration 1 mM during the 15th day, compared with the control ( $10 \mu\text{g.mL}^{-1}$ ). Where the lowest magnitude at (1 mM) was  $13.33 \mu\text{g.mL}^{-1}$  throughout the 8th and 15th day (Fig. 9). Like other living creatures, algae create several ROS as a result of oxidative metabolism, such as  $\text{H}_2\text{O}_2$ , which may be harmful at high quantities (Torres et al. 2010). The formation of these ROS is sluggish under typical circumstances. Nevertheless, contamination, especially PAHs, enhances their creation (Binark et al. 2000, Torres et al. 2010). CAT is an important antioxidant enzyme that plays a crucial role in regulating the redox state inside cells. Its primary function is to protect cells from damage caused by peroxidation. This has been demonstrated in studies conducted by Cheng et al. (2016) and Hassan et al. (2017, 2018). The enzyme catalase (CAT) may mitigate the harmful effects of hydrogen peroxide ( $\text{H}_2\text{O}_2$ ) by facilitating its transformation into water ( $\text{H}_2\text{O}$ ) (Torres et al. 2010). The

excessive generation of ROS may diminish the functioning of CAT, leading to oxidative stress (El Maghraby & Hassan 2021).

### Lipid Peroxidation (Malondialdehyde MDA)

Lipids, being crucial constituents of the membrane, are the main target of ROS and result in lipid peroxidation by the extraction of hydrogen from the unsaturated fatty acid chain. Thus, lipid peroxidation plays a crucial role in causing cellular damage in living organisms experiencing oxidative stress. Lipid peroxidation generates many harmful compounds, including malondialdehyde (MDA) and aldehydes, from polyunsaturated fatty acids. MDA is a marker for oxidative damage. Algae possess chloroplasts that include a complex network of membranes rich in polyunsaturated fatty acids. These fatty acids are particularly susceptible to peroxidation (Garg & Manchanda 2009, Halliwell & Chirico 1993).

The findings study demonstrates a significant variance ( $p \leq 0.05$ ) in the content of the MDA for the alga

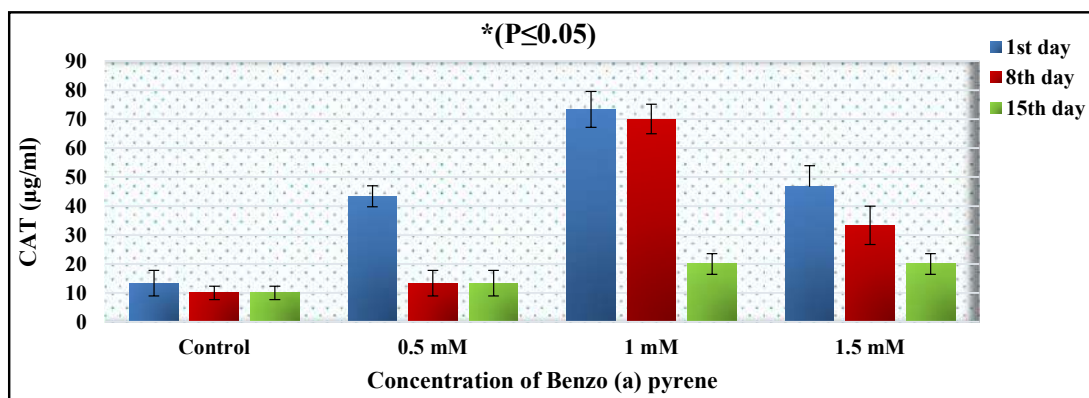


Fig. 9: CAT amount of *S. quadricauda* at various amounts of Benzo [a] pyrene.

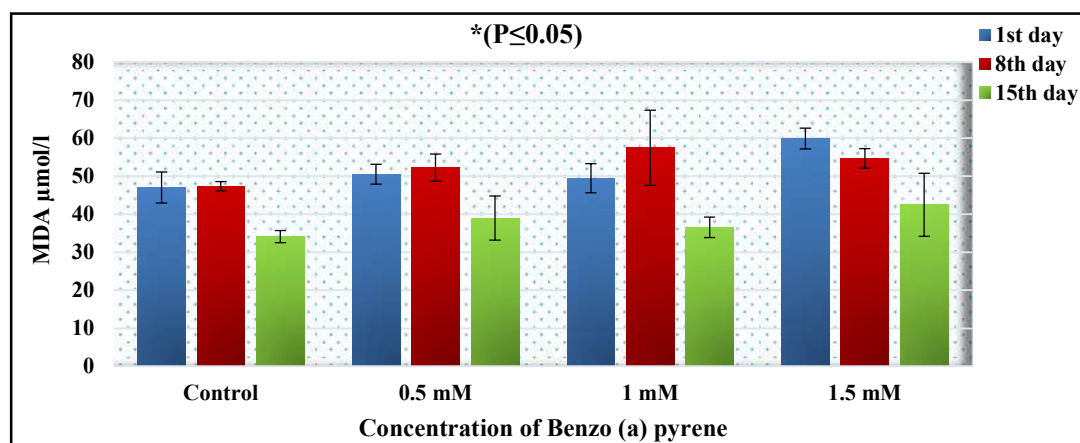


Fig. 10: MDA amount of *S. quadricauda* at various amounts of Benzo [a] pyrene.

*S. quadricauda* after treatment; the content of MDA decreased at various amounts Benzo[a]pyrene compared with control ( $34.14 \mu\text{mol.L}^{-1}$ ), the minimum value is 36.58, 39.02 and  $42.50 \mu\text{mol.L}^{-1}$  at concentration 1, 0.5 and 1.5 mM respectively, throughout 15th day (Fig. 10). This may be due to stimulated antioxidant defense in algae was efficient in eliminating ROS, and inhibiting the algal cells from oxidative damage (Zhang et al. 2018).

### Bioremediation of Benzo[a]pyrene

Researchers have extensively investigated the capacity of certain types of algae to break down PAH (polycyclic aromatic hydrocarbon) compounds found in water due to their toxicity and carcinogenic properties. In a study conducted by Kumar et al. (2018), it was discovered that PAHs interact with cytochrome P450 monooxygenase CYP in the active sites of algae through intermolecular hydrogen bonding, hydrophobic bonding  $\pi$ - $\pi$  interactions, and van der Waals interactions. These interactions enable algae to remediate PAHs more effectively than other microorganisms. The results showed the effect of different amounts of benzo[a]pyrene on the degradation of *S. quadricauda*; the highest value was 40.13 throughout the 15<sup>th</sup> with 0.5 mM, while the lowest value was 0 throughout 1<sup>st</sup> day with 0.5 and 1 mM (Fig. 11), in the present study demonstrated *S. quadeicauda* have high ability to removed Benzo[a]pyrene after 1, 8 and 15 days of treatments. Ei-Sheekh et al. (2012) suggested that the chemical structure of the molecule and the physiological metabolism of the algae appear to determine how polycyclic and heterocyclic aromatic compounds break down under them. Apart from being ingested by cells or absorbed on the wall, the results of the study imply that algae broke down the compound's high removal efficiencies by several processes, including a reduction, oxidation, and the activation

of enzymes, including cytochrome P450, diphenol oxidase, and Peroxidase, Detoxifying B[a]P and breaking down these toxic chemicals depend critically on these enzyme systems (Takáčová et al. 2014).

### CONCLUSIONS

Benzo[a]pyrene, a form of polycyclic aromatic hydrocarbon (PAH), may be efficiently removed from polluted water by use of the green alga *S. quadricauda* in the process of bioremediation. This results from harmless substances being produced all along the algal breakdown. The results of the investigation show that the alga shows great ability for BaP removal at low concentrations and that the pollution is cleared in a short period. Algae showed biological reactions in some results of exposure to different biological parameters with different amounts of B[a]P such as decreased amount, total protein, chlorophyll a, and b, increased oxidative stress ROS and carbohydrates and enzyme activity, SOD, MDA, and catalase.

### ACKNOWLEDGMENT

The authors extend their thanks and appreciation to the Department of Biology, College of Science at the University of Babylon, for their assistance in supporting this work.

### REFERENCES

- Abdul Razak, V., 1985. Physiological and Biochemical Aspects of Metal Tolerance in *Arachis hypogaea*. LM Phil. Dissertation, SV University, Tirupati. Abstr. No. XIV-25.
- Aksmann, A., Shutova, T., Samuelsson, G. and Tukaj, Z., 2011. The mechanism of anthracene interaction with photosynthetic apparatus: A study using intact cells, thylakoid membranes, and PS II complexes isolated from *Chlamydomonas reinhardtii*. *Aquatic Toxicology*, 104(3-4), pp.205-210.

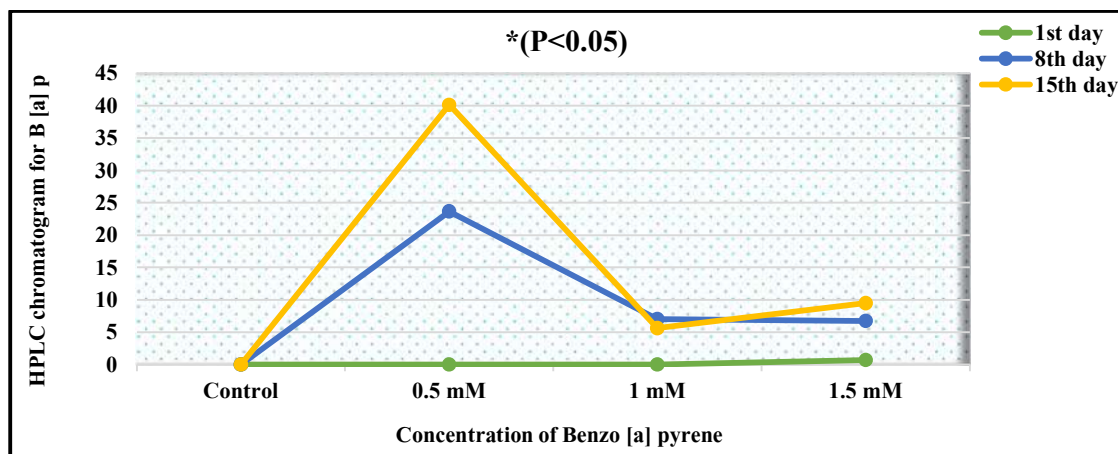


Fig. 11: HPLC Chromatogram for Benzo[a]pyrene standard at various concentrations.



- Aksmann, A. and Tukaj, Z., 2004. The effect of anthracene and phenanthrene on the growth, photosynthesis, and SOD activity of the green alga *Scenedesmus armatus* depends on the PAR irradiance and CO<sub>2</sub> level. *Archives of Environmental Contamination and Toxicology*, 47, pp.177-184.
- Aksmann, A. and Tukaj, Z., 2008. Intact anthracene inhibits photosynthesis in algal cells: A fluorescence induction study on *Chlamydomonas reinhardtii* cw92 strain. *Chemosphere*, 74(1), pp.26-32.
- Alegbeleye, O.O., Opeolu, B.O. and Jackson, V.A., 2017. Polycyclic aromatic hydrocarbons: A critical review of environmental occurrence and bioremediation. *Environmental Management*, 60, pp.758-783.
- Alexander, M., 1999. *Biodegradation and Bioremediation*. 2nd ed. Academic Press.
- Allen, J.F., 2003. State transitions—A question of balance. *Science*, 299(5612), pp.1530-1532.
- Amran, R.H., Jamal, M.T., Pugazhendhi, A., Al-Harbi, M., Ghandourah, M., Al-Otaibi, A. and Haque, M.F., 2022. Biodegradation and bioremediation of petroleum hydrocarbons in marine ecosystems by microorganisms: A review. *Nature Environment & Pollution Technology*, 21(3).
- Aust, S.D., 1985. *Handbook of Methods for Oxygen Radical Research*. Springer, pp.203-207.
- Barsanti, L. and Gualtieri, P., 2022. *Algae: Anatomy, Biochemistry, and Biotechnology*. CRC Press.
- Bhatt, K.K., Lily, M.K., Joshi, G. and Dangwal, K., 2018. Benzo(a)pyrene degradation pathway in *Bacillus subtilis* BMT4i (MTCC 9447). *Turkish Journal of Biochemistry*, 43(6), pp.693-701.
- Binark, N., Güven, K.C., Gezgin, T. and Ünlü, S., 2000. Oil pollution of marine algae. *Bulletin of Environmental Contamination & Toxicology*, 64(6).
- Bradford, M.M., 1976. A rapid and sensitive method for the quantitation of microgram quantities of protein utilizing the principle of protein-dye binding. *Analytical Biochemistry*, 72(1-2), pp.248-254.
- Burtis, C.A. and Ashwood, E.R., 1999. *Tietz Textbook of Clinical Chemistry*. Philadelphia, pp.1654-1655.
- Calow, P. and Sibly, R.M., 1990. A physiological basis of population processes: Ecotoxicological implications. *Functional Ecology*, 18, pp.283-288.
- Carfagna, S., Lanza, N., Salbitani, G., Basile, A., Sorbo, S. and Vona, V., 2013. Physiological and morphological responses of lead- or cadmium-exposed *Chlorella sorokiniana* 211-8K (*Chlorophyceae*). *SpringerPlus*, 2, pp.1-7.
- Cheng, J., Qiu, H., Chang, Z., Jiang, Z. and Yin, W., 2016. The effect of cadmium on the growth and antioxidant response for freshwater algae *Chlorella vulgaris*. *SpringerPlus*, 5, pp.1-7.
- Chia, M.A., Chimdirim, P.K. and Japhet, W.S., 2015. Lead-induced antioxidant response and phenotypic plasticity of *Scenedesmus quadricauda* (Turp.) de Brébisson under different nitrogen concentrations. *Journal of Applied Phycology*, 27, pp.293-302.
- Chia, M.A., Lombardi, A.T. and Melao, M.D.G.G., 2013. Growth and biochemical composition of *Chlorella vulgaris* in different growth media. *Anais da Academia Brasileira de Ciências*, 85(4), pp.1427-1438.
- Echeveste, P., Agustí, S. and Dachs, J., 2010. Cell size-dependent toxicity thresholds of polycyclic aromatic hydrocarbons to natural and cultured phytoplankton populations. *Environmental Pollution*, 158(1), pp.299-307.
- El Maghraby, D. and Hassan, I., 2021. Photosynthetic and biochemical response of *Ulva lactuca* to marine pollution by polyaromatic hydrocarbons (PAHs) collected from different regions in Alexandria City, Egypt. *Egyptian Journal of Botany*, 61(2), pp.467-478.
- Ei-Sheekh, M.M., Ghareib, M.M. and El-Souod, G.W., 2012. Biodegradation of phenolic and polycyclic aromatic compounds by some algae and cyanobacteria. *Journal of Bioremediation & Biodegradation*, 3(133), p.2.
- Ermis, H., Guven-Gulhan, U., Cakir, T. and Altinbas, M., 2020. Effect of iron and magnesium addition on population dynamics and high-value product of microalgae grown in the anaerobic liquid digestate. *Scientific Reports*, 10(1), p.3510.
- Frary, A., Göll, D., Keleş, D., Ökmen, B., Pınar, H., Şığva, H.Ö., Yemencioğlu, A. and Doğanlar, S., 2010. Salt tolerance in *Solanum pennellii*: Antioxidant response and related QTL. *BMC Plant Biology*, 10, pp.1-16.
- García de Llasera, M.P., Olmos-Espejel, J.D.J., Díaz-Flores, G. and Montaña-Montiel, A., 2016. Biodegradation of benzo(a)pyrene by two freshwater microalgae *Selenastrum capricornutum* and *Scenedesmus acutus*: A comparative study useful for bioremediation. *Environmental Science and Pollution Research*, 23, pp.3365-3375.
- Garg, N. and Manchanda, G., 2009. ROS generation in plants: Boon or bane? *Plant Biosystems*, 143(1), pp.81-96.
- Gour, R.S., Kant, A. and Chauhan, R.S., 2014. Screening of microalgae for growth and lipid accumulation properties. *Journal of Algal Biomass Utilization*, 5, pp.38-46.
- Halliwell, B. and Chirico, S., 1993. Lipid peroxidation: Its mechanism, measurement, and significance. *The American Journal of Clinical Nutrition*, 57(5), pp.715S-725S.
- Haritash, A.K. and Kaushik, C.P., 2009. Biodegradation aspects of polycyclic aromatic hydrocarbons (PAHs): A review. *Journal of Hazardous Materials*, 169(1-3), pp.1-15.
- Greenhaff, P.L., Hultman, E. and Harris, R.C., 2004. Carbohydrate metabolism. *Medicine and Sport Science*, 46, pp.108-151.
- Hassan, I.A., Bell, N.B., Ashmore, M.R., Cotrozzi, L., Haiba, N.S., Basahi, J.M., Summan, A., Almeelbi, T. and Ismail, I.M., 2018. Radish (*Raphanus sativus* L.) cultivar-specific response to O<sub>3</sub>: Patterns of biochemical and plant growth characteristics. *Clean-Soil, Air, Water*, 46(6), p.1800124.
- Hassan, I.A., Haiba, N.S., Badr, R.H., Basahi, J.M., Almeelbi, T., Ismail, I.M. and Taia, W.K., 2017. Effects of ambient ozone on reactive oxygen species and antioxidant metabolites in leaves of pea (*Pisum sativum* L.) plants. *Pakistani Journal of Botany*, 49(1), pp.47-55.
- Heipieper, H.J., Löffel, B., Keweloh, H. and de Bont, J.A., 1995. The *cis/trans* isomerization of unsaturated fatty acids in *Pseudomonas putida* S12: an indicator for environmental stress due to organic compounds. *Chemosphere*, 30(6), pp.1041-1051.
- Herbert, D., Phipps, P.J. and Strange, R.E., 1971. *Methods in Microbiology*. Academic Press, pp. 209-344.
- Hwang, J.H., Church, J., Lee, S.J., Park, J. and Lee, W.H., 2016. Use of microalgae for advanced wastewater treatment and sustainable bioenergy generation. *Environmental Engineering Science*, 33(11), pp.882-897.
- Juda, S.A., Salah, M.M. and Salman, J.M., 2019. Efficiency of green algae *Chlorella vulgaris* in remediation of polycyclic aromatic hydrocarbon (anthracene) from culture media. *Baghdad Science Journal*, 16(3), pp.543-549.
- Juneja, A., Ceballos, R.M. and Murthy, G.S., 2013. Effects of environmental factors and nutrient availability on the biochemical composition of algae for biofuels production: a review. *Energies*, 6(9), pp.4607-4638.
- Kapoor, K. and Arora, L., 1996. Observations on growth responses of cyanobacteria under the influence of herbicides. *Pollution Research*, 15, pp.343-351.
- Keith, L.H., 2015. The source of US EPA's sixteen PAH priority pollutants. *Polycyclic Aromatic Compounds*, 35(2-4), pp.147-160.
- Kumar, P.S., Thomas, J. and Poornima, V., 2018. Structural insights on bioremediation of polycyclic aromatic hydrocarbons using microalgae: A modeling-based computational study. *Environmental Monitoring and Assessment*, 190(92), pp.1-16.
- Lawal, A.T., 2017. Polycyclic aromatic hydrocarbons: A review. *Cogent Environmental Science*, 3(1), p.1339841.



- Lin, Y.H., Pan, K.Y., Hung, C.H., Huang, H.E., Chen, C.L., Feng, T.Y. and Huang, L.F., 2013. Overexpression of ferredoxin, PETF, enhances tolerance to heat stress in *Chlamydomonas reinhardtii*. *International Journal of Molecular Sciences*, 14(10), pp.20913-20929.
- Liu, H., Yin, H., Tang, S., Wei, K., Peng, H., Lu, G. and Dang, Z., 2019. Effects of benzo[a]pyrene (BaP) on the composting and microbial community of sewage sludge. *Chemosphere*, 222, pp.517-526.
- Lowry, O.H., Rosebrough, N.J., Farr, A.L. and Randall, R.J., 1951. Protein measurement with the Folin phenol reagent. *Journal of Biological Chemistry*, 193(1), pp.265-275.
- Luka, Y., Highina, B.K. and Zubairu, A., 2018. Bioremediation: A solution to environmental pollution: A review. *American Journal of Engineering Research*, 7(2), pp.101-109.
- McCann, J.H. and Solomon, K.R., 2000. The effect of creosote on membrane ion leakage in *Myriophyllum spicatum* L. *Aquatic Toxicology*, 50(3), pp.275-284.
- Meewes, C., Brenneisen, P., Wenk, J., Kuhr, L., Ma, W., Alikoski, J., Poswig, A., Krieg, T. and Scharffetter-Kochanek, K., 2001. Adaptive antioxidant response protects dermal fibroblasts from UVA-induced phototoxicity. *Free Radical Biology and Medicine*, 30(3), pp.238-247.
- Miller, K.P. and Ramos, K.S., 2001. Impact of cellular metabolism on the biological effects of benzo[a]pyrene and related hydrocarbons. *Drug Metabolism Reviews*, 33(1), pp.1-35.
- Mohapatra, P.K. and Schiewer, U., 2000. Dimethoate and quinalphos toxicity: Pattern of photosynthetic pigment degradation and recovery in *Synechocystis* sp. PCC 6803. *Archiv für Hydrobiologie. Supplementband, Algological Studies*, 134, pp.79-94.
- Mostafa, F.I. and Helling, C.S., 2002. Impact of four pesticides on the growth and metabolic activities of two photosynthetic algae. *Journal of Environmental Science and Health, Part B*, 37(5), pp.417-444.
- Mustafa, E.M., 2013. *Effect of Selected Chemical Contaminants on Growth, Biochemical Composition, DNA Damage, and Superoxide Dismutase Activity in Four Marine Algae*. University of Malaya (Malaysia).
- Nagajyoti, P.C., Dinakar, N., Suresh, S., Udaykiran, Y., Suresh, C., Prasad, T.N.V.K.V. and Damodharam, T., 2009. Biomass industrial effluent effect on carbohydrates, amino acids, nitrite, and nitrite enzyme activities of *Arachis hypogaea* L. *Agricultural Sciences in China*, 8(2), pp.203-215.
- Nandal, M., Solanki, P., Rastogi, M. and Hooda, R., 2015. Bioremediation: A sustainable tool for environmental management of oily sludge. *Nature Environment and Pollution Technology*, 14(1), p.181.
- Okpashi, V.E., Ogugua, V.N., Ubani, S.C., Ujah, I.I. and Ozioko, J.N., 2017. Estimation of residual polycyclic aromatic hydrocarbons concentration in fish species: Implication in reciprocal corollary. *Cogent Environmental Science*, 3(1), p.1303979.
- Pandya, D.K. and Kumar, M.A., 2021. Chemo-metric engineering designs for deciphering the biodegradation of polycyclic aromatic hydrocarbons. *Journal of Hazardous Materials*, 411, p.125154.
- Papadimitriou, E. and Loumbourdis, N.S., 2002. Exposure of the frog *Rana ridibunda* to copper: Impact on two biomarkers, lipid peroxidation and glutathione. *Bulletin of Environmental Contamination and Toxicology*, 69(6).
- Patel, A.K., Suseela, M.R., Singh, M. and Nayaka, S., 2015. Application of response surface methodology for optimization of biomass, carbohydrate, and lipid production in BG11+ by *Scenedesmus quadricauda*. *International Journal of Research in Engineering and Applied Sciences*, 5, pp.199-215.
- Richmond, A. ed., 2004. *Handbook of Microalgal Culture: Biotechnology and Applied Phycology* (Vol. 577). Oxford: Blackwell Science
- Salman, J.M., Grmasha, R.A., Stenger-Kovács, C., Lengyel, E., Al-Sareji, O.J., Al-Cheban, A.M.A. and Meiczing, M., 2023. Influence of magnesium concentrations on the biomass and biochemical variations in the freshwater algae *Chlorella vulgaris*. *Heliyon*, 9(1).
- Samanta, P., Shin, S., Jang, S. and Kim, J.K., 2019. Comparative assessment of salinity tolerance based on physiological and biochemical performances in *Ulva australis* and *Pyropia yezoensis*. *Algal Research*, 42, p.101590.
- Sánchez-Bayo, A., Morales, V., Rodríguez, R., Vicente, G. and Bautista, L.F., 2020. Cultivation of microalgae and cyanobacteria: Effect of operating conditions on growth and biomass composition. *Molecules*, 25(12), p.2834.
- Selvan, B.K., Revathi, M., Piriya, P.S., Vasan, P.T., Prabhu, D. and Vennison, S.J., 2013. Biodiesel production from marine cyanobacteria cultured in plate and tubular photobioreactors. *Journal of Bioenergy and Algal Research*, 15(2), pp.45-53.
- Shukla, K.P., Singh, N.K. and Sharma, S., 2010. Bioremediation: Developments, current practices and perspectives. *Genetic Engineering and Biotechnology Journal*, 3, pp.1-20.
- Sikkema, J., de Bont, J.A. and Poolman, B., 1994. Interactions of cyclic hydrocarbons with biological membranes. *Journal of Biological Chemistry*, 269(11), pp.8022-8028.
- Singh, O.V., 2006. Proteomics and metabolomics: The molecular make-up of toxic aromatic pollutant bioremediation. *Proteomics*, 6(20), pp.5481-5492.
- Sinha, R., Kulldorff, M., Gunter, M.J., Strickland, P. and Rothman, N., 2005. Dietary benzo[a]pyrene intake and risk of colorectal adenoma. *Cancer Epidemiology Biomarkers & Prevention*, 14(8), pp.2030-2034.
- Sun, Y., Xu, Y., Zhou, Q., Wang, L., Lin, D. and Liang, X., 2013. The potential of gibberellic acid 3 (GA3) and Tween-80 induced phytoremediation of co-contamination of Cd and benzo[a]pyrene (B[a]P) using *Tagetes patula*. *Journal of Environmental Management*, 114, pp.202-208.
- Takáčová, A., Smolinská, M., Ryba, J., Mackul'ak, T., Jokrllová, J., Hronec, P. and Čík, G., 2014. Biodegradation of benzo[a]pyrene through the use of algae. *Central European Journal of Chemistry*, 12, pp.1133-1143.
- Tewari, A., Bhutada, D.S. and Wadgaonkar, V., 2023. Heavy metal remediation from water/wastewater using bioadsorbents—A review. *Nature Environment & Pollution Technology*, 22(4), p.11.
- Torres, M.A., Barros, M.P., Campos, S.C., Pinto, E., Rajamani, S., Sayre, R.T. and Colepicolo, P., 2008. Biochemical biomarkers in algae and marine pollution: A review. *Ecotoxicology and Environmental Safety*, 71(1), pp.1-15.
- Tripranthakam, S., Duxbury, C.L., Babu, T.S. and Greenberg, B.M., 1999. *Environmental Toxicology and Risk Assessment: Standardization of Biomarkers for Endocrine Disruption and Environmental Assessment*. ASTM International.
- Wiśniewska, K.A., Lewandowska, A.U., Śliwińska-Wilczewska, S., Staniszevska, M. and Budzalek, G., 2023. The ability of airborne microalgae and cyanobacteria to survive and transfer the carcinogenic benzo[a]pyrene in coastal regions. *Cells*, 12(7), p.1073.
- Yang, B., Xue, Q.H., Qu, C.T., Lu, C., Liu, F.F., Zhang, H., Ma, L.T., Qi, L. and Wang, Y.T., 2024. Research progress on in-situ remediation of typical heavy metals in petroleum hydrocarbon-contaminated soil enrichment by plants. *Nature Environment & Pollution Technology*, 23(1), p.65.
- Zhang, M., Wang, X., Tao, J., Li, S., Hao, S., Zhu, X. and Hong, Y., 2018. PAHs would alter cyanobacterial blooms by affecting the microcystin production and physiological characteristics of *Microcystis aeruginosa*. *Ecotoxicology and Environmental Safety*, 157, pp.134-142.
- Zhao, L., 2018. Measurement of superoxide dismutase-like activity in peel and pulp of apple from Anshan acres. *AIP Conference Proceedings*, 1956(1), p.7521.

# Transforming Type 2 Diabetes Management Through Telemedicine, Data Mining and Environmental Insights

Sapna S. Basavaraddi<sup>1</sup> and A. S. Raju<sup>2</sup>

<sup>1</sup>SSIT, SSAHE, Agalakote, B.H. Road, Tumakuru-572105, Karnataka, India

<sup>2</sup>Department of Medical Electronics, SSIT, SSAHE, Agalakote, B.H. Road, Tumakuru-572105, Karnataka, India

†Corresponding author: Sapna S. Basavaraddi; sapnasbasavaraddi@gmail.com , asraju74@gmail.com

**Abbreviation: Nat. Env. & Poll. Technol.**  
**Website: www.neptjournal.com**

*Received:* 11-08-2024

*Revised:* 23-09-2024

*Accepted:* 21-10-2024

## Key Words:

Diabetes mellitus  
 Type-2 diabetes  
 Telemedicine  
 Environment  
 Arsenic  
 Machine learning  
 Data mining  
 Predictive analytics  
 Healthcare management

## Citation for the Paper:

Sapna S. Basavaraddi and A. S. Raju., 2025. Transforming type 2 diabetes management through telemedicine, data mining and environmental insights. *Nature Environment and Pollution Technology*, 24(2), p. B4256. <https://doi.org/10.46488/NEPT.2025.v24i02.B4256>

*Note: From year 2025, the journal uses Article ID instead of page numbers in citation of the published articles.*



**Copyright:** © 2025 by the authors  
**Licensee:** Technoscience Publications  
 This article is an open access article distributed under the terms and conditions of the Creative Commons Attribution (CC BY) license (<https://creativecommons.org/licenses/by/4.0/>).

## ABSTRACT

Diabetes mellitus is a prevalent chronic disease with significant implications for public health, including an expanded chance of coronary heart malady, stroke, persistent kidney illness, misery, and useful inability. In India, the predominance of diabetes among grown-ups matured 20 a long time and more seasoned rose from 5.5% in 1990 to 7.7% in 2016. Traditionally, diabetes management involves costly consultations and diagnostic tests, presenting challenges for timely diagnosis and treatment. Additionally, a comprehensive study was conducted to investigate the relationship between the incidence of type 2 diabetes mellitus (T2DM) and environmental exposure to arsenic in the form of air, water, and food pathways. The majority of the analyzed studies examined the levels of arsenic in water samples, with analyses of urine, blood, serum, and plasma samples coming next. Groundwater supplies may get contaminated by arsenic, especially in regions where arsenic deposits are naturally occurring or as a result of industrial activity. Additionally, various meals contain it, particularly rice, seafood, and poultry. Besides, it might be released into the environment by industrial processes such as coal combustion, smelting, and mining, which could lead to occupational exposure. There may be a genetic component to the association between arsenic exposure and the onset of diabetes. Ultimately, diabetes mellitus is enhanced by arsenic pollution through air, food, and drinking water. Advances in machine learning and telemedicine offer innovative solutions to address these challenges. Data mining, a crucial aspect of machine learning, facilitates the extraction of valuable insights from extensive datasets, enabling more efficient and effective diabetes management. This study explores a telemedicine-based system utilizing five classification techniques Tree, Naive Bayes, Support Vector Machine, and others to predict Type-2 diabetes. By leveraging real-time data analysis, the system aims to enhance early diagnosis and management of Type-2 diabetes, potentially preventing progression to critical conditions. The results evaluate the effectiveness of these models in a telemedicine context, identifying the best-performing model to assist healthcare professionals in making informed decisions for early intervention and improved patient outcomes.

## INTRODUCTION

Diabetes has developed as a worldwide well-being emergency, with the scourge especially articulated in Southeast Asia, eminently in India. Around 72 million individuals in India are evaluated to have diabetes, whereas an extra 80 million are accepted to have pre-diabetes. Type 2 diabetes accounts for over 90-95% of these cases (Gupta et al. 2024, Kumar 2024). According to the World Wellbeing Organization (WHO), roughly 347 million individuals around the world are influenced by diabetes, and it is anticipated to become the seventh driving cause of passing all-inclusive by 2030 (“WHO/diabetes”, Rahman et al. 2023). The management of Type 2 diabetes has evolved rapidly over the past decade, with several new therapeutic agents introduced. In 2005, the Indian Council of Medical Research (ICMR) released guidelines for the management of Type 2 diabetes, which have been extensively embraced throughout the nation. A

subsequent ICMR workshop in 2018 focused on refining these guidelines (Kumar 2024). The short-term goals of this work are to discuss certain methodological modifications related to the environment, possible fixes, and further research opportunities. At this point, the most prevalent attributes are walking distance, air pollution, food, exercise, and environmental pathways (Schulz et al. 2016).

### **Mechanism Linking the Environment and T2DM**

Environmental, biochemical, and behavioral risk variables are thought to combine to cause type 2 diabetes (Kahn et al. 2014, Chatterjee et al. 2017). If no environment encourages healthy lifestyles, it is taught that these lifestyles are undesirable. A comprehensive search was carried out in Pubmed, Scopus, web of Science, and Embase databases. The inclusion of some criteria was studied. Diabetes is a chronic metabolic disease characterized by the body's inability to appropriately control blood sugar levels. Diabetes mellitus type 2 is a chronic metabolic disease that usually shows up as adult food and a complex interaction between environmental and genetic factors causes it. This condition is characterized by insulin resistance and decreased insulin production, both of which cause long-term disruptions in glucose metabolism. As a result, high blood sugar levels can lead to many complications, such as cardiovascular disease, neurological conditions, kidney problems, and retinopathy (Barbagallo et al. 2022, Kakavandi et al. 2023, Armghan et al. 2023).

Empirical data has demonstrated a probable association between diabetes and exposure to environmental arsenic. Numerous studies have shown that extended exposure to arsenic may increase the likelihood of developing diabetes. There is evidence linking the high levels of arsenic in the population's drinking water to both occupational settings and demographics (Halim & Halim 2019). Studies revealed a 27% increase in the risk of developing diabetes is linked to a drinking water arsenic concentration rise of 15 micrograms per liter (Ke et al. 2023, Rahmani et al. 2023). Insulin signaling and secretion are negatively impacted by arsenic, which results in decreased glucose tolerance and elevated insulin resistance. This event raises the possibility that arsenic plays a role in the onset or exacerbation of diabetes mellitus 2. Furthermore, it has been demonstrated that exposure to arsenic increases oxidative stress and inflammation, two processes that are known to be important in the development and maintenance of diabetes (Nikraves et al. 2023, Colwell et al. 2023, Rangel-Moreno et al. 2022).

Arsenic's effects on the advancement of diabetes have been linked in numerous research. The data points to a possible connection between inorganic arsenic and the onset

of diabetes, especially in populations exposed to different concentrations of the metal. Chronic low-level arsenic exposure has been linked in certain publications to a higher prevalence of diabetes mellitus 2 ( Li et al. 2023, Shokat et al. 2024, Nurchi et al. 2020, Tinkelman et al. 2020). Polluted air can raise type 2 diabetes risk. Studies from the USA and Europe reveal that there is a definite link between incident diabetes mellitus 2 and ambient PM 2.5(fine particulate matter 2.5 micrometer diameter). In a systematic review and meta-analysis, some countries showed that the risk of diabetes mellitus 2 rose by 8-10% per 10 microgram/meter increase in exposure, and the association was stronger in females. However, conclusions drawn from these studies cannot be directly collated to developing countries.

Ambient pollution and the levels are low in high-income countries. There have been a few attempts to assess the risk of diabetes associated with air pollution in developing nations where the air quality tends to be much poorer. A study from China showed 155 increased hazards of incidents of diabetes from every 10 microgram/meter increase in fine particulate matter of diameter of less than or equal to 2.5 micrometers. Another study from China reported an increase in the fasting plasma glucose (FPG) and glycated hemoglobin (HBA1c) by 0.025 and 0.001 m mole/liter, respectively, for every 10 microgram/meter increase in particulate matter of diameter less than or equal to 10 micrometers and an increase by 0.061 to 0.016 m mole /liter respectively for every 10 microgram/meter increase in fine particulate matter of diameter 2.5 micrometers.

An analysis of data from nearly 4 lakh individuals showed that exposure to higher levels of fine particulate matter in air of diameter 2.5 micrometers was associated not only with the increased risk of diabetes 2 but also mortality risk from baseline of diabetes mellitus 2 and its complications. In such an environment, educational and behavioral measures may be severely reduced or completely useless. Numerous studies have demonstrated the importance of behavioral, socioeconomic, demographic, and individual-level factors in predicting type 2 diabetes (Gray-Webb et al. 2013, Agardh et al. 2011). Reviews from the past also point to a connection between the environment and conditions like obesity, cardiovascular disease, hypertension, metabolic syndrome, and physical activity that are directly linked to type 2 diabetes (Black & Macinko 2008, Sallis et al. 2008, Poortinga 2006).

The hypothetical system shown in Fig. 1 describes the various ways that unique environmental factors could influence type 2 diabetes. Socio-ecological theories form the basis of this paradigm; they highlight that human behavior is determined by capacity and is supported by the socio-demographic, psycho-social, economic, organizational, and

physical environments (Sallis et al. 2012). In Fig. 1.1, the methods by which environmental factors affect the possibility of Type-2 diabetic complications are diagrammatically represented (Northridge et al. 2023). Within this framework, newer advancements have led to the development of categorization models utilizing a range of machine-learning approaches. By leveraging extensive or real-time data sets to aid in diagnosis and prediction, these models assist medical professionals in the identification and management of Type 2 diabetes (Kumar 2024).

### Investigation

This study's main objective is to examine diabetes datasets and apply machine learning algorithms-namely Decision Tree, Random Forest, Neural Network, Support Vector Machine, and Naive Bayes-for the prediction of Type 2

diabetes (Teimoory & Keyvanpour 2024, Chakraborty et al. 2023, Uddin & Ali 2023). The research seeks to develop a robust prediction engine and a corresponding web application that enables users to predict diabetes using these algorithms. This study also explores the application of statistical models in machine learning and aims to enhance understanding of how these algorithms function in the context of diabetes prediction (Teimoory & Keyvanpour 2024).

### MATERIALS AND METHODS

The study was done with preferred reporting items for systematic reviews and meta-analysis (PRISMA) statements. Based on study criteria such as

1. Article published in English
2. Full-text records

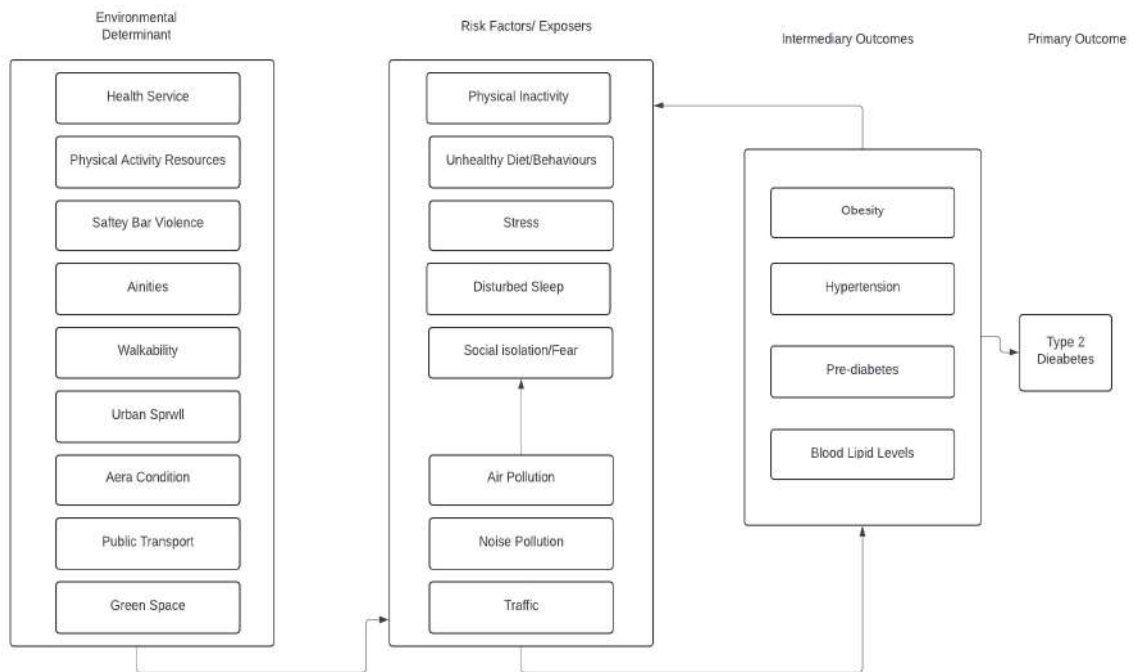


Fig. 1: Diagrammatic representation of the mechanisms by which environmental factors affect the risk of Type-2 diabetes mellitus.

Table 1: Clinical Differentiation between Type 1 and Type 2 Diabetes (LIANA 2024).

Clinical Point	Type 1 Diabetes	Type 2 Diabetes
Age	Typically diagnosed in youth	Commonly diagnosed in adults
Family History of Diabetes	Uncommon	Common
Ketosis at Diagnosis	Can occur	Rare
Insulin Markers	Absence	Presence
C-Peptide Assay	Lack of reserve beta cells	Presence of reserve beta cells
Pancreatic Autoantibodies	Presence	Absence



3. Articles relating arsenic exposure through the drinking water, air, and food pathways and its effects on diabetes mellitus 2.
4. Exclusion criteria like books, clinical trials and conference articles.

Along with these criteria, followed by a real-time data set and online dataset to study the prevalence accessibility of diabetes mellitus 2 and its management to reduce mortality rate, it also emphasizes the linkage between air pollution in the form of fine particulate matter less than or equal to 2.5-micrometer diameter and also arsenic pollution through drinking water and food and other pollutant toxins.

Diabetes mellitus is classified into the following types:

1. Type 1 Diabetes: Previously known as “Insulin-Dependent Diabetes Mellitus,” this kind of disease is caused by the body’s inability to manufacture insulin (IDDM).
2. Type 2 Diabetes: This kind is marked by an absolute insulin deficit that can occasionally coexist with insulin resistance, a condition in which cells are unable to use insulin as intended. It was once referred to as “Adult-

Onset Diabetes” or “Non-Insulin Dependent Diabetes Mellitus” (NIDDM).

3. Type 3 diabetes, often known as gestational diabetes, is characterized by increased blood glucose levels and affects pregnant women who have never been diagnosed with the disease (Chakraborty et al. 2023, Uddin & Ali 2023).
4. The following Table 1 describes the Clinical Differentiation between Type 1 and Type 2 Diabetes.

### Overview of Types-2 Diabetes

Diabetes type 2 may be a complicated metabolic and vascular condition primarily marked by insulin resistance and, to differing degrees, insulin secretory absconds. It may be a dynamic condition, as often as possible, related to central corpulence, dyslipidemia, and hypertension. Although type 2 diabetes is most common among overweight and hefty people of center to late age, it is progressively watched in more youthful populaces and those with lower body mass index (BMI). Outstandingly, South Asians display the “Asian Indian phenotype,” where, at a given BMI level, Compared to Caucasians, they typically

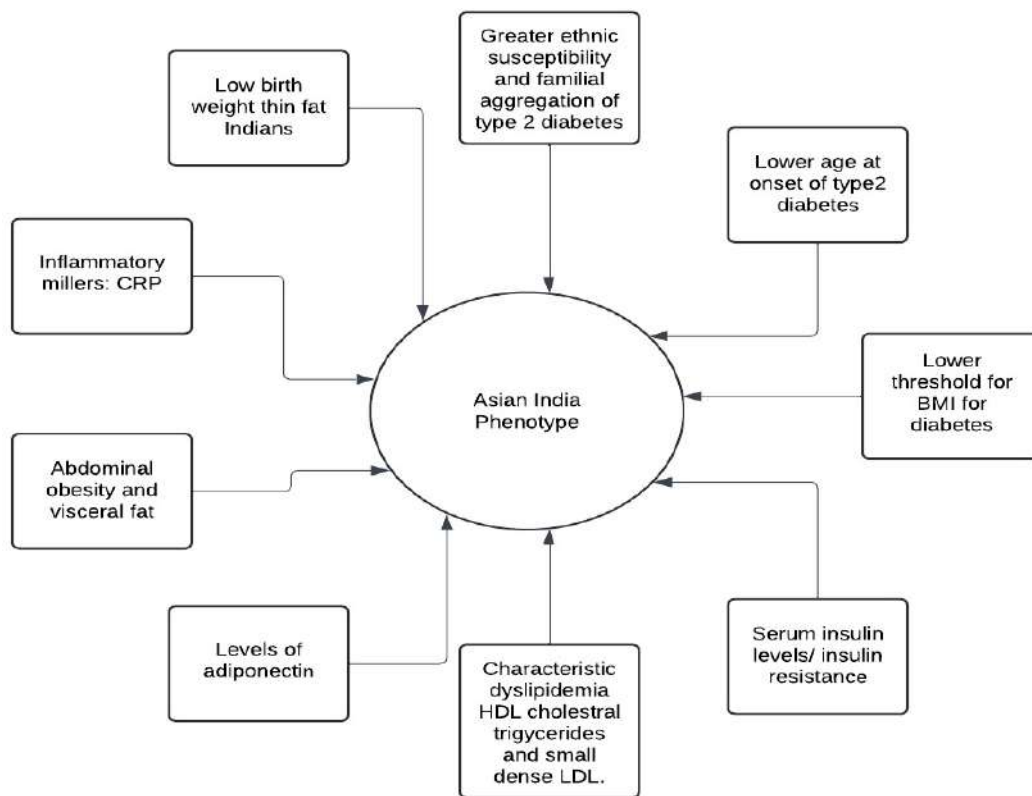


Fig. 2: Block diagram of Asian Indian phenotype.

have total body fat, extra visceral fat, increased insulin resistance, and a higher prevalence of diabetes (see Figure 2).

### Data Collection

Actual data were gathered from diagnostic facilities in accordance with accepted clinical standards for the diagnosis of diabetes. The following Table 2 describes the diagnostic criteria for Diabetes and Pre-diabetes disease. Among the diagnostic standards used are:

- Random Plasma Glucose:  $\geq 200 \text{ mg.dL}^{-1}$
- Fasting Plasma Glucose (FPG):  $\geq 126 \text{ mg.dL}^{-1}$
- 2-Hour Post 75g Glucose (hPG):  $\geq 200 \text{ mg.dL}^{-1}$
- Glycated Hemoglobin (HbA1c):  $\geq 6.5\%$

Patients presenting with symptoms such as osmotic symptoms, weight loss, tiredness, weakness, recurrent urogenital infections, and delayed wound healing were assessed. Notably, some patients with diabetes may exhibit no symptoms. Pre-diabetes, identified as impaired glucose tolerance (IGT), was also evaluated to gauge early risk.

Based on family history, symptoms of insulin resistance, hypertension, dyslipidemia, and polycystic ovarian syndrome (PCOS), specialists frequently predict Type 2 diabetes. This research leverages real-time data collected at Clinical

diagnostic centers to enhance prediction accuracy. Machine learning algorithms were applied to analyze patterns in the collected data. This approach aimed to improve the prediction and classification of diabetes and pre-diabetes, providing a valuable tool for doctors in the diagnostic process. The data mining techniques used were selected to identify underlying patterns and trends, thus supporting more accurate diabetes classification and management.

### Methodology

#### Data Description

The evaluation of the performance of various classification algorithms on two distinct datasets and reviews relating to arsenic in drinking water, food, fine particulate matter & pollution in the air to predict diabetes.

**Dataset 1:** the dataset is collected from the online Kaggle website. It consists of 5,000 samples with nine features, including gender, age, hypertension, heart disease, smoking history, BMI, HbA1c level, blood glucose level, and diabetes as the target variable. The following Table 3 is the sample table of the online dataset.

**Dataset 2:** the real-time data set is collected from the Clinical Diagnostic Center. It Comprises 48 samples with 19 features, including lab\_id, gender, age, fasting blood sugar levels,

Table 2: Diagnostic criteria for diabetes and pre-diabetes.

Parameter	WHO/ADA Criteria	Diabetes
Fasting Plasma Glucose (FPG) [mg.dL <sup>-1</sup> ]	$< 110 \text{ mg.dL}^{-1}$	$126 \text{ mg.dL}^{-1}$ or higher
2-Hour Postprandial Glucose(2-hPG) (mg/dl)	$< 140 \text{ mg.dL}^{-1}$	$200 \text{ mg.dL}^{-1}$ or higher
Glycated Hemoglobin (HbA1c)[%]	$< 5.7\%$	6.5% or higher
Random Plasma Glucose	Not specified	$200 \text{ mg.dL}^{-1}$ or higher with symptoms

Table 3: The Sample Table of Online Dataset.

SI.No	Gender	Age	hypertension	heart_disease	smoking_history	BMI	HbA1c_Level	blood_glucose_level	diabetes
1	Female	80	0	1	never	25.19	6.6	140	0
2	Female	54	0	0	No Info	27.32	6.6	80	0
3	Male	28	0	0	never	27.32	5.7	158	0
4	Female	36	0	0	current	23.45	5	155	0
5	Male	76	1	1	current	20.14	4.8	155	0

Table 4: The Sample Table of Real-Time Dataset.

SI.No	lab_id	Gender	Age	fbs1	fns1	ppbs1	ppvs1	HbA1c	Mbg	result	Remarks
1	4	M	49	209	1	354	1.5	9.3	220.21	1	dm
2	11	M	28	81	0	105	0	5.4	108.28	0	nd
3	12	F	25	76	0	99	0	5.1	99.67	0	nd
4	15	M	65	69	0	104	0	5.6	114.02	0	nd
5	19	M	51	164	0.5	238	1	7.3	162.81	1	dm

postprandial blood sugar levels, HbA1c, and a target variable indicating diabetes presence. The following Table 4 is the sample table of the real-time dataset.

## Data Preprocessing

### Dataset 1:

- **Missing Value Imputation:** Examined for any missing data. The most frequent value was used to impute categorical data, and the mean was used for numerical features.
- **Encoding Categorical Variables:** One-hot encoding was used for categorical variables like “smoking history” and “gender,” whereas label encoding was used for other variables.
- **Feature Standardization:** Standardized numerical features were given a mean of 0 and a standard deviation of 1.

### Dataset 2:

- **Missing Value Handling:** Missing values were handled appropriately, with numerical features filled using the mean and categorical features filled using the mode.
- **Feature Transformation:** Features were encoded and scaled as necessary for compatibility with the classification algorithms.

## Managing Class Disparities

### Dataset 1:

- Created synthetic samples for the minority class using the Synthetic Minority Over-sampling Technique (SMOTE), which balanced the distribution of classes.

### Dataset 2:

- The dataset was relatively balanced, but preprocessing was applied to ensure class distributions were optimal for modeling.

## Model Training And Evaluation

### Dataset 1:

- Trained and evaluated six classifiers: Support Vector Machine (SVM), Decision Tree, Random Forest, Naive Bayes and Neural Network
- Split the dataset into training (70%) and testing (30%) sets.
- Employed Stratified K-Fold cross-validation (5 folds) to assess model performance.

### Dataset 2:

1. Trained and evaluated the same classifiers with cross-validation techniques suited for smaller datasets.

2. Used the entire dataset for training and evaluation due to its smaller size.

## Classifiers and configurations

- **SVM:** RBF kernel approximation.
- **Decision Tree:** Limited maximum depth to avoid overfitting.
- **Random Forest:** 100 trees with a maximum depth of 10.
- **Naive Bayes:** classifier with probability based on the Bayes theorem.
- **Neural Network:** 100 neurons in a single hidden layer with ReLU activation.

## RESULTS AND DISCUSSION

Arsenic is a heavy metalloid that can be toxic to the body and has no place in human physiology. Type 2 diabetes is more common in people who have been exposed to high doses of arsenic over an extended period (Fan et al. 2022, Tsai et al. 1999, Guisela et al. 2022, Kile & Christiani 2008). Due to the fact that prolonged exposure to arsenic is associated with impaired glucose tolerance and insulin resistance, two conditions that are known to exist. The characteristic insulin resistance found in people with type 2 diabetes. Uncertainty exists regarding the exact mechanisms by which arsenic influences the development of type 2 diabetes (Castriota et al. 2018, Ghaedrahmat et al. 2021, Dalal et al. 2010, Spratlen et al. 2018). The likelihood of developing diabetes increases with continuous exposure to arsenic and with increasing concentrations of the element, according to weighted data (Spratlen et al. 2019, Wang et al. 2018, Chang et al. 2020). More research that looked into the quantity of arsenic in water samples was included in the review. Arsenic analysis in plasma, blood serum, and urine samples came in second. The inferior classes included food, diet, nails, and tears, in addition to air samples.

## Environmental Exposure to Arsenic and Type 2 Diabetic Mellitus

Long-term exposure to arsenic through drinking water has been linked to an increased incidence of micro and macro vascular complications of diabetes type 2-such as myocardial infarctions, heart failure, stroke, retinopathy, diabetic foot, and polyneuropathy (Jovanović et al. 2019, Hsu et al. 2016, Bräuner et al. 2014, Rahman et al. 1998, Andrew et al. 1998, Chakraborti et al. 2011). This systematic review looked at several studies that looked into the relationship between the prevalence of diabetes and long-term exposure to arsenic via food, drink, and airborne environments (D’Ippoliti et

al. 2010, Huang et al. 2014, Rao et al. 2022). Consuming arsenic-tainted water can lower insulin production and increase insulin resistance, which can lead to beta-cell dysfunction and insulin resistance. Furthermore, oxidative stress and inflammation—both of which are connected to diabetes mellitus—can result from exposure to arsenic (Diaz-Villasenor et al. 2013).

These mechanisms may explain why consuming arsenic-contaminated water results in diabetes and other associated health problems (James et al. 2013, Fevrier-Paul et al. 2021, Drobná et al. 2013, Rahman et al. 1998, Sriparaya et al. 2017). Genetics and drinking water exposure to arsenic were also associated with an increased incidence of diabetes 2. People with particular mutations in the notch Recept (Spangler 2012) or 2 Gene (NOTCH2) were more likely to develop diabetes 2 when exposed to inorganic arsenic. There is a correlation between the death rate from diabetes mellitus and the county-level air concentration of arsenic in each of the 100 counties of North Carolina, in addition to drinking water sources. Furthermore, it is well acknowledged that exposure to particulate matter containing arsenic, beryllium, cadmium, and nickel has a negative effect on health, potentially increasing death rates and elevating the risk of Type 2 diabetes (Spangler 2012, Riseberg et al. 2021).

### Demographic Characteristics and Socio-Economic Status

Based on demographic factors like gender, age, genetics, obesity, and socioeconomic level, some research demonstrates

Table 5: Test Set Accuracy.

Classifier	Dataset 1 Accuracy	Dataset 2 Accuracy
SVM	0.91	1.00
Decision Tree	0.92	1.00
Random Forest	0.98	1.00
Naive Bayes	0.86	1.00
Neural Network	0.93	0.50

a relationship between arsenic exposure and the development of Type 2 diabetes. Regarding this, some findings were noted across many populations, including those in the US, Taiwan, Korea, and China. Diabetes increases the incidence of internal malignancies, such as those of the stomach, colon, liver, pancreas, and lungs. When diabetes patients had elevated arsenic levels, the correlation was especially strong (Hendryx et al. 2021). For instance, the amount of 20 metals in the urine of middle-aged women participating in the study was measured. This finding indicated a link between T2DM in women and the excretion of metals like arsenic (Wang et al. 2020). Thus, to eliminate the accessibility of heavy metals that cause T2DM and ultimately result in mortality, the primary focus needs to be on drinking water, food, and crops. To reduce and assist physicians in identifying the primary causes of diabetes and to identify previous treatments based on reviews and datasets that are currently available, the best machine learning techniques or classifiers were developed. This allowed medical professionals to provide direct or telemedicine care while also lowering global death rates.

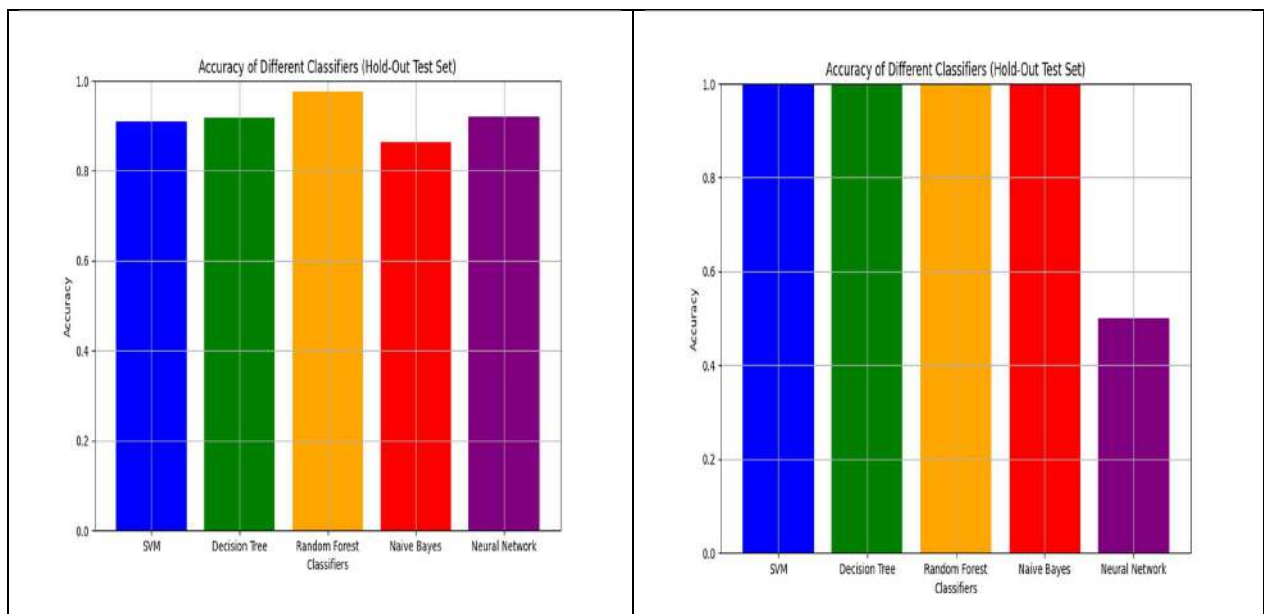


Fig. 3: Accuracy of different classifiers on Dataset 1 and Dataset 2.



Table 6: Cross-Validation Accuracy.

Classifier	Dataset-1 Accuracy	Dataset-1 Std Dev	Dataset-2 Accuracy	Dataset-2 Std Dev
SVM	0.91	0.01	1.00	0.00
Decision Tree	0.92	0.02	1.00	0.00
Random Forest	0.98	0.00	1.00	0.00
Naive Bayes	0.86	0.01	1.00	0.00
Neural Network	0.92	0.02	0.50	0.00

Dataset Results

The test accuracy of five classifiers, SVM, Decision Tree, Random Forest, Naive Bayes, and Neural Network, was evaluated across two datasets and is given in Table 5. On Dataset 1, Random Forest achieved the highest accuracy at 98%, followed by Neural Network (93%), Decision Tree (92%), SVM (91%), and Naive Bayes (86%). In contrast, for Dataset 2, all classifiers except the Neural Network reached 100% accuracy. The Neural Network, however, showed a significant drop to 50% accuracy on Dataset 2, suggesting potential challenges such as overfitting or data imbalance.

Table 7: Confusion Matrices.

Dataset 1

SVM:

	Predicted Non-Diabetic	Predicted Diabetic
Actual Non-Diabetic	1357	45
Actual Diabetic	85	513

Decision Tree:

	Predicted Non-Diabetic	Predicted Diabetic
Actual Non-Diabetic	1360	42
Actual Diabetic	72	526

Random Forest:

	Predicted Non-Diabetic	Predicted Diabetic
Actual Non-Diabetic	1392	10
Actual Diabetic	32	566

Naive Bayes:

	Predicted Non-Diabetic	Predicted Diabetic
Actual Non-Diabetic	1300	102
Actual Diabetic	95	503

Neural Network:

	Predicted Non-Diabetic	Predicted Diabetic
Actual Non-Diabetic	1362	40
Actual Diabetic	72	526

Dataset 2

SVM:

	Predicted Non-Diabetic	Predicted Diabetic
Actual Non-Diabetic	17	0
Actual Diabetic	0	31

Decision Tree:

	Predicted Non-Diabetic	Predicted Diabetic
Actual Non-Diabetic	17	0
Actual Diabetic	0	31

Random Forest:

	Predicted Non-Diabetic	Predicted Diabetic
Actual Non-Diabetic	17	0
Actual Diabetic	0	31

Naive Bayes:

	Predicted Non-Diabetic	Predicted Diabetic
Actual Non-Diabetic	17	0
Actual Diabetic	0	31

Neural Network:

	Predicted Non-Diabetic	Predicted Diabetic
Actual Non-Diabetic	17	0
Actual Diabetic	0	31

The bar graph in Fig. 3 illustrates the accuracy of five classifiers, SVM, Decision Tree, Random Forest, Naive Bayes, and Neural Network, across two datasets. Random Forest consistently achieved the highest accuracy on Dataset 1, while all classifiers except the Neural Network reached 100% accuracy on Dataset 2. The Neural Network’s significant drop in performance on Dataset 2, with only 50% accuracy, stands out, highlighting potential model-specific issues.

In Table 6, the cross-validation accuracy and standard deviation of five classifiers are compared across two datasets. On Dataset 1, Random Forest achieved the highest accuracy (0.98), while Naive Bayes had the lowest (0.86). For Dataset 2, all classifiers except the Neural Network achieved perfect accuracy (1.00) with no variation. The Neural Network showed a notable drop in performance on Dataset 2, with an accuracy of 0.50 and no deviation.

The confusion matrices compare the performance of five classifiers-SVM, Decision Tree, Random Forest, Naive Bayes, and Neural Network—across two datasets, as shown in Table 7. On Dataset 1, Random Forest exhibited the

highest accuracy, with only 10 false positives and 32 false negatives, while Naïve Bayes showed the most errors. For Dataset 2, all classifiers performed flawlessly, correctly classifying both non-diabetic and diabetic cases with no misclassifications.

## Key Findings

### 1. Dataset Characteristics and Performance

- **Dataset 1** (5,000 samples) and **Dataset 2** (48 samples) presented different challenges due to their size and feature composition. Dataset 1, with its larger size and varied features, demonstrated generally lower but still competitive accuracy scores compared to Dataset 2, which, despite its small size, showed perfect classification results for most models.

### 2. Classifier Performance

- **Random Forest** emerged as the most effective classifier for Dataset 1, achieving the highest cross-validation accuracy (0.98) and test set accuracy (0.98). This robustness indicates Random Forest's ability to handle complex feature interactions and its generalization capability.
- For Dataset 2, all classifiers achieved perfect test set accuracy except the neural network. However, permutation testing showed a p-value of 1.0000 for the SVM classifier, suggesting that while the model performed well, the results could be influenced by the small sample size.

### 3. Model Evaluation Metrics

- **Cross-Validation Accuracy:** Random Forest consistently outperformed other models in Dataset 1. For Dataset 2, classifiers achieved perfect accuracy, but this is likely influenced by the small sample size.
- **Confusion Matrices:** The confusion matrices highlighted the models' ability to correctly classify diabetic and non-diabetic instances. For Dataset 1, Random Forest had the lowest number of misclassifications. For Dataset 2, all classifiers achieved perfect results, indicating a lack of variance in the data.

### 4. Feature Importance

- In Dataset 1, Random Forest's feature importance analysis identified Blood Glucose Level, HbA1c Level, and BMI as the most influential features, aligning with clinical expectations. Dataset 2's limited feature set and size did not permit a detailed feature importance analysis.

## Implications

- The findings suggest that while Random Forest is a highly effective algorithm for larger, complex datasets, smaller datasets may yield inflated performance results due to limited data variability. Future research should focus on expanding dataset sizes, exploring additional features, and applying more advanced preprocessing techniques to enhance model performance and generalizability. This research work emphasizes the purpose of the application of data mining techniques in telemedicine.
- In the telemedicine system, regular visits to the hospitals for patients suffering from diseases are minimized since they can be expensive for rural background patients.
- During the COVID-19 pandemic, the physical presence of the patients and doctors became risky. People preferred the Telemedicine system.
- Telemedicine services are done through video conferences & smartphones, which reduce the time and cost to patients.
- Furthermore, the telemedicine system has fast and advantageous characteristics. It can streamline the workflow of hospitals and clinics.
- This method is more useful in natural calamities, floods, war zones, and rural areas all over the world.
- The telemedicine system would make it easier to monitor discharged patients, manage their recovery from disease, and reduce mortality rates.

## CONCLUSIONS

This systematic review and dataset study discusses the relationship between type 2 diabetes and arsenic exposure. Research has indicated that extended exposure to arsenic by ingestion or work-related exposure heightens the likelihood of acquiring Type 2 diabetes. Insulin resistance is thought to be caused by exposure to arsenic, which is thought to alter how the body uses insulin and how it is released. It is linked to inflammation and stress as well. The information now available suggests a possible link between T2DM and environmental arsenic exposure from food, water, and the air. The review reveals a close connection between T2DM and environmental degradation. This study presents a straightforward approach for assessing the prevalence of type 2 diabetes through dataset analysis utilizing different classifiers. It finds that the Random Forest classifier consistently delivers superior performance, achieving perfect accuracy of 100% on both real-time datasets. The research compares various classifiers, including SVM, Random Forest,

Naive Bayes, Neural Network, and Decision Tree, ultimately identifying Random Forest as the most effective method for disease prediction in telemedicine. With accuracy rates of 98% and 100% for online datasets, Random Forest is highlighted as the best option for detecting, controlling, and monitoring prevalent diseases while helping to reduce mortality rates. Thus, data mining techniques emerge as powerful tools for predicting and monitoring diseases within telemedicine systems. Doctors can use these accurate classifiers to help patients lead healthy lives, control the mortality rates in remote areas using telemedicine systems, or use a personal approach. To stop the disease's escalating burden, a fuller understanding of the connection between the environment and type 2 diabetes can assist in developing health-promoting policies and offer opportunities for people to translate their intentions into long-lasting behavioral adjustments.

### Future Work

Further investigations are needed to:

- **Expand Dataset Size:** Get more samples to make sure the models are reliable and applicable to a wider range of situations.
- **Explore Additional Features:** Integrate more relevant features that could enhance predictive performance.
- **Hyper-parameter Tuning:** Perform extensive hyper-parameter optimization to further improve model accuracy.
- **Advanced Techniques:** Implement ensemble methods and deep learning approaches to address limitations observed in smaller datasets.

For future research, several key areas warrant attention: First, expanding the dataset size is crucial to obtain a more comprehensive range of samples, which will enhance the reliability and generalizability of the models across diverse situations. Second, exploring additional relevant features may significantly improve predictive performance, as incorporating more data points can provide a richer context for classification. Third, hyperparameter tuning should be prioritized to optimize model accuracy, allowing for fine-tuning of the algorithms to achieve better results. Finally, implementing advanced techniques, such as ensemble methods or deep learning approaches, can help overcome the limitations associated with smaller datasets and improve predictive capabilities in the context of telemedicine. This study underscores the importance of selecting appropriate models and evaluation techniques based on dataset characteristics and highlights the need for careful consideration of model performance metrics, especially in cases with small sample sizes.

### REFERENCES

- Agardh, E., Allebeck, P., Hallqvist, J., Moradi, T. and Sidorchuk, A., 2011. Type 2 diabetes incidence and socio-economic position: A systematic review and meta-analysis. *International Journal of Epidemiology*, 40(3), pp.804–818. DOI
- Andrew, A.S., Jewell, D.A., Mason, R.A., Whitfield, M.L., Moore, J.H. and Karagas, M.R., 2008. Drinking water arsenic exposure modulates gene expression in human lymphocytes from a US population. *Environmental Health Perspectives*, 116(4), pp.524–531.
- Armghan, J., Logeshwaran, S.M., Sutharshan, K., Aliqab, M., Alsharari, M. and Patel, S.K., 2023. Design of biosensor for synchronized identification of diabetes using deep learning. *Results in Engineering*, 20, p.1382.
- Barbagallo, M., Veronese, N. and Dominguez, L.J., 2022. Magnesium in type 2 diabetes mellitus, obesity, and metabolic syndrome. *Biomedicine and Pharmacotherapy*, 87(3), p.714.
- Black, J.L. and Macinko, J., 2008. Neighborhoods and obesity. *Nutrition Reviews*, 66(1), pp.2–20. DOI
- Bräuner, E.V., Nordsborg, R.B., Andersen, Z.J., Tjønneland, A., Loft, S. and Raaschou-Nielsen, O., 2014. Long-term exposure to low-level arsenic in drinking water and diabetes incidence: A prospective study of the diet, cancer, and health cohort. *Environmental Health Perspectives*, 122(10), pp.1059–1065.
- Castriota, F., Acevedo, J., Ferreccio, C., Smith, A.H., Liaw, J., Smith, M.T. and Steinmaus, C., 2018. Obesity and increased susceptibility to arsenic-related type 2 diabetes in Northern Chile. *Environmental Research*, 167, pp.248–254.
- Chakraborti, D., Singh, S.K., Rashid, M.H. and Rahman, M.M., 2011. Arsenic: Occurrence in groundwater. *Encyclopedia of Environmental Health*, 2, p.117.
- Chakraborty, S., Panda, A.R., Vadiya, P., Samal, S., Gupta, I. and Ray, N.K., 2023. Predicting diabetes: A comparative study of machine learning models. *2023 OITS International Conference on Information Technology (OCIT)*, Raipur, India, pp.743–748.
- Chang, A., Ridpath, A., Carpenter, J., Kieszak, S., Sircar, K., Espinosa-Bode, A., Nelson, D. and Martin, C., 2020. Urine bisphenol A and arsenic levels in residents of the Cheyenne River Sioux Tribe, South Dakota, with and without diabetes. *Journal of Medical Toxicology*, 16, pp.276–283.
- Chatterjee, S., Khunti, K. and Davies, M.J., 2017. Type 2 diabetes. *The Lancet*, 389(10085), pp.2239–2251. DOI
- Colwell, M.L., Flack, N., Rezabek, A. and Faulk, C., 2023. Intergenerational arsenic exposure on the mouse epigenome and metabolic physiology. *Environmental and Molecular Mutagenesis*, 64(2), pp.72–87.
- Dalal, B., Nayak, K., Gangopadhyay, P. and Mukherjee, A., 2010. Identification of indicators of arsenic-induced hepatic damage in humans. *Internet Journal of Toxicology*, 7(1), p.71.
- Diaz-Villasenor, A., Cruz, L., Cebrian, A., Hernandez-Ramirez, R.U., Hiriart, M., Garcia-Vargas, G., Bassol, S., Sordo, M., Gandolfi, A.J., Klimecki, W.T. and Lopez-Carillo, L., 2013. Arsenic exposure and calpain-10 polymorphisms impair the function of pancreatic beta-cells in humans: A pilot study of risk factors for T2DM. *PLoS One*, 8(1), p.642.
- D'Ippoliti, D., Santelli, E., De Sario, M., Scorticini, M., Davoli, M. and Michelozzi, P., 2015. Arsenic in drinking water and mortality for cancer and chronic diseases in Central Italy, 1990–2010. *PLoS One*, 10(9), p.e013.
- Drobná, Z., Del Razo, L.M., García-Vargas, G.G., Sánchez-Peña, L.C., Barrera-Hernández, A. and Stýblo, M., 2013. Environmental exposure to arsenic, AS3MT polymorphism and prevalence of diabetes in Mexico. *Journal of Exposure Science and Environmental Epidemiology*, 23(2), pp.151–155.
- Fan, C., Zhan, Z., Zhang, X., Lou, Q., Guo, N., Su, M., Gao, Y., Qin, M.,

- Wu, L., Huang, W. and Zhang, M., 2022. Research for type 2 diabetes mellitus in endemic arsenic areas in central China: Role of low level of arsenic exposure and KEAP1 rs11545829 polymorphism. *Archives of Toxicology*, 96(6), pp.1673–1683.
- Fevrier-Paul, A.K., Soyibo, K., De Silva, N., Mitchell, S., Nwokocha, C. and Voutchkov, M., 2021. Addressing the challenge of potentially hazardous elements in the reduction of hypertension, diabetes, and chronic kidney disease in the Caribbean. *Journal of Health Pollution*, 11(30), Article 210613.
- Ghaedrahmat, Z., Cheraghian, B., Jaafarzadeh, N., Takdastan, A., Shabbazian, H.B. and Ahmadi, M., 2021. Relationship between urinary heavy metals with metabolic syndrome and its components in population from Hoveyeh cohort study: A case-control study in Iran. *Journal of Trace Elements in Medicine and Biology*, 66, Article 126757.
- Gray-Webb, T.L., Suglia, S.F. and Tehranifar, P., 2013. Social epidemiology of diabetes and associated conditions. *Current Diabetes Reports*, 13(6), pp.850–859.
- Guisela, B.Z., Ohana, N.D.A., Dalvani, S.D., Fermin, G.V., Francisco Hm, L. and Luis, N.-G., 2022. Adsorption of arsenic anions in water using modified lignocellulosic adsorbents. *Results in Engineering*, 13, p.340.
- Gupta, S., Sharma, N., Arora, S. and Verma, S., 2024. Diabetes: A review of its pathophysiology and advanced methods of mitigation. *Current Medical Research and Opinion*, 40(5), pp.773–780.
- Halim, M. and Halim, A., 2019. The effects of inflammation, aging, and oxidative stress on the pathogenesis of diabetes mellitus (type 2 diabetes). *Diabetes & Metabolic Syndrome: Clinical Research & Reviews*, 13(2), pp.1165–1172.
- Hendryx, M., Luo, J., Chojenta, C. and Byles, J.E., 2021. Exposure to heavy metals from point pollution sources and risk of incident type 2 diabetes among women: A prospective cohort analysis. *International Journal of Environmental Health Research*, 31(4), pp.453–464.
- Hsu, L.I., Cheng, Y.W., Chen, C.J., Wu, M.M., Hsu, K.H. and Chiou, H.Y., 2016. Cumulative arsenic exposure is associated with fungal infections: Two cohort studies based on southwestern and northeastern basins in Taiwan. *Environmental International*, 96, pp.173–179.
- Hsu, L.I., Wang, Y.H., Chiou, H.Y., Wu, M.M., Yang, T.Y. and Chen, Y.H., 2013. The association of diabetes mellitus with subsequent internal cancers in the arsenic-exposed area of Taiwan. *Journal of Asian Earth Sciences*, 73, pp.452–459.
- Huang, J.W., Cheng, Y.Y., Sung, T.C., Guo, H.R. and Shihannopkao, S., 2014. Association between arsenic exposure and diabetes mellitus in Cambodia. *BioMed Research International*, 2014, p.54.
- James, K.A., Marshall, J.A., Hokanson, J.E., Meliker, J.R., Zerbe, G.O. and Byers, T.E., 2013. A case-cohort study examining lifetime exposure to inorganic arsenic in drinking water and diabetes mellitus. *Environmental Research*, 123, pp.33–38.
- Jovanović, D., Paunović, K., Manojlović, D. and Rasic-Milutinović, Z., 2019. Arsenic exposure from drinking water and the occurrence of micro- and macrovascular complications of type 2 diabetes. *Environmental Arsenic in a Changing World*, CRC Press, pp.331–332.
- Kahn, S.E., Cooper, M.E. and Del Prato, S., 2021. Pathophysiology and treatment of type 2 diabetes: Perspectives on the past, present, and future. *Lancet*, 383, pp.1068–1083.
- Kakavandi, N.R., Mousavi, T., Asadi, T., Moradi, A., Esmaeili, M., Sezavar, A.H., Nikfar, S. and Abdollahi, M., 2023. An updated systematic review and dose-response meta-analysis on the relation between exposure to arsenic and risk of type 2 diabetes. *Toxicology Letters*, 384, pp.115–127. DOI.
- Ke, C., Narayan, K.V., Chan, J.C., Jha, P. and Shah, B.R., 2022. Pathophysiology, phenotypes and management of type 2 diabetes mellitus in Indian and Chinese populations. *Nature Reviews Endocrinology*, 18(7), pp.413–432.
- Kile, M.L. and Christiani, D.C., 2008. Environmental arsenic exposure and diabetes. *JAMA*, 300(7), pp.845–846.
- Kumar, A., Gangwar, R., Ahmad Zargar, A., Kumar, R. and Sharma, A., 2024. Prevalence of diabetes in India: A review of IDF Diabetes Atlas 10th Edition. *Current Diabetes Reviews*, 20(1), e130423215752.
- Li, W., Li, Z., Yan, Y., Zhang, J., Zhou, Q., Jia, C., Xu, Y., Cui, H., Xie, S., Liu, Q. and Guan, Y., 2023. Urinary arsenic metabolism, genetic susceptibility, and their interaction on type 2 diabetes. *Chemosphere*, 345, Article 140536.
- Nikraves, M., Mahdavinia, M., Neisi, N., Khorsandi, L. and Khodayar, M.J., 2023. Citicoline ameliorates arsenic-induced hepatotoxicity and diabetes in mice by overexpression of VAMP2, PPAR- $\alpha$ , AS3MT, and SIRT3. *Pesticide Biochemistry and Physiology*, 192, p.391.
- Northridge, M.E., Sclar, E.D. and Biswas, P., 2003. Sorting out the connections between the built environment and health: A conceptual framework for navigating pathways and planning healthy cities. *Journal of Urban Health*, 80, pp.556–568.
- Nurchi, V.M., Buha Djordjevic, A., Crisponi, G., Alexander, J., Bjørklund, G. and Aaseth, J., 2020. Arsenic toxicity: Molecular targets and therapeutic agents. *Biomolecules*, 10(2), p.235.
- Poortinga, W., 2006. Perceptions of the environment, physical activity, and obesity. *Social Science & Medicine*, 63, pp.2835–2846.
- Rahman, M., Tondel, M., Ahmad, S.A. and Axelsson, O., 1998. Diabetes mellitus associated with arsenic exposure in Bangladesh. *American Journal of Epidemiology*, 148(2), pp.198–203.
- Rahman, M., Tondel, M., Chowdhury, I.A. and Axelsson, O., 1999. Relations between exposure to arsenic, skin lesions, and glucosuria. *Occupational and Environmental Medicine*, 56(4), pp.277–281.
- Rahman, T., 2023. A proposed method to identify the occurrence of diabetes in the human body using data analysis. *International Journal of Scientific Research in Science, Engineering and Technology (IJSRSET)*, 10(3), pp.399–429.
- Rahmani, A., Khamutian, S., Doosti-Irani, A., Shokohizadeh, M.J., Shirmohammadi-Khorram, N., Sahraei, F., Khodabakhshi, M. and Ahangaran, N., 2023. The association of arsenic exposure with mortality due to cancer, diabetes, Alzheimer's, and congenital anomalies using Poisson regression. *Scientific Reports*, 13(1), p.456.
- Rangel-Moreno, K., Gamboa-Loira, B., López-Carrillo, L. and Cebrián, M.E., 2022. Prevalence of type 2 diabetes mellitus in relation to arsenic exposure and metabolism in Mexican women. *Environmental Research*, 210, p.48.
- Rao, N.S., Raju, G.N., Tiwari, M., Naidu, B. and Sarita, P., 2022. Serum elemental analysis of type 2 diabetes patients using SRXRF. *Biological Trace Element Research*, 200(4), pp.1485–1494.
- Riseberg, E., James, K.A., Woodin, M., Melamed, R., Alderete, T. and Corlin, L., 2021. Multipollutant, longitudinal analysis of the association between urinary tungsten and incident diabetes in a rural population. *Environmental Epidemiology*, 5(6), p.615.
- Sallis, J.F., Floyd, M.F., Rodriguez, D.A. and Saelens, B.E., 2012. Role of built environments in physical activity, obesity, and cardiovascular disease. *Circulation*, 125, pp.726–737.
- Sallis, J.F., Owen, N. and Fisher, E.B., 2008. Ecological models of health behavior. *Health Behavior and Health Education: Theory, Research, and Practice*, 4, pp.465–486.
- Schulz, M., Romppel, M. and Grande, G., 2016. Built environment and health: A systematic review of studies in Germany. *Journal of Public Health*, 18, pp.1–8.
- Shokat, S., Iqbal, R., Riaz, S. and Yaqub, A., 2024. Association between arsenic toxicity, AS3MT gene polymorphism, and the onset of type 2 diabetes. *Biological Trace Element Research*, 202(4), pp.1550–1558.
- Spangler, J.G., 2012. Diabetes mortality and environmental heavy metals in North Carolina counties: An ecological study. *Dubai Diabetes and Endocrinology Journal*, 20, pp.71–74.
- Spratlen, M.J., Grau-Perez, M., Umans, J.G., Yracheta, J., Best, L.G. and Francesconi, K., 2018. Arsenic, one-carbon metabolism and diabetes-



- related outcomes in the Strong Heart Family Study. *Environmental International*, 121, pp.728–740.
- Spratlen, M.J., Grau-Perez, M., Umans, J.G., Yracheta, J., Best, L.G. and Francesconi, K., 2019. Targeted metabolomics to understand the association between arsenic metabolism and diabetes-related outcomes: Preliminary evidence from the Strong Heart Family Study. *Environmental Research*, 168, pp.146–157.
- Sripaoraya, K., Siri Wong, W., Pavitratanon, S. and Chapman, R.S., 2017. Environmental arsenic exposure and risk of diabetes type 2 in Ron Phibun subdistrict, Nakhon Si Thammarat Province, Thailand: Unmatched and matched case-control studies. *Risk Management and Healthcare Policy*, 2017, pp.41–48.
- Teimoory, G.K. and Keyvanpour, M.R., 2024. An effective feature selection for Type II diabetes prediction. *Proceedings of the 10th International Conference on Web Research (ICWR)*, Tehran, Iran, pp.64–69.
- Tinkelman, N.E., Spratlen, M.J., Domingo-Relloso, A., Tellez-Plaza, M., Grau-Perez, M. and Francesconi, K.A., 2020. Associations of maternal arsenic exposure with adult fasting glucose and insulin resistance in the Strong Heart Study and Strong Heart Family Study. *Environmental International*, 137, p.553.
- Tsai, S.M., Wang, T.N. and Ko, Y.C., 1999. Mortality for certain diseases in areas with high levels of arsenic in drinking water. *Archives of Environmental Health*, 54(3), pp.186–193.
- Uddin, M. and Ali, A., 2023. Diabetes prediction with machine learning techniques. *2023 Global Conference on Information Technologies and Communications (GCITC)*, Bangalore, India, p.16.
- Wang, X., Karvonen-Gutierrez, C.A., Herman, W.H., Mukherjee, B., Harlow, S.D. and Park, S.K., 2020. Urinary metals and incident diabetes in midlife women: Study of Women's Health across the Nation (SWAN). *BMJ Open Diabetes Research and Care*, 8(1), p.233.
- Wang, X., Mukherjee, B. and Park, S.K., 2018. Associations of cumulative exposure to heavy metal mixtures with obesity and its comorbidities among US adults in NHANES 2003–2014. *Environmental International*, 121, pp.683–694.

# Assessment of Bioefficacy of *Achromobacter xylosoxidans* KUESCCHK-6, Isolated from Textile Contaminated Soil, in Treating Textile Effluent and its Impact on *Vigna mungo*

C. Chaithra<sup>1</sup> and Hina Kousar<sup>†</sup>

Department of P.G. Studies and Research in Environmental Science, Kuvempu University, Shivamogga District, 577451, Karnataka State, India

<sup>†</sup>Corresponding author: Hina Kousar; eshinakousar@gmail.com

**Abbreviation:** Nat. Env. & Poll. Technol.  
**Website:** www.neptjournal.com

Received: 03-08-2024

Revised: 06-09-2024

Accepted: 23-09-2024

## Key Words:

Bioremediation  
 Textile effluent  
*Achromobacter xylosoxidans*  
 Phytotoxicity study  
*Vigna mungo*

## Citation for the Paper:

Chaithra, C. and Kousar, H., 2025. Assessment of bioefficacy of *Achromobacter xylosoxidans* KUESCCHK-6, isolated from textile contaminated soil, in treating textile effluent and its impact on *Vigna mungo*. *Nature Environment and Pollution Technology*, 24(2), p. B4253. <https://doi.org/10.46488/NEPT.2025.v24i02.B4253>

Note: From year 2025, the journal uses Article ID instead of page numbers in citation of the published articles.



Copyright: © 2025 by the authors

Licensee: Technoscience Publications

This article is an open access article distributed under the terms and conditions of the Creative Commons Attribution (CC BY) license (<https://creativecommons.org/licenses/by/4.0/>).

## ABSTRACT

Textile effluents are major pollutants with varied contaminants. Traditional treatment methods are costly and produce sludge, necessitating alternative, eco-friendly solutions. Biological treatment methods are receiving attention as it is proven to be cheap, environment-friendly, and highly efficient treatment methods for dye effluent on an industrial scale as compared to the other available treatment methods. The present work evaluates the bioremediation of textile effluent using a pure culture of a bacterium isolated from the soil samples contaminated with textile wastewater. The strain was identified as *Achromobacter xylosoxidans* KUESCCHK-6 (GenBank Accession Number: OM475749) through 16S rRNA molecular analysis. This bacterial strain was used to treat textile effluent under specific conditions: glucose as the carbon source, urea as the nitrogen source, a C/N ratio of 6:1, a temperature of 35°C, a pH of 8.5, and a static incubation period of 5 days. The results indicated that the strain effectively reduced various physiochemical parameters of the raw textile wastewater: color by 87.94%, BOD by 80.61%, COD by 80.96%, EC by 73.11%, fluoride by 81.15%, phosphate by 79.57%, sodium by 76.88%, and turbidity by 81.02%. Additionally, metal ions, including iron, were removed by 84.83%, while other metals, such as zinc, nickel, manganese, copper, lead, cadmium, total chromium, arsenic, barium, cobalt, and boron, were reduced to below-detectable limits. Phytotoxicity tests confirmed the non-toxic nature of the treated effluent. Overall, the study concludes that *Achromobacter xylosoxidans* KUESCCHK-6 is a promising candidate for the bioremediation of textile industrial effluents, with potential for commercial application.

## INTRODUCTION

Textiles rank second after food among the substantial desires of human life. The textile industry converts fibers into yarn and fabrics, applying dyes and finishes through various processes. Numerous dyes and chemicals used in wet processing generate wastewater that poses environmental risks. Therefore, it is crucial to thoroughly treat this wastewater before release. Textile effluents are highly heterogeneous, containing substantial amounts of toxic and hard-to-treat substances from dyeing and finishing operations (Table 1).

The primary issue with textile industry wastewater is the use of dyes to impart color. Effluents contain various contaminants, including surfactants, salts, heavy metals, enzymes, and oxidizing and reducing agents. Over time, the release of these polluted effluents degrades the quality of nearby surface and groundwater. Untreated effluents from harmful and persistent chemicals in wet processing are especially detrimental to the environment (Madhav et al. 2018).

Textile effluents contain trace metals like Cr, As, Cu, and Zn, which can harm the environment. Heavy metals pose significant environmental and health risks due

Table 1: Total water consumed during the wet process.

Process	Water Consumption (L.1000 <sup>-1</sup> kg of products)
Sizing	500-8200
Desizing	2500-21000
Scouring	20000-45000
Bleaching	2500-25000
Mercerizing	17000-32000
Dyeing	10000-300000
Printing	8000-16000

to their ability to disrupt cellular structures and biomolecules. They bind strongly to essential metal ion sites, destabilizing cellular components like enzymes, DNA, and RNA, leading to replication errors, mutations, and potentially cancer. These metals are toxic, persistent, and accumulate in living organisms. Toxic heavy metals, such as chromium, nickel, zinc, cadmium, lead, and others, can hinder plant growth by adversely affecting photosynthesis, enzymatic activities, and mineral nutrition (Kuanar et al. 2022). The eradication of toxic textile dyes through wastewater treatment is essential to mitigate their harmful environmental and biological impacts. Synthetic dyes, prevalent in industries like fabric printing and leather coloring, are major pollutants, contributing to significant environmental damage. Textile effluents, rich in organic and inorganic pollutants, heavy metals, and colorants present serious ecological risks due to their high pH, color, and elevated COD and BOD levels. In aquatic environments, these dyes can form non-biodegradable, hazardous by-products. Given their mutagenic and carcinogenic properties, decolorization of these effluents is crucial before discharge (Verma et al. 2022).

Pollutants from the textile industry alter the physicochemical parameters of receiving water bodies. Parameters such as color, odor, temperature, chemical oxygen demand (COD), biological oxygen demand (BOD), pH, fats, oil, nitrogen, phosphorus, total suspended solids (TSS), total solids (TS), total dissolved solids (TDS), sulfate, calcium, magnesium, and chloride can reach their highest levels according to Bureau of Indian Standard limits (Kousar et al. 2020).

Different physicochemical methods, such as coagulation, adsorption, filtration, and ion exchange, have been developed for treating textile effluents. However, membrane filtration faces limitations due to cost and clogging issues, making adsorption a preferable method. Despite this, biological treatment methods are superior to chemical processes. They generate fewer by-products like solid wastes, have lower operational costs, and achieve complete mineralization of dyes, making them more effective for dye removal compared to physicochemical treatments (Adane et al. 2021).

The inefficiency or lack of wastewater treatment facilities is the main cause of water pollution. To achieve zero pollution, adopting alternative technologies is essential. The current focus is on sustainable wastewater treatment techniques. Bioremediation is a promising option due to its ability to detoxify effluents and its environmentally friendly approach. This process uses naturally occurring microorganisms and plants to break down hazardous substances into less toxic or non-toxic forms. It is typically more cost-effective than other remediation methods and avoids issues like atmospheric emissions and waste generation. Numerous studies have shown the effectiveness of microremediation techniques, using various microorganisms (bacteria and fungi) to remove a wide range of pollutants from industrial wastewater (Chaithra et al. 2022).

Bioremediation is a pollution remediation technique that employs naturally occurring or genetically modified organisms to degrade or transform toxic chemicals into less toxic or non-toxic substances. This method leverages bacteria, fungi, and other biological agents to remove pollutants from contaminated sites by stimulating microorganisms to use the pollutants as a source of food and energy (Chaithra & Kousar 2022).

Microorganisms like *Shewanella oneidensis*, *Pseudomonas delafieldii*, *Dehalococcoides*, *Lysinibacillus*, and species of *Sphingomonas* are effectively used in the removal of hexavalent chromium, dibenzothiophene, trichloroethane, nickel, and carbazole, respectively, in the presence of nanoparticles (Hemalatha et al. 2022).

Molecular-based techniques offer new possibilities for detecting specific microorganisms in soil or effluent and quantifying target gene expression. Recent advances in PCR amplification of the 16S rRNA gene and sequence analysis have enhanced the identification of unknown bacterial isolates. The 16S rRNA gene contains conserved sequences across all bacteria, aiding in identification. Bioremediation leverages the catalytic abilities of microorganisms to accelerate pollutant degradation, using compounds in influent waste as nutrients. The Basic Local Alignment Search Tool (BLAST) compares partial sequences to the GenBank database to identify phylogenetic relatives. Utilizing microbial communities from textile effluents for bioremediation is promising due to their genetic and biochemical adaptations to toxic compounds. Effective *in-situ* bioremediation requires sufficient indigenous microbial populations with strong degradation capacities and suitable environmental conditions (Chaithra et al. 2023).

The current research aims to isolate, identify, and describe indigenous bacteria from textile industry effluent-contaminated soil using 16S rRNA sequencing. These

identified bacteria will then be utilized for the treatment of textile effluent under optimal conditions. The effectiveness of the treatment process will be evaluated through a phytotoxicity study on *Vigna mungo* using the treated effluent.

## MATERIALS AND METHODS

### Effluent Sample Collection

The effluent for this study was collected from a textile mill in Bangalore, Karnataka, using the grab sampling technique at the inlet of an effluent treatment plant. The samples were immediately transported to the laboratory of the Department of P.G. Studies and Research in Environmental Science at Kuvempu University for further analysis. To preserve the samples, they were stored in a refrigerator at 4°C.

### Isolation of Bacterial Isolate from Soil

1g soil sample was suspended in 10 mL of sterile distilled water and further diluted. From each dilution, 100µl was spread on Petri plates containing 20 mL of sterile Nutrient Agar Media (NAM) using the L-Rod (spread plate technique) and incubated at 37°C for 24 h. Bacterial growth was observed and sub-cultured for pure culture, achieved through the quadrant streaking method (Aneja 2018).

### Identification, Morphological Characterization, and Biochemical Characterization of Isolated Bacterial Strain

The study focused on examining various characteristics of a bacterial colony, including color, shape, margin, elevation, surface, and arrangement. Standard gram staining procedures were used for the morphological characterization of the isolate. Once a pure culture was obtained, biochemical methods were employed to identify the bacterial culture. The isolated strain was preserved on a nutrient agar slant and stored in a refrigerator at 4°C. Both macroscopic and microscopic analysis, along with biochemical tests and molecular methods, were used to further characterize the isolated bacterial strain. The results were compared with those in Bergey (1994). Biochemical tests conducted included starch hydrolysis, gelatin hydrolysis, citrate utilization, nitrate reduction, the urease test, the methyl red test, the indole production test, the catalase test, the oxidase test, and hydrogen sulfide production. These tests followed the methodologies described by Cappuccino & Sherman (2013).

### Isolation, identification, and Phylogenetic Analysis Using 16S rRNA Gene Sequencing

The National Center for Biotechnology Information (NCBI)

database and MEGA version 5 verified the identity of ITS sequence fragments using the Basic Local Alignment Search Tool (BLAST) in GenBank. BLASTn in NCBI was used for searches. Additionally, 16S ribosomal RNA (rRNA) gene sequencing, a common method for bacterial identification and phylogenetic analysis, was performed. Purified 16S rRNA gene sequences were obtained and aligned with homologous sequences using NCBI BLAST. Clustal W software aligned the sequences based on maximum identity scores. MEGA 7 was then used to generate a distance matrix and construct a phylogenetic tree for accurate classification.

### Determination of Optimal Growth Conditions for Isolated Bacterial Strain

The growth characteristics of the bacterial isolate were analyzed by measuring biomass in g/L. The analysis was conducted at pH levels of 6.0 to 10.0 and temperatures of 25°C to 45°C, using nutrient broth for growth. Various carbon sources (glucose, fructose, sucrose, maltose, lactose) and nitrogen sources (peptone, beef extract, urea, yeast extract) were tested. The carbon to nitrogen (C/N) ratio was optimized at concentrations of 1:1, 2:1, 4:1, 8:1, and 16:1. After a 5-day incubation period under these varying conditions, biomass was measured. The optimal conditions for the highest biomass production were identified as the best for removing color and various physico-chemical characteristics from textile industry effluent.

### Experimental Setup for Degradation Studies

Bioremediation of textile industry effluent was undertaken at the laboratory scale. The effluent was diluted into three dilutions: 25%, 50%, and 75%, using either distilled water or deionized water. The purpose of dilution was to investigate the degradation efficiency of organisms at varying concentrations. Under aseptic conditions, 5mL of spore suspension from each organism was introduced into the effluent treatment systems (5mL/L). Treatment was then carried out for 5 days under static conditions under optimal conditions for the organisms. Static conditions were preferred to facilitate biofilm formation and enhance organism efficiency in pollution remediation. Following treatment, the effluent was analyzed for physico-chemical parameters.

The formula used to calculate the percentage reduction in physico-chemical parameters after treatment with the study microorganisms is as follows:

$$\text{Reduction \%} = \frac{\text{Initial value} - \text{Final value}}{\text{Initial value}} \times 100$$



### Physicochemical Characterization and Color Analysis

The effluent's physico-chemical properties were analyzed in the laboratory according to APHA (2017) standards (Table 2). Decolorization was assessed spectrophotometrically by measuring the absorbance peak of untreated effluent at 470 nm, expressed in mg/L. Post-treatment, samples were centrifuged at 8000 rpm, and the supernatant's absorbance was measured using a UV-visible spectrophotometer at 470 nm. The percentage of decolorization was then calculated using a specific formula.

$$\% \text{ Decolourization} = \frac{(C_0 - C_e)}{C_0} \times 100$$

Where,  $C_0$  is the initial concentration of colour ( $\text{mg.L}^{-1}$ )

$C_e$  is the color concentration after treatment ( $\text{mg.L}^{-1}$ )  
(Sharma et al. 2010)

### Bacterial Cell Counting Using Dilution Technique

Serial dilutions of a bacterial suspension were made across 10 dilution blanks. Samples from each dilution were plated on

nutrient agar petri dishes. After incubating for 24-48 hours, colonies were counted using a colony counter. The number of organisms per plate was calculated by multiplying the colony count by the dilution factor, and the cell concentration per milliliter in the spore suspension was determined using the provided formula.

$$\text{Number of cells/ mL} = \frac{\text{Number of colonies}}{\text{Amount plated} \times \text{dilution}}$$

### Phytotoxicity Studies of Treated Effluent

To assess the toxicity of treated textile industry effluent, phytotoxicity studies were conducted using *Vigna mungo* seeds at room temperature. The experiments were primarily focused on studying seed germination and root elongation. Healthy, uniform seeds were washed and sterilized at  $24^\circ\text{C}$  for 30 minutes, and 10 mature seeds were used per test. Daily, 10mL of treated effluent, untreated effluent, and distilled water (control) were administered to observe effects on seed germination and growth over a week. The number of germinated seeds, root, and shoot lengths were recorded.

Table 2: Standard methods adopted for physico-chemical characterization of textile industry effluent.

Sl. No.	Parameter	Methods APHA (2017)	Instrument Used	Units
1.	Color	Spectrophotometric Method	Spectrophotometer	$\text{mg.L}^{-1}$
2.	Electrical Conductivity	Electrometric Method	Conductivity Meter	$\mu\text{mhos.cm}^{-1}$
3.	BOD	Winkler's Method	Titration	$\text{mg.L}^{-1}$
4.	COD	Potassium dichromate Method	COD reflux	$\text{mg.L}^{-1}$
5.	Turbidity	Turbidometric Method	Turbidity meter	NTU
6.	Phosphate	Spectrophotometric Method	Spectrophotometer	$\text{mg.L}^{-1}$
7.	Fluoride	SPANDA method	Spectrophotometer	$\text{mg.L}^{-1}$
8.	Iron	Spectrophotometric Method	Spectrophotometer	$\text{mg.L}^{-1}$
9.	Sodium	Flame Photometry	Flame atomic emission Spectrometry	$\text{mg.L}^{-1}$
10.	Potassium	Flame Photometry	Flame atomic emission spectrometry	$\text{mg.L}^{-1}$
11.	Manganese	Atomic Absorption Method	Atomic Absorption Spectrometry	$\text{mg.L}^{-1}$
12.	Zinc	Atomic Absorption Method	Atomic Absorption Spectrometry	$\text{mg.L}^{-1}$
13.	Nickel	Atomic Absorption Method	Atomic Absorption Spectrometry	$\text{mg.L}^{-1}$
14.	Cadmium	Atomic Absorption Method	Atomic Absorption Spectrometry	$\text{mg.L}^{-1}$
15.	Arsenic	Atomic Absorption Method	Atomic Absorption Spectrometry	$\text{mg.L}^{-1}$
16.	Lead	Atomic Absorption Method	Atomic Absorption Spectrometry	$\text{mg.L}^{-1}$
17.	Total Chromium	Atomic Absorption Method	Atomic Absorption Spectrometry	$\text{mg.L}^{-1}$
18.	Barium	Atomic Absorption Method	Atomic Absorption Spectrometry	$\text{mg.L}^{-1}$
19.	Cobalt	Atomic Absorption Method	Atomic Absorption Spectrometry	$\text{mg.L}^{-1}$
20.	Copper	Atomic Absorption Method	Spectrophotometer	$\text{mg.L}^{-1}$
21.	Boron	Curcumin method	Spectrophotometer	$\text{mg.L}^{-1}$
22.	Spore Count	Haemocytometer Chamber	Haemocytometer	Spores. $\text{mL}^{-1}$

Results were presented using established methods to assess seed germination index (GI), relative seed germination (RSG), and relative root elongation (RRE).

$$\text{RSG}(\%) =$$

$$\frac{\text{Number of seeds germinated in the sample extracted}}{\text{Number of seeds germinated in the control}} \times 100$$

$$\text{RRE}(\%) =$$

$$\frac{\text{Mean root elongation in the sample extract}}{\text{Mean root elongation in the control}} \times 100$$

$$\text{GI}(\%) =$$

$$\frac{(\% \text{ Seed germination}) \times (\% \text{ Root elongation})}{100}$$

## RESULTS AND DISCUSSION

### Isolation of Bacteria

A bacterial colony was isolated from the effluent based on its unique colonial characteristics observed on a NAM. Gram staining tests indicated that the isolate exhibited a gram-negative reaction with smooth, bacilli-shaped morphology (Fig. 1). This isolate displayed distinct morphological and colonial features. To identify the bacteria, various biochemical tests were conducted, and the responses to different biochemical compounds were assessed. By consulting Bergey's Manual of Systematic Bacteriology, it was determined that the isolate belonged to the genus *Achromobacter*.

Table 3 summarizes the biochemical characteristics of the bacterial strain isolated from textile effluent-contaminated soil. The strain tested negative for starch hydrolysis, gelatin hydrolysis, methyl red, and indole production, indicating it does not break down starch or gelatin, perform mixed-acid fermentation, or produce indole. Conversely, it tested positive for citrate utilization, nitrate reduction, urease activity, catalase, and oxidase, showing its ability to use citrate as a carbon source, reduce nitrate, hydrolyze urea, and produce enzymes involved in hydrogen peroxide breakdown and cytochrome c oxidation. The strain was also negative for hydrogen sulfide production, indicating it does not produce this compound from sulfur-containing sources. These results reflect the strain's specific metabolic capabilities and potential for bioremediation applications.

Table 4 summarizes the morphological features of the bacterial strain isolated from textile effluent-contaminated soil. On solid media, the colonies of the strain appear round in shape, with a smooth texture and a creamy color.

Microscopically, the cells are rod-shaped and exhibit motility, which indicates that the strain is capable of moving. Additionally, the strain does not form spores, as indicated by a negative result for spore formation. These morphological characteristics provide a basic identification framework for the bacterial strain and offer insight into its growth patterns and structural features. The results revealed unique morphological and biochemical characteristics, including colony traits, suggesting distinct structures and functions.

The 16S rRNA sequence of the bacterial isolate was deposited in GenBank, identifying it as *Achromobacter xylosoxidans* KUESCCHK-6 (Accession number-OM475749) with 100% similarity in partial gene sequencing. The evolutionary relationship of this bacterial strain with



Fig. 1: Macroscopic and microscopic observation of isolated strain.

Table 3: Biochemical characteristics of the isolated strain.

Sl. No.	Biochemical Test	Bacterial Isolate
1.	Starch hydrolysis	-
2.	Gelatin hydrolysis	-
3.	Citrate utilization	+
4.	Nitrate reduction	+
5.	Urease	+
6.	Methyl red	-
7.	Indole production	-
8.	Catalase	+
9.	Oxidase	+
10.	Hydrogen Sulphide production	-

Table 4: Morphological features of isolated bacterial strain.

Morphology features		Bacterial isolate
Colony Morphology	Shape	Round
	Texture	Smooth
	Color	Creamy
Microscopic Characters	Cell shape	Rod
	Motility	Motile
	Spore Formation	-ve

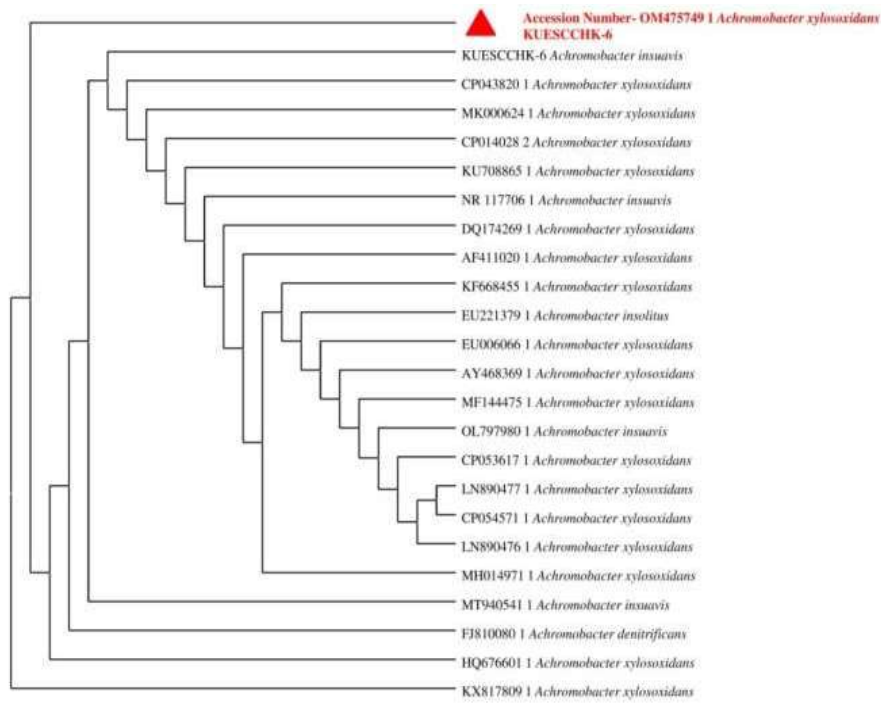


Fig. 2: Phylogenetic tree of 16S rRNA gene sequence of isolate *Achromobacter xylosoxidans*.

Table 5: Biomass production by bacterial strain *Achromobacter xylosoxidans* at optimized parameter.

Biomass production by <i>Achromobacter xylosoxidans</i>									
Temperature (°C)	Biomass Production in g.L <sup>-1</sup>	pH	Biomass Production in g.L <sup>-1</sup>	Nitrogen Source	Biomass Production in g.L <sup>-1</sup>	Carbon Source	Biomass Production in g.L <sup>-1</sup>	Carbon to Nitrogen Ratio	Biomass Production in g.L <sup>-1</sup>
25°C	1	5.5	0.5	Urea	2.7	Fructose	6.7	01:01	1.5
30°C	3.1	6.5	1	Yeast Extract	3.3	Maltose	5.1	02:01	3.1
35°C	4.2	7.5	2.9	Peptone	3.1	Glucose	7.3	04:01	5.2
40°C	3.8	8.5	4.8	Beef Extract	3.8	Lactose	6	06:01	6.8
45°C	2.9	9.5	4.6			Sucrose	9.6	08:01	3.8
50°C	0.7	10.5	3.2						

other relevant bacteria can be found in Fig. 2 within the GenBank database.

**The Impact of Varying Temperatures, pH Levels, Carbon Sources, Nitrogen Sources and Carbon-to-Nitrogen Ratios (C/N Ratio) on *Achromobacter xylosoxidans***

The optimal conditions for biomass production by *Achromobacter xylosoxidans* were identified through the variation of temperature, pH, nitrogen source, carbon source, and C/N ratio. Maximum biomass production was achieved at a temperature of 35°C and a pH of 8.5, with urea serving

as the nitrogen source and glucose as the carbon source, and a C/N ratio of 06:01. These conditions yielded the highest biomass output, which is essential for the efficient treatment of textile industry effluent as shown in Table 5 and Fig. 3.

**Bacterial Counting Using the Dilution Technique**

1mL of bacterial suspension containing 85,00,000 cells was used for textile industry effluent treatment.

**Decolorization and Physico-Chemical Parameters Reduction by *Achromobacter xylosoxidans* KUESCCHK-5**

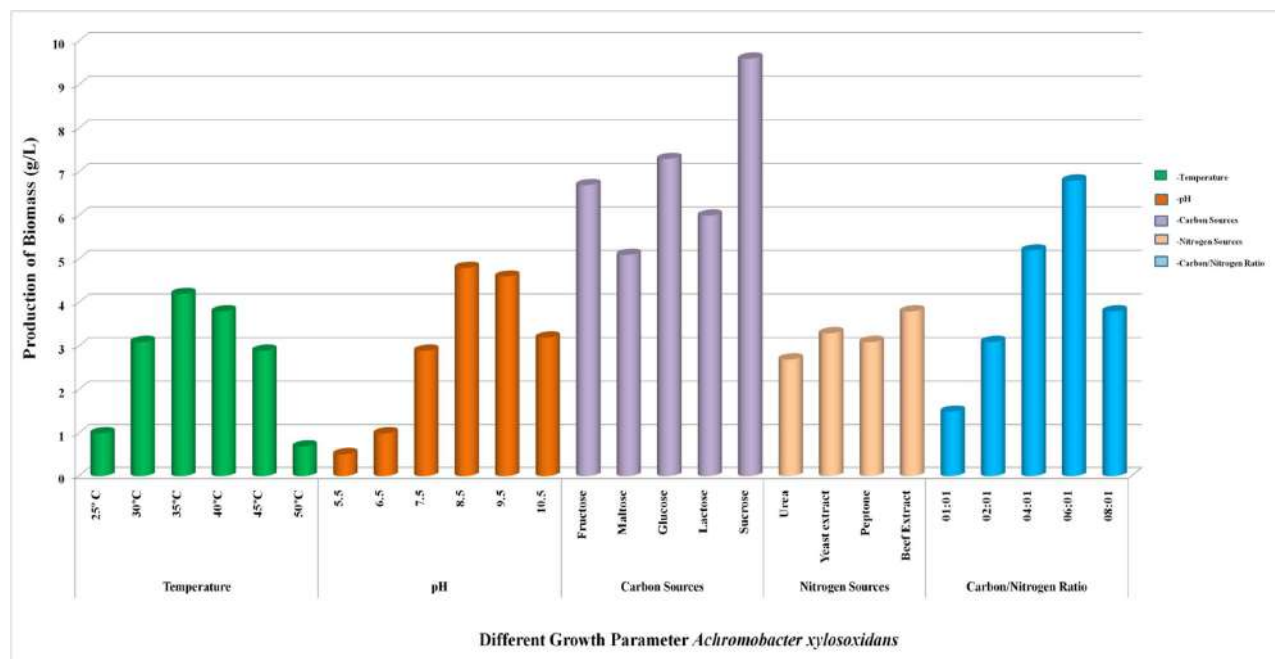


Fig. 3: Biomass production by *Achromobacter xylosoxidans* in different growth parameters.

Tables 6 and 7 illustrate the concentrations of various pollutants in textile effluent before and after treatment with *Achromobacter xylosoxidans*. Table 6 shows that the raw effluent had high pollutant levels, including a color concentration of 218.48 mg.L<sup>-1</sup>, BOD of 694.58 mg.L<sup>-1</sup>, COD of 2662.74 mg.L<sup>-1</sup>, and an EC of 7095.63 µmhos.cm<sup>-1</sup>. The concentrations of other contaminants such as fluoride, phosphate, sodium, turbidity, iron, and several heavy metals were also significantly high in the raw effluent (Fig. 4).

Table 7 shows the effectiveness of *Achromobacter xylosoxidans* in treating the effluent. After treatment, there were significant reductions in pollutant concentrations across all effluent dilutions. For instance, color concentration dropped from 26.34 mg.L<sup>-1</sup> to 6.61 mg.L<sup>-1</sup>, BOD decreased from 134.63 mg.L<sup>-1</sup> to 19.61 mg.L<sup>-1</sup>, and COD was reduced from 506.55 mg.L<sup>-1</sup> to 97.56 mg.L<sup>-1</sup>. EC, fluoride, phosphate, sodium, and turbidity also saw marked reductions. At a 25% dilution level, the effluent treatment process achieved substantial reductions across key environmental parameters. Iron content was reduced by 91.56%, effectively removing this potentially toxic metal. The color of the effluent decreased by 91.07%, indicating the successful elimination of chromophoric substances. Reductions in BOD and COD by 88.16% and 85.23%, respectively, show a significant decrease in pollution levels. EC dropped by 81.07%, reflecting a reduction in dissolved salts. Fluoride and phosphate levels were lowered by 88.34% and 86.41%, respectively, minimizing risks of fluorosis and eutrophication. Turbidity

was reduced by 89.10%, indicating clearer water, while sodium levels decreased by 83.01%, helping to prevent soil salinization. Additionally, heavy metals such as zinc, nickel, manganese, copper, lead, cadmium, total chromium, arsenic, barium, cobalt, and boron were either reduced to below detectable limits or significantly lowered. These results highlight that *Achromobacter xylosoxidans* is highly effective in reducing the concentration of pollutants in textile effluent (Fig. 5 and 6).

Chaudhary et al. (2020) investigated the removal of Cr<sup>6+</sup> using fungi isolated from tannery effluent. Their rDNA genes were subsequently identified as *Aspergillus niveus* MCC 1318, *Aspergillus flavus* MCC 1317, and *Aspergillus niger* MCC 1316. *A. niveus*, *A. niger*, and *A. flavus* were capable of removing 80%, 82%, and 88% Cr, respectively. The bioremediation efficiency of individual fungal strains for other heavy metals such as Zn, Pb, Cd, and Ni was observed to be 55%, 68%, 41%, and 69%, respectively for *A. niveus*, 60%, 59%, 59%, and 50%, respectively for *A. niger*, and 63%, 52%, 68%, and 58% for *A. flavus*. An exceptional removal of Zn, Pb, Cd, and Ni was observed in the case of fungal consortia, i.e., 80%, 70%, 80%, and 75%, respectively. Fourier transform infrared spectroscopy (FTIR) unveiled the adsorption phenomena by revealing the interactions of adsorbed Cr with methyl and methylene groups, secondary amides, and phosphate groups present in the fungal media.

Harish et al. (2024) noted similar findings in their investigations of dye decolorization utilizing immobilized



Table 6: Concentration of parameters before treatment at different effluent dilutions.

Parameters	Units	Raw effluent	75% dilution	50% dilution	25% dilution	Control
Color concentration	mg.L <sup>-1</sup>	218.48±0.04	179.51±0.04	133.74±0.03	74.07±0.07	218.48±0.04
BOD	mg.L <sup>-1</sup>	694.58±0.14	514.57±0.21	336.98±0.15	165.71±0.15	694.3±0.02
COD	mg.L <sup>-1</sup>	2662.74±0.12	1985.54±0.20	1320.49±0.15	660.57±0.17	2662.74±0.11
EC	µmhos.cm <sup>-1</sup>	7095.63±0.08	6083.60±0.11	4487.70±0.03	2656.30±0.06	7095.63±0.08
Fluoride	mg.L <sup>-1</sup>	3.91±0.03	2.96±0.02	2.15±0.07	1.37±0.11	3.91±0.0
Phosphate	mg.L <sup>-1</sup>	16.56±0.15	14.39±0.11	11.56±0.12	9.91±0.02	16.56±0.15
Sodium	mg.L <sup>-1</sup>	2287±0.02	1815.39±0.07	1302.49±0.12	798.66±0.11	2287.22±0.02
Turbidity	mg.L <sup>-1</sup>	180.66±0.09	144.25±0.10	111.76±0.12	59.91±0.02	180.66±0.09
Iron	mg.L <sup>-1</sup>	7.08±0.05	5.71±0.09	4.15±0.11	2.13±0.07	7.08±0.05
Zinc	mg.L <sup>-1</sup>	1.99±0.0003	1.59±0.001	1.09±0.0003	0.596±0.001	1.99±0.0003
Nickel	mg.L <sup>-1</sup>	2.34±0.0003	1.89±0.0003	1.24±0.0006	0.679±0.0006	2.34±0.0003
Manganese	mg.L <sup>-1</sup>	0.33±0.0003	0.26±0.001	0.18±0.0005	0.103±0.0006	0.33±0.0003
Copper	mg.L <sup>-1</sup>	0.66±0.0006	0.52±0.0006	0.35±0.0006	0.180±0.0008	0.66±0.0006
Lead	mg.L <sup>-1</sup>	1.004±0.001	0.79±0.001	0.53±0.001	0.275±0.002	1.004±0.001
Cadmium	mg.L <sup>-1</sup>	0.52±0.001	0.41±0.001	0.29±0.001	0.161±0.0006	0.52±0.001
Total Chromium	mg.L <sup>-1</sup>	0.73±0.001	0.61±0.001	0.42±0.001	0.243±0.001	0.73±0.001
Arsenic	mg.L <sup>-1</sup>	0.002±0.0003	0.0015±0	0.001±0	0.0006±0	0.002±0.0003
Barium	mg.L <sup>-1</sup>	0.04±0.003	0.036±0.001	0.027±0.0003	0.014±0	0.04±0.003
Cobalt	mg.L <sup>-1</sup>	0.20±0.003	0.15±0.0006	0.107±0.001	0.058±0.001	0.20±0.003
Boron	mg.L <sup>-1</sup>	0.32±0.01	0.23±0.002	0.164±0.002	0.080±0	0.32±0.01

Key: mg.L<sup>-1</sup> = milligram per liter. Values are expressed as mean ± SEM (n=3)

Table 7: Concentration of parameters after treatment with *Achromobacter xylosoxidans*.

Parameters	Units	Raw effluent	75% dilution	50% dilution	25% dilution	Control
Color concentration	mg.L <sup>-1</sup>	26.34±0.02	19.07±0.03	13.15±0.03	6.61±0.01	210.26±0.08
BOD	mg.L <sup>-1</sup>	134.63±0.10	83.71±0.20	47.55±0.21	19.61±0.15	660.30±0.09
COD	mg.L <sup>-1</sup>	506.55±0.12	357.55±0.17	224.52±0.21	97.56±0.20	2568.54±0.15
EC	µmhos.cm <sup>-1</sup>	1907.37±0.12	1404.72±0.08	934.16±0.06	502.82±0.10	6796.63±0.12
Fluoride	mg.L <sup>-1</sup>	0.73±0.06	0.48±0.07	0.31±0.05	0.16±0.05	3.65±0.06
Phosphate	mg.L <sup>-1</sup>	3.38±0.09	2.68±0.11	1.80±0.08	1.34±0.09	15.76±0.10
Sodium	mg.L <sup>-1</sup>	528.60±0.17	394.24±0.09	246.42±0.11	135.62±0.07	2121.27±0.04
Turbidity	mg.L <sup>-1</sup>	34.27±0.06	24.39±0.09	15.26±0.05	6.52±0.08	660.30±0.09
Iron	mg.L <sup>-1</sup>	1.07±0.04	0.74±0.05	0.49±0.11	0.18±0.08	6.42±0.21
Zinc	mg.L <sup>-1</sup>		Below detectable limit			1.99±0.0003
Nickel	mg.L <sup>-1</sup>		Below detectable limit			2.34±0.0003
Manganese	mg.L <sup>-1</sup>		Below detectable limit			0.33±0.0003
Copper	mg.L <sup>-1</sup>		Below detectable limit			0.66±0.0006
Lead	mg.L <sup>-1</sup>		Below detectable limit			1.004±0.001
Cadmium	mg.L <sup>-1</sup>		Below detectable limit			0.52±0.001
Total Chromium	mg.L <sup>-1</sup>		Below detectable limit			0.73±0.001
Arsenic	mg.L <sup>-1</sup>		Below detectable limit			0.002±0.0003
Barium	mg.L <sup>-1</sup>		Below detectable limit			0.04±0.003
Cobalt	mg.L <sup>-1</sup>		Below detectable limit			0.20±0.003
Boron	mg.L <sup>-1</sup>		Below detectable limit			0.32±0.01S

Key: mg.L<sup>-1</sup> = milligram per liter, BDL: Below detectable limit, Values are expressed as mean ± SEM (n=3)

*Achromobacter xylosoxidans* DDB6, which was isolated from textile effluent. Their study indicated that this strain effectively reduced the color of crystal violet, coomassie brilliant blue, and alizarin red by 67.20%, 28.58%, and 20.41%, respectively. Kundu et al. (2012) investigated the treatment of small-scale slaughterhouse wastewater using *Achromobacter xylosoxidans* S18. The results indicated a reduction in COD of the effluent by  $88 \pm 3\%$  in the presence of glucose and ammonium chloride.

*Achromobacter xylosoxidans* is highly effective in reducing a wide range of pollutants, including color, BOD, COD, EC, and heavy metals. Its performance is comparable or even superior to other bioremediation agents, such as fungal strains like *Aspergillus species*. The broad spectrum of pollutant reductions achieved with *Achromobacter xylosoxidans* makes it a potent and versatile bioremediation

agent for treating industrial effluents, particularly in sectors like textiles.

#### Phytotoxicity Study on Effluent Treated with *Achromobacter xylosoxidans*

The control group achieved a seed germination rate of 100%, while the treated effluent reached 90%, and the raw effluent had only a 40% germination rate. Additionally, seeds in the treated effluent exhibited more substantial root and shoot growth compared to those in the raw effluent. The germination index was notably lower for the raw effluent at 6.7%, whereas the effluent treated with *Achromobacter xylosoxidans* showed a germination index of 83.96% (Tables 8 and Fig. 7).

Rahman et al. (2018) investigated the phytotoxic effect of synthetic dye effluent on the seed germination of red amaranth.



Fig. 4: Effluent dilutions before treatment with the study organism.



Fig. 5: Effluent treated with *Achromobacter xylosoxidans*.

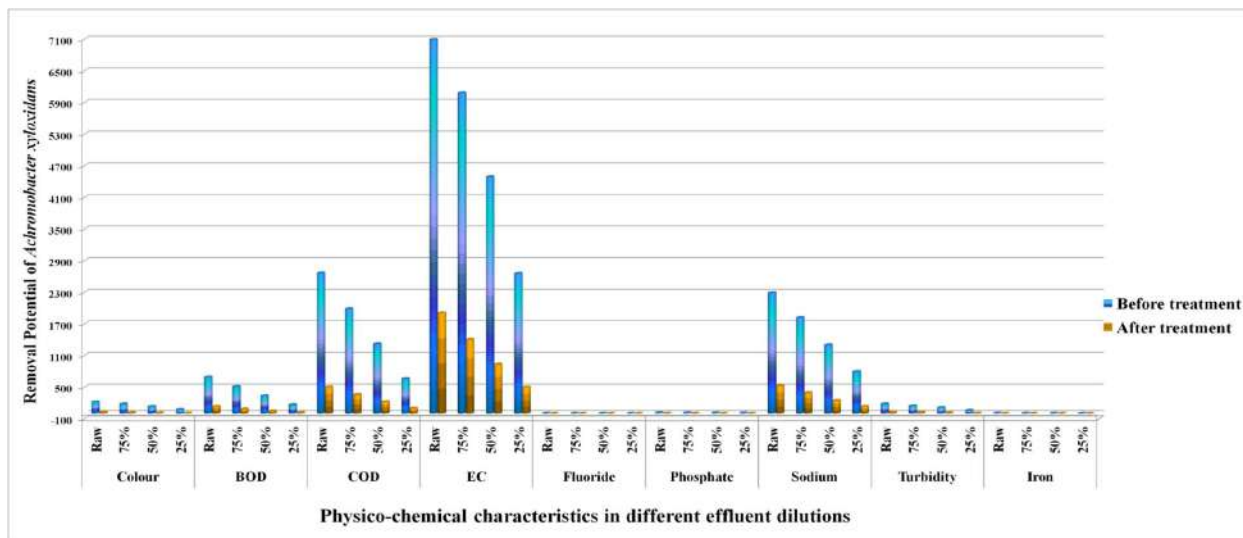


Fig. 6: Physico-chemical parameters reduction by *Achromobacter xylosoxidans* at different effluent dilutions.

Results showed that germination experiments of *Amaranthus cruentus* L. (red amaranth) were conducted in sterilized Petri dishes containing concentrations of 0%, 5%, 10%, 25%, 50%, 75%, and 100%. There was a gradual decrease in the

Table 8: Effect of effluent treated with *Achromobacter xylosoxidans* on the germination and growth of *Vigna mungo*.

Sample	Shoot length [cm]	Root length [cm]	Germination [%]	GI [%]
Control	22.4	17.9	100	100
Raw	4.9	3	40	6.7
Treated	17.6	16.7	90	83.96



Fig. 7: *Vigna mungo* grown in effluent treated with *Achromobacter xylosoxidans*.

percentage of seed germination and seedling growth with increased concentrations of effluents. Relative toxicity and phytotoxicity were extreme at 100% effluent concentration. Root and shoot lengths of seedlings exhibited the lowest values at raw effluent and peaked at 5%. Hence, it was concluded that diluted effluent favored the growth and germination of seeds, while concentrated effluent inhibited seed growth.

## CONCLUSIONS

The study effectively demonstrates that *Achromobacter xylosoxidans* KUESCCHK-6, identified through 16S rRNA molecular analysis, is a highly efficient and eco-friendly solution for the bioremediation of textile effluents. Under optimal conditions, the strain significantly reduced key physiochemical parameters of the wastewater, including color, BOD, COD, EC, fluoride, phosphate, sodium, and turbidity, as well as various metal ions, to below detectable limits. The treated effluent was confirmed to be non-toxic through phytotoxicity tests. These findings suggest that *Achromobacter xylosoxidans* KUESCCHK-6 holds great promise for large-scale, sustainable bioremediation applications in the textile industry.

## ACKNOWLEDGMENT

The author acknowledges the Department of P.G. Studies and Research in Environmental Science, Kuvempu University, Shankaraghatta, Shimoga, Karnataka, India, for their contribution to this article. This work received support from the Government of India, Ministry of Science and Technology, Department of Science and Technology under Grant Number DST/INSPIRE Fellowship/2019/IF190360.

## REFERENCES

- Adane, T., Adugna, A.T. and Alemayehu, E., 2021. Textile industry effluent treatment techniques. *Journal of Chemistry*, 2021(1), pp.5314404. DOI
- American Public Health Association (APHA), 2017. *Standard Methods for the Examination of Water and Wastewater*. 23rd ed. American Public Health Association, American Water Work Association, Water Work Federation, Washington DC.
- Aneja, K.R., 2018. *Laboratory Manual of Microbiology and Biotechnology*. ED-TECH.
- Bergey, D.H., 1994. *Bergey's Manual of Determinative Bacteriology*. Lippincott Williams and Wilkins.
- Cappuccino, J.G. and Sherman, N., 2013. *Microbiology: A Laboratory Manual*. Pearson Higher Ed.
- Chaithra, C. and Kousar, H., 2022. Molecular identification of fungal strains isolated from textile effluent and contaminated soil using 16S rRNA sequencing. *Research Journal of Biotechnology*, 17(6), pp.1–6.
- Chaithra, C., Kousar, H., Akshatha, K.U. and Dhanushree, M.S., 2023. Isolation, identification, and molecular characterization of indigenous bacterial isolates from textile effluent and contaminated soil using 16S rRNA sequencing. *Research Journal of Chemistry and Environment*, 27(8), pp.9–15.
- Chaithra, C., Kousar, H., Dhanushree, D.M., Akshatha, K.U. and Veena, H.R., 2022. Molecular identification of fungal strains using 16S rRNA sequencing and a comparative assessment of their efficiency on reduction of biological oxygen demand in textile industry effluent. *European Journal of Molecular & Clinical Medicine*, 9(07), pp.6890–6897.
- Chaudhary, P., Beniwal, V., Sharma, P., Goyal, S., Kumar, R., Alkhanjaf, A.A.M. and Umar, A., 2022. Unloading of hazardous Cr and tannic acid from real and synthetic wastewater by novel fungal consortia. *Environmental Technology & Innovation*, 26, pp.102230. DOI
- Harish, B.S., Thayumanavan, T., Subashkumar, R., Gopal, K. and Kowsik Raj, N., 2024. Kinetics of dye decolorization using the heterogeneous catalytic system with immobilized *Achromobacter xylosoxidans* DDB6. *Preparative Biochemistry & Biotechnology*, 54(5), pp.691–699. DOI
- Hemalatha, I., Harika, D. and Karnena, M.K., 2022. Sustainable nano-bioremediation approaches for the treatment of polluted soils. *Nature Environment & Pollution Technology*, 21(4), pp.1817–1826. DOI
- Kousar, H., Chaithra, C. and Akshatha, K.U., 2020. Role of certain bacterial and fungal strains in bioremediation of textile industrial effluent—a review. *Journal of Advanced Scientific Research*, 11(4 Suppl 8), pp.45–52.
- Kuanar, A., Kabi, S.K., Rath, M., Dhal, N.K., Bhuyan, R., Das, S. and Kar, D., 2022. A comparative review on bioremediation of chromium by bacterial, fungal, algal, and microbial consortia. *Geomicrobiology Journal*, 39(6), pp.515–530. DOI
- Kundu, P., Pramanik, A., Mitra, S., Choudhury, J.D., Mukherjee, J. and Mukherjee, S., 2012. Heterotrophic nitrification by *Achromobacter xylosoxidans* S18 isolated from small-scale slaughterhouse wastewater. *Bioprocess and Biosystems Engineering*, 35, pp.721–728. DOI
- Madhav, S., Ahamad, A., Singh, P. and Mishra, P.K., 2018. A review of textile industry: Wet processing, environmental impacts, and effluent treatment methods. *Environmental Quality Management*, 27(3), pp.31–41. DOI
- Rahman, M.A., Rayhan, M.Y.H., Chowdhury, M.A.H., Mohiuddin, K.M. and Chowdhury, M.A.K., 2018. Phytotoxic effect of synthetic dye effluents on seed germination and early growth of red amaranth. *Fundamental and Applied Agriculture*, 3(2), pp.480–490. DOI
- Sharma, P., Singh, L. and Mehta, J., 2010. COD reduction and color removal of simulated textile mill wastewater by mixed bacterial consortium. *Rasayan Journal of Chemistry*, 3(4), pp.731–735.
- Verma, R.K., Sankhla, M.S., Rathod, N.V., Sonone, S.S., Parihar, K. and Singh, G.K., 2022. Eradication of fatal textile industrial dyes by wastewater treatment. *Biointerface Research in Applied Chemistry*, 12, pp.567–587. DOI



# Assessment of Toxic Metals in an Open Dump Site Near PNG University of Technology, Papua New Guinea

John Ape<sup>1</sup>, Srikanth Bathula<sup>1</sup>†, Sailesh Samanta<sup>2</sup> and Krishna Kumar Kotra<sup>3</sup>

<sup>1</sup>School of Applied Sciences, Applied Chemistry, Papua New Guinea University of Technology, Lae, Morobe Province, Papua New Guinea

<sup>2</sup>School of Surveying and Land Studies, Papua New Guinea University of Technology, Lae, Morobe Province, Papua New Guinea

<sup>3</sup>School of Agriculture, Geography, Environment, Ocean and Natural Sciences (SAGEONS), The University of the South Pacific, Emalus Campus, Port Vila, Vanuatu

†Corresponding author: Srikanth Bathula; srikanth.bathula@pnguot.ac.pg

**Abbreviation:** Nat. Env. & Poll. Technol.  
**Website:** [www.neptjournal.com](http://www.neptjournal.com)

*Received:* 09-08-2024

*Revised:* 22-09-2024

*Accepted:* 10-11-2024

## Key Words:

Groundwater  
 Municipal solid waste  
 Open dump site  
 Heavy metal contaminants  
 Inverse distance weight interpolation

## Citation for the Paper:

Ape, J., Bathula, S., Samanta, S. and Kotra, K. K., 2025. Assessment of toxic metals in an open dump site near PNG University of Technology, Papua New Guinea. *Nature Environment and Pollution Technology*, 24(2), p. D1713. <https://doi.org/10.46488/NEPT.2025.v24i02.D1713>

*Note: From year 2025, the journal uses Article ID instead of page numbers in citation of the published articles.*



**Copyright:** © 2025 by the authors  
**Licensee:** Technoscience Publications  
 This article is an open access article distributed under the terms and conditions of the Creative Commons Attribution (CC BY) license (<https://creativecommons.org/licenses/by/4.0/>).

## ABSTRACT

Groundwater contamination near the municipal solid waste dump at the Papua New Guinea University of Technology (PNGUoT) has raised serious health concerns in the local communities. To testify to this, a research study was conducted to quantify the presence of heavy metals. Water sample analyses showed Cd levels ranging from 0.0002 to 0.02 mg.L<sup>-1</sup>, Pb from 0.00002 to 0.094 mg.L<sup>-1</sup>, and Hg from 0.0001 to 0.052 mg.L<sup>-1</sup>, all of which exceed the World Health Organization's (WHO) safe drinking water limits. These metals are known to cause a range of health problems, including kidney disease, cancer, brain damage, and developmental delays in children. The situation calls for urgent action to safeguard the local community's health. Immediate improvements in waste management, such as better landfill designs with systems to capture and treat leachate, are needed to prevent further contamination of groundwater. Additionally, water treatment technologies like reverse osmosis should be considered to provide safe drinking water. Regular monitoring of groundwater quality and public health education in the area are also key steps in minimizing risks. These combined efforts will help ensure safer water for the community and more responsible management of the waste disposal site.

## INTRODUCTION

Human activities, including industrial processes, urbanization, agriculture, and the open dumping of municipal solid waste (MSW), significantly contaminate water sources, adversely affecting groundwater quality (Akinbile 2012, Usman et al. 2017). Landfills and Open Dump Sites (ODS) are major threats, with ODS referring to sites where solid waste is dumped without environmental regulations (Fatta & Loizidou 1999, Fodor & Szabo 2004). Areas near these sites are at a heightened risk for groundwater contamination due to leachate pollution (Hossain et al. 2014, Hadi 2023). When electronics, paints, batteries, and plastics are mixed with MSW, they increase heavy metal concentrations at dump sites (Maiti et al. 2016, Przydatek & Kanownik 2019). ODS remains the primary disposal method in many developing countries, contributing significantly to water and environmental pollution (Omeiza et al. 2022). It is well-documented that garbage is often dumped near borewells without proper waste management, further raising the risk of groundwater contamination. The issue of MSW is universal (Aderemi et al. 2011), and its management is an issue in underdeveloped nations like PNG.

Research by Sugirtharan & Rajendran (2015) found that borewells near dumping sites have higher pollutant concentrations compared to those located farther away.

Leachate, which accumulates at the bottoms of open dumps, percolates through soil layers, reaching groundwater and introducing toxic contaminants (Mor et al. 2006, Omeiza et al. 2022). The high concentration and toxicity of leachate pose serious public health risks (Baderna et al. 2019). Chemical pollution remains a pressing issue globally, particularly in industrialized and developing nations. Studies link chemical exposure in drinking water to chronic health problems, including cancer and cardiovascular diseases, with children being especially vulnerable (Lin et al. 2022, Alao et al. 2023, Sankhla & Kumar 2019). Unsafe drinking water, inadequate sanitation, and poor hygiene create dangerous conditions, leading to water-related diseases such as diarrhea, typhoid, and cholera. In light of public concerns regarding the dump site at PNG University of Technology (PNGUoT) in Lae, this study aims to assess the impact of leachates on bore water quality in the vicinity of the dumping site.

## RESEARCH AREA

Lake City, the capital of Morobe Province, is the second largest city in Papua New Guinea (PNG) and hosts the largest cargo port, making it an industrial hub and home to the Papua New Guinea University of Technology (PNGUoT). Located between the Indonesian-Australian Plates and the Pacific Plates on the South Bismarck Plate, Lae lies at coordinates 6.7155° S, 146.9999° E and features a tropical rainforest climate, with an average annual precipitation of 4,500 millimeters (Stanaway et al. 2009).

The focus of this study is an open dump site situated near borewells from which Water PNG Limited extracts, treats, and distributes water for residential and commercial use across Lae City and surrounding areas. The dump site is located northeast of PNGUoT at the Second Seventh Landfill, positioned at 6.6598° S, 147.0123° E. Between

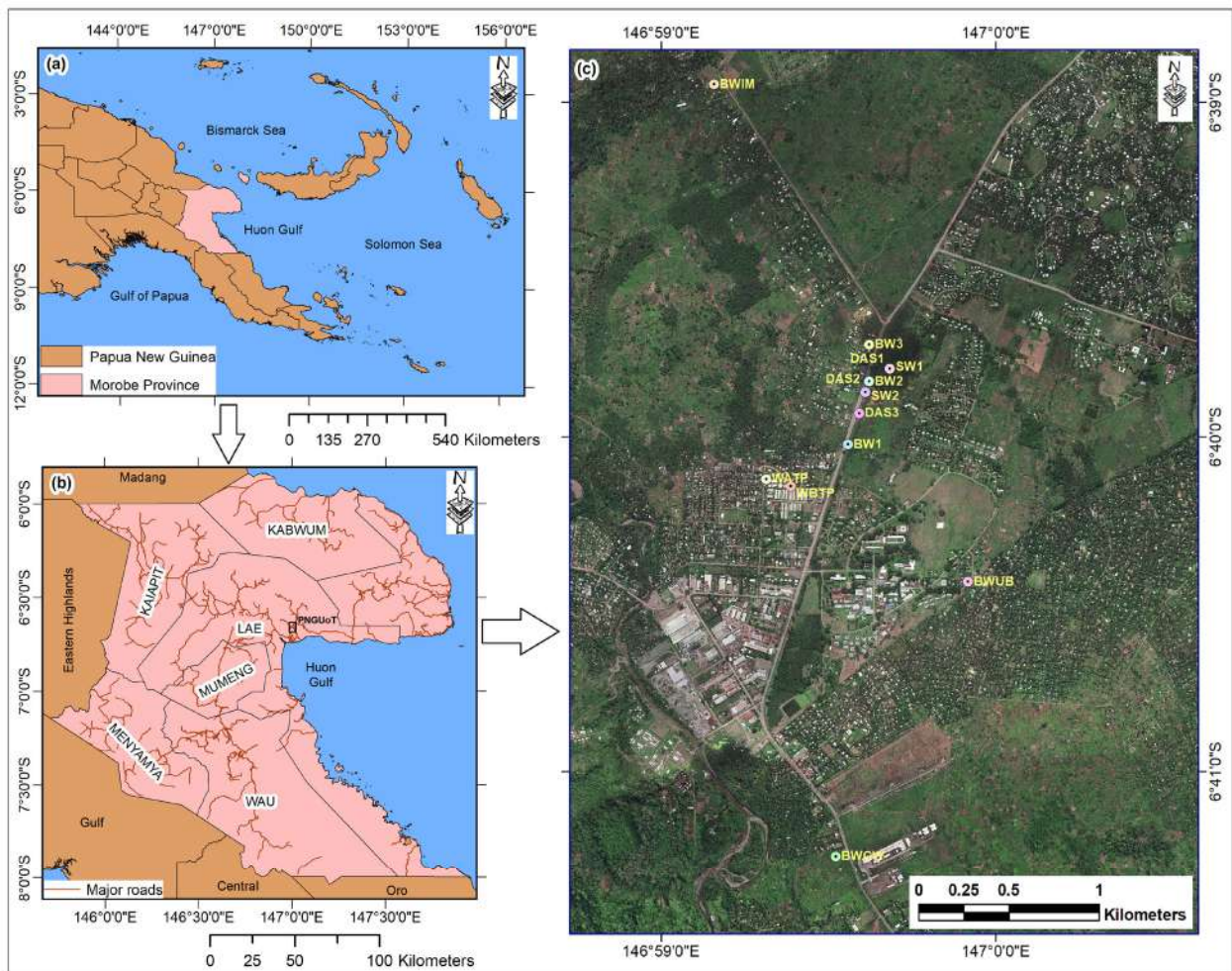


Fig. 1: Location map of the study area (a) Papua New Guinea, (b) Morobe Province, and (c) Dump site and Borewells around PNGUoT.





Fig. 2: Types of Solid waste dumped at PNGuT dump site, (a) Electronic Waste at Dump Site, (b) Disposal of polymer, (c) Pond near Dump Site, and (d) Electrical, paint waste near Dump Site.

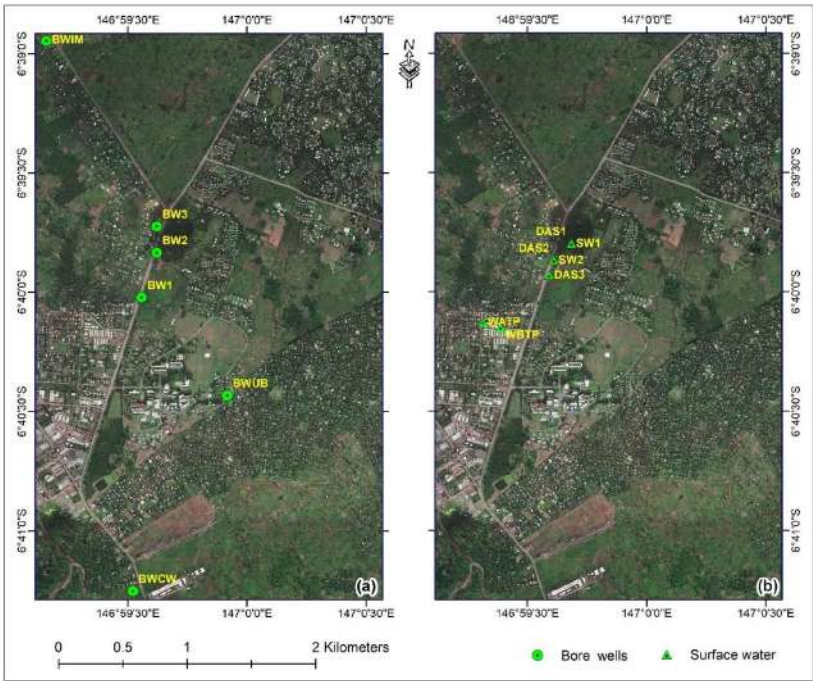


Fig. 3: Location of water sample points (a) Bore wells and (b) Surface water.

Table 1: Location of sampling point in the study area.

Sl. No.	Station Type	Sampling point	Longitude	Latitude
1.	Bore Wells (BW)	Bore Well 1 (BW1)	146.99265	-6.66704
2.		Bore Well 2 (BW2)	146.99370	-6.66391
3.		Bore Well 3 (BW3)	146.99370	-6.66207
4.		Bore Well Uni Block (BWUB)	146.99862	-6.67388
5.		Bore Well Igam Market (BWIM)	146.98597	-6.64911
6.		Bore Well Carwash (BWCW)	146.99203	-6.68756
7.	Ground Points (GP)	Dump Area Soil 1 (DAS1)	146.99474	-6.66327
8.		Dump Area Soil 2 (DAS2)	146.99352	-6.66444
9.		Dump Area Soil 3 DAS3)	146.99320	-6.66549
10.		Surface Water 1 (SW1)	146.99474	-6.66327
11.		Surface Water 2 (SW2)	146.99352	-6.66444
12.		Water Before Treatment Plant (WBTP)	146.98980	-6.66913
13.		Water After Treatment Plant (WATP)	146.98858	-6.66877

March 2022 and February 2023, a survey was conducted on the borewells adjacent to the PNGUoT disposal site. The dumping sites with various disposals are shown in Figs. 1 and 2. Thirteen sampling locations were established: three for dump soils, two for surface waters, and eight for bore waters (groundwater samples). Table 1 provides the coordinates of these sampling sites, while Fig. 3 illustrates their actual positions within the study area.

## MATERIALS AND METHODS

A streamlined process was followed as below during the assessment procedures.

**Sample Collection and Storage:** Water and soil samples were collected in clean bottles and stored in an icebox. They were transported to the National Analytical and Testing Services Limited (NATSL) laboratory and processed within 24 h.

**Water Sample Analysis:** Toxic and heavy metals in surface and groundwater were analyzed using Inductively Coupled Plasma-Mass Spectrometry (ICP-MS). Samples were acidified with 10% nitric acid, filtered through a 0.45  $\mu\text{m}$  filter, and analyzed for Cadmium (Cd), Mercury (Hg), Lead (Pb), Manganese (Mn), Molybdenum (Mo), Nickel (Ni), Silver (Ag), Chromium (Cr) and Tin (Sn).

**Soil Sample Digestion:** Soil samples were digested using 3:1 aqua regia following Soil Chemical Methods–Australasia. The mixture was heated at 70–90°C and reduced in volume, then filtered through 0.45  $\mu\text{m}$  cellulose nitrate filters. The digested samples were analyzed by ICP-MS.

**Calibration Standard Preparation:** ICP-Multi Elemental Solution IV (Merck KGaA), traceable to NIST SRM, was used for calibration. Solutions were prepared at  $\mu\text{g.L}^{-1}$

concentrations (50, 100, 150, 200  $\mu\text{g.L}^{-1}$ ), with accepted calibration graph Replicate (R) values >0.95.

**Spatial Interpolation and Mapping:** The spatial interpolation technique predicts unknown values from a set of known values for any geographic location (Samanta et al. 2012). IDWA (Inverse distance-weighted) is one of the global spatial interpolation techniques used to interpolate the known tested values of the sample point location (Burrough & McDonnell 1998). These points are named bore wells (BW) from where the water samples were collected. Contours were generated from these interpolated raster surfaces. Both these activities were executed using the ArcGIS spatial analyst tool. The other set of points, called ground points (GP), were overlaid on the interpolated map to understand the impact or relationship of surface phenomena on the groundwater.

## RESULTS AND DISCUSSION

Groundwater in the research area is used for both residential and commercial purposes, so pollutant concentrations were compared against relevant standards. Measurements were taken at ODS and nearby borewells, with results for surface water, groundwater, and waste soils summarized in Table 2. Using the IDW interpolation technique, results for each parameter across different time frames were used to generate thematic maps. The range of values (high to low) for each parameter is presented in Table 3. The values highlighted in the Table 3 exceed the limits set by WHO guidelines, further corroborated by the visual comparisons presented in Figs. 5, 8, and 11.

### Interpretation of Data

The data illustrates the contamination of borewell water with



Table 2: Analytical results of pollution sources - Dump area soils and surface waters in open dumping areas.

Sampling ID	Sampling Dates	Cd [mg.L <sup>-1</sup> ]	Hg [mg.L <sup>-1</sup> ]	Pb [mg.L <sup>-1</sup> ]	Mn [mg.L <sup>-1</sup> ]	Mo [mg.L <sup>-1</sup> ]	Ni [mg.L <sup>-1</sup> ]	Ag [mg.L <sup>-1</sup> ]	Cr [mg.L <sup>-1</sup> ]	Sn [mg.L <sup>-1</sup> ]
DAS 1	Apr-22	0.0011	0.00086	0.08	0.471	0.0002	0.03	0.00068	0.043	0.0043
	Aug-22	0.0036	0.00004	0.013	0.277	0.0002	0.019	0.00004	0.025	0.0017
	Feb-23	0.0024	0.0007	0.01	0.384	0.0002	0.001	0.00003	0.0037	0.0034
DAS 2	Apr-22	0.00024	0.00034	0.049	0.334	0.0002	0.027	0.00034	0.034	0.0016
	Aug-22	0.0004	0.00004	0.0097	0.265	0.0002	0.011	0.00004	0.012	0.0036
	Feb-23	0.0003	0.0004	0.0084	0.247	0.0002	0.001	0.00003	0.0031	0.0028
DAS3	Apr-22	0.00015	0.00043	0.02	0.342	0.0007	0.032	0.00044	0.043	0.0011
	Aug-22	0.0005	0.00004	0.0038	0.202	0.0002	0.013	0.00004	0.012	0.0012
	Feb-23	0.0025	0.00006	0.0034	0.352	0.0005	0.001	0.00004	0.024	0.0016
WHO	Guidelines(mg/L)	0.003	0.006	0.01	0.1	0.07	0.07	0.1	0.05	
SW1	Apr-22	0.0029	0.0026	0.0005	0.033	1.441	0.001	0.0062	0.0002	2
	Aug-22	0.015	0.009	0.00003	0.0013	0.1	0.26	0.5	0.0019	1
	Feb-23	0.0022	0.0054	0.0007	0.0028	1.224	0.001	0.42	0.0016	1
SW2	Apr-22	0.0024	0.0092	0.0001	0.0038	2.442	0.001	0.0078	0.0002	2
	Aug-22	0.0009	0.0026	0.071	0.0009	0.1	0.029	0.027	0.0014	0.554
	Feb-23	0.0029	0.0035	0.094	0.0021	2.134	0.001	0.0019	0.0009	2
BW1	Apr-22	0.013	0.0077	0.026	0.0074	0.1	0.001	0.0081	0.0008	0.001
	Aug-22	0.0009	0.0086	0.0005	0.0062	0.1	0.001	0.015	0.0002	0.001
	Feb-23	0.0043	0.011	0.00003	0.0084	0.1	0.001	0.00001	0.00002	0.001
BW2	Apr-22	0.02	0.0023	0.022	0.01	0.1	0.001	0.0052	0.0003	0.001
	Aug-22	0.0002	0.0038	0.0011	0.021	0.1	0.001	0.012	0.0002	0.001
	Feb-23	0.0063	0.052	0.0002	0.02	0.1	0.001	0.00001	0.0006	0.001
BW3	Apr-22	0.0002	0.0019	0.00003	0.0095	0.1	0.001	0.0048	0.0002	0.001
	Aug-22	0.0003	0.0035	0.0001	0.01	0.1	0.001	0.048	0.0002	0.001
	Feb-23	0.0033	0.029	0.0004	0.029	0.1	0.001	0.00001	0.0002	0.001
WBTP	Apr-22	0.0047	0.0012	0.018	0.0095	0.1	0.001	0.0081	0.0002	0.001
	Aug-22	0.0047	0.0022	0.0003	0.0092	0.1	0.001	0.0071	0.0002	0.001
	Feb-23	0.00005	0.018	0.0008	0.015	0.1	0.001	0.00001	0.0002	0.001
WATP	Apr-22	0.0015	0.0012	0.00003	0.0088	0.1	0.001	0.0016	0.0002	0.001
	Aug-22	0.01	0.0018	0.0003	0.0096	0.1	0.001	0.011	0.0002	0.001
	Feb-23	0.0027	0.014	0.00003	0.035	0.1	0.001	0.00001	0.0007	0.001
BWUB	Apr-22	0.0035	0.0035	0.00003	0.0001	0.1	0.001	0.00001	0.0001	0.001
	Aug-22	0.0042	0.0051	0.0003	0.0001	0.1	0.001	0.00001	0.0002	0.001
	Feb-23	0.0006	0.0061	0.00003	0.0001	0.1	0.001	0.00001	0.0004	0.001
BWIM	Apr-22	0.0028	0.0032	0.00003	0.002	0.1	0.001	0.00001	0.0002	0.001
	Aug-22	0.0024	0.0038	0.0003	0.0015	0.1	0.001	0.00001	0.0002	0.001
	Feb-23	0.0007	0.0041	0.00003	0.002	0.1	0.001	0.00001	0.0002	0.001
BUCW	Apr-22	0.003	0.005	0.00003	0.00005	0.1	0.001	0.00001	0.0003	0.001
	Aug-22	0.0034	0.004	0.0003	0.00003	0.1	0.001	0.00001	0.0001	0.001
	Feb-23	0.0026	0.004	0.00003	0.00003	0.1	0.001	0.00001	0.0002	0.001

heavy metals, specifically cadmium (Cd), lead (Pb), and mercury (Hg), which were detected above the permissible limits set by the World Health Organization (WHO 2022).

The permissible limits for these metals are 0.003 mg.L<sup>-1</sup> for Cd, 0.01 mg.L<sup>-1</sup> for Pb, and 0.006 mg.L<sup>-1</sup> for Hg. These contaminants were found in borewell samples (BW1

Table 3: The resulting interpolated data ranges.

Sl. No.	Parameters	Interpolation range value		
		April, 2022	August, 2022	February, 2023
1.	Silicon dioxide (SiO <sub>2</sub> ), mg.L <sup>-1</sup>	8.7 – 51	9.1 - 40	9.4 – 102
2.	Total dissolved solids (TDS), mg.L <sup>-1</sup>	59 – 295	60 - 560	55 – 290
3.	Total hardness (TH), mg.L <sup>-1</sup>	101 – 564	123 - 639	101 – 517
4.	Mercury (Hg), mg.L <sup>-1</sup>	0.0019 – 0.007	0.0035 – 0.0086	0.004 – 0.052
5.	Lead (Pb), mg.L <sup>-1</sup>	0.00003 - 0.026	0.0001 – 0.001	0.00003 – 0.0003
6.	Cadmium (Cd), mg.L <sup>-1</sup>	0.0002 – 0.02	0.0002 – 0.004	0.0006 – 0.006
7.	Chromium (Cr), mg.L <sup>-1</sup>	0.0001 – 0.0007	0.01 – 0.02	0.00002 – 0.0006

and BW2) near dumping sites, indicating that pollution is occurring due to the leaching of heavy metals into the groundwater, and the likely sources of contamination are items such as fluorescent lamps, batteries, and electronic waste, which are disposed of in open dump sites (Fig. 2). These observations coincide with earlier reported studies of Hossain et al. (2014), Waheed & Bhawsar (2021). The detection of Cadmium (Cd), Lead (Pb), and Mercury (Hg) in samples collected and tested in BW1, BW2, and WBT is an indication of heavy metal contamination undiluted during dry seasons. This contamination is particularly concerning as it coincides with dry seasons when the lack of rainfall leads to minimal dilution of the contaminants. The findings align with earlier studies conducted in Tamil Nadu, India, by Nagarajan et al. (2012) and Pande (2015), which also reported high levels of heavy metal contamination in groundwater near dumping sites. The situation underscores the environmental and public health risks associated with improper waste

disposal and the subsequent leaching of toxic substances into groundwater. A graphical representation and spatial diagrams of Cd, Pb, and Hg are represented in Figs. 4-12.

The highest concentration of cadmium (Cd) was detected in SW1 in August 2022, likely due to its proximity to DAS1, where leaching and percolation were particularly active during the wet season when the samples were collected. However, in April 2023, cadmium levels were found to be higher in BW1 and BW2. This increase in concentration is attributed to the samples being collected during the driest week of the month, a period when the contaminants were undiluted, leading to more concentrated levels of Cd in the groundwater. This seasonal variation highlights the impact of rainfall on the dilution and dispersion of heavy metal contaminants in groundwater systems.

The highest concentrations of lead (Pb) were measured in DAS1, DAS2, and SW2 in April 2022, August 2022,

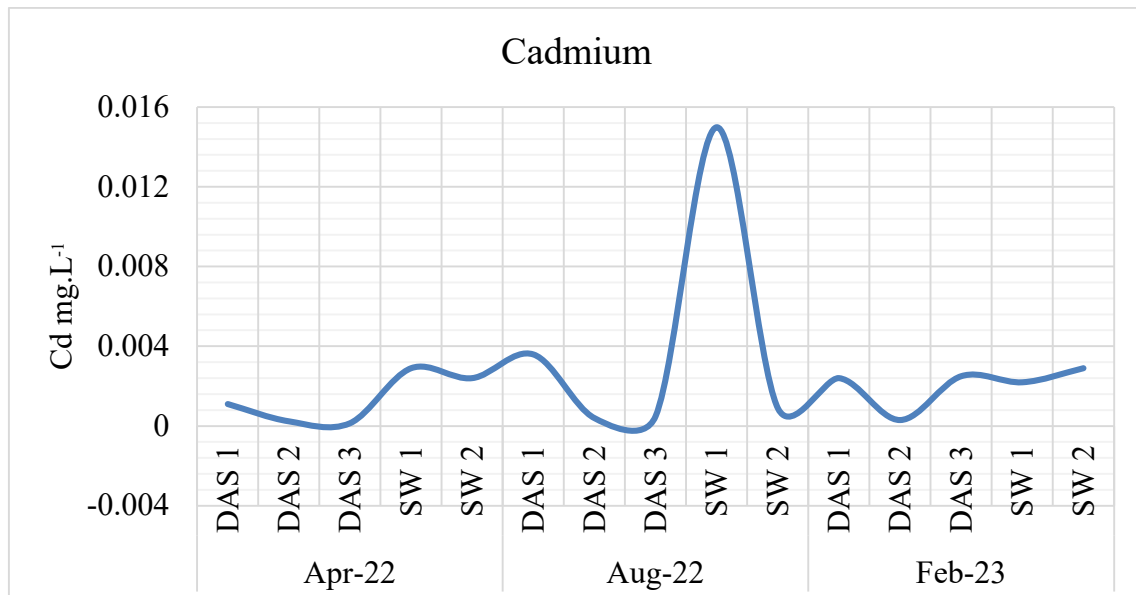


Fig. 4: Temporal Variation of Cd in Surface Point.

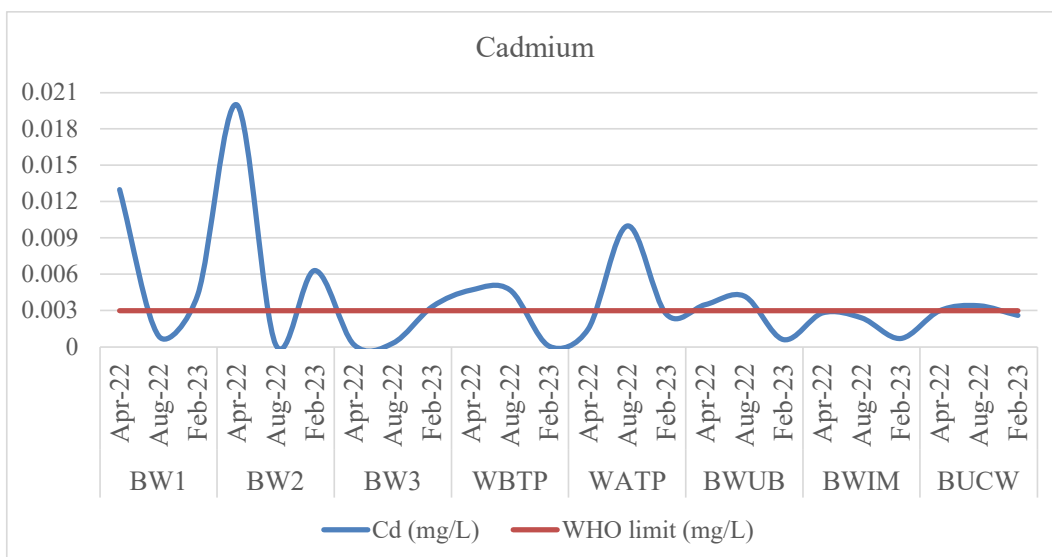


Fig. 5: Temporal Variation of Cd in Borewells.

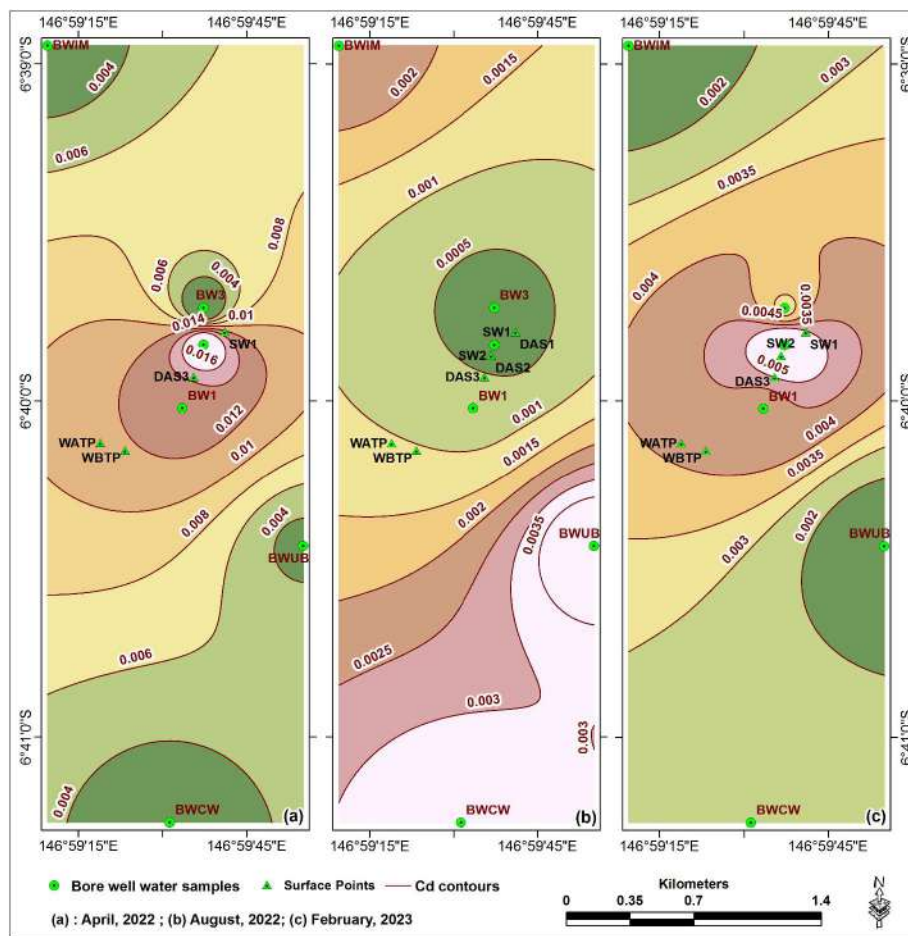


Fig. 6: Spatial Variation of Cd.

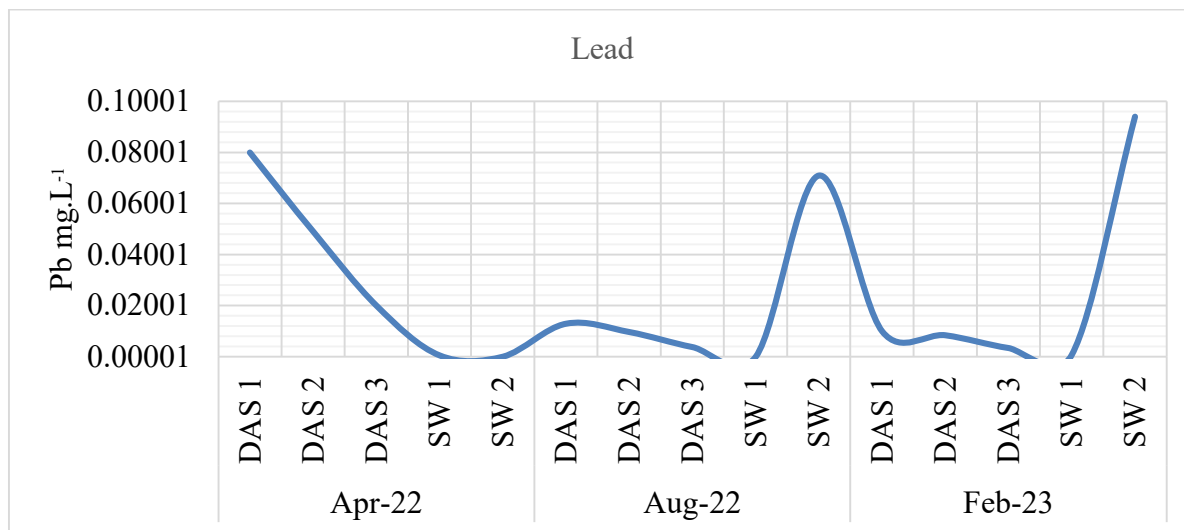


Fig. 7: Temporal Variation of Pb in Surface Point.

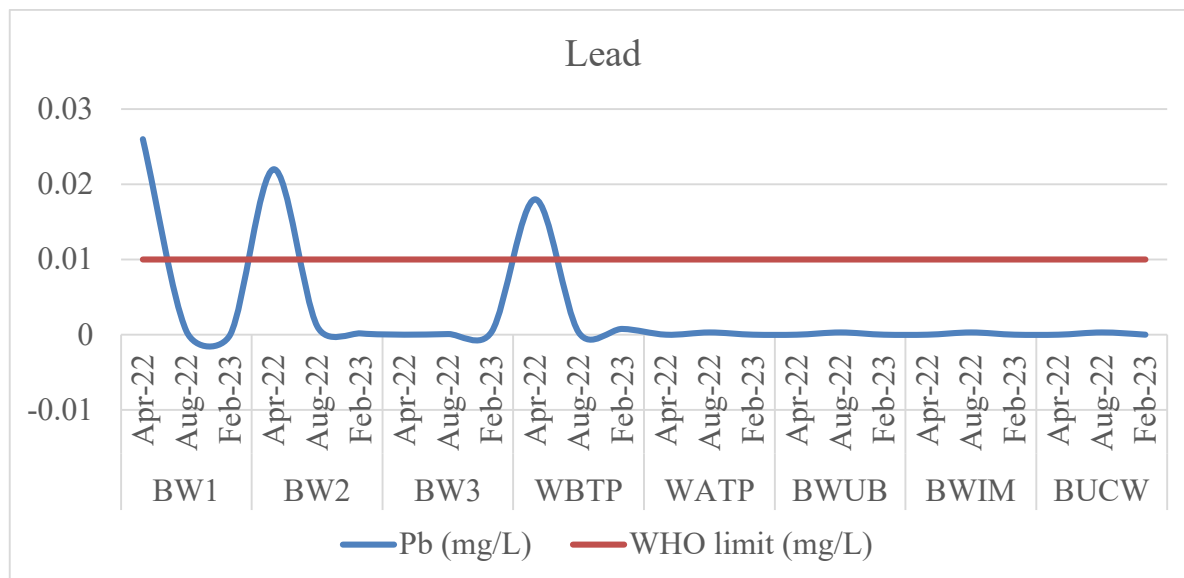


Fig. 8: Temporal Variation of Pb in Borewells.

and February 2023, respectively. Leaching and percolation of contaminants were particularly effective during the rainy seasons in August 2022 and February 2023, which likely caused an increase in Pb levels in surface water samples collected at those times. In contrast, the highest Pb concentrations in groundwater were detected in BW1, BW2, and WBTP in April 2022, when the samples were collected during the driest week. Due to the lack of rainfall, the contaminants were not effectively diluted, leading to higher Pb levels in the groundwater. This variation emphasizes the influence of seasonal rainfall on the dispersion and concentration of lead contaminants in both surface and groundwater systems.

The maximum mercury (Hg) levels were consistently detected in SW1, SW2, and BW1 throughout the investigation period. However, the highest concentrations of Hg were measured in BW2, WB3, WBTP, and WATP in February 2023. Since mercury is known to be highly persistent in the environment, it is believed that Hg pollution in SW1 and SW2 leached into the groundwater over time. This process likely contributed to the elevated concentrations of Hg detected in the groundwater samples in February 2023. The persistence of Hg and its ability to contaminate both surface and groundwater highlight the long-term environmental risks associated with mercury pollution.



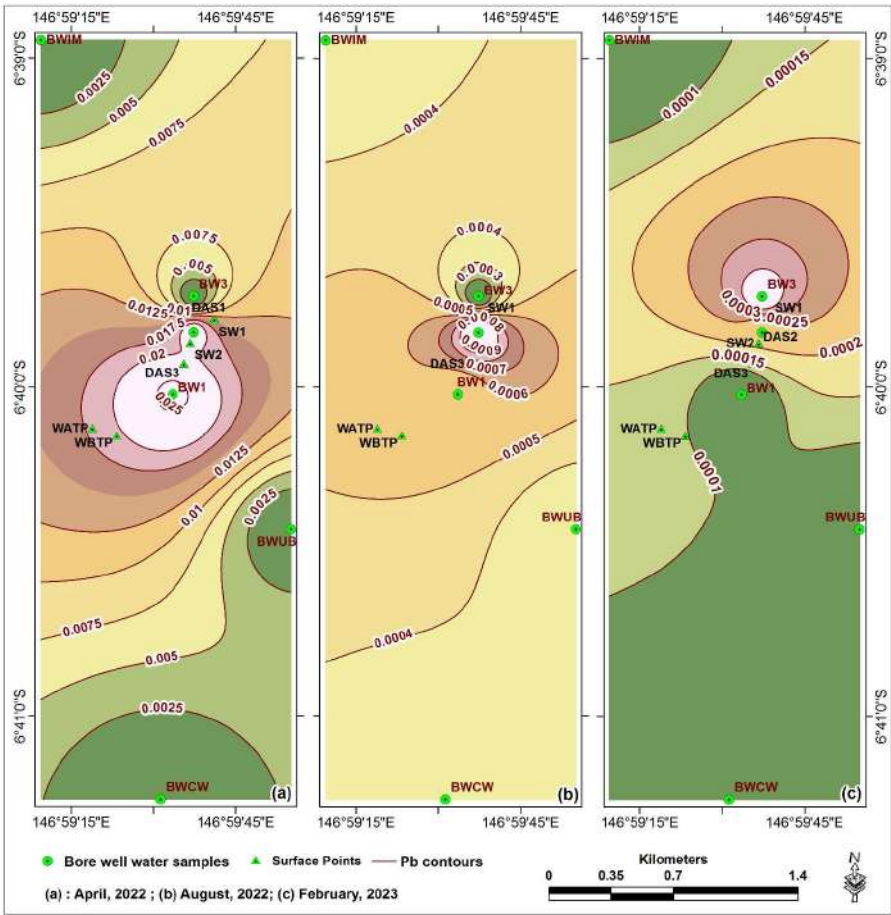


Fig. 9: Spatial variation of Pb.

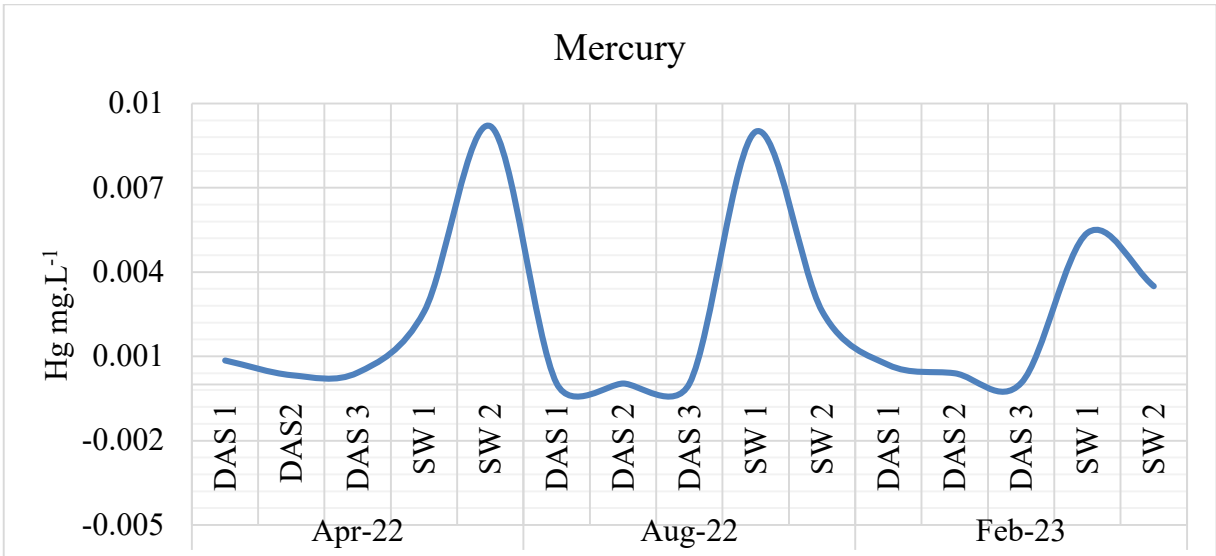


Fig. 10: Temporal Variation Hg in Surface Point.

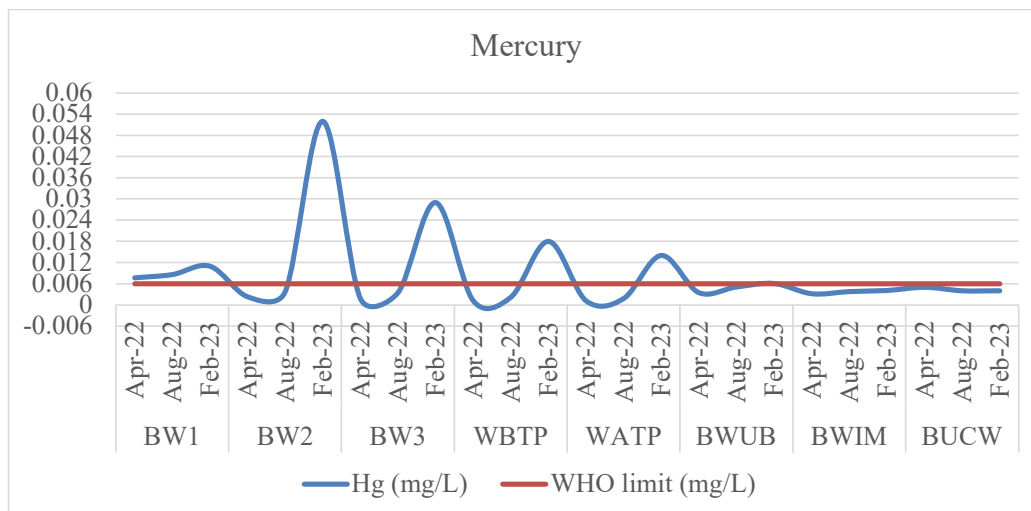


Fig. 11: Temporal Variation of Hg in borewells.

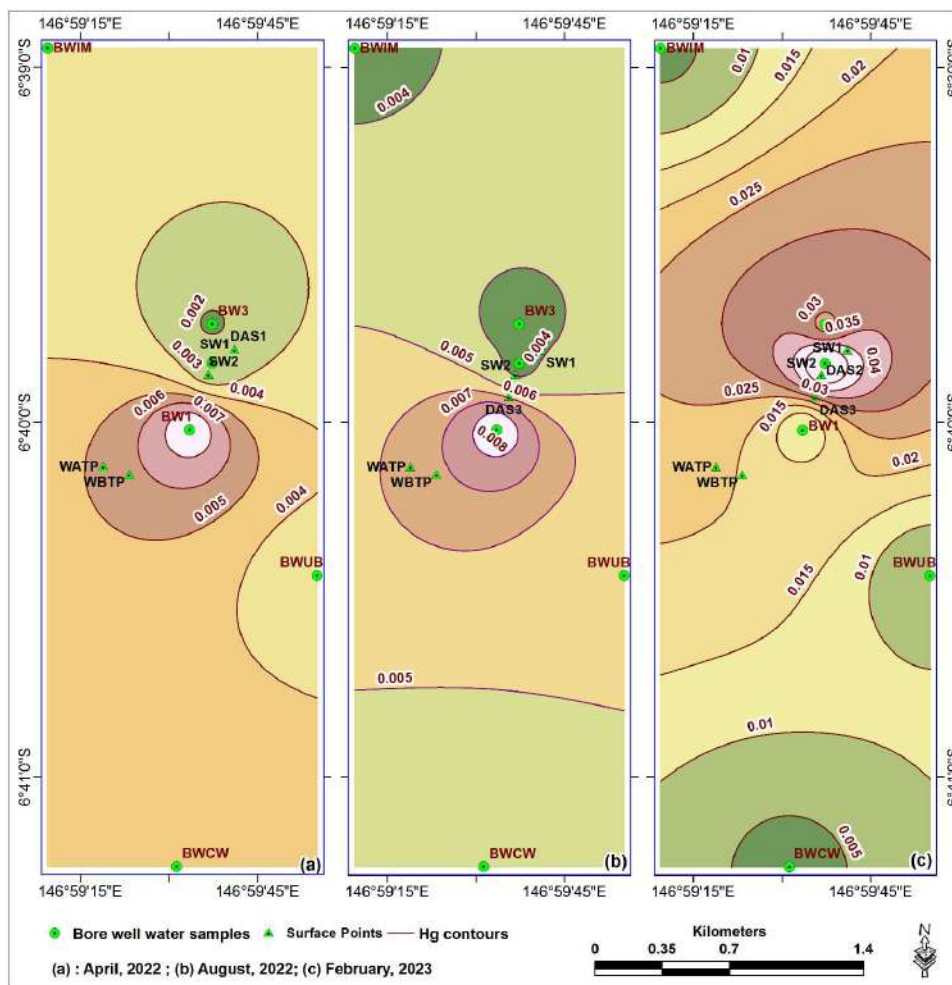


Fig. 12: Spatial Variation of Hg.

## CONCLUSIONS

Confirming the concerns of pollution at the site, the study concludes that leaching of Cadmium (Cd), Lead (Pb), and Mercury (Hg) percolated through the soils and polluted the groundwater nearer to ODS. Also concluded that leaching of chemical contaminants as confirmed by Cd, Pb, and Hg concentrations at the site under investigation, heavy metals were detected in BW1 BW2 BW3, WBTP, WATP, SW1, SW2, DAS1, DAS2, and DAS3 which signifies leaching and percolating of potential pollution sources near the dumping. Borewells further away from dumping sites and BWIM. BWUB and BWCWP detected heavy metals below the permissible limit. Therefore, an ODS along the boundary has significant impacts on groundwater quality near the dumping site. Cd and Pb were detected at greater concentrations in April 2022 at BW1, BW2, SW1 SW2. The heavy metals detection in bore water seems to have resulted from the dumping of electronic waste, electrical appliances, batteries, packaging materials, and cosmetic products, as per site observations coinciding with earlier reported studies.

Preventing groundwater pollution from open dumping requires a combination of regulatory measures, waste management practices, and environmental monitoring. Looking at the situation of the site, we herewith recommend the following best strategies to prevent open dumping from contaminating groundwater. Firstly, proper waste management systems like improved waste collection and recycling infrastructure should be considered with designed sanitary landfills. This should be followed by implementing hazardous waste regulations with strict enforcement of laws. Further, regular monitoring of the site along with real-time detection technologies would be beneficial in timely identification and remedial steps. Finally, public awareness programs should be engaged in the local communities for proper disposal and civic responsibility in maintaining public health and environmental protection. Modern environmentally friendly methods like bioremediation and phytoremediation should be considered at the site. By implementing these strategies, open dumping and its subsequent groundwater pollution can be significantly reduced, protecting both human health and the environment.

## ACKNOWLEDGMENT

The Author would like to thank Mr. Parkop Kurua, Managing Director and staff of Water PNG Limited, for granting permission to access borewells and assistance during sampling as well as to National Analytical and Testing Services Limited (NATSL) management through Executive Manager Mr. Vincent Koddy and staff for support through providing analytical services.

## REFERENCES

- Aderemi, A.O., Oriaku, A.V., Adewumi, G.A. and Otitolaju, A.A., 2011. Assessment of groundwater contamination by leachate near a municipal solid waste landfill. *African Journal of Environmental Science and Technology*, 5, pp.933–940.
- Akinbile, C.O., 2012. Environmental impact of landfill on groundwater quality and agricultural soils in Nigeria. *Soil and Water Research*, 7, pp.18–26.
- Alao, J.O., Fahad, A., Abdo, H.G., Ayejoto, D.A., Almohamad, H., Ahmad, M.S., Nur, M.S., Danjuma, T.T., Yusuf, M.A. and Francis, O.T., 2023. Effects of dumpsite leachate plumes on surface and groundwater and the possible public health risks. *Science of The Total Environment*, 897, pp. 165469.
- Baderna, D., Caloni, F. and Benfenati, E., 2019. Investigating landfill leachate toxicity in vitro: A review of cell models and endpoints. *Environment International*, 122, pp.21–30.
- Burrough, P.A. and McDonnell, R.A., 1998. *Principles of Geographical Information Systems*. Oxford University Press, p. 330.
- Fatta, D., Papadopoulos, A. and Loizidou, M., 1999. A study on the landfill leachate and its impact on the groundwater quality of the greater area. *Environmental Geochemistry and Health*, 21, pp.175–190.
- Fodor, L. and Szabó, L., 2004. Study of heavy metal leaching in the soil. Proceedings of the 13th International Soil Conservation. Organization Conference.
- Hadi, N.S., 2023. Leachate Characterization and Assessment of Soil Pollution Near Some Municipal Solid Waste Transfer Stations in Baghdad City. *Nature Environment & Pollution Technology*, 22(4), pp. 2239-2247.
- Hossain, M.L., Das, S.R., Hossain, M. K. and others, 2014. Impact of landfill leachate on surface and groundwater quality. *Journal of Environmental Science and Technology*, 7, pp.337–346.
- Lin, L., Yang, H. and Xu, X., 2022. Effects of water pollution on human health and disease heterogeneity: a review. *Frontiers in environmental science*, 10, pp.1-16.
- Maiti, S.K., De, S., Hazra, T., Debsarkar, A. and Dutta, A., 2016. Characterization of leachate and its impact on surface and groundwater quality of a closed dumpsite—a case study at Dhapa, Kolkata, India. *Procedia Environmental Sciences*, 35, pp.391–399.
- Mor, S., Ravindra, K., Dahiya, R.P. and Chandra, A., 2006. Leachate characterization and assessment of groundwater pollution near municipal solid waste landfill site. *Environmental Monitoring and Assessment*, 118, pp.435–456.
- Nagarajan, R., Thirumalaisamy, S. and Lakshumanan, E., 2012. Impact of leachate on groundwater pollution due to non-engineered municipal solid waste landfill sites of Erode City, Tamil Nadu, India. *Iranian Journal of Environmental Health Science & Engineering*, 9, pp.1-12.
- Omeiza, A.J., Abdulwahab, O.O., Nur, M.S., Danjuma, T.T., Jaiyeoba, E., Abdullahi, D., Adekanye, O.O. and Mary, E.T., 2022. Effect of an active open dumpsite on the earth's subsurface and groundwater resource. *Asian Journal of Physical and Chemical Sciences*, 10, pp. 15–24.
- Pande, G.S., 2015. Impacts of leachate percolation on groundwater quality: A case study of Dhanbad city. *Global Nest Journal*, 17, pp.162–174.
- Przydatek, G. and Kanownik, W., 2019. Impact of small municipal solid waste landfill on groundwater quality. *Environmental Monitoring and Assessment*, 191, pp.1–14.
- Samanta, S., Pal, D.K., Lohar, D. and Pal, B., 2012. Interpolation of climate variables and temperature modeling. *Theoretical and Applied Climatology*, 107, pp.35-45.
- Sankhla, M.S. and Kumar, R., 2019. Contaminant of heavy metals in groundwater & its toxic effects on human health & environment. *International Journal of Environmental Sciences & Natural Resources*, 18(5), pp. 00149-00153.

- Stanaway, R., Wallace, L., Sombo, Z., Peter, J., Palusi, T., Safomea, B. and Nathan, J., 2009. Lae, a City Caught Between Two Plates – 15 Years of Deformation Measurements with GPS. *Paper presented at the 43rd Association of Surveyors PNG Congress*, Lae, Papua New Guinea, 12–15 August 2009.
- Sugirtharan, M. and Rajendran, M., 2015. Groundwater quality near municipal solid waste dumping site at Thirupperumthurai, Batticaloa. *The Journal of Agricultural Sciences*, 10(1), pp.21-28.
- Usman, M., Yasin, H., Nasir, D.A. and Mehmood, W., 2017. A case study of groundwater contamination due to open dumping of municipal solid waste in Faisalabad, Pakistan. *Earth Sciences Pakistan*, 1, pp. 15–16.
- Waheed, A.H. and Bhawsar, A., 2021. Assessment of groundwater quality near solid waste dumping site Bhanpur, Bhopal. *International Journal of Applied Research*, 7(8), pp.314-319.
- World Health Organization (WHO), 2022. *Guidelines for Drinking-Water Quality: Fourth Edition Incorporating the First Addendum, Annex 3*. WHO.



# Evaluation of Air Quality by Particulate Matter in Junin and Huancavelica, Peru

Julio Angeles Suazo<sup>1†</sup>, Roberto Angeles Vasquez<sup>2</sup>, Esmila Yeime Chavarría Márquez<sup>1</sup>, Carmencita Lavado-Meza<sup>1</sup>, Leonel de la Cruz-Cerrón<sup>3</sup>, Nataly Angeles Suazo<sup>4</sup>, Liz Quispe Quincho<sup>1</sup> and Hugo Abi Karam<sup>5</sup>

<sup>1</sup>Universidad Nacional Autónoma de Tayacaja Daniel Hernández Morillo, Escuela Profesional de Ingeniería Forestal, Ambiental, Tayacaja, Perú

<sup>2</sup>Universidad Nacional del Centro del Perú, Facultad de Ingeniería Civil, Huancayo, Perú

<sup>3</sup>Universidad Continental, Facultad de Ingeniería, Huancayo, Perú

<sup>4</sup>Universidad Tecnológica del Perú, Facultad de ingeniería de Sistemas, Huancayo, Perú

<sup>5</sup>Universidade Federal do Rio de Janeiro, Rio de Janeiro, Brasil

†Corresponding author: Julio Angeles Suazo; jangelesambiental@gmail.com

**Abbreviation:** Nat. Env. & Poll. Technol.  
**Website:** [www.neptjournal.com](http://www.neptjournal.com)

*Received:* 14-09-2024

*Revised:* 12-11-2024

*Accepted:* 13-11-2024

## Key Words:

Particulate matter  
 Purple air  
 Hysplit model  
 Air pollution transport  
 Air quality

## Citation for the Paper:

Angeles Suazo, J., Angeles Vasquez, R., Chavarría Márquez, E.Y., Lavado-Meza, C., de la Cruz-Cerrón, L., Angeles Suazo, N., Quispe Quincho, L. and Abi Karam, H., 2025. Evaluation of air quality by particulate material in Junin and Huancavelica, Peru. *Nature Environment and Pollution Technology*, 24(2), p. D1722. <https://doi.org/10.46488/NEPT.2025.v24i02.D1722>

*Note: From year 2025, the journal uses Article ID instead of page numbers in citation of the published articles.*



**Copyright:** © 2025 by the authors

**Licensee:** Technoscience Publications

This article is an open access article distributed under the terms and conditions of the Creative Commons Attribution (CC BY) license (<https://creativecommons.org/licenses/by/4.0/>).

## ABSTRACT

Anthropogenic atmospheric particles with a diameter of less than 2.5 µm (PM<sub>2.5</sub>) and between 2.5 to 10 µm (PM<sub>10</sub>) are among the main contributors to air pollution and have become a serious pollution threat in the Junin and Huancavelica region of Peru. This increase could be due to the burning of vegetation in the Amazon region of Brazil. Therefore, data obtained with the low-cost PA-II Purpleair sensor were analyzed to measure particulate matter (fine and coarse fashions) in the Junin region (Chanchamayo, station T. Huancayo, station T1 and Chupaca, station T3) and Huancavelica (Pampas, station T2). Likewise, the Hysplit model was used to quantify the transboundary wind trajectories from the Amazon region in Brazil to the Junin region in Peru. Shows that, during the rainy season, the maximum concentrations of PM<sub>2.5</sub> and PM<sub>10</sub> are 151 µg.m<sup>-3</sup> (station T1) and 178 µg.m<sup>-3</sup> (station T1), respectively. Finally, the results of the air quality index (AQI) for PM<sub>2.5</sub> allow for the classification of the Huancayo and Chanchamayo stations with "very bad" and "moderate to bad" air quality, respectively. Also, in Pampas and Chupaca, the AQI is classified as very unhealthy and hazardous on almost 50% and 43% of days, respectively.

## INTRODUCTION

Atmospheric aerosols are a suspended mixture of solid particles or liquid droplets in the air, also known as particulate matter (PM) (Rabha & Saikia 2019). These exert a broader effect on atmospheric processes, radiative balance, climate, ecology, public health, and radiative forcing at both global and regional scales (Chang et al. 2021). Currently, air pollution is dominated by fine particulate matter whose aerodynamic diameter is less than or equal to 2.5 µm (PM<sub>2.5</sub>), resulting from the rapid urbanization and industrialization of major cities (Vo et al. 2020). It has been considered that the increase of these particles is an important factor in the cooling of the earth-atmosphere system and partially offsets the greenhouse effect (Suazo et al. 2020, Tosca et al. 2017, Vo et al. 2020).

Air pollution is becoming increasingly important in the environmental scene due to its effects on health, as it has increased the risk of death and respiratory diseases among children (César et al. 2016, Perlroth & Branco 2017). In 2016, globally, one in four child deaths was associated with the effects of air pollution; this was responsible for 4.2 million premature deaths; of these, almost 300,000 were children under 5 years old (Adair & Arroyo 2018).

On the other hand, in Huancayo (a province belonging to the Junín region, Peru), the mass concentration of PM<sub>2.5</sub> from March to November 2017 shows the average annual mass concentration, which ranged from 3.4 to 36.8.  $\mu\text{g.m}^{-3}$  (De La Cruz et al. 2019). However, in August 2007, and January, April, and May 2008, they reported results for PM<sub>10</sub> ( $64.54 \pm 30.87 \mu\text{g.m}^{-3}$ ) and PM<sub>14.75</sub> ( $\pm 34.47$ )  $2.5 \mu\text{g.m}^{-3}$ ), which exceeded annual air quality standards. Peruvian. They also showed a higher concentration of PM<sub>10</sub> and PM<sub>2.5</sub> in the dry period (Suárez-Salas et al. 2017).

However, meteorological parameters are a determining factor in PM concentrations since the dispersion processes and the mechanisms for removing atmospheric particles depend on wind speed (Chakraborty et al. 2016, Dhar et al. 2019, Galindo et al. 2011, Haque et al. 2016, Hu et al. 2018, Jayamurugan et al. 2013, Owoade et al. 2015, Zu et al. 2017, Zyromski et al. 2014).

Poor green policies, socioeconomic conditions, and weak governance practices may explain this, including the lack of research in this field (Benegas et al. 2021, Dobbs et al. 2019). However, this situation is changing globally, and there is increasing concern about the relationship between the presence of urban trees and the mitigation of pollution, noise, and so-called heat island effects in cities around the world (Pimienta-Barrios et al. 2018, Soto-Estrada 2019, Zardo et al. 2017). In this trend, more and more studies and research highlight the need to integrate the benefits of urban trees into urban planning and management, to improve the quality of life of citizens (Dobbs et al. 2018, de Mola et al. 2017, Muñoz-Pacheco & Villaseñor 2022, Romero-Duque et al. 2020).

Therefore, this research consists of determining the concentration of particulate matter and its air quality in the Junín region (Huancayo, Chupaca, and La Merced) and Huancavelica (Ahuaycha), Peru during the period 2020-2022 and 2024.

## MATERIALS AND METHODS

### Site Study

The study area is in the Junín region, in the central Andes of Peru, and has different altitudes ranging from the lowland

jungle at 250 m above sea level (a.s.l) to the cold Andean mountains at 5 500 m a.s.l. (Fig. 1), giving rise to a great diversity of climates, landscapes, and ecosystems (Ministerio de Vivienda 2016).

Precipitation in Peru is concentrated in the period between September and April, while in the period between May and August, there is very little precipitation, which is why there is a marked seasonality in the region (Aceituno 1989, Flores-Rojas et al. 2019, Garreaud 2009). The climate of the city of Huancayo is presented regularly based on data collected at the Huancayo Observatory (IGP), where the coldest temperatures are recorded in June and July (winter), and the highest values around October and December. The average annual temperature is  $11.9 \pm 1.2^\circ\text{C}$ . Precipitation from June to July is recorded with the lowest amounts of rain, while from January to March, the highest rainfall is recorded (February = 129.1 mm) and presents an average annual accumulated rainfall of  $752 \pm 44.3$  mm (IGP, 2005). On the other hand, during the rainy season, humid air from the middle troposphere, coming from the Amazon, flows over the Central Andes, where it is responsible for the occurrence of summer convective storms in this region (Garreaud et al. 2003, Garreaud 1999, Vuille 1999, Vuille et al. 2000, 2008). Various authors demonstrated that the region is affected by the burning of biomass or anthropogenic emissions released from the city of Huancayo, which are transported and dispersed over the Peruvian Andes (Magalhães et al. 2019, Vuille & Keimig 2004).

The Pampas District is located in the province of Tayacaja, in the department of Huancavelica. The district is 3280 m above sea level and has an area of 90.96  $\text{km}^2$ , with a population density of 65.29 inhabitants/ $\text{km}^2$ . The temperature varies according to the seasons of the year, ranging between  $24^\circ\text{C}$  maximum and minus  $12^\circ\text{C}$  minimum. Precipitation varies from 8 mm to 124 mm, with rainfall beginning to intensify from October to March (Ministerio de Vivienda 2002).

For the present study, the purple air sensor was used (data downloadable at: <https://map.purpleair.com/>) for six continuous particulate matter monitoring stations (Table 1).

Table 1: Measurements of particulate matter sensor.

State/Country	Province	Symbology	Coordinates	
			Latitude	Longitude
Junín/Peru	Chanchamayo	T	-11.05	-75.33
Junín/Peru	Huancayo	T1	-12.05	-75.22
Huancavelica/Peru	Pampas	T2	-12.39	-74.87
Junín/Peru	Chupaca	T3	-12.06	-75.28

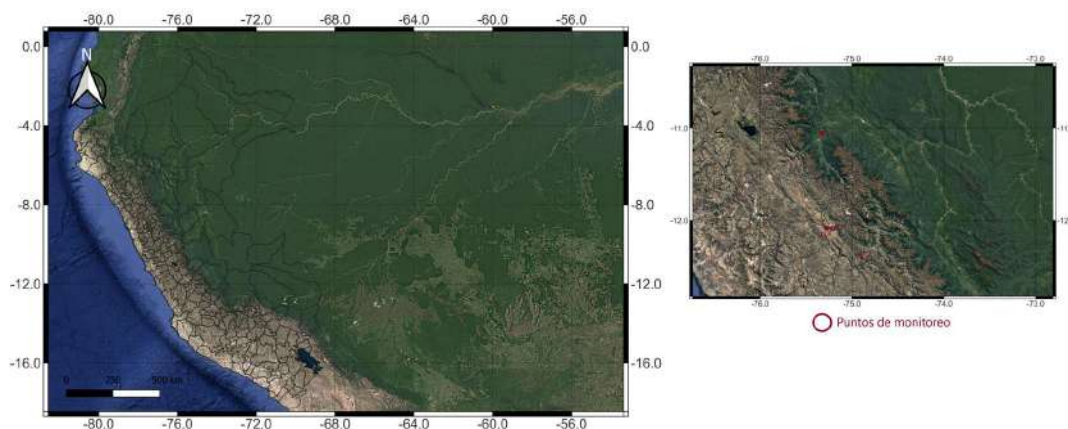


Fig. 1: A. Location of monitoring stations.

### The Purple Air PA-II Low-Cost PM Monitor

The PurpleAir sensor is a low-cost optical particle counter of PM<sub>2.5</sub>, and PM<sub>10</sub> mass concentrations in  $\mu\text{g}/\text{m}^3$ , incorporating a temperature, relative humidity, and pressure sensor with a wireless network communication module, which records and transmits data via Wi-Fi to a cloud-based platform (Ardon-Dryer et al. 2020). Furthermore, the Purple Air PA-II monitors as a component of a large-scale calibrated monitoring network, which can lead to integrated solutions for high-resolution monitoring (Bi et al. 2020).

### Air Quality Index

The air quality index (AQI) for particulate matter was calculated according to the equation used (Beringui et al. 2022).

Daily AQI was calculated from the 24-hour average particulate matter concentration and is classified into five classes, as presented in Table 2.

## RESULTS AND DISCUSSION

### Particulate Matter

**Huancayo/Junín:** Fig. 2 shows that during the rainy season, the maximum mass concentrations of PM<sub>1</sub>, PM<sub>2.5</sub>, and

Table 2: Air quality index (AQI) range and air classification according to indexed values (Beringui et al. 2022, 2023).

Classes	Range	Air classification	Color identification
I	0-40	Good	green
II	41-81	Moderate	yellow
III	81-120	unhealthy	orange
IV	121-200	Very unhealthy	red
V	201-400	hazardous	purple

PM<sub>10</sub> are  $97 \mu\text{g}/\text{m}^3$  (station T151),  $1 \mu\text{g}/\text{m}^3$  (station T1) and  $178 \mu\text{g}/\text{m}^3$  (station T1) respectively.

These results indicate that high loads of fine particles affect the study region, due to the long-range transport of regional fires driven by advection, so common during the dry season in the Amazon. At station T1, located in the Huancayo area, the rains were late, and its precipitation rate was low. This seasonal pattern is associated with differences in climatic conditions and emission sources characteristic of the rainy and dry periods. Likewise, it is shown that they exceed the quality standards established by Peru only for PM<sub>2.5</sub> (PM<sub>2.5</sub>= $50 \mu\text{g}/\text{m}^3$ , PM<sub>10</sub>= $100 \mu\text{g}/\text{m}^3$  for a period of 24 h, available SUPREME DECREE N° 003 -2017 -MINAM), however, for Brazil (PM<sub>2.5</sub>= $25 \mu\text{g}/\text{m}^3$ , PM<sub>10</sub>= $50 \mu\text{g}/\text{m}^3$  for 24 h, available Resolution CONAMA 491 of 11/19/2018) they exceed for PM<sub>2.5</sub> and PM<sub>10</sub>, and the same would happen with the standards established by the World Health Organization (PM<sub>2.5</sub>= $15 \mu\text{g}/\text{m}^3$ , PM<sub>10</sub>= $45 \mu\text{g}/\text{m}^3$  for 24 h, under the global air quality guidelines of WHO available). Also show the time series of the monthly mean of PM<sub>2.5</sub> and PM<sub>10</sub> for the study stations, illustrating the seasonal and monthly variability. All regions show maximum values before and after partial confinement due to COVID-19 (after June 2020), also in the dry season and can be attributed mainly to meteorological parameters (less precipitation) as happens in China, where in the humid season, due to the deposition process it can reduce the particles suspended in the atmosphere (Wang et al. 2018).

**La Merced/Junín:** Likewise, in Fig. 3, during the period 2021 (November and December) and in the period 2022 (January to August), very noticeable maximum values are presented (August) in La Merced (station T), which exceed the ECAs established in the Peruvian regulations for the values of PM<sub>2.5</sub> and PM<sub>10</sub>.

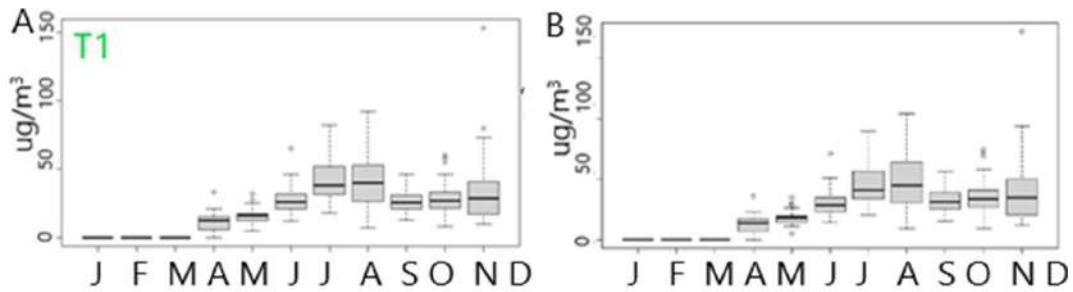


Fig. 2: Time series of monthly average A. PM<sub>2.5</sub> and B. PM<sub>10</sub> concentrations at the stations during 2020.

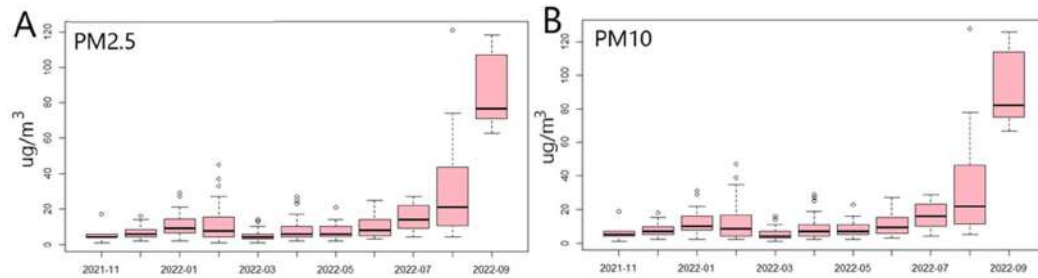


Fig. 3: Time series of monthly average concentrations of A. PM<sub>2.5</sub>, B. PM<sub>10</sub>, and C. time series at the La Merced station (T).

**Pampas/Huancavelica:** Likewise, in Fig. 4, during the period 2024 (February and July), very noticeable maximum values are presented (July) in Pampas (station T2), which doesn't exceed the ECAs established in the Peruvian regulations for the values of PM<sub>2.5</sub> and PM<sub>10</sub>.

**Chupaca/Junin:** Also, note that during February and March 2024, the concentrations of MP<sub>2.5</sub> and MP<sub>10</sub> (Fig. 5) present maximum values of 40 and 49  $\mu\text{g}\cdot\text{m}^{-3}$ , respectively, in August.

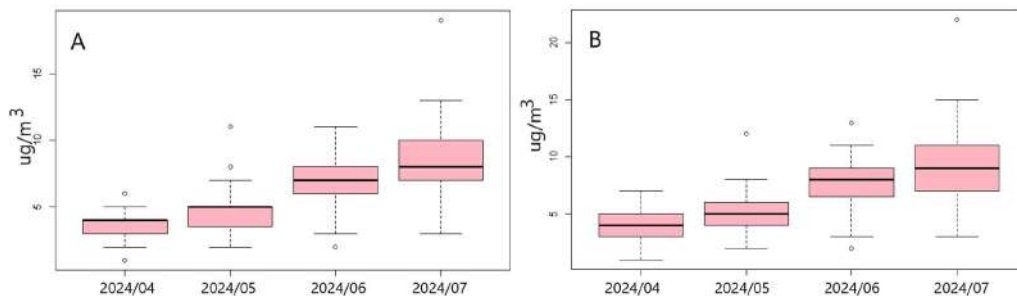


Fig. 4: Time series of monthly average concentrations of A. PM<sub>2.5</sub>, B. PM<sub>10</sub>, and C. time series at Pampas station (T2).

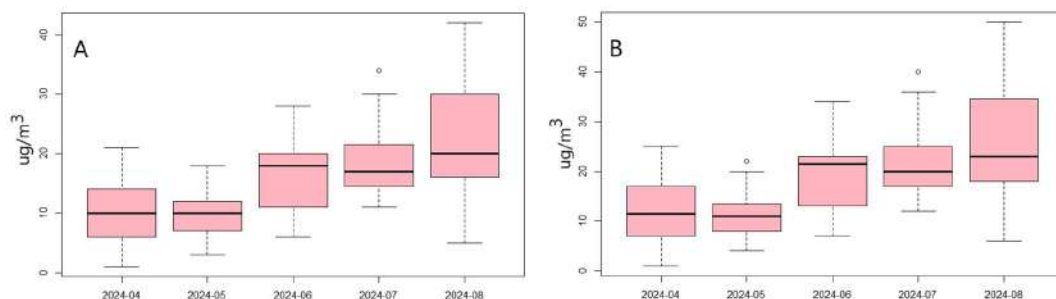


Fig. 5: Boxplot of A. PM<sub>2.5</sub> and B. PM<sub>10</sub> from February to August 2024 to Chupaca Station (T3).



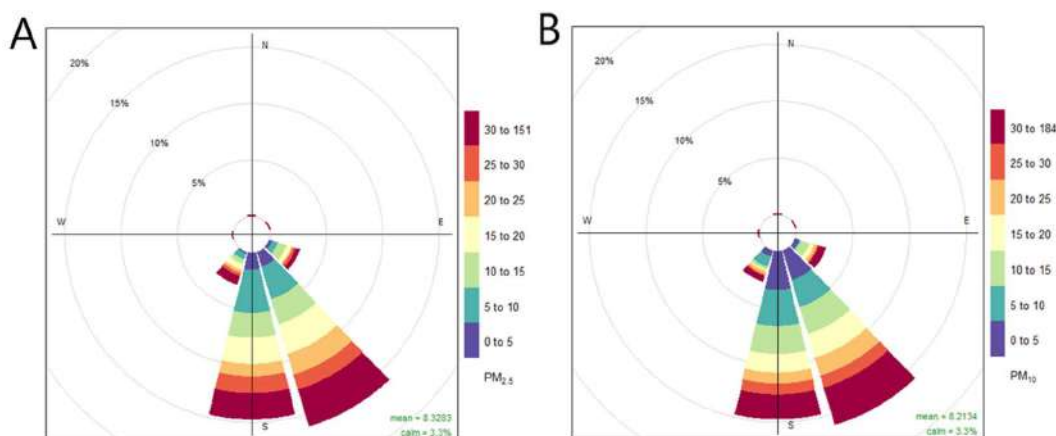


Fig. 6: Influence of wind direction and wind speed on A. PM<sub>2.5</sub> and B. PM<sub>10</sub> concentrations during 2020 for Huancayo station (T1).

### Pollution Roses Due to Particulate Matter

**Huancayo:** The pollution rose diagrams (Fig. 6) show the relationship between WD and WS, and the concentration of pollutants at the monitoring stations. The dispersion of particles towards the south and southeast of Station T1 is indicated. Where it indicates that it can influence the increase in particulate matter resulting from atmospheric dispersion. Likewise, meteorology drives large daily, seasonal, and interannual variations in PM<sub>2.5</sub>. A clear example is in China, by affects the transport of emissions and chemical production. The relationships between PM<sub>2.5</sub> and meteorological variables are complex and differ depending on the region and time of year (Shen et al. 2017). For example, PM<sub>2.5</sub> pollution events during winter in central and eastern China are associated with low wind speed and high relative humidity (HR).

### Air Quality Index

The AQI for MP<sub>2.5</sub> and MP<sub>10</sub> was calculated for stations T and T1, where it presented for La Merced and Huancayo (Fig. 7 and 8 respectively), AQI values lower than 40, classified as “good” 80% of the time in both sites for MP<sub>10</sub>. The concentrations of PM<sub>2.5</sub> were higher than the limit established by Peruvian legislation. Likewise, in La Merced (Fig. 7), the air quality was classified as “moderate” to “very poor”. The concentrations obtained in July-August-2022 were higher than those in January-June-2022, indicating poor air quality. Some days during the partial confinement presented lower concentrations of PM<sub>2.5</sub> than at the beginning of March, which is related to the decrease in the vehicle fleet for 2020 at station T1.

Overall, the air quality index ranged from “good” to “very bad” for both stations. However, during the days of partial confinement (March 2020), the index varied from “good” to

“moderate” for PM<sub>10</sub>-T1. The T1 station is in a populated area, near roads with heavy traffic. Therefore, industrial activities, which did not come to a standstill during the partial lockdown, could be the reason for the poor air quality.

On most days, the air quality for MP<sub>2.5</sub> was classified as “terrible” since the concentrations were higher than the quality standards established by MINAM. Also, mention that, on some days of the evaluated period, data collection failed or was invalidated due to the monitoring station being maintained, so the AQI was not carried out, and the days were not filled in the calendar plots.

These AQI results agree with studies carried out in other cities around the world. In India, air pollution decreased after the second week of lockdown, and the AQI for a total of 91 cities was rated as “good” and “satisfactory”, and no city was rated as “poor” (Anjum 2020). AQI for three cities in China (Wuhan, Jingmen, and Enshi) showed that 88% of days were classified as “moderate” or “good” during the lockdown, while before the lockdown, the percentage of days was 66% (Xu et al. 2020). It should be noted that the AQI of Pampas (T2) (Fig. 9) presents 54.6% of days classified as good, 42.9% moderate and 2.5% unhealthy for MP<sub>2.5</sub>. For AQI of MP<sub>10</sub>, it is classified as good due to the low concentrations of MP<sub>10</sub>. Likewise, for the province of Chupaca, good air quality for coarse mode is 97.9 and moderate of 2.1%, and unhealthy, moderate, and good air quality for fine mode is around 6.8%, 51.3%, and 41.9% of days measurements (Fig. 10).

Therefore, based on the calculated values of the air quality index, we note that it is important to measure the PM<sub>2.5</sub> levels to better manage air quality. Additionally, it is proposed to use deep learning and machine learning algorithms to forecast air quality and thus propose measures for the mitigation and control of air pollution (Saminathan & Malathy 2024).

It is also worth mentioning that PM<sub>2.5</sub> affects health; a clear example is that PM<sub>2.5</sub> is inversely related to hemoglobin and was positively associated with anemia, but

the results were not statistically significant at the alpha level of 0.05 (Deng et al. 2024). On the other hand, Alzheimer's disease (AD) has been linked to air pollution, especially with

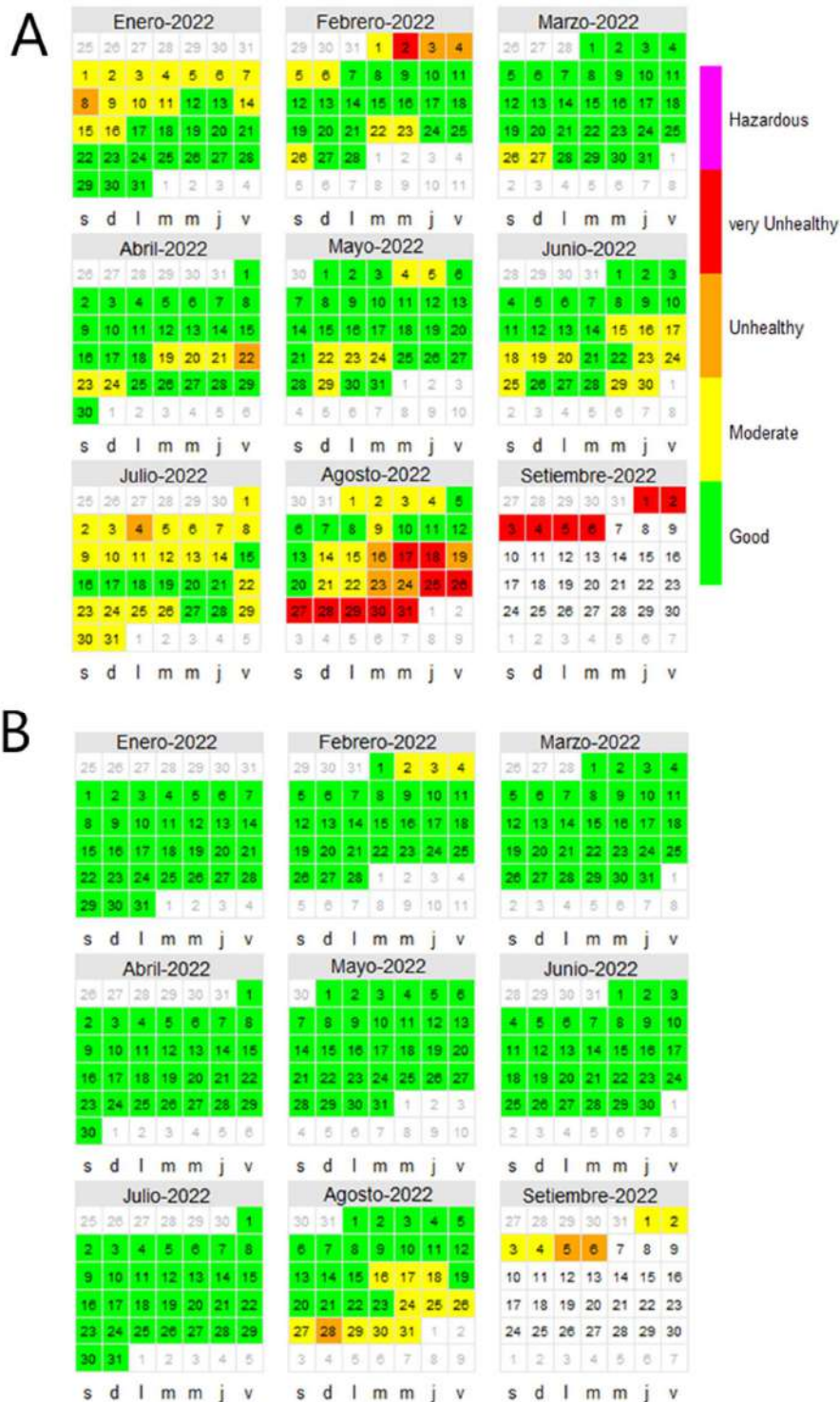
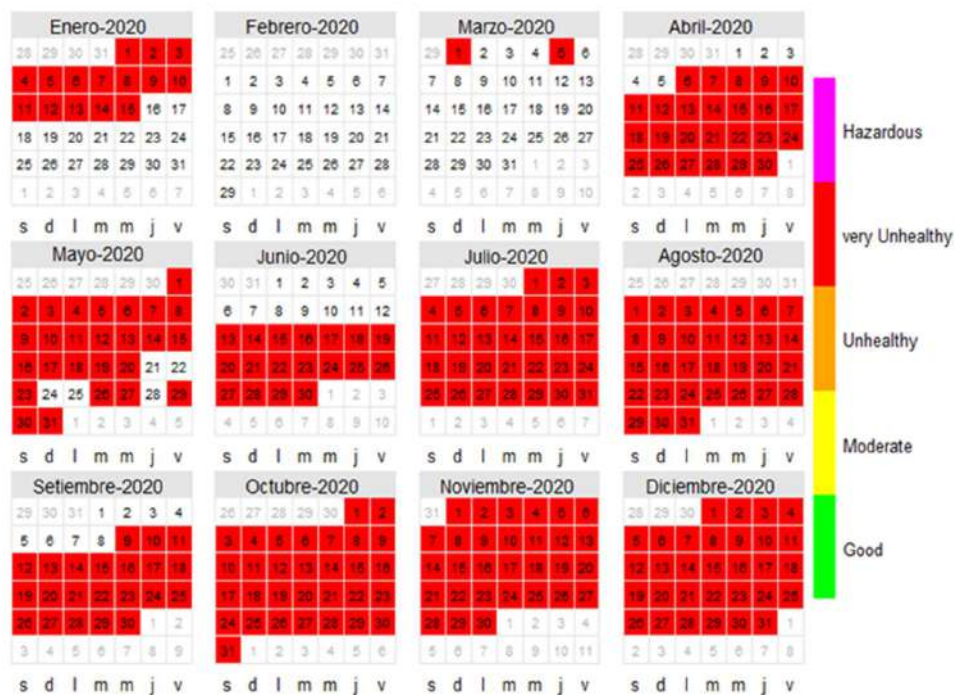
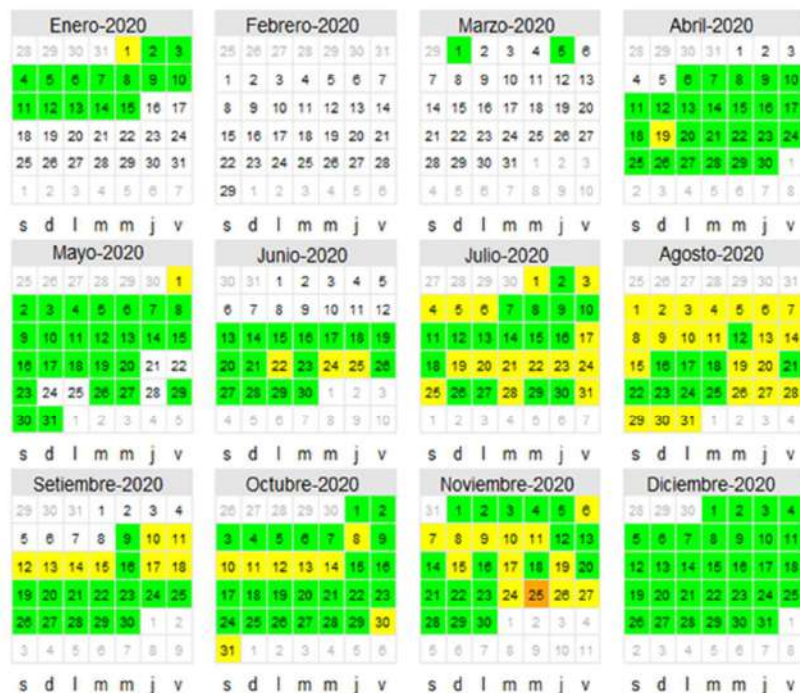


Fig. 7: Air quality index of A. MP<sub>2.5</sub> and B. MP<sub>10</sub> in La Merced (T) during 2022.

A



B

Fig. 8: Air quality index of A. PM<sub>2.5</sub> and B. PM<sub>10</sub> in Huancayo (T1) during 2020.

particulate matter (PM), since PM is composed of several elements, including iron-rich particles that can reach the

brain through inhalation; in addition, Lima, Peru, is one of the most polluted cities in Latin America, with a high rate



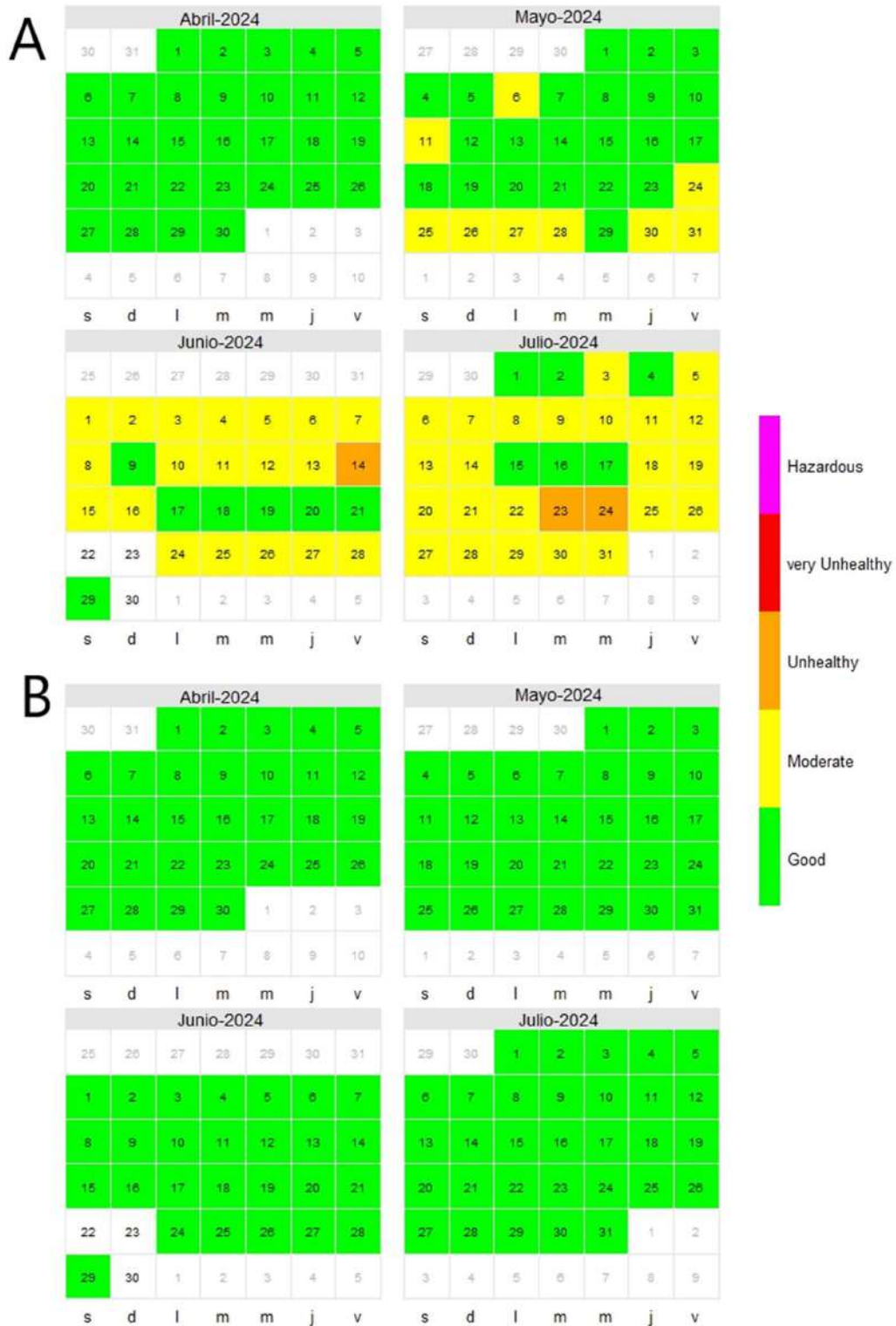


Fig. 9: Air quality index of A. MP2.5 and B. MP10 in Pampas (T2) during 2024.



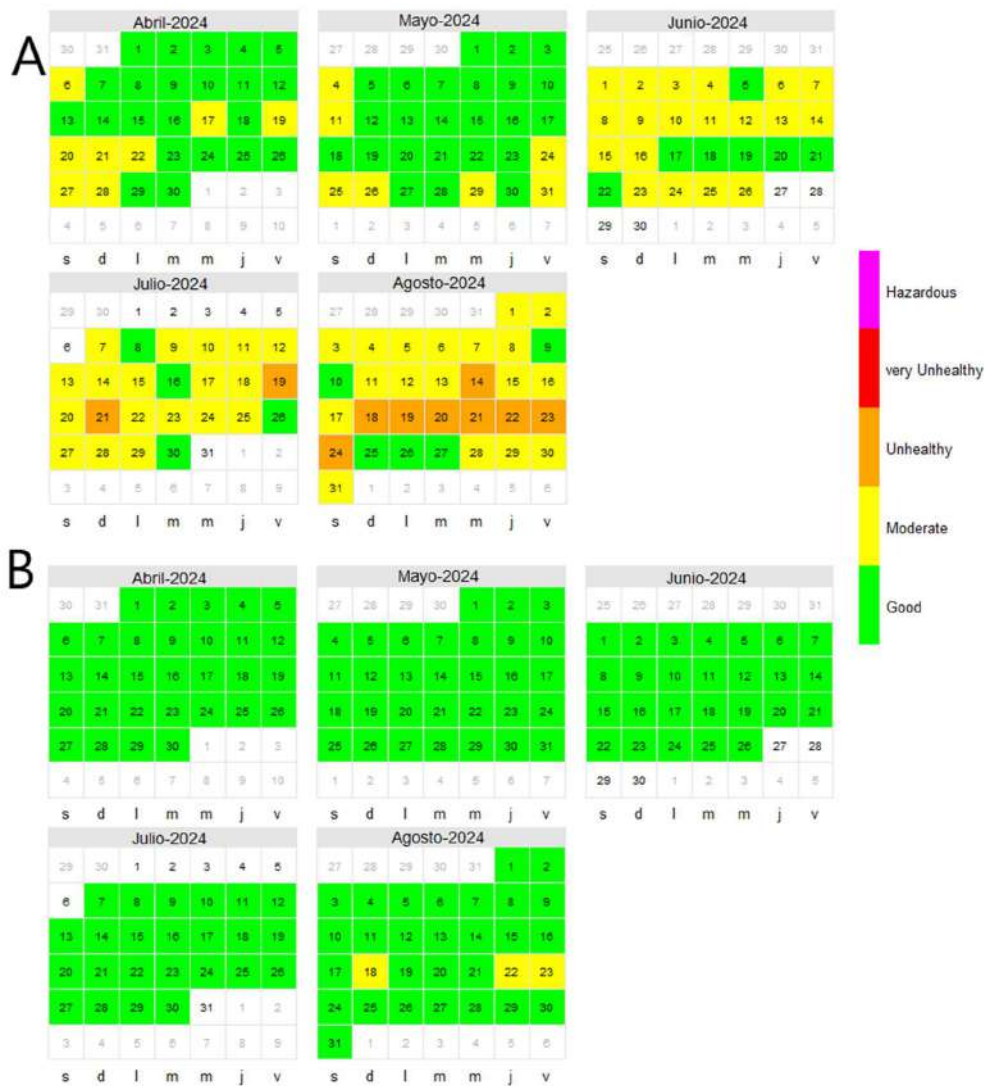


Fig. 10: Air quality index of A. MP2.5 and B. MP10 in Chupaca (T3) during 2024.

of AD, exposure to Fe through inhalation of PM10 may be associated with the presence of AD in Lima (Fano-Sizgorich et al. 2024). However, to mitigate the health effects of air pollutants, There is limited knowledge about the contribution of tree species and the general ecosystem services provided by urban trees under public management, especially in Latin America. They demonstrated that urban tree cover is very relevant to reducing these pollutants dangerous to public health by reducing PM, both PM2.5 and PM10 (Moreno et al. 2024).

Suspended particles, accepted as markers of air quality, are also indicators of health risks for the population, especially for children, due to their greater susceptibility to the quality of the air they breathe. There is a negative

correlation with temperature and a positive correlation with humidity. The correlation with temperature was also very weak compared to humidity (Zender-Świercz et al. 2024). Also, seasonal variations in PM2.5 pollution levels are closely related to changes in the thermal stability of the planetary boundary layer (PBL). During winter, daily increases in PM2.5 concentrations are often linked to atmospheric warming above 1500 m, as increasing thermal inversions and lower PBL heights lead to the accumulation of pollutants (Liang et al. 2024).

## CONCLUSIONS

This research concludes that, during the rainy season, the maximum mass concentrations of PM1, PM2.5, and PM10

are  $97 \mu\text{g.m}^{-3}$  (station T1),  $151 \mu\text{g.m}^{-3}$  (station T1) and  $178 \mu\text{g.m}^{-3}$  (station T1) respectively. Also, at station T1, located in the Huancayo area, the rains were late, and the precipitation rate was low. This seasonal pattern is associated with differences in climatic conditions and emission sources characteristic of the rainy and dry periods.

Finally, the classification of the sites according to the AQI, where in 2020, Huancayo presented the air quality classified as “good to moderate” for MP10 and MP2.5, it was classified as very unhealthy, while La Merced presented the days as “moderate” to “unhealthy” and 10% as very unhealthy. PM2.5 was the pollutant responsible for the reduction in air quality at both monitoring stations. Also, in Pampas and Chupaca, the AQI is classified as moderate and good on almost 50% of days to fine mode. In La Merced, Huancayo, Chupaca, and Pampas, fine particles predominate. These findings highlight the importance of implementing policies and measures to reduce particulate matter emissions, especially those related to motor vehicle fleets and vegetation burning, to improve air quality and reduce health risks.

## ACKNOWLEDGMENTS


To the Universidad Nacional Autónoma de Tayacaja Daniel Hernandez Morillo and Universidad Nacional del Centro del Perú as to the portal purple air.

## REFERENCES

- Aceituno, P., 1989. On the functioning of the Southern Oscillation in the South American sector. Part II. Upper-air circulation. *Journal of Climate*, 2(4).
- Adair, H. and Arroyo, V., 2018. WHO | Air pollution and child health: Prescribing clean air. *World Health Organization*, 12(1), pp.1–10.
- Ardon-Dryer, K., Dryer, Y., Williams, J.N. and Moghimi, N., 2020. Measurements of PM2.5 with PurpleAir under atmospheric conditions. *Atmospheric Measurement Techniques*, 13, pp.5441–5458.
- Benegas, L., Rojas, A., Iraheta, A. and Cárdenas, J., 2021. Analysis of the tree component and its contribution to ecosystem services in the city of Turrialba, Costa Rica. *Ecosystems*, 30(2).
- Beringui, K., Justo, E., Ventura, L., Gomes, R., LionelMateus, V., De La Cruz, A., de Almeida, A.C., Ramos, M., Angeles Suazo, J., Valle, P. and Gioda, A., 2023. The contribution of meteorological parameters and the COVID-19 partial lockdown on air quality in Rio de Janeiro, Brazil. *Journal of the Brazilian Chemical Society*, 34(1), pp.69–82.
- Beringui, K., Justo, E.P.S., De Falco, A., Santa-Helena, E., Rocha, W.F.C., Deroubaix, A. and Gioda, A., 2022. Assessment of air quality changes during COVID-19 partial lockdown in a Brazilian metropolis: From lockdown to the economic opening of Rio de Janeiro, Brazil. *Air Quality, Atmosphere and Health*, 15(7), pp.1205–1220.
- Bi, J., Wildani, A., Chang, H.H. and Liu, Y., 2020. Incorporating low-cost sensor measurements into high-resolution PM2.5 modeling at a large spatial scale. *Environmental Science and Technology*, 54(4).
- César, A.C.G., Nascimento, L.F.C., Mantovani, K.C.C. and Pompeo Vieira, L.C., 2016. Fine particulate matter estimated by a mathematical model and hospitalizations for pneumonia and asthma in children. *Revista Paulista de Pediatria*, 34(2), pp.145–152.
- Chakraborty, S., Fu, R., Massie, S.T. and Stephens, G., 2016. The relative influence of meteorological conditions and aerosols on the lifetime of mesoscale convective systems. *Proceedings of the National Academy of Sciences of the United States of America*, 113(27).
- Chang, D.Y., Yoon, J., Lelieveld, J., Park, S.K., Yum, S.S., Kim, J. and Jeong, S., 2021. Direct radiative forcing of biomass burning aerosols from the extensive Australian wildfires in 2019–2020. *Environmental Research Letters*, 16(4).
- De La Cruz, A.H., Roca, Y.B., Suarez-Salas, L., Pomalaya, J., Tolentino, D.A. and Gioda, A., 2019. Chemical characterization of PM2.5 at rural and urban sites around the metropolitan area of Huancayo (Central Andes of Peru). *Atmosphere*, 10(12), pp.1–14.
- de Mola, U.L., Ladd, B., Duarte, S., Borchard, N., La Rosa, R.A. and Zutta, B., 2017. On the use of hedonic price indices to understand ecosystem service provision from urban green space in five Latin American megacities. *Forests*, 8(12), pp.1–15.
- Deng, Y., Steenland, K., Sinharoy, S.S., Peel, J.L., Ye, W., Pillarisetti, A., Eick, S.M., Chang, H.H., Wang, J., Chen, Y., Young, B.N., Clark, M.L., Barr, D.B. and Clasen, T.F., 2024. Association of household air pollution exposure and anemia among pregnant women: Analysis of baseline data from ‘Household Air Pollution Intervention Network (HAPIN)’ trial. *Environment International*, 190, p.108815.
- Dhar, R.B., Chakraborty, S., Chattopadhyay, R. and Sikdar, P.K., 2019. Impact of land-use/land-cover change on land surface temperature using satellite data: A case study of Rajarhat Block, North 24-Parganas District, West Bengal. *Journal of the Indian Society of Remote Sensing*, 47(2), p.65.
- Dobbs, C., Escobedo, F.J., Clerici, N., de la Barrera, F., Eleuterio, A.A., MacGregor-Fors, I., Reyes-Paecke, S., Vásquez, A., Zea Camaño, J.D. and Hernández, H.J., 2019. Urban ecosystem services in Latin America: Mismatch between global concepts and regional realities? *Urban Ecosystems*, 22(1), pp.78–93.
- Dobbs, C., Hernández-Moreno, Á., Reyes-Paecke, S. and Miranda, M.D., 2018. Exploring temporal dynamics of urban ecosystem services in Latin America: The case of Bogotá (Colombia) and Santiago (Chile). *Ecological Indicators*, 85, pp.812–821.
- Fano-Sizgorich, D., Vásquez-Velásquez, C., Ordoñez-Aquino, C., Sánchez-Ccoyllo, O., Tapia, V. and Gonzales, G.F., 2024. Iron trace elements concentration in PM10 and Alzheimer’s disease in Lima, Peru: Ecological study. *Biomedicine*, 12(9), p.2043.
- Flores-Rojas, J.L., Pereira-Filho, A.J., Karam, H.A., Vemado, F., Masson, V. and Silva-Vidal, F.Y., 2019. Modeling the effects of explicit urban canopy representation on the development of thunderstorms above a tropical megacity. *Atmosphere*, 10(3), pp.1–12.
- Galindo, N., Yubero, E., Nicolás, J.F., Crespo, J., Pastor, C., Carratalá, A. and Santacatalina, M., 2011. Water-soluble ions measured in fine particulate matter next to cement works. *Atmospheric Environment*, 45(12), pp.2041–2047.
- Garreaud, R., Vuille, M. and Clement, A.C., 2003. The climate of the Altiplano: Observed current conditions and mechanisms of past changes. *Palaeogeography, Palaeoclimatology, Palaeoecology*, 194, pp.5–22.
- Garreaud, R.D., 1999. Multiscale analysis of the summertime precipitation over the central Andes. *Monthly Weather Review*, 127, p.5.
- Haque, M.M., Kawamura, K. and Kim, Y., 2016. Seasonal variations of biogenic secondary organic aerosol tracers in ambient aerosols from Alaska. *Atmospheric Environment*, 130, pp.1–10.
- Hu, R., Wang, H., Yin, Y., Zhu, B., Xia, L., Zhang, Z. and Chen, K., 2018. Measurement of ambient aerosols by single particle mass spectrometry in the Yangtze River Delta, China: Seasonal variations, mixing state and meteorological effects. *Atmospheric Research*, 213, pp.200–211.
- Instituto de Geofísico del Perú, 2005. Atlas Climático de precipitación y temperatura del aire en la Cuenca del Rio Mantaro, pp. 1–110.

- Jayamurugan, R., Kumaravel, B., Palanivelraja, S. and Chockalingam, M.P., 2013. Influence of temperature, relative humidity and seasonal variability on ambient air quality in a coastal urban area. *International Journal of Atmospheric Sciences*, 2013, pp.1–10.
- Liang, Q., Zhang, X., Miao, Y. and Liu, S., 2024. Multi-scale meteorological impact on PM<sub>2.5</sub> pollution in Tangshan, Northern China. *Toxics*, 12(9), pp.1–15.
- Magalhães, N. de, Evangelista, H., Condom, T., Rabatel, A. and Ginot, P., 2019. Amazonian biomass burning enhances tropical Andean glaciers melting. *Scientific Reports*, 9(1), pp.1–10.
- Ministerio de Vivienda, P., 2016. *Urban Development Plan Ahuaycha*, no. 112, pp.1–25.
- Moreno, R., Nery, A., Zamora, R., Lora, Á. and Galán, C., 2024. Contribution of urban trees to carbon sequestration and reduction of air pollutants in Lima, Peru. *Ecosystem Services*, 67, p.650.
- Muñoz-Pacheco, C.B. and Villaseñor, N.R., 2022. Urban ecosystem services in South America: A systematic review. *Sustainability (Switzerland)*, 14(5), pp.1–15.
- Owoade, K.O., Hopke, P.K., Olise, F.S., Ogundele, L.T., Fawole, O.G., Olaniyi, B.H., Jegede, O.O., Ayoola, M.A. and Bashiru, M.I., 2015. Chemical compositions and source identification of particulate matter (PM<sub>2.5</sub> and PM<sub>2.5–10</sub>) from a scrap iron and steel smelting industry along the Ife–Ibadan highway, Nigeria. *Atmospheric Pollution Research*, 6(1), pp.107–119.
- Perlroth, N.H. and Branco, C.W.C., 2017. Current knowledge of environmental exposure in children during sensitive developmental periods. *Journal of Paediatrics (Portuguese Edition)*, 93(6), pp.555–564.
- Pimienta-Barrios, E., Robles-Murguía, C., Carvajal, S., Muñoz-Urias, A., Martínez-Chávez, C. and De León-Santos, S., 2018. Environmental services of vegetation in urban ecosystems in the context of climate change. *Mexican Journal of Forest Sciences*, 5(22), pp.101–115.
- Rabha, S. and Saikia, B.K., 2019. *Handbook of Nanomaterials in Analytical Chemistry: Modern Trends in Analysis*, Springer, pp.453–470.
- Romero-Duque, L.P., Trilleras, J.M., Castellarini, F. and Quijas, S., 2020. Ecosystem services in urban ecological infrastructure of Latin America and the Caribbean: How do they contribute to urban planning? *Science of the Total Environment*, 728, pp.1–10.
- Saminathan, S. and Malathy, C., 2024. PM<sub>2.5</sub> concentration estimation using Bi-LSTM with Osprey Optimization Method. *Nature Environment and Pollution Technology*, 23(3), pp.1631–1638.
- Shen, L., Mickley, L.J. and Murray, L.T., 2017. Influence of 2000–2050 climate change on particulate matter in the United States: Results from a new statistical model. *Atmospheric Chemistry and Physics*, 17(6), pp.3855–3870.
- Soto-Estrada, E., 2019. Estimation of the urban heat island in Medellín, Colombia. *International Journal of Environmental Pollution*, 35(2), pp.89–96.
- Suárez-Salas, L., Álvarez Tolentino, D., Bendezú, Y. and Pomalaya, J., 2017. Chemical characterization of atmospheric particulate matter in the urban center of Huancayo, Peru. *Journal of the Chemical Society of Peru*, 83(3), pp.201–214.
- Suazo, J.M.A., Salas, L.S., Cruz, A.R.H.D. La, Vasquez, R.A., Aylas, G.R., Condor, A.R., Rojas, E.R., Curo, F.M., Rojas, J.L.F. and Karam, H.A., 2020. Direct radiative forcing due to aerosol properties at the Peruvian Antarctic station and metropolitan Huancayo area. *Annals of the Institute of Geosciences*, 43(4), pp.404–412.
- Tai, A.P.K., Mickley, L.J., Jacob, D.J., Leibensperger, E.M., Zhang, L., Fisher, J.A. and Pye, H.O.T., 2012. Meteorological modes of variability for fine particulate matter (PM<sub>2.5</sub>) air quality in the United States: Implications for PM<sub>2.5</sub> sensitivity to climate change. *Atmospheric Chemistry and Physics*, 12(14), pp.3135–3150.
- Tosca, M.G., Campbell, J., Garay, M., Lolli, S., Seidel, F.C., Marquis, J. and Kalashnikova, O., 2017. Attributing accelerated summertime warming in the southeast United States to recent reductions in aerosol burden: Indications from vertically-resolved observations. *Remote Sensing*, 9(1), pp.1–18.
- Vo, T.T.T., Wu, C.Z. and Lee, I.T., 2020. Potential effects of noxious chemical-containing fine particulate matter on oral health through reactive oxygen species-mediated oxidative stress: Promising clues. *Biochemical Pharmacology*, 178, p.114050.
- Vuille, M. and Keimig, F., 2004. Interannual variability of summertime convective cloudiness and precipitation in the central Andes derived from ISCCP-B3 data. *Journal of Climate*, 17(17), pp.3334–3348.
- Vuille, M., 1999. Atmospheric circulation over the Bolivian Altiplano during dry and wet periods and extreme phases of the Southern Oscillation. *International Journal of Climatology*, 19(14), pp.1579–1600.
- Vuille, M., Bradley, R.S. and Keimig, F., 2000. Interannual climate variability in the Central Andes and its relation to tropical Pacific and Atlantic forcing. *Journal of Geophysical Research: Atmospheres*, 105(D10), pp.12447–12460.
- Vuille, M., Kaser, G. and Juen, I., 2008. Glacier mass balance variability in the Cordillera Blanca, Peru, and its relationship with climate and the large-scale circulation. *Global and Planetary Change*, 62(1–2), pp.14–28.
- Wang, X., Dickinson, R.R.E., Su, L., Zhou, C. and Wang, K., 2018. PM<sub>2.5</sub> pollution in China and how it has been exacerbated by terrain and meteorological conditions. *Bulletin of the American Meteorological Society*, 99(1), pp.91–106.
- Xu, K., Cui, K., Young, L.H., Wang, Y.F., Hsieh, Y.K., Wan, S. and Zhang, J., 2020. Air quality index, indicator air pollutants and impact of COVID-19 event on the air quality near central China. *Aerosol and Air Quality Research*, 20(6), pp.1430–1441.
- Zardo, L., Geneletti, D., Pérez-Soba, M. and Van Eupen, M., 2017. Estimating the cooling capacity of green infrastructures to support urban planning. *Ecosystem Services*, 26, pp.225–235.
- Zender-Świercz, E., Galiszewska, B., Telejko, M. and Starzomska, M., 2024. The effect of temperature and humidity of air on the concentration of particulate matter - PM<sub>2.5</sub> and PM<sub>10</sub>. *Atmospheric Research*, 312(October), pp.1–12.
- Zu, Y., Huang, L., Hu, J., Zhao, Z., Liu, H., Zhang, H., Ying, Q. and Chen, M., 2017. Investigation of relationships between meteorological conditions and high PM<sub>10</sub> pollution in a megacity in the western Yangtze River Delta, China. *Air Quality, Atmosphere and Health*, 10(6), pp.627–638.
- Zyromski, A., Biniak-Pieróg, M., Burszta-Adamiak, E. and Zamiar, Z., 2014. Evaluation of relationship between air pollutant concentration and meteorological elements in winter months. *Journal of Water and Land Development*, 22(1), pp.33–41.

# Land Use/Land Cover (LULC) Change Classification for Change Detection Analysis of Remotely Sensed Data Using Machine Learning-Based Random Forest Classifier

H. N. Mahendra<sup>1</sup>, V. Pushpalatha<sup>2†</sup>, V. Rekha<sup>3</sup>, N. Sharmila<sup>4</sup>, D. Mahesh Kumar<sup>1</sup>, G. S. Pavithra<sup>5</sup>, N. M. Basavaraj<sup>1</sup> and S. Mallikarjunaswamy<sup>1</sup>

<sup>1</sup>Department of Electronics and Communication Engineering, JSS Academy of Technical Education (Affiliated to Visvesvaraya Technological University, Belagavi), Bengaluru-560060, Karnataka, India

<sup>2</sup>Department of Information Science and Engineering, JSS Academy of Technical Education (Affiliated to Visvesvaraya Technological University, Belagavi), Bengaluru-560060, Karnataka, India

<sup>3</sup>Department of Computer Science and Engineering, School of Engineering and Technology, Christ University, Bangalore-560060, India

<sup>4</sup>Department of Electrical and Electronics Engineering, JSS Science and Technology University, Mysuru-570015, Karnataka, India

<sup>5</sup>Pavithra G S, Department of Computer Science and Engineering (AI-ML), RNS Institute of Technology (Affiliated to Visvesvaraya Technological University, Belagavi), Bengaluru-560098, Karnataka, India

†Corresponding author: V. Pushpalatha; pushpav27@gmail.com

**Abbreviation:** Nat. Env. & Poll. Technol.

**Website:** [www.neptjournal.com](http://www.neptjournal.com)

**Received:** 11-07-2024

**Revised:** 23-08-2024

**Accepted:** 26-08-2024

## Key Words:

Remote sensing  
Multispectral data  
Machine learning  
Random forest classifier  
Linear Imaging Self-Scanning Sensor-III  
Land use/land cover

## Citation for the Paper:

Mahendra, H. N., Pushpalatha, V., Rekha, V., Sharmila, N., Kumar, D. M., Pavithra, G. S., Basavaraj, N. M., and Mallikarjunaswamy, S., 2025. Land Use/Land Cover (LULC) change classification for change detection analysis of remotely sensed data using machine learning-based random forest classifier. *Nature Environment and Pollution Technology*, 24(2), p. B4238. <https://doi.org/10.46488/NEPT.2025.v24i02.B4238>.

*Note: From year 2025, the journal uses Article ID instead of page numbers in citation of the published articles.*



**Copyright:** © 2025 by the authors

**Licensee:** Technoscience Publications

This article is an open access article distributed under the terms and conditions of the Creative Commons Attribution (CC BY) license (<https://creativecommons.org/licenses/by/4.0/>).

## ABSTRACT

Land Use and Land Cover (LULC) classification is critical for monitoring and managing natural resources and urban development. This study focuses on LULC classification for change detection analysis of remotely sensed data using a machine learning-based Random Forest classifier. The research aims to provide a detailed analysis of LULC changes between 2010 and 2020. The Random Forest classifier is chosen for its robustness and high accuracy in handling complex datasets. The classifier achieved a classification accuracy of 86.56% for the 2010 data and 88.42% for the 2020 data, demonstrating an improvement in classification performance over the decade. The results indicate significant LULC changes, highlighting areas of urban expansion, deforestation, and agricultural transformation. These findings highlight the importance of continuous monitoring and provide valuable insights for policymakers and environmental managers. The study demonstrates the effectiveness of using advanced machine-learning techniques for accurate LULC classification and change detection in remotely sensed data.

## INTRODUCTION

Land Use and Land Cover (LULC) classification is a crucial aspect of environmental monitoring and management, providing insights into the spatial distribution and temporal dynamics of the Earth's surface (Mahendra et al. 2023a). The classification and subsequent change detection of LULC are fundamental for understanding ecological dynamics, urban planning, and resource management (Kumar et al. 2008). Traditionally, LULC mapping relied on manual interpretation of satellite images, which was both time-consuming and prone to human error. With advancements in remote sensing technology, it is now possible to acquire high-resolution, multi-temporal satellite imagery, facilitating more efficient and accurate LULC classification (Ganesha et al. 2020).

In recent years, the integration of machine learning techniques with remote sensing technologies has emerged as a powerful collaboration, offering unprecedented capabilities for analyzing vast amounts of spatial data (Hosseiny et al. 2022, Mahendra et al. 2023d). This research delves into the application of a machine learning-based random forest classifier for the classification and change



detection of remotely sensed data. Remote sensing, with its ability to capture information from a distance, provides an invaluable tool for monitoring changes in the Earth's surface over time (Li et al. 2013). Leveraging the efficiency and versatility of machine learning algorithms, particularly the random forest classifier, holds the promise of enhancing the accuracy and automation of such analyses (Pande 2022, Jayabaskaran & Das 2023, Jensen et al. 2001).

The classification of remotely sensed data is a fundamental step in extracting meaningful information about land cover and land use (Belgiu & Drăguț 2016). Traditional methods often face challenges in handling the complexity and variability present in large-scale datasets (Lu & Weng 2007). This research seeks to address these challenges by exploring the random forest (RF) classifier's ability to handle high-dimensional data, nonlinear relationships, and complex interactions between spectral bands. By employing this machine learning approach, we aim to improve the precision and efficiency of land cover classification, leading to more reliable assessments of the Earth's surface characteristics.

Change detection, a critical component of land monitoring, involves identifying alterations in land cover over time (Firoz et al. 2016 Mahendra et al. 2023b). As environmental dynamics accelerate, timely and accurate detection of changes becomes paramount for informed decision-making (Vivekananda et al. 2021). The random forest classifier, known for its adaptability and robustness, presents an innovative solution for change detection in remotely sensed imagery (Gislason et al. 2004 Mahendra et al. 2023c). Through a systematic analysis of temporal datasets, this research aims to evaluate the random forest classifier's performance in detecting and characterizing land cover changes, contributing to our understanding of environmental transformations on both regional and global scales (Mahendra & Mallikarjunaswamy 2022).

The integration of machine learning algorithms into the realm of remote sensing not only promises advancements in accuracy and efficiency but also opens avenues for scalable and automated analyses (Mahendra et al. 2019). By exploring the potential of the random forest classifier in this context, we aspire to contribute to the ongoing discourse on the optimization of land cover classification and change detection methodologies (Tiwari et al. 2024). This research aligns with the broader objective of harnessing technology to address environmental challenges and facilitate sustainable land management practices, ultimately fostering a deeper understanding of our planet's ever-evolving landscape. The outcomes of this research contribute valuable insights into the effectiveness of machine learning-based random forest classifiers for remotely sensed data analysis. The findings

have implications for a range of applications, including environmental monitoring, land-use planning, and natural resource management. Eventually, this research enhances our ability to harness the power of machine learning for accurate classification and change detection in remotely sensed datasets, facilitating a more comprehensive understanding of dynamic land cover patterns.

## RELATED WORKS

The use of remotely sensed data in environmental monitoring and analysis has been widely explored in the literature. Numerous studies have investigated the application of various classification techniques to interpret and classify remote sensing data. Notable works include Davis & Townshend (2002) and Mahendra et al. (2023c), who employed Support Vector Machines (SVM) for land cover classification, and Voulgaris & Magoulas (2008), who utilized k-Nearest Neighbors (k-NN) for similar purposes.

A range of studies have demonstrated the effectiveness of random forest classifiers in analyzing remotely sensed data. Piramanayagam et al. (2016) achieved an 86.3% overall accuracy in land cover classification using this method, while Mellor et al. (2014) obtained a 73% accuracy in forest classification. Gislason et al. (2004) further highlighted the potential of random forests in handling multisource data, and Belgiu & Drăguț (2016) emphasized their ability to handle high data dimensionality and multicollinearity. Mosin et al. (2019) presented tree detection and classification in forestry applications using machine learning. A system with finely tuned filters will make possible robust species classification at a cost much lower than hyperspectral imaging. Boukir & Mellor (2017) used random forests for remote sensing classification. Targeting lower-margin training samples is a strategy for inducing diversity in ensemble classifiers and achieving better classifier performance for difficult or rare classes.

Pal (2005) developed a random forest classifier remote sensing image classification. The number of user-defined parameters required by random forest classifiers is less than the number required for SVMs. Zerrouki et al. (2019) presented LULC Change Detection analysis using a machine learning-based algorithm. The proposed detection scheme succeeds in effectively identifying land cover changes. Sheykhoumousa et al. (2013) compared the Random forest- and support vector machine-based multi-temporal classifications. Tian et al. (2016) used the random forest classifier to achieve accurate classification in the Ertix River in northern Xinjiang, China.

The Random Forest (RF) classifier has proven to be a robust and versatile machine learning algorithm for remote sensing applications. Studies such as Nguyen et al.

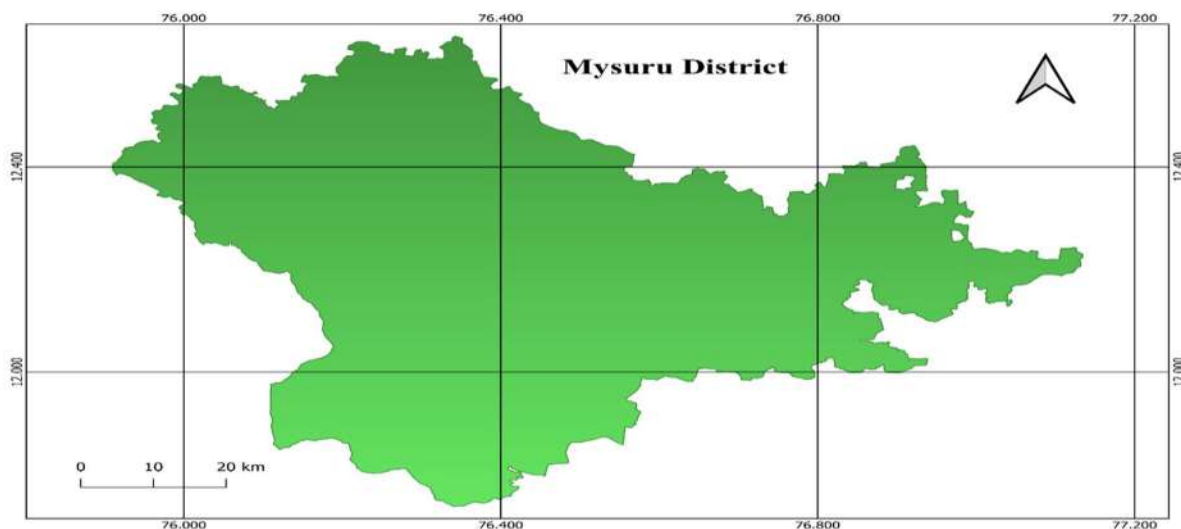


Fig. 1: Study area.

(2018) have demonstrated the effectiveness of RF in land cover mapping, showcasing its ability to handle diverse spectral information and improve classification accuracy. Additionally, Shihab et al. (2020) applied RF to detect changes in land cover over time, showcasing its utility in change detection analyses. Several studies have combined classification and change detection methodologies to monitor environmental changes over time. Abdi (2020) conducted a comprehensive analysis using a combination of machine learning classifiers and change detection algorithms to assess land cover changes in a specific region. Their work highlights the importance of integrating classification techniques with change detection methods for a more comprehensive understanding of dynamic environmental processes.

While the existing literature provides valuable insights into the application of machine learning-based classifiers for remote sensing, there is still a need for research that specifically focuses on the integration of Random Forest classifiers for both classification and change detection tasks. This research aims to address this gap by presenting a detailed analysis of the performance of Random Forest in classifying remotely sensed data and detecting temporal changes, contributing to the advancement of effective environmental monitoring techniques.

## STUDY AREA

Mysuru district, located in the southern part of the Indian state of Karnataka, is renowned for its rich historical and cultural significance. The district serves as the cultural capital of Karnataka and is steeped in the grandeur of its royal heritage. The city of Mysuru, also known as the 'City of Palaces,' is home to the iconic Mysuru Palace, a splendid

architectural masterpiece that attracts tourists from around the world. The palace, built in Indo-Saracenic style, stands as a testament to the opulence and grandeur of the Wadiyar dynasty, which ruled the region for centuries. Apart from the palace, Mysuru is known for its vibrant Dasara festival, celebrated with grandeur, featuring a procession of decorated elephants, cultural events, and a spectacular illumination of the palace.

The district is not just a historical and cultural hub but also boasts a diverse geographical landscape. Nestled in the Deccan Plateau, Mysuru is surrounded by lush greenery, picturesque hills, and serene lakes. The Chamundi Hills, with the Chamundeshwari Temple perched on top, provide a panoramic view of the city. Mysuru is also home to the enchanting Brindavan Gardens, known for its musical fountain and beautifully landscaped terraces. Additionally, the district is recognized for its educational institutions, including the historic Mysore University, contributing to the intellectual and academic development of the region. With its blend of cultural heritage, natural beauty, and educational excellence, Mysuru district stands as a unique and vibrant destination in the heart of South India. The map of the Mysuru district is shown in Fig. 1.

## MATERIALS AND METHODS

Linear Imaging Self-Scanning Sensor-III (LISS-III) is a satellite sensor data used in this work. This sensor is designed for remote sensing applications, particularly in the field of Earth observation. Developed by the Indian Space Research Organization (ISRO), LISS-III is part of the payload onboard the Indian Remote Sensing (IRS) satellites. This sensor operates in the visible and near-infrared spectral bands,

Table 1: Satellite data.

Satellite Name	Spatial resolution (meters)	Sensor Used	Year of Acquisition
Resourcesat-1	24m	LISS-III	2010
Resourcesat-1	24m	LISS-III	2020

capturing high-resolution imagery with a spatial resolution ranging from 23.5 meters to 5.8 meters, depending on the specific satellite and its orbital parameters. The multi-spectral capabilities of LISS-III enable it to provide valuable data for a variety of applications, including agriculture monitoring, land use planning, disaster management, and environmental studies.

One notable aspect of LISS-III is its ability to acquire imagery in multiple spectral bands, such as blue, green, red, and near-infrared. This spectral diversity allows for the extraction of valuable information about the Earth's surface and vegetation health. The high spatial resolution of LISS-III imagery enhances the level of detail in the captured data, making it a valuable tool for precision agriculture, urban planning, and natural resource management. Researchers, government agencies, and industries leverage LISS-III data to make informed decisions and monitor changes in the environment over time, contributing to sustainable development and effective resource utilization. Table 1 provides the details of satellite data used in the study.

## Methodology

LULC classification using RF involves a systematic methodology to accurately categorize different land use and land cover types based on remote sensing data. The first step in the process is data acquisition, where high-resolution satellite imagery is obtained for the study area. These images serve as the input data for the classification model. Preprocessing steps, such as radiometric and atmospheric correction, are performed to enhance the quality of the images and ensure consistency across the dataset. Additionally, feature extraction may be employed to identify relevant spectral, spatial, and textural characteristics that can aid in distinguishing between different land cover classes.

The second step involves the application of the RF algorithm for classification. RF is an ensemble learning technique that combines the predictions of multiple decision trees to improve overall accuracy and robustness. Training data, consisting of labeled samples representing different land cover classes, are used to train the RF model. The algorithm leverages the spectral signatures and spatial patterns present in the training data to build a robust classification model. The model is then applied to the entire dataset, classifying each pixel or image segment into specific land cover

categories. Finally, an accuracy assessment is conducted using validation data to evaluate the performance of the RF classifier and refine the model if necessary. This iterative process ensures the generation of reliable and accurate LULC maps for informed decision-making in various applications, such as environmental monitoring, urban planning, and natural resource management. The methodology followed in this research work is shown in Fig. 2.

**Data acquisition:** The first step in our methodology involves acquiring remotely sensed data covering the study area. This may include satellite imagery captured at different time points. In this work, we have obtained the LISS-III image of the study area for the years 2010 and 2020, respectively.

**Pre-Processing:** Pre-processing tasks such as atmospheric correction, radiometric calibration, and geometric correction are performed on both the LISS-III images to enhance the quality of the imagery. Atmospheric correction of satellite data involves removing the effects of the atmosphere, such as scattering and absorption) on the reflected light reaching the sensor. This process ensures that the data accurately represents surface reflectance by compensating for atmospheric distortions. Techniques include using radiative transfer models, ground-based measurements, or empirical methods. Corrected data is essential for accurate analysis in remote sensing applications. Radiometric correction of satellite data involves adjusting the pixel values in an image to account for sensor-specific errors, atmospheric conditions, and illumination differences. This ensures that the observed reflectance values represent true ground conditions. The process typically includes calibration using known reference targets and correcting for atmospheric scattering and absorption. It improves the accuracy and consistency of the satellite data for further analysis. Geometric correction of satellite data involves aligning images to a standard coordinate system by correcting distortions due to sensor geometry, satellite motion, and Earth's curvature. This process typically uses ground control points (GCPs) to match the satellite image to a reference map or coordinate system. It ensures accurate spatial representation, making the data usable for further analysis and comparison.

**Feature selection and extraction:** Next, we focus on selecting and extracting relevant features from the remotely sensed data. Feature selection in satellite data typically involves parameters like spectral bands, in which the selection of specific wavelengths relevant to the study (e.g., visible, nir, thermal), spatial resolution is choosing the pixel size that balances detail with computational efficiency, temporal resolution is selecting data from relevant time periods or frequencies of observation, topographic features is inclusion of elevation, slope, and aspect to account for

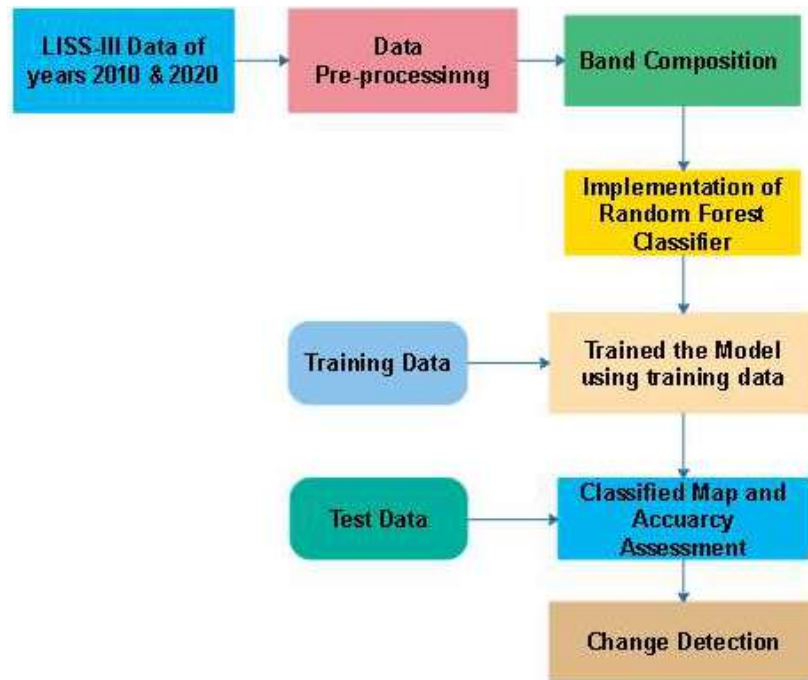


Fig. 2: Methodology.

terrain effects, and radiometric calibration is ensuring the data is corrected for sensor and atmospheric influences.

**Training data collection:** A representative set of training data is essential for training the random forest classifier. Ground truth data collected through field surveys or existing high-quality reference datasets should be used to label the training samples. These labeled samples should cover the full range of land cover classes present in the study area. Care must be taken to ensure an adequate number of samples for each class, avoiding bias in the classifier towards overrepresented classes.

**Random forest classification:** The heart of our analysis involves the application of a machine learning-based RF classifier to the pre-processed and feature-selected datasets. The classifier will be trained using the labeled training samples, learning the relationships between the selected features and the corresponding land cover classes. The algorithm's ability to handle complex and non-linear relationships makes it well-suited for classifying remotely sensed data. The resulting classification map will provide a detailed representation of land cover types in the study area.

**Change detection analysis:** To detect changes over time, a comparative analysis is performed between classification results from different time points. The classified maps for each time period are compared pixel-wise to identify areas of change. Post-classification change detection techniques

may be applied, such as image differencing or the calculation of vegetation indices for change assessment. This step allows for the identification and characterization of land cover changes, such as urban expansion, deforestation, or agricultural land conversion.

**Accuracy assessment and validation:** The final step involves assessing the accuracy of the classification and change detection results. This is done by comparing the classified maps with independent validation datasets or ground truth data not used during the training phase. Accuracy metrics, such as overall accuracy, producer's accuracy, and user's accuracy, are calculated to quantify the reliability of the classification. This step ensures the robustness of the analysis and provides insights into the effectiveness of the random forest classifier in capturing temporal changes in the remotely sensed data.

### Random Forest (RF) Classifier

RF classifier has emerged as a powerful tool for the classification and change detection analysis of remotely sensed data. In the view of Earth observation, where satellite imagery plays a crucial role, the RF algorithm stands out for its versatility and robustness. Comprising an ensemble of decision trees, RF leverages the principle of bagging (bootstrap aggregating) to construct multiple trees, each trained on a subset of the data. This diversity in the ensemble enhances the model's generalization capabilities, making it



well-suited for handling the complex and high-dimensional nature of remote sensing datasets.

In the context of classification, RF excels in distinguishing between land cover classes, a fundamental task in remote sensing applications. The algorithm's ability to consider a multitude of spectral, spatial, and temporal features allows for more accurate and comprehensive classification outcomes. Additionally, the RF model provides information about feature importance, aiding in the interpretation of the classification results and enabling users to understand the key factors influencing land cover distinctions. Change detection, a critical aspect of monitoring environmental dynamics, benefits significantly from the Random Forest classifier. By comparing classifications from different time points, RF can identify changes in land cover with high precision. The ensemble nature of the algorithm enhances its sensitivity to subtle alterations in the landscape, making it particularly effective for detecting land cover changes caused by natural phenomena or human activities.

The RF resistance to overfitting and capacity to handle noisy data contribute to its reliability in remote sensing analyses. The algorithm accommodates a wide range of input data types, such as multispectral or hyperspectral imagery, as well as ancillary information like topographic and meteorological data. This adaptability makes it a versatile choice for various remote sensing applications, from monitoring urban expansion to assessing deforestation. In summary, the RF classifier has proven to be an invaluable tool for classification and change detection analyses of remotely sensed data. Its ensemble-based approach, feature importance insights, and adaptability to different data types contribute to its widespread use in Earth observation studies. Whether applied to monitor land cover changes, map vegetation types, or assess environmental impacts, the RF algorithm stands as a robust and reliable solution in the

ever-evolving field of remote sensing. The working principle of the random forest classifier is shown in Fig. 3.

**Ensemble learning:** Random Forest is an ensemble of decision trees. Ensemble learning combines the predictions of multiple models to improve overall accuracy and robustness. In the case of Random Forest, it builds a forest of decision trees and merges their outputs to make a more informed and reliable prediction.

**Decision trees:** Each tree in the Random Forest is a decision tree. Decision trees split the input data based on features, recursively dividing it into subsets until a certain condition is met. The decision at each node is made by evaluating a feature, and the goal is to make the final decision (classification) at the tree's leaf nodes.

**Random feature selection:** Randomness is introduced in Random Forest through the selection of a random subset of features for each decision tree. This helps to decorrelate the trees and avoid overfitting specific features in the dataset. The algorithm doesn't use the entire set of features for each tree, which increases the diversity of the trees in the ensemble.

**Bootstrap sampling:** Another source of randomness is introduced through bootstrap sampling, also known as bagging (Bootstrap Aggregating). Random Forest builds each tree on a different subset of the training data, sampled with replacement. This means that some instances may be repeated in the subset while others may be left out.

**Voting or averaging:** Once all the decision trees are built, predictions are made for each tree. In classification, the final prediction is often determined by a majority vote among the trees (for binary classification, it's a simple majority). For regression tasks, the predictions are averaged.

**Robustness and generalization:** The combination of multiple trees and the randomness introduced in feature selection and data sampling makes Random Forest robust

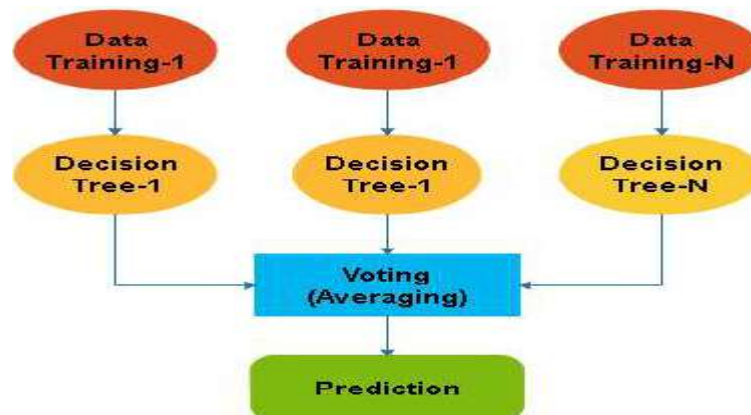


Fig. 3: Working principle of the random forest classifier.

and less prone to overfitting. It can handle noisy data and outliers better than individual decision trees.

**Feature importance:** Random Forest provides a measure of feature importance based on how often a feature is used to split the data across all trees. This can be valuable in understanding the significance of different features in the classification process.

**Change detection analysis:** In the context of change detection, random forest can be applied by training the model on historical data representing different classes (e.g., land cover types) and then using the trained model to classify new or updated data. Changes can be detected by comparing classifications over different periods.

Overall, the Random Forest classifier's strength lies in its ability to create a robust and accurate model by combining multiple decision trees and introducing randomness through feature selection and data sampling. This makes it well-suited for classification tasks, including change detection analysis in various domains.

## RESULTS AND DISCUSSION

### LULC Classification and Assessment

The study identified and delineated various land cover classes across the study area. The prominent land cover classes included built-up areas, water bodies, cultivated land, fallow land, scrubland, vegetation, and forest. In the analysis

of LULC for the year 2010, the classified maps revealed distinctive patterns across various categories. The built-up areas exhibited a significant expansion, indicating urbanization and infrastructure development. Water bodies were identified with precision, reflecting the spatial distribution of lakes, rivers, and other aquatic features. Cultivated lands showcased a mix of agricultural activities, highlighting the regions contributing to food production. Fallow lands, scrub lands, and vegetation were discerned, providing insights into transitional and natural landscapes. Forest cover was evident, emphasizing the importance of preserving biodiversity and ecological balance. The comprehensive classification of LULC in 2010 laid the foundation for understanding the baseline landscape and served as a valuable reference point for subsequent years.

Fast forward to the year 2020, the classified maps depicted dynamic changes in LULC, indicative of evolving environmental and societal factors. Built-up areas exhibited continued expansion, illustrating ongoing urban development. Water bodies maintain their distinct presence, which is crucial for monitoring aquatic ecosystems and water resource management. Cultivated lands showcased alterations in land use patterns, reflecting changes in agricultural practices. The identification of fallow lands, scrub lands, and vegetation highlighted areas undergoing transition or ecological restoration efforts. Notably, the forest cover exhibited fluctuations, underlining the importance

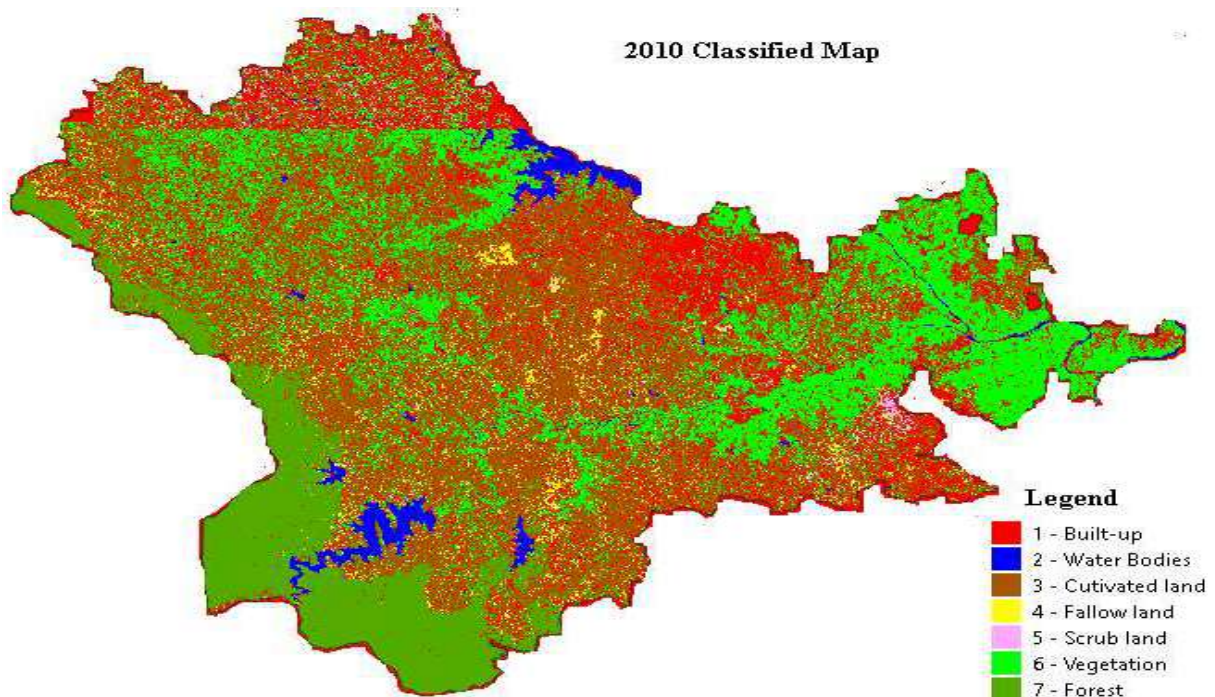


Fig. 4: LULC classified map of the Mysuru district for the year 2010.

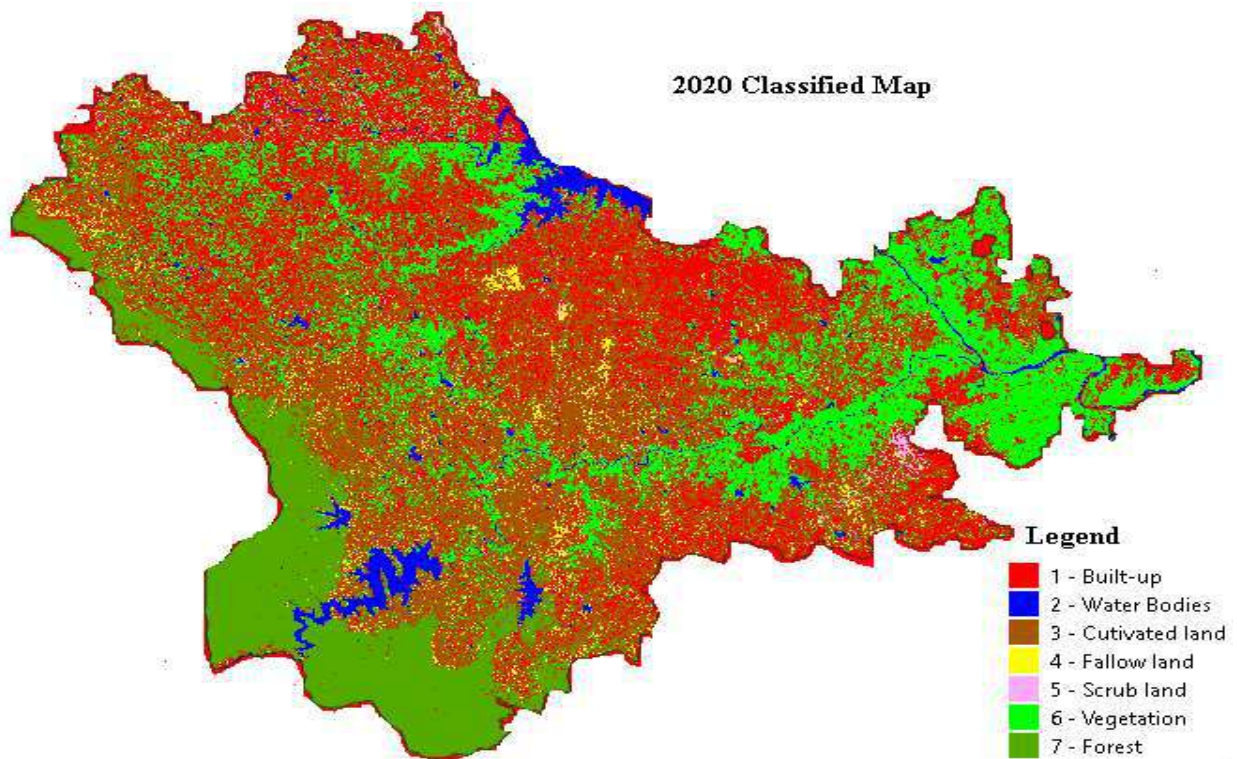


Fig. 5: LULC classified map of the Mysuru district for the year 2020.

of conservation efforts amidst increasing anthropogenic pressures. The comparative analysis between the 2010 and 2020 classified maps unveiled trends in land use dynamics, providing valuable insights for informed decision-making in the realms of urban planning, environmental conservation, and sustainable resource management. The classified map of the Mysuru district for the years 2010 and 2020 is shown in Fig. 4 and Fig. 5, respectively. The LULC assessment has been carried out for both the classified map and the corresponding assessment results of both years are shown in Table 2. The total geographical area of Mysuru district is 6307 sq. km.

Table 2: Assessment of LULC classes.

Class Name	2010	2020	Change in area (sq. km)
	Area (in sq. km)	Area (in sq. km)	
Built-up	292.24	411.78	119.54
Water bodies	287.55	346.92	59.37
Cultivated land	2986	3751.12	765.12
Fallow land	1096.51	123.26	-973.25
Scrubland	91.6	112.45	20.85
Vegetation	554.4	628.65	74.25
Forest	996.25	932.12	-64.13

### Performance Analysis

The Random Forest classifier demonstrated commendable accuracy in LULC mapping for both periods. The classification accuracy was measured at 86.56% for the year 2010 and exhibited improvement to 88.42% in 2020 as shown in Table 3. This upward trend in accuracy indicates the robustness of the classification model, suggesting its efficacy in capturing changes in land cover over time. The increase in accuracy from 2010 to 2020 underscores the classifier's ability to adapt and enhance performance, likely attributed to improvements in training data and model optimization. This increase in classification accuracy reflects the effectiveness of the chosen methodology in capturing land use and land cover changes over the decade. The higher accuracy in 2020 suggests the model's ability to adapt to the evolving landscape, highlighting its robustness in handling temporal variations. The other performance parameters such as precision, recall, and F1 is also calculated for both the classified images. Table 3 compares the performance of an RF model using satellite images from two different years, 2010 and 2020, respectively. For 2010 classified data, the model achieved a precision of 85%, recall of 84%, and F1 score of 86%, with an accuracy of 86.56% and a Kappa value of 85.86%. While 2020 classified data, the model slightly



Table 3: Accuracy assessment results.

Model	Satellite Images	Precision	Recall	F1	Accuracy (%)	Kappa Value
RF	LISS-III 2010	85	84	86	86.56 %	85.86%
	LISS-III 2020	86	85	86	88.42 %	86.32%

Table 4: Comparison analysis of different classification methods.

#	RF		Hosseiny et al (2022)	Singh et al. (2021)	Sengan et al. (2022)	Sencaki et al. (2023)	Mandla et al. (2021)	Vivekananda et al. (2021)
Classifier	2010 Data	2020 Data	Mnlogit model	RAVNet	DL	SVM	MLC	WRF
Accuracy [%]	86.56	88.42	86	81	73.3	82.83	87.46	85.30
Kappa Value	85.86	86.32	NA	NA	NA	0.81	0.857	0.87

improved with a precision of 86%, recall of 85%, and F1 score of 86%, with a higher accuracy of 88.42% and the same Kappa value of 85.86%.

Further, the performance of the RF classifier is compared with other classification methods, as shown in Table 4. Table 4 compares different classifiers used in studies by various author, focusing on their performance with 2010 and 2020 data. The classifiers listed include the Mnlogit model, RAVNet, Deep Learning (DL), Support Vector Machine (SVM), Multilayer Perceptron Classifier (MLC), and Weighted Random Forest (WRF). The comparison results show that our RF provides the highest of 88.42%.

### Temporal Changes in LULC

The comparison of LULC maps for 2010 and 2020 revealed significant temporal changes in Mysuru district. Urban expansion, agricultural transformations, and alterations in natural vegetation were notable trends. The increase in classification accuracy facilitated the identification of subtle changes, allowing for a more nuanced understanding of how human activities and natural processes have influenced the landscape over the decade. This insight is crucial for informed land management and sustainable development planning. The analysis of the classified maps reveals significant changes in land use and land cover patterns within Mysuru district over the study period. Urban expansion, agricultural transitions, and alterations in natural land covers are evident. The increase in accuracy not only indicates the model's improved performance but also enhances our understanding of the dynamics shaping the landscape. The identification of specific land cover changes, such as urban encroachment or alterations in vegetation types, can be crucial for informed land management and policy decisions.

### Urbanization and Agricultural Dynamics

The study identified a substantial increase in urban areas, reflecting the rapid pace of urbanization in Mysuru district.

This expansion is evident in the conversion of agricultural land and natural vegetation to built-up areas. Conversely, certain regions experienced agricultural intensification, possibly indicating shifts in crop patterns or land management practices. The Random Forest classifier proved effective in distinguishing between these land cover types, providing valuable information for urban planning, agricultural policy, and environmental conservation efforts.

### Implications for Sustainable Land Management

The accurate classification of LULC in the Mysuru district using the random forest classifier has important implications for sustainable land management and urban planning. The identification of areas experiencing rapid change allows policymakers to target conservation efforts or plan for infrastructure development. The observed trends in land use and land cover alterations can inform strategies to mitigate environmental impacts and promote sustainable practices. This study provides a valuable foundation for ongoing monitoring efforts and emphasizes the importance of regularly updating land cover classifications to capture dynamic changes in the landscape.

### Challenges and Limitations

Despite the overall success of the RF classifier, some challenges were encountered during the classification process. These challenges included the presence of spectral confusion in certain land cover classes and the need for careful consideration of spectral signatures. Additionally, cloud cover and atmospheric conditions in the satellite imagery posed constraints, emphasizing the importance of preprocessing techniques to mitigate these effects. Addressing these challenges is crucial for further improving the accuracy and reliability of LULC classifications. The resolution of the satellite data used in this study is 23.5m. However, classification accuracy can be further improved using high-resolution data.



## Implications and Future Directions

The results of this study have implications for land management, environmental monitoring, and urban planning in Mysuru district. The high accuracy achieved by the Random Forest classifier underscores its suitability for mapping and monitoring land cover changes. Future research should explore the integration of additional data sources, such as multi-sensor satellite imagery or ancillary data, to enhance classification accuracy further. Additionally, employing advanced machine learning techniques and incorporating ground-truth data could contribute to a more comprehensive understanding of the dynamic LULC patterns in the region.

## CONCLUSIONS

This research has demonstrated the efficiency of employing a machine learning-based random forest classifier for the classification and change detection of remotely sensed data. The utilization of a robust random forest algorithm has allowed for accurate and efficient classification of land cover classes, providing a valuable tool for applications such as environmental monitoring, urban planning, and resource management. The findings of this study show the importance of leveraging machine learning techniques, particularly the random forest classifier, in the field of remote sensing. The classifier achieved a classification accuracy of 86.56% for the 2010 data and 88.42% for the 2020 data, demonstrating an improvement in classification performance over the decade. The achieved high classification accuracy and sensitivity to temporal changes highlight the potential of this methodology for addressing the challenges associated with analyzing large-scale and dynamic environmental datasets. Future research could explore additional refinements and extensions of this methodology, as well as its application to different geographic regions and environmental contexts, to further advance the capabilities of machine learning in remote sensing applications.

## REFERENCES

Abdi, A.M., 2020. Land cover and land use classification performance of machine learning algorithms in a boreal landscape using Sentinel-2 data. *GIScience & Remote Sensing*, 57(1), pp.1-20.

Belgiu, M. and Drăguț, L.D., 2016. Random forest in remote sensing: A review of applications and future directions. *ISPRS Journal of Photogrammetry and Remote Sensing*, 114, pp.24-31.

Boukir, S. and Mellor, A., 2017. Ensemble diversity analysis on remote sensing data classification using random forests. *Journal of Image Processing*, 98, pp.1302-1306.

Davis, L.S. and Townshend, J.R.G., 2002. An assessment of support vector machines for land cover classification. *International Journal of Remote Sensing*, 23(4), pp.725-749.

Firoz, A., Laxmi, S. and Goparaj, R., 2016. Analysis of urban sprawl dynamics using geospatial technology in Ranchi city, Jharkhand, India. *Journal of Environmental Geography*, 9(1-2), pp.7-13.

Ganesha, K.R., Trivedi, S., Ramesh, K.S., Sudha, S., Rama Subramoniam, H.M. and Ravishankar, A.V., 2020. Assessment of vegetation cover of Bengaluru City, India, using geospatial techniques. *Journal of Indian Society of Remote Sensing*, 49, pp.747-758. [DOI].

Gislason, P.O., Benediktsson, J.A. and Sveinsson, J.R., 2004. Random Forest classification of multisource remote sensing and geographic data. *IGARSS 2004. 2004 IEEE International Geoscience and Remote Sensing Symposium*, 2, pp.1049-1052.

Hosseiny, B., Abdulhakim, M., Abdi, M. and Sadegh, J., 2022. Urban land use and land cover classification with interpretable machine learning – A case study using Sentinel-2 and auxiliary data. *Remote Sensing Applications: Society and Environment*, 28, p.100843. [DOI].

Jayabaskaran, M. and Das, B., 2023. Land Use Land Cover (LULC) dynamics by CA-ANN and CA-Markov model approaches: A case study of Ranipet Town, India. *Nature Environment & Pollution Technology*, 22(3), p.13. [DOI].

Jensen, J.R., Qiu, F. and Patterson, K., 2001. A neural network image interpretation system to extract rural and urban land use and land cover information from remote sensor data. *Geocarto International*, 16, pp.21-30.

Kumar, M., Garg, P.K. and Khare, D., 2008. Monitoring and modeling of urban sprawl using remote sensing and GIS techniques. *International Journal of Applied Earth Observations and Geoinformation*, 10, pp.26-43.

Li, M., Im, J. and Beier, C.M., 2013. Machine learning approaches for forest classification and change analysis using multi-temporal Landsat TM images over Huntington Wildlife Forest. *GIScience & Remote Sensing*, 50, pp.361-384.

Lu, D. and Weng, Q., 2007. A survey of image classification methods and techniques for improving classification performance. *International Journal of Remote Sensing*, 28(5), pp.823-870.

Mahendra, H.N. and Mallikarjunaswamy, S., 2022. Efficient classification of hyperspectral remotely sensed data using support vector machine. *International Journal of Electronics and Telecommunications*, 68(3), pp.609-617.

Mahendra, H.N., Kumar, D.M. and Mallikarjunaswamy, S., 2023c. An analysis of change detection in land use land cover area of remotely sensed data using the supervised classifier. *International Journal of Environmental Technology and Management*, 26, pp.61-78.

Mahendra, H.N., Mallikarjunaswamy, S. and Rama Subramoniam, S., 2023a. An assessment of vegetation cover of Mysuru City, Karnataka State, India, using deep convolutional neural networks. *Environmental Monitoring and Assessment*, 195, p.526. [DOI].

Mahendra, H.N., Mallikarjunaswamy, S. and Sudalayandi, R.S., 2023b. An assessment of built-up cover using geospatial techniques: A case study on Mysuru district, Karnataka state, India. *International Journal of Environmental Technology and Management*, 71, p.734. [DOI].

Mahendra, H.N., Mallikarjunaswamy, S., Kumar, D.M., Kumari, S., Kashyap, S., Fulwani, S. and Chatterjee, A., 2023d. Assessment and prediction of air quality level using ARIMA Model: A case study of Surat City, Gujarat State, India. *Nature Environment & Pollution Technology*, 22(1), p.16.

Mahendra, H.N., Mallikarjunaswamy, S., Rekha, V., Puspaltha, V. and Sharmila, N., 2019. Performance analysis of different classifiers for remote sensing application. *International Journal of Engineering and Advanced Technology*, 9, pp.2249-8958.

Mandla, D., Elhadi, A., George, C. and Hamandawana, H., 2021. A remote sensing-based approach to investigate changes in land use and land cover in the lower uMfolozi floodplain system, South Africa. *Transactions of the Royal Society of South Africa*, 76(1), pp.13-25.

Mellor, A., Haywood, A., Jones, S., Wilkes, P. and Mellor, A., 2014. Forest classification using random forests with multisource remote sensing and ancillary GIS data. *Australian Remote Sensing and Photogrammetry*, 27, p.12.

- Mosin, V.K., Aguilar, R., Platonov, A., Vasiliev, A., Kedrov, A. and Ivanov, A., 2019. Remote sensing and machine learning for tree detection and classification in forestry applications. *Remote Sensing*.
- Nguyen, H.T., Doan, T.M. and Radeloff, V.C., 2018. Applying random forest classification to map land use/land cover using Landsat 8 OLI. *International Archives of the Photogrammetry, Remote Sensing and Spatial Information Sciences*, 81, pp.363-367.
- Pal, M., 2005. Random forest classifier for remote sensing classification. *International Journal of Remote Sensing*, 26, pp.217-222.
- Pande, C.B., 2022. Land use/land cover and change detection mapping in Rahuri watershed area (MS), India using the Google Earth engine and machine learning approach. *Geocarto International*, 19, pp.66-72.
- Piramanayagam, S., Schwartzkopf, W.C., Koehler, F.W. and Saber, E., 2016. Classification of remotely sensed images using random forests and deep learning framework. *Remote Sensing*, 7, p.56.
- Sencaki, B.D., Mega, N., Putri, B., Santosa, H., Arfah, S., Arifandri, R., Muhammad, A.I.H., Prabu Kresna Putra, N., Anatoly, Z., Dona, O.P., Marina, C.G. and Frederik, A., 2023. Land cover multiclass classification of Wonosobo, Indonesia with time series-based one-dimensional deep learning model. *Remote Sensing Applications: Society and Environment*, 32, p.112023.
- Sengan, S., Lal Karn, A., Denis, A., Irina, V., Pustokhina, P. and Alharbi, M., 2022. A hybrid learning model for efficient classification of land use and land change from satellite images. *Physics and Chemistry of the Earth, Parts A/B/C*, 128, p.284. [DOI]
- Sheykhmousa, M., Mahdianpari, H., Ghanbari, F., Mohammadimanesh, P., Ghamisi, M. and Homayouni, S., 2020. Support vector machine versus random forest for remote sensing image classification: A meta-analysis and systematic review. *Journal of Selected Topics in Applied Earth Observations and Remote Sensing*, 13, pp.6308-6325. [DOI].
- Shihab, T.H., Al-hameedawi, A.N. and Hamza, A.M., 2020. Random forest (RF) and artificial neural network (ANN) algorithms for LULC mapping. *Engineering and Technology Journal*.
- Singh, R.K., Singh, P., Martin, D., Kumar, P., Singh, H., Gupta, A.K., Govil, H., Kaur, A. and Kumar, M., 2021. A machine learning-based classification of LANDSAT images to map land use and land cover of India. *Remote Sensing Applications: Society and Environment*, 24. [DOI].
- Tian, S., Zhang, X., Tian, J. and Sun, Q., 2016. Random forest classification of wetland landcovers from multi-sensor data in the arid region of Xinjiang, China. *Remote Sensing*, 8, p.954.
- Tiwari, A.K., Pal, A. and Kanchan, R., 2024. Mapping and monitoring of land use/land cover transformation using geospatial techniques in Varanasi City Development Region, India. *Nature Environment & Pollution Technology*, 23(1), p.31. [DOI]
- Vivekananda, G.N., Swathi, R. and Sujith, A.V., 2021. Multi-temporal image analysis for LULC classification and change detection. *European Journal of Remote Sensing*, 54(2), pp.189-199.
- Voulgaris, Z. and Magoulas, G., 2008. Extensions of the k-nearest neighbor methods for classification problems. *Proceedings of the IASTED International Conference on Artificial Intelligence and Applications (AIA 2008)*.
- Zerrouki, N., Harrou, F., Sun, Y. and Hocini, L., 2019. A machine learning-based approach for land cover change detection using remote sensing and radiometric measurements. *IEEE Sensors Journal*, 19, pp.5843-5850.

# Effect of EPS Concrete: Balancing Construction Efficiency and Environmental Sustainability

R. Rajeshwaran<sup>1†</sup>, J. Logeshwari<sup>1</sup> and R. Abirami<sup>2</sup>

<sup>1</sup>Department of Civil Engineering, Vel Tech Rangarajan Dr. Sagunthala R&D Institute of Science and Technology, Avadi, Tamil Nadu, India

<sup>2</sup>Department of Civil Engineering, Aarupadai Veedu Institute of Technology, Vinayaka Mission's Research Foundation, (Deemed to be University), Tamil Nadu, India

†Corresponding author: R. Rajeshwaran; vtd987@veltech.edu.in; rajeshwaran442@gmail.com

**Abbreviation:** Nat. Env. & Poll. Technol.  
**Website:** [www.neptjournal.com](http://www.neptjournal.com)

*Received:* 10-09-2024

*Revised:* 17-10-2024

*Accepted:* 19-10-2024

## Key Words:

Expanded polystyrene  
 Environmental pollutants reduction  
 Sustainable concrete mix  
 Replacement ratio  
 Energy saving

## Citation for the Paper:

Rajeshwaran, R., Logeshwari, J. and Abirami, R., 2025. Effect of EPS concrete: Balancing construction efficiency and environmental sustainability. *Nature Environment and Pollution Technology*, 24(2), p. B4268. <https://doi.org/10.46488/NEPT.2025.v24i02.B4268>

*Note: From year 2025, the journal uses Article ID instead of page numbers in citation of the published articles.*



**Copyright:** © 2025 by the authors

**Licensee:** Technoscience Publications

This article is an open access article distributed under the terms and conditions of the Creative Commons Attribution (CC BY) license (<https://creativecommons.org/licenses/by/4.0/>).

## ABSTRACT

Expanded polystyrene (EPS) is a material that may be harmful to human health. This is mainly because it releases specific chemicals during its manufacture, usage, and disposal. It is important to remember that the effects on health can change depending on the particular situation, exposure levels, and personal sensibilities. There are initiatives underway to address these environmental issues. Increasing EPS recycling rates, locating substitute materials, and encouraging appropriate disposal techniques are the main goals of several projects. Furthermore, studies into more environmentally friendly EPS substitutes for a variety of applications are still in progress. Creating a circular economy and lowering the total amount of single-use plastics used are two more aspects of larger plans to lessen the environmental impact of materials like EPS. The introduction of EPS cubes into concrete has reduced the adverse effects of EPS materials in the environment. This study substituted EPS, which is generated from industrial waste products, for aggregate. For an experimental study, a good-strength, sustainable concrete mix of grade M30 has been developed. In increments of 25%, five different mix proportions were evaluated for EPS cubes with size variations of 10 mm, 12 mm, and 20 mm. The range of 0 to 100% was studied. The replacement of EPS cubes by volume of course aggregates in the mixture yields the maximum increase in crushing, rupture, and bending strength, according to the mechanical properties of concrete that have been observed. This replacement ratio of 25% was shown to be efficient. The use of EPS materials in concrete is therefore shown to produce large reductions in environmental pollutants in addition to significant cost and energy savings.

## INTRODUCTION

Foamed polystyrene (PS), which can be either expanded (EPS) or extruded (XPS), is a lightweight, rigid, insulating thermoplastic widely used across various sectors such as consumer goods, packaging, construction, and marine industries. However, its properties also make it prone to generating waste that easily disperses and fragments in the environment. This review examines the impact of foamed PS in marine environments, including its sources, movement, degradation, contamination, ingestion by marine animals, and the biological effects of the chemical additives it contains. In the ocean, foamed PS is transported by wind and breaks down through photolytic degradation. It can also serve as a platform for organisms while being exposed to high levels of natural and human-made surface-active chemicals in the sea surface microlayer. Near shorelines, fragmentation is increased by the mechanical action of waves and abrasion when the material is beached, with the wind sometimes leading to its temporary burial. Various marine animals, especially those that feed at the surface or inhabit areas where foamed PS accumulates, have been documented ingesting EPS and XPS. This ingestion

can cause physical harm, such as gastrointestinal blockages, and expose animals to harmful chemicals, notably flame-retardant hexabromocyclododecane, which is still found in recycled materials. Due to the difficulty in recovering foamed PS once it becomes marine litter, reducing its environmental impact will require eliminating processes that produce foamed waste, improving storage and disposal practices, and developing more sustainable and durable alternatives (Turner 2020). Industries and post-consumer products produce trash made of expanded polystyrene (EPS). They are not biodegradable, but they are typically disposed of by burning or filling a landfill, which pollutes the environment. A very common plastic for packing is polystyrene. In the case of landfilling, it is almost non-biodegradable and takes hundreds of years to break down, while other disposal or treatment techniques have detrimental consequences on the ecosystem. However, this substance is well known for having qualities like strong heat conductivity, sound absorption, and lightweight, which makes it an excellent addition to concrete (Ubi et al. 2022). The material to address contemporary global environmental concerns about sustainability and healthier air quality is to be found for replacement as it should contain less percentage of pentane (Prasittisopin et al. 2022) and a high percentage of styrene for better structural integrity as mentioned in Table 1. Research interest has recently increased due to the potential use of EPS as a partial replacement for fine particles in concrete. (Adeniran & Soyemi 2020). A complete or partial substitute for coarse aggregate is expanded polystyrene beads, which also give better strength results (Moon et al. 2020). The weight of the concrete decreased when EPS grains were added as coarse aggregates (Salahaldeen & Al-Hadithi 2022). EPS has greater resistance to crushing and impact (Borkar & Singi 2020). The main benefits of lightweight EPS concrete are its low heat conductivity, low density, and sound-insulating qualities (Kumar et al. 2021). EPS can enhance thermal insulation and soundproofing, increasing a building's energy efficiency (Shukri et al. 2024). EPS improves workability, increasing building efficiency and utilizing recycled resources to provide acceptable structural strength and environmental sustainability (Hilal et al. 2021). Concrete enhanced with EPS (expanded polystyrene) aggregates offers environmental benefits and can be utilized for various non-load-bearing elements like partition walls, floors, ceilings, bricks, and plaster. By replacing traditional structural members such as columns and beams, this lightweight concrete can significantly reduce the overall dead load of a building (Kaya & Kar 2016). The lightweight material can also be achieved by adding EPS in bead form with a fly ash mixture (Bagde et al. 2022). EPS can be reused as an ingredient in concrete mixtures. Cement production is

resource-intensive, consuming substantial energy and raw materials. Moreover, it is responsible for approximately 7% of global CO<sub>2</sub> emissions, a significant contributor to climate change (Raja & Saravanan 2024). Treated recycled expanded polystyrene EPS concrete demonstrates a significant reduction in density, weighing about 30% less than conventional concrete (Mohammed & Hussein 2021). By incorporating EPS concrete in construction, buildings can achieve significant reductions in both structural weight and energy consumption. EPS concrete repurposes recoverable EPS particles, effectively addressing environmental pollution concerns. This material emerges as an economical, environmentally friendly, and energy-efficient option that aligns with green building principles (Pranahita et al. 2022). The recycled expanded polystyrene (EPS) into concrete as a partial replacement for fine aggregate leads to a 15% reduction in carbon dioxide emissions and a 16% decrease in energy consumption during production (Villa et al. 2023). The structural properties of recycled expanded polystyrene (EPS) and a hybrid cement blend show improved crushing strength. This eco-friendly hybrid concrete could be suitable for use as structural lightweight concrete (González-Betancur et al. 2024). The goal is to develop a concrete mixture that balances cost-effectiveness, serviceability, and compliance with lightweight concrete standards. At this 30% EPS beads replacement level, the resulting concrete exhibited density and water absorption characteristics that fell within acceptable ranges (Abah et al. 2018). The incorporation of EPS material reduces environmental pollution and alleviates storage problems associated with EPS waste (Çelikten et al. 2023). The improved EPS concrete formulation could be particularly suitable for non-structural applications in construction and addressing environmental concerns related to waste management (Mun et al. 2021). EPS-bead lightweight concrete is not only resilient and energy-efficient but also stands out as a promising technology that could help meet the growing demands for eco-friendly and high-performance building solutions (Rathore et al. 2024). The EPS-based geomaterial can also be effectively utilized, offering a practical solution for challenging soil conditions where weight reduction is crucial (Menghare et al. 2022). The higher levels of coarse aggregate replacement with EPS had a particularly detrimental impact on crushing strength. Interestingly, replacing fine aggregate with coarse aggregate at certain levels yielded more favorable outcomes, maintaining crushing strength comparable to traditional concrete mixtures (Abdel-Jabe et al. 2023). EPS concrete promotes environmental sustainability through better insulation and durability in residential and commercial structures while increasing construction efficiency by lowering energy consumption and expenses (Azzawi et al. 2023).



## EPS Waste

EPS (Expanded Polystyrene Foam) waste management in India shows that the country faces significant challenges in managing plastic waste, especially EPS, a common form of non-biodegradable plastic used in packaging. EPS waste shown in Fig. 1 is like other types of plastic and contributes to India's massive plastic pollution problem. India generates around 9 million metric tons of plastic waste every year, much of which is not properly treated or disposed of. EPS waste is particularly problematic as its lightweight structure makes it difficult to collect and recycle. Though India has put in place frameworks for plastic waste management, such as the Plastic Waste Management Rules and Extended Producer Responsibility (EPR), recycling rates remain low. Only about 12.3% of plastic waste in the country is recycled, while the remaining 20% is incinerated. Despite efforts to improve waste management infrastructure, production of single-use plastics, including EPS, continues to increase. India, along with other developing countries with limited recycling capacity, is one of the countries hardest hit by plastic waste mismanagement, accounting for over 52% of global plastic mismanagement. This trend is expected to worsen unless additional steps are taken to improve recycling and reduce single-use plastics such as EPS. India's Ministry of Environment 2024 report highlights major challenges in waste management, including the growing expanded polystyrene (EPS) waste problem. EPS is a common plastic used in packaging and insulation, but its low recyclability and high volume contribute to India's plastic waste crisis. The Centre for Science and Environment (CSE) stresses that while the plastic ban targets single-use plastics, more comprehensive measures are needed to combat EPS and other forms of plastic waste. India's entire plastic waste management system is



Fig. 1: EPS waste.

in trouble, with over 79% of the plastic produced worldwide ending up as waste. The 2024 report highlights the lack of proper infrastructure for EPS recycling, especially in urban areas where waste segregation is still limited. The Energy and Resources Institute (TERI) and CSE advocate for increased regulation of plastic manufacturers and improved recycling systems as key solutions to manage this growing problem. Regarding volume, EPS waste is a danger to the environment. This is because it tends to accumulate on discharge and navigation channels, which increases waste management issues. Decisions such as the extension of the manufacturer (EPR) and the extension treatment initiative are part of the agenda to reduce plastic waste in this format.

## MATERIALS AND METHODS

When expanded polystyrene (EPS) is used in concrete specimens, it often serves as a lightweight aggregate or filler. EPS cubes shown in Fig. 2 are incorporated into the concrete matrix to reduce the overall density of the specimen while maintaining adequate strength. This modification is commonly used in lightweight concrete applications where weight reduction is critical, such as in non-load-bearing walls or thermal insulation layers. The inclusion of EPS in concrete can also enhance its better thermal conductivity

Table 1: Chemical properties of EPS.

Properties	Value
Chemical Formula	$(C_8H_8)_n$
Molecular Weight	104.15 g.mol <sup>-1</sup> (per styrene unit)
Styrene Content	> 95%
Pentane Content (blowing agent)	< 2%

Table 2: Physical properties of EPS.

Properties	Value
Density	20 kg.m <sup>-3</sup>
Thermal Conductivity	0.036 W/(m.K)
Crushing Strength (10% deformation)	80 kPa
Bending Strength	170 kPa
Tensile Strength	150 kPa
Water Absorption (by volume)	0.5-3%
Coefficient of Linear Thermal Expansion	5-7 × 1000/K
Maximum Service Temperature	75-80°C
Glass Transition Temperature	~100°C
Specific Heat Capacity	1.3 kJ/(kg.K)
Sound Transmission Class (STC)	25 dB
Oxygen Index	24-26%
Vapor Diffusion Resistance Factor (μ)	75

properties as shown in Table 2, making it a popular choice for energy-efficient building designs. Concrete specimens are typically composed of a mixture of binder-cement whose physical properties are given in Table 3, M sand in Table 4, partial replacement of 10 mm aggregate specified in Table 5, water, and admixture-like superplasticizers. The cement acts as the binder, holding the aggregates together as the mixture hardens.

### Mix Design and Specifications

**W/C ratio:** The water-cement ratio is crucial for controlling the strength and durability of the concrete. According to IS 10262:2019, a lower W/C ratio results in higher strength, and 0.4 is used for M-30 grade concrete.

Table 3: Physical properties of cement.

Characteristics	Experimental Data
Stiffening time	36 min
Hardening time	530 min
Density ratio	3.15
Consistency	30.5%
Soundness	1.4 mm
Maximum crushing stress (MPa)	15.0 at three days 23.5 at seven days 31.5 at twenty-eight days

Table 4: Physical properties of M sand.

Physical Properties	Experimental Data
Grading index	2.80
Density	1720 kg.m <sup>-3</sup>
Impact value	15%
Density ratio	2.70

Table 5: Physical properties of 10 mm aggregate.

Physical Properties	Experimental Data
Grading index	7.00
Density	1550 kg.m <sup>-3</sup>
Density ratio	2.80



Fig. 2: EPS cubes.

**Cement content:** This amount complies with IS 456:2000, which stipulates a minimum cement content based on environmental exposure conditions. For M-30 grade concrete, 330 kg.m<sup>-3</sup> is a typical value.

**Fine aggregate and Coarse aggregate:** These M sand (675 kg.m<sup>3</sup>) and aggregate (1110 kg.m<sup>3</sup>) are calculated based on the mix design procedure outlined in IS 10262:2019. The exact quantities may vary slightly depending on the specific gravity and grade of the aggregates used.

**Water:** The water content (150 kg.m<sup>3</sup>) is calculated to achieve the desired workability with the specified W/C ratio. This aligns with IS 10262:2019.

**Mineral admixture:** Mineral admixture fly ash can replace a portion of the cement to improve durability and workability. According to IS 456:2000 and IS 10262:2019, up to 20% replacement is typical for this grade of concrete.

**Superplasticizer:** Superplasticizers are used to enhance the workability of the concrete mix without increasing the water content, which is essential for maintaining a low W/C ratio. According to IS 10262:2019, a typical dosage is around 0.5% by weight of cementitious content. A sulfonated Naphthalene Formaldehyde (SNF) - based Superplasticizer is used.



Fig. 3: Mixture for specimen casting.

Table 6. Mix design.

Ratio of ingredients	
Target crushing strength [Mpa]	30
Water/Cement ratio	0.4
Cement content [kg.m <sup>-3</sup> ]	330
M sand [kg.m <sup>-3</sup> ]	675
10 mm aggregate [kg.m <sup>-3</sup> ]	1110
Water content [kg.m <sup>-3</sup> ]	150
Supplementary Cementitious material [kg.m <sup>-3</sup> ]	20%
Dosage of superplasticizer used to improve workability [kg.m <sup>-3</sup> ]	0.5%



Fig. 4: Cube and cylinder specimens.



Fig. 5: Testing of cube specimen.



Fig. 6: Testing of cylinder specimen.



Fig. 7: Testing of beam specimen.

## Testing of Specimens

**Casting of specimens:** As per IS 516:1959, concrete specimens should be cast in clean, water-tight molds made of non-absorbent material. Fill the molds in three layers after proper mixing as shown in Fig. 3, compacting each layer with a tamping rod. After filling, level the top surface and mark the specimens for identification. The mixed proportions of specimens are referred to in Table 6. For cubes, use 15 cm x 15 cm x 15 cm molds; for cylinders, use molds with a diameter of 15 cm and height of 30 cm as shown in Fig. 4 and for beams, use 15 cm x 15 cm x 70 cm molds.

**Initial curing:** According to IS 516:1959, cover the specimens with wet burlap or similar material immediately after casting to prevent evaporation. Keep them in a place free from vibration for  $24 \pm 2$  h at a temperature of  $27 \pm 2^\circ\text{C}$ . For specimens in cold weather, maintain the temperature between  $22^\circ\text{C}$  and  $32^\circ\text{C}$ .

**Demolding:** As specified in IS 516:1959, remove the specimens from the molds after  $24 \pm 2$  h of casting. If the specimens are too weak to be handled after 24 h, leave them in the molds for up to 72 h. Handle the specimens carefully to avoid damage or distortion.

**Curing:** Following IS 516:1959 guidelines, immediately after demolding, store the specimens in clean, fresh water at a temperature of  $27 \pm 2^\circ\text{C}$  until the time of testing. Change the water in the curing tank periodically to maintain cleanliness. For specimens that will be tested at 28 days or later, you may transfer them to a moist room with 90% or more relative humidity after the initial 7 days of water curing.

**Preparation for testing:** As per IS 516:1959, remove the specimens from water storage at least 2 h before testing. For cubes and cylinders, wipe the surface water and grit from the specimens. For beams, keep them wet until testing. Measure and record the dimensions of the specimens accurately.

**Testing procedure:** Follow IS 516:1959 for the testing procedures. For cubes and cylinders, place the specimen centrally on the lower plate of the testing machine. Apply the load without shock and increase it continuously at a rate of approximately  $140 \text{ kg.sq}^{-1} \text{ cm.min}^{-1}$  until the specimen

fails. For beams, use the two-point loading method, applying the load at one-third points of the span.

**Calculations and reporting:** Calculate the strength as per IS 516:1959. A minimum of 3 specimens for each test age is required to account for variability, typically 7 days, 14 days, and 28 days.

- **Crushing strength test (Cube):** as per IS 516, 150mm cubes are cured for 28 days and loaded at a rate of  $13.7 \text{ MPa.min}^{-1}$  is applied as shown in Fig. 5. The crushing strength is calculated as  $f_c = \text{maximum load} / \text{cross-sectional area}$ .
- **Rupture strength test (Cylinder):** as per IS 5816, A cylinder of 150mm diameter x 300mm height is cast and cured for 28 days, and load at a rate of 1.2 to  $2.4 \text{ MPa.min}^{-1}$  is applied as shown in Fig. 6. The rupture strength is calculated using the formula  $f_t = 2P/(\pi LD)$ , where P = failure load, L = length, and D = diameter.
- **Bending strength test (Beam):** as per IS 516. A beam size of 100mm x 100mm x 500mm was fabricated, and curing for 28 days was done. The load at a rate of  $400 \text{ kg.min}^{-1}$  is applied as shown in Fig. 7. The bending



strength is calculated using the formula bending strength  $f_b = PL/bd^2$ , where  $P$  = failure load,  $L$  = span,  $b$  = breadth, and  $d$  = cross-sectional depth.

**Acceptance Criteria:** Refer to IS 456:2000 for concrete strength acceptance criteria. The concrete satisfies the energy requirements if the average strength of the set of test results is equal to or higher than the required strength and no single test result, except for 3 MPa, is less than the nominal strength.

### Material Blending

The specimen mixes represent various combinations of Ordinary Portland Cement (OPC), Manufactured sand (M sand), and Expanded Polystyrene (EPS) cubes of different sizes (10 mm, 12 mm, and 20 mm) with varying aggregate. These mixes are designed to explore the potential of lightweight concrete by replacing traditional 10 mm aggregates with EPS cubes, a material known for its lightweight and insulation properties. The percentages of aggregates and EPS cubes are systematically varied, ranging from 25% to 100% as mentioned in Table 7 to assess their impact on the mechanical properties of concrete, such as strength, density, and thermal insulation. Such studies are crucial in civil engineering for developing materials that are both structurally efficient and offer energy-saving benefits, particularly in applications where less self-weight is essential, like in multi-story buildings or thermal insulation applications.

## RESULTS AND DISCUSSION

### Crushing Strength Test Results

The data presented in Table 8. outlines the crushing strength performance of various Expanded Polystyrene Concrete

(EPSC) mixes with different EPS contents over a curing period of seven, fourteen, and twenty - eight days. The study shows a general trend where increasing the EPS content in the concrete mix results in a decrease in crushing strength when compared to the conventional mix. Specifically, mixes with 10%, 12%, and 20% EPS content show a reduction in strength at 28 days as EPS content increases, with the most significant drop observed at 100% EPS replacement as illustrated in Fig. 8. While some mixes (e.g., EPSC (10) 25 and EPSC (20) 25) exhibit a slight increase in crushing strength, the overall trend indicates that higher EPS content leads to a gradual decrease in crushing strength, demonstrating the trade-off between reducing the density of concrete and maintaining its structural integrity. The 28-day crushing strength test results with statistical analysis for the different concrete specimens are summarized in Table 9. below. The data exhibits variability through the use of 95% confidence intervals (CI), mean strength, and estimated standard deviations. Certain specimens, such as EPSC (10)25, demonstrate high strength and minimal variability, whereas other specimens, such as EPSC (20)100, show more variability with wider confidence intervals and lower strength. Comments emphasize relative results reliability and trends like strength retention or reduction.

### Rupture Strength Test Results

The average rupture strengths of various mixes with expanded polystyrene (EPS) aggregates at different curing ages (7, 14, and 28 days) are presented in Table 10. The mixes are labeled with different percentages (25%, 50%, 75%, 100%) and EPS bead sizes (10mm, 12mm, 20mm). The results show that % of EPS replacement increases, and the rupture strength generally decreases as illustrated in Fig. 9.

Table 7: Material Blending.

Specimen Label	Material Blending	Water in mix [kg.m <sup>-3</sup> ]	Cement in mix [kg.m <sup>-3</sup> ]	Workability [mm]
EPSC(10)25	OPC + 100 % M sand + 75 % 10 mm aggregate + 25 % EPS cubes 10 mm	157.5	350	97
EPSC(10)50	OPC + 100 % M sand + 50 % 10 mm aggregate + 50 % EPS cubes 10 mm	157.5	342	89
EPSC(10)75	OPC + 100 % M sand + 25 % 10 mm aggregate + 75 % EPS cubes 10 mm	157.5	337	84
EPSC(10)100	OPC + 100 % M sand + 100% EPS cubes 10 mm	157.5	323	79
EPSC(12)25	OPC + 100 % M sand + 75 % 10 mm aggregate + 25 % EPS cubes 12 mm	157.5	342	92
EPSC(12)50	OPC + 100 % M sand + 50 % 10 mm aggregate + 50 % EPS cubes 12 mm	157.5	331	81
EPSC(12)75	OPC + 100 % M sand + 25 % 10 mm aggregate + 75 % EPS cubes 12 mm	157.5	322	77
EPSC(12)100	OPC + 100 % M sand + 100% EPS cubes 12 mm	157.5	312	70
EPSC(20)25	OPC + 100 % M sand + 75 % 10 mm aggregate + 25 % EPS cubes 20 mm	157.5	338	88
EPSC(20)50	OPC + 100 % M sand + 50 % 10 mm aggregate + 50 % EPS cubes 20 mm	157.5	328	73
EPSC(20)75	OPC + 100 % M sand + 25 % 10 mm aggregate + 75 % EPS cubes 20 mm	157.5	315	69
EPSC(20)100	OPC + 100 % M sand + 100% EPS cubes 20 mm	157.5	306	65



The maturity strength values are compared to a conventional mix, with some mixes showing improvement (e.g., EPSC (10) 25 with a 14.19% increase) while others exhibit reduced strength (e.g., EPSC (20) 100 with a 14.52% decrease). The data suggests that smaller EPS bead sizes (10 mm) and lower replacement percentages tend to perform better in terms of rupture strength, while larger bead sizes (20 mm) and higher replacement percentages result in more significant strength reductions compared to the conventional mix.

### Bending Strength Test Results

The bending strength is measured at 7, 14, and 28 days, with the 28-day strength compared to a conventional mix. Table 11. presents data on the average bending strength

of various concrete mixes incorporating EPS as a partial substitute for aggregates. Generally, the results prove that % of EPS and its beads size increase, which tends to decrease the bending strength of the concrete. The mix EPSC (10) 25, with 25% replacement using 10 mm EPS beads, shows the highest improvement in bending strength (15% increase) compared to the conventional mix at 28 days. Conversely, EPSC (20) 100, with 100% replacement using 20mm EPS beads, exhibits the most significant decrease in bending strength (-28.57%) at 28 days as illustrated in Fig. 10. This data suggests that while EPS can be incorporated into concrete mixes, careful consideration must be given to the replacement percentage and bead size to maintain adequate bending strength for structural applications.

Table 8: Crushing strength test results.

Specimen Label	Crushing strength of three specimens at each test age [Mpa] (9 samples totally under each specimen label)			% variation in crushing strength compared with the conventional mix at 28 days.
	Early age strength (7 <sup>th</sup> Day)	Midterm strength (14 <sup>th</sup> Day)	Maturity strength (28 <sup>th</sup> Day)	
EPSC(10)25	24.11	31.20	35.45	12.54 (31.5)
EPSC(10)50	22.84	26.81	33.10	5.08
EPSC(10)75	21.11	25.02	30.15	-4.29
EPSC(10)100	18.64	24.75	29.12	-7.56
EPSC(12)25	22.65	28.47	32.35	2.70
EPSC(12)50	21.53	27.46	31.20	-0.95
EPSC(12)75	19.55	25.09	29.18	-7.37
EPSC(12)100	19.11	24.02	27.30	-13.33
EPSC(20)25	21.79	28.62	31.52	3.24
EPSC(20)50	19.77	27.07	30.42	-3.43
EPSC(20)75	18.43	24.95	28.35	-10.00
EPSC(20)100	17.79	23.54	26.16	-16.95

Table 9: Statistical analysis of Crushing strength test results.

Specimen	Mean [Mpa]	Standard Deviation [Mpa]	95% CI Lower [Mpa]	95% CI Upper [MPa]	Remarks
EPSC(10)25	35.45	3.55	26.64	44.26	High strength, narrow CI
EPSC(10)50	33.10	3.31	24.88	41.32	Slight reduction in strength
EPSC(10)75	30.15	3.02	22.66	37.64	Moderate reduction, wide CI
EPSC(10)100	29.12	2.91	21.89	36.35	Noticeable reduction in strength
EPSC(12)25	32.35	3.23	24.31	40.39	Good strength retention
EPSC(12)50	31.20	3.12	23.45	38.95	Stable strength
EPSC(12)75	29.18	2.92	21.93	36.43	Moderate strength reduction
EPSC(12)100	27.30	2.73	20.52	34.08	Lower strength, wide variation
EPSC(20)25	31.52	3.15	23.69	39.35	Good strength, narrow CI
EPSC(20)50	30.42	3.04	22.86	37.98	Stable performance
EPSC(20)75	28.35	2.84	21.31	35.39	Reduced strength, wide CI
EPSC(20)100	26.16	2.62	19.66	32.66	Lowest strength, wide variation

Table 10: Rupture strength results.

Specimen Label	Rupture strength of three specimens at each test age [Mpa] (9 samples totally under each specimen label)			% variation in Rupture strength compared with the conventional mix at 28 days.
	Early age strength (7 <sup>th</sup> Day)	Midterm strength (14 <sup>th</sup> Day)	Maturity strength (28 <sup>th</sup> Day)	
EPSC(10)25	2.40	3.15	3.54	14.19 (3.10)
EPSC(10)50	2.30	2.65	3.34	7.74
EPSC(10)75	2.15	2.55	3.01	-2.90
EPSC(10)100	1.86	2.50	2.95	-4.84
EPSC(12)25	2.23	2.81	3.25	4.84
EPSC(12)50	2.15	2.73	3.11	0.32
EPSC(12)75	1.95	2.52	2.85	-8.06
EPSC(12)100	1.91	2.40	2.70	-12.90
EPSC(20)25	2.18	2.87	3.15	1.61
EPSC(20)50	1.98	2.70	3.00	-3.23
EPSC(20)75	1.85	2.49	2.88	-7.10
EPSC(20)100	1.75	2.36	2.65	-14.52

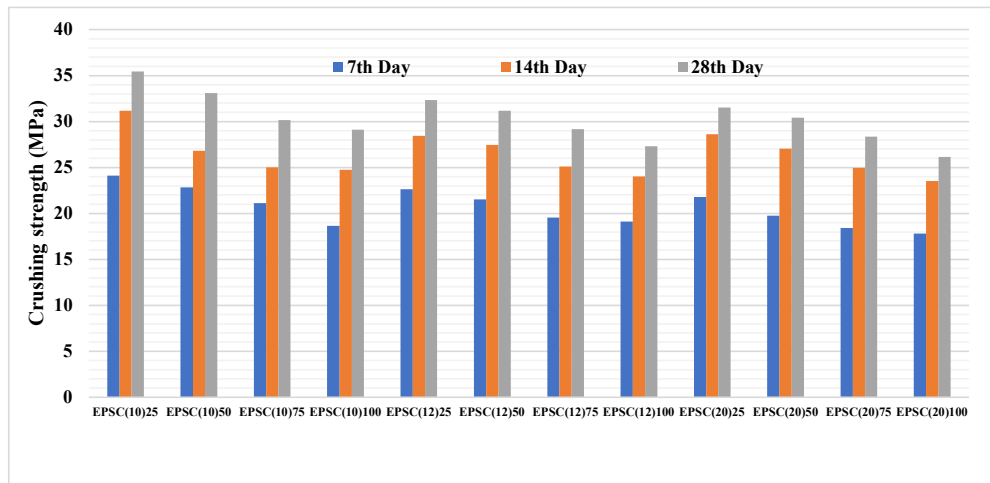


Fig. 8: Crushing strength test results.

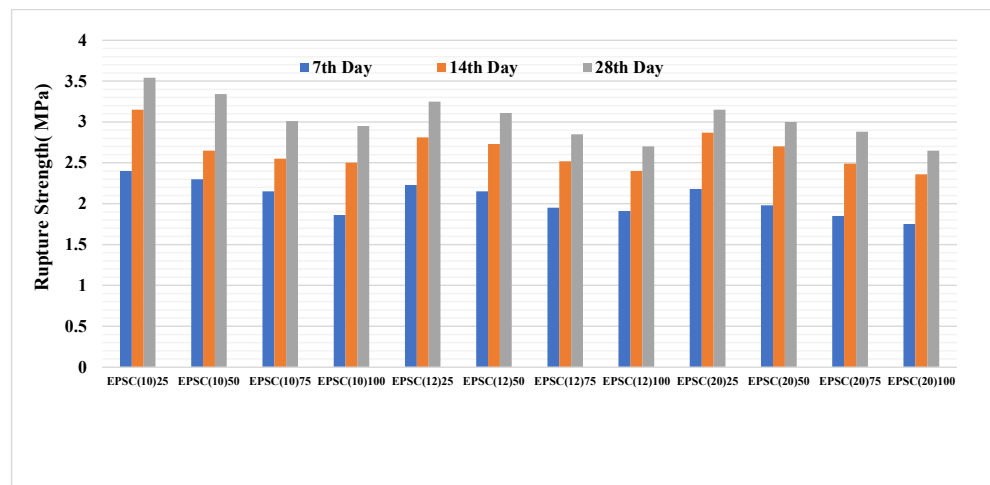


Fig. 9: Rupture strength test results.

Table 11: Bending strength test results.

Specimen Label	Bending strength of three specimens at each test age [Mpa] (9 samples totally under each specimen label)			% variation in bending strength compared with the conventional mix at 28 days.
	Early age strength (7 <sup>th</sup> Day)	Midterm strength (14 <sup>th</sup> Day)	Maturity strength (28 <sup>th</sup> Day)	
EPSC(10)25	3.28	4.25	4.83	15.00 (4.2)
EPSC(10)50	3.05	3.58	4.42	5.24
EPSC(10)75	2.91	3.44	4.15	-1.19
EPSC(10)100	2.55	3.38	3.98	-5.24
EPSC(12)25	3	3.77	4.52	7.62
EPSC(12)50	2.86	3.64	4.14	-1.43
EPSC(12)75	2.63	3.37	3.92	-6.67
EPSC(12)100	2.66	3.34	3.8	-9.52
EPSC(20)25	2.7	3.8	4.3	2.38
EPSC(20)50	2.28	3.12	3.50	-16.67
EPSC(20)75	2.08	2.82	3.20	-23.81
EPSC(20)100	2.04	2.70	3.00	-28.57

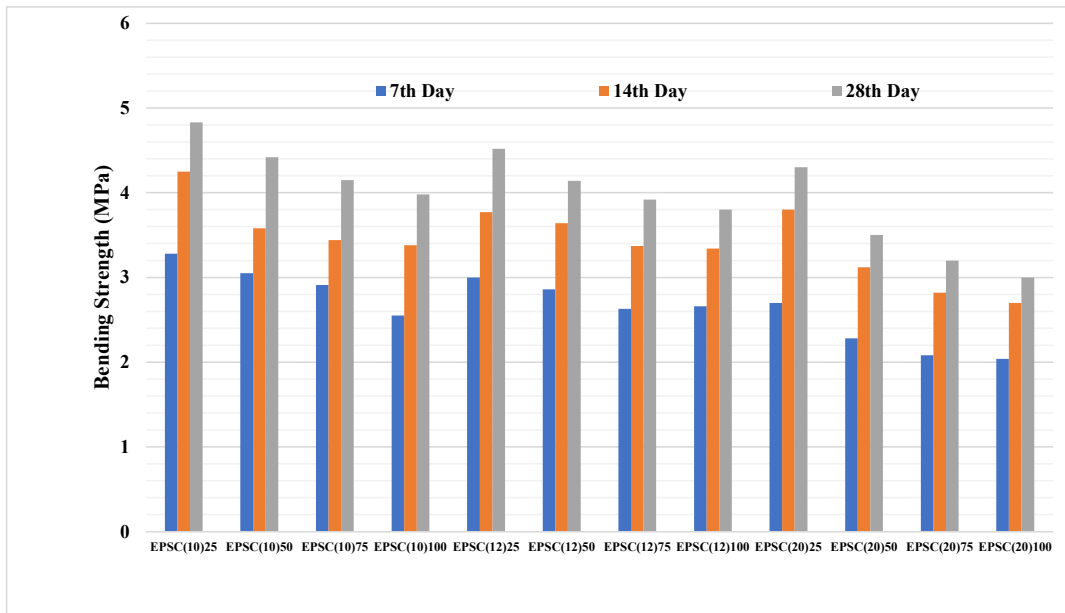


Fig. 10: Bending strength test results.

## CONCLUSION

The experimental study led to the following conclusions:

1. The expanded polystyrene concrete (EPSC) usage shows promise in reducing the environmental impact of traditional concrete while maintaining acceptable strength levels. Notably, EPSC (10) 25 and EPSC (10) 50 mixes achieved crushing strengths at 28 days, which were 12.54% and 5.08% higher than the conventional mix, respectively. This suggests that incorporating up to 50% EPSC with a 10 mm particle size can enhance

strength while potentially reducing the overall concrete volume needed. Even at higher EPSC percentages and larger particle sizes, the strength reductions were generally moderate, with many mixes still achieving over 30 MPa at 28 days. This indicates that EPSC can be a viable partial replacement for traditional aggregates, which could lead to reduced natural resource extraction and lower carbon emissions associated with aggregate production. The ability to use recycled polystyrene in EPSC further contributes to waste reduction and circular economy principles. Overall, these results demonstrate

that EPSC mixes can offer a balance between structural performance and environmental benefits, potentially leading to more sustainable construction practices.

2. A notable environmental advantage can be observed in the use of expanded polystyrene concrete (EPSC) mixes. The results show that certain EPSC mixes, particularly EPSC (10) 25 and EPSC (10) 50, exhibit improved rupture strength compared to the conventional mix at 28 days, with increases of 14.19% and 7.74%, respectively. This suggests that incorporating expanded polystyrene, a waste material, into concrete can potentially enhance its performance while simultaneously addressing environmental concerns. By utilizing expanded polystyrene in concrete production, we can reduce the amount of this non-biodegradable material ending up in landfills or polluting ecosystems. Additionally, the use of EPSC could potentially decrease the demand for traditional concrete materials, thereby reducing the environmental impact associated with their extraction and production. While some mixes show decreased strength, the overall trend indicates that with proper mix design, EPSC can offer a viable eco-friendly alternative in certain construction applications, contributing to waste reduction and resource conservation efforts.
3. The incorporation of expanded polystyrene concrete (EPSC) in various percentages shows promising results for sustainable construction practices. Notably, EPSC (10) 25 and EPSC (10) 50 mixes demonstrate improved bending strength compared to the conventional mix at 28 days, with increases of 15% and 5.24%, respectively. This suggests that the partial replacement of traditional concrete with recycled expanded polystyrene can maintain or even enhance structural performance while potentially reducing the carbon footprint associated with cement production. The use of expanded polystyrene, a common waste material, in concrete mixes addresses the issue of plastic pollution by repurposing a material that would otherwise contribute to environmental degradation. Additionally, the lighter weight of EPSC mixes could lead to reduced transportation emissions and lower energy requirements in construction, further contributing to climate change mitigation efforts. While some mixes show decreased strength at higher replacement levels, the overall trend indicates that optimized EPSC formulations could play a significant role in developing more environmentally friendly construction materials, thereby supporting pollution reduction strategies and promoting a circular economy approach in the building sector.
4. The results of this study support and broaden existing theories on material efficiency and waste

utilization in concrete production, which advances environmental engineering and sustainable construction. By showing that expanded polystyrene concrete (EPSC) may largely replace coarse aggregates without significantly compromising structural performance, EPS is challenging the conventional dependence on natural aggregates in civil engineering. Improvements in crushing and bending strengths are demonstrated by the results, especially for EPSC (10) 25 and EPSC (10) 50. This suggests that adding lightweight waste materials like EPS to concrete can preserve or even improve its mechanical qualities. Challenging traditional theories that emphasize using high-density aggregates for strength creates opportunities for creative material uses that put sustainability first without affecting loading-carrying capability. These findings, which take expanded polystyrene from landfills and repurpose it in concrete, are consistent with.

The circular economy and waste valorization concepts from the standpoint of environmental engineering. Modern sustainable engineering techniques that address plastic waste management minimize carbon emissions from aggregate extraction and manufacture, and lessen resource depletion are all in line with this. As part of the continuous transition to low-carbon, resource-efficient building technologies, the study shows that incorporating EPS into concrete is a feasible strategy to lessen the environmental impact of building materials. To establish EPSC as a competitive alternative in environmentally friendly building methods, this study expands on current frameworks by showing that optimum mix designs can strike a compromise between sustainability and structural integrity.

## FUTURE STUDIES

The following crucial areas should be investigated in further research on this project since they might also be seen as its limitations with regard to the wider economic and environmental effects of employing EPS concrete in large-scale projects:

- Durability Testing
- Structural Behavior
- Mix Design Optimization
- Life-Cycle Assessment
- Scalability and Sourcing

## ACKNOWLEDGMENT

The authors gratefully acknowledge the financial support from the Vel Tech Rangarajan Dr. Sagunthala R&D



Institute of Science and Technology, Avadi, Tamil Nadu, India.

## REFERENCES

- Abah, J.C., Ndububa, E.E. and Ikpe, E.O., 2018. An evaluation of the water absorption and density properties of expanded polystyrene sand concrete. *Open Journal of Civil Engineering*, 8(4), DOI: 10.4236/ojce.2018.84037.
- Abdel-Jabe, M., Shatarat, N.K. and El-Nimri, R., 2023. Influence of using expanded polystyrene beads on the density and crushing strength of hardened concrete. *Civil Engineering and Architecture*, 1, pp.45–53.
- Adeniran, J.A. and Soyemi, O.B., 2020. Structural use of expanded polystyrene concrete. *International Journal of Innovative Science and Research Technology*, 5(6), pp.1131–1138.
- Azzawi, R., 2023. Green construction and sustainability using modified expanded polystyrene (EPS) insulation. *9th International Engineering Conference on Sustainable Technology and Development (IEC)*, pp.102–109. <https://doi.org/10.1109/iec57380.2023.10438799>
- Bagde, R., Gajbhiye, R. and Nagdevte, P., 2022. Experimental studies on expanded polystyrene beads (fly ash geometrical). *International Journal of Innovative Research in Technology*, 8(12), pp.1557–1561.
- Borkar, Y. and Singi, M., 2020. EPS-based light weight concrete design with enhancement of strength. *International Journal of Civil and Structural Engineering Research*, 7(2), pp.44–54.
- Çelikten, S., İsa, İ., Özcan, Z.A., Durak, U., İlkentapar, S., Karahan, O. and Atiş, C.D., 2023. Recycling waste expanded polystyrene as aggregate in the production of lightweight screed mortar. *Journal of Construction*, 22(3), DOI: <https://doi.org/10.7764/RDLC.22.3.581>.
- González-Betancur, D., Hoyos-Montilla, A.A. and Tobón, J.I., 2024. Sustainable hybrid lightweight aggregate concrete using recycled expanded polystyrene. *Materials*, 17(10), Article 2368. <https://doi.org/10.3390/ma17102368>.
- Hilal, N., Hamah, N., Rabar, S. and Faraj, H., 2021. Development of eco-efficient lightweight self-compacting concrete with high volume of recycled EPS waste materials. *Environmental Science and Pollution Research*, 28(36), pp.50028–50051. <https://doi.org/10.1007/S11356-021-14213-W>
- Kaya, A. and Kar, F., 2016. Properties of concrete containing waste expanded polystyrene and natural resin. *Construction and Building Materials*, 155, pp.572–578.
- Kumar, C.V., Arun, E. and Bhaskar, B., 2021. Lightweight concrete using EPS (expanded polystyrene) beads. *International Journal of Research Publication and Reviews*, 2(8), pp.1591–1598.
- Menghare, D., Welekar, V., Shende, R., Bagde, S., Gajbhiye, R. and Nagdevte, P., 2022. Experimental studies on expanded polystyrene beads (fly ash geometrical). *International Journal of Innovative Research in Technology*, 8(12), pp.1557–1561.
- Mohammed, H.J. and Hussein, Y.G., 2021. Concrete properties using treated recycled EPS. *IOP Conference Series: Earth and Environmental Science*, 17, p.128. DOI: 10.1088/1755-1315/877/1/012028.
- Moon, A.S., Lingait, P.B., Meshram, S.B., Maske, M.S., Mohinkar, K.G. and Chimurkar, K.S., 2020. Investigation of EPS concrete. *International Research Journal of Engineering and Technology*, 7(6), pp.6269–6272.
- Mun, C.Z., Kwong, K.Z., Lee, F.W. and Lim, J.H., 2021. Mechanical, sound and thermal properties of recycled expanded polystyrene concrete reinforced with 0.5% to 5.5% kenaf fibre. *European Journal of Environmental and Civil Engineering*, 26(14), pp.7345–7358.
- Pranahita, D.L., Kumar, P., Shwetank, Banu, S., 2022. Experimental study on partial replacement of coarse aggregate by EPS (expanded polystyrene) beads in concrete blocks. *International Journal of Research Publication and Reviews*, 3(7), pp.477–485.
- Prasittisopin, L., Termkhajornkit, P. and Kim, Y.H., 2022. Review of concrete with expanded polystyrene (EPS): Performance and environmental aspects. *Journal of Cleaner Production*, 13, p.291. DOI: 10.1016/j.jclepro.2022.132919.
- Raja, R.P.S.S. and Saravanan, J., 2024. Evaluation of lightweight concrete using expanded polystyrene aggregate with montmorillonite calcined powder. *SSRG International Journal of Civil Engineering*, 11(6), pp.50–59.
- Rathore, A., Hingve, A., Singh, H., Munde, R., Yadav, R. and Prajapati, S., 2024. Lightweight concrete using expanded polystyrene beads. *International Journal of Innovative Research and Creative Technology*, 10(2), pp.1–17.
- Salahaldean, A.S. and Al-Hadithi, A.I., 2022. The effect of adding expanded polystyrene beads (EPS) on the hardened properties of concrete. *Engineering, Technology & Applied Science Research*, 12(6), pp.9692–9696.
- Shukri, Z., Umar, K. and others, 2024. Enhancing the use of expanded polystyrene (EPS) for lightweight concrete wall panels. *Journal of Advanced Research in Applied Sciences and Engineering Technology*, 47(2), pp.160–170. <https://doi.org/10.37934/araset.47.2.160170>
- Turner, A., 2020. Foamed polystyrene in the marine environment: Sources, additives, transport, behavior, and impacts. *Environmental Science and Technology*, 54(17), pp.10411–10420.
- Ubi, S.E., Ewa, D.E., Bessong, A.R. and Nyah, E.D., 2022. Effects of incorporating expanded polystyrene in concrete construction. *Journal of Building Construction and Planning Research*, 10(3), p.421. DOI: 10.4236/jbcpr.2022.103004.
- Villa, D.M., Patino, J.S., Mogrovejo, D.E. and Bernal, J.G., 2023. Influence of recycled expanded polystyrene for sustainable structural concrete. *Structural Journal*, 120(3), pp.87–89.

# Spatial Model of Fire Vulnerability Distribution Based on Multicriteria in Tropical Forest Areas, Central Sulawesi, Indonesia

Akhbar, Abdul Rosyid<sup>†</sup>, Bau Toknok, Rahmat Kurniadi Akhbar and Rizky Purnama

Universitas Tadulako, Palu, Central Sulawesi, 94148, Indonesia

<sup>†</sup>Corresponding author: Abdul Rosyid; ochidklik@gmail.com

**Abbreviation:** Nat. Env. & Poll. Technol.  
**Website:** www.neptjournal.com

*Received:* 08-07-2024

*Revised:* 10-09-2024

*Accepted:* 13-09-2024

## Key Words:

Tropical forest  
 Forest fire vulnerability  
 Forest protection  
 Spatial model  
 Land use/vegetation cover

## Citation for the Paper:

Akhbar, A. R., Bau, T., Akhbar, R. K., and Purnama, R., 2025. Spatial model of fire vulnerability distribution based on multicriteria in tropical forest areas, central Sulawesi, Indonesia. *Nature Environment and Pollution Technology*, 24(2), p. D1699. <https://doi.org/10.46488/NEPT.2025.v24i02.D1699>

*Note: From year 2025, the journal uses Article ID instead of page numbers in citation of the published articles.*



**Copyright:** © 2025 by the authors  
**Licensee:** Technoscience Publications  
 This article is an open access article distributed under the terms and conditions of the Creative Commons Attribution (CC BY) license (<https://creativecommons.org/licenses/by/4.0/>).

## ABSTRACT

The problem of fire always threatens the existence of forests in Indonesia, repeatedly occurring every year, so it becomes one of the national and regional issues, both occurring naturally and caused by human actions. This study aims to develop a spatial analysis model of the multi-criteria-based fire vulnerability distribution in tropical forest areas. Modeling using GIS and spatial correlation analysis. In a tropical forest area of 7,042.29 Ha in the Tepo Asa Aroa KPH area, North Morowali Regency, Central Sulawesi, a spatial model of the distribution of fire vulnerability based on multi-criteria was produced, which could support rapid mapping of fire-prone forest areas. The results of the analysis of variables on land use/vegetation cover, rainfall, slope, distance from roads and settlements, business permits, forest protection, and security simultaneously made it possible to lower the fire vulnerability rating from 'very high' and 'high' to a 'medium' vulnerability rating. 'to 'low' and 'very low'. All parameters tested statistically have a spatial correlation with fire vulnerability.

## INTRODUCTION

Indonesia has vast tropical forests, namely 120.6 million hectares within forest areas and 67.40 million hectares outside forest areas (Kementerian LHK 2020), with the benefits of being the lungs of the world, regulating water flow, preventing erosion and flooding, and maintaining soil fertility. In addition, forests also provide economic benefits, so the resources must be preserved to provide optimal benefits. Even so, the problem of fire always threatens the existence of forests, which occurs repeatedly every year so it becomes one of the national and regional issues.

Forest/land fire is an event of forest/land burning, both naturally and by human actions (Kementerian LHK 2016). The forest/land area that burned in Indonesia in 2020 was 296,942 Ha; in 2021 it was 358,867 Ha and up to. July 2022, covering an area of 87,704 Ha. In Central Sulawesi Province, the area of forest/land that burned in 2020 is 2,555 Ha, in 2021 it is 3,133 Ha, and in 2022, until July covering an area of 964 Ha. In 2021, North Morowali Regency has the largest burned forest/land area, namely 1,161 Ha, while up to. July 2022 reached an area of 207 Ha. During 2020-2022, Central Sulawesi Province has 11,051 hotspots (178 high confidence hotspots; 10,051 medium confidence hotspots; 822 low confidence hotspots) (Direktorat PKHL Kementerian LHK 2022)

Forest fires that occur are often only discovered after they have spread over a large area, making controlling and extinguishing fires more difficult, even impossible in some cases (Grari et al. 2022). In forest areas with arid conditions that are periodically affected by global climate change, this can generally trigger forest fires. A higher risk of forest fires can occur due to increased average temperature and decreased rainfall (Busico et al. 2019, Humam et al. 2020). The complexity of the causes of forest fires also includes social, political, and economic

problems and weak law enforcement, land conflicts, and community capacities, which can then be categorized as indirect causes of forest fires (Medrilzam et al. 2017). Meanwhile, the direct causes of forest fires are classified as including inappropriate land clearing techniques, poor water management infrastructure, weak fire monitoring, and slow response to fires.

There is a close relationship between fires and changes in land cover. Inappropriate land management systems can increase vulnerability to fire. (Pualilin et al. 2019, Adrianto et al. 2020, Samsuri et al. 2012). Forest land cover conditions such as dry land agriculture, secondary dry land forest, and shrubs have the potential to cause forest fires. Fires will occur more frequently in forest areas that have undergone land cover type conversion than those that have not undergone conversion. The greatest frequency of fires occurs in secondary forest cover that has been converted to shrubs and plantations. This is because the fire that occurs depends on the type of fuel, moisture content, and fuel coating. (Adrianto et al. 2020, Samsuri et al. 2012, Usup et al. 2004).

The unclear boundaries of forest areas and the low social capital of the community in managing land can facilitate the expansion of agricultural land into forest areas, followed by the possibility of cultivating land by burning. The production forest area is one of the forest areas that is easily accessible by the community. This allows land conversion to occur, which causes higher forest fires (Medrilzam et al. 2017, Samsuri et al. 2012). The occurrence of forest fires has a reasonably strong correlation with fire hazard locations. Concession/corporate areas such as permit areas Timber forest product businesses, natural forests, and plantation forests, as well as oil palm plantations, are the most common locations for forest fires to occur, with the spatial distribution of companies and road density having the most decisive influence on fire risk (Medrilzam et al. 2017, Rianawati et al. 2016, Song et al. 2017).

Taking into account the problem of the threat of fire in forest areas as described above, it is deemed essential to carry out a spatial analysis model for the distribution of forest fire vulnerabilities by utilizing Geomatics technology (Remote Sensing and Geographic Information System (GIS)). Remote sensing technology and GIS have been widely used in earth observation activities including spatial mapping, planning, and decision-making involving many criteria (multi-criteria) (Mohammed et al. 2021). Spatial decision-making based on multi-criteria in GIS is a collection of methods and tools for converting and combining geographic data into information. Multi-criteria-based spatial analysis is quite flexible in making decisions (Akhbar et al. 2022, Malczewski & Rinner 2015)

Making a spatial model of forest fire vulnerability level based on multi-criteria, focused on identifying important and salient variables in developing requirements and procedures for assessing forest fire vulnerability level (high, medium, low) using scoring and weighting techniques. The use of spatial knowledge, namely geospatial information systems (GIS) in various fields has been widely applied, especially by using it in spatial modeling (Rosyid et al. 2019). GIS is effectively used in combining several factors that cause forest fires in mapping forest fire risk zones (Mohammed et al. 2021, Aronoff 1989, Rikalović et al. 2013, Erten et al. 2004, Guettouche & Derias 2012). Satellite imagery data can be used to look for the effects of fires that occur in an area. Several variables affect fires, such as topography, vegetation, land use, humidity and surface temperature, population, settlements, forest fire monitoring buildings, staff characteristics, and accessibility, which are all integrated into GIS (Erten et al. 2004, Amalina et al. 2016).

The research objective was to develop a spatial analysis model for mapping the distribution of fire vulnerability based on multi-criteria in tropical forest areas. The results of this research are expected to be helpful for the development of forestry science and technology in assessing the level of vulnerability of forest fires and are expected to provide information on forest fire management.

## MATERIALS AND METHODS

### Study Area

This research was conducted in the Tepo Asa Aroa Forest Management Unit (KPH) area, Mori Atas District, North Morowali Regency, Central Sulawesi Province. The research location is at coordinates 121°7'45.03" E-121°13'15.57" E and 1°55'19.72" S-2°3'55.70" S with an area of 7,042.29 Ha. Data collection and processing were carried out from May to September 2022. Fig. 1 shows a map of the research locations.

### Materials and Tools

The materials used in this study include digital data and maps, namely maps of vegetation cover and land use (obtained from satellite imagery data), government administration maps, forest area maps, KPH work area maps, road network maps, forest business permit location maps, climate and population data, forest management data and forest fire management. The tools used in this study included personal computers and the ArcGIS software package version 10.4, compasses, Global Positioning System (GPS), digital cameras, SPOT 7 /Landsat 8 satellite imagery recorded in 2018 – 2021, and writing tools.

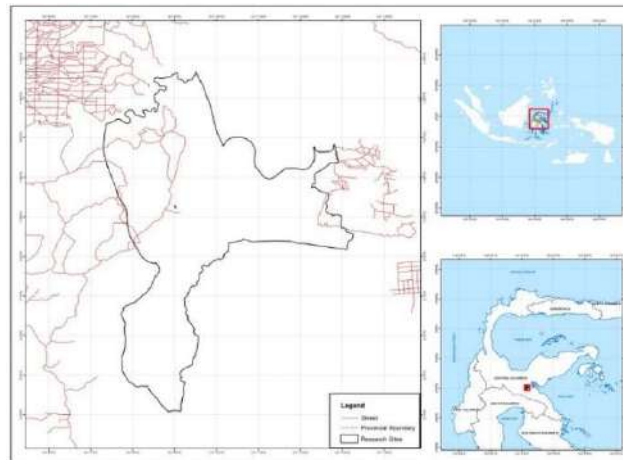


Fig. 1: Map of Research Locations.

Table 1: Variable weighting system in modeling spatial analysis of fire vulnerability distribution in tropical forest areas.

No.	Variable	Weight	Class	Score	Fire Rating Class
1.	Land Use/ Vegetation Cover (LUVIC)	7	Grassland/Savanna	5	Very High
			Uncultivated land/shrubs	4	High
			Dryland Agriculture/Seasonal Plants	3	Medium
			Plantation-Forest Plants/Perennial Plants - Timber	2	Low
			Primary Natural Forest – Secondary/ Mixed natural vegetation	1	Very Low
2.	Rainfall (R)	7	Dry (R <60 mm/Bulan)	5	Very High
			Moist (R = 60-100 mm/ bulan)	3	Medium
			Wet (R >100 mm/bulan)	1	Very Low
3.	Land Slope (S)	5	Slope $\geq 45\%$ (very steep)	5	Very High
			Slope 25-<45% (steep)	4	High
			Slope 15-<25% (rather steep)	3	Medium
			Slope 8-<15% (sloping)	2	Low
			Slope <8% (flat)	1	Very Low
4.	Distance from Road (DSt)	3	<100 m	5	Very High
			100-<200 m	4	High
			200-<300 m	3	Medium
			300-<400 m	2	Low
			$\geq 400$ m	1	Very Low
5.	Distance from Settlement (DSe)	3	<1 km	5	Very High
			1-<2 km	4	High
			2-<3 km	3	Medium
			3-<4 km	2	Low
			$\geq 4$ km	1	Very Low
6.	Existence of Forest Utilization Permit (FUP)	1	There is no forest utilization permit	5	Very High
			There is a forest utilization business permit, and it is not active	3	Medium
			There is a forest utilization business permit, and it is active.	1	Very Low
7.	Forest Protection and Security (FPS)	1	There are no forest boundaries – no patrols, and no counseling	5	Very High
			There are forest boundary markers – no patrols and counseling	3	Medium
			There are forest boundary markers – there are patrols and counseling	1	Very Low

Source: Erten et al. (2004) modified according to the research needs and conditions of the research location.



## Research Methods

The creation of a spatial analysis model for the distribution of vulnerability to forest fires is based on several incidents of forest fires in Indonesia. Forest fires can occur either intentionally or unintentionally. In many cases, forest fires start from the deliberate use of fire, such as activities to clear new land by slashing and burning, burning cattle grazing land, or hunting animals to stimulate the growth of young grass, collecting firewood, and collecting honey by driving bees out of their hives. As for forest fires due to accidents such as the negligence of smokers, tourists, adventurers, workers in the forest, and collectors of forest products.

Development of a spatial analysis model for the distribution of fire vulnerability based on multi-criteria in tropical forest areas using satellite imagery data interpretation and classification techniques, overlays, and map layouts using Geographic Information System (GIS) technology. The application of models using geomatics technology (remote sensing and GIS) makes it possible to create forest fire vulnerability maps by combining several layers of information taken from maps and the field (Guettouche & Derias 2012).

The weighting system and determining the fire vulnerability index refers to the method of determining the level of vulnerability to forest fires by Erten et al. (2004), which was further modified according to research needs. The variable weighting system in modeling the spatial analysis of the multi-criteria-based fire vulnerability distribution in tropical forest areas is shown in Table 1.

In Table 1, it appears that there are as many as 7 (seven) variables that are used as a reference in assessing forest fire vulnerability spatially, namely land use/vegetation cover, rainfall, land slope, distance from roads and settlements, business permits (existence of forest area utilization/use permits), and forest protection and security. There are several considerations in determining the weight, class, score, and class rating of fire vulnerability for each variable, as follows:

- 1) Land Use/Vegetation Cover (LUV): Land use with various types of vegetation or plants covering the land is very vulnerable to fire. The vegetation moisture factor has a significant effect on fires. Very dry vegetation is highly flammable, especially savanna or shrub species, while fresh vegetation is flammable (Erten et al. 2004).
- 2) Rainfall (R): Monthly rainfall is one of the causes of fires. Low monthly rainfall (dry months) can trigger fires, whereas high rainfall (wet months) can suppress fires (Humam et al. 2020).

- 3) Land slope (S): The topography of the plains to the mountains has various slope classes, ranging from flat, sloping, rather steep, steep to very steep. Topography is closely related to wind behavior in influencing fire susceptibility. The steeper the slope, the faster the fire spreads (Mukti et al. 2016). Fire travels the fastest up the slope and the least rapidly down the slope (Erten et al. 2004)
- 4) Distance from Road (DSt): A road network that crosses a forest area will allow humans to move, including animals and vehicles. Forest locations that are close to or crossed by a road network can make these locations vulnerable to fires. The fire risk is high in forest areas near roads (Erten et al. 2004, Mukti et al. 2016).
- 5) Distance from Settlements (DSe): Forest locations close to settlements can be categorized as fire-prone locations. Likewise, densely populated settlements can become fire-prone locations due to high human activity. High fire risk in forest areas close to settlements (Erten et al. 2004, Mukti et al. 2016, Mukti et al. 2016, Parajuli et al. 2020).
- 6) Existence of Forest Utilization Permit (FUP): Legal forest utilization following statutory regulations will be implemented by business permit holders to avoid legal sanctions. In the utilization of natural forests or plantation forests, generally, permit holders will apply a silvicultural system without having to burn. Conversely, forest locations not burdened with business permits (illegal forest utilization) are generally vulnerable to fires because there is no forest manager in that location (open access). The cause of the fires comes from uncultivated land use activities (Thoha et al. 2017, Thoha & Ahmad 2018)
- 7) Forest Protection and Security (FPS): Forest protection and security are closely related to forest management, including forest fire management. Outer boundaries of forest areas that are not clear boundaries or have no fixed boundaries, without patrols and forest counseling, will trigger conflicts over forest use, and it is easy for these forest areas to be used by people illegally, which is usually followed by land clearing by slashing and burning. Conversely, forest area boundaries with clear forest boundary markers, followed by good forest patrols and counseling, will reduce and control forest fires. Routine forest patrols and counseling are the main means of controlling forest fires (Zulkifli & Kamarubayana 2017).

To find out whether or not there is a link between the seven variables with fire vulnerability in tropical forest areas,

spatial covariation is analyzed which is the study of two or more different spatial distributions in an area or region. In several previous studies, it was reported that the theoretical basis had been tested so it confirmed that the statistical correlation test could be applied in this spatial covariation analysis.

Furthermore, by using the contingency table, a statistical correlation test is carried out for each variable related to fire vulnerability. Hypothesis testing using Chi-Square Testing ( $\chi^2$ ). With  $k$  observation frequencies, namely  $o_1, o_2, o_3, \dots, o_k$  and expected frequency (*expectation*), namely  $e_1, e_2, e_3, \dots, e_k$ , then the chi-square formula is written (Sudjana, 2005):

$$\chi^2 = \sum_{i=1}^k \frac{(o_i - e_i)^2}{e_i} \quad \dots(1)$$

If  $\chi^2 = 0$ , then there is a perfect fit between the observed results and the expected value. If  $\chi^2 > 0$ , then there is no match between the observation results and the expected value. The bigger the value  $\chi^2$ , the discrepancy between the observed results and the expected value is also getting bigger. In this analysis, we used the hypothesis:  $H_0$  accepted if the occurrence of forest fires is not related to the variable being tested ( $\chi^2_{hit} < \chi^2_{tab}$ ), while  $H_0$  is rejected if the occurrence of forest fires is related to the parameter being tested ( $\chi^2_{hit} \geq \chi^2_{tab}$ ). The significant degree is used  $\alpha = 5\%$ .

Compilation of a range of levels of vulnerability to forest fires:

$$\text{Class width} = (\text{Biggest Data Value} - \text{Smallest Data Value}) / (\text{Number of Classes}) \quad \dots(2)$$

To calculate the value *Forest Fire Vulnerability Index* (FFVI) equation is used:

$$\text{FFVI} = 7x(\text{LUVC}) + 7x(\text{R}) + 5x(\text{S}) + 3x(\text{DSt}) + 3x(\text{DSe}) + 1x(\text{FUP}) + 1x(\text{FPS}) \quad \dots(3)$$

The FFVI level values are shown in Table 2.

## RESULTS AND DISCUSSION

### Presence of Hotspots

The determination of the research location for the spatial model of the distribution of fire vulnerability in tropical

Table 2: FFVI Value.

No.	FFVI Value	Information
1	$\geq 113$	Very High (SH)
2	$91 - < 113$	High (H)
3	$70 - < 91$	Medium (M)
4	$48 - < 70$	Low (L)
5	$< 48$	Very Low (VR)

forest areas in the function of protection forest and production forest covering an area of 7,042.29 Ha in the Tepo Asa Aroa Forest Management Unit (KPH) of Tepo Asa Aroa, Mori Atas District, North Morowali Regency, Central Sulawesi Province referred to the hotspot distribution map "SiPongi PKHL Directorate of the Ministry of Environment and Forestry in 2022. In 2021, in this tropical forest area, there will be 2 (two) high confidence hotspots and 7 (seven) medium confidence hotspots, all of which will be in savanna and shrub land cover, while in 2022, Around the tropical forest area, there are 6 (six) medium confidence hotspots in dryland agriculture. Hotspots that have relatively higher temperatures compared to the surrounding temperature can be indicators of forest fires. Denser temporal hotspots will provide a high vulnerability to fire, while the occurrence of the highest number of hotspots in Indonesia is generally in June, July, August, September, and October (Humam et al. 2020, IDGA et al. 2018).

The survey results show that the hotspot location has a very high fire potential because it is generally forest land covered with flammable savanna/grass and shrubs. Considering the behavior of monthly rainfall during the 2015-2021 period from the Kasiguncu Meteorology and Geophysics Station, Poso Regency, Central Sulawesi Province, the dry months are January, August, September, October, November, and December. The existence of these dry months can trigger forest fires due to increasing air temperatures and decreasing monthly rainfall. High surface temperatures and low rainfall in forest areas contribute to forest fires (Parajuli et al. 2020).

### Land Use/Vegetation Cover

From the results of the interpretation of Landsat 8 and SPOT 7 satellite imagery and the results of field checks in 2022, in this forest area, there are types of land use/vegetation cover, namely, grazing land in the form of savanna covering an area of 842.83 Ha, uncultivated land in the form of shrubs 42.53 Ha, dry land agriculture in the form of annual crops covering an area of 664 Ha, plantations in the form of oil palm plantations covering an area of 48.55 Ha, secondary natural forest in the form of mixed natural vegetation covering an area of 5,444.38 Ha. The condition of land use/vegetation cover illustrates that this forest area has five fire vulnerability classes, namely: 'very high' area of 11.97%, 'high' area of 0.60%, 'medium' area of 9.43%, 'low' area of 0.69% and 'very low' area of 77.31% of the total forest area of 7,042.29 Ha. The amount of fuel accumulated in forest areas contributes to forest fires, while very dry vegetation cover is highly sensitive to fire (Erten et al. 2004, Parajuli et al. 2020). Savanna is a land cover with high fire vulnerability (Mukti et al. 2016).

## Rainfall

Rainfall data obtained from the Kasiguncu Meteorology and Geophysics Station, Poso District, Central Sulawesi Province for 2015-2021 with an annual average of 2,210.17 mm and a monthly average of 184.18 mm (in the wet month category,  $R > 100$  mm/month). This condition illustrates that in a forest area of 7,042.29 Ha, there is only one fire vulnerability class, namely 'very low' because it has high rainfall, while the average surface air temperature is 27.1 - 27.8 °C and average humidity -average 84.4 - 87.6%. The higher the rainfall, the lower the fire vulnerability (Humam et al. 2020)

## Slope Class

There are five classes of slopes in this forest area consisting of a very steep slope class of 356.93 Ha, a steep slope class of 588.69 Ha, a rather steep class of 1,958.80 Ha, a gentle slope class of 2,709.76 Ha, and flat slope class covering an area of 1,428.10 Ha. The condition of the slope class indicates that this forest area has five fire vulnerability classes, namely: 'very high' area of 5.07%, 'high' area of 8.36%, 'medium' area of 27.81%, 'low' area of 38.48%, and 'very low' area of 20.28% of the total forest area of 7,042.29 Ha. Class Slopes with a slope of  $> 35\%$  (steep - very steep) are very sensitive to forest fires (Erten et al. 2004).

In this forest area, there is a road network of 28,334.48 m (28.33 km). The road network connects the locations of agricultural land, plantations, grazing land, and land that is still forested. The length of the local road network is 17,204.17 m (17.20 km), other roads are 9,546.82 m (9.55 km), and footpaths are 1,583.49 m (1.58 km). The road network is concentrated in the northern and eastern parts of the location within Peonea Village, Mori Atas District, and Tiu Village, Petasia Barat District, North Morowali Regency.

The distance of the forest area from the road network in this forest area is: distance  $< 100$  m covering an area of 511.90 Ha, distance 100- $< 200$  m covering an area of 419.40 Ha, distance 200- $< 300$  m covering an area of 344.03 Ha, distance 300- $< 400$  m covering an area of 305.47 Ha, and a distance of  $\geq 400$  m covering an area of 5,461.49 Ha.

The condition of the forest area's distance from the road indicates that this forest area has five fire vulnerability classes, namely: 'very high' area of 7.27%, 'high' area of 5.96%, 'moderate' area of 4.89%, 'low' of 4.34%, and 'very low' of 77.55% of the total forest area of 7,042.29 Ha. Distance of forest areas from roads that are less than 200 m is very sensitive to forest fires (Erten et al. 2004).

## Distance from Settlements

The locations of the settlements analyzed were all settlement locations around this forest area. So, the existence of

residential areas largely determines the distance between settlement locations and forest areas. Around the forest area are 10 (10) settlement locations in Peonea Village, Kolaka, Lanumor, Ensa, Mori Atas District, Era Village, North Mori District, Togomulya Village, Petasia Barat District, North Morowali Regency. Of the 10 settlement locations, there is one settlement location in Peonea Village with a distance of 1- $< 2$  km, two settlement locations in Kolaka Village and one location in Togomulya Village with a distance of 2- $< 3$  km each, one location settlements in Era Village, one location in Ensa Village, and one location in Kolaka Village with a distance of 3- $> 4$  km each; one settlement location in Ensa Village and one location in Lanumor Village with a distance of  $\geq 4$  km each.

The distance of the forest area from the location of settlements in this forest area is: Distance  $< 1$  km covering an area of 0 Ha, distance 1- $< 2$  km covering an area of 19.09 Ha, distance 2- $< 3$  km covering an area of 421.30 Ha, distance 3- $< 4$  km covering an area of 1,211.89 Ha, and a distance of  $\geq 4$  km covering an area of 5,390.01 Ha. The condition of the distance of the forest area from the settlement location shows that there are four classes of vulnerability in this forest area: 'high' of 0.27%, 'moderate' of 5.98%, 'low' of 17.21%, and 'very high'. Low' area of 76.54% of the total forest area of 7,042.29 Ha. Distance of forest areas from settlements that are less than 1,000 m ( $< 1$  km) has a high risk of forest fires (Erten et al. 2004; Parajuli et al. 2020).

## The Existence of Business Permits for Forest Utilization

In this forest area, there are 3 (three) permits for forest utilization: a business permit for PT. Wana Rindang Lestari for forest utilization covering an area of 302.52 Ha and for harvesting natural rattan covering an area of 316.59 Ha, the business permit for the use of forest area by PT. Raya Utama Synergy for constructing a hydroelectric power plant covering an area of 33.08 Ha. In addition, there is also an area reserved for agrarian reform objects (TORA) covering an area of 2,305.76 Ha and an indicative map of social forestry areas (PIAPS) covering an area of 614.64 Ha.

Thus, the area that still needs to get a forest utilization permit is 3,469.95 Ha. Thus, the total area that already has business permits reaches 50.73%, and those that do not yet have business permits is 49.27% of the total forest area of 7,042.29 Ha. Forest utilization business permits are permits given to business actors to start and run their businesses and activities (Government of Indonesia 2021).

Of the forest area covering 50.73%, which already has a business license, 46.23% has a business license but has yet to be active, while only 4.50% has a business license and is active. The conditions for the existence of these business

permits indicate that this forest area has three classes of fire vulnerability, namely: 'very high' covering 49.27%, 'medium' covering 46.23% and 'very low' covering 4.50% of the entire forest area and covering an area of 7,042.29 ha.

### Forest Protection and Security

Forest protection and security in this forest area are quite good because this area is part of the Tepo Asa Aroa KPH management area. The entire outer boundary of the forest area has been demarcated by setting up boundary stakes to provide clear boundaries between the boundaries of forest areas and non-forest areas. Forest area patrol activities and counseling to communities around forest areas are also carried out by the FMU manager every year. These conditions indicate that there is only one fire vulnerability class in a forest area of 7,042.29 Ha, namely 'very low'.

Forest protection is an effort to prevent and limit damage to forests and forest products caused by human actions, livestock, fires, natural forces, pests, and diseases, as well as defending and safeguarding the rights of the state, communities, and individuals over forests, areas forests, forest products, investments, and tools related to forest management (Government of Indonesia 2021).

### Spatial Model of Fire Vulnerability Distribution Based on Multi-Criteria

Spatial modeling of the multi-criteria-based fire vulnerability distribution in tropical forest areas using geographic information systems (GIS) produced only three of the five available fire vulnerability classes. In the protection forest area and production forest area of 7,042.29 Ha which were analyzed using seven parameters of fire vulnerability assessment simultaneously in tropical forest areas, the three classes of fire vulnerability are referred to, namely: (a) 'medium' fire vulnerability class with an area of 287.93 Ha (4.09%), (b) 'low' fire vulnerability class with an area of 1,815.16 Ha (25.78%), and (c) 'very low' fire vulnerability class with an area of 4,939.20 Ha (70.14 %).

The results of spatial analysis of fire susceptibility to types of land use/vegetation cover in tropical forest areas show that for the three resulting fire vulnerability classes, the distribution of 'moderate' fire vulnerability classes is for savanna type 3.90% and dryland agriculture with annual crops 0.19 %, while the 'low' fire vulnerability class included savanna 8.07%, shrubs 0.60%, dryland agriculture with annual crops 7.92%, oil palm plantations 0.69%, and secondary dryland forest with mixed natural vegetation types 8.50%. The distribution of 'very low' fire susceptibility classes to dryland farming with seasonal crops was 1.32%, oil palm plantations 0.004%, and

secondary dryland forest with mixed natural vegetation 68.81%.

According to the partial analysis results, ideally, the fire vulnerability classes are distributed from the 'very high' to 'very low' class. In the results of this multi-criteria-based simultaneous analysis, it is possible that the level of fire vulnerability in tropical forest areas can be derived from the 'very high' class and 'high' being a 'moderate' to 'very low' level of vulnerability. The statistical test in the spatial covariation analysis shows that there is a correlation between fire vulnerability and the type of land use/vegetation cover because  $H_0$  is rejected at the 0.05 confidence level ( $\chi^2_{hit} = 5.233, 24 > \chi^2_{tab} = 15.51$ ). Land use/vegetation cover affects fires (Parente et al. 2023), while in this tropical forest area, grazing land/savanna or open land is prone to fire, where hotspots are most common in this type of vegetation cover (hotspot). The open land cover class is the most vulnerable to fire (Kelompok Advokasi Riau 2018, Thoha & Triani 2021).

Furthermore, the area (hectares) of each class of fire vulnerability in tropical forest areas is based on the type of land use/vegetation cover as shown in Fig. 2.

The results of the spatial analysis of fire vulnerability based on rainfall in tropical forest areas show that for the three classes of fire vulnerability resulting in the 'wet month,  $R > 100$  mm/month' class, the distribution of 'medium' fire vulnerability classes is 4.09%, in the 'wet month' class 'low' fires 25.78%, and in the 'very low' fire vulnerability class of 70.14% of all tropical forest areas covering an area of 7,042.29 Ha. This simultaneous analysis shows that the fire vulnerability class spreads into three fire vulnerability classes.

By the results of the partial analysis, which ideally is distributed only in the 'very low' class, in the results of the simultaneous analysis based on this multi-criteria, the level of forest fire vulnerability can be distributed into the 'very low' class (dominant), followed by the 'low' class and the 'moderate' class'. A forest area may be in a different class of fire vulnerability even though the climatic conditions

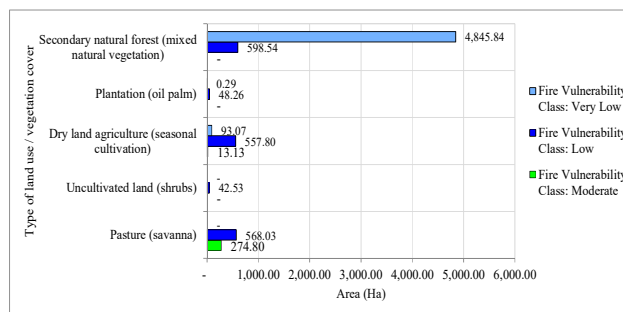


Fig. 2: Graph of fire vulnerability based on type of land use/vegetation cover.



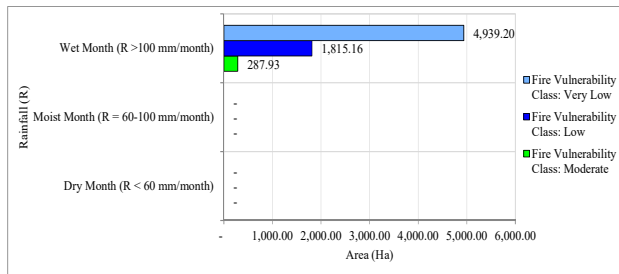


Fig 3: Graph of Fire Vulnerability Based on Rainfall.

(rainfall) are in the wet month category due to the different types of surface fuel and dryness conditions. Statistical tests in spatial covariation analysis show a correlation between fire vulnerability and climate (rainfall) because  $H_0$  is rejected at the 0.05 confidence level ( $\chi^2_{hit} = 4.789,13 > \chi^2_{tab} = 5,99$ ). Climate can cause forest fires because it can affect the dryness of surface fuels, the amount of available oxygen, and the speed at which fire spreads (Syaufina & Hafni 2018).

Furthermore, the area (hectares) of each class of fire vulnerability in tropical forest areas based on rainfall is shown in Fig. 3.

The results of the spatial analysis of fire vulnerability based on the slope of land in tropical forest areas show that for the three resulting fire vulnerability classes, the distribution of 'medium' fire vulnerability classes on flat slopes is 1.74%, sloping slopes are 0.46%, rather steep slopes are 1.70 %, steep slopes 0.12%, very steep slopes 0.06%, while in the 'low' fire vulnerability class on flat slopes 11.61%, gentle slopes 3.18%, rather steep slopes 3.67%, steep slopes 2.31%, very steep slope 5.01%. The distribution of 'very low' fire vulnerability classes on flat slopes is 6.93%, sloping slopes are 34.84%, rather steep slopes are 22.45%, and steep slopes are 5.92%.

By the results of the partial analysis, ideally, the vulnerability of fires is distributed from the 'very high' to the 'very low' class; in the results of this multi-criteria-based simultaneous analysis, the level of vulnerability to forest fires can be reduced from 'medium' to 'very low' class. A forest area may be in a lower fire vulnerability class due to the influence of other factors, such as slope aspect, wind direction, surface temperature, and humidity. The statistical test in the spatial covariation analysis shows that there is a correlation between fire vulnerability and the slope of the land because  $H_0$  is rejected at the 0.05 level of confidence ( $\chi^2_{hit} = 2.599,19 > \chi^2_{tab} = 15,51$ ). Land slope affects forest fires (Erten et al. 2004).

Furthermore, the area (hectares) of each fire vulnerability class in tropical forest areas is based on the slope of the land, as shown in Fig. 4.

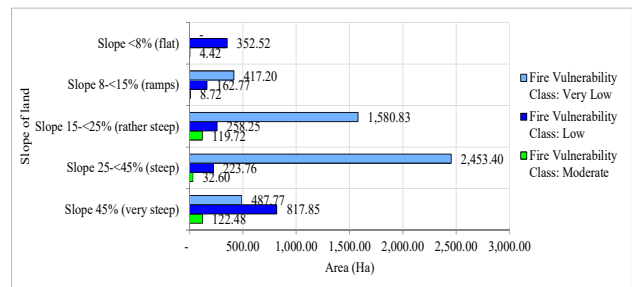


Fig. 4: Graph of fire vulnerability based on land slope.

The results of the spatial analysis of fire vulnerability based on the distance from the road in tropical forest areas show that in the three resulting fire vulnerability classes, the distribution of 'moderate' fire vulnerability classes at a distance of <100 m is 2.42%, a distance of 100 - <200 m is 1.23%, distance 200 - <300 m 0.25%, distance 300 - <400 m 0.13%, distance  $\geq 400$  m 0.05%, while in the 'low' fire vulnerability class at a distance of <100 m 3.82%, distance 100 - <200 m 3.51%, distance 200 - <300 m 3.00%, distance 300 - <400 m 2.20%, distance  $\geq 400$  m 13.25%. The distribution of 'very low' fire vulnerability classes at a distance of <100 m 1.02%, a distance of 100 - <200 m 1.21%, a distance of 200 - <300 m 1.64%, a distance of 300 - <400 m 2.00 %, distance  $\geq 400$  m 64.26%.

By the results of the partial analysis, ideally, the vulnerability of fires is distributed from the 'very high' to the 'very low' class; in the results of this multi-criteria-based simultaneous analysis, the level of vulnerability to forest fires can be reduced from 'medium' to 'very low' class. A forest area may be in a lower fire vulnerability class due to adequate forest protection and security and the presence of a legal area manager so that human activities in utilizing existing roads are safer and more controlled from causal sources. Fire. Statistical tests in spatial covariation analysis show that there is a correlation between fire vulnerability and distance from the road because  $H_0$  is rejected at the 0.05 level of confidence ( $\chi^2_{hit} = 2.892,95 > \chi^2_{tab} = 15,51$ ). A road network influences forest fires (Erten et al. 2004, Thoha & Triani 2021).

Furthermore, the area (hectares) of each fire vulnerability class in tropical forest areas is based on the distance from the road, as shown in Fig. 5.

The results of spatial analysis of fire vulnerability based on distance from settlements in tropical forest areas show that for the three resulting fire vulnerability classes, the distribution of 'medium' fire vulnerability classes at distances of 2 - <3 Km is 0.10%, distances of 3 - <4 km 1, 13%, distance  $\geq 4$  km 2.85%, while in the 'low' fire vulnerability class at distance 1 - <2 km 0.21%, distance

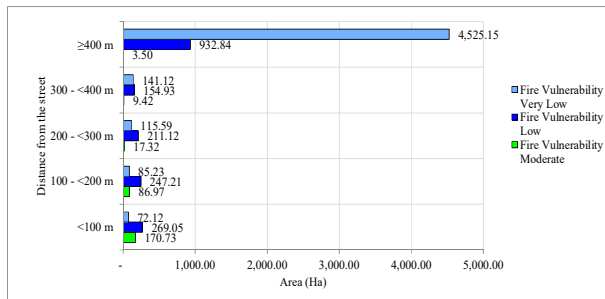


Fig. 5: Graph of fire vulnerability based on distance from the road.

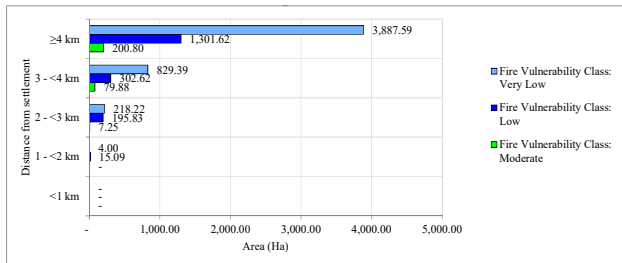


Fig. 6: Graph of fire vulnerability based on distance from settlements.

2 - <3 km 2.78%, distance 3 - <4 km 4.30%, distance ≥4 km 14.48%. The distribution of 'very low' fire vulnerability classes at a distance 1 - <2 km 0.06%, distance 2 - <3 km 3.10%, distance 3 - <4 km 11.78%, distance ≥4 km 55.20 %.

By the results of the partial analysis, ideally the vulnerability of fires is distributed from the 'high' class to the 'very low' class. In the results of this multi-criteria-based simultaneous analysis, forest fires' vulnerability level can be reduced from a 'medium' class to a 'very low' class. The 'moderate' statistical tests in spatial covariation analysis show that there is a correlation between fire vulnerability and distance from settlements because  $H_0$  is rejected at the 0.05 level of confidence ( $\chi^2_{hit}=154,12 > \chi^2_{tab} = 12,59$ ). The existence of settlements is at risk of forest fires (Erten et al. 2004, Parajuli et al. 2020, Thoha & Triani 2021).

Furthermore, the area (hectares) of each class of fire vulnerability in tropical forest areas is based on distance from settlements, as shown in Fig. 6.

The results of a spatial analysis of fire vulnerability based on forest utilization permits in tropical forest areas show that in the three resulting fire vulnerability classes, the distribution of 'moderate' fire vulnerability classes with no permits is 2.97%, there are permits and inactive 1.12%. In contrast, in the 'low' fire vulnerability class with no permits 10.13%, there are permits, and they are not active 15.58%, there are permits, and they are active 0.07%. The distribution of 'very low' fire vulnerability classes with no permits is

36.17%; there are permits and they are not active, 29.54%; there are permits, and they are active, 4.43%.

According to the results of the partial analysis, which ideally is distributed only in the 'very high' to 'very low' class, in the results of this multi-criteria-based simultaneous analysis, the vulnerability level of forest fires can be lowered from the 'very high' class to the 'moderate' to 'very low' class. Low' with a decreasing area distribution. It appears that the 'moderate' fire vulnerability class on forest land that does not have a permit or is not cultivated is wider than the area that has a permit and is not active. In statistical tests in spatial covariation analysis, it shows that there is a correlation between fire vulnerability and the existence of forest utilization permits because  $H_0$  is rejected at the 0.05 level of confidence ( $\chi^2_{hit} = 315,72 > \chi^2_{tab} = 9,49$ ). The cause of the fires comes from land use activities that are not cultivated or open access (Thoha et al. 2017, Thoha & Ahmad 2018).

Furthermore, the area (hectares) of each class of fire vulnerability in tropical forest areas is based on the existence of forest utilization permits, as shown in Fig. 7.

The results of spatial analysis of fire vulnerability based on forest protection and safety in tropical forest areas show that in the three classes of fire, vulnerability resulting in the class 'there are forest boundary markers – there are patrols and counseling', the distribution of fire vulnerability classes is 'medium' 4.09%, in the 'low' fire vulnerability class was 25.78%, and the 'very low' fire vulnerability class was 70.14% of the entire tropical forest area of 7,042.29 Ha. This simultaneous analysis shows that fire vulnerability classes based on forest protection and security (in the class 'there are forest boundary markers, there are patrols and counseling') spread into three fire vulnerability classes.

By the results of the partial analysis, which ideally is distributed only in the 'very low' class, in the results of the simultaneous analysis based on this multicriteria, the level of forest fire vulnerability can be distributed into the 'very

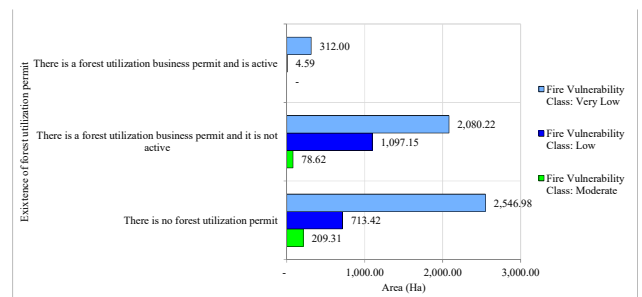


Fig. 7: Graph of fire vulnerability based on existence of forest utilization permits.

low' class (dominant), followed by the 'low' class and the 'moderate' class. A forest area may be in a different class of fire vulnerability even though the forest protection and security conditions are quite good. In statistical tests in spatial covariation analysis, it shows that there is a correlation between fire vulnerability and forest protection and security because  $H_0$  is rejected at the 0.05 level of confidence  $\chi^2_{hit} = 4.789, 13 > \chi^2_{tab} = 5,99$ ). Efforts to prevent forest fires can be carried out by carrying out preventive activities in the form of forest patrols, especially during fire-prone months or long dry seasons, putting up warning boards and prohibiting forest burning, and holding forest fire education to the community (Zulkifli & Kamarubayana 2017)

Furthermore, the area (hectares) of each class of fire vulnerability in tropical forest areas based on forest protection and security is shown in Fig. 8.

A spatial model map of the multi-criteria-based fire vulnerability distribution in tropical forest areas is shown in Fig. 9.

In the map of Fig. 9, it appears that the locations of the 'medium and low' fire vulnerability classes correspond to the existence of hotspot locations. Thus, a multi-criteria-based spatial model of fire vulnerability distribution in tropical

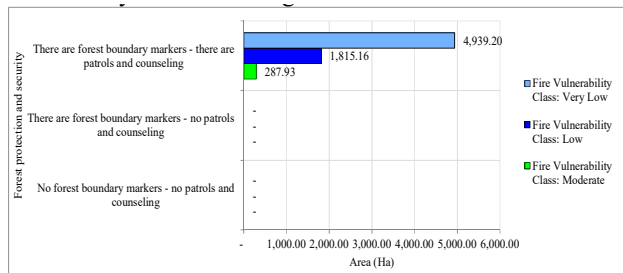


Fig 8: Graph of fire vulnerability based on forest protection and safety.

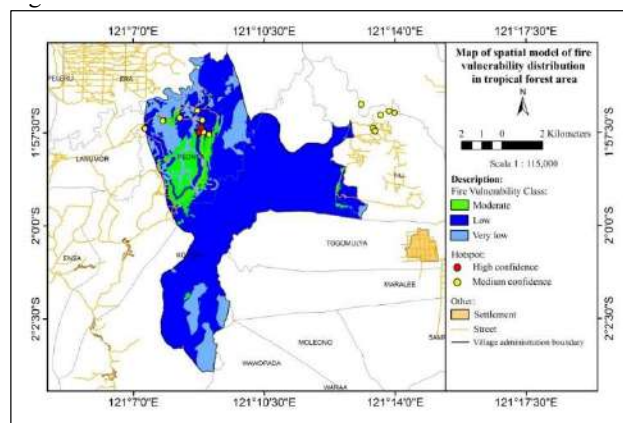


Fig. 9: Spatial model map of fire vulnerability distribution based on multicriteria in tropical forest areas.

forest areas can be used for rapid mapping of forest fire vulnerability levels. Fire risk models are a good approach to fire prevention and forest protection. Integrating remote sensing data and GIS concepts can help determine fire risk areas and forest management planning (Adab et al. 2019).

Spatial analysis based on multi-criteria mapping the distribution of fire vulnerability in this tropical forest area allows the level of fire vulnerability to be lowered from 'very high' and 'high' classes to 'moderate' to 'very low' levels of vulnerability. These results indicate that the multi-criteria-based spatial analysis approach allows each variable of land use/vegetation cover, rainfall, accessibility (distance from roads and settlements), business permits, forest protection, and security to support each other in reducing the level of fire vulnerability in a forest area.

It can be explained that the active holders of business permits in a forest area, good forest protection and security, and land use in tropical forest areas are easily controlled and controlled by various efforts to burn forests and land. On the other hand, in forest areas with open access, forest encroachers will be free to carry out their activities (Utomo & Arifianto 2019). multi-criteria decision-making is a decision-making method for determining the best alternative based on certain criteria.

## CONCLUSIONS

This research produced a spatial model of the distribution of fire vulnerability based on multi-criteria in tropical forest areas that can support rapid mapping of fire-prone forest areas. The results of the analysis of variables on land use/vegetation cover, rainfall, distance from roads and settlements, business permits, forest protection, and security simultaneously using a Geographic Information System (GIS) make it possible to rank fire vulnerability from 'very high' and 'high' classes. To 'moderate' to 'low' and 'very low' vulnerability ratings. All variables tested statistically have a spatial correlation with fire vulnerability. The results of this study can be used as a reference in the development of technology and forest management based on fire prevention and control in tropical forest areas.

## ACKNOWLEDGMENT

The authors would like to thank the PLN Institute of Technology and the University of Bangka Belitung for supporting this research activity.

## REFERENCES

Adab, H., Kanniah, K.D. and Solaimani, K., 2011. GIS-based probability assessment of fire risk in grassland and forested landscapes of

- Golestan Province, Iran. *International Conference on Environmental and Computer Science (IPCBE)*, Vol. 19, IACSIT Press, Singapore, pp. 781-807.
- Adrianto, H., Spracklen, D.V., Arnold, S.R., Sitanggang, I.S. and Lailan, S., 2020. Forest and land fires are mainly associated with deforestation in Riau Province, Indonesia. *Remote Sensing*, 12(1), p.3. DOI.
- Akhbar, N., Naharuddin, I., Arianingsih, Misrah, and Akhbar, R.K., 2022. Spatial model of forest area designation and function based on multi-criteria in dry land and mangrove forest ecosystems, Central Sulawesi, Indonesia. *Biodiversitas*, 23(7), pp.3619-3629. DOI.
- Amalina, A., Prasetyo, L.B. and Rushayati, S.B., 2016. Forest fire vulnerability mapping in Way Kambas National Park. *Procedia Environmental Sciences*, 33, pp.239-252.
- Aronoff, S., 1989. *Geographic Information System: A Management Perspective*. WDL Publication.
- Busico, G., Giuditta, E., Kazakis, N. and Colombani, N., 2019. A hybrid GIS and AHP approach for modeling actual and future forest fire risk under climate change, considering the role of water resources. *Sustainability*, 11, p.7166. DOI.
- Direktorat PKHL Kementerian LHK, 2022. Summary of Forest and Land Fire Area (Ha) per Province in Indonesia for the Years 2016-2022. *SiPongi*.
- Erten, E., Kurgun, V. and Musaolu, N., 2004. Forest fire risk mapping from satellite imagery and GIS: A case study. *ISPR*, 17, p.91.
- Government of Indonesia, 2021. *Government Regulation of The Republic of Indonesia Number 23 of 2021 Concerning Forestry Implementation*. GOI, Jakarta.
- Grari, I., Idrissi, M., Boukabous, O., Moussaoui, M., Azizi, M. and Moussaoui, M., 2022. Early wildfire detection using a machine learning model deployed in the fog/edge layers of IoT. *Indonesian Journal of Electrical Engineering and Computer Science*, 27(2), pp.1062-1073.
- Guettouche, M.S. and Derias, A., 2012. Modeling of environment vulnerability to forest fires and assessment by GIS application on the forests of Djelfa (Algeria). *Journal of Geographic Information System*, 5, pp.24-32. DOI.
- Humam, A., Hidayat, M., Nurrochman, A., Anestatia, A.I., Yuliantina, A. and Aji, S.P., 2020. Identification of forest and land fire-prone areas using geographic information systems and remote sensing in the Tanjung Jabung Barat region, Jambi Province. *Jurnal Geosains dan Remote Sensing (JGRS)*, 1(1), pp.32-42. DOI.
- Jafarzadeh, A.A., Mahdavi, A. and Jafarzadeh, H., 2017. Evaluation of forest fire risk using the Apriori algorithm and fuzzy c-means clustering. *Journal of Forest Science*, 63(8), pp.370-380.
- Kelompok Advokasi Riau, 2018. *Analysis of Hotspots in the Senepis Ecosystem Area from 2008 to 2018*. Kelompok Advokasi Riau – Belantara Foundation, Pekanbaru, Indonesia.
- Kementerian LHK, 2016. *Regulation of the Minister of Environment and Forestry of the Republic of Indonesia Number: P.32/MenLHK/Setjen/Kum.1/3/2016 on Forest and Land Fire Control*. Kementerian.
- Kementerian LHK, 2020. *Strategic Plan of the Ministry of Environment and Forestry for 2020-2024*. Kementerian.
- Malczewski, J. and Rinner, C., 2015. *Multicriteria Decision Analysis in Geographic Information Science*. Springer Science + Business Media, Berlin, Heidelberg, Germany.
- Medrilzam, N.H., Rahayu, P., Widiaryanto, L., Rosylin, R., Firdaus, U., Suprpto, S.H., Purnomo, Y.C., Wulan, M.L.P., Tarigan, L. and Nugraha, M., 2017. *Grand Design: Prevention of Forest, Plantation, and Land Fires 2017-2019*. Coordinating Ministry for Economic Affairs, National Development Planning Agency (BAPPENAS), and Ministry of Environment and Forestry (KLHK), Jakarta.
- Mohammed, A.A. and Khamees, H.T., 2021. Categorizing and measuring satellite image processing of fire in the forest Greece using remote sensing. *Indonesian Journal of Electrical Engineering and Computer Science*, 21(2), pp.846-853.
- Mukti, A., Prasetyo, L.B. and Rushayati, S.B., 2016. Mapping of fire vulnerability in Alas Purwo National Park. *Procedia Environmental Sciences*, 33, pp.290-304. DOI.
- Parajuli, A., Gautam, A.P., Sharma, S.P., Bhujel, K.B., Sharma, G., Thapa, P.B., Biste, B.S. and Poudel, S., 2020. Forest fire risk mapping using GIS and remote sensing in two major landscapes of Nepal. *Geomatics, Natural Hazards and Risk*, 11(1), pp.2569-2586. DOI.
- Parente, J., Tonini, M., Stamou, Z., Koutsias, N. and Pereira, M., 2023. Quantitative assessment of the relationship between Land Use/Land Cover Changes and wildfires in Southern Europe. *Fire*, 6(5), p.198. DOI.
- Pualilin, Y., Tjoneng, A. and Abdullah, M., 2019. Zonation mapping of forest and land fire areas in Gowa District. *Jurnal Agrotek*, 3(1), pp.89-97.
- Rianawati, F., Asyári, M., Fatriani, and Asysyifa, 2016. Mapping fire-prone areas in wetland regions of Gambut District, South Kalimantan Province. *National Seminar and Product Exhibition (SENASPRO)*, 17-18 October 2016, pp.61-89.
- Rikalović, A., Čosić, D., Popov, S. and Lazarević, D., 2013. Spatial multi-criteria decision analysis for industrial site selection: The state of the art. *XI Balkan Conference on Operational Research-Balcor*, September 2013, Belgrade, pp.645-673.
- Rosyid, A., Santosa, Y., Jaya, I.N.S., Bismark, M. and Kartono, A.P., 2019. Spatial distribution pattern of *Tarsius lariang* in Lore Lindu National Park. *Indonesian Journal of Electrical Engineering and Computer Science*, 13(2), pp.606-614.
- Samsuri, I.N.S., Jaya, P. and Yauфина, S.L., 2012. Spatial model of land and forest fire risk index: Case study in Central Kalimantan Province. *Indonesian Journal of Forestry*, 1(1), pp.12-18.
- Song, C., Kwan, M.P. and Zhu, J., 2017. Modeling fire occurrence at the city scale: A comparison between geographically weighted regression and global linear regression. *International Journal of Environmental Research and Public Health*, 14, p.396. DOI.
- Syaufina, L. and Hafni, D.A.F., 2018. Variability of climate and forest and peat fires occurrences in Bengkalis District, Riau. *Jurnal Silviculture Tropika*, 9(1), pp.60-68.
- Thoha, A.S. and Ahmad, A.G., 2018. Modeling of forest and land fires vulnerability level in North Sumatra Province, Indonesia. *Environ Asia*, 11(3), pp.1-14. DOI.
- Thoha, A.S. and Triani, H., 2021. A spatial model of forest and land fire vulnerability level in the Dairi District, North Sumatra, Indonesia. *BIODIVERSITAS*, 22(8), pp.3319-3326. DOI.
- Thoha, A.S., Saharjo, B.H., Boer, R. and Ardiansyah, M., 2017. Forest and land fires hazard level modeling: A case study of Kapuas, Central Kalimantan. In: Djalante, R., Garschagen, M., Thomalla, F. and Shaw, R. (eds.) *Disaster Risk Reduction in Indonesia. Disaster Risk Reduction (Methods, Approaches, and Practices)*. Springer, Cham, p.22. DOI.
- Usup, A., Hashimoto, Y., Takahashi, H. and Hayasaka, H., 2004. Combustion and thermal characteristics of peat fire in tropical peatland in Central Kalimantan, Indonesia. *TROPICS*, 14(1), pp.1-19.
- Utomo, A.H. and Arifianto, A.S., 2019. Fuzzy multi-criteria decision-making to classify land capability and suitability. *Food and Agriculture*, 2, p.89.
- Zulkifli, I. and Kamarubayana, L., 2017. Study on forest fire control in Merdeka Subdistrict, Samboja, East Kalimantan. *Jurnal AGRIFOR*, 16(1), pp.141-150.



# A Review on Artificial Intelligence for Water Quality Prediction in Amazonian Countries

J. E. Cruz de La Cruz<sup>1</sup>, W. A. Mamani<sup>2</sup>, F. Pineda<sup>3</sup>, V. Yana-Mamani<sup>4</sup>, R. Santa Cruz<sup>5</sup>, Í. Maldonado-Ramírez<sup>5</sup>, R. Pérez-Astonitas<sup>5</sup> and E. Morales-Rojas<sup>5†</sup>

<sup>1</sup>Facultad de Mecánica Eléctrica, Electrónica y Sistemas, Universidad Nacional del Altiplano, Puno 21001, Perú

<sup>2</sup>Universidad de Alicante, España

<sup>3</sup>Pontificia Universidad Católica del Perú, Peru

<sup>4</sup>Universidad Nacional de Moquegua, Perú

<sup>5</sup>Facultad de Ingeniería de Sistemas y Mecánica Eléctrica, Universidad Nacional Toribio Rodríguez de Mendoza de Amazonas, Calle Agropecuaria N°520, Bagua, Amazonas, Perú

†Corresponding author: E. Morales-Rojas; eli.morales@untrm.edu.pe

**Abbreviation:** Nat. Env. & Poll. Technol.  
**Website:** [www.neptjournal.com](http://www.neptjournal.com)

*Received:* 27-07-2024

*Revised:* 31-08-2024

*Accepted:* 10-09-2024

## Key Words:

Artificial intelligence  
 Water quality prediction  
 Amazonian countries

## Citation for the Paper:

Cruz de La Cruz, J. E., Mamani, W. A., Pineda, F., Yana-Mamani, V., Santa Cruz, R., Maldonado-Ramírez, Í., Pérez-Astonitas, R. and Morales-Rojas, E., 2025. A review on artificial intelligence for water quality prediction in Amazonian Countries. *Nature Environment and Pollution Technology*, 24(2), p. D1705. <https://doi.org/10.46488/NEPT.2025.v24i02.D1705>

*Note: From year 2025, the journal uses Article ID instead of page numbers in citation of the published articles.*



**Copyright:** © 2025 by the authors

**Licensee:** Technoscience Publications

This article is an open access article distributed under the terms and conditions of the Creative Commons Attribution (CC BY) license (<https://creativecommons.org/licenses/by/4.0/>).

## ABSTRACT

Water quality prediction plays an important role in environmental monitoring and ecosystem sustainability in the Amazon. Therefore, this review focuses on determining the advances in the scientific production of artificial intelligence in water quality prediction in the Amazon, as well as the limitations and perspectives compared to water quality indexes (WQI). In this sense, Boolean operators were applied, using the following terms: "artificial intelligence", "machine learning", "water quality," and "Amazonia" The databases were Scopus, web of Science, Springer, and IEEE. In this study, 14 scientific articles published during the period 2000-2024 focused on Amazonian countries were evaluated. Although in the Amazon low scientific production was evidenced and is led by Brazil, the highest scientific growth was for 2021, and 93% belongs to the Scopus database, with a compound annual rate of 12.16%. The IA is characterized by using data from governmental institutions and is only limited to parameters such as Total Suspended Solids (TSS), Total Organic Carbon, Turbidity, and Chlorophyll, using satellite imaging techniques, and the most commonly used algorithm was the Clustering Algorithms. In this context, AI applications are still very low in Amazonian countries compared to other European countries. Its limitations are in the accuracy and the limited amount of physicochemical and microbiological data used for predictions. However, AI is a tool that will replace the water quality indexes used manually.

## INTRODUCTION

Water quality is an essential ecological value for health and economic development (Villena Chávez, 2018). It is the most abundant component of the human body, so it must have proper management (Salas-Salvadó et al. 2020, Veneros et al. 2024). However, water quality has been threatened by various sources, wastewater treatment plants, mining activities (heavy metals), food processing wastes (Morales-Rojas 2020), agricultural runoff (Kaur & Sinha 2019), and chemical and household disposal. Water sources are divided into surface water and groundwater sources, These rivers are the most used water source by the population living near river Banks (Mustafa et al. 2017). In that sense, artificial intelligence (AI) plays an important role in living beings (Romero Lopez & Vargas Mato 2017) and is divided into biological, hydromorphological and physicochemical quality (Nikolaou et al. 2008, Gad et al. 2020).

Therefore, a productive and cost-effective methodology for water quality estimation is required, but they are difficult to design due to their nonlinearity, non-stationary characteristics, and constant unpredictable natural changes (Lintern et al.

2018, Perona et al. 1999). Therefore, reliable methodologies such as artificial intelligence (AI) models and their advanced tools are needed to determine water quality and achieve sustainable development (Chaudhary 2023, Tiyaisha et al. 2020). Therefore, AI is a significantly powerful resource for water monitoring (Rajae et al. 2020).

Studies have applied an artificial neural network and adaptive neuro-fuzzy inference system to calculate dissolved oxygen (DO) levels and organic matter parameters (BOD<sub>5</sub> and COD), these results were optimal with the values measured in the river water (Emamgholizadeh et al. 2014). Neural network models are studied to examine and mimic the relationship of water quality index (WQI) with water quality variables in a tropical environment, being an encouraging alternative to predict WQI, as opposed to manual calculation methods of WQI that involve long calculations and transformations (Hameed et al. 2017, Limon & Webb 1964), water quality indices have a quantitative description, it is qualitatively interpreted with the help of classification schemes (Egbueri et al. 2023). However, this process has been hampered by labor and testing costs (Agbasi & Egbueri 2023).

The adoption of AI in water has led to major revolutions and innovations with respect to water quality assessment and monitoring, and high-quality research should be prioritized (Myllyaho et al. 2021). Other studies have analyzed a variety of modeling methods, such as deep learning (DL), which have been shown to increase efficiency compared to traditional machine learning (ML) models (Irwan et al. 2023).

Water in the Amazon plays a crucial role in climate regulation, biodiversity, and ecosystem sustainability, as well as in the life and livelihood of local communities and populations (Marengo et al. 2018). The Amazon basin covers an area of approximately 7 million km<sup>2</sup>. Amazon forests cover about 5.3 million km<sup>2</sup>, representing 40% of the global tropical forest area (Laurance et al. 2001). However, water quality in this region has been affected by a number of factors, including human activities such as mining, deforestation, and land-use change, as well as by the effects of climate change (Weng et al. 2018).

In this context, the application of advanced technologies such as AI offers new opportunities to more effectively monitor and manage water resources in the Amazon. To this end, the following questions need to be addressed:

1. What will be the evolution of scientific production over time through the assessment and monitoring of water quality with AI techniques in the Amazon?
2. What are the AI algorithms used in Amazon?
3. What are the limitations and perspectives of AI versus water quality indices in the Amazon?

Based on the above, the objective of this study was to determine the advances in the scientific production of artificial intelligence in the prediction of water quality in the Amazon, as well as the limitations and perspectives of its use in the prediction of water quality in the Amazon.

## MATERIALS AND METHODS

The bibliography consulted goes back to the year 2000, up to 2024. Boolean operators were applied using the following terms: “artificial intelligence”, “machine learning”, “water quality,” and “Amazonia”. All the research was carried out through a search in Google Scholar, due to its capacity to compile free-access texts. As well as the use of the main databases Scopus, web of Science, Springer, and IEEE support all the findings on this topic by passing after a rigorous peer review (Bakhmat et al. 2022), and 95 scientific articles were found.

### Inclusion Criteria

Publications from 2000 to January 2024 in all languages were considered. Titles, abstracts, methodology (to determine the amount of data used in the study), and main results were examined to select the articles of interest. As the geographic scope was Amazon-wide, only 14 studies were rescued.

### Exclusion Conditions

Book and encyclopedia chapters, conferences, and reviews that did not consider artificial intelligence and others that did not fit the study topic were excluded. We also excluded, gray literature for not passing peer review (Valentine et al. 2019). In addition, inconclusive studies and duplicates were not taken into account.

### Compound Annual Growth Rate (CAGR)

CAGR is a factor to measure economic growth (Castillo & Powell 2019), with the purpose of describing the evolution of scientific studies, the last 23 years were studied. Calculations were performed using a CAGR calculator. An open calculator was applied because it is easier and faster to use (Calcuvio 2022).

### Limitations and Prospects

The selected research was related to the physicochemical parameters analyzed in each study and how these are contributing to the closing of gaps. The benefits of AI compared to traditional methods for determining water quality (water quality indices) were addressed. Likewise, each selected article was analyzed to determine the limitations and future perspectives for the development of research.

## Data Analysis

The data were downloaded in CSV format and processed in Microsoft Office Excel 2016. This facilitated the determination of the distribution of studies by year and country. The analysis was performed with VOSviewer software version 1.6.19, a tool widely used in the scientific community to represent and visualize bibliometric networks. VOSviewer uses several colors to help understand and discover keyword relationships (Eck, Ludo Waltman 2013).

## RESULTS AND DISCUSSION

### Research Behavior According to Countries

Table 1 shows the distribution of scientific articles according to the affiliation and country of origin of the first author, showing that Brazil (6 articles) and the USA (3 articles) lead with studies related to the application of artificial intelligence in the Amazon. These results may be related to the participation in the development and dissemination of knowledge in water resources management led by the Brazilian Association of Water Resources (ABRhidro) (de Paiva et al. 2020). Another country that leads in verified water quality prediction studies is the USA. These results may be related to the fact that it is the second country after China with the highest amount of organic pollutant emissions to water in the world, with an impressive value of 1,850,753 kg/day (Paraschiv et al. 2015).

### Behavior of Scientific Production by Year

Fig. 1 shows the evolution of publications by year, highlighting 6 articles in 2021 and only one article found for 2024 (Fig. 1A), which is related to the CAGR of 12.16%. Most publications are in the Scopus database (95%), and only 7% are in the Web of Science (Fig. 1 B). These databases are world leaders in terms of scientific content (Zhu & Liu 2020).

Fig. 2 shows the amount of data per study, with three studies using the largest amount of data, including the

Table 1: Distribution of scientific production by country.

Country	Publications
Brazil	6
USA	3
Canada	1
China	2
United Kingdom	1

studies by Valdes & Pou (2021a) with 99473 data, while Liu et al. (2023) reached 15204 data and Strobl et al. (2007) used 8097 data. Generally, the studies that used large amounts of data were obtained from public data from organizations dedicated to water quality monitoring. In that sense, the importance of the amount of data in water quality predictions is affirmed and aims to improve decision-making to improve quality indexes and public health (De Fortuny et al. 2013). However, the states devote little attention to water management in the Amazon, although, for example, in the Amazon basin of Peru, 94 percent transport it manually to their homes from rivers, and only 50% boil the water for consumption (McClain et al. 2001). Therefore, improving water quality through efficient techniques while avoiding the smallest margin of error (James et al. 2015), is through artificial intelligence that uses methods to generate highly accurate results. To counteract problems in the amount of data, studies demonstrate the application of data imputation techniques (the process of replacing missing values) (Ghapor et al. 2017) and synthetic data generation, which is widely used for exploratory data analysis (Dankar & Ibrahim 2021). These methods can be justified because of the high cost of physicochemical and microbiological analyses in water, preventing more continuous and prolonged sampling in the Amazon basin and the world.

Table 2 shows the explored studies are evidenced, the minimum female contribution as first author (3 articles) in this subject, in spite of this is evidencing the increase in the number of women working in the information technology

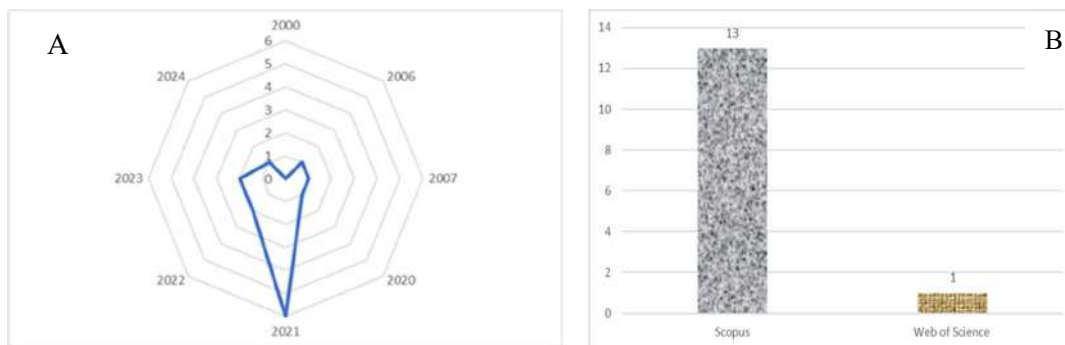


Fig. 1: Behavior of scientific production by year (A), Scientific production by database (B).

industry and even now they prefer careers related to Information and Communications Technology-ICT (Akteer et al. 2021) regarding the AI algorithms used are Support Vector Machines, Ensemble Learning, Support Vector Machines, Ensemble Learning, Correlation Maps.

With respect to data collection, it was evident that 8 studies were from the public sector, influenced by the large amount of data. This is important because the data are analyzed and visualized in open access, in this case, obtained from government institutions (Hossain et al. 2016). With this, an analysis is achieved from a holistic point of view, which proposes future directions, and the role that can be played by organizations of scientific work has the potential to advance and transform the common knowledge from which the science-based sectors are nourished (Perkmann & Schildt 2015). Only 3 studies were with data collected by the same authors, taking into account that this type of study is costly reagents and instruments for the analysis of water samples, and 3 studies used the public-public combination. Therefore, the promotion and access to water quality monitoring data by governments should be free access and artificial intelligence should be a tool for analysis and decision making by public and private institutions.

The validation methods used in the studies were the validity and accuracy index, which allows inferences to be made and hypotheses to be evaluated (Lamprea et al. 2007). Among these studies, we have the R<sup>2</sup>, standard error of the estimation, and Student's t-test analysis widely used in the studies. Prediction errors (a value that quantifies the uncertainty of a prediction), as well as the coefficient of determination, which is a function of the proportion of variability of the variable and is attributed to the linear relationship with X (Roy-García et al. 2019).

The physicochemical parameter found was the “total phosphorus” parameter that is found in water in the form of phosphates; this can be dangerous if it is not properly controlled, for example if the water is used for irrigation purposes (Morales-Rojas 2020) and total suspended solids in water are important to monitor because they carry toxic substances absorbed and limit the availability of light and photosynthesis (Park 2007). This parameter is used in predictions by using empirical models that use surface reflectance from satellite images to estimate Total Suspended Solids (TSS) concentrations (Isidro et al. 2018). Likewise, the studies analyzed are related to the evaluation of chlorophyll and dissolved organic carbon (DOC). Regarding chlorophyll in water they have distinctive spectral characteristics. Therefore, they can be measured by spectral indices in various water bodies, including lakes, ponds, rivers, and streams (Yang et al. 2017). However, it is still challenging to accurately estimate chlorophyll concentrations by remote sensing in various water bodies because the presence of suspended sediments with high inorganic content and colored dissolved organic matter can nullify the chlorophyll spectral signal (Mouw et al. 2015, Odermatt et al. 2012, Sun et al. 2014, Yacobi et al. 2011). On the other hand, from the studies, the evaluation of dissolved organic carbon in water is evidenced, this is because they carry pollutants and can negatively affect water treatment processes (Ledesma et al. 2012).

Another of the main results is the use of advances in remote sensing in landscape ecology, highlighting its contribution to the structure and function of the landscape, analysis of historical changes, and simulation of future changes, an important topic for the Amazon, which represents interdisciplinarity and will help ensure that

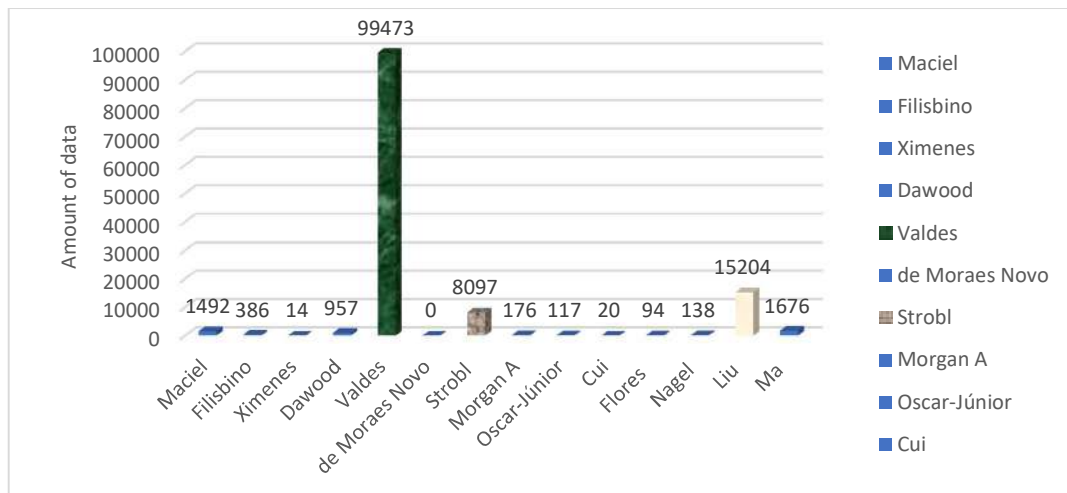


Fig. 2: Amount of data used in the studies.



Table 2: Characteristics of the studies on water quality prediction.

Cita	Quartile	Number of appointments	Database	The genre of the first author	AI algorithms used	Where data were collected	Data sources	Validation methods	Physical-chemical parameters in water quality prediction / Source.	Main results
(de Moraes Novo et al. 2006)	Q1	106	Scopus	F	Other techniques	Brazil	Own and public/historical Landsat-TM imagery	Validity and accuracy index (R2, standard error of estimation, Student's t-test)	No mention/ Lago=concentration of chlorophyll dissolved organic carbon dissolved organic carbon (DOC)	Evaluated seasonal changes in chlorophyll distribution in lakes. They used a linear mixing model on spectroradiometer reflectance data. It turned out that phytoplankton patches are concentrated in lakes close to land with clear water influence.
(Strobl et al. 2007)	Q2	10	Scopus	M	Other techniques	World Cup	Own	-	Total phosphorus/*	Describes a methodology called Critical Sampling Points (CSP) to identify crucial sampling locations in rural watersheds for total phosphorus contamination in water.
(Crowley & Cardille 2020)	SC	37	Scopus	F	Support Vector Machines	World Cup	Public	-	No mention of-	It highlights the contribution of landscape structure and function, analysis of historical changes and simulation of future changes. It underlines the importance of the continued accessibility of free imagery from satellite sources and open-access data analysis software in landscape ecology. It also emphasizes the future opportunities these advances offer for broader and more detailed studies in areas such as landscape connectivity, metapopulation dynamics, and social-ecological systems.
(Oscar-Junior 2021)	Q1	9	Scopus	M	Other techniques	Brazil	Public	Validity and accuracy index (Shapiro-Wilk)	Not mentioned/Rio	They found a correlation between precipitation and sea surface temperatures in the Pacific and Atlantic, highlighting the importance of the South Atlantic Convergence Zone in precipitation variability. These results are relevant for development planning and water resource management in the region.
(Maciel et al. 2021)	Q1	40	Scopus	M	Ensemble Learning, Support Vector Machines	Brazil	Own and public	Prediction errors	SST	Machine Learning methods outperformed Semi-Analytical methods, with Random Forest obtaining the best results (errors less than 22%). In addition, it was observed that Semi-Analytics could be useful for Zsd retrieval. The application of Random Forest to Sentinel-2 atmospherically corrected images showed reasonable feasibility with errors of 28%.

Table Cont....

Cita	Quartile	Number of appointments	Database	The genre of the first author	AI algorithms used	Where data were collected	Data sources	Validation methods	Physical-chemical parameters in water quality prediction / Source.	Main results
(Filisbino Freire da Silva et al. 2021)	Q1	7	Scopus	M	Support Vector Machines	Brazil	Own and public	Coefficient of Determination	Total Suspended Sediments (TSM)	Method for monitoring optical water types in Brazil using Sentinel-2 MSI data
(Ximenes et al. 2021)	Q1	7	Scopus	M	Clustering Algorithms	Brazil	Own	Validity and accuracy rates	NC	They mapped 14 ecoregions in the Purus-Madeira interfluvium using machine learning techniques, highlighting the environmental heterogeneity of the region. This study can help in systematic conservation planning actions to maintain a greater number of protected ecoregions (as ecoregions represent environmental heterogeneity). The study presents an integrated framework using an Adaptive Neuro-Fuzzy Inference System (ANFIS) and Fuzzy Inference System (FIS) to predict the water network condition index. The performance of the framework, superior to the multiple linear regression (MLR) model with an $R^2$ of 0.9145, demonstrates its effectiveness in optimizing prediction results and supporting sustainable urban water management.
(Dawood et al. 2021)	Q1	8	Scopus	F	Other techniques	Peru	Own	Coefficient of Determination	NC	The results highlight temporal changes in water vapor patterns. In the conclusions, it is highlighted that accurate seasonal prediction is achieved with a reduced set of features, and the association of water vapor patterns with specific events in hemispheric regions is demonstrated. Results indicate reasonable performance, even with limited annotations, and the effectiveness of incorporating Lab color space is evaluated. Spatial regularity was observed and active learning is proposed as a future approach, along with testing unsupervised clustering algorithms on artisanal gold mining datasets.
(Valdes & Pou 2021b)	SI	2	Scopus	M	Other techniques	World Cup	Public	validity and accuracy index	NC	
(Cui et al. 2022)	SI	0	Scopus	M	Support Vector Machines	Peru	Public	validity and accuracy index	NC	

Table Cont....

Cita	Quartile	Number of appointments	Database	The genre of the first author	AI algorithms used	Where data were collected	Data sources	Validation methods	Physical-chemical parameters in water quality prediction / Source.	Main results
(Flores Júnior et al. 2022)	SI	4	WOS	M	Other techniques	Brazil	Public	Prediction errors	NC	The results showed a significant improvement in the accuracy of Chl-a recovery with the hybrid semi-analytical algorithm (HSAA) compared to empirical models, with a mean absolute percent error (MAPE) of less than 37%. Furthermore, the applicability of the calibrated model for estimating Chl-a concentration in OLCI images was demonstrated, thus supporting the usefulness of semi-analytical models in highly turbid waters and their importance for monitoring Amazonian aquatic ecosystems.
(Nagel et al. 2023)	Q1	0	Scopus	M		World Cup	Public	-	NC	This paper highlights the importance of satellite data in environmental science, providing information on river migration patterns and their implications for ecosystem management and conservation.
(Liu et al. 2023)	Q1	8	Scopus	M	Correlation maps	World Cup	Public	correlation index	NC	Synergistic relationships between global nature contributions to people (PNC) were found to prevail over trade-offs, particularly in low-latitude areas vulnerable to climate change impacts. This research underscores the critical need for strategies that foster landscape multifunctionality and regional collaboration to enhance human well-being despite challenges in selection.
(Ma et al. 2024)	Q1	3	Scopus	M		World Cup	Public	-	NC	The systematic review highlights the growing application and success of Transfer Learning (TL) in environmental remote sensing in various domains, including land cover mapping and disaster management. Future directions emphasize the need for reference datasets for TL evaluation, improving model interpretability, and leveraging basic models for remote sensing tasks, indicating the crucial role of TL in improving the efficiency of environmental monitoring.

NC=No analysis of physico-chemical or microbiological parameters, SC=no quartile

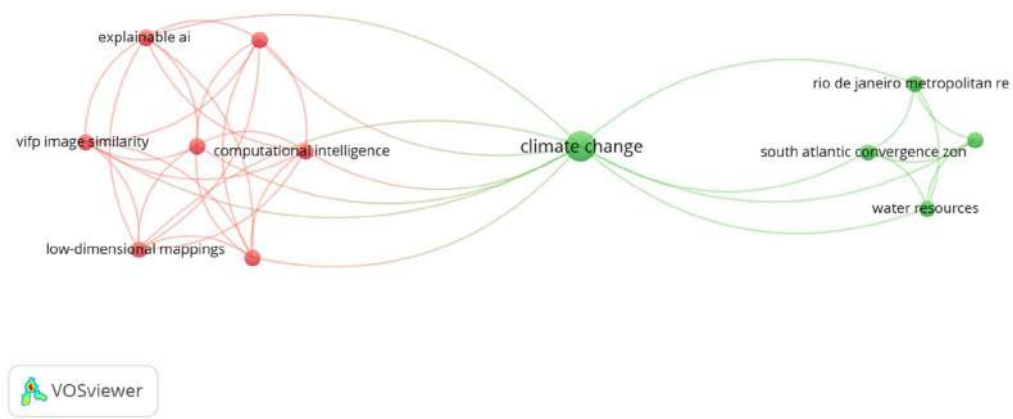


Fig. 3: Keyword analysis of the studies.

landscape ecology can benefit the most from remote sensing (Foody 2023).

Fig. 3 shows the co-occurrence of keywords where the word climate change is highlighted, and it is the node that is related to the other keywords, such as Computational intelligence. In addition, it is observed that the green nodes are the emerging words such as water resources and the South Atlantic convergence zone. The visualization of the co-occurrence of keywords is important in recent years, since they exploit the mapping of knowledge related to each topic (Radhakrishnan et al. 2017).

Limitations and Future Prospects

The limitations of the studies lie in insufficient accuracy; in the face of this, researchers are working on how to improve the accuracy of water quality prediction (Chen et al. 2023). The explored studies are based on spatial analysis of images and address a few water quality parameters such as chlorophyll, turbidity, and TSS (Feyisa et al. 2014, Su 2017). Therefore, systematic methods to estimate error should be developed and the images should be of high resolution (Burns & Nolin 2014). On the other hand, it is evident the need for future work to assess water quality in the Amazon, incorporating in the analysis several parameters (physicochemical-

Table 3: Categories of water quality indices commonly used in the Amazon countries.

Categories of ICA			
Code	Colombia		Brazil
	ICA Rojas	ICAUCA	IAP
1	Very Bad	Lousy	Lousy
2	Inadequate	Inadequate	Mala
3	Acceptable	Acceptable	Regular
4	Good	Good	Good
5	Optima	Optima	Optima

Table 4 shows the physicochemical and microbiological parameters considered by the Colombian ICAs, which are based on weighted values. However, there are few of them; in this sense, AI has the great challenge of improving and establishing evaluation patterns. Table 4: Physicochemical and microbiological parameters used by ICA and IA in Amazonia.

Parameter	Colombia		Amazonia
	Index		IA
	ICA Rojas 1991	ICAUCA 2004	Parameters used
Dissolved oxygen (DO)	0.25	0.21	-
pH	0.17	0.08	-
Biochemical oxygen demand (BOD5)	0.15	0.15	-
Nitrates			-
Fecal Coliforms	0.21	0.16	-
Temperature			-
Turbidity	0.11	0.07	-
Total Dissolved Solids	0.11	0.07	-
Total Phosphorus	-	0.08	X
Cadmium	-	-	-
Mercury	-	-	-
Electrical conductivity	-	-	-
Suspended Solids	-	0.05	X
Color	-	0.05	-
Total Nitrogen	-	0.08	-
Chlorides	-	-	-
Arsenic	-	-	-
Fluoride	-	-	-
Total Coliforms	-	-	-
Chemical Oxygen Demand (COD)	-	-	-
Alkalinity	-	-	-
Hardness	-	-	-
Phosphates	-	-	-
Cyanide	-	-	-
Selenium	-	-	-

= Parameters not contemplated, X= Parameters used in AI studies in Amazonia, Adapted from: Torres et al.(2009)



microbiological), especially the parameters of organic matter and heavy metals through in situ monitoring, associated with biological indicators of water quality and incorporating sensors for real-time evaluation.

Artificial intelligence can be used to monitor water quality in the Amazon. This is in order to have more accurate data and to replace the evaluation of quality indices applied manually, and their results are expressed in categories (Maroneze et al. 2014) (Table 3). These indices are currently classified according to values, as shown in the ICAs of Colombia and Brazil. In the future, it is expected that AI will help organizations in monitoring, decision-making, and achieving safe and improved water quality for users to support a sustainable future (Chauhan & Sahoo 2024, Mustafa et al. 2021).

## CONCLUSIONS

The IA is characterized by using data from governmental institutions, and it was evidenced that it is limited to parameters such as Total Suspended Solids (TSS), Turbidity, total organic carbon, and Chlorophyll, limiting the analysis of water quality. It is expected that this will be overcome and the IA will use monitoring with the use of a greater number of parameters. Brazil is the leading Amazonian country with AI studies, however, its application is still very low compared to other European countries. The compound annual growth rate showed a value of 12.16%, and 95% of the selected articles are hosted in Scopus 95% and only 7% are in Web of Science. This shows that these databases are the leaders in the scientific and academic world due to the high standard of review during their editorial processes.

AI is expected to increase its potential to solve the challenges faced by water monitoring in the Amazon, providing technical support for more efficient management and operation.

## REFERENCES

- Agbasi, J.C. and Egbueri, J.C., 2023. Intelligent soft computational models integrated for the prediction of potentially toxic elements and groundwater quality indicators: A case study. *Journal of Sedimentary Environments*, 8(1), pp.57–79. DOI.
- Akter, S., Siddique, S., Jahan, I., Rabeya, T. and Mim, M.R., 2021. People thoughts prediction using machine learning on women's contribution in ICT in Bangladesh. *IEEE International Conference on Computing, Communication and Automation*, 2021, pp.626–631. DOI.
- Bakhmat, N., Kolosova, O., Demchenko, O., Ivashchenko, I. and Strelchuk, V., 2022. Application of international scientometric databases in the process of training competitive research and teaching staff: Opportunities of Web of Science (WoS), Scopus, Google Scholar. *Journal of Theoretical and Applied Information Technology*, 100(13), pp.4914–4924.
- Burns, P. and Nolin, A., 2014. Using atmospherically-corrected Landsat imagery to measure glacier area change in the Cordillera Blanca, Peru from 1987 to 2010. *Remote Sensing of Environment*, 140, pp.165–178. DOI.
- Calcuvo, 2022. Calculadora de tasa de crecimiento anual compuesto o CAGR. Calcuvo.
- Castillo, J.A. and Powell, M.A., 2019. Analysis of Ecuador's scientific production and the impact of international collaboration in the period 2006–2015. *Revista Española de Documentación Científica*, 42(1), p.225. DOI.
- Chaudhary, G., 2023. Environmental sustainability: Can artificial intelligence be an enabler for SDGs? *Nature Environment and Pollution Technology*, 22(3), pp.1411–1420. DOI.
- Chauhan, M. and Sahoo, D.R., 2024. Towards a greener tomorrow: Exploring the potential of AI, blockchain, and IoT in sustainable development. *Nature Environment and Pollution Technology*, 23(2), pp.1105–1113. DOI.
- Chen, Z., Liu, L., Wang, Y. and Gao, J., 2023. Review of water quality prediction methods. *Lecture Notes in Civil Engineering*, 341, pp.237–265. DOI.
- Crowley, M.A. and Cardille, J.A., 2020. Remote sensing's recent and future contributions to landscape ecology. *Current Landscape Ecology Reports*, 5(3), pp.45–57. DOI.
- Cui, K., Camalan, S., Li, R., Pauca, V.P., Alqahtani, S., Plemmons, R., Silman, M., Dethier, E.N., Lutz, D. and Chan, R., 2022. Semi-supervised change detection of small water bodies using RGB and multispectral images in Peruvian rainforests. *Workshop on Hyperspectral Image and Signal Processing, Evolution in Remote Sensing*, 2022, pp.2–5. DOI.
- Dankar, F.K. and Ibrahim, M., 2021. Fake it till you make it: Guidelines for effective synthetic data generation. *Applied Sciences*, 11(5), pp.1–18. DOI.
- Dawood, T., Elwakil, E., Novoa, H.M. and Delgado, J.F.G., 2021. Ensemble intelligent systems for predicting water network condition index. *Sustainable Cities and Society*, 73. DOI.
- DeFortuny, E.J., Martens, D. and Provost, F., 2013. Predictive modeling with big data: Is bigger really better? *Big Data*, 1(4), pp.215–226. DOI.
- DeMoraesNovo, E.M.L., DeFariasBarbosa, C.C., Freitas, R.M., Shimabukuro, Y.E., Melack, J.M. and Filho, W.P., 2006. Seasonal changes in chlorophyll distributions in Amazon floodplain lakes derived from MODIS images. *Limnology*, 7(3), pp.153–161. DOI.
- DePaiva, R.C.D., Chaffe, P.L.B., Anache, J.A.A., Fontes, A.S., DeAraujo, L.M.N., DeAraujo, A.N., Bartiko, D., Bleninger, T., DeAmorim, P.B., Buarque, D.C., Carlotto, T., Collischonn, W., Detzel, D.H.M., Fan, F.M., Formiga-Johnsson, R.M., Kobiyama, M., Mannich, M., Marques, G., Michel, G.P. and Zanandrea, F., 2020. Advances and challenges in the water sciences in Brazil: A community synthesis of the XXIII Brazilian Water Resources Symposium. *Revista Brasileira de Recursos Hídricos*, 25, pp.1–28. DOI.
- Eck, L.W. and Waltman, N.J.V., 2013. Full-text citation analysis: A new method to enhance. *Journal of the American Society for Information Science and Technology*, 64(7), pp.1852–1863. DOI.
- Egbueri, J.C., Mgbenu, C.N., Digwo, D.C. and Nnyigide, C.S., 2023. A multi-criteria water quality evaluation for human consumption, irrigation and industrial purposes in Umuoya area, southeastern Nigeria. *International Journal of Environmental Analytical Chemistry*, 103(14), pp.3351–3375. DOI.
- Emamgholizadeh, S., Kashi, H., Marofpoor, I. and Zalaghi, E., 2014. Prediction of water quality parameters of Karoon River (Iran) by artificial intelligence-based models. *International Journal of Environmental Science and Technology*, 11(3), pp.645–656. DOI.
- Feyisa, G.L., Meilby, H., Fensholt, R. and Proud, S.R., 2014. Automated Water Extraction Index: A new technique for surface water mapping using Landsat imagery. *Remote Sensing of Environment*, 140, pp.23–35. DOI.
- FilibinoFreiredaSilva, E., MárciaLeãoDeMoraesNovo, E., DeLuciaLobo, F., ClementeFariaBarbosa, C., TressmannCairo, C., AlmeidaNoernberg,

- M. and HenriqueDaSilvaRotta, L., 2021. A machine learning approach for monitoring Brazilian optical water types using Sentinel-2 MSI. *Remote Sensing Applications: Society and Environment*, 23, pp.1–10. DOI.
- FloresJúnior, R., Barbosa, C.C.F., Maciel, D.A., Novo, E.M.L.DeM., Martins, V.S., Lobo, F.DeL., SanderDeCarvalho, L.A. and Carlos, F.M., 2022. Hybrid semi-analytical algorithm for estimating chlorophyll-a concentration in Lower Amazon floodplain waters. *Frontiers in Remote Sensing*, 3(4), pp.1–20. DOI.
- Foody, G.M., 2023. Remote sensing in landscape ecology. *Landscape Ecology*, 38(11), pp.2711–2716. DOI.
- Gad, M., Elsayed, S., Moghanm, F.S., Almarshadi, M.H., Alshammari, A.S., Khedher, K.M., Eid, E.M. and Hussein, H., 2020. Combining water quality indices and multivariate modeling to assess surface water quality in the Northern Nile Delta, Egypt. *Water (Switzerland)*, 12(8), pp.1–16. DOI.
- Ghapor, A.A., Zubairi, Y.Z. and Imon, A.H.M.R., 2017. Missing value estimation methods for data in linear functional relationship model. *Sains Malaysiana*, 46(2), pp.317–326. DOI.
- Hameed, M., Sharqi, S.S., Yaseen, Z.M., Afan, H.A., Hussain, A. and Elshafie, A., 2017. Application of artificial intelligence (AI) techniques in water quality index prediction: A case study in tropical region, Malaysia. *Neural Computing and Applications*, 28, pp.893–905. DOI.
- Hossain, M.A., Dwivedi, Y.K. and Rana, N.P., 2016. State-of-the-art in open data research: Insights from existing literature and a research agenda. *Journal of Organizational Computing and Electronic Commerce*, 26(1–2), pp.14–40. DOI.
- Irwan, D., Ali, M., Ahmed, A.N., Jacky, G., Nurhakim, A., Ping Han, M.C., AlDahoul, N. and El-Shafie, A., 2023. Predicting water quality with artificial intelligence: A review of methods and applications. *Archives of Computational Methods in Engineering*, 30(8), pp.4633–4652. DOI.
- Isidro, C.M., McIntyre, N., Lechner, A.M. and Callow, I., 2018. Quantifying suspended solids in small rivers using satellite data. *Science of the Total Environment*, 634, pp.1554–1562. DOI.
- James, D.E., Schraw, G. and Kuch, F., 2015. Using the sampling margin of error to assess the interpretative validity of student evaluations of teaching. *Assessment and Evaluation in Higher Education*, 40(8), pp.1123–1141. DOI.
- Kaur, T. and Sinha, A.K., 2019. Pesticides in agricultural run-offs affecting water resources: A study of Punjab (India). *Agricultural Sciences*, 10(10), pp.1381–1395. DOI.
- Lamprea, J.M., Jacmiel, A.L. and Gómez-Restrepo, C., 2007. Validity in scale evaluation. *Revista Colombiana de Psiquiatría*, 36(2), pp.340–348.
- Laurance, W.F., Cochrane, M.A., Bergen, S., Fearnside, P.M., Delamônica, P., Barber, C., D'Angelo, S. and Fernandes, T., 2001. The future of the Brazilian Amazon. *Science*, 291(5503), pp.438–439. DOI.
- Ledesma, J.L.J., Köhler, S.J. and Futter, M.N., 2012. Long-term dynamics of dissolved organic carbon: Implications for drinking water supply. *Science of the Total Environment*, 432, pp.1–11. DOI.
- Limon, P.J. and Webb, R.H., 1964. A magnetic resonance experiment for the undergraduate laboratory. *American Journal of Physics*, 32(5), pp.361–364. DOI.
- Lintern, A., Webb, J.A., Ryu, D., Liu, S., Bende-Michl, U., Waters, D., Leahy, P., Wilson, P. and Western, A.W., 2018. Key factors influencing differences in stream water quality across space. *Wiley Interdisciplinary Reviews: Water*, 5(1), pp.1–31. DOI.
- Liu, Y., Fu, B., Wang, S., Rhodes, J.R., Li, Y., Zhao, W., Li, C., Zhou, S. and Wang, C., 2023. Global assessment of nature's contributions to people. *Science Bulletin*, 68(4), pp.424–435. DOI.
- Ma, Y., Chen, S., Ermon, S. and Lobell, D.B., 2024. Transfer learning in environmental remote sensing. *Remote Sensing of Environment*, 301(August 2023), p.113924. DOI.
- Maciel, D.A., Barbosa, C.C.F., Novo, E.M.L.deM., Flores Júnior, R. and Begliomini, F.N., 2021. Water clarity in Brazilian water assessed using Sentinel-2 and machine learning methods. *ISPRS Journal of Photogrammetry and Remote Sensing*, 182(October), pp.134–152. DOI.
- Marengo, J.A., Souza, C.M., Thonicke, K., Burton, C., Halladay, K., Betts, R.A., Alves, L.M. and Soares, W.R., 2018. Changes in climate and land use over the Amazon region: Current and future variability and trends. *Frontiers in Earth Science*, 6(December), pp.1–21. DOI.
- Maroneze, M.M., Zepka, L.Q., Vieira, J.G., Queiroz, M.I. and Jacob-Lopes, E., 2014. A tecnologia de remoção de fósforo: Gerenciamento do elemento em resíduos industriais. *Revista Ambiente e Água*, 9(3), pp.445–458. DOI.
- McClain, M.E., Aparicio, L.M. and Llerena, C.A., 2001. Water use and protection in rural communities of the Peruvian Amazon Basin. *Water International*, 26(3), pp.400–410. DOI.
- Morales-Rojas, E., 2020. Mixed greywater treatment for irrigation uses. *Revista Ambiente e Água*, 15(6), pp.445–458. DOI.
- Mouw, C.B., Greb, S., Aurin, D., DiGiacomo, P.M., Lee, Z., Twardowski, M., Binding, C., Hu, C., Ma, R., Moore, T., Moses, W. and Craig, S.E., 2015. Aquatic color radiometry remote sensing of coastal and inland waters: Challenges and recommendations for future satellite missions. *Remote Sensing of Environment*, 160, pp.15–30. DOI.
- Mustafa, H.M., Mustapha, A., Hayder, G. and Salisu, A., 2021. Applications of IoT and artificial intelligence in water quality monitoring and prediction: A review. *Proceedings of the 6th International Conference on Inventive Computation Technologies, ICICT 2021*, February, pp.968–975. DOI.
- Myllyaho, L., Raatikainen, M., Männistö, T., Mikkonen, T. and Nurminen, J.K., 2021. Systematic literature review of validation methods for AI systems. *Journal of Systems and Software*, 181, p.111050. DOI.
- Nagel, G.W., Darby, S.E. and Leyland, J., 2023. The use of satellite remote sensing for exploring river meander migration. *Earth-Science Reviews*, 247(October), p.104607. DOI.
- Nikolaou, A.D., Meric, S., Lekkas, D.F., Naddeo, V., Belgiorno, V., Groudev, S. and Tanik, A., 2008. Multi-parametric water quality monitoring approach according to the WFD application in Evros trans-boundary river basin: Priority pollutants. *Desalination*, 226(1–3), pp.306–320. DOI.
- Odermatt, D., Gitelson, A., Brando, V.E. and Schaepman, M., 2012. Review of constituent retrieval in optically deep and complex waters from satellite imagery. *Remote Sensing of Environment*, 118, pp.116–126. DOI.
- Oscar-Júnior, A.C., 2021. Precipitation trends and variability in river basins in urban expansion areas. *Water Resources Management*, 35(2), pp.661–674. DOI.
- Paraschiv, D., Tudor, C. and Petrariu, R., 2015. The textile industry and sustainable development: A Holt-Winters forecasting investigation for the Eastern European area. *Sustainability (Switzerland)*, 7(2), pp.1280–1291. DOI.
- Park, G.S., 2007. The role and distribution of total suspended solids in the macrotidal coastal waters of Korea. *Environmental Monitoring and Assessment*, 135(1–3), pp.153–162. DOI.
- Perkmann, M. and Schildt, H., 2015. Open data partnerships between firms and universities: The role of boundary organizations. *Research Policy*, 44(5), pp.1133–1143. DOI.
- Perona, E., Bonilla, I. and Mateo, P., 1999. Spatial and temporal changes in water quality in a Spanish river. *Science of the Total Environment*, 241(1–3), pp.75–90. DOI.
- Radhakrishnan, S., Erbis, S., Isaacs, J.A. and Kamarthi, S., 2017. Correction: Novel keyword co-occurrence network-based methods to foster systematic reviews of scientific literature. *PLoS ONE*, 12(9), pp.1–16. DOI.
- Rajae, T., Khani, S. and Ravansalar, M., 2020. Artificial intelligence-based single and hybrid models for prediction of water quality in rivers: A

- review. *Chemometrics and Intelligent Laboratory Systems*, 200(August 2019), p.103978. DOI
- Romero Lopez, T. de J. and Vargas Mato, D., 2017. Uso de microorganismos eficientes para tratar aguas contaminadas. *Iha*, XXXVIII(3), pp.88–100.
- Roy-García, I., Rivas-Ruiz, R., Pérez-Rodríguez, M. and Palacios-Cruz, L., 2019. Correlation: Not all correlation entails causality. *Revista Alergia Mexico*, 66(3), pp.354–360. DOI
- Mustafa, S.A., Sulaiman, O.S. and Shahooth, H.S., 2017. Application of QUAL2K for water quality modeling and management in the lower reach of the Diyala River. *Iraqi Journal of Civil Engineering*, 11(2), pp.66–80. DOI
- Salas-Salvadó, J., Maraver, F., Rodríguez-Mañas, L., de Pipaon, M.S., Vitoria, I. and Moreno, L.A., 2020. The importance of water consumption in health and disease prevention: The current situation. *Nutricion Hospitalaria*, 37(5), pp.1072–1086. DOI
- Strobl, R.O., Robillard, P.D. and Debels, P., 2007. Critical sampling points methodology: Case studies of geographically diverse watersheds. *Environmental Monitoring and Assessment*, 129(1–3), pp.115–131. DOI
- Su, T.C., 2017. A study of a matching pixel by pixel (MPP) algorithm to establish an empirical model of water quality mapping, as based on unmanned aerial vehicle (UAV) images. *International Journal of Applied Earth Observation and Geoinformation*, 58, pp.213–224. DOI
- Sun, D., Hu, C., Qiu, Z., Cannizzaro, J.P. and Barnes, B.B., 2014. Influence of a red band-based water classification approach on chlorophyll algorithms for optically complex estuaries. *Remote Sensing of Environment*, 155, pp.289–302. DOI
- Tiyasha, Tung, T.M. and Yaseen, Z.M., 2020. A survey on river water quality modelling using artificial intelligence models: 2000–2020. *Journal of Hydrology*, 585(June), pp.2000–2020. DOI
- Torres, P., Cruz, C.H. and Patiño, P., 2009. Índices de calidad de agua en fuentes superficiales utilizadas en la producción de agua para consumo humano: Una revisión crítica. *Revista Ingenierías Universidad de Medellín*, 8(15), pp.79–94.
- Valdes, J.J. and Pou, A., 2021a. A Machine Learning—Explainable AI approach to tropospheric dynamics analysis using Water Vapor Meteosat images. 2021 IEEE Symposium Series on Computational Intelligence, SSCI 2021 - Proceedings, pp.8–11. DOI
- Valdes, J.J. and Pou, A., 2021b. A Machine Learning—Explainable AI approach to tropospheric dynamics analysis using Water Vapor Meteosat images. 2021 IEEE Symposium Series on Computational Intelligence, SSCI 2021 - Proceedings, pp.2–5. DOI
- Valentine, J.C., Hedges, L.V. and Cooper, H.M., 2019. *Handbook of Research Synthesis and Meta-Analysis* (2nd ed.). *The Lancet*, 389(10082).
- Veneros, J., Ramos, L.C., Goñas, M., Morales, E., Auquiñivín-Silva, E., Oliva, M. and García, L., 2024. Seasonal variability of water quality for human consumption in the Tilacancha conduction system, Amazonas, Peru. *Nature Environment and Pollution Technology*, 23(2), pp.899–909. DOI
- Villena Chávez, J.A., 2018. Calidad del agua y desarrollo sostenible. *Revista Peruana de Medicina Experimental y Salud Pública*, 35(2), p.304. DOI
- Weng, W., Luedeke, M., Zemp, D., Lakes, T. and Kropp, J., 2018. Aerial and surface rivers: Downwind impacts on water availability from land use changes in Amazonia. *Hydrology and Earth System Sciences*, 22(1), pp.911–927. DOI
- Ximenes, A.C., Amaral, S., Monteiro, A.M.V., Almeida, R.M. and Valeriano, D.M., 2021. Mapping the terrestrial ecoregions of the Purus-Madeira interfluvium in the Amazon Forest using machine learning techniques. *Forest Ecology and Management*, 488(February). DOI
- Yacobi, Y.Z., Moses, W.J., Kaganovsky, S., Sulimani, B., Leavitt, B.C. and Gitelson, A.A., 2011. NIR-red reflectance-based algorithms for chlorophyll-a estimation in mesotrophic inland and coastal waters: Lake Kinneret case study. *Water Research*, 45(7), pp.2428–2436. DOI
- Yang, Z., Reiter, M. and Munyei, N., 2017. Estimation of chlorophyll-a concentrations in diverse water bodies using ratio-based NIR/Red indices. *Remote Sensing Applications: Society and Environment*, 6(February), pp.52–58. DOI
- Zhu, J. and Liu, W., 2020. A tale of two databases: the use of Web of Science and Scopus in academic papers. *Scientometrics*, 123(1), pp.321–335. DOI

# Using Deep Learning for Plant Disease Detection and Classification

G. N. Balaji†, G. Parthasarathy, A. K. P. Kovendan and Aakash Jha

School of Computer Science and Engineering, Vellore Institute of Technology, Vellore, Tamil Nadu, India

†Corresponding author: G. N. Balaji; balaji.gnb@gmail.com

**Abbreviation:** Nat. Env. & Poll. Technol.  
**Website:** www.neptjournal.com

*Received:* 15-08-2024

*Revised:* 11-10-2024

*Accepted:* 16-10-2024

## Key Words:

InceptionNet  
 MobileNet  
 Plant disease classification  
 ResNet  
 ResNeXt

## Citation for the Paper:

Balaji, G. N., Parthasarathy, G., Kovendan, A.K.P. and Jha, A., 2025. Using deep learning for plant disease detection and classification. *Nature Environment and Pollution Technology*, 24(2), p. B4260. <https://doi.org/10.46488/NEPT.2025.v24i02.B4260>

*Note: From year 2025, the journal uses Article ID instead of page numbers in citation of the published articles.*



**Copyright:** © 2025 by the authors  
**Licensee:** Technoscience Publications  
 This article is an open access article distributed under the terms and conditions of the Creative Commons Attribution (CC BY) license (<https://creativecommons.org/licenses/by/4.0/>).

## ABSTRACT

In India's economy, farming is crucial, making early detection of plant diseases an important task. This helps in reducing crop damage and preventing the diseases from spreading further. Numerous plants, such as corn, tomatoes, and potatoes, display evident symptoms of diseases on their leaves. These noticeable patterns can be employed to accurately predict the diseases and facilitate prompt intervention to reduce their impact. The customary method involves farmers or plant pathologists visually inspecting plant leaves and identifying the specific disease. This project involves a deep learning model designed for classifying plant diseases, utilizing CNNs for their proficiency in image classification. The model, which utilizes architectures like MobileNet, InceptionNet, ResNet, and ResNeXt, delivers faster and more accurate predictions than traditional manual methods. Notably, ResNeXt, with its added dimension of cardinality that aids in learning more complex features, achieved the highest accuracy, reaching 98.2%.

## INTRODUCTION

Agriculture serves as the bedrock of India's economy, playing a pivotal role in human sustenance. The scrutiny of plant health is imperative for the success of agriculture. In India, an estimated 15-25% of potential crop production is lost to pests and diseases, posing a significant challenge (Baranwal et al. 2019). Early disease detection is essential, and the manual monitoring of plants is a labor-intensive and time-consuming task that requires specialized expertise. This research focuses on efficient disease identification to enhance agricultural outcomes and secure food production.

Plant leaves are a primary indicator for identifying leaf infections, as they often display visible disease symptoms (Zhao et al. 2021). The most effective method for detecting plant infections involves recognizing various symptoms indicative of different diseases on leaves. Common manifestations of plant leaf diseases include Chlorosis, which causes leaf yellowing; Stem rust in wheat; powdery mildew, common Leaf rust in corn, Sclerotinia also known as white mold; Septoria brown spot, known as Leaf spot; and Birds-eye spot on berries caused by anthracnose.

Deep Learning, a branch of Machine Learning that traces its roots back to 1943 with the advent of threshold logic, represents a pivotal step towards developing computer models that emulate human biological processes. In this context, our operational model utilizes convolutional neural networks and transfer learning to accurately classify different plant leaf diseases. Renowned for their efficacy in image classification, CNNs—a specialized type of deep learning neural network—enhance this system (Harte 2020). This approach significantly outperforms traditional methods, offering both increased speed and accuracy in detecting disease signs on plant leaves.

The paper is structured as follows: Section II encompasses a Literature Review assessing existing research. Section III explains the Models used, detailing their design and function. Section IV, 'Experimental Detail', describes our experimental



methodologies. In Section V, we present Results and Discussion, analyzing our findings with visual aids. The paper concludes with a succinct summary of our key insights in the Conclusion section.

## LITERATURE REVIEW

Lakshmanarao et al. (2021) addressed the significant challenge of plant disease detection using CNNs and Kaggle's Plant Village dataset. They experiment with datasets for Potato, Pepper Bell, and Tomato plants, training and testing the CNN models. The results of these experiments are promising, demonstrating high accuracy in disease detection across all three datasets. However, the study highlights a gap in current research, particularly in the practical implementation of such models in real-world agricultural settings. Despite the high accuracy achieved, there is a need for further research to adapt these deep learning models for large-scale, field-level applications.

Elfatimi et al. (2022) proposed an automated classification system using MobileNet models. The methodology involves employing MobileNet with TensorFlow and testing various architectures and optimizers to determine the most effective configuration for disease classification. The research showcases the performance of the MobileNet model, which was trained on a publicly available dataset comprising 1,296 bean leaf images categorized into two diseased classes and one healthy class. The results indicate that the model achieves an accuracy of over 97% on the training dataset and over 92% on the test dataset. However, it's important to note that the study's scope is limited to the classification of bean leaf diseases. Consequently, the model's applicability to other scenarios remains untested. Its performance may remain high if other datasets exhibit similar distribution and sampling characteristics as the one used in this research.

Khattak et al. (2021) tackled the crucial challenge of detecting diseases in citrus fruits and leaves using a Convolutional Neural Network (CNN) model. The proposed CNN model effectively categorizes prevalent citrus diseases, including black spot, canker, scab, greening, and Melanose, by integrating multiple layers to extract distinctive features. This system surpasses numerous existing state-of-the-art deep learning models when evaluated on the Citrus and PlantVillage datasets, achieving an impressive test accuracy of 94.55%. The methodology involves using 2293 images from these datasets, pre-processed and classified into different disease categories. The research highlights the need for improved parameter and layer selection in CNN models for more accurate classification, a gap that this study addresses by experimenting with various CNN model variants and parameters.

Zhou et al. (2021) this study addresses the pressing issue of tomato leaf disease identification amid the increasing concern for food security, especially highlighted during the COVID-19 pandemic. They present an innovative approach that leverages an RRDN, which combines the advantages of deep residual networks and dense networks. This hybrid model is designed to improve accuracy in calculations and information flow while simultaneously reducing the number of training parameters. Originally developed for image super-resolution tasks, the RRDN model has been adapted for classification tasks, demonstrating an impressive top-1 average identification accuracy of 95% on the Tomato test dataset sourced from the AI Challenger 2018 datasets. This exceptional performance represents a significant advancement over most existing state-of-the-art models for crop leaf identification, all while demanding less computational resources to achieve high performance.

Sunil et al. (2022) introduced an inventive method for detecting diseases in cardamom plants by employing the EfficientNetV2 model. This study specifically addresses two significant diseases that impact cardamom plants: Colletotrichum Blight and Phyllosticta Leaf Spot. The unique aspect of this research lies in its adoption of the EfficientNetV2 model, which is a state-of-the-art deep learning model renowned for its efficiency and exceptional performance in image classification tasks. The suggested method incorporates the utilization of U2-Net for removing unwanted backgrounds from the input images and selecting multiscale features, enhancing the model's accuracy in disease detection.

Amin et al. (2022) addressed the crucial challenge of classifying corn leaf diseases in this study. The research project introduces an end-to-end deep learning model that combines two pre-trained CNNs: EfficientNetB0 and DenseNet121. The model underwent training using a subset of the PlantVillage dataset, with a specific emphasis on corn plant diseases such as northern leaf blight, common rust, and gray leaf spot. Impressively, the proposed model achieved a remarkable classification accuracy of 98.56%, surpassing the performance of other pre-trained CNN models like ResNet152 and InceptionV3.

Hassan & Maji (2022) proposed a novel lightweight CNN model for plant disease identification, focusing on reducing the number of parameters required in deep learning models. This model incorporates depthwise separable convolution, Inception, and Residual connections, significantly cutting down computational complexity and the time required for training. Traditional methods for identifying diseases in plants, which rely heavily on visual inspections conducted by experts, are both time-consuming and expensive. The

implementation of automatic identification techniques using smart devices, especially deep learning models like CNNs, presents a promising solution to this challenge.

Wang et al. (2020) introduced a new database dedicated to classifying plant diseases and pests. They highlight the significance of employing deep learning models in the field of agriculture. This database was created by using keyword-based retrieval to gather images of various plant diseases and pests, resulting in a comprehensive dataset for analysis. The research underscores the critical role of early detection and treatment of these issues in enhancing crop yields. To classify plant diseases and pests, the authors have explored a hierarchical multi-task learning approach that capitalizes on the connections between different plant species and pests. To address the limitations of existing databases, the authors construct their database, selecting images based on relevance ranking from search engines. The database contains images of three different gramineous plants: rice, wheat, and corn, with each type having five diseases and one pest. The classification algorithms introduced in the research include classical CNN structures like AlexNet, VGG, and ResNet. In addition, hierarchical tree classifiers and fine-grained Triplet network structures are used to enhance the accuracy of disease and pest classification.

Rithik et al. (2022) emphasized the challenge of limited dataset availability in implementing deep learning frameworks and proposed the use of transfer learning with the VGG-19 model to address this issue. The model, pre-trained on the ImageNet and CIFAR 100 datasets, achieved a high accuracy of 94% in disease classification. The study suggests that such AI-based systems can be extended to other crops and used to evaluate crop protection models.

Pherry et al. (2023) investigated the use of transfer learning in machine learning models like VGG16, VGG19, ResNet50, and InceptionV3 to classify rice plant diseases. The study, utilizing a Kaggle dataset, found that data augmentation did not significantly improve results, while regularization techniques did. VGG19 emerged as the most accurate model with 84.4% accuracy. The paper highlights the potential of image-based machine learning over traditional methods for early and precise detection of plant health, although it acknowledges the challenge of overfitting in the validation phase and suggests future research should focus on more distinguishable datasets for improved performance.

A framework for detecting plant leaf damage was proposed by Roshini Polly et al. using a combination of pixel-level and image-level classification models. The suggested approach makes use of CNN for precise disease classification, DeepLabV3+ for background removal and

disease classification assistance, and YOLOv8 for identifying regions of interest from drone photos. Additionally, they increased the evaluation accuracy by employing pixel-level UNet semantic detection. This approach not only forecasted the disease's severity but also its treatment (Polly & Devi 2024.).

A deep learning-based plant disease prediction system was proposed by Ali Hussein et al. Several deep learning architectures are combined in this ensemble technique. To improve the accuracy of plant leaf disease classification, DenseNet201, efficientNetB0, inceptionresnetV2, and efficientNetB3 have been introduced. To improve the effectiveness of deep learning models, a unique image processing method is put forth in this work. An innovative approach to the problem of plant disease classification is presented in this research. After a thorough evaluation of several image processing methods, the research presents a novel image processing algorithm (CLAHE with AMF). Then, to improve photos, a brand-new image preprocessing technique is used (Ali et al.).

## MATERIALS AND METHODS

CNN models excel in recognizing and classifying objects in image datasets. However, despite their numerous advantages, CNNs do come with certain challenges. For instance, training CNNs can be time-consuming, and they often demand large datasets to perform effectively. Deep CNN models are essential for extracting detailed and minor features from images, but this requirement significantly complicates the training process. One effective way to tackle these challenges is through the use of transfer learning techniques. Transfer learning involves leveraging pre-trained networks, where the knowledge gained from training on one dataset can be applied to solve other related problems. In the next section, we explore the techniques used in this research to utilize transfer learning effectively for achieving our goals.

### Transfer Learning

Training cutting-edge models typically demands considerable time, sometimes extending to days or weeks, even on advanced GPU systems. Creating a model from scratch is especially lengthy. For example, constructing a CNN model from the beginning with a typical plant disease dataset resulted in moderate accuracy after numerous training epochs. However, using a pre-trained CNN model via transfer learning achieved significantly higher accuracy in fewer epochs. Transfer learning encompasses different approaches, and their choice depends on the kind of pre-trained network model used for classification and the unique features of the dataset (Sagar & Jacob 2020).

## ResNet

ResNet-50, a type of convolutional neural network, is notable for its depth, comprising 50 layers. The architecture of ResNet-50 is divided into five distinct stages, each containing convolution and identity blocks. These blocks are the fundamental components of the network, extensively utilized in a range of computer vision tasks. The key innovation introduced with ResNet is the concept of layer stacking, where convolution layers are piled on top of each other (Sharma & Singh 2021)

A significant feature of ResNet-50 is its utilization of skip connections. These connections enable the network to circumvent certain layers by directly transmitting the input to the output of a convolution layer. Skip connections are strategically positioned before activation functions to tackle the problem of vanishing gradients, which is prevalent in deep neural networks. This design helps mitigate the error accumulation that tends to occur in deeper models.

In ResNet-50, an input image is denoted as  $x$ , and the nonlinear layers that fit mappings are represented as  $F(x)$ . The residual mapping in this context is expressed as  $H(x)$ . Hence, the formula for the residual mapping in ResNet-50 is defined as:

$$H(x) = F(x) + x \quad \dots(1)$$

Each identity block within ResNet-50 contains three convolutional layers. The network overall boasts over 23 million trainable parameters. For the skip connection to function effectively, the dimensions of the input  $x$  and the shortcut  $x$  need to align. If the dimensions differ, the shortcut  $x$  undergoes an additional convolution layer and batch normalization to ensure compatibility in dimensions (Yadav et al. 2020).

## ResNeXt

ResNeXt is an advanced CNN architecture that extends the fundamental concepts of ResNet. It introduces “cardinality” as an additional dimension, alongside depth and width, in network architectures. The key innovation of ResNeXt lies in its block design. Each ResNeXt block comprises a set of transformations with the same topology, referred to as aggregated transformations.

The general formulation for a ResNeXt block can be expressed as:

$$Y = \sum_{i=1}^C T_i(x) \quad \dots(2)$$

Where  $x$  is the input,  $Y$  is the output,  $C$  is the cardinality (number of parallel paths), and  $T_i$  represents the transformation function of the  $i$ th path.

This aggregated transformation approach enables the network to learn more complex features without a substantial increase in computational complexity compared to widening or deepening the network. ResNeXt models are more parameter-efficient, making them easier to train and scale. The architecture is particularly effective in image recognition tasks, where it leverages its cardinality feature to handle a wide range of image types and complexities.

## InceptionNet

Images, rich in detail and varying in size, present a challenge in selecting appropriate filter sizes for feature extraction in CNNs. Smaller kernel sizes are typically used for extracting local features, while larger kernels are better suited for capturing global information. However, stacking too many convolution layers can lead to issues like overfitting and vanishing gradients. The Inception architecture addresses this by incorporating multiple kernel sizes within each block, allowing the network to become wider rather than deeper. A basic Inception module might employ filters of sizes 3x3, 1x1, and 5x5 in consecutive convolution stages. Following this, max-pooling is applied, and the results are concatenated and fed into the subsequent layer. The “stem” of the Inception layer initiates basic operations that come before the actual Inception module. Additionally, Inception V4 incorporates reduction blocks, which alter the height and width of the grid dimensions (Appel et al. 2023).

## MobileNet

MobileNet is a category of efficient convolutional neural networks crafted specifically for mobile and embedded vision applications. Its core innovation lies in the use of depthwise separable convolutions, which significantly reduce the model size and computational complexity without substantially sacrificing performance. This design makes MobileNet highly suitable for environments with limited computational resources. Depthwise separable convolutions consist of two layers: a depthwise convolution, which implements a single filter for each input channel, and a pointwise convolution, which employs a 1x1 convolution to merge the outputs from the depthwise layer. This method creates a model that is both lightweight and rapid, rendering MobileNet suitable for real-time tasks such as object detection, classification, and facial recognition on mobile devices (Gupta et al. 2023).

## Experimental Details

In this section, we outline the methodology adopted for implementing the plant disease classification project, highlighting the key steps from data handling to model evaluation and prediction. Fig. 1

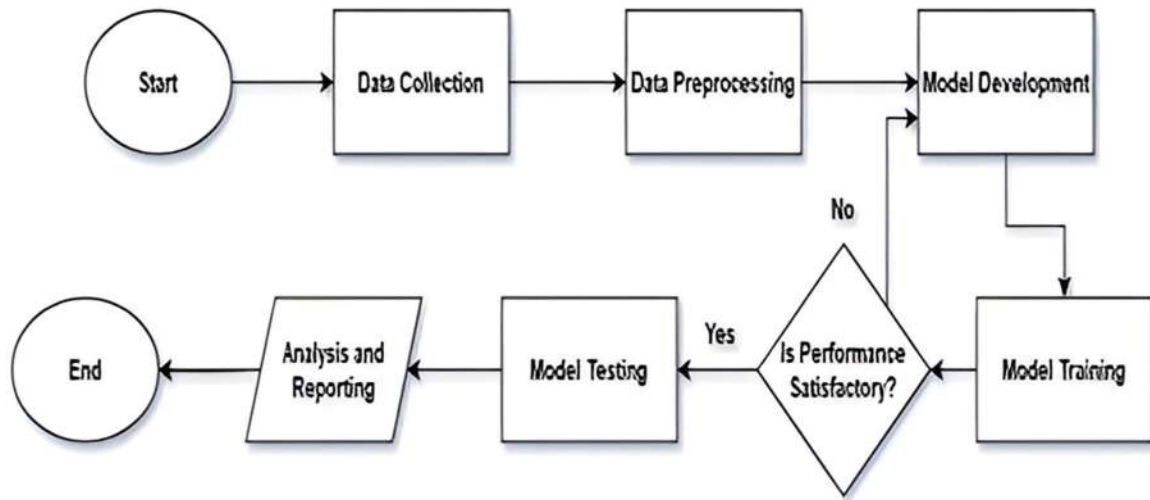


Fig. 1: Methodology flowchart.

demonstrates the methodology flowchart followed in this work.

### Experimental Setup

In this study, all models were optimized for GPU use and conducted on Google's cloud platform using a Windows 11 OS system with an Intel Core i7-10750H CPU at 2.60GHz and a 16 GB Nvidia GeForce GTX GPU. This system featured a 64-bit OS with an x64-based processor. Programming was executed using the Python framework, version 3.12.0.

### Description of Dataset

This study utilized data from the PlantVillage dataset modified and combined with the Chili dataset, which

Table 1: List of plants and diseases.

S. No.	Plant Name	Plant Disease Class
1.	Apple	Cedar Rust Scab Healthy Black Rot
2.	Cassava	Brown Streak Healthy Mosaic Disease Bacterial Blight Green Mottle
3.	Cherry	Healthy Powdery Mildew
4.	Chili	Healthy Leaf Curl Whitefly Yellowish

Table cont....

S. No.	Plant Name	Plant Disease Class
5.	Corn	Leaf Spot Leaf Spot Healthy Common Rust Leaf Blight
6.	Blueberry	Healthy
7.	Grape	Black Measles Black Rot Healthy Leaf Spot
8.	Orange	Citrus Greening
9.	Peach	Healthy Bacterial Spot
10.	Pepper	Healthy Bacterial Spot
11.	Raspberry	Healthy
12.	Potato	Late Blight Healthy Early Blight
13.	Strawberry	Healthy Leaf Scorch
14.	Squash	Powdery Mildew
15.	Tomato	Leaf Curl Virus Early Blight Bacterial Spot Mosaic Virus Leaf Mold Late Blight Target Spot Leaf Spot Spider Mite Healthy



includes over 50,000 images representing 47 classes across 15 plant species. To enhance performance and prevent overfitting, the images were resized and augmented using various techniques. The dataset was split into a training set containing 47,762 images and a validation set comprising 10,417 images, adhering to an 80:20 distribution ratio. Table 1 provides a detailed overview of the different plants and their respective diseases included in this study.

### Preprocessing

Different preprocessing techniques, including image resizing, normalization, and data augmentation (Sudhakar & Priya 2023), were applied to guarantee uniform formatting and diversity of the images. This enhances the model's capability to generalize and minimizes the risk of overfitting during training. The pictures were resized to a uniform size of 256 x 256 pixels, as the training involved the use of various pre-trained neural network models, each with its requirements for input dimensions. For ResNet and ResNeXt, the input dimensions are 256 x 256 x 3, representing height, width, and channel depth. In contrast, InceptionNet requires an input size of 150 x 150 x 3, while MobileNet operates with an input size of 224 x 224 x 3.

### Model Training

In this research, the datasets were randomly split into training and validation sets at a ratio of 80% and 20%, respectively. The training and validation datasets were exclusively utilized for training and fitting the model, while the test set was employed to assess the model's predictive performance on samples it had not previously encountered. The transfer learning approach presents the benefit of faster learning compared to models developed from the ground up. This method also allows for selective training of the model's final layers while keeping earlier layers fixed, enhancing the accuracy of classifications. In our configuration, we first standardized hyperparameters for different pre-trained models, including ResNet, ResNeXt, MobileNet, and InceptionNet (Amudha & Brindha 2022).

For each model, distinct learning rates and optimization functions were applied, as detailed in the accompanying Table 2. The training duration for each model was set at 10 epochs. During our experimentation, we observed that the

output graphs started showing convergence within these 10 epochs, which helped in mitigating issues related to overfitting and model degradation.

### Model Evaluation

The evaluation phase was designed to rigorously assess the models using two primary performance metrics: accuracy metric and validation loss.

**Accuracy Metric:** Accuracy is the principal metric, measuring the rate of correct predictions against the total predictions made. It's a direct indicator of a model's performance, with a higher accuracy reflecting a model's effectiveness in making correct classifications. The accuracy is determined by employing the following formula:

$$Acc = \frac{\text{Number of Correct Predictions}}{\text{Total Number of Predictions}} \times 100\% \dots(3)$$

**Validation Loss:** Complementing accuracy and validation loss provided insight into the model's error rate on unseen data. It served as a measure of how well the model generalized beyond the training samples. Validation Loss is often computed using a loss function, such as categorical cross-entropy for classification tasks, defined as:

$$L_{valid} = -\frac{1}{N} \sum_{i=1}^N \sum_{j=1}^M ((y_{ij} \log(p_{ij}))) \dots(4)$$

This formula for calculating accuracy takes into account various components:

N represents the total number of samples in the validation set, M stands for the total number of classes involved in the classification task,  $y_{ij}$  is a binary indicator signifying whether the class label  $j$  is the correct classification for observation  $i$  and  $p_{ij}$  Represents the predicted probability produced by the model, indicating the likelihood that observation  $i$  belongs to class  $j$ . A lower validation loss pointed to better generalizability and indicated that the model was learning the data patterns rather than memorizing specific examples.

## RESULTS AND DISCUSSION

Fig. 2a illustrates the accuracy of the InceptionNet model across different epochs throughout both the training and

Table 2: Hyperparameter specifications.

Model	Batch Size	Input Shape	Epoch	Max Learning Rate	Optimization Function	Total Parameters (M)
ResNet	32	3×256×256	5	1e <sup>-2</sup>	Adam	6
ResNext	32	3×256×256	10	1e <sup>-3</sup>	SGD	23
InceptionNet	32	3×150×150	10	1e <sup>-4</sup>	RMSprop	21
MobileNet	32	3×224×224	10	1e <sup>-3</sup>	Adam	4

validation phases. The training accuracy shows a steady increase as the number of epochs progresses, while the validation accuracy also improves, peaking at the best validation accuracy of 90.23%. This peak indicates the model's highest performance on unseen data. As the epochs continue, both accuracy lines demonstrate learning and improvement in the model's predictions. The graph in Fig. 2b represents model loss over epochs for both the training and validation phases. The loss serves as a metric to assess the model's performance, where lower values indicate better model performance. Initially, the training loss decreases sharply and then levels off, while the validation loss decreases more gradually and shows some fluctuation, suggesting areas where the model's generalization could potentially be enhanced.

The model is effectively learning the patterns in the training data, which is why the loss decreases rapidly in the initial epochs. The validation loss typically decreases more

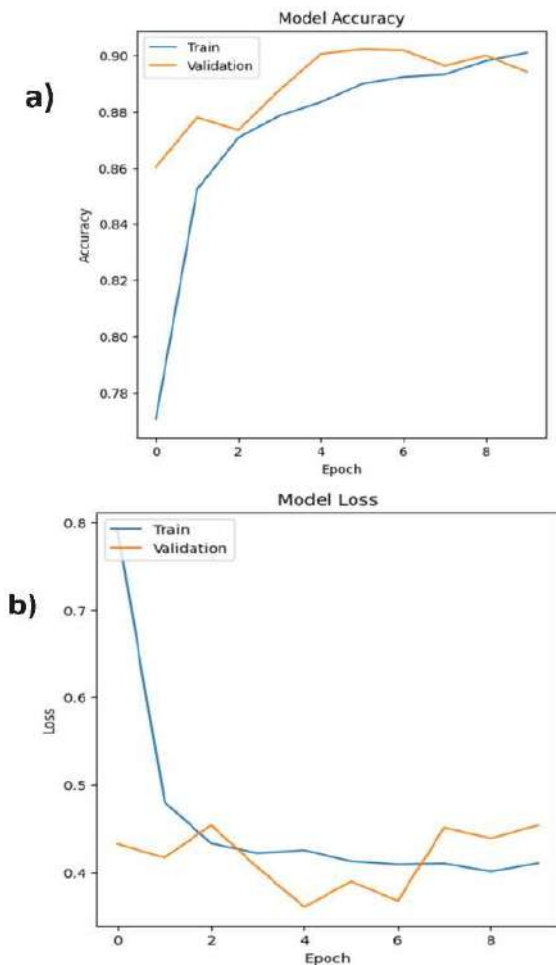


Fig. 2: Evaluation of the InceptionNet model showing (a) Training and validation accuracy, (b) Training and validation loss.

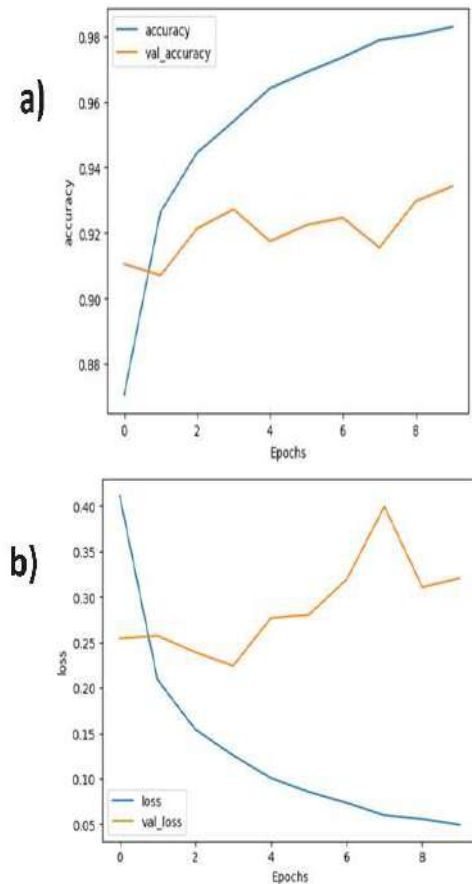


Fig. 3: Evaluation of the MobileNet model showing (a) the training and validation accuracy, (b) the training and validation loss.

slowly because the model is trying to generalize to unseen data. Validation loss shows how well the model performs on data it hasn't seen before, which is why the decrease is more gradual. Increasing the amount of training data or improving its quality can help the model generalize better.

The graph in Fig. 3a illustrates the MobileNet model's accuracy, with the training accuracy showing a consistent upward trend and the validation accuracy also improving, reaching a peak of 93.42%. The graph in Fig. 3b displays the model's loss, with training loss rapidly decreasing and leveling off, while validation loss declines with greater fluctuations, indicating some inconsistency in the model's performance on unseen data.

The accuracy graph for the ResNet model in Fig. 4a demonstrates a positive trend in learning performance across epochs. After an initial steep climb, the model's accuracy stabilizes, showcasing the effectiveness of the training process, and notably achieves a peak validation accuracy of 96.8%. The elevated validation accuracy suggests that the model possesses robustness and an aptitude for generalizing

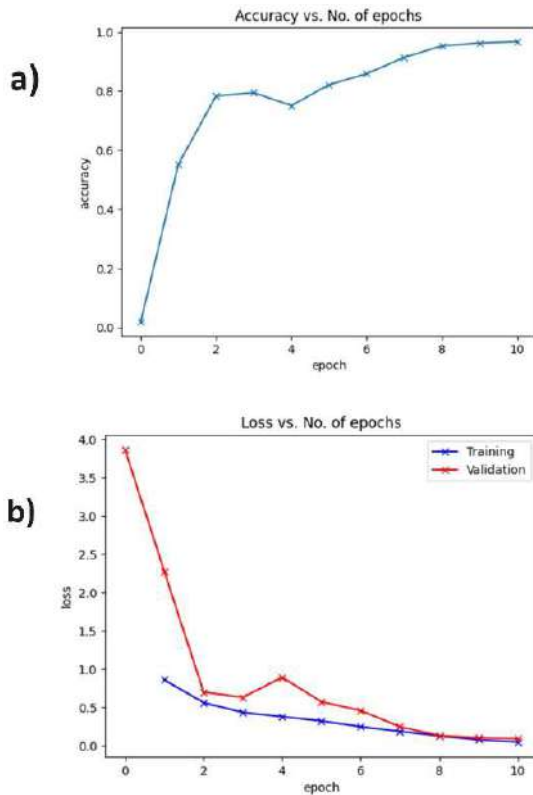


Fig. 4: Evaluation of the ResNet model showing (a) the training and validation accuracy, (b) the training and validation loss.

effectively to new, unseen data. The loss graph in Fig. 4b complements this by showing a rapid decrease in training loss, which is a sign that the model effectively minimizes errors during training. The validation loss follows a downward trend with some fluctuations, which is common in model training dynamics. These fluctuations are minor, and the overall trajectory indicates good convergence without signs of overfitting, affirming the model's strong predictive capability throughout its training epochs.

The accuracy graph for the ResNeXt model in Fig. 5a demonstrates excellent learning efficiency, with a swift rise to high accuracy levels after the initial epoch and sustaining a commendably high accuracy thereafter. Notably, the model attained a peak validation accuracy of 98.2%, reflecting its superior capability in generalizing from the training

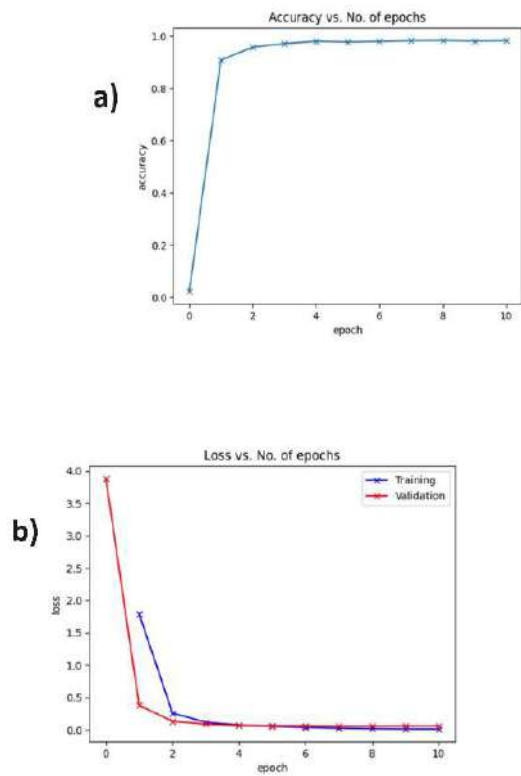


Fig. 5: Evaluation of the ResNeXt model showing (a) Validation accuracy vs Epoch (b) Training and validation loss.

data to unseen data. In parallel, the loss graph in Fig. 5b presents a favorable decrease in both training and validation loss, suggesting that the model is accurately capturing the underlying patterns without overfitting. The convergence of loss values at low levels towards the end of the training indicates that the model's performance is both stable and highly optimized.

The graphs in Fig. 6 depict the learning rate schedules for the ResNet and ResNeXt models across various batches of training. Both show a learning rate that initially ramps up, peaks at an intermediate point, and then decays. This pattern follows a cyclical learning rate policy, where the learning rate is increased to potentially help the model escape local minima and then decreased to allow for finer convergence to a minimum. The shape of the curve is smooth

Table 3: Showing comparative performance analysis of the four models used.

Model	Accuracy at the last epoch	Loss at last epoch	Train Loss Trend	Valid Loss Trend	Accuracy Stability
ResNet	0.9680	0.0925	Decreasing	Decreasing	High
ResNeXt	0.9818	0.0607	Decreasing	Decreasing	High
InceptionNet	0.8941	0.4536	Decreasing to stable	Fluctuating	Moderate
MobileNet	0.9342	0.3205	Decreasing	Fluctuate	Moderate

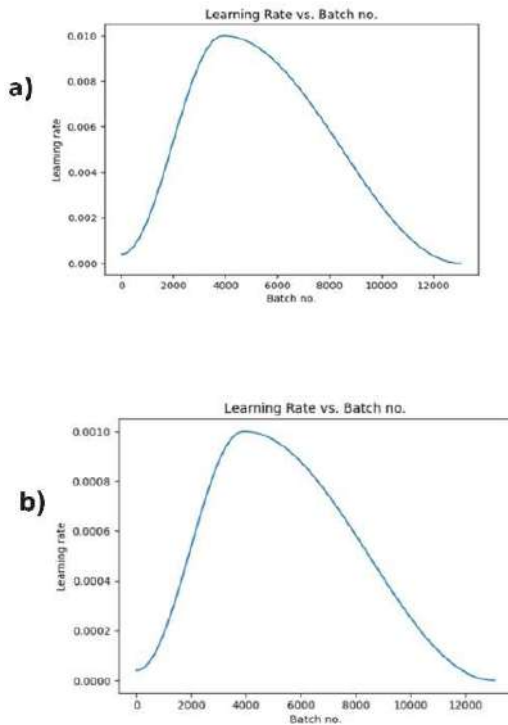


Fig. 6: Graphs showing the learning rate schedule for (a) the ResNet model and (b) the ResNeXt model.

and symmetrical for both models, suggesting a well-tuned learning rate strategy that could contribute to effective training and optimization of the neural networks.

Early detection of crop diseases plays a crucial role in achieving high agricultural yields. To ensure optimal productivity, it's vital to incorporate advanced technologies in the early identification of plant diseases. Deep learning models have been recognized for their effectiveness in image classification through a review of relevant literature. Specifically, models built upon transfer learning are well-known for their efficiency in simplifying the training process and diminishing the necessity for extensive datasets. In this study, our primary goal was to evaluate the performance of four pre-trained models—ResNet, ResNeXt, InceptionNet, and MobileNet—to identify the most effective model for the classification of various plant diseases. We evaluated these models using metrics such as accuracy and validation loss. Notably, the ResNeXt model demonstrates superior results, likely due to its more complex architecture that allows for better feature representation and generalization, especially in handling diverse plant disease image data. The validation accuracy for each model was computed, and a visual representation of these accuracies is presented in Table 2. Our analysis showed that the ResNeXt model (Fig. 5) surpassed the other models (Figs. 2-4) in performance, achieving the

highest validation accuracy of 0.982. From Table 3, we can see that the accuracy stability is high, indicating consistent performance across epochs, and the loss at the final epoch is also the lowest among the three models, which is generally a good indicator of model performance.

## CONCLUSIONS

In this study, our main focus was on conducting a comparative analysis of different transfer learning models. The goal was to determine the most efficient architecture for accurately classifying a total of 47 distinct plant disease categories. Our comparative results revealed that ResNeXt surpassed the performance of ResNet, InceptionNet, and MobileNet in terms of accuracy. Therefore, ResNeXt is preferable for the task of identifying plant diseases, especially when integrating new diseases into the model, as it shows a lower complexity in training. The model we proposed attained a noteworthy classification accuracy of 98.2%. In future research, we aim to address the challenges of creating a deep learning model that can identify plant diseases from clusters of leaves, moving beyond the analysis of individual leaves. In addition, future research will focus on how meteorological conditions such as wind, rain, or dust affect leaf appearance while forecasting plant diseases. Another issue that needs to be focused on is the possibility of images containing extraneous background elements, which lowers the classification accuracy.

## REFERENCES

- Ali, A.H., Youssef, A., Abdelal, M. and Raja, M.A., 2024. An ensemble of deep learning architectures for accurate plant disease classification. *Ecological Informatics*, 81, pp.1–10.
- Amin, H., Darwish, A., Hassani, A.E. and Soliman, M., 2022. End-to-end deep learning model for corn leaf disease classification. *IEEE Access*, 10, pp.31103–31115.
- Amudha, M. and Brindha, K., 2022. Multi techniques for agricultural image disease classification and detection: A review. *Nature Environment & Pollution Technology*, 21, pp.100–110.
- Appe, S.N., Arulselvi, G. and Balaji, G.N., 2023. Detection and classification of dense tomato fruits by integrating coordinate attention mechanism with the YOLO model. In: *Handbook of Research on Deep Learning Techniques for Cloud-Based Industrial IoT*. IGI Global, pp.278–289.
- Baranwal, S., Khandelwal, S. and Arora, A., 2019. Deep learning convolutional neural network for apple leaves disease detection. *SSRN Electronic Journal*, pp.1–8.
- Elfatimi, E., Eryigit, R. and Elfatimi, L., 2022. Beans leaf disease classification using MobileNet models. *IEEE Access*, 10, pp.9471–9482.
- Gupta, A., Yadav, D., Raj, A. and Pathak, A., 2023. Real-time object detection using SSD MobileNet model of machine learning. *International Journal of Engineering and Computer Science*, 12, pp.25729–25734.
- Harte, E., 2020. Plant disease detection using CNN. *ResearchGate*, 8(1), pp.45–52.
- Hassan, S.M. and Maji, A.K., 2022. Plant disease identification using a novel convolutional neural network. *IEEE Access*, 10, pp.5390–5401.



- Khattak, A., Khan, A., Rehman, M., Ahmed, F. and Ali, S., 2021. Automatic detection of citrus fruit and leaves diseases using deep neural network model. *IEEE Access*, 9, pp.112942–112954.
- Lakshmanarao, M.R.B. and Kiran, T.S.R., 2021. Plant disease prediction and classification using deep learning ConvNets. In: *Proceedings of the International Conference on Artificial Intelligence and Machine Vision (AIMV)*. Gandhinagar, India: IEEE, pp.1–6.
- Pherry, F., Kristanto, G.J. and Kurniadi, F.I., 2022. Rice plants disease classification using transfer learning. In: *Proceedings of the 4th International Conference on Cybernetics and Intelligent Systems (ICORIS)*. Prapat, Indonesia: IEEE, pp.1–4.
- Polly, R. and Devi, E.A., 2024. Semantic segmentation for plant leaf disease classification and damage detection: A deep learning approach. *Smart Agricultural Technology*, 9, pp.1–12.
- Rithik, J.P., Devi, S.R.S., Brendan, M.A. and R., S., 2023. Plant disease classification using deep learning approach (VGG19). In: *Proceedings of the 9th International Conference on Advanced Computing and Communication Systems (ICACCS)*. Coimbatore, India: IEEE, pp.1715–1718.
- Sagar, A. and Jacob, D., 2020. On using transfer learning for plant disease detection. *ResearchGate*, 5(2), pp.12–18.
- Sharma, V. and Singh, N., 2021. Deep convolutional neural network with ResNet-50 learning algorithm for copy-move forgery detection. In: *Proceedings of the 7th International Conference on Signal Processing and Communication (ICSC)*. Noida, India: IEEE, pp.146–150.
- Sudhakar, M. and Priya, R.M., 2023. Computer vision based machine learning and deep learning approaches for identification of nutrient deficiency in crops: A survey. *Nature Environment & Pollution Technology*, 22(3), pp.145–152.
- Sunil, C.K., Jaidhar, C.D. and Patil, N., 2022. Cardamom plant disease detection approach using EfficientNetV2. *IEEE Access*, 10, pp.789–804.
- Wang, Q., He, G., Li, F. and Zhang, H., 2020. A novel database for plant diseases and pest classification. In: *Proceedings of the IEEE International Conference on Signal Processing, Communications and Computing (ICSPCC)*. Macau, China: IEEE, pp.1–5.
- Yadav, D., Jalal, A.S., Garlapati, D., Hossain, K., Goyal, A. and Pant, G., 2020. Deep learning-based ResNeXt model in phycological studies for future. *Algal Research*, 50, pp.1–10.
- Zhao, Y., Li, J., Xu, F. and Kim, D., 2021. Plant disease detection using generated leaves based on DoubleGAN. *IEEE/ACM Transactions on Computational Biology and Bioinformatics*, 18(6), pp.1–1.
- Zhou, C., Zhou, S., Xing, J. and Song, J., 2021. Tomato leaf disease identification by restructured deep residual dense network. *IEEE Access*, 9, pp.28822–28831.

# Impact of Landfill Proximity on Soil Quality: A Comparative Study of Dumping and Non-Dumping Sites Near Srinagar, Garhwal, Uttarakhand

Ajay Negi<sup>1</sup>  and Ashok Kumar Meena<sup>2</sup> 

<sup>1</sup>School of Life Sciences, Hemvati Nandan Bahuguna Garhwal University (A Central University), Srinagar (Garhwal)-246 174, Uttarakhand, India

<sup>2</sup>Department of Environmental Sciences, Hemvati Nandan Bahuguna Garhwal University (A Central University), Srinagar (Garhwal)-246 174, Uttarakhand, India

†Corresponding Author: Ashok Kumar Meena: ashokenviro.hnbgu@gmail.com

**Abbreviation:** Nat. Env. & Poll. Technol.  
**Website:** [www.neptjournal.com](http://www.neptjournal.com)

*Received:* 21-08-2024

*Revised:* 26-09-2024

*Accepted:* 16-10-2024

## Key Words:

Municipal solid waste  
 Landfill  
 Soil quality

## ABSTRACT

The present study aims to analyze changes in the physicochemical parameters of the soil in the vicinity of a small municipal solid waste landfill site. The research results were analyzed based on general physicochemical properties, which include pH, electrical conductivity (EC), organic carbon (OC), available nitrogen (N), phosphorus (P), and potassium (K) by using standard methods. The results show that the soil from the dump sites contained higher amounts of soil properties (EC, SOC, N, P, K) than the non-dumping sites. Pearson correlation shows that pH exhibits a robust negative correlation with all other parameters while the remaining other parameters had a positive correlation with each other. Also, PCA analysis shows dumping sites mostly depict positive values in PC1, whereas the non-dumping sites indicate negative values. The final interpretation indicates that the soil in the dump site was found suitable for plant growth. However, due to improper solid waste management, this nutrient-rich soil could be mixed up with several other contaminants, such as soluble salts, plastics, heavy metals, and so on. This could make the soil unhealthy or unsuitable for plant growth. The study also suggests proper segregation, recovery, treatment, and safe disposal of solid waste and formulates an integrated municipal solid waste management plan for this particular dumping site.

## Citation for the Paper:

Negi, A. and Meena, A. K., 2025. Impact of landfill proximity on soil quality: A comparative study of dumping and non-dumping sites near Srinagar, Garhwal, Uttarakhand. *Nature Environment and Pollution Technology*, 24(2), p. B4259. <https://doi.org/10.46488/NEPT.2025.v24i02.B4259>

*Note: From year 2025, the journal uses Article ID instead of page numbers in citation of the published articles.*

## INTRODUCTION

Solid waste management is one of the important obligatory functions of the municipal authorities. Except for a few large cities, local bodies of medium and smaller towns have not undertaken regular exercises on the quantification, characterization, and disposal of municipal solid wastes. The waste characterization showed that municipal solid wastes typically contain about 50% organic waste, 17% recyclables, 11% hazardous, and 21% inert. However, some amount of all MSW is not collected at all and hence lies littered in the city/town and finds its way to nearby open areas /drains and water bodies, causing clogging of water percolation, choking of drains, and pollution of surface water. Unsegregated waste collection and transportation lead to dumping in the open, which generates leachate and gaseous emissions besides causing nuisance in the surrounding environment. Leachate contaminates the groundwater as well as surface water in the vicinity (Municipal Solid Waste (Management & Handling) Rules, 2000).

The rapid population growth in developing countries like India accelerates industrialization and urbanization which results in the generation of solid waste exponentially. Solid waste has become a major environmental issue in India. The country generates a total of 160038.9 TPD (tonnes per day) of solid waste, out of which 152749.5 TPD is collected with an efficiency rate of 95.4%. 79956.3 metric tonnes per day (50%) of trash undergoes treatment, while 29427.2 metric



**Copyright:** © 2025 by the authors  
**Licensee:** Technoscience Publications  
 This article is an open access article distributed under the terms and conditions of the Creative Commons Attribution (CC BY) license (<https://creativecommons.org/licenses/by/4.0/>).

tonnes per day (18.4%) are disposed of in landfills. 50655.4 TPD, representing 31.7% of the total garbage created, is unaccounted for. India's per capita solid waste generation in the year 2020-21 was 119.07 grams per day, according to the Central Pollution Control Board (CPCB, 2020-21).

The total amount of solid waste generated in Uttarakhand is approximately 1458.46 Tonnes Per Day (TPD). Out of this, 1378.99 TPD is collected, and 779.85 TPD undergoes treatment, according to the Central Pollution Control Board (CPCB) report for the year 2020-21. The garbage can be either incinerated or illegally deposited on vacant ground within the urban local bodies of the state, resulting in substantial environmental harm and posing a concern to human health. The creation of municipal garbage in Uttarakhand is projected to increase, resulting in an estimated total of 9.0 million tonnes of rubbish being produced between 2014 and 2041, according to the Draft Urban Municipal Garbage Management Action Plan for Uttarakhand state in 2015.

A significant amount of solid waste produced in and around Srinagar town was dumped at a dump site at Srinagar Garhwal. This municipal solid waste was an inevitable byproduct of human and constructional activities, which was disposed of through dumping. This open dump was unsightly, unsanitary, and smelly and attracted scavenging animals, rats, insects, pigs, pests, etc.

Spreading over an area of 9 sq. km, the Srinagar Municipality is divided into 9 municipal wards for undertaking solid waste management. The municipality is involved in door-to-door collection, street sweeping, drain desilting, collection, and transportation of waste from all 9 wards of the town. As per the current estimates of the Srinagar Municipality, about 7.07 tons of solid waste is generated daily in Srinagar. The physical composition of the MSW produced in Srinagar town as: Organic waste (58%), plastic (20.85%), paper (11.16%), glass (7%), rubber & textile (6.23%), and metal (1.37%) (City Sanitation Plan, Srinagar Municipality 2017).

MSW compost contains large amounts of organic matter, and macronutrients play a key role in improving soil properties such as water retention capacity, fertility, and productivity. There are various studies revealed that these valuable nutrients get mixed with toxic chemicals and spread over the surrounding soil with time damaging the upper layer of the soil, distorting soil fertility, and affecting plant life. When rainwater comes into contact with dumping yards, it produces a liquid called leachate. This leachate then seeps through the layers of soil and, over time, contaminates the groundwater and soil in the surrounding area (Deshmukh & Aher 2017). This contamination can be

harmful to plants when they absorb it through their roots. Consuming plants and animals that have been exposed to contaminated soils can have adverse effects on human health. Oyeboode et al. (2023) proposed that effective remediation methods should be applied to prevent continued contamination of groundwater and soil by leachates released from landfills and waste sites.

Therefore, the focus of the present study is to determine the nutrient status (N, P, K) and their monthly variation in and around the municipal solid waste dumping site so that we can assess the impact of solid waste on soil quality nearer to the solid waste landfill site.

## MATERIALS AND METHODS

### Study Area

The study was carried out in Srinagar town of Garhwal Himalaya in District Pauri Garhwal, Uttarakhand (Fig. 1, Table 1). Srinagar is a municipality in the district of Pauri Garhwal, Uttarakhand. The Srinagar city is divided into 9 wards. The selected study area in and around the MSW dumping yard is located in the Srinagar town of Uttarakhand, India (Fig. 1). This area is located on the left bank of the Alaknanda River. The dumping site is situated at an altitude of 534.4 masl. It lies between latitude 30° 13' 33.707" N and longitude 78° 47' 8.101" E. It covers an area of 1537.31 m<sup>2</sup> and is situated near to Nagar Palika Road.

### Demography and Literacy

The population of the Srinagar Garhwal municipality is 20,115, with 10,751 being males and 9,364 being females. The population of children aged 0-6 in Srinagar Garhwal is 2142, accounting for 10.65% of the total population. The female sex ratio in the Srinagar Garhwal Nagar municipality is 871, which is lower than the state average of 963. Furthermore, the child sex ratio in Srinagar Garhwal is approximately 864, which is lower than the average child sex ratio of 890 in the state of Uttarakhand. The literacy rate in Srinagar Garhwal city is 92.03%, which is higher than the state average of 78.82%. The male literacy rate in Srinagar Garhwal is approximately 94.22%, while the female literacy rate is around 89.51% (Census India 2011).

### Climate

The climate of Srinagar Garhwal is sub-tropical monsoon type (mild winter, hot summer). The town is situated on the bank of Alaknanda, so in winter, temperature & humidity affect the weather very much. Due to the river bank, dense fog is often seen in mild winter, but at noon, it is clear shiny weather. Opposite to this in summer, there is

very humid weather; temperature and humidity are at its top level. Maximum temperature is 40°C whereas the minimum temperature is 0.3°C and the mean annual rainfall is 1210 mm.

**Wards:** The Srinagar town is divided into nine wards by the municipal council. There are nine wards with different populations in the town (Table 2).

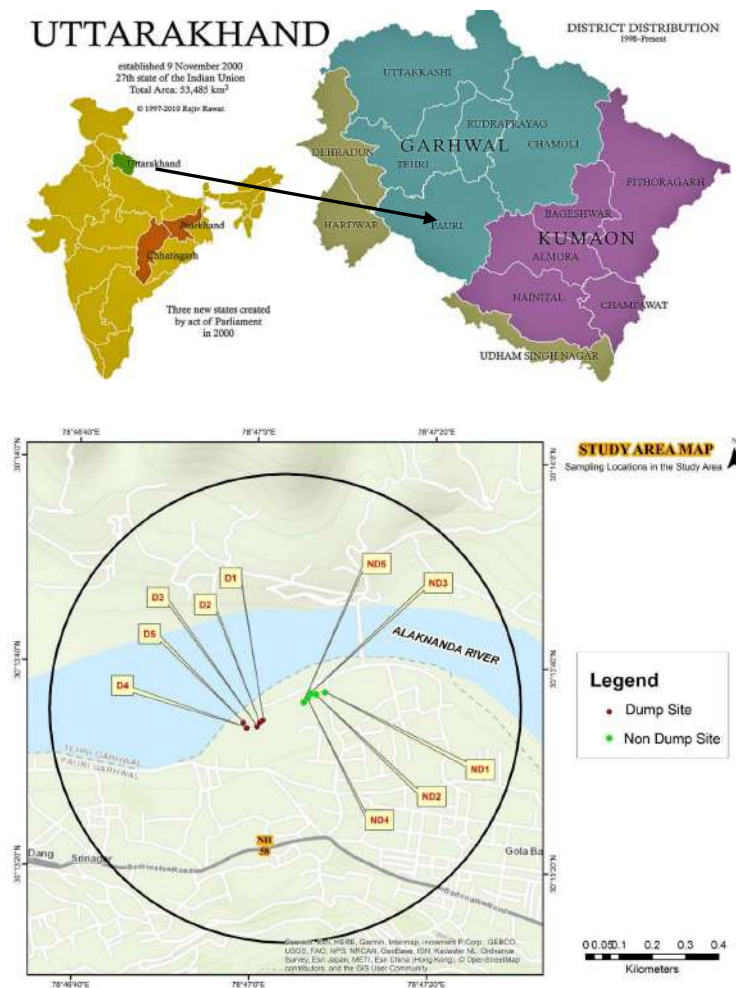


Fig. 1: Mapping of study area and demarcation of studied site.

Table 1: Location of sampling area.

Land Use	Site	Altitude (masl)	Latitude	Longitude
Municipal solid waste Dumpsite	D1	534.3	30° 13' 34.540" N	78° 47' 1.201" E
	D2	532.4	30° 13' 34.278" N	78° 47' 0.812" E
	D3	528.3	30° 13' 33.889" N	78° 47' 0.528" E
	D4	535.1	30° 13' 33.707" N	78° 46' 59.361" E
	D5	534.4	30° 13' 34.237" N	78° 46' 58.992" E
Municipal solid waste non-dump site	ND1	525.8	30° 13' 37.346" N	78° 47' 8.101" E
	ND2	531.1	30° 13' 37.118" N	78° 47' 7.139" E
	ND3	527.2	30° 13' 37.227" N	78° 47' 6.489" E
	ND4	525	30° 13' 36.750" N	78° 47' 6.148" E
	ND5	529.2	30° 13' 36.320" N	78° 47' 5.731" E



Table 2: Profile of wards, Srinagar NPP (City Sanitation Plan, 2017).

Ward No.	Name	Area (Ha.)	Families	Population	Total Solid waste production (T/day)
1.	Agency Mohalla	140	727	3946	1.246
2.	Upper Bazar	75	323	1640	0.517
3.	Ganesh Bazar	115	1029	5006	1.580
4.	Mochi Tamta Mohlla	42	328	1761	0.556
5.	Niranjani Marg	77	437	1980	0.625
6.	Mishtri Mohlla	87	313	1663	0.525
7.	Kamleshwar Bagwan	112	740	3361	1.061
8.	S.S.B.	87	145	667	0.210
9.	Shitla Mata Temple	165	372	2376	0.750
	Total	900	4414	22400	7.07

## Methodology

The Investigation to evaluate the soil properties in and around the open dumping site in Srinagar Garhwal of Uttarakhand state, soil samples were collected from two land use types i.e., open dumping site and non-dumping site. Thus, from two land uses soil samples were collected to determine soil physio-chemical properties (Texture, pH, EC, OC, N, P, K).

### Soil Sample Collection and Analysis

The soil samples were collected in and around the municipal solid waste dumping and non-dumping sites of Srinagar Garhwal. The topsoil was cleaned by removing waste and samples were collected by digging 0-15 cm depth. Soil samples were collected in fresh polythene bags and labeled properly then samples were analyzed in a laboratory for physio-chemical analysis. The samples were air-dried by spreading them on a tray. The sample was sieved using a 2 mm sieve for further chemical and nutrient analysis, i.e., pH, electrical conductivity (EC), organic carbon (OC), available nitrogen (N), phosphorus (P), and potassium (K) by using standard methods (Table 3).

Table 3: Methods used for the analysis of soil.

Parameter	Method	Reference
Texture	Sieve method	Bouyoucos (1962)
pH (1:2 soil: water)	Potentiometry	Jackson (1973)
EC (1:2 soil: water)	Conductometry	Jackson (1973)
Organic carbon (%)	Wet oxidation method	Walkley and Black (1934)
Available Nitrogen [kg.ha <sup>-1</sup> ]	Micro distillation method	Subbiah and Asija (1956)
Available Phosphorus [kg.ha <sup>-1</sup> ]	Spectrophotometry	Jackson (1973)
Available Potassium [kg.ha <sup>-1</sup> ]	Flame photometry	Jackson (1973)

## RESULTS AND DISCUSSION

### Analysis of Physical Parameter of Soil

Analysis of soil samples indicated that the texture proportions in the study area were in order of sand>silt>clay. Sand ranged from 55.42% to 68.85% with a mean value of 63.54%, silt ranged from 10.7% to 21.82% with a mean value 15.06%, and clay was ranged from 18.86 % to 24.60% with a mean value of 21.55% in the open dumping site which depicts that the soil belongs to sandy clay loam in texture whereas in non-dumping site sand is ranged from 53.42%-59.16% with mean value 56.03%, silt is ranged from 18.15%-25.51% with mean value 21.13% and clay is ranged from 20.24%-25.13% with mean value 22.87% which depicts that the soil belongs to sandy clay loam in texture (Table 4).

The higher proportion of sand followed by silt and clay could be because of the Alaknanda River bank area, where usually soil finer particles flow away, leaving coarse particles of sand. A similar kind of texture was found by Loughry (1973), who opined that the dumpsites, which dominantly contain high sand fractions and low clay content, allow water and leachates to percolate through the soil, degrade its quality and cause water pollution.

The two sites in consideration also have comparable soil textures with sandy clay loam texture classification due to the dominance of sand. However, the dump site appears to have greater fluctuations in the amount of sand and silt, which indicates that there are external factors such as dumping activities. As there is higher sand content in the dump sites, which suggests elevated permeability, this can also result in the downward migration of contaminants further down the soil and water table. This is congruent with Loughry (1973) and underscores the threat of uncontrolled dumping, for whatever reason, near river banks. The similar texture classification of sandy clay loam in both sites indicates the

Table 4: Soil texture around MSW dump sites and non-dump sites.

Site	Soil sample	Texture %			Texture class
		Sand	Silt	Clay	
Dumpsite	D1	55.73	21.82	23.38	Sandy clay loam
	D2	68.58	10.7	20.71	Sandy clay loam
	D3	68.85	12.28	18.86	Sandy clay loam
	D4	63	16.69	20.23	Sandy clay loam
	D5	61.55	13.83	24.60	Sandy clay loam
	<b>Mean</b>	<b>63.54±5.45</b>	<b>15.06±4.37</b>	<b>21.55±2.36</b>	<b>Sandy clay loam</b>
Non-dump site	ND1.	53.42	21.44	25.13	Sandy clay loam
	ND2	59.16	18.15	22.16	Sandy clay loam
	ND3	57.77	18.73	23.48	Sandy clay loam
	ND4	55.73	21.82	23.38	Sandy clay loam
	ND5	54.07	25.51	20.24	Sandy clay loam
	<b>Mean</b>	<b>56.03±2.42</b>	<b>21.13±2.93</b>	<b>22.87±1.81</b>	<b>Sandy clay loam</b>

effect of the river Alaknanda caused sedimentation and also the factors like waste disposal contributed to the soil texture. Although in the non-dump site, it is expected to be moisture-retentive silt clay soil as well, the fact that this is only slightly the case suggests that, yes, more water is available for plants in this area than in the dump site. The high level of sand in both sites means that the soil is well-drained but has little moisture and nutrient retention (especially at the dump site). According to this, too, clay content is low, which means sand is easily eroded by each swept contaminant in the waste, deteriorating soil profile as well as groundwater. The higher amount of silt in the non-dump sites means that more moisture and nutrients could be retained, suggesting fairly good quality of soil. However, it can also be concluded that the presence of sandy clay loam at the dump site increases the risk of environmental pollution by enhancing leachate movement in the soil.

### Analysis of Chemical Parameter of Soil

The present study compares the soil quality index (SQI) of two distinct sites, Dumping (D) and Non- Dumping (ND), which includes pH, Electrical Conductivity (EC), Soil Organic Carbon (SOC), Nitrogen (N), Phosphorus (P), and Potassium (K) (Fig. 2).

Dumping sites had a mean pH of 6.524, which indicates slightly acidic soil conditions, whereas non-dumping sites had a mean pH of 7.224, which indicates neutral to slightly alkaline soil (Table 5). This difference in pH may occur due to nutrient availability and may also be affected by microbial activities in both sites. The results depict the acidic nature of the soil at the dump site and the basic nature of the non-dump site. The presence of a lower value of pH at the dumping

site suggested that the soil samples were contaminated by municipal solid waste having organics, which might have decreased the pH (Kanmani & Gandhimathi 2013). The more acidic pH level identified in the dumping sites suggests waste breakdown and leachate concentration have contributed to soil acidification, which can have adverse effects on nutrient availability, microbial activities, and plant growth. There was no such geochemical alteration as in the case of the neutral pH in non-dumping sites, which is more favorable for soil and supports better vegetation growth and nutrient cycling. Under the existing dump conditions, the slightly acidic conditions in the dump sites are quite alarming as they are likely to cause soil and environmental degradation. It, therefore, calls for waste management practices and remediation measures.

Electrical Conductivity (EC), which measures soil salinity, is higher at the Dumping site (mean of  $0.7136 \text{ dS.m}^{-1}$ ) compared to the non-dumping site (mean of  $0.4296 \text{ dS.m}^{-1}$ ), indicating that the Dumping site has a higher salt concentration (Table 5). The values of EC fall under the normal rating charts. The highest EC was recorded in the soil samples collected from dump sites and the lowest from non-dump sites. High EC in the samples close to the dump yard may be due to the presence of large amounts of ionic substances and soluble salts released from the MSW dump as compared to the natural soil samples (Deshmukh 2012). Soil Organic Carbon (SOC) is much higher at dumping sites (1.0224%) compared to non-dumping sites (0.6272%), which indicates high organic matter at dumping sites (Table 5). Munoz et al. (1994) reported that biodegradable municipal solid wastes were the major contributor to increased organic matter in soil.

Nitrogen (N) levels are also higher at the Dumping site (mean of  $332.5624 \text{ kg.ha}^{-1}$ ) than at the non-dumping

Table 5: Comparative data analysis of different soil chemical parameters at dumping and non-dumping sites.

Sites	Samples	pH	EC	SOC	N	P	K
Dumping Sites	D1	6.56	0.566	0.862	332.778	27.962	303.95
	D2	6.22	0.876	1.196	342.998	29.852	309.874
	D3	6.9	0.642	0.99	333.054	27.924	297.474
	D4	6.72	0.546	0.91	319.218	26.334	297.528
	D5	6.22	0.938	1.154	334.764	29.704	306.466
	Mean	6.524 $\pm$ 0.302	0.713 $\pm$ 0.181	1.022 $\pm$ 0.147	332.562 $\pm$ 8.545	28.355 $\pm$ 1.456	303.058 $\pm$ 5.491
Non-dumping Sites	ND1	7.26	0.376	0.522	252.916	20.652	227.98
	ND2	7.04	0.392	0.568	263.246	17.998	241.298
	ND3	7.36	0.44	0.676	247.156	18.924	237.33
	ND4	7.34	0.462	0.682	254.21	20.522	227.488
	ND5	7.12	0.478	0.688	256.504	20.146	222.374
	Mean	7.224 $\pm$ 0.139	0.429 $\pm$ 0.044	0.627 $\pm$ 0.076	254.806 $\pm$ 5.843	19.648 $\pm$ 1.147	231.294 $\pm$ 7.770

site (mean of 254.8064 kg.ha<sup>-1</sup>), which could lead to more vigorous plant growth at the Dumping site (Table 5). These values reflect that the nitrogen is found in the medium range at the dump site while it is found in the low to medium range at non-dump sites. Nitrogen content in the dumping site's soil was recorded as higher than in the non-dump site's soil. Higher nitrogen content at the dumping sites might be due to higher organic matter content of the soil contributing to higher available nitrogen in the soil (Ouled et al. 2014).

Dumping sites had mean values of Phosphorus (P) and Potassium (K) 28.3552 mg.kg<sup>-1</sup> and 303.0584 mg.kg<sup>-1</sup>, respectively, compared to 19.6484 mg.kg<sup>-1</sup> of P and

231.294 mg.kg<sup>-1</sup> of K at the non-dumping site (Table 5). These differences suggest that Dumping sites were more fertile and might support higher crop yields, provided the slightly acidic pH was managed appropriately. The phosphorus availability was recorded as higher in dump sites whereas lowest in non-dump sites due to high organic matter in the dumpsite soil as a result, which in turn increased the proportion of soil phosphorus (Ouled et al. 2014). The above results reflect that the potassium found maximum in dump sites than in non-dump sites due to high organic matter at the dumpsite soil as a result which in turn increased the proportion of soil potassium present as exchangeable potassium (Ouled et al. 2014).

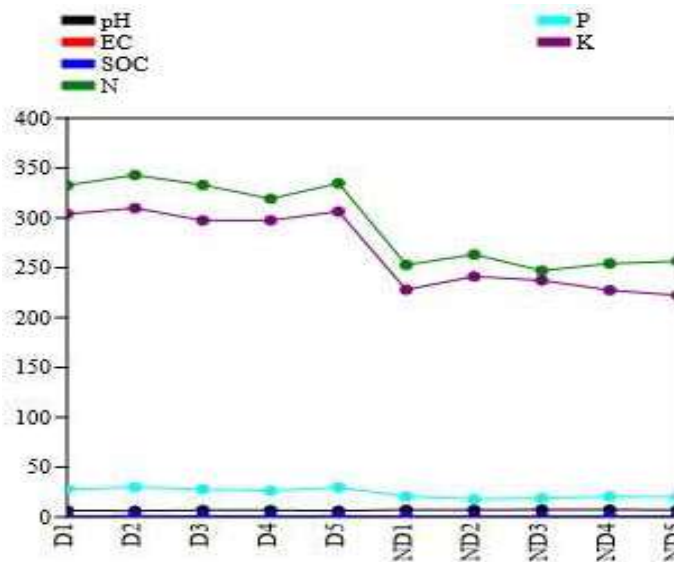


Fig. 2: Plotting of different chemical parameters of analyzed soil.

In conclusion, the dumping sites are more enriched in nitrogen, phosphorus, potassium, and SOC due to waste decomposition phenomena. It should be noted, however, that the mildly acidic pH and greater EC at the dump sites may eventually negatively affect the plant's nutrition, health, and microbiological activity. They may lead to some additional soil salinity and contamination as, a phenomenon which deteriorates the soil even further. Non-dumping sites characterized by neutral pH, lower EC, and more appropriate nutrient distribution are more favorable for soil conditions on a long-term basis. Therefore, nutrient recycling in these sites is effective and promotes sustained agronomical practice and plant development whilst lowering the risks of pollution. The present study shows that non-dumping had lower nutrient levels (particularly SOC, N, P, and K), which suggests that soil amendments are required to achieve optimal crop production. Also, the neutral to slightly alkaline pH of non-dumping sites might be more suitable for particular crops, but it could act as a limiting factor in crop growth without proper soil management.

### Statistical Analysis of SQI

Table 6 depicts the Pearson correlation in studied soil quality parameters. pH exhibits a robust inverse relationship with all other factors. This indicates that as the pH level rises, the levels of EC, SOC, N, P, and K fall. In this common situation, elevated pH levels (indicating more alkaline soil) can diminish the accessibility of vital nutrients such

as nitrogen, phosphate, and potassium, as well as organic carbon.

The EC shows a strong positive correlation with SOC, N, P, and K, which indicates that EC was increased with increasing SOC, N, P, and K. It could imply more soil fertility or more decomposition of organic matter in the soil. The SOC shows a very strong positive correlation with EC, N, P, and K. Nitrogen shows a very strong positive correlation with P and K. This indicates that soils with high nitrogen content also have high levels of phosphorus and potassium, both of which are important for plant growth. The significant correlation could be attributed to the interdependence of these nutrients on organic matter. Phosphorus shows a very strong positive correlation with N and K, suggesting that these elements mostly coexist in the soil. This phenomenon could be due to shared origins, such as the use of identical fertilizers or their response to comparable soil conditions.

PCA is a very useful multivariate statistical tool, particularly in this study, to examine the interactions of pH, EC, SOC, N, P, and K in regard to various soil quality measures and to resolve any difficulties regarding the measurement of complex datasets. Here's how it works in this study: PC1 (the first principal component) shows the greatest amount of variance and the clearest separation between such sites as dumping and non-dumping. PC1 in this study is said to be strongly influenced by SOC, nitrogen (N), phosphorus (P), and potassium (K), meaning that these factors are serviceable in giving out the functionality of soil

Table 6: The correlation table represents the Pearson correlation coefficients between different soil quality parameters.

	pH	EC	SOC	N	P	K
pH		-0.89397	-0.88651	-0.90181	-0.88953	-0.89147
EC	-0.89397		0.95845	0.81477	0.8656	0.79356
SOC	-0.88651	0.95845		0.90397	0.92939	0.89021
N	-0.90181	0.81477	0.90397		0.97203	0.98518
P	-0.88953	0.8656	0.92939	0.97203		0.94988
K	-0.89147	0.79356	0.89021	0.98518	0.94988	

Table 7: PCA data represent the relation of PC 1 to PC 6 with different dumping and non-dumping sites.

	PC 1	PC 2	PC 3	PC 4	PC 5	PC 6
D1	1.4759	0.88473	-0.26899	-0.1473	0.021069	-0.022407
D2	3.3371	-0.47804	-0.096794	0.047777	-0.10556	-0.041698
D3	1.4645	0.47049	0.66004	0.027893	-0.014499	0.15644
D4	1.0233	0.6548	0.0087711	0.14795	-0.05987	-0.13733
D5	3.258	-0.76821	-0.16491	-0.063858	0.15636	0.029423
ND1	-2.4044	0.16652	-0.10331	-0.36408	0.10575	-0.021681
ND2	-2.0723	0.1388	-0.60717	0.26804	-0.0005679	0.13385
ND3	-2.2084	-0.24797	0.27854	0.29725	0.12755	-0.092568
ND4	-2.0295	-0.31974	0.36671	-0.087519	-0.023654	-0.0062389



quality imbued with dumping and without digging. PC2 to PC6 are said to account the relatively less variance and explain primary variations. Although they offer increased understanding, they do not separate the two types slightly enough as PC1 does. PCA also assists in simplifying the data of the soil, especially in establishing the critical attributes that differentiate the soil's quality between gelatinous and non-gelatinous sites. In this way, it contributes to informing about the possible waste and its effect on soils and recommends some management parameters for soils.

The PCA analysis shows a clear segregation between the Dumping sites (D1 to D5) and non-dumping sites (ND1 to ND4), with PC1 showing a particularly pronounced split (Table 7). The Dumping sites mostly depict positive values in PC1, whereas the non-dumping sites indicate negative values. This analysis implies that PC1 may be capturing a noteworthy characteristic that differentiates these two groups. PC2 to PC6 shows a greater diversity within each study site, but the distinction between Dumping sites and non-dumping sites was not as pronounced (Table 7). This analysis indicates that the PC1 is highly influential in explaining the variability in the dataset, and it clearly distinguishes between the Dumping sites and non-dumping sites. PC2 to PC6 represent a lower amount of variance compared to the previous components (Table 7). Although they offer a further understanding of the data structure, their contributions are less impactful.

PC1 is the dominating component, majorly driven by P, N, and SOC shows a strong correlation among these soil quality parameters (Table 8). Whereas pH contrasts sharply and contributes negatively. PC2 shows secondary variability, and EC shows a strong negative correlation, which means it acts differently from other soil quality parameters. PC3 to PC6 shows regular less variance (Table 8). This PCA analysis helps in understanding the primary and secondary factors that influence soil health and fertility in the studied area.

Table 6 illustrates a prevailing pattern in which the majority of parameters exhibit either positive or negative correlations with one another. More precisely, there is a negative relationship between pH and other soil quality

indices, suggesting that soils with higher acidity or alkalinity tend to have lower nutrient levels. The parameters EC, SOC, N, P, and K have a positive correlation, suggesting that these elements collectively influence soil fertility and are likely to vary in the same direction. The correlation matrix offers useful insights into the interrelationships among different soil properties. The presence of strong positive relationships among EC, SOC, N, P, and K indicates that these parameters are interconnected and jointly impact soil fertility. Conversely, the negative associations with pH emphasize the significance of regulating soil acidity/alkalinity to uphold nutrient accessibility. Gaining insight into these relationships can provide valuable guidance for implementing more effective soil management strategies, especially in regions impacted by the disposal of solid waste, where the quality of the soil may be impaired.

## CONCLUSION

A total of seven parameters (soil texture, pH, EC, OC, N, P, K) were analyzed during the study period. Results of particle size analysis of soil samples indicated that soils in and around the MSW open dumping sites belong to sandy clay loam. The soil properties indicated that the dumping site is acidic, and the non-dumping site is alkaline in nature. The values of organic carbon and macronutrients (N, P, K) were found to be higher in the dump site than in the non-dump site. As per the soil fertility rating (FAO/WHO, 2001), the mean values of organic carbon and macronutrients (N, P, K) were found in the low category at the non-dump site, whereas the mean values were found in the medium category at the dump site.

From the above results, it is clear that the soil from the dump sites contained higher amounts of soil properties (pH, EC, OC, N, P, K) than the soil away from the dump sites. So as per the soil properties and the soil fertility rating, the soil in the dump site was found to be suitable for plant growth. But, due to improper solid waste management, this nutrient-rich soil could mix up with several other contaminants, such as soluble salts, plastics, heavy metals, and so on. This makes the soil unhealthy or unsuitable for plant growth. Proper segregation, recovery, treatment, and safe disposal, either

Table 8: PCA data represent the relation of PC 1 to PC 6 with different studied soil quality parameters.

	PC 1	PC 2	PC 3	PC 4	PC 5	PC 6
pH	-0.94982	0.067246	0.30366	0.014462	0.023003	0.01936
EC	0.92537	-0.37257	0.027386	-0.012711	0.052074	0.035394
SOC	0.96824	-0.17054	0.14933	0.082506	-0.057967	-0.030901
N	0.97088	0.22634	0.015862	-0.0020035	-0.040355	0.06541
P	0.97564	0.11125	0.10631	-0.153	0.0087144	-0.030886
K	0.95916	0.25592	-0.00065631	0.10096	0.06304	-0.018574

composting or sanitary landfill, will provide nutrient-rich organic soil for cultivating crops and for plantation purposes.

As a result, there is a need for integrated municipal solid waste management of the Srinagar dumping site to segregate the organic waste and utilize it as compost. Thus, the present study can be used in future monitoring and management of MSW in and around the dump site.

## REFERENCES

- Annual Report on Solid Waste Management, 2021. CPCB, Delhi, pp.1–50.
- Bouyoucos, G.J., 1962. Hydrometer method improvement for making particle size analysis of soils. *Agronomy Journal*, 54(2), pp.179–186.
- Census of India, 2011. Government of India, New Delhi, pp.1–100.
- City Sanitation Plan, 2017. Nagar Palika Parishad, Srinagar Garhwal, pp.1–35.
- Deshmukh, K.K., 2012. Studies on chemical characteristics and classification of soils from Sangamner area, Ahmednagar district, Maharashtra, India. *Rasayan Journal of Chemistry*, 5(1), pp.74–85.
- Deshmukh, K.K. and Aher, S.P., 2017. Assessment of soil fertility around municipal solid waste disposal site near Sangamner City, Maharashtra, India. *Current World Environment*, 12(2), pp.401–410.
- Draft Urban Municipal Waste Management Action Plan for State of Uttarakhand, 2015. Urban Development Directorate, Dehradun, 1, pp.1–60.
- Jackson, M.L., 1973. *Soil Chemical Analysis*. Prentice Hall of India Pvt. Ltd., New Delhi, pp.1–498.
- Joint FAO/WHO Expert Committee on Food Additives Meeting and World Health Organization, 2001. *Safety Evaluation of Certain Mycotoxins in Food* (No. 74). Food and Agriculture Organization, Rome, pp.1–150.
- Kanmani, S. and Gandhimathi, R., 2013. Assessment of heavy metal contamination in soil due to leachate migration from an open dumping site. *Applied Water Science*, 3(2), pp.193–205.
- Loughry, D.C., 1973. Instrument communications: A new interface system. *INTERCON 73 Conference Proceedings*, pp.150–160.
- Municipal Solid Waste Management Manual, 2000. Ministry of Urban Development, Government of India, pp.1–120.
- Municipal Solid Waste Management Manual, 2014. Ministry of Urban Development, Government of India, pp.1–150.
- Munoz, M., 1994. Use of an industrial byproduct as a liming source. *Journal of Agriculture, University of Puerto Rico*, 78(1), pp.73–86.
- Ouled, S.W., 2014. Impact of municipal rubbish dumps on major soil nutrients in north of Tunisia. *International Research Journal of Environmental Sciences*, 3(1), pp.59–69.
- Oyebode, O.J., Jimoh, F.O., Ajibade, S., Afolalu, S.A. and Oyebode, F.A., 2023. Strategic monitoring of groundwater quality around Olusosun landfill in Lagos state for pollution reduction and environmental sustainability. *Nature Environment and Pollution Technology*, 22(2), p.3. [DOI]
- Subbiah, B.V. and Asija, G.L., 1956. A rapid procedure for the estimation of available nitrogen in soils. *Current Science*, 25(4), pp.259–260.
- Walkley, A. and Black, I.A., 1934. An examination of the Degtjareff method for determining soil organic matter, and a proposed modification of the chromic acid titration method. *Soil Science*, 37(1), pp.29–38.

# Determination of the Water Quality Index (ICA-PE) of Lake Chinchaycocha, Junín, Peru

Steve Dann Camargo Hinostroza<sup>†</sup>, Carmen Andrea Taza Rojas, Diana Lizet Poma Limache and Camila Jimena Poma Romero

Environmental Engineering Academic School, Engineering Faculty, Continental University, Huancayo, Peru

<sup>†</sup>Corresponding author: Steve Dann Camargo Hinostroza; scamargo@continental.edu.pe

**Abbreviation:** Nat. Env. & Poll. Technol.  
**Website:** [www.neptjournal.com](http://www.neptjournal.com)

*Received:* 01-08-2024  
*Revised:* 11-09-2024  
*Accepted:* 23-09-2024

## Key Words:

Water quality index  
 ECA-Water  
 Lake Chinchaycocha

## ABSTRACT

The objective of the research was to determine the water quality index of Lake Chinchaycocha, which has faced pollution problems for several years. To do this, we worked with data from ten water quality monitoring points collected by the National Water Authority (ANA) during the period 2019-2023, after which the water quality index (ICA-PE) was calculated by analyzing a total of 12 parameters, using the Water Quality Standard (ECA) for water category 4 E1 (lagoons and lakes). The results of the physicochemical parameters indicated that the values of total nitrogen exceed the limits established in the ECA in 82% of the data obtained, pH in 13%, and phosphorus in 1%. In the evaluation of inorganic parameters, data from the LChin1S monitoring point showed that lead and zinc levels exceeded the values established in the ECA by 8% and 3%, respectively. Regarding the ICA-PE of the dry and wet seasons, it was determined that both present a good quality according to their averages and with the results obtained from the ICA-PE in a general way, it is concluded that Lake Chinchaycocha has a good water quality having total nitrogen as the main pollutant.

## INTRODUCTION

Water resources are essential for human survival and development. However, the quality of surface and groundwater bodies has deteriorated over time due to various human and natural activities (Aldrees et al. 2024). Primarily, industrialization, agricultural activities, and the discharge of untreated wastewater have contributed significantly to this deterioration and pollution (Lin et al. 2022), altering the chemical and biological characteristics, as well as the physical appearance of surface waters. These alterations affect the health of living beings and ecosystems, as contaminated water can cause viral and parasitic diseases in humans, in addition to modifying the composition of soil and groundwater (Kılıç 2021).

Lakes make up less than 3% of the planet's freshwater and are essential for the development and survival of humanity, as they are used for fishing, drinking water consumption, and as places of recreation, in addition to being areas that are home to a wide diversity of species. However, population growth has increased the demand for drinking water over the years (Chèvre 2018). At the same time, the advance of excessive urbanization has led human beings to pollute this primordial resource for all forms of life, and consequently, these water sources are becoming increasingly scarce. Therefore, the preservation of lakes is an issue of utmost importance for the entire population (Mohammed & Niger 2022).

Water quality refers to the conditions in which a body of water is found in relation to its physicochemical and biological characteristics, considering the alterations derived from anthropogenic activities or its natural state; therefore, to evaluate the quality of the water, the parameters of an analyzed sample are compared

## Citation for the Paper:

Camargo Hinostroza, S. D., Taza Rojas, C. A., Poma Limache, D. L. and Poma Romero, C. J., 2025. Determination of the water quality index (ICA-PE) of Lake Chinchaycocha, Junín, Peru. *Nature Environment and Pollution Technology*, 24(2), p. D1707. <https://doi.org/10.46488/NEPT.2025.v24i02.D1707>

*Note: From year 2025, the journal uses Article ID instead of page numbers in citation of the published articles.*



**Copyright:** © 2025 by the authors  
**Licensee:** Technoscience Publications  
 This article is an open access article distributed under the terms and conditions of the Creative Commons Attribution (CC BY) license (<https://creativecommons.org/licenses/by/4.0/>).

with the established quality standards (Baeza 2016). Water quality management requires the collection and analysis of a varied set of data, which can be complex to analyze and synthesize. In this context, the Water Quality Index (ICA) is used as a tool that facilitates the evaluation of a large amount of complex data, allowing the analysis of temporal and spatial variations in water quality and generating a unique easy-to-interpret value that indicates the quality of the water body (Galal et al. 2021).

Lake Chinchaycocha belongs to the Junín National Reserve and is considered the second-largest lake in Peru. Having a basin area of 529.9 km<sup>2</sup>, located at an altitude of 4080 m.a.s.l., between the regions of Pasco and Junín, it is fed by 20 streams and 12 rivers, mainly by the San Juan River. In addition, Lake Junín gives birth to the Mantaro River, the main contributor to the Amazon River. It has been recognized by the Ramsar Convention since 1997 as a wetland of international importance due to being a very productive ecosystem with a wide biological diversity housing a variety of aquatic and bird species, finding the Junín grebe and the Junín giant frog of great relevance. Species considered endangered also provide us with services, such as thermoregulation, carbon capture, and soil erosion control. It also plays a very important role in the development of electricity generation in Peru at the national level by generating around 33% of the energy consumed by the country, in addition to the fact that its waters are used for aquaculture and agricultural irrigation in different areas of the center of the country. Country, important areas to produce agricultural products (SERNANP 2020). In relation to its water quality, it is worth mentioning that it has been damaged over the years by different environmental threats when receiving effluents from different economic activities that take place in its surroundings, these being the discharge of domestic wastewater from 10 polluting sources in the towns of Villa Pasco, Vicco, Shelby, Ondores and two sectors of Carhuamayo who discharge their wastewater directly to the receiving body, while the locality of Ninacaca, a sector of Carhuamayo and two sectors of Junín discharge their wastewater into different rivers which later flow into Lake Chinchaycocha, also according to the reports presented by the National Water Authority of the monitoring carried out during the years 2013 to 2016 it was identified that the parameters of pH, dissolved oxygen and total nitrogen exceeds the ECA-Water, in the same way, it was reported that the lake had been affected by the presence of heavy metals such as lead, copper and zinc (MINAM 2017a). Likewise, different studies were carried out, such as (Flusche et al. 2005) with the measurement of dissolved strontium, which exists in smaller proportions from the amount of marine limestones and silicate rocks found in the basin to which

Lake Chinchaycocha belongs. It also mentions through a hydrogeochemical study that the measurements captured from the water discharges, in combination with the strontium isotopic data, indicate that the main sources are three rivers that contribute more than 90% of the surface water of the lake: the Chacachimpa River, the San Juan River, and the Palcamayo River. Another study such as that of (Bernal 2008), identified several potential sources of mining contamination that occurred in past years, where hydrological and hydrochemical characterizations were shown that indicated that in the northern part of Lake Chinchaycocha, one of its main sources of water entry, the San Juan River and the Upamayo Delta contained mining discharges, likewise, another research where the Water Quality Index of Lake Chinchaycocha was analyzed by different methods carried out by (Custodio et al. 2020) found that the lake has a good quality using the ICA CCME method except for point LCh1, while the Shannon-Wiener method qualified it with a moderate and extremely polluted water quality index.

To date, these problems have not been solved, as problems of contamination from mining activities, wastewater, and solid waste persist. Consequently, it is essential to evaluate the quality of the water in the water body since if the quality conditions are not met, both the environment and the health of the population will be affected. Therefore, the objective of this research is to present the evaluation of the water quality index of Lake Chinchaycocha using the methodology for the determination of the ICA-PE applied to surface continental water bodies, proposed by the National Water Authority (ANA 2018).

## MATERIALS AND METHODS

### Study Area

Lake Chinchaycocha belongs to the Junín National Reserve, located between the departments of Junín and Pasco, exactly between the districts of Carhuamayo, Ondores, Junín, Ninacaca and Vicco; the lake is located in the extreme northeast of the Pampa de Junín, with geographical coordinates of 10°50'50" S - 75°59'25" W. and 11°09'55" S - 76°15'40" W (Shoobridge 2006) (Fig. 1). It has an area of approximately 470 km<sup>2</sup> of water mirror and has an average depth that ranges between 8 to 12 m in the central areas of the lake, and it is fed by springs and infiltrations that come from the eastern and western mountain range of the San Juan River and other minor rivers (Cusiche & Miranda 2019). As for its climate, it belongs to the lower floor of the Puna region, where its temperature varies between 3° and 7°C. The coldest season occurs between May and September and has an average annual rainfall of 940 mm, having the



rainiest season between the months of December and April (SERNANP 2019).

### Data Collection and Pre-Processing

The data was collected from water quality monitors carried out by the National Water Authority (ANA) between 2019 and 2023, analyzing 10 monitoring points and 24 parameters, which include physical-chemical, inorganic, and microbiological aspects. These data are available at the following link: <https://snirh.ana.gob.pe/VisorPorCuenca/>. It should be noted that for the determination of the Water Quality Index of Peru (ICA-PE), only 12 parameters were considered since the methodology applied considers only 17 parameters, according to the assigned category of the body of water (ANA 2018), of which two were not found in the monitoring carried out, and three presented incomplete data. The data that exceeded the Environmental Quality Standard (ECA) were compared with the values of E1: Lakes and Lagoons of Category 4: Conservation of the Aquatic Environment, as established by the Ministry of the Environment (MINAM 2017b).

### Determination of the ICA-PE

To calculate the water quality index, the Canadian formula must be applied, which encompasses three factors (frequency, scope, and amplitude) that must be found with the following formulas.

**Frequency:** Indicates the total number of parameters that did not comply with the ECA-Water in relation to the total of the parameters evaluated.

Table 1: ICA-PE Rating Range.

ICA-PE	Qualification
90-100	Excellent
75-89	Good
45-74	Regular
30-44	Bad
0-29	Appalling

$$F_1 = \frac{\text{Number of parameters that do not comply with the ECA}}{\text{Total number of parameters to evaluate}} \times 100$$

**Scope:** Indicates the number of data that does not comply with the ECA-Water in relation to the total of the data evaluated.

$$F_2 = \frac{\text{Number of data that does not comply with the ECA}}{\text{Total number of data to evaluate}} \times 100$$

**Amplitude:** Indicates the measure of deviation of the data in relation to the parameters of the ECA-Water.

$$F_3 = \frac{\text{Normalized sum of surpluses}}{\text{Normalized sum of surpluses} + 1} \times 100$$

**Canadian formula:** Once the three factors have been found, the formula for the ICA-PE calculation is applied, giving us a single value result that is between 0 and 100; this value will indicate the water quality index by placing it on the five-range scale as indicated in (Table 1).

$$\text{ICA-PE} = 100 - \sqrt{\frac{F_1^2 + F_2^2 + F_3^2}{3}}$$

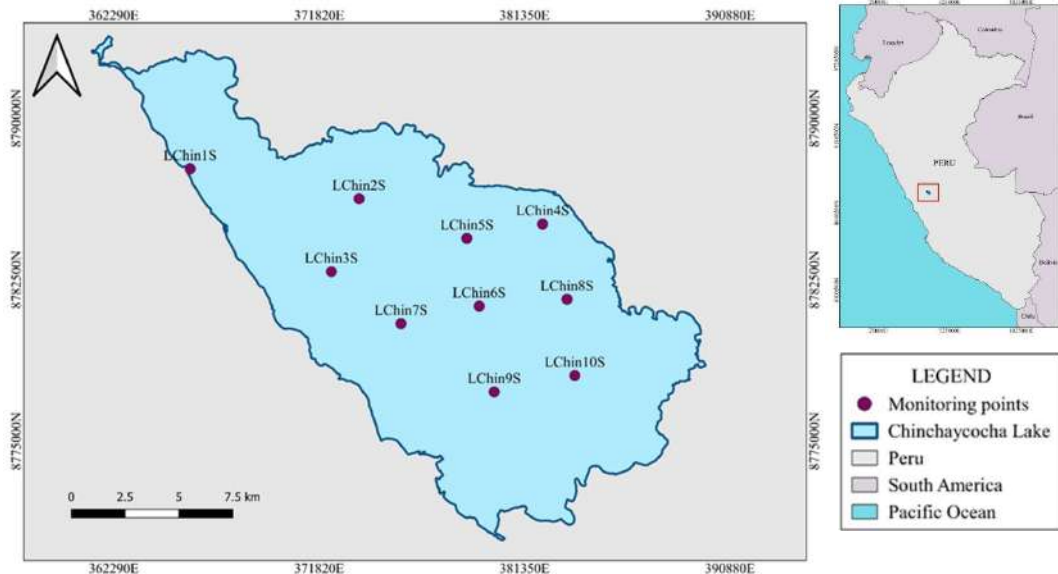


Fig. 1: Map of the study area.

## RESULTS AND DISCUSSION

The present study was carried out for 5 years considering an evaluation by seasons (dry and wet) and, in general, considering 12 parameters for the determination of the ICA-PE; it is worth mentioning that not all the parameters collected were used because complete data were not available for all monitoring points.

### Physicochemical Parameters

From the physicochemical parameters evaluated (pH, total phosphorus, oils and fats, total nitrogen, biochemical oxygen demand (BOD), and total suspended solids), it was identified that most of the values were below the Environmental Quality Standard for Water (ECA-Water). However, some parameters exceeded the values established in the ECA-Water; in particular, it was observed that the total nitrogen exceeded the values established in the ECA-Water in 82% of the data obtained from the 10 monitoring points, the data varied from the minimum value of 0.05 mg.L<sup>-1</sup> to a maximum value of 3.48 mg.L<sup>-1</sup> and an overall average of 0.59 mg.L<sup>-1</sup>, regarding pH, it was identified that 13% of the values exceeded the limits established by the ECA-Water, the data in this parameter presented a minimum value of 5.25 and a maximum of 9.17 with a general average of 8.64. In relation to total phosphorus, it was determined that 1% of the data from the monitoring carried out exceeded the ECA-Water, registering a minimum value of 0.01 mg.L<sup>-1</sup> and a maximum of 0.08 mg.L<sup>-1</sup>, with a general average of 0.10 mg.L<sup>-1</sup>. Regarding the parameters of oils and fats, BOD, and total suspended solids, none of the values analyzed did

not comply with the limits of the ECA-Water, as can be seen in (Table 2).

### Inorganic Parameters

Of the inorganic parameters evaluated (arsenic, mercury, lead, and zinc), most of the monitoring data were below the values established in the ECA-Water. However, it was determined that the LchinS1 monitoring point was the only one where the data exceeded the ECA-Water. In relation to lead, 8% of the values exceeded the ECA, registering a minimum value of 0.0002 mg.L<sup>-1</sup>, a maximum value of 0.08 mg.L<sup>-1</sup>, and a general average of 0.002 mg.L<sup>-1</sup>. Regarding zinc, it was identified that 3% of the data exceeded the ECA, with a minimum value of 0.004 mg.L<sup>-1</sup>, a maximum value of 0.25 mg.L<sup>-1</sup>, and a general average of 0.03 mg.L<sup>-1</sup>. The other parameters presented concentrations below the limits established by the ECA-Water, as indicated in (Table 2).

### Microbiological Parameters

For this study, only the microbiological parameter of thermotolerant coliforms was evaluated, of which the values collected were below the ECA-Water, registering a minimum value of 1.80 MPN.100 mL<sup>-1</sup> and a maximum value of 460 MPN.100 mL<sup>-1</sup> with an average of 10.44 MPN.100 mL<sup>-1</sup> as shown in (Table 2)

### Water Quality Index (ICA-PE)

**Dry and Wet Season:** Data were processed according to the dry and wet seasons. The dry season runs from May to September, while the wet season runs from October to

Table 2: Summary table of the parameters evaluated for the determination of the ICA-PE.

Parameters	P	F%	Min.	Max.	Prom.	ECA	Unit
Total nitrogen	82/100	82	0.05	3.48	0.59	0.315	mg/L
pH	13/100	13	5.24	9.17	8.64	6.5-9	pH unit
Lead	8/100	8	0.0002	0.08	0.002	0.0025	mg/L
Zinc	3/100	3	0.004	0.25	0.03	0.12	mg/L
Total phosphorus	1/100	1	0.01	0.08	0.015	0.035	mg/L
Oils and fats	0/100	0	0.10	1.00	0.52	5	mg/L
Dissolved oxygen	0/100	0	6.27	10.43	8.01	≥ 5	mg/L
Biochemical oxygen demand (BOD)	0/100	0	2.00	4.00	2.40	5	mg/L
Total suspended solids	0/100	0	2.00	19.00	3.68	≤ 25	mg/L
Arsenic	0/100	0	0.0001	0.013	0.004	0.15	mg/L
Mercury	0/100	0	0.00003	0.00009	0.00007	0.0001	mg/L
Thermotolerant coliforms	0/100	0	1.80	460	10.44	1000	MPN/100 ml

Q: Number of data that did not comply with the ECA-Water over the total amount of data obtained.

F%: Total percentage of data that did not comply with the ECA-Water.

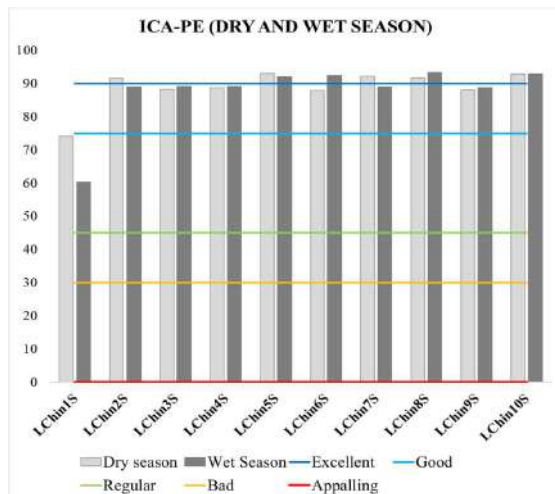


Fig. 2: Graph of ICA-PE results in dry and wet seasons.

April. To determine the Water Quality Index (ICA-PE) by season, the Canadian formula was applied. In the results of the dry season, 50% of the monitoring points qualified with excellent quality, 40% obtained good quality, and 10% presented regular quality. Also, an average of 88.56 was obtained, which qualifies it as a good quality for the dry season. Regarding the wet season, 40% of the points studied rated with an excellent quality, 50% obtained a good quality, and 10% presented a regular quality with an average of 87.03, which indicates a good quality according to (Table 3 and Fig. 2). It is important to note that the LChin1S point showed a significant variation compared to the other monitoring points in both seasons, presenting the lowest value and qualifying with a regular quality in both seasons.

### General Water Quality Index

The values of the Water Quality Index (ICA-PE) for the

Table 3: Results of the variables and ICA-PE in dry and wet seasons.

Monitoring Point	Dry Season				Wet Season			
	Variables	ICA-PE			Variables	ICA-PE		
LChin1S	F1	33.33	74.09	REGULAR	F1	41.67	60.23	REGULAR
	F2	13.33			F2	16.67		
	F3	26.92			F3	52.25		
LChin2S	F1	8.33	91.58	EXCELLENT	F1	16.67	88.97	GOOD
	F2	8.33			F2	8.33		
	F3	8.59			F3	4.20		
LChin3S	F1	16.67	88.16	GOOD	F1	16.67	89.07	GOOD
	F2	10.00			F2	6.67		
	F3	6.53			F3	6.00		
LChin4S	F1	16.67	88.69	GOOD	F1	16.67	89.06	GOOD
	F2	8.33			F2	6.67		
	F3	6.07			F3	6.07		
LChin5S	F1	8.33	92.96	EXCELLENT	F1	8.33	91.98	EXCELLENT
	F2	6.94			F2	8.33		
	F3	5.57			F3	7.35		
LChin6S	F1	16.67	87.90	GOOD	F1	8.33	92.32	EXCELLENT
	F2	10.00			F2	8.33		
	F3	7.84			F3	6.18		
LChin7S	F1	8.33	92.09	EXCELLENT	F1	16.67	88.91	GOOD
	F2	8.33			F2	8.33		
	F3	6.99			F3	4.68		
LChin8S	F1	8.33	91.72	EXCELLENT	F1	8.33	93.21	EXCELLENT
	F2	8.33			F2	6.67		
	F3	8.17			F3	4.94		
LChin9S	F1	16.67	88.13	GOOD	F1	16.67	88.59	GOOD
	F2	8.33			F2	8.33		
	F3	8.70			F3	6.56		
LChin10S	F1	8.33	92.74	EXCELLENT	F1	8.33	92.87	EXCELLENT
	F2	6.67			F2	3.33		
	F3	6.65			F3	8.49		
AVERAGE	88.56		GOOD	87.03		GOOD		

10 monitoring points of Lake Chinchaycocha ranged from a minimum value of 63.85 at the LChin1S point to a maximum value of 92.58 at the LChin5S point. Of the monitoring points evaluated, 20% rated with excellent quality, 70% with good quality, and 10% with fair quality, according to (Fig. 3 & 4 and Table 4). It is important to note that the LChin1S point presented the highest concentrations of parameters that exceeded the values established in the ECA, unlike the other monitoring points. An average value of the ICA-PE of 86.55 was obtained, which qualifies Lake Chinchaycocha, in general, with a good water quality index, according to the ranges established in (Table 1). This indicates that the lake's water quality tends to move slightly away from the desired or natural quality due to current conditions showing damage of little magnitude.

Analysis of Identified Contaminants

The results of the study carried out indicate that the parameters of total nitrogen, the potential of hydrogen, phosphorus, lead, and zinc exceed the values established in the ECA for the water of Category 4-E1 (Lagoons and Lakes) at the collection points of certain seasons.

a) Total Nitrogen

According to the results obtained, the total nitrogen parameter exceeds the limit of 0.315 mg.L<sup>-1</sup> established in the Environmental Quality Standard (ECA) in the ten monitoring points evaluated. This is the main contaminant identified. Specifically, the LChin1s point shows a high concentration of total nitrogen, registering a value of 3,479 mg/L, indicative of a greater accumulation of this parameter in the northwest region of the lake. These findings suggest that the rivers that flow into Lake Chinchaycocha

Table 4: Results of the general ICA-PE.

Monitoring Point	Variables	ICA-PE		
LChin1S	F1	41.67	63.85	REGULAR
	F2	20.00		
	F3	42.24		
LChin2S	F1	25.00	84.24	GOOD
	F2	9.17		
	F3	6.00		
LChin3S	F1	16.67	88.85	GOOD
	F2	7.50		
	F3	6.27		
LChin4S	F1	16.67	89.02	GOOD
	F2	7.50		
	F3	5.26		
LChin5S	F1	8.33	92.58	EXCELLENT
	F2	7.50		
	F3	6.29		
LChin6S	F1	16.67	88.29	GOOD
	F2	9.17		
	F3	7.02		
LChin7S	F1	16.67	88.72	GOOD
	F2	8.33		
	F3	5.85		
LChin8S	F1	8.33	92.49	EXCELLENT
	F2	7.50		
	F3	6.58		
LChin9S	F1	16.67	88.74	GOOD
	F2	8.33		
	F3	5.73		
LChin10S	F1	16.67	88.70	GOOD
	F2	6.67		
	F3	7.79		
AVERAGE			86.55	GOOD

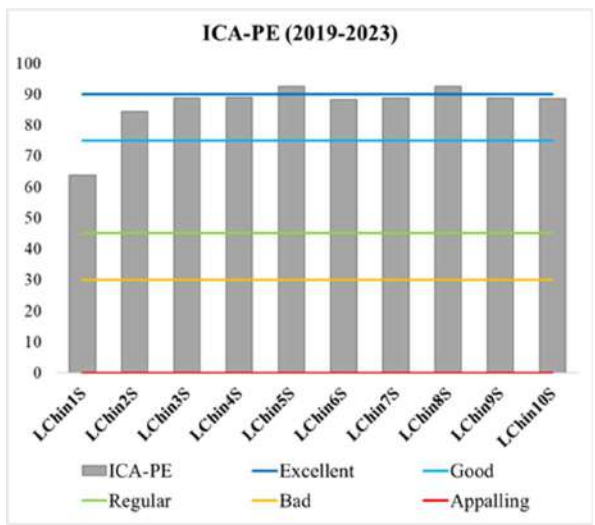


Fig. 3: General results of the ICA-PE.

are impacted by pollution, with the reservoir of the San Juan, Colorado, and Chacachimpa rivers being the main contributors to the increase in the total nitrogen load in this area. The high presence of total nitrogen probably originates from untreated domestic wastewater and the use of fertilizers applied in the production of crops such as maca and potato by local people (Porras 2023).

The excessive accumulation of total nitrogen is one of the main causes of pollution in water bodies since its increase favors the accelerated growth of algae, exceeding the natural capacity of ecosystems to manage this process (Liu et al. 2020). This leads to the eutrophication of water-receiving bodies, significantly degrading their quality (Quispe 2021).



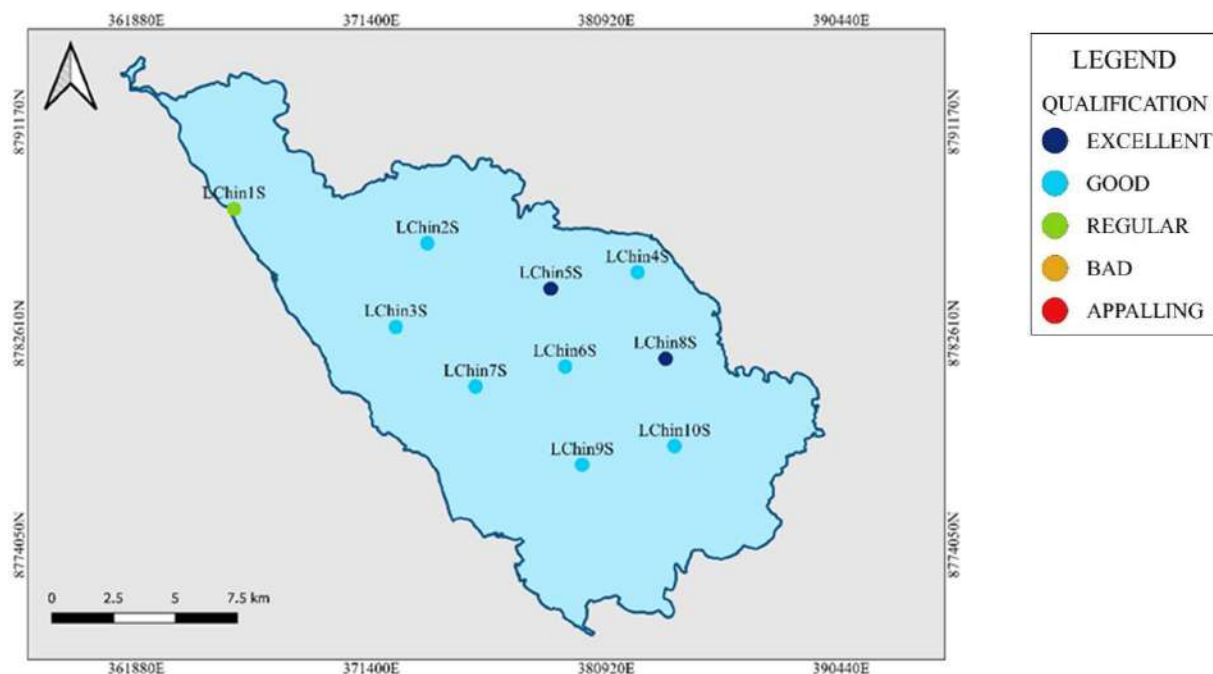


Fig. 4: Map of ICA-PE results.

### b) Hydrogen Potential

In relation to the results obtained, it is observed that the pH values exceed the limit of 9 established in the Environmental Quality Standard (ECA) at six monitoring points, which indicates that Lake Chinchaycocha experiences periods with a slightly alkaline pH. This temporary alkalinity is attributed to the presence of carbonates and bicarbonates in the water. pH is a crucial parameter in the evaluation of water quality due to its influence on the chemical and biological processes that take place in aquatic bodies (Dewangan et al. 2007). In addition, it allows the chemical evolution of several metals to be determined, as well as their solubility and bioavailability in water (ANA 2018).

### c) Total Phosphorus

The results indicated that Lake Chinchaycocha does not present significant contamination by total phosphorus since a value of  $0.08 \text{ mg.L}^{-1}$  was found, which exceeds the limit of  $0.035 \text{ mg.L}^{-1}$  established by the Environmental Quality Standard (ECA). However, it is important to mention that phosphorus is an essential component for the development of plants and animals. However, high concentrations of phosphorus can lead to an increase in algae growth in water, leading to eutrophication (Islam et al. 2016). Therefore, a eutrophic lake, characterized by high levels of phosphorus, is rich in nutrients and presents a prolific growth of algae, plants, and fish; however, this indicates poor water quality (Peña et al. 2018). In addition, eutrophication can lead to the

death of fish and other aquatic species. This accumulation of phosphorus is mainly due to anthropogenic sources, such as wastewater discharge.

### d) Lead

According to the results obtained, at the LChin1S sampling point, the value of  $0.0025 \text{ mg.L}^{-1}$  established by the Environmental Quality Standard (ECA) was exceeded, registering a maximum value of  $0.0762 \text{ mg/L}$ . The increase in lead concentration at this point is likely attributed to the fact that the water from the San Juan River and Colorado River reservoirs, which enters Lake Chinchaycocha from the northwest side, contains heavy metal contaminants, the result of mining activity (Porras 2023). Lead is a highly toxic element for flora and fauna, considered a significant potential pollutant. It is estimated that lead exposure causes approximately 143,000 human deaths each year (Bernabe 2019) because it affects the function and structure of various organs, producing adverse effects in both humans and wildlife (Clausen et al. 2011).

### e) Zinc

According to the results obtained, the concentration of zinc at the LChins1S point has exceeded the limit of  $0.12 \text{ mg/L}$  established by the Environmental Quality Standard (ECA), registering a value of  $0.246 \text{ mg/L}$ . This increase in zinc concentration is due to the influence of the reservoir of the San Juan and Colorado rivers, which flow into Lake

Chinchaycocha and contain heavy metals because of mining activity (Porras 2023). Zinc is an abundant metal on Earth, covering two-thirds of its surface (Sankhla et al. 2019). In addition, this metal is toxic to the ecosystem, posing significant health risks by directly and indirectly affecting many living organisms in Lake Chinchaycocha (Marcelo 2018). It should be noted that the lake does not have widespread zinc contamination, as only three values have been recorded that exceed the limits established by the ECA.

### Sources of Pollution

The main possible sources of contamination are domestic wastewater discharges, which reach Lake Chinchaycocha through the drainage and sewerage systems of nearby towns, such as Ondores, Junín, and Carhuamayo. This wastewater does not always receive adequate treatment before being discharged into nearby water bodies. During rainy seasons, wastewater mixes with surface runoff and is transported directly to the lake, increasing the pollutant load. In the dry season, when flows are lower, pollutant concentrations become more critical due to lower dilution (Cusiche & Miranda 2019).

Mining activity in the Junín region is also one of the main sources of pollution in Lake Chinchaycocha. Nearby mines, particularly those dedicated to the extraction of heavy metals such as lead, zinc, and copper, have contributed to the dumping of toxic waste and acidic waters into the bodies of water that flow into the lake. A relevant case is that of the Ragra River, a tributary of the San Juan River, which is seriously affected by leachate and effluents of mining waste from the Cerro SAC company. Studies carried out at the source of the Ragra River ravine, which receives the effluents from the company (Volcán Compañía Minera SAA), have shown levels of metals that considerably exceed the national limits established for the protection of the aquatic ecosystem. This has intensified pollution in the Ragra River basin, then spreading to the San Juan River basin, which in turn flows into Lake Chinchaycocha. Despite being a habitat for endemic species and being recognized as a reserve nationally and internationally as an important wetland, the lagoon continues to receive waste derived from mining exploitation, which has a negative impact on its natural ecosystem (Source 2022).

The presence of nitrogen and phosphorus induces an increase in the growth of aquatic flora and other organisms, which, together with the presence of heavy metals, generates an ecological imbalance that adversely affects the biodiversity of the lake. This phenomenon endangers threatened species, such as the giant frog of Lake Junín, the grebe of Junín, and the black redfish of Junín, whose

risk of extinction is mainly due to the degradation of their habitat caused by the destruction of riparian vegetation, mining activity and the discharge of wastewater, which significantly impact the quality of the water in the lake and its surroundings (SERNANP 2020). In addition, the degradation of these ecosystems increases the vulnerability of the local communities that inhabit the basin, reducing their capacity to adapt to climate change and affecting their productive activities, which has led to an increase in fish mortality (Wetlands 2024).

To effectively address the sources of pollution in Lake Chinchaycocha, it is crucial to implement measures such as the rehabilitation of degraded areas through reforestation and wetland restoration. These actions not only improve water quality by acting as natural filters but also restore the habitat of native and endangered species, such as the giant frog, the Junín grebe, and the Junín black hen. Carrying out projects for the development of wastewater treatment plants, likewise, the implementation of efficient solid waste and wastewater management systems in the communities surrounding the lake is essential to prevent urban waste from reaching the body of water. In addition, it is necessary to review and strengthen current environmental policies, which implies the creation of stricter regulatory frameworks and the application of effective sanctions to activities that contribute to the pollution of the lake.

### CONCLUSIONS

Based on the results analyzed from the 10 monitoring points, taking into account the 12 parameters shown in (Table 2) for the determination of the ICA-PE of Lake Chinchaycocha during the period 2019 - 2023, taking as a reference the values established in the ECA-Water in Category 4: E1 (conservation of the aquatic environment), it was determined that the physicochemical parameters that exceeded the ECA-Water are total nitrogen with 82% of data being The main pollutant compared to pH with 13% of data, as for the inorganic parameters, values were identified that exceed the ECA - Water mainly at the monitoring point Lchin1S, these being Lead with 8% and Zinc with 3% of the data in total and of the microbiological parameters having as the only parameter the thermotolerant coliforms it was determined that the data collected are below the ECA - Water.

Regarding the ICA-PE water quality index in both the dry and wet seasons, it was determined that the dry season has a higher percentage with respect to excellent quality, 50%, followed by 40% corresponding to good quality, and finally, 10% of regular quality. About the wet season, 50% was obtained in good quality, followed by 40%, which qualifies with excellent quality, and finally, 10% which

represents the regular quality. Also, according to the averages obtained in both seasons, it is concluded that they present a good water quality.

In relation to the General Water Quality Index of Lake Chinchaycocha, it can be concluded that 20% of the monitoring points have excellent water quality, 70% good quality, and 10% regular quality, considering the general average of 86.55 of the results obtained from the ICA-PE, it is also concluded that Lake Chinchaycocha has a good water quality. We delimit this result considering that, after applying the Methodology for the Determination of the ICA-PE Water Quality Index Applied to Surface Inland Water Bodies already established and completing all the necessary procedures, the result of the general average is within the range of good quality. It should be clarified that to classify water as suitable for animal or drinking consumption, it is essential to carry out a more exhaustive study. This additional analysis is crucial due to the risks associated with water consumption, which requires special care to guarantee its safety and quality since Lake Chinchaycocha presents pollutants mainly due to total nitrogen due primarily to the discharges of wastewater from nearby populations into the rivers, which subsequently flow into the lake presenting a risk to aquatic life. Likewise, the discharges of mining effluents cause a concentration of heavy metals in the lake, so the mitigation of these polluting sources is an urgent issue to address.

## REFERENCES

- Aldrees, A., Khan, M., Taha, A. and Ali, M., 2024. Evaluation of water quality indexes with novel machine learning and SHapley Additive ExPlanation (SHAP) approaches. *Journal of Water Process Engineering*, 58, p.104789. DOI.
- National Water Authority (ANA), 2018. Methodology for the Determination of the Ica-Pe Water Quality Index, Applied to Surface Inland Water Bodies. Retrieved April 18, 2024, from <https://hdl.handle.net/20.500.12543/2440>.
- Baeza, E., 2016. Water quality. Retrieved April 17, 2024, from [https://www.bcn.cl/asesoriasparlamentarias/detalle\\_documento.html?id=70193](https://www.bcn.cl/asesoriasparlamentarias/detalle_documento.html?id=70193).
- Bernabe, V.Y., 2019. Lead absorption capacity in the reed (*Scirpus californicus*) growing in the waters in the area of the Delta Upamayo-Lake Chinchaycocha. Retrieved from <http://repositorio.undac.edu.pe/handle/undac/1986>.
- Bernal, J., 2008. Study of remediation of mining liabilities in the San Juan River, Upamayo Delta and northern part of Lake Chinchaycocha. Retrieved May 29, 2024, from <http://hdl.handle.net/20.500.14076/17849>.
- Chèvre, N., 2017. *Micropollutants in Large Lakes: From Potential Pollution Sources to Risk Assessments*. First edition. EPFL Press.
- Clausen, J., Bostick, B. and Korte, N., 2011. Migration of lead in surface water, pore water, and groundwater with a focus on firing ranges. *Critical Reviews in Environmental Science and Technology*, 41(15), pp.1397-1448. DOI.
- Cusiche, L. and Miranda, G., 2019. Wastewater pollution and quality indicators in the 'Lago Junín' National Reserve, Peru. *Mexican Journal of Agricultural Sciences*, 10(6), pp.1433-1447. DOI.
- Custodio, M., Chirinos, C. and Peñaloza, R., 2020. The behavior of physicochemical parameters and potentially toxic metals in surface water evaluated by means of multimetric indices: A case study in a protected natural area of Peru. *Polish Journal of Environmental Studies*, 29(3), pp.2111-2123. DOI.
- Dewangan, K., Shrivastava, S., Tigga, V. and Lakra, M., 2007. Review paper on the role of pH in water quality implications for aquatic life, human health, and environmental sustainability. *International Advanced Research Journal in Science, Engineering and Technology*, 10(6), pp.215-218. DOI: 10.17148/IARJSET.2023.10633.
- Flusche, M., Seltzer, G., Rodbell, D., Siegel, D. and Samson, S., 2005. Constraining water sources and hydrologic processes from the isotopic analysis of water and dissolved strontium, Lake Junin, Peru. *Journal of Hydrology*, 312(1-4), pp.1-13. DOI.
- Galal, U., Stephen, N. and Agnieszka, O., 2021. A review of water quality index models and their use for assessing surface water quality. *Ecological Indicators*, 122, p.107218. DOI.
- Islam, S., Reza, M., Jeong, J.-T. and Lee, K.-H., 2016. Sensing technology for rapid detection of phosphorus in water: A review. *Journal of Biosystems Engineering*, 41(2), pp.138-144. DOI.
- Kılıç, Z., 2021. Water pollution: Causes, negative effects, and prevention methods. *İstanbul Sabahattin Zaim Üniversitesi Fen Bilimleri Enstitüsü Dergisi*, 3(2), pp.129-132. DOI.
- Lin, L., Yang, H. and Xu, X., 2022. Effects of water pollution on human health and disease heterogeneity: A review. *Frontiers in Environmental Science*, 10, p.880246. DOI.
- Liu, C., Zhang, F., Ge, X., Zhang, X., Wen Chan, N. and Qi, Y., 2020. Measurement of total nitrogen concentration in surface water using hyperspectral band observation method. *Water*, 12(7), p.1842. DOI.
- Marcelo, A., 2018. Evaluation of the Physical-Chemical Factors of the Water of Lake Chinchaycocha, Pasco-Junín. Retrieved April 30, 2024 from <https://repositorio.unfv.edu.pe/handle/20.500.13084/2645>.
- MINAM, 2017a. Chinchaycocha Sustainable Environmental Management Plan 2017-2021. Retrieved April 17, 2014, from <https://www.gob.pe/institucion/minam/informes-publicaciones/2451-plan-de-manejo-ambiental-sostenible-chinchaycocha-2017-2021>.
- MINAM, 2017b. Supreme Decree 004-2017-MINAM: Approves Environmental Quality Standards (ECA) for Water and Establishes Complementary Provisions. Retrieved April 30, 2024 from, <https://sinia.minam.gob.pe/normas/aprueban-estandares-calidad-ambiental-eca-agua-establecen-disposiciones>.
- Mohammed, A. and Niger, S., 2022. Water scarcity, pollution, and management: Chapter 18 - Pollution of water resources. *Water Scarcity, Pollution, and Management*, 5, pp.355-378. DOI.
- Peña, S.E., Cantera Kintz, J. and Muñoz, E., 2018. Evaluation of pollution in aquatic ecosystems: A case study in the Sonso Lagoon, the upper basin of the Cauca River. *Journal of Cleaner Production*, 251, p.100182. DOI.
- Porras, M., 2023. Evaluation of the environmental impact on the water quality of Lake Chinchaycocha applying the geographic information system located in the province of Junín and Pasco-2022. Retrieved April 30, 2024, from <http://repositorio.undac.edu.pe/handle/undac/3807>.
- Quispe, B.K.L., Guadalupe Baylón, N.K., Diaz Avalos, H. and Diaz Panduro, H.G., 2021. Use of *Eichhornia crassipes* and *Lemma minor* in the removal of nitrogen and phosphorus from wastewater from the oxidation lagoon of the city of Pucallpa, Peru. *Ciencia Latina Revista Científica Multidisciplinar*, 5(3), pp.2813-2827. DOI.
- SERNANP, 2020. Junín National Reserve: A mirror in the middle of the Andes. Retrieved April 18, 2024, from <https://sis.sernanp.gob.pe/biblioteca/descargarPublicacionAdjunto.action?strIdInterno=62795660449903372856322135950135912709>.
- Sankhla, M., Kumar, R. and Prasad, L., 2019. Zinc impurity in drinking water and its toxic effect on human health. *Indian Internet Journal of Forensic Medicine & Toxicology*, 17(4), pp.84-87. DOI.

- Shoobridge, D., 2006. Profile of Natural Protected Area Peru: Junín National Reserve. Retrieved June 1, 2024, from [https://www.parkswatch.org/parkprofiles/pdf/jnar\\_spa.pdf](https://www.parkswatch.org/parkprofiles/pdf/jnar_spa.pdf).
- Source, 2022. Environmental assessment of water resources and soils in the Cerro de Pasco mining area. Retrieved August 30, 2024, from <https://www.source-international.org/news/our-last-environmental-investigation-in-cerro-de-pasco>.
- United Nations Environment Programme, 2024. What is phosphorus and why is concern about its environmental impact increasing? UNEP. Retrieved April 30, 2024, from <https://www.unep.org/es/noticias-y-reportajes/reportajes/que-es-el-fosforo-y-por-que-aumenta-la-preocupacion-por-su-impacto>
- Wetlands International, 2024. Lake Junín, Peru. Retrieved August 30, 2024, from <https://www.wetlands.org/case-study/lake-junin-peru/>.



# Evaluation of Landscape Resources and Legal Protection Boundary Setting in Xinchang County, China

Ya Li<sup>1,2†</sup> and Faridah Sahari<sup>1,3</sup>

<sup>1</sup>Faculty of Applied and Creative Art, Universiti Malaysia Sarawak, 94300 Kota Samarahan, Sarawak, Malaysia

<sup>2</sup>Zhejiang Industry Polytechnic College, College of Architectural Engineering, 312000, 151 Qutun Road Yuecheng District, Shaoxing City, Zhejiang, People's Republic of China

<sup>3</sup>Institute of Creative Art and Technology, Universiti Malaysia Sarawak, 94300 Kota Samarahan, Sarawak, Malaysia

†Corresponding author: Ya Li; 20010144@siswa.unimas.my

**Abbreviation:** Nat. Env. & Poll. Technol.  
**Website:** [www.neptjournal.com](http://www.neptjournal.com)

*Received:* 02-08-2024

*Revised:* 26-09-2024

*Accepted:* 03-10-2024

## Key Words:

Landscape protection  
 Legal boundaries  
 Sustainable utilization  
 Landscape resources

## ABSTRACT

Landscapes are vital for ecological protection and cultural heritage, facing challenges from urbanization, agricultural modernization, and climate change. By setting legal boundaries, land use can be regulated to prevent unreasonable development and ensure the sustainable use of landscapes. This paper assesses the forest, geological, aquatic, cultural, and religious relic landscape resources of Xinchang County, Zhejiang Province, using the Analytic Hierarchy Process (AHP) and fuzzy evaluation methods to quantify their protection needs. The study finds that establishing nature reserves, ecological protection red lines, and historical and cultural villages can effectively maintain ecosystem stability and biodiversity, and protect cultural heritage. Legal protection has significantly improved forest coverage and water quality in Tianmu Mountain National Forest Park and Wozhou Lake Scenic Area, while Meizhu Ancient Village and Waipo Keng Village have excelled in cultural landscape protection. However, challenges such as inadequate law enforcement, low public participation, and insufficient funding hinder the execution of legal boundaries. Recommendations include strengthening law enforcement, raising public environmental awareness, and expanding funding sources. This paper provides a scientific basis and practical guidance for the formulation and implementation of landscape protection policies, contributing to the sustainable utilization and long-term protection of landscape resources in Xinchang County and other regions.

## Citation for the Paper:

Li, Y. and Sahari, F., 2025. Evaluation of landscape resources and legal protection boundary setting in Xinchang County, China. *Nature Environment and Pollution Technology*, 24(2), p. D1708. <https://doi.org/10.46488/NEPT.2025.v24i02.D1708>

*Note: From year 2025, the journal uses Article ID instead of page numbers in citation of the published articles.*



**Copyright:** © 2025 by the authors

**Licensee:** Technoscience Publications

This article is an open access article distributed under the terms and conditions of the Creative Commons Attribution (CC BY) license (<https://creativecommons.org/licenses/by/4.0/>).

## INTRODUCTION

### Importance of Landscape Protection

Landscapes are not only an essential part of environmental protection but also a key carrier of cultural heritage (Ning 2024). Globally, landscape protection faces numerous challenges, such as accelerated urbanization, agricultural modernization, and climate change. The interplay of these factors poses a collective threat to landscapes across numerous regions, elevating the risks of their degradation and potential permanent loss. Protecting landscapes is crucial for maintaining ecosystem stability and biodiversity (Mo et al. 2021). Natural elements in landscapes, such as forests, wetlands, and grasslands, play vital roles in soil and water conservation, carbon sequestration, and habitat protection.

Additionally, landscapes embody a wealth of cultural heritage, mirroring the historical, social, and cultural transformations of diverse regions. Traditional village layouts and architectural styles not only embody the lifestyle and cultural customs of residents but also demonstrate the wisdom of harmonious coexistence between humans and nature (Li et al. 2024). Therefore, landscapes not only contribute to

environmental protection but also promote cultural heritage and enhance community identity.

### **Role of Legal Boundaries**

Legal boundaries are crucial for landscape protection. By setting and enforcing legal boundaries, land use can be effectively regulated to prevent unreasonable development and destruction, ensuring the sustainable utilization of landscapes. Many countries and regions have established legal boundaries, such as protected areas, ecological red lines, and restricted development zones, through laws and regulations to limit the intensity and purpose of land development, thereby protecting the ecological environment and landscape resources. For example, the EU's Natura 2000 directive and China's Ecological Protection Red Line policy have effectively protected large areas of natural landscapes and ecosystems through legal boundaries (Patz et al. 2004). The establishment of legal boundaries promotes the institutionalization and standardization of landscape protection, ensuring the long-term effective implementation of protective measures through clear laws and policy guidance. Legal boundaries ensure public rights to information, participation, and supervision in landscape protection, enhancing protection effectiveness and social recognition (Terra et al. 2014).

### **Background of Xinchang County**

Xinchang County, located in southern Shaoxing City, Zhejiang Province, lies on the northern slope of the Tiantai Mountains, known for its scenic beauty. The county has a long history and rich cultural heritage. Its unique geographical position endows the region with distinctive natural landscapes and abundant cultural landscape resources. The county borders Ninghai and Fenghua to the east, Tiantai to the south, Pan'an and Dongyang to the southwest, and Shengzhou to the northwest. The terrain mainly consists of low mountains and hills, with low mountains in the east, hilly terraces in the center, and river valleys and low hills interspersed in the northwest. Influenced by a subtropical monsoon climate, Xinchang has four distinct seasons and a mild and humid environment conducive to biodiversity. The county's water resources are abundant, with rivers like the Chengtan River, Xinchang River, and Huangze River providing natural advantages for hydropower development.

Xinchang's landscapes not only have high ecological value but also carry rich cultural connotations (Zhang 2022). Natural scenery represented by Tianmu Mountain and cultural landscapes represented by traditional villages together form Xinchang's unique landscape system. These landscapes attract numerous tourists and are an integral part

of local residents' lives and culture. In recent years, Xinchang has accumulated some experience in landscape protection but has not formed a systematic mechanism for landscape resource protection (Chun 2023).

### **Research Objectives**

This study aims to collect data on Xinchang's landscape resources through literature analysis and field surveys to clarify their value and analyze and quantify the protection needs of these resources based on collected data. After identifying and classifying landscape resources, the study will set legal boundaries such as nature reserves, ecological protection red lines, and historical and cultural villages based on their value to ensure sustainable utilization and protection of landscape resources. It will analyze the effectiveness of legal boundaries in limiting unreasonable development, protecting the ecological environment, and preserving cultural heritage, and propose optimization suggestions to enhance the effectiveness of legal boundaries, providing scientific basis and practical guidance for Xinchang County and other regions.

## **MATERIALS AND METHODS**

### **Literature Review**

To systematically review and analyze relevant domestic and international literature on landscape protection and legal boundary setting, this study searched keywords such as "legal boundaries" and "landscape protection" in databases like CNKI, Web of Science, and Google Scholar. The authors included 80 highly relevant and representative papers (Table 1). These papers provide a theoretical foundation and practical experience for this study, which can be broadly categorized into four types:

**Legal Boundary Setting:** Research on legal boundary setting focuses on how to delineate and protect key ecological areas through scientific methods and legal means (Holder 1999). The EU's Natura 2000 directive is a typical case, limiting land development intensity through protected areas to protect ecological environments and landscape resources (Paracchini & Capitani 2011). Additionally, Sarah Blandy & Sibley (2010) explored how legal boundaries form legally significant spaces at different spatial scales, providing international experience and a scientific basis for Xinchang's legal boundary setting.

**Legal Boundary Enforcement:** Effective enforcement of legal boundaries requires strong law enforcement mechanisms and public participation (Holder 1999). Desideri (2015) pointed out that while setting legal boundaries is important, effective enforcement is crucial and requires

strong law enforcement mechanisms and broad public participation. Jennifer Nedelsky (1990) studied the role of legal boundaries in protecting personal freedom and property rights, emphasizing the importance of legal boundary enforcement. These studies highlight the challenges in legal boundary enforcement, including insufficient law enforcement and low public participation.

**Landscape Protection:** Landscape protection plays an important role in environmental protection and cultural heritage. Górka (2016) studied the legal and practical aspects

of landscape protection in Poland, emphasizing the crucial role of law in maintaining landscapes. O'Donnell (2016) discussed landscape mosaic and edge effects in forest protection, providing specific cases of landscape protection. These papers emphasize that protecting landscapes not only helps ecological environmental protection but also promotes cultural heritage and community identity enhancement.

**Policy and Governance:** Research on policy and governance explores how effective policy frameworks and governance mechanisms promote landscape protection.

Table 1: Literature Review.

Literature Classification	Author(s) and Year	Title Primary	Viewpoints	Role in This Study
Establishment of Legal Boundaries	Blandy & Sibley (2010)	Law Boundaries and the Production of Space	Discuss how legal boundaries form legally significant spaces at different spatial scales.	Provides the theoretical foundation and practical experience for establishing legal boundaries.
Establishment of Legal Boundaries	Lindahl (2010)	A-Legality: Postnationalism and the Question of Legal Boundaries	The study examines issues related to legal boundaries in the context of post-nationalism, emphasizing the necessity of legal boundaries within the legal order.	Provides the importance and basis for establishing legal boundaries in the context of globalization.
Establishment of Legal Boundaries	Nedelsky (1990)	Law Boundaries and the Bounded Self	The study explores the role of legal boundaries in protecting individual freedom and property rights.	Emphasizes the importance of establishing legal boundaries for the protection of individual rights.
Enforcement of Legal Boundaries	Purcell & Nevins (2004)	Pushing the boundary: state restructuring state theory and the case of U.S.–Mexico border enforcement in the 1990s	The study examines issues of state restructuring in the enforcement of the US-Mexico border during the 1990s.	Provides case analysis of challenges faced during the enforcement of legal boundaries.
Enforcement of Legal Boundaries	Paul (2018)	Legal Challenges of International Environmental Law Enforcement on Transnational Boundary Pollution	The study analyzes the legal challenges in the enforcement of international environmental law concerning transboundary pollution.	Emphasizes the transnational challenges and the importance of enforcement mechanisms in the execution of legal boundaries.
Enforcement of Legal Boundaries	Chang et al. (2024)	Legal or Illegal —Transferring jurisdiction in the course of maritime law enforcement	The study examines issues of jurisdictional transfer in the enforcement of maritime law.	Provides issues of jurisdiction and practical challenges in the enforcement of legal boundaries.
Landscape Protection	Górka (2018)	Threats to Landscape and Its Protection in Poland	The study describes the prerequisites for landscape protection in Poland and the threats it faces.	Provides legal and practical insights into landscape protection, serving as a reference for this study.
Landscape Protection	Zhang et al. (2015)	Landscape Approaches for Rural Environment Protection and Management	The study explores landscape approaches to rural environmental protection and management.	Provides methodological support for landscape protection and management.
Landscape Protection	Dai & Lu (2019)	Protection and Construction Strategy of Rural Landscape Based on Regional Perspective	The study examines landscape protection strategies in Wuling Town, Hunan Province.	Provides landscape protection strategies and practical experiences from a regional perspective.
Policy and Governance	Buizer et al. (2015), van Oosten et al. (2021)	Landscape governance as policy integration ‘from below’: A case of displaced and contained political conflict in the Netherlands	The study explores landscape governance practices in the Netherlands, highlighting the importance of local governance in environmental protection.	Provides case analysis of policy integration and local governance.
Policy and Governance	Kusters et al. (2018), van Oosten et al. (2021)	Capable of governing landscape restoration? Exploring landscape governance capabilities based on literature and stakeholder perceptions	The study examines the governance capacity for landscape restoration, analyzing the role of multiple stakeholders in landscape governance.	Provides theoretical support for landscape governance capacity and multi-stakeholder collaboration.

Buizer et al. (2015) explored landscape governance practices in the Netherlands, demonstrating the importance of local governance in environmental protection. Kusters et al. (2018) studied landscape restoration governance capabilities, analyzing the role of multiple stakeholders in landscape governance.

The literature review conducted has not only offered theoretical backing for the development and enforcement of landscape conservation policies in Xinchang County, but it has also enriched the theoretical underpinnings of this study by integrating findings and practical experiences from both domestic and international research. Spanning a wide array of topics, from the fundamental principles of landscape ecology to concrete examples of legal boundary implementation and from the preservation of local traditional knowledge to the management of landscape resources on a global scale, these documents have helped establish a multifaceted and interdisciplinary theoretical framework for this research. By thoroughly analyzing this body of literature, the study is able to draw on the successes and shortcomings in landscape resource assessment and legal boundary establishment from various regions, offering tailored recommendations for the specific context of Xinchang County. This academic foundation not only aids in objectively evaluating the current state of landscape resources in the county but also provides a basis for setting and adjusting legal boundaries in response to the evolving socio-economic and ecological landscape.

### Area Selection

The study selected Xinchang County as the research object due to its diverse landscape characteristics and accumulated experience in landscape protection. Xinchang's geographical position and natural environment provide rich research data; its economic structure and social development are also

representative, providing a good practical basis for studying the role of legal boundaries in landscape protection. Given the abundance of landscape resources in Xinchang, the authors chose representative landscape resource clusters within the county, including Tianmu Mountain National Forest Park, Wozhou Lake National Natural Protection Scenic Area, Meizhu Ancient Village, and Waipo Keng Village, as data collection samples. In addition to these four representative landscape resource clusters, other well-known sites within the county were also surveyed.

Through investigation, the landscape resources of Xinchang can be broadly categorized into five main types: forest landscapes, geological landscapes, water landscapes, cultural landscapes, and religious relic landscapes. Among the forest landscapes, Tianmu Mountain stands out with its majestic mountain terrain and rich vegetation, creating a magnificent natural panorama. The geological landscapes are best represented by the Chuanyan Nineteen Peaks and the National Petrified Wood Geological Park. The Nineteen Peaks are a series of interconnected mountains stretching for 2.5 kilometers, characterized by lush trees on the mountains and crystal-clear streams at their base. The central peak features a circular hole that allows passage from east to west, thus the name Chuanyan Nineteen Peaks. The Xinchang National Petrified Wood Geological Park is a significant site for displaying Earth's history and geological evolution, containing abundant fossil resources. In terms of water landscapes, Wozhou Lake Scenic Area, Chengtanjian, and Xinchang River, along with their associated reservoirs, streams, and waterfalls, offer visitors a variety of water-based activities and scenic experiences. The cultural landscapes, such as the stone carvings and inscriptions on Tianmu Mountain and the ancient buildings in Meizhu Village, bear witness to the rich historical and cultural development of the

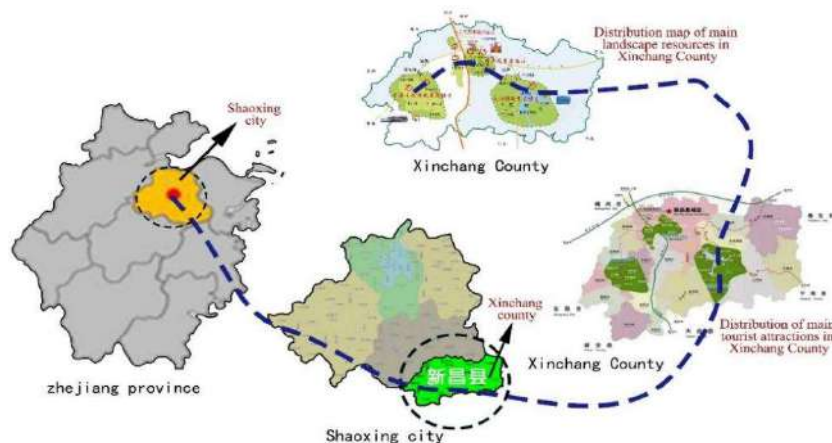


Fig. 1: The geographical location of Xinchang County and the distribution of its main scenic resources.



Xinchang region. The religious relic landscapes, including temples like Dafo Temple and Zhenjun Temple, attract numerous devotees and tourists with their long histories.

These landscape resources not only possess natural beauty but also embody profound cultural significance. In recent years, through scientific planning and reasonable management, the landscape resources of Xinchang County have gradually become a crucial force in promoting local economic development, enhancing residents' quality of life, and facilitating cultural exchange (Fig. 1).

### Data Collection

To comprehensively understand the landscape resources of Xinchang, the authors conducted field surveys from February to August 2024 at Tianmu Mountain National Forest Park, Wozhou Lake National Natural Protection Scenic Area, Meizhu Ancient Village, and Waipo Keng Village. To authentically reflect the beauty of landscape resources and strengthen comparisons between landscape resources, numerous photos were taken at each site following specific guidelines. Photos were selected based on three principles: (1) ensuring representativeness, (2) avoiding non-landscape factors, (3) maintaining consistent shooting conditions (Fig. 2).

Through field surveys, landscape resources were categorized into five types: forest landscape resources, geological landscape resources, water landscape resources, human landscape resources, and religious relics landscape resources. Human landscape resources refer to valuable landscapes created by human activities, such as architectural relics, historical towns, celebrity residences, and regional culture (Mo et al. 2021). Many scholars' landscape evaluation studies show that evaluators from different groups

or cultural backgrounds do not have significant statistical differences in aesthetic attitudes (Buhyoff et al. 1984, Tips & Savasdisara, 1986). Therefore, during the field surveys, 50 participants, including villagers, tourists, and managers from the above areas, were randomly recruited for evaluation. Fuzzy evaluation was used for assessment. Evaluators rated each indicator on a five-point scale and provided an overall evaluation of each site. Then, evaluation forms were collected, and membership degrees and scores for each indicator at each site were calculated. Finally, the total score for each site was calculated based on the evaluation system.

The fuzzy score  $Q_i$  of each evaluation indicator was calculated as follows:

$$Q_i = \sum_{a=1}^5 r_{ia} \times a \quad (a = 1, 2, 3, 4, 5)$$

$r_{ia}$  is the score membership degree of each indicator,  $a$  is the score grade, and the calculation method of membership degree  $r_{ia}$  was as follows:

$$r_{ia} = \frac{m}{M} \quad (i = 1, 2, 3, \dots, n; a = 1, 2, 3, 4, 5)$$

### Data Analysis

The data used AHP to establish the structural model for landscape resource evaluation (Ovchinnikova et al. 2021) and then applied comparative judgment to layer the typical landscape resources of Xinchang County (Balta & Atik 2022), resulting in the landscape resource evaluation results for Xinchang County. Finally, the overall scores for landscape resources were obtained. Based on field surveys and literature reviews, an evaluation system for Xinchang's landscape resources was established. The evaluation system



Fig. 2: Partial photos of 6 evaluation sites. A01 Tianmu Mountain National Forest Park, A02 Wozhou Lake National Natural Protection Scenic Area, A03 Meizhu Ancient Village, A04 Grandma Keng Village.

Table 2: The evaluation system of landscape resources of Xinchang County.

Objective Level	Criterion Level	Weight	First-level Indicator	Weight
Xinchang County Landscape Resource Evaluation System	B1 Forest Landscape Resources	0.3000	C1 Tree Morphology	0.1200
			C2 Tree Distribution Pattern	0.1800
			C3 Canopy Density	0.2000
			C4 Forest Perspective	0.1600
			C5 Coordination of Shrubs and Grasslands	0.1600
			C6 Uniformity of Shrubs and Grasslands	0.1800
	B2 Geological Landscape Resources	0.2500	C7 Terrain Variation	0.3000
			C8 Slope	0.2500
			C9 Vegetation Coverage	0.4500
	B3 Water Landscape Resources	0.2000	C10 Waterbody Morphology	0.4000
			C11 Waterbody Openness	0.3000
			C12 Waterbody Transparency	0.3000
			C13 Landscape Aesthetic Value	0.2500
	B4 Cultural Landscape Resources	0.1500	C14 Landscape Uniqueness	0.2500
			C15 Historical and Cultural Value	0.3000
			C16 Popular Science Value	0.2000
			C17 Religious Cultural Value	0.5000
	B5 Religious Relic Landscape Resources	0.1000	C18 Religious Architectural Aesthetics	0.3000
			C19 Pilgrimage Tourism Attraction	0.2000

includes five criteria: forest landscape resources, geological landscape resources, water landscape resources, human landscape resources, and religious relics landscape resources. The following is the specific evaluation system of Xinchang County and the weight of each indicator (Table 2).

## RESULTS

### Landscape Resource Evaluation Results

Using AHP and fuzzy evaluation methods, this study systematically evaluated Xinchang's landscape resources and analyzed the impact of legal boundary settings on landscape resource protection. Tables 2 and 3 show the scores and comprehensive evaluation results of typical landscape resource clusters in Xinchang County. The results indicate that Tianmu Mountain National Forest Park performs best in forest and geological resources, while Wozhou Lake National Natural Protection Scenic Area excels in water and religious resources. Meizhu Ancient Village has a strong comparative advantage in human resources, while Waipo Keng Village has weaker comparative advantages among the four sites.

From the scores of various landscape resources in Table

3 and Table 4, it can be observed that Tianmu Mountain National Forest Park (A01) in Xinchang County has the highest total score. This is mainly attributed to the high scores of its forest landscape resources (B1) and geological landscape resources (B2), both of which reach a score of 4. In A01, visitors can enjoy the majestic Tianmu Mountain range and abundant forest resources, which significantly enhance the overall value of the scenic area. Additionally, A01's cultural landscape resources (B4) also score relatively high, primarily due to its location at an important node on the Tang Poetry Road in eastern Zhejiang. Many poets of the Tang Dynasty, such as Li Bai, Du Fu, and Bai Juyi, visited this area, leaving behind numerous poems and former residences. However, there is still room for improvement in the cultural landscape resources of A01, particularly in terms of increasing cultural activities and tourism facilities.

In contrast, Wozhou Lake National Natural Protected Scenic Area (A02) scores highest in water landscape resources (B3) and religious relic landscape resources (B5). The water landscapes of A02, such as lakes and rivers, along with religious temples like Shanchan Temple and Zhenjun Temple, attract a considerable number of visitors. Its forest

landscape resources (B1) also score relatively high. However, A02 scores lower in cultural landscape resources (B4), indicating the need for further development and protection of its historical and cultural heritage. A03 (Meizhu Ancient Village) scores highest in cultural landscape resources (B4), showcasing its rich cultural history and traditional architecture. Its water landscape resources (B3) also score well, reflecting good water quality and waterbody morphology. A02 (Waipo Keng Village) has balanced scores in forest landscape resources (B1) and cultural landscape resources (B4), demonstrating an overall good ecological and cultural environment. However, there is still room for improvement in geological landscape resources (B2) and other aspects.

From these evaluation results, it can be seen that different landscape resources in Xinchang County are distributed and perform variably across different scenic areas. Tianmu Mountain National Forest Park excels in forest and geological resources, while Wozhou Lake National Natural Protected Scenic Area stands out in water and religious resources. Meizhu Ancient Village has a strong comparative advantage in cultural resources, and Waipo Keng Village maintains a good status in both forest and cultural resources. These data provide scientific evidence and practical guidance for the protection and management of landscape resources in Xinchang.

### Legal Boundary Setting

Based on the above research, this paper finds that Xinchang County can establish three types of legal boundaries: nature reserves, ecological protection red lines, and historical and cultural villages (Wei et al. 2024). These legal boundaries are primarily based on ecological and cultural values to protect key natural and cultural landscape areas. Nature reserves mainly include areas such as Tianmu Mountain National

Forest Park, Wozhou Lake Scenic Area, and Chuan Rock Nineteen Peaks, which are dominated by natural landscape resources. These areas protect rich natural landscapes and biodiversity through legal boundaries, limiting human activities that damage ecosystems.

Ecological protection red lines cover the county's main rivers, wetlands, and forest areas, focusing on ecological environment protection. By setting ecological red lines, human activities in these areas are restricted, ensuring the stability of water resources and wetland ecosystems. For river and wetland protection, the ecological red lines cover major rivers like Chengtan River and Xinchang River and surrounding wetlands, limiting development and pollution in riverine areas to protect aquatic ecosystems' health. The red lines should also cover the Tianmu Mountain range and other forest areas within the county, with legal prohibitions on large-scale logging and development activities, protecting the ecological functions and biodiversity of forests.

Historical and cultural villages like Meizhu Ancient Village and Waipo Keng Village need laws and regulations to protect their traditional buildings and cultural heritage. Legal boundaries not only protect the physical structure of historical buildings but also preserve their social value (Przybyszewski et al. 2022). Legal boundaries prevent modernization projects from damaging the traditional landscape of ancient villages, promoting cultural heritage transmission and protection.

### Landscape Protection Inside and Outside Legal Boundaries

Comparing data from typical landscape resource clusters within Xinchang County, such as Tianmu Mountain National Forest Park (A01), Wozhou Lake National Natural Protection

Table 3: Index System Evaluation of Xinchang County.

No.	Scenic spot	Type of landscape resources					Total score
		B1 Forest Landscape Resources	B2 Geological Landscape Resources	B3 Water Landscape Resources	B4 Cultural Landscape Resources	B5 Religious Relic Landscape Resources	
1	Tianmu Mountain Forest Park (A01)	4	4	3	4	3.65	3.73
2	Wozhou Lake Scenic Area (A02)	3.6	3.7	4	3	4	3.66
3	Meizhu Ancient Village (A03)	3.2	3.3	3.75	3.1	2.9	3.25
4	Waipo Keng Village (A04)	2.8	2.9	2.8	4	3.2	3.14

Table 4: A Comprehensive Evaluation of Xinchang County.

No.	Location	Excellent (5)	Good(4)	Average (3)	Poor (2)	Very Poor (1)	Total Score
1	Tianmu Mountain Forest Park (A01)	0.3	0.4	0.2	0.05	0.05	4
2	Wozhou Lake Scenic Area (A02)	0.25	0.35	0.25	0.1	0.05	3.75
3	Meizhu Ancient Village (A03)	0.2	0.25	0.3	0.15	0.1	3.45
4	Waipo Keng Village (A04)	0.15	0.3	0.35	0.1	0.1	3.35

Scenic Area (A02), Meizhu Ancient Village (A03), and Waipo Keng Village (A04), reveals that setting legal boundaries around these areas can significantly limit unreasonable development, protect the ecological environment, and preserve cultural heritage. Areas within legal boundaries show significantly higher forest coverage, water quality, and biodiversity than areas outside boundaries. Legal boundaries play a crucial role in these scenic areas. Typical landscape resource clusters within Xinchang County, such as Tianmu Mountain National Forest Park and Wozhou Lake National Natural Protection Scenic Area, effectively curb illegal development activities through legal boundary protection, preserving their rich natural landscape resources. Historical and cultural villages like Meizhu Ancient Village and Waipo Keng Village protect traditional architectural heritage and unique cultural landscapes through legal boundaries.

### Challenges Facing Legal Boundaries

Past experiences indicate that the implementation of legal boundaries may face challenges such as inadequate law enforcement, low public participation, and insufficient funding. Due to insufficient law enforcement and supervision in some areas, illegal development and destruction still occur. During the survey, villagers mentioned that illegal logging and construction still exist in some protected areas, damaging the local ecological environment. Despite the government's efforts to promote community participation in landscape protection, many residents lack awareness of its importance and show low enthusiasm for participation. Only about 40% of respondents reported participating in related activities.

Additionally, landscape protection requires sufficient funding, but due to limited fiscal budgets, protection projects are difficult to fully implement. Several respondents indicated that landscape protection funds mainly rely on government appropriations, lacking diversified funding sources, limiting the effectiveness and sustainability of protective measures. Therefore, to effectively protect landscape resources, it is necessary to strengthen law enforcement, raise public awareness, and expand funding channels (Jiahua 2023), ensuring the smooth implementation of landscape protection projects.

## DISCUSSION

Through this study's systematic evaluation of Xinchang's landscape resources and the setting of legal boundaries, the urgency and key role of legal boundaries in Xinchang's landscape resource protection can be clarified. First, the establishment of legal boundaries can effectively protect the local natural and cultural landscape resources, limit unreasonable development behaviors, and maintain ecosystem

stability and biodiversity (Yermolenko et al. 2021). Legal boundary protection has effectively maintained forest coverage and water quality in areas such as Tianmu Mountain National Forest Park and Wozhou Lake National Natural Protection Scenic Area, alleviating or curbing environmentally destructive behaviors. Of course, legal boundaries may still face challenges, such as inadequate law enforcement and low public participation during implementation, which can be quite acute in some areas.

Secondly, public awareness and participation in landscape protection significantly influence the effectiveness of legal boundaries. Some residents lack awareness of the importance of landscape protection and show low participation enthusiasm, affecting the protection effect of legal boundaries to some extent. Areas within legal boundaries perform significantly better in environmental protection and cultural heritage maintenance than areas outside boundaries, mainly due to the restrictive role of legal boundaries. However, to further enhance protection effectiveness, it is necessary to strengthen public environmental awareness and participation. The government and relevant departments should intensify publicity and education efforts to raise residents' awareness of landscape protection and encourage more people to participate in landscape protection work. Meanwhile, the establishment and implementation of legal boundaries require more funding to ensure the effective implementation of protective measures. Therefore, it is recommended that the government prioritize funding needs for landscape protection projects in fiscal budgets to ensure orderly protection work. Through these measures, the actual effectiveness of legal boundaries in landscape protection in Xinchang County can be further improved, providing strong support for achieving sustainable development goals.

Additionally, to thoroughly discuss landscape protection in Xinchang County, the researchers conducted a comparative study with Shengxian City, which faces similar landscape challenges. Bordering Xinchang County, Shengzhou City also boasts a wealth of natural scenery and a profound cultural heritage. Through this comparison, it became evident that the landscape resources in Xinchang County demand a more explicit establishment of legal boundaries, especially considering the high susceptibility of its important scenic areas, such as Tianmu Mountain and Wozhou Lake, to tourist influence and agricultural activities. Consequently, stricter legal boundaries are required to safeguard its natural resources. In contrast, Shengzhou City has achieved notable success in the protection of cultural landscape heritage, yet there remains room for improvement in the protection of natural landscapes.



This study also examined Lijiang City in Yunnan Province, which, despite differences in geographical location and climatic conditions compared to Xinchang County, offers valuable insights into the protection of both cultural and natural landscape resources. Lijiang City has implemented legislation to protect its ancient city, restrict commercial development, and actively promote cultural tourism, thereby preserving its cultural heritage while also stimulating local economic growth. These experiences provide significant guidance for Xinchang County on how to balance tourism development with the protection of cultural heritage while safeguarding natural landscapes.

## CONCLUSIONS

This study reveals the critical role and impact of legal boundaries in the landscape protection of Xinchang County through the evaluation of typical landscape resources and the establishment of legal boundaries. The study shows that rational evaluation of the advantages and disadvantages of landscape resources within the region and the establishment of legal boundaries can effectively protect the natural and cultural landscape resources of Xinchang County, limit unreasonable development behaviors, and promote the sustainable development of the ecological environment and the protection of cultural heritage. The study also finds that strengthening law enforcement and public participation is key to further enhancing the protection effectiveness of legal boundaries. By raising public environmental awareness and increasing funding for landscape protection projects, the protection goals of legal boundaries can be better achieved. The study's findings provide a scientific basis and practical guidance for Xinchang County and other regions in formulating and implementing landscape protection policies, offering new perspectives for the long-term protection and sustainable utilization of landscape resources in Xinchang County.

## ACKNOWLEDGMENTS

Firstly, I am particularly grateful to the Shaoxing City Philosophy and Social Science Work Office and the Zhejiang Federation of Humanities and Social Sciences Circles for assisting in the research project. Secondly, I would like to express my gratitude to the reviewers and editors of this manuscript for their valuable remarks. The research was financially supported by Shaoxing City Philosophy and Social Sciences Planning "Rule of Law Culture and Grassroots Governance Legalization" Collaborative Project (Project Number: 145510) and Shaoxing City Philosophy and Social Science Research "14th Five-Year Plan" 2024 Key Project (Project Number: 145472).

## REFERENCES

- Balta, S. and Atik, M., 2022. Rural planning guidelines for urban-rural transition zones as a tool for the protection of rural landscape characters and retaining urban sprawl: Antalya case from Mediterranean. *Land Use Policy*, 119(April), p.106144. DOI
- Blandy, S. and Sibley, D., 2010. Law, boundaries and the production of space. *Social & Legal Studies*, 19(3), pp.275–284.
- Buhyoff, G.J., Gauthier, L.J. and Wellman, J.D., 1984. Predicting scenic quality for urban forests using vegetation measurements. *Forest Science*, 30(1), pp.71–82.
- Buizer, M., Elands, B., Mattijssen, T., van der Jagt, A., Ambrose, B., Gerőházi, É., Santos, A. and Møller, M.S., 2015. The governance of urban green spaces in selected EU-cities: policies, practices, actors, topics. *The Urban Institute, School of Energy, Geoscience, Infrastructure and Society*.
- Chun, W., 2023. Xinchang procurators actively perform their duties to promote the construction of Tang Poetry Road in Eastern Zhejiang. Guaranteeing the most beautiful poem road scenery with high-quality rule of law. *Daily Rule of Law*, 6(1), pp.88–100.
- Cialdea, D. and Mastronardi, L., 2018. New land use in rural marginal areas: Renewable energy vs landscape preservation. *Advances in Environmental Sciences, Development and Chemistry*, 6, pp.468–474.
- Górka, A., 2016. *Krajobrazowy wymiar ruralistyki* (pp. 1–284). *Politechnika Gdańska*.
- Holder, J., 1999. Law and landscape: The legal construction and protection of hedgerows. *The Modern Law Review*, 62(1), pp.100–114. DOI
- Jiahua, Z., 2023. Defining the legal boundary of personal information protection in the digital era. *Frontiers*, 11, pp.108–111.
- Kusters, K., Buck, L., de Graaf, M., Minang, P., van Oosten, C. and Zagt, R., 2018. Participatory planning, monitoring and evaluation of multi-stakeholder platforms in integrated landscape initiatives. *Environmental Management*, 62(1), pp.170–181.
- Li, J., Liu, Y. and Wang, X., 2024. Study on the temporal and spatial characteristics of village cultural landscape and the protection and development of architecture. *Jiangsu Economic News*, 4(02), pp.7823–7830.
- Mo, L., Chen, J. and Xie, Y., 2021. Assessment of landscape resource using the scenic beauty estimation method at compound ecological system. *Environmental Science and Pollution Research*, 28(5), pp.5892–5899. DOI
- Ning, L.N.C., 2024. Design method of protecting and developing ancient village landscape—taking Dali Lutao Village as an example. *Art Education*, 04, pp.248–251.
- O'Donnell, P.M., 2016. Cultural landscape preservation: An evolving field. *Landscape Journal*, 35(2), pp.203–217. DOI
- Ovchinnikova, N., Aliyeva, N. and Petrova, I., 2021. Integrated approach to area development, preservation and protection of natural landscape. *IOP Conference Series: Earth and Environmental Science*, 937(4). DOI
- Paracchini, M.L. and Capitani, C., 2011. Implementation of an EU-wide indicator for the rural-agrarian landscape in support of COM(2006)508. *Publications Office of the European Union*, 06, p.827. DOI
- Patz, J.A., Daszak, P., Tabor, G.M., Aguirre, A.A., Pearl, M., Epstein, J., Wolfe, N.D., Kilpatrick, A.M., Foutopoulos, J., Molyneux, D., Bradley, D.J., Amerasinghe, F.P., Ashford, R.W., Barthelemy, D., Bos, R., Bradley, D.J., Buck, A., Butler, C., Chivian, E.S. and Zakarov, V., 2004. Unhealthy landscapes: Policy recommendations on land use change and infectious disease emergence. *Environmental Health Perspectives*, 112(10), pp.1092–1098. DOI
- Przybyszewski, K.R., Vicente, R.E., Ferreira, J.V.A., Pereira, M.J.B., Izzo, T.J. and Storck-Tonon, D., 2022. Legal reserves ensure alpha and beta ant diversity in highly modified agricultural landscapes. *Perspectives in Ecology and Conservation*, 20(4), pp.330–337. DOI

- Terra, T.N., dos Santos, R.F. and Costa, D.C., 2014. Land use changes in protected areas and their future: The legal effectiveness of landscape protection. *Land Use Policy*, 38, pp.378–387.
- Tips, W.E. and Savasdisara, T., 1986. The influence of the socio-economic background of subjects on their landscape preference evaluation. *Landscape and Urban Planning*, 13, pp.225–230.
- van Oosten, C., Runhaar, H. and Arts, B., 2021. Capable to govern landscape restoration? Exploring landscape governance capabilities, based on literature and stakeholder perceptions. *Land Use Policy*, 104, p.104020.
- Wei, W., Wang, N., Yin, L., Guo, S. and Bo, L., 2024. Spatio-temporal evolution characteristics and driving mechanisms of Urban–Agricultural–Ecological space in ecologically fragile areas: A case study of the upper reaches of the Yangtze River Economic Belt, China. *Land Use Policy*, 145(June).
- Yermolenko, V., Hafurova, O., Deineha, M., Novak, T., Sinitsky, J. and Ulugov, U., 2021. Landscape approach to formation of system of ecologically balanced use of natural resources: Legal framework. *E3S Web of Conferences*, 280. DOI
- Zhang, L., 2022. Xinchang practice of large garden construction. *Zhejiang Economy*, 12, pp.60–61.

# Bioremediation of Manganese by Thermophilic Bacterial Isolates of Tapt Kund, Soldhar, and Gauri Kund Hot Springs of Uttarakhand, India

A. Patil<sup>1</sup>, S. Devi<sup>2</sup>, Y. Sharma<sup>3</sup>, S. Singh<sup>4</sup>, N. K. Prabhakar<sup>5</sup>, S. Agrawal<sup>6</sup> and Mamta Arya<sup>6†</sup>

<sup>1</sup>Department of Biotechnology, Graphic Era (Deemed to be University), Dehradun-248001, Uttarakhand, India

<sup>2</sup>Department of Microbiology, Himachal Pradesh University, Shimla, Himachal Pradesh, India

<sup>3</sup>Department of Biotechnology, Kalp Laboratories, Mathura-281406, Uttar Pradesh, India

<sup>4</sup>Department of Biotechnology, Dolphin (PG) Institute of Bio-Medical & Natural Sciences, Dehradun, Uttarakhand, India

<sup>5</sup>Department of Botany, H.N.B Garhwal University, Srinagar, Uttarakhand, India

<sup>6</sup>Department of Biotechnology, H.N.B Garhwal University, Srinagar, Uttarakhand, India

†Corresponding author: Mamta Arya; mamtaarya.biotech@gmail.com

**Abbreviation:** Nat. Env. & Poll. Technol.

**Website:** [www.neptjournal.com](http://www.neptjournal.com)

*Received:* 12-09-2024

*Revised:* 11-10-2024

*Accepted:* 19-10-2024

## Key Words:

Manganese  
Minimum Inhibitory Concentration  
Bioremediation  
ICP-MS  
TA8

## Citation for the Paper:

Patil, A., Devi, S., Sharma, Y., Singh, S., Prabhakar, N.K., Agrawal, S. and Arya, M., 2025. Bioremediation of manganese by thermophilic bacterial isolates of Tapt Kund, Soldhar, and Gauri Kund, hot springs of Uttarakhand, India. *Nature Environment and Pollution Technology*, 24(2), p. B4269. <https://doi.org/10.46488/NEPT.2025.v24i02.B4269>

*Note: From year 2025, the journal uses Article ID instead of page numbers in citation of the published articles.*



**Copyright:** © 2025 by the authors

**Licensee:** Technoscience Publications

This article is an open access article distributed under the terms and conditions of the Creative Commons Attribution (CC BY) license (<https://creativecommons.org/licenses/by/4.0/>).

## ABSTRACT

Manganese (Mn) contamination in groundwater is a global concern due to its harmful effects. The high concentration of  $Mn^{2+}$  in humans creates memory issues, decreased fertility, appetite loss, sleeplessness, sperm abnormalities, and 'Manganism'. In this study, the isolation of thermophiles was followed by their assessment for MIC (minimum inhibitory concentration) and Mn bioremediation. We have isolated a total of 11 Mn-resistant bacterial strains of thermophiles with the identification of their bioremediation potential from the Tapt Kund, Soldhar, and Gauri Kund hot springs of Uttarakhand, India. Out of 11 strains, three isolates (TA8, SA9, and GA7) were identified with the highest metal resistance properties for toxic  $Mn^{2+}$ . The metal tolerance capabilities of the strains were evaluated through MIC and the metal biosorption rate was estimated by the live cells bioremediation through thermophilic bacteria. ICP-MS (inductively coupled plasma mass spectrometry) was used to assess the  $Mn^{2+}$  removal rate of bacterial bioremediation. It turned out that every strain exhibited promising bioremediation potential and proved Mn-resistant. The bacterial strain TA8 exhibits the highest MIC ( $600 \mu g.L^{-1}$ ) with a bioremediation rate of 98.34% for  $Mn^{2+}$ . The bacterial strain SA9 has a MIC value of  $525 \mu g.L^{-1}$ , with a biosorption rate of 77.74% for  $Mn^{2+}$ . The bacterial strain GA7 has a MIC of  $475 \mu g.L^{-1}$ , with an efficiency rate of 61.17% for  $Mn^{2+}$  removal. The most promising strain of thermophilic bacteria for  $Mn^{2+}$  bioremediation is the TA8, which has demonstrated the highest potential (98.34%) out of all the tested strains. The findings may have public health implications, as reducing manganese levels in groundwater can help mitigate health risks associated with Mn exposure. Also, this research enriches our knowledge of microbial bioremediation and its potential applications in environmental management. Ultimately, this research could offer a novel, economical, and environmentally beneficial approach to managing metal toxicity.

## INTRODUCTION

Heavy metals are elements that have an atomic number greater than 20, except actinoids, lanthanoids, alkaline earth, and alkali metals. Whereas the density of heavy metals is more than  $5 g.cm^{-3}$  (Arya et al. 2023, Zeng et al. 2024). At present time, technology and modernization result in an increased amount of metal contaminants in the environment (Vishwakarma et al. 2024). Some of the most toxic and hazardous heavy metal elements for the environment and health of organisms include arsenic, manganese, cobalt, selenium, zinc, copper, iron, lead, chromium, cadmium, and mercury. Manganese (Mn) is a vital trace element for both humans and plants. The presence of Mn supports the preservation of human health, including reproduction, digestion, homeostasis, metabolism, antioxidant

defenses, and brain functions (Ao et al. 2024, He et al. 2024).

In addition to being a fundamental and necessary nutrient for all living things, Mn is utilized in a wide range of industries to produce steel, electrode materials, non-ferrous metallurgy, batteries, and catalysis. Therefore, excessive atmospheric concentrations of  $Mn^{2+}$  may be produced by industrial activities. The maximum amount of metal that is permitted to be present in drinking water, according to the World Health Organization (WHO), is  $0.05\text{ mg}\cdot\text{L}^{-1}$ . Since Mn is not a metallic element that degrades naturally, it might be dangerous. In biological systems, Mn exists in eleven distinct oxidation states, but it mostly resides in two states: soluble ( $Mn^{2+}$ ) and insoluble ( $Mn^{4+}$ ) (Patil et al. 2024).

According to Wu et al. (2022) and Vishwakarma et al. (2024), Mn is a complex mineral that is involved in respiration, photosynthesis, pathogen defense, detoxification of reactive oxygen species (ROS), and hormone signaling in plants. However, Mn is an essential component needed by all living things. Amorim et al. (2018) and Patil et al. (2024) stated that a variety of industrial operations may lead to elevated hazardous  $Mn^{2+}$  concentrations that are harmful to the environment and living beings.  $Mn^{2+}$  is a migratory element that is difficult to control, hard to metabolize, and bioaccumulates in the environment (Amorim et al. 2018, Queiroz et al. 2024). Due to the risk of memory loss, insomnia, sperm abnormalities, decreased fertility, and appetite loss, exposure to high concentrations of  $Mn^{2+}$  is harmful to human health (Vishwakarma et al. 2024, He et al. 2024). “Manganism” is a disorder that emerges when the brain’s central nervous system (CNS) possesses an abnormally high concentration of  $Mn^{2+}$  (Vishwakarma et al. 2024, Siddha & Kumar 2024).

To mitigate the adverse effects of heavy metals on the environment, the World Health Organization (WHO) sets maximum permissible limits for the availability of heavy metals in the environment. For this purpose, to keep the balanced concentration of Mn in the environment, a healthy treatment method is required. Common techniques for  $Mn^{2+}$  detoxification include physical, chemical, and biological techniques (Idris et al. 2023, Krishnan et al. 2024). Although these chemical and physical processes result in hazardous byproducts, are difficult to observe for a prolonged amount of time, and ultimately introduce more contaminants into the treated effluent (Krishnan et al. 2024). Therefore, biological treatment such as bioremediation is considered an eco-friendly, economically feasible, and safe technique for metal detoxification (Vishwakarma et al. 2024, Latif et al. 2024). For this purpose, the utilization of bacteria to detoxify hazardous  $Mn^{2+}$  metal into its less complex

form is a significant approach. Bacterial bioremediation is a popular alternative for the biological treatment of toxic metal ions (Latif et al. 2024). Biosorption, bioaccumulation, bioprecipitation, and biological oxidation are the main components of the mechanism of bacterial bioremediation. Several distinct features of bacteria, such as their genetic and structural makeup, extra polymeric substances (EPS), and cell wall composition, are important to accelerate the process of bioremediation. Therefore, bacteria can evolve the genetic resistance mechanisms to handle the metal stress conditions (Vishwakarma et al. 2024). In comparison to bacteria, thermophiles are considered to be more resistant to heavy metals due to their lack of stable thermozymes (Vishwakarma et al. 2024, Singh et al. 2023). The facility of enzyme-mediated catalysis, solubilization, and precipitation of heavy metals make thermophilic bacteria more potent to detoxify heavy metal ions efficiently (Wu et al. 2022, Xu et al. 2024).

The importance of studying heavy metal bioremediation continues to rise as a result of the adverse impacts of toxic metal pollution on the ecosystem. By exploring the bioremediation potential of metal-resistant strains of thermophiles that were isolated from Taptkund hot spring (Chamoli), Soldhar hot spring (Chamoli), and Gaurikund hot spring (Rudraprayag), this study seeks to understand the effects of  $Mn^{2+}$  on these strains and their biological accumulation capacities. Inductively coupled plasma mass spectroscopy, or ICP-MS, was applied to investigate the metal bioremediation of potential thermophilic strains. Through the use of thermophiles, this investigation could offer an effective and novel approach to regulating  $Mn^{2+}$  toxicity and draw attention to the ecological importance of the hot springs located in Garhwal Himalaya, which is among Uttarakhand’s most prominent pilgrimage destinations.

## MATERIALS AND METHODS

### Bacterial Strains and Culture Conditions

A total of 11 Mn-resistant bacterial isolates (Tapt Kund: TA8, TA9, Soldhar: SA7, SA8, SA9, SA10, SA11, SA12, Gauri Kund: GA7, GA8, GA9) were isolated from three distinct hot springs named Taptkund (Chamoli), Soldhar (Chamoli), and Gauri Kund (Rudraprayag) (Fig. 1) of Uttarakhand, India. The samples of water were taken from thermal springs in sterile plastic vials and kept in sterile thermos flasks to maintain the appropriate temperature during the transportation. The sampling was done in October, although the temperature and pH of the hot spring remained the same throughout the year. The bacterial colonies were obtained by the pour plate method (Aneja 2007) that helps to culture



Mn-resistant strains on Mn-containing Tryptone Soya Agar (TSA) medium plates. 1 liter of TSA medium consists of 15g Casein peptone (pancreatic), 5g Soya peptone (papainic), 5g Sodium chloride, and 15g agar with pH 7.3  $\pm$  0.2 to provide nutritious favorable conditions for the growth of bacterial colonies. The inoculated plates were incubated at 55°C for 24-48 h. Each distinctive colony was subsequently streaked on TSA plates to obtain a pure culture.

### MIC of Mn-Resistant Bacterial Strains

The agar dilution method was used to estimate the minimum inhibitory concentration (MIC) of Mn that inhibits bacterial growth. Agar plates were prepared with 50  $\mu\text{g.L}^{-1}$  of sterilized metal as the initial concentration. After inoculating the plates with various bacterial strains, they were incubated for twenty-four hours at 55°C. The bacterial isolates were transferred using the streak plate method onto different agar plates with progressively higher metal concentrations until the isolates stopped growing. This experiment was done in triplicates to ensure the accuracy of this work. The concentration of heavy metals that halted the growth of bacterial cells in the medium was referred to as the minimum inhibitory concentration (MIC) (Srinath et al. 2002).

### Bioremediation of $\text{Mn}^{2+}$ by Live Bacterial Cell

Bacterial bioremediation employs live cells to bioremediate  $\text{Mn}^{2+}$  and to evaluate the metal removal capabilities of

bacterial strains (Özdemir et al. 2013, Vishwakarma et al. 2024). ICP-MS analysis of the samples revealed a decrease in the concentration of Mn ions throughout a 24-hour incubation period of the bacteria with the metal. For this purpose, Mn ions were generated as a heavy metal solution (1000  $\mu\text{g.L}^{-1}$ ) by dissolving its 100% pure chloride salt ( $\text{MnCl}_2 \cdot 4\text{H}_2\text{O}$ ) with sterilized distilled water (Kang et al. 2016). To prevent precipitation, a few drops of concentrated  $\text{HNO}_3$  were added to the further filtered metal solution. The heavy metal solution was diluted successively until it reached the appropriate concentration.

The overnight-cultivated bacteria inoculum was inoculated with 100 micrograms per liter ( $\mu\text{g.L}^{-1}$ ) in 20 mL of broth medium. The mixture was then incubated for 48 h at 55°C at 150 rpm. An additional 24 h were spent incubating the medium after adding 100  $\mu\text{g.L}^{-1}$  of sterilized  $\text{Mn}^{2+}$  solution (except control). To extract the bacterial cells from the broth, centrifugation was performed for 15 min at 10,000 rpm. After collecting the supernatant, it was digested with 2% conc.  $\text{HNO}_3$ , which was subsequently utilized to determine the rate at which bacteria biosorb metals using ICP-MS (Özdemir et al. 2013, Vishwakarma et al. 2024). The remaining concentration of control samples identified through ICP-MS was used as the standard to calculate the bioremediation percentage. All the experiments were performed in triplicates to ensure the accuracy of the results.

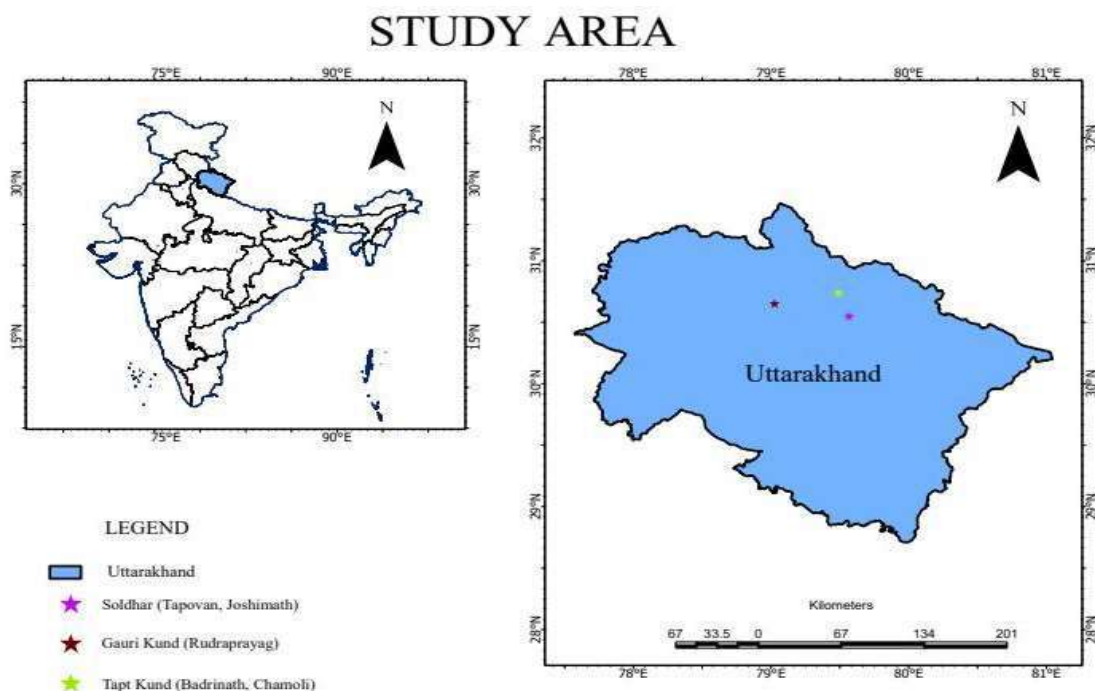


Fig. 1: Geographical locations of hot springs.

## Data Analysis and Calculations

Dilutions of the 1 g.L<sup>-1</sup> stock solution for ICP–MS were prepared to calculate the concentration of total Mn using the PerkinElmer Pure Plus instrument calibration standard 2 solution. To prepare the Mn standard solutions, the 1 g.L<sup>-1</sup> stock solution of instrument calibration standard 2 was diluted. ICP-MS was used to evaluate the bacterial isolates' capacity for heavy metal biosorption. The concentration of metal ions ingested by bacteria was measured using the Perkin-Elmer Nexlon 300x ICP-MS Model. Every sample has been processed sequentially with their standards. Using an appropriate calibration curve or, if available, simply reading the concentration provided by the instrument, the metal ion concentration was measured in micrograms per liter (µg.L<sup>-1</sup>). To determine the heavy metal degrading capability (%), the final result was compared to the control (Vishwakarma et al. 2024) as mentioned in equation (1). The initial concentration is represented as C<sub>i</sub>, the final concentration is represented as C<sub>f</sub>, and the live cell bioremediation absorption % is represented as B<sub>(L)</sub>%.

$$B(L)\% = \frac{C_i - C_f}{C_i} \times 100 \quad \dots(1)$$

## RESULTS AND DISCUSSION

### Bacterial Strains and Culture Conditions

The importance of the bacterial diversity found in the hot springs of Uttarakhand is made clear by the study of thermal springs located in the Garhwal region of the Uttarakhand state (Vishwakarma et al. 2024, Kaur et al. 2023). A total of 11 Mn-resistant bacterial isolates (Tapt Kund: TA8, TA9, Soldhar: SA7, SA8, SA9, SA10, SA11, SA12, Gauri Kund: GA7, GA8, GA9) were isolated from three distinct hot springs of Uttarakhand, India.

The optimal temperature and pH for the growth of thermophilic strains have been reported as 55°C and 7.0, respectively (Vishwakarma et al. 2024). Similarly, Kumar et al. (2020) found comparable values for temperature and pH. Generally, most thermophilic strains thrive within a temperature range of 45°C to 80°C, and those capable of growing at 80°C are classified as thermophilic bacteria, as noted by Brock (1978). Pandey et al. (2015) indicated that the temperature range of the Soldhar hot spring is between 90°C and 95°C. The most favorable pH conditions for bacterial growth are typically neutral. Previous studies have suggested that the temperature and pH parameters are relevant to the hot springs in Manikaran, Himachal Pradesh (Devi & Kanwar 2016), and Surya Kund, Yamunotri, Uttarakhand (Vishwakarma et al. 2024).

Additionally, Ortiz-Cortés et al. (2021) observed that the optimal growth of *Alicyclobacillus* species of thermophiles occurs at 65°C and within a pH range of 3 to 5. Temperature is a key factor influencing the composition of microbial communities in any given ecological niche. It impacts the morphological, physiological, and molecular traits of these communities, resulting in shifts both in composition and function. In this study, the bacterial isolates showed a remarkable capacity to survive across a temperature range of 20 to 70°C, surpassing other colonizers. Furthermore, these isolates displayed tolerance to a broad range of pH levels and moderate salt concentrations, which are also important traits.

### MIC of Mn-Resistant Bacterial Strains

The Mn metal tolerance potential of bacterial strains was determined through MIC. MIC is the lowest concentration of metals at which bacterial growth was not observed, and it was used to confirm the Mn-resistant behavior of the bacterial strains. Table 1 displays the MIC values of all the bacterial strains against toxic Mn ions. All the bacterial strains were found capable of growing in the presence of Mn. The observed Mn-resistant average count (CFU.mL<sup>-1</sup>) of Gauri Kund is 3.5 × 10<sup>4</sup>, Tapt Kund is 3.6 × 10<sup>4</sup>, and Soldhar is 7.1 × 10<sup>4</sup>.

TA8 has the highest MIC (600 µg.L<sup>-1</sup>) among all the thermophilic strains isolated from the Tapt Kund hot spring, whereas SA9 has the highest MIC value of 525 µg.L<sup>-1</sup>. Among all the strains of the Soldhar spring, GA7 was 475 µg.L<sup>-1</sup>, showing the highest MIC value among all the bacterial strains of the Gauri Kund hot spring.

The similar findings of some previous research increase the significance of this study. According to the previous study by Hou et al. (2015), *Klebsiella* species can withstand doses of metals up to 80 mM for Mn (II), among other

Table 1: MIC of Mn<sup>2+</sup> tolerated by the bacterial strains.

Hot spring	Strains	Metal concentration [µg.L <sup>-1</sup> ]
Tapt Kund	TA8	600
	TA9	350
Soldhar	SA7	500
	SA8	425
	SA9	<b>525</b>
	SA10	300
	SA11	475
Gauri Kund	SA12	475
	GA7	<b>475</b>
	GA8	400
	GA9	400

metals. *Marinomonas* sp. *S11-S-4*, isolated from arctic ocean sediment, grew at up to 100 mM (Noszczyńska et al. 2020) of  $Mn^{2+}$ , while strains isolated from Sanindipur mines in Odisha, India, showed discernible growth at up to 500 mM of Mn. Interestingly, at 1000 mM  $MnCl_2$  concentration, *Acinetobacter* sp. MSB 5 from the Sanindipur mines was still viable (Mohanty et al. 2017). *Bacillus thuringiensis* HM7, on the other hand, was able to grow at 31.78 mM after being isolated from Mn ore in Xiangtan, China. Minimal inhibitory concentrations (MIC) of *Alteromonas macleodii* ASC1 (El-Moselhy et al. 2013) isolated from Hurghada harbor in the Red Sea were examined, and resistance to multiple heavy metals was noted at 300 ppm for Mn (El-Moselhy et al. 2013). According to Özdemir et al. (2023), the thermophilic strain *Bacillus cereus* SO-16 was shown to be Mn resistant, with MIC values of Mn (II) 380 mg.L<sup>-1</sup>. Similar to this,

Vishwakarma et al. (2024) isolated eight thermophilic metal-resistant strains of *Firmicutes* and *Proteobacteria* from the Surya Kund Hot Spring in Yamunotri, Uttarakhand, and found that the strains' minimum inhibitory concentrations (MICs) varied from 300 to 375 mg.L<sup>-1</sup>.

### Bioremediation of $Mn^{2+}$ by Live Bacterial Cell

The 24-hour incubation of metal and bacterial isolates interacting solution was resulting the degradation of Mn ions concentration in ICP-MS measurement. Table 2 contains information about heavy metal and tested strains used for the bioremediation assay. The Mn concentration in the control, as determined by ICP-MS analysis, was 25.82 µg.L<sup>-1</sup>. All the strains are found capable of absorbing the toxic  $Mn^{2+}$ . The highest percentages of metal biosorption among all the Mn-resistant strains, including the Tapt Kund strains, have

Table 2: Metal absorption percentage of live bacterial isolates.

Metal	Isolate	Initial Metal concentration [µg.L <sup>-1</sup> ]	Final metal concentration [µg.L <sup>-1</sup> ]	Bioremediation [%] with live bacterial cells	Mean (Average)	Standard Deviation
$Mn^{2+}$	TA8	25.82	0.43	98.35%	13.13	17.953
	TA9		6.96	73.04%	16.39	13.336
	SA7		8.14	68.49%	16.98	12.502
	SA8		11.0	57.02%	18.46	10.409
	SA9		5.75	<b>77.74%</b>	15.79	14.192
	SA10		16.05	37.84%	20.94	6.908
	SA11		10.06	61.02%	17.94	11.144
	SA12		9.24	64.21%	17.53	11.724
	GA7		10.02	<b>61.17%</b>	17.92	11.172
	GA8		11.72	54.60%	18.77	9.970
	GA9		13.27	48.62%	19.55	8.874

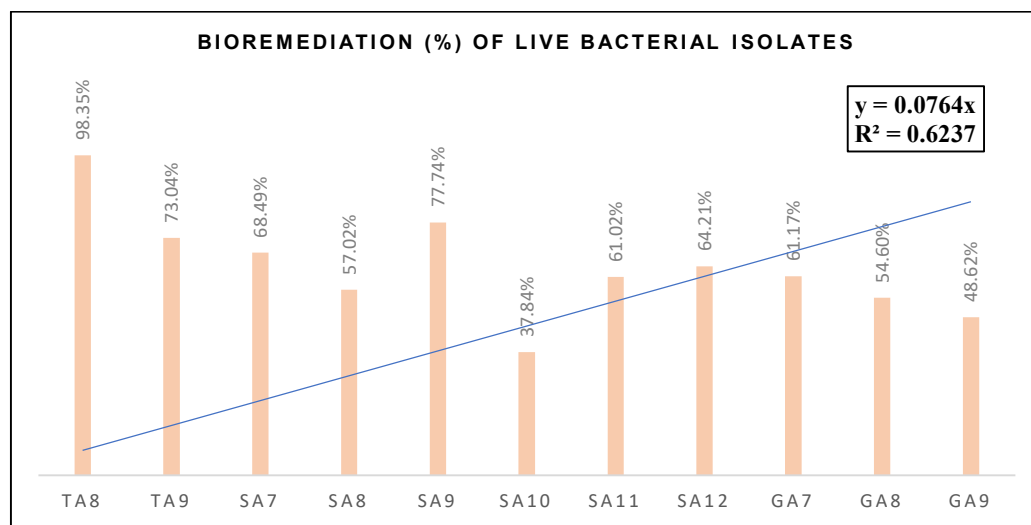


Fig. 2: Rate of  $Mn^{2+}$  absorption through live cells of bacterial isolates [X axis: Isolates, Y axis: Bioremediation%].

been observed in the TA8 isolate (98.34%). Among Gauri Kund strains, the highest percentage of Mn observation has been observed in GA7 (61.17%), and among Soldhar strains, the highest metal absorption percentage has been observed in SA9 (77.74%) respectively (Fig. 2). SA10 isolate of the Soldhar spring has observed with the least percentage (37.84%) of Mn absorption.

This finding highlights the differences in metal absorption capabilities among various strains from the same ecological niche. The SA10 isolate from the Soldhar spring showed the lowest Mn absorption rate at 37.84%, raising questions about the factors that may be contributing to its reduced effectiveness. Possible explanations could include genetic variations, differences in metabolic pathways, or adaptations to environmental conditions. Overall, these results reveal the diverse capacities of different bacterial strains to absorb manganese, suggesting that certain isolates could be effectively utilized in bioremediation efforts. Further investigation into the mechanisms driving these differences in biosorption rates could provide valuable insights for enhancing bioremediation strategies.

The  $R^2$  value is less than 1 with a straight line, indicating that the data of results are significant (Fig. 2 and Table 2). To validate the accuracy of the results, a standard deviation was calculated. This measure indicates the extent of variability within the data set. By comparing each data point to the overall average, standard deviation provides a value that reflects how closely the points cluster around the mean. A low standard deviation suggests that the data is closely aligned with the average, indicating higher accuracy, while a high standard deviation points to significant variation

from the mean. In this analysis, the observed  $R^2$  value for standard deviation is notably low at 0.87, which underscores the reliability of the bioremediation outcomes (Fig. 3). Consequently, the isolates have shown promising potential for Mn metal bioremediation.

Each isolate demonstrated robust resistance to the  $Mn^{2+}$  and demonstrated the ability to proliferate on the plates containing metal. All of the bacterial isolates used in the bioremediation experiment were able to biosorb  $Mn^{2+}$  by using live biomass. It has been demonstrated by the current study and references to other research that thermophilic bacteria are capable of bioremediating  $Mn^{2+}$  from the environment. Hussein et al. (2005) examined the bioaccumulation of heavy metals in mesophilic environments by using two strains of *Pseudomonas*. For that, two distinct metal ions were gathered for the bioaccumulation of Cu (II) ( $151.42 \text{ mg.L}^{-1}$ ) and Ni (II) ( $54 \text{ mg.L}^{-1}$ ) effectively. Vishwakarma et al. (2024) discovered that *Acinetobacter* sp. *LSN10* has the highest potential for eliminating  $Mn^{2+}$  ions in both live (41.202%) and dead (64.721%) environments. According to Majumder et al. (2015), *Acinetobacter guillouiae* and the *Enterobacter* genera were discovered to be capable of bioaccumulating harmful metal ions and of having an efficient removal mechanism for  $Cu^{2+}$  bioremediation. Firmicute members can use bioremediation to lower environmental concentrations of iron and sulfate when conditions are favorable (Banerjee et al. 2015, Vishwakarma et al. 2024). According to Imron et al. (2021), *V. damsela*, *P. fluorescens*, *P. stutzeri*, and *P. aeruginosa* are the four bacterial strains that have been isolated from leachate and exhibit a high resistance for Cu, Fe, and Mn.

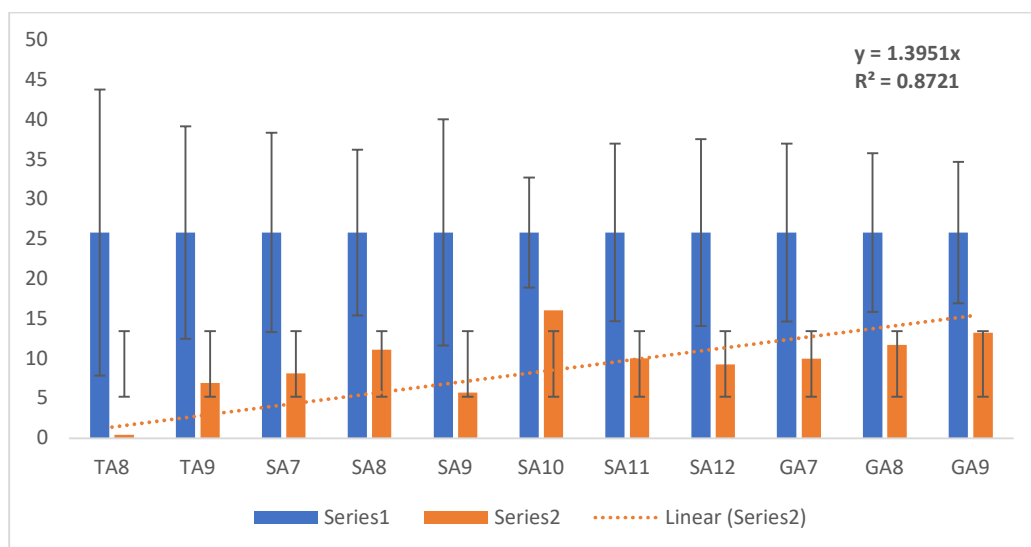


Fig. 3: Standard deviation of Mn resistant isolates.



The thermophilic bacteria *Bacillus thuringiensis* has been reported by Huang et al. (2020) to be able to withstand 4,000 mg.L<sup>-1</sup> of Mn (II) and to have a maximum clearance rate of 95.04% at 400 mg.L<sup>-1</sup>.

According to these previous studies, the most effective bacterial strains for bacterial bioremediation are thermophilic strains, which are also highly resistant to heavy metals. Additionally, it is observed that a mixture or consortium of bacterial species exhibits a significant influence on the rate of metal biosorption. The potential of the novel manganese-oxidizing bacteria (MOB) consortium AS for the removal of Mn<sup>2+</sup> was investigated by Wan et al. (2020). The MOB consortium was able to remove 98%, 91%, 99%, and 76% of metal ions by performing Mn (II) and Fe (II), Ni (II), Cu (II), and Zn (II) biosorption assay. As a result, it can also be said that the rate of Mn (II) of MOB consortium AS is increased by the presence of different organics and other metals. Therefore, a bioremediation assay through the consortium of some bacteria has been considered for further studies (Patil et al. 2024, Bee et al. 2024, Patil et al. 2024). The dead biomass of bacteria also has a significant role in heavy metal bioremediation (Patil & Arya 2024). Therefore, these strains will further explore the dead biomass bioremediation to check the comparative potential of live and dead biomass of thermophilic bacterial strains.

This research is significant for several reasons. Firstly, it deepens our understanding of bioremediation strategies for managing toxic metal contamination in groundwater, particularly manganese, which is often overlooked. Secondly, identifying effective thermophilic strains offers a sustainable and eco-friendly approach to reducing Mn<sup>2+</sup> toxicity in contaminated environments. By leveraging the natural capabilities of these bacteria, this study paves the way for the development of innovative bioremediation techniques that are both cost-effective and environmentally beneficial.

## CONCLUSION

Manganese is an important metal that is necessary for the accomplishment of several biological processes, but excessive amounts of it can be harmful. The environment and human health are more at risk due to the elevated concentration of Mn<sup>2+</sup> contaminants in the environment. As a result, it's necessary to investigate several natural remediation processes that can effectively and economically extract Mn<sup>2+</sup> from the environment. Through this study, we were able to isolate some Mn-resistant strains of bacteria from the thermal springs of Uttarakhand's Himalaya range. Among all the bacterial strains, TA8 has the highest Mn<sup>2+</sup> bioremediation rate (98.34%) with the highest minimum inhibitory concentration (MIC) of 600 µg.L<sup>-1</sup>, therefore

this strain can be considered for further in-depth study. It had been proven that the bacterial strains could bioabsorb and detoxify Mn<sup>2+</sup> from their systems when the conditions (pH, temperature, and incubation time) were ideal. This study has important implications for environmental policies and industrial practices. It can help policymakers refine regulations on manganese contamination in groundwater and establish permissible levels. Moreover, the identification of thermophilic strains with high Mn<sup>2+</sup> absorption supports industries in adopting sustainable bioremediation techniques as alternatives to chemical methods, reducing environmental impact. However, more research is needed on the comparative analysis of consortia biosorption of heavy metals and dead biomass bioremediation by utilizing different potent bacterial strains. However, molecular identification of these strains has been included in another part of the study. The results of this study could provide new optimism for managing metal toxicity in the future. The findings of this study might provide an economical, sustainable, and effective substitute for Mn<sup>2+</sup> metal biosorption.

## ACKNOWLEDGMENTS

We are thankful to the Department of Biotechnology, Hemvati Nandan Bahuguna Garhwal University, Srinagar (Uttarakhand), and National Scheduled Castes Finance and Development Corporation (NSFDC) India for providing the facility for this work.

## REFERENCES

- Amorim, S.S., Ruas, F.A.D., Barboza, N.R., de Oliveira Neves, V.G., Leao, V.A. and Guerra-Sa, R., 2018. Manganese (Mn<sup>2+</sup>) tolerance and biosorption by *Meyerozyma guilliermondii* and *Meyerozyma caribbica* strains. *Journal of Environmental Chemical Engineering*, 6(4), pp.4538–4545.
- Aneja, K.R., 2007. *Experiments in Microbiology, Plant Pathology, and Biotechnology*. New Age International, New Delhi.
- Ao, C., Tang, S., Yang, Y., Liu, Y., Zhao, H., Ban, J. and Li, J., 2024. Identification of histone acetylation modification sites in the striatum of subchronically manganese-exposed rats. *Epigenomics*, 0(0), pp.1–10.
- Arya, M., Patil, A., Singh, S. and Sharma, B., 2023. *Water: Management & Governance*. Springer, pp.194–207.
- Banerjee, G., Pandey, S., Ray, A.K. and Kumar, R., 2015. Bioremediation of heavy metals by a novel bacterial strain *Enterobacter cloacae* and its antioxidant enzyme activity, flocculant production, and protein expression in the presence of lead, cadmium, and nickel. *Water, Air, & Soil Pollution*, 226(4), pp.1–9.
- Bee, A., Kumar, S., Khamari, A. and Patil, A., 2024. A brief comparative note about the mechanisms of microbial bioremediation and phytoremediation. *Journal of Environmental Bio-Sciences*, 38, pp.59–64.
- Brock, T.D., 1978. *Thermophilic Microorganisms and Life at High Temperatures*. Springer-Verlag, New York.
- Devi, S. and Kanwar, S.S., 2016. Deciphering the diversity of aerobic culturable thermophiles in hot springs of Manikaran, Himachal Pradesh. *International Journal of Farm Sciences*, 6(1), pp.156–162.

- El-Moselhy, K.M., Shaaban, M.T., Ibrahim, H.A. and Abdel-Mongy, A.S., 2013. Biosorption of cadmium by the multiple-metal resistant marine bacterium *Alteromonas macleodii* ASC1 isolated from Hurghada harbor, Red Sea. *Archives of Science*, 66(2), pp.259–272.
- He, J., Ma, X., Zhang, J., Yang, Y.P., Qin, H., Chen, H. and Zou, Y., 2024. Manganese-induced neurological pyroptosis: Unveiling the mechanism through the ROS-activated Caspase-3/GSDME signaling pathway. *Food and Chemical Toxicology*, 184, 114322.
- Hou, Y., Cheng, K., Li, Z., Ma, X., Wei, Y., Zhang, L. and Wang, Y., 2015. Biosorption of cadmium and manganese using free cells of *Klebsiella* sp. isolated from wastewater. *PLOS ONE*, 10(10), p.e0140962.
- Huang, H., Zhao, Y., Xu, Z., Ding, Y., Zhou, X. and Dong, M., 2020. A high Mn (II)-tolerance strain, *Bacillus thuringiensis* HM7, isolated from manganese ore and its biosorption characteristics. *PeerJ*, 8, p.e8589.
- Hussein, H., Farag, S., Kandil, K. and Moawad, H., 2005. Tolerance and uptake of heavy metals by *Pseudomonads*. *Process Biochemistry*, 40(2), pp.955–961.
- Idris, M.O., Yaqoob, A.A., Ibrahim, M.N.M., Ahmad, A. and Alshammari, M.B., 2023. Introduction of adsorption techniques for heavy metals remediation. In *Emerging Techniques for Treatment of Toxic Metals from Wastewater*, pp.1–18. Elsevier.
- Imron, M.F., Kurniawan, S.B. and Abdullah, S.R.S., 2021. Resistance of bacteria isolated from leachate to heavy metals and the removal of Hg by *Pseudomonas aeruginosa* strain FZ-2 at different salinity levels in a batch biosorption system. *Sustainable Environment Research*, 31, pp.1–13.
- Kang, C.H., Kwon, Y.J. and So, J.S., 2016. Bioremediation of heavy metals by using bacterial mixtures. *Ecological Engineering*, 89, pp.64–69.
- Kaur, S., Patil, A., Singh, S. and Arya, M., 2023. Hot springs of Uttarakhand and scheme for rejuvenation of Gaurikund at Kedarnath. *ENVIS Newsletter on Himalayan Ecology*, 20(3), pp.1–3.
- Krishnan, N.B., Velmurugan, N.K., Kumar, P.S., Rangasamy, G., Palanivelu, J., Thamarai, P. and Shakoor, A., 2024. Fungal bioremediation approaches for the removal of toxic pollutants: Mechanistic understanding for biorefinery applications. *Chemosphere*, p.141123.
- Kumar, R., Kirti, V. and Sharma, R.C., 2020. Thermophilic microbial diversity and physicochemical attributes of thermal springs in the Garhwal Himalaya. *Environmental & Experimental Biology*, 18(2), pp.1–10.
- Latif, F., Perveen, S., Aziz, S., Iqbal, R. and Shahzad, M.M., 2024. Bioremediation of heavy metals from aquatic environments. In *Bioremediation for Sustainable Environmental Cleanup*, pp.223–237. CRC Press.
- Majumder, S., Gangadhar, G., Raghuvanshi, S. and Gupta, S., 2015. A comprehensive study on the behavior of a novel bacterial strain, *Acinetobacter guillouiae*, for bioremediation of divalent copper. *Bioprocess and Biosystems Engineering*, 38(9), pp.1749–1760.
- Mohanty, S., Ghosh, S., Nayak, S. and Das, A.P., 2017. Bioleaching of manganese by *Aspergillus* sp. isolated from mining deposits. *Chemosphere*, 172, pp.302–309.
- Noszczyńska, M., Łakomy, K., Nowacki, K. and Piotrowska-Seget, Z., 2020. A high manganese-tolerant *Pseudomonas* sp. strain isolated from a metallurgical waste heap can be a tool for enhancing manganese removal from contaminated soil. *Applied Sciences*, 10(16), p.5717.
- Ortiz-Cortés, L.Y., Ventura-Canseco, L.M.C., Abud-Archila, M., Ruíz-Valdiviezo, V.M., Velázquez-Ríos, I.O. and Alvarez-Gutiérrez, P.E., 2021. Evaluation of temperature, pH, and nutrient conditions in bacterial growth and extracellular hydrolytic activities of two *Alicyclobacillus* spp. strains. *Archives of Microbiology*, 203(7), pp.4557–4570.
- Özdemir, S., Kilinç, E., Poli, A. and Nicolaus, B., 2013. Biosorption of heavy metals ( $\text{Cd}^{2+}$ ,  $\text{Cu}^{2+}$ ,  $\text{Co}^{2+}$ , and  $\text{Mn}^{2+}$ ) by thermophilic bacteria, *Geobacillus thermantarcticus*, and *Anoxybacillus amylolyticus*: Equilibrium and kinetic studies. *Bioremediation Journal*, 17(2), pp.86–96.
- Ozdemir, S., Turkan, Z., Kilinc, E., Bayat, R. and Sen, F., 2023. The removal of heavy metal pollution from wastewaters using thermophilic *B. cereus* SO-16 bacteria. *Chemosphere*, 311, p.136986.
- Pandey, A., Dhakar, K., Sharma, A., Priti, P., Sati, P. and Kumar, B., 2015. Thermophilic bacteria that tolerate a wide temperature and pH range colonize the Soldhar (95°C) and Ringigad (80°C) hot springs of Uttarakhand, India. *Annals of Microbiology*, 65, pp.809–816.
- Patil, A., Kaur, S., Verma, A. and Arya, M., 2024. Manganese ( $\text{Mn}^{2+}$ ) pollution and its bioremediation: An overview. *Biochemistry and Cellular Archives*, 24, pp.1–11.
- Patil, A. and Arya, M., 2024. Water quality assessment and heavy metal analysis of Ganga River system and effluent water of SIDCUL at Haridwar through atomic absorption spectroscopy. *Journal of Mountain Research*, 19(1), pp.171–181.
- Patil, A., Chakraborty, S., Yadav, Y., Sharma, B., Singh, S. and Arya, M., 2024. Bioremediation strategies and mechanisms of bacteria for resistance against heavy metals: A review. *Bioremediation Journal*, pp.1–33.
- Patil, A., Sharma, Y., Khandelwal, V., Rajamohan, N. and Arya, M., 2024. Biochemical, molecular characteristics, and bioremediation properties of  $\text{Mn}^{2+}$ -resistant thermophilic *Bacillus* strains. *Waste and Biomass Valorization*, (in press), pp.1–12.
- Queiroz, H.M., Maki, B., Ferreira, A.D., Boim, A.G.F., Ying, S.C., Nóbrega, G.N. and Ferreira, T.O., 2024. Manganese: The rise of an unnoticed environmental contaminant. In *Inorganic Contaminants and Radionuclides*, pp.151–188. Elsevier.
- Siddha, S. and Kumar, M., 2024. Sustainable approaches for heavy metal removal from water. In *Role of Green Chemistry in Ecosystem Restoration to Achieve Environmental Sustainability*, pp.227–235. Elsevier.
- Singh, S., Das, S. and Khanna, C., 2023. Extremophiles for the textile industry. In *Extremophiles*, pp.277–298. CRC Press.
- Srinath, T., Verma, T., Ramteke, P.W. and Garg, S.K., 2002. Chromium (VI) biosorption and bioaccumulation by chromate-resistant bacteria. *Chemosphere*, 48(4), pp.427–435.
- Vishwakarma, S.K., Patil, A., Pandey, A. and Arya, M., 2024. Biosorption of heavy metal ( $\text{Mn}^{2+}$ ) by thermophilic bacterial strains isolated from Surya Kund hot spring, Yamunotri, Uttarakhand. *Applied Biochemistry and Biotechnology*, 44, pp.1–16.
- Wan, W., Xing, Y., Qin, X., Li, X., Liu, S., Luo, X. and Chen, W., 2020. A manganese-oxidizing bacterial consortium and its biogenic Mn oxides for dye decolorization and heavy metal adsorption. *Chemosphere*, 253, p.126627.
- Wu, R., Yao, F., Li, X., Shi, C., Zang, X., Shu, X. and Zhang, W., 2022. Manganese pollution and its remediation: A review of biological removal and promising combination strategies. *Microorganisms*, 10(12), p.2411.
- Xu, X., Song, F., Zhang, G., Ma, L. and Yang, N., 2024. Proteomic insights into the response of *Halomonas* sp. MNB13 to excess Mn (II) and the role of  $\text{H}_2\text{S}$  in Mn (II) resistance. *Environmental Research*, 91, p.118157.
- Zeng, Y., Lin, Y., Ma, M. and Chen, H., 2024. A review on the removal of heavy metals from water by phosphorus-enriched biochar. *Minerals*, 14(1), p.61.

# Investigating the Effectiveness of Peanut Hull as Biosorbent of Lead (Pb) from Water

Mehak Verma<sup>†</sup>  and Sarita Sachdeva

Department of Biotechnology, Manav Rachna International Institute of Research and Studies, Sector 43, Faridabad, Haryana, India

<sup>†</sup>Corresponding author: Mehak Verma; mehakverma2829@gmail.com

**Abbreviation:** Nat. Env. & Poll. Technol.  
**Website:** www.neptjournal.com

*Received:* 09-07-2024

*Revised:* 21-08-2024

*Accepted:* 26-08-2024

## Key Words:

Biosorption  
 Heavy metals  
 Lead  
 Peanut hull  
 SDG-6  
 SDG-12

## Citation for the Paper:

Verma, M. and Sachdeva, S., 2025. Investigating the effectiveness of peanut hull as biosorbent of lead (Pb) from water. *Nature Environment and Pollution Technology*, 24(2), p. B4239. <https://doi.org/10.46488/NEPT.2025.v24i02.B4239>

*Note: From year 2025, the journal uses Article ID instead of page numbers in citation of the published articles.*



**Copyright:** © 2025 by the authors

**Licensee:** Technoscience Publications

This article is an open access article distributed under the terms and conditions of the Creative Commons Attribution (CC BY) license (<https://creativecommons.org/licenses/by/4.0/>).

## ABSTRACT

Lead contamination poses a major threat to health and environmental well-being. The remediation of this heavy metal from water sources is essential to safeguard health and ensure access to clean water. In this study, Peanut hull was used as a biosorbent for lead (Pb) removal from water. It focuses on optimizing various parameters important for lead removal. Statistical analysis, such as the Kruskal-Wallis test, was done to assess the significance of these parameters on lead biosorption, and an inverse variance weighting technique was employed to derive the weighted contribution of each variable for fixed Pb removal categories in the range of 80-100% and 80% (below). On analysis, it was found that factors such as pH and biomass dosage played major roles in lead removal. Furthermore, Scanning Electron Microscopy (SEM) and Energy-dispersive X-ray Spectroscopy (EDS), were done to find out changes in the structural and elemental characteristics of peanut hull after lead sequestration. Overall, this study highlights the potential of peanut hull as a promising biosorbent for lead removal from water, thereby offering a sustainable solution to water contamination with heavy metals.

## INTRODUCTION

Water is one of the most essential resources required for the survival of living beings on earth. It plays a crucial role in physiological functions such as digestion, circulation, regulation of temperature, and waste removal. Beyond its biological importance, water also plays an important role in hydration, agriculture, sanitation, and industry, but access to clean and safe water is a cornerstone of public health, reducing the spread of diseases and improving the quality of life, along with very survival of lifeform on this planet. However, when it comes to water contamination with heavy metals, Lead contributes to significant health risks. When ingested through contaminated water, lead can accumulate in the body, leading to a range of health problems, such as developmental delays in children, neurological damage, kidney damage, and high blood pressure (Prabha & Udayashankara 2014, Tewari et al. 2023). Even low levels of lead exposure can be harmful, making it crucial to ensure that water sources are free from such contaminants. The United States Environment Protection Agency (USEPA) sets maximum permissible limits for lead (II) in drinking water at 0.015 mg.L<sup>-1</sup> and in wastewater at 0.1 mg.L<sup>-1</sup> respectively (Tanase et al. 2020).

Therefore, to address the removal of lead contamination in water, biosorption has emerged as an effective technique. This technique utilizes biological materials to adsorb and eliminate a pollutant, also offering a promising solution to mitigate Pb poisoning (Apori et al. 2018).

From the various materials used in the past, Peanut hull, the outer covering of peanut, also known as ground nut, consisting of cellulose, hemicellulose, and lignin, has proved to be a novel bioadsorbent as it is very porous and has a large surface area which makes it a good bioadsorbent. Though these hulls have no nutritional benefits, they do have health benefits as they have antioxidants such as polyphenols, amino acids, and flavonoids (Adhikari et al. 2019). They also contain Carotene, Luteolin, and Isosaponaretin (Yu et al. 2014). Peanut hulls not only exhibit antimicrobial activities, which can help reduce harmful bacteria in water, but also demonstrate inhibitory effects against pest attacks (Wee et al. 2007, Adhikari et al. 2019). These benefits are being explored in the scientific world for the benefit of humans. In addition to this, they also show good adsorbent properties in the removal of metals and dyes from water (Sattar et al. 2019, Panchal et al. 2020). In recent times, new regulations have been introduced to bolster the protection of our environment, majorly focusing on the depollution and recycling of heavy metals. These regulations emphasize the need for eco-friendly depollution methods. Plant-based materials for the treatment of water are highly encouraged because of their eco-friendly and non-toxicity nature (Dharsana & Arul Jose 2022). Among the various approaches, using low-cost natural adsorbents for the adsorption process stands out as an effective and sustainable solution for heavy metal remediation (Olabanji & Oluayemi 2021, Kali et al. 2024, Sudan et al. 2024). Therefore, peanut hull fits best as a bioadsorbent for the removal of heavy metals such as lead from water. It is environmentally friendly and cost-effective and works great in removing toxic metals and contaminants. It contains functional groups like hydroxyl, carboxyl, and amino, which enable the biosorption process (Gong et al. 2005).

In this study, Peanut hull is used as a biosorbent for the removal of Lead from water. The impact of parameters such as pH, contact time, temperature, metal concentration, particle size, and biomass dose on the adsorption efficiency of lead from water was investigated in light of the presence of lead in raw drinking water in Faridabad district, Haryana, as observed in previous study undertaken. Also, In alignment with the United Nations Sustainable Development Goals (SDGs), Goal 6 (Clean Water and Sanitation) and Goal 12 (Responsible Consumption and Production) supports the utilization of peanut hulls as biosorbents in sustainable water management and promote the efficient use of natural resources.

## MATERIALS AND METHODS

### Preparation of Biosorbent

Peanut hull was selected as biomaterials. It was sourced from

a local market and thoroughly washed with water to remove any impurities. Afterward, it was air-dried for three days. The dried husks were then ground using a grinder machine and sieved through meshes of sizes (100, 150, 200, 250, and 300 mm) to obtain particles of varying sizes. These biomass particles were stored in airtight pouches to preserve their quality and were subsequently utilized in batch experiments.

### Preparation of Metallic ion Solution

A lead standard solution ( $\text{Pb}(\text{NO}_3)_2$ ) in  $\text{HNO}_3$  at  $0.5 \text{ mol.L}^{-1}$  of 1000 ppm was purchased from Sigma Aldrich. Stock solutions of 50, 100, 150, 200, and 250 ppm were prepared using the standard solutions. pH of the samples was maintained by adding 0.1M NaOH solution or by adding 0.1M HCl solution.

### Design of Sorption Experiments

Adsorption studies were conducted by considering six major factors as operational variables. The effects of pH levels (4-8), temperature ( $20\text{-}40^\circ\text{C}$ ), particle size (100-300 mm), biomass dose ( $1\text{-}5 \text{ g.L}^{-1}$ ), initial metal concentration (50-250 ppm), and metal exposure time (30-240 min) were investigated to determine the optimal conditions for Pb removal. The experiment was designed on Minitab 17 using the Taguchi method with six variables at five levels. A 25-run experiment was designed using the software. Each run was carried out in triplicate with a specific range for each variable. A 50 mL water sample was taken, and the peanut hull biomaterial was added along with a synthetic metal solution of Lead, and the experiments were performed as shown in Fig. 1. The experiments were conducted in a 250 mL flask containing the lead synthetic solution in different concentrations containing the desired level of peanut hull biomass at the beginning of each experiment. The flasks were kept in the incubator and were agitated at 125 rpm and then centrifuged at 5000 rpm for 5 min to separate the solid from the liquid phase. The samples were filtered and the concentrations of metal in the samples were estimated by Atomic Absorption Spectroscopy (Model No. AAS429).

### Characterization

Scanning Electron Microscopy (SEM) and energy-dispersive X-ray spectroscopy (EDS) were undertaken to analyze the sorption of lead on the biomaterial. The air-dried samples of the peanut hull, before and after biosorption, were used. The samples were coated with a thin layer of gold before conducting morphological studies to ensure clear imaging and prevent charging effects. The elemental compositions of the samples were analyzed using energy-dispersive X-ray spectroscopy (EDS) integrated with the scanning electron microscope (SEM) at bar lengths of  $10 \mu\text{m}$  and a voltage



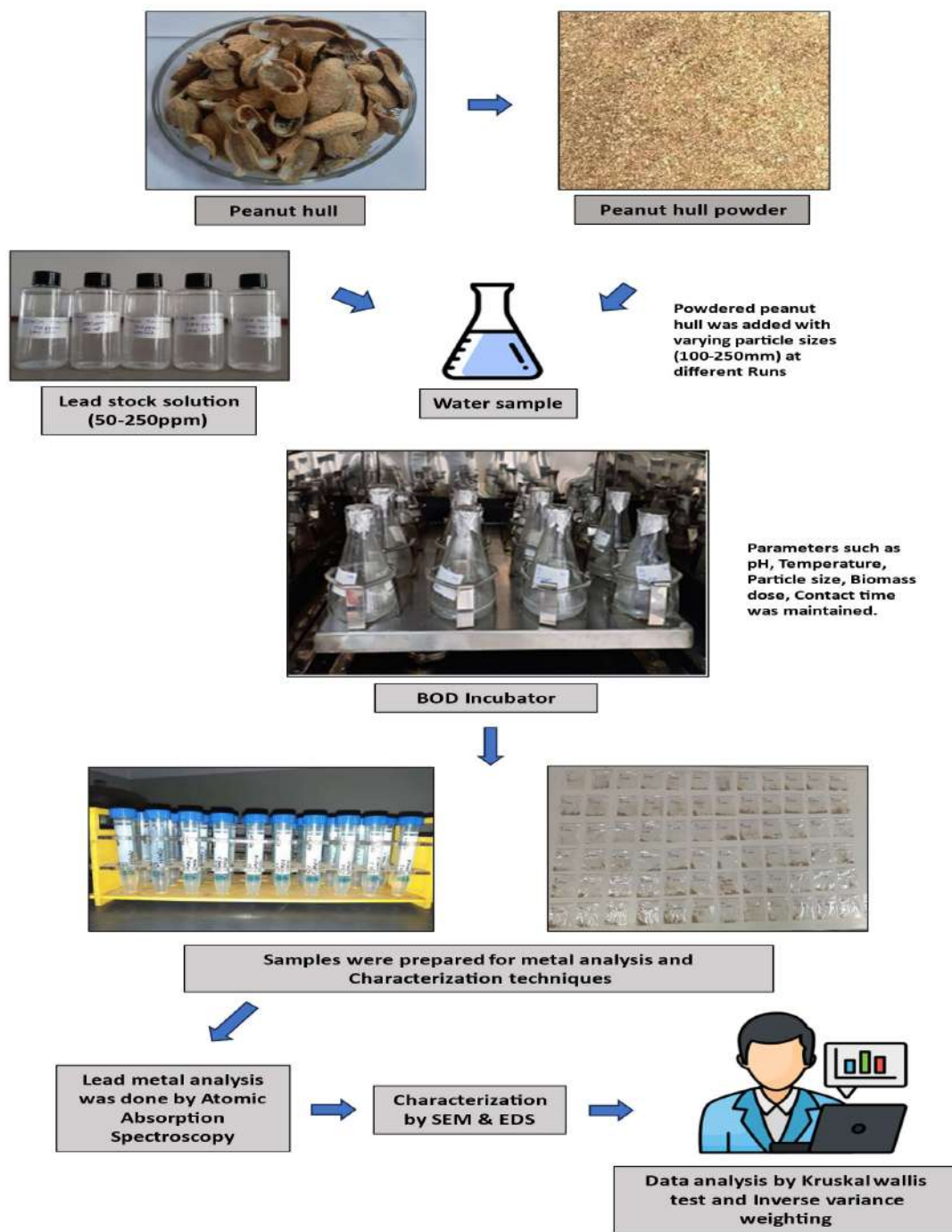


Fig. 1: Schematic diagram depicting the process of biosorption study with lead metal.

of 20 kV at 1500 magnification was recorded on a JEOL JSM-6610LV SEM.

### Statistical Analysis

Statistical analysis was conducted using Python 3.11.4 (by Anaconda) and R software. The Kruskal–Wallis test was used

to determine the significance of the adsorption parameters on metal removal. The inverse variance weighting method was used to determine the weight percent contribution of each variable towards the removal of the Lead metal. In this method, the weights of each variable are calculated as the inverse of the variance of the variable when taking multiple

measurements with varying values of the variables. In this study, several variables, each contributing towards the removal of lead, and to calculate the weighted contribution of each variable, first, the total percentage removal was fixed into two categories, namely 80-100% and below 80%, to obtain the significant number of data points. Given the percentage removal in each category, the variance (var) of the values of the contributing variables was calculated using the R statistical software. The inverse of this variance (1/var) was regarded as the weight. To calculate the weight percent, all these weights were summed up for all the variables, and the percentage was calculated as  $\text{weight}/\text{sum} \times 100$ . The assumptions include that the variables are independent and their values are expressed in their respective standard units (Team 2024).

To determine the optimum conditions, adsorption efficiency was calculated using Eq.1 -

$$\text{Adsorption efficiency (\%)} = \frac{C_0 - C_F}{C_0} \times 100 \quad \dots(1)$$

Where  $C_0$  is the initial concentration (ppm) and  $C_F$  is the Final concentration (ppm) of the metal.

## RESULTS AND DISCUSSION

### Effect of pH

The potential of hydrogen (pH) plays an important role in influencing the process of biosorption. The biosorption of lead (Pb) on the sorbent was investigated across a pH range of 4 to 8, considering various factors such as temperature, particle size, biomass dosage, metal concentrations, and contact time. The influence of pH on metal removal was

investigated across varying concentrations (50, 100, 150, 200 and 250 ppm). As seen in Fig. 2, Average maximum removal was observed at pH 5, i.e. 91.51%. Also, out of the experiments conducted, under varying variables, at an initial concentration of 150 ppm, pH 5, lead removal (100%) was observed, which indicates the efficiency of peanut hull as a biosorbent. Hence, results reveal that pH is one of the crucial factors. The competitiveness of metallic ions, the activity of the functional groups in the biomass, and the solution chemistry of the metals are all impacted by pH (Verma & Suthar 2015).

Furthermore, the Kruskal Wallis test statistically shows significant removal of Pb across all the variables. The inverse variance weighting approach gives the weighted contribution of each variable across the percentage ranges of 80-100% and below 80%. The result reveals that pH is one of the most important factors among all the adsorption parameters, with % weights ranging from 47.52-50.40%.

### Effect of Temperature

The effect of this parameter on the metal removal was investigated in the temperature range between 20-40°C. Temperature significantly impacts the adsorption capacity, kinetics, and thermodynamic properties of peanut hulls in the removal of lead (Pb) metal (Aranda-García & Cristiani-Urbina 2018). Further, temperature variations can alter the efficiency of adsorption, affect the rate at which adsorption occurs, and influence the overall thermodynamic feasibility of the process (Znad et al. 2022). The maximum average removal, i.e., 87.65% at 20°C. With the increase

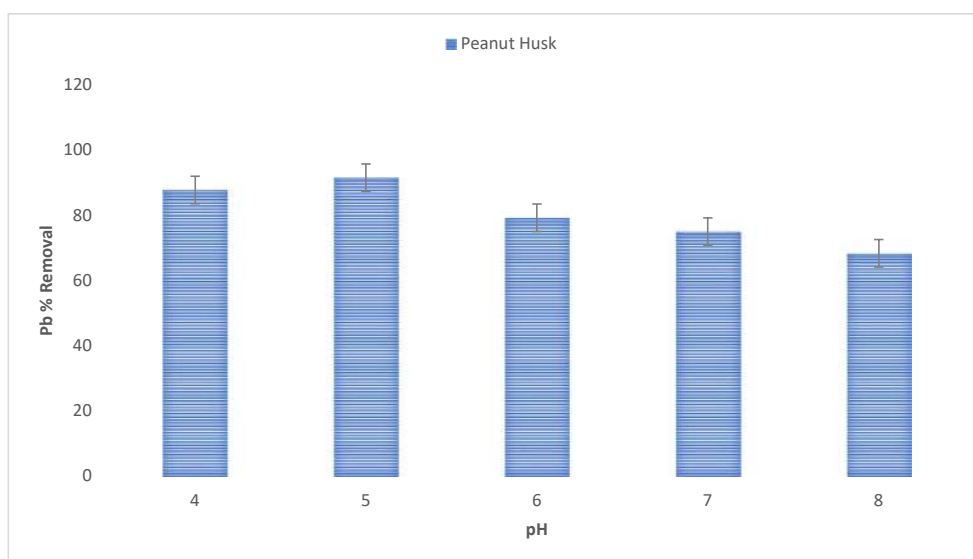


Fig. 2: Effect of pH on Lead adsorption efficiency.

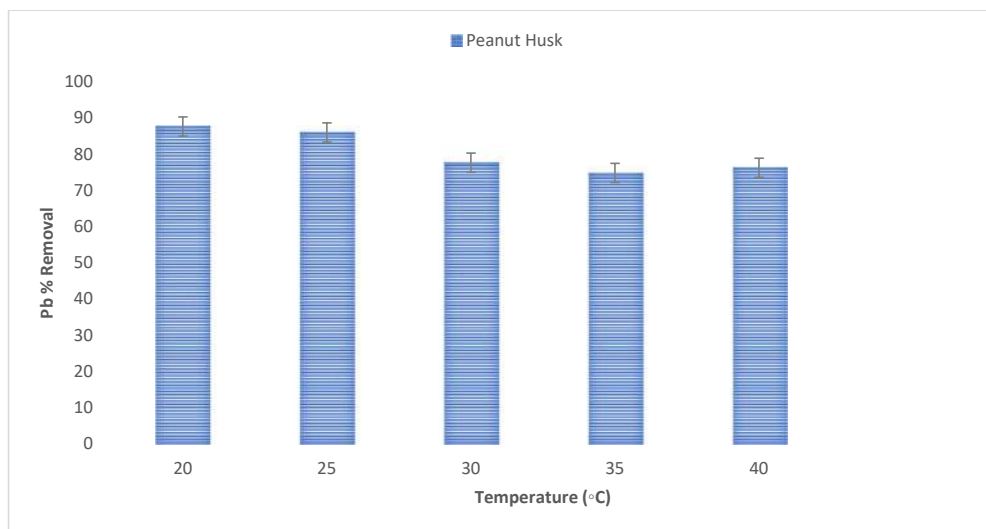


Fig. 3: Effect of temperature on lead adsorption efficiency.

in temperature, there was a decrease in lead adsorption efficiency (Tanyildizi et al. 2011, Zhao et al. 2021), as depicted in Fig. 3 below. Also, under specific conditions, At a pH range of 4-6, Temperature 20°C, metal concentration of 50-100ppm, 100% metal removal was observed. Furthermore, the Kruskal Wallis test statistically shows significant removal of Pb across all the variables. The inverse variance weighting approach reveals that Temperature also exerts influence amongst all the adsorption parameters with % weights ranging from 2.27 – 18.25%.

### Effect of Particle Size

To investigate the effect of particle size on metal sorption, particle sizes ranging from 100 to 300 mm were tested. It was

observed that particle size did not exhibit a major trend or significant difference in lead uptake. Previous studies have shown that smaller particle sizes result in higher surface areas available for sorption, leading to increased removal efficiency (Amuda et al. 2007). Smaller particles possess a greater surface area compared to larger particles, providing more adsorption sites and resulting in a higher adsorption capacity (Wang & Shadman 2013, Manyangadze et al. 2020). In this study, the highest average adsorption efficiency was recorded at a particle size of 100 mm, achieving 89.18% lead removal, as seen in Fig. 4 below. The active sites on the biomass interact with metal ions. Smaller particles expose more of these sites, leading to better metal uptake (Baker 2020). Also, out of the 25 experiments conducted

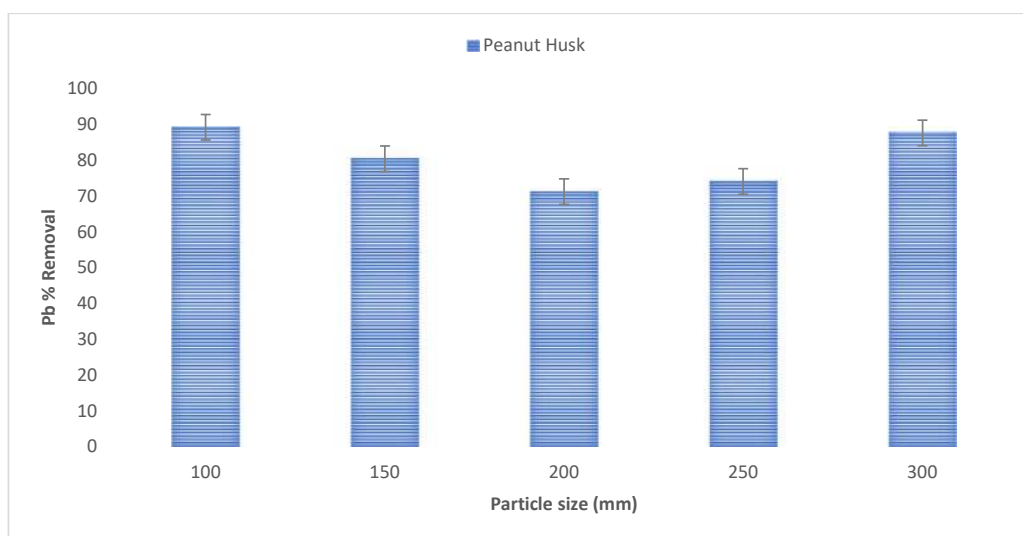


Fig. 4: Effect of particle size on lead adsorption efficiency.

in triplicates under varying variables, the best result with 100% lead removal was observed at an initial concentration of 50 ppm, pH 4, temperature of 20°C, particle size of 100 mm, biomass dose of 1 g.L<sup>-1</sup>, and contact time of 30 min. Furthermore, the Kruskal Wallis test statistically shows significant removal of Pb across all the variables. The inverse variance weighting approach reveals that particle size has less influence amongst all the adsorption parameters with % weights ranging from 0.0001-0.0002%

### Effect of Biomass Dose

The biomass dose, or the amount of biosorbent used, is a crucial factor in determining the efficiency of biosorption studies. In the present study, varying doses, ranging from 1 g.L<sup>-1</sup> to 5 g.L<sup>-1</sup>, were investigated for the removal of lead from water with different metal concentrations (50, 100, 150, 200, and 250 ppm) and varying parameters. The maximum average adsorption efficiency, i.e., 84.7%, was observed at an adsorbent dose of 5g.L<sup>-1</sup>, as seen in Fig. 5 below. As the adsorbent dose increases, the surface area available for adsorption also expands, enhancing the interaction between lead (Pb) and the adsorbent. Consequently, the removal efficiency improves with the increased adsorbent dosage (Elkhaleefa et al. 2021, Ahmad et al. 2022). This results in more adsorption sites and a stronger binding capacity, leading to more effective removal of lead from the solution (Shah et al. 2022). However, there is a great impact of other variables, which sometimes leads to the fluctuating behavior of this parameter on the adsorption efficiency. The result of the

study clearly states a dose-response relationship where the lead uptake increases with an increase in biosorbent dosage (5g) until a maximum uptake is reached. Also, under specific conditions, at an initial metal concentration of 100 ppm, pH 6, Temperature of 20°C, particle size of 200 mm, biomass dose of 5 g.L<sup>-1</sup>, and Contact time of 180 min, 100% metal removal was observed. Furthermore, the Kruskal Wallis test statistically shows significant removal of Pb across all the variables. The inverse variance weighting approach reveals that Biomass is also one of the most important factors, with % weights ranging from 31.34-50.1%.

### Effect of Contact Time

Contact time is also a crucial variable as it determines the duration needed for metal sorption onto the peanut hull biosorbent. It reflects the time period of the sorption process, influencing the efficiency and effectiveness of metal removal from the solution. The average maximum adsorption efficiency, i.e., 91.3%, was observed at 180 min. Initially, the biosorption was near to constant within a time range of 30-120 min, it gradually started increasing after 120 min, and the maximum biosorption of lead on peanut hull was observed at 180 min, and after that, it started decreasing. As contact time increases, the availability of adsorption sites also increases, leading to a higher adsorption rate (Li et al. 2022). However, after a certain point, these sites become saturated, causing the adsorption process to slow down (Abbas et al. 2020).

Also, under specific conditions, at an initial metal concentration of 150 ppm, pH 5, Temperature 40°C, Particle

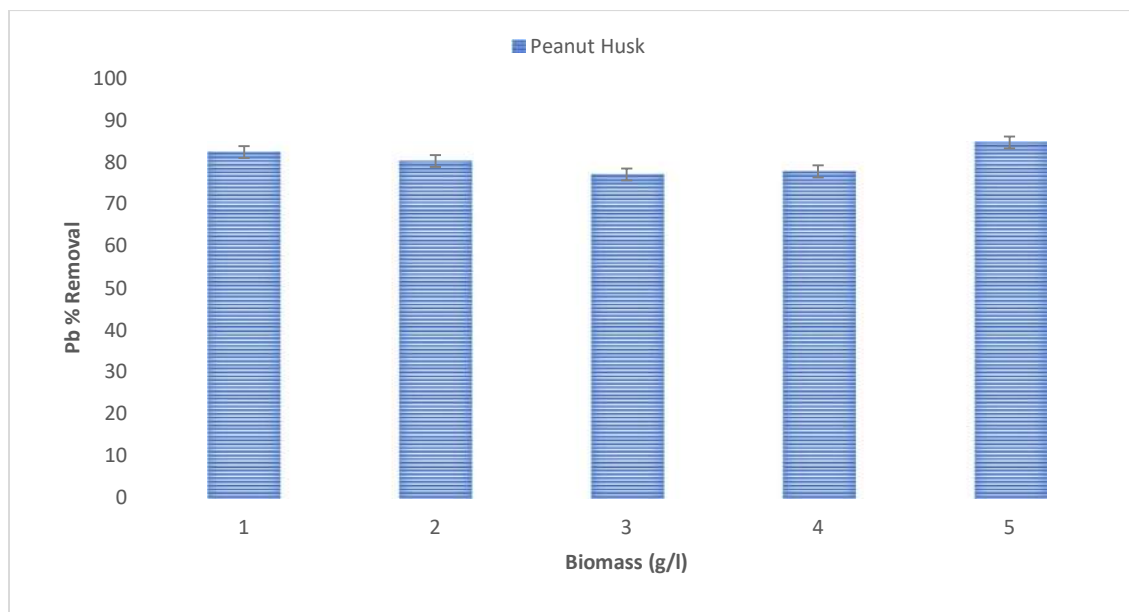


Fig. 5: Effect of biomass dose on Lead adsorption efficiency.



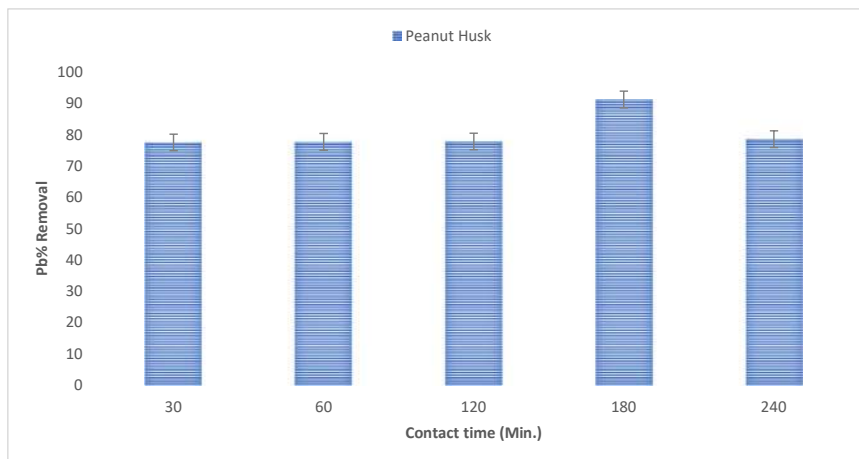
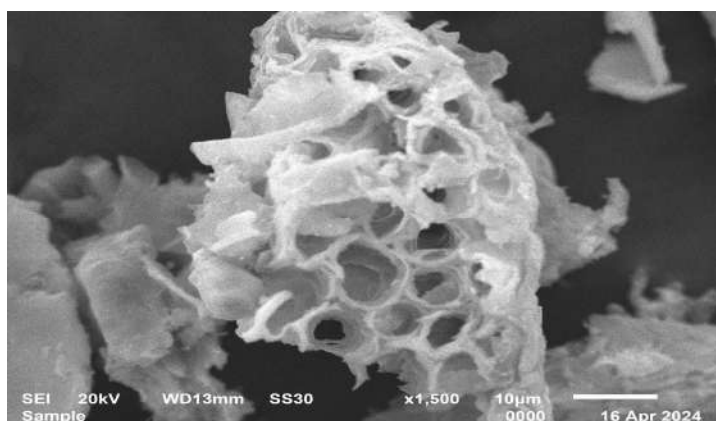
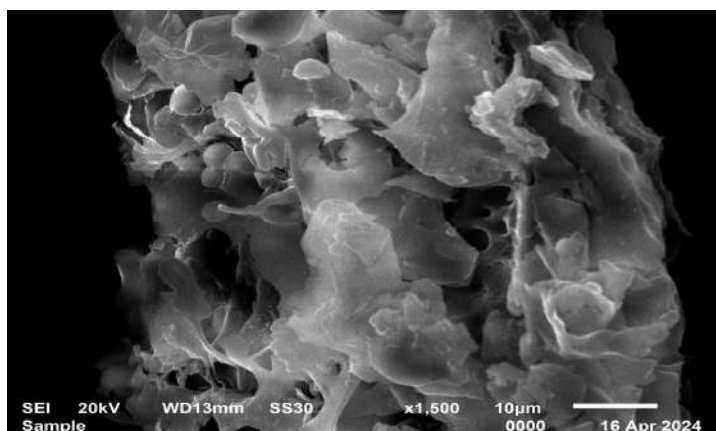


Fig. 6: Effect of Contact time on Lead adsorption efficiency.

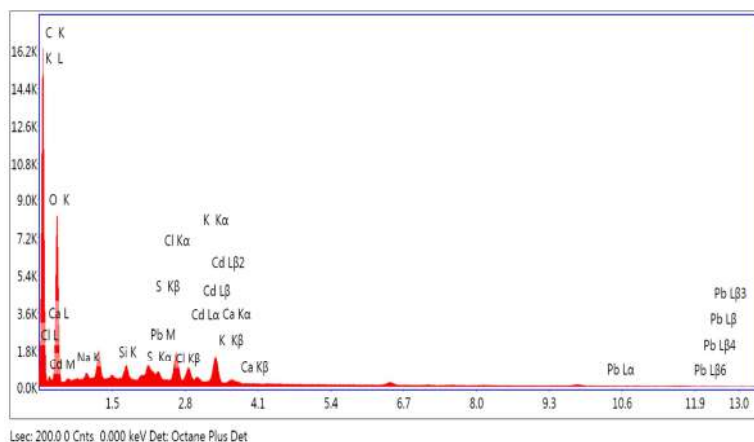


a) SEM Scans of Peanut hull before Biosorption of Lead metal

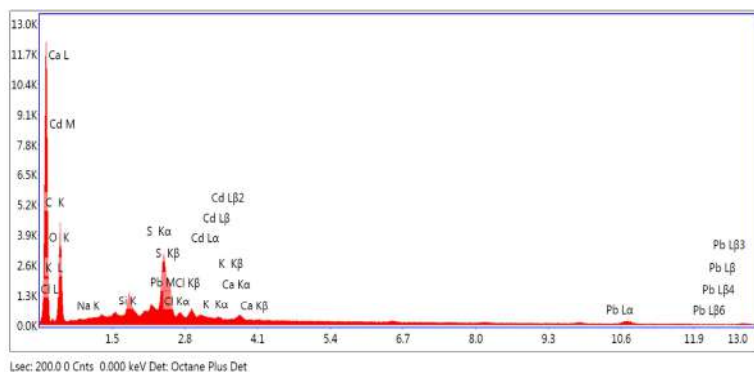


b) SEM Scans of Peanut hull after Biosorption of Lead metal

Fig. 7: a) Scanning electron micrographs before biosorption, b) After biosorption.



a) Elemental map for visualization of lead before biosorption



b) Elemental map for visualization of lead after biosorption

Fig. 8: a) Energy Dispersive X-Ray Spectroscopy graphs before biosorption b) after biosorption.

size 100 mm, Biomass 2 g.L<sup>-1</sup>, and contact time of 180 min, 100% lead removal was observed (Fig. 6). Moreover, the Kruskal Wallis test statistically shows significant removal of Pb across all the variables. The inverse variance weighting approach reveals that contact time has less influence amongst all the adsorption parameters, with % weights ranging from 0.00001-0.0001%.

### Characterization

The scanning electron micrograph of the peanut hull biomass at bar lengths of 10 μm and a voltage of 20 kV with 1500 magnification was recorded. Fig. 7a shows the porous texture of the peanut hull, which provides ample surface area and adsorption sites for biosorption. Fig. 7b reveals the changes in the surface morphology of the biomaterial after biosorption. The altered surface structure enhances the adsorption efficiency which facilitates the smooth sorption of lead on the surface of peanut hull. This type of porous surface is suitable for the retention of metals. The adsorption of Pb

on the surface of the biomaterial was further confirmed by Energy Dispersion X-ray Spectroscopy (EDS) analysis, as depicted in Fig 8a and 8b, and their elemental composition is shown in Table 1.

The characterization results indicate that the selected biomaterial effectively removes Lead (Pb) from water and demonstrates efficient performance. Further, the chemical properties of the biosorbent play an important role in its efficiency to remove a particular metal therefore, the elemental composition of the peanut hull before and after

Table 1: Elemental composition of peanut hull biosorbent before and after biosorption.

Element	Weight %		Atomic %	
	Before	After	Before	After
Carbon	55.54	44.53	63.46	56.74
Oxygen	41.24	42.97	35.38	41.11
Sodium	0.09	0.01	0.06	0.01
Lead	0.19	8.25	0.01	0.61

the process of biosorption of lead is shown in Table 1. It was generated during the SEM-EDS integrated analysis. The weight percentage of Lead increased from 0.19% to 8.25% after the biosorption process, which proves this material is a good biosorbent.

## LIMITATIONS

Our study was conducted in controlled laboratory conditions, which may not reflect real-life water treatment processes. Several additional factors could arise, thereby posing challenges during the scaling up of the process for large-scale water treatment. These include the availability and uniformity of peanut hulls for maintaining uniform biosorption efficiency, the renewal and reusability of peanut hulls after lead adsorption, and the presence of other heavy metals or contaminants in the water that could potentially interfere with lead biosorption.

These limitations highlight the need for further research and consideration in treatment applications, while they do not undermine the potential of peanut hulls as a good biosorbent, especially because peanut hulls are presently discarded as waste material.

## CONCLUSIONS

This study shows the impressive biosorption potential of peanut hulls, revealing a high adsorption efficiency for the targeted lead metal. There was significant removal of lead across all the variables with pH and biomass dose being the most influential factors. The weighted contributions on the adsorption efficiency ranged from 47.52% to 50.40% for pH 31.34% to 50.1% for Biomass dose. The Variables are aligned by their maximum weighted contributions as follows: pH > biomass dose > temperature. Thus, pH and biomass do have the highest impact, followed by temperature and other variables for peanut hull biosorbent. The findings of the studies accentuate the importance of pH and biomass dose to maximize the adsorption of peanut hulls. Hence, Peanut hulls, an agricultural by-product, can be an economically and eco-friendly solution for lead contamination in water. The use of such biosorbents could reduce reliance on expensive and chemically intensive methods of water purification. Future research should explore the reusability and regeneration of peanut hull biosorbents as well as their effectiveness in removing other heavy metals and contaminants from water. Additionally, investigations are required to refine the biosorption process, comprehend the mechanisms involved, and examine the feasibility of scaling up for industrial use. Large-scale peanut shell use needs to be studied for its long-term stability and environmental effects,

as well as its potential for promoting a circular economy by minimizing waste discard and recycling. Multidisciplinary research might also investigate the synergistic effects of integrating peanut hull biosorbents with currently used water treatment technologies. Overall, Peanut hull proves to be a potential, sustainable, and effective material for the removal of lead contamination, thereby contributing to cleaner water resources, enhanced public health, and reduced environmental footprints.

## REFERENCES

- Abbas, M.N., Ali, S.T. and Abass, R.S., 2020. Rice husks as a biosorbent agent for Pb<sup>2+</sup> ions from contaminated aqueous solutions: A review. *Biochemical & Cellular Archives*, 20(1), pp.1813-1825. DOI
- Adhikari, B., Dhungana, S.K., Ali, M.W., Adhikari, A., Kim, I.D. and Shin, D.H., 2019. Antioxidant activities, polyphenol, flavonoid, and amino acid contents in peanut shells. *Journal of the Saudi Society of Agricultural Sciences*, 18(4), pp.437-442. DOI
- Ahmad, K., Khan, M.S., Iqbal, A., Potrich, E., Amaral, L.S., Rasheed, S., Nawaz, H., Ayub, A., Naseem, K., Muhammad, A. and Yaqoob, M.R., 2022. Lead in drinking water: Adsorption method and role of zeolitic imidazolate frameworks for its remediation: A review. *Journal of Cleaner Production*, 368, p.133010. DOI
- Amuda, O.S., Giwa, A. and Bello, I.A., 2007. Removal of heavy metal from industrial wastewater using modified activated coconut shell carbon. *Biochemical Engineering Journal*, 36(2), pp.174-181. DOI
- Apori, O.S., Hanyabui, E. and Asiamah, Y.J., 2018. Remediation technology for copper contaminated soil: A review. *Asian Soil Research Journal*, 1(3), pp.1-7. DOI
- Aranda-García, E. and Cristiani-Urbina, E., 2018. Kinetic, equilibrium, and thermodynamic analyses of Ni (II) biosorption from aqueous solution by acorn shell of *Quercus crassipes*. *Water, Air, & Soil Pollution*, 229(4), pp.345-360. DOI
- Baker, H.M., 2020. Removal of lead ions from wastewater using modified Jordanian zeolite. *Chemical Science International Journal*, 29(8), pp.19-30. DOI
- Belhaj, A.F., Elraies, K.A., Mahmood, S.M., Zulkifli, N.N., Akbari, S. and Hussien, O.S., 2020. The effect of surfactant concentration, salinity, temperature, and pH on surfactant adsorption for chemically enhanced oil recovery: A review. *Journal of Petroleum Exploration and Production Technology*, 10(2), pp.125-137. DOI
- Dharsana, M. and Arul Jose, J.P., 2023. A novel green approach for lead adsorption and isotherm evaluation. *Nature Environment & Pollution Technology*, 22(1), pp.50-65. DOI
- Elkhalefa, A., Ali, I.H., Brima, E.I., Shigidi, I., Elhag, A.B. and Karama, B., 2021. Evaluation of the adsorption efficiency on the removal of lead (II) ions from aqueous solutions using *Azadirachta indica* leaves as an adsorbent. *Processes*, 9(3), pp.559-572. DOI
- Gong, R., Sun, Y., Chen, J., Liu, H. and Yang, C., 2005. Effect of chemical modification on dye adsorption capacity of peanut hull. *Dyes and Pigments*, 67(3), pp.175-181. DOI
- Kali, A., Amar, A., Loulidi, I., Jabri, M., Hadey, C., Lgaz, H. and Boukhelifi, F., 2024. Characterization and adsorption capacity of four low-cost adsorbents based on coconut, almond, walnut, and peanut shells for copper removal. *Biomass Conversion and Biorefinery*, 14(3), pp.3655-3666. DOI
- Li, H., Budarin, V.L., Clark, J.H., North, M. and Wu, X., 2022. Rapid and efficient adsorption of methylene blue dye from aqueous solution by hierarchically porous, activated starbons®: Mechanism and porosity dependence. *Journal of Hazardous Materials*, 436, p.129174. DOI

- Manyangadze, M., Chikuruwo, N.H.M., Chakra, C.S., Narsaiah, T.B., Radhakumari, M. and Danha, G., 2020. Enhancing adsorption capacity of nano-adsorbents via surface modification: A review. *South African Journal of Chemical Engineering*, 31(1), pp.25-32.
- Olabanji, I.O. and Oluyemi, E.A., 2021. Investigating the effectiveness of raw okra (*Abelmoschus esculentus* L.) and raw sugarcane (*Saccharum officinarum*) wastes as bioadsorbent of heavy metal in aqueous systems. *Materials and Green Energy Environmental Science*, 6, pp.1-12. DOI
- Panchal, V., Ghosh, A., Tomar, P.C. and Chapadgaonkar, S.S., 2020. Decolourization of Yamuna water using peanut hull in packed bed reactor. *Rasayan Journal of Chemistry*, 13(2). DOI
- Prabha, R.T. and Udayashankara, T.H., 2014. Removal of heavy metal from synthetic wastewater using rice husk and groundnut shell as adsorbents. *IOSR Journal of Environmental Science, Toxicology and Food Technology*, 8(7), pp.26-34. DOI
- Sattar, M.S., Shakoor, M.B., Ali, S., Rizwan, M., Niazi, N.K. and Jilani, A., 2019. Comparative efficiency of peanut shell and peanut shell biochar for removal of arsenic from water. *Environmental Science and Pollution Research*, 26, pp.18624-18635. DOI
- Shah, G.M., Imran, M., Aiman, U., Iqbal, M.M., Akram, M., Javeed, H.M.R., Waqar, A. and Rabbani, F., 2022. Efficient sequestration of lead from aqueous systems by peanut shells and compost: Evidence from fixed bed column and batch scale studies. *PeerJ Physical Chemistry*, 4, p.e21. DOI
- Sudan, A., Ghosh, A., Verma, M. and Tomar, P., 2024. Impact of water pollution & perspective techniques to mitigate it: An overview. *Handbook of Water Pollution*, pp.29-64. DOI
- Tanase, N.M., Barboiu, A.G., Popescu, I., Radulescu, C., Bucurica, I.A., Dulama, I.D. and Vasile, I., 2020. Health risk assessment of heavy metals in drinking waters. *Journal of Science and Arts*, 20(1), pp.187-196. DOI
- Tanyildizi, M.Ş., 2011. Modeling of adsorption isotherms and kinetics of reactive dye from aqueous solution by peanut hull. *Chemical Engineering Journal*, 168(3), pp.1234-1240.
- Team, R.C., 2020. R language and environment for statistical computing. *R Foundation for Statistical Computing*.
- Tewari, A., Bhutada, D.S. and Wadgaonkar, V., 2023. Heavy metal remediation from water/wastewater using bioadsorbents - A review. *Nature Environment & Pollution Technology*, 22(4), pp.125-136. DOI
- Verma, R. and Suthar, S., 2015. Lead and cadmium removal from water using duckweed-*Lemna gibba* L.: Impact of pH and initial metal load. *Alexandria Engineering Journal*, 54(4), pp.1297-1304. DOI
- Wang, H. and Shadman, F., 2013. Effect of particle size on the adsorption and desorption properties of oxide nanoparticles. *AIChE Journal*, 59(5), pp.1502-1510. DOI
- Wee, J.H., Moon, J.H., Eun, J.B., Chung, J.H., Kim, Y.G. and Park, K.H., 2007. Isolation and identification of antioxidants from peanut shells and the relationship between structure and antioxidant activity. *Food Science and Biotechnology*, 16(1), pp.116-122.
- Yu, J., Ahmedna, M. and Goktepe, I., 2005. Effects of processing methods and extraction solvents on concentration and antioxidant activity of peanut skin phenolics. *Food Chemistry*, 90(1-2), pp.199-206. DOI
- Zhao, H., Ouyang, X.K. and Yang, L.Y., 2021. Adsorption of lead ions from aqueous solutions by porous cellulose nanofiber-sodium alginate hydrogel beads. *Journal of Molecular Liquids*, 324, p.115122. DOI
- Znad, H., Awual, M.R. and Martini, S., 2022. The utilization of algae and seaweed biomass for bioremediation of heavy metal-contaminated wastewater. *Molecules*, 27(4), p.1275. DOI



# Sustainability Evaluation of Waste Management Using RAPWASTE Method at the 3R Temporary Waste Disposal Site in Yogyakarta City

Willis Muhammad Iqbal, Hashfi Hawali Abdul Matin<sup>†</sup> and Prabang Setyono

Department of Environmental Science, Faculty of Mathematics and Science, Universitas Sebelas Maret, Surakarta, Indonesia

<sup>†</sup>Corresponding author: Hashfi Hawali Abdul Matin; hawalihashfi@staff.uns.ac.id

**Abbreviation:** Nat. Env. & Poll. Technol.

**Website:** www.neptjournal.com

*Received:* 17-08-2024

*Revised:* 23-09-2024

*Accepted:* 20-10-2024

## Key Words:

Sustainability evaluation  
Waste management  
3R Temporary Waste Disposal Site  
RAPWASTE method

## ABSTRACT

The waste problem has become a big problem in Indonesia as the population continues to grow. The daily amount of waste generated in Yogyakarta City is 303.13 tons.day<sup>-1</sup>, with the composition of the largest waste source, namely household waste, around 63.75%. This data shows that there is a need for improvements related to management; 3R Temporary Waste Disposal Sites is an alternative for reducing waste before it is transported to the final processing place. This research aims to understand performance and waste transportation management and evaluate the level of waste management and sustainability of waste management at 3R Temporary Waste Disposal Sites Nitikan Yogyakarta. This research was conducted on 99 respondents using a *purposive* sampling method; the data analysis used was the evaluation of waste transportation, analysis of incoming, managed, and unmanaged waste data, categorization of questionnaire data, evaluation of waste management performance and analysis of the sustainability of waste management using RAPFISH software. The research results show that waste volume management at 3R Temporary Waste Disposal Sites Nitikan is 941.15 kg.day<sup>-1</sup>, and compost production is 190.65 kg.day<sup>-1</sup>. Transport management is carried out using the Stationary Container System (SCS) and is carried out 2 times. The evaluation of waste management performance is moderate, with a total relative value of 15.4, based on studies on the technical sector, institutional sector, financial sector, and the area of community participation. Based on the attribute index in each sector, it is concluded that the sustainability status of waste sorting and management at 3R Temporary Waste Disposal Sites Nitikan is 79.03, or very sustainable.

## Citation for the Paper:

Iqbal, W.M., Abdul Matin, H.H. and Setyono, P., 2025. Sustainability evaluating of waste management using RAPWASTE method at the 3R temporary waste disposal site in Yogyakarta City. *Nature Environment and Pollution Technology*, 24(2), p. D1715. <https://doi.org/10.46488/NEPT.2025.v24i02.D1715>

*Note: From year 2025, the journal uses Article ID instead of page numbers in citation of the published articles.*

## INTRODUCTION

Waste is defined as something that is no longer useful and unused and comes from human activities (Nainggolan 2019). The waste problem has become a big problem in Indonesia as the population continues to grow. Umbulharjo District is one of the 14 Districts in Yogyakarta with the largest area and is followed by a high population. Based on data from the Ministry of Environment and Forestry (KLHK 2022), the daily amount of waste generated in Yogyakarta City is 303.13 tons.day<sup>-1</sup>, with the composition of the largest waste source, namely household waste, around 63.75%. This data shows that there is a need to improve household waste management. If waste management is not appropriate, it can cause problems for the environment. In waste management, there are 4 areas supporting waste management that synergize with each other to achieve good waste management. The four areas include engineering, institutional, financial and community participation (Ihsanudin 2022). Waste management is a field related to the control of accumulation, temporary storage, collection, transfer, transportation, processing and disposal carried out in accordance with the principles of public health, economics, aesthetics, environmental considerations and community attitudes (Amaluddin et al. 2019). Problems related to waste are regulated in Law Number 18 of 2008,



**Copyright:** © 2025 by the authors

**Licensee:** Technoscience Publications

This article is an open access article distributed under the terms and conditions of the Creative Commons Attribution (CC BY) license (<https://creativecommons.org/licenses/by/4.0/>).

which states that waste reduction can be done by reusing waste through the 3R (*Reduce, Reuse, and Recycle*) system (Hidayat et al. 2020).

Regulations related to household waste management are also regulated in Presidential Regulation Number 97 of 2017 concerning National Policy and Strategy for the Management of Household Waste and Similar Household Waste, which states that 3R-based waste reduction can be carried out at 3R Temporary Waste Disposal Sites. The Yogyakarta City Government also regulates waste management in Yogyakarta City Regional Regulation Number 1 of 2022 concerning Amendments to Yogyakarta City Regional Regulation Number 10 of 2022 concerning Waste Management and Yogyakarta City Mayor Regulation Number 32 of 2023 concerning Yogyakarta City Waste Management Masterplan for 2022 – 2031 which stated that waste handling is prioritized at 3R Temporary Waste Disposal Sites. Based on 2022 KLHK data, the number of 3R Temporary Waste Disposal Sites in Yogyakarta City is 12 depots with active status, one of which is 3R Temporary Waste Disposal Sites Nitikan RT.43/RW.11, Sorosutan, Umbulharjo. RW.11, Sorosutan, Umbulharjo. 3R Temporary Waste Disposal Sites are an alternative to reduce waste before it is transported to the final processing place.

3R Temporary Waste Disposal Sites is a place for collecting, sorting, and recycling waste on a regional or communal scale (Aprizon 2019, Rizki Aziz 2019). The waste transportation process using a transfer system (TPS/TPS 3R) can be carried out using an indirect system or using a Hauled Container System (HCS) lifting container system or a Stationary Container System (SCS) fixed container system (Fauziah et al. 2022). The 3R Temporary Waste Disposal Sites program is aimed at supporting environmental policies so that they can create sustainable *development*. 3R Temporary Waste Disposal Sites is a communal scale waste management approach that requires participation from the government and community. Waste management with the 3R system emphasizes reducing, utilizing, and processing waste

starting from the source (residential areas, commercial areas, office areas, educational areas, tourist areas, etc.). Waste handling with the 3R system must also be supported by the availability of good waste transportation. The availability of waste transport and waste transport management greatly influences waste management (Prdiftha 2020). This opinion is in accordance with the statement (Gusti et al. 2019) that the waste transportation process is an important stage in waste management. So, adequate transportation facilities are needed to transport waste from upstream (waste source) to downstream (final disposal site). This research aims to understand performance and waste transportation management and evaluate the level of waste management and sustainability of waste management at 3R Temporary Waste Disposal Sites Nitikan.

## MATERIALS AND METHODS

The type of research used in this research is descriptive with a qualitative approach. Qualitative research is intended to understand phenomena that occur and are described in the form of words. The application of qualitative research in this study was used to comprehensively explain the performance of waste management at 3R Temporary Waste Disposal Sites Nitikan, Umbulharjo, Yogyakarta City. The research was conducted from February to May 2024.

The sampling technique in this research used the purposive sampling method. Sample determination was carried out using the Slovin Formula. The respondents selected were residents who had lived in the area for  $\geq 5$  years. The selection of these criteria was carried out with the hope that respondents would have a good understanding of regional conditions. The population of Sorosutan Village is 15,397 people. Based on sample calculations using the Slovin formula, the sample used was 99 respondents. The data collection phase is collected through two methods, namely primary and secondary data. Primary data was obtained through interviews, observations, and questionnaires at 3R Temporary Waste Disposal Sites Nitikan in Sorosutan

Table 1: Types and Sources of Data.

No	Data	Data Type	Data source
1.	Exiting condition of 3R Temporary Waste Disposal Sites Nitikan	Secondary	3R Temporary Waste Disposal Sites Nitikan Manager
2.	3R Temporary Waste Disposal Sites Nitikan Performance (Technical and Institutional Aspects)	Secondary	Data on Temporary Waste Disposal Sites 3R facilities and infrastructure and organizational structure
3.	The volume of waste generation	Secondary	Yogyakarta City Environmental Service
4.	Waste transportation patterns and vehicle types	Secondary	3R Temporary Waste Disposal Sites Nitikan Manager
5.	Data on community participation in the management and transportation of 3R Temporary Waste Disposal Sites Nitikan waste	Primary	Questionnaires and interviews

Village, Umbulharjo District, Yogyakarta City, regarding waste management and transportation. Details of primary and secondary data in this research are presented in Table 1.

## Data Analysis

### Waste transportation: 3R Temporary Waste Disposal Sites

waste transportation is analyzed based on SNI 19-2454-2002 regarding Operational Technical Procedures for Urban Waste Management.

**Analysis of incoming managed, and unmanaged garbage data:** In waste management at 3R Temporary Waste Disposal Sites Nitikan, data regarding incoming and managed waste

Table 2: Dimensions and Attributes.

Variables/ Dimensions	Score	Good	Bad	Attribute	Indicator
Technical	0;1;2	2	0	• Waste management	(0) < 60% of planned capacity (1) 60 - 80% of planned service capacity (2) > 80% of the planned capacity
		2	0	• Condition of facilities and infrastructure	(0) The condition of the buildings and infrastructure is not functioning (1) The condition of the buildings and infrastructure is partially functional (2) The condition of the buildings and infrastructure is functioning well
		2	0	• Management type	(0) Just a sorting process (1) The process of sorting and processing organic waste (2) Sorting process, processing of organic and inorganic waste
Institutional	0;1;2	2	0	• Management institution	(0) Individual (1) Department/Village (2) Community self-help groups
		2	0	• Legality of the institution	(0) Without a notarial deed, the establishment decree is signed by the Village Head, and it is known that the relevant SKPD and there are AD/ART. (1) There is a notarial deed still in place, the establishment decree signed by the Village Head, the relevant SKPD is known, and there is AD/ART. (2) There is a notarial deed, an establishment decree signed by the Village Head, and the relevant SKPD is known, and there is AD/ART.
				• Management administration	(0) TEMPORARY WASTE DISPOSAL SITES 3R operations were not recorded (1) TEMPORARY WASTE DISPOSAL SITES 3R operational records were carried out, but they were not good (2) TEMPORARY WASTE DISPOSAL SITES 3R operational records were carried out properly
Society Participation	0;1;2	2	0	• Waste sorting	(0) There is no waste sorting in the household (1) Only some people sort waste (2) The whole community sorts waste
		2	0	• Retribution	(0) 60% pay contributions on time (1) 60 - 90% pay contributions on time (2) 100% of people pay contributions
				• Waste management	(0) Waste management into compost and sorting according to type of waste (1) Just sorting waste (2) Not carrying out management and sorting
Economy	0;1;2	2	0	• Government assistance	(0) There is no operational funding assistance (1) There is minimal operational funding assistance (2) There is operational funding assistance as needed
		2	0	• Economic improvement	(0) There is no added economic value. (1) There is additional economic value in managing TEMPORARY WASTE DISPOSAL SITES 3R (2) There is additional economic value at the community level.
				• Waste reduction	(0) There is no economic improvement (1) Recycle (2) Recycling and sustainability in production and consumption
Ecology	0;1;2	2	0	• Concern about waste management	(0) No concern appears (1) Community service program (2) Active concern
		2	0	• Waste sorting	(0) Disrupts environmental aesthetics (1) Reduces waste accumulation (2) Protecting the environment
				• Environmental Health	(0) Environmental pollution and disease (1) Awareness of maintaining sanitation (2) Sanitation and reducing piles of rubbish

is recorded every month ( $\text{kg} \cdot \text{month}^{-1}$ ). Management involves separating organic and inorganic waste, as well as making compost from organic waste. This data is used to calculate the 3R Temporary Waste Disposal Sites Nitikan Recovery Factor value using the formula:

$$\frac{\text{Recovery Factor} = (\text{garbage in} - \text{unmanaged waste})}{\text{garbage in}} \times 100\%$$

#### Categorization of questionnaire data:

##### a. Scoring

Scoring is used to determine the maximum and minimum scores on a question or item.

$Y = \text{highest score likert scale} \times \text{number of questionnaire items}$

$X = \text{lowest score likert scale} \times \text{number of questionnaire items}$

##### b. Intervals

Intervals used to determine distance class classification or category which will be used.

$$I = \frac{(Y) - (X)}{\text{number of categories}}$$

##### c. Percentage Index

Index percentage used for percentage value in determining category class.

$$\text{Index\%} = \frac{\text{total score}}{Y \times 100}$$

#### Evaluation of Waste Management Performance

The evaluation was carried out based on the 2020 3R Temporary Waste Disposal Sites Technical Guidelines, using 5 areas, namely supporting regulations, technical, institutional, financial, and community participation. Each field has indicators with the same assessment value, namely 5, 3, and 1. Each field has a certain percentage weight. The scores for each field are added up to get a total score, which is then categorized as very good, good, poor, or poor based on predetermined evaluation criteria.

#### Analysis of the Sustainability of Waste Management

The sustainability of waste management will be analyzed using *RAPWASTE*. In this research, researchers will analyze and evaluate the sustainability of waste management at 3R Temporary Waste Disposal Sites Nitikan in terms of technical, institutional, community participation, economic, and ecological aspects. The dimensions and attributes in detail can be seen in Table 2.

## RESULTS AND DISCUSSION

### Analysis of Waste Transport and Management Performance Factors

#### Aspects of Regulations and Development Plans

Regulations related to waste management and 3R Temporary Waste Disposal Sites are regulated in Yogyakarta City Regional Regulation Number 1 of 2022 concerning Amendments to Yogyakarta City Regional Regulation Number 10 of 2012 concerning Waste Management and Yogyakarta Mayor Regulation Number 32 of 2022 concerning Yogyakarta City Waste Management Masterplan for 2022 – 2031.

**Technical aspects:** Waste volume management at 3R Temporary Waste Disposal Sites Nitikan is planned to be able to accommodate 10 tons of waste per day, based on data from the Yogyakarta City Environmental Service. 3R Temporary Waste Disposal Sites Nitikan manages  $941.15 \text{ kg} \cdot \text{day}^{-1}$ , meaning this amount is  $>80\%$  of the planned capacity. Compost production at 3R Temporary Waste Disposal Sites Nitikan is  $190.65 \text{ Kg} \cdot \text{Day}^{-1}$ , which means  $70 - 99\%$  of organic waste is processed into compost. Organic waste at 3R Temporary Waste Disposal Sites Nitikan consists of slurry, leaf material, and maggot feed. Furthermore, the indicator for the residual volume of waste to the landfill is 2,242,582.00 of the total segregated waste of 343,519.74, which indicates that there is processing of  $<40\%$  of the total waste managed.

**Institutional aspects:** 3R Temporary Waste Disposal Sites Nitikan is managed by the Department/Village of the 3R Temporary Waste Disposal Sites Nitikan area. The management of 3R Temporary Waste Disposal Sites is equipped with an organizational structure and functions actively.

**Financing aspects:** The financing or financial aspects at 3R Temporary Waste Disposal Sites Nitikan receive operational funding assistance from the government according to needs.

#### Aspects of Community Participation

The 3R Temporary Waste Disposal Sites Nitikan customer community actively participates in membership. This active participation is demonstrated by awareness of sorting waste, even though not all people do this. Then, in terms of community contribution indicators, around  $60 - 90\%$  of people pay their contributions on time. Regulations related to the Yogyakarta City Regional Waste Levy are regulated in Yogyakarta City Regional Regulation Number 21 of 2012 Cleaning Levy. Payment of waste levies, especially for 3R Temporary Waste Disposal Sites Nitikan, is IDR. 2,500 – Rp.



3,000 for private parties who collect waste using carts. The economic impact felt due to the existence of 3R Temporary Waste Disposal Sites Nitikan is in the form of added value or the increase in value of goods whose benefits have been lost, then added value is given so that they have use value (Amalia 2020). The results of this study are in accordance with research conducted by (Oyebode & Abdulazeez 2023), which states that the community does not carry out proper sorting. In addition, most correspondents prefer the inclusiveness of scavenger garbage collectors for various reasons ranging from laziness to not having time.

### **Waste Transport Patterns in Nitikan Village, Umbulharjo District, Yogyakarta Special Region**

The waste collection process is carried out by collecting waste from waste sources using transport vehicles such as waste carts to the Transfer Depo or waste containers, and then the collected waste will be transported by dump trucks or armroll trucks to 3R Temporary Waste Disposal Sites Nitikan. The availability of waste transportation and waste transportation management greatly influences waste management (Pradiftha, 2020). Based on data from the Yogyakarta City Environmental Service, the amount of waste transported to the landfill was  $181.37 \text{ tonnes.day}^{-1}$ . Garbage transportation in Nitikan Village, Umbulharjo District, is carried out using several vehicles such as pick-ups, arm roll cars, and dump trucks. Transportation using the *Stationary Container System* (SCS) system is influenced by the number of officers on duty during transportation (Putri et al. 2023, Gustiabani et al. 2023). Transport vehicles with a lifting system (Hauled Contained System) have advantages over fixed system transport vehicles (Stationary Contained System) in terms of transport time per trip (Dzakwan et al. 2020).

### **Evaluation of Waste Transport Performance**

The amount of waste entering 3R Temporary Waste Disposal Sites Nitikan in 2023 is 2,700,947.75, with an average of 225,078.98 and a total of  $7,399.86 \text{ kg.day}^{-1}$ . Then, the amount of residual waste was  $6,144.06 \text{ kg.day}^{-1}$ , and the total segregated waste was  $941.15 \text{ kg.day}^{-1}$ . The amount of waste generation that enters 3R Temporary Waste Disposal Sites Nitikan, if it is assumed that using  $1 \text{ m}^3$  of waste is  $\frac{1}{4}$  ton of waste, then the waste generation at 3R Temporary Waste Disposal Sites Nitikan is  $29,600 \text{ m}^3$  or around  $81 \text{ m}^3.\text{day}^{-1}$  and the potential for waste accumulation is  $38,429.5 \text{ L.day}^{-1}$ .

### **Waste Management Performance Evaluation**

Evaluation of waste management performance at 3R Temporary Waste Disposal Sites Nitikan was carried out

in several areas, namely regulatory, technical, institutional, and community participation in accordance with research conditions. Each indicator has the same assessment level, namely 5.3 and 1. Then, the scores for each aspect will be added up into the categories Good ( $>19.0$ ), Medium ( $\leq 19.0-9.50$ ), and Bad ( $< 9.5$ ). Relative scores in waste management evaluations are used to determine areas in the good, medium, or poor categories. The relative value is obtained by multiplying the field value and the weight. In the regulatory sector, the relative value is 0.8 points, the technical sector is 7.8 points, the institutional sector is 4.6 points, the financial sector is 0.25 points, the community participation sector is 1.95 points, and the total relative value is 15.4. So, the evaluation of waste management performance is included as Medium.

### **Percentage of Waste Processing and Transport Indicators**

The age level of respondents in this study was dominated by people aged 20-30 years. At this age, people tend to use their time more often to read and develop their intellectual abilities. This is as per the results of research by Suwaryo et al. (2017), which states that at the age of 20 - 35 years, individuals will play a more active role in society.

The waste management indicator shows a good category with a percentage of 82%. Public knowledge regarding waste management can be influenced by information obtained regarding how to process organic and inorganic waste (Dalimuthe & Nasution 2022). Then, research conducted by (Agyustia 2022) with a percentage related to waste knowledge of 80% shows that there is a need to increase information regarding household waste management through socialization.

The public knowledge indicator shows a good category with a percentage of 84%. This is in line with research conducted by (Nurin et al. 2021), where 90% of people actively participate in waste sorting, which means that people are aware of the impact that waste will have on the environment and health. The waste processing facilities indicator gets a percentage of 84% and is included in the good category. The results of this research are as per the research conducted by (Niskiyya & Zalmita 2023), which states that in the waste management process, which involves the utilization and use of facilities and infrastructure, the government provides facilities in the form of placing waste containers for organic and inorganic waste, moving and transporting waste and processing waste to processing. In the waste transportation indicator, the percentage value is 83% and is included in the good category.

### Waste Incoming, Managed, and Residue at 3R Temporary Waste Disposal Sites Nitikan

3R Temporary Waste Disposal Sites Nitikan received 2,700,947.75 rubles with a monthly average of 225,078.98 kg.month<sup>-1</sup>. Total incoming waste is 225,078.98 kg.month<sup>-1</sup>, residual waste is 186,881.83 kg.month<sup>-1</sup>, and total segregated waste is 28,626.64 kg.month<sup>-1</sup>. The recovery factor value is obtained from waste that can be composted and resold. Based on the calculation results, the recovery factor for 3R Temporary Waste Disposal Sites Nitikan is 16.9% of the total incoming waste for 1 year. The recovery factor can be used as a form of waste reduction as well as increasing the use value and economic value of waste (Syafudin et al. 2020).

### Analysis of the Sustainability of Waste Transportation and Management at 3R Temporary Waste Disposal Sites Nitikan

**Technical dimensions:** RAPWASTE analysis of the sustainability index in the technical dimension produces a value of 73.09 with a *Stress* value of 0.32. This value is included in the quite sustainable category because, based on the index value, it is between 50 -75. Meanwhile, the results of the *Leverage of Attributes* sustainability analysis in the technical dimension show that the waste management attribute value has the highest value, namely 15.18. The

results of this research are in accordance with research conducted by (Gifari et al. 2023), which states that 72% of people have reduced the volume of waste (Fig. 1).

**Institutional dimensions:** RAPWASTE analysis of the sustainability index on the institutional dimension produces a value of 83.98 with a stress value of 0.29. This value is included in the very sustainable category because, based on the index value, it is between 75 - 100. Meanwhile, the results of the *Leverage of Attributes* analysis of sustainability in the institutional dimension show that the attribute value of the management institution is (12.72), the legality of the institution is (12.16), and management administration is (6.79) (Fig. 2). In this institutional dimension, for management institutions, collaboration between institutions such as the private sector and environmentally concerned communities is needed, which can encourage improvements in the quality of public services (Sukwika & Noviana 2020). Apart from that, the opinion of Gifari et al. (2023) stated that laws and regulations have an important role in making waste management decisions. The existence of national laws and regional regulations that apply should be strictly implemented so that they can have an impact on the amount of waste produced, the irresponsible use of various single-use plastic products, and the mixing of various types of waste (Latugan et al. 2024).

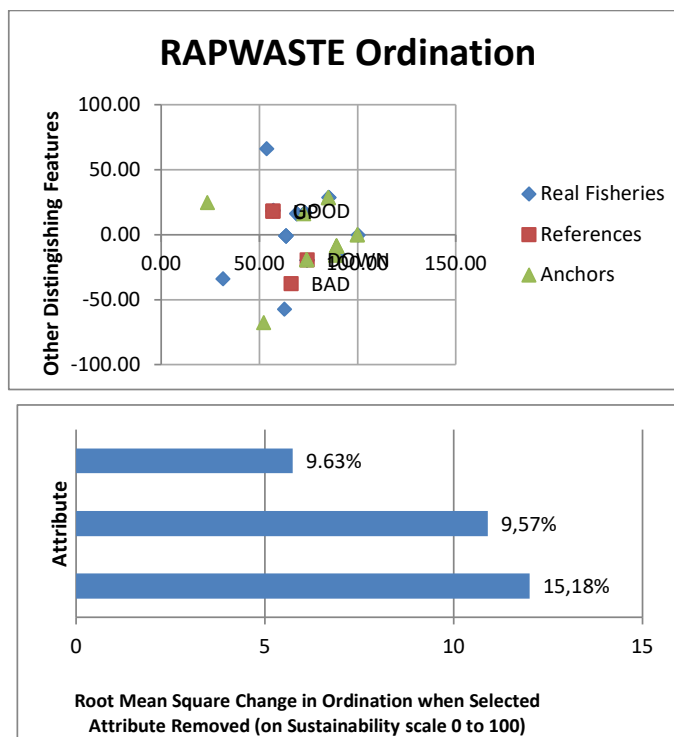


Fig. 1: RapWaste Graph and Leverage of Attributes on Technical Dimensions.

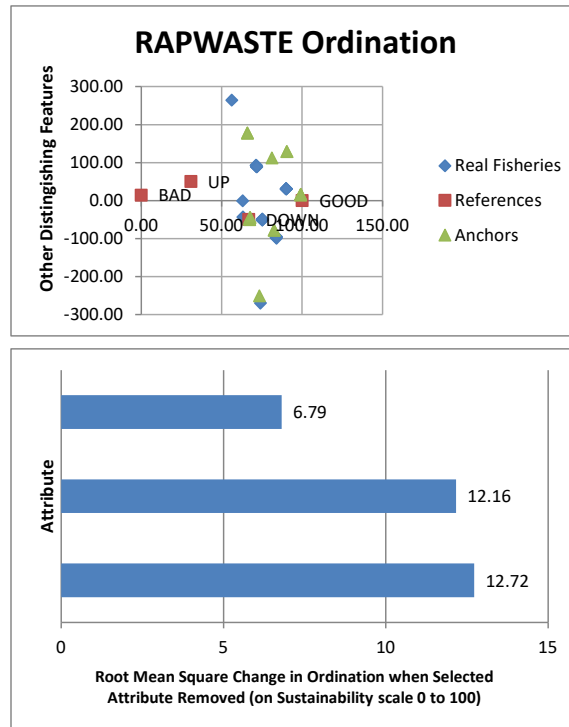


Fig. 2: RapWaste Graph and Leverage of Attributes on Institutional Dimensions.

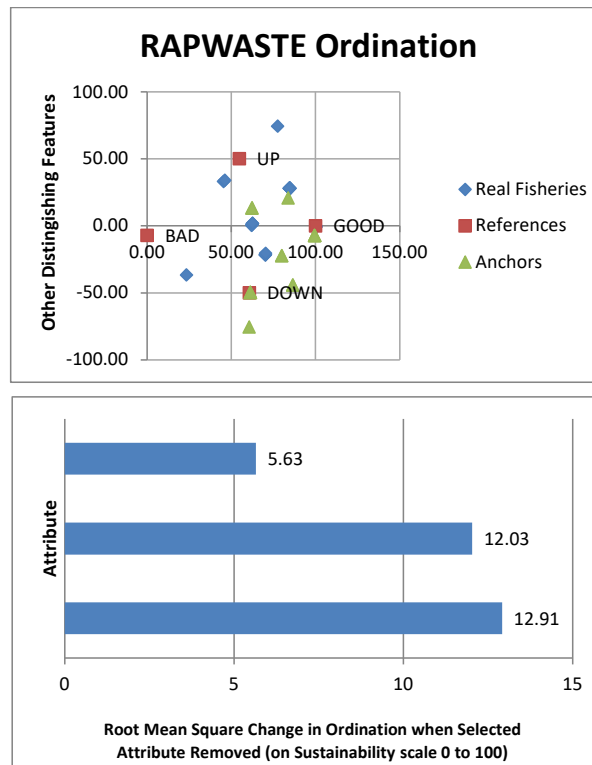


Fig. 3: RapWaste Graph and Leverage of Attributes on Dimensions of Community Participation.

**Dimensions of community participation:** RAPWASTE analysis of the sustainability index on the community participation dimension produces a value of 100 with a stress

value of 0.27. This value is included in the very sustainable category. Meanwhile, the results of the Leverage of Attributes analysis of sustainability in the institutional dimension show

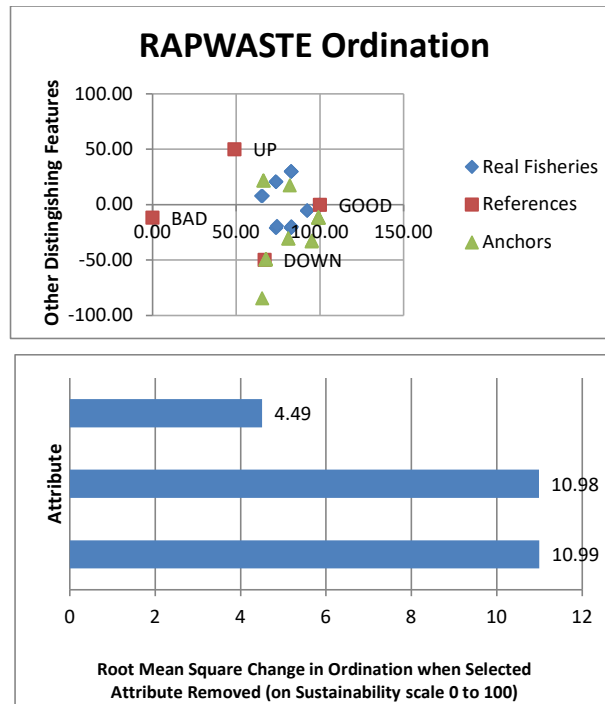


Fig. 4: RapWaste Graph and Leverage of Attributes on Economical Dimensions.

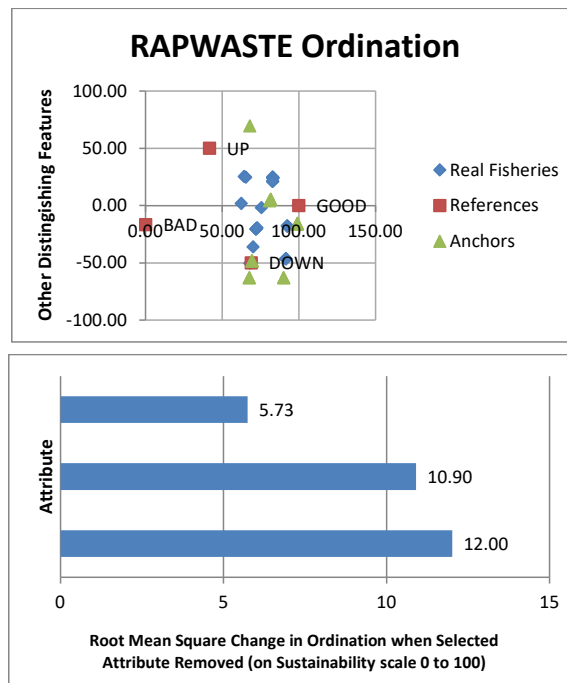


Fig. 5: RapWaste Graph and Leverage of Attributes on Ecological Dimensions.



the attribute values for waste sorting by the community (12.91), retribution (12.03), and waste management (5.63) (Fig. 3). Amalia (2020) stated that the main factor driving people to recycle is the internal motivation of the individual. So, it is important to carry out programs to form and support this program.

**Economic dimensions:** RAPWASTE analysis of the sustainability index in the economic dimension produces a value of 73.73 with a stress value of 0.29. Leverage of Attributes sustainability in the dimensions of government assistance (10.99), economic improvement (10.98), and waste reduction (4.49) (Fig. 4). This waste reduction activity is included in a circular economy with the principles of reducing waste and pollution, preserving used products and materials as long as possible, and regenerating natural systems (Otivriyanti et al. 2023).

**Ecological dimensions:** RAPWASTE analysis of the sustainability index in the economic dimension produces a value of 64.39 with a stress value of 0.32. As for the results of the Leverage of Attributes analysis of sustainability in the dimensions of awareness of waste management (12.00), waste sorting (10.09), and waste reduction (5.73) (Fig. 5). Based on the two most prominent attributes, namely concern for waste management and waste sorting. The community is one of the important elements in realizing this concern (Idris et al. 2023).

## CONCLUSIONS

The conclusion of this research is that performance in technical aspects consists of waste management, condition of facilities and infrastructure, type of management, condition of equipment, compost products, and volume of waste residue. Waste volume management at 3R Temporary Waste Disposal Sites Nitikan is 941.15 kg.day<sup>-1</sup>. The type of management is the process of sorting and processing organic and inorganic waste with sufficient supporting equipment. Compost production at 3R Temporary Waste Disposal Sites Nitikan was 190.65 Kg.Day<sup>-1</sup>. Institutional aspects: 3R Temporary Waste Disposal Sites Nitikan is managed by the Department/ Village in the 3R Temporary Waste Disposal Sites Nitikan area. In the aspect of community participation, some people are active in sorting waste and paying fees, and there is an economic impact in the form of added economic value. Waste transportation management at 3R Temporary Waste Disposal Sites Nitikan is carried out using a *Stationary Container System* (SCS) and carried out in 2 cycles. The evaluation of waste management performance is moderate, with a total relative value of 15.4. Each indicator in the regulatory sector has a relative value of 0.8 points, the technical sector is 7.8 points, the institutional sector is 4.6 points, and the financial

sector is 0.25 points. The area of community participation is 1.95 points. The average sustainability status of waste sorting and management at 3R Temporary Waste Disposal Sites Nitikan is 79.03, or very sustainable. The technical attribute index is 73.09, the institutional attribute is 83.98, the community participation attribute is 100, the economic attribute is 73.73, and the ecological attribute is 64.39.

## REFERENCES

- Agyustia, R., 2022. Factors Related to Household Waste Management in the Kuranji Health Center Work Area (Doctoral dissertation, Stikes Alifah Padang).
- Amalia, S., 2020. Factors that hinder community participation in the waste bank program in the city of Yogyakarta. *Journal of Administrative Science: Media for the Development of Administrative Science and Practice*, 17(2), pp.306-323. DOI
- Amaluddin, L.O. and Putra, A., 2019. Community behavior in disposing of household waste in Wali Village, Tan Watopute District. *Journal of Geography Education Research*, 4(2), pp.65-71. DOI
- Aprizon, P.D., 2019. Juridical review of the existence of environmental regulations in the 1945 Constitution of the Republic of Indonesia and the Constitution of the Fifth Republic of France. *Journal of Islamic Government and Politics*, pp.26-40.
- Dalimunthe, K.T. and Nasution, A., 2022. The Relationship of Knowledge Towards Organic and Non-Organic Waste Management in The Community of Kampung Banjar 1, Kotapinang District. *Jurnal Education and Development*, 10(1), pp.191-194
- Dzakwan, M.A., Pramestyawati, T.N. and Alala, P.S., 2020. Comparison of garbage transport with compactor trucks and arm roll trucks. *Proceedings of the National Seminar on Applied Science and Technology*, 1(1), pp.419-426.
- Fauziah, R. and Suparmi, S., 2022. Jambi City waste transport system. *Jambura Health and Sport Journal*, 4(2), pp.127-138.
- Gifari, O.I., Kusriani, K. and Yuana, K.A., 2023. Analysis of Land Cover Changes Using the Supervised Classification Method on Remote Sensing Image Data of Samarinda City-East Kalimantan. *Informatika Mulawarman: Jurnal Ilmiah Ilmu Komputer*, 18(2), pp.71-77. DOI
- Gusti, G.I., Wahyu, D. and Pratama, I.G., 2019. Waste transport management in Kuta District, Badung Regency. *Civil Engineering Infrastructure Electronic Scientific Journal*, pp.1-7.
- Gustiabani, Z. and Lingga, Y.S., 2023. Issues relating to the waste transport system in Sekupang Batam City. *Sigma Teknika Journal*, pp.214-222. DOI
- Hidayat, E. and Faizal, L., 2020. Waste management strategy as an effort to improve waste management in the era of regional autonomy. *ASAS*, 12(2), pp.69-80.
- Idris, I.H., Narawida, T., Agustin, R.D., Oktaviani, D. and Hidayat, M.B., 2023. RAPWASTE analysis of the sustainability study of the development of the Kaoetangan Heritage Tourism Area in Malang City. *Brawijaya Journal of Social Sciences*, 2(2), p.71.
- Ihsanudin, M.D., 2022. *Spatial Analysis of Waste Management Sites*. Muhammadiyah University of Surakarta.
- Latugan, P., Carabacan, J.J., Bonicillo, G., Cayog, J., Eyawa, M.Q., Cairel, M.T. and Ngohayon, J.M., 2024. Analysis and characterization of municipal solid wastes generated in Ifugao State University Potia Campus: A basis for planning of waste management. *Nature Environment & Pollution Technology*, 23(1). doi:10.46488/NEPT.2024.v23i01.024. DOI
- Nainggolan, R.R., 2019. Analysis of willingness to pay (WTP) waste management levy in Cileunyi District, Bandung Regency. *Widya Praja Journal of Government Science*, pp.33-46. DOI

- Niskiyya, N. and Zalmita, N., 2023. Level of Community Understanding in Managing Waste in Gampong Jojo, Mutiara Timur District, Pidie Regency. *Jurnal Pendidikan Geosfer*, 1, pp.10-16. DOI
- Nurin, L.A., Rhomadhoni, M.N. and Syafiuddin, A., 2021. The Influence of Community Characteristics and Waste Disposal Facilities on Waste Processing in Urban and Rural Areas. *Jurnal Ilmiah Permas: Jurnal Ilmiah STIKES Kendal*, 11(4), pp.731-738.
- Otivriyanti, G., Fani, A.M., Yusuf, N.R., Haris, K.A., Alfatri, P. and Purwanta, W., 2023. A study on the implementation of a circular economy in municipal solid waste management in the new capital city of Indonesia. *IOP Conf. Ser.: Earth Environ. Sci.*, 1201, p. 012005. DOI
- Oyebode, O.J. and Abdulazeez, Z.O., 2023. Optimization of supply chain network in solid waste management using a hybrid approach of genetic algorithm and fuzzy logic: A case study of Lagos State. *Nature Environment & Pollution Technology*, 22(4). DOI
- Pradifitha, M.D., 2020. *Evaluation of Waste Transport Performance in Polewali District, Polewali Mandar Regency*. Thesis.
- Putri, I.A., Rini, I.D.W.S. and Hayati, R.N., 2023. Study on optimizing stationary container system waste transport routes based on geospatial information systems (GIS) in East Balikpapan District. *Journal of Environmental Pollution Control (JPPL)*, 5(2), pp.168-176.
- Rizki Aziz, T.I., 2019. West Pasaman Regency waste management system development scenario with a waste processing scale approach at regional and city levels. *Serambi Engineering Journal*, pp.444-450.
- Sukwika, T. and Noviana, L., 2020. Sustainability status of integrated waste management at temporary waste disposal sites Bantargebang, Bekasi: Using RapWaste with R statistics. *Journal of Environmental Science*, 18(1), pp.107-118.
- Suwaryo, P.A.W. and Yuwono, P., 2017. Factors Influencing the Level of Public Knowledge in Mitigating Natural Disasters Landslides. *University Research Colloquium 2017 Universitas Muhammadiyah Magelang*, pp.305-314.
- Syafurudin, S., Nugraha, W.D., Matin, H.H.A., Saputri, E.S. and Budiyo, B., 2020. The Effectiveness of Biogas Method from Rice Husks Waste: Liquid Anaerobic Digestion and Solid-State Anaerobic Digestion. *IOP Conf. Ser.: Earth Environ. Sci.*, 448, p. 012007. DOI

# Deep Learning Approach for Evaluating Air Pollution Using the RFM Model

Jannah Mohammad† and Mohammad Abul Kashem

Department of Computer Science and Engineering, Dhaka University of Engineering and Technology,  
Gazipur, Bangladesh

†Corresponding author: Jannah Mohammad; jmgodhuli@gmail.com

**Abbreviation:** Nat. Env. & Poll. Technol.  
**Website:** [www.neptjournal.com](http://www.neptjournal.com)

*Received:* 10-09-2024

*Revised:* 19-09-2024

*Accepted:* 20-10-2024

## Key Words:

RFM model  
Neural network  
Air pollution  
Air Quality Index

## ABSTRACT

Air pollution is a required environmental and public health issue in India, with multiple municipalities repeatedly ranking among the most polluted in the world. This study leverages large datasets to construct a predictive model for forecasting air quality trends using a novel approach that integrates the Recency Frequency Monetary (RFM) model with deep learning. The research aims to efficiently quantify pollution events frequency and assess the impact of air quality variations on public health, offering a more flexible and adaptive system for air quality monitoring. As a result, a large volume of air quality data provided by RFM (Recency, Frequency, and Monetary) will be flexible and frequently handled and analyzed. In this research, the performance of the integrated RFM technology is examined using Python and Google Colab, and the simulation results are compared to air pollution information from neural networks for structures in additional data using existing air quality monitoring systems in India. Performance examination of both regression and classification techniques in RFM. The execution of RFM can be one of the models and its potential to enhance air quality monitoring and urban sustainability.

## INTRODUCTION

Urban air pollution is an escalating problem that severely impacts public health and energy consumption. In North India, the burning of agricultural waste has degraded air quality, with pollutants like PM<sub>2.5</sub> affecting regions as far as the central Himalayas and even doubling air pollution levels in cities like Kathmandu due to cross-border pollution (Khanal et al. 2022). Rapid urbanization, especially in countries like India, makes air pollution issues more severe. Kanpur City, for instance, has serious air quality problems, leading the Indian government to create an Environmental Management Plan (EMP) (Gupta 2008). This plan emphasizes the urgent need for effective strategies to reduce pollution and protect health. Many areas in India have pollution levels far above World Health Organization guidelines (Brauer et al. 2019), resulting in significant health problems and highlighting the need for better monitoring and prediction tools.

Effective air pollution monitoring involves measuring and analyzing pollutant levels to guide mitigation efforts. Traditional methods are being improved with advanced technologies, such as neural networks, which can predict pollution levels more accurately (Wesolowski et al. 2006). A comparison of Indigenous Structures (Kumar & Gupta 2023) compared Support Vector Machines (SVM) with deep learning models, finding SVMs competitive but lagged in temporal dynamics. Research from institutions like the Spanish Ministry of Science and Education has shown that neural networks can provide detailed insights and forecasts (Ibarra-Berastegi et al. 2009). For example, the Greater Istanbul Area uses neural networks for short-term pollution predictions to help reduce emissions (Kurt

## Citation for the Paper:

Mohammad, J. and Mohammad, A. K., 2025. Deep learning approach for evaluating air pollution using the RFM Model. *Nature Environment and Pollution Technology*, 24(2), p. D1718. <https://doi.org/10.46488/NEPT.2025.v24i02.D1718>

*Note: From year 2025, the journal uses Article ID instead of page numbers in citation of the published articles.*



**Copyright:** © 2025 by the authors

**Licensee:** Technoscience Publications

This article is an open access article distributed under the terms and conditions of the Creative Commons Attribution (CC BY) license (<https://creativecommons.org/licenses/by/4.0/>).

et al. 2008), and research in Bilbao, Spain, uses multiple neural network models for forecasting (Ibarra-Berastegi et al. 2008). According to (Lisboa 2002), Artificial Neural Networks (ANNs) are valuable for analyzing complex data and improving early disease detection.

Recent advancements in machine learning offer new ways to analyze air pollution (Mohammad & Kashem 2022) using the Recency, Frequency, Monetary (RFM) model with k-means clustering to compare pollution levels, achieving 50% accuracy in clustering. Integrating neural networks with the RFM model enhances data analysis and pattern recognition (Liao et al. 2022), which is useful for managing large and complex datasets (Mena et al. 2023). RFM analysis has been effective in customer segmentation for marketing (Anitha & Patil 2022), but predicting air pollution with neural networks has faced challenges, particularly with short-term forecasts. In this research, The RFM model integrates neural networks to learn from the most relevant information, which can improve air quality prediction by evaluating regression and classification metrics.

This research paper proposes a unique approach by combining the RFM model with neural networks to enhance air pollution predictions and attain more in-depth insights into pollution conventions in India. The RFM model can evaluate pollution instances based on their frequency and intensity. Integrating neural networks is intended to increase prediction accuracy and provide a better knowledge of air quality patterns. This research evaluates the effectiveness of regression and classification techniques within the RFM model. Regression helps predict the quantity of pollution, while classification categorizes pollution levels. This combined approach allows for a thorough analysis and more manageable interpretation of pollution data.

The paper's organization is as follows: Section 2 covers data assemblage and exploratory analysis. Section 3 describes the AQI computation and the proposed methodology for operating neural networks and RFM models. Section 4 presents simulation consequences and assesses the performance of regression and classification procedures. Section 5 concludes with insights and propositions for prospective research.

### Exploratory Data Analysis

The research investigation collects air pollution data from 2015 to 2020 in India. The dataset includes the following cities: Amravati, Amritsar, Chandigarh, Delhi, Gurugram, Hyderabad, Kolkata, Patna, and Visakhapatnam. After collecting the data, an Exploratory Data Analysis (EDA) has been conducted to determine the dataset's structure and features. The subsequent efforts involved straining for null

values and using data-cleaning techniques to provide the dataset's integrity and reliability for additional analysis. Latitude is followed by ° N (for the Northern Hemisphere). Longitude is followed by ° E (for the Eastern Hemisphere) (Fig. 1, Table 1).

### Dataset Description

The dataset provides comprehensive data for various cities, with no missing values in the City and Date columns, ensuring complete information for these entries.

$PM_{2.5}$  and  $PM_{10}$ : These columns contain concentrations of fine particulate matter  $PM_{2.5}$  and coarser particulate matter

$PM_{10}$  units of microgram m<sup>3</sup>, The  $PM_{2.5}$  and  $PM_{10}$  columns, representing concentrations of fine particulate matter and coarser particulate matter, respectively, are critical for understanding air quality issues in India. Due to factors like industrial operations, automobile emissions, and seasonal crop burning,  $PM_{2.5}$  and  $PM_{10}$  levels are a significant concern in major Indian cities (WHO 2021). In this research, the dataset reveals 4,598 missing values in the  $PM_{2.5}$  column and 11,140 missing values in the  $PM_{10}$  column.

The NO, NO<sub>2</sub>, and NO<sub>x</sub> columns units of parts per million (ppm) measure nitric oxide, nitrogen dioxide, and

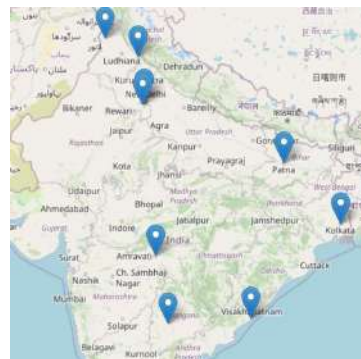


Fig. 1: Location map of India.

Table 1: Latitude and longitude of Indian cities.

City	Latitude	Longitude
Amravati	20.9374° N	77.7796° E
Amritsar	31.6340° N	74.8723° E
Chandigarh	30.7333° N	76.7794° E
Delhi	28.7041° N	77.1025° E
Gurugram	28.4575° N	77.0263° E
Hyderabad	17.3850° N	78.4867° E
Kolkata	22.5726° N	88.3639° E
Patna	25.5941° N	85.1376° E
Visakhapatnam	17.6868° N	83.2185° E



total nitrogen oxide levels. These nitrogen oxides, produced from combustion processes and atmospheric reactions, are important pollutants to monitor (USEPA 2021). The data shows 3,582 missing values in the NO column, 3,585 missing values in the NO<sub>2</sub> column, and 4,185 missing values in the NO<sub>x</sub> column. Additionally, the NH<sub>3</sub> (ammonia) units of parts per million (ppm) columns have 10,328 missing values.

The CO column units of parts per million (ppm), which tracks carbon monoxide levels, is also vital due to the high levels of CO in India caused by traffic emissions, industrial activities, and biomass burning, leading to significant air quality and health issues in urban areas (CPCB 2023). This column has 2,059 missing values.

The SO<sub>2</sub> column units of parts per million (ppm), measuring sulfur dioxide levels, reflect the impact of coal-fired power plants, industrial operations, and vehicular emissions on air pollution and health (MoEFCC 2022), with 3,854 missing values. The O<sub>3</sub> column records ground-level ozone levels in units of parts per million (ppm), an air pollutant linked to respiratory and cardiovascular risks (EEA 2022), and has 4,022 missing values. The Benzene, Toluene, and Xylene columns units of parts per million (ppm) represent volatile organic compounds (VOCs) that pose soundness threats and donate to ozone construction. These VOCs are primarily radiated by industrial operations, conveyance emissions, and chemical solvents in India (ATSDR 2021), with 5,623 missing values in the Benzene column, 8,041 in the Toluene column, and 18,109 in the Xylene column.

Lastly, the AQI (Air Quality Index) column provides a composite index reflecting overall air quality based on the concentrations of the pollutants mentioned above. There are 4,681 missing values in the AQI column, which corresponds to the same number of missing values in the  $AQI_{bucket}$  column that categorizes AQI into qualitative buckets.

**Data Cleaning:** An air pollution dataset contains missing values for pollutant concentrations, which are set to 0 to indicate that no measurement has been taken. The dataset contains comprehensive air quality data for several Indian cities, with complete entries for the City and Date columns. However, pollutant concentration data exhibited significant missing values. It found 29,531 rows and 16 columns of air pollution data; substituting null values with a predetermined value is a standard method for dealing with missing data points.

## MATERIALS AND METHODS

This analysis operates the Recency Frequency Monetary (RFM) model, which is commonly used in customer segmentation (Anitha & Patil 2022) to assess air pollution occurrences. The model is adapted to measure the recency,

frequency, and severity (monetary impact) of pollution occurrences. The proposed methodology is given in Fig. 2. A deep learning neural network is employed to predict air quality using the RFM data, with both regression and classification techniques tested for accuracy. The Air Quality Index (AQI) is an important instrument for expressing the health effects of air pollution. It employs classifications to describe the severity of air quality, ranging from Good to Hazardous (USEP 2014) (Table 2).

## RFM

RFM (Recency, Frequency, Monetary) principles can be adapted to analyze air pollution data by considering analogous factors:

**Recency:** Recency of air pollution station from location. In air pollution, this could refer to the timeliness of the air quality measurements or the most recent pollution events area.

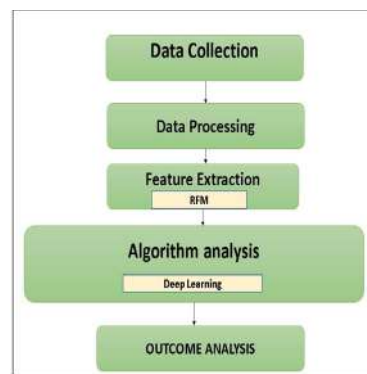


Fig. 2: Proposed methodology.

Table 2: Air Quality Index.

AQI status	Index Range	Characterization of Air Quality Index
GOOD	0 to 50	The level of air pollution is acceptable.
Moderate	51 to 100	The air is in good condition. But some individuals might be concerned.
Unhealthy for sensitive groups (Caution)	101 to 150	Health issues may affect members of sensitive groups. Less likely to be impacted is the general public.
Unhealthy	151 to 200	Members of weak residents may face more intense sound consequences than available resident participants.
Very Unhealthy	201 to 300	Everybody is additionally at hazard for negative soundness repercussions.
Hazardous (Extremely Unhealthy)	301 to 500	Everyone has additional potential to be affected by circumstances in an emergency.

**Frequency:** The frequency of pollution events or measurements. This could mean how often the air quality measurements are taken or the number of times a particular pollution level has been recorded.

**Monetary:** Although not directly applicable, this could be adapted to represent the severity or impact of the pollution. The severity of pollution levels and their environmental and health consequences. Perhaps it is appropriate to be based on pollutant concentration levels and their subsequent health or environmental effects. The customer segmentation approach successfully assesses and categorizes customers by combining ABC and RFM strategies (Liu et al. 2019). Panus (2016) employed ABC classification to identify commodities based on their economic or technological relevance. While ABCXYZ analysis is described as an approach that integrates ABC and XYZ categories over two dimensions, similar to the BCG matrix, it is incapable of offering a detailed analysis (Teslenko 2023). In this research, The RFM classification ranges help in categorizing the data into different air pollution levels of predicted pollution (Table 3).

### Algorithm Analysis

#### Neural Network

Layers of connected nodes, or neurons, make up neural networks. During training, the weights of each connection are changed. Neural network fundamental equations include the following: **Weighted Sum:** Each neuron computes a weighted sum of its inputs. If  $x_1, x_2, \dots, x_n$  are the inputs and  $w_1, w_2, \dots, w_n$  are the corresponding weights, the weighted sum  $z$  for a neuron is given by:

$$Z = \sum_{i=1}^n w_i x_i + b \quad \dots(1)$$

Where  $b$  is the bias term (Goodfellow et al. 2016). **Activation Function:** The weighted sum  $z$  is then passed through an activation function to produce the neuron's output  $a$ . Common activation functions include the sigmoid function, tanh function, and Rectified Linear Unit. For a generic activation function, the output  $a$  is:  $a = \sigma(z)$  (Deng 2014).

**Forward propagation:** In a neural network with multiple layers, the output of each layer is passed as input to the next

layer. For each layer  $l$ , the output  $a^{(l)}$  is computed as :

$$\mathbf{a}^{(l)} = \sigma \left( \mathbf{W}^{(l)} \mathbf{a}^{(l-1)} + \mathbf{b}^{(l)} \right) \quad \dots(2)$$

Where  $\mathbf{w}^{(l)}$  is the weight matrix for layer  $l$ ,  $\mathbf{a}^{(l+1)}$  is the output from the previous layer, and  $\mathbf{b}^{(l)}$  is the bias vector for layer  $l$  (LeCun et al. 2015). **Loss Function:** The performance of the neural network is evaluated using a loss function  $L$ , which measures the difference between the predicted output and the actual target. For a given set of predictions  $y$  and actual values  $y$ , the loss function  $L$  could be Mean Squared Error (MSE), Cross-Entropy, or another appropriate function (Bishop 2006).

**Back propagation:** Backpropagation is used to determine the gradients of the loss function for each weight and bias to train the network. Gradient descent or its derivatives are then used to update the weights and biases:

$$\mathbf{w}(l) \leftarrow \mathbf{w}(l) - \eta \frac{\partial L}{\partial \mathbf{w}l} \quad \dots(3)$$

$$\mathbf{b} \leftarrow \mathbf{b} - \eta \frac{\partial L}{\partial \mathbf{b}} \quad \dots(4)$$

Where  $\eta$  is the learning rate (Rumelhart et al. 1986).

#### Predict Model Performance Metrics

The statistical Mean Absolute Error (MAE), Root Mean Square Error (RMSE), Mean Square Error (MSE), Relative Absolute Error (RAE), and coefficient of determination ( $R^2$ ). These metrics are widely recognized and utilized in various research contexts, including the development of hybrid models that integrate neural networks with traditional statistical methods for air quality forecasting (Zhang 2019). Their application allows for a comprehensive evaluation of model performance, ensuring that the predictions are both accurate and meaningful (Huang 2020). Moreover, in a study by Yadav & Malik (2020), neural network-based predictive models for air quality indices demonstrated the effectiveness of these statistical performance metrics in enhancing prediction accuracy. Similarly, Ma (2020) conducted a comparative study of neural networks and traditional statistical models for air quality forecasting.

**Mean Absolute Error (MAE):** The average of the absolute errors is known as the mean absolute error (MAE). Understanding whether the amount of the error deserves concern or not is made easier by the fact that the MAE units are the same as the expected target

$$\frac{1}{N} \sum_{i=1}^N |w_i - w'_i| \quad \dots(5)$$

**Mean Squared Error (MSE) -** The term Mean Squared Error (MSE) refers to the average or mean of the square of the discrepancy between actual and estimated data.

$$\frac{1}{N} \sum_{i=1}^N (w_i - w'_i)^2 \quad \dots(6)$$

Table 3: RFM classification ranges and descriptions.

Recency	Frequency	Monetary
A	0-50	Very low values or scores
B	51-100	Low values
C	101-150	Moderate-low values
X	151-200	Moderate values
Y	201-300	High values
Z	301-500	Very high values

Here,  $n$  is the number of statements, and  $i$  the indicated True value.

The Relative Absolute Error (RAE) measures the total absolute error as a proportion of the total absolute difference between the true values and their mean. It provides a normalized view of the error, making it easier to understand the model's performance relative to a simple model that always predicts the mean of the target variable. The Relative Absolute Error (RAE) is defined as RAE.

$$= \frac{\sum_{i=1}^N |w_i - w'_i|}{\sum_{i=1}^N |w_i - \bar{w}|} \quad \dots(7)$$

Where:

- $N$  is the number of observations,
- $w_i$  is the true value,
- $w'_i$  is the predicted value,
- $\bar{w}$  is the mean of the true values.

Root Mean Squared Error (RMSE) - MSE's squared root.

$$\sqrt{\frac{1}{N} \sum_{j=1}^N (w_j - w'_j)^2} \quad \dots(8)$$

Squared Error (RSE) - The ratio of value from the square of the fundamental error.

$$\frac{\sum_{j=1}^N (w_j - w'_j)^2}{\sum_{j=1}^N (w_j - w)^2} \quad \dots(9)$$

R Squared Error: The proportion of the error's square.

$$R^2 = 1 - \left( \frac{\sum_{j=1}^N (w_j - w'_j)^2}{\sum_{j=1}^N (w_j - w)^2} \right) \quad \dots(10)$$

**Classification Metrics:** When evaluating classification models, several metrics are commonly used to assess performance. These include Precision, Recall, F1-Score, Accuracy, and their corresponding averages (Macro Avg and Weighted Avg).

**Precision:** Precision is the ratio of correctly predicted positive observations to the total predicted positives. It determines the proportion of predicted positive cases that are correctly identified as positive.

$$\text{Precision} = \frac{\text{True Positives(TP)}}{\text{True Positives(TP)} + \text{False Positives(FP)}} \quad \dots(11)$$

**Recall:** Recall (also known as Sensitivity or True Positive Rate) is the ratio of correctly predicted positive observations to all observations in the actual positive class. The amount of positive instances are correctly identified?

True Positives(TP)

$$\text{Recall} = \frac{\text{True Positives(TP)}}{\text{True Positives(TP)} + \text{False Negatives(FN)}} \quad \dots(12)$$

**F1-Score:** The F1-Score is the harmonic mean of Precision and Recall. It provides a single metric that balances both the concerns of false positives and false negatives.

$$\text{F1-Score} = 2 \times \frac{\text{Precision} \times \text{Recall}}{\text{Precision} + \text{Recall}} \quad \dots(13)$$

**Support:** Support refers to the number of actual occurrences of each class in the dataset. It is used to weigh the average of metrics such as Precision, Recall, and F1-Score. Accuracy

Accuracy is the ratio of correctly predicted observations to the total observations. It works well when the classes are well-balanced.

$$\text{Accuracy} = \frac{\text{TP} + \text{True Negatives (TN)}}{\text{Total Observations}} \quad \dots(14)$$

### Macro Average

The Macro Average computes the average of Precision, Recall, and F1-Score for each class independently, without considering the class imbalance.

$$\text{Macro Avg} = \frac{1}{N} \sum_{i=1}^N \text{Metric}_i \quad \dots(15)$$

Where  $N$  is the number of classes.

### Weighted Average

Weighted Average calculates the average of Precision, Recall, and F1-Score while considering the support (the number of true instances for each label). It accounts for class imbalance by giving more importance to classes with higher support.

$$\text{Weighted Avg} = \frac{\sum_{i=1}^N \text{Support}_i \times \text{Metric}_i}{\sum_{i=1}^N \text{Support}_i} \quad \dots(16)$$

**Confusion Matrix:** The Confusion Matrix is a tabular representation of the actual versus predicted classifications. It provides insights into the RFM model's performance by showing the count of true positive (TP), false positive (FP), true negative (TN), and false negative (FN) predictions, which are then used to calculate metrics like Precision, Recall, F1-Score, and Accuracy (Kök et al. 2017). These metrics are commonly used in classification tasks to assess how well the model distinguishes between different air quality states.

A Confusion Matrix for a binary classification problem is structured as follows:

	Predicted Positive	Predicted Negative
Actual Positive	TP	FN
Actual Negative	FP	TN

## RESULTS AND DISCUSSION

The Simulation Result analysis of the air quality data across various cities reveals significant insights into the distribution and concentration of key pollutants across different cities in India. This result includes Air pollution data on several air quality indicators such as PM<sub>2.5</sub>, PM<sub>10</sub>, NO, NO<sub>2</sub>, NO<sub>x</sub>, NH<sub>3</sub>, CO, SO<sub>2</sub>, O<sub>3</sub>, Benzene, Toluene, Xylene, and the specified Air Quality Index (AQI). The data set is used to concoct and stretch a deep-learning model for forecasting AQI based on pollution statuses in India. Utilizing Google Colab and Python is an applicable method for examining and offering regression and classification experimental data. Regression training and testing sets with 20% of the data reserved for the arbitrary form materialized to 42 testings, batch size of 32, and Training the classification model with a learning rate of 0.1 and 5000 iterations.

As shown in Table 4 provides information on recent high pollution levels in India, the frequency of these events, and the severity of the pollution, suggesting an unhealthy air quality level in Monetary.

The neural network model has been trained to predict air pollution levels over 150 epochs (Table 5), showing rapid initial improvement. As training continued, loss values decreased, indicating convergence. The final epoch recorded a training loss of 8,301.5947 and a validation loss of 8,923.1963, demonstrating the model's ability to learn and stabilize.

The RFM model has been trained and validated using a neural network over 150 epochs, resulting in a mean squared error (MSE) of 557.68. This relatively low MSE indicates that the model can accurately predict air pollution levels with a reasonable degree of precision. A lower MSE indicates a better fit of the model to the data.

Table 4: RFM model predicts air pollution in India.

Recency	Frequency	Monetary
India	190	Unhealthy

Table 5: RFM model hyperparameters.

Hyperparameters	Significances
Input Sequence	12
Hidden Layer	1
Output Layer	1
Number of Epochs	150

Table 6: Training and Validation Metrics Per Epoch (First 50 Epochs).

Training Accuracy	Training Loss	Validation Accuracy	Validation Loss
0.1333	5.7914	0.1533	4.6140
0.1543	4.5265	0.1538	4.4378
0.1560	4.3593	0.1531	4.3554
0.1513	4.2842	0.1570	4.3306
0.1571	4.2104	0.1574	4.3196
0.1549	4.1714	0.1586	4.3149
0.1625	4.0927	0.1608	4.3170
0.1587	4.0802	0.1599	4.3051
0.1579	4.0707	0.1579	4.3413
0.1615	4.0069	0.1596	4.3587
0.1619	4.0050	0.1595	4.3467
0.1623	4.0040	0.1604	4.3194
0.1629	4.0032	0.1610	4.3120
0.1630	4.0030	0.1608	4.3195
0.1636	4.0028	0.1609	4.3186
0.1640	4.0026	0.1613	4.3125
0.1635	4.0025	0.1610	4.3069
0.1637	4.0024	0.1614	4.3095
0.1638	4.0023	0.1613	4.3090
0.1639	4.0023	0.1616	4.3101
0.1642	4.0022	0.1614	4.3078
0.1641	4.0022	0.1615	4.3103
0.1643	4.0021	0.1615	4.3112
0.1644	4.0021	0.1617	4.3109
0.1645	4.0020	0.1617	4.3098
0.1646	4.0020	0.1616	4.3087
0.1647	4.0020	0.1618	4.3082
0.1648	4.0020	0.1618	4.3089
0.1648	4.0020	0.1618	4.3088
0.1649	4.0019	0.1619	4.3091
0.1649	4.0019	0.1619	4.3089
0.1650	4.0019	0.1620	4.3086
0.1650	4.0019	0.1621	4.3084
0.1651	4.0019	0.1621	4.3087
0.1651	4.0018	0.1622	4.3086
0.1652	4.0018	0.1622	4.3089
0.1652	4.0018	0.1622	4.3087
0.1653	4.0018	0.1623	4.3085
0.1653	4.0018	0.1623	4.3088
0.1653	4.0018	0.1624	4.3086
0.1654	4.0018	0.1624	4.3085
0.1654	4.0018	0.1624	4.3088
0.1654	4.0018	0.1624	4.3087
0.1655	4.0018	0.1625	4.3086
0.1655	4.0018	0.1625	4.3086
0.1655	4.0018	0.1625	4.3086
0.1656	4.0018	0.1625	4.3087
0.1656	4.0018	0.1626	4.3087
0.1656	4.0018	0.1626	4.3086
0.1656	4.0018	0.1626	4.3086



The neural network model, trained over 150 epochs, demonstrated rapid initial improvement in predicting air pollution levels, over the first 150 epochs of training (Table 6).

A Deep Learning model's training and validation metrics have been collected. Metrics include training accuracy and loss, as well as validation accuracy and loss. The training accuracy begins low and increases over epochs, peaking about epoch 77. Validation accuracy varies while lack of success improves significantly, hovering around 0.16 to 0.17. Training loss typically reduces, whereas validation loss swings and occasionally increases, indicating model architectural flaws. A final epoch produces a training loss of 8,301.5947 and a validation loss of 8,923.1963.

As shown in Table 7, the classification system exhibits varied performance across different classes. Class A has modest precision and recall, resulting in an F1 score of 0.64. Class B outperforms with excellent precision (0.75) and recall (0.70), yielding an F1-Score of 0.72. Alternatively, Class C has lower performance, reflected in an F1-Score of 0.51 due to its lower recall (0.43). Class X struggles with poor performance, as evidenced by an F1-Score of 0.40, indicating substantial challenges. Class Y demonstrates moderate performance with an F1-Score of 0.57.

In contrast, Class Z delivers the best results, with high precision (0.68) and recall (0.88), culminating in an F1-Score of 0.77. The overall accuracy of 66% reflects the proportion of correctly classified instances, while the macro average provides an unweighted mean across all classes, highlighting balanced performance. The weighted average, which accounts for the support of each class, offers a balanced view of the system's performance.

As shown in Table 6 and Table 7, the model has excellent overall accuracy and a decent fit, as evidenced by the  $R^2$  value. However, the high error metrics indicate potential difficulties with prediction accuracy. The

Table 7: Classification of air pollution RFM model in India.

Class	Precision	Recall	F1-Score	Support
A	0.67	0.62	0.64	836
B	0.75	0.70	0.72	2614
C	0.64	0.43	0.51	1507
X	0.45	0.37	0.40	694
Y	0.54	0.60	0.57	806
Z	0.68	0.88	0.77	2403
Accuracy		0.66		
Macro Avg	0.62	0.60	0.60	8860
Weighted Avg	0.66	0.66	0.65	8860

Table 8: Evaluation of the RFM.

Class	TP	FN	FP	TN
A	522	314	262	6793
B	1839	775	622	3655
C	641	866	1000	4384
X	256	438	572	5625
Y	484	322	419	5666
Z	2121	282	1019	4469

classification metrics reveal varied performance across different classes, though some classes show poorer results.

Despite the model's overall high accuracy (Table 8), performance issues have been observed in specific classes, particularly in distinguishing between moderate and severe pollution levels. A substantial number of false positives and false negatives indicate that the categorization process needs further improvement. The model demonstrated better accuracy in predicting air pollution for regions with high variability in pollution levels. Classes C and Z show a large number of incorrect classifications, indicating the model's difficulty in distinguishing these classes. As shown in Table 9, a deep learning algorithm predicts the air quality index (AQI) with an accuracy of 94%. However, a large Mean Squared Error (454.09) indicates considerable errors. Low metrics such as MAE (14) and RMSE (21.31) indicate that the model's predictions are generally close to true AQI values.

Table 9: Evaluation metrics for the RFM.

Metric	Value
Test Accuracy	94%
Mean Squared Error (MSE)	454.09
Root Mean Squared Error (RMSE)	21.31
Mean Absolute Error (MAE)	14.64
Relative Absolute Error (RAE)	0.215
Relative Squared Error (RSE)	0.055
R Squared Error ( $R^2$ )	0.945

Table 10: RFM performance metrics in back propagation.

Metric	Value
Test Accuracy	99%
Mean Squared Error (MSE)	0.48
Root Mean Squared Error (RMSE)	0.06
Mean Absolute Error (MAE)	0.05
Relative Absolute Error (RAE)	0.11
Relative Squared Error (RSE)	0.03
R Squared Error ( $R^2$ )	0.99

As shown in Table 10, using backpropagation, various performance metrics provide insights into the model's accuracy and efficacy. Mean Squared Error (MSE) measures the average squared difference between estimated and actual values, indicating the model's accuracy. A low MSE suggests a relatively low degree of error, reflecting good model performance. In conjunction, the Root Mean Squared Error (RMSE) assesses the average magnitude of prediction errors, and a low RMSE signifies that the errors are small. In addition, the Mean Absolute Error (MAE) quantifies the average absolute difference from actual values; an MAE of 0.05 indicates model accuracy. The Relative Absolute Error (RAE) stands at 11% of the baseline error, offering that the model performs significantly better than the baseline.

Furthermore, the Relative Squared Error (RSE) is 0.03, indicating a 97% reduction in error compared to the baseline. Finally, the  $R^2$  value, representing the proportion of variance explained by the model, is 0.9, signifying an excellent fit. The RFM model using backpropagation regression achieves 99% test highest accuracy for air quality predictions, with low MSE and RMSE, excellent accuracy, and strong performance compared to baseline models. It explains 99% of the dependent variable's variance with an  $R^2$  of 0.99, demonstrating robustness.

As shown in Table 11, the model's failure to identify Class A and high false positives for Class B raises concerns about its accuracy. The confusion matrix reveals that while the model performs well for Classes C, X, Y, and Z, it significantly underperforms in Classes A and B. The model's failure to correctly classify Class A and high false positives for Class B

As shown in Table 12, the RFM model's precision, recall, and F1-score for classes A, C, X, Y, and Z are 0.00, indicating it failed to predict any instances. Class B has a precision of 0.27, a recall of 1.00, and an F1-score of 0.43, suggesting it properly recognized all cases but assembled a large number of false positives. The overall accuracy is 0.27, indicating underperformance, especially considering imbalanced performance across different classes. The Macro average values are low, indicating poor performance across all classes

Table 11: Evaluation back propagation for RFM.

Class	TP	FN	FP	TN
A	0	1209	0	2688
B	1601	0	1209	2087
C	1289	0	0	2608
X	510	0	0	3387
Y	609	0	0	4288
Z	689	0	0	4208

Table 12: Classification report for back propagation.

Class	Precision	Recall	F1-Score	Support
A	0.00	0.00	0.00	1209
B	0.27	1.00	0.43	1601
C	0.00	0.00	0.00	1289
X	0.00	0.00	0.00	510
Y	0.00	0.00	0.00	609
Z	0.00	0.00	0.00	689
Accuracy		0.27		
Macro Avg	0.05	0.17	0.07	5907
Weighted Avg	0.07	0.27	0.12	5907

Table 13: RFM performance metrics in forward propagation.

Metric	Value
Test Accuracy	93%
Mean Squared Error (MSE)	39085.58
Root Mean Squared Error (RMSE)	197.70
Mean Absolute Error (MAE)	137.63
Relative Absolute Error (RAE)	1.44
Relative Squared Error (RSE)	1.93
R Squared Error ( $R^2$ )	0.93

without considering class distribution. They perform well for class B but struggle to generalize across other classes,

As shown in Table 13, the model has a high test accuracy of 99%, indicating its exceptional performance in classifying or predicting the target variable correctly. However, the mean squared error (MSE) is significantly higher than expected, suggesting a notable difference between predicted and actual values. Moreover, the root mean squared error (RMSE) is considerable, indicating significant inaccuracies in predictions. In addition, the mean absolute error (MAE) is relatively high, reflecting a considerable average error in predictions. Furthermore, the model's absolute error is 144% of the baseline error, implying worse performance compared to a baseline model. Similarly, the relative squared error (RSE) is 193% of the total squared error, indicating large errors relative to the baseline. Despite these issues, the  $R^2$  value is high, suggesting that 93% of the variance in the

Table 14: Evaluation forward propagation for RFM.

Class	TP	FN	FP	TN
A	1209	0	4698	6793
B	0	2107	1209	3575
C	0	1289	1209	3874
X	0	510	1209	3384
Y	0	609	1209	3384
Z	0	689	1209	6682

Table 15: Classification report forward propagation.

Class	Precision	Recall	F1-Score	Support
A	0.20	1.00	0.34	1209
B	0.00	0.00	0.00	1601
C	0.00	0.00	0.00	1289
X	0.00	0.00	0.00	510
Y	0.00	0.00	0.00	609
Z	0.00	0.00	0.00	689
Accuracy		0.20		
Macro Avg	0.03	0.17	0.06	5907
Weighted Avg	0.04	0.20	0.07	5907

target variable is explained by the model, which indicates a very good fit.

As shown in Table 14, the confusion matrix for ward propagation reveals that the model is underperforming significantly, with a strong bias towards Class A and failure to classify other classes. The increased amount of false positives for Class A and zero true positives for the additional classes. Table 15, The model's performance in class A has been analyzed, with a recall of 1.00 and a precision of 0.20, indicating a correct labeling of class A instances. However, the model also misclassified many instances of classes B, C, X, Y, and Z, resulting in zero precision, recall, and F1-Score. The overall accuracy has been 20%, indicating only 20% of the total predictions are correct.

The model's performance across all classes has been poor, with a significant failure to predict instances of classes B, C, X, Y, and Z. Classes with relatively fewer samples have larger weights than the majority classes to balance their contribution to the loss function. The neural network model demonstrated a strong ability to capture complex patterns in the air pollution data. The RFM model integration appeared to increase forecast accuracy, particularly in metropolitan regions with varying pollution levels. The RFM model's integration with neural networks enhanced air pollution forecast accuracy, as indicated by higher metrics, including MSE and R-squared, compared with standard models without RFM integration. Combining RFM models A, B, C, X, Y Z with deep learning can yield better predictive performance. The model's ability to effectively account for recency, frequency, and monetary value in pollution data has been evident, particularly when predicting air quality index (AQI) values.

## CONCLUSIONS

The integration of the RFM model with neural networks has proven effective in enhancing air quality predictions across various Indian cities. By incorporating recency,

frequency, and severity, the model provides a detailed and accurate representation of air pollution trends. The neural network demonstrated significant reductions in loss and effective convergence, offering valuable insights into temporal patterns and high-risk pollution areas. Regression performs better in Air pollution levels in predicting continuous outcomes and effectively apprehending the nuanced variations in air quality metrics. However, the strength of classification in the RFM model keeps the focus on their practical application in air quality analysis. Performance issues have been observed in distinguishing between moderate and severe pollution levels, highlighting the need for further refinement of the classification model. Regularization techniques and more complex neural network architectures could improve robustness and generalization. Evaluating the RFM with neural networks complex model on prior observed assessment air pollution data and comparing training and validation errors is critical for preventing overfitting from occurring.

Additionally, future research should focus on optimizing the model's performance through better tuning and exploring advanced architectures. Regression techniques show promise for determining precise pollutant levels, while classification methods are more suitable for assessing overall pollution risk. These improvements will help develop targeted interventions to mitigate urban air pollution effectively.

## REFERENCES

- Agency for Toxic Substances and Disease Registry (ATSDR), 2021. Toxicological Profile for Benzene. Retrieved 7 Oct. 2024, from <https://www.atsdr.cdc.gov/toxprofiles/tp3.html>.
- Anitha, P. and Patil, M.M., 2022. RFM model for customer purchase behavior using K-Means algorithm. *Journal of King Saud University - Computer and Information Sciences*, 34(5), pp.1785–1792. DOI
- Bishop, C.M., 2006. *Pattern Recognition and Machine Learning*. Springer. DOI
- Brauer, M., Guttikunda, S.K., Dey, S., Tripathi, S.N., Weagle, C. and Martin, R.V., 2019. Examination of monitoring approaches for ambient air pollution: A case study for India. *Atmospheric Environment*, 216, p.116940.
- Central Pollution Control Board (CPCB), 2023. National Ambient Air Quality Status & Trends. Retrieved 7 Oct. 2024, from <https://cpcb.nic.in/air-quality-status/>.
- Deng, L., 2014. A tutorial survey of architectures, algorithms, and applications for deep learning. *APSIPA Transactions on Signal and Information Processing*, 3, p.39. DOI
- European Environment Agency (EEA), 2022. Air Quality in Europe – 2022 Report. Retrieved 7 Oct. 2024, from <https://www.eea.europa.eu/publications/air-quality-in-europe-2022>.
- Goodfellow, I., Bengio, Y. and Courville, A., 2016. *Deep Learning*. MIT Press. DOI
- Gupta, U., 2008. Valuation of urban air pollution: A case study of Kanpur City in India. *Environmental Resources and Economics*, 41, pp.315–326. DOI
- Huang, C., 2020. Evaluation of neural network model performance using statistical metrics in predicting air pollutant concentrations. *IEEE*

- Transactions on Neural Networks and Learning Systems*, 31(5), pp.1450–1460. DOI
- Ibarra-Berastegi, G., Elias, A., Barona, A., Saenz, J., Ezcurra, A. and de Argandoña, J.D., 2008. From diagnosis to prognosis for forecasting air pollution using neural networks: Air pollution monitoring in Bilbao. *Environmental Modelling & Software*, 23(5), pp.622–637. DOI
- Ibarra-Berastegi, G., Saenz, J., Ezcurra, A., Elias, A. and Barona, A., 2009. Using neural networks for short-term prediction of air pollution levels. In: *Proceedings of the 2009 International Conference on Advanced Computing Tools for Engineering Applications (ACTEA)*. Zouk Mosbeh, Lebanon, 2009. pp.498–502. DOI
- Khanal, S., Pokhrel, R.P., Pokharel, B., Becker, S., Giri, B., Adhikari, L. and LaPlante, M.D., 2022. An episode of transboundary air pollution in the central Himalayas during agricultural residue burning season in North India. *Atmospheric Pollution Research*, 13(1), p.101270. DOI
- Kök, M.U., Şimşek, M. and Özdemir, S., 2017. A deep learning model for air quality prediction in smart cities. In: *2017 IEEE International Conference on Big Data (Big Data)*, 11–14 Dec. 2017, Boston, MA, US, IEEE, pp.1983–1990. DOI
- Kumar, P. and Gupta, A., 2023. Comparative analysis of SVM and deep learning methods for predicting air quality index. *Environmental Monitoring and Assessment*, 195(6), pp.12–24. DOI
- Kurt, A., Gulbagci, B., Karaca, F. and Alagha, O., 2008. An online air pollution forecasting system using neural networks. *Environment International*, 34(5), pp.592–598. DOI
- LeCun, Y., Bengio, Y. and Hinton, G., 2015. Deep learning. *Nature*, 521(7553), pp.436–444. DOI
- Liao, J., Jantan, A., Ruan, Y. and Zhou, C., 2022. Multi-behavior RFM model based on improved SOM neural network algorithm for customer segmentation. *IEEE Access*, 10, pp.122501–122512. DOI
- Lisboa, P.J., 2002. A review of evidence of health benefit from artificial neural networks in medical intervention. *Neural Networks*, 15(1), pp.11–39.
- Liu, M., Du, Y. and Xu, X., 2019. Customer value analysis based on Python crawler. In: *2019 Chinese Control and Decision Conference (CCDC)*, 3–5 June 2019, Nanchang, China, IEEE, pp.4345–4350. DOI
- Ma, Y., 2020. A comparative study of neural networks and traditional statistical models for air quality forecasting. *Journal of Cleaner Production*, 256, p.120461. DOI
- Mena, G., Coussement, K., De Bock, K.W., De Caigny, A. and Lessmann, S., 2023. Exploiting time-varying RFM measures for customer churn prediction with deep neural networks. *Annals of Operations Research*, pp.1–23. DOI
- Ministry of Environment, Forest and Climate Change (MoEFCC), 2022. *Annual Report 2021–22*. Retrieved 7 Oct. 2024, from <https://moef.gov.in/annual-report/>
- Mohammad, J. and Kashem, M.A., 2022. Air pollution comparison RFM model using machine learning approach. In: *Proceedings of the 2022 IEEE 7th International Conference on Convergence Technology (I2CT)*. Pune, India, 2022. pp.1–5. DOI
- Panus, J., 2016. Customer segmentation utilization for differentiated approach. In: *2016 International Conference on Information and Digital Technologies (IDT)*, 5–7 July 2016, Rzeszow, Poland, IEEE, pp.227–233. DOI
- Rumelhart, D.E., Hinton, G.E. and Williams, R.J., 1986. Learning representations by back-propagating errors. *Nature*, 323(6088), pp.533–536. DOI
- Teslenko, D., 2023. Comparative analysis of the applicability of five clustering algorithms for market segmentation. In: *2023 IEEE Open Conference of Electrical, Electronic and Information Sciences (eStream)*, 27 April 2023, eStream, IEEE, pp.1–6. DOI
- U.S. Environmental Protection Agency (USEPA), 2014. *Air Quality Index: A Guide to Air Quality and Your Health*. Retrieved 7 Oct. 2024, from <https://www.epa.gov/airquality-index>
- U.S. Environmental Protection Agency (USEPA), 2021. *Nitrogen Dioxide (NO<sub>2</sub>) Pollution*. Retrieved 7 Oct. 2024, from <https://www.epa.gov/no2-pollution>
- Wesolowski, M., Suchacz, B. and Halkiewicz, J., 2006. The analysis of seasonal air pollution patterns with the application of neural networks. *Analytical and Bioanalytical Chemistry*, 384, pp.458–467. DOI
- World Health Organization (WHO), 2021. *Ambient Air Pollution: A Global Assessment of Exposure and Burden of Disease*. Retrieved 7 Oct. 2024, from <https://www.who.int/publications/i/item/9789240061311>
- Yadav, R. and Malik, H., 2020. Neural network-based predictive models for air quality index using statistical performance metrics. *Neural Computing and Applications*, 32(9), pp.4591–4603. DOI
- Zhang, D., 2019. A novel hybrid model based on neural networks and statistical methods for air quality forecasting. *IEEE Access*, 7, pp.109415–109427. DOI



# Systematic Review of Phytoremediation: Efficacy of Aquatic Plants in Wastewater Treatment and Pollutant Removal

Mangesh Jabade<sup>id</sup> and Jasneet Kaur<sup>†id</sup>

Symbiosis College of Nursing, Symbiosis International (Deemed) University, Pune, Maharashtra, India

<sup>†</sup>Corresponding author: [jasneetkaur@scon.edu.in](mailto:jasneetkaur@scon.edu.in)

**Abbreviation:** Nat. Env. & Poll. Technol.  
**Website:** [www.neptjournal.com](http://www.neptjournal.com)

*Received:* 26-06-2024

*Revised:* 14-08-2024

*Accepted:* 30-08-2024

## Key Words:

Aquatic plants  
 Phytoremediation  
 Water pollutants  
 Wastewater  
 Environmental health

## ABSTRACT

The swift process of industrialization and urbanization in our society has resulted in a growing issue of wastewater production, which presents a substantial danger to ecosystems and human well-being. This study examines the efficacy of aquatic plants in wastewater treatment by using their innate ability to remove pollutants. Water hyacinth (*Eichhornia crassipes*), water lettuce (*Pistia stratiotes*), and duckweeds (Lemnaceae) are types of aquatic plants that have been thoroughly researched due to their capacity to cleanse domestic, industrial, agricultural, and wastewater. This study encompasses a range of studies completed from 2014 to 2024, which investigate the efficacy of different aquatic plants in eliminating contaminants and provide insights into the specific mechanisms employed by these plants. Research has revealed remarkable findings, indicating that specialist plants can eliminate pollutants, including nitrogen, phosphate, and heavy metals, with an efficiency of up to 100%. Furthermore, the incorporation of these plants into wetlands and natural purification systems has been demonstrated to enhance the purification process by stimulating increased biomass production and the absorption of noxious gases. Future research should give priority to genetically modifying plants to enhance their capacity for absorbing contaminants and to develop integrated systems for treating wastewater. In summary, this study showcases the capacity of aquatic plants to serve as a highly effective and eco-friendly substitute for wastewater treatment. Implementing phytoremediation techniques can enhance the sustainability of water management practices and aid in safeguarding our ecosystems and the health of society.

## INTRODUCTION

As the outcome of industry, population growth, and urbanization, a significant quantity of wastewater is discharged into the environment. Population increase and economic development have a significant influence on water pollution, causing detrimental effects on ecosystems and presenting the most significant environmental hazard (Bashir et al. 2020). Wastewater treatment is a very efficient method of restoring wastewater to its initial condition following industrial, home, or municipal utilization. Phytoremediation, utilizing aquatic plants, has gained popularity during the past twenty years. The objective of this assessment is to determine the most effective aquatic plants for the treatment of wastewater by doing a thorough examination of current models. Phytoremediation is a sort of biological treatment that can be implemented in different ways, including phytoextraction, rhizosphere filtration, phytostabilization, and phytotransformation. This technique facilitates the photosynthesis and proliferation of specific plants, enabling them to acclimate to pollution and eliminate organic or inorganic contaminants (Silva 2023). The fundamental aspects and qualities of the operation rely on the process of degradation, extraction, transformation, or detoxification. This procedure is conducted within a well or pond that has a depth ranging from 0.4 to 1.5 meters. Employ strategies to regulate the proliferation of aquatic vegetation in wetland ecosystems (Kaur et al. 2020).

## Citation for the Paper:

Jabade, M. and Kaur, J., 2025. Systematic review of phytoremediation: efficacy of aquatic plants in wastewater treatment and pollutant removal. *Nature Environment and Pollution Technology*, 24(2), p. B4243. <https://doi.org/10.46488/NEPT.2025.v24i02.B4243>

*Note: From year 2025, the journal uses Article ID instead of page numbers in citation of the published articles.*



**Copyright:** © 2025 by the authors  
**Licensee:** Technoscience Publications  
 This article is an open access article distributed under the terms and conditions of the Creative Commons Attribution (CC BY) license (<https://creativecommons.org/licenses/by/4.0/>).

Rendering to the United Nations, a portion of the wastewater from both public and industrial sources is released without undergoing any treatment in developing countries. Wastewater can be utilized for irrigation in underdeveloped nations with scarce water supplies, which presents a health risk to the population while also supplying nutrients to agricultural systems (Mishra et al. 2023). Wastewater may contain non-biodegradable heavy metals such as zinc (Zn), nickel (Ni), copper (Cu), chromium (Cr), mercury (Hg), cadmium (Cd), lead (Pb), and arsenic (As), along with a substantial quantity of agriculturally significant nutrients (Zaynab et al. 2022). As an effect, there is an increasing worldwide interest in environmentally sustainable technology for treating wastewater that allows for the reuse of essential nutrients (Ugwuanyi et al. 2024). In addition to industrial activities, the photoengraving technique, which is also referred to as metal engraving, photochemical treatment, or chemical milling, has the potential to contaminate water sources with different amounts and combinations of metal ions. Annually, substantial amounts of agricultural waste are generated globally. Some of these agricultural wastes are directly disposed of in water bodies, resulting in significant water pollution (Bokov et al. 2021). In addition, disposing of kitchen trash into untreated or improperly treated wastewater can result in several detrimental environmental consequences, such as the introduction of hazardous materials (HMs). Exceeding the sensitivity threshold of specific metals can be hazardous to both humans and other biological systems. As a result, the issue of water contamination by heavy metals is a significant worry in many developing countries, impacting both the quality of drinking water and the health of the aquatic ecosystem (Elbasiouny et al. 2021a). Consequently, it is imperative to meticulously regulate and supervise HM levels to guarantee compliance with the specific environmental criteria for each type of water source. The majority of heavy metals (HMs) are regarded as elemental remnants, present in small quantities (parts per billion: < 10 ppm) in different environmental matrices. Significant quantities of municipal waste, untreated industrial waste, and significant quantities of agrochemicals have been discharged into exposed lakes and rivers at alarming concentrations, leading to a rise in the concentration of heavy metals (HMs) and a deterioration in water quality (US EPA 2015). The escalating global need for drinkable water, coupled with the need to address water pollution, has become a critical concern owed to its potential to induce cancer, Parkinson's disease, Alzheimer's disease, anemia, and negative impacts on the gastrointestinal, neurological, skeletal, and cutaneous systems (Shetty et al. 2023).

Plants serve as the main reservoir of nourishment, textiles, and energy. Nevertheless, many aquatic plants

possess the ability to eliminate contaminants present in wastewater. The presence of toxic contaminants in synthetic compounds has experienced a significant surge throughout ecosystems in recent times. Water supplies are contaminated with toxic contaminants, including solvents, pesticides, dyes, and other chemicals, resulting in ecological harm (Aziz et al. 2023). Aquatic plants have a significant role in the removal of detrimental pollutants. Aquatic plants, such as Water Typha, Colocasia Hyacinth, Canna, Arabica, and other plant species are employed to eliminate toxic substances from water. These aquatic plants effectively absorb both organic and inorganic contaminants in their environment through competition (Carvajal-Flórez & Santiago-Alonso 2019, Hendrasarie & Redina 2023). Water hyacinth plants could potentially treat almost all types of wastewater (Panday 2023). The term used to describe this process is "phytoremediation". The presence of polluted water, coupled with a limited supply of water, has exerted a substantial burden on the environment. Water scarcity impacts more than 40% of the global population due to climate change, increasing food demand, rapid urbanization, and unsustainable utilization of natural resources (World-Scientific-News 2023). Discharging waste material and residues into water bodies can have fatal repercussions for marine ecosystems, presenting significant hazards to both the environment and human life. Therefore, it is crucial to expose wastewater to suitable treatment and purification procedures before releasing it into the environment. Currently, traditional methods of wastewater treatment do not consistently achieve the desired level of contaminant reduction in the water (Medeiros et al. 2022). Therefore, trace levels of contaminants may still be present in the purified water. Due to the hazardous properties of pollutants, these substances have the potential to pose a threat to the ecosystem and disrupt many cellular processes in plants. Contaminated wastewater poses significant risks to both the well-being of aquatic organisms and the total health of the environment. Wastewater reclamation is the sole remaining option to address the increasing need for water in the agricultural and industrial fields (Mishra et al. 2023).

Although phytoremediation utilizing aquatic plants for wastewater treatment has been increasingly popular in the last twenty years, there is a significant lack of systematic research on identifying the most efficient aquatic plants for this specific purpose. Prior research has predominantly concentrated on individual plant species or limited features of phytoremediation, lacking a comprehensive evaluation that compares diverse species and their capacities in varied situations. In addition, while the individual processes of phytoremediation, such as phytoextraction and rhizosphere filtration, have been studied, there is a lack of comprehensive research that combines these findings to provide a clear

evaluation of the overall efficacy of phytoremediation techniques. In light of the increasing global attention towards sustainable wastewater treatment technologies and the urgent need to address water pollution and scarcity, it is imperative to carry out a methodical evaluation. This evaluation aims to collect and arrange up-to-date material, determine the most efficient approaches, and offer direction for future research and implementation efforts. This review aims to resolve the issue by doing a comprehensive analysis of existing models and identifying the most effective aquatic plants for wastewater treatment.

## Aims

The objective of this systematic review is to assess and determine the most efficient aquatic plants for the removal of contaminants and the purification of wastewater. This review aims to assess the efficacy and versatility of various phytoremediation techniques, offering a thorough examination of current models and practices to inform future research and use in sustainable wastewater treatment technologies. The review question involves,

1. What are the effective aquatic plants for removing pollutants and purifying wastewater?
2. What are the methods for eliminating pollution in wastewater?
3. What are the Wastewater treatment mechanisms employed by aquatic plants?
4. How do different phytoremediation methods compare in terms of efficiency and adaptability in various environmental contexts?

## MATERIALS AND METHODS

This is a comprehensive and methodical review. To locate databases containing references, a variety of internet search engines were also employed. The review questions had a direct impact on the exact criteria that were employed to select the research. Written justifications were provided for both inclusion and exclusion.

The inclusion criteria were as follows.

1. Studies published within the last 10 years (2014-2024) to ensure the review includes recent advancements.
2. Research focusing on various aquatic plants used for phytoremediation, including but not limited to Water Hyacinth, Canna, Colocasia, and Typha.
3. Studies examine different phytoremediation methods, such as phytoextraction, phytostabilization, and phytotransformation.
4. Studies addressing a range of pollutants, including

heavy metals, organic contaminants, nutrients, and other common wastewater pollutants.

5. Research conducted in various environmental contexts, including industrial, domestic, municipal wastewater, and agricultural runoff.
6. Studies published in English.

The Exclusion criteria were as follows,

1. Non-peer-reviewed articles, editorials, opinion pieces, and conference abstracts.
2. Research focusing on terrestrial plants or non-plant-based wastewater treatment methods.
3. Studies focusing on pollutants not typically found in wastewater or not relevant to water purification

The chosen studies underwent a comprehensive quality review utilizing broad criteria for critical evaluation. The PEO factors were considered to assess any potential impact of aquatic plants in removing pollutants from wastewater.

**Search Strategy:** The selected databases were utilized throughout the entire data collection process in this investigation. We conducted a thorough search on Pubmed, CINAHL, and Medline. To minimize data saturation, keywords were searched using logical operators and keywords like {"plants" (MeSH Terms) OR ("Phytoplankton" (All Fields) AND "water" (All Fields) AND "pollution" (All Fields)) OR "Biodegradation" (All Fields) OR ("Phytoremediation" (All Fields) AND "Environmental Pollutants" (All Fields)) OR "metals, heavy" (All Fields))}. Furthermore, the reference lists of all the discovered papers were examined to find other qualifying publications. The study adhered to the Preferred Reporting Items for Systematic Reviews and Meta-analyses (PRISMA) standards. To ensure that the updates are based on reliable research, we have only included papers from the past 10 years.

## Study Selection

The procedure for choosing these papers entailed an initial assessment of the titles and abstracts, followed by a comprehensive analysis of the whole article. After the selection process, a consensus meeting was organized to resolve the disagreements, and the third author's input was used as a deciding factor. Disputes among researchers on the appropriateness of an article for inclusion were settled by convening a meeting of the three authors to reach a consensus.

## Data Extraction

Two researchers independently collected data using a standardized form and later verified the accuracy of the

information. Disagreements were settled by reaching a consensus. Each study collected data on the name of the initial author, the year of publication, the geographic location, the methodology used in the study, the types of plants studied, the type of wastewater used, and the nutrient uptake or removal efficiency that was of interest.

### Assessment of Quality of Papers

The majority of studies focused on school-age children and adolescents up to 18 years of age. The median quality score of the included studies, calculated using the modified Newcastle-Ottawa Quality Assessment Scale (Herzog et al. 2013), was seven points (range 2–9). Eleven papers were deemed to be of better quality. The remaining studies were of lesser quality generally because of the research samples' poorer representativeness, their lack of study power, or their insufficient ability to adjust for potential confounding

variables during analysis. The quality check was done by two authors.

After performing a Boolean search to identify relevant phrases, the terms were sorted using various filters based on the inclusion criteria. This process resulted in the identification of 320 pertinent records, with 165 entries discovered in Web of Science, 75 in SCOPUS, and 80 in PubMed. The review adhered to the PRISMA (Preferred Reporting Items for Systematic Reviews and Meta-Analyses) guidelines for documenting findings, and flow diagrams were created to illustrate the selection process (Fig. 1).

During the initial stages, various aspects were excluded due to their lack of relevance to the subject matter of the study. Specifically, 180 duplicate articles were eliminated. Subsequently, a thorough examination of each article's abstract was conducted. Two independent reviewers screened 140 records, excluding 80 for the following

### Search Results

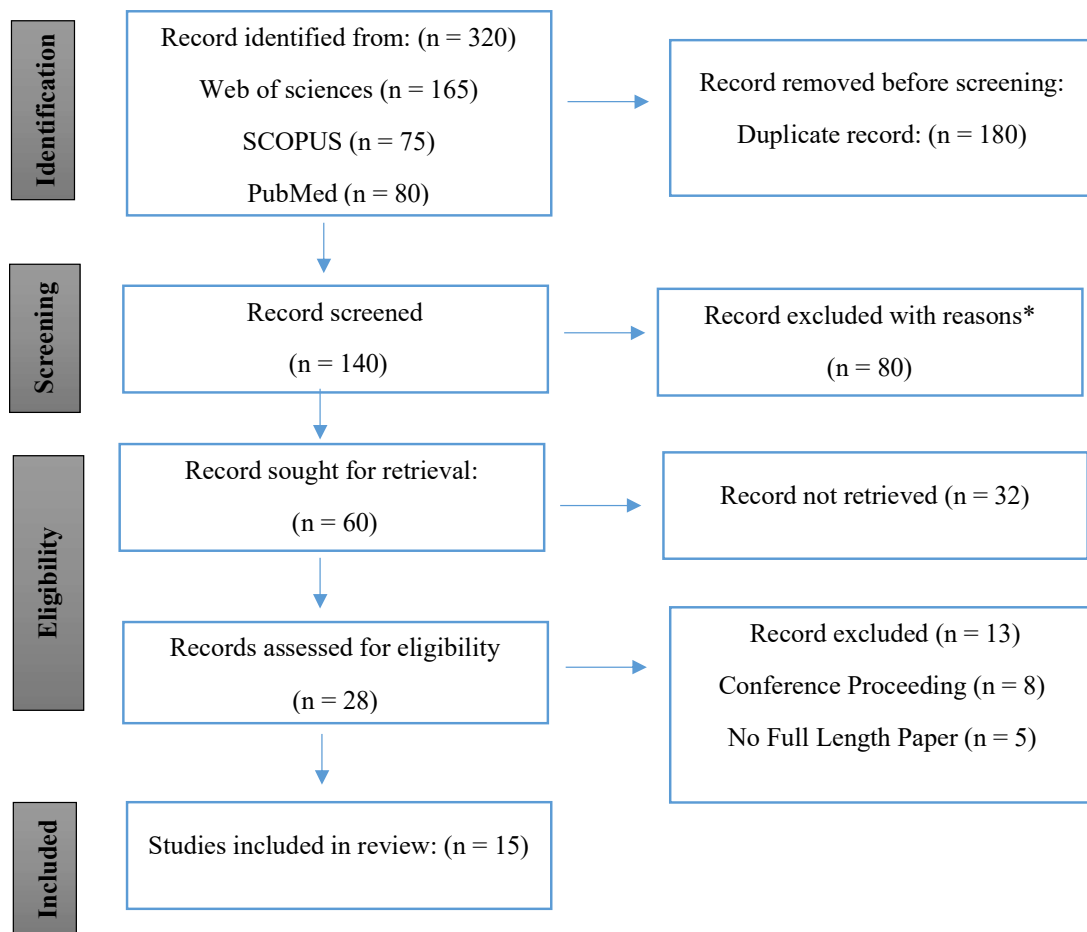


Fig. 1: Prisma Flowchart. [\*Insufficient data (22), non-English language (14), Outcomes are not relevant (44)].



Table 1: Depicts the study characteristics, and details are discussed as follows.

Authors	Type of Study	Plants	Classification of wastewater	Remediation	Desired nutrient absorption/ Efficiency of nutrient removal
Lu et al. (2018) Shanghai, China	Experimental Research Study	Water hyacinth and Water lettuce	polluted rural rivers	Situ remediation.	TN and $\text{NH}_4^+\text{-N}$ & phosphorus
Ansari et al. (2020) India	Literature review	water hyacinth (Eichhornia) and Lemnaceae Azolla, Eichhornia, Lemna, Potamogeton, Spirodela, Wolfia, and Wolfiella	Bioremediation of contaminated waters	Phytoremediation, Bioaccumulation	Despite their hazardous attributes, there are elevated levels of heavy metals, phenols, formaldehyde, formic acids, acetic acids, and oxalic acids. Similarly, the proportion of biological oxygen demand (BOD), chemical oxygen demand (COD), and different ionic forms of nitrogen and phosphorus.
Maine et al. (2022) Argentina	Experimental Research Study	Pontederia rotundifolia, Typha domingensis	peri-urban wetlands	Phytoremediation	Chromium, Nickel, Zinc, Lead, total phosphorus (TP), and total Kjeldahl nitrogen (TKN)
Escoto et al. (2019) Brazil	Experimental Research Study	Pistia stratiotes	clomazone in water	Phytoremediation	LCT and HCT
Chen et al. (2019) China	Experimental Research Study	Duckweed	rural wastewater	Phytoremediation and bioremediation	$\text{NO}_3\text{-N}$ and TN
Zhou et al. (2019) China	Experimental Research Study	Duckweed	swine wastewater	Phytoremediation	ammonia nitrogen ( $\text{NH}_3$ single bond N) and total phosphorus (TP) increased at 0.1–1.0 mg/L of $\text{Cu}^{2+}$ while dropping at 2.0–5.0 mg/L of $\text{Cu}^{2+}$ .
Raza et al. (2023) Pakistan	Experimental Research Study	water lettuce (WL), alligator weed (AW), pennywort (PW), and duckweed (DW)	household and industrial wastewater	Phytoremediation	lead (Pb), zinc (Zn), phosphate, sulfate, and potassium.
Mohd Nizam et al. (2020) Malaysia	Experimental Research Study	Centella asiatica, Ipomoea aquatica, Salvinia molesta, Eichhornia crassipes, and Pistia stratiotes	Aquaculture Wastewater	Phytoremediation	Suspended solids (TSS), ammoniacal nitrogen ( $\text{NH}_3\text{-N}$ ), and phosphate.
Sricoth et al. (2018) Thailand	Experimental Research Study	Typha angustifolia and Eichhornia crassipes	Market wastewater	Phytoremediation	$\text{NO}_3^-\text{-N}$ , $\text{NH}_3\text{-N}$ , and metal (Pb, Cd, and Zn)
Wickramasinghe and Jayawardana (2018) Sri Lanka	Experimental Research Study	Eichhornia crassipes (water hyacinth), Pistia stratiotes (water lettuce) and Salvinia molesta (water fern)	Textile wastewater	Phytoremediation	Chemical oxygen demand (COD), total solids (TS), total suspended solids (TSS), total dissolved solids (TDS), nitrates, phosphates, and heavy metals such as cadmium (Cd), nickel (Ni), and zinc (Zn).
Mustafa and Hayder G. (2021) Malaysia	Review paper	S. molesta plants	Domestic wastewater	Phytoremediation	turbidity, phosphate, ammoniacal nitrogen, and nitrate
Kumar and Deswal (2020) India	Experimental Research Study	water hyacinth, water lettuce, salvinia, and duckweed	rice mill wastewater	Phytoremediation	phosphorus (TP) and chemical oxygen demand (COD)
Saleh et al. (2019) Egypt	Experimental Research Study	Ludwigia stolonifera	Biological treatment of wastewater	Stabilization and Solidification	Cu, Fe, and Mn
Gupta and Tyagi (2022) India	Experimental Research Study	E. crassipes	Industrial wastewater	Phytoremediation	Cd, Cr, Co, Ni, Pb, and Hg
Sompura et al. (2024) India	Literature review	Eichhornia crassipes, Pistia stratiotes, and Lemna minor	Polluted wastewater	Phytoremediation with Genetic Engineering Enhancements	Iron (Fe), manganese (Mn), zinc (Zn)

reasons: 22 records contained insufficient data, 14 were in non-English languages, and 44 had outcomes not relevant to the study.

Out of the remaining 60 records sought for retrieval, 32 could not be retrieved. Ultimately, 28 records were assessed for eligibility, resulting in the exclusion of 13 additional records. Consequently, a total of 15 papers met the inclusion criteria and were included in the final evaluation.

## RESULTS AND DISCUSSION

The studies are summarized in Table 1 below. The synthesis of results adopted a convergent approach, amalgamating a plethora of outcomes gathered. The publications from different countries, such as China (Chen et al. 2019, Lu et al. 2018, Zhou et al. 2019), India (Ansari et al. 2020, Gupta & Tyagi 2022, Mishra et al. 2023, Sompura et al. 2024), Argentina (Maine et al. 2022), Brazil (Escoto et al. 2019), Pakistan (Raza et al. 2023), Malaysia (Mohd Nizam et al. 2020, Mustafa & Hayder 2021), Thailand (Sricoth et al. 2018), Sri Lanka (Wickramasinghe & Jayawardana 2018) and Egypt (Saleh et al. 2020), to explore the possible usage of aquatic plants for this purpose. For this work, a systematic mapping review procedure was employed. The primary objective of this review paper is to examine the latest advancements in wastewater phytoremediation methods. It aims to identify the limitations and places within the phytoremediation process that may necessitate future research. Up until this point, over 20 aquatic plants have been mentioned in this article. This document offers comprehensive guidance for researchers in selecting suitable facilities and determining the optimal hydraulic retention period for conducting wastewater treatment tests.

### Efficacy of the Plants

Several extensive research has been carried out to explore the possible applications of plants in the treatment of wastewater. Only research conducted from 2015 onwards that focused on the use of aquatic plants for wastewater treatment was chosen for link with this review article. Table 1 summarises the findings of our study, which examined several papers on wastewater phytoremediation. Some researchers focused on individual plants and provided detailed information on their effectiveness in treating wastewater. Meanwhile, other researchers studied multiple species for this purpose.

A combination of aquatic plants, such as water hyacinth and water lettuce, can effectively improve water quality. The researchers found that water hyacinth had the highest removal rates for TN (89.4%) and  $\text{NH}_4^+\text{-N}$  (99.0%), whereas water lettuce had the highest removal efficiency for total

phosphorus (93.6%) (Lu et al. 2018).

However, Azolla, Eichhornia, Lemna, Potamogeton, Spirodela, Wolfia, and Wolfialla are effective phytoremediators. These aquatic plant species can significantly reduce water pollution by accumulating pollutants in their tissues (Ansari et al. 2020). Water hyacinth (*Eichhornia crassipes*) is extremely resilient and can withstand high levels of heavy metals (Lu et al. 2018). Phenols, formaldehyde, formic acids, acetic acids, and oxalic acids are toxic chemicals that are frequently present in water (Ansari et al. 2020). *P. stratiotes* demonstrates notable resilience to clomazone exposure and efficiently eliminates as much as 90% of the herbicide residues. *Pistia stratiotes* is a potent phytoremediation agent for the herbicide clomazone in water, according to a study (Escoto et al. 2019). The review demonstrated the efficacy of five aquatic plants, namely *Centella asiatica*, *Ipomoea aquatica*, *Salvinia molesta*, *Eichhornia crassipes*, and *Pistia stratiotes*, in effectively eliminating three pollutants, specifically total suspended solids (TSS), ammoniacal nitrogen ( $\text{NH}_3\text{-N}$ ), and phosphate, from aquaculture wastewater (Mohd et al. 2020).

The potential of using locally abundant aquatic plants, such as *Eichhornia crassipes* (water hyacinth), *Pistia stratiotes* (water lettuce), and *Salvinia molesta* (water fern), for phytoremediation in the treatment of textile wastewater has also been highlighted. The efficacy of lowering chemical oxygen demand (COD), total solids (TS), total suspended solids (TSS), total dissolved solids (TDS), nitrates, phosphates, heavy metals (Cd, Ni, and Zn), as well as total and fecal coliform was measured by the wastewater treatment plants (Wickramasinghe & Jayawardana 2018). *Salvinia molesta* and *Pistia stratiotes*, two species of aquatic plants, have been widely used for the treatment of agricultural, household, and industrial wastewater. The widespread use of these plants can be due to their wide availability, ability to thrive in unfavorable environments, capacity for bioaccumulation, invasive nature, and great potential for biomass production (Mustafa & Hayder 2021). Water lettuce has shown the most effectiveness in decreasing phosphorus (TP) and chemical oxygen demand (COD), with water hyacinth, duckweed, and *Salvinia* following suit (Kumar & Deswal 2020). *E. crassipes* is an aquatic invasive plant that has a strong inclination to absorb toxins from water, particularly heavy metals. This facility is very conducive for the utilization of living organisms to cleanse industrial wastewater contaminated with the heavy metals Cd, Cr, Co, Ni, Pb, and Hg. In addition, *E. crassipes* can eliminate pollutants aside from heavy metals, including cyanide, making it highly beneficial in regions involved in gold mining (Gupta & Tyagi 2022).

Similarly, multiple plants belonging to the Lemna family can significantly reduce levels of biochemical oxygen demand (BOD) and chemical oxygen demand (COD) and also alleviate the effects of heavy metals (HM) and different types of ions. The citation (Ansari et al. 2020) Aquatic macrophytes, including *Eichhornia crassipes*, *Pistia stratiotes*, and *Lemna minor*, have shown promise in utilizing phytoremediation to cleanse wastewater and eliminate heavy metals (Sompura et al. 2024).

Roots of *Pontederia rotundifolia* had the most elevated concentration of Pb. *Typha domingensis* had the greatest levels of Cr, Ni, and Zn, which aligns with the highest concentration found in the sediment. Peri-urban wetlands require plants with a large amount of biomass, such as *T. domingensis*, to effectively remove metals from water (Maine et al. 2022)

The introduction of a microbial carrier did not affect the growth and biomass components of duckweed. The CDW system unveiled the subsequent characteristics. The removal efficiencies of  $\text{NO}_3^-$ -N and TN were much higher compared to the other two systems, reaching a maximum of 80.02% and 56.42%, respectively. Furthermore, Illumina sequencing demonstrated the utmost microbial diversity. Furthermore, a clear and sequential progression of microbial community was found (Chen et al. 2019). The efficiency of removing ammonia nitrogen ( $\text{NH}_3$ -N) and total phosphorus (TP) rose when the concentration of  $\text{Cu}^{2+}$  was between 0.1 and 1.0 mg/L but decreased when the concentration of  $\text{Cu}^{2+}$  was between 2.0 and 5.0 mg.L<sup>-1</sup>. A unique kinetic model incorporating  $\text{Cu}^{2+}$  was subsequently created and utilized to optimize the concentration of  $\text{Cu}^{2+}$  at 0.96 mg/L for efficient nutrient removal in duckweed systems (Zhou et al. 2019). The use of duckweed and pennywort in treating effluent resulted in the complete removal of lead (Pb) from industrial wastewater while achieving an 81% removal rate. Additionally, the treatment using AW achieved a complete removal of Pb from domestic wastewater (Raza et al. 2023). *T. angustifolia* and *E. crassipes* have comparable carbon content (about 35%), hydrogen content (around 6%), and gross calorific value. *Eichhornia crassipes* had an ash content of up to 16.9% and a moisture content of 65.4%. *T. angustifolia* has the potential to serve as an alternate energy source in addition to its ability to cleanse wastewater, according to its significant biomass production (Sricoth et al. 2018). The efficacy of *Ludwigia stolonifera*, a wetland plant, displayed effective removal of three hazardous metals, namely Pb, Cd, and Cr. The plant's ability to survive has been examined in solutions with varying concentrations of three individual metals or as a combination, and the long-term accumulation of these harmful metals has been assessed (Saleh et al. 2019).

## Methods for Eliminating Pollution in Wastewater

Prioritization of treatment has been given to polluted aqueous solutions to prevent their entry into natural water bodies. Bioremediation, electrocoagulation, chemical precipitation, membrane separation, ion-exchange resins, adsorption, coagulation, reduction, reverse osmosis, evaporation, solvent extraction, and flocculation are various techniques used to eliminate heavy metals from water-based solutions. Each of these strategies has advantages and disadvantages. However, most of these procedures are costly and inefficient in terms of removing dangerous substances from large amounts of water. Furthermore, these advantages include non-selectivity, elevated energy consumption, and dependence on chemical compounds, all of which necessitate meticulous removal of the resultant perilous waste. Adsorption is the preferred method for eliminating hazardous pollutants due to its high efficiency, cost-effectiveness, simple design, and user-friendly nature (Elbasiouny et al. 2021b). Adsorption is a well-recognized and reliable technology that is preferred by many sectors. Activated carbon, fly ash, peat, woody biomass, zeolites, sewage sludge ash, and other biomaterials have demonstrated significant efficacy in the removal of certain metals, such as lead and cadmium, from wastewater. Aquatic plants such as water primrose (*Ludwigia stolonifera*), water hyacinth (*Eichhornia crassipes*), blue water well (*Veronica anagallis-aquatica*), and duckweed (*Lemna gibba*) have effectively eliminated heavy metals (HMs) from aquatic settings. Aquatic organisms can absorb and immobilize hazardous metals (HMs), leading to the buildup of these chemicals as solid waste. This technique results in the purification of the liquid solutions containing water (Hamad & Idrus 2022). The method offers two notable benefits: cost-effectiveness and ease. It only necessitates the organic development of plants. The dissolved elements are extracted from the liquid solution by the process of adsorption onto the roots or transportation within the plant's stem. Subsequently, the elements are secured through physical and/or chemical interactions. Consequently, phytoremediation is increasingly employed for the treatment of wastewater contaminated with heavy metals (Saleh et al. 2020). While numerous land-based and water-based plants have been examined, it remains crucial to assess their performance and effectiveness in various scenarios in the majority of instances. Furthermore, it is imperative to examine plant species that have not yet been investigated for their capacity to cleanse aquatic habitats (Sree et al. 2023).

## Wastewater Treatment Mechanisms Employed by Aquatic Plants

Recently, natural treatment systems have become increasingly popular as effective treatment solutions for several types of

wastewater. Examples of natural systems encompass soil systems, aquatic systems, and wetlands. These systems depend on sustainable energy sources such as solar power, wind power, and the energy stored in biomass and soil. Phytoremediation and wetland systems have become widely used natural methods for treating wastewater in many countries, especially developed ones, with the establishment of stable pond systems (Sharma et al. 2023). Presently, there is an increasing fascination with investigating the ability of plants to efficiently decompose and eliminate detrimental microorganisms and pollutants. This has led to expanded utilization of plant systems and a broader variety of studies in this field (Bala et al. 2022)

Plants in this system have the main function of providing the necessary oxygen for heterotrophic bacteria in the root zone, as well as absorbing nutrients and improving the stability and flow of water in the substrate. Wetlands, functioning as a highly efficient secondary treatment system, can decrease the concentration of contaminants, such as organic waste, inorganic matter, and various harmful bacteria, to a level that is considered acceptable. Criteria for selecting land treatment or technology include the success of treatments in achieving rehabilitative goals, reducing pollutants, reducing pollutant toxicity, and being cost-effective in both the short- and long-term (Thakur et al. 2023). Typically, common plant species, such as lichens, plankton, and higher plants, provide vital insights into the well-being of an ecosystem. Plants serve as reliable markers for predicting and detecting ecological disruptions. The process of industrialization and urbanization has resulted in a recent increase in pollution in both terrestrial and marine ecosystems. Plants are essential in evaluating the extent of pollution in an ecosystem because they are stationary and can adjust to their environment (Zaghloul et al. 2020). Aquatic plants function as the main providers of nutrients and oxygen for the water. They have a vital function in preserving the equilibrium of the aquatic ecosystem. Aquatic plants serve as the primary source of nourishment and oxygen for the water, which plays a crucial role in maintaining the balance of the aquatic ecosystem (Irfan & Alatawi 2019). The marine environment is an efficient and economical way to clean up aquatic plants in a large contaminated area. Aquatic plants naturally mitigate pollution and heavy metals. Utilizing aquatic plants is the most optimal and economical approach for eliminating heavy metals and other contaminants from the environment (Kristanti & Hadibarata 2023).

Aquatic vegetation and engineered wetlands have been widely employed for wastewater treatment on a global scale. Choosing aquatic plant species that have a high capacity for accumulating heavy metals is crucial for the treatment of aquatic plants. Aquatic plants have gained

a commendable reputation for their ability to remediate contaminated areas worldwide throughout time. Aquatic plants possess a complex root system that allows them to accumulate pollutants in their roots and stems, rendering them highly suitable for this purpose (Ali et al. 2024). The growth & cultivation of aquatic plants need a significant amount of time, which could impede the increasing demand for the treatment of aquatic plants. However, the drawbacks of this issue are overshadowed by the numerous benefits that this technology provides in the field of wastewater treatment (Harun et al. 2021). An essential benefit of aquatic plant treatment is its status as an environmentally friendly technology that supports sustainable growth over an extended period. This approach harnesses the natural resources of plants and microbes, mitigates environmental degradation, protects ecosystems, and enhances the quality of life and well-being (Obaideen et al. 2022). Aquatic plants have the benefit of efficiently remedying both organic and inorganic contaminants. These mechanisms, including Phytoaccumulation, Phytodegradation, Phytotransformation, Phytovolatilization, and Phytoextraction, make them highly effective in treating mixed types of pollutants. These systems facilitate the elimination and refinement of impurities. At concentrations varying from low to moderate, it effectively restores soil that has been contaminated with significant amounts of pollutants that are spread over a wide area. The task can be accomplished on-site without causing any adverse impact on the soil's texture and structure. This approach is distinguished by its environmentally sustainable methods and aesthetically pleasant architecture, offering the civic a stunning view of the surroundings (Pathak et al. 2022). By applying pollution mitigation techniques and pursuing specific development objectives, it is possible to rehabilitate damaged soil for agricultural purposes and utilize treated wastewater for sanitation or landscaping. This approach effectively minimizes the adverse effects on the ecosystem. Furthermore, phytotechnology is more economically efficient than alternative chemical and physical treatment methods since it is easy to install and maintain (Wang & Aghajani Delavar 2023)

**Limitations:** The review presents a meticulous and methodical examination of the existing body of literature, providing a comprehensive comprehension of the present level of expertise regarding aquatic plants and their diverse applications and effects. The work of literature contributes to conservation efforts by examining the potential ecological advantages and disadvantages of aquatic plants. Nevertheless, there are specific constraints associated with the review. The efficacy of aquatic vegetation might vary considerably depending on the geographical location and environmental circumstances. The variability observed in the data may



restrict the applicability of the results to wider or distinct circumstances. The data utilized in the evaluation may originate from a variety of studies with distinct techniques, scales, and levels of quality. The presence of heterogeneity can lead to biases and impact the consistency and reliability of the results made.

## CONCLUSIONS

Aquatic plants have shown a notable ability to remove diseases from wastewater. Plants counteract infections by several mechanisms, such as the absorption by plant roots, interactions with biofilms, and alterations in soil or water chemistry. Aquatic plants provide a multitude of benefits to people, and there are still countless unexplored opportunities for their utilization. At now, the introduction of problematic aquatic plant species is posing a threat to both marine and freshwater habitats. These plant species are commonly imported from other regions for medicinal or horticultural purposes. However, they gradually evade human control and establish self-sustaining populations in the wild. These aquatic plants possess the capacity to effectively eliminate diverse contaminants, including hydrocarbons and other perilous and cancer-causing compounds, from water. Utilizing growth-promoting bacteria to enhance plant development in the rhizosphere and manage overgrown plants is a potential change that can have a substantial therapeutic effect. Aquatic plants are frequently used in wastewater treatment due to their significantly reduced cost and superior efficiency. A multitude of research has demonstrated that aquatic plants serve as effective repositories for wastewater treatment. They are utilized in the treatment process to diminish or restrict the presence of pollutant-laden wastewater. The quality of the treated wastewater met the worldwide effluent criteria for irrigation. In the future, there is potential to utilize genetically modified plants to enhance their ability to absorb heavy metals and facilitate the decontamination process. These modified plants should have accelerated growth cycles, allowing them to complete their life cycle in a shorter period while also possessing a high capacity for phytoremediation. These plants can eliminate additional pollutants from water, including hydrocarbons and other harmful and cancer-causing substances. Applying growth-promoting bacteria to enhance plant development in the rhizosphere and regulate overgrown plants is a promising intervention that can lead to substantial treatment results.

## REFERENCES

- Ali, M., Aslam, A., Qadeer, A., Javied, S., Nisar, N., Hassan, N., Hussain, A., Ali, B., Iqbal, R., Chaudhary, T., Alwahibi, M.S. and Elshikh, M.S., 2024. Domestic wastewater treatment by *Pistia stratiotes* in constructed wetland. *Scientific Reports*, 14, p.7553. DOI
- Ansari, A.A., Naeem, M., Gill, S.S. and AlZuaibr, F.M., 2020. Phytoremediation of contaminated waters: An eco-friendly technology based on aquatic macrophytes application. *Egyptian Journal of Aquatic Research*, 46, pp.371–376. DOI
- Aziz, K.H.H., Mustafa, S.F., Omer, K.M., Hama, S.F., Hamarawf, R.F. and Rahman, K.O., 2023. Heavy metal pollution in the aquatic environment: Efficient and low-cost removal approaches to eliminate their toxicity: A review. *RSC Advances*, 13, pp.17595–17610. DOI
- Bala, S., Garg, D., Thirumalesh, B.V., Sharma, M., Sridhar, K., Inbaraj, B.S. and Tripathi, M., 2022. Recent strategies for bioremediation of emerging pollutants: A review for a green and sustainable environment. *Toxics*, 10, p.484. DOI
- Bashir, I., Lone, F.A., Bhat, R.A., Mir, S.A., Dar, Z.A. and Dar, S.A., 2020. Concerns and threats of contamination on aquatic ecosystems. *Bioremediation and Biotechnology*, pp.1–26. DOI
- Bokov, D., Turki Jalil, A., Chupradit, S., Suksatan, W., Javed Ansari, M., Shewael, I.H., Valiev, G.H. and Kianfar, E., 2021. Nanomaterial by sol-gel method: Synthesis and application. *Advances in Materials Science and Engineering*, 2021, p.e5102014. DOI
- Carvajal-Flórez, E. and Santiago-Alonso, C.G., 2019. Technologies applicable to the removal of heavy metals from landfill leachate. *Environmental Science and Pollution Research*, 26, pp.15725–15753. DOI
- Chen, G., Huang, J., Fang, Y., Zhao, Y., Tian, X., Jin, Y. and Zhao, H., 2019. Microbial community succession and pollutants removal of a novel carrier-enhanced duckweed treatment system for rural wastewater in Dianchi Lake basin. *Bioresource Technology*, 276, pp.8–17. DOI
- Elbasiouny, H., Darwesh, M., Elbeltagy, H., Abo-alhamd, F.G., Amer, A.A., Elsegaiy, M.A., Khattab, I.A., Elsharawy, E.A., Ebehiry, F., El-Ramady, H. and Brevik, E.C., 2021a. Ecofriendly remediation technologies for wastewater contaminated with heavy metals with special focus on using water hyacinth and black tea wastes: A review. *Environmental Monitoring and Assessment*, 193, p.449. DOI
- Escoto, D.F., Gayer, M.C., Bianchini, M.C., da Cruz Pereira, G., Roehrs, R. and Denardin, E.L.G., 2019. Use of *Pistia stratiotes* for phytoremediation of water resources contaminated by clomazone. *Chemosphere*, 227, pp.299–304. DOI
- Gupta, A. and Tyagi, T., 2022. Phytoremediation and therapeutic potential of neglected plants: An invasive aquatic weeds and ornamental plant. In: S. Arora, A. Kumar, S. Ogita and Y.-Y. Yau, eds. *Biotechnological Innovations for Environmental Bioremediation*. Springer Nature, pp.259–290. DOI
- Hamad, H.N. and Idrus, S., 2022. Recent developments in the application of bio-waste-derived adsorbents for the removal of methylene blue from wastewater: A review. *Polymers*, 14(4), p.783. DOI
- Harun, I., Pushiri, H., Amirul-Aiman, A.J. and Zulkeflee, Z., 2021. Invasive water hyacinth: Ecology, impacts, and prospects for the rural economy. *Plants*, 10(8), p.1613. DOI
- Hendrasarie, N. and Redina, C., 2023. Ability of water lettuce (*Pistia stratiotes*) and water hyacinth (*Eichhornia crassipes*) to remove methylene blue anionic surfactant (MBAS) from detergent wastewater. *Nature Environment and Pollution Technology*, 22(4), pp.1961–1970. DOI
- Herzog, R., Álvarez-Pasquin, M.J., Díaz, C., Del Barrio, J.L., Estrada, J.M. and Gil, Á., 2013. Are healthcare workers' intentions to vaccinate related to their knowledge, beliefs and attitudes? A systematic review. *BMC public health*, 13, pp.1–17.
- Irfan, S. and Alatawi, A.M.M., 2019. Aquatic ecosystem and biodiversity: A review. *Open Journal of Ecology*, 9(1), p.1. DOI
- Kaur, R., Talan, A., Tiwari, B., Pilli, S., Sellamuthu, B. and Tyagi, R.D., 2020. Constructed wetlands for the removal of organic micro-pollutants. In: S. Varjani, A. Pandey, R.D. Tyagi, H.H. Ngo and C. Larroche, eds. *Current Developments in Biotechnology and Bioengineering*. Elsevier, pp.87–140. DOI

- Kristanti, R.A. and Hadibarata, T., 2023. Phytoremediation of contaminated water using aquatic plants, its mechanism and enhancement. *Current Opinion in Environmental Science & Health*, 32, p.100451. DOI
- Kumar, S. and Deswal, S., 2020. Phytoremediation capabilities of *Salvinia molesta*, water hyacinth, water lettuce, and duckweed to reduce phosphorus in rice mill wastewater. *International Journal of Phytoremediation*, 22(11), pp.1097-1109. DOI
- Lu, B., Xu, Z., Li, J. and Chai, X., 2018. Removal of water nutrients by different aquatic plant species: An alternative way to remediate polluted rural rivers. *Ecological Engineering*, 110, pp.18-26. DOI
- Maine, M.A., Hadad, H.R., Camaño Silvestrini, N.E., Nocetti, E., Sanchez, G.C. and Campagnoli, M.A., 2022. Cr, Ni, and Zn removal from landfill leachate using vertical flow wetlands planted with *Typha domingensis* and *Canna indica*. *International Journal of Phytoremediation*, 24(1), pp.66-75. DOI
- Medeiros, A.D.M.de, Silva Junior, C.J.G.da, Amorim, J.D.P.de, Durval, I.J.B., Costa, A.F. and Sarubbo, L.A., 2022. Oily wastewater treatment: Methods, challenges, and trends. *Processes*, 10(4), Article 4. DOI
- Mishra, R.K., Mentha, S.S., Misra, Y. and Dwivedi, N., 2023. Emerging pollutants of severe environmental concern in water and wastewater: A comprehensive review on current developments and future research. *Water-Energy Nexus*, 6, pp.74-95. DOI
- Mishra, S., Kumar, R. and Kumar, M., 2023. Use of treated sewage or wastewater as an irrigation water for agricultural purposes—Environmental, health, and economic impacts. *Total Environment Research Themes*, 6, p.100051. DOI
- Mohd Nizam, N.U., Mohd Hanafiah, M., Mohd Noor, I. and Abd Karim, H.I., 2020. Efficiency of five selected aquatic plants in phytoremediation of aquaculture wastewater. *Applied Sciences*, 10(8), Article 8. DOI
- Mustafa, H.M. and Hayder, G., 2021. Recent studies on applications of aquatic weed plants in phytoremediation of wastewater: A review article. *Ain Shams Engineering Journal*, 12(1), pp.355-365. DOI
- Obaideen, K., Shehata, N., Sayed, E.T., Abdelkareem, M.A., Mahmoud, M.S. and Olabi, A.G., 2022. The role of wastewater treatment in achieving sustainable development goals (SDGs) and sustainability guidelines. *Energy Nexus*, 7, p.100112. DOI
- Panday, A.B., 2023. The potential of phytoremediation to treat different types of wastewater—A review. *Nature Environment and Pollution Technology*, 22(2), pp.969-975. DOI
- Pathak, V.M., Verma, V.K., Rawat, B.S., Kaur, B., Babu, N., Sharma, A., Dewali, S., Yadav, M., Kumari, R., Singh, S., Mohapatra, A., Pandey, V., Rana, N. and Cunill, J.M., 2022. Current status of pesticide effects on the environment, human health and its eco-friendly management as bioremediation: A comprehensive review. *Frontiers in Microbiology*, 13, p.962619. DOI
- Raza, M., Nosheen, A., Yasmin, H., Naz, R., UsmanShah, S.M., Ambreen, J. and El-Sheikh, M.A., 2023. Application of aquatic plants alone as well as in combination for phytoremediation of household and industrial wastewater. *Journal of King Saud University - Science*, 35(7), p.102805. DOI
- Saleh, H.M., El-Saied, F.A., Salaheldin, T.A. and Hezo, A.A., 2019. Influence of severe climatic variability on the structural, mechanical, and chemical stability of cement kiln dust-slag-nano-silica composite used for radwaste solidification. *Construction and Building Materials*, 218, pp.556-567. DOI
- Saleh, H.M., Moussa, H.R., Mahmoud, H.H., El-Saied, F.A., Dawoud, M. and AbdelWahed, R.S., 2020. The potential of the submerged plant *Myriophyllum spicatum* for treatment of aquatic environments contaminated with stable or radioactive cobalt and cesium. *Progress in Nuclear Energy*, 118, p.103147. DOI
- Sharma, K.S., Panchal, K., Chhimwal, M. and Kumar, D., 2023. Integrated detection and natural remediation technology as a low-cost alternative for wastewater treatment. *Health Sciences Review*, 8, p.100111. DOI
- Shetty, S.S., Sonkusare, S., Naik, P.B., Kumari, N.S. and Madhyastha, H., 2023. Environmental pollutants and their effects on human health. *Heliyon*, 9(9), p.e19496. DOI
- Silva, J.A., 2023. Wastewater treatment and reuse for sustainable water resources management: A systematic literature review. *Sustainability*, 15(14), p.10940. DOI
- Sompura, Y., Bhardwaj, S., Selwal, G., Soni, V. and Ashokkumar, K., 2024. Unrevealing the potential of aquatic macrophytes for phytoremediation in heavy metal-polluted wastewater. *Journal of Current Opinion in Crop Science*, 5, pp.48–61. DOI
- Sree, K.S., Appenroth, K.J. and Oelmüller, R., 2023. Sustainable stress management: Aquatic plants vs. terrestrial plants. *Plants*, 12(11), p.2208. DOI
- Sricoth, T., Meeinkuirt, W., Pichtel, J., Taepayoon, P. and Saengwilai, P., 2018. Synergistic phytoremediation of wastewater by two aquatic plants (*Typha angustifolia* and *Eichhornia crassipes*) and potential as biomass fuel. *Environmental Science and Pollution Research International*, 25(6), pp.5344–5358. DOI
- Thakur, T.K., Barya, M.P., Dutta, J., Mukherjee, P., Thakur, A., Swamy, S.L. and Anderson, J.T., 2023. Integrated phytobial remediation of dissolved pollutants from domestic wastewater through constructed wetlands: An interactive macrophyte-microbe-based green and low-cost decontamination technology with prospective resource recovery. *Water*, 15(22), p.3877. DOI
- Ugwuanyi, E.D., Nwokediegwu, Z.Q.S., Dada, M.A., Majemite, M.T. and Obaigbena, A., 2024. Review of emerging technologies for nutrient removal in wastewater treatment. *World Journal of Advanced Research and Reviews*, 21(2), p.520. DOI
- US EPA, 2015. *Sustainable Materials Management: Non-Hazardous Materials and Waste Management Hierarchy*. U.S. Environmental Protection Agency.
- Wang, J. and Aghajani Delavar, M., 2023. Techno-economic analysis of phytoremediation: A strategic rethinking. *Science of The Total Environment*, 902, p.165949. DOI
- Wickramasinghe, S. and Jayawardana, C.K., 2018. The potential of aquatic macrophytes *Eichhornia crassipes*, *Pistia stratiotes*, and *Salvinia molesta* in phytoremediation of textile wastewater. *Journal of Water Security*, 4(0). DOI
- World-Scientific-News, 2023. Phytoremediation of Heavy Metals and Organic Pollutants Using Aquatic Macro- and Macro-phytes. Retrieved 30 December 2024. Available at Link
- Zaghloul, A., Saber, M., Gadow, S. and Awad, F., 2020. Biological indicators for pollution detection in terrestrial and aquatic ecosystems. *Bulletin of the National Research Centre*, 44(1), p.127. DOI
- Zaynab, M., Al-Yahyai, R., Ameen, A., Sharif, Y., Ali, L., Fatima, M., Khan, K.A. and Li, S., 2022. Health and environmental effects of heavy metals. *Journal of King Saud University - Science*, 34(1), p.101653. DOI
- Zhou, Q., Li, X., Lin, Y., Yang, C., Tang, W., Wu, S., Li, D. and Lou, W., 2019. Effects of copper ions on the removal of nutrients from swine wastewater and on the release of dissolved organic matter in duckweed systems. *Water Research*, 158, pp.171–181. DOI

# Geospatial Analysis of the Relationship Between Land Surface Temperature and Land Use/Land Cover Indices: A Study of Raiganj Municipality, West Bengal, India

Bapi Sarkar<sup>1</sup>, Sribas Patra<sup>2</sup> and Mallikarjun Mishra<sup>2†</sup>

<sup>1</sup>Department of Geography, Raiganj University, Raiganj-733134, West Bengal, India

<sup>2</sup>Department Geography, Ravenshaw University, Cuttack-753003, Odisha, India

†Corresponding author: Mallikarjun Mishra, mallikarjungeog@ravenshawuniversity.ac.in

**Abbreviation:** Nat. Env. & Poll. Technol.

**Website:** www.neptjournal.com

*Received:* 11-07-2024

*Revised:* 03-10-2024

*Accepted:* 11-10-2024

## Key Words:

Geospatial techniques  
Land surface temperature  
LU/LC indices

## Citation for the Paper:

Sarkar, B., Patra, S. and Mishra, M., 2025. Geospatial analysis of the relationship between land surface temperature and land use/land cover indices: A study of Raiganj municipality, West Bengal, India. *Nature Environment and Pollution Technology*, 24(2), p. B4245. <https://doi.org/10.46488/NEPT.2025.v24i02.B4245>

*Note: From year 2025, the journal uses Article ID instead of page numbers in citation of the published articles.*



**Copyright:** © 2025 by the authors

**Licensee:** Technoscience Publications

This article is an open access article distributed under the terms and conditions of the Creative Commons Attribution (CC BY) license (<https://creativecommons.org/licenses/by/4.0/>).

## ABSTRACT

The present study is focused on the estimation of Land Surface Temperature (LST) and its relationship with three Land Use and Land Cover (LULC) indices--Normalised Difference Vegetation Index (NDVI), Normalised Difference Water Index (NDWI), and Normalised Difference Built-up Index (NDBI) in Raiganj Municipality, India. Landsat-5 TM (2001 & 2011) and Landsat-8 OLI (2021) satellite images were used, processed, and analyzed in the ArcGIS. The study observed that the values of LST and NDBI were increased by +0.9°C and +0.71, and the values of NDVI and NDWI were decreased by -0.20 and -0.34 during 2001-2021. The highest LST is observed over the built-up spaces and the lowest over vegetation cover and water bodies. The result indicates LST has a significant positive correlation with NDBI and a negative correlation with NDVI and NDWI. LST is increased due to dramatic changes in LULC especially in unplanned infrastructural development and losses in green and blue spaces.

## INTRODUCTION

Land Use/ Land Cover in urban spaces is rapidly changing, which creates many environmental issues (Herold et al. 2016, Lambin et al. 2003). In a mixed and complex urban environment, the concept of Land Surface Temperature (LST) is utilized to interpret the changing pattern of land use/land cover (LULC) (Guha et al. 2020a, Pal & Ziaul, 2017, Saha et al. 2021). The study of the intensity of LST in major global cities like Beijing, Columbia, Shanghai, Chicago, Mumbai, and New Delhi used to address a variety of environmental issues (Asgarian et al. 2015, Das & Das 2020, Kuang et al. 2014, Mukherjee & Singh 2020, O'Connor 2003, Peng et al. 2020). The nature and distribution of LST are influenced by various LULC indices (Bindajam et al. 2020, Bokaie et al. 2016, Guha & Govil 2020, 2021, 2022, Hua & Ping 2018, Kafy et al. 2020). Vegetation index, built-up index, bareness index, water index, and other normalized difference LULC indices were frequently utilized in recent LST-related studies to quantify their impact on the changing environmental status of urban areas (Aboelnour et al. 2018, Gantumur et al. 2017). The relationship between LST and LULC indices using statistical techniques has been explored by scholars for different cities (Ferreira & Duarte 2019, Mallick et al. 2012, Naserikia et al. 2019, Rasul & Ibrahim 2017, Sekertekin et al. 2015). The linear correlation analysis between the LST and LULC indices was discussed in the context of big global cities but very limited to small cities like Raiganj. Li & Zhou (2019) assessed the seasonal impact of thermal conditions of Ohio City using simple regression analysis, and Guha et al. (2020b) also assessed the seasonal impact of LST on LULC indices in Jaipur City of Rajasthan. Seoul in South Korea (Kim et

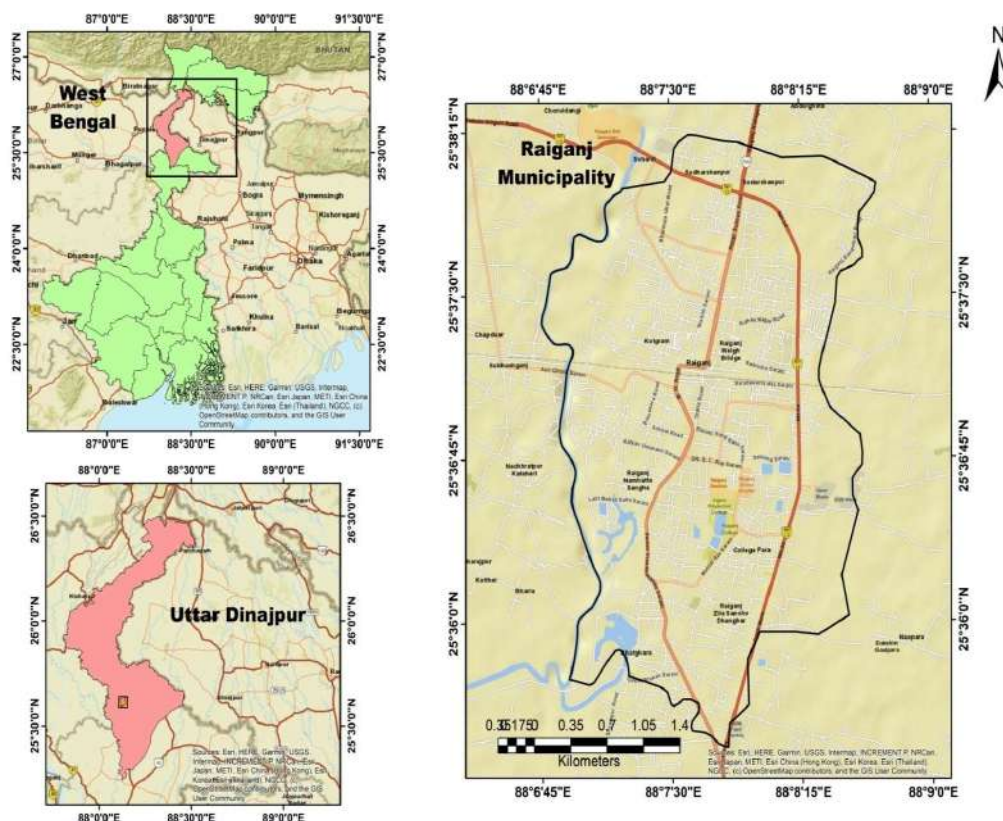


al. 2022), the Anatolian region of Turkey (Karakus 2019), Dhaka in Bangladesh (Kafy et al. 2021), Yangon City of Myanmar (Yee et al. 2016), Bucharest of Romania (Grigora & Urişescu 2019) are some examples where the relationship between LST and LULC indices has been studied using a different model to depict the seasonal fluctuation (Hassan et al. 2021). Major Indian cities are not an exception. They are also affected by the ongoing phenomenon of large-scale land-use changes as a result of globalization (Chadchan & Shankar 2012). LST of Indian cities like Bengaluru (Govind & Ramesh 2020), Chennai (Kaaviya & Devadas 2021), Delhi (Kant et al. 2009), and Jaipur City (Guha et al. 2020) is continuously increasing due to high concretization, urbanization, industrialization, transportation, losses in green spaces, changes in local climate, and the establishment of urban heat islands (UHI). Changes in demographic structure create pressure on the physical environment and its resources (Alberti 2016, Mersal 2016, Smyth & Royle 2000). At a local level, a study on the English Bazar Municipality of Malda District, West Bengal, by Pal & Ziaul (2017) shows seasonal and temporal LST increased from  $0.070^{\circ}\text{C}/\text{year}$  to  $0.114^{\circ}\text{C}/\text{year}$  during 1991-2014. Hoque & Lepcha (2019) study on the Siliguri Jalpaiguri Development Region shows LST

increased  $0.34^{\circ}\text{C}/\text{year}^{-1}$  from 1991 to 2017, and Sultana & Satyanarayana (2019) noticed that LST of Kolkata Municipal Corporation (KMC) increased from  $10.5^{\circ}\text{C}$  (2002) to  $11.7^{\circ}\text{C}$  (2013). The present study assessed the relationship between land surface temperature and different LULC indices and evaluated its impact on the urban environment of the Raiganj Municipality. Three major LULC Indices--Normalised Difference Vegetation Index (NDVI), Normalised Difference Built-up Index (NDBI), and Normalised Difference Water Index (NDWI) were used in this study to investigate the statistical relationships between these land use indices and LST. The study can be helpful in land use planning by bridging the knowledge gap between present and past conditions and mitigating environmental concerns.

### Study Area

The Raiganj municipality is situated in the southwestern part of the Uttar Dinajpur district in West Bengal, India. The city received municipal status on August 15, 1951, and it is also popularly known as the Raiganj Wildlife Sanctuary (popularly known as Kulik Bird Sanctuary). Geographically, it is situated between  $25^{\circ}34'57''\text{N}$  and  $25^{\circ}38'27''\text{N}$  and latitude, and  $88^{\circ}6'24''\text{E}$  and  $88^{\circ}9'6''\text{E}$  longitude, located 30





meters above sea level. (Fig. 1). The area of the municipality is 10.75 sq. km. and is located 425 kilometers away from Kolkata, the state capital of West Bengal. The city of Raiganj is split into 27 wards. With the massive economic expansion and urban agglomeration, the city is designated the district headquarters of Uttar Dinajpur.

## MATERIALS AND METHODS

### Remote Sensing Data

Landsat images are updated and available regularly to assist in large-scale landscape studies efficiently. This study uses cloud-free multi-temporal Landsat-5 TM (Thematic Mapper) data from 2001 and 2011, as well as Landsat-8 OLI/TIRS (Operational Land Imager/ Thermal Infra-Red Sensor) data from 2021 (Table 1). The data are obtained from the United States Geological Survey Earth Explorer Portal (<https://earthexplorer.usgs.gov>).

### Satellite Image Processing

ERDAS Imagine 14, and Arc GIS 10.3 were used to calcu-

late, analyze, and prepare various thematic maps of LST, NDVI, NDBI, and NDWI derived from satellite images. Calculation of spectral indices and assessment of the relationship between LST and other land use indices are the two stages of the present study. The methodological procedure for the study has been summarised in the flowchart (Fig. 2).

### The Derivation of Land Surface Temperature (LST)

Landsat-5 TM of 2001 and 2011 and Landsat-8 OLI of 2021 with 0% cloud cover were used to calculate the land surface temperature (LST). Landsat-5 TM provides 7 bands of data in which band-6 is a thermal band, while Landsat-8 OLI imagery provides 11 bands of data, in which bands 10 and 11 are thermal bands. The following steps were used for the calculation of LST.

**Step 1:** Conversion of Landsat-5 TM Band-6 digital values to spectral radiances.

The following formula was used to convert band 6 digital values into radiance values ( $L\lambda$ ) (Landsat Project Science Office, 2002).

Table 1: Characteristics of Landsat satellite images used in the present study.

Dataset	Sensor	Year	Acquisition date	Resolution	Path/row	Projections/Datums
Landsat 5	TM	2001	04-02-2001	30m (Band-6, 60 m)	139/42	UTM-WGS1984
Landsat 5	TM	2011	31-01-2011	30m (Band-6, 60 m)	139/42	UTM-WGS1984
Landsat 8	OLI_TIRS	2021	11-02-2021	30m (Band-10- 11, 100 m)	139/42	UTM-WGS1984

(Source: USGS Earth Explorer)

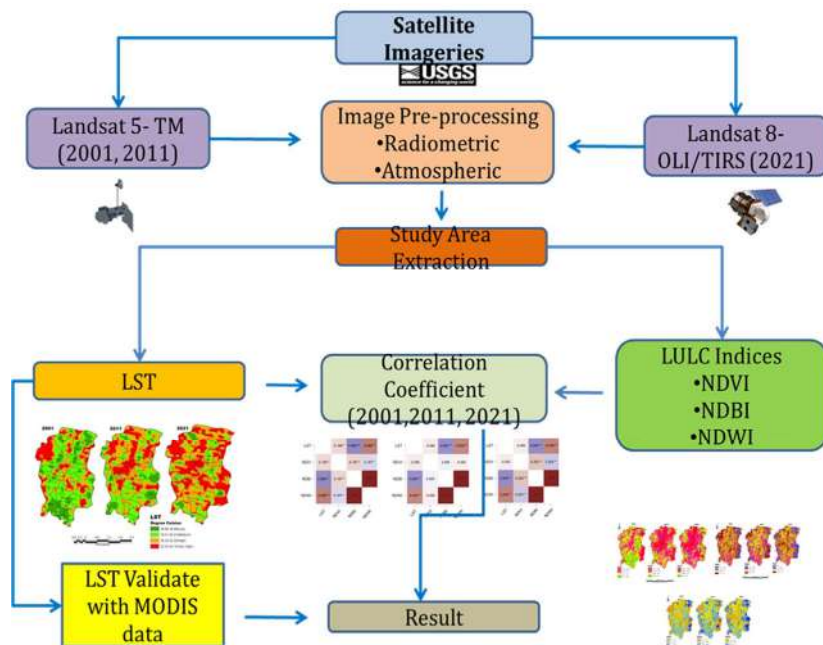


Fig. 2: Details of the methodology used in this study.

$$L\lambda = \frac{LMAX\lambda - LMIN\lambda}{QCALMAX - QCALMIN} \times (QCAL - QCALMIN) + LMIN\lambda \quad \dots(1)$$

Here,  $L\lambda$  is the atmospherically corrected cell value as the radiance,  $QCAL$  is the digital image value,  $LMIN\lambda$  is the spectral radiance scaled to  $QCALMIN$ ,  $LMAX\lambda$  is the spectral radiance scaled to  $QCALMAX$ , and  $QCALMIN$  is the minimum quantization calibration. The radiance pixel value (usually 1) and  $QCALMAX$  are the maximum values of quantized calibrated pixels (usually 255).

The following formula was used to convert the Landsat-8 OLI/TIRS Band-10 digital values to spectral radiances.

$$L\lambda = ML \times QCAL + AL \quad \dots(2)$$

Where  $L\lambda$  is the spectral radiance at the top of the atmosphere,  $ML$  denotes the radiance multi-band X,  $AL$  denotes the radiance add band X,  $QCAL$  denotes the quantized and calibrated standard product pixel value, and X denotes the band number. The band-specific multiplicative rescaling factor  $ML$  and the band-specific additive rescaling factor  $AL$  are obtained from the metadata file (MTL file).

**Step 2:** Satellite brightness spectral radiance temperature conversion and emissivity modification were added to radiant temperature based on the land cover nature following.

$$T = \frac{K_2}{\ln\left(\frac{K_1}{L\lambda} + 1\right)} - 273 \quad \dots(3)$$

Where  $T$  is the satellite brightness temperature in Kelvin (K),  $L\lambda$  is the satellite radiance in  $W/(m^2sr\mu m)$ , and the thermal calibration constants in  $W/(m^2sr\mu m)$ , respectively. The values of  $K_1 = 607.76$ ,  $K_2 = 1260.56$  for band 6 in Landsat-5 TM, and  $K_1 = 774.8853$ , and  $K_2 = 1321.0789$  in Landsat-8 OLI for bands 10 used in the present study taken from (metadata file). For better understanding, the thermal constant values for Landsat TM and Landsat OLI are converted from Kelvin (K) to degrees Celsius ( $^{\circ}C$ ) using the equation  $0^{\circ}C = 273.15K$ .

**Step 3:** Emissions from the ground surface are measured (E)

The temperature values derived above are compared to a black body. As a result, spectral emissivity (E) adjustments are required. These can be done according to the land cover type or by calculating the emissivity values for each pixel from the proportion of vegetation (Pv) data.

$$E = 0.004 \times PV + 0.986 \quad \dots(4)$$

Where, the proportion of vegetation (PV) can be calculated as:

$$P_V = \left\{ \frac{(NDVI_{max} - NDVI_{min})}{(NDVI_{max} - NDVI_{min})} \right\}^2 \quad \dots(5)$$

**Step 4:** Calculation of Land Surface Temperature (LST).

LST is calculated using the equation given below.

$$\frac{BT}{1} + W \times \left( \frac{BT}{P} \right) \times \ln(E) \quad \dots(6)$$

Where  $BT$  is the brightness temperature at the satellite image,  $W$  is the wavelength of emitted radiance,  $P = h \cdot c / s$  ( $1.438 \cdot 10^{-2}$  m K),  $h$  is the Planck's constant ( $6.626 \cdot 10^{-34}$  Js),  $s$  is the Boltzmann constant ( $1.38 \cdot 10^{-23}$  J/K), and  $c$  is the velocity of light ( $2.998 \cdot 10^8$  m/s).

### Retrieval of LULC Indices

The following methods were used to determine the relationship between LST and three spectral indices-NDVI (Normalized Difference Vegetation Index), NDWI (Normalized Difference Water Index), and NDBI (Normalized Difference Built-Up Index) (Equations 7 to 9).

#### Calculation of Normalized Difference Vegetation Index (NDVI)

The NDVI values was extracted using the approach given by Cityshend & Justice (1986 )

$$NDVI = \frac{(NIR \text{ band} - R \text{ band})}{(NIR \text{ band} + R \text{ band})} \quad \dots(7)$$

Where  $NIR$  is the Near-InfraRed band's DN (digital number) value (Band-4 for Landsat 5 and band-5 for Landsat 8), and  $R$  is the red band's DN value (Band-3 for Landsat 5 and band-4 for Landsat 8). The NDVI value is a number that ranges between -1 to +1. Low vegetation cover is indicated by values close to 0, and high vegetation density is indicated by values close to 1.

#### Calculation of Normalized Difference Water Index (NDWI)

$$NDWI = \frac{(Greenband - NIRband)}{(Green \text{ band} - NIR \text{ band})} \quad \dots(8)$$

To avoid the problem of the built-up area being included in the  $NIR$  band (Band-4 for Landsat 5 and Band-5 for Landsat 8), NDWI is used, where green refers to the green band (Band-2 Landsat for 5 and Band-3 for Landsat 8), and  $NIR$  refers to the near-infrared band.

#### Calculation of Normalized Difference Built-up Index (NDBI)

The formula used by Zha et al. (2003) is used to calculate NDBI with a value closer to 1, indicating a high density of built-up land.

$$NDBI = \frac{(MIR \text{ band} - NIR \text{ band})}{(MIR \text{ band} + NIR \text{ band})} \quad \dots(9)$$

Where  $MIR$  (Band-5 for Landsat-5 and Band-6 for

Landsat-8) is the DN from the Mid-InfraRed band, and NIR (Band-4 for Landsat 5 and band-5 for Landsat 8) is the Near-InfraRed band.

The following formula of Pearson's product-moment correlation coefficient ( $r$ ) is used in the present study. is used in (Patra & Gavsger 2021).

$$r = \frac{n(\sum xy) - (\sum x)(\sum y)}{\sqrt{[n\sum x^2 - (\sum x)^2][n\sum y^2 - (\sum y)^2]}} \quad \dots(10)$$

$$y_i = \beta_0 + \beta^1 x_i^1 + \beta^2 x_i^2 + \dots + \beta_p x_{ip} + \epsilon \quad \dots(11)$$

where, for  $i = n$  observations,

$y_i$  = dependent variable,

$x_i$  = explanatory variables,

$\beta_0$  = y-intercept (constant term),

$\beta_p$  = slope coefficients for each explanatory variable,

$\epsilon$  = the model's error term

Maps derived from the calculation of spectral indices NDVI, NDWI, and NDBI show the geographical distribution of vegetation cover, water coverage, and built-up areas of the municipality during the study period.

## RESULTS AND DISCUSSION

### Spatio-Temporal Distribution of Land Surface Temperature (LST)

The land surface temperature (LST) of Raiganj Municipality has been derived from knowing how the LST distribution has changed over a period of time (Table 2 & Fig. 3). The result shows that the value of the LST increases throughout the study period. LST in 2001 with low radiant temperature ranges between 16.50-18.40°C covers an area of 2.02 sq. km. (17.77% of the total study area) distributed over wards--1,3,10, 25, 26, and 27. And, very high radiant temperature ranges between 22.23°C-24.13°C cover an area of 1.96 sq. km. (17.31% of the total area) distributed over wards 7, 9, 13, 20, and 21. Medium to high temperature

Table 2: Statistical description of land surface temperature of years 2001, 2011, and 2021.

Year	2001	2011	2021
Maximum	22.821	21.066	23.717
Minimum	17.023	16.565	19.382
Mean	19.465	18.527	21.680
SD	0.967	0.544	0.548

ranges between 18.41°C-22.22°C cover the rest of the wards accounts 7.37 sq.km. area (64.92% of the total area).

LST in 2011, with low radiant temperature ranges between 16.50°C -18.40°C, covers an area of 1.88 sq.km. (16.56% whole area) distributed over wards--13,20, and 27. The very high radiant temperature ranges between 22.23°C -24.13°C and covers an area of 2.02 sq.km (17.80 % of total area) distributed over wards 2, 5, 7, 10, 13, 14, 15, and 21 (Fig. 3). Medium to high temperatures were observed in parts of wards 2-3, 5, and 9. The low radiant temperature ranges between 16.50°C-18.40°C and covers an area of 1.05 sq.km, which is distributed over wards--6, 20, and 27 in 2021. Very high radiant temperature ranges between 22.23°C-24.13°C covers an area of 2.46 sq.km. (21.67% of the study area) mainly distributed over wards 7, 9,13,14,15, 20, 21, and 22 (Table 3). The result indicates that LST has changed over time in different land-use units, particularly in the north-western portion, noticed a high range of temperature prevailed from 2001 to 2021. LST has increased significantly over each land cover unit, particularly over built-up spaces, sand-deposited areas, and water bodies. For the validation of Landsat-derived LST, Terra MODI11A2 products were used. The MOD11A2 product is available from 2001 to 2021. The Root Mean Square Error (RMSE) value acquired was 0.81°C, and the  $r$  (Pearson correlation coefficient) value was seen as 0.94. the result shows the LST value acquired from Landsat imageries is highly reliable for this study area. According to the correlation value, LST values for MODIS and Landsat are highly correlated.

Table 3: Decadal descriptive statistics of land surface temperature.

Category	Temperature (°C)	Years					
		2001		2011		2021	
		Area[sq.km]	Percentage	Area(sq.km.)	Percentage	Area(sq.km.)	Percentage
Low	16.50-18.40	2.02	17.77	1.88	16.56	1.05	9.24
Medium	18.41-20.31	4.77	41.99	4.71	41.53	3.60	31.73
High	20.32-22.22	2.60	22.93	2.74	24.11	4.24	37.35
Very High	22.23-24.13	1.96	17.31	2.02	17.80	2.46	21.67
Total	11.35		100	11.35	100	11.35	100

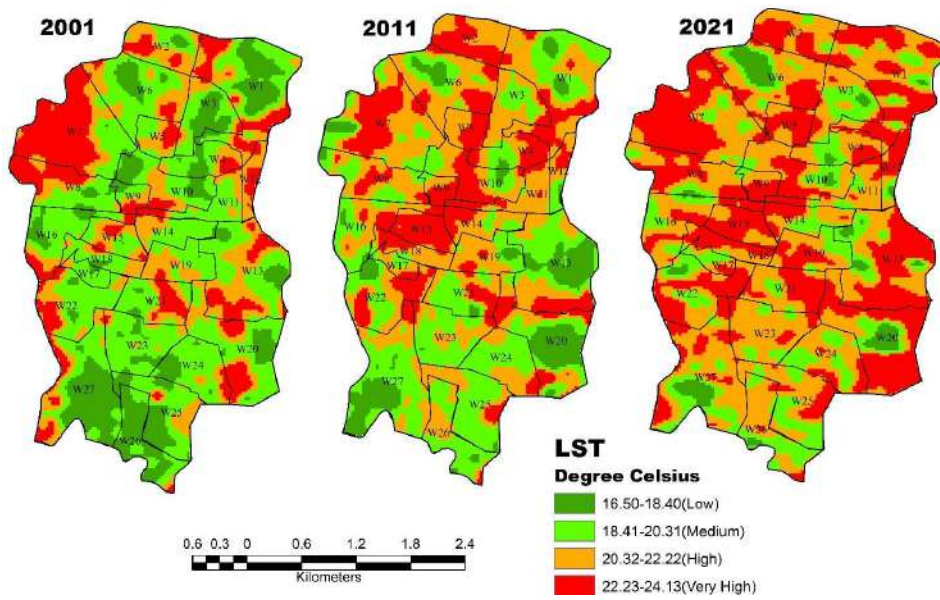


Fig. 3: Spatial distribution of LST of 2001, 2011, and 2021.

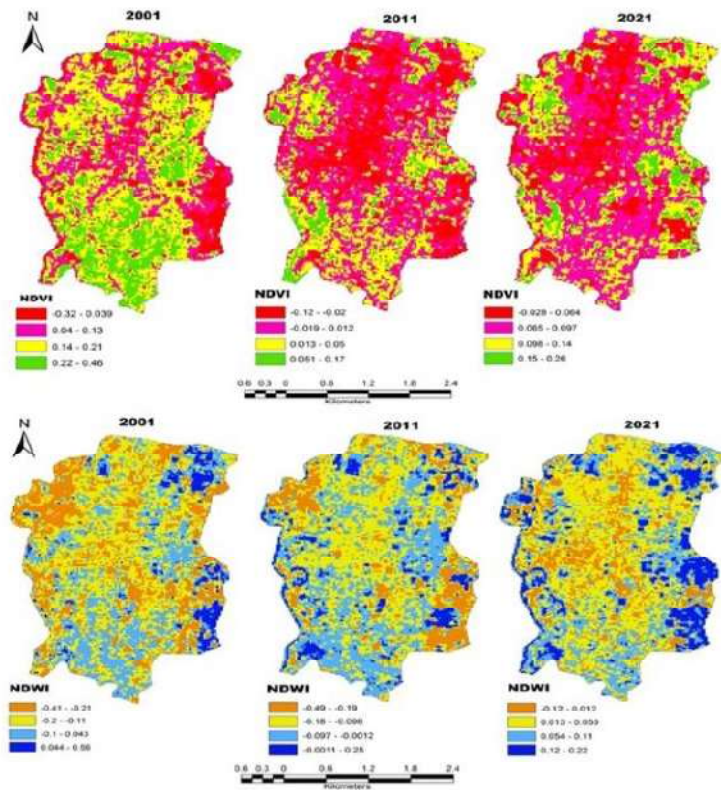


Fig. 4: Spatial distribution of NDVI of 2001, 2011, and 2021.



Table 4: The statistical description of NDVI, NDWI, and NDBI in study years.

LULC indices	YEAR	2001	2011	2021
NDVI	Minimum	-0.31	-0.123	-0.027
	Maximum	0.466	0.171	0.264
	Mean	0.146	0.005	0.089
	SD	0.087	0.033	0.035
NDWI	Minimum	-0.405	-0.494	-0.117
	Maximum	0.565	0.25	0.224
	Mean	-0.137	-0.109	0.050
	SD	0.110	0.083	0.046
NDBI	Minimum	-0.565	-0.25	-0.224
	Maximum	0.405	0.494	1.117
	Mean	0.137	0.109	-0.050
	SD	0.110	0.083	0.046

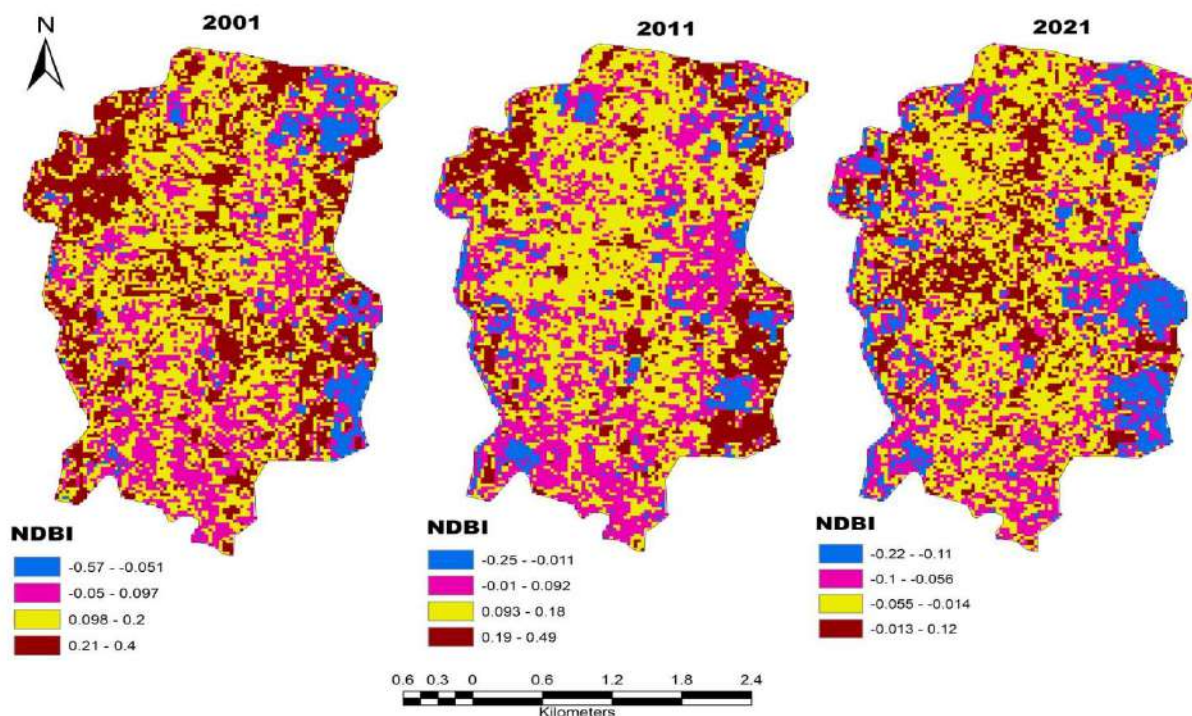


Fig. 6: Spatial distribution of NDBI of 2001, 2011, and 2021.

### Analysis of Spatial Characteristics of NDVI, NDBI and NDWI

NDVI, NDBI, and NDWI were used to create maps and statistical analyses over different periods (2001, 2011 and 2021). Decadal descriptive statistics of NDVI, NDWI, and NDBI are given in Table 2. For the years 2001, 2011, and 2021, NDVI was used to determine the vegetation condition of the study area (Fig. 4). NDVI maps extracted from the Landsat images of the years--2001, 2011, and 2021 show

impervious surface there is a notable decrease of vegetation cover (scattered vegetation and woodland). The area covered with waterbodies also shows low values. The highest value of the NDVI in 2001 is 0.466, and in 2021 is 0.264 which means there is a decreasing trend in vegetation cover and loss in conditions and an increasing trend in impervious surface (built-up spaces) (Table 3).

NDWI maps of years 2001, 2011, and 2021 show the NDWI pattern (Fig. 5). There is a significant change in the

coverage of the water bodies, as the maximum NDWI value was decreased from 0.56 (2001) to 0.22 (2021). The highest NDWI value belongs to a water body, and the lowest NDWI concentration indicates the impervious surface (buildings, roads, bridges, etc.). To some extent, the presence of water bodies aids in lowering its own and the surrounding areas' temperatures (Table 4).

Built-up maps are created by visualizing the area's built-up growth using the NDBI (Normalised Difference Built-up Index) (Fig. 6). Built-up and densely populated areas have high NDBI values. Due to land use conversion in industrial and commercial buildings, residential buildings, roads, and

transportation communication from other land use features (Green and Blue Cover). Maximum NDBI value significantly increased over these land use areas. As a result, high NDBI values can be seen in built-up areas and other impervious surfaces, whereas low NDBI values can be seen over water bodies and vegetation cover (Table 4).

### Correlation and Regression Between LST and LULC Indices

In 2001, a significant negative relation was observed mainly between LST and all three LULC indices--NDVI, NDBI, and NDWI (Fig.7). In 2021, it was shown that there

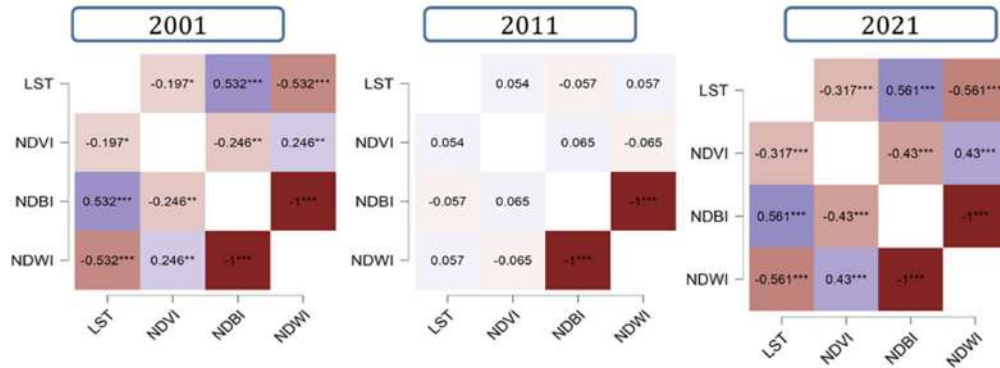


Fig. 7: Correlation diagram among the LST, NDVI, NDBI, and NDWI.

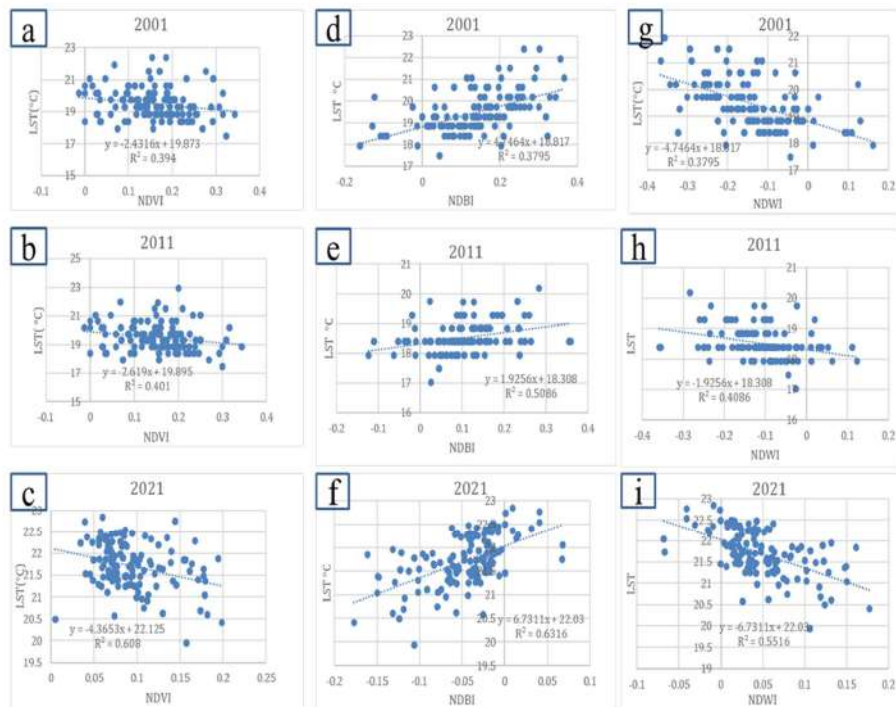


Fig. 8: Correlation between LST and NDVI (a, b, and c), LST and NDBI (d, e, and f), LST and NDWI (g, h, and i).

was a significant negative relationship between LST and NDVI and a positive relationship between LST and NDBI (Fig. 7). Result indicates that temperature increases over built-up land and gradually decreases over vegetation cover. Here also retrieved values of the selected parameters (LST, NDVI, NDWI, and NDBI) were used to build a regression model. The association between LST and various LULC indices of LULC was studied using a linear regression model for each land use type separately. The area where the  $R^2$  (coefficient of determination) produced from the regression model is 0.394, 0.401, and 0.608 for 2001, 2011, and 2021 years shows there is a strong negative connection (Fig. 8) between land surface temperature (LST) and vegetation cover. The high  $R^2$  value in 2021 shows that vegetation cover is significantly reduced and surface radiative temperature is gradually increased (Fig. 8).

LST and NDWI have a negative connection, signifying lower temperatures over water bodies and higher temperatures in non-water body areas. The linear regression model reveals association with an  $R^2$  of 0.379, 0.4086, and 0.551 in the years--2001, 2011, and 2021, respectively (Fig. 8). The higher  $R^2$  value in 2021 (Fig. 8) shows that water bodies play an important role in reducing surface radiative temperature (Fig. 5). The perfect positive relationship between LST and NDBI can be seen in Fig. 8. In 2021, the  $R^2$  value generated by the model was 0.6316, which is higher than in 2001. The fact that a rise in built-up or impermeable surfaces captured the radiation that positively controls LST was established by such a high value of  $R^2$  (Fig. 8). As a result, the land surface temperature (LST) is sensitive to each form of land use, it can be used to detect changes in land use and land cover.

## CONCLUSION

Landsat-5 TM and Landsat-8 OLI of different years have been used to investigate the dynamic relationship between LST with NDVI, NDWI, and NDBI and evaluate the environmental impact of urbanization in terms of reduced green space and increased land surface temperature, UHI intensity effect in the area. At the pixel level, the associations between LST and NDVI, NDWI, and NDBI have been quantified using linear regression analysis. Conclusions drawn from the present study are given below.

1. The land use pattern in Raiganj city is changing at a faster rate. Vegetation cover and agricultural land have been occupied, and open spaces and wetlands have been converted into infrastructural areas.
2. The study found that changing LULC significantly influences land surface temperature.
3. LST has a significant positive association with NDBI and a moderate to strong negative correlation with

NDVI and NDWI.

4. The study shows that the radiative surface temperature is regulated by green space, and the distribution of the UHI is significantly influenced by plant cover in the urban area.
5. UHIs have been identified through the spatial distribution of LST, which mainly existed in bare land and built-up areas; this area is primarily responsible for accumulating high LST values in the city. LST level is reduced significantly due to the presence of vegetation cover and water bodies.

The researcher, policy-maker, and administrators of Raiganj City can benefit from the present study for urban planning and management. This study has its own limitations. First, LST can be derived by using other high-resolution satellite datasets--IKONOS (1m), Quickbird (0.6m), ASTER (15m), and Sentinel-2A (10m) to carry out the complete research. Second, the in-situ measurement or validation of the satellite-derived LST with temperature data collected from the field can give a better outcome.

## ACKNOWLEDGMENT

The authors are thankful to the reviewers for giving critical comments to improve the quality of the manuscript.

## REFERENCES

- Aboelnour, M., Engel, B.A., Aboelnour, M. and Engel, B.A., 2018. Application of remote sensing techniques and geographic information systems to analyze land surface temperature in response to land use/land cover change in Greater Cairo Region, Egypt. *Journal of Geographic Information System*, 10(1), pp.57–88. DOI
- Alberti, M., 2008. Modeling the urban ecosystem: a conceptual framework. *Urban ecology: An international perspective on the interaction between humans and nature*, pp.623–646. DOI
- Asgarian, A., Amiri, B.J. and Sakieh, Y., 2015. Assessing the effect of green cover spatial patterns on urban land surface temperature using landscape metrics approach. *Urban Ecosystems*, 18(1), pp.209–222. DOI
- Bindajam, A.A., Mallick, J., AlQadhi, S., Singh, C.K. and Hang, H.T., 2020. Impacts of vegetation and topography on land surface temperature variability over the semi-arid mountain cities of Saudi Arabia. *Atmosphere*, 11(7), pp.1–28. DOI
- Bokaie, M., Zarkesh, M.K., Arasteh, P.D. and Hosseini, A., 2016. Assessment of urban heat island based on the relationship between land surface temperature and land use/land cover in Tehran. *Sustainable Cities and Society*, 23, pp.94–104. DOI
- Chadchan, J. and Shankar, R., 2012. An analysis of urban growth trends in the post-economic reforms period in India. *International Journal of Sustainable Built Environment*, 1(1), pp.36–49. DOI
- Das, M. and Das, A., 2020. Assessing the relationship between local climatic zones (LCZs) and land surface temperature (LST) – A case study of Sriniketan-Santiniketan Planning Area (SSPA), West Bengal, India. *Urban Climate*, 32(January), 100591. DOI
- Ferreira, L.S. and Duarte, D.H.S., 2019. Exploring the relationship between urban form, land surface temperature and vegetation indices in a subtropical megacity. *Urban Climate*, 27, pp.105–123. DOI



- Gantumur, B., Wu, F., Zhao, Y., Vandansambuu, B., Dalaibaatar, E., Itiriphan, F. and Shaimurat, D., 2017. Implication of relationship between natural impacts and land use/land cover (LULC) changes of urban area in Mongolia. *Journal of Environmental Studies*, 10431, pp.139–157. DOI
- Govind, N.R. and Ramesh, H., 2020. Exploring the relationship between LST and land cover of Bengaluru by concentric ring approach. *Environmental Monitoring and Assessment*, 192(10). DOI
- Grigoraş, G. and Urişescu, B., 2019. Land use/land cover changes dynamics and their effects on surface urban heat island in Bucharest, Romania. *International Journal of Applied Earth Observation and Geoinformation*, 80(February), pp.115–126. DOI
- Guha, S. and Govil, H., 2020. Seasonal impact on the relationship between land surface temperature and normalized difference vegetation index in an urban landscape. *Journal of Climate Studies*, 45(3), pp.67–85. DOI
- Guha, S., Govil, H., Gill, N. and Dey, A., 2020a. Analytical study on the relationship between land surface temperature and land use/land cover indices. *Annals of GIS*, 26(2), pp.201–216. DOI
- Guha, S., Govil, H., Gill, N. and Dey, A., 2020b. Analytical study on the relationship between land surface temperature and land use/land cover indices. *Annals of GIS*, 26(2), pp.201–216. DOI
- Guha, S. and Govil, H., 2021. A long-term monthly analytical study on the relationship of LST with normalized difference spectral indices. *European Journal of Remote Sensing*, 54(1), pp.487–511. DOI
- Guha, S. and Govil, H., 2022. Annual assessment on the relationship between land surface temperature and six remote sensing indices using Landsat data from 1988 to 2019. *Geocarto International*, 37(15), pp.4292–4311. DOI
- Hassan, T., Zhang, J., Prodhan, F. A., Pangali Sharma, T. P. and Bashir, B., 2021. Surface urban heat islands dynamics in response to LULC and vegetation across South Asia (2000–2019). *Remote Sensing*, 13(16), pp.1–24. DOI
- Herold, M., Scepan, J. and Clarke, K.C., 2016. The use of remote sensing and landscape metrics to describe structures and changes in urban land uses. *Environment and Planning A*, 34(8), pp.1443–1458. DOI
- Hoque, I. and Lepcha, S.K., 2019. A geospatial analysis of land use dynamics and its impact on land surface temperature in Siliguri Jalpaiguri development region, West Bengal. *Applied Geomatics*, 12(2), pp.163–178. DOI
- Hua, A.K. and Ping, O.W., 2018. The influence of land-use/land-cover changes on land surface temperature: A case study of Kuala Lumpur metropolitan city. *European Journal of Remote Sensing*, 51(1), pp.1049–1069. DOI
- Kaaviya, R. and Devadas, V., 2021. Water resilience mapping of Chennai, India using analytical hierarchy process. *Ecological Processes*, 10(1), pp.1–22. DOI
- Kafy, A.A., Rahman, M.S., Faisal, A.A., Hasan, M.M. and Islam, M., 2020. Modelling future land use land cover changes and their impacts on land surface temperatures in Rajshahi, Bangladesh. *Remote Sensing Applications: Society and Environment*, 18, p.100314. DOI
- Kafy, A.A., Dey, N.N., Al Rakib, A., Rahaman, Z.A., Nasher, N.M.R. and Bhatt, A., 2021. Modeling the relationship between land use/land cover and land surface temperature in Dhaka, Bangladesh using CA-ANN algorithm. *Environmental Challenges*, 4(May), p.100190. DOI
- Kant, Y., Bharath, B.D., Mallick, J., Atzberger, C. and Kerle, N., 2009. Satellite-based analysis of the role of land use/land cover and vegetation density on surface temperature regime of Delhi, India. *Journal of the Indian Society of Remote Sensing*, 37(2), pp.201–214. DOI
- Karakuş, C.B., 2019. The impact of land use/land cover (LULC) changes on land surface temperature in Sivas city center and its surroundings and assessment of urban heat island. *Asia-Pacific Journal of Atmospheric Sciences*, 55(4), pp.669–684. DOI
- Kim, M., Kim, D. and Kim, G., 2022. Examining the relationship between land use/land cover (LULC) and land surface temperature (LST) using explainable artificial intelligence (XAI) models: A case study of Seoul, South Korea. *International Journal of Environmental Research and Public Health*, 19(23). DOI
- Kuang, W., Liu, Y., Dou, Y., Chi, W., Chen, G., Gao, C., Yang, T., Liu, J. and Zhang, R., 2014. What are hot and what are not in an urban landscape: Quantifying and explaining the land surface temperature pattern in Beijing, China. *Landscape Ecology*, 30(2), pp.357–373. DOI
- Lambin, E.F., Geist, H.J. and Lepers, E., 2003. Dynamics of land-use and land-cover change in tropical regions. *Annual Review of Energy and the Environment*, 28, pp.205–241. DOI
- Li, T., Cao, J., Xu, M., Wu, Q. and Yao, L., 2020. The influence of urban spatial pattern on land surface temperature for different functional zones. *Landscape and Ecological Engineering*, 16(3), pp.249–262. DOI
- Mallick, J., Singh, C.K., Shashtri, S., Rahman, A. and Mukherjee, S., 2012. Land surface emissivity retrieval based on moisture index from LANDSAT TM satellite data over heterogeneous surfaces of Delhi city. *International Journal of Applied Earth Observation and Geoinformation*, 19(1), pp.348–358. DOI
- Mersal, A., 2016. Sustainable Urban Futures: Environmental Planning for Sustainable Urban Development. *Procedia Environmental Sciences*, 34, pp.49–61. DOI
- Mukherjee, F. and Singh, D., 2020. Assessing land use–land cover change and its impact on land surface temperature using LANDSAT data: A comparison of two urban areas in India. *Earth Systems and Environment*, 4(2), pp.385–407. DOI
- Naserikia, M., Shamsabadi, E.A., Rafieian, M. and Filho, W.L., 2019. The urban heat island in an urban context: A case study of Mashhad, Iran. *International Journal of Environmental Research and Public Health*, 16(3). DOI
- O'Connor, K., 2003. Global air travel: Toward concentration or dispersal? *Journal of Transport Geography*, 11(2), pp.83–92. DOI
- Pal, S. and Ziaul, S., 2017. Detection of land use and land cover change and land surface temperature in English Bazar urban centre. *Egyptian Journal of Remote Sensing and Space Science*, 20(1), pp.125–145. DOI
- Patra, S. and Gavsner, K.K., 2021. Land use and land cover change-induced landscape dynamics: A geospatial study of Durgapur Sub-Division, West Bengal (India). *Acta Universitatis Carolinae, Geographica*, 56(1), pp.79–94. DOI
- Peng, X., Wu, W., Zheng, Y., Sun, J., Hu, T. and Wang, P., 2020. Correlation analysis of land surface temperature and topographic elements in Hangzhou, China. *Scientific Reports*, 10(1), pp.1–16. DOI
- Rasul, G. and Ibrahim, F., 2017. Urban land use land cover changes and their effect on land surface temperature: Case study using Dohuk City in the Kurdistan Region of Iraq. *Journal of Cleaner Production*, 33(9), p.10013. DOI
- Saha, S., Saha, A., Das, M., Saha, A., Sarkar, R. and Das, A., 2021. Analyzing spatial relationship between land use/land cover (LULC) and land surface temperature (LST) of three urban agglomerations (UAs) of Eastern India. *Remote Sensing Applications: Society and Environment*, 22(4), p.100507. DOI
- Sekertekin, A., Kutoglu, S.H. and Kaya, S., 2015. Evaluation of spatio-temporal variability in land surface temperature: A case study of Zonguldak, Turkey. *Environmental Monitoring and Assessment*, 188(1), pp.1–15. DOI
- Smyth, C.G. and Royle, S.A., 2000. Urban landslide hazards: Incidence and causative factors in Niterói, Rio de Janeiro State, Brazil. *Applied Geography*, 20(2), pp.95–118. DOI
- Sultana, S. and Satyanarayana, A.N.V., 2019. Impact of urbanisation on urban heat island intensity during summer and winter over Indian metropolitan cities. *Environmental Monitoring and Assessment*, 191. DOI
- Yee, K.M., Ahn, H., Shin, D. and Choi, C., 2016. Relationship assessment among land use and land cover and land surface temperature over downcity and suburban areas in Yangon City, Myanmar. *Korean Journal of Remote Sensing*, 32(4), pp.353–364. DOI



# Thermodynamic Modeling Studies on Biosorption of Reactive Amoxicillin Antibiotic by *Pithophora* Macroalgae in Aqueous Solution

Murad M. Khamayseh<sup>1†</sup>  and Rana Kidak<sup>2</sup> 

<sup>1</sup>Department of Environmental Sciences, Cyprus International University, Nicosia 99010, Turkey

<sup>2</sup>Department of Environmental Engineering, Faculty of Engineering, Cyprus International University, Nicosia 99010, Turkey

†Corresponding author: Murad M. Khamayseh; murad.kha32@gmail.com

**Abbreviation:** Nat. Env. & Poll. Technol.

**Website:** www.neptjournal.com

*Received:* 05-09-2024

*Revised:* 16-11-2024

*Accepted:* 20-11-2024

## Key Words:

Amoxicillin  
Biosorption  
Biosorbent  
*Pithophora* Macroalgae

## ABSTRACT

Antibiotic removal poses a serious risk to the environment due to its intricate structure. Consequently, scientists are developing new and efficient techniques to remove antibiotic compounds from wastewater. The goal of this study is to employ green *Pithophora* macroalgae to remove the antibiotic amoxicillin (AMX) from a water-based solution. With a focus on understanding the process, this study assesses the application of reacting AMX biosorption on the biomass of *Pithophora* algae in aqueous solutions using thermodynamic modeling. The determined thermodynamic characteristics show that an endothermic process is used in the biosorption of the antibiotic AMX, considering that AMX has a positive electrical charge of  $\Delta H^\circ$  at 49.796 kJ.mol<sup>-1</sup>. As  $\Delta G^\circ$  has a positive charge (2.982 kJ.mol<sup>-1</sup>, 3.718 kJ.mol<sup>-1</sup>, and 4.793 kJ.mol<sup>-1</sup>) for AMX at (298 K, 303 K, and 308 K, respectively). This positive result indicates that the reaction is not feasible or spontaneous. The decrease in chaos at the liquid/solid interface caused by AMX biosorption on *Pithophora* macro algae is reflected in the negative charge of  $\Delta S^\circ$ , which was -176.735 kJ.mol<sup>-1</sup>. The effect of temperature on the biosorption of AMX was investigated for different initial AMX concentrations. At a lower temperature of 298 K, the AMX molecules were more likely to diffuse into the internal pores of the *Pithophora* algae. This suggests that the diffusion rate of the adsorbate (AMX) across the bulk and pore boundaries of the biosorbent particles may be increased at lower temperatures. The findings of this study indicate that the biomass of the macroalgae *Pithophora* is a valuable biosorbent for the biosorption of AMX antibiotics, and it may have potential applications in the treatment of wastewater.

## Citation for the Paper:

Khamayseh, M. M. and Kidak, R., 2025. Thermodynamic modeling studies on biosorption of reactive amoxicillin antibiotic by *Pithophora* macroalgae in aqueous solution. *Nature Environment and Pollution Technology*, 24(2), p. D1725. <https://doi.org/10.46488/NEPT.2025.v24i02.D1725>

*Note: From year 2025, the journal uses Article ID instead of page numbers in citation of the published articles.*

## INTRODUCTION

Biosorption is a sustainable method for removing contaminants and heavy metals from aqueous solutions (Balarak et al. 2017). It is a process where contaminants are extracted from water or wastewater using a biosorbent. Biosorbents are materials that can be found naturally or produced artificially, and they can selectively bind contaminants and other chemicals from aqueous solutions (Arihilam & Arihilam, 2019). They are frequently employed in the cleanup of polluted soils and water. Because of its straightforward operation, low cost of raw materials, ability to reduce spent water, and ability to keep contaminants out of natural resources, biosorption has become a viable method for removing toxins from water and soil (Abd & Mohammed-Ridha 2021).

Amoxicillin (AMX) is a beta-lactam antibiotic that is used for the treatment of bacterial infections. Because amoxicillin is so inexpensive, it is prescribed extensively throughout the world. With a half-life of roughly one to two hours, it is known that this antibiotic is very vulnerable to hydrolytic and oxidative degradation in aqueous solutions (Aljeboree et al. 2020). It is well known that this antibiotic is extremely reactive, acting much like hydroxyl radicals. Due to its reactivity, using it in water systems may cause the creation of hazardous intermediates,



Copyright: © 2025 by the authors

Licensee: Technoscience Publications

This article is an open access article distributed under the terms and conditions of the Creative Commons Attribution (CC BY) license (<https://creativecommons.org/licenses/by/4.0/>).

which may have an impact on aquatic life (Matsubara et al. 2020).

One potential method for removing AMX from water systems is biosorption. The majority of AMX is allegedly released into the sewage system unaltered, as stated by Jung et al. (2012). Water samples contain about  $1.3 \mu\text{g}\cdot\text{mL}^{-1}$  of it (Välitalo et al. 2017). Before AMX is released into the environment, the sewage system does not adequately remove it (Lai et al. 2017). On the other hand, amoxicillin can be removed more successfully via genetic engineering, and the biological process of removing antibiotics from macroalgae does not require chemical intervention (Chakhtouna et al. 2021). Many methods, including adsorption, coagulation, electrolysis, filtration, photocatalysis, coagulation, accelerated oxidation, and biological degradation, have been used to eradicate antibiotics (Yan et al. 2022).

The high energy consumption, high material costs, and additional pollution caused by the addition of additional chemicals are some of the disadvantages of these technologies (Boukhelkhal et al. 2016). Adsorption is the most widely used and successful technique for removing contaminants from wastewater (Asim et al. 2021). Its uncomplicated appearance and ease of usage make it simple to install. Because biosorption is inexpensive, efficient, and safe for the environment, it has attracted a lot of attention as an alternative to antibiotics. This method binds and concentrates pollutants in water by using biological material from live and dead biomass that has been heat-dried and chemically treated (Dimitrakopoulou et al. 2012). Because of its straightforward operation, low cost of raw materials, ability to minimize spent water, and ability to keep contaminants out of natural resources, biosorption has become a promising method for removing pollutants from soil and water (Limousy et al. 2017). With a focus on comprehending its mechanism, this paper reviews some recent developments in equilibrium and kinetics research on the biosorption of reactive Amoxicillin Antibiotic (AMX) on Pithophora Macroalgae in aqueous solutions. Pithophora is a type of filamentous green algae. It can grow in dense mats either on the surface or at the bottom. This algae is often described as having a rough, coarse texture, and its growth pattern resembles a tangled mass of cotton or wool. One of the most economical adsorbents is green algae, which contains cellulosic polysaccharides that react with a large number of proteins to form glycoproteins. Numerous functionalized groups, such as amino, carboxyl, sulfate, and hydroxyl, are present in these materials and are essential to the biosorption process (Romera et al. 2007). The thermodynamic values obtained from the study suggest that the sorption of levofloxacin (LVX) antibiotics is governed by an endothermic process. The findings indicate that the biomass of Pithophora macroalgae

serves as an effective biosorbent for the removal of LVX antibiotics, presenting a promising alternative method for the elimination of antibiotics from aqueous environments. Furthermore, Pithophora demonstrates potential applicability in real-world wastewater treatment scenarios, having proven its efficacy as a biosorbent for antibiotic compounds (Khamayseh & Kidak 2023). According to the study conducted by Kalyani et al. (2021), the thermodynamic analysis revealed that the biosorption processes are both exothermic and spontaneous. The biosorbents derived from *Pithophora cleveana* Wittrock and *Mimusops elengi* exhibited maximum removal efficiencies of 74.11% and 73.11%, respectively, with corresponding maximum uptake capacities of  $13.58 \text{ mg}\cdot\text{g}^{-1}$  and  $12.96 \text{ mg}\cdot\text{g}^{-1}$ . Furthermore, the thermodynamic parameters, including  $\Delta G^\circ$ ,  $\Delta H^\circ$ , and  $\Delta S^\circ$ , indicated that the biosorption process is spontaneous and exothermic. These findings suggest that the biosorbents derived from Pithophora cleveana Wittrock and Mimusops elengi possess significant potential for the removal of lead metal ions from aqueous solutions, attributable to their effective absorption capabilities (Gaddam et al. 2020). Additionally, Pithophora has demonstrated its applicability in real-world wastewater treatment scenarios and has proven to be an effective biosorbent for the biosorption of antibiotics.

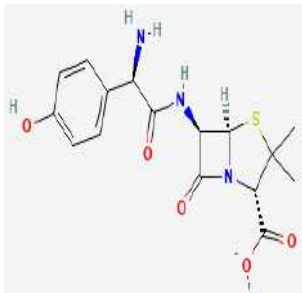
Algal biomass treated with an alkaline solution will bio-absorb pharmaceutical chemicals. The primary goal of this research is to use the readily available green Pithophora macroalgae to extract AMX from aqueous solutions. The starting pH, temperature, agitation speed, and adsorbent dosage all have an impact on how well the green macroalgae biosorb antibiotic is. For equilibrium studies, the isotherm biosorption and kinetics models and thermodynamic modeling are also assessed. Therefore, our objective was to examine the effectiveness of Pithophora macroalgae in the removal of AMX from aqueous solutions. Pithophora is a filamentous green alga that creates free-floating mats, which refers to Cladophorales members (O'Neal et al. 1985).

## MATERIALS AND METHODS

### Materials and Instruments

The following materials and instruments were used in this experiment: 10 L distilled water; 10 L tap water; 1 L Methanol; 1 g Amoxicillin antibiotic; 8 Erlenmeyer flasks; 8 Lab shaker bottles; one measuring cylinder; 2 Pipettes; 1 Flask; 1 beaker; volumetric cylinder; 0.1 NaOH; 0.1 HCL solution; and weighing Scale (Saturius CP, model CPA 2250). In addition, 1 mortar and pestle, 1 magnetic stirrer or batch, a Bath water shaker, and a UV-visible spectrophotometer

Table 1: The characteristics of the Amoxicillin antibiotic (Khamayseh &amp; Kidak 2024).

Amoxicillin (AMX) (penicillin antibiotic)	
Structure	
Molecular formula	$C_{16}H_{19}N_3O_5S$
Molecular weight	$365.4 \text{ g.mol}^{-1}$
pKa	2.67, 7.11 and 9.55

were used. (National Center for Biotechnology Information 2022).

### The Procedure for Preparing the Stock Solution

The amoxicillin (AMX) antibiotic component was obtained from a local pharmacy in Istanbul, Turkey, for analytical reference purposes without undergoing any further processing. The antibiotics' characteristics are listed in Table 1; the following process was used to use the AMX: The antibiotic was precisely weighed by weighing scale. The stock solution ( $1\text{g.L}^{-1}$ ) was prepared by grounding the antibiotics, 1 g of AMX antibiotic using mortar and pestle to make them as powders in the lab. Dissolving accurately weighted amounts of the antibiotics in suitable solvents.

Table 2: The concentrations of AMX and its absorptions.

Conc. $\text{mg.L}^{-1}$	absorbance
10	0.345
30	1.108
50	1.512
70	1.912
100	2.89
115	3.31
125	3.59
150	4.56

The AMX antibiotic was dissolved in methanol and water. Then, the antibiotic powders were added to the magnetic stirrer for around 2 h at  $70^\circ\text{C}$  to speed up the dissolving. After that, the stock solutions were put in the refrigerator at  $4^\circ\text{C}$  further to use it. 0.1 M NaOH and 0.1 M HCl were used to adjust the pH.

Many standards calibration charts were prepared for a wide range of concentrations that were close to the anticipated concentration of the analyte, measuring the absorbance of different Antibiotic (AMX) concentrations at different ( $\lambda$ ) nanometers and unknown concentrations of antibiotics before and after adsorption were computed from the calibration chart. In this work, the calibration curve was plotted using different wavelengths as given for the AMX at 231 nm. UV spectrometer, which would be based on the wavelength obtained during spectrum research. As shown in Fig. 1, the calibration curve was obtained for the range of 10 to 150  $\text{mg.L}^{-1}$ . N.B: the experiment was repeated three times, and the mean values and standard deviations from the mean values

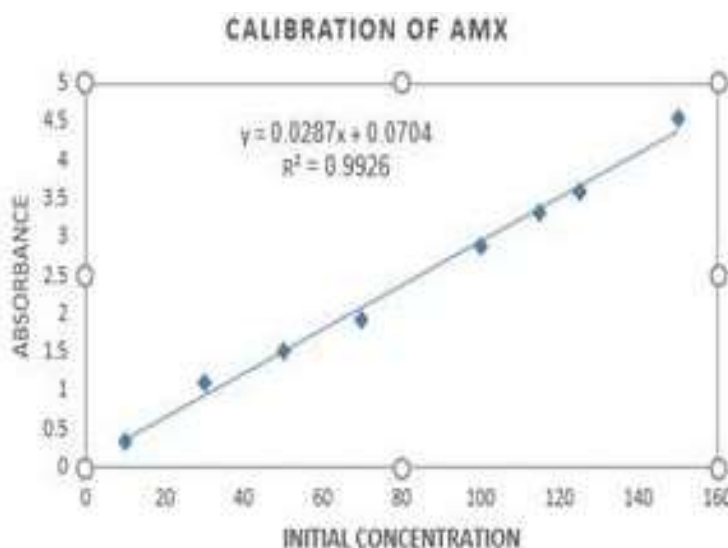


Fig. 1: Calibration curve of AMX at different concentrations.

were recorded. Table 2 presents the various concentrations of AMX alongside their corresponding absorbance values. A double beam/visible spectrophotometer (Shimadzu UV-2450) was employed to measure absorbance at the specific wavelength characteristic of the compound, facilitating the determination of an unknown antibiotic concentration.

The measurement of antibiotic concentration is widely regarded as one of the most commonly utilized methodologies. When appropriately calibrated, this technique can exclusively analyze the UV-visible spectral properties of the substance, thereby providing accurate estimations of AMX concentration. The UV spectrophotometer utilized in the laboratory during the experiments is depicted by the spectrophotometer device (Fig. 2). The standard deviation of the measurements is reported to be 1.41. The best-fitting

isotherm has been found in recent years using a variety of error analysis techniques, including the coefficient of determination ( $R^2$ ), the sum of the errors squared, a hybrid error function, Marquardt's percent standard deviation, the average relative error, and the sum of absolute errors which noted that the  $R^2$  of linear regression analysis alone is not a suitable metric for assessing an isotherm model's fit quality (Allen et al. 2003).

### Determination of pH and Zeta Potential Charge

The pH of the growth media was assessed at the commencement and conclusion of each trial, as well as on designated sample days and during the preparation of the medium, utilizing a pH meter (WTW Inolab pH 7110 masa Tipi pH meter). Additionally, the pH of the metal removal media was adjusted



Fig. 2: Shimadzu UV-2450 double-beam UV/visible spectrophotometer.

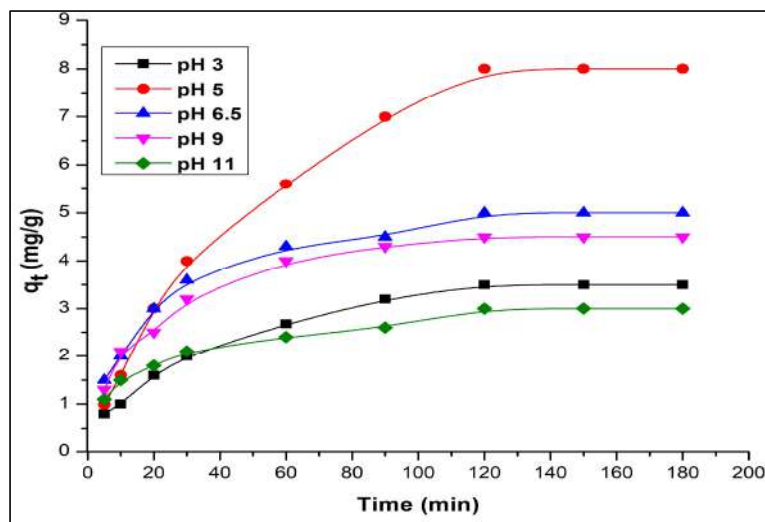


Fig. 3: Effect of initial pH and contact time on sorption of AMX (Khamayseh & Kidak 2024).



before the initiation of the experiment. To ensure accurate pH measurements, a two-point calibration with buffer solutions was routinely conducted. The determination of the zero-point charge (ZPC) of the *Pithophora* algae was carried out at a pH of 7.6, following the mass titration method as described by Cristiano et al. (2011). Specifically, fifty milliliters of 0.01 M  $\text{NaNO}_3$  were placed in Erlenmeyer flasks, and appropriate biosorbent dosages ranging from 0.1 to 1.5 grams were introduced. The samples were agitated in a mechanical shaker for twenty-four hours, after which the residual pH value was measured.

The neutral charge of the bio-sorbent was assessed utilizing the pH drift method. Under optimal conditions,

the kinetic profiles illustrating the biosorption removal of AMX, employing non-linear forms across varying solution pH levels, are presented in Fig. 3. A gradual biosorption process was observed, characterized by an increase in contact time across all pH levels investigated. The AMX antibiotic was effectively removed at an initial pH level, reaching equilibrium after 120 min, beyond which no further sorption occurred. The influence of pH on the adsorption process can be attributed to the solubility of pollutants and the presence of active functional groups on the adsorbents, which facilitate electrostatic interactions between the antibiotic molecules and the surface of the algae. (Khamayseh & Kidak 2024).



Fig. 4: Fresh *Pithophora* macroalgae harvested from the CIU University (2022).



Fig. 5: *Pithophora* cells under electron microscope, CIU labs-North Cyprus.

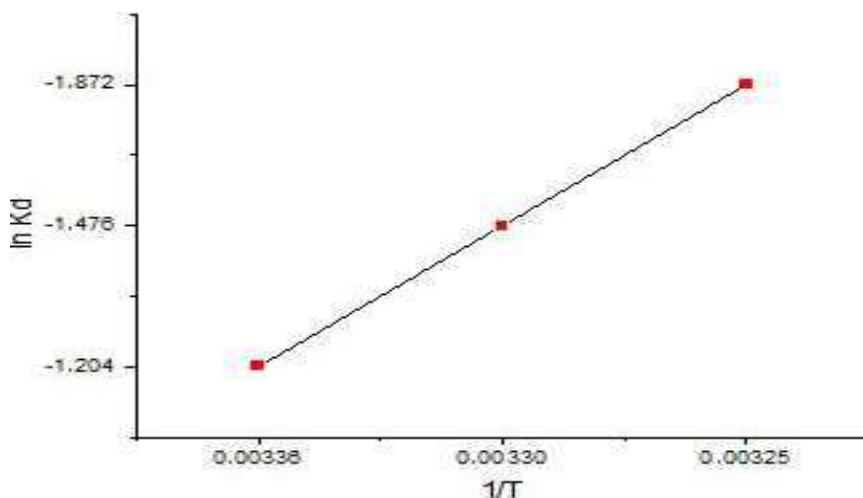


Fig. 6: The relation between  $\ln K_d$  and  $1/T$  of AMX.

Table 3: Thermodynamics for biosorption of AMX at different temperatures.

Adsorbate	T[°C]	$q_e$ [mg.g <sup>-1</sup> ]	Thermodynamic parameters		
			$\Delta G^\circ$ [kJ.mol <sup>-1</sup> ]	$\Delta H^\circ$ [kJ.mol <sup>-1</sup> k]	$\Delta S^\circ$ [J mol <sup>-1</sup> K]
AMX	25	18.0	2.982	49.796	-176.735
	30	16.0	3.718		
	35	12.1	4.793		

### Collection and Identification of the Algae

This study made use of the (seaweed) Green *Pithophora* Macroalgae (GPM) as in Fig. 4. Between October and November 2021, during the winter months, they were gathered from the pond at Cyprus International University (CIU). To create the 40 g powdery form, around 8 kg of pond-harvested material was pulverized in a milling machine. After which they were dried at 40 degrees and grounded at 45 microns.

Under the electron microscope shown in Fig. 5, *Pithophora* was seen, which is made up of filaments irregularly branching and frequently include akinetes; many inflated reproductive cells resemble spores. From lime green to a dark greenish brown, it can be any color. When gas bubbles created by the plant are caught within the thick algal growth, they become buoyant, and the surface mats typically form in warmer weather. These mats may momentarily sink to the bottom if they are disturbed by significant wind or rain events.

## RESULTS AND DISCUSSION

### Effects of Temperature

The temperature is typically affected by processes involving heat or mass transport. A thermodynamic process alters the thermodynamic state of a system.  $r$  is defined as the degree

of chaos or uncertainty in a system. Enthalpy is a key concept in thermodynamics. It is the overall amount of heat in the system. This indicates that as more energy is provided, the enthalpy rises. To determine whether antibiotic adsorption by *Pithophora* algae occurs spontaneously, entropy and energy factors should be considered. An experimental investigation was conducted to examine the influence of temperature on the adsorption of AMX by *Pithophora* algae. The findings indicated that the capacity for antibiotic adsorption diminishes as the temperature increases. (Khamayseh & Kidak 2024).

At temperature ranges of 298 K to 308 K, the removal effectiveness of AMX medication at various start concentrations was investigated. A 100 mL solution was applied to 0.5 g of biomass in Erlenmeyer flasks. After that, it was shaken in a temperature-controlled shaker at 150 rpm. Samples were taken anywhere from five to eighty-one minutes apart at various times. The equations were used to calculate Gibb's free energy ( $\Delta G^\circ$ ). (4.1), (4.2), and (4.3) (Aravindhan et al. 2009).

$$\Delta G^\circ = \Delta H^\circ - T\Delta S^\circ \quad \dots(4.1)$$

$$\Delta G^\circ = -RT \ln K_d \quad \dots(4.2)$$

$$K_d = \frac{q_e}{C_e} \quad \dots(4.3)$$

Where  $T$  is the absolute temperature (K),  $R$  is the gas

constant ( $8.314 \text{ J mol}^{-1} \cdot \text{K}^{-1}$ ),  $q_e$  is the amount of antibiotic absorbed onto the biosorbent at equilibrium time (mg/g), and  $C_e$  is the equilibrium concentration of the sorbate present antibiotics ( $\text{mg} \cdot \text{L}^{-1}$ ).

Van't Hoff plots  $\ln K_d$  vs.  $1/T$  (Fig. 6) can be used to determine entropy ( $\Delta S^\circ$ ) and enthalpy ( $\Delta H^\circ$ ) based on their slope and intercept. Also, entropy ( $\Delta S$ ) and enthalpy ( $\Delta H$ ) can be determined using the following equations (4.4) and (4.5).

$$\Delta H^\circ = \text{Slope} * R \text{ gas constant} \quad \dots(4.4)$$

$$\Delta S^\circ = \text{Intercept} * R \text{ gas constant} \quad \dots(4.5)$$

The Langmuir isotherm equilibrium constants at 298 K, 303 K, and 308 K were used to calculate  $\Delta G^\circ$ ,  $\Delta H^\circ$ , and  $\Delta S^\circ$  for AMX adsorption by *Pithophora* (Table 3). At increasing temperatures, the biosorption % shows a trend toward decline. This decrease may be explained by an increase in the propensity of ions to break bonds and move from the solid to the bulk state, the destruction or deactivation of active sites on the surface of the biosorbent as a result of bond breaks, or the mobilization of ions in solution as a result of highly energized metal ions (Sulaymon et al. 2013). The coefficient of correlation value,  $R^2$ , of the van't Hoff plot in Fig. 6 was deemed satisfactory at 0.996 for AMX. For the necessary system, the thermodynamic parameters  $\Delta G^\circ$ ,  $\Delta S^\circ$ , and  $\Delta H^\circ$  were measured. As can be shown in Table 3, the

charge of  $\Delta G^\circ$  for AMX is positive ( $2.982 \text{ kJ} \cdot \text{mol}^{-1}$ ,  $3.718 \text{ kJ} \cdot \text{mol}^{-1}$ , and  $4.793 \text{ kJ} \cdot \text{mol}^{-1}$ ) at (298 K, 303 K, and 308 K, respectively). This positive value suggests that the reaction is neither possible nor spontaneous.

According to the  $\Delta H^\circ$  values, the biosorption process could be viewed as a physical sorption that is facilitated by a chemical reaction. Given that the electrical charge of  $\Delta H^\circ$  for AMX is positive at  $49.796 \text{ kJ} \cdot \text{mol}^{-1}$ . This shows that the method of biosorption was endothermic, indicating that the antibiotics and biomass have a significant interaction. This finding indicates that the biosorption process is endothermic, suggesting a significant interaction between the biomass and the antibiotics. Consequently, algal biomass can be effectively utilized for the removal of AMX at ambient temperature. Entropy effects can be considered as the driving force of the biosorption process. Consequently, the biomass of algae demonstrates efficacy in the removal of AMX at ambient temperature. It can be posited that entropy effects are instrumental in driving the biosorption process. The reduction in disorder at the liquid/solid interface, resulting from the biosorption of AMX onto *Pithophora* macroalgae, is indicated by the negative value of  $\Delta S^\circ$ , which is measured at  $-176.735 \text{ kJ} \cdot \text{mol}^{-1}$ .

The measured  $q_e$  values of the biomass of AMX decreased substantially from 18.0 to 12.1 mg/g when the

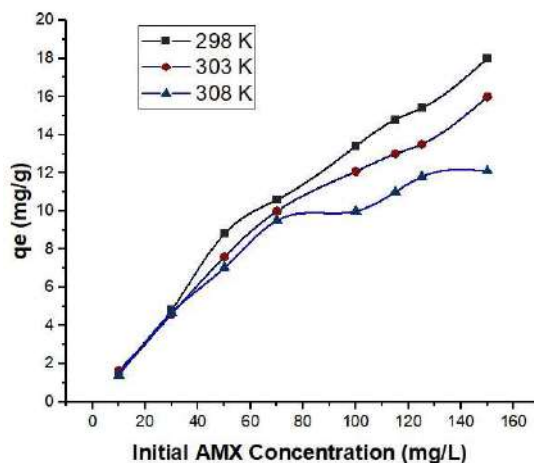


Fig. 7: Effect of temperature on the equilibrium AMX and uptake capacity.

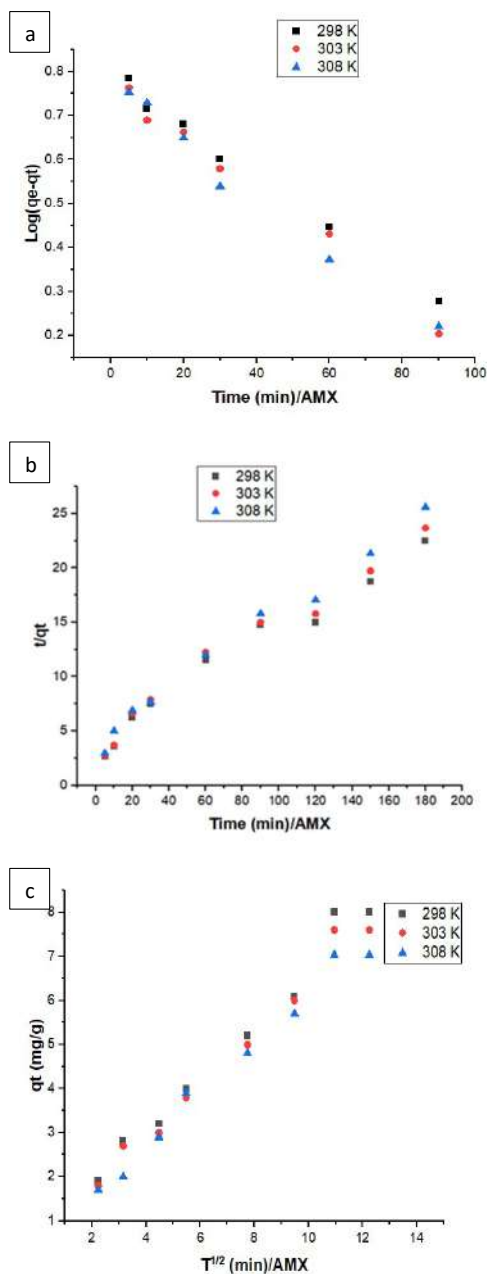
Table 4: Biosorption isotherm constants obtained for various models obtained through linear regression analysis for AMX removal by *Pithophora* biosorbent at different temperature.

Antibiotic	T [K]	$q_e \text{ EXP (mg/g)}$	Freundlich			Langmuir		
			$K_f [\text{mg} \cdot \text{g}^{-1}]$	N	$R^2$	$Q_m [\text{mg} \cdot \text{g}^{-1}]$	$K[\text{L} \cdot \text{mg}^{-1}]$	$R^2$
AMX	298	18.0	1.17	1.43	0.930	25.83	0.0345	0.944
	303	16.0	1.07	1.51	0.921	18.79	0.0367	0.954
	308	12.1	1.03	1.63	0.841	15.69	0.076	0.942

temperature of an antibiotic solution rose from 298 K to 308 K, as depicted in Fig. 7's plot of the influence of the biosorption of AMX antibiotic. This may indicate a decrease in the viscosity of the antibiotic-containing aqueous solution. As a result, the total volume of the biosorbent particles and the adsorbate's diffusion rate across pore borders may both rise (Mohammed et al. 2020).

### Biosorption Isotherm at Different Temperatures

At all the temperatures investigated, Table 4 demonstrates that the adsorption data of AMX can be better described by the Langmuir isotherm than the Freundlich isotherm. According to the Langmuir isotherm's values for  $q_m$ , the two antibiotics under study have a significant amount of



For AMX biosorption at 298 K, 303 K, and 308 K, pseudo-first order, pseudo-second order, and intraparticle diffusion kinetics are presented. a) Pseudo-first order of AMX b) Pseudo-second- order of AMX, c) intraparticle diffusion

Fig. 8: Biosorption Kinetics at different temperatures: (a-c).



Table 5: Results comparison between Pseudo-first order, pseudo-second order kinetics and intraparticle diffusion for AMX biosorption at 25°C (Khamayseh &amp; Kidaz 2024).

Adsorbent	$C_o$ [mg. <sup>-1</sup> L]	$q_{e,EXP}$ [mg.g <sup>-1</sup> ]	Pseudo-first order			Pseudo-second order			Intraparticle diffusion		
Pithophora Algae			$K_1$ ([])	$q_{e,cal}$ [mg.g <sup>-1</sup> ]	$R_2$	$K_2(g/mg$ $min^{-1})$	$q_{e,cal}$ [mg.g <sup>-1</sup> ]	$R_2$	$K_{DIF}$ [g.g <sup>-1</sup> min <sup>-1/2</sup> ]	C [g.g <sup>-1</sup> ]	R <sup>2</sup>
	10	1.52	0.0091	1.31	0.985	0.0641	1.60	0.999	0.0687	0.7059	0.965
	30	4.80	0.0047	2.91	0.942	0.0093	5.32	0.993	0.2932	1.2117	0.976
	50	8.00	0.0057	6.18	0.996	0.0031	9.48	0.986	0.5830	0.7619	0.986
	70	10.60	0.0052	7.89	0.988	0.0025	11.79	0.988	0.7532	1.1859	0.984
	100	13.40	0.0094	10.93	0.989	0.0026	15.40	0.994	0.9256	2.3055	0.979
	115	14.80	0.0092	11.70	0.991	0.0025	16.88	0.996	1.0127	2.7025	0.977
	125	15.40	0.0104	11.38	0.993	0.0033	17.08	0.999	0.9851	3.8705	0.956
	150	18.00	0.0135	14.66	0.983	0.0029	20.02	0.998	1.1795	4.4310	0.944

adsorption capacity for algae biosorbent and adsorption capacity for AMX. The experimental  $q_m$  values of the biomass of AMX dramatically dropped from 25.83 to 15.69 mg.g<sup>-1</sup>. This may indicate a decrease in the viscosity of the antibiotic-containing aqueous solution. As a result, the adsorbate's diffusion rate may rise through the biosorbent particles' pores and bulk borders (Mohammed et al. 2020). The greater  $R^2$  of the Langmuir isotherm model in Table 4 for all AMX values indicates that it provides the best fitting for the experimental data. Having a 25.83 mg/g maximal capacity for sorption, the experimental data for AMX biosorption most closely resembles the Langmuir isotherm model (Khamayseh & Kidak 2024).

### Biosorption Kinetics at Different Temperatures

The Biosorption kinetics determine the sorption mechanism, which involves mass transfer, diffusion, and reaction on the biosorbent surface, as well as the reaction rate. This involves how the system sorption qualities vary over time and how much of the surface is covered, which in turn provides information about how quickly a process is happening. The design and regeneration of the biosorbent rely heavily on the rates of adsorption since sorption and desorption processes are both time-dependent. The experimental data are analyzed

using dynamic models to study the component of biosorption, the potential rate and governing steps, mass transfer, and the chemical reaction process (Ho & McKay 1999). In other words, the sorption equilibrium also reveals details about the adsorption process dynamics. Based on the physicochemical characteristics of the antibiotic and the bio-sorbent, the kinetics of the biosorption process aid in assessing the effectiveness and identifying the type of sorption mechanism (Kerkez-Kuyumcu et al. 2016). The capacity for biosorption at equilibrium and the rate of solute binding on the surface of the biological material may both be calculated using biosorption kinetics. This material gives crucial details regarding a potential biosorption mechanism that includes chemical reactions and diffusion (Kratochvil & Volesky 1998). Three kinetic models—pseudo-first-order (PFO), pseudo-second-order (PSO), and intraparticle diffusion models—were employed to investigate the biosorption kinetics of AMX. The rate constants for these models were determined through linear regression analysis of the experimental data, as presented in Table 5. The experiment was conducted under optimal conditions, utilizing an initial concentration of 50 mg.L<sup>-1</sup>, and the kinetics were examined at a temperature of 25°C.

The pseudo-second-order (PSO) model demonstrated a superior fit to the experimental data, exhibiting a

Table 6: Results comparison between Pseudo-first order, pseudo-second order kinetics and Intraparticle diffusion for AMX biosorption at different temperatures.

	Temp.	$q_{e,EXP}$ [mg.g <sup>-1</sup> ]	Pseudo-First Order			Pseudo-Second Order			Intraparticle Diffusion		
			$K_1$ [[min <sup>-1</sup> ]	$q_{e,cal}$ [mg.g <sup>-1</sup> ]	$R^2$	$g/K_2$ (mg/min)	$q_{e,cal}$ [mg.g <sup>-1</sup> ]	$R^2$	$K_{dif}$ [mg/g min <sup>1/2</sup> ]	C [mg.g <sup>-1</sup> ]	$R^2$
AMX	298 K	8.00	0.0057	6.18	0.996	0.0031	9.48	0.999	0.5830	0.7619	0.986
	303 K	7.60	0.0064	6.10	0.986	0.0029	9.18	0.975	0.5687	0.593	0.971
	308 K	7.03	0.0062	5.49	0.943	0.0034	8.40	0.981	0.529	0.546	0.961

regression coefficient ( $R^2$ ) of 0.999 and a rate constant of  $0.0641 \text{ g.mg}^{-1}.\text{min}^{-1}$  at an initial amoxicillin (AMX) concentration of  $10 \text{ mg.L}^{-1}$ . Additionally, at the maximum AMX concentration of  $150 \text{ mg.L}^{-1}$ , the PSO rate constant ( $K_2$ ) was determined to be  $0.0029 \text{ g.mg}^{-1}.\text{min}^{-1}$ , with an  $R^2$  value of 0.998 at a temperature of  $25^\circ\text{C}$ . The PSO model was more obvious to fit with the experimental data (Table 5), demonstrating that the PSO model fitted better with the experimental data than the PFO model and the intraparticle diffusion data in terms of regression coefficients for all AMX concentrations. This is further shown by contrasting the experimental data's  $q_e$  values with the one inferred from the plots ( $q_e.\text{CAL}$ ). The intraparticle diffusion method was then used to examine the data to gain additional insight into the adsorption mechanism. The potential of intra-particle diffusion was explored using experimental data and the Weber-Morris intra-particle diffusion model. The lower  $R^2$  values obtained corroborate the conclusion drawn from Table 5 data analysis: intraparticle diffusion is not able to explain the experimental results, the intraparticle diffusion cannot explain the experimental results, which is confirmed by the lower  $R^2$  values attained in the AMX antibiotic. All things considered, the PSO model appears to have the greatest match to the study data, indicating that the biosorption of AMX onto Pithophora algae is caused by chemisorption interaction which is responsible for the biosorption of AMX. This correlates with previous research (Oba & Aydinlik 2022, Dan et al. 2021, Hamadeen et al. 2021, Pezoti et al. 2016). Pseudo-first-order and pseudo-second-order kinetic model equations were used to model the experimental data (Fig. 8 a, b). To determine whether film diffusion or intraparticle diffusion is the rate-controlling step, kinetic parameters were calculated using the Weber and Morris kinetic model to investigate intraparticle diffusion Fig. 8 (c). It can be said that the pseudo-second-order kinetic model and the experimental data closely match each other. Additionally,  $q_e$ ,  $q_{e,\text{calc}}$  based on the pseudo-second-order isotherm has values that are comparable to  $q_e$ ,  $q_{e,\text{exp}}$ . The temperature has an impact on parameter values like  $k_2$ ,  $q_e$ ,  $q_{e,\text{calc}}$ , but not in a way that makes it necessary to treat it less than 298 K. For Kinetic analyses, Table 6 displays the values for the  $K_{\text{diff}}$  and C parameters from the modeling along with the rate constants, k, and adsorption capacity. The regression coefficient, or  $R^2$ , values are also displayed in the same table. According to Table 6, the experiment was carried out on the optimal condition at  $50 \text{ mg.L}^{-1}$  initial concentration, and the kinetic was studied at different temperatures. It was seen the  $q_e$  decreased by increasing the temperature in all types of the kinetics under 298 K, 303 K, and 308 K. So, the best-fit temperature is 298 K, which indicates high  $q_e$  in pseudo-second order as the following order 9.48, 9.18, and  $8.40 \text{ (mg.g}^{-1}\text{)}$  for AMX

at 298 K, 303K, and 308K, respectively. We looked at the Freundlich and Langmuir isotherms to see which model fit the experimental data best. The experimental results' kinetic model adheres to the pseudo-second-order ( $R^2 = 0.999$ ). In practical water and wastewater treatment applications, the biomass of the macroalgae Pithophora has been demonstrated in this study to be a potential biosorbent for the biosorption of AMX antibiotics (Khamayseh & Kidak 2024).

## CONCLUSIONS

There is significant interest in identifying effective strategies for the removal of highly hazardous organic chemicals from water and wastewater. Among these strategies, adsorption has emerged as a recognized method for eliminating organic contaminants, noted for its efficiency, cost-effectiveness, and ability to yield high-quality treated effluent. Thermodynamic analyses have indicated that the biosorption process is endothermic and nonspontaneous. The findings of this study suggest that Pithophora algae represent a promising biosorbent for the extraction of the antibiotic amoxicillin from aqueous environments in practical wastewater applications. Pithophora was selected for this research due to its prevalence in urban areas, propensity for algal blooms, and natural dominance in nutrient-rich or eutrophic conditions. Furthermore, its filamentous structure contributes to reduced harvesting costs. When compared to other materials, algal biomass is the most frequently utilized biosorbent. Algae possess a high capacity for binding metal ions due to their untreated state and the characteristics of their cell walls, rendering them a cost-effective biosorbent option. Future investigations should focus on the specific functional characteristics of Pithophora's cell wall, particularly the presence of chlorophyll and its implications for the biosorption process. Additionally, further research is necessary to explore modeling, the regeneration of biosorbent materials, and the testing of adsorbed raw biomasses in relation to antibiotics. Advancements in techniques that enhance biosorbent processing will be essential for optimizing the application of biosorbent technology and regenerating biomass. • It is advised to use modified pithophora algae in a subsequent isotherm study to compare raw, unmodified algae with modified macroalgae treated with NaOH, formaldehyde, and  $\text{CaCl}_2$  under different temperatures related to the thermodynamics methods. The potential for biological process improvement is limited because cells are not metabolizing, and there is no ability to biologically change the metal cationic and anionic state. The scientific understanding of the ion-binding mechanisms of these materials remains limited, highlighting the need for ongoing research and development in this area.

## REFERENCES

- Abd, I.N. and Mohammed-Ridha, M.J., 2021. Simultaneous adsorption of tetracycline and amoxicillin by *Cladophora* and *Spirulina* algae biomass. *Iraqi Journal of Agricultural Sciences*, 52(5), pp.1290–1303.
- Aljeboree, A.M., Alshirifi, A.N. and Alkaim, A.F., 2020. Removal of amoxicillin drug onto nanocomposite surface using ultrasound assistance. *Plant Archives*, 20(1), pp.3135–3140.
- Allen, S.J., Gan, Q., Matthews, R. and Johnson, P.A., 2003. Comparison of optimized isotherm models for basic dye adsorption by kudzu. *Bioresource Technology*, 88(2), pp.143–152.
- Aravindhan, R., Rao, J.R. and Nair, B.U., 2009. Application of a chemically modified green macro alga as a biosorbent for phenol removal. *Journal of Environmental Management*, 90(5), pp.1877–1883.
- Arihilar, N. and Arihilar, E., 2019. Impact and control of anthropogenic pollution on the ecosystem – A review. *Journal of Bioscience and Biotechnology Discovery*, 4, pp.54–59. DOI.
- Asim, N., Amin, M.H., Alghoul, M.A., Sulaiman, S.N.A., Razali, H., Akhtaruzzaman, M. and Sopian, K., 2021. Developing chemically treated waste biomass adsorbent for dye removal. *Journal of Natural Fibers*, 18(7), pp.968–977.
- Balarak, D., Joghatayi, A., Mostafapour, F.K. and Azarpira, H., 2017. Biosorption of amoxicillin from contaminated water onto palm bark biomass. *International Journal of Life Science and Pharma Research*, 7(1), pp.L-9.
- Boukheikhal, A., Benkortbi, O., Hamadache, M., Ghalem, N., Hanini, S. and Amrane, A., 2016. Adsorptive removal of amoxicillin from wastewater using wheat grains: Equilibrium, kinetic, thermodynamic studies, and mass transfer. *Desalination and Water Treatment*, 57(56), pp.27035–27047.
- Chakhtouna, H., Benzeid, H., Zari, N. and Bouhfid, R., 2021. Functional CoFe<sub>2</sub>O<sub>4</sub>-modified biochar derived from banana pseudostem as an efficient adsorbent for the removal of amoxicillin from water. *Separation and Purification Technology*, 266, 118592.
- Cristiano, E., Hu, Y.J., Siegfried, M., Kaplan, D. and Nitsche, H., 2011. A comparison of point of zero charge measurement methodology. *Clays and Clay Minerals*, 59(2), pp.107–115.
- Dan, A., Chen, C.X., Zou, M.Y., Deng, Y.Y., Zhang, X.M., Du, J.J. and Yang, Y., 2021. Removal efficiency, kinetic, and behavior of antibiotics from sewage treatment plant effluent in a hybrid constructed wetland and a layered biological filter. *Journal of Environmental Management*, 288, 112435.
- Dimitrakopoulou, D., Rethemiotaki, I., Frontistis, Z., Xekoukoulotakis, N.P., Venieri, D. and Mantzavinos, D., 2012. Degradation, mineralization, and antibiotic inactivation of amoxicillin by UV-A/TiO<sub>2</sub> photocatalysis. *Journal of Environmental Management*, 98, pp.168–174.
- Gaddam, K., SivananainthaPerumal, M. and Ravindiran, G., 2020. Removal of lead metal ion using biowaste of *Pithophora cleveana* Wittrock and *Mimusops elengi*. *Energy Sources, Part A: Recovery, Utilization, and Environmental Effects*, pp.1–19.
- Hamadeen, M., Elsayed, A., Elkhatib, A., Mohamed, E., Badawy, A., Samir, A. and Abdelgaleil, M., 2021. Novel low-cost nanoparticles for enhanced removal of chlorpyrifos from wastewater: Sorption kinetics, and mechanistic studies. *Arabian Journal of Chemistry*, 14, 102981. DOI
- Ho, Y.S. and McKay, G., 1999. Pseudo-second order model for sorption processes. *Process Biochemistry*, 34(5), pp.451–465. DOI
- Jung, Y., Kim, W., Yoon, Y., Kang, J., Hong, Y. and Kim, H., 2012. Removal of amoxicillin by UV and UV/H<sub>2</sub>O<sub>2</sub> processes. *Science of The Total Environment*, 420, pp.160–167. DOI
- Kalyani, G., Gokulan, R. and Sujatha, S., 2021. Biosorption of zinc metal ion in aqueous solution using biowaste of *Pithophora cleveana* Wittrock and *Mimusops elengi*. *Desalination and Water Treatment*, 218, pp.363–371.
- Kerkez-Kuyumcu, Ö., Bayazit, Ş.S. and Salam, M.A., 2016. Antibiotic amoxicillin removal from aqueous solution using magnetically modified graphene nanoplatelets. *Journal of Industrial and Engineering Chemistry*, 36, pp.198–205.
- Khamayseh, M.M. and Kidak, R., 2023. Equilibrium, kinetics, and thermodynamics study on the biosorption of reactive levofloxacin antibiotic on *Pithophora* macroalgae in aqueous solution. *Environmental Monitoring and Assessment*, 195(2), 301.
- Khamayseh, M.M. and Kidak, R., 2024. Biosorption of reactive amoxicillin antibiotic on *Pithophora* macroalgae in aqueous solution. Equilibrium and kinetic studies. *Desalination and Water Treatment*, 100669.
- Kratochvil, D. and Volesky, B., 1998. Advances in the biosorption of heavy metals. *Trends in Biotechnology*, 16(7), pp.291–300.
- Lai, C., Liu, X., Qin, L., Zhang, C. and Zeng, G., 2017. Chitosan-wrapped gold nanoparticles for hydrogen-bonding recognition and colorimetric determination of the antibiotic kanamycin. *Microchimica Acta*, 184(7), pp.2097–2105. DOI
- Limousy, L., Ghouma, I., Ouederni, A. and Jeguirim, M., 2017. Amoxicillin removal from aqueous solution using activated carbon prepared by chemical activation of olive stone. *Environmental Science and Pollution Research*, 24(11), pp.9993–10004.
- Matsubara, M.E., Helwig, K., Hunter, C., Roberts, J., Subtil, E.L. and Coelho, L.H.G., 2020. Amoxicillin removal by pre-denitrification membrane bioreactor (A/O-MBR): performance evaluation, degradation by-products, and antibiotic resistant bacteria. *Ecotoxicology and Environmental Safety*, 192, 110258.
- Mohammed, A.A., Al-Musawi, T.J., Kareem, S.L., Zarrabi, M. and Al-Ma'abreh, A.M., 2020. Simultaneous adsorption of tetracycline, amoxicillin, and ciprofloxacin by pistachio shell powder coated with zinc oxide nanoparticles. *Arabian Journal of Chemistry*, 13(3), pp.4629–4643.
- National Center for Biotechnology Information., 2022. PubChem Compound Summary for CID 149096, Levofloxacin. Retrieved November 9, 2022 from <https://pubchem.ncbi.nlm.nih.gov/compound/Levofloxacin>
- Oba, O.A. and Pasaogulari Aydinlik, N., 2022. Preparation of mesoporous activated carbon from novel African walnut shells (AWS) for deltamethrin removal: kinetics and equilibrium studies. *Applied Water Science*, 12(7), pp.1–20.
- O'Neal, S.W., Lembi, C.A. and Spencer, D.F., 1985. Productivity of the filamentous alga *Pithophora oedogonia* (Chlorophyta) in Surrey Lake, Indiana. *Journal of Phycology*, 21(4), pp.562–569.
- Pezoti, O., Cazetta, A.L., Bedin, K.C., Souza, L.S., Martins, A.C., Silva, T.L. and Almeida, V.C., 2016. NaOH-activated carbon of high surface area produced from guava seeds as a high-efficiency adsorbent for amoxicillin removal: kinetic, isotherm and thermodynamic studies. *Chemical Engineering Journal*, 288, pp.778–788.
- Romera, E., González, F., Ballester, A., Blázquez, M.L. and Muñoz, J.A., 2007. Comparative study of biosorption of heavy metals using different types of algae. *Bioresource Technology*, 98(17), pp.3344–3353.
- Sulaymon, A.H., Mohammed, A.A. and Al-Musawi, T.J., 2013. Removal of lead, cadmium, copper, and arsenic ions using biosorption: equilibrium and kinetic studies. *Desalination and Water Treatment*, 51(22–24), pp.4424–4434.
- Válitalo, P., Kruglova, A., Mikola, A. and Vahala, R., 2017. Toxicological impacts of antibiotics on aquatic micro-organisms: a mini-review. *International Journal of Hygiene and Environmental Health*, 220(3), pp.558–569.
- Yan, L., Yan, N., Gao, X.Y., Liu, Y. and Liu, Z.P., 2022. Degradation of amoxicillin by newly isolated *Bosea* sp. Ads-6. *Science of The Total Environment*, 828, 154411.

# A Comprehensive Study on the Environmental Features of Green Buildings in Dhaka, Bangladesh: Prospects, Challenges and Mitigation Strategies

Md. Sultanul Islam<sup>1†</sup> , Nafis Ibna Oli<sup>2</sup> and Md. Hasibul Hassan<sup>1</sup>

<sup>1</sup>Department of Civil Engineering, School of Civil, Environment and Industrial Engineering, Uttara University, Dhaka-1230, Bangladesh

<sup>2</sup>Department of Civil Engineering, Bangladesh University of Engineering and Technology, Dhaka-1000, Bangladesh

†Corresponding author: Md. Sultanul Islam; sultanul.islam@uttarauniversity.edu.bd

**Abbreviation:** Nat. Env. & Poll. Technol.  
**Website:** www.neptjournal.com

*Received:* 13-09-2024

*Revised:* 11-11-2024

*Accepted:* 13-11-2024

## Key Words:

Green buildings  
 Leadership in energy and environmental design  
 Environmental features  
 Mitigation strategies

## Citation for the Paper:

Islam, M.S., Oli, N.I. and Hassan, M.H., 2025. A comprehensive study on the environmental features of green buildings in Dhaka, Bangladesh: Prospects, challenges and mitigation strategies. *Nature Environment and Pollution Technology*, 24(2), p. D1724. <https://doi.org/10.46488/NEPT.2025.v24i02.D1724>

*Note: From year 2025, the journal uses Article ID instead of page numbers in citation of the published articles.*



**Copyright:** © 2025 by the authors  
**Licensee:** Technoscience Publications  
 This article is an open access article distributed under the terms and conditions of the Creative Commons Attribution (CC BY) license (<https://creativecommons.org/licenses/by/4.0/>).

## ABSTRACT

The construction industry has played a significant role in causing environmental degradation, primarily due to its substantial energy use. Focusing on green building development projects is gaining momentum as a sustainable solution for mitigating environmental challenges. This study assessed several environmental features of 22 green buildings in Dhaka, the capital of Bangladesh. In addition, the challenges were discussed, and mitigation strategies were recommended. The Leadership in Energy and Environmental Design (LEED) certification technique is widely acknowledged and globally accepted as the leading green building certification standard. Three LEED versions, v3 for new construction and major renovations and v4 and v4.1 for building design and construction, were investigated. Seven environmental features of three versions, including rainwater management, renewable energy, enhanced commissioning, optimized energy performance, construction and demolition waste management, water use reduction, and water efficient landscaping, were considered in this work. A survey questionnaire was prepared to receive information about these LEED-certified (or applied for certification) buildings. The findings of our study suggested that the general trend for seven environmental features of the selected green buildings was positive except for renewable energy, where 72.72% of buildings were in 'very poor' condition. Regarding rainwater management, enhanced commissioning, and optimized energy performance, 40.91% of buildings were in 'very good' condition. Despite satisfactory responses for several environmental features, the survey found that renewable energy integration remains challenging for all buildings. Solar energy should be extensively employed to enhance energy utilization efficiency, reduce energy demand, and minimize environmental impact. It was suggested that a few challenges, including the government's lack of action and initiatives, financial incentives, investor hesitation, and knowledge gaps, must be overcome to create a truly green building market in Bangladesh. Bridging this disparity requires policy reforms, public awareness, industry development, and capacity building. This study provides a basic understanding of the green building situation and guides future research and policy initiatives to accelerate Bangladesh's commitment to sustainable development goals.

## INTRODUCTION

Anthropogenic activities have led to a significant increase in greenhouse gas emissions. The construction industries are substantial contributors to global emissions, although they play a crucial role in establishing necessary infrastructure, generating employment opportunities, and contributing to the nation's overall economy (Zuo & Zhao 2014). Consequently, the management of environmental effects in the construction industry has emerged as a significant concern.

The construction is plagued with various environmental issues, such as noise, dust, traffic congestion, water contamination, and waste disposal. Building construction, installation, transportation, and manufacturing, all require large amounts of energy and emit large amounts of greenhouse gases, mostly carbon



dioxide (CO<sub>2</sub>) (Yan et al. 2010). 35% of the world's CO<sub>2</sub> emissions and 45-65% of the waste that ends up in landfills are caused by the building sector. The construction industry and its linked activities also generate considerable harmful emissions; construction-related activities account for about 30% of global greenhouse gas emissions. 18% of these emissions are attributed to the preparation and transportation of building materials alone (Lima 2021). The Intergovernmental Panel on Climate Change (IPCC) predicts that by 2050, global temperatures will increase by 1.5°C (2.7°F) compared to the levels before the industrial era (IPCC 2022). The energy-related carbon dioxide (CO<sub>2</sub>) emissions totaled 32.3 billion metric tons in 2012 and are forecasted to rise to 43.4 billion metric tons by 2040 (Zhang et al. 2017).

Green buildings, or green infrastructures, have gained significant attention recently because of their potential to minimize the adverse effects of buildings on the environment and the people who use them. Although green building lacks a universally recognized and agreed-upon definition (Li et al. 2017), in the context of “green building”, the term “green” denotes explicitly a symbol or concept that signifies a building that does not cause harm to the environment. It does not encompass the broader meaning of green roofs or rooftop gardens (Zheng 2021). Instead, it refers to a form of construction that reduces its impact on the natural environment and human well-being.

The technique of designing and constructing buildings with responsible and resource-efficient methods at every stage of their life cycle, from siting to design, construction, operation, maintenance, and renovation, is known as “green building.” Green buildings are designed and built using recycled materials, less water, less energy, and resource-efficient techniques; they also feature water-sensitive design to reduce their vulnerability to flooding; they minimize pollutant emissions to the air, water, and soil; and they minimize light and noise pollution (Hussin et al. 2013, Olubunmi et al. 2016). Green buildings often maintain higher indoor air quality (Darko et al. 2017).

Green building materials play a crucial role in sustainable architecture due to their low environmental impact and high resource efficiency, leading to reduced emissions and resource conservation. Achieving long-term sustainability requires ongoing innovation, supportive legislation, and collaboration among architects, builders, legislators, and consumers (Iwuanyanwu 2024).

Green buildings offer significant economic and social benefits by improving energy efficiency, lowering operational costs, and promoting environmental sustainability. Economically, they result in substantial savings on energy, water, and materials, which reduces overall expenses

and increases property values (Zhao 2023). They cut infrastructure costs, lower waste disposal expenses, and mitigate risks while enhancing durability and maintenance efficiency. Socially, green buildings foster healthier living and working environments, which improve occupants' health, comfort, and productivity (Vasilevna & Trofimovich 2021).

Multiple international green rating systems have been devised to assess the sustainability of construction projects. The Leadership in Energy and Environmental Design (LEED) certification technique is widely acknowledged and considered the leading green certification standard globally. Although the US Green Building Council (USGBC) created LEED as a discretionary benchmark, it is widely regarded as the most extensively implemented grading scheme based on the number of countries. LEED primarily assesses environmental elements like sustainable sites, water efficiency, energy and atmosphere, materials and resources, and the indoor environment (Doan et al. 2017). The LEED green building certification system is a voluntary and consensus-driven procedure for measuring the impacts of the constructed environment and construction activities across multiple impact categories. The categories encompass crucial global environmental, social, health, and economic concerns. They offer performance measures, best practices, and procedures for enhancing buildings in these domains. Over the past decade, LEED has undergone multiple revisions with the addition of stricter sustainability criteria and credit rating systems. LEED classifies several interrelated rating systems into four main construction types (USGBC 2017, Dorsey & Hedge 2017):

- i. Building Design and Construction (BD+C)
- ii. Interior Design and Construction (ID+C)
- iii. Building Operations and Maintenance (O+M)
- iv. Neighbourhood Development (ND)

LEED v3 or LEED 2009 for New Construction and Major Renovations had seven main categories: Sustainable Sites, Water Efficiency, Energy and Atmosphere, Materials and Resources, Indoor Environmental Quality, Innovation and Design Process, and Regional Priority Credits, totaling 110 points (LEED 2009). LEED v4 (2013) comprised 21 rating systems designed to cater to various building types, whereas v4.1 (2019) raised the bar on building standards to address energy efficiency, water conservation, and carbon emission reduction. The LEED rating system requires fulfilling prerequisites in all credit categories to obtain certification at any level. Additionally, optional credits can be pursued to collect points that contribute to achieving higher certification levels. Project teams can choose any combination of credits

to reach the required level of certification. The weighting technique assigns 110 points to each LEED rating system, considering their respective social, environmental, and economic implications. The degree of certification for a project is determined by the number of points it has earned (Worden et al. 2020).

- Certified: 40-49 points
- Silver: 50-59 points
- Gold: 60-79 points
- Platinum: 80 points or more

Bangladesh currently lacks an officially recognized green building grading system. Bangladesh Bank has recognized LEED as the main green building rating system for the formal certification process (Saba 2019). The introduction of LEED certification fosters constructive competition to create a more environment-friendly, sustainable, and ecologically balanced Bangladesh. Most of the 177 buildings in Bangladesh that have received LEED certification are industrial structures. The composition comprises 31% platinum, 58% gold, 8% silver, and 2% certified (Assure Group 2022). Most of the commercial green buildings are in Dhaka city. The Cityscape Tower, located on Gulshan Avenue, Dhaka, is under LEED Platinum Certification. In addition, Simpletree Anarkali and Simpletree Lighthouse, situated on Gulshan Avenue, are also under LEED Gold Certification (Fig. 1).

Due to the increasing need for environment-friendly construction, academia has significantly emphasized researching green buildings. Developed countries are working towards shifting to eco-friendly building technologies. Bangladesh, a developing nation, strives to increase knowledge regarding green building practices; however, the actual construction of such buildings is still limited. Construction professionals in Bangladesh rarely adhere to the many laws, regulations, and recommendations outlined in the national policies. Despite the ongoing research on green

buildings in Bangladesh, the environment-related features of these buildings are not well-studied. The objective of this study was to investigate the existing condition of the environmental features of selected green buildings situated in Dhaka North City Corporation, Bangladesh. The challenges and mitigation strategies were also suggested to overcome the shortcomings of the necessary environmental features of these buildings.

## MATERIALS AND METHODS

### Study Area

This study considered 22 buildings in the Dhaka North City Corporation area (Fig. 2). The buildings were selected based on the accessibility to reach out to the stakeholders or concerned personnel easily for collecting necessary information regarding their LEED certification. Among the buildings, sixteen of them are located in Gulshan Avenue, while the rest are in Tejgaon, North Badda, Uttara, Kazi Nazrul Islam Avenue, and Bashundhara. Table 1 lists the buildings considered during this study and their LEED certification status.

### Scope of Study

Seven environmental features of the LEED rating system were considered to understand the current conditions of the selected 22 green buildings in the capital city of Bangladesh, Dhaka. The environmental features included rainwater management, renewable energy, enhanced commissioning, optimized energy performance, construction and demolition waste management, water use reduction, and water-efficient landscaping. Three LEED versions – version 3 (v3) for new construction and major renovations and version 4 (v4) and version 4.1 (v4.1) for building design and construction were considered as the buildings were certified under these versions. A total LEED score



(a)



(b)



(c)

Fig. 1: (a) Cityscape Tower, (b) Simpletree Lighthouse, and (c) Simpletree Anarkali.

Table 1: List of considered buildings and their LEED certification status.

Sl. No.	Name of the Building	LEED Certification
1.	Simpletree Anarkali	LEED Gold Certification
2.	Cityscape Tower	LEED Platinum Certification
3.	Hadi Tower	LEED Gold Certification
4.	Saiham Tower	LEED Platinum Certification
5.	bti Landmark	LEED Gold Certification
6.	Mobil House	LEED Platinum Certification
7.	SouthBreeze Square	LEED Platinum Certification
8.	Simpletree Lighthouse	LEED Gold Certification
9.	HSBC Bangladesh Gulshan Branch	LEED Platinum Certification
10.	Palmal Tower	LEED Gold Certification
11.	Shahjalal Islami Bank Corporate Headquarters	LEED Gold Certification
12.	Shanta Pinnacle	LEED Platinum Pre-certified
13.	Simpletree GSR	Registered for LEED Certification, LEED v4 BD+C CS
14.	Rangs RK Square	Applied for LEED Certification
15.	JCX Business Tower	Registered for LEED Certification, LEED v4 BD+C CS
16.	InnStar Trade Intercontinental	LEED Platinum Pre-certified
17.	Standard Bank Limited Head Office	Registered for LEED Certification, LEED v4 BD+C NC
18.	Suvastu Skyline Avenue	Registered for LEED Certification, LEED v4 BD+C CS
19.	The Pearl Trade Center	Certification in Progress
20.	Ishtiak Thal Green	Certification in Progress
21.	BIFFL Corporate Office	LEED Platinum Certification
22.	Rangs Z Square	Applied for LEED Certification

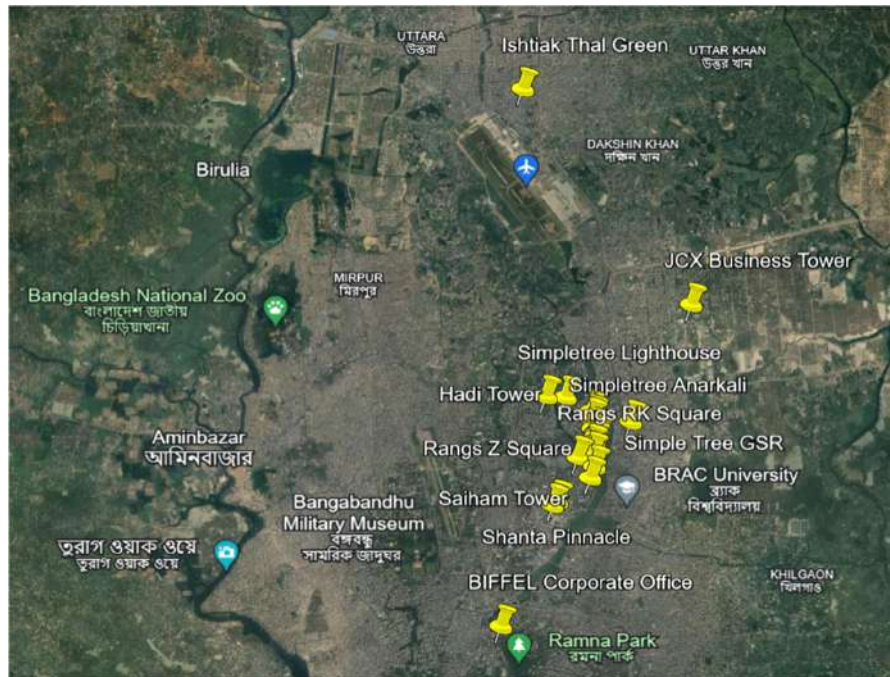


Fig. 2: Study area and location of the buildings (Google Earth).

of 42 out of 110 for these seven features was taken into consideration.

### Data Collection

This study required the collection of both qualitative and quantitative data. To begin with, a detailed analysis of research papers and articles on green buildings was carried out to prepare a survey questionnaire. The survey was intended only for research purposes on knowledge-sharing outcomes. The questionnaire featured a Likert scale with four weight categories: ‘very lightweight,’ ‘lightweight,’ ‘moderate weight,’ and ‘heavyweight.’ Environmental features were weighted based on their contributions to a total LEED score of 110 points.

Furthermore, the questionnaire featured a Likert scale with five points, which assessed the fulfillment of the criteria. The available alternatives were ‘very poor condition,’ ‘poor condition,’ ‘neutral condition,’ ‘good condition,’ and ‘very good condition.’ A Likert scale was chosen because it allowed for the systematic quantification of subjective evaluations of different environmental characteristics and their conditions. Individuals working in constructing those buildings provided most of the primary data. In addition to conducting a Likert-

Table 2: Environmental features and their associated weights.

Percentage of LEED score covered	Weightage
Up to 1%	Very Light Weight
More than 1% up to 2%	Light Weight
More than 2% up to 3%	Moderate Weight
More than 3% and above	Heavy Weight

scale survey, technical people were also interviewed to gather their ideas and suggestions about adopting green construction practices, specifically about environmental aspects. Hence, the survey targeted engineers and technicians responsible for implementing sustainable technologies in the construction industry. The responses to the questionnaire and project data were recorded in 2023. To ensure participant anonymity and confidentiality, the survey provided anonymous responses, assured participants that their data would be used only for research, and securely stored the data, thereby enhancing the study’s reliability and validity.

## RESULTS AND DISCUSSION

### Environmental Features

The questionnaire, featuring a Likert scale with four

Table 3: Environmental features and their associated weights.

Environmental Features	Main Category	LEED Version	Score	Weight
Rainwater Management	Sustainable Sites	v4	3	Moderate
Renewable Energy	Energy and Atmosphere	v4.1	5	Heavy
Enhanced Commissioning	Energy and Atmosphere	v4.1	6	Heavy
Optimize Energy Performance	Energy and Atmosphere	v4.1	18	Heavy
Construction and Demolition Waste Management	Materials and Resources	v4	2	Light
Water Use Reduction	Water Efficiency	v3	4	Heavy
Water Efficient Landscaping	Water Efficiency	v3	4	Heavy

Table 4: Considered criteria for each environmental feature.

Environmental Features	Number of Criteria
Rainwater Management	i. Catchment, ii. Conveyance system, iii. Flush and Filter, iv. Tank and the recharge structure, v. Regular maintenance
Renewable Energy	i. Solar power, ii. Wind power, iii. Waste to electric energy, iv. Biogas, v. Maintenance
Enhanced Commissioning	i. Engage commissioning authority, ii. Design review, iii. Construction review and as-built drawing, iv. Quality v. Durability
Optimize Energy Performance	i. HVAC system (Heating, Ventilation, and Air Conditioning), ii. Daylight system, iii. Solar heating and water saving technology, iv. CO <sub>2</sub> sensor and double-glazed thermal glass, v. Regular maintenance
Construction and Demolition Waste Management	i. Eliminating waste, ii. Minimize waste, iii. Recycling and salvage value, iv. Disposal and diversion, v. Govt. regulation and management
Water Use Reduction	i. Sensor type dual flush (Water Closets), ii. Sensor type (Lavatory Faucet), iii. Ultra-low flow (Urinals & Shower), iv. Sensor type (Water Pump), v. Regular maintenance
Water Efficient Landscaping	i. Native and adapted plants, ii. Smart sensors and controls for watering, iii. Healthy soil and retain moisture, iv. Rainwater and recycled wastewater, v. Regular maintenance



Table 5: Condition assigned of seven environmental features of the buildings under consideration.

Rainwater Management	No or one criterion	Very Poor	0	0.00%
	Two criteria	Poor	3	13.64%
	Three criteria	Neutral	4	18.18%
	Four criteria	Good	6	27.27%
	Five criteria	Very Good	9	40.91%
	<b>Total</b>		<b>22</b>	<b>100%</b>
Renewable Energy	No or one criterion	Very Poor	16	72.73%
	Two criteria	Poor	6	27.27%
	Three criteria	Neutral	0	0.00%
	Four criteria	Good	0	0.00%
	Five criteria	Very Good	0	0.00%
	<b>Total</b>		<b>22</b>	<b>100%</b>
Enhanced Commissioning	No or one criterion	Very Poor	3	13.64%
	Two criteria	Poor	2	9.09%
	Three criteria	Neutral	3	13.64%
	Four criteria	Good	5	22.73%
	Five criteria	Very Good	9	40.91%
	<b>Total</b>		<b>22</b>	<b>100%</b>
Optimize Energy Performance	No or one criterion	Very Poor	2	9.09%
	Two criteria	Poor	2	9.09%
	Three criteria	Neutral	3	13.64%
	Four criteria	Good	6	27.27%
	Five criteria	Very Good	9	40.91%
	<b>Total</b>		<b>22</b>	<b>100%</b>
Construction and Demolition Waste Management	No or one criterion	Very Poor	3	13.64%
	Two criteria	Poor	3	13.64%
	Three criteria	Neutral	4	18.18%
	Four criteria	Good	5	22.73%
	Five criteria	Very Good	7	31.82%
	<b>Total</b>		<b>22</b>	<b>100%</b>
Water Use Reduction	No or one criterion	Very Poor	4	18.18%
	Two criteria	Poor	2	9.09%
	Three criteria	Neutral	4	18.18%
	Four criteria	Good	6	27.27%
	Five criteria	Very Good	6	27.27%
	<b>Total</b>		<b>22</b>	<b>100%</b>
Water Efficient Landscaping	No or one criterion	Very Poor	5	22.73%
	Two criteria	Poor	4	18.18%
	Three criteria	Neutral	3	13.64%
	Four criteria	Good	5	22.73%
	Five criteria	Very Good	5	22.73%
	<b>Total</b>		<b>22</b>	<b>100%</b>

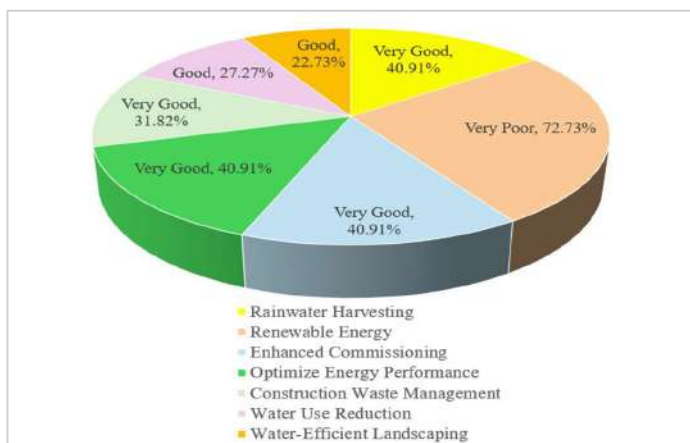


Fig. 3: Dominant condition of all environmental features in the buildings.

weight categories, assigned weights of ‘very lightweight,’ ‘lightweight,’ ‘moderate weight,’ and ‘heavyweight’ to the environmental features based on the percentage of total LEED score covered by each feature (Table 2 and Table 3).

For example, according to LEED, the total scorecard is 110, and the score of rainwater management is 3. The weight of rainwater management =  $\left(\frac{3}{110}\right) \times 100 = 2.73\%$ . Therefore, it is a moderate weight criterion.

Table 4 displays the five criteria considered among others for each environmental feature and Table 5 shows the conditions assigned based on the fulfillment of criteria for each environmental feature of the buildings.

### Conditions of the Environmental Features

Table 5 shows that nine buildings are in ‘very good’ condition, and none are in ‘very poor’ condition regarding rainwater management. The maximum percentage of buildings, 40.91%, is in ‘very good’ condition. Sixteen buildings lie in ‘very poor’ condition which accounts for 72.72% of the buildings for renewable energy, as shown in Table 5. Therefore, the highest proportion is in ‘very poor’ condition. This data shows that renewable energy is yet to be properly implemented in green buildings in Dhaka city. Being a heavy-weight environmental feature of the LEED certification system, this feature must be implemented regularly. In the case of enhanced commissioning, nine buildings are in ‘very good’ condition, which accounts for 40.91% of the total buildings under consideration.

Similarly, the maximum percentage of buildings, 40.91%, is in ‘very good’ condition for optimizing energy performance. However, more than 18% of the buildings fail to fulfill even two criteria, which is undesirable, as this heavy-weight environmental feature has a LEED score of 18.

The maximum percentage is in ‘very good’ condition (seven buildings), whereas ‘very poor’ and ‘poor’ conditions are the lowest (three buildings each) for construction and demolition waste management. In the case of water use reduction, six buildings lie in both ‘very good’ and ‘good’ conditions respectively (27.27%), whereas four buildings are in ‘very poor’ condition. Lastly, five buildings are categorized separately into ‘very good’ and ‘good’ conditions regarding water-efficient landscaping. However, almost 41% of buildings are either in ‘very poor’ or ‘poor’ condition. Being a heavy-weight environmental feature, all the buildings are expected to fulfill more than two criteria for water-efficient landscaping.

Fig. 3 summarizes the dominant conditions of seven environmental features among 22 buildings under consideration for this investigation. The figure also indicated that most buildings have either very good or good conditions for environmental features except for renewable energy. In all the buildings surveyed, the state of renewable energy was either very poor or poor since they failed to fulfill either any criteria or just fulfilled one criterion. The main challenges behind the non-compliance of criteria for renewable energy may be a lack of proper awareness, lack of LEED construction teams, vendors, and consultants in Bangladesh, limitations in training of engineers and other technical teams, and limitations of Government incentives and enforcement. Mitigation may be possible by establishing organizational supportive policies and regulations, creating awareness through education and training programs, and deploying the appropriate green consultant to implement. Nevertheless, the seven environmental features did not inherently indicate that all buildings were in a state of sufficient condition to be considered green buildings. The actual objective of green building necessitates the enhancement

of several features and the satisfaction of additional criteria.

The study found that the state of renewable energy in most buildings is quite inadequate, posing a significant obstacle to the implementation of environment-friendly structures. Renewable energy, renowned for its environmental sustainability, could be substantial for tackling the increasing need for energy and reducing the impact of global warming. This will facilitate achieving a 10% reduction in energy cost savings, which is the requirement of any building for LEED certification (Dobiáš & Macek 2014). As Bangladesh is a tropical country with abundant sunlight, solar energy can significantly increase the contribution of renewable energy to a higher level. Previous studies found that the energy requirement of buildings can be met by up to 83% in the case of solar energy integration and 15% when wind energy is incorporated into buildings (Chen et al. 2024).

Active solar building integration systems can modify the attributes of buildings and mitigate the adverse environmental effects of constructing public spaces. Furthermore, the combined exploitation of solar energy with photovoltaic technology may offer a significant advantage in enhancing energy efficiency and decreasing energy consumption (Vassiliades et al. 2022).

There are numerous challenges associated with the implementation of green buildings in Bangladesh. The most likely challenges are the absence of government incentives, the hesitation of building owners, and the lack of environmental awareness (Khan & Shammi 2022). Myths regarding the cost-effectiveness of green buildings, market understanding, and lack of knowledge regarding the planning and construction of green buildings are other considerable obstacles, in addition to the scarcity of resources and skills (Chowdhury & Hossain 2021, Al-Fahim & Shahriar 2024).

Current construction policies incorporate sustainability, but they do not rigorously enforce it. A comprehensive strategy is necessary to resolve these issues. This necessitates increased public and academic awareness, robust government support, funds, strict laws, and industry development that emphasize skill development, material availability, and market promotion of green structures. Financial incentives, for instance, a 30% subsidy for adopting renewable technologies, could enhance the appeal of these innovations (Chen et al. 2024).

Implementing new legislation that mandates sustainable practices in new construction and government certifications for green developers is imperative. Green certification enhances innovation and motivation for more energy and water-efficient equipment (Dobiáš & Macek 2014). Individuals and institutions must collaborate to share knowledge and overcome technical obstacles and material scarcity. Fostering research in

engineering institutions and incorporating green construction into higher education is critical for developing a competent workforce and promoting sustainable practices.

## CONCLUSIONS

The environmental features of 22 green buildings in Dhaka North City Corporation were studied in this work. Furthermore, this study reviewed the challenges to implementing green buildings in Bangladesh and recommended mitigation strategies. It has been shown that while some green construction features, such as rainwater management and water efficiency, are generally effectively implemented, integrating renewable energy remains a considerable challenge. The widespread use of solar energy, a form of renewable energy, is necessary to enhance energy usage efficiency, decrease energy demand, and eventually fulfill the objectives of constructing green buildings.

Various challenges should be overcome to achieve a completely green building sector in Bangladesh, including government apathy, financial incentives, investor hesitancy, and knowledge shortages. To close this gap, a multifaceted strategy encompassing policy reforms, public awareness, industry development, and capacity building. Focusing on these areas may create a long-term built environment in Bangladesh that benefits both the environment and the economy.

Green building implementation in Bangladesh must address renewable energy concerns to increase energy efficiency, lower carbon emissions, potential energy security, and improve economic outcomes. Establishing legislative frameworks, offering financial incentives like tax credits, subsidies, and low-interest loans, and raising public awareness are necessary for the government to encourage sustainable construction.

This study provides a fundamental understanding of the green building scenario in Dhaka North City Corporation. It serves as a road map for future research and policy interventions to speed up Bangladesh's adoption of sustainable development goals. Future research should explore alternative green certifications for Bangladesh, public-private partnerships, and the impact of government policies and financial incentives on green building development. It should also address industry knowledge gaps and methods for integrating renewable energy, particularly solar, to enhance energy efficiency and sustainability.

## ACKNOWLEDGEMENTS

The authors would like to take this opportunity to express sincere appreciation to those who worked very hard to

physically visit the buildings and collected information through questionnaires for this investigation. We are also grateful to the people who were present in the buildings for their assistance in completing the survey.

## REFERENCES

- Al-Fahim, M.A. and Shahriar, S., 2024. Hindrances in Constructing Green Buildings in Bangladesh: A Comprehensive Study. 7th International Conference on Civil Engineering for Sustainable Development, Khulna, Bangladesh, 7-9 February 2024, pp.1-6. [http://www.iccesd.com/proc\\_2024/index.html](http://www.iccesd.com/proc_2024/index.html)
- Assure Group, 2022. Green Buildings - The Future of Sustainable Living in Bangladesh. Retrieved June 12, 2023, from <https://www.assuregroupbd.com/media/blog/green-buildings-the-future-of-sustainable-living>
- Chen, L., Hu, Y., Wang, R., Li, X., Chen, Z., Hua, J., Osman, A.I., Farghali, M., Huang, L., Li, J. and Dong, L., 2024. Green building practices to integrate renewable energy in the construction sector: a review. *Environmental Chemistry Letters*, 22(2), pp.751-784. DOI.
- Chowdhury, M.R. and Hossain, M.E., 2021. Green Building and Sustainable Development: Prospects and Challenges to Infrastructure Advancement of Bangladesh. In *International Conference on Planning, Architecture and Civil Engineering*, Rajshahi, Bangladesh.
- Darko, A., Zhang, C. and Chan, A.P., 2017. Drivers for green building: A review of empirical studies. *Habitat International*, 60, pp.34-49. DOI.
- Doan, D.T., Ghaffarianhoseini, A., Naismith, N., Zhang, T., Ghaffarianhoseini, A. and Tookey, J., 2017. A critical comparison of green building rating systems. *Building and Environment*, 123, pp.243-260. DOI.
- Dobiáš, J. and Macek, D., 2014. Leadership in Energy and Environmental Design (LEED) and its impact on building operational expenditures. *Procedia Engineering*, 85, pp.132-139. DOI.
- Dorsey, J. and Hedge, A., 2017. Re-evaluation of a LEED Platinum Building: Occupant experiences of health and comfort. *Work*, 57(1), pp.31-41. DOI.
- Hussin, J.M., Rahman, I.A. and Memon, A.H., 2013. The way forward in sustainable construction: issues and challenges keyword: Construction waste cost overrun green building issues in construction sustainable construction time overrun. *International Journal of Advances in Applied Sciences (IJAAS)*, 2(1), pp.15-24.
- Intergovernmental Panel on Climate Change (IPCC), 2022. Global Warming of 1.5°C. Cambridge University Press, UK. DOI.
- Iwuanyanwu, N.O., 2024. The role of green building materials in sustainable architecture: Innovations, challenges, and future trends. *International Journal of Applied Research in Social Sciences*, 6(8), pp.1935-1950. DOI.
- Khan, F.I. and Shammi, M., 2022. Perceptions and barriers to the construction of green buildings (GB) in Bangladesh. *Bangladesh Journal of Environmental Research*, 13, pp.13-27.
- Leadership in Energy and Environmental Design (LEED), 2009. LEED 2009 for New Construction and Major Renovations. Retrieved May 20, 2023, from <https://www.usgbc.org/resources/leed-new-construction-v2009-current-version>
- Li, Y., Chen, X., Wang, X., Xu, Y. and Chen, P.H., 2017. A review of studies on green building assessment methods by comparative analysis. *Energy and Buildings*, 146, pp.152-159. DOI.
- Lima, L., 2021. Sustainability in the construction industry: A systematic review of the literature. *Journal of Cleaner Production*, 12, p.730. DOI.
- Olubunmi, O.A., Xia, P.B. and Skitmore, M., 2016. Green building incentives: A review. *Renewable and Sustainable Energy Reviews*, 71, pp.1611-1621. DOI.
- Saba, S.S., 2019. Report A: The Construction Industry in Bangladesh, its Impact on the Economy and its Challenges. Retrieved June 18, 2023, from <https://www.researchgate.net/publication/336956702>
- US Green Building Council (USGBC), 2017. LEED US Green Building Council. Retrieved July 10, 2024, from <http://www.usgbc.org/leed>
- Vasilevna, A. and Trofimovich, V., 2021. Economic, environmental, and social benefits of green building. *Alfa Build*, 20, pp.1-9. DOI.
- Vassiliades, C., Savvides, A. and Buonomano, A., 2022. Building integration of active solar energy systems for façades renovation in the urban fabric: Effects on the thermal comfort in outdoor public spaces in Naples and Thessaloniki. *Renewable Energy*, 190, pp.30-47. DOI.
- Worden, K., Hazer, M., Pyke, C. and Trowbridge, M., 2020. Using LEED green rating systems to promote population health. *Building and Environment*, 172, p.106550. DOI.
- Yan, H., Shen, Q., Fan, L.C., Wang, Y. and Zhang, L., 2010. Greenhouse gas emissions in building construction: A case study of One Peking in Hong Kong. *Building and Environment*, 45(4), pp.949-955. DOI.
- Zhang, Y., Chen, W. and Gao, W., 2017. A survey on the development status and challenges of smart grids in main driver countries. *Renewable and Sustainable Energy Reviews*, 79, pp.137-147. DOI.
- Zheng, L., 2021. Research on the application of green building in building design. In *IOP Conference Series: Earth and Environmental Science*, 783(1), p.012160. DOI.
- Zhao, W., 2023. Comprehensive social, cultural, and economic benefits of green buildings based on improved AHP-FCE method. *Buildings*, 13(2), p.311. DOI.
- Zuo, J. and Zhao, Z.Y., 2014. Green building research—current status and future agenda: A review. *Renewable and Sustainable Energy Reviews*, 30, pp.271-281. DOI.



# Enabling Environment for Climate-Smart Agriculture: A Critical Review of Climate Smart Practices from South Asia and Sub-Saharan Africa

Arpita Ghosh<sup>1</sup>✉, Puneet Sharma<sup>2</sup>, Arnab Mondal<sup>3</sup> and Surajit Mondal<sup>4</sup>

<sup>1</sup>Symbiosis Centre for Management Studies, Symbiosis International (Deemed University), Pune, India

<sup>2</sup>Indian Institute of Management, Sirmaur, Rampur Ghat Road, Paonta Sahib, 173025, Himachal Pradesh, India

<sup>3</sup>Banaras Hindu University, Varanasi-221005, India

<sup>4</sup>Electrical Cluster, School of Advanced Engineering, University of Petroleum and Energy Studies, Dehradun-248007, Uttarakhand, India

✉Corresponding author: Arpita Ghosh; arpi.335@gmail.com, arpita.ghosh@scmstpune.ac.in

**Abbreviation:** Nat. Env. & Poll. Technol.  
**Website:** www.neptjournal.com

*Received:* 05-07-2024

*Revised:* 14-08-2024

*Accepted:* 25-08-2024

## Key Words:

Climate change  
 Smallholders  
 Climate-smart agriculture  
 Enabling environments

## Citation for the Paper:

Ghosh, A., Sharma, P., Mondal, A. and Mondal, S., 2025. Enabling environment for climate-smart agriculture: A critical review of climate-smart practices from South Asia and Sub-Saharan Africa. *Nature Environment and Pollution Technology*, 24(2), p. B4236. <https://doi.org/10.46488/NEPT.2025.v24i02.B4236>

*Note: From year 2025, the journal uses Article ID instead of page numbers in citation of the published articles.*



**Copyright:** © 2025 by the authors  
**Licensee:** Technoscience Publications  
 This article is an open access article distributed under the terms and conditions of the Creative Commons Attribution (CC BY) license (<https://creativecommons.org/licenses/by/4.0/>).

## ABSTRACT

In South Asian and Sub-Saharan African nations, climate change offers numerous hurdles to growth and development. These regions are susceptible to climate change due to their vast population reliance on agriculture, high demand for natural resources, and comparatively limited strategies for coping. Reduced food grain yields, crop losses, feed scarcity, lack of potable water for livestock during the summer, forceful animal migrations, and severe losses in the poultry and fishery industries have all been documented, posing a threat to the lives of the rural poor. As global food security and agricultural productivity become increasingly vulnerable, the focus has shifted towards adopting climate-smart agricultural practices and techniques. The present study discussed the need to identify and prioritize regionally evolving climate-smart farming practices and the enabling environment required for CSA uptake. The popular CSA practices in South Asia and Sub-Saharan Africa are crop rotation, cultivation of drought/flood-tolerant crops, legume intercropping, changing planting dates, rainwater harvesting, agroforestry, micro-irrigation technologies, minimum tillage, and integrated crop-livestock farming. A solid institutional structure, policy environment, infrastructure, agricultural insurance, climate information services, and gender and social inclusion provide the required enabling environment to alleviate farmer issues, lower CSA adoption obstacles, and improve operational sustainability. Highlights of the study are: This study examines how climate-smart farming practices are evolving in South Asia and Sub-Saharan Africa. We used a systematic approach to categorize and characterize agricultural adaptation alternatives to climate change. Our specific goals are to gain knowledge of the CSA adoption-enabling environments and the climate-smart agriculture practices employed in South Asia and Sub-Saharan Africa.

## INTRODUCTION

By 2050, the world's population is projected to increase by three billion people, with emerging nations accounting for 90% of that growth and putting pressure on the planet's current resources for food and wellness (Mishra et al. 2024, Ghosh et al. 2024a, Searchinger et al. 2019). The warming of the climate system is indisputable and has become increasingly intense since the 1950s (Seppelt et al. 2024). Less snow and ice and an increase in sea level result from warming oceans and climate. According to Lima and Wethey (2012), the earth's surface has warmed by 0.85°C since 1880, making the last three decades warmer than the decade before based on data from the global averaged composite ocean and land surface temperatures. The year 2015 was the warmest on record (WMO 2015).

In Low and Middle-income countries, mainly South Asian and Sub-Saharan African nations, climate change offers numerous hurdles to growth

and development (Teklewold et al. 2017, Prasad et al. 2014, Nyasimi et al. 2017). The agriculture production system in these areas faces the complex problem of feeding the world's population with limited land and water resources. These regions are susceptible to climate change due to their vast population reliance on agriculture, high demand for natural resources, and comparatively limited strategies for coping (Rao et al. 2016, Makate et al. 2018). Global warming increased by 0.6°C over the past 100 years, which anticipates impacting numerous crops and jeopardizing millions of farmers' food and livelihood security (Mensah et al. 2020, Jiri et al. 2017). Ipsos (2017) surveyed India's most pressing environmental challenges, and air pollution came out on top with 50% of respondents, followed by global warming/climate change with 43%, which highlights the need to act aggressively to combat and adapt to climate change (Fig. 1).

Agriculture is the backbone of many South Asia and Sub-Saharan African countries, contributing to food and nutrition security and economic growth, accounting for around 60 percent of the workforce and 30 percent of GDP (Khurshid et al. 2024, Yaongam 2024). Agriculture is rainfed (50 percent) in these regions, where 70 percent of farmers are smallholders (farmland < 0.5 hectares) from various socio-economic backgrounds, and roughly 35 percent of the population remains undernourished (WHO 2021). As a result of climate change or variability, migration from rural to urban regions, child hunger, and other challenges have grown more sensitive. Droughts, cyclones, and hailstorms have been more common in the last decade, with severe droughts occurring in 2002, 2004, 2009, 2012, and 2014. Drought-prone areas have seen an increase in cyclones and severe hailstorms. Reduced food grain yields, crop losses, feed scarcity, lack of potable water for livestock during the summer, forceful animal migrations, and severe losses in the poultry and fishery industries have all been documented, posing a threat to the lives of the rural poor (Khatri - Chhetri et al. 2016, Jellason et al. 2021, Ghosh et al. 2024b, Srivastava et al. 2020). Any change in climate poses serious risks threatening the food security situation in developing nations because of their dependence on agricultural production and limited capacities to adapt effectively (Sardar et al. 2020). Fig. 2 depicts the consequences of continuous climate change on grain yields between 2000 and 2050, based on NCAR climate change projections (Nelson et al. 2009). Climate change is expected to reduce the yield of irrigated maize (without CO<sub>2</sub> fertilization) by 2.8 percent in developing countries throughout this period.

Therefore, increasing agricultural productivity is essential for maintaining food and nutritional security

for everyone, especially the most vulnerable smallholder, disadvantaged, and resource-poor farmers (Ghosh et al. 2024a). Long-term climate change could severely affect the poor's livelihood security if adaptation is not planned. Increased adaptive capacity and resilience are the best strategies to deal with climate challenges since they can deliver immediate advantages while lowering climate change's adverse effects. The Sustainable Development Goals (SDGs) are visions for a sustainable future for all, highlighting the urgency to substantially reduce poverty and achieve food and nutrition security and sustainable agriculture by 2030 (UN 2015). As global food security becomes increasingly vulnerable, the focus has shifted towards adopting climate-smart agricultural practices and techniques.

Despite growing agreement that climate change makes agricultural expansion more complicated, no consensus exists on how agricultural practices should alter in response (Goli et al. 2024). There is a need to identify diverse climate-smart practices as adaptation methods in a period when climate change is a significant factor in agricultural development. Land, crop, livelihood, and water management practices are examples of climate-smart practices that have the potential to increase climate resilience and productivity while also lowering greenhouse gas (GHG) emissions per unit of output (Lipper et al. 2014). Protecting agrobiodiversity through Climate-Smart Agriculture (CSA) practices has recently been recommended as an approach for attaining numerous SDGs and subgoals related to no poverty, zero hunger, good health and well-being, responsible consumption and production, climate action, and life on land (Goli et al. 2024).

The present study emphasizes the need for regionally tailored practices, effective strategies like crop rotation and agroforestry, and supportive institutional structures. This review examines climate-smart farming practices in South Asia and Sub-Saharan Africa, focusing on long-term livelihoods for smallholder farmers. The study calls for increased awareness of climate-smart agriculture as a climate change mitigation strategy and identifies gaps in understanding barriers and motivations affecting smallholder farmers' adoption. It calls for cross-sector collaboration to build resilient agricultural frameworks.

## MATERIALS AND METHODS

The study used online databases and search engines to conduct a comprehensive literature search on climate change, focusing on peer-reviewed scientific publications from 2010 to 2022. The research included recent articles from South

Table 1: Criteria for literature selection for review.

Criteria for inclusion	Criteria for exclusion
The text is in English.	Text available in non-English language
Focus purely on climate-smart agriculture.	Focus on non-farm sectors.
Mentions Climate-Smart practices and focuses on smallholder farmers	Do not mention climate-smart practices and no focus on smallholder farmers
The study is based in Sub-Saharan Africa or South Asia	The study location is not from our concerned focus areas
Studies respond to the research question.	Studies did not respond to the research question.

Table 2: Climate-Smart Agriculture Practices/ Strategies.

Crop Management	Water Management	Land Management	Livelihood Management
<i>Crop Rotation</i>	<i>Improving irrigation use efficiency</i>	<i>Soil Conservation</i>	<i>Agro-forestry</i>
Mensah et al.(2020), Ochieng et al. (2016), Jellason et al. (2021) Issahaku and Abdulai (2019)	Rao et al. (2016), Issahaku and Abdulai (2019), Teklewold et al. (2017)	Issahaku and Abdulai (2019), Teklewold et al. (2017), Ochieng et al. (2016)	Rao et al. (2016), Aggarwal et al. (2018), Rahaman et al. (2019), Nyasimi et al. (2017), Mensah et al.(2020), Khatri - Chhetri et al. (2016), Teklewold et al. (2017), Ochieng et al. (2016)
<b><i>Drought /Flood Tolerant Seed varieties</i></b>	<b><i>Micro-irrigation technologies</i></b>	<b><i>Mulching</i></b>	<b><i>Crop Livestock integrated farming</i></b>
Rao et al. (2016), Aggarwal et al. (2018), Rahaman et al. (2019), Jiri et al. (2017), Issahaku and Abdulai (2019), Bairagi et al. (2020), Makate et al. (2018)	Jellason et al. (2021), Sardar et al. (2020), Khatri - Chhetri et al. (2016), Ochieng et al. (2016)	Rao et al. (2016), Rahaman et al. (2019), Mensah et al.(2020), Jellason et al. (2021)	Rao et al. (2016), Aggarwal et al. (2018), Rahaman et al. (2019), Ochieng et al. (2016)
<b><i>Short duration crops</i></b>	<b><i>Rainwater Harvesting</i></b>	<b><i>Minimum Tillage/ Zero Tillage</i></b>	<b><i>Crop Diversification</i></b>
Rao et al. (2016), Rahaman et al. (2019), Jiri et al. (2017),	Aggarwal et al. (2018), Rahaman et al. (2019), Prasad et al. (2014), Jellason et al. (2021), Khatri - Chhetri et al. (2016)	Aggarwal et al. (2018), Rahaman et al. (2019), Nyasimi et al. (2017), Sardar et al. (2020), Khatri - Chhetri et al. (2016), Issahaku and Abdulai (2019), Teklewold et al. (2017), Aryal et al. (2017), Makate et al. (2018)	Nyasimi et al. (2017), Jiri et al. (2017), Teklewold et al. (2017), Aryal et al. (2017), Ochieng et al. (2016)
<b><i>Legume Intercropping/ Cover cropping</i></b>	<b><i>Solar Pumps</i></b>		<b><i>Climate Smart Housing for livestock</i></b>
Rao et al. (2016), Nyasimi et al. (2017), Mensah et al.(2020), Jellason et al. (2021), Khatri - Chhetri et al. (2016), Makate et al. (2018)	Aggarwal et al. (2018)		Khatri - Chhetri et al. (2016) Rao et al. (2016)
<b><i>Changing Planting Dates/ Early Planting</i></b>	<b><i>Onsite moisture conservation</i></b>		<b><i>Fodder production and storage</i></b>
Rao et al. (2016), Rahaman et al. (2019), Nyasimi et al. (2017), Mensah et al.(2020), Sardar et al. (2020), Ochieng et al. (2016)	Rao et al. (2016), Jiri et al. (2017)		Rao et al. (2016) Rahaman et al. (2019) Nyasimi et al. (2017) Khatri - Chhetri et al. (2016)
<b><i>Integrated Nutrient Management</i></b>	<b><i>Aquifer recharge/recharge of wells</i></b>		
Aggarwal et al. (2018), Jellason et al. (2021), Sardar et al. (2020), Khatri - Chhetri et al. (2016), Teklewold et al. (2017), Aryal et al. (2017), Ochieng et al. (2016)	Aggarwal et al. (2018) Prasad et al. (2014)		
<b><i>Improved crop varieties</i></b>	<b><i>Optimized drainage</i></b>		
Sardar et al. (2020), Khatri - Chhetri et al. (2016), Aryal et al. (2017), Ochieng et al. (2016)	Rao et al. (2016), Khatri - Chhetri et al. (2016)		
<b><i>Integrated Pest management</i></b>	<b><i>Community tanks/ ponds</i></b>		
Khatri - Chhetri et al. (2016) Bairagi et al. (2020)	Prasad et al. (2014)		
	<b><i>Laser Land leveling</i></b>		
	Khatri - Chhetri et al. (2016), Aryal et al. (2017)		

Asia and Sub-Saharan Africa and was filtered down to 17 studies using the search term “climate AND smart AND agricultural AND Sub-Saharan African OR South Asian AND countries.” The criteria for the section of literature is given in Table 1.

## RESULTS AND DISCUSSION

### Climate-Smart Agriculture

The application of adaptation and resilient strategies in agriculture to increase the system’s capability to react to various climate-related shocks by preventing harm and ensuring a quick rebound is called CSA (Mathews 2016, Newsham et al. 2024). Droughts, floods, heat/cold waves, unpredictable rainfall patterns, insect outbreaks, and other climate-related risks are such disruptions (Rao et al. 2016, Aggarwal et al. 2018, Rahaman et al. 2019, Jiri

et al. 2017, Bairagi et al. 2020, Makate et al. 2018). In the wake of the climate crisis, CSA provides a strategy for meeting short- and long-term agricultural output targets while also serving as a doorway to other developmental activities. Its objective is to assist nations and other stakeholders in setting up the legislative, technological, and financial frameworks necessary to (a) enhance farm yields and earnings sustainably to fulfill goals for food security and development, (b) establish resilient agricultural food networks to cope with climate change, and (c) try to find ways to reduce greenhouse gas (GHG) emissions and boost carbon sinks. The “triple win” of overall CSA is food security, adaptation, and mitigation (Mwongera et al. 2017, Sardar et al. 2020). Food security, adaptation, mitigation, and ecosystem restoration are the four pillars that underpin our understanding of CSA (Fig. 3). For example, “sustainability” has important

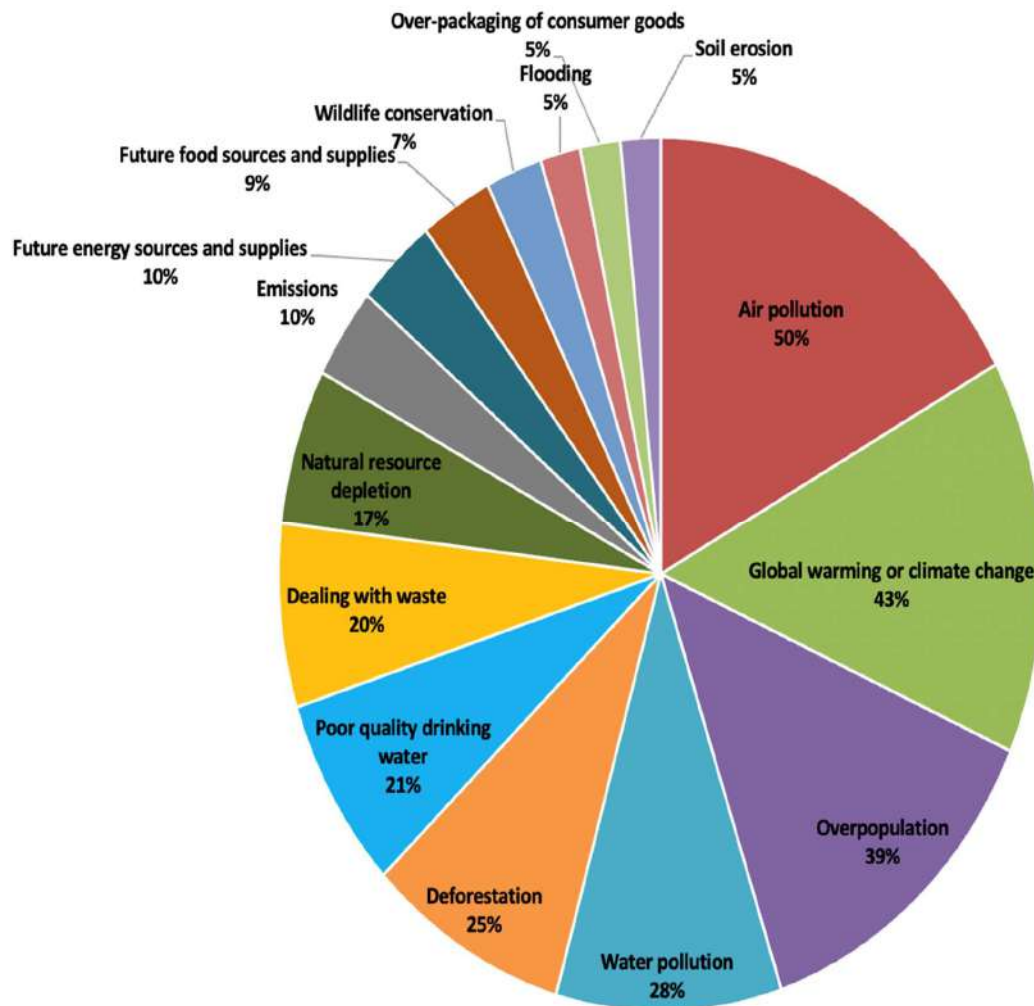


Fig. 1: Most concerning environmental issues according to citizens across India (Statista 2019).



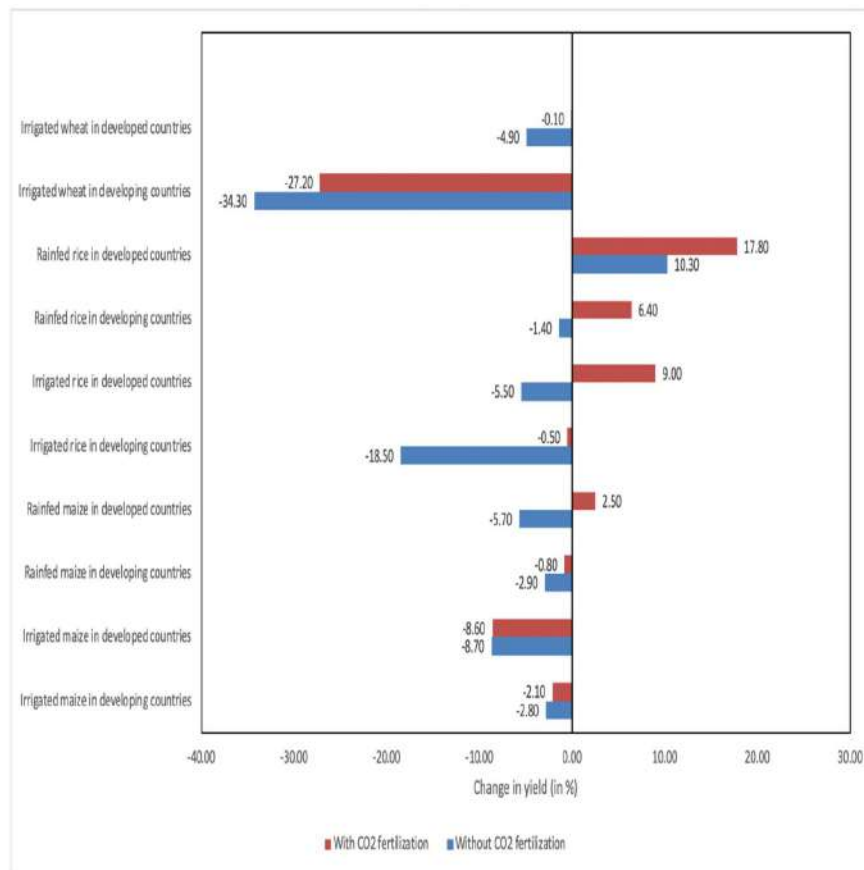


Fig. 2: Climate-change-induced yield effects from 2000 to 2050 by grain, based on NCAR estimates (in percent).

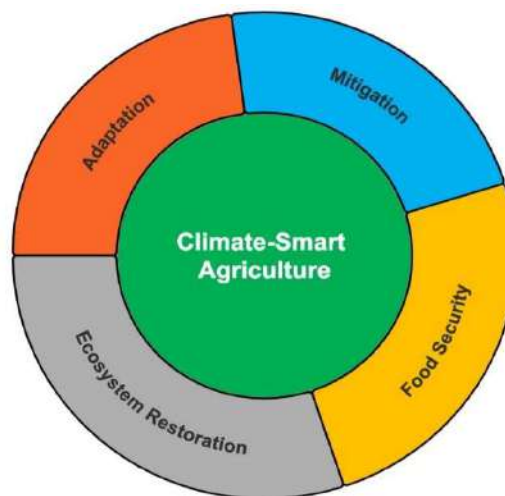


Fig. 3: Description of the Framework to Understand CSA.

implications and nuances for food and nutrition security and adaptability pillars. Although the environmental component of sustainability can be put under the

mitigation pillar, ecosystem restoration requires its pillar. The authors feel that explicitly mentioning ecosystem restoration will help CSA acceptance.

Adaptation relates to physical resilience in the face of climatic sensitivity, such as increasing temperatures, improved efficiency of rainwater utilization, and uncertain or shrinking seasons (Priya & Rahamathunnisa 2024, Subbarayudu & Kubendiran 2024). Adaptation attempts can reduce the adverse effects of climate shocks, ranging from minor to significant adjustments in strategy that can result in farming system transformation. Enhancing water storage options and intensifying institutional arrangements promoting coordinated effort, information sharing, and local adaptation planning are all benefits of developing an ecosystem beneath an agro-ecology that increases resilience, makes it possible to acquire poultry, livestock, and crop varieties that are heat, drought, and flood-tolerant (Guja & Bedeke 2024).

Mitigation is a crucial CSA pillar that reduces environmental impact on the food supply, as agriculture is a major source of anthropogenic emissions and ecological degradation. Measuring mitigation actions using GHG emissions, such as carbon dioxide, methane, and nitrogen oxides, helps compare them to natural emissions and other industries. Continuous observations can detect emissions variations and extremes (Nisbet et al. 2020). The pillar of food security, often equated with production, overlooks two essential features: sustainability and oversimplification (Dyball et al. 2020). Sustainable farming involves producing target output over decades, recovering from climatic stresses, and maintaining ecological sustainability (Ghosh et al. 2024b). Developing indicators and metrics to apply general principles in specific settings has increased the complexity of dividing the CSA into three distinct pillars. CSA practices can contribute to ecosystem restoration, promoting sustainable development and boosting agricultural productivity. They address food insecurity, climate change, and environmental protection. Farmers in underdeveloped countries embrace CSA as a reassuring way to increase crop yield and ensure food security. Rural transformation and decision-making support for adaptation are essential, and resources must be allocated to maximize agricultural system gains under climatic variability. Implementing CSAs helps develop a robust, sustainable farming system capable of increasing productivity regardless of the changing climate (Dyball et al. 2020).

### **Climate-Smart Agriculture Practices**

Farmers and other stakeholders worldwide are embracing various climate-smart practices, technologies, and initiatives to alleviate the adverse impacts of changing climate. In such endeavors, both traditional and modern farming methods are used (Ma & Rahut 2024). We classify and describe agricultural adaptation options to

climate change in a systematic approach. Climate-smart farming approaches are primarily concerned with (a) crop management, (b) water management, (c) land management, and (d) livelihood management from a broader viewpoint. The following is a summary of these approaches as documented in the literature. Table 2 summarizes the essential CSA practices described in the literature.

### **Crop Management Strategies**

Many agricultural systems grow crops for food, textiles, and feedstock. Each system is influenced by various socio-economic, climatic, and soil elements. Some are irrigated, while others rely on rain. There is much focus on the variety of crop production methods that could be deemed “climate-smart,” either in terms of adaptation or mitigation capacity. This section will examine how ‘crop-specific’ technologies can help farmers become climate-smart.

Crop rotation (Mensah et al. 2020, Issahaku & Abdulai 2019, Ochieng et al. 2016), drought/flood tolerant seed varieties (Rao et al. 2016, Aggarwal et al. 2018, Rahaman et al. 2019, Jiri et al. 2017, Bairagi et al. 2020, Makate et al. 2018), short-season crops (Rao et al. 2016), legume intercropping (Nyasimi et al. 2017, Khatri - Chhetri et al. 2016), Integrated Nutrient Management (Teklewold et al. 2017, Aryal et al. 2015), Improved crop varieties (Sardar et al. 2020), Integrated Pest Management (Bairagi et al. 2020) and changing planting dates (Sardar et al. 2020) are all standard climate-smart crop management practices.

Farmers have traditionally produced long-lasting local crops, exposing a portion of the crop’s growth to rainfall shortages or excesses and lowering crop production (Rao et al. 2016). Numerous factors impact crop development and yield depending on the amount and length of dry periods or excessive moisture circumstances (Nyasimi et al. 2017, Jiri et al. 2017). Most improved and high-yielding cultivars resist dryness, which happens toward the close of the agricultural growing season, especially in regions with rainfall of less than 750 mm, because they have a short growing season.

In rainfed locations, moisture deficits and excesses are common throughout the season, especially in places with more than 1000 mm of rainfall (Rashid & Rasul 2011). These cultivars ought to be resilient to both excessive and insufficient rainfall. A stable strategy for intercropping that allows the system to function better in the face of unpredictable rainfall is using a balance of short-term and long-term crops, shallow- and deep-

root plants, and leguminous and non-leguminous crops. Furthermore, synergy and complementarity are better used when legume and nonlegume crops are cultivated together (Makate et al. 2018). When compared to single cropping, crop rotation that allows for dual cropping is among the resilient strategies because it enables the farmer to boost earnings from both harvests during years of abundant rainfall and to sustain the second harvest even though the first crop is damaged by either an excess or a shortage of moisture (Mensah et al. 2020). During the rainy and post-rainy seasons, short-duration crops can help farmers achieve sustainable agricultural intensification (Rao et al. 2016). Both crops must complete their life cycles between June and October when most rainfall occurs.

### Water Management

Agriculture uses most of the world's freshwater resources, accounting for 70% of the total supply, with rice accounting for over 40% (Mancosu et al. 2015). The water crisis is a serious concern as the global population grows and demands more food, industry develops, and urbanization intensifies. New water management techniques are required. Water management has a broad and complex scope, given the significance of water for agricultural purposes, as shown by numerous other studies (Langemeyer et al. 2021). Improved water management in rainfed agriculture can be achieved through Improving irrigation use efficiency (Teklewold et al. 2017), Micro-irrigation technologies (Sardar et al. 2020, Ochieng et al. 2016), solar pumps (Aggarwal et al. 2018), (rainwater harvesting (Prasad et al. 2014), Onsite moisture conservation (Jiri et al. 2017), Aquifer recharge/ recharge of wells (Aggarwal et al. 2018), Optimised drainage (Rao et al. 2016), Community tank/ ponds (Prasad et al. 2014) and, Laser Land leveling (Khatri - Chhetri et al. 2016). Water management can be improved at several stages of irrigation, including water supply through transportation and delivery methods, scheduling, and water availability in the plant's root system to boost water consumption effectiveness in irrigated systems.

Water management is crucial for agriculture's survival in a world with depleting and contaminated freshwater resources (Ding et al. 2021). Irrigation management techniques like deficit irrigation, desalination, and water market mechanisms are evolving to address climate change. Water-conserving micro-irrigation systems are more common in drought-prone areas (Dhawan 2017). Integrated water management encourages using discarded and surplus

water for farming purposes. Water storage, an ancient Indian tradition, increases agricultural productivity and resilience (Rao et al. 2016). Laser leveling, a technique that flattens the ground surface, can decrease irrigation duration and boost yield. Rainwater collection is a time-honored method for saving water (Prasad et al. 2014). Rejuvenating existing watersheds is an effective technique for reducing climate unpredictability and droughts (Nyasimi et al. 2017, Ali et al. 2018). Aryal et al. (2020) found that compared to conventionally leveled regions, laser leveling in paddy fields decreased irrigation duration by 40-70 hours per hectare per season and boosted yield by about 7%. In arid locations, rainwater collection is a time-honored means of saving water.

### Land Management

Sustainable land management is "the use of land resources, such as soils, water, animals, and plants, for the production of goods to fulfill changing human demands while ensuring these resources' long-term productive potential and environmental functions" (Branca et al. 2013). For agriculture to be sustainable and productive, soil health must be maintained or enhanced (Ochieng et al. 2016, Teklewold et al. 2017). With 'healthy' soil, agricultural productivity will be pushed closer to the limits determined by soil type and climate. Soil conservation (Issahaku & Abdulai, 2019), Mulching (Rao et al. 2016, Rahaman et al. 2019), and Minimum tillage/ Zero tillage (Aryal et al. 2017, Makate et al. 2018) are all land management techniques used by smallholder farmers as resilience strategies.

Soil health is a significant concern in many regions due to human and animal populations, overstocking, and overgrazing (Mensah et al. 2020). The minimum tillage concept, which avoids primary tillage, offers benefits such as less soil compaction, more fertile soils, reduced moisture evaporation, lower fuel and labor costs, and reduced soil erosion (Aggarwal et al. 2018, Makate et al. 2018). Conservation agriculture, which combines reduced tillage, soil cover preservation, and crop rotation variation, produces agricultural output similar to conventional agriculture (Rahaman et al. 2019). Research in West Africa has shown higher cereal yields through parkland management, mulching, crop rotation, and conventional soil and water conservation techniques (Bayala et al. 2012).

### Livelihood Management

Agriculture is the lifeblood of many rural households in the study area. Thus, establishing climate-smart agricultural systems is crucial, particularly for

developing and emerging economies (Pretty 2008). In developing countries, many poor rural households are compelled to relocate to urban areas in the hope of employment (Alam et al. 2017). Climate-induced migration is seen as an economic or survivability strategy in many emerging countries (Jha et al. 2017), with agricultural communities seeing migration as a way to supplement their income or maintain their livelihood security. South Asian and African countries use agroforestry and integrated farming as additional livelihood management measures (Dhyani et al. 2021). Over 1 billion people in developing nations use agroforestry to preserve farming output and livelihood (Quandt et al. 2019).

Agroforestry systems involve integrated activities like upgraded fallows, multilayered trees, and crop gardens. They are widely adopted for climate adaptation and mitigation, boosting crop productivity and food security (Dagar & Tewari 2017). Forests provide essential services to over 65 million native people and contribute to one-fourth of global emissions. Afforestation can increase forestry capacity on farms, acting as carbon sinks, but agriculture is the primary driver of deforestation (Maja & Ayano 2021).

Agroforestry (Khatri - Chhetri et al. 2016), Crop Livestock integrated farming (Rahaman et al. 2019), Climate Smart Housing for livestock (Rao et al. 2016) and Crop Diversification (Jiri et al. 2017), Fodder production and storage (Nyasimi et al. 2017) are all viable methods. Still, they must be addressed in the backdrop of the greater landscape. Improved shelters for reducing heat stress in livestock, managing fish ponds/tanks during water scarcity, and excess water act as climate-smart housing strategies (Khatri-Chhetri et al. 2016).

Agroforestry and cocoa agroforestry are effective systems for providing high-quality timber and fruits in Vietnam and West and Central Asia (Nguyen et al. 2013). Long-term solutions involve integrated agricultural systems, combining crop production with livelihood practices like livestock management (Béné et al. 2019). This promotes agrobiodiversity, food-based land resource management, and agroecosystem resilience. Small farmers in Asia use crop-livestock-integrated farming for resource utilization, diversification, and production (Aggarwal et al. 2018, Rahaman et al. 2019). Integrated rice-fish farming is better than monoculture farming as it increases soil fertility, decreases chemical fertilizers, and reduces greenhouse gas emissions.

According to our review, rural households worldwide are experimenting with various climate-smart practices linked to crop management, land

and water management, and livelihood maintenance. However, the success and scalability of these approaches differ by region (Mwongera et al. 2017). Many of these solutions, nevertheless, necessitate substantial legislative, organizational, and assistance from states, which the private sector's technology and service providers ably offer. Considering the importance of laws and institutions in supporting the uptake of novel and innovative climate-smart agricultural systems, we will investigate the role of enabling environments for CSA adoption in the next section.

### **Enabling Environment for CSA**

Enabling environments for Climate Change (CSA) are framework conditions that encourage the adoption of climate-smart technology and practices, including policy, institutional systems, stakeholder engagement, facilities, insurance schemes, and advisory services, facilitating a long-term transition and broader CSA deployment.

### **Agricultural Insurance**

Smallholder farmers in low-income countries are frequently locked in poverty due to their inability to invest in better farm practices due to climate uncertainties (Hansen et al. 2019). Agricultural insurance, a popular risk-management approach, is often based on directly assessing a farmer's damage. Furthermore, evaluating field losses is expensive and time-consuming, especially when many smallholder farmers cannot incur cost overruns.

However, Index-based insurance provides a viable option as it is based on meteorological data (Hochrainer-Stigler et al. 2014). A weather index is based on specific meteorological parameters measured at a given weather station over a pre-determined period. Using weather indexes to aim for insurance pay-outs may make insurance schemes more accessible and appealing to farmers than standard agricultural insurance. Farmers may be readier to take on the risk of investing in climate-smart agriculture due to this safety net., such as rainfall, to establish pay-outs for clearly defined dangers. Payments are made swiftly, with fewer administrative costs and lower rates than traditional crop insurance (Sun et al. 2024).

Index insurance, typically linked with credit facilities, enables farmers to take further risks by investing in resilience practices that surprisingly boost production and food security in severe climate circumstances. Rainfall in various parts of the world



varies significantly regarding overall season levels and geographic distribution. Smallholders are necessarily exposed to the danger of animal loss, crop output decline, or crop failure under such circumstances. Index insurance mitigates these risks and hence contributes significantly to farmer resilience. According to climate change forecasts, rainfall levels would likely decrease, and rainfall unpredictability will likely increase in many locations. Index insurance will become an essential adaptation method in such areas, but premiums may also have to rise (Sun et al. 2024, Hansen et al. 2019).

### **Climate Information Services**

Climate change increases the frequency and severity of extreme weather events, making small-scale farmers vulnerable. They rely on traditional coping strategies to manage risks and capitalize on favorable conditions. However, the availability of climate information is inadequate for smallholder farmers. By effectively using weather information services, farmers can control the negative consequences of climate hazards during bad seasons and reap the benefits of regular and better-than-average seasons. This will help them adapt to climate change and minimize their sensitivity to climate hazards (Tall et al. 2018).

### **Infrastructure**

Agriculture relies heavily on infrastructural and physical capital, like roads, machinery, and facilities, which are all sensitive to severe weather (Reardon & Zilberman 2018). Climate disasters pose an extreme risk to the farming sector regarding possible economic loss (Sivakumar 2021). This is especially the case when fixed assets are valued at a high percentage of annual productivity and agriculture income. As a result, preventative activities and tools to deal with possible harm to agriculture facilities are required. Additionally, for these efforts to be successful, they must be adapted to area features.

Adaptation measures in policy-making, planning, and financing can enhance rural infrastructure resilience (Kuhl 2021). Climate change necessitates changes to building standards and norms. Indigenous methods are used in low-cost climate-proofing construction projects (Brown & Kernaghan 2011). National structural responses include revamping transport corridors, bridges, dams, and distribution centers (Dale et al. 2011). Inter-sectoral planning is crucial for coordination and sensitivity to climate change fluctuations. Climate-smart infrastructure investments boost farm output and livelihoods but insulate assets from climate change's adverse effects. They can withstand short-term

threats and help the agricultural sector adapt to long-term implications (Shakou et al. 2019).

### **Policy Engagement**

The adoption of Climate Change Strategies (CSA) requires the development and execution of policies that create an enabling environment for efficient and sustainable development. This environment includes economic, legal, organizational, political, and cultural issues (Lipper et al. 2014, Visser et al. 2019). Stakeholders, including agriculture, food security, commerce, economics, agrarian, and environmental, must collaborate to reconcile disputes and establish the necessary institutional framework. The policy should include various actors, not just state policy (Campbell et al. 2016, Anderl & Hißen 2024). Regulations, policies, and funding can significantly enhance the viability of CSA by removing barriers, increasing competencies, engaging marginalized groups, and making resources available (Makate 2019). Climate adaptation policies can incentivize adaptation, while popular initiatives can enhance adaptive capacity and sustainable agriculture.

### **Institutional Arrangements**

Institutions play a crucial role in agricultural growth and sustainable lives, facilitating climate-smart farming practices and guiding farm owners and decision-makers (Fusco et al. 2020). Proper institutional frameworks are essential for CSA policy implementation. Local frameworks should promote farmer-driven uptake and adaptability, requiring the establishment of new institutions and strengthening ties among existing organizations. Local governments and state agencies are essential for directing climate change adaptation and mitigation assistance.

The lack of suitable structures, institutional competency, and higher-level coordination thwarts efforts to aid CSA. To execute changes on the ground, farmers need incentives and enabling conditions, which institutions and practices must provide. The development and dissemination of knowledge about technology possibilities and management strategies, climatic variability, and value chain circumstances are particularly crucial for state entities. Furthermore, national institutions are critical in providing farmers with safety nets and insurance plans. Developing knowledge base and capabilities, strengthening institutional procedures, incorporating climate change and CSA into strategic policy plans, bolstering horizontal and vertical institutional and sector collaboration, and analyzing deconcentration and decentralization options are among the offerings

for boosting institutional efficiency (Lipper et al. 2014, Campbell et al. 2016).

### Gender and Social Inclusion

Climate-smart agriculture techniques require local solutions, but understanding stakeholders' needs and challenges is crucial. Gender relationships, power structures, and societal norms can impact the adoption of CSA. Stakeholder involvement can identify gender discrepancies and socio-economic injustices (Aggarwal et al. 2018, Mutenje et al. 2019). Addressing these inequities is crucial for sustainable agriculture and societies. Gender-sensitive and socially inclusive CSA projects should consider the varying awareness levels, attitudes, and constraints of diverse social groups and stakeholders (Mwongera et al. 2017, Khoza et al. 2019).

### RECOMMENDATIONS AND CONCLUSIONS

- Prioritize climate-smart agriculture (CSA) to support sustainable and equitable transitions in agroecosystems and livelihoods across scales, given the emphasis on economic development, poverty reduction, and food security.
- Investigate the situation of CSA in South Asian and Sub-Saharan agricultural systems, identifying priority climate-smart farming practices and enabling conditions for adoption.
- Implement popular CSA practices in South Asia and Sub-Saharan Africa, including crop rotation, drought/flood tolerant crops, legume intercropping, changing planting dates, rainwater harvesting, agroforestry, micro-irrigation, minimum tillage, and integrated crop-livestock farming.
- Create an enabling environment for CSA adoption by establishing solid institutions, supportive policies, infrastructure, agricultural insurance, climate information services, and promoting gender and social inclusion.
- Mainstream CSA into agriculture policies and programs, as technology-oriented interventions alone are insufficient for sustainable agricultural transformation.
- Increase awareness of CSA as a viable approach for mitigating the negative effects of climate change.
- Facilitate and support decision-making for adaptation by considering the complexities of farming systems while also understanding the contextual factors and motivations that influence smallholder farmers' capacity to adopt various climate-smart agriculture (CSA) practices.

- Build the capacity of agricultural households and institutions to comprehend and address the multifaceted problems posed by climate change.
- Research and development play a vital role in identifying and disseminating CSA practices that enhance smallholder livelihoods and employment.

### REFERENCES

- Aggarwal, P.K., Jarvis, A., Campbell, B.M., Zougmore, R.B., Khatri-Chhetri, A., Vermeulen, S.J., Loboguerrero, A.M., Sebastian, L.S., Kinyangi, J., Bonilla-Findji, O., Radeny, M., Recha, J., Martinez-Baron, D., Ramirez-Villegas, J., Huyer, S., Thornton, P., Wollenberg, E., Hansen, J., Alvarez-Toro, P. and Yen, B.T., 2018. The climate-smart village approach: Framework of an integrative strategy for scaling up adaptation options in agriculture. *Ecology and Society*, 23(1), pp.230-246. [DOI]
- Alam, G.M.M., Alam, K. and Mushtaq, S., 2017. Climate change perceptions and local adaptation strategies of hazard-prone rural households in Bangladesh. *Climate Risk Management*, 17, pp.52-63. [DOI]
- Ali, A., Hussain, I., Rahut, D.B. and Erenstein, O., 2018. Laser-land leveling adoption and its impact on water use, crop yields, and household income: Empirical evidence from the rice-wheat system of Pakistan Punjab. *Food Policy*, 77, pp.19-32. [DOI]
- Anderl, F. and Hißen, M., 2024. How trust is lost: the Food Systems Summit 2021 and the delegitimation of UN food governance. *European Journal of International Relations*, 30(1), pp.151-175.
- Aryal, J.P., Jat, M.L., Sapkota, T.B., Khatri-Chhetri, A., Kassie, M., Rahut, D.B. and Maharjan, S., 2017. Adoption of multiple climate-smart agricultural practices in the Gangetic plains of Bihar, India. *International Journal of Climate Change Strategies and Management*, 10(3), pp.407-427. [DOI]
- Aryal, J.P., Mehrotra, M.B., Jat, M.L. and Sidhu, H.S., 2015. Impacts of laser land leveling in rice-wheat systems of the north-western Indo-Gangetic plains of India. *Food Security*, 7(3), pp.725-738. [DOI]
- Aryal, J.P., Sapkota, T.B., Rahut, D.B., Krupnik, T.J., Shahrin, S., Jat, M.L. and Stirling, C.M., 2020. Major climate risks and adaptation strategies of smallholder farmers in coastal Bangladesh. *Environmental Management*, 66(1), pp.105-120. [DOI]
- Bairagi, S., Mishra, A.K. and Durand-Morat, A., 2020. Climate risk management strategies and food security: Evidence from Cambodian rice farmers. *Food Policy*, 95, 101935. [DOI]
- Bayala, J., Sileshi, G.W., Coe, R., Kalinganire, A., Tchoundjeu, Z., Sinclair, F. and Garrity, D., 2012. Cereal yield response to conservation agriculture practices in drylands of West Africa: A quantitative synthesis. *Journal of Arid Environments*, 78, pp.13-25. [DOI]
- Béné, C., Oosterveer, P., Lamotte, L., Brouwer, I.D., de Haan, S., Prager, S.D., Talsma, E.F. and Khoury, C.K., 2019. When food systems meet sustainability—Current narratives and implications for actions. *World Development*, 113, pp.116-130. [DOI]
- Branca, G., Lipper, L., McCarthy, N. and Jolejole, M.C., 2013. Food security, climate change, and sustainable land management. A review. *Agronomy for Sustainable Development*, 33(4), pp.635-650. [DOI]
- Brown, A. and Kernaghan, S., 2011. Beyond climate-proofing: Taking an integrated approach to building climate resilience in Asian Cities. *UGEC Viewpoints*, 6, pp.4-7.
- Campbell, B.M., Vermeulen, S.J., Aggarwal, P.K., Corner-Dolloff, C., Girvetz, E., Loboguerrero, A.M., Ramirez-Villegas, J., Rosenstock, T., Sebastian, L., Thornton, P.K. and Wollenberg, E., 2016. Reducing risks to food security from climate change. *Global Food Security*, 11, pp.34-43. [DOI]
- Dagar, J.C. and Tewari, V.P., 2017. Evolution of agroforestry as a modern science. In *Agroforestry*, pp.13-90. Springer.

- Dale, V.H., Efromymson, R.A. and Kline, K.L., 2011. The land use–climate change–energy nexus. *Landscape Ecology*, 26(6), pp.755–773. [DOI]
- Dhawan, V., 2017. Water and agriculture in India. In *Background paper for the South Asia expert panel during the Global Forum for Food and Agriculture*, p.28.
- Dhyani, S., Murthy, I.K., Kadaverugu, R., Dasgupta, R., Kumar, M. and Gadpayle, K.A., 2021. Agroforestry to achieve global climate adaptation and mitigation targets: Are South Asian countries sufficiently prepared? *Forests*, 12(3), 303. [DOI]
- Ding, Z., Ali, E.F., Elmahdy, A.M., Ragab, K.E., Seleiman, M.F. and Kheir, A.M.S., 2021. Modeling the combined impacts of deficit irrigation, rising temperature, and compost application on wheat yield and water productivity. *Agricultural Water Management*, 244, p.106626. [DOI]
- Dyball, R., Davila, F. and Wilkes, B., 2020. A human ecological approach to policy in the context of food and nutrition security. *Handbook of Systems Sciences*, 1, pp.1–26.
- Fusco, G., Melgiovanni, M., Porrini, D. and Ricciardo, T.M., 2020. How to improve the diffusion of climate-smart agriculture: What the literature tells us. *Sustainability*, 12(12), p.5168. [DOI]
- Ghosh, A., Kumar, A. and Biswas, G., 2024a. Exponential population growth and global food security: challenges and alternatives. *Bioremediation of Emerging Contaminants from Soils*, pp.1–20.
- Ghosh, A., Sharma, P., Vashisht, D., Malik, P., Mondal, A. and Mondal, S., 2024b. Socio-economic-environmental challenges at Himachal villages: Findings from five Unnat Bharat Abhiyan adopted villages. *GeoJournal*, 89(1), p.3. [DOI]
- Goli, I., Kriauciūnienė, Z., Zhang, R., Bijani, M., Koohi, P.K., Rostamkalaei, S.A. and Azadi, H., 2024. Contributions of climate-smart agriculture toward climate change adaptation and food security: The case of Mazandaran Province, Iran. *Trends in Food Science & Technology*, p.104653.
- Guja, M.M. and Bedeke, S.B., 2024. Smallholders' climate change adaptation strategies: exploring effectiveness and opportunities to be capitalized. *Environment, Development and Sustainability*, pp.1–30.
- Hansen, J., Hellin, J., Rosenstock, T., Fisher, E., Cairns, J., Stirling, C., Lamanna, C., van Etten, J., Rose, A. and Campbell, B., 2019. Climate risk management and rural poverty reduction. *Agricultural Systems*, 172, pp.28–46. [DOI]
- Hochrainer-Stigler, S., van der Velde, M., Fritz, S. and Pflug, G., 2014. Remote sensing data for managing climate risks: Index-based insurance and growth-related applications for smallholder farmers in Ethiopia. *Climate Risk Management*, 6, pp.27–38. [DOI]
- Ipsos, 2017. Most concerning environmental issues according to citizens across India as of March 2019. *Statista* [viewed 12 June 2022]. Available at Link
- Issahaku, G. and Abdulai, A., 2019. Can farm households improve food and nutrition security through the adoption of climate-smart practices? Empirical evidence from Northern Ghana. *Applied Economic Perspectives and Policy*, 42(3), pp.559–579. [DOI]
- Jarvis, A., Upadhyaya, H.D., Gowda, C.L.L., Agrawal, P.K., Fujisaka, S. and Anderson, B., 2008. Climate Change and Its Effect on Conservation and Use of Plant Genetic Resources for Food and Agriculture and Associated Biodiversity for Food Security. *FAO*.
- Jellason, N.P., Conway, J.S. and Baines, R.N., 2021. Understanding impacts and barriers to adoption of climate-smart agriculture (CSA) practices in North-Western Nigerian drylands. *Journal of Agricultural Education and Extension*, 27(1), pp.55–72. [DOI]
- Jha, C.K., Gupta, V., Chatopadhyay, U. and Amarayil Sreeraman, B.A., 2017. Migration as an adaptation strategy to cope with climate change: A study of farmers' migration in rural India. *International Journal of Climate Change Strategies and Management*, 10(1), pp.121–141. [DOI]
- Jiri, O., Mafongoya, P.L. and Chivenge, P., 2017. Building climate change resilience through adaptation in smallholder farming systems in semi-arid Zimbabwe. *International Journal of Climate Change Strategies and Management*, 9(2), pp.151–165. [DOI]
- Khatri-Chhetri, A., Aggarwal, P.K., Joshi, P.K. and Vyas, S., 2016. Farmers' prioritization of climate-smart agriculture (CSA) technologies. *Agricultural Systems*, 151, pp.184–191. [DOI]
- Khoza, S., Van Niekerk, D. and Nemaconde, L.D., 2019. Understanding gender dimensions of climate-smart agriculture adoption in disaster-prone smallholder farming communities in Malawi and Zambia. *Disaster Prevention and Management: An International Journal*.
- Khurshid, N., Sharif, H., Tabash, M.I. and El Refae, G.A., 2024. An assessment of the asymmetric impact of financial stability and agricultural subsidies on agricultural production in Pakistan. *Journal of Agribusiness in Developing and Emerging Economies*.
- Kuhl, L., 2021. Policy making under scarcity: Reflections for designing socially just climate adaptation policy. *One Earth*, 4(2), pp.202–212. [DOI]
- Langemeyer, J., Madrid-Lopez, C., Mendoza Beltran, A. and Villalba Mendez, G., 2021. Urban agriculture—A necessary pathway towards urban resilience and global sustainability? *Landscape and Urban Planning*, 210, p.104055. [DOI]
- Lima, F.P. and Wethey, D.S., 2012. Three decades of high-resolution coastal sea surface temperatures reveal more than warming. *Nature Communications*, 3(1), p.704. [DOI]
- Lipper, L., Thornton, P., Campbell, B.M., Baedeker, T., Braimoh, A., Bwalya, M., Caron, P., Cattaneo, A., Garrity, D., Henry, K., Hottle, R., Jackson, L., Jarvis, A., Kossam, F., Mann, W., McCarthy, N., Meybeck, A., Neufeldt, H., Remington, T. and Torquebiau, E.F., 2014. Climate-smart agriculture for food security. *Nature Climate Change*, 4(12), pp.1068–1072. [DOI]
- Ma, W. and Rahut, D.B., 2024. Climate-smart agriculture: adoption, impacts, and implications for sustainable development. *Mitigation and Adaptation Strategies for Global Change*, 29(5), p.44.
- Maja, M.M. and Ayano, S.F., 2021. The impact of population growth on natural resources and farmers' capacity to adapt to climate change in low-income countries. *Earth Systems and Environment*, 5(2), pp.271–283.
- Makate, C., 2019. Effective scaling of climate-smart agriculture innovations in African smallholder agriculture: A review of approaches, policy, and institutional strategy needs. *Environmental Science and Policy*, 96, pp.37–51.
- Makate, C., Makate, M., Mango, N. and Siziba, S., 2018. Increasing resilience of smallholder farmers to climate change through multiple adoptions of proven climate-smart agriculture innovations. Lessons from Southern Africa. *Journal of Environmental Management*, 231, pp.858–868.
- Mancosu, N., Snyder, R.L., Kyriakakis, G. and Spano, D., 2015. Water scarcity and future challenges for food production. *Water*, 7(12), pp.975–992.
- Mathews, J.A., 2016. Building resilience to climate risk in the agricultural sector through adaptation education using a climate-smart approach: the case of the Mooifontein region, North-West province. *Doctoral dissertation, North-West University (South Africa), Potchefstroom Campus*.
- Mensah, H., Ahadzie, D.K., Takyi, S.A. and Amponsah, O., 2020. Climate change resilience: Lessons from local climate-smart agricultural practices in Ghana. *Energy, Ecology and Environment*, 6(3), pp.271–284.
- Mishra, N., Ghosh, A. and Biswas, G., 2024. Perspectives of crop improvement techniques and green chemistry towards sustainable agriculture. In *Role of Green Chemistry in Ecosystem Restoration to Achieve Environmental Sustainability*, pp.343–351.
- Mutenje, M.J., Farnworth, C.R., Stirling, C., Thierfelder, C., Mupangwa, W. and Nyagumbo, I., 2019. A cost-benefit analysis of climate-smart agriculture options in Southern Africa: Balancing gender and technology. *Ecological Economics*, 163, pp.126–137.
- Mwongera, C., Shikuku, K.M., Twyman, J., Läderach, P., Ampaire, E.,



- Van Asten, P., Twomlow, S. and Winowiecki, L.A., 2017. Climate-smart agriculture rapid appraisal (CSA-RA): A tool for prioritizing context-specific climate-smart agriculture technologies. *Agricultural Systems*, 151, pp.192–203.
- Nelson, G.C., Rosegrant, M.W., Koo, J., Robertson, R., Sulser, T., Zhu, T. and Lee, D., 2009. Climate change: Impact on agriculture and costs of adaptation. *International Food Policy Research Institute (Vol. 21)*.
- Newsham, A., Naess, L.O., Mutabazi, K., Shonhe, T., Boniface, G. and Bvute, T., 2024. Precarious prospects? Exploring climate resilience of agricultural commercialization pathways in Tanzania and Zimbabwe. *Climate and Development*, 16(5), pp.395–409.
- Nisbet, E.G., Fisher, R.E., Lowry, D., France, J.L., Allen, G., Bakkaloglu, S. and Zazzeri, G., 2020. Methane mitigation: Methods to reduce emissions on the path to the Paris agreement. *Reviews of Geophysics*, 58(1), e2019RG000675.
- Nyasimi, M., Kimeli, P., Sayula, G., Radeny, M., Kinyangi, J. and Mungai, C., 2017. Adoption and dissemination pathways for climate-smart agriculture technologies and practices for climate-resilient livelihoods in Lushoto, Northeast Tanzania. *Climate*, 5(3), p.63. [DOI]
- Ochieng, J., Kirimi, L. and Mathenge, M., 2016. Effects of climate variability and change on agricultural production: The case of small-scale farmers in Kenya. *NJAS*, 77(1), pp.71–78. [DOI]
- Prasad, Y.G., Maheswari, M., Dixit, S., Srinivasarao, C., Sikka, A.K., Venkateswarlu, B., Sudhakar, N., Kumar, S.P., Singh, A.K., Gogoi, A.K. and Singh, A.K., 2014. Smart practices and technologies for climate-resilient agriculture.
- Pretty, J., 2008. Agricultural sustainability: Concepts, principles, and evidence. *Philosophical Transactions of the Royal Society of London. Series B, Biological Sciences*, 363(1491), pp.447–465. [DOI]
- Priya, R.S. and Rahamathunnisa, U., 2024. A comprehensive study of remote sensing technology for agriculture crop monitoring. *Nature Environment & Pollution Technology*, 23(2). [DOI]
- Quandt, A., Neufeldt, H. and McCabe, J.T., 2019. Building livelihood resilience: What role does agroforestry play? *Climate and Development*, 11(6), pp.485–500. [DOI]
- Rahaman, M.A., Rahman, M.M., and Hossain, M.S., 2019. Climate-resilient agricultural practices in different agroecological zones of Bangladesh. *Handbook of Climate Change Resilience*, pp.1–27. Springer International Publishing.
- Rao, S.C., Gopinath, K.A., Prasad, J.V.N.S., Prasannakumar and Singh, A.K., 2016. Climate resilient villages for sustainable food security in tropical India: Concept, process, technologies, institutions, and impacts. *Advances in Agronomy*, 140, pp.101–214. [DOI]
- Rashid, K. and Rasul, G., 2011. Rainfall variability and maize production over the Potohar Plateau of Pakistan. *Pakistan Journal of Meteorology*, 8(15), pp.63–74.
- Reardon, T. and Zilberman, D., 2018. Climate-smart food supply chains in developing countries in an era of rapid dual change in agrifood systems and the climate. *Natural Resource Management and Policy*, pp.335–351. Springer. [DOI]
- Sardar, A., Kiani, A.K. and Kuslu, Y., 2020. Does adoption of climate-smart agriculture (CSA) practices improve farmers' crop income? Assessing the determinants and its impacts in Punjab Province, Pakistan. *Environment, Development and Sustainability*, 23(7), pp.10119–10140.
- Searchinger, Waite, T.R., Hanson, C., Ranganathan, J., Dumas, P., Matthews, E. and Klirs, C., 2019. *Creating a Sustainable Food Future: A Menu of Solutions to Feed Nearly 10 Billion People by 2050*. World Resource Institute
- Seppelt, R., Klotz, S., Peiter, E. and Volk, M., 2024. Agriculture in a hot world: Why efficiency improvements are not enough to secure our food supply. *Nature*, 91, pp.41–62.
- Shakou, L.M., Wybo, J.L., Reniers, G. and Boustras, G., 2019. Developing an innovative framework for enhancing the resilience of critical infrastructure to climate change. *Safety Science*, 118, pp.364–378. [DOI]
- Sivakumar, M., 2021. Climate change, agriculture adaptation, and sustainability. *Climate Resilience and Environmental Sustainability Approaches*, 67, pp.87–109.
- Srivastava, A., Mondal, A., Siddiqui, N.A. and Tauseef, S.M., 2020. Analysis and quantification of airborne heavy metals and RSPMs in Dehradun City. *Nature Environment and Pollution Technology*, 19(1), pp.325–331.
- Subbarayudu, C. and Kubendiran, M., 2024. A comprehensive survey on machine learning and deep learning techniques for crop disease prediction in smart agriculture. *Nature Environment & Pollution Technology*, 23(2). [DOI]
- Sun, J.L., Tao, R., Wang, J., Wang, Y.F. and Li, J.Y., 2024. Do farmers always choose agricultural insurance against climate change risks? *Economic Analysis and Policy*, 81, pp.617–628.
- Tall, A., Coulibaly, J.Y. and Diop, M., 2018. Do climate services make a difference? A review of evaluation methodologies and practices to assess the value of climate information services for farmers: Implications for Africa. *Climate Services*, 11, pp.1–12. [DOI]
- Teklewold, H., Mekonnen, A., Kohlin, G. and Di Falco, S., 2017. Does adoption of multiple climate-smart practices improve farmers' climate resilience? Empirical evidence from the Nile Basin of Ethiopia. *Climate Change Economics*, 08(1), p.1750001. [DOI]
- United Nations (UN), 2015. *Transforming our world: The 2030 agenda for sustainable development*. UN Publishing.
- Visser, S., Keesstra, S., Maas, G., De Cleen, M. and Molenaar, C., 2019. Soil as a basis to create enabling conditions for transitions towards sustainable land management as a key to achieve the SDGs by 2030. *Sustainability*, 11(23), p.6792. [DOI]
- World Health Organization (WHO), 2021. *The State of Food Security and Nutrition in the World 2021: Transforming Food Systems for Food Security, Improved Nutrition, and Affordable Healthy Diets for All*. WHO
- World Meteorological Organization (WMO), 2015. *Status of the Global Observing System for Climate*. World Meteorological Organization
- Yaongam, R., 2024. *Participation in Agriculture and Well-Being Among Women in Ukhrul District, Manipur*. Doctoral dissertation, Mizoram University.



# Studies on the Effect of the Zinc Oxide Nano Additives along with Rice Bran Biodiesel Diesel Blends into CI Engine to Reduce Pollution

Abhijeet Maurya<sup>1†</sup>, Bhanu Pratap Singh<sup>1</sup> and Ajay Kumar Sharma<sup>2</sup>

<sup>1</sup>Maharishi University of Information Technology, Lucknow, Uttar Pradesh, India

<sup>2</sup>Institute of Engineering and Technology, Lucknow, Uttar Pradesh, India

†Corresponding author: Abhijeet Maurya; abhijeetmaurya007@gmail.com

**Abbreviation:** Nat. Env. & Poll. Technol.

**Website:** www.neptjournal.com

*Received:* 04-06-2024

*Revised:* 23-07-2024

*Accepted:* 06-08-2024

## Key Words:

Rice bran  
Carbon monoxide  
Zinc oxide nano additive  
Biodiesel  
Exhaust emission  
Pollution

## ABSTRACT

Pollution is a major problem for urban cities and their associated industries. The pollution caused by industries is mainly because of the burning of fossil fuels. Some of the pollutants can be controlled by plantation, but the oxides of nitrogen cannot be controlled only by planting trees. Some extra efforts are required to minimize pollution associated with the normal functioning of the shop floor of the industries concerned but not affecting its performance. The fuel that is best for industrial use is the need of the hour. In this study, zinc oxide nanoparticles are used as an additive to the rice bran blended biodiesel and analyze the combustion, performance, and emission parameters in the single-cylinder four-stroke engine water-cooled powered by diesel normally utilized in industries at a constant speed and compression ratio. The available fuel alternatives for testing consist of multiple combinations of diesel fuel and RB biodiesel, each with varying proportions. Furthermore, many gasoline mixes additionally have Zinc Oxide nanoparticles at a concentration of 30 parts per million (ppm). The findings suggest that the brake-specific fuel consumption of Rice bran biodiesel combined with Zinc oxide nano additive exhibits a consistent enhancement, but the brake thermal efficiency declines in comparison to diesel fuel. The concentrations of hydrocarbon (HC) and oxides of nitrogen (NO<sub>x</sub>) have been reduced. However, there has been a small rise in carbon dioxide (CO<sub>2</sub>) and carbon monoxide (CO). When rice bran biodiesel fuel combined with Zinc Oxide nano additive was used, an abnormally high exhaust gas temperature (EGT) was detected. According to this research, the addition of Zinc Oxide nano additive to rice bran biodiesel blends improves performance and decreases the noxious exhaust emissions generated by diesel engines.

## Citation for the Paper:

Maurya, A., Singh, B. P., and Sharma, A. K., 2025. Studies on the effect of zinc oxide nano additives along with rice bran biodiesel diesel blends into CI engine to reduce pollution. *Nature Environment and Pollution Technology*, 24(2), p. B4225. <https://doi.org/10.46488/NEPT.2025.v24i02.B4225>

*Note: From year 2025, the journal uses Article ID instead of page numbers in citation of the published articles.*



**Copyright:** © 2025 by the authors

**Licensee:** Technoscience Publications

This article is an open access article distributed under the terms and conditions of the Creative Commons Attribution (CC BY) license (<https://creativecommons.org/licenses/by/4.0/>).

## INTRODUCTION

Rapidly increasing pollution in the urban cities of popular countries is harmful to human health. Most of the polluted content raised by diesel engine-driven industries is inevitable, and reducing these toxic elements from the atmosphere becomes impossible. The use of fossil fuels in industries is responsible for greenhouse gases and affects human health directly. Due to the unexpected rise in harmful toxicities, numerous alternative fuels have been taken for compensation in place of diesel fuel, taking into consideration the accessibility, financial, and technical suitability. Thus, because it is possible to lower the maximum toxicity and increase the life of the engines in comparison to diesel fuel, biodiesel is an alternative energy source that is appropriate and sustainable enough to be used (Verma et al. 2021). Possible developing countries like India are producing biodiesels such as mahua oil, neem oil, rice bran oil, Pongamia oil, soyabean oil, jatropha oil, etc., from non-edible oils (van Gerpen 2004). Rice bran biodiesel is mandatory because the large waste of rice bran is readily available in India.

Diesel engines that run on biodiesel may cut emissions the sulfur, hydrocarbon, and carbon monoxide exhaust emissions while increasing the NO<sub>x</sub> because higher oxygen content is available in the biodiesel. The immense availability of

oxygen is ascribed to complete combustion. Due to this, the temperature increases in the chamber, and it leads to nitrogen oxide. To accomplish these issues from biodiesel, the zinc oxide nanoparticle is used as an additive because it has catalytic properties, and due to this property, it reduces the temperature during the combustion. On the other hand, biodiesel has a few advantages and disadvantages like higher viscosity, lower volatility, and pour point. These disadvantages are ascribed to improper combustion (Sinha et al. 2008, Sivakumar et al. 2018). Although biodiesel is prepared under an Indian version of the American Standard ASTM D-6751 and the European Standard EN-14214 has previously been developed by the Bureau of Indian Standards (BIS) in the form of a standard known as IS-15607 for biodiesel (B 100). For motor petrol mixed with 5% ethanol and motor petrol blended with 10% ethanol, the Bureau of Indian Standards (BIS) has also released IS: 2796: 2008, which contains the specifications for both products.

The emission parameters of the diesel engine on necons methyl ester of algae oil along with ZnO in the concentration of 25, 50, 75, and 100 ppm reported that BTE and HRR are enhanced and emission of CO and HC is reduced at 100 ppm ZnO nano additive (Kalaimurugan et al. 2021). Outcomes of the study on the efficiency of the engine's performance, and combustion parameters using 80 ppm zinc oxide with cottonseed oil biodiesel reported a better increment in performance and combustion characteristics along with a reduction in exhaust emission. Nayak et al. (2021) experimented by using the WCO biodiesel (B20) along with 3gm of ZnO, GO, and  $Al_2O_3$  nano additives into fuel and compared the results with pure diesel. It was observed that the BTE has increased at a higher load for fuels with ZnO and GO nano additives, while the BSFC has been enhanced for fuels with ZnO and  $Al_2O_3$  at a higher load. They reported that the exhaust emissions of carbon monoxide, hydrogen carbon, and nitrogen oxide are lowered in comparison to diesel fuel; however, smoke emissions are found to be higher for all blended fuel at full load. Gavhane et al. (2020) performed the findings after using the soybean biodiesel (B25) and 25, 50, and 75 ppm ZnO nanoparticles with surfactant at many variations of loads (0% to 100%) and compression ratio (18.5 to 21.5 mm). They found an increment in BSFC and BTE and decreased exhaust emissions like carbon monoxide, carbon dioxide, hydrogen carbon, and nitrogen oxide at a 21.5 mm compression ratio for 50 ppm ZnO nanoparticles added fuel. They also analyzed the HRR and MGT increased and the reduction in ignition delay at the same blended fuel and engine operating conditions. Rajak et al. (2022) conducted a comparative examination of the outcomes obtained from numerical and experimental investigations. The researchers introduced ZnO nanoparticles into diesel

fuel at concentrations of 250, 500, and 1000 parts per million (ppm). The addition was carried out at different rotational speeds ranging from 2000 to 3000 revolutions per minute (RPM), fuel injection timings (FITs) between 19.50 and 24.50, and compression ratios ranging from 15.5 to 16.5 millimeters (mm). They found the increment in BTE and marginal improvement in BSFC after numerical analysis as compared to experimental data. However, the BSFC is found lower in the numerical analysis as compared to experimental data between 2750 to 3000 rpm speed. They mentioned a reduction in PMM at all compression ratios, and till 2500 rpm, speed and diminishment are found in smoke and There are no emissions whatsoever at any compression ratio. However, the emissions are larger when using gasoline combined with 500 ppm ZnO. They also saw an increase in EGT across all operating speeds and FITs. Praveena et al. (2020) studied the impact of grapeseed oil with 50 ppm and 100 ppm ZnO and  $CeO_2$  nanoparticles with 1% span and 80% surfactant using the nano-emulsion process. According to their findings, the BTE and HRR values of 100 ppm ZnO and  $CeO_2$  nanoparticles combined with grapeseed oil biodiesel fuel were much higher than those of GSBD. The study observed a decrease in the levels of NO<sub>x</sub>, HC, and CO when using fuel blended with 100 ppm ZnO nanoparticles. The study conducted by Khond et al. (2021) compares the results of the 200 ppm of  $Fe_2O_3$ , ZnO, and  $SiO_2$  nanoparticles along with neem biodiesel (B25). They used diesel expert software to find the relation between the performance of the engine (BSFC and BTE) and also the relation between exhaust emissions (CO, NO<sub>x</sub>, and Smoke) in their study. They found a reduction in BSFC for  $Al_2O_3$  and ZnO blended fuel, while the BSFC is improved for  $SiO_2$  and B25 blended fuel. When they checked for the result of BTE, they found an enhancement in BTE and maximum efficiency found for ZnO blended fuel as compared to B25,  $Al_2O_3$ , and  $SiO_2$  blended fuel. They reported that the pollutant of NO<sub>x</sub> increases for all blended fuel as well as CO<sub>2</sub> is enhanced from ZnO blended fuel only. However, CO and CO<sub>2</sub> are decreased from  $Al_2O_3$  and  $SiO_2$  blended fuels.

Fayad & Dhahad (2021) investigated the  $Al_2O_3$  nanoparticles with butanol-diesel (B20) blended fuel in the concentration of 30, 50, and 100 ppm nanoparticles. The result reported HRR and an increase in cylinder pressure. They also mentioned the result of the performance, such as BSFC was reduced, and BTE was enhanced. The emission parameters such as HC, CO, and NO<sub>x</sub> had been reduced for B20. They mentioned that the combustion is better for the butanol-diesel (B20)  $Al_2O_3$  blended fuel. Yadav & Srivastava (2022) investigated diesel engines using SSCR technology that have met EURO-VI emission criteria rapidly. Uniform ammonia stream homogeneity improves droplet generation and evaporation across the SCR catalyst.

An appropriate mixer may improve ammonia flow. In SCR systems, line mixers, swirl mixers, and combinations of both are common. However, line and swirl mixers perform best for SCR efficiency. This article discusses many ammonia flow uniformity methods. Due to reduced droplet residence time, a line-swirl mixer combination converts urea optimally. These mixers provide consistent flow and temperature. Uniform temperature distribution improves catalyst performance and reduces deposits. The study gives enough data for diesel engine NO<sub>x</sub> reduction researchers. A good mixer will reduce ammonia slip, helping diesel engine makers meet strict emission standards (Chethan et al. 2023). ASFAME synthesis is studied utilizing *Azadirachta indica* and *Simarouba glauca* oil blends with GO-CaO, a heterogeneous catalyst produced from discarded eggshells. Optimizing ASFAME production with varying catalyst concentrations provided 94.69% biodiesel from 0.5 g of GO-CaO. Additionally, the physicochemical properties of ASFAME were compared to conventional diesel, resulting in high-quality biodiesel meeting ASTM Standards 6751D. This work utilizes the eco-friendly heterogeneous catalyst GO-CaO to fulfill fuel demand and enable its recovery and reuse. This article enables small-scale biodiesel makers to get affordable catalysts and use leftover wastes for catalyst production. This project aims to reduce disposal issues and promote sustainability by combining various biodiesel oils.

## PREPARATION OF RICE BRAN BIODIESEL

Srivastava et al. (2000) analyzed the literature review and identified various physical and chemical properties of rice

bran oil fatty acids (FA). The chemical properties include Oleic (18:1) at 43.1%, Arachidic (C20:0) at 0.7%, Linoleic (18:2) at 32.2%, Linolenic (18:3) at 0.6%, and Free Fatty Acids (FFA) at 2.8%. Most of the physical properties have been tested in the fuel laboratory. Due to these properties, firstly, choose the 0.5% (W/W<sub>oil</sub>) alcohol whose molar ratio is 6:1. Two types of base catalysts, such as NaOH and KOH, are selected, and after splitting the glycerol, water washing is applied to remove the impurities from the biodiesel. 1 L of hot distilled water (70°C) was used for the catalyst removal and settled into the furnace under gravity. Through the application of these processes, two distinct layers were discovered. The lower layer reveals the presence of water and impurities, while the second layer signifies the presence of biodiesel. The pH of distilled water suggests that biodiesel does not contain any catalysts.

## PREPARATION OF NANO FUEL BLEND

The Zinc oxide nanoparticles with a size of 40 nm are manufactured by Ad-nano Pvt. Ltd. Karnataka, India. Fig. 1 and Fig. 2 show the SEM and EDX pictures, respectively. Table 1 presents the parameters of ZnO nanoparticles. The process of blending diesel with biodiesel involves using a magnetic stirrer set at a speed of 1500 revolutions per minute (RPM) for 20 min. The ultrasonicator (24kHz) was used for 30 min to disperse nanoparticles at a concentration of 30 parts per million (ppm) into the biodiesel-mixed fuel. The prepared samples of fuel are stable after using the ultrasonication process. The properties of nano additive blended fuels are shown in Table 2, which is tested according to the ASTM standards. The fuel properties, as

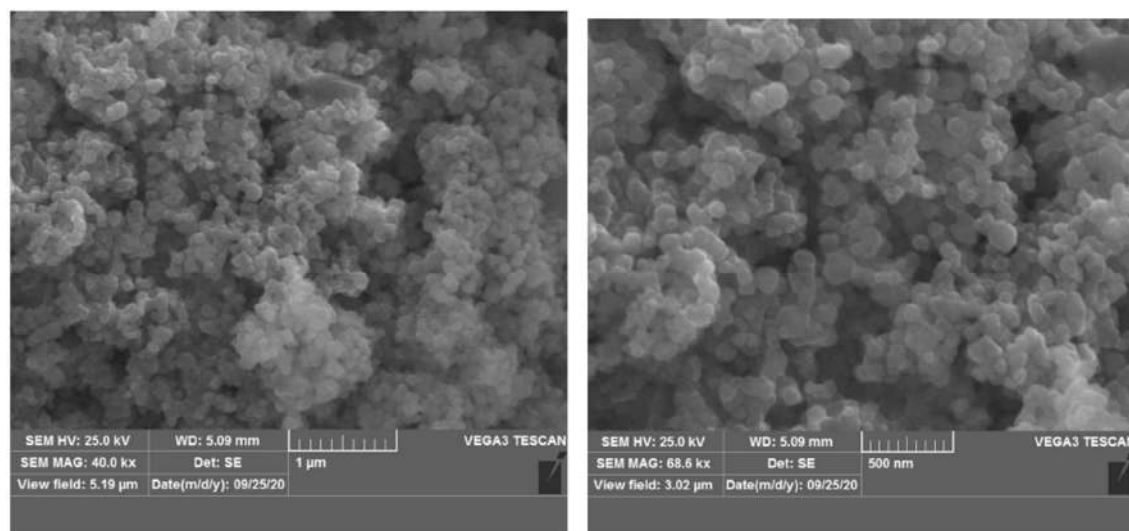


Fig. 1: SEM images of 40 nm ZnO nanoparticles.

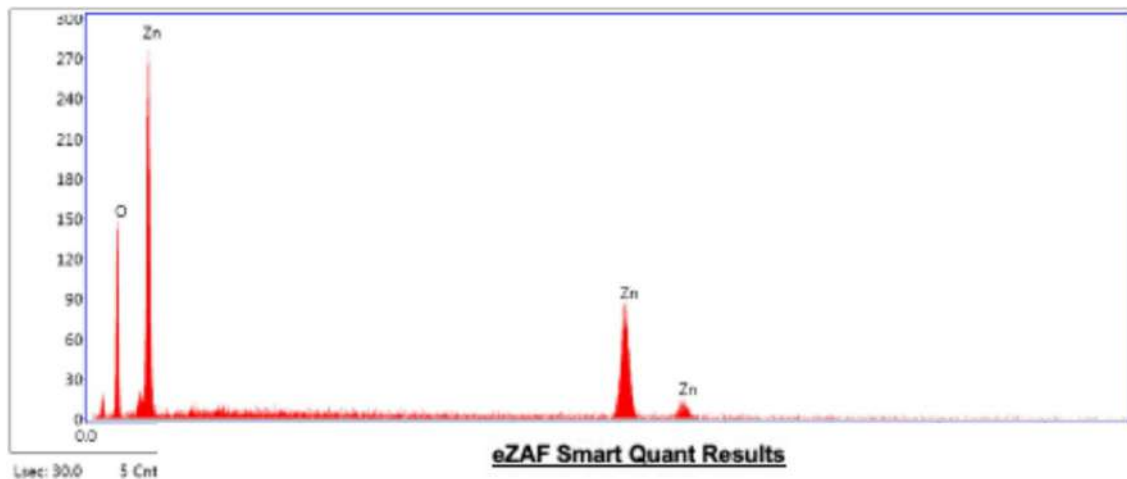


Fig. 2: EDX graph for the ZnO nanoparticles.

Table 1: Characteristics of zinc oxide nanoparticles.

Item	Value
Molecular Formula	ZnO
Purity	99.9%
Particle Size	10-40 nm
Molecular Weight	81.408 g.mol <sup>-1</sup>
Bulk density	0.58g.cm <sup>-3</sup>
SSA	100-120 m <sup>2</sup> .g <sup>-1</sup>
Manufacturer	Ad-nano Technologies Pvt. Ltd.

in Table 2 measured by a hydrometer, bomb calorimeter, Viscometer, and Cleveland open-cup apparatus.

Zinc oxide nanoparticles exhibited smooth and homogeneous shapes, including spherical-like structures, cube-like structures, and layer-like structures. Furthermore, there was no agglomeration identified, which indicates that these nanoparticles are acceptable for treatment. Investigations using energy-dispersive X-rays on the nanoparticles of zinc oxide provide evidence that the samples are free of impurities. The ultra purity of the zinc oxide nanoparticles that were produced was quite high, as shown in Fig. 1.

Fig. 2 displays the elemental composition analyses of the ZNPs that were derived from the EDX plot of the SEM

images. A high level of purity was validated for the ZNPs that were synthesized, as shown by the EDX spectra, which demonstrated that the samples contain the requisite phase of zinc and oxygen.

## MATERIALS AND METHODS

This experimentation involves the use of a single-cylinder, four-stroke agricultural diesel engine manufactured in Bharat (Table 3). The engine operates at a consistent speed and compression ratio. The dynamometer is utilized for load and speed control, while the thermocouple heating filament (ranging from 0 kW to 3.5 kW) is employed to calculate data at different loads. There are five different types of temperature sensors, labeled T1 to T5, that are utilized for measuring various temperatures. These include the water inlet temperature, water outlet temperature to the engine, water outlet temperature to the calorimeter, exhaust gas temperature, and ambient temperature. The Airvisor 4 gas analyzer is utilized for measuring the emissions of CO, CO<sub>2</sub>, HC, and NO<sub>x</sub> (Fig. 3).

### Uncertainty Analysis

Uncertainty analysis is important for finding out the exact value after experimentation. Various types of uncertainty

Table 2: Characteristics of all fuel samples.

Properties/fuel	D100 (Neat)	B10	B20	B30	B10ZnO30	B20ZnO30	B30ZnO30	Standard
Density, kg.m <sup>-3</sup> , 15°C	837	839	847	852	839.2	848	854	ASTM D-1298
Heating Value [MJ.kg <sup>-1</sup> ]	44.0	43.6	42.90	40.05	44.01	46.23	46.54	ASTM D240
Kinematic Viscosity, 40°C	3.8	4.1	4.32	4.9	4.0	4.14	4.5	ASTM 7042
Flashpoint [°C]	74	185	188	76	83	85	86	ASTM D-93



Table 3: Key specifications of the diesel engine.

Item	Value
Engine manufacturer	Bharat
Rated power	3.5 kW
Engine Capacity	8 HP
Cooling Method	Water-Cooled
Injection Method	Direct Injection
Bore × Stroke	(87.5 × 110) mm.
Compression Ratio	17.5:1 mm
Speed	1500 RPM
Number of cylinders	1

(inaccuracies), such as weighting of nanoparticles, engine or test fuel components, some environmental effects, and calculation errors by humans, were found during the research work. The accuracies and inaccuracies are displayed in Table 4.

## RESULTS AND DISCUSSION

Within this industry, we analyzed the performance results such as BSFC and BTE of diesel, as well as combustion parameters like EGT and emissions including CO, CO<sub>2</sub>,

Table 4: Exploring the analysis of uncertainty.

Parameters	Accuracy	Uncertainty [%]
Electronic balance [ppm]	-	± 0.007
Heat release rate [J.sec <sup>-1</sup> ]	-	± 0.22
BTE	-	± 0.25
BSFC	-	± 0.30
CO	± 0.001	± 0.16
CO <sub>2</sub>	± 10 ppm	± 0.002
HC	± 10 ppm	± 0.001
NO <sub>x</sub>	± 10 ppm	± 0.002

HC, and NO<sub>x</sub>. These are compared to the neat diesel fuel (D100). All these effects are measured under consistent conditions, including a constant speed and compression ratio of the diesel engine at four different loads: 0 kW, 1.5 kW, 2.5 kW, and 3.5 kW.

### Effect of All Fuel Samples on the Performance of the Engine

**Effect on BSFC of nano additive mixed fuel:** The BSFC is the major parameter of engine performance. The results of the BSFC are shown in Fig. 4. The results show an increase in BSFC for all fuel blends, except for B30 and B10 at



Fig. 3: Experimental Diesel engine image.

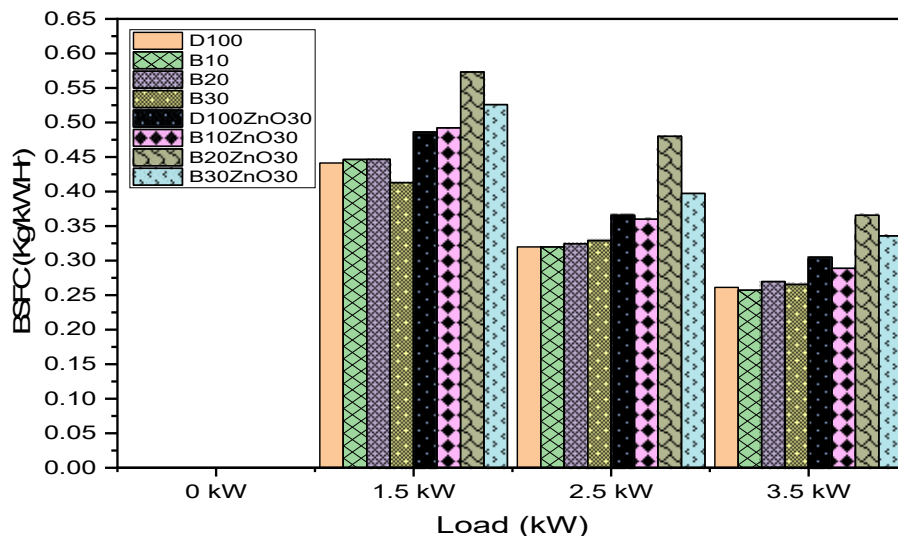


Fig. 4: Graph for Load vs BSFC.

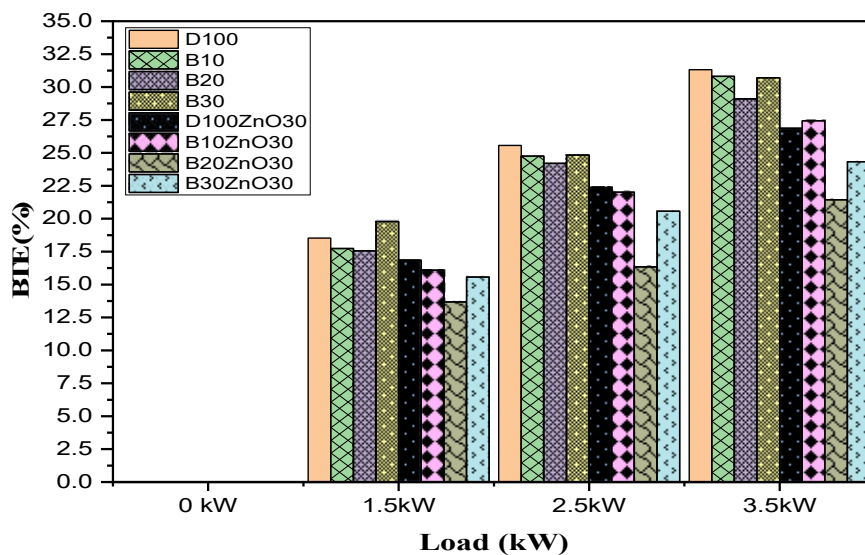


Fig. 5: Graph for Load vs BTE.

1.5 kW and 3.5 kW loads, respectively. The fuel consumption reached its highest levels at 29.86%, 50.04%, and 40% for the B20ZnO30 fuel blend when operating at 1.5 kW, 2.5 kW, and 3.5 kW loads, respectively, in comparison to neat diesel (D100). The improvements were demonstrated due to the utilization of Zinc Oxide nanoparticles, which contribute to enhanced oxidation. The addition of zinc oxide nanoparticles to a fuel significantly improves the combustion response in the combustion chamber. This is due to the superior volume-to-surface area ratio and high thermal efficiency of the nanoparticles, which increase the accessible volume for burning. Using the Zinc Oxide nano additive in the fuel

blends improves the air-fuel ratio and decreases the ignition delay period. In addition, it enhances the flash point of the fuel blends, resulting in improved combustion.

**Effect of nano additive blended fuel on BTE:** The BTE increases when the loads increase. It depends on the dosage level of nanoparticles. If the dosage of nanoparticles improves, then BTE will increase (Fig. 5). The addition of ZnO nanoparticles lowers the ignition delay and evaporation time. The addition of nano additive improves the fuel-burning properties and air-fuel ratio of fuel. This causes fuel droplets to increase. Due to these droplets, fuel evaporates rapidly. This process affects thermal efficiency. At a 1.5 kW load,

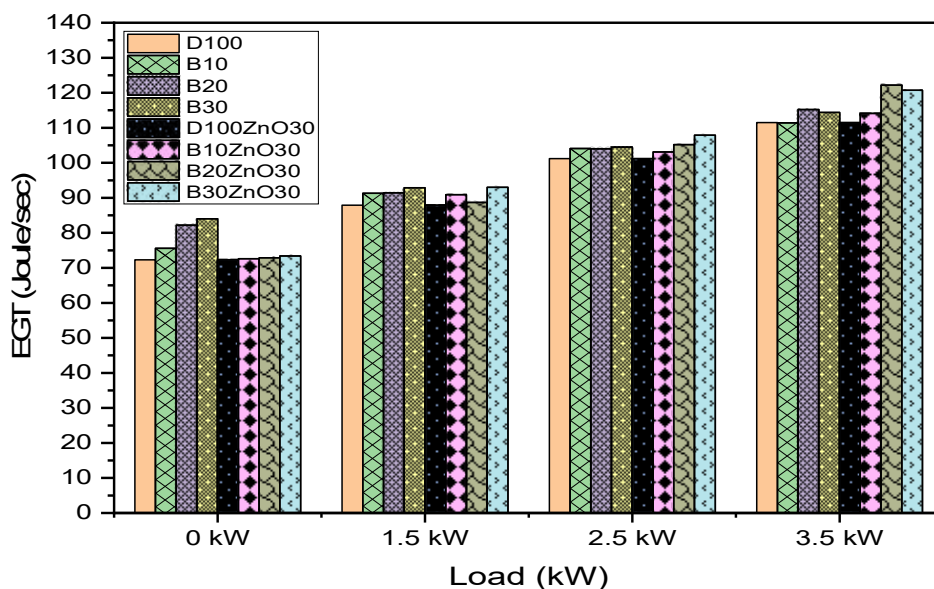


Fig. 6: Graph for Load vs EGT.

the use of B30 fuel resulted in a 6.79% increase in BTE compared to neat diesel fuel.

### The Impact of Nano-Additive Mixtures on Engine Combustion

**Examining the impact of nano additive blended fuel on EGT:** Increasing the temperature in the combustion chamber improves the exhaust gas temperature (EGT). In this experimental study, the temperature of exhaust gas is higher for some blended fuels. The maximum EGT values for different fuel blends were recorded at various load levels (Fig. 6). B30, B30ZnO30, B30ZnO30, and B20ZnO30 fuel blends exhibited EGT values of 16.18%, 5.80%, 6.62%, and 9.59%, respectively, compared to neat diesel fuel (D100). The presence of ZnO in the fuel blends acted as a catalyst, controlling the temperature rise in the cylinder. Additionally, the high pressure inside the cylinder contributed to the increase in temperature. The temperatures of exhaust gas for D100ZnO30 fuel blends are identical to those of neat diesel fuel (D100) across all loads.

### The Impact of Using Nano Additives on Exhaust Emissions from the Engine

**The nano additive mixed fuel's impact on CO exhaust:** Carbon monoxide is generated as a result of an increase in the temperature of the combustion chamber. A fuel's combustion response in the combustion chamber is considerably improved when zinc oxide nanoparticles are added to the fuel via the addition process. This occurs because of the nanoparticles' high thermal efficiency and higher volume-to-

surface area ratio, both of which contribute to an increase in the volume that is potentially available for combustion. As a result of excessive oxygen and the higher reactive surface of ZnO, which improves the temperature, as well as pressure due to the higher heating value of fuel, which results in complete combustion, and due to the higher oxygen content, it converts the CO into CO<sub>2</sub>, the maximum decrement in CO content for the D100ZnO30 fuel blend was found to be 80% at 0 kW load in this experimental study (Fig. 7). This was found to be the case when compared to neat diesel (D100). The carbon monoxide (CO) levels for various fuel blends, including B10, B20, B30, D100ZnO30, B10ZnO30, and B30ZnO30, at 1.5 kW, as well as B10 and B10ZnO30 at 2.5 kW, are equivalent to that of pure diesel (D100) fuel.

**The impact of incorporating nano additives into gasoline on the release of CO<sub>2</sub> emissions:** CO<sub>2</sub> is produced due to the higher oxidation of fuel during combustion. In this experiment, maximum diminishment in CO<sub>2</sub> is obtained from B10, B20, B30, and B10ZnO30 fuel blends that are 3.4%, 3.1%, 3.6%, and 3.7%, respectively, at 0 kW load, and CO<sub>2</sub> decreases 2.94% for B10 fuel blend at 1.5 kW as compared to D100 due to better atomization of fuel (Fig. 8). At a 2.5 kW load, the CO<sub>2</sub> value for B10 fuel blends is equivalent to that of neat diesel fuel in the experiment.

**Effect of the nano additive blended fuel on HC exhaust emission:** Because of the viscosity of the fuel's combination with air and the spraying of fuel within the combustion chamber, the hydrocarbon (HC) emission is mostly determined by these two factors. It involved determining

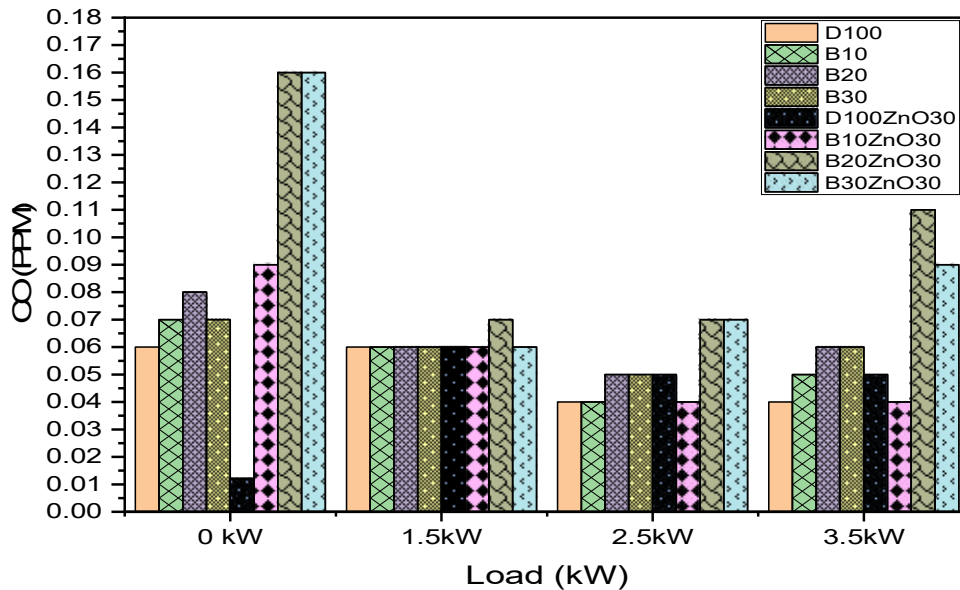
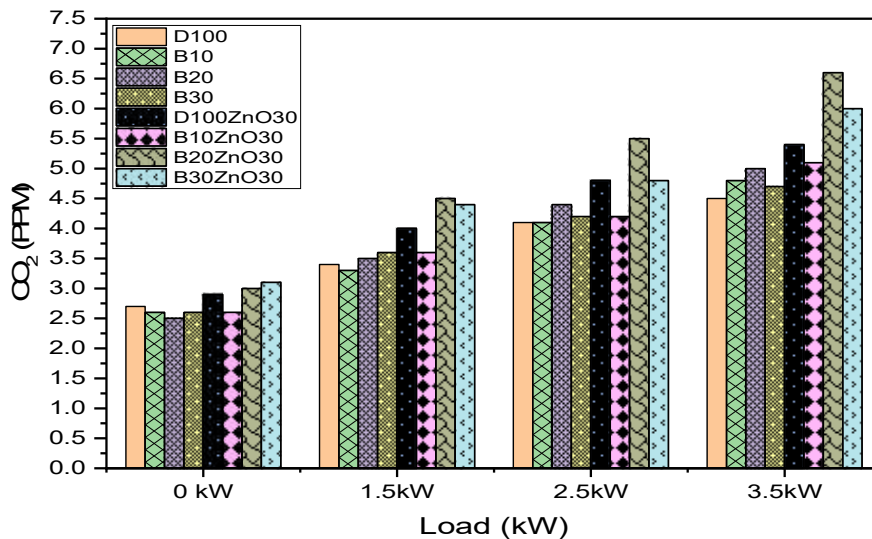


Fig. 7: Graph for Load vs CO.

Fig. 8: Graph for Load vs CO<sub>2</sub>.

the ratio of air to fuel, ranging from a lean mixture to a rich mixture. Certain fuel blends have demonstrated a decrease in HC emissions under various load conditions (Fig. 9). At 0 kW, 1.5 kW, and 2.5 kW loads, B10ZnO30, D100ZnO30, and D100ZnO30 showed significant reductions in HC levels when compared to neat diesel fuel (D100). The reason for the above phenomena is the addition of nano additives in the blended fuel, which effectively eliminated unwanted fuel and provided an excess of oxygen. Therefore, nanoparticles are commonly referred to as oxygen buffers that aid in enhancing

the air-fuel equivalence ratio. When operating at a 3.5 kW load, the HC emission levels are higher for all blended fuels compared to neat diesel fuel (D100). This is primarily due to the higher viscosity characteristics of the blended fuels, which leads to difficulties in fuel spraying and ultimately results in poor combustion.

**Effect of the nano additive blended fuel on NO<sub>x</sub> exhaust emission:** The emission of NO<sub>x</sub> is influenced by the elevated temperature and pressure within the cylinder. It is directly related to the engine's loads. As the engine load increases, the



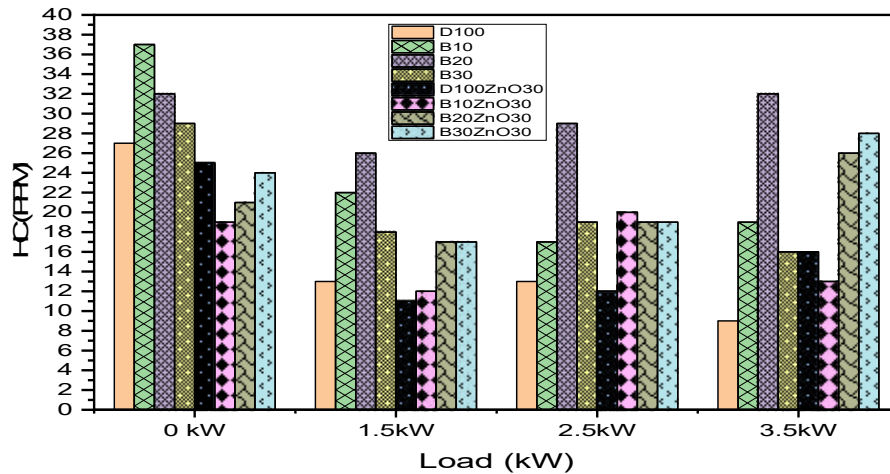
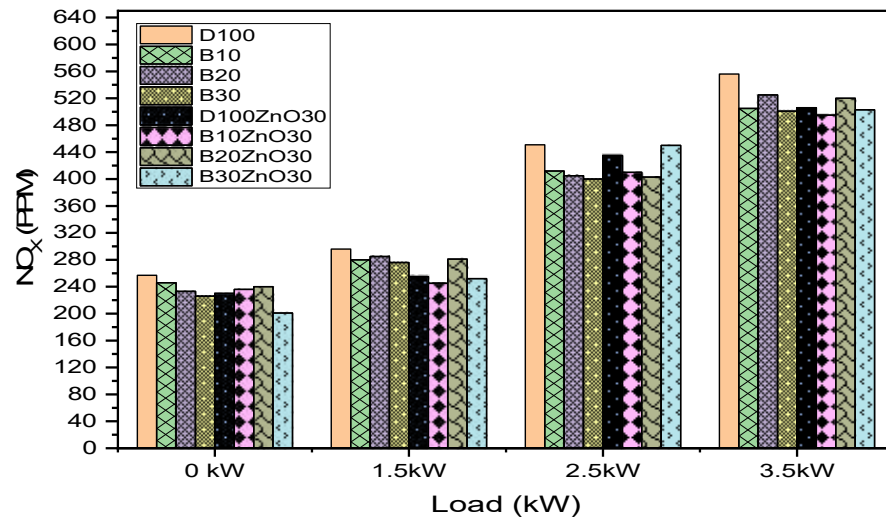


Fig. 9: Graph for Loads vs Hydrocarbon (HC).

Fig. 10: Graph for Load vs NO<sub>x</sub>.

NO<sub>x</sub> levels will also rise. Fig. 10 illustrates the decrease in NO<sub>x</sub> emissions when using all-fuel blends compared to neat diesel fuel (D100). The fuel blends B30ZnO30, B10ZnO30, B30ZnO30, and B10ZnO30 showed significant reductions of 21.78%, 17.22%, 11.30%, and 10.97% respectively at different power levels. The reason for the thermal stability of ZnO nanoparticles and their ability to promote shorter ignition delay, resulting in improved air-fuel mixing. Through their catalytic properties, zinc oxide nanoparticles can absorb oxygen content, resulting in a reduction in NO<sub>x</sub> exhaust emissions.

## CONCLUSIONS

This research examined the impact of adding a ZnO additive

to biodiesel and diesel fuel blends on the performance, combustion, and exhaust emissions of a diesel engine. The data are presented in a columnized format below, comparing them to plain diesel.

- The BSFC is 29.86%, 50.04%, and 40% improved for the B20ZnO30 fuel at various loads due to the characteristics of the biodiesel.
- The Brake thermal efficiency value should be enhanced by increasing the concentrations of nano additives in fuel. The maximum 6.79% improvement is recorded on B30 fuel at a 1.5 kW load.
- The EGT shows a significant improvement of 16.18% thanks to the catalytic properties of ZnO and its large surface area.

- The highest reduction in carbon monoxide (CO) emissions for B20 fuel is 7.69% when the load is 0 kW, while the value of CO emission for B10 fuel is the same as that of plain diesel fuel when the load is 2.5 kW. This leads to an improvement in CO<sub>2</sub> levels as well. Plantations of trees can help control emissions, but they are unable to control NO<sub>x</sub>, which directly harms the ozone (O<sub>3</sub>).
- The maximum reduction in HC is 29.2% and 15.38% for B10ZnO30 and D100ZnO30 because nanoparticles are the oxidation catalyst that improves the combustion property and leads to shorter ignition delay.
- Very good results were found for NO<sub>x</sub> emission. NO<sub>x</sub> emission slightly decreases for the all-fuel blends at all loads. The better results of reduction in NO<sub>x</sub> emission are 21.78% and 17.22% found for B30ZnO30 and B10ZnO30 fuel blends respectively. Because of the excessive content in biodiesel, mixing the catalytic-based ZnO nanoparticles enhances the cylinder temperature. Nitrogen is converted into nitric acid, which causes to decrease in NO<sub>x</sub> content from the exhaust.

Thus, it has been summarized that Zinc Oxide nanoparticles are better additive, enhancing performance and reducing exhaust emissions. Zinc Oxide nanoparticles are efficient and improve concentration for better combustion results for future recommendation. The above-archived combination of biodiesel and nanoparticles seems to be the solution for reducing industrial pollution and reducing the related health hazards for its workers.

## ABBREVIATIONS

RB	Rice bran	SEM	Scanning Electron Microscope
WCO	Waste cooking oil	EDX	Energy dispersive X-ray Spectroscopy
PMM	Particulate matter	MGT	Mean gas temperature
GO	Graphene Oxide	FA	Fatty acid
EGT	Exhaust gas temperature	HRR	Heat release rate
FFA	Free fatty acid		
GSD	Grapeseed oil biodiesel		
FITs	Fuel injection timings		

## REFERENCES

- Chethan, S.G., Khan, M.M. and Sreepathi, L.K. 2023. An approach for biodiesel production from blends of *Azadirachta indica* and *Simarouba glauca* triglycerides by graphene-doped calcium oxide catalyst and its comparative studies. *Nature Environment and Pollution Technology*, 22(3), pp.1607–1614. [DOI]
- Deepak Kumar, T., Hussain, S.S. and Ramesha, D.K. 2019. Effect of a zinc oxide nanoparticle fuel additive on the performance and emission characteristics of a CI engine fuelled with cotton seed biodiesel blends. *Materials Today: Proceedings*, 811, pp.2374–2378. [DOI]
- Fayad, M.A. and Dhahad, H.A. 2021. Effects of adding aluminum oxide nanoparticles to butanol-diesel blends on performance, particulate matter, and emission characteristics of diesel engine. *Fuel*, 286. [DOI]
- Gavhane, R.S., Kate, A.M., Pawar, A., Safaei, M.R., Soudagar, M.E.M., Abbas, M.M., Ali, H.M., Banapurmath, N.R., Goodarzi, M., Badruddin, I.A., Ahmed, W. and Shahapurkar, K. 2020. Effect of zinc oxide nano-additives and soybean biodiesel at varying loads and compression ratios on VCR diesel engine characteristics. *Symmetry (Basel)*, 12, pp.1–31. [DOI]
- Kalaimurugan, K., Somasundaram, D., Thirugnanam, C. and Dharmaprabhakaran, T. 2021. Combustion behaviour of ZnO nanoparticles added algae biodiesel on CI engine. *Materials Today: Proceedings*, 90, pp.46–63. [DOI]
- Khond, V.W., Rambhad, K. and Shahadani, V. 2021. New diesel-neem biodiesel blend (D75NB25) containing nano iron oxide, silicon dioxide and zinc oxide for diesel engine: An experimental investigation. *Materials Today: Proceedings*, 47, pp.2701–2708. [DOI]
- Nayak, V., Karthik, A.V., Sreejith, B.K., Prasad, B.G. and Kini, K.S. 2021. Performance, combustion and emission characteristics of single-cylinder I engine with WCO biodiesel and nanoparticles. *Materials Today: Proceedings*, 612, pp.1127–1136. [DOI]
- Praveena, V., Martin, M.L.J. and Geo, V.E. 2020. Experimental characterization of CI engine performance, combustion, and emission parameters using various metal oxide nanoemulsions of grapeseed oil methyl ester. *Journal of Thermal Analysis and Calorimetry*, 139, pp.3441–3456. [DOI]
- Rajak, U., Ağbulut, Ü., Veza, I., Dasore, A., Sandemir, S. and Verma, T.N. 2022. Numerical and experimental investigation of CI engine behaviours supported by zinc oxide nanomaterial along with diesel fuel. *Energy*, 239, p.12242. [DOI]
- Sinha, S., Agarwal, A.K. and Garg, S. 2008. Biodiesel development from rice bran oil: Transesterification process optimization and fuel characterization. *Energy Conversion and Management*, 49, pp.1248–1257. [DOI]
- Sivakumar, M., Shanmuga Sundaram, N., Ramesh Kumar, R. and Syed Thasthagir, M.H. 2018. Effect of aluminium oxide nanoparticles blended *Pongamia* methyl ester on performance, combustion and emission characteristics of diesel engine. *Renewable Energy*, 116, pp.518–526. [DOI]
- Srivastava, A. and Prasad, R. 2000. Triglycerides-based diesel fuels. *Renewable and Sustainable Energy Reviews*, 4, pp.111–133. [DOI]
- van Gerpen, J. 2004. Biodiesel processing and production. *Fuel Processing Technology*, 86(10), pp.1097–1107. [DOI]
- Verma, T.N., Shrivastava, P., Rajak, U., Dwivedi, G., Jain, S., Zare, A., Shukla, A.K. and Verma, P. 2021. A comprehensive review of the influence of physicochemical properties of biodiesel on combustion characteristics, engine performance, and emissions. *Journal of Traffic and Transportation Engineering*, 8, pp.510–533. [DOI]
- Yadav, M.K. and Srivastava, A.K. 2022. Effective mixer design: an important factor in SSCR systems for the reduction of NO<sub>x</sub> from the exhaust of diesel engines. *Nature Environment and Pollution Technology*, 21(4), pp.1753–1760. [DOI]

# Biomonitoring of Bedog River Water Quality Using Dragonfly Diversity as Bioindicators in Yogyakarta, Indonesia

Sapta Suhardono<sup>1</sup>, Muhammad Amin Sunarhadi<sup>1</sup>, Iva Yenisi Septiariva<sup>2</sup>, Hening Triandika Rachman<sup>3</sup> and I. Wayan Koko Suryawan<sup>4†</sup>

<sup>1</sup>Department of Environmental Sciences, Faculty of Mathematics and Natural Sciences, Universitas Sebelas Maret, Surakarta, 57126, Indonesia

<sup>2</sup>Department of Civil Engineering, Faculty of Engineering, Universitas Sebelas Maret, Surakarta, 57126, Indonesia

<sup>3</sup>Department of Life Sciences, National Central University, Taoyuan City, Taiwan

<sup>4</sup>Department of Environmental Engineering, Faculty of Infrastructure Planning, Universitas Pertamina, Jakarta Selatan 12220, Indonesia

†Corresponding author: I. Wayan Koko Suryawan; i.suryawan@universitaspertamina.ac.id

**Abbreviation:** Nat. Env. & Poll. Technol.  
**Website:** [www.neptjournal.com](http://www.neptjournal.com)

*Received:* 28-08-2024

*Revised:* 15-09-2024

*Accepted:* 23-09-2024

## Key Words:

Water quality  
 Bioindicators  
 Dragonfly diversity  
 River pollution

## Citation for the Paper:

Suhardono, S., Sunarhadi, M. A., Septiariva, I. Y., Rachman, H. T. and Suryawan, I. W. K., 2025. Biomonitoring of Bedog river water quality using dragonfly diversity as bioindicators in Yogyakarta, Indonesia. *Nature Environment and Pollution Technology*, 24(2), p. D1711. <https://doi.org/10.46488/NEPT.2025.v24i02.D1711>

*Note: From year 2025, the journal uses Article ID instead of page numbers in citation of the published articles.*



**Copyright:** © 2025 by the authors

**Licensee:** Technoscience Publications

This article is an open access article distributed under the terms and conditions of the Creative Commons Attribution (CC BY) license (<https://creativecommons.org/licenses/by/4.0/>).

## ABSTRACT

The quantity of contaminants being released into rivers is rising in direct correlation with the growth of the human population. Bedog River is a tributary located in the vicinity of Mount Merapi. This river flows through agricultural, residential, and cattle sectors, making it easier to detect river contamination. The objective of this study is to evaluate the water quality of the Bedog River. The research employs a methodology that evaluates water quality by considering biological indicators, specifically the existence of dragonfly species, with the analysis of other chemical and physical properties in river water. The water quality research findings indicate that the physical and chemical characteristics remain satisfactory, with the water falling into the moderately polluted category. It also meets the water quality criteria outlined in PPRI No. 82 of 2001, specifically the class 2 threshold. A total of 23 Odonata species were identified. The upstream section, as indicated by the presence of *Neurobasis chinensis florida* and *Helioecypha fenestrata*, which are endemic, along with *Macrogomphus parallelogramma*, which is rare, is considered an optimal habitat capable of supporting sensitive dragonfly species. The dragonfly variety index in the Bedog River is relatively high, with values of 2.08, 2.79, and 1.47 for the upstream, middle, and downstream sections, respectively. The Pearson correlation coefficient indicates a strong positive correlation of 0.961, while the significance level of 0.179 suggests a statistically meaningful association. The findings highlight the potential of using dragonflies as bioindicators for long-term monitoring of river health and pollution levels. This study contributes to the understanding of how water quality impacts biodiversity and provides a basis for future research and river management practices. This research fills a gap by integrating biological indicators with traditional water quality assessments in a specific regional context. It provides new insights into the relationship between water quality and dragonfly diversity, offering valuable information for environmental monitoring and conservation efforts.

## INTRODUCTION

Several land use activities, including agriculture and housing development, will have an impact on the hydrological conditions in the nearest river basin (Aflizar 2008). Converting forests into agricultural and residential land increases surface runoff, carrying along the soil layer it passes through (Agustiniingsih et al. 2012). This is related to one of the river functions as a water reservoir for the surrounding area (Ali et al. 2013). The level of pollutants in the water can have an impact on aquatic organisms, and it can kill certain species or support the life of others. The increasing population is one of the factors affecting environmental pollution, including water pollution (Amneera et al. 2012). The growing population leads to

an increase in the number of people competing to fulfill their needs and driving rapid development. On the other hand, the increasing population is also proportional to the increasing demand for clean water, but the availability of clean water for daily consumption is disrupted by water pollution (Anwar et al. 2016).

The decrease in water quality can reduce the usefulness, productivity, carrying capacity, and sustainability of water resources, which ultimately reduces the natural resource wealth (PPRI No. 82 of 2001). In the hydrological cycle, rivers function as a raw water source for irrigation storage and are utilized as water catchment areas, making rivers a very important role in an aquatic ecosystem (Setiari et al. 2012). The amount of water supply on earth is about 0.036% derived from rivers and lakes, then the majority of it, as much as 76%, is used for household sectors (Kumar Reddy & Lee 2012). The use of river water for various needs must be done sustainably. Rivers are very important ecosystems for humans. They also provide water for various activities such as agriculture, industry, and household needs. Therefore, river resources must be protected so that they can be well utilized by humans and other living creatures (Djaja et al. 2018). Increasing domestic, agricultural, and industrial activities can affect the quality of river water. Specifically, domestic activities contribute the largest BOD concentration to the river body (Ministry of Environment 2003). Large companies or industries can overcome wastewater management problems because they have more capital, but it will be different for small or medium-scale industries. Small-scale industries are not yet able to overcome wastewater problems (Asmadi & Suharno 2012).

The presence or distribution of species is closely related to the conditions of the environment in which they live (Setyawan et al. 2021, 2020). This close relationship between environmental conditions and the presence of species underpins the concept of biomonitoring. This concept has been applied to evaluate organic pollution based on the diversity of algae (Alombro et al. 2023). It is expected that using biotic methods can become a benchmark in water quality monitoring by identifying the presence of macroinvertebrates that can be used as bioindicators of changes in the quality of a water source. In identifying the presence of macroinvertebrates, the type, composition, and domination of a particular species of macroinvertebrates that inhabit the area must be considered. Macroinvertebrates are invertebrates that live on the riverbed and can be an important component in the food chain of an aquatic ecosystem. Some macroinvertebrate groups that can be used as bioindicators of water quality in a water source include worms and leeches (Annelida), flatworms (Platyhelminthes), insects

(Insecta), shrimps and crabs (Decapoda), as well as snails and mussels (Mollusca). The main advantage of biotic methods over chemical and physical methods is the potential for this method to be used by the public widely, thus opening opportunities for participatory river water quality monitoring activities by the community.

The Bedog River is a tributary that traverses the Bedog River Basin, situated in Sleman Regency, Yogyakarta City, and Bantul Regency. Presently, the Bedog River serves as a primary water source for local inhabitants to fulfill their home and industrial requirements. The water sourced from the Bedog River is utilized for various purposes, such as domestic, industrial, and agricultural uses, among others. The assessment of water quality status is conducted by employing the Pollution Index Method. The Pollution Index is utilized to assess the comparative pollution level in relation to the authorized water quality indicators. The Pollution Index (PI) is initially established for a specific objective and subsequently extended to encompass several other objectives pertaining to the entire body of water or specific segments of a river, as outlined in the Ministry of Environment (2003). The Water Quality Index (WQI) is frequently employed to evaluate the water quality in wetlands. The river water quality index, as described by Bordalo et al. (2006) and Phong et al. (2023), is a measure that can be used to determine the quality status of a river's water.

Nevertheless, alterations in the plant cover inside wetlands have been observed to have an impact on Water Quality Index (WQI) values, both directly and indirectly. Wetland ecosystem restoration is achieved through restoration initiatives. Improving existing ecosystems has gained significant attention (Menberu et al. 2017). Moreover, revegetation is a deliberate undertaking aimed at restoring an area (Waluyo & Nurlia 2017).

The current study aims to fill this gap by evaluating the water quality of the Bedog River using both chemical and physical water parameters and biological indicators, specifically dragonfly diversity. The primary objectives of this study are to assess the current water quality status of the Bedog River, determine the diversity of dragonfly species in different segments of the river, and explore the correlation between water quality and dragonfly diversity. By addressing these objectives, the study seeks to provide a more integrated understanding of river health and the potential of dragonflies as bioindicators for long-term water quality monitoring.

Moreover, this study aims to contribute to scientific knowledge by providing new insights into the use of dragonflies as bioindicators, particularly in the context of Indonesian river systems. The authors hypothesize that there is a strong positive correlation between water quality and



dragonfly diversity, with higher water quality supporting greater species richness and diversity. This research not only addresses the existing gaps in the integration of biological and physicochemical assessments but also aims to inform future river management and conservation strategies by highlighting the importance of maintaining and improving water quality to preserve aquatic biodiversity.

## MATERIALS AND METHODS

### Materials and Tools

The tools used in this research are GPS (Global Positioning System), insect nets, dragonfly identification guidebooks, Horiba Multi parameters, and digital cameras.

### Data Analysis Method

This study was conducted by segmenting the flow of the Bedog River into three areas, namely upstream, middle, and downstream (Table 1). Chemical and physical water quality measurements were carried out using a Horiba multi-parameter instrument that can measure temperature, pH, TDS, DO, conductivity, salinity, depth, and turbidity. Meanwhile, for biological parameters, observations were made visually and records were made of the presence of dragonflies in the water. The research activities were generally divided into surveys, data collection of dragonfly species and quantity, data collection of chemical and physical parameters, data processing, and analysis. Water samples were taken from the river using the grab sampling technique, which is a direct sampling technique from the observed body of water and only informs the characteristics of the water at the time the sample is taken.

The water quality state is assessed utilizing the Pollution Index Model by the following sequential procedures:

- 1) Systematic collecting of water quality data to create a time series dataset.
- 2) The data from each water quality parameter is compared to the quality threshold based on the water class.

This study used the Pollution Index approach [KLHK 2001] to determine the status of river water quality. The Pollution Index equation used is as follows:

$$PIj = \sqrt{\frac{\left(\frac{Ci}{Lij}\right)^2 M^2 + \left(\frac{Ci}{Lij}\right)^2 R^2}{2}} \quad \dots(1)$$

Table 1: Coordinates of sample collection locations.

Segmentation	Coordinate X	Coordinate Y
Upstream	-7.67987	110.3545
Middle	-7.77942	110.3278
Downstream	-7.88725	110.3112

Where:

PIj : Pollution Index for its designation (j)

Ci : Concentration of water quality parameters (i)

Lij : Concentration of water quality parameters (i) listed in the water quality standards (j)

M : Maximum

R : Average

The Pollution Index values indicate the extent of pollution in the Bedog River by comparing it to the quality standard specified in Government Regulation 82/2001 for the respective water class. By doing this, it is anticipated that significant data will be obtained to ascertain whether the water in the river is suitable for its intended uses based on its water classification. The collected data on physical and chemical parameters of water quality were examined in accordance with the water quality standard of class 2, as outlined in Government Regulation Number 82 of 2001. Based on the results of the Pollution Index calculation that has been obtained, then an assessment of the quality status of river water quality can be carried out with 4 assessment categories following Table 2 below:

The obtained dragonfly data were analyzed using the Shannon-Wiener Diversity Index formula to determine the level of diversity and the evenness index to indicate the number of individuals spread across each species, obtained as follows:

$$H' = \sum(pi \cdot \ln(pi)) \quad \dots(2)$$

$$pi = \frac{ni}{N} \quad \dots(3)$$

H' = diversity index

pi = proportion of individuals of species i

ni = number of individuals of species i

N = total number of individuals of all species

The criteria for species diversity are determined as follows:

H' < 1 = low diversity type

1 < H' < 3 = moderate diversity type

H' > 3 = high diversity type

Table 2: Pollution Index Category (Decree of the Minister of Environment Number 115 of 2003).

Pollution Index Score	Quality Status
0 ≤ PI ≤ 1.0	Good
1.1 < PI ≤ 5.0	Lightly Polluted
5.1 < PI ≤ 10	Moderately Polluted
PI > 10	Heavily Polluted

The collected data is then tabulated, processed, and analyzed descriptively. Data analysis includes the calculation of the diversity index (Hasyim & Asmuni 2009). The final analysis stage of this study is to correlate the previously known water quality values with the diversity index of dragonflies.

## RESULTS AND DISCUSSION

### Bedog River Water Quality

Based on field measurements, several values of chemical and physical parameters were obtained, namely temperature, pH, DO, TDS, turbidity, conductivity, salinity, and depth, which are presented in Table 3. In the table, it can be compared that there is a temperature difference in the upstream, middle, and downstream sections caused by the elevation and time of measurement. For the pH parameter, the obtained value is above the specified threshold, which is due to the potential contamination from wastewater originating from households or agricultural activities. Therefore, further research needs to be conducted on parameters that affect the pH value.

According to Table 3, the temperature variations in the Bedog River at the three observation stations remain rather constant, with a variation of approximately 3 degrees compared to the initial state before alterations in land use along the river. The temperature parameter of the Bedog River indicates that its water quality remains within the designated threshold for its intended use since it does not deviate more than (+3) from its natural condition, which is the requirement for class II water quality. Observations of pH levels at each station indicate varying results from the upstream, middle, and downstream locations. The pH values are arranged in the following order: 5.61, 5.36, and 5.03. The pH of the Bedog River is still below the water quality threshold necessary for its authorized use, as specified by Government Regulation 82/2001 (6-9), which sets the pH range for class II water quality. The height and time of measurement result in a temperature disparity between the

upstream, middle, and downstream regions. Based on the provided information, it can be inferred that the water quality of Sungai Bedog at stations 1 and 2 fulfills the required standards for the TDS parameter. However, station 3 has an acceptable water quality limit for its intended use.

The increase in TDS values may be due to water pollution from agricultural activities and domestic waste that contains heavy metals and harmful chemicals. The salinity value at each station indicates the absence of salt content in the water, with salinity values at all stations being 0 mg.L<sup>-1</sup>.

The pH levels fluctuate due to the release of organic waste from domestic activities, the decomposition of plants and animals, and the garbage generated by industrial planting forests near the Bedog River. Furthermore, the proper management of inorganic waste also plays a substantial role. Nevertheless, variations in pH have minimal impact on the overall quality of the river water. Water that is suitable for sustaining life typically has a pH level between 6.5 and 7.5 (Wardhana 2004). Typically, unpolluted water has a pH level that is close to neutral, about pH 7, which is suitable for the majority of aquatic creatures (Sutriati 2018). The Bedog River is not now a suitable environment for aquatic species due to its pH level being below 6.

Dissolved oxygen (DO) serves as a reliable measure of the freshness of water. Oxygen is crucial for assessing water quality because dissolved oxygen (DO) facilitates the oxidation and reduction of both organic and inorganic substances. The oxidation and reduction processes play a crucial role in naturally reducing pollutant burdens in water. The recorded measurements of the dissolved oxygen (DO) parameter at each station showed variability in the upstream, middle, and downstream sections. Specifically, the DO levels were observed to be 7.9 mg.L<sup>-1</sup> at point 1, 8.8 mg<sup>-1</sup>.L at station 2, and 6.79 mg.L<sup>-1</sup> at station 3. The water quality conditions of the Bedog River at all stations have surpassed the minimal standards for their classification, as specified by PP 82/2001, with regards to the quality threshold limit for Class II water parameters for dissolved oxygen (DO),

Table 3: Chemical and physical parameters of water in the Bedog River.

Parameter	Unit	Upstream	Middle	Downstream
Temperature	°C	25.74	27.81	28.71
pH		5.61	5.36	5.03
DO	mg.L <sup>-1</sup> O <sub>2</sub>	7.9	8.8	6.79
TDS	Mg.L <sup>-1</sup> TDS	313	361	503
Turbidity	NTU	3.5	5.5	10.8
Conductivity	mS.cm <sup>-1</sup>	0.481	0.565	0.785
Salinity	mg.L <sup>-1</sup>	0	0	0
Depth	°C	0.25	0.15	0.25

Table 4: Water pollution levels in the Bedog River.

Segmentation	Score	Result
Upstream	1.933504	Lightly Polluted
Middle	2.055469	Lightly Polluted
Downstream	1.635416	Lightly Polluted

which is set at  $4 \text{ mg.L}^{-1}$ . In general, our analysis discovered only a minute portion of contaminated water (Table 4). As the amount of organic waste increases, the level of dissolved oxygen in the water decreases. Anthropogenic activities, such as agricultural practices and waste disposal, have led to a decline in the levels of dissolved oxygen in the environment (Anhwange et al. 2012).

### Dragonfly Diversity Index

In the upstream area, 12 dragonfly species were found, with *Heliocypha fenestrata* being the most commonly found species with 11 individuals (Table 5). *Heliocypha fenestrata* is a Javan endemic dragonfly species that can be found along the Bedog River. The dragonfly species diversity index in the upstream area is 2.08, indicating that the dragonfly diversity in the upstream area is categorized as moderate. *Neurobasis chinensis florida*, a rare Javanese endemic dragonfly species, was also found in the upstream area.

The middle area is the region with the highest number of species and individuals compared to the other two regions (Table 6). Nineteen species of dragonflies were found in this region, with a total of 59 individuals. The diversity index value for this area is almost 3, at 2.79, which categorizes this region as having a moderate diversity index.

Table 5: Dragonfly diversity index in the upstream part of Bedog River.

Number	Species	ni	pi ln pi	H'
1	<i>Copera marginipes</i>	10	-0.32927	0.329269
2	<i>Heliocypha fenestrata</i>	11	-0.33989	0.339889
3	<i>Orthetrum testaceum</i>	1	-0.08192	0.081918
4	<i>Euphaea variegata</i>	9	-0.31652	0.316517
5	<i>Pseudagrion pruinsum</i>	1	-0.08192	0.081918
6	<i>Libellago lineata</i>	1	-0.08192	0.081918
7	<i>Neurothemis ramburii</i>	2	-0.13434	0.13434
8	<i>Macrogomphus parallelogramma</i>	1	-0.08192	0.081918
9	<i>Neurobasis chinensis florida</i>	2	-0.13434	0.13434
10	<i>Orthetrum sabina</i>	1	-0.08192	0.081918
11	<i>Prodaseineura autumnalis</i>	3	-0.17563	0.17563
12	<i>Neurothemis terminata</i>	5	-0.23837	0.238373
	N	47	Index	2.08

Table 6: Dragonfly diversity index in the middle part of the Bedog River.

Number	Species	ni	pi ln pi	H'
1	<i>Neurobasis chinensis florida</i>	7	-0.2529	0.252905
2	<i>Potamarcha congener</i>	2	-0.11473	0.114725
3	<i>Orthetrum testaceum</i>	1	-0.06911	0.069111
4	<i>Orthetrum chrysis</i>	3	-0.15147	0.151471
5	<i>Neurothemis terminata</i>	2	-0.11473	0.114725
6	<i>Neurothemis ramburii</i>	3	-0.15147	0.151471
7	<i>Pseudagrion pruinsum</i>	2	-0.11473	0.114725
8	<i>Prodaseineura autumnalis</i>	3	-0.15147	0.151471
9	<i>Libellago lineata</i>	5	-0.20916	0.209161
10	<i>Onychothemis culminicola</i>	1	-0.06911	0.069111
11	<i>Heliocypha fenestrata</i>	7	-0.2529	0.252905
12	<i>Anax guttatus</i>	2	-0.11473	0.114725
13	<i>Rhodothemis rufa</i>	3	-0.15147	0.151471
14	<i>Pseudagrion microcephalum</i>	2	-0.11473	0.114725
15	<i>Ictinogomphus decoratus</i>	1	-0.06911	0.069111
16	<i>Brachythemis contaminata</i>	3	-0.15147	0.151471
17	<i>Orthetrum sabina</i>	3	-0.15147	0.151471
18	<i>Copera marginipes</i>	6	-0.23245	0.232452
19	<i>Crocothemis servilia</i>	3	-0.15147	0.151471
	N	59	Index	2.79

Table 7: Dragonfly Diversity Index in the downstream area of Bedog River.

Number	Species	ni	pi ln pi	H'
1	<i>Brachythemis contaminata</i>	51	-0.34804	0.34804
2	<i>Pseudagrion microcephalum</i>	22	-0.32972	0.329719
3	<i>Orthetrum sabina</i>	3	-0.10299	0.102994
4	<i>Ictinogomphus decoratus</i>	1	-0.045	0.044997
5	<i>Heliocypha fenestrata</i>	2	-0.07654	0.076536
6	<i>Libellago lineata</i>	17	-0.29734	0.297338
7	<i>Potamarcha congener</i>	2	-0.07654	0.076536
8	<i>Tholymis tillarga</i>	3	-0.10299	0.102994
9	<i>Orthetrum testaceum</i>	1	-0.045	0.044997
10	<i>Zyxomma obtusum</i>	1	-0.045	0.044997
	N	103	Index	1.47

The downstream area has the lowest diversity index compared to the two previous areas, which is 1.47, although it still falls into the moderate category (Table 7). The index is





	
<i>Heliocypha fenestrata</i>	<i>Brachythemis contaminata</i>
	
<i>Macrogomphus parallelogramma</i>	<i>Neurobasis chinensis florida</i>

Fig. 1: Types of dragonflies found in the Bedog River.

obtained from the number of species found, which is 10, and the number of individuals is 103. The most commonly found species in this area is *Brachythemis contaminata*, with 51 individuals. As the name suggests, this species has the highest tolerance level to contaminants, making it more commonly found in the downstream area compared to other species.

Based on the measurements of the three areas, the overall value of the dragonfly diversity index in the Bedog River is at a moderate level. It can be concluded that ecologically, the Bedog River area has good productivity and relatively balanced ecosystem conditions. Fig. 1 shows some of the dragonfly species encountered during field data collection.

### Relationship between Water Quality and Dragonfly Diversity Index

Table 8 displays a correlation coefficient of 0.961 between water quality and the diversity index, demonstrating a robust link. This is further reinforced by the  $r$  value lying within the range of 0.5 to 0.75. Nevertheless, the correlation coefficient ( $r$ -value) of 0.179 indicates a somewhat weak relationship between water quality and diversity index since it falls

Table 8: Correlation of water quality values and Dragonfly Diversity Index.

Correlation result	Score
Correlation	0.961
Significance	0.179

below the threshold of 0.5. This juxtaposition emphasizes the intricacy of the correlation between water quality and biodiversity indices, indicating that although there may be a broad pattern, the intensity of the connection might fluctuate depending on unique circumstances or supplementary factors.

The intricacy of this matter is further clarified by studies that show a direct relationship between the quality of water and the diversity of dragonflies. Areas with higher water quality have been found to have greater species richness and abundance of dragonflies (Jacob 2016, Bora 2019, Agus et al. 2017). Dragonfly populations in Indonesia, India, and Malaysia have been evaluated in terms of water quality using diversity indices such as Shannon-Wiener and Simpson's (Hidayat et al. 2019, Bora 2019, & Rohman 2016). According to Jacob (2016), certain species of dragonflies, such as *Brachythemis contaminata* and *Bradinopyga geminata*, have been recognized as reliable markers of contaminated and non-polluted waters, respectively. The parameters that affect the distribution of species, such as pH, conductivity, and the concentration of dissolved oxygen, also have a substantial impact (Bora 2019, Perron & Pick 2020). Hence, although there may be overall associations indicating a robust connection between water quality and biodiversity indices, the specific connections can be affected by various environmental and biological factors (Rachmawati et al.



2023). Dragonflies serve as bioindicators, indicating water quality over an extended period rather than at a specific moment, highlighting their significance in long-term ecological monitoring. This comprehensive method affirms the concept that the variety of odonates can serve as a beneficial means of evaluating and tracking water quality in various habitats.

## CONCLUSIONS

The main objective of this study was to assess the water quality of the Bedog River by employing a range of chemical, physical, and biological indicators, with a specific emphasis on the diversity of dragonflies. According to PPRI No. 82 of 2001, the data suggest that the water quality of the Bedog River is moderately contaminated. The water's physical and chemical properties, including temperature, pH, dissolved oxygen, and total dissolved solids, were evaluated and determined to meet the criteria for Class II water quality. However, certain parameters, such as pH and TDS, showed variations from the desired thresholds. The study found that the Bedog River has a reasonably high level of diversity in dragonflies, as a total of 23 dragonfly species were observed. The diversity index was 2.08 in the upstream section, 2.79 in the middle section, and 1.47 in the downstream section. The indices indicate a modest level of diversity in the different sections of the river, with the middle part showing the highest level of diversity. The Pearson correlation value of 0.961 indicates a robust positive association between water quality and dragonfly diversity. However, the significance level of 0.179 suggests that although the correlation is strong, it is not statistically significant.

The novel scientific findings of this study reside in the amalgamation of biological and physicochemical studies to offer a thorough evaluation of river health. Based on the diversity of dragonfly species present and the variation in species richness across observation stations (upstream, middle, and downstream), the observed dragonfly diversity demonstrates potential applicability as an aquatic bioindicator. However, knowledge of species-specific habitat preferences in relation to environmental quality, whether pristine or polluted, is highly dependent on observer experience. Increased frequency, duration, and spatial coverage of field studies on dragonflies will enhance the depth of understanding regarding their ecological significance and bioindicator potential. Utilizing dragonfly diversity as a bioindicator, in conjunction with conventional water quality measurements, addresses a crucial deficiency in river monitoring by providing a more nuanced comprehension of biological circumstances. This approach emphasizes the efficacy of dragonflies as indicators of water

quality and emphasizes their potential for ongoing ecological monitoring. This work presents new opportunities for river management and conservation initiatives by highlighting the significance of preserving water quality to sustain a wide range of aquatic species. Furthermore, it creates opportunities for future investigations into the interaction between biological indicators and water quality, which could result in enhanced approaches for assessing river health and managing the environment.

## REFERENCES

- Aflizar, 2008. Design of watershed management information system (DAS) for rehabilitation and conservation of Sumani Watershed in Solok Regency.
- Agus, M., Pujiastuti, Y. and Windusari, Y., 2017. The diversity of the dragonfly (Odonata) as an indication of water quality. *Science and Technology Indonesia*, 2(4), pp.80-84. DOI.
- Agustiniingsih, D., Setia, B.S. and Sudarno, 2012. Analysis of water quality and water pollution control strategies in Blukar River, Kendal Regency. *Jurnal Presipitasi*, 9(2), September 2012, ISSN 1907-187X. DOI
- Anhwange, B.A., Agbaji, E.B. and Gimba, E.C., 2012. *International Journal of Science and Technology*, 2(5), pp.248-254.
- Ali, A., Soemarno and Mangku, P., 2013. Study of water quality and water quality status of Metro River in Sukun District, Malang City. *Jurnal Bumi Lestari*, 13(2), pp.265-274.
- Alombro, N.C., Guiamadil, R.C., Datumama, W.U., Catipay, J.P.A. and deVera, P.J.D., 2023. Evaluation of organic pollution using algal diversity in rivers of Cotabato City, Bangsamoro Autonomous Region in Muslim Mindanao (BARMM), Mindanao Island, Philippines. *Nature Environment and Pollution Technology*, 22(4), pp.2231-2237. DOI.
- Amneera, N., Najib, N., Rawdhoh, S., Yusof, M. and Rangunathan, S., 2012. Water quality index of Perlis River. *International Journal of Civil & Environmental Engineering*, 13(2), pp.65-73. DOI
- Anwar, M., Budiyo, L. and Syafrudin, S., 2016. Analysis of river water quality to determine allocation from an environmental aspect. *Jurnal Ilmu Lingkungan*, 14, pp.63-71. DOI
- Asmadi, S. and Suharno, S.K.M., 2012. Dasar-dasar teknologi pengolahan air limbah. *Yogyakarta: Gowsen Publishing*.
- Bora, A., 2019. Odonate (Dragonflies and damselflies) diversity as a marker of water quality in Sivasagar, Assam, India. *International Journal on Emerging Technologies*, 10(3), pp.51-54.
- Bordalo, A.A., Teixeira, A.R. and Wiebe, A.W.J., 2006. A water quality index applied to an international shared river basin: The case of the Douro River. *Environmental Management*, 38, pp.910-920. DOI.
- Djaja, I., Purwanto, P. and Sunoko, H.R., 2018. Evaluation of water quality at Bian River in Merauke, Papua. *Web 3 Conference*, 108, p.8016 DOI.
- Hasyim, K. and Asmuni, M., 2009. Study of Soil Fauna Diversity in Organic and Non-Organic Orange Plantations in Batu City. Thesis. Faculty of Science and Technology, Maulana Malik Ibrahim State Islamic University, Malang.
- Hidayat, S., Husnia, F., Rohmah, E. and Mukhlisoh, S., 2019. Study on diversity of dragonfly (Odonata) as a bioindicator of water quality in Mount Muria area, Central Java. *Journal of Natural Sciences and Mathematics Research*, 5(2), pp.53-61. DOI.
- Jacob, S., 2013. The potential of odonate (Dragonflies and damselflies) diversity as a bioindicator of water quality. *International Journal of Science and Research*, 5(7), pp.2319-7064. www.ijsr.net.
- Ministry of Environment, 2003. Decree of the State Minister for the Environment Number 115 of 2003 concerning guidelines for determining water quality status. Ministry of Environment of the Republic of Indonesia, Jakarta.

- Kumar Reddy, D.H. and Lee, S.M., 2012. Water pollution and treatment technologies. *Journal of Environmental & Analytical Toxicology*. DOI.
- Menberu, M.W., Marttila, H., Tahvanainen, T., Kotiaho, J.S., Hokkanen, R., Kløve, B. and Ronkanen, A.K., 2017. Changes in pore water quality after peatland restoration: Assessment of a large-scale, replicated before-after-control-impact study in Finland. *Water Resources Research*, 53, pp.8327-8343. DOI.
- Perron, M.A.C. and Pick, F.R., 2020. Water quality effects on dragonfly and damselfly nymph communities: A comparison of urban and natural ponds. *Environmental Pollution*, 263, 114472. DOI.
- Phong, N.T., Vinh, P.T., Luan, N.D., Dung, P.H., Tanim, A.H., Gagnon, A.S., Lohpaisankrit, W., Hoa, P.T., Truong, P.N. and Vuong, N.D., 2023. Assessment of water quality during 2018-2022 in the Vam Co River Basin, Vietnam. *Nature Environment and Pollution Technology*, 22(4), pp.1747-1763. DOI.
- Rachmawati, A., Yustian, I., Pujiastuti, Y., Shk, S. and Arinafril, 2023. Biotic and dragonfly diversity indices as ecological quality evaluation in Lahat District Rivers, South Sumatra, Indonesia. *Biodiversitas*, 24(11), pp.6059-6068. DOI.
- Rachman, H.T. and Rohman, A., 2016. Dragonflies diversity (Odonata) in Menoreh Karst Central Java – Yogyakarta. *International Journal of Advances in Agricultural and Environmental Engineering*, 3(2), pp.0–4. DOI.
- Setiari, N.M., Mahendra, M.S. and Suyasa, I.W.B., 2012. Identification of pollution sources and water quality analysis of Tukad Yeh Sungai in Tabanan Regency using the pollution index method. *Ecotrophic: Jurnal Ilmu Lingkungan*, 7(1), pp.40-46.
- Setyawan, A.D., Supriatna, J., Nisyawati, Nursamsi, I., Sutarno, Sugiyarto, Sunarto, Pradan, P., Budiharta, S., Pitoyo, A., Suhardono, S., Setyono, P. and Indrawan, M., 2020. Anticipated climate changes reveal shifting in habitat suitability of high-altitude selaginellas in Java, Indonesia. *Biodiversitas*, 21(11), pp.5482-5497. DOI.
- Setyawan, A.D., Supriatna, J., Nisyawati, Nursamsi, I., Sutarno, Sugiyarto, Sunarto, Pradan, P., Budiharta, S., Pitoyo, A., Suhardono, S., Setyono, P. and Indrawan, M., 2021. Projecting expansion range of *Selaginella zollingeriana* in the Indonesian archipelago under future climate conditions. *Biodiversitas*, 22(4), pp.2088-2103. DOI.
- Sutriati, A., 2011. Water quality assessment of urban rivers in Indonesia. *Jurnal Sumber Daya Air*, 7, pp.61-76.
- Wardhana, W.A., 2004. *Impact of Environmental Pollution*. Andi Publisher, Yogyakarta.
- Waluyo, E.A. and Nurlia, A., 2017. Potential development of Liberica coffee (*Coffea liberica*) agroforestry patterns and marketing prospects to support peatland restoration in South Sumatra (Learning from the District of Tanjung Jabung Barat, Jambi Province). *National Seminar Proceeding of Suboptimal Lands*, 2017, pp.978-979.

# From Preservative to Environmental and Health Hazards: A Review on Diverse Applications, Health Impacts and Detection Methods of Paraben(s)

Pooja Upadhyay<sup>ID</sup>, Pammi Gauba<sup>ID</sup> and Ashwani Mathur<sup>†ID</sup>

Department of Biotechnology, Jaypee Institute of Information Technology, A-10, Sector-62, Noida, Uttar Pradesh-201309, India

<sup>†</sup>Corresponding author: Ashwani Mathur; ashwani.mathur@jiit.ac.in

**Abbreviation:** Nat. Env. & Poll. Technol.  
**Website:** www.neptjournal.com

*Received:* 21-05-2024

*Revised:* 10-06-2024

*Accepted:* 19-06-2024

## Key Words:

Parabens  
 Endocrine disruptor  
 Environmental epidemiology  
 Health hazards

## Citation of the Paper:

Upadhyay, P., Gauba, P. and Mathur, A., 2025. From preservative to environmental and health hazards: A review on diverse applications, health impacts and detection methods of paraben(s). *Nature Environment and Pollution Technology*, 24(2), p. B4209. <https://doi.org/10.46488/NEPT.2025.v24i02.B4209>

*Note: From year 2025, the journal uses Article ID instead of page numbers in citation of the published articles.*



**Copyright:** © 2025 by the authors

**Licensee:** Technoscience Publications

This article is an open access article distributed under the terms and conditions of the Creative Commons Attribution (CC BY) license (<https://creativecommons.org/licenses/by/4.0/>).

## ABSTRACT

Paraben(s), or p-hydroxybenzoate derivatives, have been extensively used as preservatives in catalogs of products for decades. The chemical(s) of the group are well known for their water solubility, chemical stability, and low production costs. Additionally, these synthetic organics can be used as supplements in cosmetics, packaged foods, pharmaceuticals, and many other products requiring prolonged shelf lives. However, recent reports of paraben-mediated endocrine disruptions, allergic responses, cancer, loss of fertility, and respiratory disorders are alarming and are the signs of growing health and environmental hazards. The unregulated disposal of packaged products supplemented with parabens and unintended uses may increase the environmental burden in the time to come. Recent studies exploring the health hazards associated with the use or consumption of compounds have provided insight into the underlying mechanisms of action. The paraben(s) are assimilated through two routes: oral administration and skin permeation. The ability to detect compounds in different environmental habitats with robust and specific techniques is important due to the unintended public health burdens of these compounds. This review presents the recent findings on the health burden of the compounds, fallacies in detection, and chronological advancements in the detection of paraben(s). This review assesses the impact of the increasing use of parabens on different cohorts, health hazards, and the need to develop more robust and accurate tools for detecting parabens in different environments.

## INTRODUCTION

Growing industrialization, globalization, and the intervention of modern techniques and technologies have revolutionized the world by meeting the pressing needs of humans. However, this has also created an economic imbalance between the resources and their negative effects. Chemical additives, pesticides, preservatives, taste enhancers, and several other products that have affected human life are an intriguing part of daily life and hold a special significance in the existing food web. One economically obtruding product range is personal care products (PCPs), with diverse compositions, including creams, soaps, shampoos, face washes, toothpaste, deodorants, conditioners, and sun protectants. Often, the ingredients have been tested for their negative health impacts and bioaccumulation (of hazardous chemicals) (Berger et al. 2020). Most of these hazardous chemicals were associated with endocrine disruption, mutagenic, carcinogenic, and other health burdens towards cohorts (Aeling & Nuss 1974, Harvey 2003, Handa et al. 2006, Tavares et al. 2009, Ali & Elgoly 2013, Jia et al. 2015, Vitku et al. 2018). Paraben(s), the alkyl (and often aryl) esters of p-hydroxybenzoic acid, have been exploited as low-cost preservatives due to their excellent preservation activities, biodegradability, thermal stabilities, neutral pHs, lack of color, nonvolatile nature, imperceptible taste and odor, broad antimicrobial spectra (particularly antifungal),

and relatively non-irritating and non-sensitizing properties (Michalkiewicz 2013, Calafat et al. 2010). Furthermore, the low frequencies of sensitization, adequate solubilities in aqueous solutions, and inertness of paraben add to its features (Francisco & Fonseca 2016).

## PARABEN: AN EMERGING ENVIRONMENTAL CONTAMINANT

Paraben(s) use has greatly expanded in daily life products, and with limited knowledge of its health impact for different cohorts, it is difficult to avoid (Yang et al. 2018, Lincho et al. 2021). The urgent need to regulate the use of Paraben(s) in different daily need products has already been mentioned as a concern by different government agencies throughout the world (Vale et al. 2022). Previous studies exploring the

existence of Paraben in different environment matrices have reported half-life time of paraben(s) differing in demography, ranging from around 28h in Spain to 36,000 h in China (Delgado et al. 2016, Song et al. 2017, Vale et al. 2022)

Concerning the severe health impact paraben(s) can pose, and their reported abundance in water bodies and effluents, different physical, biological, and chemical approaches have been noted for their removal or the removal of their transformational products (Ma et al. 2018) (Table 1).

Although the compound has been in use for more than a few decades, utilization has increased since the 1990s as a preservative in food items, drinks, medications, cosmetics, and personal care products (Haman et al. 2015). The alkyl derivatives of paraben are often used in catalogs of products like methylparaben (MP), ethylparaben (EP), propylparaben

Table 1: A few techniques for the removal of Paraben(s) (as reported in prior studies).

Name of Paraben	Removal Percentage (%)	Source	Removal Strategy	Amount of Paraben present initially	References
Methylparaben, Propylparaben	100	Wastewater	Adsorption by Magnetic waste tire-activated carbon-chitosan composite	$1293 \pm 20, 2113 \pm 15 \text{ ng.L}^{-1}$	Mashile et al. 2020
Paraben	99.7	Synthetic solution	Ceramic ultrafiltration membrane developed natively from CuO/TiO <sub>2</sub> nanoparticles	500 ppb	Bhattacharya et al. 2021
Methylparaben, Ethylparaben, Butylparaben	77.2, 88.0, 96.3 (at 90 min)	Water Samples	Photodegradation by direct UV irradiation	$0.6 \times 10^{-3} \text{ mol.L}^{-1}$	Álvarez et al. 2020
Paraben	100	Pure Compound	Transition- and lanthanide-metal co-doped manganese oxide octahedral molecular sieve (Cu-Nd-OMS-2) in peroxymonosulfate (PMS)	$30 \text{ mg.L}^{-1}$	Wang et al. 2022
Paraben	100	Pure Compound	Photo-Fenton process	$5 \text{ mg.L}^{-1}$	Alvarado et al. 2022
Methylparaben, Ethylparaben, Propylparaben, Butylparaben	91.6, 94.0, 97.1, 95.3	Wastewater	aerobic granular sludge (AGS) system-biodegradation and adsorption on sludge	205, 245, 235, $214 \mu\text{g.L}^{-1}$	Argenta et al. 2021
Ethylparaben	92	Pure Compound	CoxNi1-xTiO <sub>3</sub> nanorods as visible light responsive photocatalysts (Calcined at 600 °C)	$250 \text{ mg.L}^{-1}$	Moschogiannaki et al. 2020
Methylparaben	62.16	Wastewater	Adsorption onto oxalic acid pretreated organo-modified bentonite and direct organo-modified bentonite adsorbent	-	Abdulsalam et al. 2023
Benzylparaben	61.3	Pure Compound	S-scheme heterojunction photocatalyst, consisting of monoclinic bismuth vanadate (BiVO <sub>4</sub> ) and graphitic carbon nitride (g-C <sub>3</sub> N <sub>4</sub> )	$20 \text{ mg.L}^{-1}$	Hu et al. 2022
Methylparaben	100, 34.2	Pure Compound	Biodegradation by microalgae <i>Phaeodactylum tricornutum</i> and <i>Chlorella vulgaris</i>	$80 \text{ mg.L}^{-1}$	Chang et al. 2023
Benzylparaben	85.7 in 150 min	Pure Compound	Modified g-C <sub>3</sub> N <sub>4</sub> (GCN) and BiVO <sub>4</sub> (BVO) composite under Irradiation through visible light by carbon quantum dots (CQDs)	-	Tian et al. 2023
Benzylparaben dye	100	Wastewater	Zeolitic Imidazolate-67 Modified by Fe <sub>3</sub> O <sub>4</sub> Nanoparticles	$10 \text{ mg.L}^{-1}$	Pourmohammad et al. 2024



(PP), and butylparaben (BP) (Liao et al. 2013). The paraben(s) have been found in various natural resources as well, including carrots, mulberries, blueberries, olives, vanilla, strawberries, and mangoes, preserving by protecting against various microorganisms and pathogens (Sellappan et al. 2002, Kang et al. 2008, Kirchhof & de Gannes 2013, Li et al. 2016). Prior studies have also noted associations between antimicrobial activities and the alkyl chain lengths of parabens, coupled with a reduction in water solubility (Flasiński et al. 2016).

In recent years, there have been mounting concerns about the health impacts of parabens as the rate of human exposure to these compounds has increased. The paraben(s) have been used in more than thousands of personal care products at concentrations up to 0.4% to 0.8% (by weight) (Andersen et al. 2007). In a recent study by Li et al. 2020, several noninvasive biomarkers, such as human fingernails, were used to assess paraben contamination. The concentrations reached 39.9 to 27400 ng.g<sup>-1</sup> of methylparaben, propylparaben, or ethylparaben in fingernails, indicating their use in cosmetics (Li et al. 2020). Most of these studies have reported endocrine disruption effects and imbalanced reproductive function due to paraben in humans and animals (Koeppe et al. 2013, Boberg et al. 2010, Aker et al. 2016, Darbre & Harvey 2008). The paraben(s) enter the human body mainly through absorption or ingestion and are generally detected in blood, breast milk, and urine (Popa et al. 2011, Leppert et al. 2020). Parabens are excreted through the urinary system as mixtures of various paraben metabolites (Ye et al. 2006, Upadhyay et al. 2020). Further analyses of the antimicrobial activity showed better efficacy against fungi than against bacteria, and the impact was greater against gram-positive bacteria than against their gram-negative bacteria counterparts (Wang et al. 2013). The efficiencies of parabens in combination with each other agents have also been explored (Soni et al. 2002). Parabens disturb the hypothalamic-pituitary-gonadal axis by imitating female hormone actions, thereby hindering or destabilizing normal hormonal functions and compromising male reproductive abilities. This endocrine disruptor interferes with overall hormone activity, synthesis, transport, and metabolism. The composites may induce changes in the typical operations of the nervous system, thyroid function, immune system, glucose levels, and lipid balance. Additionally, they can serve as epigenetic regulators, initiating effects that span generations (Bledzka et al. 2014, Lincho et al. 2021). It has been reported that paraben(s) exposure can also cause mitochondrial dysfunction (Martins et al. 2020). In recent studies, their associations with breast cancer and changes in the ovarian and pituitary hormone levels have been discovered (Amin et al. 2019, Khanna et al. 2013, Charles et al. 2013, Hajizadeh et al. 2020). These compounds are responsible

for the dislocation of [3H]estradiol from the estrogen receptor in the MCF7 cell cytosol, increased expression of a stably transfected estrogen-responsive reporter gene in MCF7 cells, and increased growth of estrogen-dependent human breast cancer cells (MCF7 and ZR-75-1). This association connects the estrogenic response of breast tumor cells with the presence of parabens in human breast tissue, as estrogen plays a role in breast cancer development. (Lincho et al. 2021). The health impacts of these treatments are not limited to this, but a study by Meeker et al. 2011 showed a positive correlation between the concentration of urinary butyl paraben (BP) and male sperm DNA damage. Due to the widespread use of parabens, human exposure to these chemicals is inevitable. Therefore, a suitable, specific, cost-effective detection technique is necessary to regulate the increasing exposure to these adverse effects.

Numerous studies have shown the presence of parabens in diverse personal care products and food items at the nanomolar level (Table 2).

## DETECTION METHODS FOR ALKYL DERIVATIVES OF PARABEN

### Qualitative and Quantitative Estimates of Paraben Concentrations

A permanent tool for primary detection and monitoring of this preservative is vital (Alhadrami et al. 2017). Various analytical

Table 2: Amounts of Paraben present in various products (as reported in prior studies).

S. No	Sample Product	Concentration of Methylparaben	Reference
1.	Iced tea	97 ng.g <sup>-1</sup>	(Liao et al. 2013)
2.	Pudding	51 ng.g <sup>-1</sup>	
3.	Muffins	83 ng.g <sup>-1</sup>	
4.	Turkey Roast	44 ng.g <sup>-1</sup>	
5.	Hair conditioner	21.6 ± 0.79 nM	(Baytak et al. 2017)
6.	Baby wipes	24.0 ± 0.67 nM	
7.	Shaving lotion	31.8 ± 0.95 nM	
8.	Hair gel	34.7 ± 0.88 nM	
9.	Syrup	13.1 ± 0.39 nM	(Mendonca et al. 2017)
10.	Eye drop	15.8 ± 0.40 nM	
11.	Mouthwash	21.0 ± 0.67 nM	
12.	Deodorant	2.89 x10 <sup>-3</sup> mol/L	
13.	Cyprodien Syrup	1.57 mM	(Dhahir & Hussein 2013)
14.	Ketofen Syrup	4.21 mM	
15.	Conditioner	20 nM	(Gholivand et al. 2014)

techniques with different principles and methodologies have been used for the detection of these pollutants in ecosystems. However, the selectivities and sensitivities differed. Furthermore, with the increasing need for early detection of carcinogens, mutagenic agents, and various other toxic materials, there is also a need for bioassays that monitor and report bio-availabilities and their impacts on humans. All optimized and tested techniques are thought to be highly accurate with a low detection limit, although they are laborious and expensive (Gurban et al. 2011).

- a) **Spectrophotometric analysis:** Spectrophotometric methods determine the presence of paraben in pure and combined forms, as reported by Dhahir and Hussein (2013). The process is based on the diazotization of the compound with sodium nitrite, which is subsequently coupled with ortho-aminobenzoic acid to produce an orange-colored product. The method requires an acidic medium and a low temperature to reach a concentration range of  $1\text{--}9\text{ }\mu\text{g.mL}^{-1}$  for detection at 442 nm (in accordance with Beer's law). The detection limit of this procedure was  $0.0065\text{ }\mu\text{g.mL}^{-1}$ , and the limit of quantitation was  $0.02\text{ }\mu\text{g/mL}$ . Different variables were studied to optimize the reaction, including the concentrations of the reagents, reaction time, mole ratio, and color stability period. The analytical results were statistically validated with recovery studies. These methods successfully determined the concentrations of methylparaben in some oral solutions (Dhahir & Hussein 2013). Even though the method is simple, repetition of the method with promising results exhibited limitations (Wasito & Phechkrajung 2015).
- b) **Chromatographic analysis:** Many analytical techniques have been designed for quantitative determinations of parabens. These include microbiological assays, which are less accurate than HPLC and insensitive to low concentrations of parabens, while colorimetric and spectrophotometric methods are tedious and nonspecific (Abuirjeie et al. 1990). Gas chromatography, although specific and sensitive, is not commonly used with pharmaceuticals because prior derivatization is needed. Thin-layer chromatography is suitable for qualitative determinations of parabens in preservative mixtures, and more recently, thin-layer HPLC densitometry has been employed for quantitative determinations (Tománková

& Pinkasová 1990). Esters of p-hydroxybenzoic acids undergo hydrolysis to the parent acid and subsequent degradation to phenol via decarboxylation. The process is faster at  $\text{pH}>5$  (Lachman 1968, Dhaliwal & Theobald 1995). Chromatography is undoubtedly an accurate method, but it has various limitations related to the costly instruments used, locations, skilled labor, and method of operation (Wasito & Phechkrajung 2015).

- c) **Sensor-based analysis:** The prevailing need for field monitoring has spurred the advancement of sensors into analytical tools that offer swift, cost-efficient, precise, and highly sensitive analysis. Other analytical methods cannot be applied at the location or site of analysis. Therefore, alternative robust analytical methods with high accuracies, selectivities, and sensitivities for the detection of many such analytes need to be developed and explored. Additionally, sensors often provide versatile solutions for on-site monitoring. A sensor is an instrument that responds to changes in environmental variables such as pressure, heat, movement, humidity, etc. These changes alter the chemical, physical, or electromagnetic properties of the sensor, which are converted into more usable and comprehensible forms (Fig. 1). The signal produced by the equipment corresponds to the quantity to be determined. Sensors measure a particular characteristic of any object, compound, or disease.

Sensors have been used in many fields, such as the food industry and the marine and medical sectors, and they exhibit better stabilities and sensitivities than traditional methods (Mehrotra 2016). The types of sensors used depend on the reaction, analyte, and element involved and include physical sensors, chemical sensors, and biosensors (Naresh & Lee 2021). Food contaminants, environmental pollutants, and medical applications require the same limits of detection, sensitivities, and stabilities. However, various parameters, such as the sample volume, matrix density, and continuous on-site monitoring, complicate the development of these sensors. The sensor must be stable in a normal storage environment. In the case of *in vivo* monitoring, the sensor should be sterile, biocompatible, and non-toxic. Additionally, the sensor should be small, portable, easy to use, and inexpensive, and the various parameters on which the performance of a sensor depends are listed in Table 3.

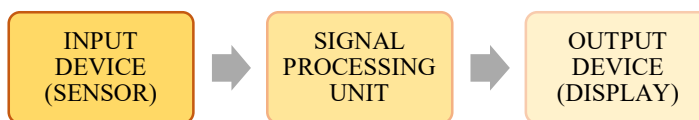


Fig. 1: Principal operation of electrochemical (bio)sensors (Alhadrami et al. 2017).

The typical sensor structure can be segregated into three major parts: recognition components, interfaces (immobilization techniques), and transducing elements (Fig. 2).

### Different Sensor Design/Immobilization Techniques for the Detection of Paraben

Parabens are found in various environmental niches and exert both acute and chronic effects on living beings. Recently, numerous sensors and biosensors have been deployed for the determination of paraben concentrations based on the techniques and methods used. Significant achievements in sensing have been attained by the integration of biomolecules into devices. Various studies have shown the use of different techniques for sensing parabens, ranging from the use of nanomaterials to hemoglobin, glassy carbon electrodes, and screen-printed electrodes

have been used for the detection of various parabens (Tables 4-7).

The diverse development of paraben sensors with different electrodes, receptor systems, and immobilization methods makes every sensor unique and shows the growing scientific interest in harnessing sensor technology for the detection of paraben(s). The limits of detection are also affected by changes in the transducer and receptor used. It is evident that the unique reactions between receptor(s) and parabens, along with signal transduction with electrochemical methods, play pivotal roles in the development of paraben sensors with dynamic accuracies and limits of detection. These studies may be extended further to explore the potential roles of biomolecules, including enzymes, as alternative receptors. However, exploratory studies on potential enzyme sources are limited by major bottlenecks (such as enzyme stability and cost of production), which may be specific to paraben detection.

Table 3: Parameters that affect the analytical capabilities of the sensors (Slaughter 2018).

Parameters of Biosensor	Description
Sensitivity	The slope of the calibration curve (ratio of the change in the output signal for a given change in the analyte concentration)
Selectivity	The ratio of the change in the output signal for a given change in the concentrations of analyte and interfering species
Specificity	The biocatalyst used for detection is highly specific and displays adequate stability over many assays (>>100)
Signal-to-noise ratio	Measure of the statistical instability in a blank signal (ratio of the suitable analytical signal to the background noise)
Limit of detection (LOD)	Certain concentrations obtained from the smallest detectable output signal
Reproducibility	Precision of the output signal when engaged over a long time interval/performed in different locations
Repeatability	Precision in the output signal over a brief time
Response time	The time required for the output signal to reach 90% steady-state value.

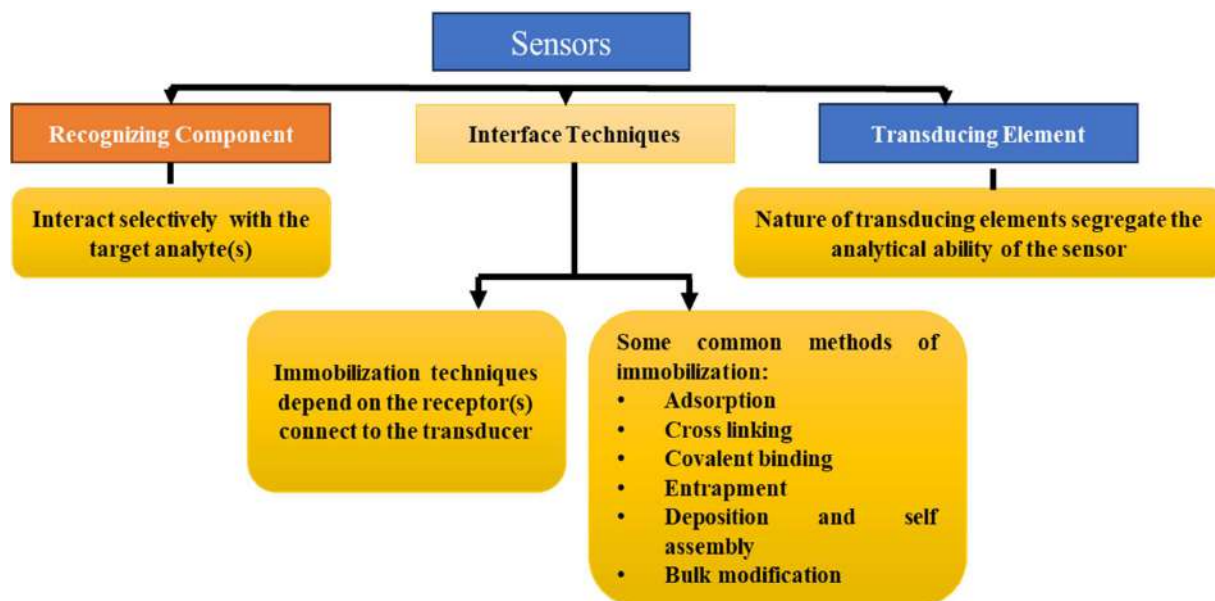


Fig. 2: Paraben detection, component, and properties of the sensors.

Table 4: Advances in sensors for the detection of methylparaben.

Receptor used	Immobilization technique used	Transducer	Reaction	Modification of Electrode	Range of Detection	Limit of Detection	Advantages	Reference
The ability of reduced Graphene Oxide (rGO) to adsorb MP	Drop-coating Nanocomposite onto the electrode surface	Carbon Nanocrystal (CNC)	Formation of benzoquinone due to the oxidation of phenolic group in the methylparaben	Nanocomposite of Cellulose nanocrystal – reduced Graphene Oxide (CNC–rGO) modified electrode	$2 \times 10^{-4}$ M to $9 \times 10^{-4}$ M	$1 \times 10^{-4}$ M	Reproducibility and reusability	(Khalid et al. 2019)
Langmuir Blodgett (LB) film	Vertical dipping of compressed LB film on the layer of MWCNTs-ODA (Multi-Walled Carbon Nano Tubes-Octadecylamine) Composite of hemoglobin-MWCNTs was packed by piston piston-driven CPE holder	Glassy Carbon Electrode (GCE)	Release of electron	Langmuir Blodgett film of Multi-Walled Carbon Nano Tubes (MWCNTs) on GCE	$1 \times 10^{-6}$ mol.L <sup>-1</sup> to $8 \times 10^{-5}$ mol.L <sup>-1</sup>	$4 \times 10^{-7}$ mol.L <sup>-1</sup>	Stability and reproducibility	(Wang et al. 2015)
Hemoglobin		Carbon Paste Electrode (CPE)	Hemoglobin acts as an electron transfer mediator between MP and electrode.	Hemoglobin and MWCNTs on CPE	0.1 to 13 $\mu$ mol.L <sup>-1</sup>	25 nmol.L <sup>-1</sup>	Accurate, rapid response and Adequate sensitivity, stability, and repeatability.	(Haijin et al. 2015, Haijin et al. 2016)
Nanoparticles of Carbon Nanofibers and Cobalt-Nickel-Palladium	The composite was cast and left to dry	Glassy Carbon Electrode (GCE)	One-electron transfer accompanied by one proton.	Carbon Nanofibers and Nanoparticles Complex of Cobalt-Nickel-Palladium ((Co-Ni-Pd) NPs) and Nanofibers of Carbon on GCE	3–300 nM	1.2 nM	Reproducibility, excellent accuracy, decreased overpotential, Precision, lower limit of detection, and increased sensitivity.	(Baytak et al. 2017)
Reduced Graphene Oxide decorated along with Ruthenium Nanoparticles Reduced Graphene Oxide (CNC–rGO) nanocomposite	Dropped over GCE	Glassy Carbon Electrode (GCE)	electro-oxidization of Hydroxyl group on the aromatic ring, releasing one electron and one proton generating a quinone	Reduced Graphene Oxide decorated along with Ruthenium Nanoparticles (rGO/Ru NPs) on GCE	$5.00 \times 10^{-7}$ to $3.00 \times 10^{-6}$ mol.L <sup>-1</sup>	$2.40 \times 10^{-7}$ mol.L <sup>-1</sup>	Low LOD	(Mendonca et al. 2017)
Nanoparticles Reduced Graphene oxide (CNC–rGO) nanocomposite	Drop coating	Screen Printed Electrode (SPE)	The electrochemically active surface area of the electrode (i.e., CNC-rGO, rGO)	Cellulose Nanocrystal-Reduced Graphene Oxide Nanocomposite (CNC-rGO) on SPE	$2 \times 10^{-4}$ to $9 \times 10^{-4}$ M	$1 \times 10^{-4}$ M	Stability	(Khalid et al. 2019)
Nafion Film	Coating	Glassy Carbon Electrode (GCE)	Oxidation of MP	MWCNT-Nafion Film on GCE	$3.00 \times 10^{-6}$ to $1.00 \times 10^{-4}$ mol.L <sup>-1</sup>	$1.00 \times 10^{-6}$ mol.L <sup>-1</sup>	Good Sensitivity	(Luo et al. 2012)
Zinc Hydroxide	Not mentioned	Carbon Paste Electrode (CPE)	Electrocatalytic oxidation	Zinc Hydroxide Nanoparticles on CPE	$4.00 \times 10^{-6}$ to $1.26 \times 10^{-3}$ mol.L <sup>-1</sup>	$3.21 \times 10^{-6}$ mol.L <sup>-1</sup>	Not mentioned	(Hasanzadeh et al. 2012)
Molecularly imprinted polymers (MIPs)	Tripropylene glycol diacrylate cross-linking the functional monomer (i.e., Methacrylic acid) on Molecularly Imprinted Polymer film.	Glassy Carbon Electrode (GCE)	Analyte Specific recognition sites by formation of a vacant shape, same as the analyte, Cross-linking (functional groups rebind target using the same noncovalent bonds)	For the dual templates sensor, Methylparaben and Propylparaben were imprinted on the surface of the sensor.	$2.0 \times 10^{-5}$ to $1.0 \times 10^{-4}$ M	$4.0 \times 10^{-7}$ M	Less Response Time	(Wang et al. 2010)



Table 5: Advances in propylparaben sensors.

Receptor used	Recognition method	Transducer	Reaction	Mechanism	Range	Limit of Detection	References
Molecularly imprinted polymers (MIPs)	Tripropylene glycol diacrylate cross-linking the functional monomer (i.e., Methacrylic acid) on Molecularly Imprinted Polymer film.	GCE	Analyte Specific recognition sites by formation of a vacant shape, same as the analyte, Cross-linking (functional groups rebind target using the same noncovalent bonds)	For the dual templates sensor, Methylparaben and Propylparaben were imprinted on the surface of the sensor.	$5.0 \times 10^{-6}$ – $1.0 \times 10^{-4}$ M	$2.0 \times 10^{-7}$ M	(Wang et al. 2010)
Poly(methacrylic acid) (PMAA)	Poly(methacrylic acid) and functionalized carbon nanotubes nanocomposite	GCE	synergetic effect of f-CNTs and PMAA	synergetic effect of f-CNTs and PMAA	$5 \times 10^{-6}$ to $1 \times 10^{-4}$ M	$2 \times 10^{-7}$ M	(Xin et al. 2023)

Table 6: Advances in sensors for ethylparaben.

Receptor used	Immobilization technique used	Transducer	Mechanism	Modification of Electrode	Range	Limit of Detection	Advantages	Reference
poly-(2-hydroxyethyl methacrylate-N-meth acryloyl-L-phenylalanine) (PHEMA-MAPA) nanofilm	Polymerization of paraben imprinted polymeric film	SPE	Unavailable	N-methacryloyl-(L)-cysteine (MAC) Coating	1 to 30 mM	$\mu$ M	Highly selective	(Yücebaşı et al. 2020)
Fullerene nanorods (f-NR)	C <sub>60</sub> NRs were immobilized at the surface of GCE–Ph–NH <sub>2</sub> by N–H addition over a p-bond of fullerene	GCE	Electrooxidation of ethyl paraben at the ERC <sub>60</sub> NRs–NH–Ph–GCE sensor	ERC <sub>60</sub> NRs–NH–Ph–GCE sensor	0.01–0.52 mM	3.8 nM	High electrocatalytic detection activity	(Rather et al. 2016)
Poly(methacrylic acid)	Crosslinking	GCE	synergetic effect of f-CNTs and PMAA	Poly(methacrylic acid) and functionalized carbon nanotubes nanocomposite	$2 \times 10^{-5}$ to $10 \times 10^{-5}$ M	$4 \times 10^{-7}$ M	Sensitive detection	(Xin et al. 2023)

Table 7: Advances in sensors for butylparaben.

Receptor used	Immobilization technique used	Transducer	Reaction	Modification of Electrode	Range	Limit of Detection	Advantages	References
ds DNA	electrochemically entrapped on CPE	Silver nanoparticles	Not mentioned	Not mentioned	0.362 to 100 $\mu$ g.L <sup>-1</sup>	0.109 $\mu$ g.L <sup>-1</sup>	Electrochemically large active surface area, good selectivity, excellent reproducibility and sensitivity.	(Karastogianni et al. 2017)
Poly (methacrylic acid)	Crosslinking	GCE	synergetic effect of f-CNTs and PMAA	Poly(methacrylic acid) and functionalized carbon nanotubes nanocomposite	$5 \times 10^{-6}$ to $8 \times 10^{-5}$ M	$2 \times 10^{-7}$ M	Sensitive detection	(Xin et al. 2023)
In <sub>2</sub> O <sub>3</sub> nano bricks	Not mentioned	GCE	OH Benzoquinone (Single electron oxidation)	Indium Oxide (In <sub>2</sub> O <sub>3</sub> ) Nano brick on GCE	Not mentioned	0.08 $\mu$ M	Increased conductivity and surface area	(Qurashi et al. 2015)

## CONCLUSIONS

The presence of paraben alkyl derivatives to meet the daily needs of humans is of paramount importance, and the possibility that these compounds may be present in ecological niches cannot be ruled out. The irreplaceable property of paraben is that it is a preferred choice for society. Previous studies have highlighted the advantages of sensor technology as a suitable, highly sensitive approach to supersede the conventional technique. Growing health-related concerns associated with different alkyl derivatives of parabens may impose a negative burden on the health of society at large. Early detection via the design of POC (point of care) devices would aid in the detection of parabens through more accurate analyses and with lower limits of quantification. These techniques could be extended by exploring a more diverse range of analytes to improve their accuracy and make them economically viable and sustainable solutions for society at large.

## ACKNOWLEDGMENT

This work was funded by the Department of Biotechnology (DBT), Ministry of Science and Technology, Government of India [vide Project No. BT/PR40549/MED/32/756/2020]. We acknowledge Jaypee Institute of Information Technology, Noida, Uttar Pradesh, India for providing the required infrastructure.

## REFERENCES

- Abdulsalam, A., Ibrahim, Y.S., Yaro, N.A., Olanrewaju, O.A., Alhassan, B., Iyayosa, D.A. and Lawal, K., 2023. Emerging contaminants removal from wastewater using organo-modified bentonite clay. *Journal of Engineering Research and Reports*, 25(10), pp.121–144. [DOI]
- Abuirjeie, M.A., Abdel-Hamid, M.E., Abdel-Aziz, A.A. and Ibrahim, E.A., 1990. A comparative study on HPLC and microbiological determination of p-hydroxybenzoate esters (parabens) in pharmaceutical formulations. *Analytical Letters*, 23(1), pp.67–82. [DOI]
- Aeling, J.L. and Nuss, D.D., 1974. Letter: Systemic eczematous “contact-type” dermatitis medicamentosa caused by parabens. *Archives of Dermatology*, 110(4), p.640.
- Aker, A.M., Watkins, D.J., Johns, L.E., Ferguson, K.K., Soldin, O.P., Anzalota Del Toro, L.V., Alshawabkeh, A.N., Cordero, J.F. and Meeker, J.D., 2016. Phenols and parabens in relation to reproductive and thyroid hormones in pregnant women. *Environmental Research*, 151, pp.30–37. [DOI]
- Alhadrami, H., 2017. Biosensors: Classifications, medical applications, and future prospective. *Biotechnology and Applied Biochemistry*, 65(3), pp.497–508. [DOI]
- Ali, E.H. and Elgoly, A.H., 2013. Combined prenatal and postnatal butylparaben exposure produces autism-like symptoms in offspring: comparison with the valproic acid autistic model. *Pharmacology Biochemistry and Behavior*, 111, pp.102–110. [DOI]
- Álvarez, M.A., Martínez, M.M.R., Quesada, G.C., Ramón, M.V.L., Utrilla, J.R., Polo, M.S. and Mota, A.J., 2020. Removal of parabens from water by UV-driven advanced oxidation processes. *Journal of Chemical Engineering*, 379, p.122334. [DOI]
- Amin, M.M., Tabatabaeian, M., Chavoshani, A., Amjadi, E., Hashemi, M., Ebrahimpour, K., Klishadi, R., Khazaei, S. and Mansourian, M., 2019. Paraben content in adjacent normal-malignant breast tissues from women with breast cancer. *Biomedical and Environmental Sciences*, 32(12), pp.893–904. [DOI]
- Andersen, H.R., Lundsbye, M., Wedel, H.V., Eriksson, E. and Ledin, A., 2007. Estrogenic personal care products in a greywater reuse system. *Water Science and Technology*, 56(12), pp.45–49. [DOI]
- Argenta, T.S., Barros, A.R.M., Carvalho, C.A., Santos, A.B. and Firmino, P.I.M., 2021. Parabens in aerobic granular sludge systems: impact on granulation and insights into removal mechanisms. *Science of the Total Environment*, 753, p.142105. [DOI]
- Baytak, A.K., Duzmen, S., Teker, T. and Aslanoglu, M., 2017. Voltammetric determination of methylparaben and its DNA interaction using a novel platform based on carbon nanofibers and cobalt-nickel-palladium nanoparticles. *Sensors and Actuators B: Chemical*, 239, pp.330–337. [DOI]
- Berger, K., Coker, E., Rauch, S., Eskenazi, B., Balmes, J., Kogut, K., Holland, N., Calafat, A.M. and Harley, K., 2020. Prenatal phthalate, paraben, and phenol exposure and childhood allergic and respiratory outcomes: Evaluating exposure to chemical mixtures. *Science of the Total Environment*, 725, p.138418. [DOI]
- Bhattacharya, P., Mukherjee, D., Deb, N., Swarnakar, S. and Banerjee, S., 2021. Indigenously developed CuO/TiO<sub>2</sub> coated ceramic ultrafiltration membrane for removal of emerging contaminants like phthalates and parabens: Toxicity evaluation in PA-1 cell line. *Materials Chemistry and Physics*, 258, p.123920. [DOI]
- Bledzka, D., Gromadzińska, J. and Wasowicz, W., 2014. Paraben: From environmental studies to human health. *Environment International*, 67, pp.27–42. [DOI]
- Boberg, J., Taxvig, C., Christiansen, S. and Hass, U., 2010. Possible endocrine-disrupting effects of parabens and their metabolites. *Reproductive Toxicology*, 30(2), pp.301–312. [DOI]
- Calafat, A.M., Ye, X., Wong, L.Y., Bishop, A.M. and Needham, L.L., 2010. Urinary concentrations of four parabens in the U.S. population: NHANES 2005–2006. *Environmental Health Perspectives*, 118, pp.679–685. [DOI]
- Chang, X., He, Y., Song, L., Ding, J., Ren, S., Lv, M. and Chen, L., 2023. Methylparaben toxicity and its removal by microalgae *Chlorella vulgaris* and *Phaeodactylum tricornutum*. *Journal of Hazardous Materials*, 454, p.131528. [DOI]
- Charles, A.K. and Darbre, P.D., 2013. Combinations of parabens at concentrations measured in human breast tissue can increase the proliferation of MCF-7 human breast cancer cells. *Journal of Applied Toxicology*, 33(5), pp.390–398. [DOI]
- Darbre, P.D. and Harvey, P.W., 2008. Paraben esters: Review of recent studies of endocrine toxicity, absorption, esterase, and human exposure, and discussion of potential human health risks. *Journal of Applied Toxicology*, 28(5), pp.561–578. [DOI]
- Dhahir, S.A. and Hussein, H.J., 2013. Spectrophotometric determination of methyl paraben in pure and pharmaceutical oral solution. *Advances in Natural Science*, 6(4), pp.69–74. [DOI]
- Dhaliwal, K. and Theobald, A.E., 1995. The determination of paraben preservatives in syrup formulations. *Pharmaceutical Science*, 1(2), pp.99–101. [DOI]
- Alvarado, D.V., Santos-Juanes, L., Arques, A. and Amat, A.M., 2022. Mild Fenton processes for the removal of preservatives: Interfering effect of methylisothiazolinone (MIT) on paraben degradation. *Catalysts*, 12(11), p.1390. [DOI]
- Flasiński, M., Gawryś, M. and Broniatowski, M., 2016. Studies on the interactions between parabens and lipid membrane components in monolayers at the air/aqueous solution interface. *Biochimica et Biophysica Acta (BBA) - Biomembranes*, 1858(4), pp.836–844. [DOI]
- Francisco, A. and Fonseca, A.P., 2016. Parabens paradoxes in cosmetic

- formulations: A review. *International Journal of Medical Research & Pharmaceutical Sciences*, 3(8). [DOI]
- Gholivand, M.B., Shamsipur, M., Dehdashtian, S. and Rajabi, H.R., 2014. Development of a selective and sensitive voltammetric sensor for propylparaben based on a nanosized molecularly imprinted polymer-carbon paste electrode. *Materials Science and Engineering: C*, 36, pp.102–107. [DOI]
- Gurban, A.M., Rotariu, L., Baibarac, M., Baltog, I. and Bala, C., 2011. Sensitive detection of endocrine disrupters using ionic liquid–single-walled carbon nanotubes modified screen-printed based biosensors. *Talanta*, 85, pp.2007–2013. [DOI]
- Haijin, A., Ghodsi, J., Afraz, A., Rafati, A.A., Shoja, Y., Yurchenko, O. and Urban, G., 2015. Development of a novel biosensor for nanomolar detection of methylparaben. *Procedia Engineering*, 120, pp.552–555. [DOI]
- Haijin, A., Ghodsi, J., Afraz, A., Yurchenko, O. and Urban, G., 2016. Nanomolar detection of methylparaben by a cost-effective hemoglobin-based biosensor. *Materials Science and Engineering: C*, 69, pp.122–127. [DOI]
- Hajizadeh, Y., Feizabadi, K.G., Ebrahimpour, K., Shoshtari-Yeganeh, B., Fadaei, S., Darvishmotevali, M. and Karimi, H., 2020. Urinary paraben concentrations and their implications for human exposure in Iranian pregnant women. *Environmental Science and Pollution Research*, 27, pp.14723–14734. [DOI]
- Haman, C., Dauchy, X., Rosin, C. and Munoz, J.F., 2015. Occurrence, fate, and behavior of parabens in aquatic environments: A review. *Water Research*, 68, pp.1–11. [DOI]
- Handa, O., Kokura, S., Adachi, S., Takagi, T., Naito, Y., Tanigawa, T., Yoshida, N. and Yoshikawa, T., 2006. Methylparaben potentiates UV-induced damage of skin keratinocytes. *Toxicology*, 227(1–2), pp.62–72.
- Harvey, P.W., 2003. Parabens, oestrogenicity, underarm cosmetics, and breast cancer: A perspective on a hypothesis. *Journal of Applied Toxicology*, 23(5), pp.285–288. [DOI]
- Hasanzadeh, M., Shadjou, N., Saghatforoush, L., Mehdizadeh, R. and Sanati, S., 2012. Electrocatalytic oxidation of selected parabens on zinc hydroxide nanoparticles. *Catalysis Communications*, 19, pp.10–16. [DOI]
- Hu, C., Tian, M., Wu, L. and Chen, L., 2022. Enhanced photocatalytic degradation of paraben preservative over designed g-C<sub>3</sub>N<sub>4</sub>/BiVO<sub>4</sub> S-scheme system and toxicity assessment. *Ecotoxicology and Environmental Safety*, 231, p.113175. [DOI]
- Jia, M., Dahlman-Wright, K. and Gustafsson, J.A., 2015. Estrogen receptor alpha and beta in health and disease. *Best Practice & Research Clinical Endocrinology & Metabolism*, 29(4), pp.557–568. [DOI]
- Kang, Y.H., Parker, C.C., Smith, A.C. and Waldron, K.W., 2008. Characterization and distribution of phenolics in carrot cell walls. *Journal of Agricultural and Food Chemistry*, 56(18), pp.8558–8564. [DOI]
- Karastogianni, S. and Girousi, S., 2017. A novel electrochemical bioimprinted sensor of butylparaben on a modified carbon paste electrode with safranin-O capped to silver nanoparticles. *International Journal of Current Research*, 9(11), pp.61118–61124.
- Khalid, W.E.F.W., Arip, M.N.M., Jasmani, L. and Lee, Y.H., 2019. A new sensor for methylparaben using an electrode made of a cellulose nanocrystal-reduced graphene oxide nanocomposite. *Sensors*, 19(12), p.2726. [DOI]
- Khanna, S. and Darbre, P.D., 2013. Parabens enable suspension growth of MCF-10A immortalized, non-transformed human breast epithelial cells. *Journal of Applied Toxicology*, 33(5), pp.378–382. [DOI]
- Kirchhof, M.G. and de Gannes, G.C., 2013. The health controversies of parabens. *Skin Therapy Letter*, 18(2), pp.5–7.
- Koeppe, E.S., Ferguson, K.K., Colacino, J.A. and Meeker, J.D., 2013. Relationship between urinary triclosan and paraben concentrations and serum thyroid measures in NHANES 2007–2008. *Science of the Total Environment*, 445–446, pp.299–305. [DOI]
- Lachman, L., 1968. The instability of antimicrobial preservatives. *Bulletin of the Parenteral Drug Association*, 22(3), pp.127–144.
- Leppert, B., Strunz, S., Seiwert, B., Schlittenbauer, L., Schlichting, R., Pfeiffer, C., Röder, S., Bauer, M., Borte, M., Stangl, G.I., Schöneberg, T., Schulz, A., Karkossa, I., Rolle-Kampczyk, U.E., Thürmann, L., Bergen, M.V., Escher, B.J., Junge, K.M., Reemtsma, T., Lehmann, I. and Polte, T., 2020. Maternal paraben exposure triggers childhood overweight development. *Nature Communications*, 11, p.561. [DOI]
- Li, C., Cui, X., Chen, Y. and Liao, C., 2020. Paraben concentrations in human fingernails and their association with personal care product use. *Ecotoxicology and Environmental Safety*, 202, p.110933. [DOI]
- Li, W., Gao, L., Shi, Y., Wang, Y., Liu, J. and Cai, Y., 2016. Spatial distribution, temporal variation and risks of parabens and their chlorinated derivatives in urban surface water in Beijing, China. *Science of the Total Environment*, 539, pp.262–270. [DOI]
- Liao, C., Liu, F. and Kannan, K., 2013. Occurrence of and dietary exposure to parabens in foodstuffs from the United States. *Environmental Science & Technology*, 47(8), pp.3918–3925. [DOI]
- Lincho, J., Martins, R.C. and Gomes, J., 2021. Paraben compounds—Part I: An overview of their characteristics, detection, and impacts. *Applied Sciences*, 11(5), p.2307. [DOI]
- Luo, P., Liu, J., Li, Y., Miao, Y.H. and Ye, B., 2012. Voltammetric determination of methylparaben in cosmetics using a multi-wall carbon nanotubes/Nafion composite modified glassy carbon electrode. *Analytical Letters*, 45, pp.2445–2454. [DOI]
- Ma, W.L., Zhao, X., Zhang, Z.F., Xu, F.J. and Li, Y.F., 2018. Concentrations and fate of parabens and their metabolites in two typical wastewater treatment plants in northeastern China. *Science of the Total Environment*, 644, pp.754–761. [DOI]
- Martins, F.C., Videira, R.A., Oliveira, M.M., Silva-Maia, D., Ferreira, F.M. and Peixoto, F.P., 2020. Parabens enhance the calcium-dependent testicular mitochondrial permeability transition: Their relevance on the reproductive capacity in male animals. *Journal of Biochemical and Molecular Toxicology*, 35(3), pp.1–8. [DOI]
- Mashile, G.P., Mpupa, A., Nqombolo, A., Dimpe, K.M. and Nomngongo, P.N., 2020. Recyclable magnetic waste tire-activated carbon-chitosan composite as an effective adsorbent for rapid and simultaneous removal of methylparaben and propylparaben from aqueous solution and wastewater. *Journal of Water Process Engineering*, 33, p.101011. [DOI]
- Meeker, J.D., Yang, T., Ye, X., Calafat, A.M. and Hauser, R., 2011. Urinary concentrations of parabens and serum hormone levels, semen quality parameters, and sperm DNA damage. *Environmental Health Perspectives*, 119(2), pp.252–257. [DOI]
- Mehrotra, P., 2016. Biosensors and their applications—A review. *Journal of Oral Biology and Craniofacial Research*, 6, pp.153–159. [DOI]
- Mendonça, C.D., Prado, T.M., Cincotto, F.H., Verbinen, R.T. and Machado, S.A.S., 2017. Methylparaben quantification via electrochemical sensor based on reduced graphene oxide decorated with ruthenium nanoparticles. *Sensors and Actuators B: Chemical*, 251. [DOI]
- Michalkiewicz, S., 2013. Anodic oxidation of parabens in acetic acid–acetonitrile solutions. *Journal of Applied Electrochemistry*, 43(1), pp.85–97. [DOI]
- Delgado, M.D., Cruz, D.M.S. and Barceló, D., 2016. Ecological risk assessment associated with the removal of endocrine-disrupting parabens and benzophenone-4 in wastewater treatment. *Journal of Hazardous Materials*, 310, pp.143–151. [DOI]
- Moschogiannaki, M., Frontitis, Z., Kiriakidis, G., Mantzavinos, D. and Binas, V., 2020. Porous CoxNi<sub>1-x</sub>TiO<sub>3</sub> nanorods for solar photocatalytic degradation of ethylparaben. *Journal of Materials*, 6(4), pp.788–799. [DOI]
- Naresh, V. and Lee, N., 2021. A review on biosensors and recent development of nanostructured materials-enabled biosensors. *Sensors*, 21(4), p.1109. [DOI]

- Popa, D.S., Kiss, B., Vlase, L., Pop, A., Iepure, R., Păltinean, R. and Loghin, F., 2011. Study of oxidative stress induction after exposure to bisphenol A and methylparaben in rats. *Farmacia*, 59(4), pp.539–549.
- Pourmohammad, M., Ghadi, A. and Beni, A.A., 2024. Removal of benzyl paraben from wastewater using zeolitic imidazolate-67 modified by Fe<sub>3</sub>O<sub>4</sub> nanoparticles with response surface methodology. *Journal of Applied Chemistry Research*, 18(1), pp.88–107.
- Qurashi, A., Rather, J.A., Yamazaki, T., Sohail, M., Wael, K.D., Merzougui, B. and Hakeem, A.S., 2015. Swift electrochemical detection of paraben, an endocrine disruptor by In<sub>2</sub>O<sub>3</sub> nanobricks. *Sensors and Actuators B: Chemical*, 221, pp.167–171. [DOI]
- Rather, J.A., Harthi, A.J.A., Khudaish, E.A., Qurashi, A., Munam, A. and Kannan, P., 2016. An electrochemical sensor based on fullerene nanorods for the detection of paraben, an endocrine disruptor. *Analytical Methods*, 8(28), pp.5690–5700. [DOI]
- Sellappan, S., Akoh, C.C. and Krewer, G., 2002. Phenolic compounds and antioxidant capacity of Georgia-grown blueberries and blackberries. *Journal of Agricultural and Food Chemistry*, 50(8), pp.2432–2438. [DOI]
- Slaughter, G., 2018. Current advances in biosensor design and fabrication. *Encyclopedia of Analytical Chemistry*. John Wiley, Chichester. [DOI]
- Song, C., Hu, H., Ao, H., Wu, Y. and Wu, C., 2017. Removal of parabens and their chlorinated by-products by periphyton: influence of light and temperature. *Environmental Science and Pollution Research*, 24, pp.5566–5575. [DOI]
- Soni, M.G., Taylor, S.L., Greenberg, N.A. and Burdock, G.A., 2002. Evaluation of the health aspects of methyl paraben: a review of the published literature. *Food and Chemical Toxicology*, 40(10), pp.1335–1373. [DOI]
- Tavares, R.S., Martins, F.C., Oliveira, P.J., Ramalho-Santos, J. and Peixoto, F.P., 2009. Parabens in male infertility—is there a mitochondrial connection? *Reproductive Toxicology*, 27, pp.1–7. [DOI]
- Tian, M., Hu, C., Yu, J. and Chen, L., 2023. Carbon quantum dots (CQDs) mediated Z-scheme g-C<sub>3</sub>N<sub>4</sub>-CQDs/BiVO<sub>4</sub> heterojunction with enhanced visible light photocatalytic degradation of paraben. *Chemosphere*, 323, p.138248. [DOI]
- Tománková, H. and Pinkasová, M., 1990. Determination of parabens and their degradation product p-hydroxy-benzoic acid in pharmaceutical dosage forms by HPTLC densitometry. *Analytical Letters*, 23(7), pp.1319–1332. [DOI]
- Upadhyay, P., Gauba, P. and Mathur, A., 2020. Paraben: A boon or bane for society. In: P. Gauba, I.P. Sarethy, and A. Mathur, eds. *Advances in Bioresources, Biodiversity and Therapeutics*, 16, pp.79–93.
- Vale, F., Sousa, C.A., Sousa, H., Santos, L. and Simões, M., 2022. Parabens as emerging contaminants: Environmental persistence, current practices, and treatment processes. *Journal of Cleaner Production*, 347, p.131244. [DOI]
- Vitku, J., Kolatorova, L., Franekova, L., Blahos, J., Simkova, M., Duskova, M., Skodova, T. and Starka, L., 2018. Endocrine disruptors of the bisphenol and paraben families and bone metabolism. *Physiological Research*, 67(Suppl 3), pp.S455–S464. [DOI]
- Wang, L., Li, Y., Li, G. and Ye, B., 2015. A new strategy for enhancing electrochemical sensing from MWCNTs modified electrode with Langmuir-Blodgett film and used in the determination of methylparaben. *Sensors and Actuators B: Chemical*, 211, pp.332–338. [DOI]
- Wang, S., Wang, X., Poon, K., Wang, Y., Li, S., Liu, H., Lin, S. and Cai, Z., 2013. Removal and reductive dechlorination of triclosan by *Chlorella pyrenoidosa*. *Chemosphere*, 92, pp.1498–1505. [DOI]
- Wang, X., Bi, X., Yao, N., Elmaci, G., Ertürk, A.S., Lv, Q., Zhao, P. and Meng, X., 2022. Doping strategy-tuned non-radical pathway on manganese oxide for catalytic degradation of parabens. *Journal of Chemical Engineering*, 442(Part 1), p.136180. [DOI]
- Wang, Y., Cao, Y., Fang, C. and Gong, Q., 2010. Electrochemical sensor for parabens based on molecular imprinting polymers with dual-templates. *Analytica Chimica Acta*, 673(2), pp.145–150. [DOI]
- Wasito, H. and Phechkrajung, C., 2015. Validated visible spectrophotometry for quantitative analysis of pirenixine in the presence of paraben preservatives in eye drop preparations. *4th International Conference on Instrumentation, Communications, Information Technology, and Biomedical Engineering (ICICI-BME)*, Bandung, Indonesia, pp.327–331. [DOI]
- Xin, T., Chen, W., Su, N. and Wang, Z., 2023. Synthesis of poly(methacrylic acid)/functionalized carbon nanotubes nanocomposite modified electrode for electrochemical sensitive determination of acrylamide in food sample. *International Journal of Electrochemical Science*, 18(3), p.541. [DOI]
- Yang, H., Zhang, F. and Wu, H., 2018. Review on the life cycle of parabens: synthesis, degradation, characterization, and safety analysis. *Current Organic Chemistry*, 22(8), pp.769–779. [DOI]
- Ye, X., Bishop, A.M., Reidy, J.A., Needham, L.L. and Calafat, A.M., 2006. Parabens as urinary biomarkers of exposure in humans. *Environmental Health Perspectives*, 114, pp.1843–1846. [DOI]
- Yücebaş, B.B., Yaman, Y.T., Bolat, G., Özgür, E., Uzun, L. and Abaci, S., 2020. Molecular imprinted polymer-based electrochemical sensor for selective detection of paraben. *Sensors and Actuators B: Chemical*, 305, p.127368. [DOI]



# Enhanced Microplastics Removal from Paper Recycling Industry Wastewater Using Membrane Bioreactor Technology

Savita Kalshan<sup>1</sup>, Rajesh Dhankhar<sup>1</sup>✉, Shivani Narwal<sup>1</sup>, Amit Chhillar<sup>1</sup>, Manju Desondia<sup>2</sup>, Poonam Yadav<sup>1</sup> and Sashi Yadav<sup>3</sup>

<sup>1</sup>Department of Environmental Science, Maharshi Dayanand University, Rohtak-124001, Haryana, India

<sup>2</sup>Rajiv Gandhi Govt College for Women, Bhiwani, Haryana, India

<sup>3</sup>University Institute of Engineering and Technology, Maharshi Dayanand University, Rohtak-124001, Haryana, India

✉Corresponding author: Rajesh Dhankhar: savita.rs.evs@mdurohtak.ac.in

**Abbreviation:** Nat. Env. & Poll. Technol.  
**Website:** www.neptjournal.com

*Received:* 11-07-2024

*Revised:* 15-08-2024

*Accepted:* 28-08-2024

## Key Words:

Microplastics  
 Membrane bioreactor  
 Waste treatment  
 Pulp and paper  
 Industrial wastewater

## Citation for the Paper:

Kalshan, S., Dhankhar, R., Narwal, S., Chhillar, A., Desondia, M., Yadav, P. and Yadav, S., 2025. Enhanced microplastic removal from paper recycling industry wastewater using membrane bioreactor technology. *Nature Environment and Pollution Technology*, 24(2), p. B4240. <https://doi.org/10.46488/NEPT.2025.v24i02.B4240>.

*Note: From year 2025, the journal uses Article ID instead of page numbers in citation of the published articles.*



**Copyright:** © 2025 by the authors  
**Licensee:** Technoscience Publications  
 This article is an open access article distributed under the terms and conditions of the Creative Commons Attribution (CC BY) license (<https://creativecommons.org/licenses/by/4.0/>).

## ABSTRACT

Urbanization and industrialization have caused a ubiquity of microplastics in the environmental system. An effective elimination technique is required for microplastics from industrial effluent and other wastewater systems due to its growing threats to the ecosystem and human health. The present study endeavors to evaluate the potential of the membrane bioreactor (MBR) technique in the removal of microplastics from paper recycling industry wastewater effluent. The effectiveness of the MBR system was evaluated relative to the conventional method used in industry for wastewater treatment. The paper recycling industrial effluent consists of 148 pieces/L of microplastics. The conventional treatment plant's effluent is used as an MBR system influent, and MBR removes 64.9% of the microplastic present after the conventional treatment plant, which is ascribed to the complementary actions of membrane filtration. MBR technology offers a reliable and workable plan to decrease the quantity of microplastics in industrial wastewater. It also offers a scalable solution that is consistent with sustainable environment management.

## INTRODUCTION

Global plastic production was 370 million tonnes in 2019, with European production accounting for nearly 58 million tons. By 2020, the largest consumers of plastics in Europe were the packaging industry (39.6%) and the building and construction sector (20.4%). Despite advancements in recycling technologies, only 32.5% of plastics are recycled in Europe, while 42.6% are used for the production of energy, and 24.9% end up in landfills (Mishra et al. 2021, Yadav et al. 2024a).

Although recycling rates have been increasing, it is significant to note that around 50% of plastics are designed for single-use application, contributing significantly to environmental accumulation. Single-use plastics are widely used in disposable consumer goods, packaging, and agricultural films. By comparison, just twenty to twenty-five percent of plastics are used in long-term items such as structural materials, cable coatings, and pipelines. The remaining polymers are utilized in furniture, automobiles, and electronic devices that have intermediate lifespans. The significant increase in global plastic production has resulted in a massive amount of plastic waste on land, much of which eventually enters aquatic environments, causing growing concerns (Yadav et al. 2022, Yadav et al. 2023).

Smaller than 5 mm plastic particles are known as microplastics (MPs), and they constitute a major ecological hazard for the Earth's biosphere. MPs are produced when larger plastic garbage breaks down (Ahmed et al. 2023). With an estimated 51 trillion plastic particles floating in surface waterways globally, the microplastic problem is a direct result of global plastic pollution (Edo et al. 2020). Numerous

freshwater bodies, estuaries, and oceans have been found to contain these microscopic particles. Microplastics can build up in aquatic food webs and the biota because of their widespread and incredibly slow rate of biodegradation (about 100 years) (Andrady 2017).

Numerous studies indicate that a substantial portion of microplastic fibers in aquatic environments originates from the washing of synthetic clothes. Ingestion of microplastics can obstruct the digestive tracts of aquatic organisms and facilitate the transfer of adsorbed contaminants, with uncertain consequences for the health of both aquatic life and humans.

Microplastics are widely present, as evidenced by samples taken from surface water, beaches, marine sediment, and marine creatures (Bellasi et al. 2020). MPs in waterbodies cannot be efficiently collected for recycling or management, in contrast to bigger plastic waste. MPs have been discovered in wastewater treatment plant effluents in addition to being present in oceans and other bodies of water (Sun et al. 2019). According to Li et al. (2018), MPs can also find their way into ecosystems through food, clothing, cosmetics, and other industrial emissions. These dangerous materials eventually find their way into the environment if they are not adequately recycled or treated, endangering both human health and aquatic species. According to research by Li et al. (2020), a lot of MPs come from wastewater treatment operations because of their tiny size and restricted treatability.

The capacity of microplastics to adsorb different common environmental pollutants, such as metals, medications, personal care items, and others, is a significant problem. Therefore, diseases like cancer, abnormalities in humans and animals, decreased immunological response, and impaired reproductive function can all be brought on by microplastics.

The removal of microplastics from aquatic environments has become an urgent challenge in the past decade due to their negative impact on aquatic animals as well as human health. The microplastics were detected in several aquatic ecosystems, including oceans, rivers, lakes, and sewage waste-water effluent. Based on their size, these plastics are classified as microplastics (MP) and nanoplastics (NP) (Poerio et al. 2018). Most existing studies have predominantly focused on municipal wastewater treatment plants (WWTPs) (Park 2020, Yuan 2022, Lee et al. 2023), focusing on a significant research gap concerning microplastics (MPs) in industrial wastewater sludge.

The production operations of the pulp and paper industry yield a substantial amount of wastewater, which in turn produces a substantial amount of sludge as a byproduct (Upadhyay & Bajpai 2023, Upendra & Kaur 2023). Historically, landfilling and incineration have been used as sludge disposal techniques. But there are also possible

uses for these byproducts in land alteration and agriculture (Rissanen 2020).

The process of pulp and paper making includes wood preparation by chipping and debarking for the production of pulp, pulp bleaching, and the production of the papers. The recovered papers are separated chemically or mechanically method for the removal of ink, adhesives as well as other impurities, which are further rewetted and reduced into pulp to provide a valuable supply of fiber for the paper-making process. Pressing and drying process used for water removal.

Over the past several years, developing countries have seen an increase in demand for recycled paper of more than 7%–8% annually (Recycling Magazine 2018). The basic material for recycled paper is supplied from recovered paper. Recycling paper helps preserve natural resources like trees and water while significantly lowering production costs (Lares et al. 2018).

Its recycling material is stored and processed using plastic material, and it is the major source of microplastic generation from paper recycling plants (Yadav et al. 2024b). The wastewater or paper industry effluent involves primary treatment including neutralization, screening, and sedimentation for the removal of suspended solids. These solids are subsequently dewatered into a sludge that needs to be disposed of. Secondary and tertiary treatments are used less frequently to remove harmful organics and color from wastewater and lower its organic concentration. Consequently, it is essential to research MPs in pulp and paper wastewater sludge to monitor sludge quality and stop MPs from building up in terrestrial ecosystems (Pham 2023).

Membrane bioreactor (MBR) technology, a modern advancement in wastewater treatment, offers significant advantages over traditional activated sludge treatment. With its ability to operate at higher sludge ages and densities, MBR technology enhances the removal of pollutants, including microplastic particles. Unlike conventional methods, which struggle to eliminate microplastics effectively, MBR processes achieve more efficient elimination, preventing these particles from entering aquatic environments through final effluents. Scientific studies have shown that nearly 99% of the microplastic particles can be eliminated using activated sludge processes, particularly over the use of membrane bioreactor. The MBR technique reduces the average concentration of microplastic from the primary to final effluent by 96.2%, highlighting the crucial role of this tertiary treatment step in addressing this emerging pollutant (Mishra et al. 2021). The primary aim of the present study is to the identification of MPs and their extraction protocol specifically for effluent and waste sludges from the recycling paper industry.

## MATERIALS AND METHODS

### Sample Collection

The paper recycling industry wastewater samples were collected from the Yamuna Nagar Industrial area, Haryana, India. Samples were collected on October 16, 2023 to December 20, 2023. The industry set up a conventional treatment plant for wastewater treatment, which consists of a primary treatment plant that includes screening and grit chamber, then secondary conventional activated sludge with sedimentation. The samples collected for the study were influent-industrial raw wastewater (S1), effluent from the primary chamber (S2), and the final effluent sample from the conventional wastewater treatment plant (S3) were collected in 5-10L of water bottles. Sludge sample (SS) also collected 1kg packet. The final effluent wastewater sample (S3) and sludge (SS) were kept in a clean and dried container and stored in the refrigerator. Then, the collected sample S3 used as an inlet, was run in a design pilot setup of membrane bioreactor, and outlet/ effluent of MBR (S4) was also studied for microplastic.

### Sample Processing/ Analysis and Chemical Reagents

The NOAA Marine Debris Programme defines microplastics (MPs) as particles with a size range of 0.3 mm to 5.0 mm. Samples were analyzed following this technique. Samples were sieved using mesh sizes of 0.3 mm and 5 mm to achieve this size requirement. Particles falling within the designated size range were washed with deionized water and gathered in a beaker to be subjected to wet peroxide oxidation (WPO), a process that separates MPs from other particles. To oxidize organic matter for WPO, 20 mL of 0.05 mol.L<sup>-1</sup> Fe(II) solution and 20 mL of 30% hydrogen peroxide solution were added to the samples. After five minutes at room temperature, the mixtures were heated to 75°C and stirred. If there was still visible biological matter, this process was repeated. All the chemical reagents were analytical grade and obtained from Merck.

The WPO solution was then transferred to a density separator. To ensure that all the remaining particles were included, the samples were rinsed with deionized water (dH<sub>2</sub>O) and transferred to the density separator, where microplastics (MPs) were allowed to settle down overnight. The settled MPs were then drained and manually removed. These collected MPs were dried at 75°C for 24 hours and subsequently stored in a desiccator until analysis.

Using a microscope with ×40 magnification, microplastics were counted and classified into the following categories: (i) spherical shape, (ii) fiber type, (iii) fragmented pieces, (iv) thin sheets, or (v) irregular shape, according to protocols from the NOAA Marine Debris Program (2015) and Hidayatullah & Lee (2019), as illustrated in Fig. 1.

Infrared micro-spectroscopic analysis was conducted using a Bruker ALPHA Fourier Transform Infrared (FTIR) spectrometer. Individual MP samples were transferred to the FTIR base. IR spectra were examined at a wavenumber range of 600 cm<sup>-1</sup>– 4000cm<sup>-1</sup> and compared against a material database as per Qiu et al. (2016).

## RESULTS AND DISCUSSION

### Occurrence of Microplastic in Pulp and Paper Industrial Effluent

Microplastic production from the chosen paper recycling industry is measured and characterized. These emissions wind up in municipal sewage water. According to reports, a significant source of MPs was the effluent from the pulp and paper industries (Kay et al. 2018). With an average value of 148 pieces/L, the average number of MPs in the industrial influent was greater (Table 1). In the primary treatment plant (S2), the MP number increased as well, reaching 67 pieces/L. Sludge was held in the reactor for a considerable amount of time until biofilm grew on the MP surface (Michels et al. 2018), which would facilitate particle settling. The microplastic content of the sludge sample (SS) was 131 pieces/L.

The effluent's MP number decreased to 13 pieces/L, which explained the 91.2% total MP removal capacity. In contrast, MPs were removed in the range of 82-189 percent in China's sophisticated drinking water treatment facilities by the use of coagulation, flocculation, sedimentation, and sand and GAC filtration procedures (Wang et al. 2020). It was discovered that MPs were able to pass through the screening and grit chamber primary treatment processes by overflow and that these processes were unable to eliminate MPs.

Conversely, the traditional plant utilized in activated sludge processes significantly contributed to the increased removal of microplastics (MPs) in WWTPs (Table 2). This is because MPs have a hydrophobic characteristic, allowing them to quickly attach to organisms or sludge in the treatment plant (Crawford & Quinn 2016). In light of this, MPs are kept in the sludge, some are transferred to the drying bed for disposal or drying, and some are recycled back into the aeration tank. According to Murphy et al. (2016), these MPs may, therefore, be discharged into the environment or accumulate in the soil and food chain, where they may eventually endanger both humans and the environment.

Pham et al. (2023) studied the WWTP of Kraft Paper Factory A, which has a capacity of 24,000 m<sup>3</sup>day<sup>-1</sup>. It uses treatment facilities such as level I (Dissolved Air Flotation-DAF), level II (Up-flow Anaerobic Sludge Banket-UASB and Conventional Activated Sludge-CAS), and level III (DAF and Fenton). The findings indicate that, despite a

99.8% removal rate and 12 items per  $\text{m}^{-3}$  concentration of microplastics in treated effluent, the microplastic load of this factory was 288,000 pieces per day. The microplastics were removed most efficiently by the primary and secondary treatment methods (75.8–97.9%), with DAF having a microplastic removal effectiveness of >95%.

The sludge sample had a microplastic content of 22,772 items  $\text{kg}^{-1}$  of dry weight. Regarding morphologies, the only forms of microplastics found in the wastewater and sludge samples were fragments (55% and 91%) and fibers (44% and 9%), respectively. The proportion of blue and white microplastics in the total was 37% and 30%.

Throughout the tropic chain, exposure to MP has been linked to a wide range of toxic insults, including disturbances in eating and reproductive outcomes, as demonstrated by numerous studies (Anbumani & Kakkar 2018). Consequently, to stop MP pollution and the consequences that come with it, the management of this sludge needs to be taken seriously.

### Shapes of Microplastics

The findings of the MPs' classification into the four shapes—with a fifth type known as “irregular shape”—are displayed in Table 1 and Fig. 1 & Fig. 2. The findings show that all 20 pieces/L of the sample (S1, S2, S3, S4, and SS having 15, 1, 2, 0, and 2 pieces/L, respectively) had low concentrations of spherical-shaped MP. According to Table 2, fiber was the most prevalent fraction in all samples, accounting for roughly 30.5% of all MPs in wastewater samples and 35% in sludge samples. Another significant portion was thin sheets, which ranged from 20% in WW. Plastic bags, packaging, covering, and lining materials are the main sources of thin sheet MPs (Efimova et al. 2018).

Furthermore, samples from all sites showed almost the same proportions of MPs, even though sample 1 uses wastewater from Yamuna Nagar's paper recycling industry. The MP compositions (i.e., five forms) of wastewater and sludge samples are contrasted in Table 2. Fiber, fragments, thin sheets, and irregular shapes make up the majority of MPs

in WWTPs. According to a recent study (Kay et al. 2018), fiber and fragments made up more than 75% of the total MP number in WWTP samples that were collected throughout the north of England.

The present study's findings show that the mean composition of fiber MPs is higher in the water phase (30.5%) than in the sludge (32%). However, for MPs with irregular shapes, the distribution is different, with fewer in the water phase (22.6%) than in the sludge (29%). Regarding thin-sheet and fragmented MPs, slight variations were observed between the sludge and water phases. It is important to highlight that certain MPs in the sludge could not be identified based on their shape, most likely due to microbial attachment on the surface of the microplastic. As a result, the unidentified fraction was relatively high at 29%, compared to 22.6% in the water phase.

The average MP shape distribution for the samples under study is shown in Table 2. The four main portions of the sludge (solid phase) were equally divided among MP shapes: fragment, thin sheet, fiber, and unclassified. In total, fibers make up 30% of MPs.

### Microplastics-Polymer Type

Fourier transform infrared spectroscopy (FTIR) is the most widely used method for examining the individual chemical bonds or surface chemical composition of plastic particles (Hidalgo-Ruz et al. 2012). By comparing the unique infrared spectra produced by the FTIR technique with known reference spectra, MPs can be identified. The FTIR technology detects changes in the dipole moment of chemical bonds. According to Doyle et al. (2011) and Harrison et al. (2012), plastics may be clearly distinguished from other organic or inorganic particles by their distinct FTIR spectra, which also allow for the determination of the MPs particle composition and particular polymer type. The physicochemical weathering of measured MP particles may be determined by utilizing FTIR spectroscopy to analyze various band patterns (Corcoran et al. 2009, Ahmed et al. 2021).

Table 1: Classification based on the shape of microplastic in different samples.

Samples	Microplastics (pieces/L)				
	Spherical	Fiber	Fragmented	Thin sheet	Irregular shape
S1	15	38	30	25	40
S2	1	26	12	18	10
S3	2	15	8	8	4
S4	0	2	3	2	6
SS	2	42	28	21	38



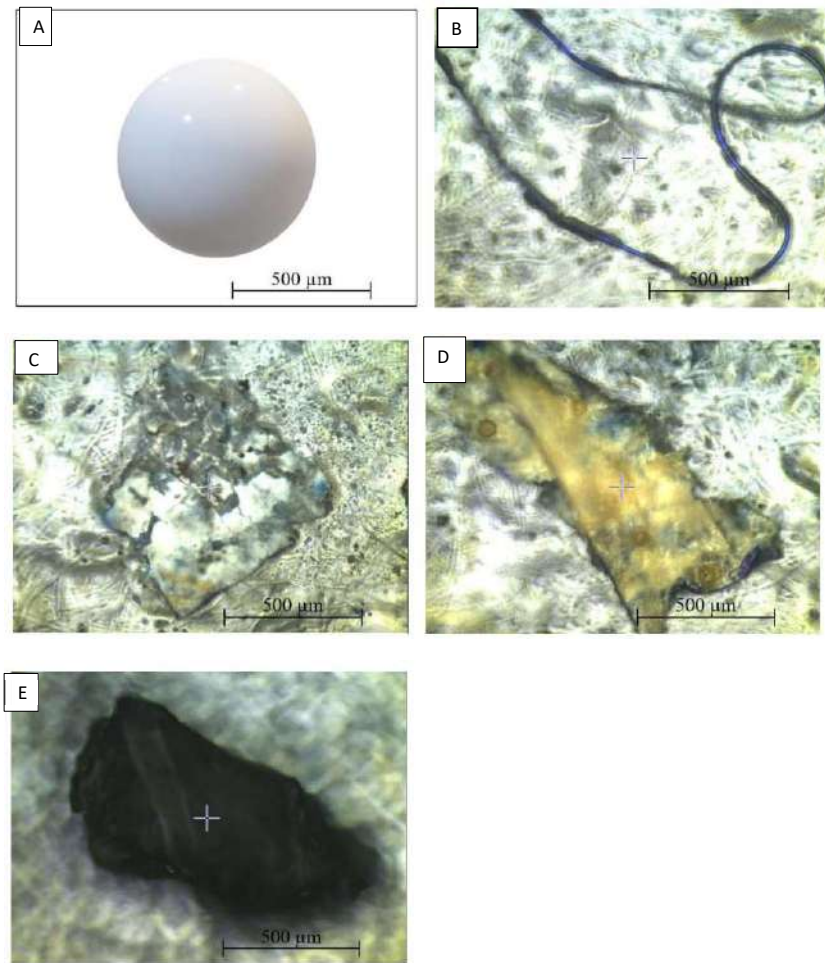


Fig 1: Shapes of Microplastic: A- Spherical, B- Fiber, C- Fragmented, D- Thin Sheet, and E- Irregular shape (Environmental and Climate Change Canada 2015, Hongprasith et al. 2020).

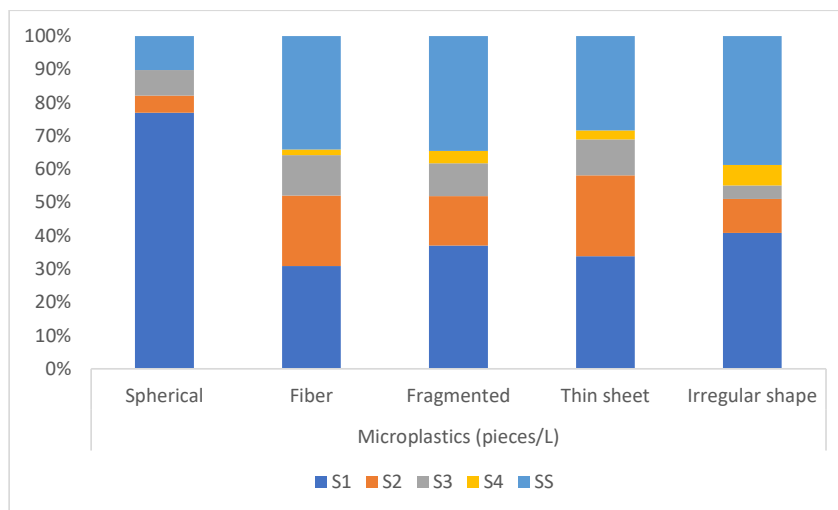


Fig. 2: Classification of microplastics (Pieces/L) in samples.

Table 2: Mean composition of total MP in wastewater sample and sludge.

MP Shapes	Wastewater samples [%]	Sludge sample [%]
Spherical	6.7	1.5
Fiber	30.5	32
Fragmented	20	21.3
Thin sheet	20	16.03
Irregular Shape	22.6	29

Following the recovery of microplastic particles from the samples, several polymers were found (Fig.3). Polyester (PES), polyethylene (PE), polyamide (PA), and polypropylene (PP) are on the list. FTIR microscopy was widely used to identify and validate these polymers.

The proportion of different polymers remained relatively consistent across different sampling dates when considering all sampling points. Throughout the sampling campaign industrial effluent (S1) represents polyester constituted 80% of the MP and 85% polyester in the sludge sample collected. Most of the remaining MPFs were polyamide, accounting for 3.1% of all MPFs. Microplastic fibers typically exhibit a uniform thickness with three-dimensional bending, distinguishing them from cellulose-based fibers, which have a ribbon-like appearance (Noren 2007, Murphy et al., 2016). This study also found polyester fibers with a flat, cotton-like appearance. For the MP, polyethylene was the prevalent polymer, representing 30% of MP in S2 and 25% in S3 of the total MPs. The polyester represents 67% of all the wastewater samples (Fig. 4) and 85% of sludge samples (Fig. 5).

Throughout the sampling campaign, there were significant variations in the quantity of microplastics in the sludge and wastewater samples (Fig. 6). Consequently, the number of MPs in WWTPs reported for individual sample events does not provide a consistent set of data that may be used to appropriately assess and address the microplastics pollution issue. Automatic composite sampling could be used to gather more representative samples and account for diurnal variation in the estimation of microplastic concentrations in WWTP (Talvitie et al. 2017).

The majority of research investigations carried out to date took place over a few days. However, only a few numbers of additional research (Talvitie et al. 2017) noted the significant change in MP concentrations in wastewater for weeks and seasons. To determine the prevalence of MPs in wastewaters during the fall and winter seasons in a Nordic setting, a sampling program was carried out between the third week of October and the first week of December.

Municipal wastewater treatment plant in Hungary, the microplastic study was performed, and it found seventh and sixteenth weeks of 2023 saw variations in the fiber content, ranging from 1.88–2.84 and 4.25–6.79 pieces/L, respectively. The percentage of microfibrers in the solid particles was 94.7% in April and 78.3% in February. Microfibrers based on cellulose predominated in the effluent (53–91%), whereas polyester predominated among those based on petroleum. In April, the median length of cellulose-based fibers grew significantly from February to April (650 vs. 1250  $\mu\text{m}$ ), while at the same time, the median diameter increased

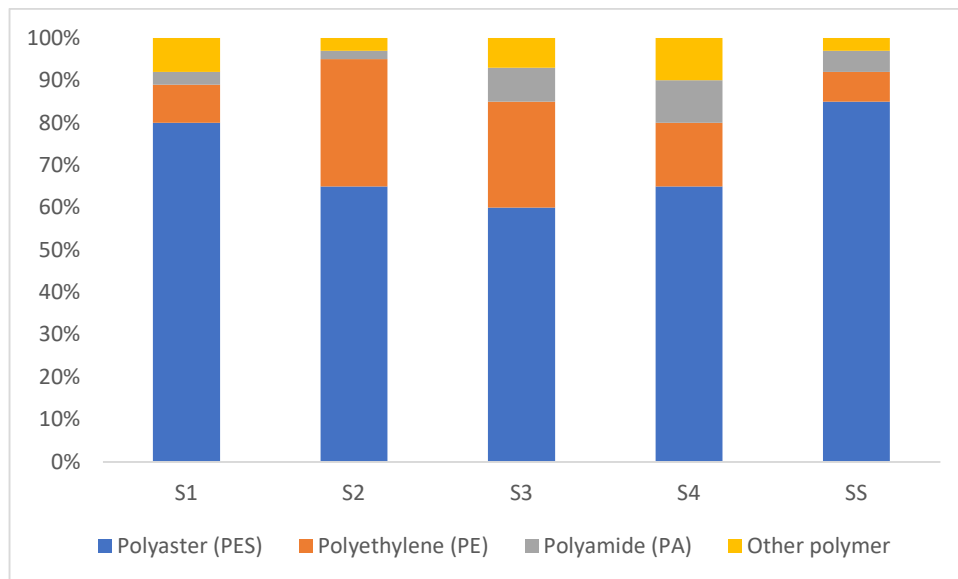


Fig. 3: Type of polymers in microplastics.

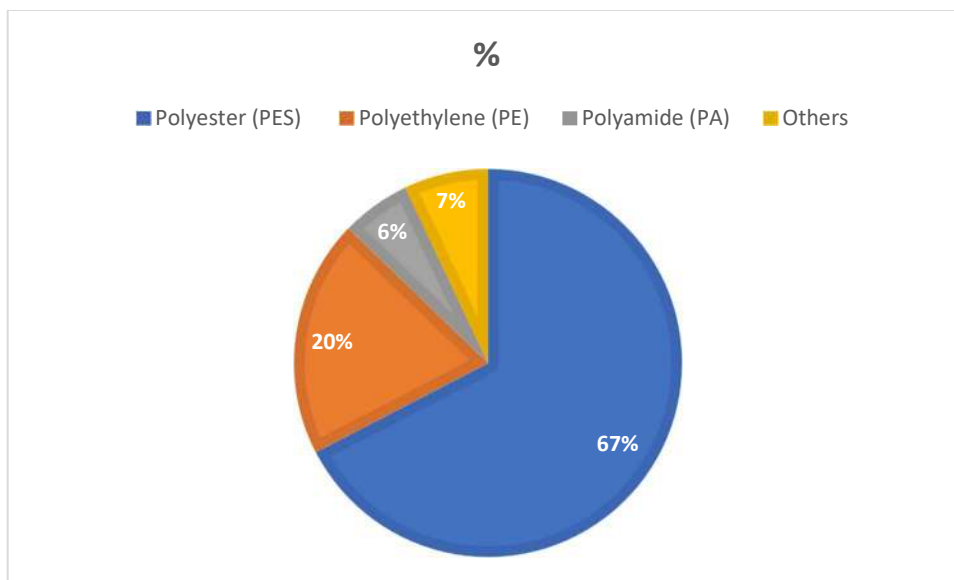


Fig. 4: Type of polymer present in wastewater samples

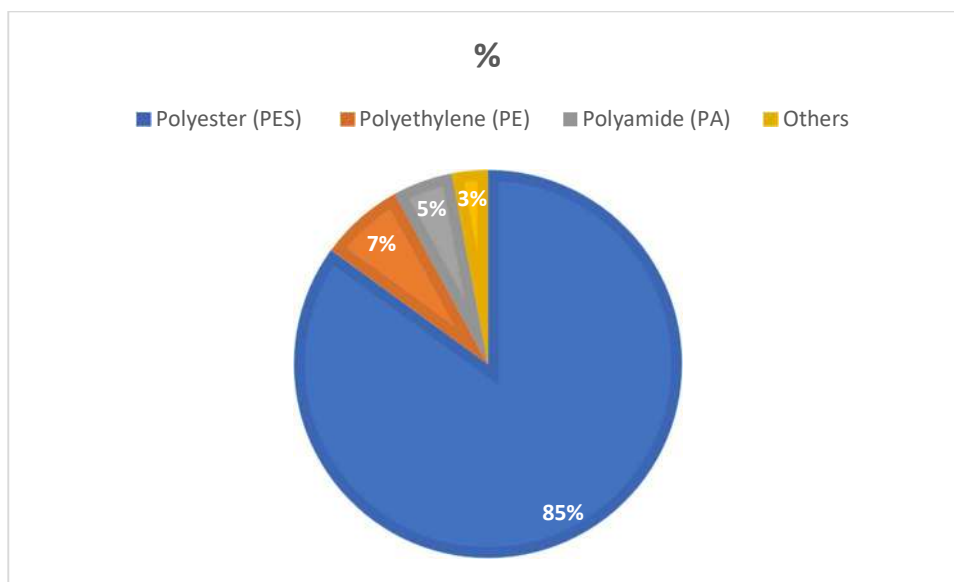


Fig. 5: Type of polymer present in sludge sample.

from 21 to 29  $\mu\text{m}$ . This behavior was observed in relation to microfibers made of petroleum but to a lower degree. In February and April of 2023, the daily average transfer of treated wastewater to the Danube River varied between 0.44 – 0.69 and 0.94–1.53 billion, respectively (et al. 2024).

The study's authors highlight the necessity of expanding the monitoring campaign to include the spring and summer months to estimate the annual variation of MPs in wastewater and the corresponding capacity of WWTPs to manage such

seasonal variation, based on the study's results. The MP concentrations in the influent may vary during the day in addition to seasonal variations. This might have increased some uncertainty in the published results because it was not taken into consideration during the sampling and computation of the MP removal efficiency in the WWTP under study.

Therefore, for more accurate evaluations, long-term sample campaigns should take the hydraulic retention time in various process components into account.

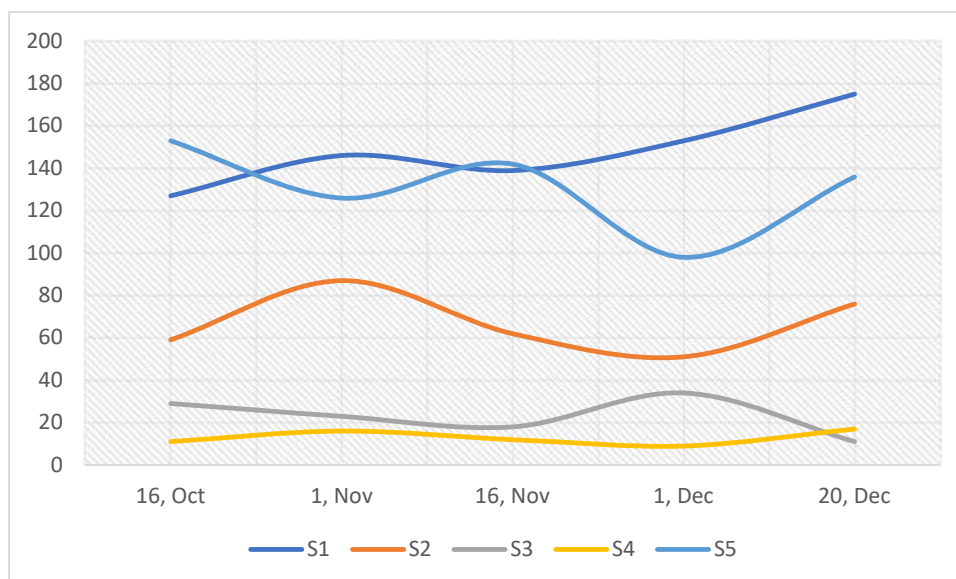


Fig. 6: Microplastic concentration with sampling dates.

## CONCLUSIONS

The study's results highlight the great potential of membrane bioreactor (MBR) technology for improving the removal of microplastics from effluent from the recycled pulp and paper industry. It is clear by comparing the MBR system's performance to traditional wastewater treatment techniques that it is capable of achieving a significant 64.9% decrease in microplastics by utilizing the complementing processes of membrane filtration and biodegradation. This significant advancement emphasizes how much better the MBR system is at capturing microplastic pollutants, which are becoming more and more common as a result of industrialization and urbanization.

An effective and scalable solution that adheres to sustainable environmental management principles is provided by the MBR technology. Its efficacious treatment of industrial effluents indicates that it can be used in a wide range of industries with comparable pollution problems. Because the MBR system effectively removes microplastics, it presents a viable option for widespread implementation in industrial wastewater treatment plants, addressing a significant environmental and public health concern.

Subsequent studies ought to concentrate on refining operating parameters, examining the system's long-term stability and economic viability, and examining how well the technology works with various kinds of industrial effluents. Overall, this study offers strong evidence in favor of the use of MBR technology as a major approach to reducing the

negative environmental effects of microplastics improving the quality of water bodies and ecosystems.

## ACKNOWLEDGMENT

The authors are thankful to the Department of Environmental Sciences, Maharshi Dayanand University, Rohtak, India, for their laboratory facility.

## REFERENCES

- Ahmed, M.B., Rahman, M.S., Alom, J., Hasan, M.S., Johir, M., Mondal, M.I.H., Lee, D., Park, J., Zhou, J.L. and Yoon, M., 2021. Microplastic particles in the aquatic environment: A systematic review. *Science of The Total Environment*, 775, p.145793. DOI
- Ahmed, S.F., Islam, N., Tasannum, N., Mehjabin, A., Momtahn, A., Chowdhury, A.A., Almomani, F. and Mofijur, M., 2023. Microplastic removal and management strategies for wastewater treatment plants. *Chemosphere*, 347, p.140648. DOI
- Anbumani, S. and Kakkar, P., 2018. Ecotoxicological effects of microplastics on biota: A review. *Environmental Science and Pollution Research*, 25, pp.14373–14396.
- Andrady, A.L., 2017. The plastic in microplastics: A review. *Marine Pollution Bulletin*, 119(1), pp.12–22.
- Bellasi, A., Binda, G., Pozzi, A., Galafassi, S., Volta, P. and Bettinetti, R., 2020. Microplastic contamination in freshwater environments: A review, focusing on interactions with sediments and benthic organisms. *Environments*, 7(4), p.30.
- Corcoran, P.L., Biesinger, M.C. and Grifi, M., 2009. Plastics and beaches: A degrading relationship. *Marine Pollution Bulletin*, 58(1), pp.80–84.
- Crawford, C.B. and Quinn, B., 2016. *Microplastic Pollutants*. Elsevier Science.
- Doyle, M.J., Watson, W., Bowlin, N.M. and Sheavly, S.B., 2011. Plastic particles in coastal pelagic ecosystems of the Northeast Pacific Ocean. *Marine Environmental Research*, 71(1), pp.41–52.



- Edo, C., González-Pleiter, M., Leganés, F., Fernández-Piñas, F. and Rosal, R., 2020. Fate of microplastics in wastewater treatment plants and their environmental dispersion with effluent and sludge. *Environmental Pollution*, 259, p.113837.
- Efimova, I., Bagaeva, M., Bagaev, A., Kileso, A. and Chubarenko, I.P., 2018. Secondary microplastics generation in the sea swash zone with coarse bottom sediments: Laboratory experiments. *Frontiers in Marine Science*, 5, p.313. DOI
- Environment and Climate Change Canada, 2015. Microbeads - A science summary - July 2015. *IOP Publishing Physics Web*. Available at: Link
- Harrison, J.P., Ojeda, J.J. and Romero-González, M.E., 2012. The applicability of reflectance micro-Fourier-transform infrared spectroscopy for the detection of synthetic microplastics in marine sediments. *Science of the Total Environment*, 416, pp.455-463.
- Hidalgo-Ruz, V., Gutow, L., Thompson, R.C. and Thiel, M., 2012. Microplastics in the marine environment: A review of the methods used for identification and quantification. *Environmental Science & Technology*, 46(6), pp.3060-3075.
- Hidayaturrehman, H. and Lee, T.G., 2019. A study on characteristics of microplastic in wastewater of South Korea: Identification, quantification, and fate of microplastics during treatment process. *Marine Pollution Bulletin*, 146, pp.696-702. DOI
- Hongprasith, N., Kittimethawong, C., Lertlucksanaporn, R., Eamchotchawalit, T., Kittipongvises, S. and Lohwacharin, J., 2020. IR microspectroscopic identification of microplastics in municipal wastewater treatment plants. *Environmental Science and Pollution Research*, 27, pp.18557-18564.
- Kalshan, S., Dhankhar, R., Narwal, S., Chhillar, A., Yadav, P. and Yadav, S., 2024. Achieving high removal efficiency and membrane sustainability in pulp and paper industry MBR system. *Oriental Journal of Chemistry*, 40(1), p.65.
- Kay, P., Hiscoe, R., Moberley, I., Bajic, L. and McKenna, N., 2018. Wastewater treatment plants as a source of microplastics in river catchments. *Environmental Science and Pollution Research*, 25, pp.20264-20267. DOI
- Lares, M., Ncibi, M.C., Sillanpää, M. and Sillanpää, M., 2018. Occurrence, identification and removal of microplastic particles and fibers in conventional activated sludge process and advanced MBR technology. *Water Research*, 133, pp.236-246. DOI
- Lee, J.H., 2023. Detection of microplastic traces in four different types of municipal wastewater treatment plants through FT-IR and TED-GC-MS. *Environmental Pollution*, 333, p.122017. DOI
- Li, J., Liu, H. and Chen, J.P., 2018. Microplastics in freshwater systems: A review on occurrence, environmental effects, and methods for microplastics detection. *Water Research*, 137, pp.362-374.
- Li, X., Chen, L., Ji, Y., Li, M., Dong, B., Qian, G. and Dai, X., 2020. Effects of chemical pretreatments on microplastic extraction in sewage sludge and their physicochemical characteristics. *Water Research*, 171, p.115379.
- Michels, J., Stippkugel, A., Lenz, M., Wirtz, K. and Engel, A., 2018. Rapid aggregation of biofilm-covered microplastics with marine biogenic particles. *Proceedings of the Royal Society B*, 285, p.1203. DOI
- Mishra, S., Singh, R.P., Rout, P.K. and Das, A.P., 2021. Membrane bioreactor (MBR) as an advanced wastewater treatment technology for removal of synthetic microplastics. *Development in Wastewater Treatment Research and Processes*, 78, pp.45-60. DOI
- Murphy, F., Ewins, C., Carbonnier, F. and Quinn, B., 2016. Wastewater treatment works (WwTW) as a source of microplastics in the aquatic environment. *Environmental Science & Technology*, 50, pp.5800-5808. DOI
- NOAA Marine Debris Program, 2015. *Laboratory Methods for the Analysis of Microplastics in the Marine Environment: Recommendations for Quantifying Synthetic Particles in Waters and Sediments*.
- Noren, F., 2007. *Small Plastic Particles in Coastal Swedish Waters*. KIMO.
- Park, H.J., 2020. National reconnaissance survey of microplastics in municipal wastewater treatment plants in Korea. *Environmental Science & Technology*, 54, pp.1503-1512. DOI
- Pham, T., 2023. *Microplastics Extraction from Pulp and Paper Industry Wastewater Sludges*. Master's Thesis, Tampere University
- Pham, T.T., Kieu-Le, T.C., Truong, T.N.S., Nguyen, P.D., Le, Q.D.T., Le, T.M.T. and Strady, E., 2023. Evaluation of microplastic removal efficiency at the wastewater treatment plant of a kraft paper factory in Vietnam. *Sustainable Civil Engineering and Architecture*, 140, pp.1855-1863.
- Poerio, T., Piacentini, E. and Mazzei, R., 2018. Membrane processes for microplastic removal. *Molecules*, 24, p.4148. DOI
- Qiu, Q., Tan, Z., Wang, J., Peng, J., Li, M. and Zhan, Z., 2016. Extraction, enumeration, and identification methods for monitoring microplastics in the environment. *Estuarine, Coastal and Shelf Science*, 176, pp.102-109. DOI
- Recycling Magazine, 2018. *Paper Recycling Market Expected to Grow Significantly*. Retrieved from Recycling Magazine
- Rissanen, A., 2020. *Study on Different Effluent Treatment Sludge Utilizing Methods in Pulp and Paperboard Mills*. Lappeenranta-Lahti University of Technology (LUT).
- Sun, J., Dai, X., Wang, Q., Van Loosdrecht, M.C. and Ni, B.J., 2019. Microplastics in wastewater treatment plants: Detection, occurrence and removal. *Water Research*, 152, pp.21-37.
- Talvitie, J., Mikola, A., Koistinen, A. and Setälä, O., 2017. Solutions to microplastic pollution—removal of microplastics from wastewater effluent with advanced wastewater treatment technologies. *Water Research*, 123, pp.401-407. DOI
- Tserendorj, D., Illés, Á., Károly, Á., Sandil, S., Mireisz, T., Dobosy, P., Pomázi, F., Baranya, S., Adányi, M. and Zárny, G., 2024. Microfiber emission from a municipal wastewater treatment plant in Hungary. *Scientific Reports*, 14, pp.1-8. DOI
- Upadhyay, K. and Bajpai, S., 2023. Abundance, characteristics, and microplastic load in informal urban drainage system carrying intermixed liquid waste streams. *Nature Environment & Pollution Technology*, 22, p.4. DOI
- Upendra, S. and Kaur, J., 2023. Microplastic pollution in seawater: A review study. *Nature Environment & Pollution Technology*, 22, p.50. DOI
- Wang, Z., Lin, T. and Chen, W., 2020. Occurrence and removal of microplastics in an advanced drinking water treatment plant (ADWTP). *Science of the Total Environment*, 700, p.134520. DOI
- Yadav, S., Bajar, S., Hemraj, Rohilla, R., Chhikara, S.K. and Dhankhar, R., 2023. Assessment of groundwater quality near municipal solid waste landfill by using multivariate statistical technique and GIS: a case study of Bandhwari (Gurugram) landfill site, Haryana, India. *Sustainable Water Resources Management*, 9, p.174. DOI
- Yadav, S., Dhankhar, R. and Chhikara, S.K., 2022. Significant changes in urban air quality during the COVID-19 pandemic lockdown in Rohtak City, India. *Asian Journal of Chemistry*, 34, pp.3189-3196.
- Yadav, S., Rohilla, R. and Chhikara, S.K., 2024a. Review on landfill leachate treatment: Focus on the applicability of adsorbents. *Proceedings of the National Academy of Sciences, India Section B: Biological Sciences*, 87, pp.1-9. DOI
- Yadav, S., Yadav, A., Goyal, G., Dhawan, M., Kumar, V., Yadav, A. and Chhikara, S.K., 2024b. Fly ash-based adsorption for hexavalent chromium removal in aqueous systems: A promising eco-friendly technique. *Oriental Journal of Chemistry*, 40, p.614.
- Yuan, F., 2022. Investigation of microplastics in sludge from five wastewater treatment plants in Nanjing, China. *Journal of Environmental Management*, 301, p.113793. DOI

# Exploring Institutional Climate Capacity Assessment Indicators of Community-Based Organizations in the Conservation Projects: A Participative Approach

Ravi Sharma<sup>1†</sup>  and Vinayak Patil<sup>2</sup> 

<sup>1</sup>Symbiosis Institute of International Business, Symbiosis International (Deemed University), Pune-411057, India

<sup>2</sup>Department of Forestry, Dr. Balasaheb Sawant Konkan Krishi Vidyapeeth, Dapoli, Maharashtra, India

†Corresponding author: Ravi Sharma; ravi.sharma@siib.ac.in; ravisharma\_16@yahoo.co.in

**Abbreviation:** Nat. Env. & Poll. Technol.  
**Website:** www.neptjournal.com

*Received:* 16-07-2024

*Revised:* 10-08-2024

*Accepted:* 28-08-2024

## Key Words:

Climate change  
 Adaptive capacity  
 Climate assessment tools  
 Coastal forests  
 Institutional resilience

## ABSTRACT

The present comprehensive study seeks to evaluate the institutional climate capacity of Community-based Organizations (CBOs) involved in coastal ecotourism conservation projects along the Maharashtra coastal region in India. The primary objective is to understand the community interactions, organizational structures, and adaptive capacities of CBOs in the face of climate change, utilizing an integrated approach through participative and stakeholder interaction. The research methodology employed through the integrated investigated assessment, which includes- focused group discussions (n=06) and a survey of key informants' interviews and community participants (n=143), additionally were added to this set of data combined for a total of 204 respondents, to comprehensively evaluate the institutional climate capacity of the CSOs engaged in coastal ecotourism projects. The findings identify key dimensions influencing CBO-led conservation projects, emphasizing the importance of different actors' interplay and processes reflected through the communities. Notable strengths include effective communication, inclusive planning, and budgetary processes contributing to climate action orientation, emphasizing strengths in communication, inclusive planning, and budgetary processes. Socially excluded groups actively participate, underscoring the significance of their involvement for project success. Integrating socio-cultural factors into climate change planning is highlighted, emphasizing the need for quantitative research in this area. These identified key dimensions influence the CSO's institutional climate capacities.

## Citation for the Paper:

Sharma, R. and Patil, V., 2025. Exploring institutional climate capacity assessment indicators of community-based organizations in the conservation projects: A participative approach. *Nature Environment and Pollution Technology*, 24(2), p. B4244. <https://doi.org/10.46488/NEPT.2025.v24i02.B4244>

*Note: From year 2025, the journal uses Article ID instead of page numbers in citation of the published articles.*



**Copyright:** © 2025 by the authors

**Licensee:** Technoscience Publications

This article is an open access article distributed under the terms and conditions of the Creative Commons Attribution (CC BY) license (<https://creativecommons.org/licenses/by/4.0/>).

## INTRODUCTION

Climate change poses a significant threat to human societies and natural ecosystems, presenting challenges extending to social systems. Global attention has been increasing in recent years in adapting to these changes. International efforts, such as the United Nations Framework Convention on Climate Change (UNFCCC), National Adaptation Plans (NAPs), global institutions, and the Intergovernmental Panel on Climate Change (IPCC), have structured frameworks to assess climate impacts and vulnerabilities (Ingram & Hamilton 2014).

Civil society organizations (CSOs), Community-based organizations (CBOs), and Non-Governmental Organizations (NGOs) play crucial roles at local and regional levels in guiding stakeholders on climate actions and policies through grassroots engagement. Their contributions are integrated into governance processes, reviewing policy impacts through action research. CBOs particularly drive environmental governance, including efforts related to climate change and biodiversity conservation (Dupuits 2016). Climate adaptation involves adjusting to the current and anticipated effects of climate change. Institutional participation across various domains is essential for local and regional development, bridging

gaps in climate change response. At both macro and micro levels, institutions like CBOs and NGOs are pivotal in implementing climate awareness at the community level and contributing to achieving sustainable development goals (SDGs) (Patterson 2021). CSOs are key actors in climate action strategies, facing the challenge of effective adaptation within evolving climate governance frameworks (Bhardwaj & Khosla 2021, Patterson 2021). On the other hand, these institutions bridge the gap between local institutions and communities and climate change adaptation at the macro level. These organizations provide an extended organizational arm to society in increasing citizen engagement in public policy problems and creating solutions by providing answers to society development processes, including livelihood and social security net.

CBOs encompass a range of local self-governance bodies, including elected municipal councils, urban local bodies, village councils, self-help groups (SHGs), intermediate governing bodies, and various economic and social NGO associations. Through diverse approaches and action plans, these CBOs and NGOs have effectively mapped out strategies to conserve ecological systems while locally enhancing rural communities' social and economic fabric. Studies are advocated through a focus on protected area networks, assessing the specific strategies NGOs utilize in the planning, adopting, and managing those networks (White et al. 2022). Bridging an organization's connections among the actors or stakeholders at various levels of governance and indigenous knowledge of local communities, including capacity building, improves access to resources and information, thereby building local governance institutions (Berdej & Armitage 2016). It was found that countries have unique ways of producing and using indigenous community knowledge adopted by the different institutional structures involved in their formal and informal practices (Tosun & Howlett 2021). Such institutional structures are crucial and play a dominant role in shaping the responses to strategic and policy issues, including the policies and actions on climate change (Njuguna et al. 2022). The capacity building of these CBOs to address climate change at the grassroots level will provide more meaning in recognizing climate change adaptation and mitigation measures among coastal communities. Therefore, there is a shortage of knowledge enhancement on the climate capacity assessments of these CBOs, which will help in understanding the key challenges and issues these CBOs are facing and addressing the gaps to explore the opportunities for these CBOs to address climate change.

The success and long-term viability of community-based natural resource management initiatives have been mixed,

often hindered by challenges in institutional sustainability. To address this, the research employs a participatory approach, using focus group discussions (FGDs) to assess the institutional climate capacity of coastal-forest community-based organizations (CBOs). Drawing on field research with CBO members and communities involved in ecotourism projects, the study aims to identify key factors influencing the ability of these organizations to effectively govern and manage coastal forest resources, highlighting their climate resilience and adaptability capacity. This study will attempt to provide the existing capacity level studies with the CBO communities required for addressing the climate action at the ground level. In addition, what are the specific indicators within the approaches and frameworks implemented for institutional capacity assessments regarding adaptive capacity assessment and risk management through community-based conservation projects; what are the specific existing gaps in the approaches, and how are the CBOs required to address them while dealing with the climate to address at the community level in understanding adaptive capacities towards their goals and priorities would be the key agenda objectives of carrying this study? Specifically, the study examines the role of local institutions, the legitimacy and accountability of management structures, and the interplay between community needs, forest resource dependency, and conservation objectives.

By engaging community stakeholders through the FGDs, the research aims to capture their perspectives, experiences, and insights, allowing for a more comprehensive understanding of the institutional climate and the barriers or enabling factors that shape the capacity of these organizations. The findings of this study will contribute to the growing body of knowledge on community-based natural resource management, providing valuable insights for policymakers, practitioners, and community leaders working to enhance the long-term sustainability of coastal forests.

## MATERIALS AND METHODS

Field investigators engaged with coastal forest communities and organizations to map the institutional climate capacity of community-based organizations (CBOs). Organizations involved in coastal ecotourism or environmental conservation projects in mangrove forests were selected. A participative approach combined focused group discussions (FGDs) with iterative surveys to assess CBOs' climate capacity. The surveys, conducted after FGDs, focused on identifying influencing factors and assessing stakeholders' agreement on the climate resilience of community-based ecotourism (CbET) projects. The surveying approach was conducted after the completion of FGDs at the specific areas of the

study. The essential items in the surveying schedule include the following: The assessment focused on basic information about the ecotourism project model, type, and community engagement level. It evaluated the community's climate change adaptive capacity and resilience, gauging opinions on climate impacts and response capabilities using a Likert scale. The assessment categorized indicators into anticipated climate responses, emotional reactions, risk mitigation expectations, readiness for implementation, and overall climate risk management approaches.

The approach of FGDs and surveying yielded descriptive information about the project activities, level of engagements, institutional structure, and the project's outcome relating it to the institutional adaptive capacity of the CBOs.

### Sample and Analysis of Data

The study sample consists of ecotourism projects in the Ratnagiri and Sindhudurg districts of the Maharashtra State coastal belt. Five village projects were identified and led by some CBOs, and the community-engaged projects through the self-help groups (SHGs) were the key to the project. The projects are mostly related to the livelihood generation and conservation of mangroves and coastal resources through the involvement of local coastal communities. The three projects were in Sindhudurg district, while two were in Ratnagiri. To characterize the community's perceptions of the CBO's climate capacity, the stakeholders' engagements and interactions were organized through a participative approach, conducting small FGDs at different study area locations. These FGDs were conducted from August 2022 to December 2023, and six small FGD sessions were conducted at the suitable villages.

Along with these FGD Sessions, parallel interviews through the pre-tested questionnaires were implemented to survey the CBO community members, staff, officials, and SHG members individually to mark the agreement on

the factors considered for the climate capacity assessment of the study. During the survey with the SHGs and CBO staff members, we used the snowball approach using participants' responses to identify up to three individuals they would consult through their work. This approach helps us better represent community members involved through the project with the CBOs. The details of the community and stakeholder participation in FGDs in the study area are explained in Table 1.

Our sampling included 6 FGD sessions with 61 participants and survey data (n=143), totaling 204 participants. We used basic descriptive coding for analysis and transcribing and coding audio recordings from FGDs. These discussions provided insights into the interactions between the community and CBO members, focusing on CBO structure, engagement, resources, project execution, and climate adaptation strategies. Thematic content analysis was conducted, supported by observational field notes. Emerging themes were categorized by typology, validated through literature and expert opinions, and used to identify key strengths and gaps in climate adaptation. The key themes were divided into motor, niche, basic, and emerging themes, further helping identify institutional climate capacity factors.

## RESULTS AND DISCUSSION

### Preliminary Identification of Relevant Themes

The literature study and expert validation have identified the key thematic evolution of the various aspects of climate capacity assessments of the organizations based on their work and contribution through community projects. The experts validated the key emerging themes and motor themes, which originated through their project models and community involvements (Fig. 1). The emergent themes identified that the key climate-related issues, like flooding, conservation, etc., were emphasized through the governance approach

Table 1: FGD Participants' details from the study area.

Location of FGD	Key Stakeholders participated	No. of Participants
Anjarle (Ratnagiri)	SHG members, Village council members, Project Specialists from CBOs, Project beneficiaries	23
Songaon & Chiplun (Ratnagiri)	SHG members, Village council members, Project Specialists from CBOs, Project beneficiaries	06
Mithmumbari (Sindhudurg)	Women SHG members, Village council members, Project Specialists from CBOs, Project beneficiaries	17
Achara (Sindhudurg)	Women SHG members, Village council members, Project Specialists from CBOs, Project beneficiaries	07
Mandavi	Women SHG members, Village council members, Project Specialists from CBOs, Project beneficiaries	03
Nivati(Sindhudurg)	Women SHG members, Project Specialists from CBOs, Project beneficiaries	05
Total 06 FDPs		61



and capacity-building initiatives integrated through the CBO-Community project models. This has resulted in better coastal management and decision-making at the community level, enhancing their adaptive capacity and depicting important factors for determining institutional resilience while dealing with climate issues. The other key aspects that CBOs, through their community engagement model, depict showcasing their climate resilience and adaptive capacity were stakeholder engagements, local participation (a participative and institutional mechanism), and climate vulnerability assessment through their project approaches with communities. The NGOs/CBOs/and SHGs at the grassroots levels addressed the risk management of climate hazards and their social consequences.

### Factors Defining Institutional Climate Capacity of the CBOs through Community Perceptions

The factors and key criteria under each factor were categorized from the various FGD sessions, qualitative analysis of communities' perceptions, and validation through renowned agencies' publications and published research. The categorization and the factors required for the assessment of climate capacity and resilience of community-based ecotourism projects through the CBOs as identified from the participatory approaches are explained below:

### Institutional Climate Capacity Factors

- Governance and Leadership Mandate:** Clear roles, responsibilities, authorities, and public availability of mandates.
- Organizational Structure:** Involves CbET beneficiaries, socio-cultural drivers, knowledge management, objectives, implementation capacity, transparency, legal knowledge, proactive goals, Indigenous knowledge integration, adaptive co-management, and leadership coordination.
- Information Accessibility:** Involves ICT use, best practices dissemination, stakeholder engagement, and access to sectoral funding and public information.
- Resource Management:** Focuses on collaborations, resource allocations, organizational assets, skilled human resources, and stakeholder engagement for context-specific knowledge.
- Strategic Planning:** Includes stakeholder participation, risk assessment, partnerships, feedback, and rule adjustments.
- Design-Plan Implementation:** Enhances spatial planning and climate change mitigation objectives.

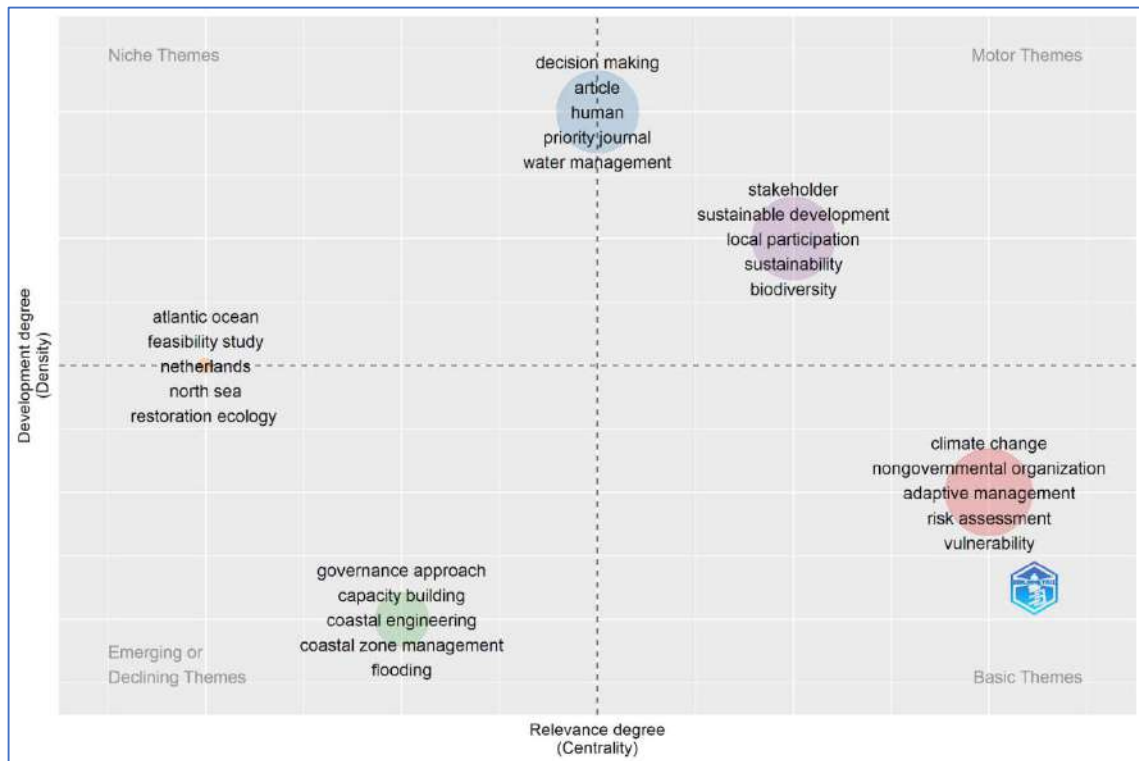


Fig. 1: Key themes showcasing interlinkage of CBOs and Community associations related to climate change factors.

- g) **Monitoring and Evaluation:** Covers policy and project assessments, performance evaluation, social impact, and resilience measures.
- h) **Knowledge Management:** Involves learning, network efficiency, spatiotemporal knowledge, knowledge-based planning, and risk modeling.

The participative approach identified key institutional climate capacity indicators for assessing CBOs, focusing on how stakeholders in coastal ecotourism influence and are influenced by CBOs in formulating plans and processes. These interactions highlight the conditions necessary for climate-resilient ecotourism, enhancing the knowledge and climate resilience of communities and CBOs. The CBOs' processes and engagement with communities reflect their climate capacity, shaping mutual learning and improving institutional capabilities. This interaction-driven learning empowers communities to implement sustainable ecotourism practices, with the resulting actions evaluated to assess the effectiveness and impact of CBOs in addressing identified challenges and opportunities. In the relationship, the interaction of CBO with the communities through an initiative reflects on learning among the staff and community members captured through their perceptions and group interactions. This learning, in turn, empowers the community to take 'actions' by providing them with the knowledge and skills needed to implement sustainable ecotourism practices on the ground. Finally, the actions would lead to the 'performance', which is evaluated as the impact of those actions, ensuring that the project effectively addresses the challenges and opportunities identified, showcasing the strengths or weaknesses of the CBOs.

### **Inter-component Matrix Interpreting Institutional Climate Capacity Through Community Projects**

The FGD interactions with the community SHGs and stakeholders of the community and projects have resulted in the understanding of various situations and actions involved in the processes, including the planning for the project towards conservation and resilience—the cross-interaction matrix translating the relation between learning into actions as illustrated in Table 2.

The inter-relational matrix indicates a strong influence of climate action plans based on planning (L\*1) with the actions resulting in their capacity and resilience. The key actions displayed by these institutions working in the CbET reveal enhanced participation among themselves, resulting in knowledge management and capacity building related to conservation, environmental issues, and climate change (L\*1- A\*2, A\*3) and (L\*2- A\*4). Those SHGs and communities have shown positive and perceptual solid

focus on this, which have achieved confidence and maturity in understanding the business of ecotourism and addressing the environmental issues through their ecotourism approach. Such institutions or cooperative groups (Women SHGs) based on their recognition and accolades received in this field. A women's SHGs group from Vengurla reveals that the recognition and interaction with the outside world have brought a lot of courage to deal with environmental issues and spread awareness among the women members in their group on biodiversity and coastal degradation issues. They can now sustain ecotourism and conservation practices because of support, knowledge sharing, and capacity building provided by the Mangrove Foundation and the United Nations Development Programme India (UNDP). The Global Environment Facility funded the UNDP project. The Swamini SHG group has received many accolades and recognition because of their initiative and work at the national and international levels. With the appreciation and support from these agencies, the all-Women SHG group is working on mainstreaming biodiversity in the region and presented the idea of a mangrove safari. Their initiatives have raised awareness among the villagers and the tourists. These groups have received support from various institutions and forest departments in terms of developing capacity and participation at regional and state levels. All such efforts have resulted into an effective communication among members and resolution of conflicts among each others.

The other key outcome actions revealed as an indicator of the institutional climate capacity of these community-based organizations (CBOs) focused on the interaction between the quality of resources and its importance in setting realistic targets and assessing stakeholders' needs and their satisfaction from the initiatives [L\*3-A\*3; L\*4-A\*5]. The importance of design-plan implementation in relation to resources and knowledge management has been advocated in the previous chapter. The same has been revealed through the participatory approach. The SHGs and other stakeholders indicated that the organizations could set targets consistent with the targets and outcomes to achieve and address the priorities of stakeholders aligned with their objectives of conservation and awareness. The study could not find any relational matrix between the formats of archived data to identify the indicators of knowledge management and planning or assess the needs and satisfaction of the stakeholders engaged with the organization or among the members (L\*6- A\*1-5= 0). The participant's discussion revealed the difficulty of accessing the existing relevant climate and performance parameters due to its technical nature or lack of coordination. However, no consensus was developed on the same due to a lack of knowledge in the domain. The solution to such gaps can be addressed

Table 2: Cross interaction Matrix between Learnings (L\*) and Actions (A\*).

	A*1: Monitoring and evaluating climate change work and Implementing results/project	A*2: Participation in knowledge management regarding climate change	A*3: Climate change plan and setting realistic targets	A*4: Providing climate change services and programs	A*5: Assessing stakeholder's needs and satisfaction
L*1: Climate action plan based on scenario planning for management decision	-	The organization has a system for documenting, storing, and disseminating climate change knowledge, which is accessible both externally and internally (1).	-	The extent to which services and programs align with the priorities and make progress against the objectives laid out in the strategic plan (1)	-
L*2: Awareness regarding climate information, mitigation practices, and influencing policy	-	-	-	The organization provides climate change services and programs aligning with the risks and opportunities identified in the strategic plan (1).	-
L*3: Quality of realistic resource requirement	-	-	The targets are set yearly and can be revised, and proper actions are taken if they are not met (1).	-	-
L*4: Mutually beneficial knowledge management	-	-	-	-	There is a transparent process for prioritizing services and programs; services and programs address stakeholders' climate change needs and priorities (1)
L*5: Knowledge of indicators and preventive risk modeling and data management	-	-	The organization consistently sets realistic targets for appropriately chosen climate change quantitative and qualitative indicators (1)	-	-
L*6: Helpful format of the archived data	-	-	-	-	-

Source: Compiled by Authors based on FGD and survey analysis

through a collaborative approach among the institutions and CBOs in developing information and data in prescribed understandable formats for a resilient and informative institutions for the community.

The key inter-relational matrix of the actions as an influence of institutional actions and processes resulting in the learning process of communities further leading to the performance of the CBOs has been illustrated in Table 3. The performance of the CBOs could be an outcome because of the improved situation, resulting in the enhanced capacity level of actors, institutions, and workflow simultaneously. Analyzing performances and actions leads to identifying gaps and issues these CBOs must address to develop their

climate capacity and resilience. The crucial performance variables, as revealed through the study, affecting the capacity of the institutions are their capacity to achieve adaptation and mitigation initiatives, employ approaches to ensure maximum and effective participation among the actors involved, capacity to recognize their roles and functions, and clarity on the requirement of data to manage to have the capability of leading to informed management decisions.

The actions taken by the communities, as influenced by various situations and processes factors by the organization's interaction with community members, lead to the performance of the institutions, depicting the strengths and weaknesses of these institutions in addressing the climate change requirements

Table 3: Cross interaction Matrix between Actions (A\*) and Performances (P\*).

	P*1: Achieving clear and measurable climate change adaptation and mitigation results	P*2: Employing approaches to ensure the participation of other actors	P*3: Recognition of functions and roles	P*4: Intended to clearly and accurately monitor data	P*5: Data leads informed management decisions
A*1: Monitoring and evaluating climate change work and Implementing results/project	The organization generates climate data, information, or analysis, and the generated data satisfies the purpose (1).	-	-	The organization often monitors and evaluates climate change work and results (1)	It is measured consistently over time and has sufficient precision and timeliness to inform management decisions (1).
A*2: Participation in knowledge management regarding climate change	Efforts are made to prioritize needed climate information, data, and analysis; the prioritization matches the organization's stated climate change goals and objectives (1)	The organization employs approaches to ensure the participation of other actors in accomplishing its objectives, particularly on climate change (1)	Local communities and other actors recognize the organization's functions and roles: (1)	-	-
A*3: Climate change plan and setting realistic targets	Performance monitoring data clearly and accurately represents intended results (1)	-	-	-	-
A*4: Providing climate change services and programs	services and programs achieve clear and measurable climate change adaptation and mitigation results (1)	-	Clear timelines, responsibilities, and resources are assigned for the climate change services and programs (1)	Services and programs are based on adequate and appropriate climate information, data, and analysis (1).	-
A*5: Assessing stakeholder's needs and satisfaction	-	-	-	Projects are monitored regularly, and the needs and satisfaction of customers of the organization's climate change services and programs are assessed often (1)	-

Source: Compiled by Authors based on FGD and survey analysis

and their capacity. The performance can be enhanced through the learnings over a period of time. Also, because of the influencing factors, the performance outcomes lead to multiple learning, which cumulatively directly or indirectly leads to the organization's overall performance. It has been found from the discussions that the key learnings that these communities value for their association with the CBOs or as CBOs are in the form of experiential learning through stakeholders' feedback and collaborations. There is no set format for data monitoring and evaluation that generates the input analysis or a formal setup intriguing into the improvement aspects. They also believe that the key umbrella organizations (Nationally & International levels) have skilled resources and staff, providing opportunities to these institutions at the different platforms

and recognizing their roles and functions at the broader level. The community participants and local institutions agreed that collaborative strategies and feedback mechanisms among the group members, irrespective of their locations, have helped in identifying different risks and opportunities affecting the community projects. For the monitoring and evaluation of the projects, the level of knowledge regarding resource management and evaluations needs to be established through learning feedback mechanisms and expertise knowledge by the supporting institutions and channels for improved performance. At present, the forest department staff and their livelihood specialists provide the initial support associated with the project for each location and are the only resource for the community group projects.



The key learning or re-learning factors influencing the community values towards the association with the CBOs or reflecting the capabilities of their internal structure are perceived strongly through opportunities provided and recognition at the different levels and platforms. The collaborative effort and internal management decisions are based on experiential learning. Feedback mechanisms (informal & formal) and staff competencies are essential for assessing these institutions' climate capacity.

To sum up the results, it is envisaged that the study identifies the determinants of the value and the capacities of the local CBOs dealing with the conservation projects, determining or reflecting the adaptive capacity of these CBOs in terms of their resilience when dealing with the local communities through the conservation model intervention. This will also provide input for the CBO working with the communities to identify their strengths and opportunities to improve in managing and enhancing their adaptive capacities to deal with climate change through such initiatives. Such results are significant in informing policy and practice at a local, regional, and national level.

## CONCLUSION

The study deployed conceptualized dimensions based on the CBO's interaction with the communities in certain situations where there is an interplay of various stakeholders and processes leading to the learning model development. The data was collected through consultative approaches involving CBOs, NGOs, and SHGs, using FGDs and key informant interviews in the conservation project areas. The interpretive stance of this exploratory qualitative framework is helpful for systematically inducing a learning outcome on climate risk mitigation of coastal ecotourism activities/services provided by the local communities. The perceived community value is an indication of assessing the climate institutional capacity of the CBOs capable of defining their key strengths, weaknesses, and gaps related to climate actions through conservation models. The consequential actions need to be further planned and executed. Within the scope of the present baseline study, the interconnections were explored by collaborating the institutional climate capacity through the perceptions of the community stakeholders engaged with these CBOs. The outcome discusses the awareness, learning dimensions, and adaptive capacities of CBOs about climate change, adaptive capacity, mitigation, and knowledge management. The study outcome accurately reflects the focus on evaluating the institutional climate capacity of CBOs and their role in addressing climate change challenges. It emphasizes the assessment aspect and highlights the

importance of understanding the capacity of CBOs in dealing with climate change issues.

The findings presented that the CBOs operating through the conservation-based approaches through the local communities can demonstrate a high level of awareness regarding emerging information on climate change. Community-based institutions can effectively coordinate with internal and external organizations for collaborations, capacity building, and sharing similar mandates. Such collaborations are considered crucial for the success of conservation efforts and enhance the climate resilience of CBOs engaged. Most institutions have established formal mechanisms for inter-organizational coordination, such as task forces, self-help groups, cooperative societies, village management committees, task forces, and capacity-building programs, to pool resources and amplify their impact. The study envisaged the involvement of socially excluded groups in implementing the CBO plan to ensure relevance and effectiveness. By participating in the planning, implementation, and evaluation processes, these groups can play a significant role in the plan's success. The staff and stakeholders are actively involved in developing the mandate/mission, and there are effective communication and coordination mechanisms within the CBOs & CBOs. Overall, the perceived values of the actor processes reflect the strengths and weaknesses of CBOs' institutional climate capacities, which are crucial for capacity building and sustainable conservation efforts.

The synthesized key interaction components highlight an integrated approach to learning and action, informing the design and delivery of experiences that empower communities to take informed actions; learning bridges the gap between understanding community needs and empowering them to implement sustainable practices, with knowledge dissemination and skill-building initiatives by CBOs and agencies like the Maharashtra Mangrove Foundation, Forest Department, UNDP, and Global Environment Facility playing crucial roles. Participation in ecotourism and conservation practices enhances community resilience and recognition, exemplified by the successes of groups like the Swamini Women SHG and Dapoli ELP unit. However, challenges such as technical expertise and resource availability hinder data collection and implementation, emphasizing the need for formalized feedback mechanisms and capacity-building. The performance of CBOs is shaped by the interaction between situations, actors, processes, and learning components, with continuous learning and partnerships contributing to their adaptive capacity in addressing climate change. Understanding community values and capacities informs policy and practice, empowering CBOs

to enhance their effectiveness in managing conservation projects and community engagement.

The findings highlight and determine the adaptive capacity of local CBOs and provide insights for improving their resilience and adaptive capacities in managing climate actions through conservation initiatives. The findings have implications for informing policies and practices at local, regional, and national levels. Additionally, the findings underscore the importance of holistic approaches to learning and action, collaborative partnerships, and continuous capacity-building efforts in fostering community resilience and sustainable environmental practices. These insights serve as valuable inputs for policymakers, practitioners, and funding agencies seeking to support community-based conservation initiatives and address climate change challenges effectively.

## ACKNOWLEDGMENT

This work was supported by the Indian Council of Social Science Research (ICSSR) under Grant No. 02/111/GN/2021-22/ICSSR/RP/MJ. The scholar, namely Dr Ravi Sharma, is the awardee of the ICSSR Research Project (Major Project). However, the author is responsible for the facts stated, opinions expressed, and conclusions drawn.

## REFERENCES

- Berdej, S.M. and Armitage, D.R., 2016. Bridging organizations drive effective governance outcomes for the conservation of Indonesia's marine systems. *PloS One*, 11(1), p.e0147142.
- Bhardwaj, A. and Khosla, R., 2021. Superimposition: How Indian city bureaucracies are responding to climate change. *Environment and Planning E: Nature and Space*, 4(3), pp.1139-1170.
- Dupuits, E., 2016. Civil society and NGOs as Drivers of Change in Environmental Governance. E-International Relations Retrieved August 20, 2023, from <https://www.e-ir.info/2016/06/13/actors-other-than-states-the-role-of-civil-society-and-ngos-as-drivers-of-change/>.
- Ingram, J. and Hamilton, C., 2014. *Planning for Climate Change—Guide: A Strategic, Values-based Approach for Urban Planners* UN-Habitat, pp. 1–160.
- Njuguna, L., Biesbroek, R., Crane, T.A., Tamás, P. and Dewulf, A., 2022. Designing fit-for-context climate change adaptation tracking: Towards a framework for analyzing the institutional structures of knowledge production and use. *Climate Risk Management*, 35, p.100401.
- Patterson, J.J., 2021. More than planning: Diversity and drivers of institutional adaptation under climate change in 96 major cities. *Global Environmental Change*, 68, p.102279.
- Tosun, J. and Howlett, M., 2021. Managing slow onset events related to climate change: The role of public bureaucracy. *Current Opinion in Environmental Sustainability*, 50, pp.43-53.
- White, C.M., Mangubhai, S., Rumetna, L. and Brooks, C.M., 2022. The bridging role of non-governmental organizations in the planning, adoption, and management of the marine protected area network in Raja Ampat, Indonesia. *Marine Policy*, 141, p.105095.

# Larval Age-Dependent Parasitization Performance of *Cotesia flavipes* on *Sesamia inferens*

V. K. Sonawane<sup>1</sup>, S. K. Gharde<sup>1†</sup>, K. S. Ghodekar<sup>1</sup>, A. M. Raut<sup>1</sup> and Amine Assouguem<sup>2</sup>

<sup>1</sup>Department of Entomology, School of Agriculture, Lovely Professional University, Phagwara, Jalandhar, Punjab, India

<sup>2</sup>Ethnopharmacology and Pharmacognosy Team, Faculty of Sciences and Technology, Errachidia, Moulay Ismail University, Meknes, Morocco

†Corresponding author: S.K. Gharde: sgharde@rediffmail.com

**Abbreviation:** Nat. Env. & Poll. Technol.  
**Website:** www.neptjournal.com

Received: 26-07-2024

Revised: 01-09-2024

Accepted: 21-09-2024

## Key Words:

*Cotesia flavipes*  
*Sesamia inferens*  
 Parasitism  
 Mass rearing  
 Braconidae

## Citation for the Paper:

Sonawane, V.K., Gharde, S.K., Ghodekar, K.S., Raut, A.M. and Assouguem, A., 2025. Larval age-dependent parasitization performance of *Cotesia flavipes* on *Sesamia inferens*. *Nature Environment and Pollution Technology*, 24(2), p. B4249. <https://doi.org/10.46488/NEPT.2025.v24i02.B4249>

Note: From year 2025, the journal uses Article ID instead of page numbers in citation of the published articles.



Copyright: © 2025 by the authors

Licensee: Technoscience Publications

This article is an open access article distributed under the terms and conditions of the Creative Commons Attribution (CC BY) license (<https://creativecommons.org/licenses/by/4.0/>).

## ABSTRACT

*Cotesia flavipes* is an important hymenopteran larval parasitoid that belongs to the family Braconidae. Its usage in pest management strategies is promising due to its parasitic impact on the larval stage of lepidopteran pests. The current investigation aims to determine the optimal host age for the parasitoid's mass proliferation and augmentative releases. The experiments showed that the female *C. flavipes* parasitizes all larval age groups of *Sesamia inferens*. Among all the larval ages, *C. flavipes* preferred second to third instars for parasitism during the spring (up to 90%) and kharif (up to 80%) seasons. There was no substantial difference in the development period between stinging, cocoon production, and the adult emergence of parasitoids. The age of the host has a substantial impact on adult longevity, with females taking longer than males. Thus, larval instars (second and third) are also recommended for high-quality mass-rearing larval parasitoids, especially *C. flavipes*, due to their strong parasitism and high net reproductive rate. Therefore, the second and third instars of *S. inferens* will recommend the mass rearing of *C. flavipes* and the release of these parasitoids in the field as a successful bio-control program.

## INTRODUCTION

Biological control with various living organisms such as predators, parasitoids, and entomopathogens has significant potential in integrated pest management (Sedaratian-Jahromi 2021). Adult parasitoids are free-living, whereas their egg and larval stages live in or on a single host to complete their life cycle to reach the adult stage (Dodiya & Pathan 2022, Fei et al. 2023, Holmes et al. 2023). Parasitoids eventually kill their hosts throughout the parasitism process by inducing paralysis (Quicke 2014, Butcher & Quicke 2023, Dai et al. 2024). It lays eggs in the hemocoel of the host insect (Jervis et al. 2023), complete larval development inside the host, and emerge just before the pupal formation in the silken cocoons (Van Noort & Broad 2024, Virla et al. 2023, Farahani et al. 2012). However, larval endoparasitoids like *Cotesia* are being used in biological pest control programs worldwide (Chepkemai et al. 2023, Parker & Kingsolver 2024) and parasitize various lepidopteran pests, including *Sesamia inferens*. Pink stem borer, *Sesamia inferens*, is a polyphagous pest reported on wheat, sorghum, oats, rice, pearl millet, barley, sugarcane, finger millet, and grasses (Jeer et al. 2021, Jadhao et al. 2020, Baladhiya et al. 2018). This pest caused damage of up to 78% in maize (Deole et al. 2017, Upadhyay et al. 2023).

Chemical communication is a very important factor in the host selection of parasitoids (Han et al. 2024). When the plant is infested by the insect pest, which emits volatile cues that are responsible for the identification of the host location for the parasitoid (Penaflor et al. 2011, Uefune et al. 2012, Furstenberg

et al. 2013, Bogka et al. 2023, Yi et al. 2023) or emitted by herbivores and their frass after feeding on plants (de Rijk et al. 2016, Liu et al. 2024), host preference could influence the host-parasitoid interaction (Furstenberg-Hagg et al. 2013), the development, success of reproduction, and the percentage of survival of the parasitoid on the hosts in field condition (Kher et al. 2024, Han et al. 2013, Ehteshami et al. 2023, Gomes et al. 2024). Consequently, numerous parasitoids exhibit host preferences based on particular stages of host or species and enhance the percentage of parasitism in invitro conditions (Stacconi et al. 2013, Yazdani et al. 2015, Hegazi et al. 2024, Kher et al. 2024).

The ability of parasitoids to search behavior is based on the parasitism rate against hosts (Hardy & Wajnberg 2023). After the parasitism of the host by the parasitoid, it goes through various phases such as host habitat location, host location, host acceptance, host suitability, and host regulation (Harris et al. 2012 Kuramitsu et al. 2019 Benrey 2023 Kathirvelu et al. 2024 Fei et al. 2023 Abram et al. 2023). The steps to be followed for effective colonization of a host by a parasitoid according to chemical cues are employed by the male wasps to find conspecific females in the field or an artificial cage (Malek et al. 2021). Certain parasitoids possess the capability to locate potential mates over a considerable distance through the emission of highly volatile pheromones, whereas, in certain instances, less volatile pheromones are employed for short-range (Ruther 2013). It is believed that male wasps may use cues other than female pheromones to locate females, other cues that help to find mates through host-associated volatiles or host-induced plant volatiles (Reddy & Guerrero 2004, Xu et al. 2017). Female parasitoids use plant volatiles to locate host habitats (McCormick et al. 2012, Wäschke et al. 2013, Turlings & Erb 2018). Some insects also take volatile stimuli from the habitat for mating (male dung flies are attracted to the odor of fresh cow manure) (Parker 1978, McAuslane et al. 1990, Webster & Cardé 2017).

The biocontrol program is successful when bio-agents are available at ground level, and natural enemies are mass culturing in the laboratory. The natural population available in the field will not survive for a longer period due to the application of pesticides to protect the crops. In agriculture, crops are protected through synthetic pesticides, causing several problems like the development of resistance and resurgence in pests, habitat loss, the decline of ecological service members, environmental pollution, and many more (Onaho et al. 2023, Ahmad & Akhtar 2016, Shimeng et al. 2001, Mruthunjayaswamy et al. 2016, Nwankwo et al. 2016). Therefore, the laboratory mass culture of braconid wasps requires lepidopteran larvae as a feeding

source. However, one issue encountered during laboratory production of *Cotesia flavipes* is parasitoid quality (Prezotti & Parra 2002). The parasitoid's inferior quality is the reason for its production failure and lack of demand (Ramalho et al. 2012). Hence, the knowledge of the parasitoid is most important for the suitable host age used for augmentative parasitoid releases (Li et al. 2006). Therefore, the present study mainly focuses on the performance of *Cotesia flavipes* on parasitization and net reproductive rate on different larval instars of the pink stem borer, *Sesamia inferens*, to enhance the mass-rearing process of parasitoids.

## MATERIALS AND METHODS

The experiment entitled Parasitization performance of *Cotesia flavipes* on different larval instars of pink stem borer, *Sesamia inferens*, was conducted under laboratory conditions at the School of Agriculture, Lovely Professional University, Phagwara (Punjab). The experiments were conducted during the spring and kharif seasons of 2023.

### Mother Culture of *Sesamia inferens*

A fourth and fifth instar of the pink stem borer, *Sesamia inferens* Walker, were collected from a maize field and reared under laboratory conditions. The insects were kept in in-vivo conditions at  $26 \pm 2^\circ\text{C}$ , RH  $65 \pm 5\%$ , and a 12L:12D photoperiod. The emerged adult from this culture was reared on a maize plant in the ovipositional chamber (Kumar et al. 2011) by providing 10% honey solution to emerging adults. After five to six days, remove the potted plant from the ovipositional chamber, separate the leaf sheath from the plant where the egg mass was, and rear in the incubator up to the hatching of neonate larvae. These larvae were reared on a maize stem (7×2.5 cm) in tubes, with this method, culture was maintained for future study (Sharma et al. 2017). The old stems were replaced by fresh stems every day. Two generations were reared under laboratory conditions before starting the experiments.

### Mother Culture of *Cotesia flavipes*

Parasitized cadavers were collected from the maize field and brought into the laboratory for further mass culturing. The cocoons were kept at  $26 \pm 2^\circ\text{C}$ , RH  $65 \pm 5\%$ , with a photometer for 12 hours of equal day and night length. The cocoons of parasitoids were reared in the rearing chamber by covering them with brown paper (22×15×5 cm). The observations were recorded daily until adults emerged. Emerged adults were then shifted to the rearing cage by providing a 20% honey solution in cotton swabs as food for adult parasitoids. After 24 hours, keep the old larvae separate and the fresh larvae with the parasitoids,



and continue this process till the death of the parasitoid. All parasitized larvae of *S. inferens* were reared at  $26 \pm 2^\circ\text{C}$ , RH  $65 \pm 5\%$ , with a photoperiod of 12 hours equal to the length of day and night. The honey solution was provided daily to the adult parasitoid, and three generations of *Cotesia flavipes* were reared in laboratory conditions with the same procedure.

### Preference of *Cotesia flavipes* on Different Larval Instars

To study the preference of female parasitoid *Cotesia flavipes* on different larval instars of pink stem borer, a pair of adult parasitoids were released for 24 hours in a glass tube for mating (Saini et al. 2019) with a 20% honey solution in a cotton swab as food. For mating, a no-choice experiment was carried out, with 10 larvae of each instar in a rearing box ( $22 \times 15 \times 5$  cm). The separation of the larvae was done (instar-wise) according to their size and color (Sharma et al. 2017, Nagarjuna et al. 2015). The parasitized host larvae of different instars of pink stem borer were then reared individually and observed until the pupation and emergence of the adult parasitoid.

### Impact on the Developmental Biology of *Cotesia flavipes*

The experiment on the developmental biology of the parasitoid *Cotesia flavipes* on the larval instars of pink stem borer was investigated through a series of experiments involving the parasitization of various larval instars of stem borer. The eclosion of adults was sorted by sex, and a pair of parasitoids were exposed separately to batches of ten larvae of host II to VI instars in a no-choice

experimental design. After 24 hours, the old larvae were replaced with new ones.

The old larvae were reared according to the prescribed procedure to facilitate the emergence of parasitoids (Saini et al. 2019). Since immature stages (egg and larvae) of the parasitoid were present in the body of the host, various parameters like duration of egg and larval stages (stinging to cocoon formation stage), pre-pupa and pupal stage (cocoon stage), longevity of adults, and sex ratio were recorded throughout the experimental period.

### Statistical Analysis

Different parameters recorded during the study were subjected to a one-way analysis of variance (ANOVA) using SPSS 22.0 software. We investigated the interactions of season and instar on the parasitization and developmental period of *Cotesia flavipes*, considering season and instar as fixed effects. The means that showed significant differences were distinguished using the least significant difference (LSD) method.

## RESULTS

### Parasitization Rate of *Cotesia flavipes* on Different Larval Instars

The *C. flavipes* parasitization rate significantly differs between the different larval instars of *S. inferens*. The most preferred stage and the highest level of parasitism (80% and 90%) were observed in third-instar larvae in the spring ( $F_{(4,9)} = 3.68$   $p = 0.011$ ) and kharif ( $F_{(4,9)} = 5.07$

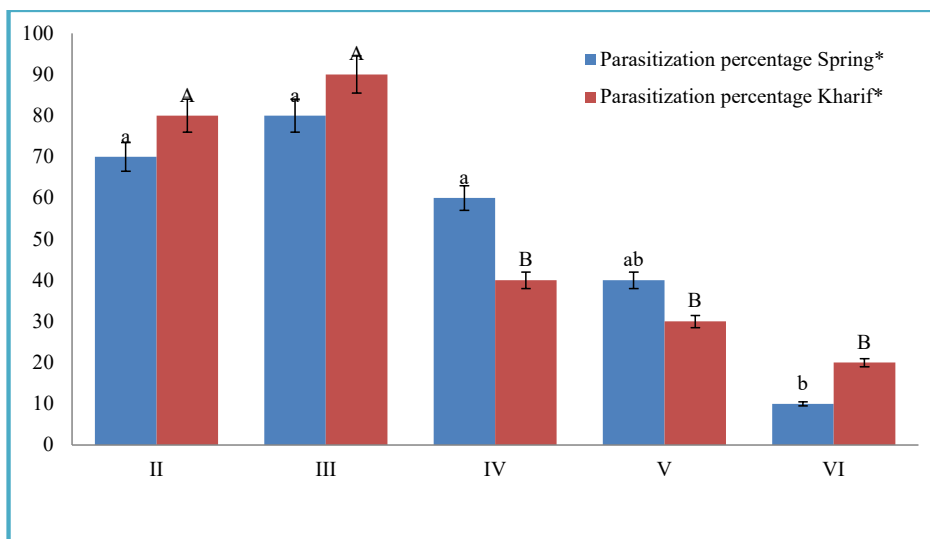


Fig. 1: Parasitization capability of *Cotesia flavipes* on different larval instars. <sup>a</sup>, <sup>A</sup> values with the same letters in a column are non-significant, as per DMRT. <sup>\*</sup> significant at 5% level of significance.

$p=0.002$ ) seasons, respectively (Fig 1). The parasitization rate gradually decreased after the third instar until the sixth instar during both seasons. However, there was no statistically significant impact of season on the parasitization of *C. flavipes* with respect to larvae host age.

### Impact on the Developmental Biology of *Cotesia flavipes*

The development period of immature parasitoids on host age was not significantly different ( $p > 0.05$ ) in both seasons (Table 1). The age of the parasitized host showed a substantial effect on adult longevity ( $p < 0.05$ ), with females living longer in both seasons. In *spring* 2023, the third instars had the longest development period, followed by the second, fourth, fifth, and sixth instars, and a similar pattern was seen in *Kharif* 2023 (Table 1).

### Net Reproductive Rate

The maximum oviposition period of *C. flavipes* was up to 96 hours observed in the second and third instars and then gradually decreased with host age in the *spring* season, and the same trend was observed in the *Kharif* season (Fig. 2). However, the female adult who emerged from the cocoon was twice as old as the male adult in all the time periods and

the age of the host in both seasons. Overall, there was no significant variation in the cocoon-forming population and adult emergence between seasons (Fig. 2). The sex ratio was 0.40:1 and 0.37:1 (male: female) found in the *spring* and *kharif* seasons, respectively.

## DISCUSSION

Bio-agents have the potential to check pest populations in the available ecosystem and therefore They are an important tool in the integrated pest management (IPM) system (Sampaio et al. 2009). The biological control includes predators, parasitoids, and entomopathogens successfully accommodated in the environment by the availability of suitable habitat, the application of eco-friendly pesticides, etc. Among the natural enemies, parasitoids are usually the best option for pest management due to their high host specificity and free-living behaviors (Colmenarez et al. 2018, Trejo & Contreras 2024). Therefore, mass culturing of parasitoids is an important step, and a temperature of 25-30°C indicates a faster development rate (Adamo et al. 2012, Huey et al. 2012, Moore et al. 2020). However, the mass production of *Cotesia* species in the laboratory is very cost-effective for pest management (Zang et al. 2021). Our research study showed that the *Cotesia flavipes* preferred

Table 1: Development time and adult longevity of parasitoids at different ages of the host.

<b>Spring 2023</b>					
Host instars	Development time (days) $\pm$ SD			Adult longevity (days) $\pm$ SD	
	Stinging to cocoon formation	Cocoon stage	Stinging to Adult emergence	Male	Female
II	8.2 $\pm$ 4.42 <sup>a</sup>	3.3 $\pm$ 1.83 <sup>ab</sup>	11.5 $\pm$ 6.13 <sup>a</sup>	4.9 $\pm$ 3.48 <sup>a</sup>	5.1 $\pm$ 3.57 <sup>a</sup>
III	8.5 $\pm$ 7.40 <sup>a</sup>	4.0 $\pm$ 3.5 <sup>a</sup>	12.5 $\pm$ 10.8 <sup>a</sup>	5.2 $\pm$ 2.86 <sup>a</sup>	5.5 $\pm$ 3.10 <sup>a</sup>
IV	7.1 $\pm$ 5.02 <sup>ab</sup>	3.0 $\pm$ 3.89 <sup>ab</sup>	10 $\pm$ 7.04 <sup>ab</sup>	4.5 $\pm$ 4.00 <sup>a</sup>	4.7 $\pm$ 4.1 <sup>a</sup>
V	6.2 $\pm$ 8.01 <sup>ab</sup>	2.9 $\pm$ 2.08 <sup>ab</sup>	9.2 $\pm$ 11.89 <sup>ab</sup>	2.9 $\pm$ 3.78 <sup>b</sup>	3.2 $\pm$ 4.21 <sup>ab</sup>
VI	1.7 $\pm$ 5.38 <sup>b</sup>	0.8 $\pm$ 2.53 <sup>b</sup>	2.5 $\pm$ 7.91 <sup>b</sup>	0.7 $\pm$ 2.21 <sup>b</sup>	0.9 $\pm$ 2.85 <sup>b</sup>
F <sub>value</sub>	2.25	2.00	2.17	3.72	3.19
P <sub>value</sub>	0.116 <sup>NS</sup>	0.159 <sup>NS</sup>	0.129 <sup>NS</sup>	0.022*	0.041*
<b>Kharif 2023</b>					
Host instars	Development time (days) $\pm$ SD			Adult longevity (days) $\pm$ SD	
	Stinging to cocoon formation	Cocoon stage	Stinging to Adult emergence	Male	Female
II	8.0 $\pm$ 4.37 <sup>a#</sup>	3.5 $\pm$ 1.90 <sup>a</sup>	11.5 $\pm$ 6.15 <sup>a</sup>	4.7 $\pm$ 2.71 <sup>a</sup>	5.6 $\pm$ 3.17 <sup>a</sup>
III	8.8 $\pm$ 7.60 <sup>a</sup>	4.0 $\pm$ 3.50 <sup>a</sup>	12.8 $\pm$ 11.08 <sup>a</sup>	5.1 $\pm$ 3.03 <sup>a</sup>	5.3 $\pm$ 2.95 <sup>a</sup>
IV	6.0 $\pm$ 3.27 <sup>a</sup>	3.2 $\pm$ 4.16 <sup>a</sup>	9.2 $\pm$ 11.93 <sup>a</sup>	4.0 $\pm$ 3.53 <sup>ab</sup>	4.3 $\pm$ 3.74 <sup>ab</sup>
V	6.0 $\pm$ 7.79 <sup>a</sup>	2.9 $\pm$ 1.66 <sup>a</sup>	8.9 $\pm$ 4.91 <sup>a</sup>	2.5 $\pm$ 3.37 <sup>ab</sup>	2.8 $\pm$ 3.65 <sup>ab</sup>
VI	3.1 $\pm$ 6.54 <sup>a</sup>	1.7 $\pm$ 3.59 <sup>a</sup>	4.8 $\pm$ 10.13 <sup>a</sup>	1.2 $\pm$ 2.57 <sup>b</sup>	1.4 $\pm$ 2.95 <sup>b</sup>
F <sub>value</sub>	1.27	0.761	1.088	2.803	2.44
P <sub>value</sub>	0.293 <sup>NS</sup>	0.556 <sup>NS</sup>	0.374 <sup>NS</sup>	0.037*	0.035*

# The values with the same letters in a column are non-significant, as per DMRT.

‘\*’ significant at 5% level of significance (P<0.05), NS - non-significant

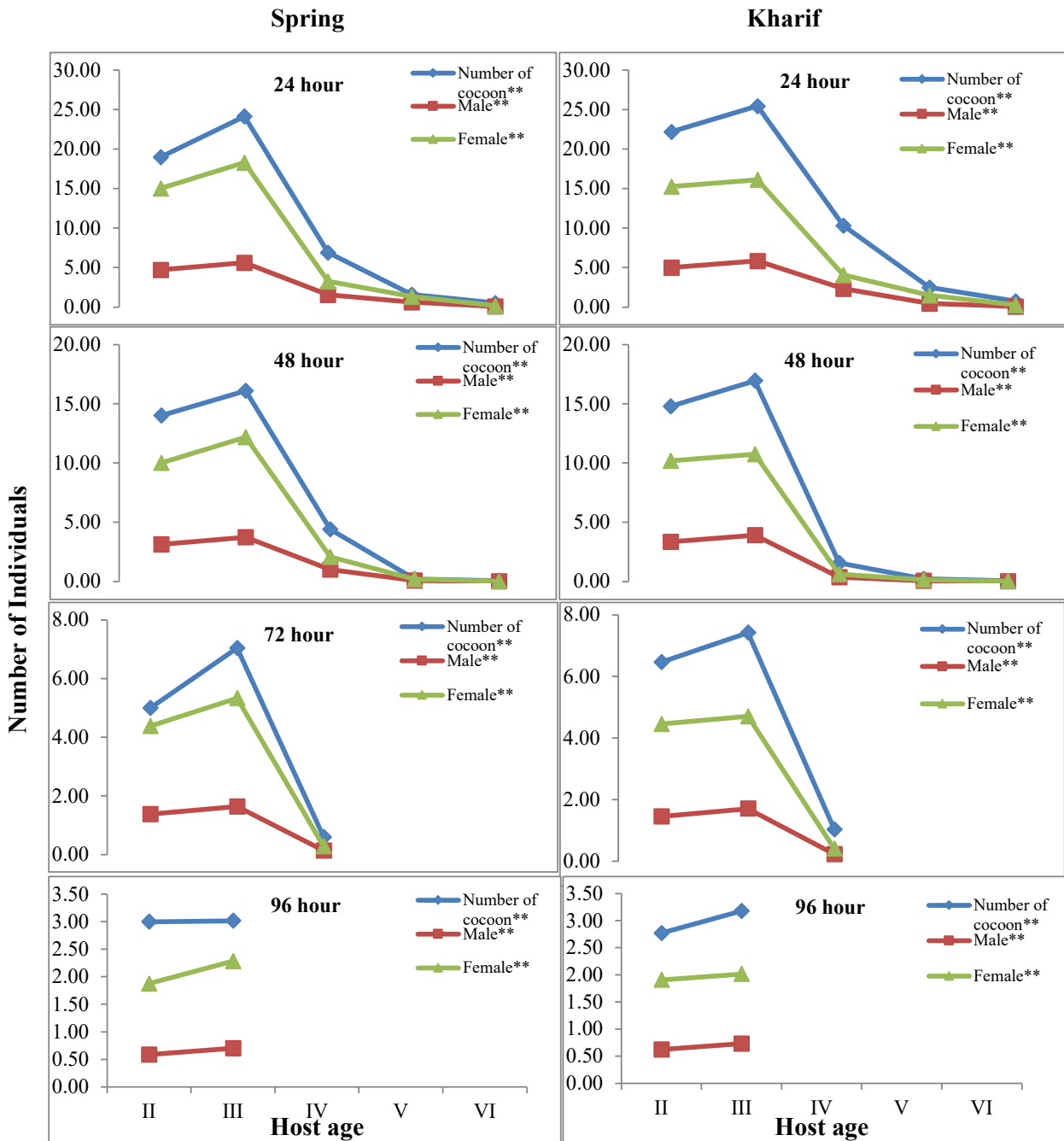


Fig. 2: Variation in the larval Parasitoid Reproductive Rate Across Different Host Ages  
\*\*\* Significant level at  $P \leq 0.01$

the second and third instars of the host for parasitism at a temperature of 25°C due to the availability of high protein, sugar, and lipid content in early instars larvae (Shekharappa & Kulkarni 2003, Jervis et al. 2008, Silva-Torres et al. 2009, Sokame et al. 2021).

However, the old age instars were not preferred by the

female *C. flavipes* for parasitization because the old larval instars developed defense mechanisms themselves and were aggressive, which led to the death of parasitoids (Potting et al. 1997).

Abiotic factors, especially temperature, play a crucial role in parasitoid growth and development (Adamo et

al. 2012, Huey et al. 2012). However, parasitoid wasp emergence and survival rate were maximum at 20°C and 25°C, but when it exceeded 30°C exhibited the rate of wasp emergence and survival rate (Moore et al. 2020). The longer development process, cocoon formation, and duration from stung to the emergence of adult parasitoids were observed at 25°C in the present investigation. A similar result was observed in *Cotesia* species; development periods were longer in the second instar of *Chilo partellus* (Sarkar et al. 2020 Khan et al. 2017), and the formation of the highest number of parasitoid cocoons was recorded in the third instar of *Spodoptera frugiperda* (Obala et al. 2023).

Augmentation is the release of natural enemies or environmental manipulation to increase the effectiveness of naturally occurring natural enemies (Hoy 2008). Environmental manipulation can include supplying alternate hosts or prey, food or nesting locations, or changing agricultural methods to benefit bioagents (Hoy 2008). The periodic release of natural enemies is evaluated based on fitness factors such as offspring sex ratio (Mohamad et al. 2015, Kruitwagen et al. 2018). Our research reported that males emerged early as compared to females, and the population of female adults was almost double the of male adults. This result may be due to mated female parasitoids being able to manage progeny sex ratios by regulating fertilization during oviposition. The present result, supported by (Heimpel & de Boer 2008), revealed that females develop from fertilized eggs and are diploid, while males develop from unfertilized eggs and are haploid. However, the previous research showed that the female adult emerged more than the male adult of *Cotesia* sp. when the host was *Spodoptera frugiperda* (Obala et al. 2023) and *S. littoralis* (Agbodzavu et al. 2018).

## CONCLUSIONS

The present investigation concludes that *Cotesia flavipes* preferred the second or third instars of *Sesamia inferens* for parasitization. These larval stages are used for mass rearing of *C. flavipes* in laboratory conditions and are periodically relived in the field to manage the lepidopteron pest. In laboratory conditions, a temperature of 25–30°C will enhance the fecundity, cocoon formation, and emergence rate of *C. flavipes*. However, for the conservation of parasitoids, we will provide alternate hosts and food by planting nectarine plants and avoiding the application of non-selective pesticides. The conservation of the larval parasitoid *C. flavipes* enhances the efficacy of biological pest management strategies aimed at mitigating the impact of lepidopteran pest infestations in field conditions.

## ACKNOWLEDGMENT

All the authors are thankful to Lovely Professional University for providing the facility for conducting the experiments.

## REFERENCES

- Abram, P.K., Haye, T., Clarke, P., Grove, E., Thiessen, J. and Garipey, T.D., 2023. Partial refuges from biological control due to intraspecific variation in protective host traits. *Ecological Applications*, 33(4), e2796. [DOI]
- Adamo, S.A., Baker, J.L., Lovett, M.M. and Wilson, G., 2012. Climate change and temperate zone insects: The tyranny of thermodynamics meets the world of limited resources. *Environmental Entomology*, 41(6), pp.1644-1652. [DOI]
- Agbodzavu, M.K., Lagat, Z.O., Gikungu, M., Rwomushana, I., Ekesi, S. and Fiaboe, K.K.M., 2018. Performance of the newly identified endoparasitoid *Cotesia icipe* Fernandez-Triana & Fiaboe on *Spodoptera littoralis* (Boisduval). *Journal of Applied Entomology*, 142(7), pp.646-653. [DOI]
- Ahmad, M. and Akhtar, S., 2016. Development of resistance to insecticides in the invasive mealybug *Phenacoccus solenopsis* (Hemiptera: Pseudococcidae) in Pakistan. *Crop Protection*, 88, pp.96-102. [DOI]
- Baladhiya, H.C., Sisodiya, D.B. and Pathan, N.P., 2018. A review on pink stem borer, *Sesamia inferens* Walker: A threat to cereals. *Journal of Entomology and Zoology Studies*, 6(3), pp.1235-1239.
- Benrey, B., 2023. The effects of plant domestication on the foraging and performance of parasitoids. *Current Opinion in Insect Science*, 57, 101031. [DOI]
- Bogka, G., Anastasaki, E., Milonas, P.G., Psoma, A., Kabourakis, E.M., Zwaan, B.J., Pannebakker, B.A. and Fatouros, N.E., 2023. Chemical cues involved in the host foraging behavior of *Psytalia concolor* wasps to locate the olive fruit fly *Bactrocera oleae*. *Frontiers in Ecology and Evolution*, 11, pp.1-10. [DOI]
- Butcher, B.A., 2023. *Parasitoid Wasps of South East Asia*. GB: CABI.
- Colmenarez, Y., Corniani, N., Mundstock, S., Sampaio, M. and Vásquez, C., 2018. Use of parasitoids as a biocontrol agent in the Neotropical region: Challenges and potential. In *Horticultural Crops*, pp.171-185. London: IntechOpen. [DOI]
- de Rijk, M., Krijn, M., Jenniskens, W., Engel, B., Dicke, M. and Poelman, E.H., 2016. Flexible parasitoid behaviour overcomes constraint resulting from position of host and nonhost herbivores. *Animal Behaviour*, 113, pp.125-135. [DOI]
- Deole, S., Dubey, V.K., Rana, D.K. and Gauraha, R., 2017. Evaluation of newer insecticides against maize pink stem borer: Major constraint insect pest of maize in Raipur, Chhattisgarh. *Journal of Plant Development Sciences*, 9(4), pp.335-339.
- Dodiya, R.D. and Pathan, N.P., 2022. Host searching behaviour of parasitoids and predators. *A Monthly Peer Reviewed Magazine for Agriculture and Allied Sciences*, 14, pp.1-10.
- Ehteshami, F., Aleosfoor, M., Allahyari, H., Kavousi, A. and Fekrat, L., 2023. Comparative demography, population projection, functional response and host age preference behavior of the parasitoid *Goniozus legneri* on two lepidopteron insect hosts. *Egyptian Journal of Biological Pest Control*, 33(1), pp.2-10. [DOI]
- Farahani, H.K., Bell, H. and Goldansaz, S.H., 2012. Biology of *Apanteles myeloenta* (Hymenoptera: Braconidae), a larval parasitoid of carob moth *Ectomyelais ceratoniae* (Lepidoptera: Pyralidae). *Journal of Asia-Pacific Entomology*, 15(4), pp.607-610. [DOI]
- Fei, M., Gols, R. and Harvey, J.A., 2023. The biology and ecology of parasitoid wasps of predatory arthropods. *Annual Review of Entomology*, 68, pp.109-128. [DOI]



- Fürstenberg-Hägg, J., Zagrobelny, M. and Bak, S., 2013. Plant defense against insect herbivores. *International Journal of Molecular Sciences*, 14(5), pp.10242-10297. [DOI]
- Gao, Y., Hu, Y., Fu, Q., Zhang, J., Oppert, B., Lai, F. and Zhang, Z., 2010. Screen of *Bacillus thuringiensis* toxins for transgenic rice to control *Sesamia inferens* and *Chilo suppressalis*. *Journal of Invertebrate Pathology*, 105(1), pp.11-15. [DOI]
- George-Onaho, J.A., Moore, J.C., Haastруп, N.O., Agboola, I.S., Ete, J.A. and Ajao, O.I., 2023. Insecticidal efficacy of *Tithonia diversifolia* extracts against pink stem borer (*Sesamia calamistis* (Hampson)). *Ethiopian Journal of Environmental Studies & Management*, 16(1), pp.117-123. [DOI]
- Gomes, E., Lemaître, J.F., Rodriguez-Rada, V., Débias, F., Desouhant, E. and Amat, I., 2024. Foraging at night under artificial light: impacts on senescence and lifetime reproductive success for a diurnal insect. *Animal Behaviour*, 210, pp.85-98. [DOI]
- Gornard, L., Mougél, S., Germon, F., Borday-Birraux, I. and Kaiser, L., 2024. Cellular dynamics of host-parasitoid interactions: insights from the encapsulation process in a partially resistant host. *Journal of Experimental Biology*, 227(4), pp.1-12. [DOI]
- Han, L.B., Huang, L.Q. and Wang, C.Z., 2013. Host preference and suitability in the endoparasitoid *Campoletis chloridae* is associated with its ability to suppress host immune responses. *Ecological Entomology*, 38(2), pp.173-182. [DOI]
- Hardy, I.C. and Wajnberg, E., 2023. *Jervis's Insects as Natural Enemies: Practical Perspectives*. Springer Nature.
- Harris, C.M., Ruberson, J.R., Meagher, R. and Tumlinson, J.H., 2012. Host suitability affects odor association in *Cotesia marginiventris*: implications in generalist parasitoid host-finding. *Journal of Chemical Ecology*, 38, pp.340-347.
- Hegazi, E. and Khafagi, W., 2024. Host-instar selection, interspecific competition, and reproductive capacity of extant and novel parasitoids (Hymenoptera: Braconidae) on Egyptian cotton leafworm. *Egyptian Journal of Biological Pest Control*, 34(1), p.10.
- Heimpel, G.E. and de Boer, J.G., 2008. Sex determination in the Hymenoptera. *Annual Review of Entomology*, 53, pp.209-230. [DOI]
- Holmes, L.A., Nelson, W.A. and Loughheed, S.C., 2023. Strong effects of food quality on host life history do not scale to impact parasitoid efficacy or life history. *Scientific Reports*, 13(1), p.3528.
- Hoy, M.A., 2008. Augmentative biological control. In: Capinera, J.L. (ed.) *Encyclopedia of Entomology*. Springer, Dordrecht.
- Huey, R.B., Kearney, M.R., Krockenberger, A., Holtum, J.A., Jess, M. and Williams, S.E., 2012. Predicting organismal vulnerability to climate warming: roles of behaviour, physiology and adaptation. *Philosophical Transactions of the Royal Society B: Biological Sciences*, 367(1596), pp.1665-1679. [DOI]
- Jadhao, K.R., Bansal, A. and Rout, G.R., 2020. Silicon amendment induces synergistic plant defense mechanism against pink stem borer (*Sesamia inferens* Walker) in finger millet (*Eleusine coracana* Gaertn.). *Scientific Reports*, 10(1), p.4229. [DOI]
- Jeer, M., Yele, Y., Sharma, K.C. and Prakash, N.B., 2021. Exogenous application of different silicon sources and potassium reduces pink stem borer damage and improves photosynthesis, yield and related parameters in wheat. *Silicon*, 13(3), pp.901-910. [DOI]
- Jervis, M.A., Ellers, J. and Harvey, J.A., 2008. Resource acquisition, allocation, and utilization in parasitoid reproductive strategies. *Annual Review of Entomology*, 53, pp.361-385. [DOI]
- Kathirvelu, C., Manickavasagam, S. and Gopianand, L., 2024. Host preference of *Xanthopimpla Saussure* parasitising *Sesamia inferens* Walker. *Indian Journal of Entomology*, pp.1-7.
- Khan, J., Ali, R., Blouch, A., Javed, H.I., Haq, E.U., Mehmood, T. and Rasool, A., 2017. Biological parameters of *Cotesia flavipes* reared on different larval instars of *Chilo partellus* under laboratory conditions. *Journal of Entomology and Zoology Studies*, 5(3), pp.829-832.
- Kher, S.V., Kulkarni, S.S., Dosdall, L.M. and Cárcamo, H.A., 2024. Life history and host preferences of *Tetrastichus julis* (Walker) (Hymenoptera: Eulophidae), the principal parasitoid of the cereal leaf beetle, *Oulema melanopus* (L.) (Coleoptera: Chrysomelidae). *Biological Control*, 188, p.105432. [DOI]
- Kruitwagen, A., Beukeboom, L.W. and Wertheim, B., 2018. Optimization of native biocontrol agents, with parasitoids of the invasive pest *Drosophila suzukii* as an example. *Evolutionary Applications*, 11(9), pp.1473-1497. [DOI]
- Kumar, P., Suby, S.B., Sekhar, J.C. and Kumar, R.S., 2011. A collapsible insect rearing cage. *Patent Application No.* 0923/DEL/2011.
- Kuramitsu, K., Vicencio, E.J.M. and Kainoh, Y., 2019. Differences in food plant species of the polyphagous herbivore *Mythimna separata* (Lepidoptera: Noctuidae) influence host searching behavior of its larval parasitoid, *Cotesia kariyai* (Hymenoptera: Braconidae). *Arthropod-Plant Interactions*, 13(1), pp.49-55. [DOI]
- Li, J., Coudron, T.A., Pan, W., Liu, X., Lu, Z. and Zhang, Q., 2006. Host age preference of *Microplitis mediator* (Hymenoptera: Braconidae), an endoparasitoid of *Mythimna separata* (Lepidoptera: Noctuidae). *Biological Control*, 39(3), pp.257-261. [DOI]
- Liu, G., Wang, Q., Chen, H., Wang, Y., Zhou, X., Bao, D. and Fu, J., 2024. Plant-derived monoterpene S-linalool and  $\beta$ -ocimene generated by CsLIS and CsOCS-SCZ are key chemical cues for attracting parasitoid wasps for suppressing *Ectopis obliqua* infestation in *Camellia sinensis* L. *Plant, Cell & Environment*, 47(3), pp.913-927.
- Malek, R., Kaser, J.M., Anfora, G., Ciolli, M., Khirman, A., Weber, D.C. and Hoelmer, K.A., 2021. *Trissolcus japonicus* foraging behavior: implications for host preference and classical biological control. *Biological Control*, 161, p.104700. [DOI]
- McAuslane, H.J., Vinson, S.B. and Williams, H.J., 1990. Influence of host plant on mate location by the parasitoid *Campoletis sonorensis* (Hymenoptera: Ichneumonidae). *Environmental Entomology*, 19(1), pp.26-31.
- McCormick, A.C., Unsicker, S.B. and Gershenson, J., 2012. The specificity of herbivore-induced plant volatiles in attracting herbivore enemies. *Trends in Plant Science*, 17(5), pp.303-310. [DOI]
- Mohamad, F., Mansour, M. and Ramadan, A., 2015. Effects of biological and environmental factors on sex ratio in *Ascogaster quadridentata* Wesmäl (Hymenoptera: Braconidae), a parasitoid of *Cydia pomonella* L. (Tortricidae). *Journal of Plant Protection Research*, 55(2), pp.151-155. [DOI]
- Moore, M.E., Kester, K.M. and Kingsolver, J.G., 2020. Rearing temperature and parasitoid load determine host and parasitoid performance in *Manduca sexta* and *Cotesia congregata*. *Ecological Entomology*, 45(1), pp.79-89. [DOI]
- Mruthunjayawamy, P., Thiruvengadam, V. and Kumar, J.S., 2016. Resistance in *Maconellicoccus hirsutus* (Green) in India to selected insecticides and quantification of detoxifying enzymes imparting resistance. *Crop Protection*, 89, pp.116-122. [DOI]
- Nagarjuna, B., Manjunatha, M. and Latha, M., 2015. Biology of maize stem borer, *Sesamia inferens* (Walker) Noctuidae: Lepidoptera. *Journal of Eco-friendly Agriculture*, 10(1), pp.90-91.
- Nwankwo, E.N., Onuseleogu, D.C., Ogbonna, C.U. and Okorocho, A.O.E., 2016. Effect of neem leaf extracts (*Azadirachta indica*) and synthetic pesticide (Carbofuran) on the root-knot nematode (*Meloidogyne* spp.) of cowpea (*Vigna unguiculata* L. Walp.). *International Journal of Entomological Research*, 3(1), pp.1-6.
- Obala, F., Mohamed, S.A., Magomere, T.O. and Subramanian, S., 2023. Old and new association of *Cotesia icipe* (Hymenoptera: Braconidae) with alien invasive and native *Spodoptera* species and key stemborer species: implication for their management. *Pest Management Science*, 79(12), pp.5312-5320. [DOI]
- Parker, A.L. and Kingsolver, J.G., 2024. The interactive effects of heat stress, parasitism and host plant quality in a host-parasitoid system. *Functional Ecology* (in press). [DOI]

- Parker, G.A., 1978. Evolution of competitive mate searching. *Annual Review of Entomology*, 23(1), pp.173-196. [DOI]
- Penaflo, M.F.G.V., Erb, M., Miranda, L.A., Werneburg, A.G. and Bento, J.M.S., 2011. Herbivore-induced plant volatiles can serve as host location cues for a generalist and a specialist egg parasitoid. *Journal of Chemical Ecology*, 37, pp.1304-1313. [DOI]
- Potting, R.P.J., Overholt, W.A., Danso, F.O. and Takasu, K., 1997. Foraging behavior and life history of the stemborer parasitoid *Cotesia flavipes* (Hymenoptera: Braconidae). *Journal of Insect Behavior*, 10, pp.13-29. [DOI]
- Prezotti, L. and Parra, J.P., 2002. Quality control in mass rearing of parasitoids and predators. In: Parra, J.R.P., Botelho, P.S.M., Corrêa-Ferreira, B.S. and Bento, J.M.S. (Eds.), *Biological Control in Brazil: Parasitoids and Predators*. Manole, São Paulo, pp.295-296.
- Quicke, D.L., 2014. *The Braconid and Ichneumonid Parasitoid Wasps: Biology, Systematics, Evolution and Ecology*. John Wiley & Sons.
- Ramvalho, D.G., Viel, S.R., Vacari, A.M., De Bortoli, S.A., Lopes, M.M., Laurentis, V.L. and Veiga, A.C.P., 2012. Criteria for optimization of mass rearing of the parasitoid *Cotesia flavipes* in the laboratory. *Journal of Research in Biology*, 2(5), pp.529-536. [DOI]
- Reddy, G.V. and Guerrero, A., 2004. Interactions of insect pheromones and plant semiochemicals. *Trends in Plant Science*, 9(5), pp.253-261. [DOI]
- Ruther, J., 2013. Novel insights into pheromone-mediated communication in parasitic hymenopterans. *Chemical Ecology of Insect Parasitoids*, pp.112-144.
- Saini, A., Sharma, P.L. and Chandel, R.S., 2019. Host age influence on the parasitism of the species *Cotesia vestalis* (Haliday) (Hymenoptera: Braconidae). *Egyptian Journal of Biological Pest Control*, 29, pp.1-6. [DOI]
- Sampaio, M.V., Bueno, V.H.P., Silveira, L.C.P. and Auad, A.M., 2009. Biological control of insect pests in the tropics. *Tropical Biology and Conservation Management*, 3, pp.28-70.
- Sarkar, S., Babu, A., Chakraborty, K. and Deka, B., 2020. Biology and life history of *Cotesia ruficrus* (Hymenoptera: Braconidae), a potential parasitoid of *Hyposidra talaca* (Lepidoptera: Geometridae) larvae, a major tea pest. *Journal of Biopesticides*, 13(1), pp.79-84.
- Sedaratian-Jahromi, A., 2021. Effects of entomopathogens on insect predators and parasitoids. *Microbes for Sustainable Insect Pest Management: Hydrolytic Enzyme & Secondary Metabolite—Volume 2*, pp.183-231. [DOI]
- Sharma, H., Jaglan, M.S. and Yadav, S.S., 2017. Biology of pink stem borer, *Sesamia inferens* (Walker) on maize, *Zea mays*. *Journal of Applied and Natural Science*, 9(4), pp.1994-2003.
- Shekharappa, S. and Kulkarni, K.A., 2003. Cultural practices for the management of stem borer, *Chilo partellus* (Swinhoe) in sorghum. *Journal of Agricultural Research*, 12(2), pp.45-51.
- Shimeng, H., Shijie, X., Shangang, X. and Guomeng, M., 2001. Resistance of rice stem borer (*Chilo suppressalis* Walker) to insecticides in Cixi, Zhejiang Province. *Acta Agriculturae Zhejiangensis*, 13(1), pp.38-41.
- Silva-Torres, C.S., Barros, R. and Torres, J.B., 2009. Effect of age, photoperiod, and host availability on the parasitism behavior of *Oomyzus sokolowskii* Kurdjumov (Hymenoptera: Eulophidae). *Neotropical Entomology*, 38, pp.512-519.
- Sokame, B.M., Obonyo, J., Sammy, E.M., Mohamed, S.A., Subramanian, S., Kilalo, D.C. and Calatayud, P.A., 2021. Impact of the exotic fall armyworm on larval parasitoids associated with the lepidopteran maize stemborers in Kenya. *BioControl*, 66, pp.193-204.
- Stacconi, R., Grassi, A.L., Dalton, D.T., Miller, B., Ouantar, M., Loni, A. and Anfora, G., 2013. First field records of *Pachycrepoides vindemiae* as a parasitoid of *Drosophila suzukii* in European and Oregon small fruit production areas. *Entomologia*, 1(e3), pp.11-16.
- Tang, L.D., Smagghe, G., Wang, S., Lü, Z.X. and Zang, L.S., 2024. Dead-end trap plants as an environment-friendly IPM tool: A case study of the successful use of vetiver grass in China. *Entomologia Generalis*, 45(2), pp.67-89.
- Turlings, T.C. and Erb, M., 2018. Tritrophic interactions mediated by herbivore-induced plant volatiles: Mechanisms, ecological relevance, and application potential. *Annual Review of Entomology*, 63, pp.433-452. [DOI]
- Uefune, M., Choh, Y., Abe, J., Shiojiri, K., Sano, K. and Takabayashi, J., 2012. Application of synthetic herbivore-induced plant volatiles causes increased parasitism of herbivores in the field. *Journal of Applied Entomology*, 136(8), pp.561-567. [DOI]
- Upadhyay, A., Ranjitha, M.R. and Mishra, P.K., 2023. Major pests of maize and their control. *Agricultural Research Journal*, 15(3), pp.121-135.
- Van Dam, N.M., Qiu, B.L., Hordijk, C.A., Vet, L.E. and Jansen, J.J., 2010. Identification of biologically relevant compounds in aboveground and belowground induced volatile blends. *Journal of Chemical Ecology*, 36, pp.1006-1016. [DOI]
- Van Noort, S. and Broad, G., 2024. *Wasps of the World: A Guide to Every Family* (Vol. 8). Princeton University Press.
- Virla, E.G., Moya-Raygoza, G. and Guglielmino, A., 2023. A review of the biology of the pincer wasps (Hymenoptera: Dryinidae). *Austral Entomology*, 62(3), pp.274-299. [DOI]
- Wäschke, N., Meiners, T. and Rostás, M., 2013. Foraging strategies of parasitoids in complex chemical environments. *Chemical Ecology of Insect Parasitoids*, pp.37-63.
- Webster, B. and Cardé, R.T., 2017. Use of habitat odour by host-seeking insects. *Biological Reviews*, 92(2), pp.1241-1249. [DOI]
- Xu, H., Desurmont, G., Degen, T., Zhou, G., Laplanche, D., Henryk, L. and Turlings, T.C., 2017. Combined use of herbivore-induced plant volatiles and sex pheromones for mate location in braconid parasitoids. *Plant, Cell & Environment*, 40(3), pp.330-339. [DOI]
- Yazdani, M., Feng, Y., Glatz, R. and Keller, M.A., 2015. Host stage preference of *Dolichogenidea tasmanica* (Cameron, 1912) (Hymenoptera: Braconidae), a parasitoid of *Epiphyas postvittana* (Walker, 1863) (Lepidoptera: Tortricidae). *Austral Entomology*, 54(3), pp.325-331. [DOI]
- Yi, S.C., Wu, Y.H., Yang, R.N., Li, D.Z., Abdelnabby, H. and Wang, M.Q., 2023. A highly expressed antennae odorant-binding protein involved in the recognition of herbivore-induced plant volatiles in *Dastarcus helophoroides*. *International Journal of Molecular Sciences*, 24(4), p.3464. [DOI]
- Zang, L.S., Wang, S., Zhang, F. and Desneux, N., 2021. Biological control with *Trichogramma* in China: History, present status, and perspectives. *Annual Review of Entomology*, 66, pp.463-484. [DOI]

# Sustainable Biomass Conversion: Impact of NaCl Pretreatment on Cabbage Waste

Sunder, Sangita Yadav and Jitender Pal†

Department of Environmental Sciences and Engineering, Guru Jambheshwar University of Science and Technology, Hisar-125001, Haryana, India

†Corresponding author: Jitender Pal; j\_pal2k1@yahoo.com

**Abbreviation:** Nat. Env. & Poll. Technol.

**Website:** [www.neptjournal.com](http://www.neptjournal.com)

*Received:* 06-08-2024

*Revised:* 23-09-2024

*Accepted:* 14-10-2024

## Key Words:

Cabbage waste  
Lignocellulosic biomass  
NaCl pretreatment  
Circular economy

## ABSTRACT

Vegetable waste, particularly cabbage waste (CW), is a valuable raw material for various applications, including bioenergy production, owing to its high lignocellulosic content. However, the potential of lignin in biomass conversion remains largely untapped. This study is significant as it aims to optimize the pretreatment of CW biomass using different chemical reagents and concentrations (sulphuric acid, acetic acid, sodium hydroxide, potassium hydroxide, and sodium chloride) at 12 and 24 h for 50, 75, and 100°C. In this study, a novel pretreatment approach was introduced with 2% NaCl at 50°C for 12 h for CW biomass. At this optimized condition, 2% NaCl led to 28% delignification for CW biomass. The study examined the impact of pretreatment efficacy on biomass characterization using SEM, XRD, and FTIR analytical techniques. Results showed that 2% NaCl pretreatment significantly improved digestibility, increased surface area and porosity, altered the crystallinity index, and confirmed delignification through shifts in peaks and intensity changes. Furthermore, reduced hemicellulose and reduced lignin were noted in comparison to untreated biomass. This reassures us of the effectiveness of the pretreatment method. This promising result underscores the feasibility, economics, sustainability, and environmental friendliness of this pretreatment method. The method not only offers a cost-effective solution but also aligns with the principles of sustainability and environmental protection, thereby reassuring the researchers about its potential for various industrial applications.

## INTRODUCTION

India is a country that grows more than 70 different kinds of vegetables. One of the most popular vegetables grown worldwide is cabbage including India, a cruciferous vegetable used as an herbal medicine and nutritional supplement (Šamec et al. 2017). People eat cabbage worldwide since it is a healthful vegetable renowned for its high nutritional value, delicious taste, and medicinal properties (Pradhan 2020). It provides essential nutrients and fiber. It is usually cooked like a green vegetable, consumed raw, and frequently turned into a pickle (Sarkar et al. 2021). Cabbage makes up around 6.5% of global vegetable production (Pradhan 2020). It is grown on 0.40 million hectares in India, accounting for 4% of the total vegetable area, and produces 9.04 million metric tonnes annually (Patra et al. 2024). Although cabbage meets quality criteria and is typically consumed by humans as food, over thirty percent of the cultivated cabbage is rejected as solid waste. CW comprised 50 million metric tonnes, or 8%, of all vegetable and fruit garbage in 2017 (Eom et al. 2024). CW is often collected from various sources and disposed of in landfills or dumpsites, leading to severe environmental impacts such as greenhouse gas emissions, groundwater pollution, malodor, and microbial contamination (Bamisaye et al. 2022). The dumping of food waste also affects the environment's health in ways such as acidification and eutrophication of local water bodies. These impacts underscore the urgent need for sustainable waste management solutions.

## Citation for the Paper:

Sunder, Yadav, S. and Pal, J., 2025. Sustainable biomass conversion: Impact of NaCl pretreatment on cabbage waste. *Nature Environment and Pollution Technology*, 24(2), p. B4254. <https://doi.org/10.46488/NEPT.2025.v24i02.B4254>

*Note: From year 2025, the journal uses Article ID instead of page numbers in citation of the published articles.*



**Copyright:** © 2025 by the authors

**Licensee:** Technoscience Publications

This article is an open access article distributed under the terms and conditions of the Creative Commons Attribution (CC BY) license (<https://creativecommons.org/licenses/by/4.0/>).

Crop waste biomass, including (CW), contains high concentrations of cellulose, hemicelluloses, and lignin, making them potential value-added products for lignocellulose biorefinery, as per research by Bamisaye et al. (2022). The stalks of cabbage have about 37% cellulose on a dry weight basis, making it relatively cellulose-rich (Pradhan 2020). The hydrolysis of cellulose in plant cells is hindered by lignin and hemicellulose, which bind to the cellulose microfibrils, making pretreatment crucial for enhancing efficiency by solubilizing these components (Dharmalingam et al. 2023). Pretreatment procedures are also crucial to converting lignocellulosic feedstocks into reducing sugars. Pretreatments with alkali, acid, organic solvent, and mechanical methods have all been shown to improve the release of structural carbohydrates from different types of lignocellulosic biomass (He et al. 2021). Plant materials undergo various pretreatment methods, including thermal and ultrasonic, to improve structural modifications, but thermal pretreatment can potentially cause bioactive compound degradation, while ultrasonic pretreatment disrupts cell walls (Pongmalai et al. 2015). As a result, the development of alkali treatment utilizing NaOH, CaO, NaCl, ammonia, urea, etc., was required to modify the biomass matrix (Bamisaye et al. 2022). Organic salts have certain qualities, such as low volatility, high stability, recyclability, non-toxic, and non-explosive (Xie et al. 2020).

This research analyses chemical pretreatment in converting lignocellulosic biomass, considering factors like research breakthroughs, technology development, application strengths and weaknesses, and potential economic and environmental impacts. Cellulose, lignin, and hemicellulose yields from acid, base, and salt pre-treatment processes were compared 1stly. Then, this study introduces a novel pretreatment method for CW biomass degradation with sodium chloride within 24 h. The method optimizes the pretreatment of cabbage residue based on temperature, time, and chemical reagent. Before and after pretreatment, the selected biomass samples were characterized by FTIR, XRD, and SEM for their physicochemical composition. This study offers the development of a cost-effective, environmentally friendly pretreatment method that contributes to the circular economy by using agro-waste as raw material while solving the waste management problem. The results offer valuable insights for designing pretreatment processes for agricultural waste.

## MATERIALS AND METHODS

### Sample Collection and Processing

Lignocellulose biomass (CW) was collected from the nearby village of Dhana in the district of Hisar. The biomass samples

were prepared by washing them with distilled water to remove dirt and surface impurities and then drying them in the sun. After that, biomass was chopped and ground into powdered form, and it was sieved using a 40–60 mesh sieve. All the samples were prepared in atmospheric conditions. For subsequent use, powdered CW was kept in hermetically sealed bags.

### Chemicals

The chemicals employed in this study are acetic acid, Sulfuric acid, Sodium hydroxide, Potassium hydroxide, sodium chloride, and ethanol in the pretreatment process. EDTA, sodium borate, sodium dodecyl sulfate, disodium phosphate, and 2-ethoxyethanol were used to analyze lignin, cellulose, and hemicellulose. All the chemicals used were analytical grade and procured by Merck (Sigma-Aldrich, Chemicals Pvt. Ltd., Bangalore, India). The experiments were conducted with deionized water.

### Pretreatment Optimisation Experiment Design

The purpose of statistically designing an experiment is to collect common relationships between various factors affecting the process of finding the most suitable conditions. An experimental design methodology must be economical for extracting the maximum amount of complex information, significantly reducing experimental time and saving material and cost. Four factors, namely, chemicals, chemical concentration, temperature, and time, were studied to optimize the process parameters for pretreatment, as shown in Table 1. The experimental scheme employed in this study is depicted in Fig. 1.

### Estimation of Lignocellulosic Biomass

The lignocellulosic composition of lignin, cellulose, and hemicellulose in biomass in powder form was investigated, and data were analyzed both before and after the biomass was pretreated. The lignocellulosic content, lignin, cellulose, and hemicelluloses in CW were investigated using a modified version of the Van Soest method.

Calculation for Lignocellulosic Biomass (dry weight percentage):

Hemicelluloses = neutral detergent fiber (NDF) - acid detergent fiber (ADF)

Cellulose = ADF-ash

Lignin = acid detergent lignin (ADL)

### Characterization of Biomass

The X-ray diffractometer (Smart Lab 3kW/Rigaku) was used to analyze the crystalline structure of lignocellulosic biomass,



Table 1: Experimental design for optimization of the process parameters for pretreatment.

Type of Biomass	Pretreatment Conditions			
	Chemical	Concentration [%]	Temperature [°C]	Time [h]
CW	Control	0	37	12
				24
	CH <sub>3</sub> COOH	2	37	12
				24
	H <sub>2</sub> SO <sub>4</sub>	2	37	12
				24
	KOH	2	37	12
				24
CW	NaOH	2	37	12
				24
	NaCl	2	37	12
				24
CW	Control	0	50	12
				12
	NaCl	2	50	12
				12
CW	NaCl	4	50	12
				12
	NaCl	6	50	12
				12
CW	Control	0	75	12
				12
	NaCl	2	75	12
				12
CW	NaCl	4%	75	12
				12
	NaCl	6%	75	12
				12
CW	Control	0	100	12
				12
	NaCl	2%	100	12
				12
CW	NaCl	4%	100	12
				12
CW	NaCl	6%	100	12
				12

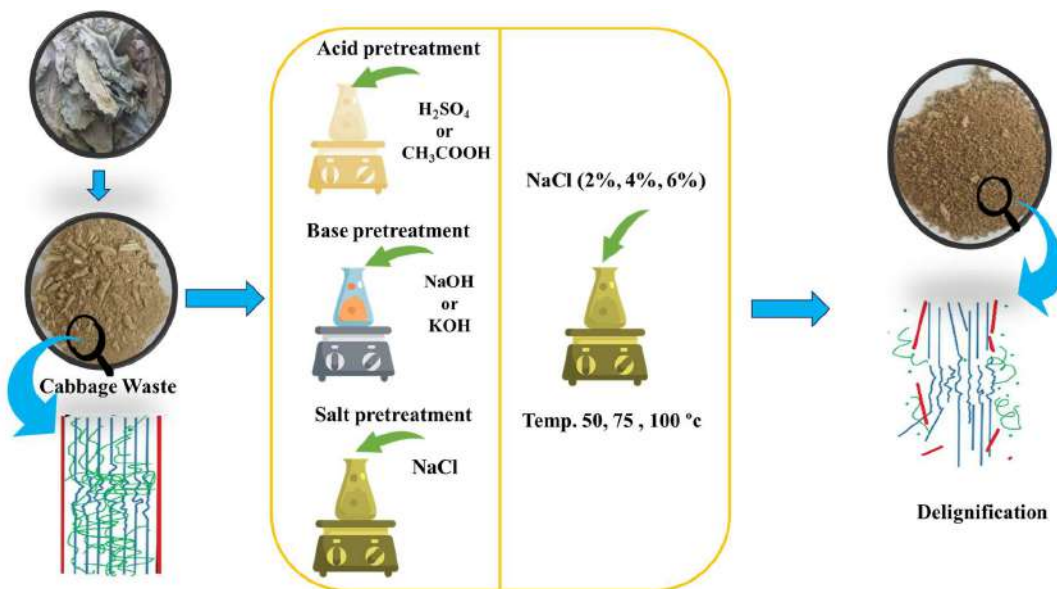


Fig. 1: Schematic illustration of experimental design for pretreatment of biomass.

examining its inherent crystalline nature across a  $2\theta$  scan range of  $3^\circ$  to  $60^\circ$  (Vydrina et al. 2023). The crystallinity index (CrI) was determined using the following equation;

$$\text{CrI (\%)} = \frac{A_c}{A_c + A_a} \times 100 \quad \dots(1)$$

Where CrI represents the relative degree of crystallinity (%),  $A_c$  is the under-crystalline peak, and  $A_a$  is the area under the amorphous peak at  $2\theta$ . FTIR (PerkinElmer, USA) analysis was performed in a range of 400 to  $4000 \text{ cm}^{-1}$  to analyze the functional groups of biomasses before and after pretreatment. The morphology of lignocellulosic biomass was analyzed using scanning electron microscopy (Leica EM SCD050) before and after pretreatment.

## RESULTS AND DISCUSSION

This study investigates the impact of different pretreatment technologies on CW biomass. NaCl pretreatment is best suited for the delignification of the CW, which was further proved using characterization like FTIR, XRD, and SEM.

### Optimization Study

**Optimization of chemical reagents and time:** The effect of five different chemicals, acetic acid, Sulfuric acid, Sodium hydroxide, Potassium hydroxide, and sodium chloride, and time on the lignin, cellulose, and hemicellulose was studied for CW at  $37^\circ\text{C}$  while varying time (12 and 24 h), as presented in Table 1. The lignin in the supernatant was measured as an indicator of pretreatment efficiency, as depicted in Fig. 2. The pretreatment process leads to the disruption of the fiber, which is demonstrated by a drop in the biomass's lignin concentration as well as a reduction in the biomass matrix's degree of polymerization and crystallinity (Bamisaye et al. 2022). These were the preliminary experiments conducted to

determine a suitable time and chemical for the pretreatment process.

The study reveals that the pretreatment of CW biomass leads to delignification, a reduction in lignin, and an increase in cellulose composition. This is attributed to the observed delignification of the biomass samples. Fig. 2 shows that when NaCl pretreatment is compared with the control and other chemical reagents, it is observed to have the most delignification. Yiga et al. (2021) indicated that the biomass samples' observed delignification, a decrease in their lignin and extractive contents, and the concomitant rise in their cellulose composition are caused by the alkali pretreatment of cabbage waste. Fig. 2 shows that 12 h and 24 h of pretreatment do not differ much; that is why 12 h is selected as an optimized condition to make the process economical, sustainable, and environmentally friendly. The findings show that pretreatment with NaCl for 12 h was selected as the optimized condition for CW biomass.

**Optimization of salt concentration and temperature:** After optimizing chemical reagents and time, this study also optimizes chemical concentration and temperature. As discussed in the above section 3.1.1, NaCl is the optimized chemical at 12 h. So, the effect of the different concentrations of NaCl (2, 4, and 6% w/w) at different temperatures on the lignin, cellulose, and hemicellulose was studied for CW at 12 h, as presented in Table 1. The lignin in the supernatant was measured as an indicator of pretreatment efficiency. From Fig. 3, it can be concluded that lignin degradation also increased with an increase in temperature from 50 to  $100^\circ\text{C}$ . This is because a higher reaction temperature enhances hemicellulose solubilization and modifies lignin in biomass. It was found that  $50^\circ\text{C}$  is best suited for the pretreatment experiments to make the process more economical and environmentally friendly. Especially

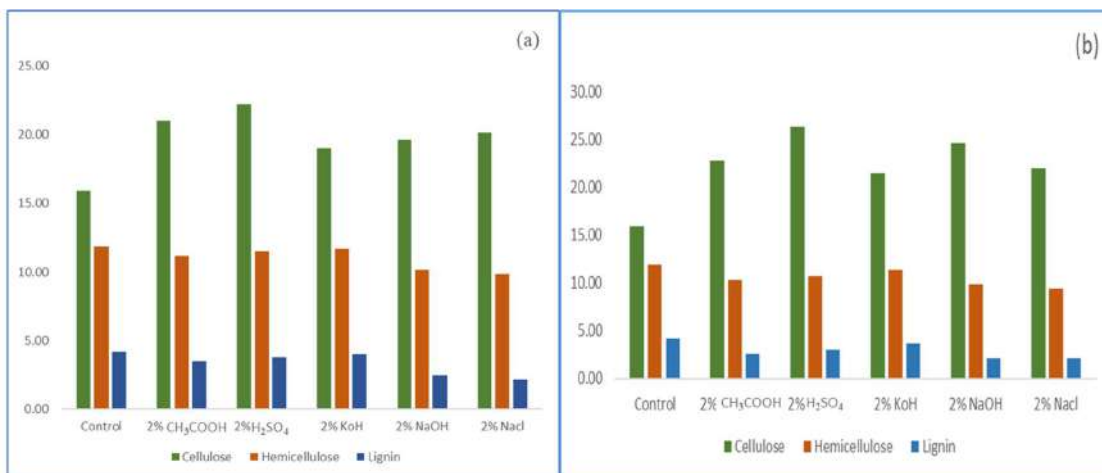


Fig. 2: Optimization study of different chemicals for CW biomass at 12 h (a) and 24 h (b).

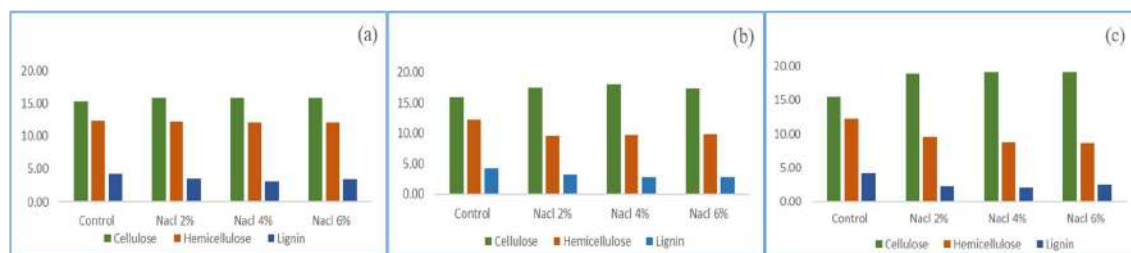


Fig. 3: Optimization study of NaCl concentration for CW biomass at 50°C (a), 75°C (b) and 100°C (c).

at higher temperatures, specifically in hydrothermal pretreatment, the lignin recondensation occurred in the solid matrix, and biomass browning at higher temperatures was observed in this study. The browning effect can be attributed to carbohydrate degradation products, caramelization of polysaccharides, or the recondensation of pseudo-lignin aromatic polycondensates (Batista et al. 2019). From Fig. 3, it can also be observed that with an increase in NaCl conc, there is a decrease in lignin degradation, and 2% NaCl shows maximum lignin degradation when compared to control and 4 and 6% NaCl conc. Dharmalingam et al. (2023) also showed that the reducing sugar yield decreased for samples pretreated with acetic acid when the temperature increased from 100 to 140°C and the acid concentration increased from 2 to 10% w/v. Thus, 2% NaCl at 50°C is an optimized condition for further pretreatment experiments.

### Effect of Pretreatment on the Lignocellulosic Biomass Characteristics

The simplest method of overcoming biomass recalcitrance is to modify the structural properties through an appropriate pretreatment process. Milling biomass samples could increase specific surface area and decrease cellulose crystallinity, but these changes were not significant enough to have a significant pretreatment effect. Therefore, a more effective method should be applied to alter both structural and chemical properties significantly (Lee & Park 2020). Table 2 shows the CW lignocellulosic biomass characteristics, determining weight percentage composition for raw and

Table 2: Characteristics of NaCl treated biomass at optimized conditions.

Biomass structural characteristics	Agro waste (Cabbage)		
	Raw [%]	Pretreated [%]	Change [%]
Lignin	4.33	3.10	28
Cellulose	15.34	15.95	2.9
Hemicellulose	12.39	12.05	2.7

pretreated biomass with 2% NaCl at 50°C for 12 h using a modified Van Soest approach. The composition of lignocellulosic biomass varies globally due to factors like soil type, nutrient availability, and crop harvesting timing. NaCl pretreatment decreases lignin concentration with the increase in the availability of cellulose and hemicellulose. Meng et al. (2020) also reported the delignification in biomass of *Populus trichocarpa deltoidea* through organosolv pretreatment. Saratale et al. (2020) suggested the alkaline pretreatment as a potential treatment for wheat waste biomass. Table 3 presents the comparison of previous studies with the present study to show the crucial benefits of this study,

### Characterization of Wheat and Rice Straw before and after Pretreatment

The study assessed CW's surface morphology, functional groups, and crystallinity before and after NaCl pretreatment at optimum conditions using FTIR, XRD, and SEM analytical techniques. The results were used to understand the lower and higher saccharification yields after pretreatment. The efficiency of saccharification performance was linked

Table 3: Pretreatment efficiency comparison with previous studies.

Pretreatment methods	Reagent Used	Pretreatment conditions	Change [%]			Reference
			Lignin	Cellulose	Hemicellulose	
Acidic	H <sub>2</sub> SO <sub>4</sub>	2%, 4%	10.6	22.8	21.8	Song et al. 2014
Acidic	H <sub>2</sub> SO <sub>4</sub>	1.1%	41.36	31.2	47.5	Christopher et al. 2023
Alkali	NaOH	4%	10.66	28.3	17.36	Song et al. 2014
Alkali	NaOH	8%	62	--	81	Mansour et al. 2024
Salt Solution	NaCl CW biomass	2%, 12 hr, 50°C	28	2.9	2.7	Present Study

to the substrate's structural characteristics, with biomass pretreatment causing structural changes like the removal of lignin and modification of cellulose crystallinity (Saratale et al. 2020, Selvakumar et al. 2022).

### Surface Morphological Analysis

Scanning Microscope Electronic Microscopy (SEM) examined the morphology of the untreated and pretreated biomass samples, as depicted in Fig. 4. A smooth, fibrillary, stiff, and dense structure was seen in the SEM analysis of the raw biomass (Fig. 4a), which may have been caused by the lignin and hemicellulose in the tightly wrapped cellulose. However, after NaCl pretreatment, the pretreated biomass surfaces were disordered, rougher, conglomerated, and agglomerated. SEM micrographs showed increased porosity and surface area. However, pretreatment with NaCl increased biomass fragmentation and cellulose fiber surface roughness, suggesting that NaCl improved the depolymerization effect on CW biomass, as presented (Fig. 4 b, c, d, e, f). Pongmalai et al. (2015) showed that ultrasonic-assisted pretreatment of CW biomass also showed space, cell rupture, and cell structure collapse. Blanched cabbage showed a wilt appearance and flattened surface, while pretreated samples with acetic acid showed deformation, with higher acid concentrations causing more deformation (Chiewchan et al. 2010). Eom et al. (2024) showed that the untreated mixed cabbage residue (MCR) had a rigid, smooth structure, limiting enzyme access, while the pretreated MCR had a rough, conglomerated, and agglomerated surface morphology. This may be due to matrix disruption brought on by the dissolution of lignin and hemicellulose (Ziaei-Rad et al. 2021). Additionally, the structural modification enhanced

the porosity of cellulose, increasing its hydrolyzability (Eom et al. 2019).

Fig. 4 shows that 2% and 4% NaCl pretreatment do not differ much; that is why 2% NaCl is taken as Optimised conditions to make the process economical, sustainable, and environmentally friendly. The figure also depicts the images taken at different magnifications for optimized 2% NaCl for CW biomass, showing the profound changes in biomass surface compared to raw biomasses. Overall, incorporating salt solutions facilitated the breakdown of surface structure and enhanced biomass depolymerization.

### Fourier-Transform Infrared Spectroscopy (FTIR) Analysis

FTIR spectroscopy was utilized to analyze the functional groups of raw and pretreated biomass samples, specifically CW, with NaCl pretreatment. It revealed conformational variations of functional groups. FTIR is particularly useful for qualitative analysis of cellulose, hemicellulose, and lignin in lignocellulosic biomass, focusing on structural analysis. The FTIR spectra ranged from 4000-500  $\text{cm}^{-1}$ . FTIR analysis revealed significant chemical changes in CW biomass samples, with an increase or decrease in cellulose, hemicellulose, and lignin peaks in the pretreated samples compared to raw CW biomass, as depicted in Fig. 5 (a) and analysis of FTIR spectra are presented in Table 4. The FT-IR spectra indicate the presence of alkali lignin, which range from 1850 to 500  $\text{cm}^{-1}$  (Wang et al. 2016). Changes in C=O bonds following pretreatment (Xie et al. 2020) might also be connected to hemicellulose's partial elimination. The intermolecular decomposition of hydrogen bonding due to

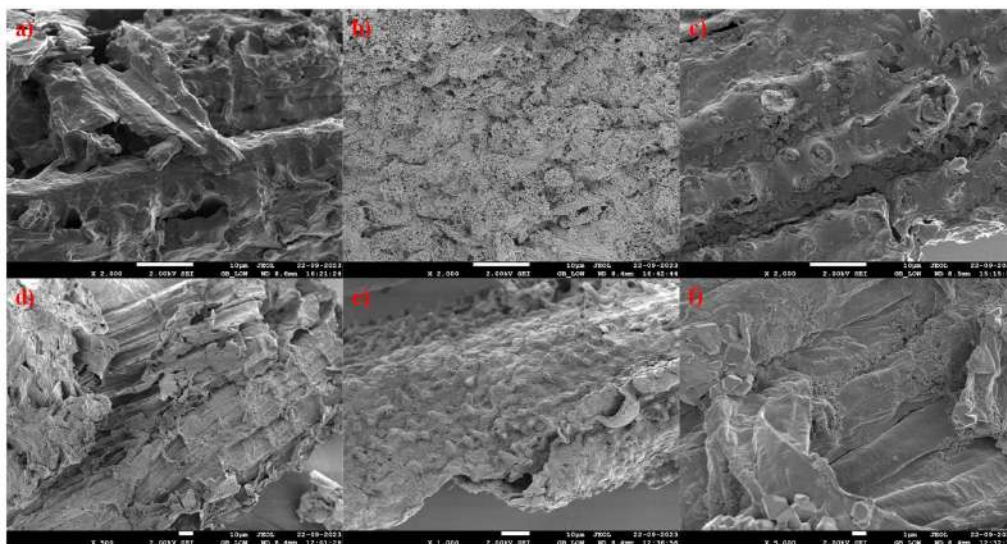


Fig. 4: SEM images of cabbage waste biomass; a) Raw, b) 2% NaCl, c) 4%NaCl, (d-f) Optimized 2% NaCl at different magnifications.



Table 4: FTIR analysis of CW biomass.

Raw CW biomass	2% pretreated CW biomass	4% pretreated CW biomass	Range [ $\text{cm}^{-1}$ ]	Functional group	Characteristic and Reference
3412.3	3411	3417	3570-3200	O-H	Alcohol/water molecules
2917.9	2922.3	2917.9	3000-2840	C-H	Alkane
2855	2841.7	2855	3000-2800	N-H	Amine
1735.8	1744	1747.5	1750-1735	C=O	Esters
1631.3	1611.1	1627.6	1650-1566	C=C	Cyclo alkene
1382.08	1377.6	1382.08	1390-1380	C-H	Aldehyde
1060.44	1104.4	1096.2	1250-1020	C-N	Amine

the change in peak in the  $3200\text{--}3570\text{ cm}^{-1}$  range is associated with hemicellulose and cellulose (Eom et al. 2024). The change in all the peaks presented in Table 4 before and after the pretreatment could be attributed to the delignification in the biomass surface, increasing the particle size and porosity. From the FTIR figure, it can also be concluded that 2% NaCl pretreatment is more effective as the change in peak intensity and shifting of the peaks is more profound for CW.

### X-Ray Diffraction (XRD) Analysis

X-ray diffractograms (XRD) are crucial for analyzing cellulosic fraction morphology and conformational changes. XRD is also an essential analytical technique for determining the materials' structure, i.e., crystalline or amorphous. Alkali delignification treatments can affect the crystalline structure of cellulose. The XRD spectra of wheat and rice straw before and after pretreatment are presented in Fig. 5 (b). The XRD pattern showed distinct peaks at  $2\theta$  are 20.74, 29.54, 31.74, and 45.34 for raw CW biomass, 20.76, 29.54, 31.72, and 45.44 for 2% NaCl pretreatment, and 20.28, 27.46, 31.84 and 45.56 for 4% NaCl pretreatment of CW biomass. Compared

with the control, the positions of these peaks of different pretreated samples had no noticeable change, while their intensities varied greatly. This phenomenon indicated that the crystal form of cellulose was not affected by pretreatment, while cellulose structures were changed to different degrees after pretreatments (Zhang et al. 2020).

The untreated and pretreated CW biomass was characterized using XRD to calculate the cellulose crystallinity index (CrI). The CrI value changed from 19.37% for raw to 15.14% for 2% NaCl pretreatment and 24% for 4% NaCl pretreatment for the CW biomass. According to these results, the amorphous areas of the CW biomass, such as lignin, hemicellulose, and a small portion of cellulose, were removed during pretreatment (Eom et al. 2024). These results are consistent with those of earlier research. Eom et al. (2024) showed that the pretreated MCR had a higher CrI (44.4% vs. 38.03%) than untreated MCR. A 3-hour ionic liquid (IL) pretreatment of wheat straw increased crystallinity by about 3% (Ziaei-Rad et al. 2021). Quinoa straw treated with IL has more crystallinity than untreated biomass (40.0% vs. 33.3%), according to Xie et al. (2020).

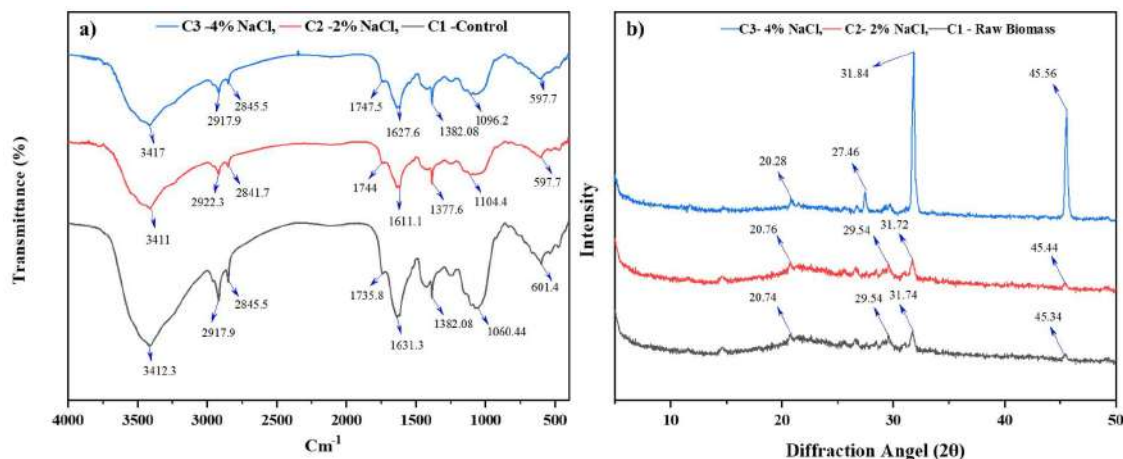


Fig. 5: Characterization of cabbage waste biomass before and after pretreatment a) FTIR spectra b) XRD spectra.

## CONCLUSION

Mixed vegetable and food wastes left from consumption and processing were important uncontrolled sources of greenhouse gas emissions. The application of vegetable waste is ineffective due to the recalcitrant structure of lignocellulose. However, this biomass must be pretreated to break down the lignin structure and interrupt the cellulose crystalline makeup. The CW biomass was obtained locally, dried, and pretreated using acid, base, and salt-based chemical processes, with salt being the most effective for delignification at 12 h and 50°C temperature. The results of the FTIR and composition analysis of the biomass indicated that hemicellulose and lignin were extracted from the biomass by pretreatment with various chemical reagents. NaCl pretreatment was observed to be more effective in removing lignin than other chemical reagents. Compared to untreated CW biomass, the pretreated biomass showed a greater cellulose conversion. The SEM picture, XRD pattern, and FT-IR spectra of the CW biomass after pretreatment revealed a noteworthy impact of the NaCl pretreatment, as pretreated biomass showed a significant structural and morphological difference from the raw biomass. This study provides valuable insights into the effectiveness of NaCl pretreatment and offers a promising avenue for sustainable biomass applications, inspiring further research and development in the field.

## REFERENCES

- Bamisaye, A., Ige, A.R., Adegoke, A.I., Idowu, M.A. and Elinge, C.M., 2022. Evaluation and characterization of the combustion properties of alkaline pretreated bio-solid fuel derived from cabbage waste. *Biomass Conversion and Biorefinery*, pp.1–11. DOI
- Batista, G., Souza, R.B., Pratto, B., dos Santos-Rocha, M.S. and Cruz, A.J., 2019. Effect of severity factor on the hydrothermal pretreatment of sugarcane straw. *Bioresource Technology*, 275, pp.321–327. DOI
- Chiewchan, N., Prapraipetch, C. and Devahastin, S., 2010. Effect of pretreatment on surface topographical features of vegetables during drying. *Journal of Food Engineering*, 101(1), pp.41–48. DOI
- Dharmalingam, B., Tantayotai, P., Panakkal, E.J., Cheenkachorn, K., Kirdponpattara, S., Gundupalli, M.P. and Sririyanun, M., 2023. Organic acid pretreatments and optimization techniques for mixed vegetable waste biomass conversion into biofuel production. *BioEnergy Research*, 16(3), pp.1667–1682. DOI
- Eom, T., Chaiprapat, S. and Charnnok, B., 2019. Enhanced enzymatic hydrolysis and methane production from rubber wood waste using steam explosion. *Journal of Environmental Management*, 235, pp.231–239. DOI
- Eom, T., Isanapong, J., Kumnorkaew, P., Sririyanun, M. and Pornwongthong, P., 2024. 1-ethyl-3-methylimidazolium acetate pretreatment for maximizing reducing sugar recovery from mixed cabbage residue. *Environmental Science and Pollution Research*, 31(10), pp.15491–15502. DOI
- He, F., Chen, J., Gong, Z., Xu, Q., Yue, W. and Xie, H., 2021. Dissolution pretreatment of cellulose by using levulinic acid-based protic ionic liquids towards enhanced enzymatic hydrolysis. *Carbohydrate Polymers*, 269, p.118271. DOI
- Lee, J. and Park, K.Y., 2020. Impact of hydrothermal pretreatment on anaerobic digestion efficiency for lignocellulosic biomass: Influence of pretreatment temperature on the formation of biomass-degrading byproducts. *Chemosphere*, 256, p.127116. DOI
- Mansour, M., Ince, O., Uzun, O., Ozbayram, E.G., Miraloglu, H.I. and Ince, B., 2024. Enhanced anaerobic mono-digestion and co-digestion of crop residues by NaOH alkali pre-treatment: digestion performance and microbial community dynamics. *Waste and Biomass Valorization*, 15(5), pp.3003–3015. DOI
- Meng, X., Bhagia, S., Wang, Y., Zhou, Y., Pu, Y., Dunlap, J.R. and Yoo, C.G., 2020. Effects of the advanced organosolv pretreatment strategies on structural properties of woody biomass. *Industrial Crops and Products*, 146, p.112144.
- Patra, S.K., Poddar, R., Panda, R., Sarkar, A., Gaber, A. and Hossain, A., 2024. Response of cabbage (*Brassica oleracea* var. capitata L.) to different frequencies of irrigation and levels of soil fertilization in a non-saline coastal Typic Endoaquept. *Journal of Coastal Conservation*, 28(1), pp.6.
- Pongmalai, P., Devahastin, S., Chiewchan, N. and Soponronnarit, S., 2015. Enhancement of microwave-assisted extraction of bioactive compounds from cabbage outer leaves via the application of ultrasonic pretreatment. *Separation and Purification Technology*, 144, pp.37–45.
- Pradhan, S., 2020. Optimization of process and properties of biochar from cabbage waste by response surface methodology. *Biomass Conversion and Biorefinery*, 1, pp.1–13.
- Šamec, D., Pavlović, I. and Salopek-Sondi, B., 2017. White cabbage (*Brassica oleracea* var. capitata f. alba): Botanical, phytochemical and pharmacological overview. *Phytochemistry Reviews*, 16, pp.117–135.
- Saratale, G.D., Saratale, R.G., Varjani, S., Cho, S.K., Ghodake, G.S., Kadam, A. and Shin, H.S., 2020. Development of ultrasound-aided chemical pretreatment methods to enrich saccharification of wheat waste biomass for polyhydroxybutyrate production and its characterization. *Industrial Crops and Products*, 150, pp.112425.
- Sarkar, A., Rahman, S., Roy, M., Alam, M., Hossain, M.A. and Ahmed, T., 2021. Impact of blanching pretreatment on physicochemical properties and drying characteristics of cabbage (*Brassica oleracea*). *Food Research*, 5(2), pp.393–400.
- Selvakumar, P., Adane, A.A., Zelalem, T., Hunegnaw, B.M., Karthik, V., Kavitha, S. and Kim, W., 2022. Optimization of binary acids pretreatment of corncob biomass for enhanced recovery of cellulose to produce bioethanol. *Fuel*, 321, pp.124060.
- Vydrina, I., Malkov, A., Vashukova, K., Tyshkunova, I., Mayer, L., Faleva, A. and Chukhchin, D., 2023. A new method for determination of lignocellulose crystallinity from XRD data using NMR calibration. *Carbohydrate Polymer Technologies and Applications*, 5, pp.100305.
- Wang, M., Zhou, D., Wang, Y., Wei, S., Yang, W., Kuang, M. and Du, S.K., 2016. Bioethanol production from cotton stalk: A comparative study of various pretreatments. *Fuel*, 184, pp.527–532.
- Xie, W., Ren, Y., Jiang, F., Liang, J. and Du, S.K., 2020. Pretreatment of quinoa straw with 1-butyl-3-methylimidazolium chloride and physicochemical characterization of biomass. *Renewable Energy*, 146, pp.1364–1371.
- Yiga, V.A., Lubwama, M. and Olupot, P.W., 2021. Effect of alkaline surface modification and carbonization on biochemical properties of rice and coffee husks for use in briquettes and fiber-reinforced plastics. *Journal of Natural Fibers*, 18(4), pp.620–629.
- Zhang, T., Jiang, D., Zhang, H., Lee, D.J., Zhang, Z., Zhang, Q. and Xia, C., 2020. Effects of different pretreatment methods on the structural characteristics, enzymatic saccharification, and photo-fermentative bio-hydrogen production performance of corn straw. *Bioresource Technology*, 304, pp.122999.
- Ziaei-Rad, Z., Fooladi, J., Pazouki, M. and Gummadi, S.N., 2021. Lignocellulosic biomass pre-treatment using low-cost ionic liquid for bioethanol production: An economically viable method for wheat straw fractionation. *Biomass and Bioenergy*, 151, pp.106140.

# Expository Assessment of Air Quality Scenario with Sentinel-5 Precursor TROPOMI Explorer Sensor

Abhay Yadav, Divya Srivastava<sup>†</sup> and Vivek Mathur

Department of Civil Engineering, Amity University, Lucknow, Uttar Pradesh, India

<sup>†</sup>Corresponding author: Divya Srivastava; dsrivastava4@lko.amity.edu

**Abbreviation:** Nat. Env. & Poll. Technol.  
**Website:** www.neptjournal.com

*Received:* 15-06-2024

*Revised:* 15-08-2024

*Accepted:* 24-08-2024

## Key Words:

Air quality  
 Sentinel-5 precursor  
 Tropomi explorer  
 Geographic information systems

## ABSTRACT

Air pollution is the atmospheric state in which the concentration of specific elements has adverse impacts on human health as well as the environment, including global warming, transportation disruptions, acid rain, and ozone layer depletion. Nowadays, a large portion of the world's population lives in urban areas, where population growth and the increasing number of vehicles have significantly worsened air quality. Clean air is essential for the health and well-being of any region's environment and its inhabitants. Henceforth, the primary focus of this research endeavor is to meticulously scrutinize the levels of key air pollutants, notably nitrogen dioxide (NO<sub>2</sub>) and sulfur dioxide (SO<sub>2</sub>), leveraging satellite remote sensing data obtained from TROPOMI EXPLORER across a network of monitoring stations dispersed throughout Lucknow City. Additionally, it aims to meticulously dissect ground-based air quality monitoring data to validate and amalgamate the observations derived from satellite technology. Furthermore, it analyzes the distribution of concentrations of primary air pollutants, encompassing NO<sub>2</sub>, SO<sub>2</sub>, and PM<sub>10</sub>, within Lucknow City, juxtaposing them against the stringent benchmarks stipulated by the World Health Organization (WHO) for air quality standards. Moreover, it endeavors to ascertain the deleterious health ramifications of air pollution by correlating air quality metrics with health outcomes among the denizens of Lucknow City through a meticulously crafted questionnaire survey. The scrutiny of satellite imagery unveiled a conspicuous escalation in the concentration of air pollution parameters vis-à-vis the WHO's prescribed thresholds, portending consequential adverse ramifications for both the environment and human health.

## Citation of the Paper:

Yadav, A., Srivastava, D. and Mathur, V., 2025. Expository assessment of air quality scenario with Sentinel-5 Precursor Tropomi Explorer sensor. *Nature Environment and Pollution Technology*, 24(2), p. B4232. <https://doi.org/10.46488/NEPT.2025.v24i02.B4232>

*Note: From year 2025, the journal uses Article ID instead of page numbers in citation of the published articles.*

## INTRODUCTION

In Indian megacities, Lucknow is one of the most polluted with respect to particulate pollution. Due to this, air pollution has emerged as a serious environmental challenge, especially in urban areas. According to the World Air Quality Report 2019, Lucknow ranks 11th for poor air quality among the top 15 most polluted cities worldwide (IQ Air 2019). The major sources of air pollution in Lucknow include urbanization, industrialization, vehicular exhaust, construction work, and burning activities (Bharti et al. 2017, Kumar & Dwivedi 2021). As a result of the increasing pace of anthropogenic activities, Lucknow has become one of the most polluted cities in the world, especially in the winter season.

Air pollution means the contamination of air. In the Air (Prevention and Control of Pollution) Act, 1981, section 2(a), air pollution is characterized as "any solid, liquid, or gaseous substance (including noise) present in the atmosphere in such concentration as may be or tend to be injurious to human beings or other living creatures or plants or property or the environment" (Government of India 1981). Over the past two decades, there has been a significant increase in urbanization and industrialization in many Indian cities. This urbanization has had both positive and negative effects on air quality in cities worldwide. Various chemicals, whether from natural or man-made sources, continuously enter the atmosphere and interact



**Copyright:** © 2025 by the authors  
**Licensee:** Technoscience Publications  
 This article is an open access article distributed under the terms and conditions of the Creative Commons Attribution (CC BY) license (<https://creativecommons.org/licenses/by/4.0/>).

with the environment, causing diseases, pollution, and environmental degradation; these substances are known as pollutants. Both developed and developing countries are striving to balance climate issues with economic development. There is a strong correlation between population growth and environmental contamination, with environmental damage escalating as the population increases (Barck et al. 2005). Poor environmental conditions adversely affect the biological sections of ecosystems.

In Asia, air pollution has worsened with the progression of industrialization and urbanization. In Lucknow, studies on air pollution have primarily focused on atmospheric pollution (Barman et al. 2010, Pandey et al. 2012, 2013, Kim 1992). Geographical Information System (GIS) technology is extensively used to assess, inventory, identify, model, and manage the natural environment. Air pollution, a major environmental issue, is concentrated in urban areas. Burning fuel releases particulate matter and diverse types of unburned or waste oil into the environment (Khan et al. 2010).

Analyzing air pollution, particularly regarding Respirable Suspended Particulate Matter (RSPM), is a significant challenge. According to a WHO report, particulate matter (PM<sub>10</sub>) affects more people than any other air pollutant. Even low levels of PM<sub>10</sub> have been associated with adverse health effects (Agarwal 2012). As modern research continues to uncover the health impacts of tiny particles and pollutants, the issue of particulate matter and gaseous emissions in the atmosphere is gaining increased attention.

Lucknow, the most populous city, and capital of Uttar Pradesh, is the second-largest city in northern and central India. It is one of India's fastest-growing metropolitan areas, rapidly emerging as a hub for manufacturing, business, and retail. Air pollution contributes to many outstanding environmental issues and human health risks, triggering a substantial mortality rate affecting developed and developing countries worldwide (Sinha et al. 2013, Saber et al. 2020, Biswas et al. 2020, Filonchyk 2022). Air pollution includes particulate matter (PM<sub>2.5</sub> and PM<sub>10</sub>), nitrogen oxide and dioxide (NO, NO<sub>2</sub>), sulfur dioxide (SO<sub>2</sub>), carbon monoxide (CO), and ozone (O<sub>3</sub>). The WHO defines air pollution as the contamination of indoor and/or outdoor environments through chemical, physical, or biological factors that cause changes in the normal features of the ambient air. Additionally, the World Health Organization (WHO) announced that air pollution kills millions worldwide every year. Industrial areas worldwide are considered the main contributors to air pollution and are responsible for deteriorating human health (Salman et al. 2021).

The Air Quality Index (AQI) of Lucknow is adopted through the Central Pollution Control Board to provide

information on the levels of air pollutants. Table 1 shows air quality guidelines established by the WHO and CPCB.

Several authors utilized in-situ ground measurements and TROPOMI/Sentinel-5P high spatial-resolution images to study and monitor the nitrogen dioxide (NO<sub>2</sub>) levels in the ambient air, including Zhao et al. (2020), Shikwambana et al. (2020), Lalongo et al. (2020), Vîrghileanu et al. (2020), and Al-Alola et al. (2022). These studies suggested using TROPOMI/Sentinel-5P images only to monitor the NO<sub>2</sub> concentration. Lalongo et al. (2020) suggested using TROPOMI images with NO<sub>2</sub> observations collected from ground-based measurements.

Theys et al. (2021) examined the SO<sub>2</sub> emissions using Sentinel-5P data obtained during 2019. The authors found biases in the SO<sub>2</sub> emissions using TROPOMI data due to surface-related effects such as elevated terrain and albedo. Opio et al. (2021) utilized TROPOMI to monitor the sulfur dioxide (SO<sub>2</sub>) over East Africa. The results of the analysis revealed an increasing trend in SO<sub>2</sub>. Anil and Alagha (2021) studied CO, SO<sub>2</sub>, NO<sub>2</sub>, O<sub>3</sub>, and PM<sub>10</sub> in the Eastern Province using data collected from the General Authority of Meteorology and Environment Protection during the COVID-19 lockdown. The study encompassed monitoring stations in Jubail, Qatif, Dammam, and Al Ahsa. It was observed that the concentrations of NO<sub>2</sub>, SO<sub>2</sub>, CO, and PM<sub>10</sub> decreased at certain stations to levels below the WHO standards. Conversely, O<sub>3</sub> concentrations increased at most of the stations. Farahat (2016) examined dust events, SO<sub>2</sub>, and NO<sub>2</sub> in the Arabian Peninsula, including the United Arab Emirates, Qatar, Kuwait, Oman, Bahrain, and Saudi Arabia. The study in Saudi Arabia concentrated on the cities of Taif, Jeddah, and Mecca. The findings indicated that NO<sub>2</sub> tropospheric column density was high and SO<sub>2</sub> concentrations exceeded the WHO guideline mean values in these major cities.

The project aims to analyze the levels of key air pollutants, such as nitrogen dioxide (NO<sub>2</sub>) and sulfur dioxide (SO<sub>2</sub>), utilizing satellite remote sensing data (TROPOMI Explorer) collected from various stations across Lucknow City. Additionally, it involves the examination of ground-based air quality monitoring data to validate and integrate the observations obtained from satellites. The project will compare key air pollutant levels (NO<sub>2</sub>, SO<sub>2</sub>, and PM<sub>10</sub>)

Table 1: Mean concentration standards and AQI of primary air pollutants.

Pollutants	Average Time period	WHO [ $\mu\text{g.m}^{-3}$ ] <sup>a</sup>	CPCB [ $\mu\text{g.m}^{-3}$ ] <sup>b</sup>
PM <sub>10</sub>	24- h	45	60
NO <sub>2</sub>	24- h	25	40
SO <sub>2</sub>	24- h	40	50



obtained from CAAQM stations of CPCB and UPPCB with WHO standards. Furthermore, the project intends to evaluate the health impacts of air pollution by conducting surveys among residents of Lucknow City and correlating air quality indicators with health outcomes.

## MATERIALS AND METHODS

### Study Site Description

Lucknow, the capital of the state of Uttar Pradesh, India, is located in northern India between 26°85' N latitude and longitude 80°95' E. Lucknow lies at the upper Gangetic plains of India, 123m (404 ft) above sea level (Sen 2017); experiences a great variation in temp (45°C in summer and 5°C in winter) and average rainfall is 100 cm (Singh et al. 2017). Fig. 1 shows the study area.

### Air Quality Data

For this study, air quality data were obtained from Continuous Ambient Air Quality Monitoring (CAAQM) stations operated by the Central Pollution Control Board (CPCB) and the Uttar Pradesh Pollution Control Board (UPPCB). In Lucknow, six monitoring stations located in various areas (industrial, commercial, and residential) continuously monitor air pollutants daily (Table 2).

### Satellite Data

Multiple spatial and temporal data types and sources were collected for monitoring the air pollutant parameter as shown in Table 3.

Table 2: List of Monitoring Stations.

Station Name	Monitoring Station	Latitude	Longitude
B R Ambedkar University	MS 1	26.8632	80.90845
Gomti Nagar	MS 2	26.850017	80.9833163
Kendriya Vidyalaya	MS 3	26.9004194	80.9484125
Kukrail Picnic Spot-1	MS 4	26.8632	80.90845
Lalbagh	MS 5	26.165998	80.970673
Talkatora District Industries Center	MS 6	26.840503	80.8792761

Access to Sentinel-5P (Tropomi Explorer) satellite data has been obtained. The application has been launched and ensured its latest data is available. Relevant atmospheric composition data, including measurements of pollutants like nitrogen dioxide (NO<sub>2</sub>) and sulfur dioxide (SO<sub>2</sub>), is being acquired. Preprocessing is being performed to correct for sensor artifacts and atmospheric effects.

Integration of the satellite data with ground-based measurements from monitoring stations has been done for validation and calibration purposes. Then, different maps showing concentration levels of different pollutants across various regions have been generated, and air quality data obtained from CAAQM station operated by CPCB and UPPCB is compared with WHO standard.

### Questionnaire

The questionnaire used in this study aimed to assess residents'

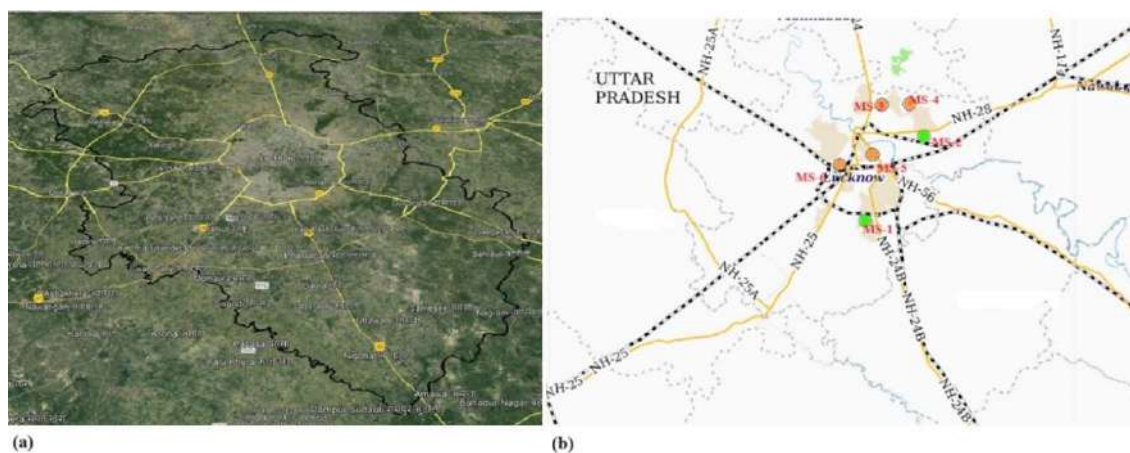


Fig. 1: Study area.

Table 3: Multiple spatial and temporal data types.

Platform/instrument	Sensor	Bands	Image format	Spatial resolution	Units	Extracted data
Sentinel-5P	Tropomi	7	HDF5	5.5 × 3.5 km	MoL.m <sup>-2</sup>	NO <sub>2</sub> , CO <sub>2</sub> , PM <sub>10</sub>

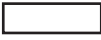



opinions on air pollution levels and their respiratory health status. Created with Google Forms and distributed via email to 200 residents, the questionnaire had two main sections. The first section focused on residents' demographics, their understanding and experiences regarding air quality, and their views on existing air pollution laws. The second section addressed their respiratory health conditions, awareness of pollution, and its impact on both the built environment and their health.

## RESULTS AND DISCUSSION

### Comparison of Key Air Pollutant Level ( $\text{NO}_2$ , $\text{SO}_2$ ) Obtained from Satellite Data with Ground Level Monitoring

Analysis of temporal trends in air pollution levels over one year from January 1 to December 31, 2023, has been made, observing fluctuations in pollutant concentrations across

Table 4: Four official seasons designated by the Indian Meteorological Department (IMD).

Colors Representation	Season
	Winter
	Summer or pre-monsoon
	Monsoon or rainy
	Post-monsoon

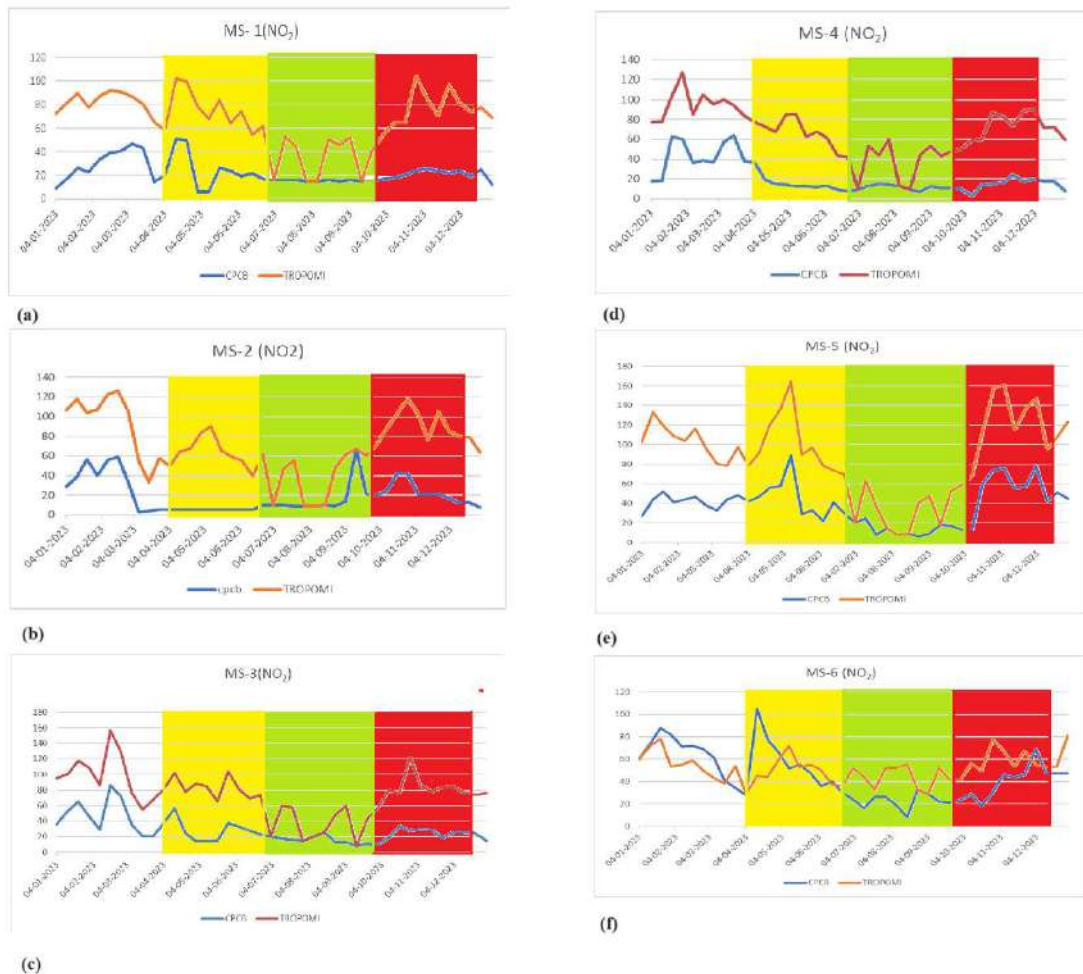


Fig. 2: Comparative prediction of monthly variation of  $\text{NO}_2$  level in (a) MS 1,(b) MS 2,(c) MS 3,(d) MS 4,(e) MS 5 and (f) MS 6.

different seasons and involving the examination of ground-based air quality monitoring data to validate and integrate the observations obtained from satellites. The seasonal variations in the data were categorized based on color representation, as shown in Table 4. These categories include Winter, Summer or Pre-Monsoon, Monsoon or Rainy, and Post-Monsoon.

Fig. 2 presents the monthly variation in  $\text{NO}_2$  levels and the examination of ground-based air quality monitoring data to validate and integrate the observations obtained from satellites in MS 1, MS 2, MS 3, MS 4, MS 5, and MS 6. Higher concentrations during winter months were observed due to increased emissions from heating sources and stagnant atmospheric conditions. During winter, temperature inversion phenomena are common, especially in urban areas like Lucknow. Inversions trap pollutants, including  $\text{NO}_2$ , close to the ground as colder air near the surface is denser and prevents vertical mixing. This leads to the accumulation

of pollutants, resulting in higher  $\text{NO}_2$  concentrations. Rainy months showed much lower concentrations due to rainfall acts as a natural cleanser by washing pollutants, including  $\text{NO}_2$ , out of the atmosphere. The precipitation effectively removes  $\text{NO}_2$  molecules from the air, leading to reduced concentrations. During rainy weather, increased humidity levels and the presence of water vapor can facilitate chemical reactions that result in the transformation or removal of  $\text{NO}_2$  from the atmosphere through processes like dissolution and oxidation. Enhanced atmospheric dispersion due to windy and turbulent conditions associated with rain can result in the dilution of pollutants, including  $\text{NO}_2$ , leading to lower concentrations in the air.

Fig. 3 presents the monthly variation in  $\text{SO}_2$  levels in MS 1, MS 2, MS 3, MS 4, MS 5, and MS 6, showing higher concentrations during winter months due to increased emissions from combustion sources and stagnation of air

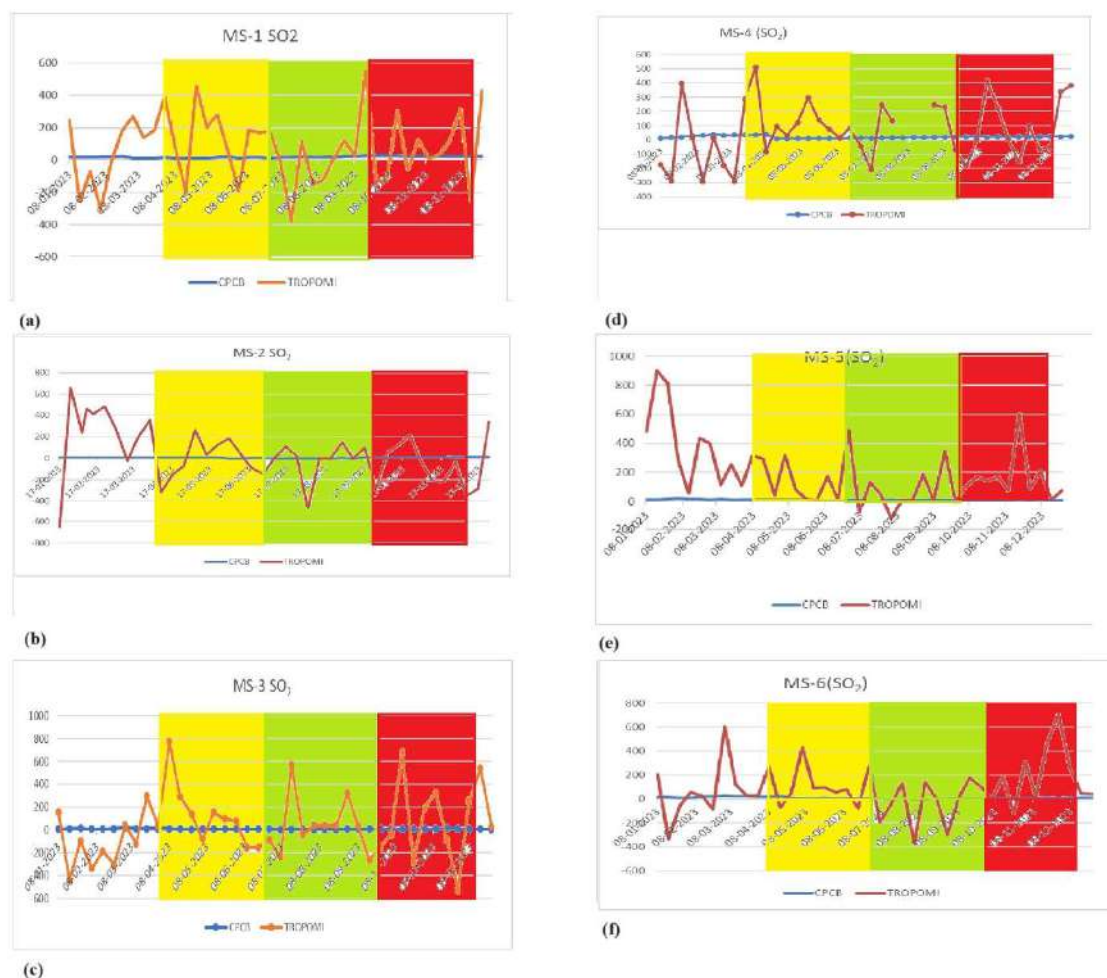


Fig. 3: Comparative prediction of monthly variation of  $\text{SO}_2$  level in (a) MS 1, (b) MS 2, (c) MS 3, (d) MS 4, (e) MS 5 and (f) MS 6.

leading to the accumulation of pollutants like  $\text{SO}_2$ , especially in urban areas where emissions are high.

### Comparison of Key Air Pollutant Levels ( $\text{NO}_2$ , $\text{SO}_2$ , and $\text{PM}_{10}$ ) Obtained from CAAQM Stations of CPCB and UPPCB with WHO Standard

A comparison of measured pollutant concentrations with WHO standards has been done to assess compliance and identify areas of concern. Fig. 4(a) and 4(c) indicate that MS-1 of Lucknow city exceeds permissible limits for  $\text{NO}_2$  in the winter season and  $\text{PM}_{10}$  in all seasons, highlighting the need for targeted interventions to mitigate air pollution and safeguard public health. This is mainly because, during winter, meteorological conditions such as temperature inversions can trap pollutants close to the ground, leading to higher concentrations of  $\text{NO}_2$  and other pollutants. In colder months, there is typically an increase in the use of fossil fuels for heating purposes, particularly in residential areas. This can lead to higher emissions of  $\text{NO}_2$  from sources such as residential heating systems and vehicles.

Winter months often experience stagnant air masses, which can result in the accumulation of pollutants, including  $\text{NO}_2$ , in the atmosphere. Cold weather can affect vehicle engines and reduce the efficiency of emission control systems, leading to higher emissions of  $\text{NO}_2$  from vehicles.

The high  $\text{PM}_{10}$  concentration in the MS-1 of Lucknow city throughout the year could be attributed to several factors: MS-1 experiences heavy traffic congestion, especially during peak hours. Vehicle emissions, particularly from diesel engines, contribute significantly to  $\text{PM}_{10}$  levels due to the release of particles from exhaust fumes and brake wear. There are ongoing construction projects nearby, and activities such as excavation, demolition, and material transport can generate dust particles, contributing to  $\text{PM}_{10}$  level. There are large open spaces or bare soil areas nearby, and wind erosion can lift dust particles into the air, adding to the  $\text{PM}_{10}$  concentration. Fig. 4(b) shows the  $\text{SO}_2$  level is below baseline. This is due to MS-1 having less industrial activity compared to other areas, leading to lower emissions of sulfur dioxide. Industries like power plants, refineries, and manufacturing facilities are major sources of  $\text{SO}_2$  emissions.

Similarly, Fig. 5(a) and 5(c) show that MS-2 of Lucknow city exceeds permissible limits for  $\text{NO}_2$  in the winter season and  $\text{PM}_{10}$  in all seasons, highlighting the need for targeted interventions to mitigate air pollution and safeguard public health. Fig. 5(b) indicates  $\text{SO}_2$  level is below the baseline.

Similarly, Fig. 6(a) and 6(c) indicate that MS-3 of Lucknow city exceeds permissible limits for  $\text{NO}_2$  in the winter season and  $\text{PM}_{10}$  in all seasons, highlighting the need for targeted interventions to mitigate air pollution and

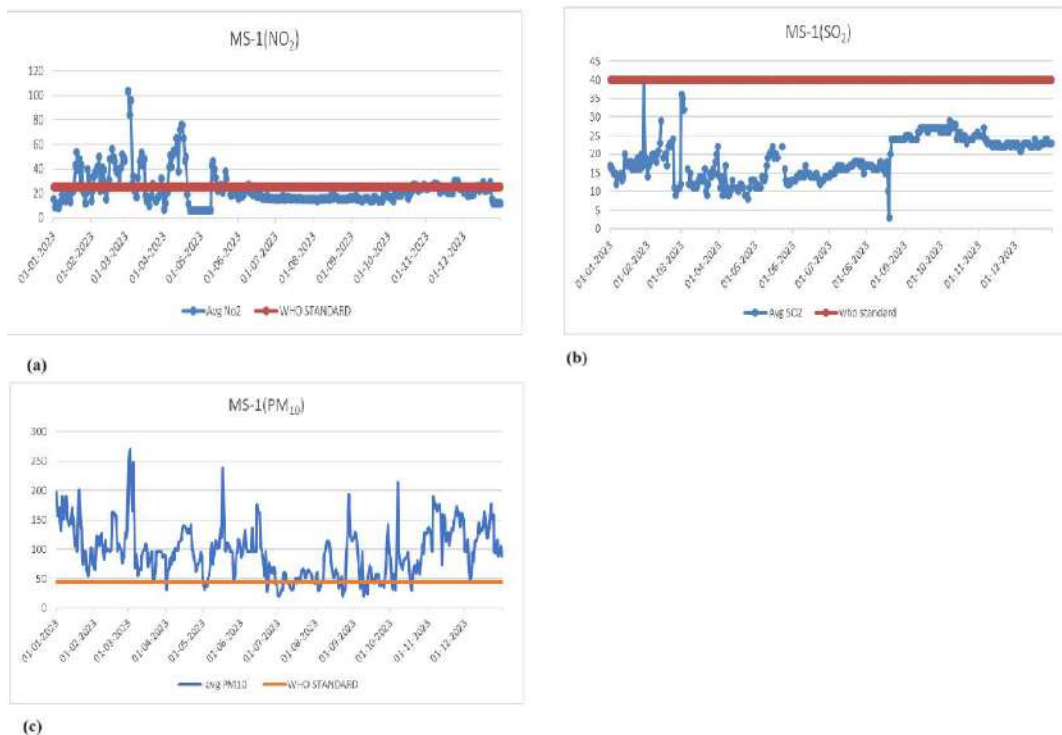


Fig. 4: Comparative prediction of ground truth (a)  $\text{NO}_2$ , (b)  $\text{SO}_2$ , and (c)  $\text{PM}_{10}$  with WHO standards of MS-1.



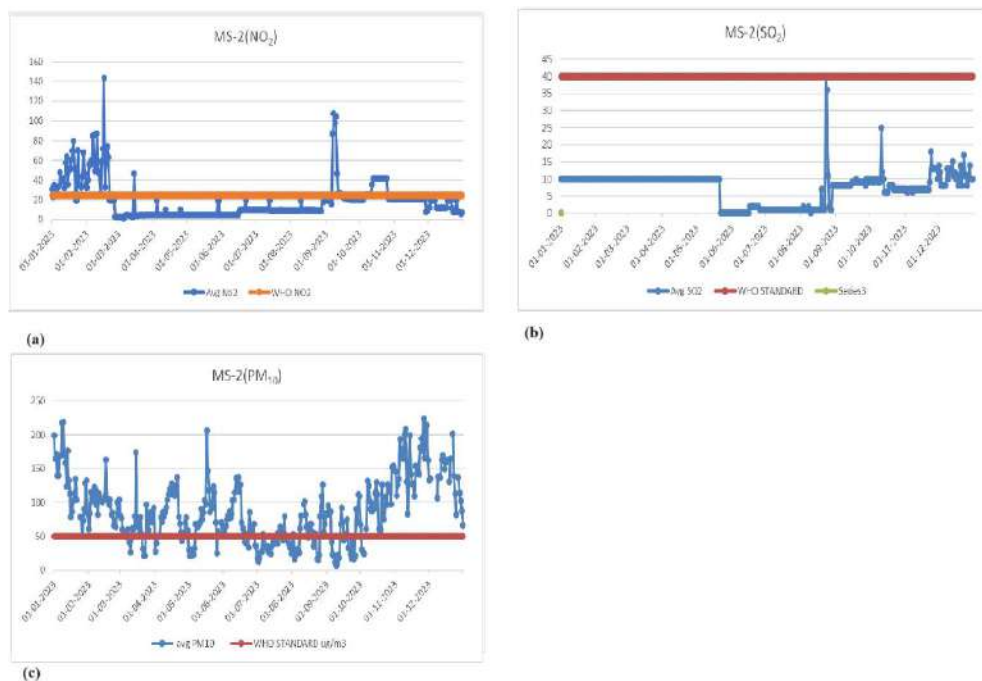


Fig. 5: Comparative prediction of ground truth (a)  $\text{NO}_2$ , (b)  $\text{SO}_2$ , and (c)  $\text{PM}_{10}$  with WHO standards of MS-2.

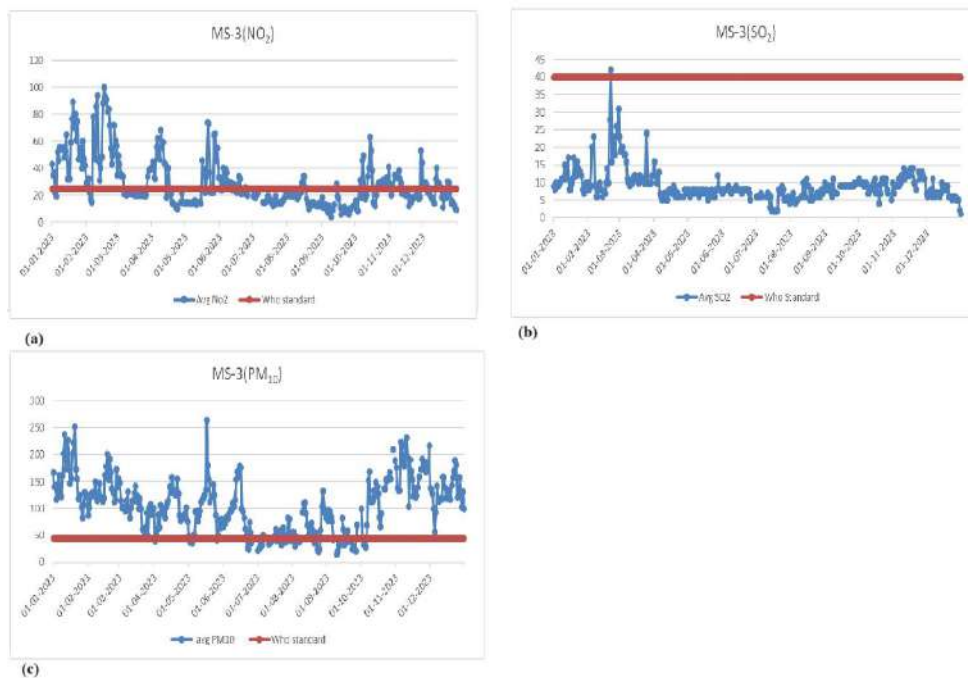


Fig. 6: Comparative prediction of ground truth (a)  $\text{NO}_2$ , (b)  $\text{SO}_2$ , and (c)  $\text{PM}_{10}$  with WHO standards of MS 3.

safeguard public health. Fig. 6(b) indicates  $\text{SO}_2$  level is below the baseline.

Similarly, Fig. 7(a) and 7(c) indicate that MS-4 of Lucknow city exceeds permissible limits for  $\text{NO}_2$  in the

winter season and  $\text{PM}_{10}$  in all seasons, highlighting the need for targeted interventions to mitigate air pollution and safeguard public health. Fig. 7(b) indicates  $\text{SO}_2$  level is below the baseline.

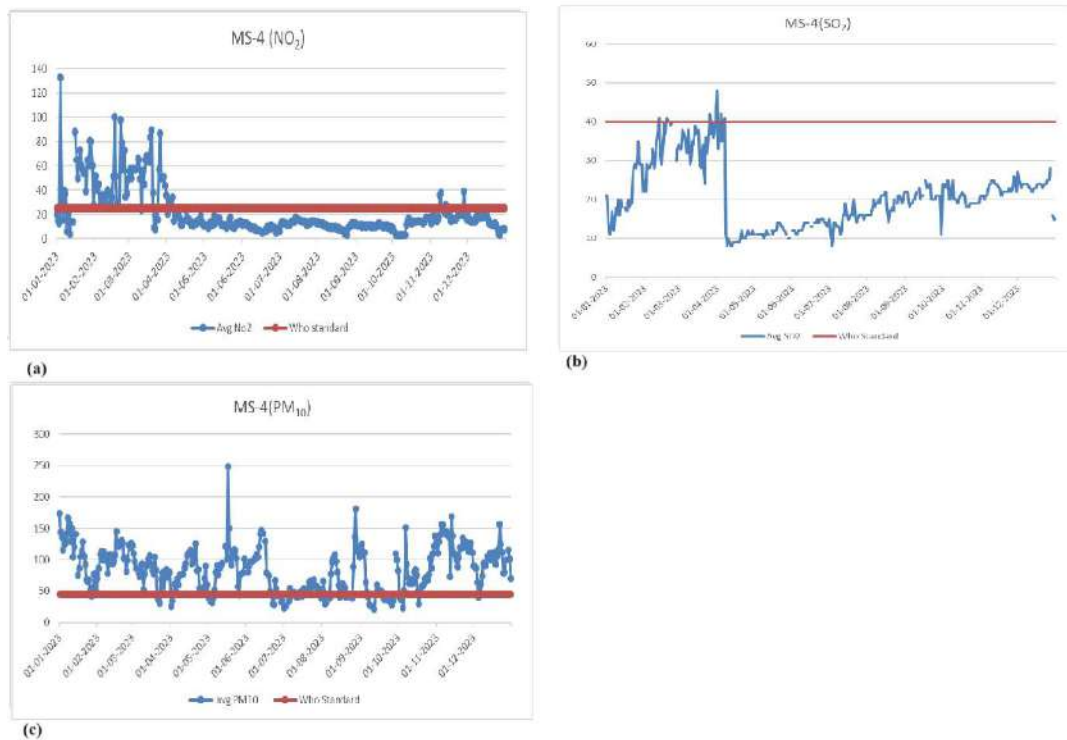


Fig. 7: Comparative prediction of ground truth (a)NO<sub>2</sub>, (b) SO<sub>2</sub>, and (c) PM<sub>10</sub> with WHO standards of MS 4.

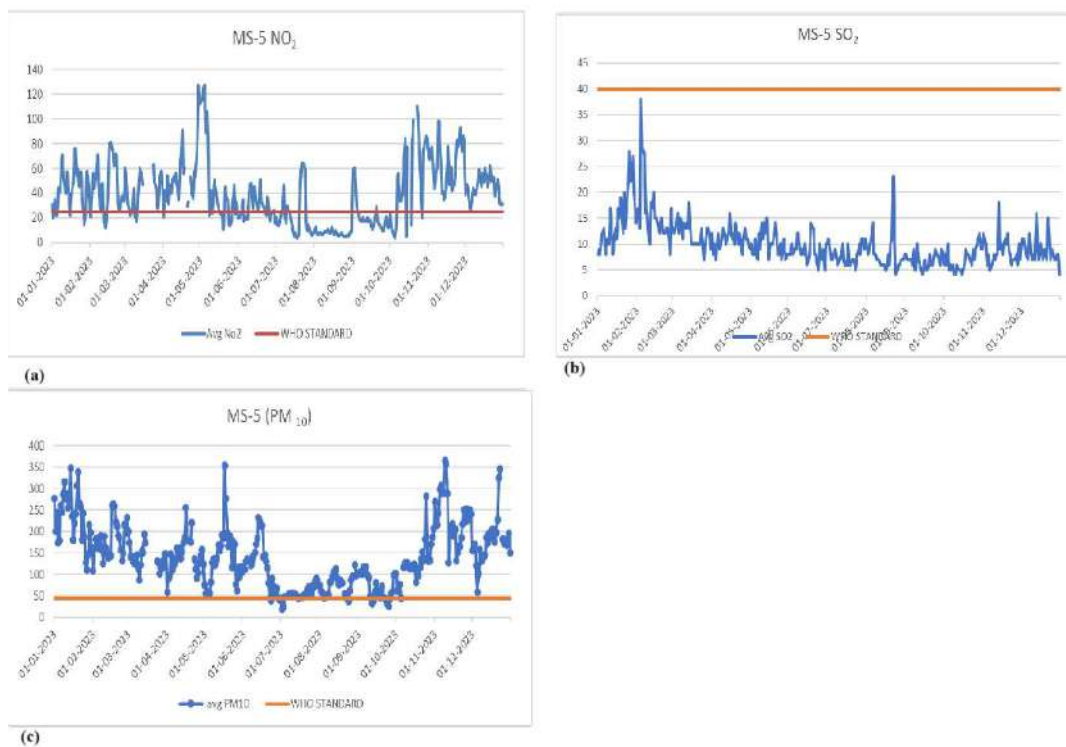


Fig. 8: Comparative prediction of ground truth (a)NO<sub>2</sub>, (b) SO<sub>2</sub>, and (c) PM<sub>10</sub> with WHO standards of MS 5.

Similarly, Fig. 8(a) and 8(c) indicate that MS-5 of Lucknow city exceeds permissible limits for  $\text{NO}_2$  and  $\text{PM}_{10}$  in all seasons, highlighting the need for targeted interventions to mitigate air pollution and safeguard public health. MS-5 is situated in a commercial area, so Commercial areas typically experience heavy traffic flow, leading to increased emissions of  $\text{NO}_2$  from vehicles.  $\text{NO}_2$  is a common pollutant produced by combustion engines, especially diesel vehicles, and traffic congestion can exacerbate its levels. It also hosts small-scale industrial activities, such as workshops or small factories, which can emit pollutants, including  $\text{NO}_2$  and  $\text{PM}_{10}$ . These emissions are continuous throughout the year. Fig. 8(b) indicates  $\text{SO}_2$  level is below the baseline.

Similarly, Fig. 9(a) and Fig. 9(c) indicate that MS-6 of Lucknow city exceeds permissible limits for  $\text{NO}_2$  and  $\text{PM}_{10}$  in all seasons, highlighting the need for targeted interventions to mitigate air pollution and safeguard public health. MS-6 is situated in an industrial area. Industrial areas typically experience heavy traffic flow due to transportation of goods, employees commuting to work, and logistics operations. This can lead to increased emissions of  $\text{NO}_2$  from vehicles, especially diesel-powered trucks and industrial vehicles. Many industries in MS-6 may rely on the combustion of fossil fuels such as coal, oil, and natural gas for energy

generation and production processes. These combustion processes release  $\text{NO}_2$  and  $\text{PM}_{10}$  as byproducts, contributing to air pollution in the area. MS-6 has fewer green spaces compared to residential or commercial areas. Greenery helps in absorbing pollutants and improving air quality. The absence of vegetation in MS-6 exacerbates air pollution by allowing pollutants to accumulate without being absorbed.

The spatial distribution of air pollutants in Lucknow city reflects the influence of both anthropogenic and natural factors, including industrial activities, vehicular emissions, and meteorological conditions. Hotspots of  $\text{NO}_2$  and  $\text{SO}_2$  concentrations coincide with industrial zones and major roadways, emphasizing the contribution of vehicular traffic and industrial emissions to local air quality degradation. The observed spatial patterns provide valuable insights for urban planners and policymakers to prioritize mitigation efforts and implement zoning regulations to reduce exposure to harmful pollutants.

The observed seasonal variability in air pollution levels underscores the influence of seasonal meteorological patterns and seasonal anthropogenic activities on air quality.

Winter months exhibit higher concentrations of pollutants such as  $\text{NO}_2$  and  $\text{PM}_{10}$  due to increased emissions

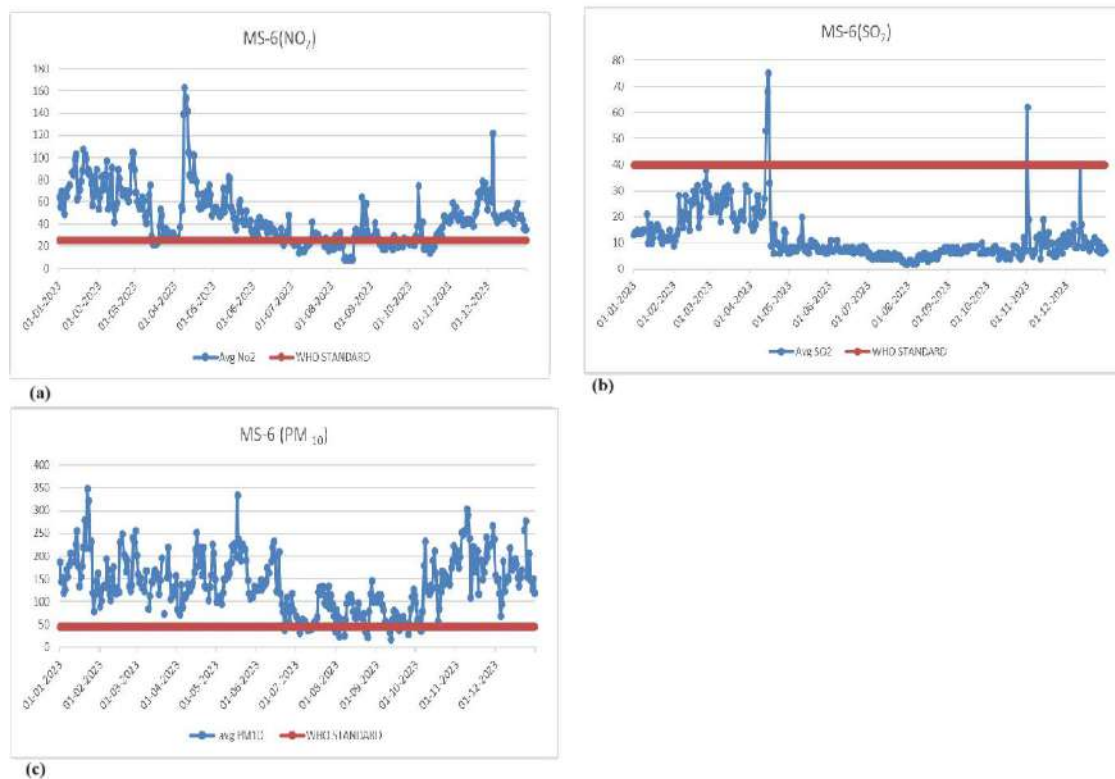


Fig. 9: Comparative prediction of ground truth (a)  $\text{NO}_2$ , (b)  $\text{SO}_2$  and (c)  $\text{PM}_{10}$  with WHO standards of MS 6.

from heating sources, agricultural residue burning, and atmospheric stagnation. Understanding these seasonal trends is essential for implementing targeted interventions and seasonal pollution control measures to mitigate the adverse effects of air pollution on public health and the environment.

Our findings have significant implications for air quality management and policy development in Lucknow city, emphasizing the importance of implementing stringent emission controls and promoting sustainable urban development practices.

Future research efforts should focus on refining spatial modeling techniques, integrating additional data sources, and conducting longitudinal studies to monitor changes in air pollution levels and assess the effectiveness of pollution control measures over time.

### Evaluating the Health Impacts of Air Pollution in Lucknow City

The analysis of the questionnaire yields significant insights into the demographics and perceptions regarding air pollution in the study area of Lucknow. Most respondents, approximately 53.2%, fall within the age group of 20-25 years. This indicates that younger individuals are actively engaged in the survey, reflecting a potential concern among the youth regarding air pollution. About 36.4% of the respondents are employed in the private sector, while 16.5% are from the government sector, and the remaining respondents are from other sectors (Fig. 10). This distribution suggests a diverse representation across various employment sectors.

All respondents were selected to be residents in the study area Fig. 34, ensuring that the survey accurately reflects the opinions and experiences of individuals directly affected by local air pollution issues.

The survey results confirm a correlation between air pollution and deteriorated respiratory health status, especially among sensitive groups and different age cohorts. This highlights the urgent need for interventions to address air quality issues, particularly for vulnerable populations. The survey identifies traffic and transportation, rapid urbanization, and population growth as the primary contributors to air pollution in Lucknow.

These findings underline the multifaceted nature of the problem, implicating both anthropogenic activities and urban development patterns. Despite acknowledging the presence of strong air pollution laws in the country (33.8%), a substantial portion of respondents (55.3%) also believe that air pollution is contributing to the extinction of flora and fauna. This suggests a perception of regulatory inadequacy or enforcement challenges in mitigating environmental degradation.

### CONCLUSIONS

In conclusion, this research paper has provided a comprehensive analysis of key air pollutants, namely nitrogen dioxide (NO<sub>2</sub>) and sulfur dioxide (SO<sub>2</sub>), utilizing satellite remote sensing data from TROPOMI Explorer in Lucknow City. Through the utilization of advanced satellite technology, we were able to gather valuable insights into the spatial distribution and concentration levels of these pollutants across the city.

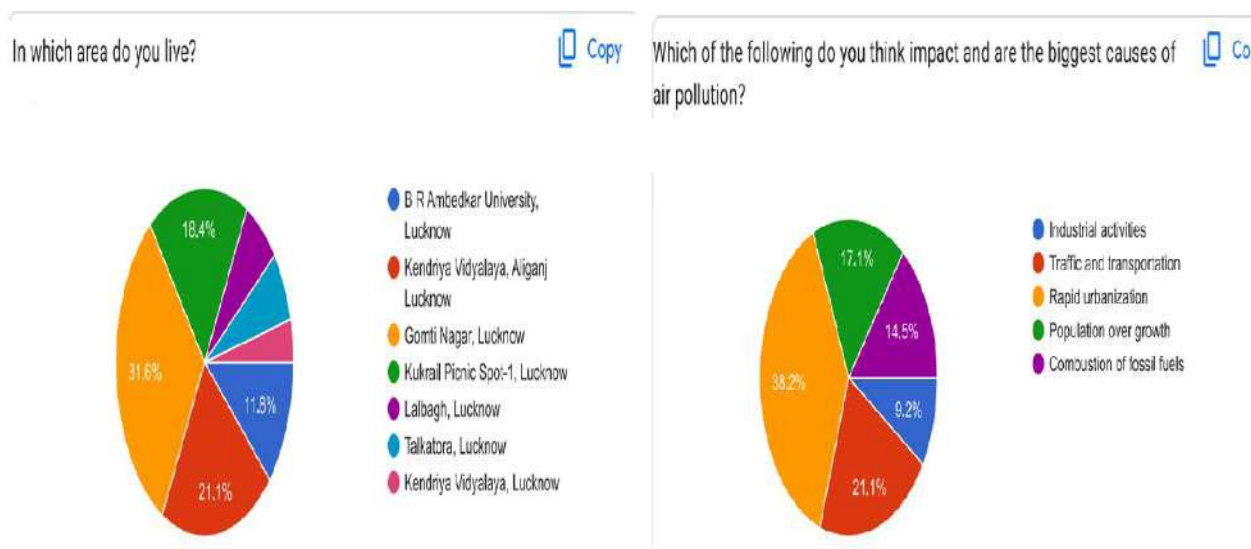


Fig. 10: Resident area.



The findings of this study shed light on the extent of air pollution in Lucknow City, highlighting areas of elevated pollutant levels and potential sources of emissions. This information is crucial for policymakers and stakeholders in formulating effective strategies to address air quality issues and protect public health.

Furthermore, the use of satellite remote sensing data has provided a cost-effective and efficient means of monitoring air quality on a large scale, complementing ground-based monitoring efforts. This integrated approach enhances our understanding of air pollution dynamics and facilitates informed decision-making towards mitigating its adverse impacts.

This research paper has successfully utilized Geographic Information Systems (GIS) and remote sensing techniques to map and analyze air pollution levels in Lucknow City. By integrating these advanced technologies, we have gained valuable insights into the spatial distribution and concentration of air pollutants within the urban environment.

Comparisons with WHO air quality standards have highlighted areas where pollution levels exceed recommended thresholds, emphasizing the urgent need for targeted interventions to improve air quality and safeguard public health in Lucknow City.

The application of GIS and remote sensing has proven to be a powerful tool in environmental monitoring, providing policymakers and stakeholders with actionable data for informed decision-making. This research underscores the importance of continued investment in technological innovations to address the complex challenges of urban air pollution and create healthier, more sustainable cities for future generations.

This research underscores the significance of leveraging satellite remote sensing technology for monitoring air quality and emphasizes the importance of continued efforts in addressing environmental challenges for the well-being of present and future generations.

### Limitations and Future Scope

The Sentinel-5P TROPOMI sensor provides valuable data for air quality assessment, but it has some limitations. Its spatial resolution may not capture localized pollution variations within Lucknow, potentially missing critical hotspots. The temporal resolution is another limitation, as satellite data were collected only at specific times, which may not reflect daily variations in pollution levels. Cloud cover and adverse weather conditions can obscure satellite observations, leading to data gaps. Additionally, TROPOMI measures total column concentrations, lacking detailed vertical profiles

that distinguish surface-level pollution from higher altitudes. Regular calibration with ground-based sensors is essential to ensure accuracy, and discrepancies may arise if calibration is not maintained. Furthermore, TROPOMI does not cover all pollutants, missing critical data on particulate matter and volatile organic compounds.

Future research should integrate satellite data with ground-based monitoring to improve accuracy and resolution. Advanced analytics, including machine learning, can enhance data processing and pattern recognition. High-resolution satellite sensors in future missions will provide more detailed data. Longitudinal studies using TROPOMI data can reveal long-term trends and policy impacts. Combining air quality data with health studies will elucidate the impact of pollution on public health. Public awareness initiatives and multi-sensor platforms can provide comprehensive air quality insights. Additionally, studying the interplay between air quality and climate change using TROPOMI data will be crucial for developing holistic environmental strategies.

### REFERENCES

- Agarwal, S., 2012. Effect of indoor air pollution from biomass and solid fuel combustion on prevalence of self-reported asthma among adult men and women in India. *Journal of Asthma*, 49(4), pp.355-365. [DOI]
- Al-Alola, S.S., Alkadi, I.I., Alogayell, H.M., Mohamed, S.A. and Ismail, Y., 2022. Air quality estimation using remote sensing and GIS-spatial technologies along Al-Shamal train pathway, Al-Qurayyat City in Saudi Arabia. *Environmental and Sustainability Indicators*, 15(6), p.100184. [DOI]
- Anil, I. and Alagha, O., 2021. The impact of COVID-19 lockdown on the air quality of Eastern Province, Saudi Arabia. *Air Quality, Atmosphere & Health*, 14, pp.117-128. [DOI]
- Barck, C., Lundahl, J., Halldén, G. and Bylin, G., 2005. Brief exposures to NO<sub>2</sub> augment the allergic inflammation in asthmatics. *Environmental Research*, 97(1), pp.58-66. [DOI]
- Barman, S.C., Kumar, N., Singh, R., Kisku, G.C., Khan, A.H. and Kidwai, M.M., 2010. Assessment of urban air pollution and its probable health impact. *Journal of Environmental Biology*, 31(6), pp.913-920. [PDF]
- Bharti, S.K., Kumar, D., Anand, S., Poonam, Barman, S.C. and Kumar, N., 2017. Characterization and morphological analysis of individual aerosol of PM<sub>10</sub> in the urban area of Lucknow, India. *Micron*, 103, pp.90-98. [DOI]
- Biswas, K., Chatterjee, A. and Chakraborty, J., 2020. Comparison of air pollutants between Kolkata and Siliguri, India, and its relationship to temperature change. *Journal of Geovisualization and Spatial Analysis*, 4, p.25. [DOI]
- Farahat, A., 2016. Air pollution in the Arabian Peninsula (Saudi Arabia, the United Arab Emirates, Kuwait, Qatar, Bahrain, and Oman): causes, effects, and aerosol categorization. *Arabian Journal of Geosciences*, 9, p.196. [DOI]
- Filonchik, M., 2022. Characteristics of the severe March 2021 Gobi Desert dust storm and its impact on air pollution in China. *Chemosphere*, 287(3), p.132219. [DOI]
- Government of India, 1981. The Air (Prevention and Control of Pollution) Act, 1981. PDF
- Ialongo, I., Virta, H., Eskes, H., Hovila, J. and Douros, J., 2020. Comparison

- of TROPOMI/Sentinel-5 Precursor NO<sub>2</sub> observations with ground-based measurements in Helsinki. *Atmospheric Measurement Techniques*, 13, pp.205-218. [DOI]
- IQ Air, 2019. World air quality report 2019. PDF
- Khan, A.H., Ansari, F.A., Patel, D.K., Siddiqui, H., Sharma, S. and Ashquin, M., 2010. Indoor exposure to respirable particulate matter and particulate-phase PAHs in rural homes in North India. *Environmental Monitoring and Assessment*, 170(1-4), pp.491-497. [DOI]
- Kumar, S. and Dwivedi, S.K., 2021. Impact on particulate matters in India's most polluted cities due to long-term restriction on anthropogenic activities. *Environmental Research*, 200, p.111754. [DOI]
- Opio, R., Mugume, I. and Nakatumba-Nabende, J., 2021. Understanding the trend of NO<sub>2</sub>, SO<sub>2</sub>, and CO over East Africa from 2005 to 2020. *Atmosphere*, 12(10), p.1283. [DOI]
- Pandey, P., Khan, A.H., Verma, A.K., Singh, K.A. and Kisku, G.C., 2012. Seasonal trends of PM<sub>2.5</sub> and PM<sub>10</sub> in ambient air and their correlation in ambient air of Lucknow City, India. *Bulletin of Environmental Contamination and Toxicology*, 88(2), pp.265-270. [DOI]
- Pandey, P., Patel, D.K., Khan, A.H., Barman, S.C., Murthy, R.C. and Kisku, G.C., 2013. Temporal distribution of fine particulates (PM<sub>2.5</sub>, PM<sub>10</sub>), potentially toxic metals, PAHs, and metal-bound carcinogenic risk in the population of Lucknow City, India. *Journal of Environmental Science and Health*, 48(7), pp.730-745. [DOI]
- Saber, A., Abdel Basset, H., Morsy, M., El-Hussainy, F.M. and Eid, M.M., 2020. Characteristics of the simulated pollutants and atmospheric conditions over Egypt. *NRIAG Journal of Astronomy and Geophysics*, 9, pp.402-419.
- Salman, A., Al-Tayib, M., Hag-Elsafi, S., Zaidi, F.K. and Al-Duwarij, N., 2021. Spatiotemporal assessment of air quality and heat island effect due to industrial activities and urbanization in southern Riyadh, Saudi Arabia. *Applied Sciences*, 11, p.2107.
- Sen, A., Abdelmaksoud, A.S., Ahammed, Y.N., Banerjee, T., Bhat, M.A., Chatterjee, A., Choudhuri, A.K., Das, T., Dhir, A., Dhyani, P.P. and Gadi, R., 2017. Variations in particulate matter over Indo-Gangetic Plains and Indo-Himalayan Range during four field campaigns in winter monsoon and summer monsoon: role of pollution pathways. *Atmospheric Environment*, 154, pp.200-224.
- Shikwambana, L., Mhangara, P. and Mbatha, N., 2020. Trend analysis and first-time observations of sulphur dioxide and nitrogen dioxide in South Africa using TROPOMI/Sentinel-5P data. *International Journal of Applied Earth Observation and Geoinformation*, 91, p.102130.
- Singh, P., Kikon, N. and Verma, P., 2017. Impact of land use change and urbanization on urban heat island in Lucknow city, Central India. *Sustainable Cities and Society*, 32, pp.100-114.
- Sinha, P.R., Manchanda, R.K., Kaskaoutis, D.G., Kumar, Y.B. and Sreenivasan, S., 2013. Seasonal variation of surface and vertical profile of aerosol properties over a tropical urban station Hyderabad, India. *Journal of Geophysical Research: Atmospheres*, 118(2), pp.749-768.
- Theys, N., Fioletov, V., Li, C., De Smedt, I., Lerot, C., McLinden, C., Krotkov, N., Griffin, D., Clarisse, L., Hedelt, P. and Loyola, D., 2021. A sulfur dioxide Covariance-Based Retrieval Algorithm (COBRA): application to TROPOMI reveals new emission sources. *Atmospheric Chemistry and Physics*, 21(22), pp.16727-16744.
- Vîrghileanu, M., Săvulescu, I., Mihai, B., Nistor, C. and Dobre, R., 2020. Nitrogen dioxide (NO<sub>2</sub>) pollution monitoring with Sentinel-5P satellite imagery over Europe during the coronavirus pandemic outbreak. *Remote Sensing*, 12, p.3575.
- Zhao, X., Griffin, D., Fioletov, V., McLinden, C., Cede, A., Tiefengraber, M., Müller, M., Bogner, K., Strong, K., Boersma, F., Eskes, H., Davies, J., Ogyu, A. and Lee, S.C., 2020. Assessment of the quality of TROPOMI high-spatial-resolution NO<sub>2</sub> data products in the Greater Toronto Area. *Atmospheric Measurement Techniques*, 13, pp.2131-2159.

# Flood Frequency Analysis of Kadamaian and Wariu Rivers in Kota Belud, Sabah, Malaysia

K. Sharir<sup>1</sup>, A. Saidin<sup>2</sup> and R. Roslee<sup>2†</sup>

<sup>1</sup>Faculty of Engineering (FKJ), Universiti Malaysia Sabah, 88400 Kota Kinabalu, Sabah, Malaysia

<sup>2</sup>Faculty of Science & Natural Resources (FSSA), Universiti Malaysia Sabah, 88400 Kota Kinabalu, Sabah, Malaysia

†Corresponding author: R. Roslee; rodeano@ums.edu.my

**Abbreviation:** Nat. Env. & Poll. Technol.  
**Website:** www.neptjournal.com

*Received:* 19-06-2024

*Revised:* 09-08-2024

*Accepted:* 22-08-2024

## Key Words:

Annual recurrence interval  
 Flood hazards  
 Flood frequency analysis  
 Gumbel distribution  
 Probability distribution  
 Weibull plotting position

## Citation for the Paper:

Sharir, K., Saidin, A. and Roslee, R., 2025. Flood frequency analysis of Kadamaian and Wariu Rivers in Kota Belud, Sabah, Malaysia. *Nature Environment and Pollution Technology*, 24(2), p.D1691. <https://doi.org/10.46488/NEPT.2025.v24i02.D1691>

*Note: From year 2025, the journal uses Article ID instead of page numbers in citation of the published articles.*



*Copyright:* © 2025 by the authors

*Licensee:* Technoscience Publications

This article is an open access article distributed under the terms and conditions of the Creative Commons Attribution (CC BY) license (<https://creativecommons.org/licenses/by/4.0/>).

## ABSTRACT

Flood frequency analysis is crucial for understanding flood risks in specific regions. This study applied the Gumbel Distribution Method to analyze flood frequency using river discharge data from the Kadamaian and Wariu Rivers in Kota Belud, Sabah, Malaysia. The analysis involved data collection, parameter estimation, goodness-of-fit testing, and determination of annual recurrence intervals (ARIs). The study found that the ARIs for the Kadamaian and Wariu Rivers are 50 years and 30 years, respectively, highlighting the need for targeted flood mitigation strategies in these areas. These findings emphasize the higher flood risk in the Kadamaian River basin, necessitating more robust flood control measures compared to the Wariu River basin. The Gumbel distribution provided accurate flood frequency estimations validated by the Kolmogorov-Smirnov test and correlation coefficient ( $R^2$ ). The calculated ARIs offer valuable insights for flood hazard assessment and contingency planning. These findings underscore the importance of accurate flood frequency analysis in enhancing flood mitigation strategies and disaster preparedness. It is recommended that local authorities incorporate these results into flood management and urban planning initiatives.

## INTRODUCTION

Flood frequency analysis is a technique for preparing and calculating the size of floods that occur in a specific area based on recurring factors (Hamzah et al. 2021, Pankaj & Sunil, 2015, Sharir et al. 2022). It is a tool for determining the design of rainfall levels, river discharge rates, and drainage structures, focusing on the hydraulic capacity required for a drainage system to control flooding (Mohamad Hamzah et al. 2019, Sharir et al. 2022, Sharir & Roslee 2022). In this analysis, the flood probability distribution is frequently paired with the maximum annual discharge data (Shabri 2012). Recent studies have demonstrated the effectiveness of using advanced hydrodynamic models, such as HEC-RAS, in simulating flood events, which significantly enhances flood risk management and mitigation strategies (Garg & Ananda Babu 2023).

Current studies on flood frequency analysis in the Kota Belud region have primarily focused on traditional methods without incorporating modern approaches or comparing different methodologies. There is a lack of comprehensive studies that validate the Gumbel Distribution Method against recent advancements in flood frequency analysis. This study aims to fill this gap by providing a detailed comparison and highlighting the significance of using the Gumbel Distribution Method in this region. The novelty of this study lies in its application of the Gumbel Distribution Method in the context of the Kadamaian and Wariu Rivers in Kota Belud, a region that has not been extensively studied using this approach. The analysis not only provides a detailed assessment of flood frequencies but also validates the method's applicability in this unique geographical area, offering

valuable insights for local flood management strategies. The integration of hydrodynamic models, such as the WRF model, has shown that accurate flood simulations are crucial for assessing the impact of heavy precipitation events and improving flood management practices (Nabi & Kumar 2022).

The Gumbel Distribution Method, also known as the Extreme Value Distribution (EV Type I), Generalized Extreme Value Distribution (GEV), Normal Log, Pearson Log III (LP3), and Pareto Distribution, are several widely used methods for analyzing the best flood frequency distribution based on the goodness-of-fit test scale (Bhagat 2017, Farooq et al. 2018, Kordrostami et al. 2020, Pankaj & Sunil 2015, Romali et al. 2018, Romali & Yusop 2017, Selaman et al. 2007). Depending on the range of data available in the area, the researcher may use hydrological data like rainfall intensity rate, water level, and maximum annual discharge to analyze flood frequency (Hamzah et al. 2021, Kordrostami et al. 2020, Pankaj & Sunil 2015, Romali & Yusop 2017).

The frequency distribution of floods is analyzed to estimate the return of the flood recurrence time at a particular site. The predicted return is then compared to the observed value of the current data. The flood recurrence period is conceptually represented by the symbol  $T$ , which is expressed in years. A flood intensity with a probability of  $1/T$  exceeding a specific year is referred to as a  $T$ -year flood. This is known as the exceedance probability. For instance, “100 years of floods” does not always imply that a flood happens once every 100 years. This refers to the likelihood of it occurring — 1 in 100, or 1%, within a year. This means that regardless of when the most recent incident of this nature occurred, there is a 1% probability that it will happen in any given year. In other words, it has a 10% probability and is ten times less likely to occur than a flood with a 10-year recurrence period. Calculating flood intensities for exceeding possibilities or recurrence times (from 0.1 to 0.001) is essential, especially when flood mitigation design is factored in. This is a typical source of misunderstandings and confusion over the concept of a recurrent period, which results in inaccurate evaluations of the risk or hazard of flooding.

Generalized Logistics and Gumbel Distribution (EV Type 1) is appropriate for representing the severity and frequency of floods in Malaysia (Department of Irrigation and Drainage 2018). Although both distribution systems are suitable for Peninsular Malaysia, the Gumbel Distribution (EV Type 1) is more practicable for distribution in Sabah and Sarawak (Jefferin et al. 2017, 2018, Selaman et al. 2007). For each sample of the flood frequency distribution, the plotting position is calculated using a variety of formulas

(techniques), including Weibull, Gringorten, and L-moment (Jefferin et al. 2017, Mohamad Hamzah et al. 2019, Romali & Yusop 2017, Selaman et al. 2007). In Peninsular Malaysia, the plotting position of each frequency distribution is determined using the Weibull formula (Department of Irrigation and Drainage 2018). For flood frequency analysis in Sarawak, the Gumbel distribution using the L-moment technique is best for plotting the flood probability distribution (Selaman et al. 2007). In contrast, the Gumbel distribution approach utilizing the Weibull plotting position technique is the most appropriate since it receives good validation in Sabah (Jefferin et al. 2018).

The data are validated, and the best distribution to suit the observed data is chosen in flood frequency analysis using the model-fitting goodness score (Millington et al. 2011). Several practical tests have been suggested to evaluate the effectiveness of flood frequency distributions, including the Kolmogorov-Smirnov (KS), Chi-Squared, Root Mean Square Error (RMSE), Mean Absolute Error (MAE), and relative mean absolute error (RMAE) tests (Bezak et al. 2014, Farooq et al. 2018, Millington et al. 2011). The level of significance was assessed using the P-value. Meanwhile, the optimal model evaluation for the flood frequency distribution is estimated based on  $R^2$  in  $0.7 < R^2 < 1$  (Department of Irrigation and Drainage 2018).

## STUDY AREA

The research area is located in a section of the Kota Belud district on Sabah's west coast and faces the South China Sea (Fig. 1). Kota Belud is approximately 70 kilometers from Sabah's capital, Kota Kinabalu (Sharir et al. 2022, Sharir & Roslee 2022). This district is estimated to be 1,385.6 square kilometers ( $\text{km}^2$ ) (Pejabat Daerah Kota Belud 2017). The section contains three major river basins. Three river basins include the Tempasuk River Basin (122 square kilometers), the Kadamaian River Basin (445 square kilometers), and the Wariu River Basin (343 square kilometers) (Sharir & Roslee 2023a, 2023b).

## MATERIALS AND METHODS

The flood frequency study is defined by four steps: data collection, plotting distribution and estimating parameters, good-of-fit test, and annual recurrence interval result.

### Data Collection

Hourly river discharge data from the Kadamaian River and Wariu River stations provided by the Sabah Department of Irrigation and Drainage covers a period of 50 years, from 1969 to 2018. The data is measured in cubic meters per



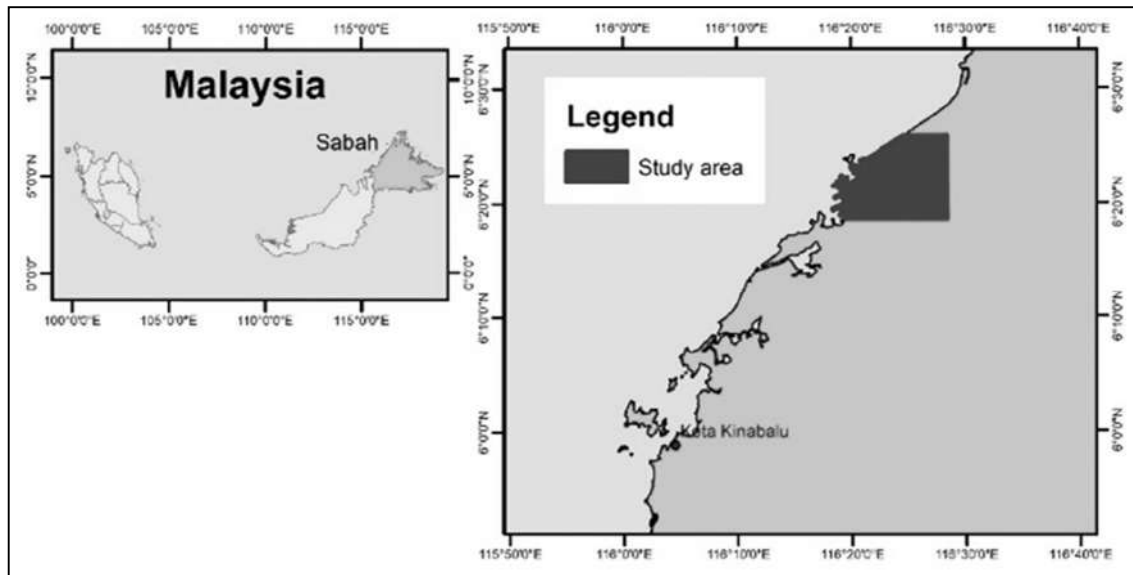


Fig. 1: Location of Kota Belud area, Sabah, Malaysia.

second ( $\text{m}^3/\text{s}$ ), and missing or untraceable hourly discharge data will be estimated using the hours before and after.

There are two ways to determine flood frequency using hourly river discharge data: annual maximum series data and partial duration series data. Annual maximum series data is derived from the peak river discharge of each year, while partial duration series data considers all values that exceed a certain threshold during the recording period.

For this study, the annual maximum series data will be used as the primary data to create a flood frequency distribution model since it avoids selecting corresponding data from the same event period throughout the year, which could lead to larger values when using partial duration series data. The hourly discharge data was collected from two hydrological stations, the Kadamaian River (Tamu Darat) at 6.2644 latitudes and 116.4547 longitudes, and the Wariu River (Bridge No. 2) at 6.3245 latitudes and 116.483 longitudes, and consists of 50 independent data points selected from 439,000 hourly river discharge series data.

### Plotting Distribution and Estimation Parameters

Once the series data for river discharge is obtained, the statistical distribution function is determined to accurately depict the results of flood frequency analysis. The Gumbel Distribution Method (EV Type I) with the Weibull plot position technique was selected for this study, but the validity of this model depends on the validation value obtained. The flood frequency distribution analysis involves two steps: determining the Weibull plot position and selecting the appropriate distribution for the Gumbel method.

### Gumbel Distributions

The flood recurrence period can be defined as the average number of attempted flood events occurring in a year with an event magnitude more significant than the designated event (Benjamin & Cornell 1970). Today's flood management policies and plans focus on 100-year flood events with a 1% chance of occurring each year. Additionally, there is a proposal to raise the flood recurrence period to 200 years (Pusat Ramalan & Amaran Banjir Negara 2021). Extreme value distribution is also referred to as Gumbel's distribution. It is a type of probability analysis frequently used in hydrologic studies to anticipate floods for extreme values. The inflow for each return period was calculated using the Eq. (1) below:

$$X_t = \bar{X} + K.S \quad \dots(1)$$

Where,  $X_t$  is the value of variate with a return period,  $T$ ,  $\bar{X}$  Is the Mean of the variate,  $S$  is the standard deviation of the sample,  $K$  is the frequency factor expressed as in Eq. (2):

$$K = \frac{Y_t + Y_n}{S_n} \quad \dots(2)$$

$Y_t$  is Gumbel's reduced variate, as shown in Eq. (3) below:

$$Y_t = -\ln \ln \frac{T}{T-1} \quad \dots(3)$$

### Weibull Plotting Position

The maximum annual river discharge data is arranged according to the highest to the lowest magnitude, and the probability  $P$  for each event is equal to or greater than (plot

position) calculated with the Weibull plot position formula. The formula of Weibull is, Eq. (4):

$$P = \frac{m}{N + 1} \quad \dots(4)$$

Where  $m$  is the order of numbers,  $N$  is the record number, and  $P$  is the probability of exceedance. The probability will be obtained using the following relationships, Eq. (5):

$$T = \frac{1}{p} \quad \dots(5)$$

$$F = 1 - \frac{1}{T} \quad \dots(6)$$

Where in Eq. 6,  $p$  is the probability of exceedance (Probability that an event will exceed in a year),  $T$  is the return Period, and  $F$  is the frequency (rate of an event occurring). The river discharge will be plotted against the flood recurrence period. The flood recurrence period of 1 to 200 years is estimated through the plotted graph.

### Goodness-of-Fit Test

Objective quantitative tests are employed to evaluate the goodness of fit of the model because they offer an unbiased approach to the analysis. In this study, the Kolmogorov-Smirnov statistical tests were utilized to assess the distribution's performance. The test statistics for evaluating the goodness of fit are as follows:

$H_0$ : The data adheres to a specific distribution

$H_A$ : The data does not adhere to a specific distribution

The calculated  $p$ -value is used to evaluate the tests. If the calculated  $p$ -value is less than 0.05 ( $p < 0.05$ ),  $H_0$  is rejected. Rejection of  $H_0$  implies that the specific distribution does not explain the data adequately. The Kolmogorov-Smirnov (KS) test is suitable for continuous data and is known to have an independent distribution. It is also appropriate for small sample sizes. However, to use this test, it is necessary to determine the location, shape, and scale parameters, as they cannot be estimated directly from the data.

### Annual Recurrence Interval (ARI)

The recurrence interval, also known as the return period, predicts the likelihood of an event occurring. The magnitude of an event at a selected return period can be mathematically calculated by taking the inverse of the cumulative distribution function, which is also called the quantile function. In this study, the Gumbel Extreme Value Distribution method is used to determine the return period. The obtained return period will then be utilized in the hydrodynamic model analysis to determine the probability of flood frequency and generate a flood inundation map of the study area.

## RESULTS AND DISCUSSION

Flooding is the most common geological hazard that can happen everywhere, especially in floodplain areas where people might choose to dwell along the population growth. Knowing the potential size of significant floods and how often they are likely to occur helps minimize flood damage and loss of life. The analysis revealed that the Annual Recurrence Interval (ARI) for significant flood events varies considerably between the Kadamaian and Wariu Rivers, with the former showing a higher frequency of severe events. This suggests the need for tailored flood management strategies in the region. For instance, the higher ARIs observed for the Kadamaian River indicate a greater vulnerability to extreme flood events, which necessitates the implementation of enhanced flood mitigation measures, such as the construction of additional retention basins and improved early warning systems. Conversely, the lower ARIs in the Wariu River may allow for different management strategies focused on periodic maintenance and community preparedness.

### Annual Maximum Series

Flood frequency analysis primarily uses annual maximum flood series data observed at gauging stations (hydrologic stations) to estimate flood magnitude. A statistical distribution method and historical flood data are needed for this purpose. There is a total of 439,000 data for 50 years. Only one maximum data is taken to represent the year, making it only 50 data required in the annual maximum series. The y-axis represents river discharge data in cubic meters per second ( $\text{m}^3 \cdot \text{s}^{-1}$ ), and the x-axis represents years from 1969 to 2018. Hourly data descriptive statistics are shown in Table 1 for the Kadamaian River Station and Wariu River Station.

The annual maximum series (AMS) consists of the highest maximum data between 1969 and 2018 (Fig. 2). AMS descriptive statistics are summarized in Table 1. For Kadamaian River Station, the hydrology station recorded the highest discharge flow in 2010, which was  $1,362.05 \text{ m}^3 \cdot \text{s}^{-1}$ , while the hydrology station recorded the minimum discharge flow of  $248.05 \text{ m}^3 \cdot \text{s}^{-1}$  in 1982. The average maximum discharge flow for Kadamaian River Station is  $759.36 \text{ m}^3 \cdot \text{s}^{-1}$ , the median of the maximum discharge flow is  $736.36 \text{ m}^3 \cdot \text{s}^{-1}$ , and the standard deviation is  $291.39 \text{ m}^3 \cdot \text{s}^{-1}$ . For Wariu River Station, the hydrology station recorded the highest discharge flow in 2010, which was  $891.48 \text{ m}^3 \cdot \text{s}^{-1}$ , while the hydrology station recorded the minimum discharge flow of  $127.55 \text{ m}^3 \cdot \text{s}^{-1}$  in 1990. The average maximum discharge flow for Wariu River Station is  $442.06 \text{ m}^3 \cdot \text{s}^{-1}$ , the median of the maximum discharge flow is  $407.14 \text{ m}^3 \cdot \text{s}^{-1}$ , and the standard deviation is  $166.87 \text{ m}^3 \cdot \text{s}^{-1}$ .

Table 1: Descriptive analysis of river discharge data at both hydrological stations.

	Kadamaian River		Wariu River	
	Hourly river discharge	Annual maximum series	Hourly river discharge	Annual maximum series
Min [ $\text{m}^3 \cdot \text{s}^{-1}$ ]	0.71	248.05	0.63	127.55
Average [ $\text{m}^3 \cdot \text{s}^{-1}$ ]	34.82	759.36	19.06	442.06
Max [ $\text{m}^3 \cdot \text{s}^{-1}$ ]	1362.05	1362.05	891.48	891.48
S.D [ $\text{m}^3 \cdot \text{s}^{-1}$ ]	10.05	291.39	5.45	166.87

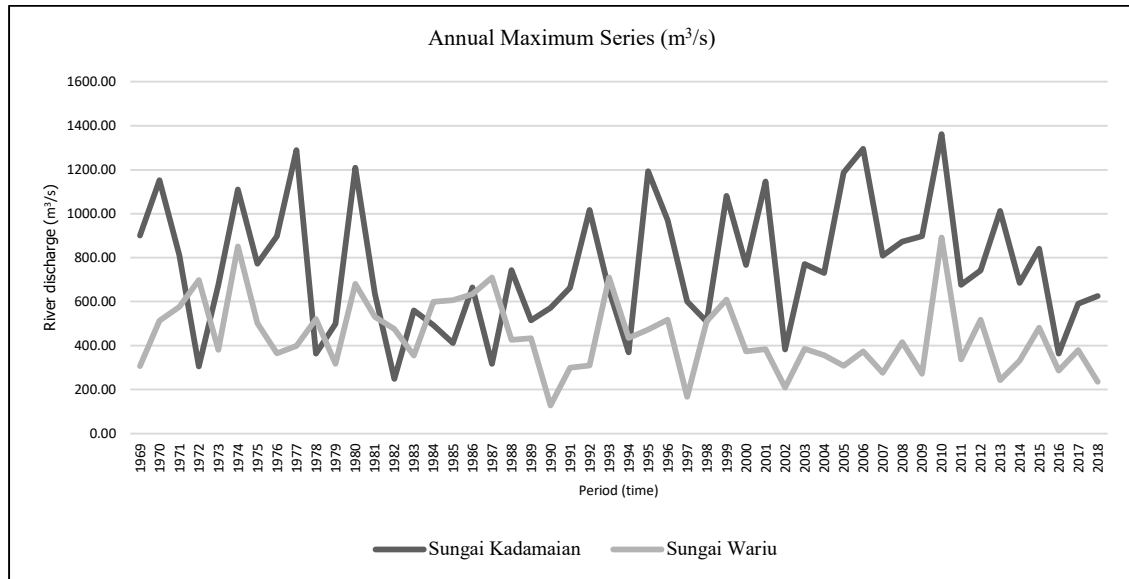


Fig. 2: Maximum annual discharge series (AMS) for Kadamaian River Hydrological Station and Wariu River Hydrological Station.

### Flood Frequency Distribution

This section presents the results of probability distribution analysis using the Gumbel Distribution (EV I) technique for both hydrological stations. The method of plotting this distribution uses the Weibull formula. The results of this analysis were used to produce probability plots and flood frequency curves for the Kadamaian River and Wariu River Stations.

The probability of exceeding (P) means that it is possible that, in a certain period, the flood will reach or exceed a certain magnitude. In contrast, the probability of not exceeding (F) means that the likelihood of flooding will not occur in a certain repetition period.

This research will use this probability in determining the flood discharge for a specific flood recurrence period (ARI) which will be discussed in the following sub-topic. The Empirical Curve (x) is the observation value obtained from the maximum annual series discharge data used to get the Gumbel value and measure the goodness of the resulting distribution. Fig. 3 illustrates the Gumbel distribution's probability plot and flood frequency curve using the

Weibull Formula for the Kadamaian River and Wariu River Stations.

### Goodness-of-Fit of the Model

To assess the suitability of the probability distribution that fits the given data, a goodness-of-fit test was conducted on the maximum annual discharge data spanning 50 years. This test involves comparing the empirical distribution function (EDF) based on the data with the cumulative distribution function (CDF) to determine if they are in good agreement. This test aims to identify the best probability distribution to use for the analysis (Hamzah et al. 2021).

In this study, the Kolmogorov-Smirnov (KS) test is used to evaluate the goodness of fit of the probability distribution model. Fig. 4 shows a comparison graph of empirical values (obtained from observational data) and Gumbel values (theoretical values) produced from the Gumbel distribution (EV I) to get the p-value in the KS test for both hydrological stations.

The p-value is the observed value, while the significant alpha value is the tabulated value. If the p-value is smaller

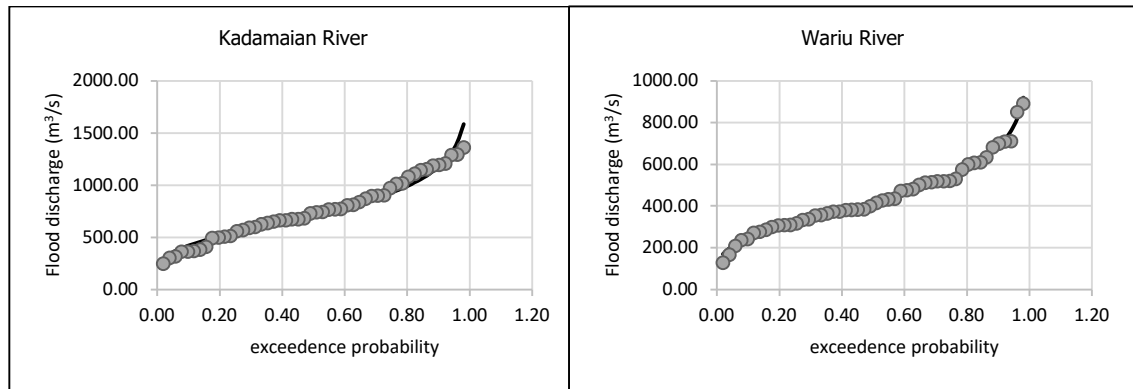


Fig. 3: Gumbel Distribution using Weibull Formula for Kadamaian River Station and Wariu River Station.

than the significant alpha value,  $\alpha = 0.05$ , the null hypothesis,  $H_0$ , will be accepted. Thus, the tested data are consistent with the defined distribution (Farooq et al. 2018, Suhaimi et al. 2020). If the value of  $p$  is greater than the significant alpha value, then the alternative hypothesis,  $H_a$ , will be accepted.

In other words, the data does not follow a specific distribution. The KS test on the results of the Gumbel distribution analysis (EV I) shows that both hydrological stations have a  $p$ -value that is smaller than the significant alpha value ( $p < 0.05$ ). Consequently, this distribution is consistent with the null hypothesis, which claims that the data provided would follow a specific distribution.

In addition to the KS test, the accuracy measurement method using the correlation coefficient ( $R^2$ ) is also used to evaluate the extent to which the flood frequency distribution produced matches the observation data. The results of the calculations show that the coefficient correlation value,  $R^2$ , is equal to 0.9681 for the Kadamaian River Station data and 0.9906 for the Wariu River Station data. If the value of  $r$  approaches one (1), this graph shows a good correlation. The  $r$  values shown for Kadamaian River Station ( $r = 0.9839$ ) and Wariu River Station ( $r = 0.9953$ ) show that the distribution pattern is narrow, and the Gumbel distribution method is seen as ideal for predicting river discharge flow.

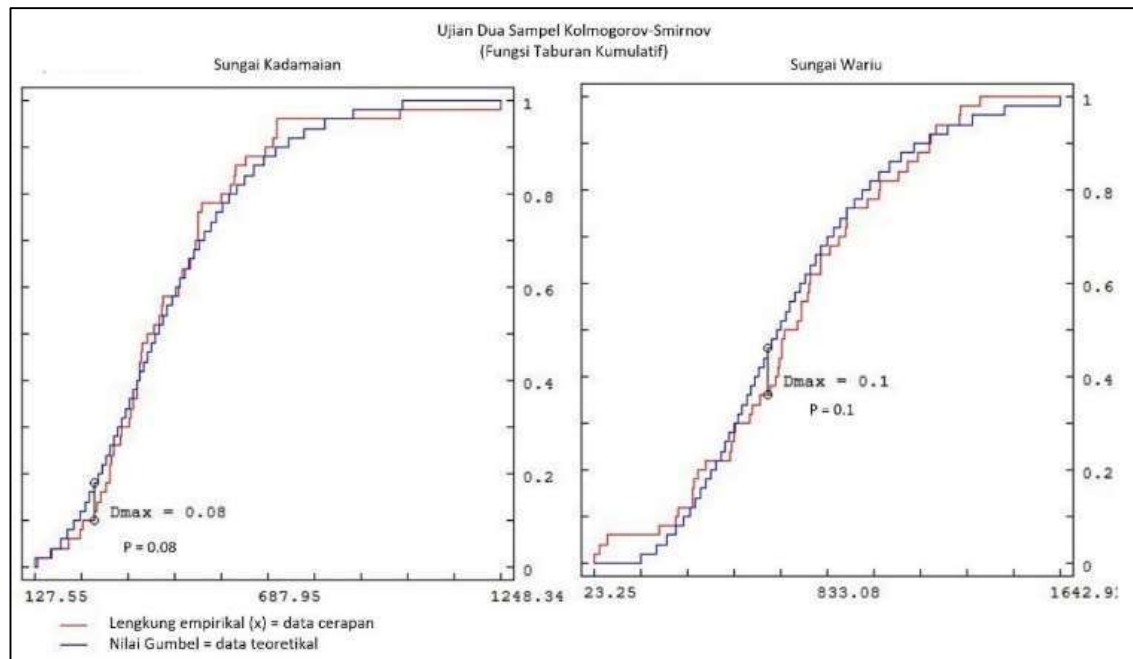


Fig. 4: Kolmogorov-Smirnov Test Graph to obtain  $p$ -values for both hydrological stations.



### Annual Recurrence Interval (ARI)

Estimating the value of flood recurrence for a certain recurrence period is essential and needs to be done after looking at the probability distribution. This is because the frequency and size of floods in a region can be influenced by the flood recurrence period. This information is crucial for lowering the risk of future flooding. Using Gumbel distribution analysis, floods with different recurrence periods of 5, 10-, 20-, 50- and 100 years were calculated. The magnitude value for each ARI is given in Table 2. This demonstrates how the following techniques can be used to extrapolate or calculate additional values that aren't depicted in the chart.

According to Hydrological Procedure 11, it is assumed that the design recurrence interval (ARI) of floods is the same as the design recurrence interval (ARI) of storms (Department of Irrigation and Drainage 2018). The observational data obtained only show ARI up to 50 years. As mentioned before, ARI values for 100-, 150- and 200 years can be estimated through the Gumbel distribution method. This fits with how the stormwater system in Malaysia is made, which is meant to handle storms, especially those that happen only once every 100 years (Daniel 2020, Zakaria et al. 2017). The result of the Annual Recurrence Interval will be used to create a 2D flood model using a hydrodynamic model. The flood simulation produced through this analysis can then serve as a baseline for flood contingency planning in assessing flood hazards in the future.

### Flood Pattern

The findings from the Kadamaian and Wariu Rivers show similarities with flood patterns observed in other tropical regions, such as the flood frequency studies conducted in the Kelantan River basin. However, the unique topography and

land use patterns in Kota Belud present additional challenges that are not observed in those regions. For example, the higher frequency of extreme events in the Kadamaian River may be attributed to the steep terrain and rapid runoff characteristics, which differ significantly from the relatively flatter regions studied elsewhere. These differences underscore the need for localized flood management strategies that consider the specific geographical and environmental conditions of each basin.

### CONCLUSIONS

Flood frequency analysis using the Gumbel Distribution Method in conjunction with the Weibull plot position technique has proven effective in estimating flood magnitudes and recurrence intervals for the Kadamaian River and Wariu River hydrological stations in Sabah, Malaysia. The goodness-of-fit tests, including the Kolmogorov-Smirnov test and correlation coefficient evaluation, indicated a strong agreement between the distribution model and observed data. The analysis provides a comprehensive understanding of flood hazards by estimating annual recurrence intervals for various return periods.

This study is limited by the availability of long-term hydrological data, which could affect the robustness of the frequency analysis. The data used, while extensive, may not fully capture the variability of flood events due to possible gaps in record-keeping or changes in land use over time. Future research should focus on improving data collection methods, possibly incorporating remote sensing and satellite data to enhance the accuracy of flood frequency predictions. Additionally, exploring the impact of climate change on flood frequency in this region could provide valuable insights for adapting flood management strategies in the future.

### ACKNOWLEDGMENT

Sincere appreciation to the Natural Disaster Research Centre (NDRC) and the Faculty of Science and Natural Resources (FSSA) at Universiti Malaysia Sabah (UMS) for providing access to laboratories and research equipment. The research was supported by the following grants: SDK0012-2017, GUG0534-2/2020, and GKP0036-2021, which covered all research expenses.

### REFERENCES

- Benjamin, J. R. and Cornell, C. A., 1970. *Probability, Statistics, and Decision for Civil Engineers*. McGraw-Hill.
- Bezak, N., Brilly, M. and Sraj, M., 2014. Comparison between the peaks-over threshold method and the annual maximum method for flood frequency analysis. *Hydrological Sciences Journal*, 59(5), pp. 959-977.

Table 2: Flood recurrence interval (ARI) for both hydrological stations.

ARI (Year)	Exceedance probability	Flood peak discharge [ $\text{m}^3 \cdot \text{s}^{-1}$ ]	
		Kadamaian River	Wariu River
2	0.500	714.85	416.28
5	0.200	992.01	576.84
10	0.100	1175.50	683.14
20	0.050	1351.52	785.11
30	0.033	1452.78	843.77
50	0.020	1579.35	917.10
100	0.010	1750.08	1016.01
150	0.007	1849.64	1073.69
200	0.005	1920.19	1114.56

- Bhagat, N., 2017. Flood frequency analysis using Gumbel's distribution method: A case study of Lower Mahi Basin, India. *Journal of Water Resources and Ocean Science*, 6(4), pp.51–54. [DOI]
- Daniel, W., 2020. Kuala Lumpur: A model of resilience. *The Flood People*. Link
- Department of Irrigation and Drainage, 2018. *Hydrological Procedure HP4: Magnitude and Frequency of Flood in Malaysia (Revised and Updated 2018)*. Link
- Farooq, M., Shafique, M. and Khattak, M. S., 2018. Flood frequency analysis of River Swat using Log Pearson Type 3, Generalized Extreme Value, Normal, and Gumbel Max distribution methods. *Arabian Journal of Geosciences*, 11(9), p.853. [DOI]
- Garg, C. and Ananda Babu, K., 2023. Extreme flood calibration and simulation using a 2D hydrodynamic model under a multipurpose reservoir. *Nature Environment and Pollution Technology*, 22(2), pp.977–983. [DOI]
- Hamzah, F. M., Tajudin, H. and Jaafar, O., 2021. A comparative flood frequency analysis of high-flow between annual maximum and partial duration series at Sungai Langat Basin. *Sains Malaysiana*, 50(7), pp.1843–1856. [DOI]
- Jefferin, N., Bolong, N., Sentian, J., Abustan, I., Mohammad, T. A. and Ayog, J. L., 2018. Comparison of GEV and Gumbel's distribution for development of intensity-duration-frequency curve for the flood-prone area in Sabah. *Malaysian Journal of Geosciences*, 2(1), pp.42–44. [DOI]
- Jefferin, N., Bolong, N., Sentian, J., Abustan, I., Mohammad, A. and Ayog, J. L., 2017. The development of intensity-duration-frequency curve for Ulu Moyog and Kaiduan Station of Sabah. *Transactions on Science and Technology*, 4(2), pp.149–156.
- Kordrostami, S., Alim, M. A., Karim, F. and Rahman, A., 2020. Regional flood frequency analysis using an artificial neural network model. *i*, 1–15.
- Millington, N., Das, S. and Simonovic, S. P., 2011. The comparison of GEV, Log-Pearson Type 3, and Gumbel distributions in the Upper Thames River Watershed under global climate models. Link
- Mohamad Hamzah, F., Mohd Yusoff, S. H. and Jaafar, O., 2019. L-moment-based frequency analysis of high-flow at Sungai Langat, Kajang, Selangor, Malaysia. *Sains Malaysiana*, 48(7), pp.1357–1366. [DOI]
- Nabi, Z. and Kumar, D., 2022. Sensitivity of WRF model for simulation of 2014 massive flood over Kashmir region: A case of very heavy precipitation. *Nature Environment and Pollution Technology*, 21(5), pp.2177–2187. [DOI]
- Pankaj, R. and Sunil, K. De., 2015. A comparative approach to flood frequency analysis of the Puthimari River in Assam, India. *Asian Journal of Spatial Science*, 3, pp.90–99. [DOI]
- Pejabat Daerah Kota Belud., 2017. *Pencapaian dan Impak Komuniti Pintar Kota Belud*. Link
- Pusat Ramalan and Amaran Banjir Negara., 2021. *Type of flood in Malaysia. Webinar JPS 2021*. Link
- Romali, N. S. and Yusop, Z., 2017. Frequency analysis of annual maximum flood for Segamat River. *MATEC Web of Conferences*, 103, p.4003. [DOI]
- Romali, N. S., Yusop, Z. and Ismail, A. Z., 2018. Application of HEC-RAS and ArcGIS for floodplain mapping in Segamat Town, Malaysia. 14(43), pp.125–131.
- Selaman, O. S., Said, S. and Putuhen, F. J., 2007. Flood frequency analysis for Sarawak using Weibull, Gringorten, and L-Moments formula. *Journal of The Institution of Engineers, Malaysia*, 68(1), pp.43–52.
- Shabri, A., 2012. The use of Pareto distribution is common in analyzing flood extreme values using a series of peak flows over level. *Jurnal Teknologi*, 39, p. 454. [DOI]
- Sharir, K., Lai, G. T., Simon, N., Ern, L. K., Abd Talip, M. and Roslee, R., 2022. Assessment of flood susceptibility analysis using analytical hierarchy process (AHP) in Kota Belud Area, Sabah, Malaysia. *IOP Conference Series: Earth and Environmental Science*, 1103, p.012005. [DOI]
- Sharir, K. and Roslee, R., 2022. Flood Susceptibility Assessment (FSA) Using GIS-Based Frequency Ratio (FR) Model in Kota Belud, Sabah, Malaysia. *International Journal of Design and Nature and Ecodynamics*, 17(2), pp.203–208. [DOI]
- Sharir, K. and Roslee, R., 2023a. Analisis Indeks Kemudahterancaman Banjir Secara Fizikal, Sosial dan Persekitaran di Kawasan Kota Belud, Sabah, Malaysia. *Sains Malaysiana*, 52(6), pp.1619–1633. [DOI]
- Sharir, K. and Roslee, R., 2023b. Peta Ketumpatan Fizikal bagi Menentukan Unsur Berisiko Banjir di Kawasan Kota Belud, Sabah, Malaysia. *Sains Malaysiana*, 52(7), pp.1939–1954. [DOI]
- Suhaimi, Y., Hazriesyam, Amir, M. and Affendi, I., 2020. Kajian Penyelidikan Bagi Pembinaan Lengkung Keamatan-Tempoh Frekuensi (IDF Curve) Bagi Daerah Pekan, Pahang Menggunakan Kaedah Gumbel. *ANP Journal of Social Science and Humanities*, 2(1), pp.26–35. [DOI]
- Zakaria, S. F., Zin, R. M., Mohamad, I., Balubaid, S., Mydin, S. H. and Mdr, E. M. R., 2017. The development of flood map in Malaysia. *AIP Conference Proceedings*, 1903, p.11632. [DOI]

# Spatial Analyses of Reliability of Solar Power in the Western Part of Iraq

Raid Khider Salman<sup>1†</sup> , Sabah Sultan Farhan<sup>1</sup>, Muneer Naji Al-Falahi<sup>2</sup> and Thaer Eyada Mohammed<sup>1</sup>

<sup>1</sup>Renewable Energy Research Center, University of Anbar, Iraq

<sup>2</sup>Upper Euphrates Basin Development Center, University of Anbar, Iraq

†Corresponding author: Raid Khider Salman; eps.raaidk.salman@uoanbar.edu.iq

**Abbreviation:** Nat. Env. & Poll. Technol.

**Website:** www.neptjournal.com

*Received:* 09-05-2024

*Revised:* 04-07-2024

*Accepted:* 06-07-2024

## Key Words:

Iraq solar power feasibility

Anbar solar energy

Meteorological data

## ABSTRACT

This study presents a comprehensive statistical and meteorological investigation of the western part of Iraq, specifically focusing on the Anbar governorate. To facilitate a detailed analysis, the study area was divided into four sections corresponding to the geographical directions: north, south, east, and west. The primary objective was to evaluate the potential for solar power exploitation in this region by analyzing a wide range of physical and meteorological data. The study encompassed various parameters including solar irradiation, air temperature, and other climatic variables that influence solar power generation. The physical and meteorological data demonstrated a strong correlation in most cases, indicating a consistent trend across the study area. However, two variables—diffuse horizontal irradiation and air temperature—showed inverse trends, deviating from the general pattern. These deviations were carefully analyzed to understand their impact on solar power potential. Furthermore, the analysis revealed that regions with elevated terrains, particularly in the western and southern parts of the Anbar governorate, exhibited higher solar power gains. This finding is significant as it highlights the influence of topography on solar energy potential. The combination of statistical and meteorological data provided a robust framework for assessing the feasibility of solar power projects in the region. The results of this study indicate the promising potential for solar power generation in the Anbar governorate. The integration of statistical and meteorological analyses offers valuable insights for policymakers and stakeholders involved in renewable energy planning and development. This investigation paves the way for future research and practical applications aimed at harnessing solar energy in western Iraq.

## Citation for the Paper:

Salman, R.K., Farhan, S.S., Al-Falahi, M.N. and Mohammed, T.E., 2025. Spatial analyses of reliability of solar power in the western part of Iraq. *Nature Environment and Pollution Technology*, 24(2), p.D1681. <https://doi.org/10.46488/NEPT.2025.v24i02.D1681>

*Note: From year 2025, the journal uses Article ID instead of page numbers in citation of the published articles.*



**Copyright:** © 2025 by the authors

**Licensee:** Technoscience Publications

This article is an open access article distributed under the terms and conditions of the Creative Commons Attribution (CC BY) license (<https://creativecommons.org/licenses/by/4.0/>).

## INTRODUCTION

It is a clear fact that the energy demand has enormously increased during the last few decades due to population expansion. Fossil fuel is no longer the best energy source due to its negative effect on the environment (Balat 2005). Moreover, fossil fuel is a depleted source of energy, so it may be exhausted after a couple of decades (Nacke et al. 2022), leaving us in total darkness and stopping vital systems. Therefore, the demand for clean and renewable energy resources become one of the highest priorities of recent researchers (Sankari & Kumar 2023). The sun is the main source of the whole biological, physical, and chemical activities on Earth. Thus, its power can be considered as the major renewable energy source that can be used to produce clean and non-depleted amounts of energy. According to the literature, solar energy has been used since the 7th century B.C., either in lighting fires using the solar concentrating glassware (Glassmeier 2007, Schoch 2012) or in sustainable nutrition applications such as drying seeds and fruits for consumption in other seasons (Delyannis 2003, Silvi 2008). Therefore, solar energy is considered to be the eldest renewable source used by the human being. After discovering electricity, several solar energy techniques were developed to help generate electric power. However, only two among them maintained the world energy demands for thermal and electric applications (Quaschnig 2016). The first technique is the photovoltaic solar panels, in which solar radiation photons are

absorbed by semiconductor-based material layers to produce electric current via the photoelectric effect (Techo et al. 2024, Salman 2019, Rabehi 2017). The other technique is the solar concentrators, in which the electrical energy is produced by the thermal solar radiation in special power plants besides their fundamental purpose of buildings' heating (Tyagi et al. 2018).

Iraq has one of the longest daylight intervals countries during the whole year (Al-Kayiem & Mohammad 2019). Baghdad receives more than 3,000 hours of sun radiation each year. The intensity of sun radiation ranged between  $416 \text{ W.m}^{-2}$  in January to  $833 \text{ W.m}^{-2}$  in June (Kazem & Chaichan 2012, Al-Kayiem and Mohammad 2019). The western part of Iraq, represented by the Anbar governorate, is the largest part of the country with an open desert enclosure.

With a total population of 1,780,467 people, Anbar needs a huge amount of energy that reaches a peak estimated value of 1500MW(1.5GW) (International Organization for Migration (IOM) 2024). This amount of power comes due to the expansion in publicity during the last decades. However, due to the conflicts that the country generally and the nominated region specifically undergone, the real amount of power provided to the province is only about 400M. This enormous shortage of power needs to be substituted, which urged the engineers and researchers to search for the best solution for this issue. The geographic location of Anbar makes it exposed to high solar radiation in comparison with the other parts of Iraq (see Fig. 1), with the longest interval during the day. Therefore, solar power is the key to the power shortage problem solution. The provincial capital of Anbar is Al-Ramadi, which lies 100 km northwest of Baghdad. Al-Ramadi contains the highest population among the other province districts, with about 620,480 individuals.

Many relative studies have been conducted. One of the most common studies focused on the design and optimization of solar energy systems to improve their efficiency and reduce costs (Al-Naffakh & Al-Qassab 2021, Alturki 2021, Aziz 2022). These studies focused on factors such as the selection of solar panels, the design of the electrical system, and the integration of energy storage systems. Another study related to evaluating the economic feasibility of a hybrid power station that combines solar panels and wind turbines and connects it to the national grid in Al-Hayy City in the center of Iraq. That study involved a detailed analysis of the technical and financial aspects of the project, including the cost of the solar panels and wind turbines, the projected revenues from the sale of electricity, and the potential savings on fuel costs. It has also considered the current state of the electricity grid in the city and the potential benefits and challenges of connecting the hybrid power station to the

national grid (Abass 2021). Another comprehensive study looked at the potential for solar energy in Iraq, covering the topic from the early stages of development to the present day. That article covered the historical background of solar energy development in Iraq, including the current state of solar energy infrastructure and technology in the country, as well as the current policies and regulations that impact the development of solar energy in Iraq (Istepanian 2020).

Overall, the literature studies either concentrated on solar technology or aimed at other parts of Iraq in their research.

The current study aims to investigate the reliability of Anbar, the Iraqi governorate, for solar power exploitation. It looks into the specific geographical, topological, and physical characteristics of different areas in the governorate that can determine its ability to host solar power and what is the best technology that can be utilized within.

## MATERIALS AND METHODS

### Assessment of Solar Radiation in Iraq

It is well known that the solar constant on the earth is  $1353 \text{ W.m}^{-2}$  (Green 1981). The high value of solar radiation in Iraq indicates its high potential for solar energy development, but it is also important to take into account other factors, such as cost, the availability of financing, and the regulatory environment when evaluating the feasibility of solar energy projects in the country. However, the first task in this field is to assess the region's potential itself and the solar physical parameters related to its location. It's noteworthy

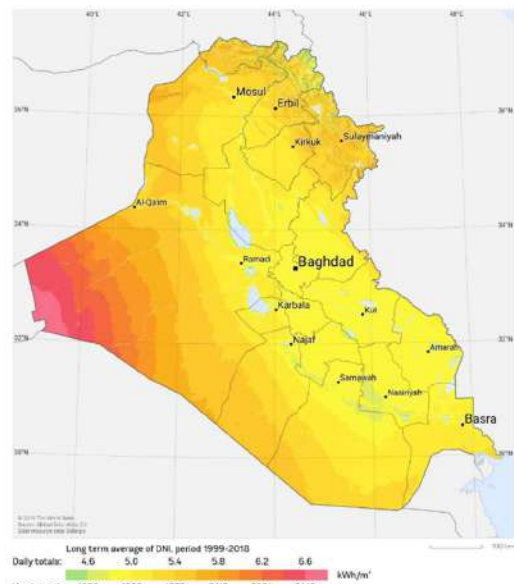


Fig. 1: Iraq's normal solar irradiation means during the year.



to mention that using the solar constant alone isn't enough to estimate the actual solar energy that can be harnessed, and it's important to use other solar parametric measures to estimate the solar energy depending on the location, weather conditions, and other factors that can affect the solar energy reaching the earth surface. Therefore, statistical techniques are essential along with the meteorological data for acquiring precise determinations in this type of investigation. Global Solar Atlas (GSA) was used to collect the location solar parameters. It is an online tool that provides information on the solar resource potential of different locations around the world. It is a comprehensive, interactive map that displays data on solar radiation, temperature, and other meteorological parameters (GSA 2022). Meteorological data were collected by selecting the areas under consideration by navigating the map controls and acquiring their coordinates. The map was then investigated using (the layers) feature to view the types of data such as Global Horizontal Irradiation, Direct Normal Irradiation, etc. The result data were then downloaded using CSV and Excel format. The downloaded data were then analyzed using Pearson's correlation statistical technique to finally get the required data and collect valuable information.

### Determination of the Study Locations

Anbar is the western part of Iraq. It is the largest governorate in the country, bordered by Syria, Jordan, and Saudi Arabia. The capital of Anbar is Al-Ramadi. The other major cities are Fallujah, Haditha, Ana, Rawa, and Al-Qaim. Anbar is an important region in Iraq as it contains several key oil fields, as well as the Haditha Dam, which is one of the largest hydroelectric power stations in the country. Four distinctive locations were chosen as areas of this study, distributed according to the four geographical directions (west, North, East, and South), as illustrated in Fig. 2. The reason behind this procedure is to collect meteorological data from different parts of the province with variations in

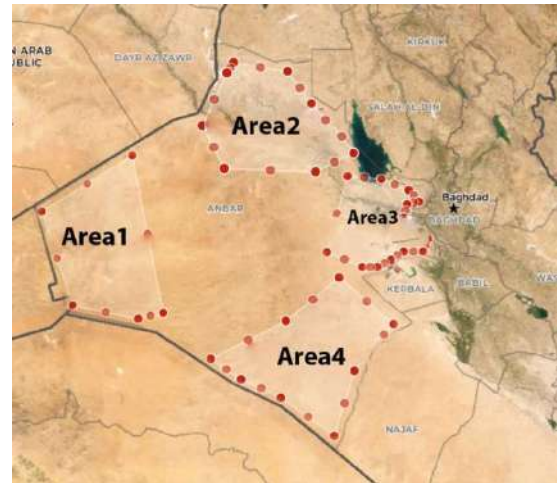


Fig. 2: Areas of study chosen in Anbar governorate.

topological and geographical environments. This information may help optimize the province's reliability statistically for solar power exploitation. The specific regions within the four areas were selected according to security, population density, and social criteria. For instance, due to the conflict status in the regions, the areas were selected to be near the defense and security formations around the governorate. Regarding the social factor, the study gives attention to community structure since some of the areas include conscious and well-educated individuals who can use power sources rationally. Meanwhile, other areas have less awareness about power exploitation.

## RESULTS AND DISCUSSION

### Spatial Optimization

Table 1 illustrates the physical and meteorological data for each one of the nominated areas. Where  $PV_{OUT}$  is the specific photovoltaic power output, DNI is the direct normal

Table 1: Spatial chosen areas and their meteorological data.

Region	Centre (deg)		PVout	DNI	GHI
	Lat	Long	kWh/kW <sub>p</sub>	kWh/m <sup>2</sup>	kWh/m <sup>2</sup>
Areal (West)	32.861449	40.166016	5.03 - 5.22	5.86 - 6.51	5.62 - 5.84
Area2 (North)	31.448154°	42.539063	4.71 - 4.94	5.05 - 5.55	5.28 - 5.51
Area3 (East)	33.431718	43.483887	4.62 - 4.87	4.72 - 5.20	5.29 - 5.51
Area4 (South)	31.298118	42.539063	4.96 - 5.07	5.40 - 5.71	5.65 - 5.75

Region	DIF	GTI <sub>opta</sub>	TEMP	OPTA	ELE
	kWh/m <sup>2</sup>	kWh/m <sup>2</sup>	°C	°	m
Areal (West)	1.71 - 1.93	6.41 - 6.65	19.0 - 20.7	32 - 33	513 - 812
Area2 (North)	1.99 - 2.15	6.03 - 6.29	21.2 - 23.1	31 - 34	125 - 387
Area3 (East)	2.15 - 2.26	5.92 - 6.26	23.2 - 24.6	29 - 33	41 - 185
Area4 (South)	2.08 - 2.17	6.39 - 6.51	22.4 - 23.6	32 - 33	266 - 412

irradiation, GHI is the global horizontal irradiation, DIF is the diffuse horizontal irradiation,  $GTI_{opta}$  is the global tilted irradiation at the optimum angle, TEMP is the air temperature, OPTA optimum tilt of PV modules and ELE is the terrain elevation.

All the physical properties illustrated in Table 1 meet the meteorological trends except for the air temperature and the diffuse horizontal irradiation, which showed distinctive behavior, as Fig. 3 shows. This behavior required statistical correlation between the anomaly parameters and the other regular trended parameters, which will be shown in the next section including the statistical tests and their potential in this study. The variation of the specific photovoltaic power output within the different parts of the governorate may be attributed to the topological characteristics. This is confirmed by the elevation graph, which shows that the north region with the greatest height has the highest photovoltaic output capacity PVout. Meanwhile, the least high area (the west region) also has opposite low PVout. The north and east areas exhibit very similar behavior. Very low variation was shown in direct normal irradiation, though the north surface area is still slightly dominant.

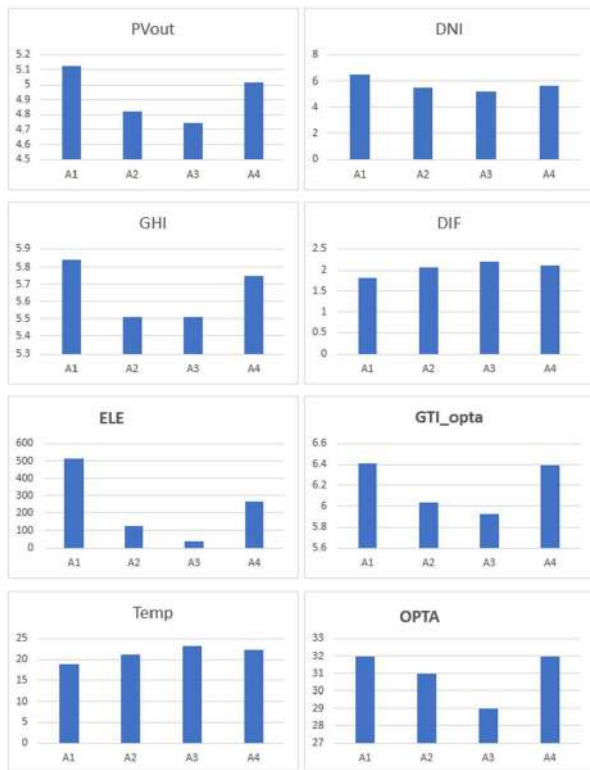


Fig. 3: Physical and meteorological characteristics comparison.

## Statistical Analyses

**Correlation analysis:** As shown before, most parameters show a good agreement with each other, but the Diffuse horizontal irradiation and temperature data showed different trends that need to be investigated statistically. The best technique for this issue is Pearson's correlation test for one of the common parameters and one of the anomaly variables, which can be given by the following equation (Emerson 2015):

$$r = \frac{\sum_{i=1}^n (X_i - \bar{X})(Y_i - \bar{Y})}{\sqrt{\sum_{i=1}^n (X_i - \bar{X})^2 \sum_{i=1}^n (Y_i - \bar{Y})^2}}$$

Where n is the number of data points (sample size)

$X_i$  and  $Y_i$  are the individual data points of the two variables being correlated.

$\bar{X}$  and  $\bar{Y}$  Are the mean (average) of the data points for X and Y, respectively?

The result of r suggests three probabilities

$r=+1$  indicating perfect positive correlation (if X increases, Y linearly increases)

$r=-1$  indicating perfect negative correlation (if X increases, Y linearly decreases)

$r=0$  indicating no correlation between the tested variables

SPSS was used to run the correlation test. Table 2 shows Pearson's correlation test between the two distinctive variables, the specific photovoltaic power output, and the diffuse horizontal irradiation. The Pearson correlation coefficient is -0.799, indicating a strong negative correlation between the two variables. However, the negative correlation suggests an inverse relation between diffuse horizontal irradiation (DIF) and the specific photovoltaic output (SPVout). These statistical indications render an atmospheric factor that can negatively affect the solar power output. This may be attributed to the cloudy and/or overcast days that can disperse and hence reduce the light reaching the photovoltaic panels. Which in turn leads to a reduction in the photovoltaic power output.

Table 2: Statistical Correlation data.

		SPVout	DIF
PVout	Pearson Correlation	1	-0.799
	Sig. (2-tailed)	0.201	
	N	4	4
DIF	Pearson Correlation	-0.799	1
	Sig. (2-tailed)	0.201	
	N	4	4

**Cumulative distribution graphs:** A cumulative distribution graph is of high importance graph that can help predict the behavior of the variable under consideration. Fig. 4 shows the cumulative distribution graph for the different areas. In general, all the areas follow the same pattern with slight variation in the west and south areas. The photovoltaic output probabilities from east and north areas show steadiness at lower profiles (from 4.4- 4.7 KW/KWp), after which they increased dramatically. No such steadiness can be observed in the west and south regions. Indicating that the optimized areas in relation to the photovoltaic technology exploitation are the west and south areas. The output is also greater within these regions than in the remaining areas. The cumulative data for the four areas propose the following indications:

1. Area 1: This area exhibits a gradual increase in the output of SPV, which implies solar radiation consistency. In other words, it suggests minimal cloudy times and more clear skies.
2. Area 2: The area 2 curve shows stepping behavior, in which the SPV values are higher at lower percentages. This implies intensive sunlight receiving throughout specific intervals. In other words, this area might occasionally undergo cloudy days.
3. Area 3: This area shows balanced weather and moderate solar irradiation, which is revealed by the flat curve and the consistency in the curve developing with the percentage.
4. Area 4: lastly, Area 4 shows similar behavior to Area 1, but might be with additional factors such as topological factors that affect the solar irradiation.

## CONCLUSIONS

The western region of Iraq, represented by Anbar governorate, showed promising indications regarding with possibility of using solar photovoltaic panels. The west and south areas

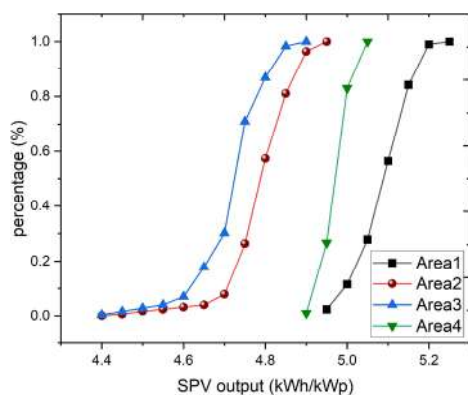


Fig. 4: Cumulative distribution graph for SPVout for the four areas.

of the governorate exhibited greater potential regarding the nominated technology. The elevation of terrains plays a major role in photovoltaic gain. Air temperature and diffuse horizontal irradiation have a negative potential on the solar power gain within these areas.

The four selected areas in the governorate show inconsistency regarding their meteorological parameters. The west and southwestern areas have more stable sunny days in comparison with the other two areas. The eastern area has modest weather, so the solar power output from it would be more stable but less than the output of the western and southwestern areas. The northern part of the governorate exhibits fluctuated intervals of sunny days, so on some days, high solar power output may be yielded. Meanwhile, on other days, the weather is more cloudy, and only minimum output may be produced.

Overall, the analyzed data revealed promising indications and significant feasibility for the governorate to exploit solar power technology.

## REFERENCES

- Abass, A.Z., 2021. Economic feasibility study of a hybrid power station between solar panels and wind turbine with the national grid in Al-Hayy City in the central of Iraq. *IOP Conference Series: Materials Science and Engineering*, 75, pp.10213-10236.
- Al-Kayiem, H.H. and Mohammad, S.T., 2019. Potential of renewable energy resources with an emphasis on solar power in Iraq: *International Journal of Energy Studies*, 8(1), p.42.
- Al-Naffakh, J. and Al-Qassab, S., 2021. Comparing the growth of renewable energy sources in Turkey, Iran, and Iraq. *Journal of Renewable Energy Studies*, 2(2), pp.21-26.
- Alturki, F.A., 2021. Optimal sizing of autonomous hybrid energy system using a supply-demand-based optimization algorithm. *International Journal of Energy Research*, 45(1), pp.605-625. [DOI]
- Aziz, A.S., 2022. Design and optimization of a grid-connected solar energy system: Study in Iraq. *Sustainability*, 14(13), p.8121. [DOI]
- Balat, M., 2005. Usage of energy sources and environmental problems. *Energy Exploration & Exploitation*, 23(2), pp.141-167. [DOI]
- Delyannis, E., 2003. Historic background of desalination and renewable energies. *Solar Energy*, 75(5), pp.357-366. [DOI]
- Emerson, R.W., 2015. Causation and Pearson's correlation coefficient. *Journal of Visual Impairment and Blindness*, 109(3), pp.242-244. [DOI]
- Glassmeier, K.H., 2007. The Rosetta mission: Flying towards the origin of the solar system. *Space Science Reviews*, 128(1), pp.1-21. [DOI]
- Green, M.A., 1982. *Solar cells: Operating principles, technology, and system applications*. Englewood Cliffs.
- GSA, 2022. *Global Solar Atlas*. Available at: Global Solar Atlas
- International Organization for Migration (IOM), 2024. *Progress toward durable solutions in Iraq: Anbar*. IOM, Iraq. Available at: IOM Report
- Istepanian, H.H., 2020. *Iraq solar energy: From dawn to dusk*. Friedrich-Ebert-Stiftung Jordan et Iraq.
- Kazem, H.A. and Chaichan, M.T., 2012. Status and future prospects of renewable energy in Iraq. *Renewable and Sustainable Energy Reviews*, 16(8), pp.6007-6012. [DOI]
- Nacke, L., Cherp, A. and Jewell, J., 2022. Phases of fossil fuel decline: Diagnostic framework for policy sequencing and feasible transition pathways in resource-dependent regions. *Oxford Open Energy*, 1, p.26. [DOI]

- Quaschnig, V., 2016. *Understanding Renewable Energy Systems*. Routledge. [DOI]
- Rabehi, A., 2017. Direct and diffuse solar radiation components estimation based on RBF model: Case study. *Renewable Energy Studies*, 31, pp.93-110.
- Salman, R., 2019. Research note: Light-emitting diodes as solar power resources. *Lighting Research & Technology*, 51(3), pp.476-483. [DOI]
- Sankari, S.S. and Kumar, P.S., 2023. A review of deep transfer learning strategy for energy forecasting. *Nature Environment and Pollution Technology*, 22(4), pp.1781-1793. [DOI]
- Schoch, R.M., 2012. *Forgotten Civilization: The Role of Solar Outbursts in Our Past and Future*. Simon and Schuster.
- Silvi, C., 2008. History and future of renewable solar energy. *Desalination*, 51(3), pp.409-414. [DOI]
- Techo, J., Techo, S., Palamanit, A., Saniso, E., Chand, A.A. and Prasanna, P., 2024. Enhanced solar photovoltaic power production approach for electric vehicle charging station: Economic and environmental aspects. *Nature Environment and Pollution Technology*, 23(1), pp.215-223. [DOI]
- Tyagi, H., Agarwal, A.K., Chakraborty, P.R. and Powar, S., 2018. *Introduction to applications of solar energy* (pp. 10-3). Springer Singapore.



# Effect of Biochar and Silicon with Different Phosphorus Levels on Maize Yield and Soil Chemical Properties

Muhammad Wasil Bin Abu Bakar<sup>1</sup>, M. K. Uddin<sup>1†</sup>, Susilawati Kasim<sup>1</sup>, Syaharudin Zaibon<sup>1</sup>, S. M. Shamsuzzaman<sup>2</sup> and A. N. A. Haque<sup>3</sup>

<sup>1</sup>Department of Land Management, Faculty of Agriculture, Universiti Putra Malaysia, 43400, UPM Serdang, Selangor, Malaysia

<sup>2</sup>Soil Resources Development Institute, Dhaka, Bangladesh

<sup>3</sup>Bangladesh Agricultural Research Council, BARC, Dhaka, Bangladesh

†Corresponding author: M. K. Uddin; mkuddin@upm.edu.my

**Abbreviation:** Nat. Env. & Poll. Technol.  
**Website:** www.neptjournal.com

*Received:* 28-08-2024

*Revised:* 15-10-2024

*Accepted:* 21-10-2024

## Key Words:

Phosphorus  
 Biochar  
 Silicon  
 Fertilizer  
 Productivity of maize

## ABSTRACT

Silicon fertilizer combined with biochar improved the utilization of phosphorus fertilization applications. The experiment was carried out with eight treatment combinations with varying proportions of rice husk biochar, silicon, and phosphorus in a completely randomized design with 75 days of growth in the greenhouse. To identify the optimum rate of phosphorus combined with rice husk biochar and Si for maximizing maize yield and soil chemical properties. This experiment showed that the application of biochar combined with silicon has the potential to reduce the amount of phosphorus fertilizer requirement. The application of 5 t ha<sup>-1</sup> RHB + 100% Si + 25% TSP showed the highest pH compared to other treatments. While application of 2.5 t ha<sup>-1</sup> RHB + 100% Si + 100% TSP showed the highest exchangeable K, Ca and Mg. Moreover, the application of 5 t ha<sup>-1</sup> RHB + 100% Si + 100% TSP recorded the highest dry biomass compared to other treatments. Lastly, the application of 5 t ha<sup>-1</sup> RHB + 100% Si + 50% TSP Showed the highest cob length(cm), cob weight(g), no of grain per cob, and grain yield (t.ha<sup>-1</sup>) compared to other treatments. The combined application of biochar and silicon, along with 50% phosphorus, is recommended for improving maize yield and soil health in greenhouse conditions.

## INTRODUCTION

Maize is one kind of important crop that is being used in daily life and has started to increase in demand all around the world (He et al. 2023). The cultivation of this crop has to face many problems in today's world that cause its production to be reduced and fail to fulfill the demand (Ali et al. 2023). The available soil mostly being affected by a few factors such as alkalinity, acidity, imbalance of nutrient toxicity, and water stress (Msimbira & Smith 2020).

This suffering by crops in soil because the acidic soil is high in hydrogen ions with a high concentration of Al content (Neina 2019). Adding cation (Mg, K & Ca) by application of chemical fertilizer can be one of the solutions to reduce soil acidity (Shankara et al. 2022). Other than that, adding silicon would also be practical to reduce the effect of aluminum and manganese while at the same time handling the P deficiency problem in acidic soil (Pontingo et al. 2015). Thus, as an alternative to single silicon, biochar should be applied together to improve its function (Sattar et al. 2022). Moreover, applying biochar together with the fertilizer would promote N retention and C stability together with improving N uptake and minimizing the loss of N (Peng et al. 2021). The biochar would also improve phytoremediation and lower health risks caused by fertilizer (Ibrahim et al. 2016). Different types of biochar would have different content of elemental compositions (i.e., wood

## Citation for the Paper:

Abu Bakar, M.W.B., Uddin, M.K., Kasim, S., Zaibon, S., Shamsuzzaman, S.M. and Haque, A.N.A., 2025. Effect of biochar and silicon with different phosphorus levels on maize yield and soil chemical properties. *Nature Environment and Pollution Technology*, 24(2), p. D1727. <https://doi.org/10.46488/NEPT.2025.v24i02.D1727>

*Note: From year 2025, the journal uses Article ID instead of page numbers in citation of the published articles.*



Copyright: © 2025 by the authors

Licensee: Technoscience Publications

This article is an open access article distributed under the terms and conditions of the Creative Commons Attribution (CC BY) license (<https://creativecommons.org/licenses/by/4.0/>).

mixture biochar has a higher content of H, O, N, and S than biochar from maize and meadow grass) (Ullah et al. 2018).

To solve the problem regarding acidity in the soil, the focus needs to be given to the functional group (carboxylic and phenolic) that needs to be neutral (Mosharrof et al. 2022). Unfortunately, freshly prepared biochar has low carboxylic and phenolic groups that give less effect to the neutralization (Mia et al. 2017). Most researchers agree that biochar combined with other compounds would have a beneficial effect in lowering the acidity effect and raising the pH (Islam et al. 2021, Haque et al. 2021, Mosharrof et al. 2022), soil carbon removal (Zheng et al. 2020), promote rapid growth, (Brennan et al. 2014), adjust soil structure together with improvement nutrient uptake (Peng et al. 2019), and some biochar also seemed to be practical to remove few types of pollutant (i.e., blue, tetracycline, pesticide and phosphate) (Li et al. 2020). Biochar is also applicable to reduce the effect of Al & Fe concentration that causes the effect to increase in pH (Shetty & Prakash 2020).

These suggest that biochar could help to reduce the acidity effect and improve production. The effects of biochar with silicon should be further enhanced because both have the same function to control the acidity of soil through alkaline and cation properties. The combining of both of these materials should have more impact on the soil quality (Pontigo et al. 2015, Abukari 2014). Moreover, previous studies showed that the silicon application would benefit by increasing the pH (De Sousa et al. 2019), boosting the photosynthesis rate (Pitann et al. 2021), and supporting plant development (Zhiming et al. 2014). To get optimal outcomes, the rate of biochar and silicon needs to be justified. Other than that, low pH values can be highly caused by phosphorus deficiency and high potential for N<sub>2</sub>O emissions (Xie et al. 2020). Mensah and Frimpong (2018) report that in sub-Saharan Africa (SSA), soil also faces problems through continuous cultivation and rapid organic matter mineralization that will affect the properties of soil. However, these studies were conducted in various rates of biochar and silicon without the reduction of any supply of NPK fertilizer.

The application of biochar and silicon fertilizer helps to reduce the phosphorus fertilizer application and improve the maize growth and soil properties. Hence, the main objective of the study was to examine the performance of maize after the application of biochar with silicon fertilizer and with variable rates of P fertilizer.

## MATERIALS AND METHODS

### Experimental Site

A pot experiment was conducted for 75 days (October to

December 2022) in the greenhouse UPM at 2°98'36.6" N (north) latitude and 101°73'81.9" E (east) longitudes with an elevation of 56.8 m from sea level at the west coast of Peninsular Malaysia.

### Experimental Design and Treatments

The pot experiment was laid out in a completely randomized (CRD) with three replications having a pot size of 38 cm(height) and 32 cm(diameter). The Bungor (Typic Paleudult; Order: Ultisol) soil series was collected in depth from 0–20 cm from Taman Pertanian, UPM, Puchong, Selangor (2°58'59.7" N latitude; 101°38'47.5" E longitude). It was air-dried and sieved through a 2 mm before chemical analysis. For the greenhouse experiment, the soil was sieved to 4mm and applied in all of the pots at a rate of 20 kg of soil pot<sup>-1</sup>. The biochar treatment was applied to the soil based on the dose required with a recommended rate of 10 t.ha<sup>-1</sup>, mixed well, and left for about one week before adding silicon 150 kg.ha<sup>-1</sup> was recommended as the optimal amount for maize by Xie et al. (2014). Additional N & K based on MARDI recommendation fertilizer: 120 kg N.ha<sup>-1</sup> in the form of urea and 100 kg Potassium in the form of Muriate of potash 45 (MOP) was applied. Two recommended treatments from previous studies (Bakar et al. 2024). It was (50% RHB+ 100%Silicon) and (25% RHB+ 100%Silicon) and continues to implement together with various rates (0%,50%,75% & 100%)

Table 1: Treatments for conducting the experiment.

Treatment	
1.	(50% RHB) + (100% Si) + (0%P)
2.	(50% RHB) + (100% Si) + (25%P)
3.	(50% RHB) + (100% Si) + (50%P)
4.	(50% RHB) + (100% Si) + (100%P)
5.	(25% RHB) + (100% Si) + (0%P)
6.	(25% RHB) + (100% Si) + (25%P)
7.	(25% RHB) + (100% Si) + (50%P)
8.	(25% RHB) + (100% Si) + (100%P)

Table 2: Equivalent amount in the experiment setup.

Element	Application	Recommended rate [kg.ha <sup>-1</sup> ]	Experiment setup rate (g/20kg soil)
Biochar	Rice Husk	10000	700
Silicon	Silicon (SiO <sub>2</sub> :40%)	150	1
Nitrogen	Urea	120	0.8
Phosphorus	Triple Superphosphate (TSP)	60	0.4
Potassium	Muriate of Potash (MOP)	90	0.6

of Triple Superphosphate (TSP) for this research. In this experiment, the F1 Hybrid Sweet Corn variety was collected from a local market as a test crop, and it is also a common variety used by Malaysian farmers. The maize seedling was put and watered regularly to maintain a soil moisture content of 60-70% of water holding capacity during the growth period and being destructively harvested 75 days after planting. Tables 1 and 2 show the treatment combination:

### Post-Harvest Soil Analysis

**Acidity (pH):** Soil Ph was determined in water at a soil-to-solution ratio of 1:10 (Tan 1995). 1g oven-dried soil sample was placed into a vial and 10 mL Distilled water was added to it. It was shaken thoroughly for 5 min and allowed to stand for 2 h, and the pH of the suspension was then measured using a pH meter for soil samples respectively.

**Soil available P:** 0.5M sodium bicarbonate,  $\text{NaHCO}_3$ , was prepared (21g of sodium bicarbonate was dissolved in about 450 mL distilled water and was adjusted to 8.5 pH with 1N NaOH and marked up to volume). 1 g of soil sample was weighed into the plastic vial, and 20 mL of the 0.5M sodium bicarbonate was added. It was shaken for 30 min, filtered by filter paper no. 2, and sent to ICP for phosphorus analysis (Olsen et al. 1954)

### Exchangeable cation(magnesium, potassium & calcium):

The exchangeable cations were extracted using 100 mL of 1N ammonium acetate (Schollenberger & Simon 1945). Ashless cotton was put down at the hole of the leaching tube to prevent the soil from passing through the tube and covered with filter paper of small size before putting the 10g soil sample. Another filter paper was put on the soil sample to prevent the soil from being inverted when the solution was poured. The leaching valve was adjusted to make sure that the ammonium acetate flowed through the soil sample slowly with the speed of one drop to another drop, around 6 to 8 seconds. The concentration of K, Ca and Mg in the solutions was determined by the inductively coupled plasma-atomic emission spectrometry (ICP).

**Soil exchangeable aluminium:** 1N KCL solution was prepared. Then, 5 g of soil was in a plastic vial, added with 50 mL KCL solution, the cap was closed, and the solution was shaken for 30 min. After that, the supernatant was slowly passed through the Whatman No. 42 filter paper and sent to ICP for aluminum analysis.

### Plant Material Analysis

**Leave number and plant height analysis:** The leave number of open leaves was counted at (75 DAS), and the plant height was determined using a measuring tape at harvest (75 DAS) from the base to the tip of the longest leaf (Lai 2019).

**Leaf photosynthesis rate ( $\mu\text{mol CO}_2\text{m}^{-2}\text{s}^{-1}$ ) and conductance ( $\text{mol H}_2\text{O m}^{-2}\text{s}^{-1}$ ):** The leaf chlorophyll content was measured using a portable chlorophyll meter (SPAD-502 Konica Minolta, Inc., Tokyo, Japan). The Chlorophyll reading was taken from the middle part of the largest leave of each plant using the meter (SPAD-502, Konica Minolta, Osaka, Japan) (Alarefee et al. 2021), and the conductance reading was recorded at the same time.

**Plant fresh weight and biomass(g):** After harvest, the shoot (stem and leaves) were washed and dammed with tissue paper before being dried in an oven at 60°C for 72 h and weighed again for the biomass with consistent weight (Mosharrof et al. 2021a)

**Shoot nutrient uptake (ppm):** The dried shoot was blended and again dried in the crucible in an oven, then put in a glass desiccator before 0.25g was taken to extract the macro element of the shoot by using the drying ashing method (Yuan et al.2016). The concentration of P, K Ca, and Mg were determined using inductively coupled plasma-atomic emission spectrometry (ICP). The result is then converted into (ppm) by this formula:

$$\text{Nutrient concentration(ppm)} = \text{Mean(mg/L)} \times$$

$$\left( \frac{\text{mark up volume(50mL)}}{\text{weight(0.25g)}} \right)$$

The maize nutrient uptake was later calculated by multiplying with the respective dry-weight oven--the dry weight of the plant part with the nutrient content (Alarefee et al. 2021).

$$\text{Nutrient Uptake} = \text{Nutrient Content(ppm)} \times \text{Biomass(g)}$$

### Cob Yield Component

**Cob length, weight, grain per cob, and grain yield:** The cob length was measured before destroying the plant. While the cob weight(g) was measured using weight balance after harvest. Then, total grain weight and 100-grain weight per cob were measured to calculate the grain per cob. Lastly, the grain yield was recorded as stated in the formula below:

$$\text{grain yield} \frac{\text{t}}{\text{ha}} =$$

$$\left( \frac{\text{Total grain weight per cob} \times (3 \times 10^6 \text{ Kg Soil per Ha})}{20 \text{ Kg Soil}} \right)$$

### Statistical Analysis

Analysis of Variance (ANOVA) procedure was used to analyze all of the data, and Tukey's Honestly

A significant Difference (HSD) test was used to separate the means. Repeated measures analyses were performed

on all parameters using John's Macintosh Project (JMP) Analysis Software ( $p \leq 0.05$ ).

## RESULTS AND DISCUSSION

### Effect of RHB, Silicon Fertilizer, and Varying Doses of Phosphorus on the Post-Harvest Soil Properties

It was noticed that pH from post-harvest soil was significantly affected by biochar and silicon with varied phosphorus fertilizer applications ( $p < 0.05$ ) (Table 3). The available pH was higher in T2(6.70) followed by T1, T3 & T7(6.47). This finding was similar to Mosharrof et al. (2021b), which observed 6.14 pH with the application of recommended RHB and phosphorus. The acidity also reduced with the low dose of phosphorus may be caused by the effectiveness applied after reducing the Al and Fe stress, making the pH increase and improving the plant development (Xiong et al. 2024, Bakar et al. 2024, Ahmad et al. 2018). The available P was significantly affected by the application of different rates of biochar, silicon, and phosphorus fertilizer. The highest P was recorded by T7(10.75), followed by T8(8.85), while T6(2.3) recorded the lowest P. Biochar application would increase phosphorus availability (Seleiman et al. 2020). Thus, the low dose of phosphorus with an application of biochar still shows high results (Glaser & Lehr 2019). The combining of silicon and fertilizer would become an agent to make a binding that will make the fertilizer embedded in soil that would reduce the leaching of it, and remain available in the soil (Nguyen 2021).

The application of Silicon, biochar and phosphorus fertilizer significantly affected the Al content in soil. The highest total Al in soil was observed from T<sub>2</sub>(0.031), followed by T<sub>1</sub>(0.023/kg), and the lowest was recorded by T<sub>6</sub>(0.001 CmoL.kg<sup>-1</sup>). One finding shows that the application of rice husk with high silicon would reduce the phytotoxicity

(Wang et al. 2019). The lower dose of phosphorus seemed to be still effective in reducing the Al may be caused by the addition of silicon with the presence of its silicate surface would absorb and reduce the Al effect (Pontigo et al. 2015, Haynes 2014).

The application of different rates of phosphorus with biochar and silicon fertilizer significantly affected the exchangeable cation of the soil (Ca, K, and Mg). The highest Exchangeable Ca, K & Mg recorded by T8(2.96, 2.09 & 1.94) cmoL.kg<sup>-1</sup> and lowest K & Ca recorded by T2(1.52 & 0.67) cmoL.kg<sup>-1</sup>. While the lowest exchangeable Mg was recorded by T5(0.42 cmoL.kg<sup>-1</sup>). This cation may increase through the high consumption of H<sup>+</sup> promoted by biochar (Mosharrof et al. 2021b), and applying biochar and silicon together seemed to be the medium to change the property of hydrophilic into hydrophobic. That would delay nutrient release from the soil (Weeks & Hettiarachchi 2019)

### Effect of RHB, Silicon Fertilizer, and Varying Doses of Phosphorus on Plant Height, Leaf Number, Conductance, Photosynthesis Rate and Dry Biomass of Maize Plant

Different availability of phosphorus significantly together with silicon and biochar application affected (Appendix F1) the plant height(cm) of the maize measure at 65 DAS. T5 showed the shortest height(119.63cm) compared to other treatments. All the remaining treatments resulted in higher height, ranging from 154.27 cm to 180.23 cm in 65 days. It was noticed that the Biomass of maize was significantly affected by the availability of biochar with biochar and silicon application ( $p < 0.05$ ) (Table 4). The highest biomass was recorded by T4(81.47), Followed by T5(76.74), while the lowest biomass was recorded by T1(52.13). One research recorded that the maize treated with Silicon 40 kg ha<sup>-1</sup> and 80 kg.ha<sup>-1</sup> showed results of shoot heights 130.4cm and 133.5 cm while 128.5 cm for control (Younas et al. 2021). While

Table 3: Post-harvest soil properties.

Treatment	pH	P[Mg.kg <sup>-1</sup> ]	EXC Ca	EXC K	EXC Mg	Al [CmoL.kg <sup>-1</sup> ]
T1	6.47ab±0.07	7.75ab±0.49	2.54b±0.04	1.08bc±0.02	0.96b±0.02	0.023ab±0.004
T2	6.7a±0.06	8.1ab±1.91	1.52c±0.04	0.67e±0.02	0.43f±0.01	0.031a±0.001
T3	6.47ab±0.07	5.9ab±0.29	2.63ab±0.04	1.04bc±0.02	0.67cd±0.01	0.005c±0.001
T4	6.33ab±0.07	3b±1.50	2.60ab±0.20	1.10b±0.04	0.71c±0.01	0.012bc±0.004
T5	5.2d±0.00	8.53ab±0.18	1.54c±0.06	0.88d±0.01	0.42f±0.003	0.012bc±0.001
T6	6.27bc±0.07	2.3b±0.12	1.83c±0.02	0.76e±0.01	0.49e±0.01	0.001c±0
T7	6.47ab±0.07	10.75a±0.38	2.43b±0.04	0.97cd±0.01	0.65d±0.004	0.006c±0.002
T8	5.87c±0.18	8.85ab±3.15	2.96a±0.02	2.09a±0.03	1.94a±0.02	0.007c±0.002

Means within the same column followed by the different letters are significantly different at  $p \leq 0.05$  (Tukey's HSD test). The column represents the mean values ± standard error. T1 = (50% RHB) + (100% Si) + (0%P), T2=(50% RHB) + (100% Si) + (25%P), T3= (50% RHB) + (100% Si) + (50%P), T4= (50% RHB) + (100% Si) + (100%P), T5= (25% RHB) + (100% Si) + (0%P), T6= (25% RHB) + (100% Si) + (25%P), T7= (25% RHB) + (100% Si) + (50%P), T8= (25% RHB) + (100% Si) + (100%P).



Table 4: Plant morphological and physiological parameters.

Treatment	Plant height	Leaf no	Conductance ( $\text{mol H}_2\text{O m}^{-2}\text{s}^{-1}$ )	Photosynthesis rate [ $\mu\text{mol CO}_2\text{m}^{-2}\text{s}^{-1}$ ]	Dry biomass
T1	174.07b $\pm$ 0.31	11a $\pm$ 0.25	0.206b $\pm$ 0.001	32.5a $\pm$ 0.31	52.13d $\pm$ 0.98
T2	157.37d $\pm$ 0.37	10b $\pm$ 0.00	0.268a $\pm$ 0.003	32.7a $\pm$ 0.95	64.86c $\pm$ 1.59
T3	166.40c $\pm$ 1.14	11a $\pm$ 0.00	0.136c $\pm$ 0.001	28.5b $\pm$ 0.49	54.22d $\pm$ 1.22
T4	154.27d $\pm$ 0.43	10b $\pm$ 0.00	0.146c $\pm$ 0.004	23.8c $\pm$ 0.78	81.47a $\pm$ 0.30
T5	119.63e $\pm$ 0.19	10b $\pm$ 0.00	0.274a $\pm$ 0.006	30.6ab $\pm$ 0.01	76.74b $\pm$ 0.43
T6	174.60ab $\pm$ 2.87	10ab $\pm$ 0.00	0.174bc $\pm$ 0.017	33.4a $\pm$ 1.18	67.97c $\pm$ 1.01
T7	180.23a $\pm$ 1.54	11a $\pm$ 0.47	0.208b $\pm$ 0.001	18.8d $\pm$ 0.00	69.05c $\pm$ 0.69
T8	168.87bc $\pm$ 1.10	11a $\pm$ 0.50	0.211b $\pm$ 0.023	24.4c $\pm$ 0.06	66.90c $\pm$ 0.58

Means within the same column followed by the different letters are significantly different at  $p \leq 0.05$  (Tukey's HSD test). The column represents the mean values  $\pm$  standard error. T1 = (50% RHB) + (100% Si) + (0%P), T2=(50% RHB) + (100% Si) + (25%P), T3= (50% RHB) + (100% Si) + (50%P), T4= (50% RHB) + (100% Si) + (100%P), T5= (25% RHB) + (100% Si) + (0%P), T6= (25% RHB) + (100% Si) + (25%P), T7= (25% RHB) + (100% Si) + (50%P), T8= (25% RHB) + (100% Si) + (100%P).

Opala (2017) stated that a high rate of phosphorus would have more impact on the Plant height after 6 weeks. The application of biochar and silicon increases the development of plants by promoting a rise in solubilizing organic phosphate, mineralizing inorganic phosphate, and nutrient uptake (Raza et al. 2021).

In this study, it was noticed that the silicon and biochar with different phosphorus availability significantly affected (Appendix F3) ( $p < 0.05$ ) the conductance ( $\text{mol H}_2\text{O m}^{-2}\text{s}^{-1}$ ) from maize leaf (Table 4). The conductance was higher in T5(0.274), followed by T2(0.268), while T3(0.136) recorded the lowest conductance. Phosphorus application on the soil would probably tend to improve the stomata opening and increase the conductance (Zangani et al. 2021). Although the dose of phosphorus in this research was not constant, still outcome with not high range in the conductance may be caused by the presence of silicon that covers the function of phosphorus to reduce chlorophyll synthesis and lower the the leaf water potential (Rehman et al. 2021).

### Effect of RHB, Silicon Fertilizer, and Varying Doses of Phosphorus on Cob Length, Cob Weight, Number of Grains Per Cob, and Grain Yield

Cob length, Cob weight, number of grains per cob, and grain yield of maize were enhanced significantly (Appendix F6, F7, F8 & F9) by various treatments (Table 5). A longer but statistically similar cob length was observed in T3, T4, and T5 (up to 20.77 g), while the lightest was observed in T5 (16.4g). The maximum cob weight, No of grain, and yield grain were noted in T3 (160.56 g, 417.08 g, and  $14.6 \text{ t.ha}^{-1}$ , respectively), while the lowest rate of biochar, silicon, and phosphorus recorded the lowest T5(61.23g, 120.24 g, and  $4.21 \text{ t.ha}^{-1}$ ). Application of biochar with NPK would produce a high yield compared to sole biochar (Arif et al. 2012), and higher doses would produce a higher yield (Islam et al. 2018). Biochar improves the soil structure, root growth, and nutrient uptake and promotes high yield (Liu et al. 2021). Although biochar has a high content of phosphorus, TSP fertilizer still needs to be implied as targeted for the high yield because

Table 5: Cob development and maize yield parameters.

Treatment	Cob length [cm]	Cob weight [g]	No grain per cob	grain yield [ $\text{t.ha}^{-1}$ ]
T1	19.4ab $\pm$ 1.15	112.21b $\pm$ 8.14	360.14a $\pm$ 7.89	12.60a $\pm$ 0.28
T2	19.13ab $\pm$ 0.91	135.76ab $\pm$ 14.41	180.11bc $\pm$ 24.99	6.30bc $\pm$ 0.87
T3	21.27a $\pm$ 0.52	160.56a $\pm$ 7.12	417.08a $\pm$ 11.84	14.60a $\pm$ 0.41
T4	20.77a $\pm$ 0.318	151.87ab $\pm$ 12.76	400.38a $\pm$ 15.24	14.01a $\pm$ 0.53
T5	16.4b $\pm$ 0.25	61.23c $\pm$ 7.95	120.24c $\pm$ 22.41	4.21c $\pm$ 0.78
T6	20.77a $\pm$ 0.63	125.96ab $\pm$ 7.61	218.8b $\pm$ 2.70	7.66b $\pm$ 0.09
T7	18.73b $\pm$ 1.07	119.22ab $\pm$ 10.32	337.36a $\pm$ 16	11.81a $\pm$ 0.56
T8	19.53ab $\pm$ 1.08	118.79ab $\pm$ 6.0	339.38a $\pm$ 19.25	11.88a $\pm$ 0.67

Means within the same column followed by the different letters are significantly different at  $p \leq 0.05$  (Tukey's HSD test). The column represents the mean values  $\pm$  standard error. T1 = (50% RHB) + (100% Si) + (0%P), T2=(50% RHB) + (100% Si) + (25%P), T3= (50% RHB) + (100% Si) + (50%P), T4= (50% RHB) + (100% Si) + (100%P), T5= (25% RHB) + (100% Si) + (0%P), T6= (25% RHB) + (100% Si) + (25%P), T7= (25% RHB) + (100% Si) + (50%P), T8= (25% RHB) + (100% Si) + (100%P).

Table 6: Nutrient uptake.

Treatment	Uptake P [ppm.g <sup>-1</sup> ]	Uptake K[ppm.g <sup>-1</sup> ]	Uptake Ca[ppm.g <sup>-1</sup> ]	Uptake Mg[ppm.g <sup>-1</sup> ]
T1	378.59de+20	17337.2d+18.22	2138.24d+8.67	578.76f+14.71
T2	422.15de+15.4	20789.1b+28.5	3221.23b+7.33	984.65bc+13.2
T3	698.09b+7.09	17129.6d+38.1	2346.87cd+2.11	812.15e+8.88
T4	426.27d+8.81	26980.9a+31.2	4273.6a+18.63	1074.65ab+34.57
T5	510.1c+3.98	20713.9b+16.6	3270.59b+7.91	980.95bc+16.89
T6	363.46de+9.15	18525.3c+20.7	2672.78c+3.75	915.23cd+20.74
T7	352.79e+18.79	19286.9c+9.16	2618.04c+1.72	863.91de+9.2
T8	1143.62a+22.82	21050.1b+9.47	2543.41cd+1.1	1135.4a+32.1

Means within the same column followed by the different letters are significantly different at  $p \leq 0.05$ ; (Tukey's HSD test). The column represents the mean values  $\pm$  standard error. T1 = (50% RHB) + (100% Si) + (0%P), T2=(50% RHB) + (100% Si) + (25%P), T3= (50% RHB) + (100% Si) + (50%P), T4= (50% RHB) + (100% Si) + (100%P), T5= (25% RHB) + (100% Si) + (0%P), T6= (25% RHB) + (100% Si) + (25%P), T7= (25% RHB) + (100% Si) + (50%P), T8= (25% RHB) + (100% Si) + (100%P).

biochar will act as slow-releasing phosphorus (P) fertilizers and will increase P use efficiency (Li et al. 2020).

### Effect of RHB, Silicon Fertilizer, and Varying Doses of Phosphorus on P, K, Ca & Mg Uptake of Maize Plant

There was a significant difference in plant nutrient uptake of maize, represented in Table 6. With T8, the total uptake of P(1143.62 ppm.g<sup>-1</sup>) and Mg (1135.4 ppm.g<sup>-1</sup>) taken up by the maize plant was statistically higher than other treatments. The highest uptake of K (26980.9 ppm.g<sup>-1</sup>) and Ca (4273.6 ppm.g<sup>-1</sup>) was obtained from T4 (50% RHB + 100% Si + 100% TSP). The lowest Uptake of P was recorded by T7(352.79 ppm.g<sup>-1</sup>), the lowest uptake of K was showed by T3(17129.6 ppm.g<sup>-1</sup>), lowest Ca and Mg were recorded by T1(2138.24 ppm.g<sup>-1</sup> & 578.76 ppm.g<sup>-1</sup>). The high phosphorus and potassium uptake is observed with the application of biochar as the treatment (Ullah et al. 2018). According to Zaidun et al. (2019), the application of biochar would increase the exchangeable K together with the increasing dose of biochar. The high uptake of K shows that the good sign to help improve photosynthesis, carbohydrate metabolism, and protein formation, then affect the good development of yield (Mikkelsen 2017).

### CONCLUSIONS

To conclude, treatment 3, the combined application of biochar and silicon, along with 50% phosphorus, is recommended for enhancing the pH, K and Ca uptake, biomass, and yield. This treatment is practical and can be applied for further trials in field plots to get more stable results. This approach will help for conducive application, environmental benefits, and gain more profit for farmers.

### ACKNOWLEDGMENTS

This work was supported under research grant FRGS

5540389. The authors thank the Ministry of Higher Education Malaysia (MOHE) and Universiti Putra Malaysia for sponsoring the research work.

### REFERENCES

- Abukari, A., 2014. Effect of rice husk biochar on maize productivity in the Guinea Savannah zone of Ghana. *Unpublished doctoral dissertation*, University for Development Studies, Ghana, 1(1), pp.1–100.
- Ahmad, M., Usman, A.R., Al-Faraj, A.S., Ahmad, M., Sallam, A. and Al-Wabel, M.I., 2018. Phosphorus-loaded biochar changes soil heavy metals availability and uptake potential of maize (*Zea mays* L.) plants. *Chemosphere*, 194, pp.327–339.
- Alarefee Ahmed, H., Ishak, C.F., Karam, D.S. and Othman, R., 2021. Efficiency of rice husk biochar with poultry litter co-composts in Oxisols for improving soil acidity physico-chemical properties and enhancing maize performance. *Agronomy*, 11(12), pp.2409.
- Ali, S.A., Mumtaz, M.Z., Rahi, A.A., Irshad, I., Hussain, G.S., Dawar, K. and Danish, S., 2023. Impact of acidified carbon on maize growth, yield and grains nutrients concentration under normal irrigation and osmotic stress. *Journal of King Saud University – Science*, 35(2), pp.102505.
- Amin, M., Ahmad, R., Ali, A., Hussain, I., Mahmood, R., Aslam, M. and Lee, D.J., 2018. Influence of silicon fertilization on maize performance under limited water supply. *Silicon*, 10, pp.177–183.
- Brennan, A., O'Reilly, C., Doyle, E., Daly, K. and Coxon, C.E., 2014. Effects of biochar amendment on root traits and contaminant availability of maize plants in a copper and arsenic impacted soil. *Plant and Soil*, 379(1–2), pp.351–360.
- Arif, M., Ali, A., Umair, M., Munsif, F., Ali, K., Inamullah, M.S. and Ayub, G., 2012. Effect of biochar FYM and mineral nitrogen alone and in combination on yield and yield components of maize. *Sarhad Journal of Agriculture*, 28(2), pp.191–195.
- Bakar, M.W.B.A., Uddin, M.K., Kasim, S., Zaibon, S., Shamsuzzaman, S.M., Haque, A.N.A. and Reza, A., 2024. Combined application of biochar and silicon fertilizer for improved soil properties and maize growth. *Nature Environment and Pollution Technology*, 23(3), pp.1527–1535.
- De Sousa, A., Saleh, A.M., Habeeb, T.H., Hassan, Y.M., Zrieq, R., Wadaan, M.A. and AbdElgawad, H., 2019. Silicon dioxide nanoparticles ameliorate the phytotoxic hazards of aluminum in maize grown on acidic soil. *Science of the Total Environment*, 693, pp.133636.
- Glaser, B. and Lehr, V.I., 2019. Biochar effects on phosphorus availability in agricultural soils: A meta-analysis. *Scientific Reports*, 9(1), pp.9338.

- Haque, A.N.A., Uddin, M.K., Sulaiman, M.F., Amin, A.M., Hossain, M., Solaiman, Z.M. and Mosharrof, M., 2022. Rice growth performance, nutrient use efficiency, and changes in soil properties influenced by biochar under alternate wetting and drying irrigation. *Sustainability*, 14(13), pp.7977.
- Haque, A.N.A., Uddin, M.K., Sulaiman, M.F., Amin, A.M., Hossain, M., Aziz, A.A. and Mosharrof, M., 2021. Impact of organic amendment with alternate wetting and drying irrigation on rice yield, water use efficiency and physicochemical properties of soil. *Agronomy*, 11(8), pp.1529.
- Haynes, R. J., 2014. A contemporary overview of silicon availability in agricultural soils. *Journal of Plant Nutrition and Soil Science*, 177(6), pp.831–844.
- He, Y., Qiu, B., Cheng, F., Chen, C., Sun, Y., Zhang, D. and Xu, A., 2023. National scale maize yield estimation by integrating multiple spectral indexes and temporal aggregation. *Remote Sensing*, 15(2), pp.414.
- Hossain, A., Krupnik, T.J., Timsina, J., Mahboob, M.G., Chaki, A.K., Farooq, M. and Hasanuzzaman, M., 2020. *Environment, Climate, Plant and Vegetation Growth*. Springer International Publishing, pp.17–61.
- Ibrahim, M., Khan, S., Hao, X. and Li, G., 2016. Biochar effects on metal bioaccumulation and arsenic speciation in alfalfa (*Medicago sativa* L.) grown in contaminated soil. *International Journal of Environmental Science and Technology*, 13, pp.2467–2474.
- Islam, M.U., Jiang, F., Guo, Z. and Peng, X., 2021. Does biochar application improve soil aggregation? A meta-analysis. *Soil and Tillage Research*, 209, p.104926.
- Lai, L., 2019. *Utilization of Rice Straw Biochar and Urea to Mitigate Greenhouse Gases Emission in Sustainable Rice Production*. Ph.D. Thesis, Universiti Putra Malaysia, Selangor, Malaysia, pp.1–200.
- Li, H., Li, Y., Xu, Y. and Lu, X., 2020. Biochar phosphorus fertilizer effects on soil phosphorus availability. *Chemosphere*, 244, p.125471.
- Liu, L., Li, J., Wu, G., Shen, H., Fu, G. and Wang, Y., 2021. Combined effects of biochar and chicken manure on maize (*Zea mays* L.) growth, lead uptake and soil enzyme activities under lead stress. *PeerJ*, 9, p.e11754.
- Ma, J.F. and Takahashi, E., 2002. *Soil, Fertilizer, and Plant Silicon Research in Japan*. Elsevier, Tokyo, pp.1–300.
- Mensah, A.K. and Frimpong, K.A., 2018. Biochar and/or compost applications improve soil properties, growth, and yield of maize grown in acidic rainforest and coastal savannah soils in Ghana. *International Journal of Agronomy*, 2018, pp.1–12.
- Mia, S., Dijkstra, F.A. and Singh, B., 2017. Long-term aging of biochar: A molecular understanding with agricultural and environmental implications. *Advances in Agronomy*, 141, pp.1–51.
- Mikkelsen, R., 2017. The importance of potassium management for horticultural crops. *Indian Journal of Fertilisers*, 13(11), pp.82–86.
- Mosharrof, M., Uddin, M.K., Jusop, S., Sulaiman, M.F., Shamsuzzaman, S.M. and Haque, A.N.A., 2021a. Changes in acidic soil chemical properties and carbon dioxide emission due to biochar and lime treatments. *Agriculture*, 11(3), p.219.
- Mosharrof, M., Uddin, M.K., Mia, S., Sulaiman, M.F., Shamsuzzaman, S.M. and Haque, A.N.A., 2022. Influence of rice husk biochar and lime in reducing phosphorus application rate in acid soil: A field trial with maize. *Sustainability*, 14(12), p.7418.
- Mosharrof, M., Uddin, M.K., Sulaiman, M.F., Mia, S., Shamsuzzaman, S.M. and Haque, A.N.A., 2021b. The combined application of rice husk biochar and lime increases phosphorus availability and maize yield in acidic soil. *Agriculture*, 11(8), p.793.
- Msimbira, L.A. and Smith, D.L., 2020. The roles of plant growth promoting microbes in enhancing plant tolerance to acidity and alkalinity stresses. *Frontiers in Sustainable Food Systems*, 4, p.106.
- Neina, D., 2019. The role of soil pH in plant nutrition and soil remediation. *Applied and Environmental Soil Science*, 2019, pp.1–9.
- Nguyen, M.N., 2021. Potential use of silica-rich biochar for the formulation of adaptively controlled release fertilizers: A mini review. *Journal of Cleaner Production*, 307, p.127188.
- Olsen, S.R., 1954. Estimation of available phosphorus in soils by extraction with sodium bicarbonate. *U.S. Department of Agriculture Bulletin*, 939, pp.1–20.
- Opala, P.A., 2017. Influence of lime and phosphorus application rates on growth of maize in an acid soil. *Advances in Agriculture*, 2017, pp.1–7.
- Peng, J., Han, X., Li, N., Chen, K., Yang, J., Zhan, X., Liu, N., 2021. Combined application of biochar with fertilizer promotes nitrogen uptake in maize by increasing nitrogen retention in soil. *Biochar*, 3, pp.367–379.
- Peng, Y., Sun, Y., Sun, R., Zhou, Y., Tsang, D.C., Chen, Q., 2019. Optimizing the synthesis of Fe/Al (hydr)oxides-biochars to maximize phosphate removal via response surface model. *Journal of Cleaner Production*, 237, p.117770.
- Pitann, B., Bakhat, H.F., Fatima, A., Hanstein, S., Schubert, S., 2021. Silicon-mediated growth promotion in maize (*Zea mays* L.) occurs via a mechanism that does not involve activation of the plasma membrane H<sup>+</sup>-ATPase. *Plant Physiology and Biochemistry*, 166, pp.1121–1130.
- Pontigo, S., Ribera, A., Gianfreda, L., de la Luz Mora, M., Nikolic, M., Cartes, P., 2015. Silicon in vascular plants: Uptake, transport and its influence on mineral stress under acidic conditions. *Planta*, 242, pp.23–37.
- Raza, M.A.S., Haider, I., Farrukh Saleem, M., Iqbal, R., Usman Aslam, M., Ahmad, S., Abbasi, S.H., 2021. Integrating biochar, rhizobacteria and silicon for strenuous productivity of drought stressed wheat. *Communications in Soil Science and Plant Analysis*, 52(4), pp.338–352.
- Rehman, M.U., Ilahi, H., Adnan, M., Wahid, F., Rehman, F.U., Ullah, A., Raza, M.A., 2021. Application of silicon: A useful way to mitigate drought stress: An overview. *Current Research in Agriculture and Farming*, 2, pp.9–17.
- Sattar, A., Sher, A., Abourehab, M.A., Ijaz, M., Nawaz, M., Ul-Allah, S. and Javaid, M.M., 2022. Application of silicon and biochar alleviates the adversities of arsenic stress in maize by triggering the morpho-physiological and antioxidant defense mechanisms. *Frontiers in Environmental Science*, 10, p.2086.
- Schollenberger, C.J. and Simon, R.H., 1945. Determination of exchange capacity and exchangeable bases in soil-ammonium acetate method. *Soil Science*, 59, pp.13–24.
- Seleiman, M.F., Alotaibi, M.A., Alhammad, B.A., Alharbi, B.M., Refay, Y. and Badawy, S.A., 2020. Effects of ZnO nanoparticles and biochar of rice straw and cow manure on characteristics of contaminated soil and sunflower productivity, oil quality, and heavy metals uptake. *Agronomy*, 10(6), p.790.
- Shankara, M.H., Chandrakala, M., Prakash, H.C., Nalina, C.N., Sudhir, K. and Rani, S.S., 2022. Maize (*Zea mays*) yield response to application of calcium, magnesium, and boron on acid soil. *International Journal of Environment and Climate Change*, 12(11), pp.2980–2988.
- Shetty, R. and Prakash, N.B., 2020. Effect of different biochars on acid soil and growth parameters of rice plants under aluminium toxicity. *Scientific Reports*, 10(1), pp.1–10.
- Tan, K.H., 2005. *Soil Sampling, Preparation, and Analysis*. CRC Press, Boca Raton, pp.1–240.
- Ullah, Z., Akmal, M.S., Ahmed, M., Ali, M., Khan, A.Z. and Ziad, T., 2018. Effect of biochar on maize yield and yield components in rainfed conditions. *International Journal of Agronomy and Agricultural Research*, 12, pp.46–51.
- Wang, Y., Xiao, X., Xu, Y. and Chen, B., 2019. Environmental effects of silicon within biochar (sichar) and carbon-silicon coupling mechanisms: A critical review. *Environmental Science & Technology*, 53(23), pp.13570–13582.
- Weeks, J.J. and Hettiarachchi, G.M., 2019. A review of the latest in phosphorus fertilizer technology: Possibilities and pragmatism. *Journal of Environmental Quality*, 48(5), pp.1300–1313.

- Xiangping, Z., Chang, W., Liu, C. and Li, D., 2020. Preparation and application of magnetic biochar in water treatment: A critical review. *Science of the Total Environment*, 711, p.134847.
- Xie, X., Yang, S., Liu, H., Pi, K. and Wang, Y., 2020. The behavior of cadmium leaching from contaminated soil by nitrilotriacetic acid: Implication for Cd-contaminated soil remediation. *Water, Air, & Soil Pollution*, 231, pp.1-12.
- Xie, Z., Song, F., Xu, H., Shao, H. and Song, R., 2014. Effects of silicon on photosynthetic characteristics of maize (*Zea mays* L.) on alluvial soil. *The Scientific World Journal*, 2014, pp.1-8.
- Xiong, M., Dai, G.Q., Sun, R.G. and Zhao, Z., 2024. Passivation effect of corn vinasse biochar on heavy metal lead in paddy soil of Pb-Zn mining area. *Nature Environment & Pollution Technology*, 23(1), pp.57-65.
- Younas, H.S., Abid, M., Shaaban, M. and Ashraf, M., 2021. Influence of silicon and chitosan on growth and physiological attributes of maize in a saline field. *Physiology and Molecular Biology of Plants*, 27, pp.387-397.
- Yu, H., Zou, W., Chen, J., Chen, H., Yu, Z., Huang, J. and Gao, B., 2019. Biochar amendment improves crop production in problem soils: A review. *Journal of Environmental Management*, 232, pp.8-21.
- Yuan, Z., Cao, Q., Zhang, K., Ata-Ul-Karim, S.T., Tian, Y., Zhu, Y., Cao, W. and Liu, X., 2016. Optimal leaf positions for SPAD meter measurement in rice. *Frontiers in Plant Science*, 7, p.719.
- Zaidun, S.W., Jalloh, M.B., Awang, A., Sam, L.M., Besar, N.A., Musta, B. and Latifah, O.M.A.R., 2019. Biochar and clinoptilolite zeolite on selected chemical properties of soil cultivated with maize (*Zea mays* L.). *Eurasian Journal of Soil Science*, 8(1), pp.1-10.
- Zangani, E., Afsahi, K., Shekari, F., Mac Sweeney, E. and Mastinu, A., 2021. Nitrogen and phosphorus addition to soil improves seed yield, foliar stomatal conductance, and the photosynthetic response of rapeseed (*Brassica napus* L.). *Agriculture*, 11(6), p.483.
- Zheng, X.J., Chen, M., Wang, J.F., Liu, Y., Liao, Y.Q. and Liu, Y.C., 2020. Assessment of zeolite, biochar, and their combination for stabilization of multimetal-contaminated soil. *ACS Omega*, 5(42), pp.27374-27382.



# Management of Grapevine Fungal Diseases by Using Antagonistic Endophytes - An Environment-Friendly Approach

Akhilesh Chandrapati<sup>1</sup>, Jay Prakash Singh<sup>2</sup>, Yenda Damodhara Rao<sup>3</sup>, Meenakshi Rana<sup>1</sup>, Somnath K. Holkar<sup>4</sup> and Seweta Srivastava<sup>1†</sup> 

<sup>1</sup>Department of Plant Pathology, School of Agriculture, Lovely Professional University, Phagwara-144 411, Punjab, India

<sup>2</sup>Department of Plant Pathology, SMMTD College, Balia-277001, Uttar Pradesh, India

<sup>3</sup>Department of Plant Pathology, Chandra Shekhar Azad University of Agriculture and Technology, Kanpur 208 002, Uttar Pradesh, India

<sup>4</sup>Department of Plant Pathology, ICAR-National Research Centre for Grapes (NRCG), Pune-412307, Maharashtra, India

†Corresponding author: Seweta Srivastava; seweta.21896@lpu.co.in

**Abbreviation:** Nat. Env. & Poll. Technol.

**Website:** [www.neptjournal.com](http://www.neptjournal.com)

*Received:* 12-07-2024

*Revised:* 02-09-2024

*Accepted:* 19-09-2024

## Key Words:

Endophytes  
Antagonistic properties  
Secondary metabolites  
Eco-friendly disease management  
Defense mechanism in plants

## Citation for the Paper:

Chandrapati, A., Singh, J.P., Rao, D. Y., Rana, M., Holkar, S.K. and Srivastava, S. 2025. Management of grapevine fungal diseases by using antagonistic endophytes - An environment-friendly approach. *Nature Environment and Pollution Technology*, 24(2), p. B4246. <https://doi.org/10.46488/NEPT.2025.v24i02.B4246>

*Note: From year 2025, the journal uses Article ID instead of page numbers in citation of the published articles.*



**Copyright:** © 2025 by the authors

**Licensee:** Technoscience Publications

This article is an open access article distributed under the terms and conditions of the Creative Commons Attribution (CC BY) license (<https://creativecommons.org/licenses/by/4.0/>).

## ABSTRACT

Grapevine (*Vitis vinifera* L.) is one of the major crops grown commercially throughout the world. In recent years, there have been major losses to grapevine production due to the challenges caused mainly due to fungal diseases like downy mildew, powdery mildew, grey mold, black rot, and anthracnose. In the last few decades, rampant chemical fertilization and bio-magnification of hazardous chemicals have posed a threat to human health and destroyed the health of the soil as well as crops. For effective management of these fungal diseases of grapes, nowadays, many researchers are conducting various studies on endophytes, which are proven to be better bio-control agents to suppress the growth and development of grapevine phytopathogens. Endophytes are eco-friendly, effective, and easy to apply at field levels, making endophyte-based formulations suppress the growth and development of grapevine pathogens without causing any detrimental effects to the beneficial micro-organisms present at the rhizospheric zone of soil and host plants as compared to the traditional fungicides usage. It also competes with these pathogens for nutrition, space, and colonization. It helps in the production of secondary metabolites with antifungal properties for preventing the growth of fungal pathogens that cause damage to the grapevine crop. It also induces a defense mechanism in grapevine crops against disease-causing fungal phytopathogens. In this review article, biocontrol mechanisms of endophytes and their potential application in the management of grapevine fungal diseases have been discussed.

## INTRODUCTION

Grapevine is one of the major commercial fruit crops grown across 7.3 million hectares worldwide and is used for juice, wine, raisin production, and fresh consumption (Karlsson & Karlsson 2021). The total productivity of grapevine throughout the world in recent years is about 27.42 million metric tons (Statista 2023). In India the grapevine is regarded as a major revenue-generating commercial fruit crop produced for export to other countries; it is expected that India is producing about 2,46,133 tons of fresh grapes with an income value of 334.79 million dollars. Maharashtra is the leading grapevine-producing state of India, which produces over 81% of total grapevine production in India (Indian Grape Forum 2019). The major grapevine fungal diseases that are causing heavy losses to grapevine production throughout the world are Downy mildew, Powdery mildew, Anthracnose, Grey mold, Black rot, etc (Armijo et al. 2016). Endophytes are pervasive and mainly colonize inside the tissues of 300,000 various plant species without causing any detrimental effects to the plants (Narayanan et al.

2022). These endophytes mainly belong to Ascomycota, Actinobacteria, Basidiomycota, Bacteroidetes, Firmicutes, Proteobacteria, and Zygomycota, which are some major prokaryotic and eukaryotic endophytes that were identified till now (Yakop et al. 2019). These endophytes produce various enzymes, hormones, and secondary metabolites, which cause antagonistic effects and antimicrobial activity that inhibit plants from pathogen infection and play a major role in biotechnology (Gunatilaka 2006). Using these natural symbionts provides a chance to increase the production of grapevine while minimizing the use of hazardous pesticides against pathogens (Srivastava et al. 2023).

Endophytes must slowly adapt to these living conditions by gradually interacting with their host plant, including mutualism and antagonism (Dudeja et al. 2012), and can establish themselves in the plant after a process of molecular crosstalk that produces a cornucopia of favorable modifications for the host (Pavithra et al. 2020, Das et al. 2021, Pavithra et al. 2021, Maurya et al. 2024). These endophytes promote the growth and development of their host plant and help them to adapt to environmental changes, and they produce various compounds to sustain symbiosis between host plant and endophytes (Das & Varma 2009). In the present situation, increasing crop production and maintaining ecological sustainability in an eco-friendly manner is possible by using microbial bio-products that include various types of bio-formulations like bio-fertilizers, bio-pesticides, bio-stimulants, bio-inoculants, etc. (Singh et al. 2016). To sustain the goal of increasing crop production and controlling various diseases throughout the world, there is an urgent need to develop microbe-based bio-formulations that are greener and safer alternatives to agrochemicals (Mishra et al. 2015). These microbe-based bio-formulations are strong in comparison to agrochemicals as the formulation includes a single microbe that interacts with the pathogen directly and suppresses its growth and development, which leads to a decrease in disease rate and improves plant growth (Rodrigo et al. 2011).

## GRAPEVINE FUNGAL DISEASES AND THEIR IMPACT ON GRAPE PRODUCTION

The major fungal diseases of grapevine (*Vitis vinifera*) as mentioned in Table 1 are powdery mildew, downy mildew, grey mold, black rot, anthracnose which are caused by these phytopathogens like *Uncinula necator*, *Plasmopara viticola*, *Botrytis cinerea*, *Guignardia bidwelli* and *Elsinoe ampelina* (Armijo et al. 2016). Downy mildew disease causes severe yield losses to the grapevine in vivo when optimum temperate and humidity are present, which is suitable for survival and increases infection-causing capacity, leading to

losses of about 40-90% of grapevine (Toffolatti et al. 2018). Powdery mildew disease causes severe losses to the quality and quantity of grapevine. If not managed properly during high disease pressure years, it leads to yield losses of about 75-100% (Fermaud et al. 2016). Anthracnose disease causes yield losses to crop productivity of grapevine about 10-15% and on highly susceptible grapevine varieties due to severe infection on them, crop losses occur up to 100% (Zhi Li et al. 2021). Grey mold disease causes major economic yield losses to the grapevine, about 20-50% throughout the world at post-harvest season, mainly due to rotting of ripe berries (Fedorina et al. 2022). Black rot disease causes yield losses to the grapevine by about 80% due to the availability of its optimum humid condition to produce its primary inoculum and causes infection to the grapevine (Jackson 2014).

## VARIOUS TYPES OF ANTAGONISTIC ENDOPHYTES ASSOCIATED WITH HOST PLANTS

Endophytes can reside inside (intercellular) and outside (intracellular) the cells of the host plant, and they can live inside (systematically) and outside (locally) of the host body in a symbiotic relationship with the host without causing any harm to the host plant (Kusari et al. 2012, Lo Presti et al. 2015, Schulz et al. 2015). Endophytes are found existing all over the places of agricultural ecosystems and natural forests and are mainly present in the plant tissues of spermatophytes, ferns, equisetopsids, mosses, liverworts, lycophytes, hornworts, etc. (Kusari et al. 2012, Jeewon et al. 2013, Doilom et al. 2017, Potshangbam et al. 2017). Clavicipitaceous endophytes live as intracellular symbionts, mainly in various grasses. They are found more in the leaves and stems of mother plants as compared to young plants, and these endophytes are transmitted both vertically and horizontally through sexual or asexual spores and seeds, etc. (Yan et al. 2015, Santangelo et al. 2015). Both the fungal and bacterial endophytes have great potential as bio-control agents as they have antagonistic activity (Table 2), which produces various secondary metabolites like antioxidants, bioactive antimicrobial and antiviral metabolites that help in suppressing the growth of various disease-causing phytopathogens, thus reducing the losses caused by them (Gouda et al. 2016).

De Bary (1866) introduced the endophyte term. He defined it as an organism that grows inside of the plant tissues and has a symbiotic relationship with its host without causing any detrimental effects to its host, sometimes helping in providing essential nutrients for the host for its growth and development. Its types are fungal and bacterial endophytes, which act as both obligate or facultative relationships with

Table 1: List of major fungal diseases of grapevine with their causal organisms and peculiar symptoms.

Diseases	Causal organism	Symptoms	References
Downy mildew	<i>Plasmopara viticola</i>	Rough circular yellow discoloration and oily spots on leaves. Whitish downy fungal growth appearance on the lower side of leaves and stem (sporulation of fungi). Infected shoot tips turn curl (Shepherd's crook). Severely infected leaves turn yellow to brown and finally get dry and dropdown.	Koledenkova et al. (2022)
Powdery mildew	<i>Uncinula necator</i>	Lesions first occur on the lower side of the leaves. Minute orange to black circular structures, <i>i.e.</i> , cleistothecia, appear on both the upper and lower surfaces of leaves and berries. Affected berries finally dried out and dropped down.	Kunova et al. (2021)
Anthraco-nose	<i>Elsinoe ampilina</i>	It causes small round spots on the surface of leaves. These spots later become holes on leaves (shot-hole appearance). The appearance of deep elongated cankers with a greyish color in the center and with a black border on the stem. Violet color spots with a greyish appearance in the center appearance on berries. Finally, these infected berries dried and dropped prematurely.	Li et al. (2021)
Grey mold	<i>Botrytis cinerea</i>	It causes necrotic brown spots. Infected berries are covered with greyish substances consisting of spores of the fungus.	Shen et al. (2021)
Black rot	<i>Guignardia Bidwell</i>	It causes small brown lesions with a border of dark marginal rings consisting of black pustules (fruiting body of fungi). Infected berries first turns white, then purple, and finally turns black color. Severely infected berries are covered by black pustules.	Szabó et al. (2023)
Ripe rot	<i>Colletotrichum</i> spp.	It causes tiny, sunken, reddish-brown spots with yellow halos. Infected berries become soft and concentric rings are formed on berries consisting of small fruiting body structures (acervuli). Infected fruits turn from light to brown color. The final stage of infection results in the drying and mummification of decaying berries.	Hsieh et al. (2023)
Angular leaf scorch	<i>Psuedopezizula tetraspora</i>	The first appearance of symptoms occurs on leaves. Lesions appear as faint, yellow spots on the leaf surface and leaf veins and later turn to reddish-brown color. At severe infection, death of leaf tissue occurs.	Fischer et al. (2022)
Armillaria root rot	<i>Armillaria mellea</i>	The first appearance of symptoms occurs as stunting of shoots. Later white mycelial mat appears below the bark of the plant. At severe infection, and trunk and root of the plant get rotten with a soft and spongy appearance, and its color changes from white to dark brown.	Calamita et al. (2021)
Bot Canker	<i>Lasiodiplodia theobromae</i>	Foliar symptoms may be observed as mild chlorosis or wilting due to inhibition of water transport. Berries of infected white-fruited varieties may develop small, flat lesions with pycnidia, with berries turning light brown.	DeKrey et al. (2022)
Phomopsis dieback	<i>Phomopsis viticola</i>	Small, black spots on the internodes at the base of developing shoots are probably the most common disease symptom. These spots are usually found on the first three to four basal internodes. It is also known as the "dead arm".	Úrbez-Torres et al. (2013)
Grapevine leaf stripe	<i>Phaeomoniella chlamydospora</i> and several species of <i>Phaeoacremonium</i>	Foliar symptoms on established grapevines have been widely described and include various types of discoloration, typically interveinal discolorations evolving into necrotic areas resembling "tiger stripes".	Serra et al. (2018), Calzarano et al. (2021)
Botryosphaeria dieback	It is caused by several pathogens, primarily <i>Neofusicoccum parvum</i> , <i>Diplodia seriata</i> , <i>Botryosphaeria stevensii</i> , and <i>Botryosphaeria dothidea</i> .	Symptoms of Botryosphaeria dieback include dead spurs, stunted shoots, and bud mortality.	Kenfaoui et al. (2022)
Eutypa dieback	<i>Eutypa lata</i>	It is a major trunk disease in grapevines associated with the heavy loss of production.	Gramaje et al. 2018
Leaf blight/ Fruit rot	<i>Alternaria alternata</i> , <i>A. vitis</i>	The disease attacks both leaves and fruits. Small yellowish spots first appear along the leaf margins, which gradually enlarge and turn into brownish patches with concentric rings.	Li et al. (2023)
Grapevine Esca disease colonizing the xylem tissues of vine plants	<i>Phaeomoniella chlamydospora</i> <i>Phaeoacremonium aleophilum</i>	The typical Esca internal symptoms are vascular discoloration with the production of dark tarry drops and wood necrosis. In leaves, both chlorotic and necrotic areas have typically been described as tiger-striped leaves and later as grapevine leaf stripe disease.	Mugnai et al. 1999, Gramaje et al. 2018

Table 2: Effectiveness of antagonistic endophytes against grapevine phytopathogens.

Endophytes	Effective against grapevine phytopathogens	Reference
<i>Pseudomonas</i> spp.	Phytoplasmas <i>Botrytis cinerea</i>	Gamalero et al. (2017) Gruau et al. (2015)
<i>Burkholderia</i> spp.	Phytoplasmas	Bulgari et al. (2014).
<i>Methylobacterium</i> spp.	Phytoplasmas	Bulgari et al. (2014).
<i>Pantoea</i> spp.	Phytoplasmas <i>Neofusicoccum parvum</i>	Andreolli et al. (2016) Haidar et al. (2021)
<i>Bacillus</i> spp.	<i>Botrytis cinerea</i> <i>Plasmopara viticola</i>	Andreolli et al. (2016). Zhang et al. (2017).
<i>B. subtilis</i> strain AG1	<i>Phaeomoniella chlamydospora</i> and <i>Phaeoacremonium aleophilum</i>	Alfonzo et al. 2009
<i>Bacillus pumilus</i> and <i>Paenibacillus</i> sp. (S19)	<i>Phaeomoniella chlamydospora</i>	Haidar et al. (2016b)
<i>Pseudomonas protegens</i> MP12 strain	<i>Phaeomoniella chlamydospora</i> and <i>Phaeoacremonium aleophilum</i>	Andreolli et al. (2019)
<i>Brevibacillus</i> spp. <i>Lysinibacillus</i> spp. <i>Nocardioides</i> spp. <i>Stenotrophomonas</i> spp. <i>Microbacterium</i> spp. <i>Streptomyces anulatus</i>	<i>Botrytis cinerea</i>	Andreolli et al. (2016)
<i>Paraburkholderia phytofirmans</i> strain PsJN	<i>Botrytis cinerea</i>	Vatsa-Portugal et al. (2017) Ait Barka et al. (2000), MiottoVilanova et al. (2016)
<i>Acinetobacter lwoffii</i>	<i>Botrytis cinerea</i>	Verhagen et al. (2011)
<i>Enterobacter</i> spp. <i>Rahnella aquatilis</i> <i>Paenibacillus</i> spp. <i>Staphylococcus</i> spp. <i>Acremonium</i> spp. <i>Alternaria alternata</i> <i>Epicoccum nigrum</i>	<i>Botrytis cinerea</i> , <i>Plasmopara viticola</i> , <i>Agrobacterium vitis</i> , <i>Xylella fastidiosa</i>	Pacifico et al. (2019)
<i>Paenibacillus</i> spp.	<i>Botrytis cinerea</i> , <i>Plasmopara viticola</i> , <i>Agrobacterium vitis</i> , <i>Xylella fastidiosa</i> <i>Neofusicoccum parvum</i>	Pacifico et al. (2019), Haidar et al. (2021)
<i>Albifimbria verrucaria</i>	<i>Botrytis cinerea</i> , <i>Lasiodiplodia theobromae</i> , <i>Elsinoe ampelina</i>	Li et al. (2000)
<i>Beauveria bassiana</i>	<i>Plasmopara viticola</i>	Rondot and Reineke (2019)
<i>Cochliobolus</i> , <i>Bipolaris</i> , <i>Fusarium</i> , <i>Alternaria</i> , <i>Diaporthe</i> , <i>Phoma</i> and <i>Phomopsis</i> .	<i>Alternaria</i> sp., <i>Sphaceloma</i> sp. And <i>Glomerella</i> sp.	Felber et al. (2016)
<i>Lophiostoma cortisol</i> (from leaves)	<i>Botrytis cinerea</i>	Kulišová et al. (2021)
<i>Alternaria alternata</i> and <i>Fusarium proliferatum</i>	<i>Plasmopara viticola</i>	Mondello et al. (2019), Aleynova et al. (2021)
<i>Acremonium byssoides</i>	<i>Plasmopara viticola</i>	Burruano et al. (2008)

the host plant (Brader et al. 2017). These endophytes colonize the plant tissues, both intercellular and intracellular, and have a mutualistic association with the host in their lifetime. Recent studies show that the health, survival, growth, and development of these host plants are mostly dependent on these endophytes (Hardoim et al. 2015, Potshangbam et al. 2017). Obligate endophytes are those that depend on the host plant metabolism for their survival, and their movement inside the plant occurs through different vectors or vertical transmission (Hardoim et al. 2008). Facultative

endophytes are those that can survive outside of the host plant for a certain period of their life cycle, and they are mostly associated with host plants as compared to their natural environment in soil (Abreu-Tarazi et al. 2010).

## ROLE OF ANTAGONISTIC ENDOPHYTES IN GRAPEVINE FUNGAL DISEASE MANAGEMENT

Endophytes are helpful in plant growth and provide biotic/



abiotic stress resistance by the production and release of secondary metabolites, plant hormones, antibiotics, and biocides, which leads to improving resistance in plants against abiotic stress and various diseases (Lugtenberg & Kamilova 2009, Compant et al. 2013). The endophytic colonization in the grapevine helps the plant to be in an active state to respond to any attack by grapevine disease-causing pathogens (Martinez-Medina et al. 2016, Mauch-Mani et al. 2017). It is proved by many researchers believe that these endophytes help in triggering defense responses in plants, which provide resistant against various fungal, oomycete, bacterial, and viral pathogens and insects (De Vleeschauwer & Höfte 2009, Van der Ent et al. 2009, Pineda et al. 2010). Some endophyte bacteria like *Pseudomonas* spp. and *Bacillus* spp. can produce HCN which helps in breaking summer bud dormancy in grapevine (Shameer & Prasad 2018, Sudawan et al. 2016). The endophytic bacteria *Pseudomonas migulae* can act as a biocontrol agent against phytoplasmas which causes grapevine yellows disease in grapevine (Gamalero et al. 2017). The bacterial species associated with induced systemic resistance (ISR), such as *Burkholderia* spp., *Methylobacterium* spp., and *Pantoea* spp. the population increased and helped in triggering defense responses for resistance when phytoplasmas attack the grapevine (Bulgari et al. 2014). The endophytic fungus *Alternaria alternata*, isolated from grapevine leaves, has been reported to be efficacious in controlling downy mildew disease through the production of toxic diketopiperazines metabolites (Musetti et al. 2006, Srivastava et al. 2024). Several other microorganisms, isolated either from rhizosphere or grape fruit surfaces, have also been selected as BCAs over the last decades to control *Plasmopara viticola*, such as *Bacillus subtilis* KS1, *Lysobacter capsici* AZ78, *Trichoderma harzianum* T39 and *Fusarium proliferatum* G6 (Perazzolli et al. 2008, Zhang et al. 2017).

In recent studies, the researchers identified various new potential endophytes as biocontrol agents *in vitro*. Among these potential endophytes, *Bacillus licheniformis* can secrete lipoproteins, which are biocontrol molecules that help in inhibiting the growth and development of various phytopathogenic fungi in grapevine, mainly against *Botrytis cinerea*, which causes grey mold disease in grapevine (Favaro et al. 2016, Nigris et al. 2018). The endophytic bacteria *i.e.*, *Bacillus* spp., *Brevibacillus* spp., *Lysinibacillus* spp., *Nocardioideis* spp., *Stenotrophomonas* spp., *Microbacterium* spp. and *Pantoea* spp. also exhibits antifungal activity and induce resistance against *Botrytis cinerea* phytopathogen causing grey mold disease in grapevine (Andreolli et al. 2016). The most effective endophytes against *Botrytis cinerea* are *Bacillus* spp., *Pantoea* spp., and *Pseudomonas* spp., respectively. Among them, the bacterial endophyte

*Pseudomonas* spp. helps in activating defense responses against *Botrytis cinerea* at both local and systemic levels in grapevine (Trotel-Aziz et al. 2008, Verhagen et al. 2011, Gruau et al. 2015).

The endophyte *i.e.*, *Pseudomonas* spp. Colonize the roots of grapevine and exhibits systemic defense response by transfer of molecular signals from roots to leaves, and it shows distinct defense-related gene expression patterns in roots and leaves of grapevine where some genes are associated with causing cell death and hypersensitive response (HR), which stops the infection from *Botrytis cinerea* from spreading into other cells and tissues of grapevine. It leads to the activation of oxidative burst and production of phytoalexins which helps in reducing the infection caused by *Botrytis cinerea* in grapevine (Gruau et al. 2015). *Streptomyces anulatus* is a potential endophytic plant growth-promoting rhizobacterium (PGPR) that exhibits resistance against *Botrytis cinerea* by activating defense responses in grapevine-like ion fluxes, extracellular alkalinization, protein kinases, oxidative burst, gene expression, and phytoalexin production (Vatsa-Portugal et al. 2017). *Paraburkholderia phytofirmans* is a potential endophytic plant growth-promoting rhizobacterium (PGPR) which helps in the activation of local immune response by inflation of phenolic compounds, ion fluxes, salicylic acid, and defense gene regulation for inhibiting growth and development of grapevine fungal pathogens mainly *Botrytis cinerea* (Compant et al. 2005, Bordiec et al. 2011, Miotto-Vilanova et al. 2016, Patya et al. 2023).

These all of the above-mentioned bacterial endophytes trigger oxidative bursts in tissues of the leaf, callose deposition in stomata, induction of salicylic acid, jasmonic acid, and pathogenesis-related (PR) genes (PR1, PR2, and PR5) in grapevine when infected by grapevine fungal disease-causing pathogens. (Miotto-Vilanova et al. 2016). Some researchers studied and observed that *Pseudomonas protegens* could colonize inside grapevine tissues, and it helps in inhibiting the growth and development of various phytopathogens such as *P. chlamydospore*, *P. aleophilum*, *B. cinerea*, *Alternaria alternata*, *Aspergillus niger*, *Penicillium expansum*, and *N. parvum* at *in vitro* and *in vivo* (Andreolli et al. 2019). Some bacterial and fungal endophytes such as *Curtobacterium* spp., *Erwinia* spp., *Pantoea* spp., *Pseudomonas* spp., *Xanthomonas* spp., *Biscogniauxia* spp., *Cladosporium* spp., and *Didymella* spp., can produce secondary metabolites (stilbene content) in the grapevine cell suspension under *in vitro* conditions (Aleynova et al. 2021). Grapevine, when inoculated with some endophytes like *Acinetobacter lwoffii*, *Bacillus subtilis*, and *Pseudomonas fluorescens*, is effective in suppressing the growth and development of *Botrytis cinerea*, causing grey mold disease in grapevine due to the help of these endophytes in synthesis of stilbene

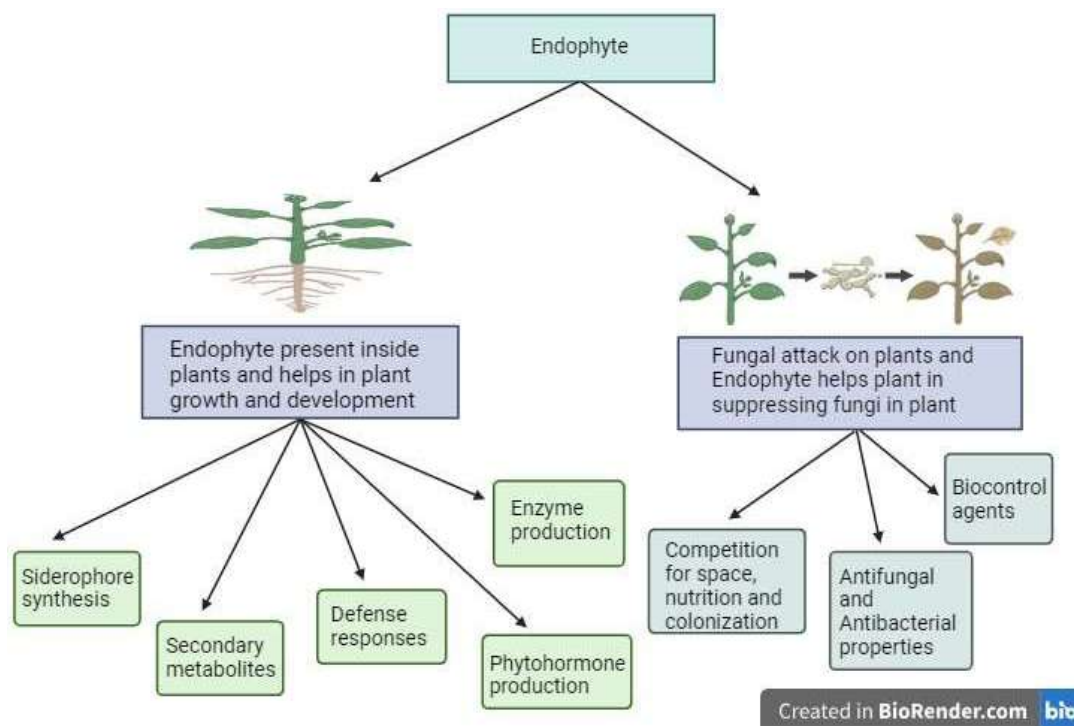
Table 3: Role played by antagonistic endophytes in the management of grapevine diseases.

Endophytes	Role played	Effective against grapevine disease	References
<i>Proteobacteria</i> spp.	Phyto-hormones production	NA	Baldan et al. (2015)
<i>Streptomyces anulatus</i> S37	Activation of protein kinases, induction of defense gene expression, and phytoalexin accumulation	Triggers early and late defense responses, such as ion fluxes, oxidative burst, extracellular alkalinization	Vatsa-Portugal et al. (2017)
<i>Acinetobacter lwoffii</i>	Enzyme Production	Grey mold	Magnin-Robert et al. (2007)
<i>Lophiostoma corticola</i>	Antifungal and antibacterial properties	Grey mold	Kulisova et al. (2021)
<i>B. velezensis</i>		Grey mold, Ripe rot, Downy mildew	Hamaoka et al. (2021)
<i>Bacillus</i> spp. <i>Variovorax</i> spp. <i>Pantoea</i> spp. <i>Staphylococcus</i> spp. <i>Herbaspirillum</i> spp. <i>Sphingomonas</i> spp.	Biocontrol Agents	Grey mold Downy mildew	Bruisson et al. (2019)
<i>Proteobacteria</i> spp. <i>Bacillus</i> spp.	Bio-fertilizers	Grey mold	Baldan et al. (2015)
<i>Proteobacteria</i> spp.	Phosphate solubilization	NA	Baldan et al. (2015)
<i>Penicillium custom</i>	Siderophore synthesis	Grey mold	Kulisova et al. (2021)
<i>Bacillus</i> spp.			Baldan et al. (2015)
<i>Pseudomonas fluorescens</i>	Secondary metabolites production	Grey mold	Gruau et al. (2015)
<i>Aspergillus pseudodeflectus</i>	Defense responses in host plant	Grey mold	Kulisova et al. (2021)
<i>Beauveria bassiana</i>		Downy mildew	Rondot and Reineke (2019)
<i>Aureobasidium pullulans</i>		Grapevine trunk	Pinto et al. (2018)
<i>Bacillus subtilis</i>		Grapevine trunk	Trotel-Aziz et al. (2019)
<i>Paenibacillus</i> spp.		Downy mildew	Hao et al. (2017)
<i>Paenibacillus</i> spp.	Induce resistance in host plants.	Downy mildew	Haidar et al. (2016)
<i>Penicillium</i> , <i>Aspergillus</i> , <i>Mucor</i> , <i>Alternaria</i> , <i>Cephalosporium</i> , and <i>Geotrichum</i>	Resveratrol	As an antioxidant compound known to increase resistance to biotic stress	Shi et al. (2012), Yang et al. (2016)
<i>Paraburkholderia phytofirmans</i> strain PsJN	Activation of a local immune response characterized by the accumulation of phenolic compounds, salicylic acid (SA) accumulation, ion fluxes, and defense gene regulation	Grey mold	Miotto-Vilanova et al. (2016)

phytoalexins, resveratrol which help activating metabolite composition and triggering defense mechanism in grapevine (Verhagen et al. 2011). It is observed that the endophyte *Arcopilus aureus* produces high resveratrol content in grapevine. A study was conducted on 53 isolates of potential endophytes obtained from various grapevine varieties to observe the resveratrol content produced by various endophytes. Among the endophytes that produce resveratrol content mainly belong to seven genera, i.e., *Aspergillus* spp., *Botryosphaeria* spp., *Penicillium* spp., *Fusarium* spp., *Alternaria* spp., *Arcopilus* spp. and *Lasiodiplodia* spp. (Dwibedi & Saxena 2018). Some important role played by endophytes against grapevine pathogens is mentioned in Table 3.

## RECENT APPLICATIONS OF ANTAGONISTIC ENDOPHYTES IN GRAPEVINE FUNGAL DISEASE MANAGEMENT

Nowadays, both fungal and bacterial endophytic applications in agriculture *in vivo* are very beneficial for host plants in which they colonize because these endophytes are eco-friendly with the host plant by promoting growth and development of the plant, act as a biocontrol, help in disease suppression, and stress tolerance, etc (Firdous et al. 2019). Some endophytes application helps the host plants acquire nutrients, production of phytohormones, phytoenzymes, and secondary metabolites, act as biocontrol agents, biofertilizers, exhibit antifungal and antibacterial properties, phosphate



(Source: made by authors).

Fig. 1: Role of endophytes in the growth and development of plants by suppressing the pathogenic microbes.

solubilization, siderophore synthesis, defense responses and induce resistance for suppressing various phytopathogens by inhibiting their growth and development in host plants and prevent them from causing diseases which leads to major losses in crop yield (Santoyo et al. 2016).

Recent studies in endophytes application to grapevine show that some endophytes are helpful in the production of siderophores and exhibit antioxidant and antifungal activity to inhibit grapevine disease-causing pathogens (Fig. 1). Application of *Diatrype stigma*, *Aspergillus niger* and *Penicillium crustose* endophytes *in vivo* helps in the production of siderophores in grapevine. Application of *Penicillium crustosum* and *Aspergillus pseudodeflectus* endophytes *in vivo* helps in exhibiting antioxidant activity in grapevine. Application of *Lophiostoma corticola*, and *Penicillium crustosum* endophytes *in vivo* helps in exhibiting antifungal activity in grapevine. (Kulisova et al. 2021). Application of *Bacillus subtilis* and *Bacillus pumilus* *in vivo* acts as a biocontrol agent against downy mildew disease of grapevine caused by *Plasmopara viticola* and helps in the reduction of disease incidence and severity in grapevine (Zhang et al. 2017).

Application of some endophytes like *Pantoea agglomerans*, *Enterobacter* spp., *Rahnella aquatilis*,

*Pseudomonas* spp., *Paenibacillus* spp., *Staphylococcus* spp., *Bacillus* spp., *Burkholderia phytofirmans*, *Acremonium* spp., *Alternaria alternata*, and *Epicoccum nigrum* can act as bio-control agents for effective control of various grapevine diseases i.e. grey mold, crown gall, pierce, and downy mildew (Pacifico et al. 2019). In recent days, many endophytic bacteria like *Streptomyces* spp., *Pseudomonas fluorescens*, *Bacillus* spp., *Pantoea agglomerans*, *Acinetobacter aeruginosa*, *Burkholderia phytofirmans*, and *Rahnella aquatilis* when applied at *in vivo* these can trigger defense responses and activate secondary metabolites in grapevine which help in effective defense mechanism against various disease-causing pathogens of grapevine. (Compant et al. 2013). It is observed that the application of both *Pantoea agglomerans* and *Paenibacillus* sp helps in the control of grapevine trunk disease caused by *Neofusicoccum parvum*. (Haidar et al. 2021). The potential roles and mechanisms of the main endophytes involved in the biotic stress tolerance of grapevine are given in Table 4.

A survey was conducted on various vineyards and observed that there are about 381 culturable bacteria isolated from the inner portion of stems and leaves. Of these isolated bacteria, 30% belongs to genus *Bacillus* spp., and the latter include *Paenibacillus* spp., *Microbacterium* spp.,

Table 4: Potential roles and mechanisms of main endophytes involved in biotic stress tolerance of grapevine.

Pathogen	Endophytes	Mechanism associated with the tolerance	Reference
<i>Botrytis cinerea</i>	<i>Acinetobacter lwoffii</i> (PTA-113 and PTA-152), <i>Pseudomonas fluorescens</i> (PTA-268 and PTA-CT2), <i>Pantoea agglomerans</i> (PTA-AF1 and PTA-AF2), <i>Bacillus subtilis</i> (PTA-271).	Induced the activities of lipoxygenase (LOX), phenylalanine ammonia-lyase (PAL), $\beta$ -1,3 glucanase, and chitinase. Induced the oxidative burst. Accumulated the stress-related metabolites phytoalexin (trans-resveratrol and trans- $\epsilon$ -viniferin).	Magnin-Robert et al. (2007) Trotel-Aziz et al. (2008) Verhagen et al. (2011)
	<i>Ulocladium atrum</i> <i>Pseudomonas fluorescens</i> (PTA-CT2).	Enhanced chitinase activity. Regulated the expression of defense-related genes in leaf and root, including those with transcriptional factor functions (JAZ9, NAC1, and ERF1), of secondary metabolism (PAL, STS, LOX9, ACCsyn, GST, CHS, CHI, LAND, and ANR), and PR proteins (PR1, PR2, PR3, PR5, and PR6). Induced callose deposition and H <sub>2</sub> O <sub>2</sub> production.	Ronseaux et al. (2013) Gruau et al. (2015)
	<i>Bukholderia phytofirmans</i> (PsJN).	Primed the expression of PR1, PR2, PR5, and JAZ in bacterized plantlets after pathogen challenge.	Miotto-Vilanova et al. (2016)
	<i>Bacillus subtilis</i> (BBG-127, BBG-131, Bs2504, and BBG-125).	Modulated carbohydrate metabolism. Treatment with <i>Bacillus subtilis</i> strains with non-producing lipopeptides, overproducing surfactin, overproducing plipastatin, and overproducing mycosubtilin differentially activated the plant's innate immune response.	Farace et al. (2015)
	<i>Microbacterium imperial</i> (Rz19M10) <i>Kocuria erythromyxa</i> (Rt5M10) <i>Terribacillus saccharophilus</i> (Rt17M10)	Modulated genes encode a chitinase (chit4c), a protease inhibitor (pin), a salicylic acid (SA) regulated marker (W17.3), and a glucanase (gluc). Induced a systemic response that triggers increases in monoterpenes, sesquiterpenes, tocopherols, and membrane sterols (enhanced antioxidant capacity).	Salomon et al. (2016)
	<i>Streptomyces annulus</i> (S37)	Induced rapid and transient generation of H <sub>2</sub> O <sub>2</sub> , extracellular alkalization, and activation of two mitogen-activated protein kinases (MAPKs) followed by the expression of LOX9, PAL, STS, and GST genes in primed cells. Induced defenses modulated by Ca <sup>2+</sup> signaling.	Vatsa-Portugal et al. (2017)
	<i>Botrytis cinerea</i> , <i>Plasmopara viticola</i> , <i>Xiphinema index</i> nematodes	<i>Paenibacillus</i> spp. strain (B2) Modulated the expression of defense-related genes CHI, PAL, STS, GST, and LOX and pathogenesis-related protein PR-6. Reduced nematode root infection associated with the expression of genes resistant to nematodes Hero and Hs 1 <sup>pro-1</sup> .	Hao et al. (2017)
	<i>Rhizobium vitis</i> (Ti) VAT03-9 (tumorigenic)	<i>Rhizobium vitis</i> (ARK-1) Co-inoculation of ARK-1 with a Ti strain (VAT03-9) into grapevine shoots suppressed the expression of the virulence genes VirA, VirD3, and VirG of VAT03-9.	Kawaguchi et al. (2019)
	<i>Flavescence dorée</i> phytoplasma	<i>Pseudomonas migulae</i> (8R6) Production of 1-aminocyclopropane-1-carboxylate (ACC) deaminase enzyme helps the plant to regulate the level of the stress-related hormone ethylene.	Gamalero et al. (2017).
	<i>Diplodia seriata</i> (strains F98.1 and Ds99.7) (Botryosphaeria dieback)	<i>Aureobasidium pullulans</i> strain (Fito-F278) Modulated genes encoded for plant defense proteins: PR protein 6 (PR-6) and $\beta$ -1,3 glucanase (Gluc), detoxification and stress tolerance: haloacid dehalogenase hydrolase (Hahl), $\alpha$ -crystalline heat shock protein (HSP), $\beta$ 1,3- glucanase (GST5), phenylpropanoid pathway: (STS) cell wall (fascAGP) and water stress (Pip2.2).	Pinto et al. (2018).

Table Cont....



Pathogen	Endophytes	Mechanism associated with the tolerance	Reference
<i>Neofusicoccum parvum</i> (Botryosphaeria dieback)	<i>Bacillus subtilis</i> (PTA-271)	Antagonized <i>Neofusicoccum parvum</i> by delaying its mycelial growth and detoxifying both (R)-mellein and (-) teremutin. Primed defense genes including PR2 ( $\beta$ -1,3 glucanase), NCED2 (involved in ABA synthesis), and PAL at systemic level after pathogen inoculation.	Trotel-Aziz et al. (2019).
<i>Phaeoemoniella chlamydospora</i> (Trunk diseases)	<i>Paenibacillus</i> spp. (S19) <i>Bacillus pumilus</i> (S32)	Induced resistance against trunk disease fungi: induced the expression of defense-related genes PR1, PR10, CHIT3, PAL, STS, CHS, ANTS, CALS, GST, and GLU.	Haidar et al. (2016).

*Staphylococcus* spp., *Micrococcus* spp., *Stenotrophomonas* spp., *Variovorax* spp., *Curtobacterium* spp. and *Agrococcus* spp., etc (Baldan et al. 2014). These are the major endophytic bacteria in the grapevine that provide both environmental and economic benefits by exhibiting plant growth-promoting hormones, providing required nutrients to the host plant, activating various beneficial microorganisms in soil rhizosphere, protecting host plant against biotic stress (pathogen) attack by aggressively competing against them for nutrient, space, and colonization. These endophytes are eco-friendly and improve the environment surrounding the grapevine without causing any detrimental effects on the soil microbiome in the rhizospheric zone. (Marasco et al. 2018).

Some endophytes like *Bacillus* spp., *Pseudomonas* spp., and *Micrococcus* spp., exhibit beneficial effects to resist various abiotic stresses like arsenic contamination, high temperature, drought, chilling, and salinity, respectively (Pacifico et al. 2019, Parashar & Mudgal 2024). The bacterial endophyte *Paraburkholderia phytofirmans* slowly gathers trehalose in grapevine to resist various abiotic stress by forming a gel during cellular dehydration to stop excess water loss from the host plant (Fernandez et al. 2012). *Pseudomonas* spp. is an endophytic bacteria that helps grapevine in resisting against cold conditions by inducing various PR (Pathogenesis) genes that encode chitinase, phenylalanine ammonia-lyase (PAL), lipoxygenase (LOX), and glucanase. Some endophytes can convert detoxification compounds into signaling molecules by decreasing ROS (Reactive oxygen species) concentration with the help of some genes, which particularly encode the enzymes in ROS accumulation in grapevine (Theocharis et al. 2012).

The bacterial endophyte *Bacillus licheniformis* can able to exhibit various secondary metabolites such as monoterpenes (antioxidant activity) and sesquiterpenes (antimicrobial activity) in grapevine to protect the host plant from various abiotic stress (Salomon et al. 2014). *Bacillus licheniformis* is an endophytic bacteria that produces catenoids (antioxidants) in the grapevine that help the host plant survivability under various extremely unfavorable conditions to stop both plant growth and development; it may be due to abiotic/biotic/

environmental changes (Cohen et al. 2018). It is observed that bacterial endophytes like *Bacillus licheniformis* and *Pseudomonas fluorescens* can able to encode genes that induce the expression of ABA synthesis and signaling pathways in grapevine plants (Salomon et al. 2014). Some endophytic fungi like *Septaglomerum deserticola*, *Funneliformis mosseae*, *Rhizoglomerum intraradices*, *Rhizoglomerum clarum*, and *Glomus aggregatum* can alter ABA metabolism when these endophytes are inoculated into grapevine so that they can survive effectively under drought condition (Torres et al. 2018).

Recently, many endophytes have been observed that can help grapevine accumulate protective molecules like melatonin, proline, and carotenoids, which are activated when the host plant suffers from various abiotic stress to help survive through that stress condition (Liu & Brettell 2019). Certain endophytes from grapevine orchards that have been isolated for further investigation can modify the chemical and physical characteristics of both leaves and berries as they ripen. Particularly, fungal endophytes alter the modify the total content of reduced sugar, total flavonoids, total phenols, resveratrol, and PAL activity in grapevine. These endophytes can determine the quality of wine and other edible products produced from grapevine (Yang et al. 2016). Some endophytes, when inoculated, help in enhancing growth and development, improving fruit quality and yield of grapevine, which help in relieving farmers' economic burden by improving profits gained with each fruit sold in the market (Huang et al. 2018). some of the endophytes can exhibit secondary metabolites inside grapevine, which lowers the cost of buying pesticides to control various grapevine diseases and improves economic value by large-scale production of grapevine (Suryanarayanan et al. 2009).

## BIOFORMULATION

### Role of Endophyte-Based Bioformulation in Sustainable Agriculture

Bioformulations are microbial-based products consisting of beneficial microbes called endophytes, which help in

improving plant growth, supply nutrients to plants, and control various diseases caused by phytopathogens in an eco-friendly manner without causing any detrimental effects to the beneficial microbes in the rhizospheric zone and host plants (Burragoni & Jeon 2021). The bio-formulation process in agriculture involves the selection of beneficial microbial strains and a suitable carrier. An appropriate carrier is a vehicle that houses latent live microorganisms and provides a supportive niche to the microbial population (Khan et al. 2023). A bioformulation of an endophyte is said to be good when it is effective, non-polluting, readily biodegradable, with high water retention capacity and sufficient shelf life (Chaudhary et al. 2020).

Endophytic bioformulation products can serve as a sustainable substitute for chemical fertilizers and pesticides. This is because chemical fertilizers can decrease soil fertility when used excessively, increase the possibility of pathogen mutation, and cause resistance to pesticides altogether (Arora & Mishra 2016, Sharma et al. 2023). Bioformulation products comprise active ingredients and inert ingredients. The active ingredient may be living microbe, spores, and their products, which should be in living conditions. It also requires some inert ingredients, *i.e.*, peat, talc, vermiculate, carboxymethylcellulose, and polymers like xanthan gum and diatomaceous earth, for bioformulation to be developed successfully. The inert carrier-based bioformulations helped insert antagonistic microbial cells into both the rhizospheric region and plant system through both foliar and soil application for a longer duration (Ardakani et al. 2010, Jorjani et al. 2011). Some additives, *i.e.*, gum, silica gel, methyl-cellulose, and starch, help protect these endophyte bio-formulated products from extreme environmental conditions, which also improve the physical, chemical, and nutritional properties of these products (Schisler et al. 2004).

Nowadays, endophyte-based bioformulation products are essential in sustainable agriculture to protect crops from phytopathogens and decrease disease-prone agricultural zones because of the resistance risk of pathogen mutation caused by using pesticides. Additionally, these bio-formulations either directly or indirectly enhance plant growth and development in their native environments (Lugtenberg & Kamilova 2009). There are also some limitations in successfully producing endophyte-based bioformulation products as we know that they consist of living microbes, so extreme care should be taken to maintain microbial load and vigor without contamination of the original product, which determines the quality of the product sold to the market (Kashyap et al. 2023). The development of these products is highly constricted due to a lack of advanced technology, instruments, lack of knowledge,

improper distribution, inexperienced manpower, technical difficulties, and importation laws, which leads to a loss of endophyte viability and decreases the efficacy of these products. Some other major limitations are high production costs and inconsistent performance. These living endophyte cells used in making bioformulations are highly sensitive to external factors, and the person handling them should follow caution during culture, distribution, and application (Arora & Mishra 2016, Xia et al. 2022).

## LIMITATIONS OF ENDOPHYTES IN SUSTAINABLE AGRICULTURE

Many endophytes are uncultured and unidentified because databases for endophytes and their metabolites are still unavailable (Xia et al. 2022). Endophytes show specific characteristics towards certain plant species, and they may not act the same on the other plant species, which limits their effectiveness in the application of various crops in the world. Their effectiveness is influenced by some environmental factors like temperature, moisture, and soil characteristics, etc respectively. Their compatibility with agricultural requirements like fertilizers and pesticides is to be considered till now. Some combinations may be synergistic, while some may be antagonistic (Watts et al. 2023). It requires large investments to develop and commercialize endophytic products through numerous research, production, and marketing methods. It may be a challenge for the product to get profits exceeding its initial investment as the small-scale farmers cannot afford it if the price is higher. It is a complex and time-consuming process to get approval from regulatory governing bodies regarding endophytic products as they change from region to region and its landscape navigation difficulty by regulatory bodies limits its commercialization. Even with the recent accomplishments and advancements in endophyte research, there is still a knowledge gap. The relationship between endophytes and plants is still developing, and our understanding of their means of action, long-term impacts, and molecular interactions with the host plant is limited. Their risk in introducing into agricultural systems without proper knowledge about them is more as we must face the unknown consequences (Kaur et al. 2023).

In the quadrutrophic system involving fruits, pathogens, and endophytes, the host faces limitations in terms of nutrition and space (Kashyap et al. 2023). Competition with pathogenic microorganisms for niche and nutrition, namely niche exclusion, is a promising mechanism for the use of endophytes in plant disease control (Liarzi & Ezra 2013). Both endophytes and pathogens rely on essential nutrients such as nitrogen, carbon, macro, and micronutrients for their survival (Kumari et al. 2022). However, after the application

of microbial biocontrol agents, these agents compete with the target pests or pathogens for space and nutrients by colonizing the same ecological niches or habitats as the target organisms, such as plant surfaces, soil, or water, and trying to establish themselves and proliferate. The biocontrol agents can out-compete the pests or pathogens by utilizing available resources more efficiently, depriving them of essential nutrients, or occupying physical spaces that prevent their establishment. In addition to competing with the target organisms, microbial biocontrol agents may also compete with the native microbial communities (Kumari et al. 2022). Native microorganisms are naturally present in ecosystems and play important roles in nutrient cycling, disease suppression, and maintaining ecosystem balance. The introduction of biocontrol agents can disrupt the existing microbial communities and create competition for resources (Kumar et al. 2020). Endophytes might also be ineffective when the disease is caused by a high presence of pathogens (Lahlali et al. 2014).

## FUTURE ASPECTS OF ENDOPHYTES

We must explore, identify, and characterize various new species of endophytes to improve our understanding of their habitat, mode of action, how they interact with host plants, they will have any beneficial effect on that host plant or not as we explore various plant species, we can find novel endophytes with unique characteristics as we know that the endophytes are plant specific. We know that there are many microorganisms in the world. Some may be beneficial to some plants, and the remaining may be harmful to other plants. These beneficial microorganisms we name them as endophytes as their role in plant growth and development is diverse: To create products from these endophytes and apply them at the *in vivo* level for sustainable agriculture, we must first examine their properties and the impact they will have on the plant to which we intend to apply them.

Additionally, we need to gain a deeper understanding of the molecular interactions between the endophyte and the host plant to gain insight into potential future applications. For conducting molecular studies, we can use techniques such as transcriptomics, proteomics, and metabolomics to know the signaling pathways and gene regulation they do inside the plant. Now, as our understanding of these endophytes improves, we must select endophytes that are beneficial to a specific plant, and we can make bioformulation products of these endophytes, which can improve their survival, colonization, and efficacy on targeted plants when applied *in vivo*. These endophytes-based products are new as they have no records of their effectiveness in reducing abiotic/biotic stress in plants. So, we must investigate their efficacy under

real-world conditions long-term to check their effectiveness in reducing the effect of both abiotic/biotic stress on targeted plants so we can apply them risk-free in sustainable agriculture. As the application of these endophytes-based products increases day by day, there is a need for some guidelines and safety standards should be framed by the regulatory bodies so that we can follow these guidelines. Following that these safety standards can be commercialized into the market to be used in agricultural practices.

## CONCLUSIONS

In the past three decades, remarkable progress has been made in research on plant disease resistance mechanisms and plant-microbe interactions. Endophytes, colonizing plant tissues, are regarded as naturally occurring agents in plant disease suppression. Most of their success is attributed to the production of a vast array of metabolites. In this review, we studied the management of various fungal diseases of grapevine with the help of various endophytes (may be bacterial or fungal), which are eco-friendly. These endophytes also play a major role in growth and development of grapevine by acquiring nutrients, production of phytohormones, phytoenzymes, secondary metabolites, acting as biocontrol agents, phosphate solubilization, siderophore synthesis, defense responses, and inducing resistance for suppressing various phytopathogens by inhibiting their growth and development in host plants and prevent them from causing diseases which leads to major losses in crop yield of grapevine. Some endophytes help in reducing abiotic stress in the grapevine. Endophytes are reliable and environmentally friendly in plant disease management and crucial for sustainable agriculture. However, to truly achieve their large-scale commercial production and application, we still have some challenges to overcome. Biocontrol effects of endophytes are not stable in field trials. It is necessary to elevate the exploitation of endophytes and their metabolites in the biological control of plant diseases to the multi-omics level as a promising research frontier.

## REFERENCES

- Abreu-Tarazi, M.F., Navarrete, A.A. Andreote, F.D., Almeida, C.V., Tsai, S.M. and Almeida, M. 2010. Endophytic bacteria in long-term *in vitro* cultivated "axenic" pineapple microplants revealed by PCR-DGGE. *World Journal of Microbiology and Biotechnology*, 26, pp.555-560. DOI
- Ait Barka, E., Belarbi, A., Hachet, C., Nowak, J. and Audran, J.C. 2000. Enhancement of *in vitro* growth and resistance to grey mold of *Vitis vinifera* co-cultured with plant-promoting rhizobacteria. *FEMS Microbiology Letters*, 186, pp.91-95. DOI
- Aleynova, O.A., Suprun, A.R., Nityagovsky, N.N., Dubrovina, A.S. and Kiselev, K.V. 2021. The influence of the grapevine bacterial and fungal

- endophytes on biomass accumulation and stilbene production by the in vitro cultivated cells of *Vitis amurensis* Rupr. *Plants*, 10, p.1276. DOI
- Alfonzo, A., Conigliaro, G., Torta, L., Burruano, S. and Monschietti, G. 2009. Antagonism of *Bacillus subtilis* strain AG1 against vine wood fungal pathogens. *Phytopathologia Mediterranea*, 48, pp.155–158. DOI
- Andreolli, M., Lampis, S., Zapparoli, G., Angelini, E. and Vallini, G. 2016. Diversity of bacterial endophytes in 3 and 15-year-old grapevines of *Vitis vinifera* cv. Corvina and their potential for plant growth promotion and phytopathogen control. *Microbiological Research*, 183, pp.42–52. DOI
- Andreolli, M., Zapparoli, G., Angelini, E., Lucchetta, G., Lampis, S. and Vallini, G. 2019. *Pseudomonas protegens* MP12: a plant growth-promoting endophytic bacterium with broad-spectrum antifungal activity against grapevine phytopathogens. *Microbiological Research*, 219, pp.123–131. DOI
- Ardakani, S.S., Heydari, A., Khorasani, N. and Arjmandi, R. 2010. Development of new bioformulations of *Pseudomonas fluorescens* and evaluation of these products against damping-off of cotton seedlings. *Journal of Plant Pathology*, 92, pp.83–88. DOI
- Armijo, G., Schlechter, R., Agurto, M., Muñoz, D., Nuñez, C. and Arce-Johnson, P. 2016. Grapevine pathogenic microorganisms: Understanding infection strategies and host response scenarios. *Frontiers in Plant Science*, 7, p.382. DOI
- Arora, N.K. and Mishra, J. 2016. Prospecting the roles of metabolites and additives in future bioformulations for sustainable agriculture. *Applied Soil Ecology*, 107, pp.405–407. DOI
- Baldan, E., Nigris, S., Populin, F., Zottini, M., Squartini, A. and Baldan, B. 2014. Identification of culturable bacterial endophyte community isolated from tissues of *Vitis vinifera* “Glera”. *Plant Biosystems: An International Journal Dealing with All Aspects of Plant Biology*, 148, pp.508–516. DOI
- Baldan, E., Nigris, S., Romualdi, C., D’Alessandro, S., Clocchiatti, A., Zottini, M. and Baldan, B. 2015. Beneficial bacteria isolated from grapevine inner tissues shape *Arabidopsis thaliana* roots. *PLOS ONE*, 10, p.e0140252. DOI
- Bordiec, S., Paquis, S., Lacroix, H., Dhondt, S., Ait Barka, E., Kauffmann, S., Jeandet, P., Mazeyrat-Gourbeyre, F., Clement, C., Baillieul, F. and Dorey, S., 2011. Comparative analysis of defense responses induced by the endophytic plant growth-promoting rhizobacterium *Burkholderia phytofirmans* strain PsJN and the non-host bacterium *Pseudomonas syringae* pv. *pisi* in grapevine cell suspensions. *Journal of Experimental Botany*, 62, pp.595–603. DOI
- Brader, G., Compant, S., Vescio, K., Mitter, B., Trognitz, F., Ma, L.J. and Sessitsch, A., 2017. Ecology and genomic insights into plant-pathogenic and plant-nonpathogenic endophytes. *Annual Review of Phytopathology*, 55, pp.61–83. DOI
- Bruisson, S., Zufferey, M., L’Haridon, F., Trutmann, E., Anand, A., Dutartre, A., Vrieze, M.D. and Weisskopf, L., 2019. Endophytes and epiphytes from the grapevine leaf microbiome as potential biocontrol agents against phytopathogens. *Frontiers in Microbiology*, 10, p.2726. DOI
- Bulgari, D., Casati, P., Quagliano, F. and Bianco, P.A., 2014. The endophytic bacterial community of grapevine leaves is influenced by sampling date and the phytoplasma infection process. *BMC Microbiology*, 14, pp.1–11. DOI
- Burragoni, S.G. and Jeon, J., 2021. Applications of endophytic microbes in agriculture, biotechnology, medicine, and beyond. *Microbiological Research*, 245, p.126691. DOI
- Burruano, S., Alfonzo, A., Lo Piccolo, S., Conigliaro, G., Mondello, V., Torta, L., Moretti, M. and Assante, G., 2008. Interaction between *Acremonium byssoides* and *Plasmopara viticola* in *Vitis vinifera*. *Phytopathologia Mediterranea*, 47, pp.122–131. DOI
- Calamita, F., Imran, H.A., Vescovo, L., Mekhalif, M.L. and La Porta, N., 2021. Early identification of root rot disease by using hyperspectral reflectance: The case of pathosystem grapevine/*Armillaria*. *Remote Sensing*, 13, p.2436. DOI
- Calzarano, F., Pagnani, G., Pisante, M., Bellocci, M., Cillo, G., Metruccio, E.G. and Di Marco, S., 2021. Factors involved in Tiger-stripe foliar symptom expression of esca of grapevine. *Plants*, 10, p.1041. DOI
- Chaudhary, T., Dixit, M., Gera, R., Shukla, A.K., Prakash, A., Gupta, G. and Shukla, P., 2020. Techniques for improving formulations of bioinoculants. *3 Biotech*, 10, pp.1–9. DOI
- Cohen, A.C., Dichiar, E., Jofré, V., Antonioli, A., Bottini, R. and Piccoli, P., 2018. Carotenoid profile produced by *Bacillus licheniformis* Rt4M10 isolated from grapevines grown at high altitude and their antioxidant activity. *International Journal of Food Science & Technology*, 53, pp.2697–2705. DOI
- Compant, S., Brader, G., Muzammil, S., Sessitsch, A., Lebrhi, A. and Mathieu, F. 2013. Use of beneficial bacteria and their secondary metabolites to control grapevine pathogen diseases. *Biological Control*, 58, pp.435–455. DOI
- Compant, S., Reiter, B., Sessitsch, A., Nowak, J., Clément, C. and Ait Barka, E. 2005. Endophytic colonization of *Vitis vinifera* L. by plant growth-promoting bacterium *Burkholderia* spp. Strain PsJN. *Applied and Environmental Microbiology*, 71, pp.1685–1693. DOI
- Das, A. and Varma, A. 2009. Symbiosis: The Art of Living. *Symbiotic Fungi: Principles and Practices*, 1, pp.1–28. DOI
- Das, A.K., Chosdon, T., Nawale, R., Koder, S.B., Bhosale, R.K., Rana, M. and Srivastava, S. 2021. Role of rhizospheric microbiome against soil-borne pathogens. *Biopesticides International*, 17, pp.1–15. DOI
- De Vleeschauwer, D. and Höfte, M. 2009. Rhizobacteria-induced systemic resistance. *Advances in Botanical Research*, 51, pp.223–281. DOI
- DeKrey, D.H., Klodd, A.E., Clark, M.D. and Blanchette, R.A. 2022. Grapevine trunk diseases of cold-hardy varieties grown in Northern Midwest vineyards coincide with canker fungi and winter injury. *PLOS ONE*, 17, e0269555. DOI
- Doilom, M., Manawasinghe, I.S., Jeewon, R., Jayawardena, R.S., Tibpromma, S., Hongsan, S., Meepol, W., Lumyong, S., Jones, E.B.G. and Hyde, K.D. 2017. Can ITS sequence data identify fungal endophytes from cultures? A case study from *Rhizophora apiculata*. *Mycosphere*, 8, pp.1869–1892. DOI
- Dudeja, S.S., Giri, R., Saini, R., Suneja-Madan, P. and Kothe, E. 2012. Interaction of endophytic microbes with legumes. *Journal of Basic Microbiology*, 52, pp.248–260. DOI
- Dwibedi, V. and Saxena, S. 2018. *Arcopilus aureus*, a resveratrol-producing endophyte from *Vitis vinifera*. *Applied Biochemistry and Biotechnology*, 186, pp.476–495. DOI
- Favaro, G., Bogianni, S., Di Gangi, I.M., Nigris, S., Baldan, E., Squartini, A., Pastore, P. and Baldan, B. 2016. Characterization of lipopeptides produced by *Bacillus licheniformis* using liquid chromatography with accurate tandem mass spectrometry. *Rapid Communications in Mass Spectrometry*, 30, pp.2237–2252. DOI
- Fedorina, J., Tikhonova, N., Ukhatova, Y., Ivanov, R. and Khlestkina, E. 2022. Grapevine gene systems for resistance to Gray mold *Botrytis cinerea* and Powdery mildew *Erysiphe necator*. *Agronomy*, 12, p.499. DOI
- Felber, A.C., Orlandelli, R.C., Rhoden, S.A., Garcia, A., Costa, A.T., Azevedo, J.L. and Pamphile, J.A. 2016. Bioprospecting foliar endophytic fungi of *Vitis labrusca* Linnaeus, Bordô and Concord cv. *Annals of Microbiology*, 66, pp.765–775. DOI
- Fermaud, M., Smits, N., Merot, A., Roudet, J., Thierry, D., Wéry, J. and Delbac, L. 2016. New multipest damage indicator to assess protection strategies in grapevine cropping systems. *Australian Journal of Grape and Wine Research*, 22, pp.450–461. DOI
- Fernandez, O., Vandesteene, L., Feil, R., Baillieul, F., Lunn, J.E. and Clément, C. 2012. Trehalose metabolism is activated upon chilling in grapevine and might participate in *Burkholderia phytofirmans*-induced chilling tolerance. *Planta*, 236, pp.355–369. DOI



- Firdous, J., Mona, R. and Muhamad, N. 2019. Endophytic bacteria and their potential application in agriculture: A review. *Indian Journal of Agricultural Research*, 53, pp.1-7. DOI
- Fischer, M., 2022. *Pseudopezizicola tracheiphila* (Rotbrenner). *CABI Compendium*, 45251. DOI
- Gamaleri, E., Marzachi, C., Galetto, L., Veratti, F., Massa, N., Bona, E., Novello, G., Glick, B. R., Ali, S., Cantamessa, S., D'Agostino, G. and Berta, G. 2017. A 1-Aminocyclopropane-1-carboxylate (ACC) deaminase-expressing endophyte increases plant resistance to *Flavescence dorée* phytoplasma infection. *Plant Biosystems: International Journal of Plant Biology*, 151, pp.331-340. DOI
- Gouda, S., Das, G., Sen, S.K., Shin, H.S. and Patra, J.K. 2016. Endophytes: A treasure house of bioactive compounds of medicinal importance. *Frontiers in Microbiology*, 7, p.1538. DOI
- Gramaje, D., Úrbez-Torres, J.R. and Sosnowski, M.R. 2018. Managing grapevine trunk diseases with respect to etiology and epidemiology: Current strategies and prospects. *Plant Disease*, 102, pp.12-39. DOI
- Gruau, C., Trotel-Aziz, P., Villaume, S., Rabenoelina, F., Clément, C., Baillieul, F. and Aziz, A. 2015. *Pseudomonas fluorescens* PTA-CT2 triggers local and systemic immune response against *Botrytis cinerea* in grapevine. *Molecular Plant-Microbe Interactions*, 28, pp.1117-1129. DOI
- Gunatilaka, A.L. 2006. Natural products from plant-associated microorganisms: Distribution, structural diversity, bioactivity, and implications of their occurrence. *Journal of Natural Products*, 69, pp.509-526. DOI
- Haidar, R., Amira, Y., Roudet, J., Marc, F. and Patrice, R. 2021. Application methods and modes of action of *Pantoea agglomerans* and *Paenibacillus* spp. to control the grapevine trunk disease-pathogen, *Neofusicoccum parvum*. *OENO One*, 55(3), pp.1-16. DOI
- Haidar, R., Roudet, J., Bonnard, O., Dufour, M.C., Corio-Costet, M.F., Fert, M., Gautier, T., Deschamps, A. and Fermaud, M. 2016. Screening and modes of action of antagonistic bacteria to control the fungal pathogen *Phaeoemoniella chlamydospora* involved in grapevine trunk diseases. *Microbiological Research*, 192, pp.172-184. DOI
- Hamaoka, K., Aoki, Y. and Suzuki, S., 2021. Isolation and characterization of endophyte *Bacillus velezensis* KOF112 from grapevine shoot xylem as a biological control agent for fungal diseases. *Plants*, 10, p.1815. DOI
- Hao, Z., Van Tuinen, D., Wipf, D., Fayolle, L., Chataignier, O., Li, X., Chen, B., Gianinazzi, S., Gianinazzi, P., Vivienne, and Adrian, M., 2017. Biocontrol of grapevine aerial and root pathogens by *Paenibacillus* sp. strain B2 and paenimycin in vitro and in planta. *Biological Control*, 109, pp.42-50. DOI
- Hardoim, P.R., van Overbeek, L.S. and van Elsas, J.D., 2008. Properties of bacterial endophytes and their proposed role in plant growth. *Trends in Microbiology*, 16, pp.463-471. DOI
- Hardoim, P.R., Van Overbeek, L.S., Berg, G., Pirttilä, A.M., Compant, S., Campisano, A., Doring, M. and Sessitsch, A., 2015. The hidden world within plants: ecological and evolutionary considerations for defining functioning of microbial endophytes. *Microbiology and Molecular Biology Reviews*, 79, pp.293-320. DOI
- Hsieh, T.F., Shen, Y.M., Huang, J.H., Tsai, J.N., Lu, M.T. and Lin, C.P., 2023. Insights into grape ripe rot: A focus on the *Colletotrichum gloeosporioides* species complex and its management strategies. *Plants*, 12, p.2873. DOI
- Huang, L.H., Yuan, M.Q., Ao, X.J., Ren, A.Y., Zhang, H.B. and Yang, M.Z., 2018. Endophytic fungi specifically introduce novel metabolites into grape flesh cells in vitro. *PLoS One*, 13, p.e0196996. DOI
- Indian Group Forum, 2019. Indian Grape Forum. Retrieved, November 2019, from <https://www.freshplaza.com/article/9164030/indian-grape-forum-2019-to-launch-november-17th>.
- Jackson, R.S., 2014. Vineyard practice. *Wine Science*, pp.143-306.
- Jeewon, R., Ittoo, J., Mahadeb, D., Jaufeerally-Fakim, Y., Wang, H.K. and Liu, A.R., 2013. DNA-based identification and phylogenetic characterization of endophytic and saprobic fungi from *Antidesma madagascariense*, a medicinal plant in Mauritius. *Journal of Mycology*, pp.1-10. DOI
- Jorjani, M., Heydari, A., Zamanizadeh, H.R., Rezaee, S. and Naraghi, L., 2011. Development of *Pseudomonas fluorescens* and *Bacillus coagulans*-based bio formulations using organic and inorganic carriers and evaluation of their influence on growth parameters of sugar beet. *Journal of Biopesticides*, 4, p.180. DOI
- Karlsson, P. and Karlsson, B., 2021. Vineyard Area In The World In 2020, A Detailed Look [WWW Document]. Forbes. Available at <https://www.forbes.com/sites/karlsson/2021/12/28/vineyard-area-in-the-world-in-2020-a-detailed-look/>.
- Kashyap, N., Singh, S.K., Yadav, N., Singh, V.K., Kumari, M., Kumar, D., Shukla, L., Bhardwaj, N.K. and Kumar, A., 2023. Biocontrol screening of endophytes: applications and limitations. *Plants*, 12, p.2480. DOI
- Kaur, G., Patel, A., Dwibedi, V. and Rath, S.K., 2023. Harnessing the action mechanisms of microbial endophytes for enhancing plant performance and stress tolerance: current understanding and future perspectives. *Archives of Microbiology*, 205, p.303. DOI
- Kenfaoui, J., Lahlali, R., Mennani, M., Radouane, N., Goura, K., El Hamss, H., El Ghadraoui, L., Fontaine, F., Tahiri, A., Barka, E.A. and Amiri, S., 2022. *Botryosphaeria Dieback* (*Lasioidiplodia viticola*): An imminent emerging threat to Moroccan vineyards. *Plants*, 11, p.2167. DOI
- Khan, A., Singh, A.V., Gautam, S.S., Agarwal, A., Punetha, A., Upadhyay, V.K., Kukreti, B., Bundela, V., Jugran, A.K. and Goel, R., 2023. Microbial bioformulation: a microbial-assisted biostimulating fertilization technique for sustainable agriculture. *Frontiers in Plant Science*, 14, p.1270039. DOI
- Koledenkova, K., Esmacel, Q., Jacquard, C., Nowak, J., Clément, C. and Ait Barka, E., 2022. *Plasmopara viticola*, the causal agent of downy mildew of grapevine: from its taxonomy to disease management. *Frontiers in Microbiology*, 13, p.889472. DOI
- Kulišová, M., Vrublevska, M., Lovecká, P., Vrchotová, B., Stránská, M., Kolařík, M. and Kolouchová, I., 2021. Fungal endophytes of *Vitis vinifera*—plant growth promotion factors. *Agriculture*, 11, p.1250. DOI
- Kumari, M., Kamat, S., Dixit, P., Pandey, S., Giri, V.P. and Mishra, A., 2021. Microbial formulation approaches in postharvest disease management. *Food Security and Plant Disease Management*, pp.279-305. DOI
- Kumari, M., Qureshi, K.A., Jaremko, M., White, J.F., Singh, S.K., Sharma, V.K., Singh, K.K., Santoyo, G., Puopolo, G. and Kumar, A., 2022. Deciphering the role of endophytic microbiome in postharvest disease management of fruits: opportunity areas in commercial up-scale production. *Frontiers in Plant Science*, 13, p.1026575. DOI
- Kunova, A., Pizzatti, C., Saracchi, M., Pasquali, M. and Cortesi, P., 2021. Grapevine powdery mildew: fungicides for its management and advances in molecular detection of markers associated with resistance. *Microorganisms*, 9, p.1541. DOI
- Kusari, S., Hertweck, C. and Spiteller, M., 2012. Chemical ecology of endophytic fungi: origins of secondary metabolites. *Chemistry & Biology*, 19, pp.792-798. DOI
- Lahlali, R., McGregor, L., Song, T., Gossen, B.D., Narisawa, K. and Peng, G., 2014. *Heteroconium chaetospora* induces resistance to clubroot via upregulation of host genes involved in jasmonic acid, ethylene, and auxin biosynthesis. *PLOS One*, 9, p.e94144. DOI
- Li, H., Ding, J., Liu, C., Huang, P., Yang, Y., Jin, Z. and Qin, W., 2023. Carvacrol treatment reduces decay and maintains the postharvest quality of red grape fruits (*Vitis vinifera* L.) inoculated with *Alternaria alternata*. *Foods*, 12, p.4305. DOI
- Li, Z., Chang, P., Gao, L. and Wang, X., 2000. The endophytic fungus *Albifimbria verrucaria* from wild grape as an antagonist of *Botrytis cinerea* and other grape pathogens. *Phytopathology*, 110, pp.843-850. DOI
- Li, Z., DosSantos, R.F., Gao, L., Chang, P. and Wang, X., 2021. Current

- status and future prospects of grapevine anthracnose caused by *Elsinoe ampelina*: An important disease in humid grape-growing regions. *Molecular Plant Pathology*, 22, pp.899-910. DOI
- Liarzi, O. and Ezra, D., 2013. Endophyte-mediated biocontrol of herbaceous and non-herbaceous plants. In: *Advances in endophytic research*. Springer, pp.335-369. DOI
- Liu, H. and Brettell, L.E., 2019. Plant defense by VOC-induced microbial priming. *Trends in Plant Science*, 24, pp.187-189. DOI
- Lo Presti, L., Lanver, D., Schweizer, G., Tanaka, S., Liang, L., Tollot, M., Zuccaro, A., Reissmann, S. and Kahmann, R., 2015. Fungal effectors and plant susceptibility. *Annual Review of Plant Biology*, 66, pp.513-545. DOI
- Lugtenberg, B. and Kamilova, F., 2009. Plant-growth-promoting rhizobacteria. *Annual Review of Microbiology*, 63, pp.541-556. DOI
- Magnin-Robert, M., Trotel-Aziz, P., Quantinet, D., Biagianti, S. and Aziz, A., 2007. Biological control of *Botrytis cinerea* by selected grapevine-associated bacteria and stimulation of chitinase and  $\beta$ -1,3-glucanase activities under field conditions. *European Journal of Plant Pathology*, 118, pp.43-57. DOI
- Marasco, R., Rolli, E., Fusi, M., Michoud, G. and Daffonchio, D., 2018. Grapevine rootstocks shape underground bacterial microbiomes and networking but not potential functionality. *Microbiome*, 6, p.17. DOI
- Martinez-Medina, A., Flors, V., Heil, M., Mauch-Mani, B., Pieterse, C.M., Pozo, M.J., Ton, J., van Dam, N.M. and Conrath, U., 2016. Recognizing plant defense priming. *Trends in Plant Science*, 21, pp.818-822. DOI
- Mauch-Mani, B., Baccelli, B., Luna, E. and Flors, V., 2017. Defense priming: An adaptive part of induced resistance. *Annual Review of Plant Biology*, 68, pp.485-512. DOI
- Maurya, S., Ntakirutimana, R., Debnath, B., Rana, M., Kaushik, D. and Srivastava, S., 2024. *Trichoderma* and their secondary metabolites – A potential approach in plant disease management. *Biopesticides International*, 20, pp.21-33. DOI
- Mendes, R., Kruijt, M., DeBruijn, I., Dekkers, E., VanDerVoort, M., Schneider, J.H., Piceno, Y.M., DeSantis, T.Z., Andersen, G.L., Bakker, P.A.H.M. and Raaijmakers, J.M., 2011. Deciphering the rhizosphere microbiome for disease-suppressive bacteria. *Science*, 332, pp.1097-1100. DOI
- Miotto-Vilanova, L., Jacquard, C., Courteaux, B., Wortham, L., Michel, J., Clément, C., Barka, E.A. and Sanchez, L., 2016. *Burkholderia phytofirmans* PsJN confers grapevine resistance against *Botrytis cinerea* via a direct antimicrobial effect combined with better resource mobilization. *Frontiers in Plant Science*, 7, p.1236. DOI
- Mishra, J., Tewari, S. and Singh, S., 2015. Biopesticides: Where do we stand? *Plant Microbe Symbiosis*. DOI
- Mondello, V., Spagnolo, A., Larignon, P., Clement, C. and Fontaine, F., 2019. The phyto-protection potential of *Fusarium proliferatum* for control of *Botryosphaeria* dieback pathogens in grapevine. *Phytopathologia Mediterranea*, 58, pp.293-306. DOI
- Mugnai, L., Graniti, A. and Surico, G., 1999. Esca (Black Measles) and Brown wood-streaking: Two old and elusive diseases of grapevines. *Plant Disease*, 83, pp.404-418. DOI
- Musetti, R., Vecchione, A., Stringher, L., Borselli, S., Zulini, L., Marzani, C., D'Ambrosio, M., Sanità di Toppi, L. and Pertot, I., 2006. Inhibition of sporulation and ultrastructural alterations of grapevine downy mildew by the endophytic fungus *Alternaria alternata*. *Phytopathology*, 96, pp.689-698. DOI
- MuthuNarayanan, M., Ahmad, N., Shivanand, P. and Metali, F., 2022. The role of endophytes in combating fungal- and bacterial-induced stress in plants. *Molecules*, 27, p.6549. DOI
- Nigris, S., Baldan, E., Tondello, A., Zanella, F., Vitulo, N., Favaro, G., Guidolin, V., Bordin, N., Telatin, A., Barizza, E., Marcato, S., Zottini, M., Squartini, A., Valle, G. and Baldan, B., 2018. Biocontrol traits of *Bacillus licheniformis* GL174, a culturable endophyte of *Vitis vinifera* cv. Glera. *BMC Microbiology*, 18, pp.1-16. DOI
- Pacifico, D., Squartini, A., Crucitti, D., Barizza, E., LoSchiavo, F., Muresu, R., Carimi, F. and Zottini, M., 2019. The role of the endophytic microbiome in the grapevine response to environmental triggers. *Frontiers in Plant Science*, 10, p.1256. DOI
- Parashar, M. and Mudgal, G., 2024. The Prostrate Spurge-isolated PGPB endophytes, EP1-AS and EP1-BM, can tolerate high levels of salinity and heavy metals and allow wheat growth under these stressors. *Natural Environment and Pollution Technology*, 23(2). DOI
- Patya, U., Kumar, V., Singh, M. and Singh, K., 2023. Plant growth-promoting efficacy of endophytic fungi isolated from the terrestrial plants of North India. *Natural Environment and Pollution Technology*, 22(3). DOI
- Pavithra, G., Bindal, S., Rana, M. and Srivastava, S., 2020. Role of endophytic microbes against plant pathogens: A review. *Asian Journal of Plant Science*, 9, pp.54-62. DOI
- Pavithra, G., Manda, R.R., Addanki, V.A. and Srivastava, S., 2021. Evaluation of isolated endophytes, bio-agents, and fungicides against anthracnose of chilli. *Biopesticides International*, 17, pp.143-149. DOI
- Perazzolli, M., Dagostin, S., Ferrari, A., Elad, Y. and Pertot, I., 2008. Induction of systemic resistance against *Plasmopara viticola* in grapevine by *Trichoderma harzianum* T39 and benzothiadiazole. *Biological Control*, 47, pp.228-234. DOI
- Pineda, A., Zheng, S.J., van Loon, J.J., Pieterse, C.M. and Dicke, M., 2010. Helping plants to deal with insects: The role of beneficial soil-borne microbes. *Trends in Plant Science*, 15, pp.507-514. DOI
- Pinto, C., Custódio, V., Nunes, M., Songy, A., Rabenoelina, F., Courteaux, B., Clement, C., Gomes, A.C. and Fontaine, F., 2018. Understand the potential role of *Aureobasidium pullulans*, a resident microorganism from the grapevine, in preventing the infection caused by *Diplodia seriata*. *Frontiers in Microbiology*, 9, p.3047. DOI
- Potshangbam, M., Devi, S.I., Sahoo, D. and Strobel, G.A., 2017. Functional characterization of endophytic fungal community associated with *Oryza sativa* L. and *Zea mays* L. *Frontiers in Microbiology*, 8, p.325. DOI
- Rondot, Y. and Reineke, A., 2019. Endophytic *Beauveria bassiana* activates the expression of defense genes in the grapevine and prevents infections by grapevine downy mildew *Plasmopara viticola*. *Plant Pathology*, 68, pp.1719-1731. DOI
- Salomon, M.V., Bottini, R., de Souza Filho, G.A., Cohen, A.C., Moreno, D., Gil, M. and Piccoli, P., 2014. Bacteria isolated from roots and rhizosphere of *Vitis vinifera* retard water losses, induce abscisic acid accumulation, and synthesis of defense-related terpenes in in vitro cultured grapevine. *Physiologia Plantarum*, 151, pp.359-374. DOI
- Santangelo, J.S., Turley, N.E. and Johnson, M.T., 2015. Fungal endophytes of *Festuca rubra* increase in frequency following long-term exclusion of rabbits. *Botany*, 93, pp.233-241. DOI
- Santoyo, G., Moreno-Hagelsieb, G., del Carmen Orozco-Mosqueda, M. and Glick, B.R., 2016. Plant growth-promoting bacterial endophytes. *Microbiological Research*, 183, pp.92-99. DOI
- Schisler, D.A., Slininger, P.J., Behle, R.W. and Jackson, M.A., 2004. Formulation of *Bacillus* spp. for biological control of plant diseases. *Phytopathology*, 94(11), pp.1267-1271. DOI
- Schulz, B., Haas, S., Junker, C., André, N. and Schobert, M., 2015. Fungal endophytes are involved in multiple balanced antagonisms. *Current Science*, 108(1), pp.39-45.
- Serra, S., Ligios, V., Schianchi, N., Prota, V.A. and Scanu, B., 2018. Expression of grapevine leaf stripe disease foliar symptoms in four cultivars in relation to grapevine phenology and climatic conditions. *Phytopathologia Mediterranea*, 57, pp.557-568. DOI
- Shameer, S. and Prasad, T.N.V.K.V., 2018. Plant growth-promoting rhizobacteria for sustainable agricultural practices with special reference to biotic and abiotic stresses. *Plant Growth Regulation*, 84, pp.603-615. DOI

- Sharma, I., Raina, A., Choudhary, M., Apra, Kaul, S. and Dhar, M.K., 2023. Fungal endophyte bioinoculants as a green alternative towards sustainable agriculture. *Heliyon*, 9, e19487. DOI
- Shen, F., Wu, W., Han, X., Wang, J., Li, Y. and Liu, D., 2021. Study on the occurrence law and green control of grape grey mold from the perspective of ecological balance. *Bioengineered*, 12, pp.779-790. DOI
- Shi, J., Zeng, Q., Liu, Y. and Pan, Z., 2012. *Alternaria* sp. MG1, a resveratrol-producing fungus: Isolation, identification, and optimal cultivation conditions for resveratrol production. *Applied Microbiology and Biotechnology*, 95, pp.369-379. DOI
- Singh, D.P., Singh, H.B. and Prabha, R., 2016. Microbial inoculants in sustainable agricultural productivity. *Springer*, 2, p.308. DOI
- Srivastava, S., Aspak Rana, M., Katyayani, K.K.S., Kaushik, D., Kumar, R., Shukla, M., Kumar, S., Manda, R.R. and Singh, V.P., 2023. Exploring the bioefficacy of endophytic bacteria against important plant pathogens. *Journal of Biopesticides*, 16(1), pp.79-99. DOI
- Srivastava, S., Rana, M., Sarma, B.K. and Meshram, S., 2024. Endophyte-mediated modulation of secondary metabolism in crops for biotic stress management. In: *Plant Endophytes and Secondary Metabolites*. Elsevier Inc., pp.205-233. DOI
- Statista, 2024. Grape production worldwide 2024 [WWW Document]. Statista. Available at: <https://www.statista.com/statistics/237600/world-grape-production-in-2007-by-region/>
- Sudawan, B., Chang, C.S., Chao, H.F., Ku, M.S. and Yen, Y.F., 2016. Hydrogen cyanamide breaks grapevine bud dormancy in the summer through transient activation of gene expression and accumulation of reactive oxygen and nitrogen species. *BMC Plant Biology*, 16, pp.1-18. DOI
- Suryanarayanan, T.S., Thirunavukkarasu, N., Govindarajulu, M.B., Sasse, F., Jansen, R. and Murali, T.S., 2009. Fungal endophytes and bioprospecting. *Fungal Biology Reviews*, 23, pp.9-19. DOI
- Xia, Y., Liu, J., Chen, C., Mo, X., Tan, Q., He, Y., Wang, Z., Yin, J. and Zhou, G., 2022. The multifunctions and prospects of endophytes and their metabolites in plant disease management. *Microorganisms*, 10, p.1072. DOI
- Yakop, F., Taha, H. and Shivanand, P., 2019. Isolation of fungi from various habitats and their possible bioremediation. *Current Science*, 116, pp.733-740.
- Yan, J.F., Broughton, S.J., Yang, S.L. and Gange, A.C., 2015. Do endophytic fungi grow through their hosts systemically? *Fungal Ecology*, 13, pp.53-59. DOI
- Yang, M.Z., Ma, M.D., Yuan, M.Q., Huang, Z.Y., Yang, W.X., Zhang, H.B., Huang, L.H., Ren, A.Y. and Shan, H., 2016. Fungal endophytes as a metabolic fine-tuning regulator for wine grapes. *PLOS ONE*, 11, e0163186. DOI
- Zhang, X., Zhou, Y., Li, Y., Fu, X., and Wang, Q., 2017. Screening and characterization of endophytic *Bacillus* for biocontrol of grapevine downy mildew. *Crop Protection*, 96, pp.173-179. DOI

... Continued from inner front cover

- The text of the manuscript should run into Abstract, Introduction, Materials & Methods, Results, Discussion, Acknowledgement (if any) and References or other suitable headings in case of reviews and theoretically oriented papers. However, short communication can be submitted in running with Abstract and References. The references should be in full with the title of the paper and mentioning names of all the authors.
- The figures should preferably be made on a computer with high resolution and should be capable of withstanding a reasonable reduction with the legends provided separately outside the figures. Photographs may be black and white or colour.
- Tables should be typed separately bearing a short title, preferably in vertical form. They should be of a size, which could easily be accommodated in the page of the Journal.
- References in the text should be cited by the authors' surname and year. In case of more than one reference of the same author in the same year, add suffix a,b,c,... to the year. For example: (Thomas 1969, Mass 1973a, 1973b, Madony et al. 1990, Abasi & Soni 1991).

## List of References

The references cited in the text should be arranged alphabetically by authors' surname in the following manner: (Note: The titles of the papers should be in running 'sentence case', while the titles of the books, reports, theses, journals, etc. should be in 'title case' with all words starting with CAPITAL letter). The references should be given in the "**Harvard Pattern**" as exemplified below.

- Dutta, A. and Chaudhury, M., 1991. Removal of arsenic from groundwater by lime softening with powdered coal additive. *Journal of Water Supply: Research and Technology—Aqua*, 40(1), pp.25-29. **(For Papers Published in Journals)**
- Goel, P.K., 2006. *Water pollution: Causes, Effects and Control*. New age international, New Delhi. **(For Authored Books)**
- Environmental Protection Agency (EPA), 2023. Air Quality and Pollution Data. Retrieved June 25, 2024, from <https://www.epa.gov/air-quality-and-pollution-data> **(For Data Retrieved from a Website)**
- Hammer, D.A. (ed.), 1989. *Constructed Wetlands for Wastewater Treatment-Municipal, Industrial and Agricultural*. Lewis Publishers Inc., pp.831. **(For Edited Book)**
- Haynes, R.J., 1986. Surface mining and wetland reclamation. In: J. Harper and B. Plass (eds.) *New Horizons for Mined Land Reclamation*. Proceedings of a National Meeting of the American Society for Surface Reclamation, Princeton, W.V. **(For Papers published in Edited Books)**

## Submission of Papers

- The papers have to be submitted online in a single WORD file through the online submission portal of journal's website: **[www.neptjournal.com](http://www.neptjournal.com)**

## Attention

1. Any change in the authors' affiliation may please be notified at the earliest.
2. Please make all the correspondence by e-mail, and authors should always quote the manuscript number.

**Note:** In order to speed up the publication, authors are requested to correct the galley proof immediately after receipt. The galley proof must be checked with utmost care, as publishers owe no responsibility for mistakes. The papers will be put on priority for publication only after receiving the processing and publication charges.



# Nature Environment and Pollution Technology

**(Abbreviation: Nat. Env. Poll. Technol.)**  
**(An International Quarterly Scientific Journal)**

Published by



## **Technoscience Publications**

A-504, Bliss Avenue, Opp. SKP Campus  
Balewadi, Pune-411 045, Maharashtra, India

In association with

## **Technoscience Knowledge Communications**

Mira Road, Mumbai, India

For further details of the Journal, please visit the website. All the papers published on a particular subject/topic or by any particular author in the journal can be searched and accessed by typing a keyword or name of the author in the 'Search' option on the Home page of the website. All the papers containing that keyword or author will be shown on the home page from where they can be directly downloaded.

**[www.neptjournal.com](http://www.neptjournal.com)**

**©Technoscience Publications:** The consent is hereby given that the copies of the articles published in this Journal can be made only for purely personal or internal use. The consent does not include copying for general distribution or sale of reprints.

Published for Proprietor, Printer and Publisher: Ms T. P. Goel, A-504, Bliss Avenue, Balewadi, Pune, Maharashtra, India; Editors: Dr. P. K. Goel (Chief Editor), Prof. K. P. Sharma (Honorary Editor) and Ms Apurva P. Goel (Executive Editor)